



UNITED NATIONS
UNIVERSITY



ORKUSTOFNUN

Geothermal Training in Iceland *2016*



Reports of the 6-month UNU Fellows
at the United Nations University
Geothermal Training Programme, 2016



UNITED NATIONS
UNIVERSITY

UNU-GTP

Geothermal Training Programme

Orkustofnun, Grensásvegur 9
IS-108 Reykjavík, Iceland

Geothermal Training in Iceland 2016

**Reports of the 6-month UNU Fellows at the
United Nations University
Geothermal Training Programme in 2016**

*Edited by
Málfríður Ómarsdóttir,
Lúdvík S. Georgsson and
Ingimar G. Haraldsson*

**ISBN 978-9979-68-428-2
ISSN 1670-7400**

The photo on the front page shows the Fellows of the 38th annual 6-month training at the UNU Geothermal Training Programme in 2016 at the Theistareykir high-temperature field, NE-Iceland with a geothermal drill rig in the background.

Back row from left (standing behind): Ionut Emil Tanase (Romania), Daniel Wanga Odongo (Kenya), Gideon Gitonga Gitobu (Kenya), Theoneste Nzayisenga (Rwanda), Anna Medgyesy (Hungary), James Karanja Kahutu (Kenya), Adrian George Foghis (Romania), Zsófia Unyi (Hungary), Harrison Kiplimo Keter (Kenya), Erios N. Sembatya (Uganda), Kristóf Boda (Hungary), Domokos Pásztor, (Hungary).

Mid row (standing in front): Winnie A. Apiyo (Kenya), Catherine Ndinda Leech (Kenya), Esther Mtimbaru Range (Tanzania), Nasim Saber (Iran), Sadock Josephat (Tanzania), Sarantsetseg Lkhagvasuren (Mongolia), Wang Wanli (China), Damaris Wacera Njoroge (Kenya), Rokiya Houssein Hassan (Djibouti), Pham Dieu Linh (Viet Nam), Birhan Abera Kebede (Ethiopia), Bertha A. Arenivar Marroquin (El Salvador), Mesay Fekadu Biru (Ethiopia), Zoltan Békés (Hungary).

Front row (kneeling): Andrei Lup (Romania), Fahman Hassan Abdallah (Djibouti), Byron F. Pilicita Masabanda (Ecuador), András Kovács (Hungary), Chagaka J. Kalimbia (Tanzania), Moses Kipsang Kachumo (Kenya), Danny Miguel Revilla Vargas (Bolivia), Valentin-Cristian Petrica (Romania).

INTRODUCTION

The 38th annual session of UNU-GTP was held from April into October 2016. A record number of thirty four UNU Fellows from 15 countries in five continents completed the traditional 6-month training, thereof 14 were women. They came from Bolivia (1), China (1), Djibouti (2), Ecuador (1), El Salvador (1), Ethiopia (2), Hungary (6), Iran (1), Kenya (8), Mongolia (1), Romania (4), Rwanda (1), Tanzania (3), Uganda (1), and Vietnam (1). UNU Fellows were trained in all eight lines of specialization: Geothermal Utilization (7 Fellows), Project Management and Finances (5), Reservoir Engineering and Borehole Geophysics (5), Chemistry of Thermal Fluids (4), Drilling Technology (4), Geothermal Geology (4), Geophysical Exploration (3), and Environmental Sciences (2). All were on fellowships from the Icelandic Government and UNU. Six UNU Fellowships were co-funded by the Kenya Electricity Generating Company (KenGen), while the six Hungarians and four Romanians were co-funded by the EES-Grants system, and one of each from Djibouti and Ethiopia by ICEIDA. One new country was added to the 6-month training repertoire with the six UNU Fellows from Hungary. Thus, during 1979-2016, 647 scientists and engineers from 60 countries have completed the annual 6-month training. Of the total, 38% have come from Africa, 35% from Asia, 14% from Latin America and the Caribbean, 12% from Central and Eastern Europe, and 1% from Oceania. The share of women grows steadily, with 141 women (22%) having attended. Over 90 professionals have received shorter training.

Seventeen UNU Fellows undertook MSc studies in 2016 under our cooperation agreements with University of Iceland (UI), and Reykjavík University (RU), coming from Bolivia (1), Djibouti (1), Ethiopia (1), Indonesia (1), Kenya (8), Malawi (2), St. Vincent and the Grenadines (1), Tanzania (1), and Yemen (1). The 6-month training at UNU-GTP can constitute up to 25% of the MSc studies. Six (from Ethiopia 1, Kenya 3, Malawi 1, and Tanzania 1) defended their MSc theses, while six started their MSc studies in 2016. At the end of 2016, 51 Fellows had completed an MSc degree on a UNU Fellowship. Furthermore, four UNU Fellows (from Kenya 3 and China 1) undertook their PhD studies at UI. One defended her dissertation in September, the second UNU Fellow to receive a PhD degree from UI (both are Kenyan women), while one started her studies (from China).

In April UNU-GTP signed a formal agreement with LaGeo S.A. de C.V. of El Salvador of increased cooperation on the development and running of the Diploma Course given at the University of El Salvador intended for Spanish speaking geothermal experts. The annual short course series for the region are now a part of the Diploma Course and Icelandic lecturers participate in the teaching. The Nordic Development Fund has agreed to support the course for 2016-2017, through the ICEIDA department of Ministry for Foreign Affairs (MFA) and UNU-GTP is responsible for the implementation with LaGeo.

Also new on the agenda was a cooperation with the Germany-based UNU-EHS in hosting four Kenyan and Ugandan MSc students from the PanAfrican University in Algeria. The students participated in lectures, but emphasis was on the MSc theses. UNU-GTP provided supervision during their 3-month stay in Iceland in the spring, and to the end of their studies in September when they graduated.

Our annual UNU Visiting Lecturer for 2016 was Mr. James Koenig from USA, the retired founder of the well-known geothermal company, GeothermEx. He gave a series of excellent lectures on geothermal development, which were very well presented and received.

In 2016, the annual series of short courses, given for E-Africa and Latin America and the Caribbean (LAC), were reorganized to better support the ideas set forward in the UN Sustainable Development Goals (SDG). The first event in the LAC region, the “*SDG Short Course I on Sustainability and Environmental Management of Geothermal Resource Utilization and the Role of Geothermal in Combatting Climate Change*” was held in El Salvador, September 4-10, in cooperation with LaGeo. A record number of 68 participants from 14 countries took part, with lecturers coming from El Salvador and Iceland, and with participants contributing as well. In E-Africa, the first event was the “*SDG Short Course I on Exploration and Development of Geothermal Resources*”, held in Kenya, November 10-30, in cooperation with KenGen and GDC. In all, 61 individuals from 16 countries participated in the Short

Course, with most of the lecturing done by Kenyan experts, with support from 5 Icelandic teachers, and 5 from the neighbouring countries. The SDG Short Courses were very well received by the participants.

UNU-GTP's intense activities in customer-designed courses continued in 2016. Short courses were given in Africa financed through the "*Geothermal Exploration Project in E-Africa*", in cooperation with the MFA-ICEIDA department and the Nordic Development Fund (NDF). These included three events: *A Short Course on Drilling Technology* given in May 14-26 in Djibouti, *A Short Course on Borehole Geophysics* in June 6-18 in Ethiopia, and *A Short Course on Project Management* given during October 31 – November 1 in Ethiopia before the ARGeo-C6 conference. Participation was good in all events. Two short courses were given in the Azores series, *Short course V on Well Design and Geothermal Drilling Technology* during January 18-30, and *Short Course VI on Geophysical Exploration for Geothermal Resources*, during April 4-16. Three events were given in Romania, a *Workshop on Utilization of Geothermal Resources for Decision Makers from Romania*, held May 27-28, *Short Course on Utilization of Low- to Medium-Enthalpy Geothermal Resources*, held April 4-8, and *Short Course II on Geothermal Resource Exploration*, held May 30 - June 3. Finally, *A Short Course on Status of Geothermal Energy* was given in Reykjavik during October 11-14, for a group of Hungarian experts. The European events were mainly financed through the EEA-funds initiative. All were well received.

Teaching and research supervision at the UNU-GTP in 2016 was carried out by geothermal specialists from ÍSOR (Iceland GeoSurvey), the University of Iceland and Reykjavik University, and specialists at other institutions, energy utilities and consulting engineering offices. In all, more than 100 teachers contributed to the training in this busiest year ever for UNU-GTP. Thanks are due to the teachers and supervisors, and their institutions. The availability of top quality supervisors for the various lines of study offered is of vital importance to our operations. Warm thanks are also due to our dedicated staff, Ingimar G. Haraldsson, Málfríður Ómarsdóttir, Markús A.G. Wilde and Thórhildur Ísberg.

The UNU programmes in Iceland had the honour of presenting their activities to the UN General Secretary, Mr. Ban Ki-Moon, during his October visit to Iceland. During his last year in office his focus was on ensuring that everybody pulls their weight in realising the UN Sustainable Development Goals, accepted at the UN meeting in Paris in late 2015, which certainly is something we can agree on.

Finally, we want to remind the readers that the reports presented here are written as a part of an academic exercise, and in most cases under a considerable time pressure. The reports have been written under close guidance of the supervisors. We are grateful for the dedication of the UNU Fellows and the teachers in their work at the UNU Geothermal Training Programme. Furthermore, we would like to point out that all the reports of the UNU-GTP from the start in 1979 are available at our website: www.unugtp.is, where they are published in colour.

With warmest regards from Iceland,
Lúdvík S. Georgsson, director

Information about the UNU Geothermal Training Programme

The Geothermal Training Programme of the United Nations University has operated at Orkustofnun (the National Energy Authority) in Iceland since 1979 with 6-month annual training for professionals who come mostly from developing countries. Candidates must have a minimum of one-year practical experience in geothermal work in their home countries prior to the training, and, preferably, be within 40 years of age. Specialized training is given in geothermal geology, geophysical exploration, reservoir engineering and borehole geophysics, environmental studies, chemistry of thermal fluids, geothermal utilization, drilling technology and project management and finances. Each trainee attends only one specialized course. The training is conducted in English. All candidates are selected by private interviews and receive scholarships (covering tuition, per diem and international travel) financed by the Government of Iceland and the UNU, or others. Upon completion of their training the participants receive a UNU Certificate. Further description can be found at our website: www.unugtp.is.

TABLE OF CONTENTS

	Page
8. Abera, B.: Geology, hydrothermal alteration and geological structures of well HE-59, Hellisheidi geothermal field, SW-Iceland.....	1
9. Apiyo, W.: Centralised monitoring and control dispatch centre for the geothermal wellhead power plants in Kenya	27
10. Arenivar Marroquín, B.A.: Environmental considerations in production tests and geothermal well stimulation.....	63
11. Békés, Z.: Geothermal district heating modelling for typical Hungarian residential buildings in Debrecen	97
12. Boda, K.: Fostering geothermal development in Hungary: Opportunities and bottlenecks.....	125
13. Fekadu Biru, M.: Analysis of well testing, temperature and pressure in high-temperature wells of Aluto-Langano, Ethiopia	169
14. Foghiş, A.G.: Geothermal development opportunities in Oradea	197
15. Gitobu, G.G.: Model organic Rankine cycle for brine at Olkaria geothermal field, Kenya.....	227
16. Hassan Abdallah, F.: Monitoring micro-earthquakes in a geothermal field.....	247
17. Houssein Hassan, R.: Geochemical interpretation of thermal water and gas samples from Lake Abbe, Djibouti.....	271
18. Josephat, S.: Geothermometry and quantifying of mixing and water-rock interactions in the Ngozi geothermal field, SW-Tanzania	289
19. Kachumo, M.K.: Financial viability of developing 35 MW of geothermal power at Menengai field, Kenya.....	311
20. Kahutu, J.K.: Challenges of directional well drilling in Kenya: Case study of Olkaria, Kenya and Theistareykir, Iceland geothermal fields	335
21. Kalimbia, C.: Business case of Ngozi geothermal power project, Mbeya, SW-Tanzania	359
22. Keter, H.K.: Methodology for optimizing pipeline route selection, separator and power plant placement in geothermal projects – case of Olkaria IV in Kenya.....	395
23. Kovács, A.: Electromagnetic exploration of the Eyjafjörður low-temperature geothermal area, N-Iceland.....	433
24. Leech, C.N.: Modelling the geochemical effects of geothermal fluid injection in the Olkaria geothermal field, Kenya.....	449
25. Lkhagvasuren, S.: Resistivity surveying in geothermal exploration with an application to the Eyjafjörður low-temperature area, N-Iceland	469
26. Lup, E.N.: Borehole geology, hydrothermal alteration and structure of well SV-26 in the Svartsengi area, SW-Iceland.....	495

	Page
27. Medgyesy, A.: Cogeneration of power and heat in Hungary	537
28. Njoroge, D.W.: Monitoring and evaluation framework for geothermal projects: Olkaria I unit 6, Kenya	557
29. Nzayisenga, T.: The basis for well design and drilling programme for geothermal exploration in Kinigi, Rwanda	575
30. Odongo, D.W.: Optimised pipeline route design for connection of a make-up production well: case study of well OW-906 for Olkaria IV power plant, Kenya	611
31. Pásztor, D.: Model review and sensitivity analysis of the Sárospatak reservoir model, NE-Hungary	647
32. Petrică, V.C.: Common geothermal well design and a case study of the low-temperature geothermal reservoir in Otopeni, Romania	669
33. Pham Dieu Linh: Chemistry of geothermal fluids in Dienbien and Sonla provinces, NW-Vietnam	693
34. Pilicita Masabanda, B.F.: A 3D model of the Chachimbiro geothermal system in Ecuador using Petrel	715
35. Range, E.M.: EIA of geothermal exploration in Tanzania: The laws and regulations, EIA process and preliminary EIA of exploration drilling in Ngozi area, SW-Tanzania	751
36. Revilla Vargas, D.M.: Analysis of bit operations: Laguna Colorada geothermal project, Bolivia	771
37. Saber, N.: Feasibility of private sector's participation in geothermal power generation in Iran	797
38. Sembatya, E.N.: Borehole geology, hydrothermal alteration and structural mapping of well HE-30, Hellisheidi, SW-Iceland	817
39. Tanase, I.E.: Geothermal reinjection in sedimentary basins	847
40. Unyi, Z.: Geothermal reservoir model of Dombóvár area, SW-Hungary	875
41. Wang Wanli: Modelling of tracer tests in a geothermal reservoir in Tianjin, China	891



UNITED NATIONS
UNIVERSITY

UNU-GTP

Geothermal Training Programme

Orkustofnun, Grensasvegur 9,
IS-108 Reykjavik, Iceland

Reports 2016
Number 8

GEOLOGY, HYDROTHERMAL ALTERATION AND GEOLOGICAL STRUCTURES OF WELL HE-59, HELLISHEIDI GEOTHERMAL FIELD, SW- ICELAND

Birhan Abera

Geological Survey of Ethiopia
P.O. Box 2302 Addis Ababa
ETHIOPIA
birhanabera@rocketmail.com

ABSTRACT

Well HE-59 is located in Hellisheidi geothermal field within the Hengill high-temperature geothermal area. It was drilled directionally to a total depth of 2400 m with a western bearing into Mt. Reykjafell. Binocular microscopy, petrographic analysis, X-ray diffraction analysis and fluid inclusion analysis were the major tools used to interpret the cutting samples that were collected from the upper 902 m, but subsequently total circulation loss occurred and cuttings were not retrieved at the surface. Beside these, the study was supported by borehole geophysical data and a surface structural study. The stratigraphy of well HE-59 is represented by dominant sub-glacial eruptions of hyaloclastite and thin layers of interglacial and postglacial basaltic lava flows and intrusions. The hyaloclastite formation is basaltic in composition and characterized by the inter-layering of basaltic tuff, breccia and pillow or glassy basalt. Structural correlation of the well path with the surface faults and fissures shows that the well crosses a nearby, narrow, postglacial volcanic fissure at 900 m and this is evidenced from the gyro survey, circulation losses and lithological and intrusion findings. The alteration zones in this well are challenging, where the hydrothermal mineral distribution and clay analysis show different outlines. However, the combination of the two approaches infers the presence of four alteration zones in the well. These zones are unaltered zones (0-150 m), a smectite-zeolite zone (150-616 m), a chlorite-epidote zone (616-716 m) and an epidote-wollastonite zone (716-902 m). From the temperature logs and circulation losses, four minor and five major aquifers were identified, which are related to geological boundaries and structures. The formation temperature, which is based on the temperature logs before the recovery of the well, together with fluid inclusions study and alteration temperatures indicate a cooling down of the system in this well. However, further temperature logs are necessary as they may change this assumption.

1. INTRODUCTION

Iceland is an island, surrounded by the North-Atlantic Ocean, situated between Greenland and continental Europe, close to the Arctic Circle. The country has a number of active geological areas, where geothermal resources are extensively exploited and supply steam and water both for power generation and different direct use purposes. Hengill is one of the largest high-temperature geothermal areas in Iceland, located in the southwestern part, about 30 km east of Reykjavik. Hellisheidi is one of the production field located within the Hengill geothermal field together with other two production fields and one exploration fields, namely Nesjavellir, Hverahlíð and Bitra respectively (Figure 1) (Franzson et al., 2010a and b; Gasperikova et al., 2015). The Hengill area has three power plants; two of them are situated at Hellisheidi and one at Nesjavellir geothermal field.

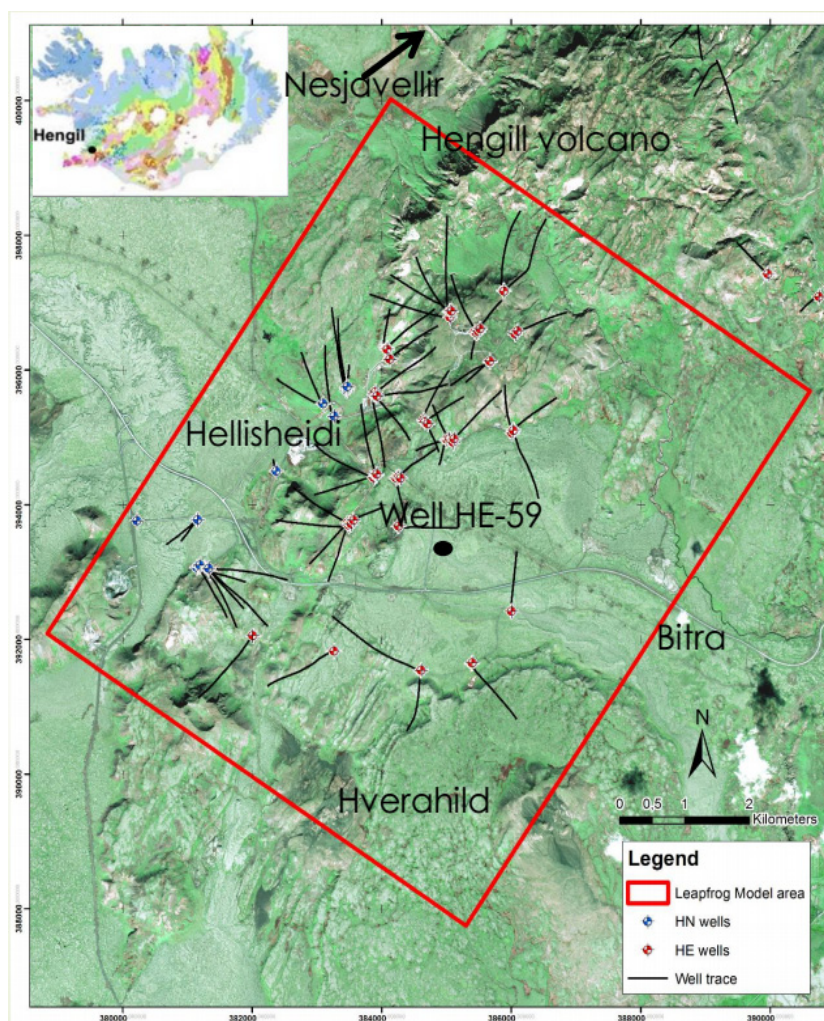


FIGURE 1: Map of Hengill area showing the four geothermal fields and location of well HE-59 (modified from Gunnarsdóttir, and Bastien, 2016)

Hellisheidi power plant is located in the southern part of Hengill volcanic complex, comprising a total of 59 deep (1300-3300 m) exploration and production wells which are currently producing about 303 MWe, and 133 MWth (Hardarson et al., 2015). Hengill geothermal area is within the SW rift zone of Iceland and has a size of 110 km², with a capacity of about 5500 GWh/y for 50 years (Franzson et al., 2010).

Surface thermal manifestations (Figure 2) in the area, are controlled by fractures and the central volcano and mainly found close to the volcanic fissures (Gasperikova et al., 2015). These include fumaroles, hot springs and altered ground.

Well HE- 59 is situated to the southern part of Hellisheidi geothermal field (Figure 1). The well is drilled to a total depth of 2400 m directionally aimed at intersecting volcanic fissures to the west. The objective of the well was to increase and keep up the production power capacity of the Hellisheidi power plant (make-up well).

This paper summarizes the results of geological, hydrothermal alteration and structural relationships in well HE-59.

2. GEOLOGY AND GEOTHERMAL SYSTEMS OF ICELAND

Geologically, Iceland is young and on the diverging Mid-Atlantic Ridge, which was created about 60 million years ago along the diverging American and the Eurasian plates, after the northwestward migration of Greenland, Eurasia and NE Atlantic plates over the Iceland plume (Sigmundsson, 2006). The continuous plate migration over the stationary mantle plume resulted in the complicated pattern of the present Icelandic rift zones, where rift jumps leave fossil rifts to the west and new ones forming to the east (Hardarson et al., 1997). The Icelandic volcanic rift zones (Reykjanes, Western Volcanic Zone, Eastern Volcanic Zone, and Northern Volcanic Zone) extend from Reykjanes peninsula in the southwest to the north through the country and divide into two parallel branches in southern Iceland (Figure 3). The rift zones are 40-50 km wide with 5-15 km wide en-echelon arrays and up to 200 km long volcanic fissure swarms (Saemundsson 1979; Sigmundsson, 2006). It has a general trend of NE-SW and N-S in the northern part.

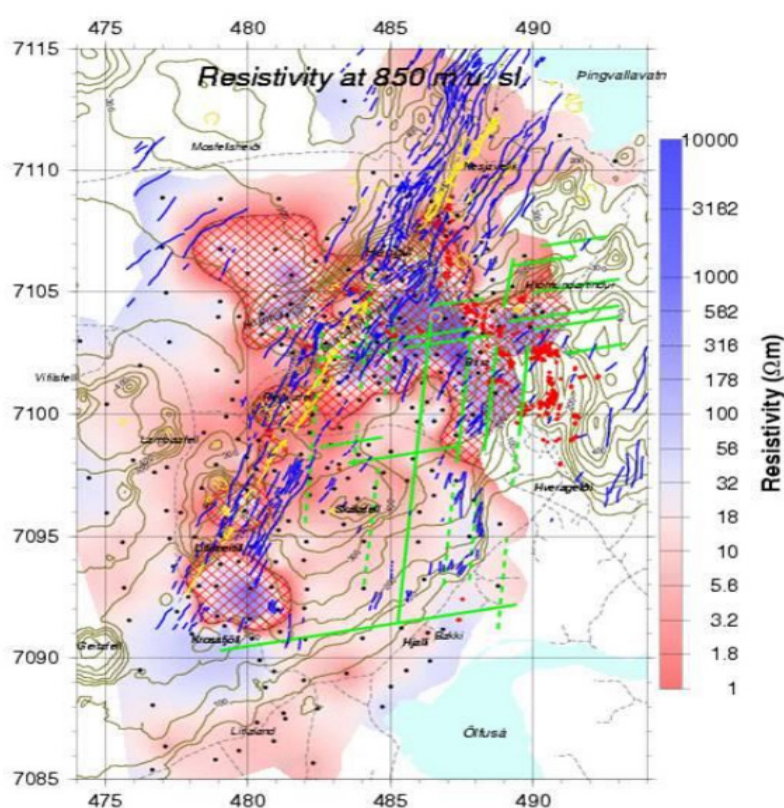


FIGURE 2: Resistivity at 850 m b.s.l. according to TEM surveys. High resistivity cores are shown with red, crossed lines. Surface geothermal springs as red dots. Postglacial surface fissure swarms and faults as blue lines. Green lines are fissures and faults defined by earthquake locations and yellow lines are postglacial fissures (Árnason, 2007)

Iceland is mainly made up of basaltic volcanic products of subglacial (hyaloclastites and pillow lavas), interglacial (lava flows) and postglacial (fissure eruptions) volcanic origin. Subglacial eruptions (eruptions under glacier ice), are the results of glacial periods during the last 3 Ma. According to Saemundsson (1979), the Icelandic volcanic pile is grouped into four stratigraphic series as Tertiary (> 3.3 Ma), Plio Pleistocene (0.8-3.3 Ma), Upper Pleistocene (0.8 Ma-11,000 yrs) and Postglacial (<11,000 yrs). The main rock type in Iceland is basalt, which covers 80-85% of the country, while intermediate-acidic rocks and sedimentary rocks cover 10% and 5-10% respectively. The oldest rock on the surface is dated to 16 million years old and located in the northwest and east parts of the country (Hardarson et al., 1997).

Geothermal systems in Iceland are classified as high- and low-temperature geothermal systems. High-temperature geothermal systems (>200°C at 1 km depth), are confined to active volcanism and rifting areas, while low-temperature geothermal systems (< 150°C at 1 km depth) are found outside the rift zones (Figure 3) within the Tertiary and Quaternary formations (Arnórsson et al., 2008). The Icelandic high-temperature geothermal systems have a heat source from magmatic intrusions while stratigraphic boundaries, faults and fractures are means of permeability. However, the heat source of low-temperature areas is crustal heat being conducted and convected upwards (Arnórsson et al., 2008; Franzson et al., 2010b).

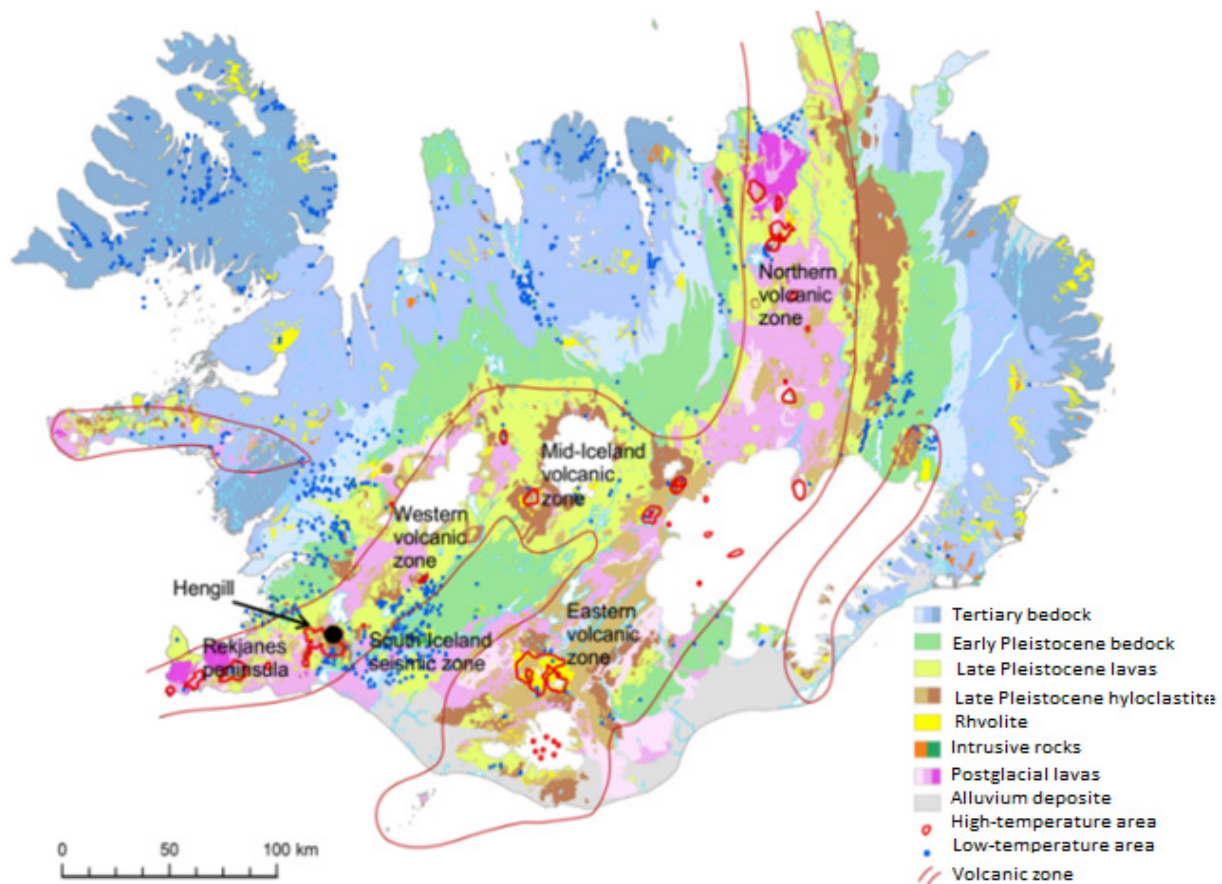


FIGURE 3: Geological and geothermal map of Iceland (modified from Hjartarson and Saemundsson, 2014)

3. GEOLOGY AND TECTONIC SETTING OF THE HENGILL-HELLISHEIDI AREA

About 0.4 Ma year old, Hengill central volcano is situated between the American and Eurasian diverging plate boundary, in the middle of the Western Volcanic Zone (Figure 3). It is a place where the three active tectonic zones; the Reykjanes Peninsula, the Western Volcanic Zone and the South Iceland Seismic Transform Zone form a triple junction (Gunnlaugsson and Gíslason, 2005; Franzson et al., 2005) which results in active tectonism, volcanism and seismic activity in the area. Hengill volcano is represented by elevated, dominant subglacial hyaloclastites (mostly consisting of pillow basalts, breccia and tuff), interglacial lava flows and postglacial eruptions of 9000, 5000 and 2000 years along NE-SW trending fissure swarms (Franzson et al., 2005). The Hengill fissure swarm is 60-70 km long to the north and south of the central volcano and 5-10 km wide. These are the main outflow zones for the geothermal system and the main drilling targets in the Hellisheidi geothermal field (Franzson et al., 2005). Tectonically, Hengill area is active and dominated by several NE-SW striking minor and well identified major normal faults, which are tilted to the east and west with a total down throw of 200 to 250 m (Hardarson et al., 2009; Hardarson et al., 2015; Helgadóttir et al., 2010; Franzson et al., 2005).

From recent studies, a narrow NNE-SSW running mini-graben, called Reykjafell mini-graben, has been identified along the western flank of Hengill volcano within the major fissure system (Figure 4 and 11). The mini-graben is 150-400 m wide with down-throws of up to 200 m at depth. Crossing the mini-graben in this area was the main drilling target for several production wells, which proved to be powerful producers (Hardarson et al., 2015).

3.1 Previous studies

3.1.1 Surface studies

Detailed geological mapping, geophysical and geochemical studies carried out on the surface, have revealed the existence of a large geothermal high-temperature anomaly in the Hengill area. The geophysical studies in the area carried out since 1971 include aeromagnetic, gravity and DC-resistivity surveys, seismic refraction and passive seismic surveys (Franzson et al., 2010).

The resistivity surveys (MT and TEM) have identified a 110 km² thermal anomaly at 850 m depth (Figure 2) and a low resistivity structure below 4 km depth. The high-resistivity anomaly also shows the dominant NNE-SSW alignment structures (Árnason, 2007; Franzson et al., 2010) (Figure 2).

Geochemical studies from fumarole samples show that the concentration of gases in the area is in equilibrium with mineral buffers at different temperatures. Gas geothermometry studies in the area have revealed a decrease in temperature towards the east (Gunnlaugsson and Gíslason, 2005).

3.1.2 Subsurface studies and hydrogeology

The first exploration well in Hengill geothermal field was drilled in 1985 (Franzson et al., 2005), followed by numerous vertical and later, dominantly directional production and reinjection wells. The directional wells generally have a “kick off point” at approximately 300 m and are subsequently aimed at intersecting major feed zones associated with boundary faults and fissures. The reservoir temperature at Hengill ranges from 200 to 340°C (Haraldsdóttir et al., 2015).

From borehole geology studies, the upper 1000 m b.s.l. in the Hengill area is dominantly hyaloclastites followed by extensive lava successions. These are mostly basaltic with occasional intermediate to acidic intrusives (dikes and/or sills), which are dominant below 800 m b.s.l. The intrusions form heat sources as well as permeability in the reservoir together with major faults (Franzson et al., 2005). The hydrothermal alteration distribution in Hengill reaches up to epidote-amphibole zone. The comparison of this with the formation temperature suggests equilibrium conditions, except some cooling at the western boundary of the Hellisheidi, cooling from the east towards Reykjafell and heating up towards the southern part of the area (Helgadóttir et al., 2010).

According to Franzson et al. (2005), the groundwater model of the area shows fluids from the outer boundaries of the system recharging the upflow. The main recharge channel is deep within the NE-SW fault zone that crosses the Hengill volcano where the permeability is believed to be highest. Higher up under Hengill the upflow divides, with some fluid flows to the NE into the fissure swarm towards Nesjavellir and some to the SW towards Hellisheidi.

4. RESULTS

4.1 Methodology and analytical methods

Binocular analysis: used to analyse cutting samples that were collected at every 2 m interval from well HE-59, to delineate the rock lithology, primary and secondary minerals and alteration, fracture fillings, oxidation and also intrusions. This analysis was carried out by using ‘Olympus’ binocular microscope.

Thin section analysis: played an important role, next to binocular analysis, which covers the major portion of the overall analysis. The analysis was conducted using ‘Leica’ petrographic microscope with 4x and 10x magnification power. A total of 11 samples were selected for thin section analysis, where

the result added some valuable data on primary and secondary mineral identification, alteration and alteration mineral sequences.

X-ray diffraction analysis (XRD): identifies clay minerals from 14 cutting samples, which were selected from different depths. The objective of these analyses is to outline different zones of clay alteration.

Fluid inclusion analysis: started by selecting appropriate quartz and calcite mineral grains from different depths and subjecting to polishing, so that the inclusions could be clearly seen under the microscope. Then micro thermometry was used to homogenise the temperature of the fluids trapped in the crystal.

Apart from these techniques, maps and GPS were used to track fissures and faults on the surface during structural studies. Software like Log plot and Leapfrog was used to plot geological and drilling logs and to compile the well's data with a 3D Leapfrog model of the area.

4.2 Drilling history of well HE-59

Well HE-59 is a make-up well for the Hellisheidi power plant. It was directed to the southwest towards a mini-graben, which is found in Mt. Reykjafell (Figure 4). Some of the most productive wells on Hellisheidi intersect that mini-graben (Hardarson et al., 2015). The well also transects a 12,300 years old volcanic fissure. Kick off point was planned at 352 m and build-up 3°/30 m, resulting in an inclination of 35° at 700 m. The azimuth was set at 252° (Figure 4). The drilling of HE-59 was achieved in four phases during February and March 2016. Drilling depths, casing depths and drill bits are presented in Table 1. The pre-drilling was done by the rig Nasi (Shcramm T130XD), but phases 1-3 by the rig Thor (Bentec Euro Rig 350).

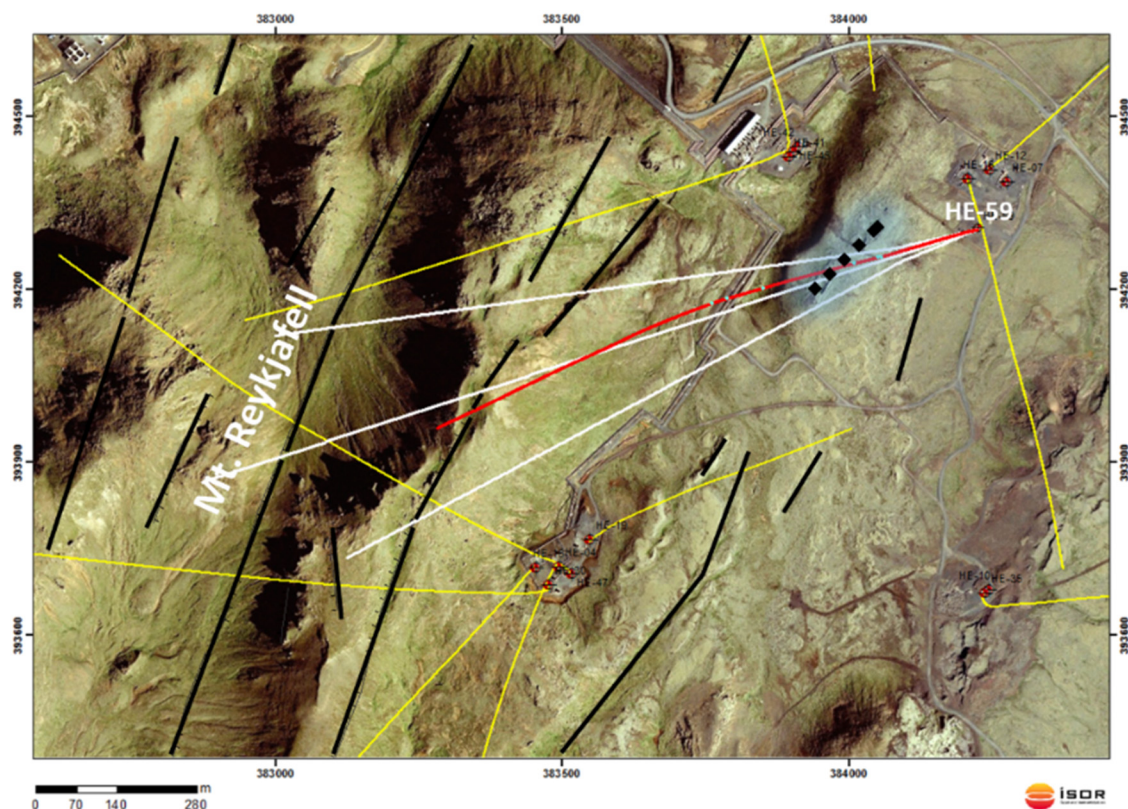


FIGURE 4: The well path of HE-59 extrapolated to the surface (red line). White lines show the planned track and allowed deviation. Yellow lines are nearby wells, black lines represent faults and fissures and black dotted line is the small fissure west of the wheel pad (Helgadóttir et al., 2016)

TABLE 1: Drilling depth, casing depth and drill bits in well HE-59. Depths refer to the platform of Thor, 9 m above ground level (Helgadóttir et al., 2016)

Rig (Drill pad)	Phase	Drill bit	Depth (m)	Casing depth (m)	Casing Diameter
Nasi (1.9 m)	Pre-drilling	26"	114.7	113.7	18 $\frac{5}{8}$ "
Thór (9 m)	1. phase	17 $\frac{1}{2}$ "	317	314.2	13 $\frac{3}{8}$ "
Thór (9 m)	2. phase	12 $\frac{1}{4}$ "	800	798.7	9 $\frac{5}{8}$ "
Thór (9 m)	3. phase	8 $\frac{1}{2}$ "	2183	762-1130	7"

Pre-drilling

Well HE-59 was spudded on April 17th 2016 using the rig Nasi and pre-drilling was completed at a depth of 114.7 m on April 23rd. The well was cased with 18 $\frac{1}{4}$ " surface casing to 113.7 m and cemented using 29 m³ of slurry. No circulation losses were observed. Drilling fluid was mud.

Phase 1. After setting up the rig Thor on the well, phase 1 commenced on May 17th and was completed on May 19th at 317 m depth. Following a logging program (temperature, calliper, resistivity, NN and gamma) the well was cased with 13 $\frac{3}{8}$ " anchor casing to a depth of 314.2 m. The casing was set with 33 m³ of cement slurry. No circulation losses were encountered during drilling of phase 1. Drill fluid was mud.

Phase 2. After WOC (weight on cement), welding a flans and testing the BOP (blowout preventer) unit, phase 2 started on May 25th, on Thor's 9th working day. Drilling was achieved using a 12 $\frac{1}{4}$ " bit, motor and MWD (Measure While Drilling). Drill fluid was mud. The drilling was completed at 800 m depth on May 28th and no circulation losses were observed. Gyro logging showed that the azimuth at 785 m depth was 254° and the inclination 34,5°, which is close to the targets. The 9 $\frac{5}{8}$ " production casing was RIH (Run In Hole) to a depth of 798,7 m and set with 42,5 m³ of cement slurry.

Phase 3. Following preparations and BOP tests phase 3 commenced on June 2nd using water. This phase proved to be rather complicated and several problems were encountered. Early in the drilling phase circulation losses occurred and had to be plugged with cement. However, as drilling cement commenced, the well side-tracked. Total loss was encountered in the side-tracked well at 904 m depth and no cuttings were retrieved after this. Drilling continued and the string got stuck a few times but the crew managed to get it loose every time. Drilling was stopped at 2381 m depth when the string got stuck once again. After several attempts to loosen the string it was cut by explosives at 1130 m and a 7" slotted liner was RIH. Drilling of HE-59 was completed at July 11th, 2016. Circulation losses during phase 3 are shown in Table 2.

TABLE 2: Circulation losses during drilling phase 3 of HE-59 (Helgadóttir et al., 2016)

Depth (m)	Losses (l/s)
833	18
835	26
840	45
850	30
885	30
890	18
902	>45

4.3 Stratigraphy of well HE-59

The cutting samples from the well were only collected down to 902 m due to total circulation loss below that depth. From the upper 902 m of the well, different lithologies were identified with the help of binocular microscope. The lithology of well HE-59 falls into two groups; hyaloclastites and crystalline basaltic rocks. Hyaloclastites incorporates subglacial eruption products of basaltic tuff, basaltic breccia and pillow lava, while crystalline basalt encompasses lava flows. The detailed lithological description of each of these rock units is described below, and shown in Figure 5.

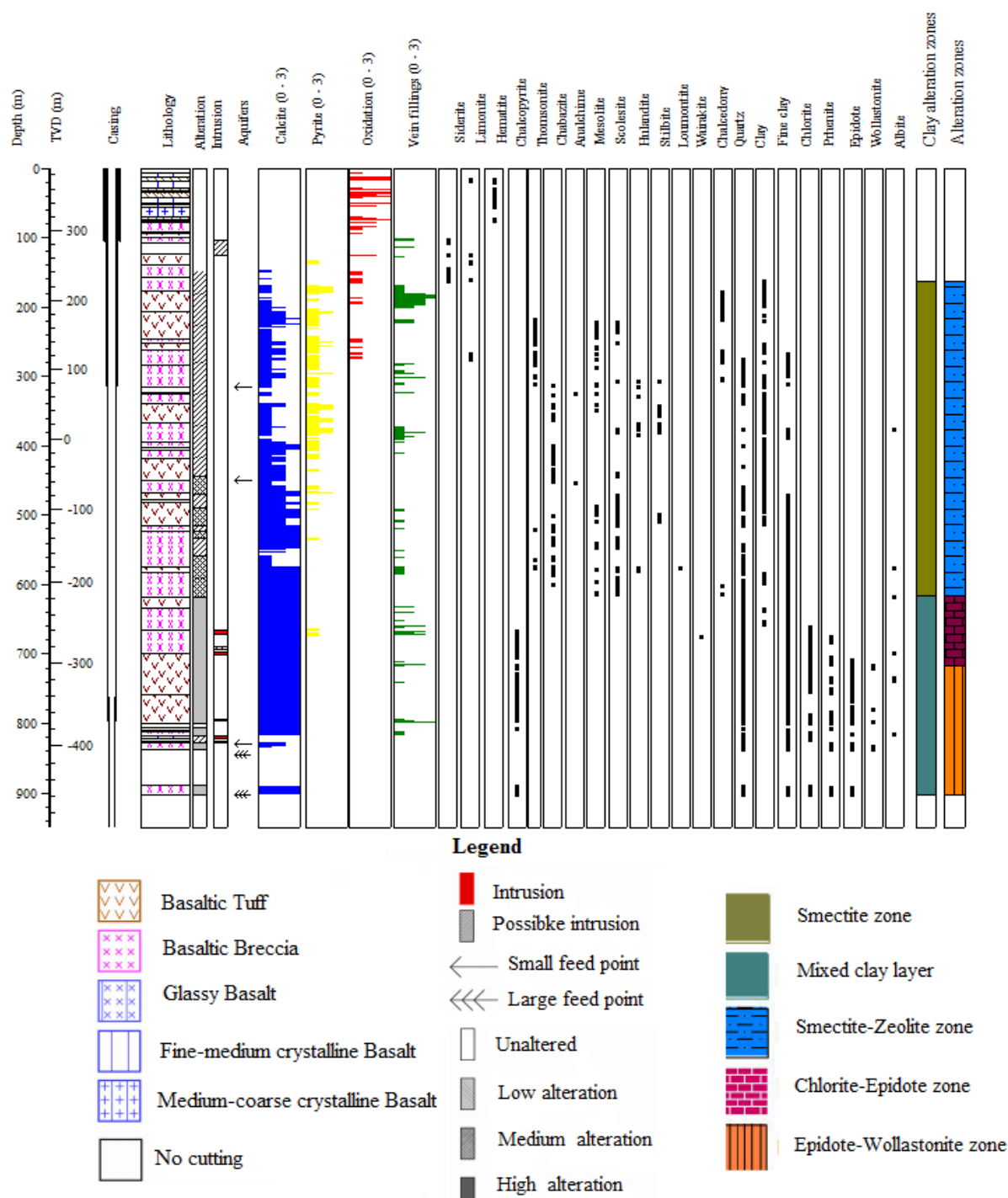


FIGURE 5: Lithology and hydrothermal minerals distribution in well HE-59. Feed zones are shown as arrows. Alteration zones are indicated far right

0-6 m: No cuttings

6-12 m: *Fine- to medium-grained crystalline basalt*

Fine- to medium-grained, greyish and partly porous unaltered basalt with very slight oxidation at 8 m. It has primary minerals like plagioclase, olivine and pyroxene.

12-18 m: *Scoria*

Reddish scoria with plagioclase phenocrysts and abundant hematite and limonite.

18-28 m: *Fine- to medium-grained crystalline basalt*

Fine- to medium-grained, greyish crystalline basalt with crystals of plagioclase, olivine and abundant pyroxene.

28-32 m: *Scoria*

Slight to highly oxidized reddish and few black scoria, having crystals of olivine and plagioclase phenocrysts, rich in hematite.

32-34 m: *Fine- to medium-grained crystalline basalt*

Fine- to medium-grained, greyish basalt with few olivine and plagioclase phenocrysts. The cuttings are slightly mixed with scoria from the upper sections.

34-42 m: *Scoria*

Oxidized reddish and a few black and brownish scoria. Plagioclase as a primary mineral and hematite are common.

42-50 m: *Fine- to medium-grained crystalline basalt*

Fine- to medium-grained, greyish basalt. Plagioclase is the dominant primary mineral, but some olivine and pyroxene are also occurring. The cuttings are slightly mixed with oxidized scoria.

50-52 m: *Scoria*

Highly oxidized reddish scoria with plagioclase phenocrysts.

52-56 m: *Fine- to medium-grained crystalline basalt*

Light greyish medium-grained basalt. At 56m, the cuttings are mixed with oxidized scoria from the upper section.

56-70m: *Medium-to coarse-grained crystalline basalt*

Light greyish pyroxene rich basalt with small olivine.

70-74 m: *Scoria*

Moderately oxidized scoria, has hematite in vesicles.

74-76m: *Basaltic tuff*

Oxidized, medium- to coarse-grained reddish brown tuff and fragments of glass.

76-78 m: *No cuttings*

78-92 m: *Basaltic breccia*

Medium-to coarse-grained reddish brown, light greyish and dark greyish oxidized moderate to highly welded tuff with slightly oxidized porous fine- to medium-grained basalt. The depth 84 to 92 m consists of a mixture of this rock unit with light yellowish sandstone. Plagioclase crystals and glass fragments are common.

92-94 m: *Glassy basalt*

Black, shiny holocrystalline basalt (pillow basalt).

94-100 m: *Basaltic tuff*

Fine- to medium-grained oxidized reddish brown, light greyish, and greyish strongly welded tuff with common glass and crystals of plagioclase and olivine.

100-107 m: *Basaltic breccia*

Light greyish very slightly altered tuff, abundant with glass together with yellow to light greyish and light reddish brown fine sand stone. Fine-grained black fresh basalt (probably intrusive) is also mixed

from 104 m with the cuttings. Glass and plagioclase crystals are common with secondary mineral siderite. At 106 and 107m, the cuttings are slightly oxidized.

107-124 m: No cuttings

124-140 m: *Basaltic tuff*

Light greyish and dark greyish moderately to highly welded tuff with plagioclase crystals and little glass. Pyrite emerges at 136 m as very fine and dispersed.

140- 158 m: *Basaltic breccia*

Light greyish and greyish moderately welded tuff and greyish partially porous fine basalt with plagioclase and glass. Siderite is a common secondary mineral. From 150 to 158 m the cuttings are slightly altered.

158-176 m: *Basaltic breccia*

Greenish and greyish tuff with greyish, fine-grained basalt consisting of black xenoliths in abundance (164-176 m). At 160 m the greenish tuff shows an increase in alteration. At 162 m, siderite, amorphous silica and at 172 m calcite is occurring. Other secondary minerals include sparse, very fine pyrite and greenish clay. Plagioclase and minor olivine are the primary minerals encountered.

176- 206 m: *Basaltic tuff*

Greyish, moderate to highly welded and slightly altered tuff, where the pore spaces and veins are extensively filled by chalcedony. Pyrite (at 188, 192 and 204 m) and calcite are also found. Plagioclase with some olivine present as primary crystals. Chalcedony is quite abundant from 180 to 190 m. Zeolites (thomsonite) emerge at 176 m.

206- 246 m: *Basaltic tuff*

Dominantly light greenish, grey and dark greyish, fine- to medium-grained, slightly altered tuff, with plagioclase crystals. At 222 m the tuff has vesicles are filled with green clay. There is an increased amount of calcite with dispersed fine pyrites. Chalcedony and zeolites (chabazite, thomsonite, mesolite and scolecite) are also increasing after 218 m.

246-252 m: *Basaltic breccia*

Fine to medium, light greenish grey tuff, with plagioclase crystal mixed with fine black basalt. Alteration minerals include green clay and zeolites. The cuttings are slightly altered.

252-262 m: *Basaltic tuff*

Fine- to medium, light greenish grey and dark greyish, slight to moderately welded tuff. The cuttings are faintly altered and consist of some pyrites, crystalline calcite, zeolites and clay.

262-284 m: *Tuff rich basaltic breccia*

Dominantly black, fragile tuff, with fine- to medium-grained light greenish and greyish, poorly to moderately welded tuff. Minor black fine-grained basalt is also occurring. The cuttings have zeolites, chalcedony and sparse limonite.

284-316 m: *Basaltic breccia*

Light greenish grey and dark greyish, fragile and moderately welded tuff, which is slightly to moderately altered, with black fine porphyritic, relatively unaltered basalt (has crystals of plagioclase and micro olivine). At 308-314 m, the basalt is partially porous and some are filled by zeolites at 314 m. The cuttings include calcite, pyrite, quartz, zeolites, clay and minor siderite.

316-324 m: No cuttings

324- 326 m: Fine- to medium-grained crystalline basalt

Dark greyish, fine- to medium-grained basalt, with micro olivine crystals. Zeolite (analcime) is found at this depth.

326-340 m: Basaltic breccia

Fine-grained, slightly porous, dark greyish basalt (some of the pore spaces are filled with zeolites) mixed with fine, greyish, slightly welded tuff and glass. Abundance of fragments of cement grout. Small amounts of calcite, pyrite, quartz, zeolites, clay and limonite are also present.

340-366 m: Basaltic tuff

Fine-grained, poorly welded black tuff, with partially altered glasses. Below 352 m, light greenish grey tuff is mixed in. At 342 m, the amount of calcite and alteration is increasing. There is also an increase in pyrite, but constant amount of zeolites (chabazite and mesolite) and quartz.

366- 402 m: Tuff rich basaltic breccia

Minor, fine- to medium-grained black basalt, mixed with greenish grey, very slightly to somewhat compacted tuff. At 394-402 m the tuff is moderately altered and more compacted, dominated by white secondary minerals like calcite.

402-406 m: Basaltic tuff

Poorly to moderately welded black and greyish tuff. The cuttings have zeolites (e.g. chabazite) and black clays with abundant calcite and rare pyrite.

406-418 m: Tuff rich basaltic breccia

Few, fine-grained black basalts with moderately welded black and greyish tuff. The cuttings are slightly altered and commonly have secondary minerals like calcite, pyrite and zeolites.

418-450 m: Basaltic tuff

Fine- to medium-grained and loose and moderately welded, some coarse grained, light greyish and greyish tuff. Moderately welded with the commonly partly altered dark brownish glass. Black medium-grained with high amount of zeolites (e.g. thomsonite) and remnant of altered glass. Moderately altered.

450-468 m: Tuff rich basaltic breccia

Fine-grained, light greenish grey, poorly and moderately welded, mixed with some greyish fine- to medium-grained basalt.

468-478 m: Basaltic tuff

Fine- to medium-grained, light greenish grey, greyish and black, slightly to moderately welded tuff. Quartz, zeolites, and clays are present as secondary minerals.

478- 482 m: Basaltic breccia

Fine-grained, light greenish grey, moderate to highly welded tuff, together with dark greyish fine porphyritic (with crystals of plagioclase and few olivine) basalt. Clays, zeolite, quartz with common pyrite and calcite are also occurring.

482-516 m: Basaltic tuff

Dominantly greenish grey, and slightly to moderate welded tuff with some black fragile tuff. Zeolites (scolecite and mesolite), quartz and clays are also found.

516-524 m: Basaltic breccia

Fine- to medium, mixed light greenish, greyish and black, moderate to highly compacted tuff, together with fine black basalt, which has plagioclase and minor olivine phenocrysts. Some glassy basalt at 520-522 m is also mixed in.

524- 574 m: Tuff rich basaltic breccia

Dominantly fine- to medium-grained, greenish grey and few black, slight to moderately welded tuff. The tuff is mixed with light brownish grey, partly porous tephra at 534-538 m. Some of the pores are filled with scolecite. Calcite and some pyrite are occur.

574-582 m: Basaltic tuff

Fine-grained, light greenish grey, slightly to moderately welded tuff. It is relatively altered and has some glass fragments. An increase in calcite with some clay, zeolites and quartz are observed.

582- 618 m: Basaltic breccia

Greenish and greyish slightly to moderately welded and moderately altered tuff, together with slightly altered light brownish grey, partly porous (filled with greenish clay and quartz) tephra. Well crystallized coarse pyroxene is observed in high amounts.

618-634 m: Basaltic tuff

Fine- to course grained, light greenish, moderate to strongly welded and highly altered tuff with few black tuffs. Green clay and quartz are common with high amount of calcite.

634-666 m: Basaltic breccia (tuff rich)

Light greenish and greenish grey, moderately to strongly welded and highly altered tuff, together with fine-grained, fresh and slightly altered black and greyish basalt.

666-700 m: Basaltic breccia

Fine- to medium-grained, greyish, light greyish and black basalt (intrusive) together with light greenish grey slight to moderately welded and heavily altered tuff.

700- 758 m: Tuff rich basaltic breccia

Moderately altered, black fine-grained basalts with dominant fine light greyish, strongly welded and highly altered tuff. Plagioclase is common. From 716 m, greyish basalt and greenish tuff become dominant. There is slight oxidation from 724 to 736 m which might be part of a fault breccia. An emergence of epidote is recorded at 708 m, prehnite at 676 m and wollastonite at 716 m. Well defined cubic pyrite crystals are occurring at 726 m. Primary crystals of pyroxene and plagioclases are common.

758-800 m: Basaltic tuff

Fine- grained, light greyish, strongly welded and highly altered tuff with common plagioclase crystals. For the upper parts, minor, fairly altered, black fine-grained basalt is mixed.

800-806 m: Cement grout

The cement is very lightly mixed with light greenish tuff, calcite and quartz at 806 m.

806-810 m: Basaltic breccia

Heavily altered greenish tuff and fine-grained greyish basalt with dominant white primary and secondary minerals (plagioclase, calcite and quartz).

810-812 m: Basaltic tuff

Dominated by white primary and secondary minerals (plagioclase, calcite and quartz), with very strongly altered light greenish tuff.

812-818 m: Basaltic breccia

Highly altered, greenish tuff and slightly altered fine-grained dark greyish and greyish basalt, with dominant white primary and secondary minerals

818-822 m: Fine- to medium-grained crystalline basalt

Fine- to medium-grained, black and grey basalt (intrusive) mixed with few tuffs.

822-826 m: Basaltic breccia

The cuttings contain highly altered, greenish tuff and fragments of the basalt from the intrusive.

826-828 m: Fine- to medium-grained crystalline basalt

Black and fresh, fine- to medium-grained basalt (intrusive).

828-838 m: Basaltic breccia

A mixture of black, fine- to medium-grained basalt and highly altered greenish tuff with common plagioclase, quartz, chlorite, prehnite, chalcopyrite, epidote and wollastonite.

838-888 m: No cuttings

At 843 m there is black shiny and fresh basalt with secondary minerals of chlorite and chalcopyrite. The depth 865 m has light greenish moderate to highly welded tuff.

888-902 m: Basaltic breccia

Dominated by highly altered, light greenish tuff, with some fine-grained shiny black basalt. Hydrothermal minerals include quartz, chlorite, and chalcopyrite.

4.4 Intrusions

Several intrusive rocks were encountered in well HE-59. The depths 104-126, 690-694 and 794-796 m are marked by probable intrusions and 666-672, 698-702, 818-822 and 826-828 m are identified as intrusions (Figure 5). An intrusion is fresh or slightly altered compared to the surrounding rocks and sometimes it can be identified by the oxidation and increased precipitation of hydrothermal minerals (e.g. calcite and pyrite) at their margins, as at the depth of 104-124 m. The intrusions in well HE-59 are dominantly black and greyish, fine- to medium-grained crystalline basalt, while from 666 to 672 m it is characterized by medium- to coarse-grained, dark and fresh basalt. Petrographic analysis of the intrusions shows poikilitic texture from 822 m (Figure 6), where the plagioclase crystals are enclosed by pyroxene (augite) and olivine.

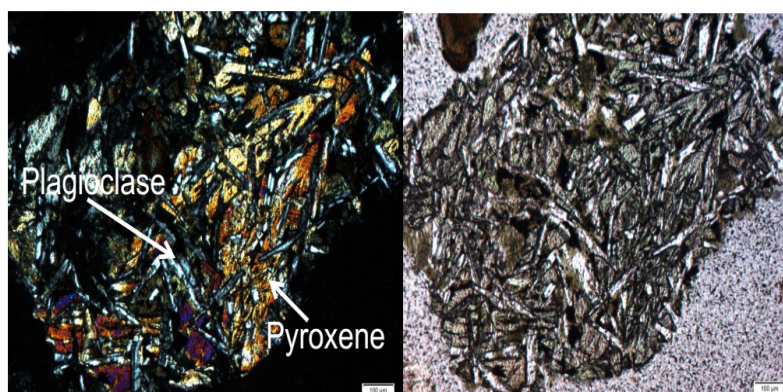


FIGURE 6: Crossed (to the left) and plane polarized (to the right) view of thin section picture showing poikilitic texture in the basaltic intrusion. The scale is 100

4.5 Hydrothermal alteration

4.5.1 Alteration of primary minerals

In high-temperature geothermal systems like Hengill, the replacement of primary minerals by secondary minerals (hydrothermally altered minerals), as a result of fluid-rock interaction, is a common process and one of the most important part of borehole studies.

Primary minerals, including olivine, pyroxene and plagioclase, are found in the form of phenocrysts and micro phenocrysts. Plagioclase is the most abundant primary mineral throughout this well, in the form of euhedral and subhedral crystals, and typically after 450 m, it is found as coarse-grained regularly

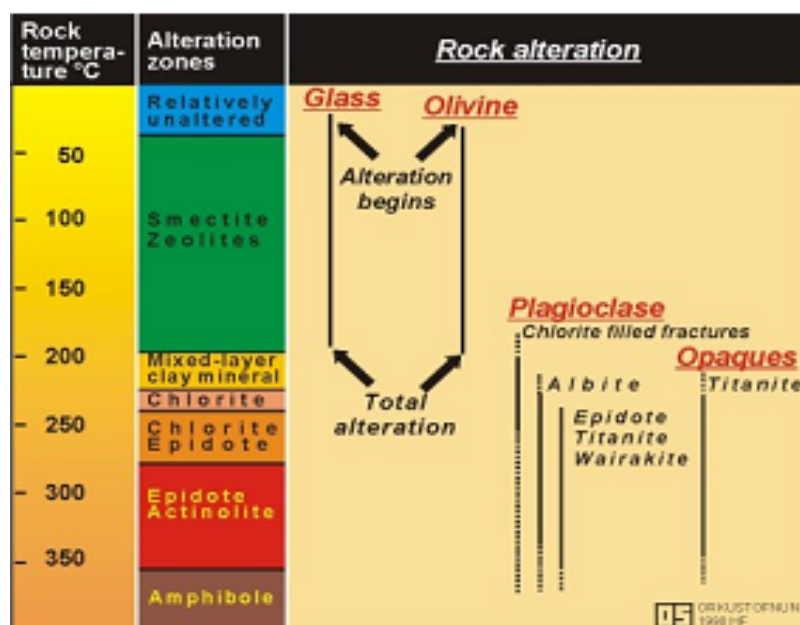


FIGURE 7: Zones of rock and mineral alteration in Iceland (Franzson, 1998)

crystallized grains. In the hydrothermal process it will be transformed to albite, calcite, epidote and wairakite. The second abundant mineral in the well, pyroxene, is very common with its well defined prismatic crystal shape and coarse grains, especially from 586 to 618 and 714 to 742 m. Olivine is mostly found as micro crystalline in the lava flows. The replacement mineral for pyroxene and olivine can be pyrite, chlorite, quartz, calcite and actinolite at high temperatures ($> 280^{\circ}\text{C}$). Volcanic glasses are susceptible to hydrothermal alteration (Figure 7) at low-temperature and are easily changed to clay, chlorite, zeolites and calcite.

The replacement of these minerals, and some opaque minerals, by secondary minerals is dependent on temperature, composition of fluids, and permeability of the rocks. The hydrothermal minerals encountered in well HE-59 that have been identified, mainly by using binocular microscope as well as in thin sections and XRD, are described below.

Hematite: is a secondary mineral replacing magnetite in the shallow alteration environment. It is steel-black, shiny with metallic lustre and well-rounded spherical shape. It was seen at the very first depths of analysis and becomes dominant from 30 to 56 m, mostly hosted by scoria.

Limonite: is yellowish brown in colour and is the result of oxidation at shallow depths. In well HE-59, it appears at 14 m.

Siderite: is an iron carbonate mineral with a reddish brown colour and spherical appearance. Siderite mostly occurs at the edges of intrusions, as seen in this well. Siderite is appearing generally rarely but at shallower depths, it is fairly common. It is associated with pyrite.

Pyrite: is amongst the most common hydrothermal minerals. It is encountered throughout the well from 136 to 838 m. It is found as disseminated, small, micro cubic crystals, except at some depths, like 382 m and 602 m, where it is coarser with perfect regular cubic shape. The occurrence is mainly dispersed in the rock matrices and within fractures and vesicles. It is associated with calcite, quartz, and zeolite. Pyrite and Chalcopyrite may indicate permeability.

Calcite: is the most common secondary mineral in the well, as it can be formed at a minimum temperature of 50°C and up to 300°C . It is found associated with clay, quartz, and zeolites. It emerges at shallow depths, 150 m in the basaltic tuff unit, and found as veins and vesicle fillings. At some depths, like 222 m, 252-258, 326, 416, 472, 482, 488, 512, 574-576 and 590 m, it is platy and transparent. Platy calcite may indicate boiling conditions in the formation. From 784 to 796 m it shows an increase in amount.

Chalcedony: is an amorphous form of quartz, with milky white to light bluish colour as it appeared in well HE-59. Its first appearance is recorded at 178 m and it extensively appeared down to 202 m in the form of veins and vesicle fillings, and it shows strong association with zeolites.

Zeolites: are low-temperature, hydrous, hydrothermal minerals that are common at shallow depths in geothermal systems. Different varieties of zeolites appeared in the well according to their specific temperature of formation. These can be identified by their definite shape of tabular, fibrous and granular (Saemundsson and Gunnlaugsson, 2014).

Zeolites from the well HE-59 were identified by binocular microscope and thin section, first found at 214 m and last observed at 614 m, but wairakite was seen at 676 m. Their occurrence is in the form of vesicle fills and rarely as veins within the basaltic tuff and breccia rock units. The distribution of different kinds of zeolites in this well is described below.

Chabazite: appeared as a granular cubic shape and as a bunch of small and compacted cubic crystals together forming rounded shapes. It is found as a cavity filling. Chabazite represent the lowest temperature, 50-70°C (Saemundsson and Gunnlaugsson, 2014) and is the first zeolite to emerge at 214 m. It mostly appears with thomsonite.

Thomsonite: is a flattened and fibrous radiating zeolite. It is dominant and occurs as vesicle and vein fillings. Thomsonite first appeared at 218 m, and was lastly seen at 614 m. Its occurrence shows the association with chabazite and scolecite/mesolite. Based on Saemundsson and Gunnlaugsson (2014), 50-120°C is the temperature where thomsonite occurs.

Analcime: is a granular type of zeolite group, found as white, multi-faced shaped, trapezohedron crystal, white in colour. It is stable at wide range of temperatures (50-160°C) but is rare in this well. The first appearance of analcime is recorded at 326 m.

Scolecite/mesolite: form aggregates of fibrous and elongated slender crystals. Scolecite is thicker and has flattened surfaces, while mesolite is thinner and spiky. They are white and occurred as vesicle and vein fills from 222 to 614 m associated with different zeolites. Scolecite/mesolite represent the temperature range 70-120°C (Saemundsson and Gunnlaugsson, 2014).

Stilbite: prismatic group of zeolites. It resembles quartz with its milky-white appearance. It is formed at temperatures of 70-140°C. Stilbite was first seen at 368 m and thin section analysis revealed its presence at 308 m.

Heulandite: appeared as a colourless, transparent, tabular crystal with a perfect cleavage. It is formed in a temperature range of 60-150°C and first found at 330 m, but under thin section it appeared at 308 m (Figure 8).

Laumontite: is tabular and white in the cuttings. It is rare in this well and it appeared only at 576 m representing the wide temperature range of 110-230°C.

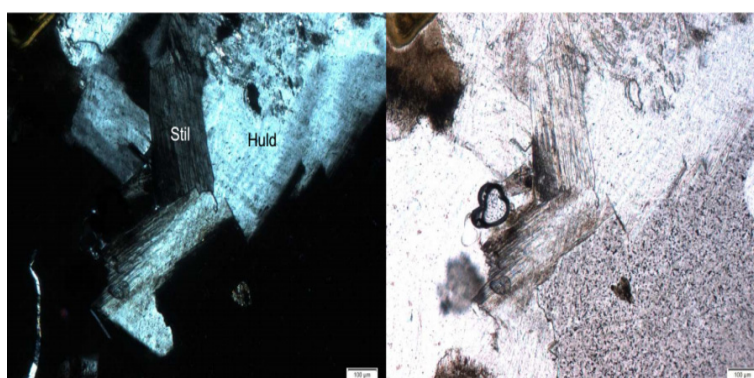


FIGURE 8: Crossed (to the left) and plane polarized (to the right) view of stilbite and heulandite from 376 m. The scale is 100 μ m

Wairakite: is a high-temperature, granular zeolite with trapezohedron crystal shape, resembles analcime, since it is Ca-substitute of the analcime. It is associated with quartz and found only at 676 m, indicating a temperature of at least 200°C (Table 3).

Clays: are among the most abundant and most common alteration minerals in geothermal systems.

Clay formation is mostly the result of the alteration of glass, in a wide range of temperatures ranges from below 200 to above 300°C (Table 3). The temperature range results in different types of clays. In this well, three different clay varieties have been studied, namely smectite, mixed layer clay and chlorite, as described below. Clays were found as both vein and vesicle fillings. The analysis was achieved by using binocular microscope, thin section and XRD analysis.

TABLE 3: Common alteration minerals and respective temperature ranges in high-temperature geothermal systems (Kristmannsdóttir, 1979; Franzson, 1998)

Minerals	Min. temp. °C	Max. temp. °C
zeolites	40	120
*laumontite	120	180
quartz	180	>300
*wairakite	200	
smectite		<200
**MLC	200	230
chlorite	230	>300
calcite	50-100	280-300
prehnite	240	>300
epidote	230-250	>300
wollastonite	260	>300
actinolite	280	>300

*Belong to the zeolite group.

**Mixed layer clay.

Smectite: is light greenish in colour and fragile, a common clay mineral at shallow depths. In well HE-59, smectite was seen first at 220 m from the XRD analysis and from the binocular analysis, it is identified first at 164 m.

Mixed layer clay: represents the presence of different clay minerals that can form at a temperature range of 200 to 230°C (Table 3). It is seen from 616 m and is confirmed by the XRD analysis to extend continuously all the way down to the end of the cutting analysis at 902 m. As the name implies, it consists of varied colour clays, but commonly smectite is black and greenish.

Chlorite: is a high-temperature clay mineral (Table 3). From the binocular analysis, it starts to occur at 662 m and frequently occurs throughout down to the 902 m. Generally, it is deep greenish in colour with its flaky appearance, mainly found as vesicle fill.

Quartz: appeared as colourless to white, and under thin section both subhedral and euhedral crystals are present from 276 m to 902 m. Apart from these, prismatic hexagonal amygdaloids of quartz are also encountered (e.g. 544, 578, 594, 604, 638 and 654 m). Quartz is normally formed at a minimum temperature of 180°C, and stable even after 300°C.

Albite: identified from the petrographic study at 376 m. It is the replacement of plagioclase by a process called albitization. As can be seen in Figure 9, it has a dirty white to greyish colour, with the absence of twinning. The presence of albite indicates the temperature to be above 220°C (Kristmannsdóttir, 1979).

Prehnite: appears in this well at 676 m. It is white colour forming clusters of perfect spherical shapes. It is formed at a minimum temperature of 240°C.

Epidote: emerges at 708 m indicating that the minimum temperature of alteration is 230-250°C. It has yellow, greenish colour, with tiny prismatic elongated appearance in this well. Epidote was found as vein fill and as individual crystals frequently growing on quartz grains. It is associated with quartz and chlorite.

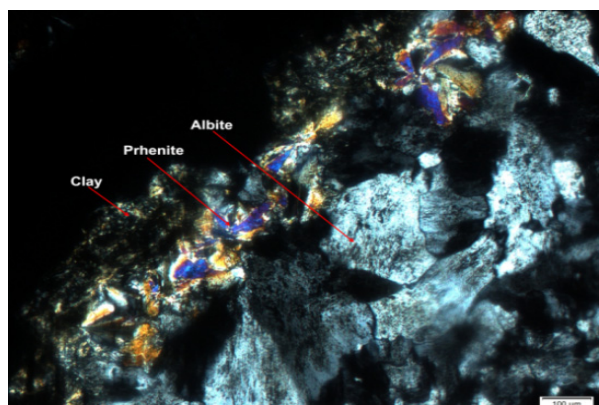


FIGURE 9: Showing depositional sequence filling the vesicle at 738 m.

The scale is 100 μm

Wollastonite: is one of the high-temperature hydrothermal minerals formed at a minimum temperature of 270°C and can be found above 300°C. The first appearance of wollastonite in well HE-59 is at 716 m. Generally, it is white in colour and has fibrous radiating pattern growing above the quartz grains. The depths 716, 718, 798, 832, 834 and 838 m are marked by the presence of wollastonite.

4.5.2 Alteration mineral zonation

Secondary minerals have their own range of temperatures at which they form. The temperature range allows us to distinguish different zones of minerals at different and specific depths.

Volcanic glass, dominant in Icelandic hyaloclastites, is partly responsible for the alteration zones to occur depending on temperature and depth (Figure 5) (Franzson, 1998).

Glass is susceptible to alteration and starts changing to clay at low-temperatures resulting in smectite. Based on clay analysis, different alteration zones can be outlined. The top most part of the wells is usually unaltered. Then as the down-hole temperature increases, smectite forms followed by mixed layer clay and then chlorite at the highest temperature (Franzson, 1998). According to the results of XRD (see the appendix) and petrographic analysis of well HE-59, three clay alteration zones were identified. These include unaltered zone (0-220 m), smectite zone (220-616) and lastly mixed layer clay zone (616-902 m). The XRD analysis did not recognize chlorite in this well. However, the combined study of XRD clay analysis, the general hydrothermal minerals distribution and petrography studies outlined four main alteration zones in well HE-59, as described below.

Unaltered zone (0-150 m): unaltered zone, where there is no alteration of rocks, except oxidation and precipitation of oxidation products.

Smectite-zeolite zone (150-616 m): marked by the abundance of smectite and different types of zeolites. The first appearance of smectite, identified by the binocular and also petrographic analysis, was at shallow depth. Smectite covers a wide range of depths, down to 616 m indicating the temperature of formation is < 200°C (Franzson, 1998) and the upper temperature limit for zeolites is also 200°C.

Chlorite-epidote zone (616-716 m): defined by the appearance of chlorite and epidote. Although the XRD analysis failed to detect the existence of chlorite, which might be caused by sampling error, petrographic analysis revealed the existence of chlorite in the well. The zone is defined by the temperature range of more than 230 to over 300°C (Table 3).

Epidote-wollastonite zone (716-902 m): represented by temperatures of 230-250 to over 300°C and the existence of epidote, wollastonite and also minor chlorite and prehnite. Within this zone, from 784-796 m (Figure 5), the amount of calcite is significantly increased. This implies the high-temperature (boiling) condition of the zone in the past hydrothermal history of the area.

4.5.3 Depositional sequences of hydrothermal minerals

Secondary minerals are deposited in the pre-existing fractures and pore spaces and as a result, vein and vesicle fillings will be formed. The replacement of a mineral into another form of mineral and precipitate is dependent on the different conditions of the geothermal system, mainly temperature, parent rock/mineral and composition of fluids. During precipitation, the former mineral sometimes leaves its traces so that one can trace it back to tell what the parent mineral was. The other important and common phenomenon is, that the low-temperature hydrothermal minerals deposited, are followed by the high-temperature ones as we go deeper into the high-temperature geothermal system. Veins and vesicle fillings are the prominent way to access the minerals depositional sequence. Studying the minerals depositional sequence will provide prevalent information on the past and present condition of the geothermal system.

The deposition sequence from well HE-59 shows the dominant fill, identified mainly through binocular studies as well as petrographic analysis. The fills occurred dominantly in the hyaloclastite successions (tuff and breccia) rather than in the lava flows. In Table 4 below, the deposition sequences of different minerals at different depths in the well are presented.

TABLE 4: Sequences of hydrothermal minerals in well HE- 59

Depth (m)	Minerals sequences (younger....older)	Host rock (formation)
284	Siderite.... Calcite.... Zeolite	Basaltic breccia
314	Pyrite.... Quartz Calcite.... Pyrite	Basaltic breccia
326	Pyrite.... Calcite	Fine- to medium-grained crystalline basalt
330	Pyrite.... Zeolite	Tuff rich basaltic breccia
390	Pyrite... Calcite.... Pyrite	Tuff rich basaltic breccia
532	Zeolite (chabazite).... Zeolite (scolecite)	Tuff rich basaltic breccia
586	Calcite.... Zeolite	Basaltic breccia
624	Pyrite.... Calcite	Basaltic tuff
628	Clay.... Quartz.... Clay	Basaltic tuff
630	Clay.... Quartz.... Clay	Basaltic tuff
640	Clay.... Calcite.... Zeolite	Basaltic breccia
662	Clay.... Calcite.... Clay	Basaltic breccia
664	Clay... Pyrite... Calcite... Pyrite... Calcite ... Clay	Basaltic breccia
672	Clay.... Calcite.... Quartz	Basaltic breccia
674	Pyrite.... Quartz	Basaltic breccia
708	Clay.... Epidote	Tuff rich basaltic breccia
738	Clay.... Prehnite.... Albite	Tuff rich basaltic breccia
740	Pyrite.... Calcite	Tuff rich basaltic breccia
772	Clay.... Pyrite.... Calcite	Basaltic tuff
796	Quartz.... Epidote	Basaltic tuff
800	Clay.... Quartz.... Epidote	Basaltic tuff
	Quartz.... Chlorite	Basaltic breccia
	Quartz.... Chlorite.... Quartz	Basaltic breccia

The dominant fill encountered in this well is calcite, followed by quartz and clay, hosted mainly by basaltic breccia and basaltic tuff. In the upper portion of the well (Table 4), one can tell that the system has been experiencing fluctuation in the geothermal environment, where the high-temperature minerals overlain by the low ones and vice versa. While the bottom portion of the well shows high-temperature minerals precipitate on top of the low-temperature minerals, implying heating up of the system.

4.6 Fluid inclusions

Formation and alteration temperature comparison is one way of estimating the conditions in a geothermal system, whether it is heating up, cooling down or in equilibrium. A fluid inclusion study in the geothermal context is a method of finding temperature from the fluids that had been trapped during crystallization of the secondary minerals.

For the well HE-59 study, two quartzes and one calcite grains were selected from suitable and appropriate depths at 700-726 m, 760-800 m and 812 m. Below these depths, the crystals were too fine grained and total circulation loss occurred below 902 m. From a total of 21 fluid inclusions, which were

examined under micro thermometry, the homogenization temperatures range between 275 - 320°C. The homogenization temperature for the first depth, 700-726 m, ranges between 275-290°C. From the second depth (760-798 m) the homogenization temperatures range is between 285-320°C. The deepest inclusions (812 m) have a range of 275-320°C. Table 5 shows histograms of fluid inclusions with depth and homogenization temperatures.

TABLE 5: Homogenization temperature of fluid inclusions in well HE-59

Depth (m)	Mineral	No of inclusions	Histogram = homog. Temperature (°C)
700-726	Calcite	10	
760-798	Quartz	4	
812	Quartz	7	

The comparison between fluid inclusion homogenization temperatures and alteration and formation temperature will be deliberated later in the discussion section.

4.7 Aquifers (feed-points)

Temperature logs, circulation losses and gains, penetration rate, alteration and standpipe pressure, are the main parameters to identify the permeable water bearing rock and aquifers/feed-points. In well HE-59, four minor and five major feed zones are identified mainly from the upper 902 m. Interpretation of temperature logs, the temperature measured during and after drilling (Figure 10) and circulation losses, supported by the cutting analysis (alteration extent, lithological boundaries and the presence of intrusions), and geophysical logs like neutron-neutron and gamma logs were used to identify feed-points. The minor feed-points are found from 316 and 830 m, while at about 450, 845, 902, 1100, 1050 and 1140 m, larger feed-points are believed to be present. The description of each feed-point is given below.

Feed-point 1: is a minor feed-point found at 316 m. It is identified from the temperature logs and circulation loss, as well as the presence of lithological contact between basaltic breccia and fine- to medium-grained crystalline basalt. The neutron- neutron and gamma loge also shows an elevated peak at this depth.

Feed-point 2: a major feed-point, located at 450 m, showing a sharp curve on the temperature logs (Figure 5). The depth is marked by an increase in intensity of alteration and also the stratigraphic contact between basaltic tuff and tuff rich basaltic breccia.

Feed-point3: indicated by the elevated temperature log at 830 m and circulation loss of about 26 l/s. It is within the basaltic breccia unit and marked by the presence of a high-temperature mineral zone, chlorite-epidote-wollastonite.

Feed-point 4: located at 845 m and has similar conditions as feed-point 3, except feed-point 4 has much higher (45 l/s) loss of circulation.

Feed-point 5: is the major feed-point at 902 m where the loss of circulation was > 45 l/s and cutting returns were not encountered below this depth.

Feed-point 6, 7 and 8: are major and minor feed-points, represent the depth at 1100, 1050 and 1140 m, based on the temperature logs.

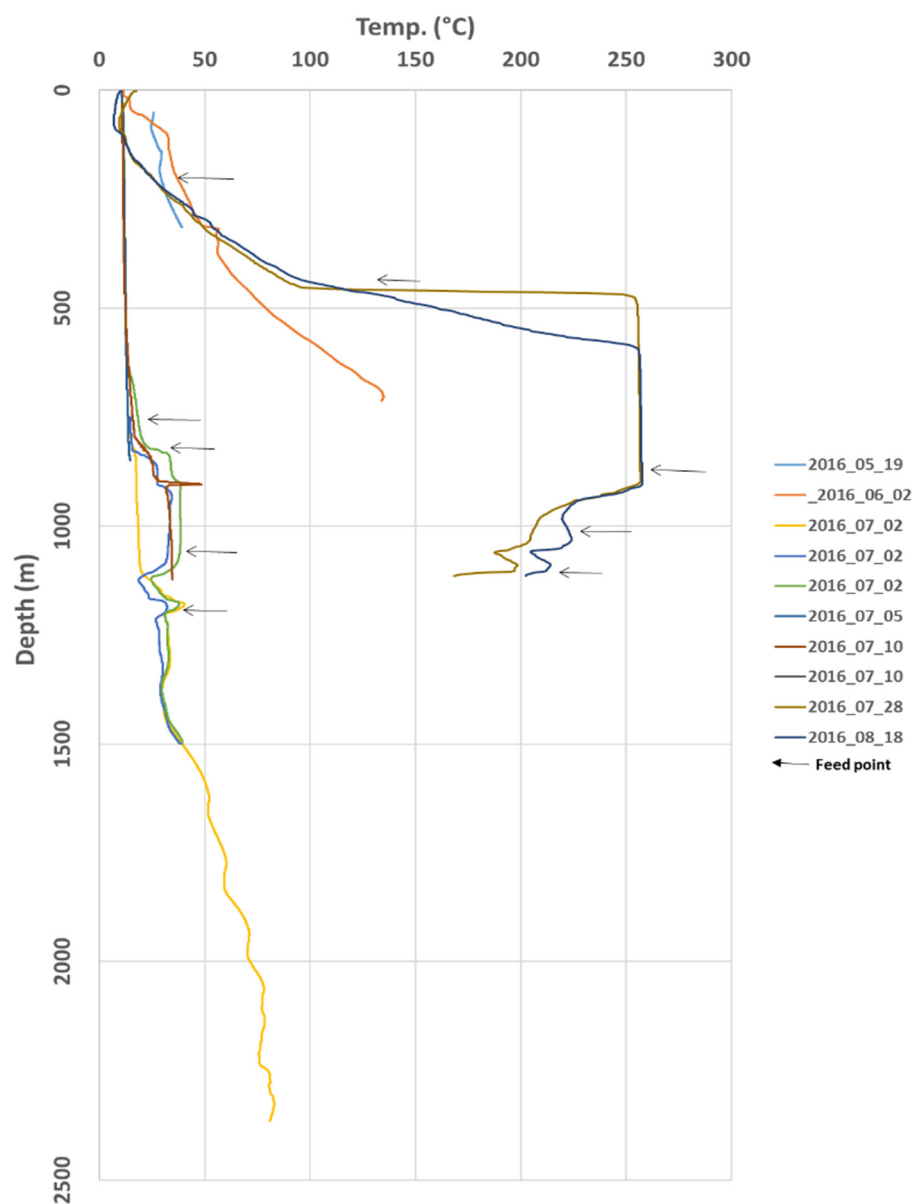


FIGURE 10: Temperature logs and feed-points in well HE-59

5. SURFACE AND SUBSURFACE STRUCTURAL RELATIONSHIPS

The aim of directional drilling of HE-59 in the Hellisheidi geothermal area, was to cross cut the major faults and the mini-graben that is situated within the major graben, locally called Reykjafell mini-graben (Figure 11). The graben is found at the western part of the area consisting of a number of localized faults and 2000, 5000, 8000 and 10,000-year-old fissures (Saemundsson, 1995; Hardarson et al., 2015).

During a surface structural study in the vicinity of well HE-59, a narrow and localized minor volcanic fissure was identified (Figure 11). This fissure lies between the well HE-59 (west) and the Reykjafell

mini-graben (east) about 250 m and 760 m away from each respectively (Figure 11). It is believed to be about 8000 year old (Saemundsson, 1995).

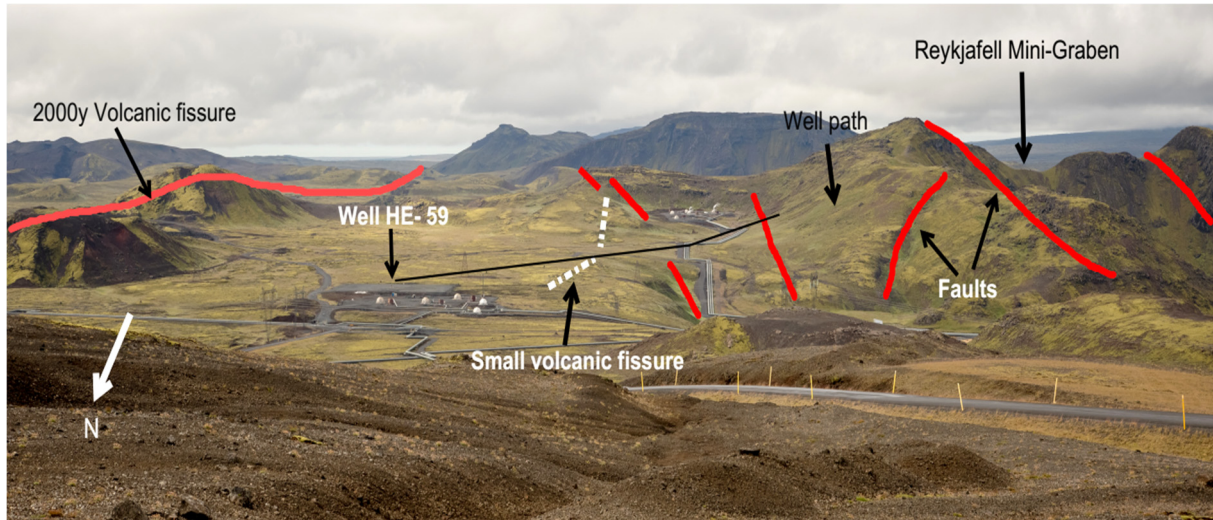


FIGURE 11: Surface structures and volcanic fissures around well HE-59

The gyro survey of well HE-59 shows that at 900 m the well is deviated 255.70° to the SW, having an inclination of 33.7° (Helgadóttir et al., 2016) and the extrapolation of this distance to the surface reaches 220 m, which is related to the small fissure that is about 250 m away from the wellhead. This can be evidenced from the circulation loss at 902 m (Table 1) and from the cutting analysis, which revealed the presence of a fine- to medium-grained crystalline basalt intrusion from 796 to 828 m (Figure 5). On the surface, the volcanic fissure was found as an oxidized scoraceous lava flow, being about 220 m long and 25-35 m wide, running NE-SW following the trend of the main fault system.

6. SUMMARY AND DISCUSSION

Well HE-59 is characterized by postglacial basaltic lava flows on the surface, followed by dominant hyaloclastite formations (basaltic tuff, basaltic breccia and glassy/ pillow lava) and interglacial lavas, based on cutting analyses from the upper 902 m. The deeper formations are intruded by fine- to medium-grained and medium- to coarse-grained basaltic intrusions. The stratigraphic relationship between the intrusions and the host rock, and also within the boundaries of the rock units, reveals permeability, resulting in aquifers/feed-points to be formed. In addition to this, the structural setting of the area, NE-SW running faults and transform faults, are the main cause of permeability. In the upper portion the well, above 900 m, the feed-points are controlled both by structure and stratigraphic boundaries (Figure 5). Alteration of the rocks and secondary mineral precipitation starts below 150 m, followed by precipitation of low-temperature minerals (zeolites). High-temperature minerals include prehnite, chlorite, epidote and wollastonite. Below 150 to 616 m, the zone is identified as a smectite-zeolite zone, as it is dominated by the presence of smectite clay and different types of zeolites with their respective temperatures reaching up to 200°C . The chlorite-epidote zone is the zone which covers 616-716 m and the last alteration mineral zone is the epidote-wollastonite zone (716-902 m), which is marked by high intensity of alteration. The clay analysis shows the absence of chlorite in this well and the presence of smectite zone from 220 to 616 m, and mixed clay below 616 m to 902 m. For this contradiction the reason could be the sampling error, but it requires further analysis.

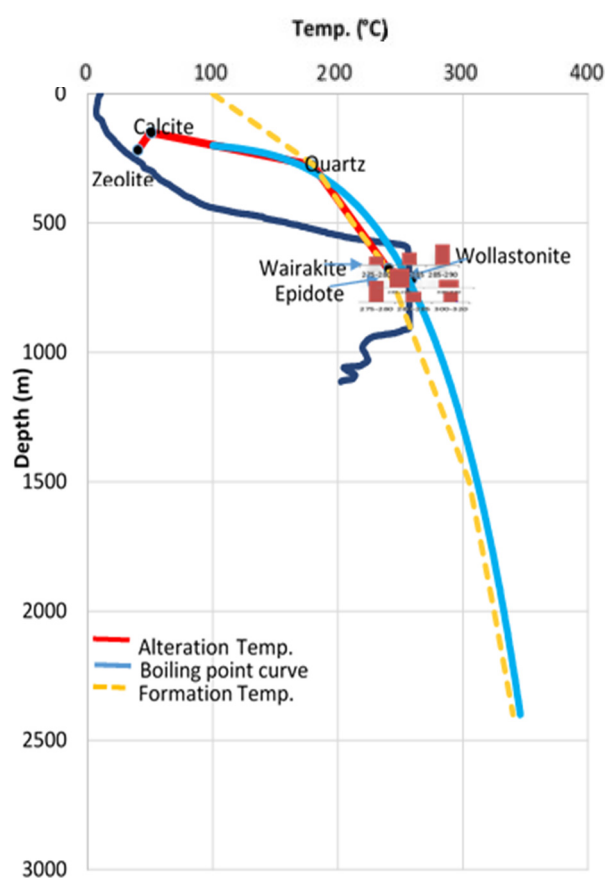


FIGURE 12: comparison between formation temperature, alteration temperature, fluid inclusions and boiling point curve

Understanding the thermal conditions of a well, i.e. whether it is cooling, heating or in equilibrium, is one of the main purposes of studying borehole geology. In this respect, studying the depositional sequence of hydrothermal minerals, alteration temperature, formation temperature and fluid inclusion plays an important role. The depositional sequences taken from 284-800 m of well HE-59 show that the system has experienced fluctuations in the geothermal environment, where apparent over growths of high and low-temperature minerals seems irregular. However, the lower section of the well shows high-temperature minerals growing on low-temperature minerals, implying a heat up of the system, or at least equilibrium conditions. Figure 12 shows the comparison between alteration temperature, formation temperature and fluid inclusion with respect to the boiling point curve. Alteration temperature (a temperature curve found from the first appearance of the alteration minerals and their specific formation temperature) and formation temperature, the present temperature in the well, shows equilibrium condition above 700 m, while below this depth the alteration temperature exceeds formation temperature implying cooling. However, it is very likely that the true formation temperature has not been revealed by the latest temperature logs, as the well had not recovered, implying that there is probably no cooling present.

The application of the fluid inclusions analysis method on samples taken from depths of 700-812 m, consists of homogenization temperatures between 275 and 317°C, and thus shows temperature conditions which exceed both the formation temperature and alteration temperature, as well as the boiling point curve (Figure 12). From this comparison, one could conclude that the system in this well is cooling. Nevertheless, since the well is new and the formation temperature curves are based on temperature logs measured during and soon after drilling, this is probably not reliable. Further temperature measurements after recovery of the well are, therefore, crucial to understand the thermodynamic conditions. On the other hand, the high-temperature records from the alteration temperature and fluid inclusions might represent past condition of the system and the young postglacial volcanic fissure triggered fresh input to the heat source (Figure 13).

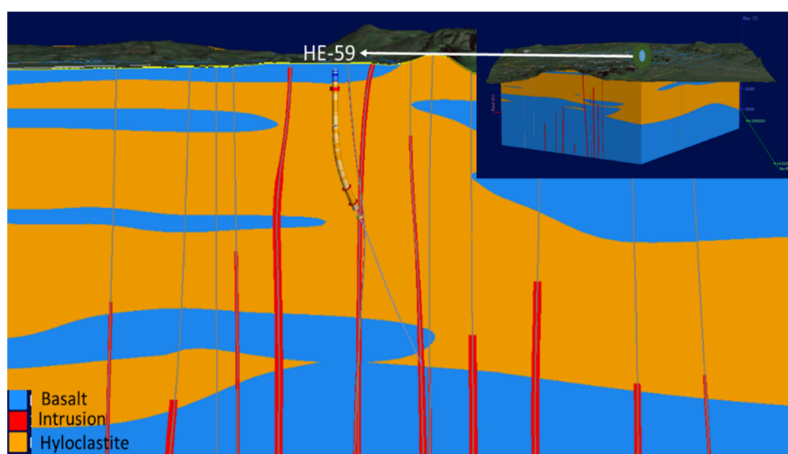


FIGURE 13: 3D model of Hellisheidi area showing subsurface track of well HE-59 related to structures, lithology and intrusions

7. CONCLUSIONS

- Well HE-59 was directionally drilled on May 17 2016 to a total depth of 2400 m into the Reykjafell mini graben, but total circulation loss was encountered below 902 m.
- The uppermost 902 m of well HE-59 is characterized by dominant hyaloclastite and basaltic lava flows, together with basaltic intrusives. The hyaloclastites consist of basaltic breccia, basaltic tuff and glassy basalt (pillow basalt), while the lava flows are dominantly fine- to medium-grained, crystalline basalt.
- About six intrusions have been identified from the stratigraphy of the well, where three of them are probable intrusions. The intrusions are fine- to medium-grained and medium- to coarse-grained crystalline basalt.
- The alteration zones in this well are challenging, where the hydrothermal mineral distribution and clay analysis shows different outlines of alteration zones. However, the combination of the two approaches infers the presence of four alteration zones. These include an unaltered zone (0-150 m), smectite-zeolite zone (150-616 m), chlorite-epidote zone (616-716 m) and epidote-wollastonite zone (716-902 m).
- Nine aquifers were identified which relate to the geological boundaries and structures. Five of them are major feed points and four are minor feed points.
- The combined result of formation temperature, fluid inclusions study and alteration temperature may indicate some cooling of the well, but the temperature logs after recovery of the well could indeed amend this conclusion.
- The structural relationship, based on gyro surveys, circulation losses and geological findings from well HE-59 shows a clear relationship between surface faults, fissures and the well path.

ACKNOWLEDGEMENTS

I would like to express my gratitude to the United Nations University, Geothermal Training Programme (UNU-GTP) and the government of Iceland for funding this project. I would also like to thank Mr. Lúdvík S. Georgsson, director of United Nations University, Geothermal Training Programme and the deputy director Mr. Ingimar Gudni Haraldsson, for giving me this opportunity. The UNU-GTP staff Ms. Thórhildur Ísberg, Ms. Málfríður Ómarsdóttir and Mr. Markús A. G. Wilde are also thanked for their support and guidance throughout my stay in the programme.

My special thanks go to my supervisor Dr. Björn S. Hardarson for his excellent guidance, patience and kindness. Dr. Hjalti Franzson and Ms. Helga Helgadóttir are thanked for the guidance during fluid inclusion analysis. Mr. Sigurdur S. Jónsson is acknowledged for his support on the XRD preparation and analysis. I would also like to thank Dr. Tobias Weisenberger for his guidance during petrographic analysis. Bastien Poux is also thanked for his guidance and patience during field study and introducing Leapfrog software. Ms. Saeunn Halldórsdóttir is thanked for her assistance on the study of reservoir temperatures.

Reykjavik Energy is sincerely acknowledged for allowing generous access to data regarding well HE-59 in the Hellisheidi geothermal field. I am grateful to my company, Geological Survey of Ethiopia (GSE), for my participation in the six-month training program.

I would like to thank all the UNU-GTP 2016 fellows for their unforgettable friendship throughout my time. Special thanks for my course mates, Erios Naiga and Andrei Lup for their cooperation and the idea sharing.

Finally, my sincere gratitude goes to my beloved family. I am sincerely thankful to the lord of all who will make everything possible, Jesus Christ.

REFERENCES

- Árnason, K., 2007: *TEM survey in Hengill area 2006 and suggested well sites at Eldborg*. ÍSOR – Iceland GeoSurvey, Reykjavík, report 2007/005, 34 pp.
- Arnórsson, S., Axelsson, G., and Saemundsson, K., 2008: Geothermal systems in Iceland. *Jökull*, 58, 269-302.
- Franzson, H., 1998: Reservoir geology of the Nesjavellir high-temperature field in SW-Iceland. *Proceedings of the 19th Annual PNOC-EDC Geothermal Conference, Manila*, 13-20.
- Franzson, H., Árnason, K., Saemundsson, K. and Gunnlaugsson E., 2010a: The Hengill geothermal system, *Proceedings of the World Geothermal Congress 2010, Bali, Indonesia*, 9 pp.
- Franzson, H., Gunnlaugsson E., Árnason, K., Saemundsson, K., Steingrímsson, B., and Hardarson, B.S., 2010b: The Hengillgeothermal system, conceptual model and thermal evolution. *Proceedings of the World Geothermal Congress 2010, Bali, Indonesia*, 19pp.
- Franzson, H., Kristjánsson, B.R., Gunnarsson, G., Björnsson, G., Hjartarson, A., Steingrímsson, B., Gunnlaugsson, E., and Gíslason G., 2005: The Hengill Hellisheidi geothermal field. Development of a conceptual geothermal model. *Proceedings World Geothermal Congress 2005, Antalya, Turkey*, 7 pp.
- Gasperiakova, E., Rosenkjaer, K.G., Árnason, K., Newman, A.G., and Lindsey, I.N., 2015: Resistivity characterization of Krafla and Hengill geothermal fields through 3D MT inversion modelling. *Geothermics* 57, 246-257.
- Gunnlaugsson, E. and Gíslason, G., 2005. Preparation for a new power plant in the Hengill geothermal area, Iceland. *Proceedings of the World Geothermal Congress, Antalya, Turkey*, 24-29.
- Gunnarsdóttir, S.H. and Bastien, P., 2016: *3D modelling of Hellisheidi geothermal field using leapfrog: data, workflow and preliminary models*. ÍSOR – Iceland GeoSurvey, Reykjavík, report 2016/039, 22 pp.
- Haraldsdóttir, S., Franzson, H., and Árnason, K., 2015: Comparison of down hole data and surface resistivity data from S-Hengill, a high-temperature geothermal field in SW-Iceland. *Proceedings of World Geothermal Congress 2015 Melbourne, Australia*, 12pp.
- Hardarson B.S., Einarsson, G.M., Franzson, H., and Gunnlaugsson, E., 2009: Volcano-tectonicgeothermal interaction at the Hengill triple junction, SW Iceland. *Geothermal Resources Council, Transactions*, 33, 49-55.
- Hardarson, B.S., Fitton, J.G., Ellam, R.M. and Pringle, M.S. 1997: Rift relocation - a geochemical and geochronological investigation of a palaeo rift in northwest Iceland. *Earth Planet. Sci. Lett.*, 153, 181-196.
- Hardarson B.S., Kristinsson, S.G., Karlsdóttir, R., and Einarsson, G.M., 2015: Geothermal implications of rift zone mini-grabens. Geological and geophysical structure of the Reykjafell mini-graben, Hengill geothermal field, SW-Iceland. *Proceedings of World Geothermal Congress 2015, Melbourne Australia*, 11pp.
- Helgadóttir, H.M., Snaebjörnsdóttir, S., Nielsson S., Gunnarsdóttir, S.H., Matthíasdóttir, T., Hardarson, B.S., Einarsson, G.E., and Franzson, H., 2010: Geology and hydrothermal alteration in the reservoir of the Hellisheidi high temperature system, SW-Iceland. *Proceedings of World Geothermal Congress 2010, Bali Indonesia*, 10 pp.

Helgadóttir, H.M., Sveinborg, H.G., Tryggvason, H., Sigurgeirsson, M.A., and Weisenberger, T., 2016: *Hellisheidi, well HE-59. Pre-drilling, and 1., 2. and 3. phase: Drilling for surface casing down to 115 m, safety casing to 317 m, production casing down to 800 m depth and perforated liner to 1130 m (depth of well 2381 m)*. ÍSOR – Iceland GeoSurvey, Reykjavík, report 2016/46 (in Icelandic) 101 pp.

Hjartarson Á. and Saemundsson K., 2014: *Bedrock map of Iceland, 1:600 000*. ÍSOR – Iceland GeoSurvey, Reykjavík.

Kristmannsdóttir, H., 1979: Alteration of basaltic rocks by hydrothermal activity at 100-300°C in: Mortland, M.M., and Farmer, V.C. (eds.), *International Clay Conference 1978*. Elsevier Scientific Publishing Co., Amsterdam, 359-367.

Saemundsson, K., 1979: Outline of the geology of Iceland. *Jökull*, 29, 7-28.

Saemundsson, K., 1995: Hengill geological map (bedrock) 1:50000. Orkustofnun, Reykjavík, Reykjavík Energy and Iceland Geodetic Survey.

Saemundsson, K., and Gunnlaugsson, E., 2014: *Icelandic rocks and minerals* (2nd ed.). Forlagid ehf., Reykjavík, 223 pp.

Sigmundsson, F., 2006: *Iceland geodynamics crustal deformation and divergent plate tectonics*. Praxis Publishing, Ltd., Chichester, UK, 231 pp.

APPENDIX I: XRD analyses

518 m - No clay

220 m - Smectite

308 m - Smectite

378 m - Smectite

500 m - Smectite

616 m - Smectite

672 m - Mixed layer clay

708 m - Mixed layer clay

744 m - Mixed layer clay

798 m - Mixed layer clay

822 - Mixed layer clay

832 m - Mixed layer clay

898 m - Mixed layer clay

58847/HE-59 #01 UNT

518 m-No clay

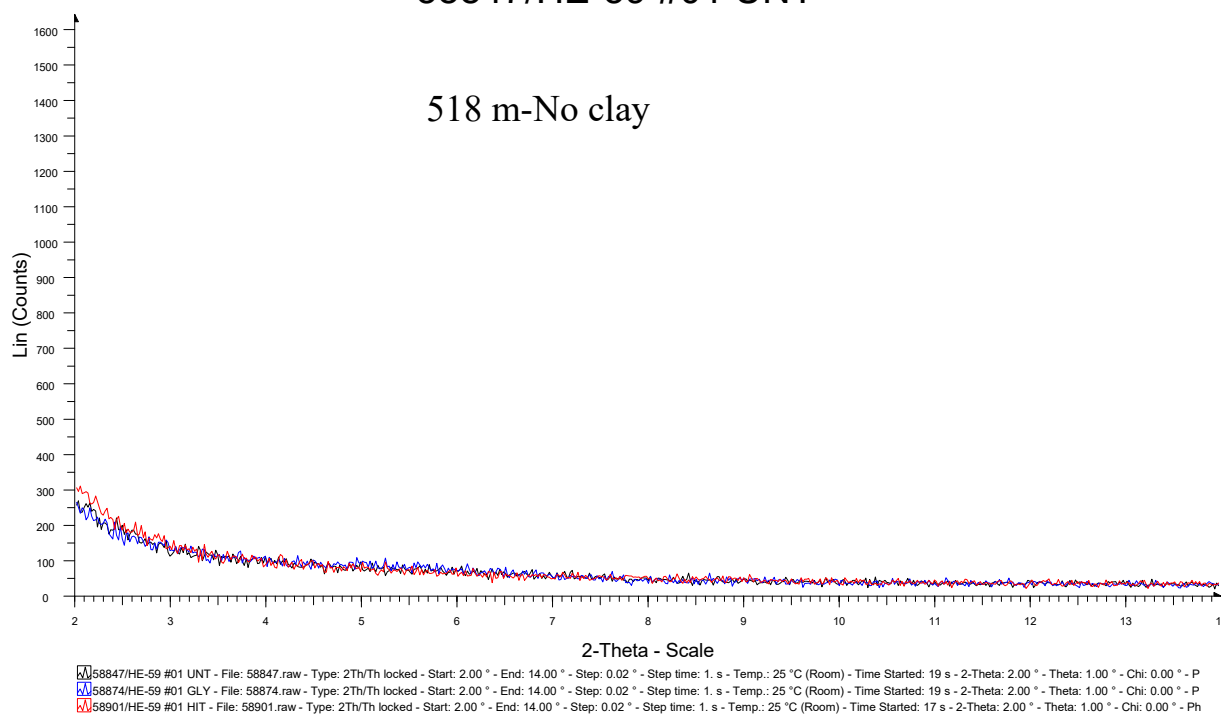


FIGURE 14: XRD-clay analysis of well HE-59



UNITED NATIONS
UNIVERSITY

UNU-GTP

Geothermal Training Programme

Orkustofnun, Grensasvegur 9,
IS-108 Reykjavik, Iceland

Reports 2016
Number 9

CENTRALISED MONITORING AND CONTROL DISPATCH CENTRE FOR THE GEOTHERMAL WELLHEAD POWER PLANTS IN KENYA

Winnie Apiyo

Kenya Electricity Generating Company, Ltd. – KenGen

P.O. Box 785

20117 Naivasha

KENYA

wapiyo@kengen.co.ke; winnieapiyo86@gmail.com

ABSTRACT

Wellhead geothermal power plants in Kenya's Eburru and Olkaria geothermal fields are mostly located in remote and inconvenient places. These plants are located far apart from each other making operation and maintenance expensive and a challenge. Remote monitoring and control of these units will enhance the power plants availability, reduce maintenance, operational, and other related costs. Supervisory control and data acquisition (SCADA) systems are used to monitor and control geographically dispersed plants. A good SCADA technology with a good communication infrastructure will enable the collection of real time data from all these scattered wellhead power plants to one control room. The real time monitoring and control of KenGen's wellhead power plants in a centralised control centre will assist with rapid detection of faults, diagnosis and repair so that downtime of the units due to faults can be reduced, thereby increasing availability and efficiency. Design of a centralised SCADA system and communication network for the wellhead units and economic and financial analysis of this project is discussed in this paper. Optimisation of operation and maintenance costs without compromising safety and technical performance of a power plants is also discussed.

1. INTRODUCTION

Kenya Electricity Generating Company, Ltd. – KenGen produces 80% of the electricity consumed in the country. The company utilizes various sources to generate electricity ranging from hydro, geothermal, thermal and wind. The east African rift passes through Kenya and this is the main reason why the country is vastly endowed with geothermal resources. Commercial generation of geothermal electricity in Olkaria started in 1981. Today (late 2016), the installed capacity of geothermal power plants in the area is about 673 MWe. The rapid economic growth and industrialization in the country accelerated the need for drilling more geothermal wells, as well as avoiding dependence on hydro power plants. Long droughts resulted in reduced power production from the hydro power plants and leading to high reliance on expensive diesel engines. In 2010, KenGen embarked on execution of developing geothermal wellhead plants under a *Research and Development Programme* culminating in the successful implementation of a pioneer plant in early 2012. Now, the total installed capacity amounts to about 84 MW. Wellhead power plants are small modular plants installed next to a wellhead. The plants have a shorter construction time, are modular and can be relocated to newly drilled wells.

Following reservoir productivity by monitoring over time during operation helps to gather data to access the potential of the resource. The units are used to generate power to the grid during resource development of a large project and for utilization of wells that have small-scale application potential.

2. OVERVIEW OF OLKARIA GEOTHERMAL WELLHEAD POWER PLANTS

2.1 Description of the location of Olkaria geothermal wellhead power plants

The first geothermal wellhead plant was located in the Eburru geothermal field, located in Kenya's rift valley approximately 140 km from Nairobi, 11 km northwest of Lake Naivasha. The field is located to the north of Olkaria at the foot of the Mau escarpment. The Eburru and Olkaria geothermal fields are about 40 km apart. Surface exploration studies at Eburru were done in the early 1980's, with four wells drilled by KenGen between 1988 and 1994. For the pilot plant, well EW-01 was selected to serve as the production well (GDA, 2011). Geothermal Development Associates (GDA) from Reno, Nevada, USA commissioned the Eburru wellhead station in 2012. The modular power plant has an installed capacity of 2.44 MW.

Olkaria geothermal field, which is estimated to be approximately 80 km², is divided into seven sectors: Olkaria East, Olkaria Northeast, Olkaria Central, Olkaria Southwest, Olkaria Northwest, Olkaria Southeast and Olkaria Domes (Ouma, 2007). Wellhead power plants have been installed in the Olkaria Domes, Olkaria East and Olkaria Northeast fields (Figure 1).

The Olkaria OW37 wellhead power plant, which has a design generation capacity of 5.5 MWe, was commissioned in January 2012 (Table 1). It was the first plant installed by Green Energy Geothermal,

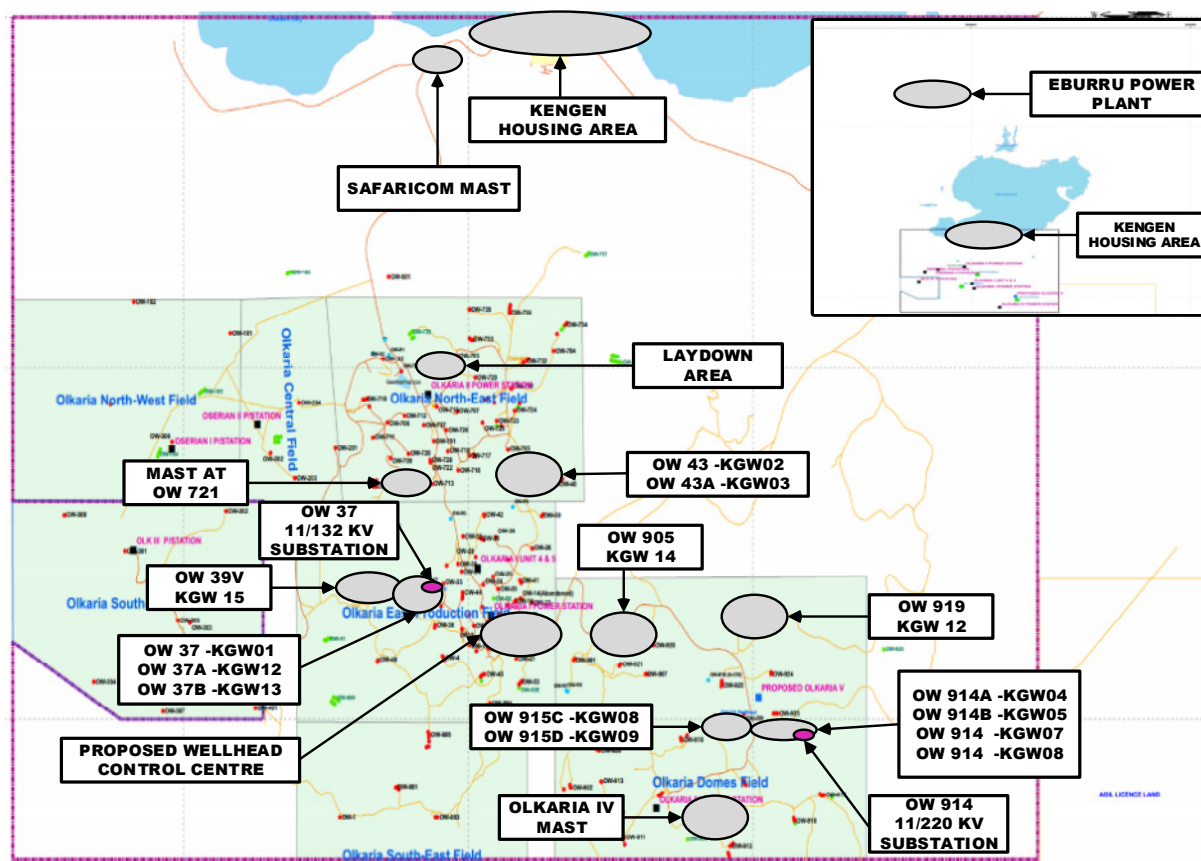


FIGURE 1: Map showing location of wellhead power plants, and associated stations

TABLE 1: Wellhead power plants key information

Field	Well	Wellhead no.	Plant model	Installed power [kW]	Year installed
Eburru	EW-01	EBURRU	Elliott Model DYRPE8	2440	2012
Olkaria east	OW-37	KGW01	C64	5500	2012
Olkaria North East	OW-43	KGW02	C64	6400	2013
Olkaria North East	OW-43A	KGW03	C64	6400	2013
Olkaria domes	OW-914A	KGW04	C64	6400	2013
Olkaria domes	OW-914B	KGW05	C64	6400	2014
Olkaria domes	OW-914	KGW06	C50	5000	2014
Olkaria domes	OW-914	KGW07	C50	5000	2015
Olkaria domes	OW-914C	KGW08	C50	5000	2015
Olkaria domes	OW-915C	KGW09	C50	5000	2015
Olkaria domes	OW-915D	KGW10	C50	5000	2015
Olkaria domes	OW-919A	KGW11	C50	5000	2016
Olkaria east	OW-37A	KGW12	C50	5000	2016
Olkaria east	OW-37B	KGW13	C50	5000	2016
Olkaria domes	OW-905	KGW14	C50	5000	2016
Olkaria east	OW-39	KGW15	C50	5000	2016

Iceland. Since then, a total of 16 wellhead plants have been installed for KenGen, and a total of 21 turbines (Figure 2). The total installed capacity is 83.54 MW.

2.2 Wellhead power plant models

Eburru power plant has an 8-stage, axial flow turbine Model DYRPE8 manufactured by the Elliot company, Jeanette, PA. It is a single-flash geothermal power plant. The gas extraction system has only a single-stage gas extraction using a liquid ring vacuum pump due to the relatively low non-condensable content (Mendive and Green, 2012). Green Energy Geothermal (GEG)

has two types of wellhead power plants installed in the Olkaria geothermal field: C50 and C64 wellhead units. The C50 single turbine setup is a modular type geothermal wellhead power plant, which consists of a single turbine generator unit (1×5 MW) that operates on one single steam and condensing system. The C64 plant consists of two identical turbine and generator (TG) units (2×3.2 MW) that operate on one single steam system and two separate condensing systems. The two types of plants consist of four main systems:

- Steam system;
- Condensing system;
- Turbine Generator set;
- Electrical & Control system.

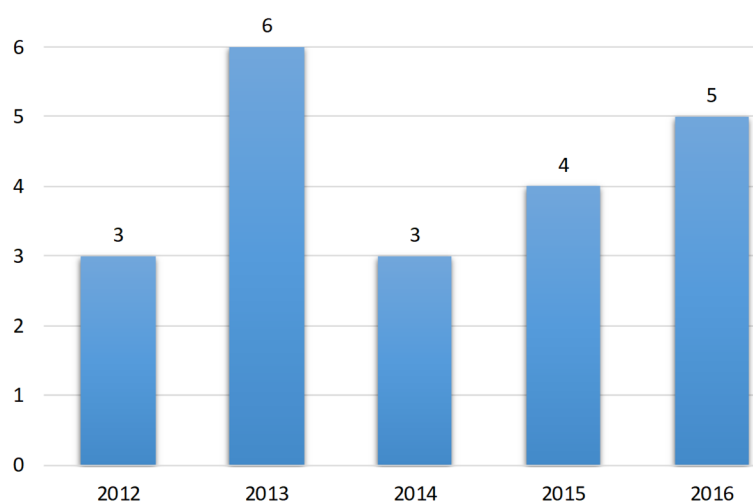


FIGURE 2: Installed wellhead power plants – historical development

Steam is discharged from the well and supplied into the steam separators. The separators remove any liquid, droplets or mist from the steam before it enters the turbine. The steam is then expanded through the turbine. In the condenser, the steam is mixed with cooling water, which condenses the steam creating the desired back-pressure vacuum. The condenser further cools down non-condensable gases that are extracted with a two-stage steam ejection system. The condensed steam/cooling water mixture is then pumped in to the cooling towers where it is cooled down and re-used as coolant.

3. CONTROL AND PROTECTION HARDWARE ARCHITECTURE

The protection relays and control equipment used in the wellhead power plants come from different manufacturers and are designed with a complete line of protection and control (Table 2).

TABLE 2: Wellhead units' control and protection equipment

	Plant PLC	Generator protection relay	Digital excitation control system	Steam turbine control (Governor)	11 kV transformer protection relay	Feeder protection
Eburru	Productivity 3000 programmable automation controller (PAC)	Basler electric BE1-11G	Basler electric DECS-200	WOODWARD 2301D-ST	Basler electric BEI-CDS220	SEPAM S80
OW37	Siemens Simatic S7 300	Unit 1: WOODWARD MFR32 Unit 2: Siemens SIPROTEC 7UM62	Basler electric DECS-200	WOODWARD 505	Electro-mechanical relays	11 kV circuit breaker: WOODWARD MRA4 33 kV circuit breaker: WOODWARD MRDT4
C64	Siemens Simatic S7 300	Siemens SIPROTEC 7UM62	Basler electric DECS-200	WOODWARD 505	SEL 787	SEL 751A
C50	Siemens Simatic S7 1500	SEL 700G	Basler electric DECS-250	WOODWARD 505	SEL 787	SEL 751A

3.1 Wellhead power plant protection scheme

The main function of a protection system in a power plant is to detect and isolate faults occurring in a power system. Generators and transformers can be subjected to internal or external faults or both. Faults occurring in the power system should be cleared as soon as possible to avoid expensive equipment damage and failure while maintaining system performance and increasing availability of the plants. The main equipment protected are the generators, transformers and feeders.

3.2 Excitation control system

The excitation control system of a generator is used to control the generator's terminal voltage as well as the generator's reactive power (MVar) output. The level of DC excitation current supplied to the field winding determines the generator's terminal voltage and reactive power output. The digital excitation system has been interfaced with the plant's control system via digital input/output cards. The Basler Digital Excitation system (DECS 200 and DECS 250) installed in the Olkaria and Eburru geothermal wellhead units have four control modes:

- Automatic voltage regulations;
- Manual or field current regulation (FCR);
- Power factor regulation (PF);
- Reactive power regulation (RP);

3.3 Turbine governor

The WOODWARD governor system drives the steam turbine valves to control turbine parameters. The main controlled parameter is speed (or load). The WOODWARD communicates directly to the plant control system and the Human Machine Interface (HMI) through Modbus communication ports.

3.4 Turbine supervisory instrument – TSI

Information provided by the TSI units is very critical and ensures that the turbine generator is operating within the safety limits. The parameters monitored by the TSI are: turbine generator bearing vibrations, rotor eccentricity, high-pressure turbine casing expansion, high-pressure and low-pressure turbine axial differential expansions, shaft axial position, assorted turbine generator temperatures, turbine speed (over speed and zero speed) and steam valve position. Vibration monitoring is very critical. The aim is to detect defects early by analysing changes in the vibration condition of the equipment during operation (Karani, 2008). The information is trended over time and analysed to detect defects or anomalies.

3.5 Olkaria geothermal wellhead power plant Distributed Control System (DCS)

3.5.1 Eburru power plant control system

Eburru plant control and monitoring system is networked on an Ethernet backbone (Figure 3). The network allows connected devices to communicate using several Transmission Control Protocol (TCP) protocols including Modbus TCP and Transmission Control Protocol/Internet Protocol (TCP/IP) (GDA, 2011). The Programmable Logic Controller (PLC) monitor and control plant systems, issue alarms and trips, and provide real-time data to the Human Machine Interface (HMI) and historical data server. Remote Input/output (I/O) Systems are used to minimize field wiring. They collect data between the plant instrumentation and the PLC. These remote I/O systems are located remotely near the field instrumentations. Energy meters via current transformers and voltage transformers provide accurate and real-time power information to the PLC and the operators via the HMI. The intelligent motor starters and controllers are used to start and stop motors and display motor status information to the PLC. Generator Management Relay (GMR), which is a generator protection relay, monitors the generator status, alarms and trips isolating the generator when there is a fault in the system. GMR functions independently from the PLC, but sends its status to the PLC for monitoring.

3.5.2 Green Energy Geothermal C64 wellhead power plants control system

The plant is run by a Siemens SIMATIC S7 300 PLC controller (GEG, 2015a). The PLC controller handles supervisory control and data acquisition for all signals and devices from the plant's systems. Signals to this PLC are read from the Ethernet communication bus from devices through MOXA MGATE 41101-MB-PBS gateway, which provides a communication portal between Profibus PLCs (Siemens S7-300) and Modbus devices (Figure 4). The rest of the signals are transmitted via a redundant Ethernet link to and from the PLC. A 19" SIMATIC human machine interface touch screen is installed at the panel door.

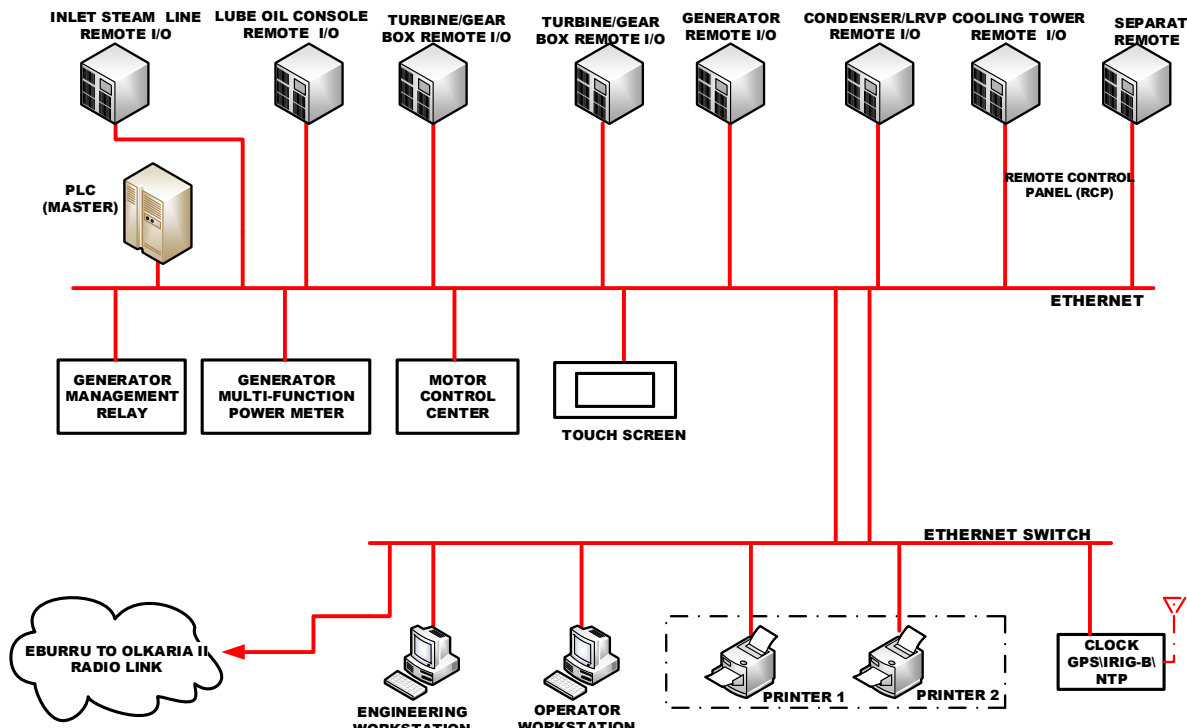


FIGURE 3: Eburru control system architecture

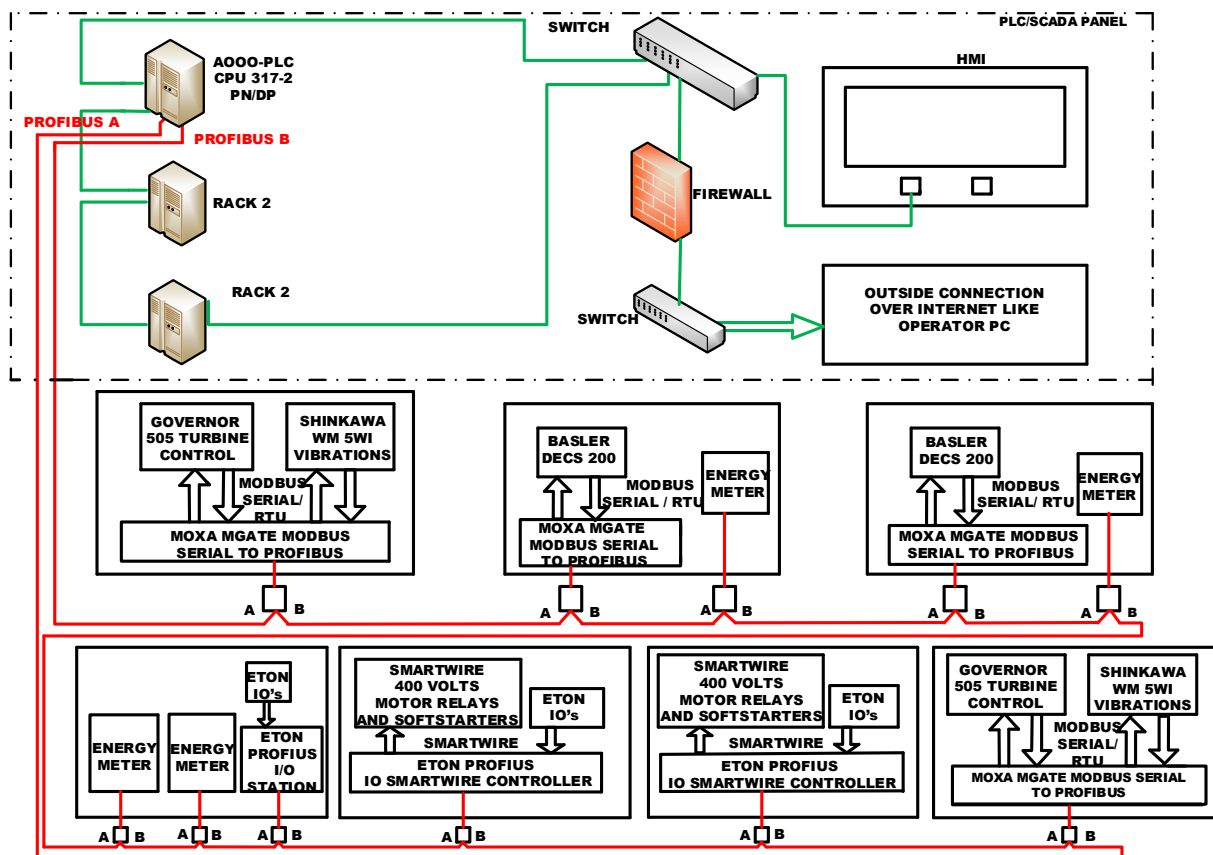


FIGURE 4: C64 wellhead unit control system

3.5.3 Green Energy Geothermal C50 well head power plant control system

The plant is run by a Siemens SIMATIC S7 1500 PLC controller. The C50 wellhead units' plant control elements are connected together through communication buses (Modbus TCP /IP) to form a distributed control system (Figure 5). The common PLC controller handles supervisory control and data acquisition for all signals and devices from the plant's common systems. Signals from instruments used for protection purposes of the steam supply system are hardwired to the electronic control unit where electrical marshalling cubicle are located, while the rest are connected to a remote-IO and transmitted via a redundant Ethernet link to and from the PLC (GEG, 2015a). Other signals to this PLC are either connected to IO cards located in the PLC rack or read from the Ethernet communication bus from other devices: DC distribution panel, AC distribution panel (PLC) or feeder Protection relay. A 19" SIMATIC human machine interface touch screen is installed at the panel door. The unit control system PLC controller handles all unit systems signals and devices. Signals from the cold end are routed through a terminal box and signals from instruments are connected to a remote-IO and transmitted via a redundant Ethernet link to and from the PLC. Turbine signals are routed through a turbine terminal box, protection signals from various instruments are hardwired to the ECU, while the other signals are connected to a remote-IO and transmitted via a redundant Ethernet link to and from the PLC (GEG, 2015a). Other signals that originated from the ECU itself to this PLC are either connected to IO cards located in the PLC rack or read from the Ethernet communication bus from vibration monitoring system, excitation control and generator protection relay.

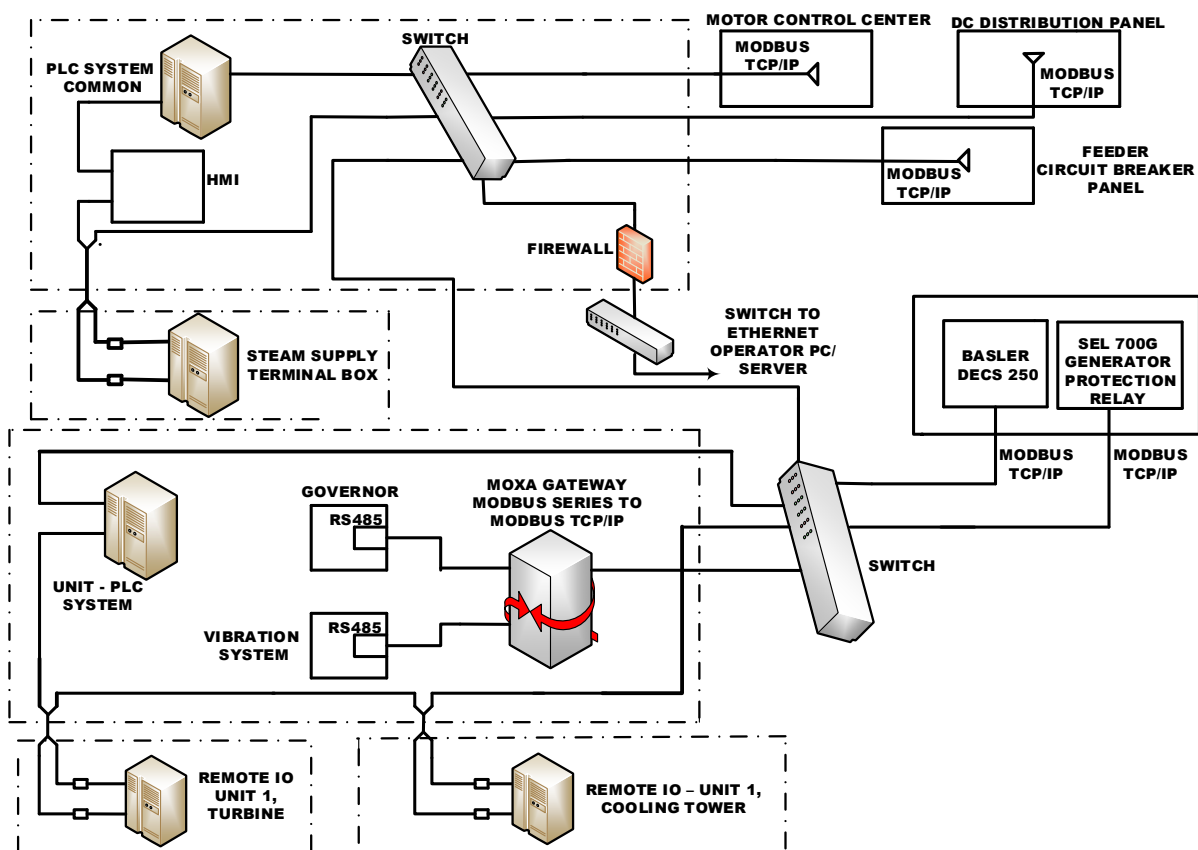


FIGURE 5: C50 wellhead unit control system

3.6 OW914 substation automation

A SEL-3530 Time Automation Controller (RTAC) is used as a protocol gateway and a Remote Terminal Unit (RTU) in OW914 to collect downstream data from all the relays connected to OW914

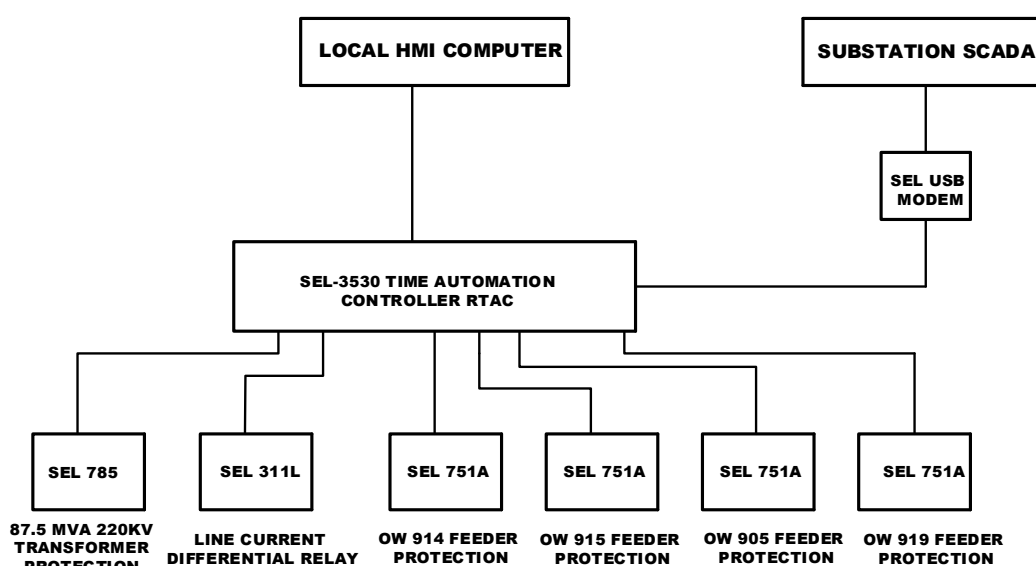


FIGURE 6: Substation automation

substation (Figure 6). These relays, which are used to protect the feeders and transformers are:

- SEL 311L line differential relay at OW914;
- SEL 311L line differential relay at Olkaria IV substation;
- SEL 787 transformer protection relay at OW914;
- OW915 feeder protection relay SEL 751A at OW914;
- OW919 feeder protection relay SEL 751A at OW914;
- OW905 feeder protection relay SEL 751A at OW914;
- SEL energy meters.

The RTAC uses IEC61850 GOOSE protocol to collect data from these relays. The messages are then converted to Distributed Network Protocol (DNP3) for connection to the SCADA. RTAC has been used as the substation SCADA data concentrator, logic processor and to collect station-wide sequential events records, events report and metering updates. This enhances system reliability providing more and better information to the operator.

3.7 Existing wellhead communication network architecture

3.7.1 Eburru radio link network

A 30 km point to point radio link over water from Eburru power plant to KenGen housing site has been implemented. A Safaricom radio tower is located near the housing unit. Two Nano station M5 radio transceivers have been installed at both Eburru power plant and on top of the Safaricom radio tower. Additionally, two rocket dishes 5G-30 are installed on top of the tower and the geothermal housing site. There, an existing fibre Ethernet cable is connected to Olkaria II power plant. At Olkaria II power plant, the fibre Ethernet cable is converted to a copper Ethernet cable connected to an operator station. Time synchronization between the two network levels has been coordinated. Time synchronization is essential to ensure all alarms and events are recorded in a sequential manner to help in emergency response and fault finding activities.

3.7.2 C64 and C50 wellhead units' communication network

Radio is used as the media of communication. Radio links exist from OW914, OW905, OW919 and OW915 to the Olkaria IV radio mast, and from OW43, OW37, OW39 to a radio mast at OW721 (Figure

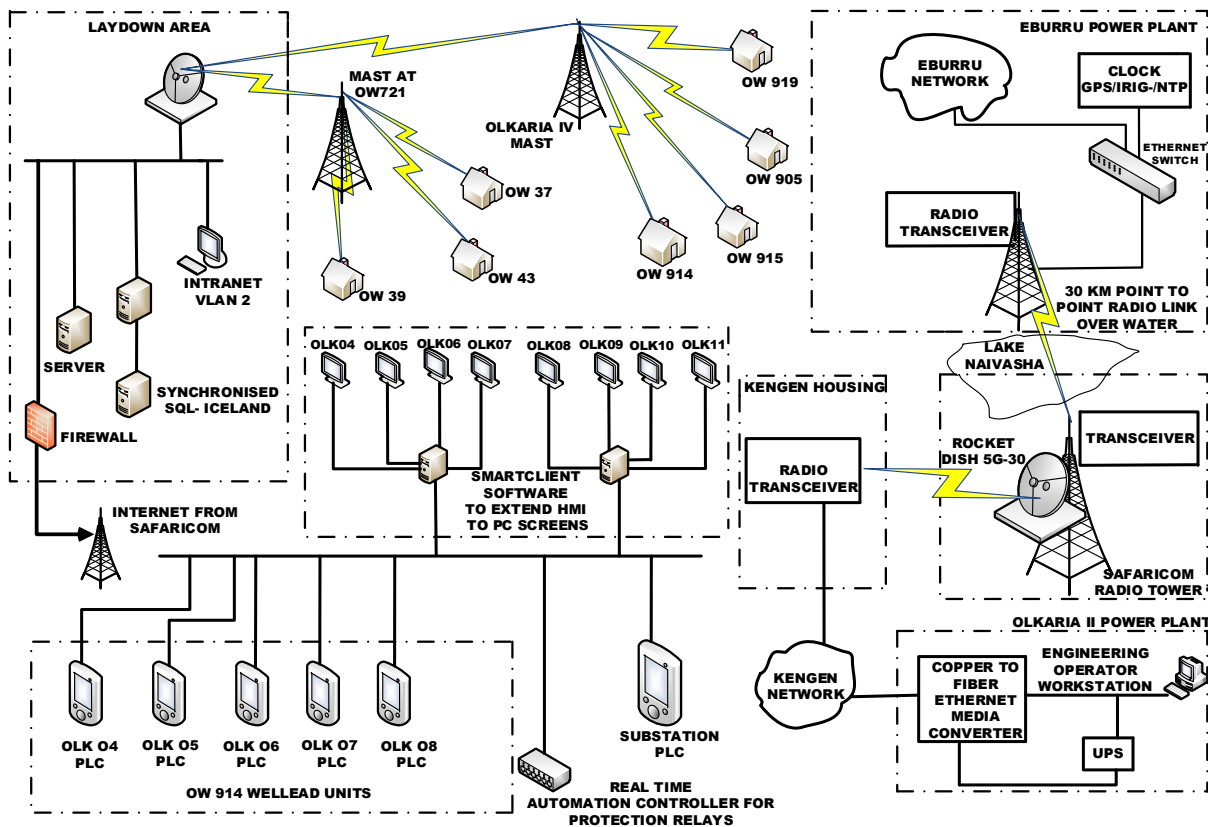


FIGURE 7: Wellhead units' telecommunication network architecture

7). There is another radio link from OW72 to the laydown station. At OW37 well pad, wellhead OW37A, 37B, OW39, OW37 are all connected to the same Virtual Local Area Network (VLAN). These plants are able to be remotely accessed from OW37 as a Siemens remote viewer is connected to an individual local HMI in each plant. At OW914, monitoring of OW915, OW905 and OW919 is also possible through remote desktop. Currently there is no GPS clock for the C64 and C50, making fault finding difficult and even impossible as time is not synchronised. GEG owns the current communication network and KenGen needs to negotiate the take-over of the network.

3.8 Olkaria geothermal power evacuation

The typical design of the wellhead power plants is such that the station auxiliary transformers are connected to the system side of the synchronizing circuit breakers. The separation point between KenGen and Kenya Power who are the grid operators is the high voltage bushing of the generator step-up transformers. Bulk energy meters capable of capturing both export and import energy are located at the separation points. At Eburru, power is generated at 11 kV and stepped to 33 kV through a 3000 kVA transformer before evacuation. The station has a 300 kVA Auxiliary transformer connected to the associated 415 V auxiliary supply board through a 415 V circuit breaker. For wellhead power plants located at Olkaria East production field: OW37, OW37A, OW37B and OW39 generation is at 11 kV channelled to the 11kV bus bar at the OW37 substation. The 11 kV is then stepped up to 132 kV via a 45 MVA 11 kV/132 kV transformer and evacuated to Olkaria I substation. Power from the OW43 units is evacuated to a 33 kV network. There is a proposed plan to step down the 33 kV to OW37 substation after which it is stepped up to 132 kV to Olkaria I substation. At the wellhead power plants located at Olkaria Domes field: OW914, OW905, OW915 and OW919 11 kV generated power is evacuated from OW914 substation 11 kV bus bar via an 87.5 MVA 11/220kV step-up transformer to Olkaria 4 substation. Figure 8 shows the Olkaria geothermal wellhead units' power evacuation scheme. Proposed future wellhead projects are also shown.

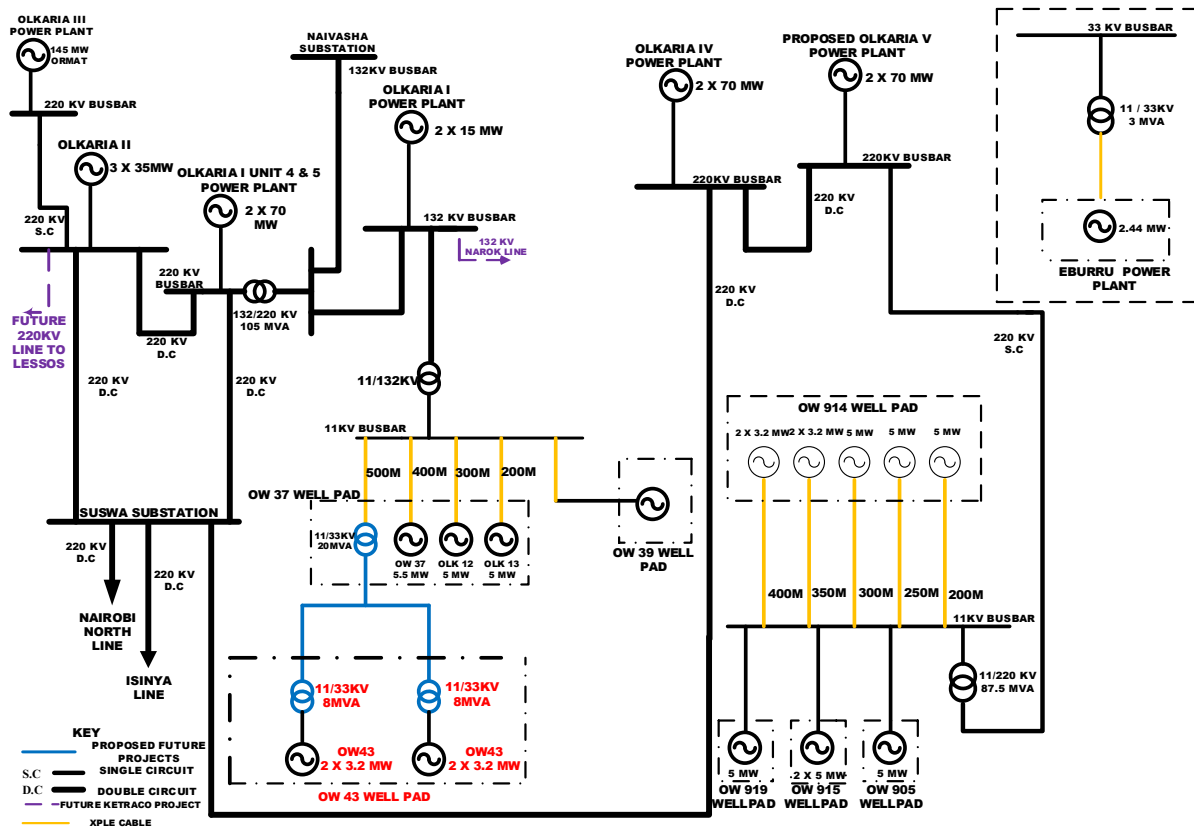


FIGURE 8: Olkaria geothermal wellhead units' power evacuation scheme

4. NEED OF SCADA MONITORING AND CONTROL CENTRE FOR THE WELLHEAD UNITS

4.1 Improved plant availability and reduced process operating and maintenance costs

The geothermal wellhead units are located in remote and inconvenient places. Therefore, it is important to install remote control and monitoring system in a centralised control centre. Also Closed Circuit TV (CCTV) is becoming popular for remote monitoring of geothermal power plants. (Magnússon, 2003). The wellhead centralized monitoring and control centre will streamline the geothermal area operations and optimise staff utilization. This will reduce the cost of operation and maintenance and prepare for ongoing market shifts and changes in Power Purchase Agreement (PPA) requirements. Different power plants control systems are connected via communication links to a SCADA in a conveniently located control centre. The real time monitoring of the wellhead unit's entire operation will assist with rapid detection of faults so that outage times due to faults can be reduced thereby increasing the availability and efficiency of the power plants. Careful consideration of all factors affecting plant availability is needed when planning for remote control (Magnússon, 2003). Operation of a geothermal power plant includes:

- Overall control and monitoring of the whole power plant;
- Adjust controls to regulate the power flow from the plant and coordinate with the grid operator;
- Cold and hot start-up of a power plant;
- Emergency shutdown of the plant in case there is a problem with any of the systems;
- Safe shutdown of the plant;
- Read and maintains logs, i.e. charts, energy meters and gauges to monitor voltage and electricity flow;
- Take hourly and shift checks of running equipment to ensure proper running of various systems.

The operators are responsible for maintaining power plant components to ensure the safety of both the plant and the personnel and to optimize the plant output and availability. They usually work on rotating shifts of 12 hours. The wellhead units have totally 84 staff members, 64 of which are operators (Figure 9). A separate centralized team of electrical, instrumentation and control engineers gives support during breakdowns and planned outages. Having one remote centre will reduce the number of operators to minimize the cost to an absolute minimum. Figure 9 shows the organizational structure.

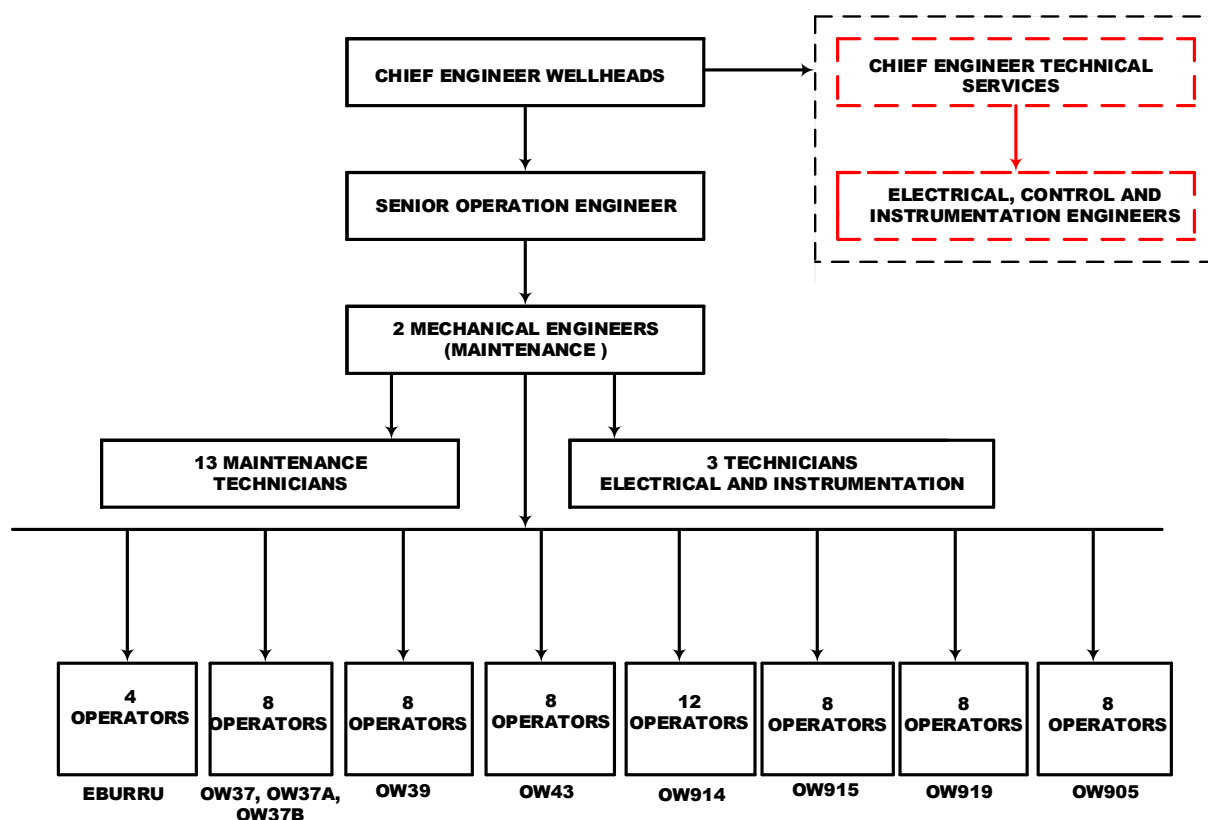


FIGURE 9: Wellhead organizational structure

It is quite common for plants, which have been operated locally for some time without remote monitoring and control that some actions require manual operator intervention since some equipment or automation functions are not working properly anymore. Some of these malfunctions can sometimes lead to outages or delays during the starting of a unit. When remote monitoring and control is installed and commissioned, these malfunctions need to be remedied which then in many cases reduces outages and speeds up starting of a unit. This is an indirect benefit of installing a central SCADA.

4.2 Comparison between plants controlled centrally with a common SCADA system and plants without a central SCADA

Troubleshooting and repair has three key areas: situation analysis, problem solving and decision making (Tomal and Agarajanian, 2014). Situation analysis, which is more of an analysis of the problem, involves discussing the defect with the operator and the overall condition of the problem. A well-trained operator should be able give a detailed background of the device and previous trips caused by it (Table 3). Decision making involves selecting the optimal option to solve the problem. The existence of a SCADA system effects the troubleshooting and repair work as explained in Table 3.

TABLE 3: Comparison between systems with SCADA and without SCADA

	Without a centralised SCADA system	With a new centralised SCADA system
Trip – initial response	The respective wellhead operator notifies the engineer-in-charge. The operator as per the alarm list reports, gives details of the trip or fault. The engineer-in-charge appoints a team to investigate the incident and carry out the necessary repairs to restore operations. This involves getting a standby vehicle and mobilising the team, which can take up to one hour to get to site.	The control room operator notifies the engineer-in-charge who appoints a team to investigate the incident. This can in many cases or to a large extent be done remotely through the Central SCADA in addition to remote desktop or remotely connected engineering system, reducing the need for traveling to wellhead site.
Situation analysis or fault analysis	Trouble shooting starts on site If the operators fails to analyse the trip correctly and maintenance team is not able to relate or understand the issue, trips to the office and back to the plant to pick proper tools or equipment will increase the downtime of the plant. Not always the correct maintenance team is sent to site due to lacking information.	Alarm list and detailed information from engineering system can be investigated from the central control room or in the office or at home using remote desktop. Complete analysis of the problem is done at the centralised control room or office through remote desktop. This enables the team to carry required tools, manuals, equipment and spare parts to site. The correct maintenance team is sent to site after proper central analysis.
Decision making	Problem is fixed. During start up, the plant might encounter normal start up issues, which may trigger a need to call for more people that further increases downtime.	Problem is fixed. In case of any start-up problems, these can be solved through remote desktop or remotely connected engineering system, eliminating the need for specialists to travel to site.

Maintenance engineers using SCADA and/or remote desktop and/or remote connected engineering system reduce the downtime of the machine and improve the availability of the power plants. The operators at the wellhead control room should be well trained in order to be able to interpret alarms and faults. The operators must understand the full operation of the power plant and all its auxiliaries. Operating a centralised SCADA centre reduces the downtime of the plant, overtime paid for off-shift callouts and capital and maintenance costs of vehicles. SCADA is also a tool used in Condition-Based Maintenance, CBM. CBM improves system reliability, availability and security and reduces direct maintenance costs by predicting equipment failures through changes in certain performance parameters (Bore, 2008). Remote engineering from manufacturers and other specialists is an additional advantage as it will enable them to find quick solutions to problems encountered while operating the plants.

Today advanced CCTV with automatic person and vehicle detection are available. Such a system is in operation in at least one large geothermal power plant in Iceland. The system promptly issues an alarm if unexpected traffic is detected. With this kind of a system a large area can be efficiently monitored with few staff.

4.3 Proposed new operation structure for wellhead power plants

The size of the operating staff depends on the system size, complexity and its operating philosophy as it is the largest non-maintenance costs (Boyer, 2004). Table 4 sums up the need for operators for the two different options discussed below.

TABLE 4: Number of operators

Existing scheme	Option 1	Option 2
64	52	36

4.3.1 Option 1

This operating structure allows highly qualified operators to monitor and control all the wellhead power plants at the wellhead central control centre. A few operators are stationed at each wellhead plant to man the plants and manually operate them when needed (Figure 10). This significantly lowers the number of operators stationed at each wellhead unit per shift and reduces the risk of accidents since it decreases the staff's exposure to high voltage equipment.

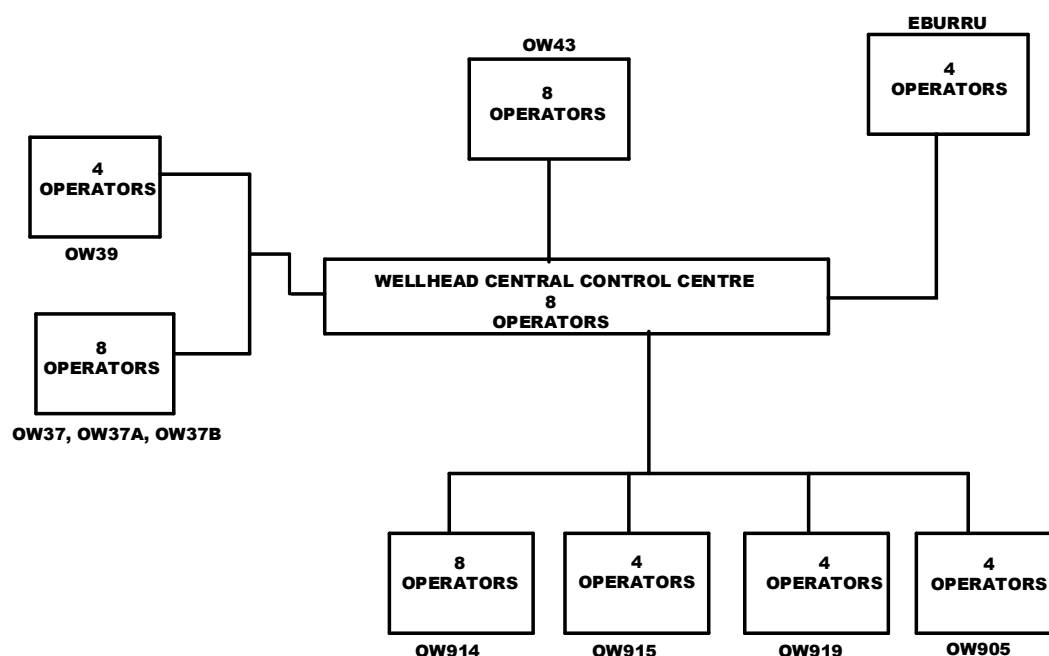


FIGURE 10: Option 1- wellhead operations structure

4.3.2 Option 2

Well trained operators are stationed at the central control centre to monitor and control all the units. Two operators per shift are stationed to monitor and operate OW37, OW37A, OW37B and OW39 at OW37 via SCADA and remote desktops and two operators per shift to monitor and operate OW914, OW915, OW905 and OW919 at OW914 via SCADA and remote desktops (Figure 11). This scheme can only work if the control system is made redundant, this means having standby/backup pumps starting up automatically in case of failure. The disadvantage of leaving the plants unmanned can negatively affect the availability of the plants as it takes time to respond to faults.

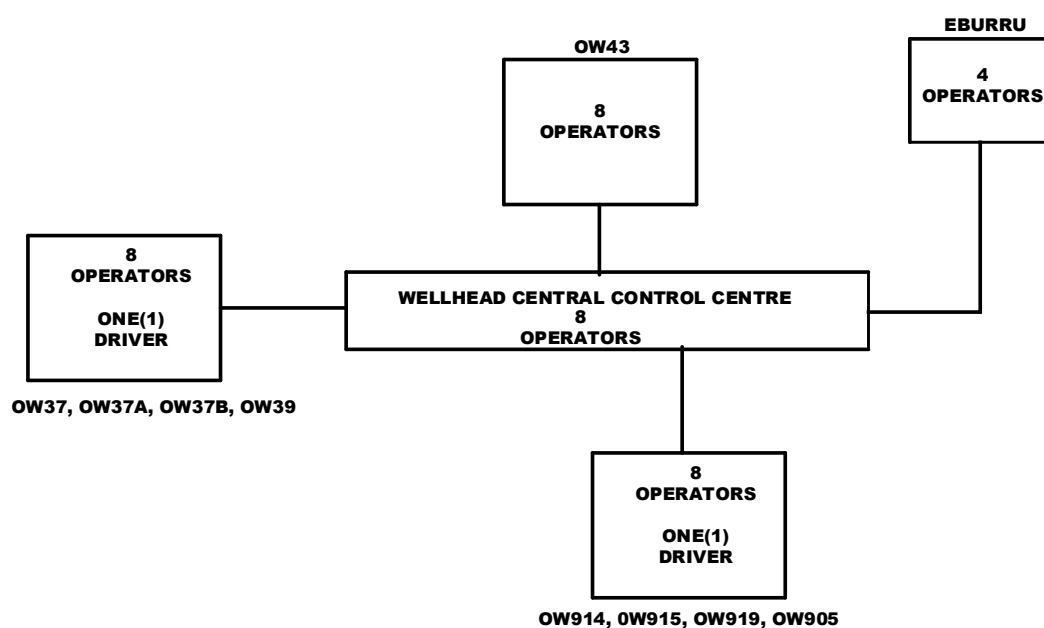


FIGURE 11: Option 2 - wellhead operations structure

5. TELECOMMUNICATION ARCHITECTURE FOR THE WELLHEAD POWER PLANTS.

5.1 General overview of SCADA communication

A comprehensive telecommunication infrastructure needs to be installed to provide the communication links between the wellhead power plants and the centralised control centre. All supervisory control and data acquisition aspects of the SCADA entirely depends on the communication system for an organised flow of data between wellhead units and the SCADA master. The communication at the wellhead units is either handled by specialized communication cards in the PLCs, by specialized remote terminal units (RTUs) or via connection with operator computers. Speech, video and data signals can be transmitted over a telecommunication network via:

- Fibre optic links
- Microwave radio links
- Power Line Carrier (PLC) links
- Metallic cables
- Leased circuits

5.1.1 Fibre optic

Fibre optic is the most powerful and versatile communication medium due to its high bandwidth capability and immunity to electromagnetic interference. The use of optical fibre as digital communication medium has therefore become common in most power utilities as the benefits of implementing fibre optic communication systems and decreasing costs have become more apparent. The advantages of using fibre optic cable links are: long distance transmission without repeater, unaffected by the topology of the terrain of the area, no interference from other communications system, not affected by electromagnetic induction, large potential bandwidth and approval from regulatory authority is not required. The disadvantages of using fibre optic links are: high investment costs, it requires right of way and investment costs are proportional to the length of the transmission link.

5.1.2 Microwave radio

Microwave radio links are used to provide communication services for both speech and data. They operate with radio frequencies ranging from 1.5 GHz up to 50 GHz. The selection of frequency depends on various parameters: the distance, transmission capacities, environmental conditions and restriction on available frequencies. The system design must include a path study between the transmitter and receiver (Boyer, 2004). It is easy to use radio system as they require no physical connection, needs little time to install and low capital costs compared to the fibre optical if large numbers of very tall radio antenna supporting structures are not involved. However, there are problems involved in the initial planning of these systems:

- Radio frequency licences from the regulatory authority is needed and a fee has to be paid annually for these licenses.
- Electromagnetic interference levels and atmospheric conditions are likely to be encountered because radio signals propagate through space as electromagnetic waves and are hard to distinguish from other electromagnetic waves of the same frequency (Boyer, 2004).
- Interference from neighbouring frequency assignments.
- Path loss and possible fading effects.
- Limited to 'line-of-sight', so repeater stations, antenna towers or mast structures for transmission over hilly terrain need to be installed.

5.1.3 Leased circuits

Dedicated leased circuits from local telecommunication service providers can be used as a communication media with minimal investment cost and high flexibility when routing signals. Full dependence on the telecommunication service provider regarding permanent availability, reliability and repair times is an issue when it comes to using leased circuits.

5.1.4 Power line carrier

A power line carrier (PLC) is used by electrical power utilities as communications media, they are the conductors in overhead power lines. PLC links operate in a frequency range between 40 and 500 kHz. The performance of these PLCs depends on the sound/noise ratio and attenuation characteristics of the lines. PLC performance is unaffected by the topology of the terrain and setup cost is independent of transmission length. However, there are disadvantages in using PLC. These include limited bandwidth, the system suffers from electromagnetic interference and adjacent channel interference.

5.2 Communication network design philosophy

The main function of the wellhead telecommunication system is to provide reliable speech, video and data channels between the wellhead power plants and the wellhead centralised control centre. The Open Systems Interconnection model (OSI model) allows the system or network to exchange signals, message packets or addresses. The first layer which is the physical layer defines the relationship between a device and a physical transmission media. A duplex type of communication will allow information to be transmitted and received at the same time. The proposed telecommunication network backbone should use fibre optic and a microwave radio system as communication medium. For security needed for SCADA operations the telecommunication network should be designed in such a way that the SCADA data network is separate from the corporate data network. Equipment shelters and power supply systems are required at the wellhead power plants and the housing site for powering up the radio equipment. Properly rated battery chargers and battery systems provide emergency power to the communication equipment in case of a main power supply failure. Power supplies for electronic equipment, especially in remote locations, are the foundation stones on which a reliable communication system is built (Bailey, 2003). A good communication network should be reliable and have a high availability.

Installation of fibre optic lines from OW915, OW905 and OW919 to OW914, and similarly from OW37A, OW37B and OW39 to OW37 is shown schematically in Figure 12. Optic fibre can be installed in the ground wire of the Overhead Power Transmission Line (OPGW) to OW914 11/220 kV substation and OW37 11/132 kV substation. A microwave radio links OW914 and OW37 to the new centralised wellhead control centre. A 30 km point to point radio link over water from Eburru power plant to KenGen housing site also exists. A Safaricom radio tower is located near the housing unit. A radio links the mast at the housing site and the wellhead control centre.



The proposed telecommunication network backbone for the convectional plants and the wellhead central control centre should use Synchronous Digital Hierarchy (SDH) fibre communication medium (Figure 13) (Parsons Brinckerhoff, 2013). SDH technology offers transmission capacity ranging from synchronous transport modules STM-1 (155 megabits per second) to STM-16 (2.5 Gb/s or higher). The new fibre optic communication system and existing communication system should employ SDH technology capable for providing STM-1 (155 Mb/s) transmission level. All the SDH nodes on the fibre optic cable will be monitored and supervised by a telecommunication Network Management System (NMS) at the proposed Geothermal Remote Control Centre – GRCC at Olkaria I Additional Units power plant (Olkaria I AU). All the geothermal convectional power plants and the wellhead units will be monitored at Olkaria I AU (Parsons Brinckerhoff, 2013).

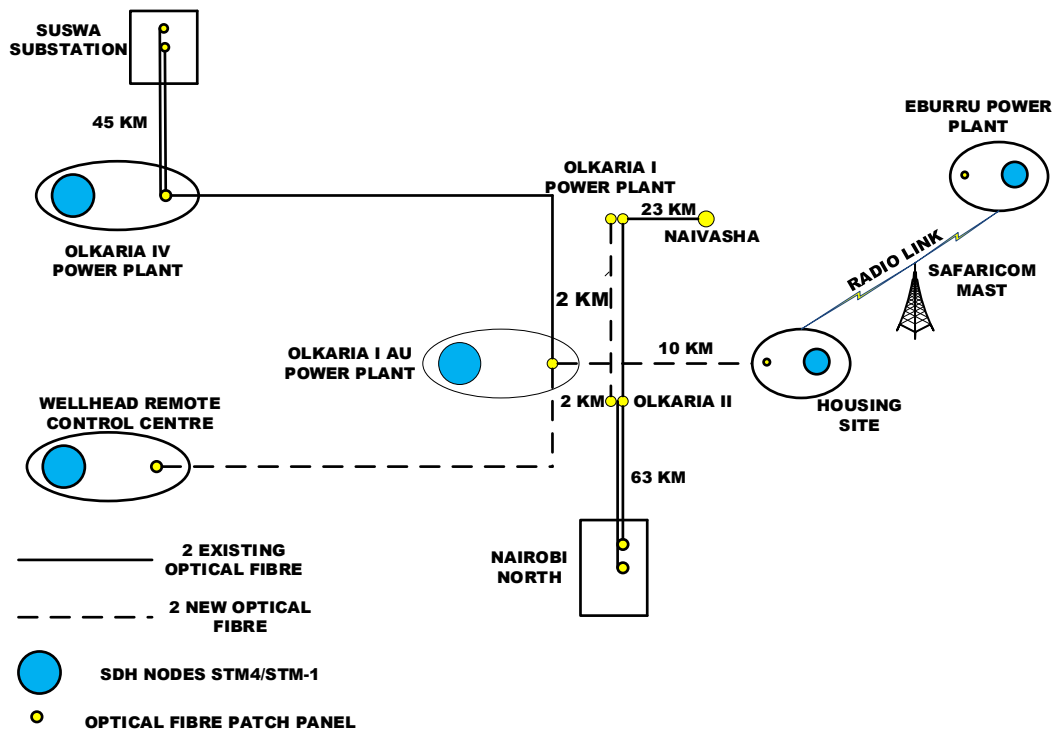


FIGURE 13: Olkaria remote control centre network communication for all the plants
(Parsons Brinckerhoff, 2013)

6. OPTIMISED WELLHEAD CONTROL CENTRE SUPERVISORY CONTROL AND DATA ACQUISITION SCADA SYSTEM

6.1 SCADA system functions

6.1.1 Dispatching of generation

One of the primary functions of the new SCADA system will be the provision of facilities for the centralized dispatch centre to receive dispatch requests from the grid operator, and to accurately and efficiently implement those instructions in accordance with the requirements of the power purchase agreements. Proper coordination with the grid operator for energy management will enhance improvement of system stability and quality of energy.

6.1.2 Operational control

Real time information on the status of the plant will be made available to the wellhead control centre operators to enable them to effectively manage the plants remotely and to take any necessary remedial action when alarms are raised. Alarms are retained in lists to which the operators can refer to be reminded of outstanding fault conditions that are pending action.

6.1.3 Rapid fault detection and accurate fault analysis

The real time monitoring of the entire area operation will assist with rapid detection of faults and dispatch of the right maintenance staff to the site. This will reduce outages, thereby increasing the availability and efficiency of the wellhead units. The SCADA system can assist the operators and the maintenance team to quickly identify the root causing the faults in order to reduce downtime. The system

can be configured to transmit critical messages by email and/or SMS to a mobile phone, for the person in charge to respond in the shortest time possible (Karani, 2008).

6.1.4 Plant condition monitoring

Many plant parameters such as temperatures, pressures, vibration levels and hours of running time can be collected or derived by the SCADA system. SCADA can be used to determine the condition of the wellhead power plants and identify operating limits and maintenance requirements. Using predictive techniques, condition monitoring and observation can be used to predict a possible time of failure and enhance the ability of the plant to plan in the best way possible (Mulugeta, 2009). Condition based maintenance allows the lowest cost and the most effective type of maintenance. The main objective of condition based maintenance is to enhance system reliability, increase the plant availability and to limit maintenance costs to an absolute minimum.

6.1.5 Analysis of historical recorded data

The historical information system will store and ultimately archive all incoming and outgoing data and internally generated values, alarms and events arising from operator actions, software applications and diagnostic routines. The main advantage is the analysis of the plant performance including faults, which aids in troubleshooting and optimization of operation.

6.1.6 Revenue collection

Data from the power plants revenue energy meters at each site are presently collected manually every half hour by staff at each site and entered into a spreadsheet. The proposed design should be able to fully automate this process by retrieving the data directly from the meters then transmitting it via the SCADA system to the centralized dispatch centre.

6.2 The location of the centralized wellhead control centre

The proposed location of the wellhead dispatch centre is at the Olkaria East field near Olkaria I power plant. The area is located centrally to all the wellhead units. Movement from the proposed dispatch centre location to the wellhead power plants is more flexible. The proposed site is about 2 km from Olkaria II power plant where all the maintenance teams are located. The road from Olkaria II to the area is tarmacked.

6.3 Monitoring and control of existing wellhead units

6.3.1 Option A – minimum monitoring

Minimum monitoring of the wellhead units includes unit active power and a few key alarms connected to the central SCADA. This limited remote monitoring will require limited modification of the existing control system. This will benefit the area as the plants do not have to be manned all the time. Key alarms and faults are identified quickly and a maintenance team is dispatched immediately and this will reduce the downtime of the plant.

6.3.2 Option B – minimum monitoring and control

This system will allow minimal control of the plant. This will allow control of active and reactive power and a few controls like tripping the plants by opening the generator circuit breakers.

6.3.3 Option C – full monitoring and control of the power plants

This type of system will allow full control and monitoring of new wellhead power plants. All the plants key information is connected to the control centre and most of the commands from the wellhead unit control system are made available from the control centre, including automatic starting and synchronization of the unit.

6.4 Retrieving data from the existing wellhead control system

The major difficulty in this project is to find an economically viable means of retrieving the desired data from each site. Once retrieved locally at each site, the technical issues of transferring that data to the wellhead control centre and processing, displaying and storing is done by the SCADA and the telecommunication network. Transducers and sensors provide the interface between the equipment and the SCADA system by converting physical phenomena into electrical signals that the signal conditioning and/or data acquisition hardware can accept (Park and Mackay, 2003):

- 4 – 20mA field analogue signals from transducers for voltages, currents, active and reactive power and frequency or from measuring probes for level, flow, pressure and temperature;
- Auxiliary switches that provide information in digital form about the status of an item of plant, i.e. 0 or 24 V equipment status signals or 0 or 24 V alarm switch signals;
- Pulse train meter signal;
- Serial input from field equipment.

6.4.1 Option 1: RTU – hardwired

Signals from and to the field are hardwired to a new SCADA Remote Terminal Unit (RTU) at each site and then the new RTUs are linked to the wellhead centralised control centre via a reliable communication network. This may be the best option for existing wellhead power plants in the case that a bus connection to a RTU is not feasible for some reason. This hardwired approach can be very expensive because the PLC design requires extensive I/O wiring. Few signals are usually hardwired to the new RTU since this option is expensive (Appendix I). The sensors, actuators and the wiring that SCADA uses to interface with the processes that are monitored and controlled form the biggest part of the total project cost (Boyer, 2004).

6.4.2 Option 2: RTU with bus connection to PLC

If there is easy access to a programmer with knowledge of the wellhead PLC programs, then probably a bus connection from the PLC to a bus connected RTU (often called gateway) might be the best solution for retrieving data from control system (Appendix II) (GEG, 2015b). For any control to be possible, the control system must be able to implement control commands received from the remote system. The existing wellhead control system should be able to allow the remote system to interrogate the data stored in its database. The wellhead control centre and SCADA systems both need to support a common communications protocol for the transfer of data and control commands between the two systems. This approach requires additional protocol modules and can be difficult or impossible to implement because of the needed configuration expertise to modify the existing programme to suit the new scheme. The wellhead control system and RTU could communicate using several TCP protocols including Modbus TCP and other TCP/IP based protocol or popular SCADA-RTU protocols such as for example DNP3.

6.5 Central SCADA design philosophy

The most important things to consider when designing a SCADA system are redundancy for a more reliable system, a routable protocol, reliable communication network, time stamping and an

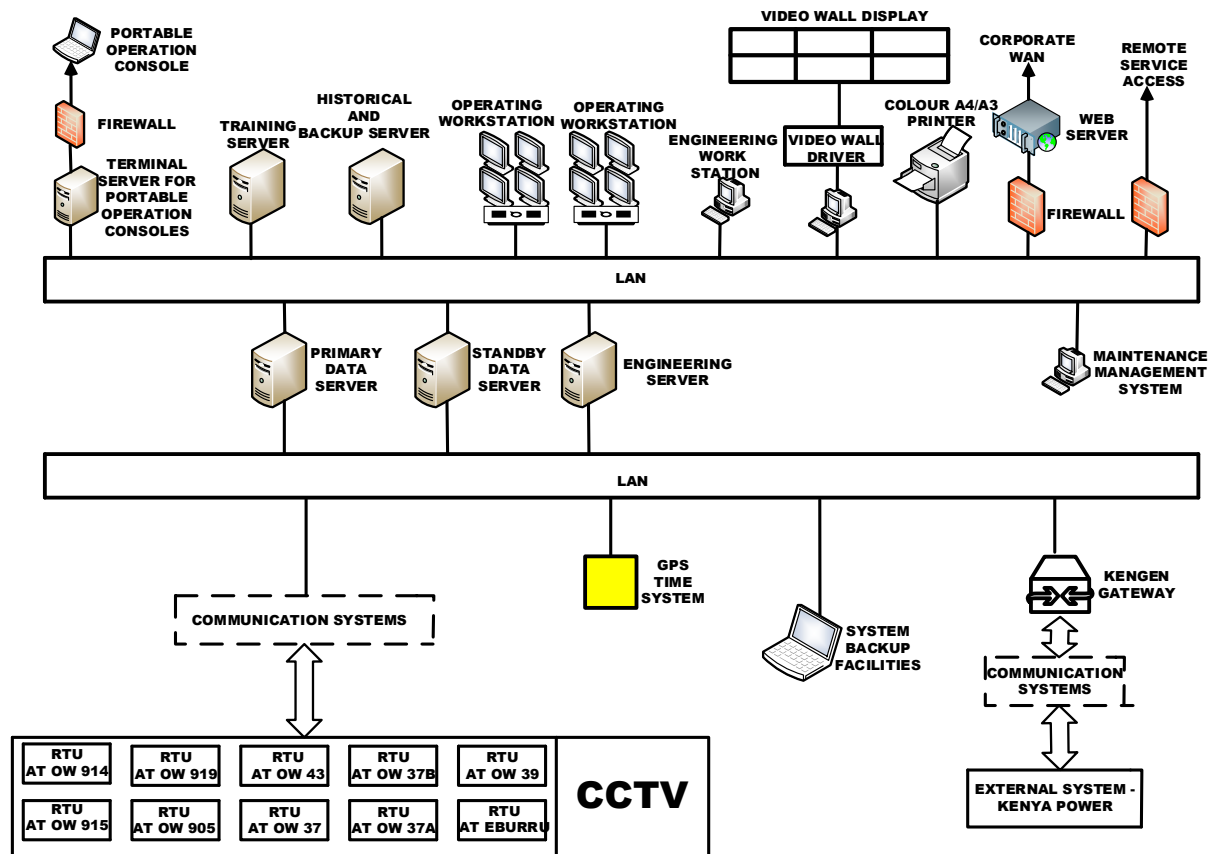


FIGURE 14: SCADA architecture for the wellhead power plants

uninterruptable power supply. Key features of a SCADA system are the user interface, graphics displays, alarms, trends, RTU/PLC interface, access to data, database, networking, fault tolerance and client/server distributed processing (Figure 14) (Bailey and Wright, 2003).

6.5.1 Data servers

Redundant server-client based SCADA architecture with distributed resources along a TCP/IP wide area network (WAN) ensures high availability and guards the system against loss of any critical functionality due to single failures. The systems must have the capacity to retrieve large quantities of real time data from multiple communication channels. The data servers communicate with field devices through process RTUs. Data servers are connected to each other and to client operating stations and engineering stations via an Ethernet LAN. Servers are responsible for data acquisition and handling of the data from the wellhead units and the two 11/132 kV and 11/220 kV substations. Under normal operating conditions both servers should run and are connected to each other. The primary server (Primary Data Server) has the active role and backup server (Standby Data Server) has the standby role. The standby data server does not communicate directly with devices to have access to all data (current and historical) and alarms/events are acquired from the data server. Instead, the primary data server will constantly communicate with the secondary server updating its status and the appropriate databases. If the primary data server fails, the standby data server will take over as the primary server and transfer information to the clients on the network.

6.5.2 Operating work stations

Workstations present process data to an operator through which the human operator controls the process. Operating and engineering work stations are linked to the SCADA system's databases and software programs and help visualize and control all processes. The video display is capable of presenting both

computer display graphics and real-time moving image video from other sources and zoom in on the problem, after being identified.

The SCADA system will maintain an overview display of the real time data coming from the grid operator (Kenya Power Company) and other external customers via dual redundant communications utilising the Inter Control Centre Protocol (ICCP - IEC 60870-6 TASE.2).

6.5.3 Historical data servers

The historical information system is based on a dual redundant server architecture with secure mass storage facilities, reliable database management system and a reporting package for extracting (via SQL like queries) and presenting the data in the acceptable formats.

6.5.4 Training servers

A training platform for the operators for plant and network simulation should also be considered to improve the skills and competency of the operators. Training simulators give valuable insight into the main factors affecting the operation of a modern geothermal plant and have proved to be the most effective and economical method in engineering teaching and training (Magnússon, 2003).

6.5.5 Web servers

A web server in a SCADA system allows using a normal web browser to access the SCADA web data server pages. The function of a webserver is to store, process and deliver web pages to clients via HyperText Transfer Protocol (HTTP) network protocol (Wikipedia, 2016). This allows managers and engineers to monitor the plant through a standard web browser from any desktop. The web server allows access according to IP address and selected webpages. Network firewall has to be incorporated to filter any traffic from the corporate network.

6.5.6 Printers

A A3/A4 printer for printing reports is installed. Printing should be minimal because all required information is available on the screen.

6.5.7 Time synchronisation

The global positioning system (GPS) clock system is an accurate representation of time using Network Time Protocol (NTP) in order to synchronize the computers, process data sub-systems and a networked NTP server. The GPS receiver located at the wellhead control centre via DNP3 protocol synchronises the RTUs and the RTAC with the SCADA.

6.5.8 Protection against hydrogen sulphide (H₂S)

Electrical equipment associated with control, instrumentation and protection is vulnerable to corrosion and failure due to hydrogen sulphide. H₂S is a very corrosive gas and it is advisable to minimize the adverse effects by making a careful selection of materials and maintain appropriate environmental conditions (Rivera, 2007).

6.5.9 Cyber security

The performance of the system depends entirely on the network credibility. Threats and attacks are dangerous to the plant network. Some of these threats include unauthorised access by outsiders and access by authorised users to unauthorised database. Controlling accesses to the network is done by means of authentication, routers, firewalls, intrusion detection system and encryption. Authentication is

TABLE 5: Comparison between SCADA and remote desktop

Remote desktop	Scada
Pros Green Energy Geothermal are already using remote desktops at OW37 and OW914. Show same information as the local plant Human Machine Interface (HMI).	Pros All information in one database. Overview display of all the wellhead units. Easy comparison of data logging. Centralised alarm system. Centralised HMI display. Easy to learn.
Cons Not all equipment is connected (protection relays are sometimes connected). One computer per wellhead is needed for continuous monitoring. HMI not standardized between wellheads. No overview displays of all the wellhead units. Data logging is not in one data server. No good centralised alarm system.	Cons Costly. Connection to existing equipment such as PLCs is uncertain as programming/modification of the PLC programme is expensive.

- *Preventive maintenance* is a time based type of maintenance which is intended to prevent failure by following routine or overhaul maintenance procedures allowing the team to predict, budget and plan maintenance.
- *Condition based maintenance* where an early detection of an equipment failure is noted through monitoring of parameters and periodic testing.
- *Root cause finding*.

A maintenance management system should be used to record maintenance history and control maintenance costs. This system controls all the work orders, routine inspections, man power, tools and spare parts. The maintenance management system should be located at the wellhead control centre. Proper maintenance planning focuses on reduction of maintenance costs, improvement of the plant availability and reducing failures to an absolute minimum.

6.9 Training strategy of the wellhead power plants operation and maintenance staff

Training is key to power plant maintenance and operation, as it encourages knowledge and improves performance of the staff. Training improves skills, knowledge, abilities and the overall availability and performance of the plants. A good strategic plan starts with identification of the training needs of the staff and understanding the equipment and systems to be operated and maintained in a safe, professional and reliable manner. The most common methods used are classroom training, on job training and self-study. Use of simulators, which illustrate general concepts and display all the process in a power plant, enhances better understanding of all the physical process, basic operation and overall operation of the plant. There is need to identify specific roles and corresponding job description and establish the starting baseline in terms of existing capability and the requirement for training. Emphasis should be on proper understanding of all the main and auxiliary components of the power plant, communication and SCADA system. The testing and commissioning of a new plant is a most important opportunity for thorough training. It is therefore very important that the staff, who will become operators and maintenance personnel of the plant, participate as much as possible in the testing and commissioning activities.

6.10 Management of spare parts

Since plant data will be interfaced with the existing enterprise resource planning system that is implemented on SAP software the control of plants spare parts is manageable. With a properly designed maintenance strategy all assets are recorded in the maintenance system and spare parts are connected to the assets. This helps the team to have spare parts available for maintenance during both planned and forced outages. The team is also able to plan and procure spare parts in advance. The timely availability of the power plant, communication and SCADA spare parts, materials and services is a key element of a strong and effective maintenance program (Mulugeta, 2009).

6.11 Transport

In order for the maintenance team based in one or two locations to maintain the dispersed wellhead power plant a more reliable transport system will be required to support the maintenance effort without wasting time, thus reducing the downtime of the plants.

7. IMPROVING PLANT AVAILABILITY - SUMMARY

No chain is stronger than its weakest link and such is the case with availability improvements that typically rest on several factors or links. The following chapter summarizes some of the key factors mentioned in previous chapters for improving plant availability.

7.1 Commitment

Significant improvements in availability require strong commitment and backup from the plant owners and management to ensure allocation of sufficient resources for the availability improvements.

7.2 The pillars of availability

Any significant improvement in plant availability rests on several pillars, a central SCADA system is only one of the necessary ingredients. Some examples of the key issues here are:

- *Staff skills* through natural talents, proper education, plant specific training, on site operational experience and resourcefulness and initiative. Staff motivation is also important in this context. A SCADA system with built in training simulator can also help here.
- *Organization*. An effective organization chart is evidently important for a cost effective and efficient plant operation. Related to this is the proper location of the staff, availability of vehicles etc. A modern central SCADA system facilitates flexible location of staff and reduces need for staff travel through easy access to online plant information almost anywhere.
- *Spare parts*. The availability of spare parts that can be rapidly brought on site is evidently important for availability. The lack of critical spare parts can potentially keep the plant shut-down for a long time. A SCADA system that keeps track of failure statistic for different types of equipment, counts operations and operating hours can be of help in the planning of preventive maintenance work and in the planning of spare parts procurement.
- *Proper tools for plant maintenance*. It is not enough to have spare parts on site, it is also necessary to have the right tools for prompt repair work available on site. The staff must have the right training in applying the tools for repair work. This also applies to each plant control and protection system (i.e. engineering system) and the central SCADA.

- *Weed out unreliable equipment.* In plants of new design or with new equipment, low availability is often experienced during the first few years of operation. Through methodical analysis of the root causes of failures and other unavailability causes, unreliable equipment will gradually be weeded out and improved or replaced by more suitable equipment. A central SCADA with its accurate event logging, trend analysis etc. is essential in this work. It should also be noted here, that when a plant has been operated for a long time without the use of remote monitoring and control, then some equipment may not work well enough for remote operation due to lacking maintenance. The equipment may only work when operated manually by an operator. In this case the equipment in questions must be repaired or replaced by better functioning equipment in preparation for remote operation.
- *Design improvements such as redundancy of critical and/or failure prone equipment.* In some instances, it may be difficult to achieve sufficient availability through simple weeding out of unreliable equipment. In this case, an acceptable improvement in availability may be reached through design changes based on redundancy of equipment. For example, if a single pump does not provide the sought after plant availability, then redundant pumps may be the solution, i.e. adding a backup pump. Triple redundant measurements are an example of another availability improvement solution.
- *Accelerate troubleshooting of failures.* In some cases, it can be time consuming to find the root cause of a trip or other failure. As an example, the root cause cannot found due to lack of information or lacking staff skills. The plant may then be re-started without fixing the root cause first, and may possibly trip again soon. A central SCADA together with other tools such as remotely connected engineering systems can greatly facilitate the search for the root cause of a failure.
- *Accelerate repair and re-starting.* KenGen experts and/or experts from the manufacturer or appropriate consultants can easily assist here, through a central SCADA and other tools such as remotely connected engineering systems. This expert advice can be made immediately available on site and thus helps in fixing the problem and assistance with re-starting can also be provided.

8. COST, ECONOMICS AND FINANCIAL ANALYSIS

8.1 Capital costs

Capital costs are costs used to acquire or upgrade fixed assets with a useful life extending beyond the taxable year. Basic project costs are estimated and economic and financial analysis of the project is made based on these costs. This includes cost related to the SCADA hardware including spare parts and software devices, telecommunication devices, engineering and management works at the plants and the control centre, technical services offered by specialists, training, warehousing and transport. Assuming existing communication masts and radio communication system will be used and the lifetime of the SCADA and telecommunication systems for the purpose of calculating overall lifetime cost is 15 years, SCADA capital cost estimate can be divided into three sections:

- Works required at the power wellhead control centre;
- Works required at OW37 and OW914 substation automation using RTAC;
- Works required at the wellhead power plants.

8.1.1 Items required at the power wellhead control centre

Table 6 shows items required at main wellhead control centre.

TABLE 6: Wellhead control centre works – bill of quantities

No.	Description	Quantity
1	<i>GPS reference time signal receiver</i>	1
2	Gateway to grid company dispatch centre (Kenya Power)	
	Gateway (redundant pair)	1
	Software (implementation of all signals and communication signal table)	1
3	<i>HMI hardware - wellhead dispatch centre</i>	
	Control Cubicles (computer equipment cabinets (for servers, gateways, DC/DC converters, switches etc.)	2
	Hardware, operator stations and associated equipment	
	Operator station computers - DCS clients + maintenance management computer	5
	Portable operator consoles	4
	Terminal server for remote access	1
	DCS servers including database servers (virtual server) redundant	1
	Monitors for operator consoles and servers (24") LCD, including a monitor stand with each OS	12
	Video wall display	1
	CCTV (in all the wellhead power plants)	LOT
	Colour laser printer for the SCADA system	2
4	<i>SCADA dispatch centre software (operating system and basic software)</i>	
	Operating system and other server software, all included (backup software, graphical user interface, real-time clock, power failure restart etc.) including engineering, historian, and database programming tools	1
	Client software for operator stations	1
	Software for portable operator consoles	1
	Engineering software	1
	Maintenance management software (for years)	1
5	<i>The station and PAC networks</i>	
	Station LAN main network switches - layer 3	1
	External connections - firewalls (redundant pair)	2
	Other PAC LAN main network switches - layer 2	2
	Firewall for service access to the station and PAC LANs	1

8.1.2 Items required at OW37 and OW914 substation

Table 7 shows items required at the OW37 and OW 914 substation. This includes acquiring existing data from the two RTAC at OW37 and OW914 to an RTU and interfacing it with the new SCADA.

TABLE 7: OW37 and OW914 RTAC – bill of quantities

<i>RTU - bus connection to RTAC</i>	
RTU software, including installation and configuration: Software I/O, DCS programming and display design for RTU signals	2
<i>Basic objects</i>	
Digital	25
Analog	25
Process displays	2

8.1.3 Items required at the wellhead power plants

Option 1: RTU with hardwired connection to the PLC

Table 8 shows the items needed for the hardwired connection to PLC.

TABLE 8: Hardwired connection to PLC – bill of quantities – RTU

<i>Control cubicles (remote I/O - wellhead): Remote I/O</i>	1
<i>Equipment in remote I/O control cubicles:</i>	
CPU and communication card (DNP 3 or similar) including installation and configuration	1
110 V/24 V DC converters (redundant pair)	1
Digital output units (16 DO)	1
Digital input units (16 DI)	4
Analogue output units (8 AO)	1
Analogue input units (8 AI)	4
Bus connection to RTU (redundant pair)	1
Optical converters for connecting remote I/O to fibre optic cable (pairs)	1
Isolating 4-20 mA / 4-20 mA amplifiers for analogue signals	32
Wiring per signal (wellhead marshalling cubicle to RTU)	87
<i>Software I/O, DCS programming and display design</i>	
Digital monitoring	55
Analogue with alarming	32
Control valve	3
Process displays	2

Option 2: RTU with bus connection to the PLC

Table 9 shows the items needed for the bus connection to PLC.

TABLE 9: RTU-bus connection to PLC – bill of quantities

<i>RTU, including installation and configuration</i>	1
Software I/O, DCS programming and display design for RTU signals	
<i>Basic objects</i>	
Digital	106
Analog	83
Process displays	4

8.2 Total capital cost

Table 10 presents the total capital cost estimates to implement the wellhead central SCADA control system. This includes installation, testing, project management costs, training and cost of spares parts – i.e., overall cost estimates to implement the SCADA

8.3 Economic and financial benefits of the SCADA project

Economic benefits from the new dispatch centre are based on evaluating the potential savings in operating costs and energy saved due to reduction in outages for unscheduled and scheduled maintenance, hence higher availability for dispatch.

8.3.1 Pre-feasibility study of investment in improved operation and increased availability

The first step in deciding whether to invest in improved operation and increased availability should be a pre-feasibility study of the potential improvements. This should be done in the light of the current operation and obvious availability and operation issues today. It is possible for example that this will reveal that most trips or other operation disturbances and problems can be traced to external grid problems or are due to fundamental design or material selection problems in the turbine rotor for example. The conclusion could then possibly be that it is more economical to operate the unit with the

TABLE 10: Overall project costs to implement the SCADA system

	Unit price (USD)	Number of wellhead units	Option 1 - Only hardwired RTUs (USD)	Option 2- Only bus connected RTUs (USD)
<i>RTU – Hardwired</i>	54,000	16	864,000	
RTU – hardwired, cubicle and wiring cubicle design and prototype construction and testing			67,200	
<i>RTU with bus connection to PLC</i>	27,000	16		432,000
RTU with bus connection to PLC. Program design and prototype construction and testing				224,000
RTU with bus connection to RTAC (OW37 and OW914)			18,000	18,000
RTU with bus connection to RTAC-planning of configuration and testing			22,400	22,400
GPS clock			3,400	3,400
Gateway to grid company dispatch centre			14,600	14,600
HMI hardware - wellhead dispatch centre			90,000	90,000
SCADA software - wellhead dispatch centre			64,400	64,400
The station and PAC networks			8200	8200
Installation, configuration and testing, 15% of above			172,830	131,550
Training and documentation, 7% of above			92,800	70,600
Specified spare parts, 4% of above			56,700	43,200
Project management costs, 20% of above			294,900	224,500
Miscellaneous cost, 15% of above			265,400	202,000
Total project cost			2,034,800	1,548,800
VAT 16%			325,568	247,808
Overall project cost			2,360,368	1,796,608

current problems rather than invest in expensive remedies with questionable return on investment. As a result, a shortened lifetime of the wellhead unit may then have to be accepted. In the light of such a situation an investment in availability improvements, including central SCADA may not be financially justifiable. In other words, if a wellhead unit has very difficult operational problems, caused by for example a problem prone turbine rotor, then investment in the connection of the unit to a central SCADA will hardly be economically feasible.

8.3.2 Reduced operation and maintenance costs

The output of the wellhead units for 363 days per year is:

$$83,540 \text{ kW} \times 363 \text{ days} \times 24 \text{ hours} = 727,800,480 \text{ kWh}$$

The income with an energy price of 0.085 USD/kWh, as per the power purchase agreement (PPA), is:

$$727,800,480 \times 0.085 = \text{USD } 61,863,040$$

The KenGen operating and maintenance staff costs of the power plant is assumed to be 2.3% of the income or USD 1.4 million. It is estimated that this cost can be reduced by at least 20% through SCADA and a new staff organisation. The economic benefit due to this is USD 280,000 annually.

8.3.3 Economic benefits of increased availability

Here it is assumed that the yearly income from electricity sales from the Olkaria wellhead units today is around USD 60 million and the average yearly availability is estimated 90%. Official availability figures are not available, so this is an estimate based on available information, with the availability probably having been somewhat lower in recent years.

The availability of exemplary geothermal power plants around the world can be 95% or even higher. A target availability improvement of 2%, i.e. to estimated 92% can be considered realistic if the plants do not have serious problems that are not economical to fix, and provided sufficient strong commitment and backup from the plants owners and management to ensure allocation of sufficient resources can be secured.

It should however be emphasized here that a precondition for this assumption is that a pre-feasibility study of potential availability improvements (see Section 8.3.1 – assessment of investment in improved operation and increased availability), has shown that problems in the operation of the unit are of such a nature that investment in operation and availability improvements are economically feasible.

If the result of the mentioned pre-feasibility study is positive, then it should be possible to increase the availability of the power plants by 2% through a central SCADA, better education and training, new staff organisation, better maintenance and spares management, access to service backup from equipment manufacturers, gradual improvement of reliability by root cause analysis and subsequent wellhead improvement. Then the economic benefit or income due to increasing the availability of the plants is USD 1.20 million annually. See also section on improving plant availability above.

8.3.4 Total economic benefits of increased availability and reduced operating costs

The yearly economic benefit (income) from reduced operating costs and increased availability is USD 1.48 million based on previous assumptions. However, this benefit might take time to be realised. For the first 3 years, it could look like this: an example USD 0.5 million in the first year, 1 million in the second year, 1.48 million in the third year etc. In this case, the calculated Net Present Value (NPV) will be lower. This economic viability analysis, based on a calculated NPV of the forecast economic benefit (income) associated with implementation of the selected SCADA options and other improvements. Furthermore it assumes an operational life of 15 years with an annual discount rate of 8% in accordance with the assumptions for the Least Cost Development Plan for Kenya (ERC, 2011), and indicates a total amount of 11,3 million USD.

With an approximate investment cost of 2 million USD for SCADA Option 1 and approximately 2.4 million USD for the Option 2 and assuming a 15% yearly cost for SCADA maintenance, retraining etc. subtracted, the benefits minus costs for the NPV is reduced to 7.5 million and 6.7 million USD, respectively. Simply said, it could be stated that this is the amount available for other investments needed before the project shows loss.

In this paper, only the cost of a central SCADA equipment has been calculated with some accuracy. An investment in increased availability and reduced operating costs will involve many other investments that are outside the scope of this paper. Housing for central SCADA is one example. A more comprehensive feasibility study, involving many more items than the central SCADA will have to be completed before the final decision can be made regarding investments in increased availability and reduced operating costs.

9. DISCUSSION AND RECOMMENDATIONS

The centralised control and monitoring SCADA scheme for the KenGen wellhead power plants is potentially viable when considering the impact it has on the economy of the wellhead plants and Kenya. Having a reliable and improved availability will result in additional electricity to consumers. The project is potentially financially viable to KenGen and will save both operations and maintenance costs. Efforts have to be made at the plant project design stage to factor in and ensure full remote monitoring and control of future plants. For the existing wellhead units, minimum remote monitoring and control is feasible with only key information from the wellhead control system connected to the central dispatch centre. For more reliable power plants, the following key improvements are recommended for even greater reliability:

1. The wellhead power plants have limited redundancy. It is possible to reduce the impact of equipment failures by introducing a more reliable equipment design, such as 2×50% instead of 1×100% which has control equipment that starts automatically in order to keep the power plant running at least on partial load in case of failure of one piece of equipment such as a pump or control valve. Related to this is the weeding out of unreliable equipment.
2. Wellhead plants need to be connected to a more stable grid to minimize the frequent trips due to line faults.
3. From the beginning of operation, critical spare parts should be purchased and stored at site to increase reliability. Purchase of appropriate tools and software for maintenance work should also be included.
4. Proper and regular equipment inspections, maintenance and routine tests should be carried out.
5. Training of all operations for maintenance staff and organisation improvements should be done regularly.

ACKNOWLEDGEMENTS

My sincere gratitude is expressed to the Government of Iceland, The United Nations University Geothermal Training Programme (UNU-GTP) and my employer, Kenya Electricity Generating Company (KenGen), for the opportunity to attend this training programme. I owe my sincere appreciation to Mr. Lúðvík S. Georgsson, director of UNU-GTP. I am sincerely grateful to my supervisors Mr. Jóhann Thór Magnússon and Lýður Skúlason for their tireless effort in advice, guidance, knowledge transfer, support and patience during all stages of this work. Many thanks to Mr. Ingimar Haraldsson, Málfríður Ómarsdóttir, Mr. Markús A. G. Wilde and Ms. Thórhildur Ísberg for their assistance during my stay in Iceland.

I am indebted to my colleagues Eng. Teresa Karani and Nathaniel Mugo for the support and providing me with valuable information towards this project.

I give special thanks and heartfelt gratitude to my parents, John Apiyo and Millicent Odera, and my siblings, Effie, Juliet, Faith and Jaffa for their love, unwavering moral and emotional support and encouragement throughout the six months.

Above all, utmost appreciation to the almighty God for the divine intervention in this academic endeavour.

REFERENCES

- Bailey, D., 2003: *Practical radio engineering and telemetry for industry*. Newness – Elsevier, Oxford, 320 pp.
- Bailey, D., and Wright, E., 2003: *Practical SCADA for industry*. Elsevier, Amsterdam, 304 pp.
- Bore, C.K., 2008: *Analysis of management methods and application to maintenance of geothermal power plants*. University of Iceland, MSc thesis, UNU-GTP, Iceland, report 5, 60 pp.
- Boyer, S., 2004: *SCADA, supervisory control and data acquisition* (3rd ed.). ISA – Instrumentation System and Automation Society, USA, 240 pp.
- ERC, 2011: *Updated least cost power development plan for Kenya - study period 2011-2013*. Energy Regulatory Commission, Kenya, 203 pp.
- GDA, 2011: *Preliminary control system function specification*. Geothermal Development Associates, report, 29 pp.
- GEG, 2015a: *Geothermal power plants operational manual*. Green Energy Geothermal, document number: C50-00-0401-MAN-001_1.0, 97 pp.
- GEG, 2015b: *C50 operation and maintenance manual*. Green Energy Geothermal, Electrical as-built drawings, drawing number: C50-4-E0033-DW, 189 pp.
- Karani., T.W., 2008: Improved operations and reliability by upgrading Olkaria I control system and installing remote monitoring and control system for Olkaria I and II geothermal power plants in Kenya. Report 21 in: *Geothermal training in Iceland 2008*. UNU-GTP, Iceland, 331-364.
- Magnússon, J.Th., 2003: Operational simulators and automatic control systems. In: Fridleifsson, I.B., and Gunnarsson, M.V. (eds.), *Lectures on sustainable use and operating policy for geothermal resources*. UNU-GTP, Iceland, publication 1, 185-194.
- Mendive, D.L., and Green, L.H., 2012: Wellhead geothermal power plant at Eburru, Kenya. *Geothermal Resources Council, Transactions*, 36, 4 pp.
- Mulugeta, A.A., 2009: *Evaluation of maintenance management through benchmarking in geothermal power plants*. University of Iceland, MSc thesis, UNU-GTP, Iceland, report 3, 52 pp.
- Ouma, P.A., 2007: Geothermal exploration and development of the Olkaria geothermal field. *Paper presented at Short Course II on Surface Exploration for Geothermal Resources, organized by UNU-GTP and KenGen, at Lake Naivasha, Kenya*, 17 pp.
- Park, J., and Mackay, S., 2003: *Practical data acquisition for instrumentation and control system*. Elsevier – Newness, Amsterdam, 425 pp.
- Parsons Brinckerhoff., 2013: *SCADA phase II and central dispatch centre inception report*. Parsons Brinckerhoff, report for Kenya Electricity Generating Company - KenGen, 147 pp.
- Rivera, M.A., 2007: Design considerations for reliable electrical, control and instrumentation systems in geothermal power plants with emphasis on hydrogen sulphide related problems. Report 20 in: *Geothermal Training in Iceland 2007*. UNU-GTP, Iceland, 461-490.
- Tomal, D.R., and Agajanian, A.S., 2014: *Electronic troubleshooting* (4th ed.). McGraw-Hill Education, NY, USA, 448 pp.
- Wikipedia, 2016: *Web server*. Wikipedia, website: en.m.wikipedia.org/wiki/Web_server.

APPENDIX I: Option 1, RTU – Hardwired**DIGITAL INPUT**

- | | |
|--|--|
| 1. Turbine exhaust pressure HIGH HIGH | 29. Auxiliary transformer 11 KV Earth Switch CLOSED |
| 2. Lube oil system trip oil pressure low | 30. Auxiliary transformer 415 V AC TRIP |
| 3. Turbine vibration system trip | 31. Auxiliary transformer 415 V AC TRIP |
| 4. Turbine control turbine governor TRIP | 32. Back generator 415 V CB TRIP |
| 5. Turbine control turbine governor FAULT | 33. Compressed air compressor fault TRIP |
| 6. Excitation control TRIP | 34. Cooling tower 1 fan motors FAULT TRIP |
| 7. Turbine control speed sensor 1 FAULT | 35. Cooling tower 2 fan motors FAULT TRIP |
| 8. Turbine control speed sensor 2 FAULT | 36. Cooling tower 3 fan motors FAULT TRIP |
| 9. Turbine governor actuator # 1 | 37. Cooling tower 4 fan motors FAULT TRIP |
| 10. Turbine governor actuator # 2 | 38. Cooling tower 1 fan vibration TRIP |
| 11. Turbine governor over speed | 39. Cooling tower 2 fan vibration TRIP |
| 12. Turbine governor emergency trip | 40. Cooling tower 3 fan vibration TRIP |
| 13. Turbine governor Manual External trip | 41. Cooling tower 4 fan vibration TRIP |
| 14. Generator circuit breaker CLOSED | 42. Cooling auxiliary H ₂ O pump FAULT TRIP |
| 15. Generator circuit breaker earth switch OPEN | 43. Fire alarm system annunciation 1 st stage ALARM |
| 16. Generator circuit breaker earth switch CLOSED | 44. Fire alarm system annunciation 2 nd stage ALARM |
| 17. Generator circuit breaker protection relay TRIP | 45. Fire alarm system annunciation FAULT |
| 18. 11 KV feeder circuit breaker OPEN | 46. Fire alarm system annunciation ALARM |
| 19. 11 KV feeder circuit breaker CLOSED | 47. PLC/SCADA system main DC supply alarm |
| 20. 11 KV feeder earth switch CLOSED | 48. PLC/SCADA system back up DC supply alarm |
| 21. 11 KV feeder circuit breaker protection relay TRIP | 49. PLC/SCADA system power supply ALARM |
| 22. Auxiliary transformer 11 KV circuit breaker CLOSED | 50. DC distribution 110V DC rectifier fault |
| 23. Auxiliary transformer 11KV circuit breaker OPEN | 51. DC distribution DC/DC converter FAULT |
| 24. Steam separator brine level HIGH HIGH | 52. DC distribution unit 1 110V DC CBD FAULT |
| 25. Condenser water level HIGH HIGH (TRIP) | |
| 26. Turbine drain drum water level HIGH HIGH | |
| 27. Lube oil system oil level in tank LOW | |
| 28. Auxiliary transformer 415 V AC CLOSED | |

ANALOG INPUT

- | | |
|---|---|
| 1. Well head outlet pressure value | 8. Turbine steam inlet 1 temperature value |
| 2. Two phase distribution supply pressure value | 9. Turbine control valve 1 position |
| 3. Steam separator brine level value | 10. Turbine emergency shutoff valve 1 |
| 4. Steam outlet to silencer pressure control valve position | 11. Turbine control valve 2 position |
| 5. Turbine inlet 1 pressure value | 12. Turbine emergency shutoff valve 2 |
| 6. Turbine steam inlet 2 pressure value | 13. Cooling circuit water to cooling tower pressure value |
| 7. Lube oil system pressure value | 14. Condenser water level value |

- | | |
|--|--|
| 15. Cooling circuit water to cooling tower temperature value | 24. Turbine bearing rotor rear journal temperature value |
| 16. Turbine HP radial X vibration | 25. Transmission gear pinion front journal temperature value |
| 17. Generator voltage | 26. Transmission gear pinion rear journal temperature value |
| 18. Generator current | 27. Transmission gear pinion wheel front journal temperature value |
| 19. Frequency | 28. Transmission gear pinion wheel rear journal temperature value |
| 20. Generator active power | 29. Turbine steam inlet 2 temperature value |
| 21. Generator reactive power | |
| 22. Turbine bearing rotor front thrust temperature bearing | |
| 23. Turbine bearing front journal temperature bearing value | |

DIGITAL OUTPUT

- | | |
|--|--|
| 1. Vacuum breaker valve CLOSE COMMAND | 3. Turbine control turbine governor trip turbine |
| 2. Governor Circuit Breaker Relay Trip command | |

ANALOG OUTPUT

- | | |
|---|---|
| 1. Turbine control valve 1 control | 5. Turbine emergency shut off valve 2 control |
| 2. Turbine control valve 2 control | 6. Turbine control active power feedback output value |
| 3. Turbine pressure inlet steam output value | |
| 4. Turbine emergency shut off valve 1 control | |

APPENDIX II: Option 2, RTU with bus connection to PLC

DIGITAL INPUT

- | | |
|---|---|
| 1. Turbine exhaust pressure HIGH HIGH | 15. Turbine control and protection PLC power supply ALARM |
| 2. Lube oil system trip oil pressure low | 16. Turbine control and protection IE Switch ALARM |
| 3. Turbine vibration system trip | 17. Generator circuit breaker OPEN |
| 4. Turbine control turbine governor ALARM | 18. Generator circuit breaker CLOSED |
| 5. Turbine control turbine governor TRIP | 19. Generator circuit breaker spring charged |
| 6. Excitation control Fault | 20. Generator circuit breaker Earth switch OPEN |
| 7. Excitation control TRIP | 21. Generator circuit breaker Earth switch CLOSED |
| 8. Lube oil system emergency oil pump Running | 22. Generator circuit breaker protection relay ALARM |
| 9. Lube oil system emergency oil pump FAULT | 23. Generator circuit breaker protection relay TRIP |
| 10. Turbine control and protection 110V supply FAULT | 24. 11 KV feeder circuit breaker OPEN |
| 11. Turbine control and protection main DC supply ALARM | 25. 11 KV feeder circuit breaker CLOSED |
| 12. Turbine control and protection backup DC supply ALARM | 26. 11 KV feeder circuit breaker spring charged |
| 13. Turbine terminal box 24 V DC FAULT | 27. 11 KV feeder earth switch CLOSED |
| 14. Cooling circuit terminal box fault | |

28. 11 KV feeder circuit breaker protection relay ALARM
29. 11 KV feeder circuit breaker protection relay TRIP
30. Auxiliary transformer 11KV circuit breaker OPEN
31. Auxiliary transformer 11KV circuit breaker CLOSED
32. Auxiliary transformer 11KV circuit breaker FAULT
33. Auxiliary transformer 11KV Earth Switch CLOSED
34. Auxiliary transformer temperature protection ALARM
35. Auxiliary transformer temperature protection FAULT
36. Steam separator brine level LOW
37. Steam separator brine level HIGH
38. Steam separator brine level HIGH HIGH
39. DC distribution 110V DC rectifier fault
40. DC distribution unit 0 110V DC CBD FAULT
41. Condenser water level LOW
42. Condenser water level HIGH HIGH
43. Turbine drain drum water level HIGH HIGH
44. DC distribution DC/DC converter FAULT
45. Lube oil system oil level in tank LOW
46. Lube oil system oil level in tank LOW
47. Lube oil system oil differential pressure AOP/MOP LOW
48. Ejector system motive steam 1st stage valve CLOSED
49. Ejector system motive steam 2st stage valve CLOSED
50. Ejector system inter-condenser inlet valve CLOSED
51. Cooling circuit vacuum breaker valve CLOSED
52. Auxiliary transformer 415 V AC CLOSED.
53. Auxiliary transformer 415 V AC TRIP.
54. Back generator 415 V CB CLOSED.
55. Back generator 415 V CB TRIP
56. Compressed air compressor READY
57. Compressed air compressor fault TRIP
58. Compressed air compressor RUNNING
59. Air conditioning system cooling unit 1 RUNNIG
60. Air conditioning system cooling unit 2 RUNNIG
61. Ventilation system 1 H₂S filter fan running
62. Ventilation system 2 H₂S filter fan running
63. Fire alarm system AC power supply ON
64. Cooling tower 1 fan motors READY
65. Cooling tower 2 fan motors READY
66. Cooling tower 3 fan motors READY
67. Cooling tower 4 fan motors READY
68. Cooling tower 1 fan motors OVERHEAT
69. Cooling tower 2 fan motors OVERHEAT
70. Cooling tower 3 fan motors OVERHEAT
71. Cooling tower 4 fan motors OVERHEAT
72. Cooling tower 1 fan motors FAULT TRIP
73. Cooling tower 2 fan motors FAULT TRIP
74. Cooling tower 3 fan motors FAULT TRIP
75. Cooling tower 4 fan motors FAULT TRIP
76. Cooling tower 1 fan vibration TRIP
77. Cooling tower 2 fan vibration TRIP
78. Cooling tower 3 fan vibration TRIP
79. Cooling tower 4 fan vibration TRIP
80. Cooling auxiliary H₂O pump READY
81. Cooling auxiliary H₂O pump FAULT TRIP
82. Cooling tower1 switch disconnecter CLOSED
83. Cooling tower 2 switch disconnecter CLOSED
84. Cooling tower3 switch disconnecter CLOSED
85. Cooling tower 4 switch disconnecter CLOSED
86. Cooling tower1 switch disconnecter CLOSED
87. Cooling tower 2 switch disconnecter CLOSED
88. Cooling tower3 switch disconnecter CLOSED
89. Cooling tower 4 switch disconnecter CLOSED
90. Fire alarm system annunciation 1st stage ALARM
91. Fire alarm system annunciation 2nd stage ALARM
92. Fire alarm system annunciation FAULT
93. Fire alarm system annunciation ALARM

- | | |
|--|---|
| <ul style="list-style-type: none"> 94. PLC/SCADA system main DC supply alarm 95. PLC/SCADA system back up DC supply alarm 96. Steam supply terminal box 24 V DC FAULT | <ul style="list-style-type: none"> 97. PLC/SCADA system main alarm buzzer off COMMAND 98. PLC/SCADA system power supply ALARM |
|--|---|

ANALOG INPUT

- | | |
|--|---|
| <ul style="list-style-type: none"> 1. Well head outlet pressure value 2. Two phase distribution supply pressure value 3. Steam separator brine level value 4. Steam outlet to silencer pressure control valve position 5. Steam outlet to silencer pressure value 6. Brine outlet to silencer level control valve 7. Wellhead outlet temperature value 8. Two phase distribution supply temperature 9. Turbine inlet 1 pressure value 10. Turbine steam inlet 2 pressure value 11. Turbine nozzle box pressure turbine exhaust pressure value 12. Lube oil system MOP discharge pressure value 13. Lube oil system AOP discharge pressure value 14. Lube oil system EOP discharge pressure value 15. Lube oil system pressure value 16. Gland steam system pressure value 17. Lube oil system trip oil pressure 18. Turbine steam inlet 1 temperature value 19. Turbine steam inlet 2 temperature value 20. Turbine exhaust temperature value 21. Steam supply steam value 22. Turbine bearing rotor front thrust temperature bearing 23. Turbine bearing front journal temperature bearing value 24. Turbine bearing rotor rear journal temperature value 25. Transmission gear pinion front journal temperature value 26. Transmission gear pinion rear journal temperature value 27. Transmission gear pinion wheel front journal temperature value 28. Transmission gear pinion wheel rear journal temperature value 29. Lube oil system oil cooler inlet temperature value | <ul style="list-style-type: none"> 30. Lube oil system oil cooler outlet temperature value 31. Gland system steam temperature value 32. Generator Bearing #3 Radial X vibration 33. Generator Bearing #4 Radial X vibration 34. Generator Bearing #3 Radial Y vibration 35. Generator Bearing #4 Radial Y vibration 36. Generator voltage 37. Generator current 38. Frequency 39. Generator Active Power 40. Generator Reactive Power 41. Turbine control valve 1 position 42. Turbine emergency shutoff valve 43. Turbine control valve 2 position 44. Turbine emergency shutoff valve 2 45. Turbine control turbine governor actuator output 1 46. Turbine control turbine governor actuator output 2 47. Cooling circuit condenser inlet valve position 48. Cooling circuit condenser level valve position 49. Cooling circuit condenser bypass valve position 50. Cooling circuit hot well pressure value 51. Cooling circuit water to cooling tower pressure value 52. Cooling circuit sump water level value 53. Cooling circuit inlet pressure value 54. Ejector system inter condenser pressure value 55. Condenser water level value 56. Condenser pressure value 57. Cooling circuit hot well outlet temperature value 58. Cooling circuit water to cooling tower temperature value 59. Oil cooling circuit inlet temperature value 60. Oil cooling circuit turbine outlet temperature value 61. Oil temperature generator outlet temperature value |
|--|---|

- | | |
|---|---|
| 62. Ejector system condenser outlet gas temperature value | 67. Electrical control unit air temperature 2 value (RTD INPUT) |
| 63. Ejector system inter-condenser temperature value | 68. Electrical control unit air temperature 2 value (RTD INPUT) |
| 64. Ejector system inter condenser gas temperature value | 69. Electrical control unit outside temperature value (RTD INPUT) |
| 65. Electrical control unit air temperature 1 value (RTD INPUT) | 70. Electrical control unit outside temperature value (RTD INPUT) |
| 66. Electrical control unit air temperature 1 value (RTD INPUT) | 71. Air compression system air pressure |

DIGITAL OUTPUT

- | | |
|---|--|
| 1. Ejector system motive steam 1 steam 1 st stage valve OPEN COMMAND | 5. Turbine control turbine governor trip turbine |
| 2. Ejector system motive steam 1 steam 2 nd stage valve OPEN COMMAND | 6. Turbine control turbine governor enable CAS |
| 3. Ejector system inter condenser inlet valve OPEN COMMAND | 7. Governor circuit breaker relay trip command |
| 4. Vacuum breaker valve CLOSE COMMAND | 8. Lube oil system emergency oil pump stop COMMAND |

ANALOG OUTPUT

- | | |
|--|--|
| 1. Steam outlet to silencer pressure control valve control | 7. Gland steam system pressure control valve 2 control |
| 2. Brine outlet to silencer level control valve control | 8. Turbine control valve 1 control |
| 3. Cooling circuit condenser inlet valve control | 9. Turbine control valve 2 control |
| 4. Cooling circuit condenser level valve control | 10. Turbine emergency shut off valve 1 control |
| 5. Cooling circuit condenser bypass valve control | 11. Turbine emergency shut off valve 2 control |
| 6. Gland steam system pressure control valve 1 control | 12. Turbine pressure inlet steam output value |
| | 13. Turbine control active power feedback output value |



UNITED NATIONS
UNIVERSITY

UNU-GTP

Geothermal Training Programme

Orkustofnun, Grensasvegur 9,
IS-108 Reykjavik, Iceland

Reports 2016
Number 10

ENVIRONMENTAL CONSIDERATIONS IN PRODUCTION TESTS AND GEOTHERMAL WELL STIMULATION

Bertha A. Arenivar Marroquín

LaGeo S.A de C.V

15 Avenida Sur, Colonia Utila

Santa Tecla, La Libertad

EL SALVADOR C.A

barenivar@lageo.com.sv

ABSTRACT

The production test is one of the most important activities in geothermal development because through the production test the properties of a reservoir become known, and in this way, the amount of energy that can be extracted from it, can be evaluated. However, these tests involve certain environmental aspects that will have to be managed, such as the emission of gases and wastewater, generation of noise, etc. During well production tests in the Hengill geothermal field, environmental aspects involved in well discharges were investigated for well HE-58, using a 35-day data period with records of water amount, steam discharge, and gas emissions to the atmosphere and the ground. For well HE-21 the amount of Fluoride (as KF) discharge into the water and the amount sulphur hexafluoride (SF₆) is discharged in the steam was monitored.

Another important activity is stimulation which is used when there is a decline in pressure in the well. This activity, though necessary, may have undesirable environmental effects.

In this report discharge tests using lip pressure, tracer flow, and stimulation through matrix acidification, are analysed. For environmental analysis, the DASI method for identifying effects is used, and the RIAM method to evaluate the magnitude of the impacts. Finally, activities to minimize environmental effects are considered such as: using of a muffler, mitigation of H₂S emissions, designing and planning a monitoring system for air and water, checking equipment and leakage, and other considerations for the minor impacts.

1. INTRODUCTION

Well tests are important for field development decisions, because this is the first step in evaluating the amount of energy that can be extracted. Discharge tests after warm up of the well are a key to the estimation of the capacity and the success of the well. During energy production from a geothermal reservoir, monitoring data is collected to continuously upgrade the model of the reservoir. All this information is essential for a successful assessment of a reservoir. The capacity of a geothermal field

can be determined from its size, heat content and production response. The first assessment of a geothermal field capacity is usually done by a volumetric method (Muffler and Cataldi, 1978).

In this paper, two different methods for evaluating the flow of a well are analysed: lip pressure and tracer flow tests, in wells HE-58 and HE-21, respectively. These wells are a part of a production well system in the Hellisheidi and Hverahlíð areas in the Hengill geothermal field.

Production tests are important to obtain knowledge of the potential energy and other characteristics of a reservoir. However, this activity involves different environmental aspects: such as gas emission, noise, wastewater, etc., so it is necessary to establish the possible environmental effects and actions to be taken when performing a production test in order to prevent possible negative environmental and social impacts on different environmental components such as water, air, soil, flora, wildlife etc.

One activity that may be important during production tests is stimulation, because it involves the injection of different chemicals in quantities that need to be considered in the environmental study. Stimulation is needed when flow has declined because of scaling or for other reasons. Sometimes it is not possible to discharge a well, because some wells develop scales or encounter other ways of flow restriction. Different methods of well stimulation exist, such as the use of chemicals that are injected into the well and upon discharge the fluid composition changes, because of reactions in the well. In this paper, an environmental analysis will be conducted to define environmental effects to be monitored.

2. OVERVIEW OF DRILLING

2.1 Short description of drilling

Well drilling is a vital component of geothermal exploration and the future utilization of a geothermal field. Well studies provide information such as enthalpy, steam fraction and chemical composition of the fluid that permits the estimation of the amount of energy that can be extracted from the reservoir. The main characteristics of the reservoir are size, temperature and permeability.

There are three different types of wells, production wells that are used for power generation, reinjection wells that contribute to the sustainability of the resource, and monitoring wells that are used to study the behaviour of the geothermal reservoir.

In general, geothermal wells are controlled by a main valve system that is used to ensure the stability of the well. A geothermal well is connected to the geothermal reservoir through feed-zones of open sections or intervals. Feed-zones are either particular open fractures or permeable aquifer layers. In volcanic rocks, feed-zones are often fractures or permeable layers such as interbeds (layers between different rock formations) while in sedimentary systems, feed-zones are most commonly associated with thin aquifer layers or thicker permeable formations. Fractures can also play an important role in sedimentary systems. In some instances, a well is connected to a reservoir through a single feed-zone while in other cases several feed-zones may exist in the open section, but often one of these is the dominant one; see Figure 1 (Axelsson and Franzson, 2012).

2.1.1 Classification of geothermal wells

Different types of geothermal wells with different roles are drilled into geothermal fields such as described by Axelsson and Franzson (2012): temperature gradient, exploration, production, step out, make up, reinjection, monitoring and unconventional wells. These are all important at different stages of the development of a new or existing geothermal field. The three principal types for environmental considerations are: production, reinjection and monitoring wells.

Production wells: Their main purpose is to enable the production of geothermal energy (such as hot liquid, two-phase mixture, or steam) from a specific target, or a geothermal reservoir. Production wells are designed either for spontaneous discharge through boiling (high-temperature reservoirs) or for the application of downhole pumps (low temperature reservoirs).

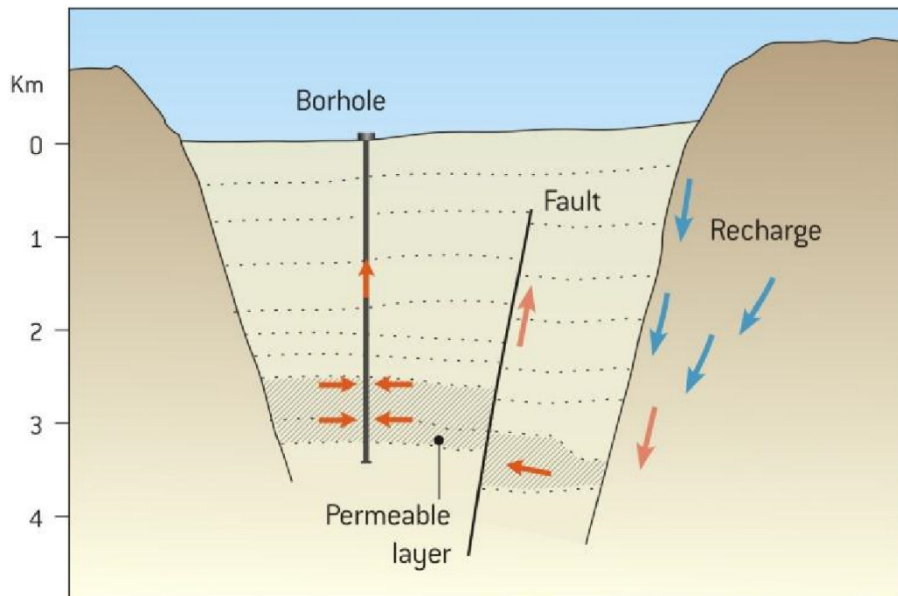


FIGURE 1: Schematic representation of a reservoir
(Axelsson and Franzson, 2012)

Reinjection wells: Reinjection wells are used to return fluid to the geothermal system or to inject water of a different origin as supplemental recharge. The location of reinjection wells is variable. Reinjection can be applied inside a production reservoir, on its periphery, below or above it or outside the main production field, depending on conditions and the purpose of the reinjection.

Monitoring wells: These are used to monitor changes in geothermal systems, mainly after utilization starts, mostly pressure and temperature changes. These are in most cases already existing wells, such as exploration wells or abandoned production wells.

Production wells can also be classified into three principal types depending on fluid enthalpy:

1. **Dry-steam high-temperature wells** where the flow from the feed-zone(s) to the well-head is steam-dominated.
2. **Two-phase high-temperature wells** where the flow from the feed-zone(s) is liquid or two-phase but the wells produce a two-phase mixture.
3. **Liquid-phase low temperature wells**, which produce liquid water at the well-head

3. PRODUCTION TESTING

The information obtained through production tests is needed to confirm whether a well was satisfactorily drilled and to decide how to utilize the reservoir. Some important reservoir and wellbore parameters are: temperature, permeability, formation storage (storability), type of reservoir (porous or fractured). Skin factor and location of the reservoir boundaries are also important. Based on the well test objectives, several kinds of tests may be designed to determine these parameters and reservoir properties. Grant et al. (1982)

3.1 Description of study area for production testing

The Hengill mountain is one of the highest mountains in the region east of Reykjavík, Iceland's capital. It is located in the centre of the western volcanic zone in Iceland, on the plate boundary between the North American and the European crustal plates; this boundary runs from Reykjanes in a north easterly direction towards Langjökull. The plates are diverging at a relative rate of 2 cm/year. Hengill mountain is on the triple junction of the Reykjanes Peninsula volcanic zone, the Western volcanic zone and the South Iceland Seismic Zone.

Within the Hengill complex, several potential geothermal fields can be distinguished. Two of these have been developed where Reykjavík Energy operates co-generation geothermal plants at Nesjavellir and Hellisheidi. The installed capacity at Nesjavellir power plant is 120 MWe and 290 MWth. The Hellisheidi power plant is also a co-generation plant with 303 MWe and 133 MWth installed. The Nesjavellir power plant is located on the northern side of the Hengill Mountain and the Hellisheidi power plant on the southern side. Other possible production fields on the southern side of the Hengill Mountain are Bitra, Hverahlíð, Gráuhnúkar, and Meitill (Figure 2).

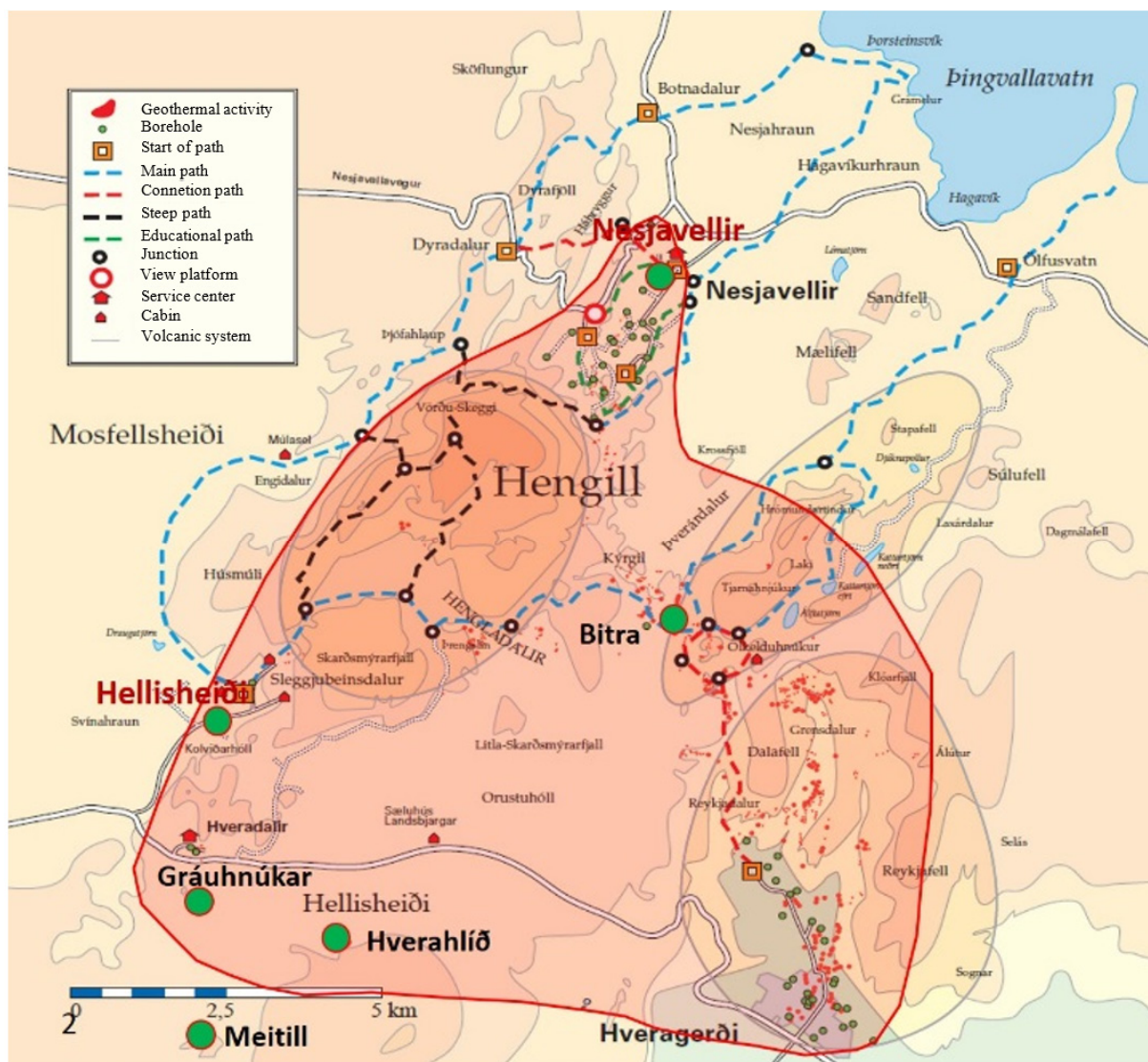


FIGURE 2: The Hengill geothermal area and some of its subfields (modified from Gunnlaugsson, 2012)

The present well field in Hellisheidi covers some 12 km². The first exploration well was drilled in 1985 at Kolvidarhóll (KhG-1) on the western boundary of the Hellisheidi field. A total of 49 exploration and production wells have been drilled in the Hellisheidi field, the last one was drilled in 2016. The depths of these wells are in the range 1400 m to 3300 m. A total of 35 production wells in this field are connected to the power plant. A total of 17 reinjection wells have been drilled for the Hellisheidi power plant at two locations, Gráuhnúkar and Húsmúli. The depths of these wells are 1000 m to 3000 m. The majority of both the production and reinjection wells, are deviated wells (Gunnlaugsson, 2012).

In the Hverahlíd field, a geothermal power plant was planned and it was described in an Environmental Impact Assessment report (Reykjavik Energy, 2005). Six exploration and production wells have been drilled at Hverahlíd. Four of the six wells in this field have now been connected to the Hellisheidi power plant.

Data from flow tests of two wells were made available for this study. These wells are HE-58 in Hellisheidi, which is a deviated well and HE-21 in Hverahlíd, which is a vertical well. The main features of these wells are shown in Table 1.

TABLE 1: Wells used in this study

Well no.	Field	Location Latitude	Location Longitude	Drilling date	Depth m	Length m
HE-21	Hverahlíd	385369,47	391637,00	Feb. 2006	2159	2159
HE-58	Hellisheidi	383860,83	394397,07	Nov. 2015	2237	2531

Some features that describe the environment surrounding the field are:

- The main characteristics of the **weather** are that the air temperature is on average 2.6°C lower than in Reykjavik. Humidity is higher and the wind speed on Hellisheidi is generally 70% higher than in the capital area. Rainfall is three times that of Reykjavik.
- The main characteristic of the **groundwater system** in the area investigated is that it is divided from southwest to northeast by a range of the mountains Hengill, Stóra-Reykjafell, Stóri-Meitill and Litli-Meitill. On the eastern side, water flow is to the east from Hellisheidi. The hydrology is a little more complex on the western side, with a characteristic area of 15 km² west of Hengill where the level of the groundwater table is at around 172 m above sea level. From there, groundwater flows in three directions: West to the Ellidaár catchment area, northeast to Lake Thingvallavatn and to the south where it reaches the sea at Selvogur. Apart from small streams in Sleggjubeinsdalur, from Draugatjörn and in Engidalur there is little surface water in the development area. The river Hengladalsá runs out of Innstidalur in the eastern part of the Hengill region.
- The **vegetation** is mostly moss, grass and small shrubs. Grassland is less widespread than the moss-covered areas. About a quarter of the area is lava covered with moss. A large part of the development on Skardsmýrarfjall has little or no vegetation. The **animal life** is rather scarce, possibly because of shortage of surface water in the area. Fifteen to seventeen breeding bird species have been recorded at Kolvidarhóll, some of which seem to be found at Kolvidarhóll and surroundings only. Raven, which is an endangered species, has bred at Hellisskard. Five to six breeding bird species were found on Skardsmýrarfjall, golden plover being the most common one.
- **Cultural remains** in the area are particularly linked to transportation and many old trails crossing the area.
- **Habitation and recreation.** There are no residential houses but some summer houses in the area. The Hengill area is popular for recreation and marked hiking trails and the publication of maps have increased its accessibility. Some old trails are also used for horseback riding (Reykjavik Energy, 2005).

3.2 Purpose and importance of the production tests

The main purpose of well production tests is to obtain relevant information about the reservoir, especially during new geothermal field exploration because it can give an idea of the main reservoir parameters such as temperature, permeability and storativity, and also other important factors such as type of reservoir (porous or fractured), skin factor and location of the reservoir boundaries (Axelsson, 2013), that can be used to construct a conceptual model of the new field, or even make an update of an existing conceptual model, in which the main production and recharge zones can be included.

3.3 Types of production tests

When a well has been drilled it is necessary to measure fluid flow, determine its energy content and analyse its characteristics. High enthalpy wells are expected to have a warmup period of 2-4 months after drilling is completed. The well is opened up and allowed to flow to the atmosphere. High-temperature geothermal wells are usually discharged into a silencer which also acts as a steam-water separator at atmospheric pressure.

There are many methods used to estimate flow from wells during production testing but two methods are most commonly used in Iceland for two-phase flow measurements: the lip pressure method and the chemical tracer method. The production tests can be classified as:

3.3.1 The pressure diffusion equation

The basic equation of well testing theory is the pressure diffusion equation. It is used to calculate the pressure (P) in the reservoir at a certain distance (r) from a production well producing at a given rate (q) as a function of time (t). The most commonly used solution to the pressure diffusion equation is the so-called Theis solution or the line source solution (Earlougher, 1977).

3.3.2 Lip pressure method

The lip pressure method is based on an empirical formula developed by Russel James (James, 1962). To use this method, a steam-water mixture is discharged through an appropriately sized pipe into a silencer or some other simple device to separate the steam and water phases at atmospheric pressure. This is the most common method used for two-phase mixtures (Steingrímsson, 2016).

Assuming that we have a fairly large amount of steam/water mixture flowing at sonic velocity through an open-ended pipe to the atmosphere, the absolute pressure at the external end of the pipe is then proportional to the mass flowrate and enthalpy (Figure 3). The flow in geothermal wells is assumed to be isenthalpic (adiabatic). Water flow from the silencer is commonly measured by the weir-box method (Grant et al., 1982).

The formula that Russel James deduced is (Equation 1):

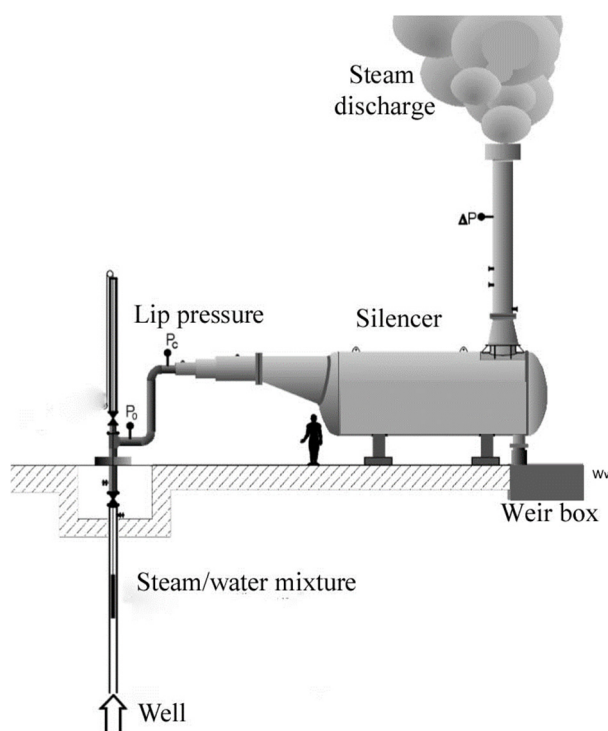


FIGURE 3: Schematic representation of the Lip Pressure method (Steingrímsson, 2016)

$$\frac{W_t H_t^{1.102}}{A P_{lip}^{0.96}} = 1680 \quad (1)$$

where:

P_{lip} = lip pressure at the end of the pipe (MPa)

W_t = total mass flow rate (kg/s)

A = cross-section area of the lip (cm²)

H_t = Total fluid enthalpy (kg/kJ)

The lip pressure is measured at the extreme end of the discharge pipe using a liquid-filled gauge to dampen out pressure fluctuations. Water flow from the silencer is measured using a V sharp-edged weir box near the silencer outlet, shown in Figure 3. When water flow W_w (kg/s) from the atmospheric silencer, measured in the weir-box, and the lip pressure are known, the total fluid enthalpy is given by Equation 2:

$$\frac{W_w}{A P_{lip}} = Y = \frac{0.74(2675 - H_t)}{H_t^{1.102}} \quad (2)$$

This equation can also be solved for H_t between 400 and 2800 kJ/kg as a function of Y with an accuracy of 1.5% (Grant et al., 1982).

The water flow W_w is related to the total mass flow as shown by equation (3), where X is the steam mass fraction ratio.

$$W_t = \frac{W_w}{1 - X} \quad (3)$$

3.3.3 Chemical tracer (tracer flow test)

In this method two different tracers are used, one for the liquid phase and one for the steam phase. The principle of this method involves measuring the dilution when a solution containing a chemical indicator is injected into the well discharge. The solution is injected at a known constant rate at an upstream location. Analysis of a downstream sample will then make it possible to determine the well discharge by the formula (Equation 4):

$$Q = q \frac{C_1 - C_2}{C_2 - C_0} \quad (4)$$

where q is the injection rate of the chemical solution and C_0 , C_1 and C_2 are respectively the concentrations of the chemical indicator in the well fluid, the solution injected and the downstream sample. For the steam phase, the same principle as for liquid water is applied. Instead of injecting solution into the flow stream, a non-condensable gas (SF_6 diluted in N_2) is more commonly used (See Figure 4). The tracers used by Reykjavik Energy are sulphur hexafluoride (SF_6) for the steam and fluoride (KF) for the liquid (Elmi 2008).

3.3.4 Injection tests

Injection testing is in principle a simple variant of discharge flow testing, with the flow reversed. Water is injected into a well and the flow rate recorded along with changes in down-hole pressure or depth to water level. A quasi-stable flow versus pressure curve can be obtained, and transient behaviour measured as changes in flow rate.

Injection is a simple inverse of production, if the fluid injected is of the same enthalpy (quality or temperature) as that produced. Generally, the fluid injected is water that is cooler than the reservoir fluid, then it has different viscosity and compressibility from the reservoir fluid (Grant et al., 1982). The

non-isothermal injectivity index obtained from these tests depends on the mobility ratio of the cold region to the hot reservoir and the extent of the cold spot.

During injection tests, the injectivity index is often used as a rough estimate of the connectivity of the well to the surrounding reservoir. Here it is given in the units $[(L/s)/bar]$ and it is defined as the change in injection flow rate divided by the change in stabilized reservoir pressure (Grant et al., 1982).

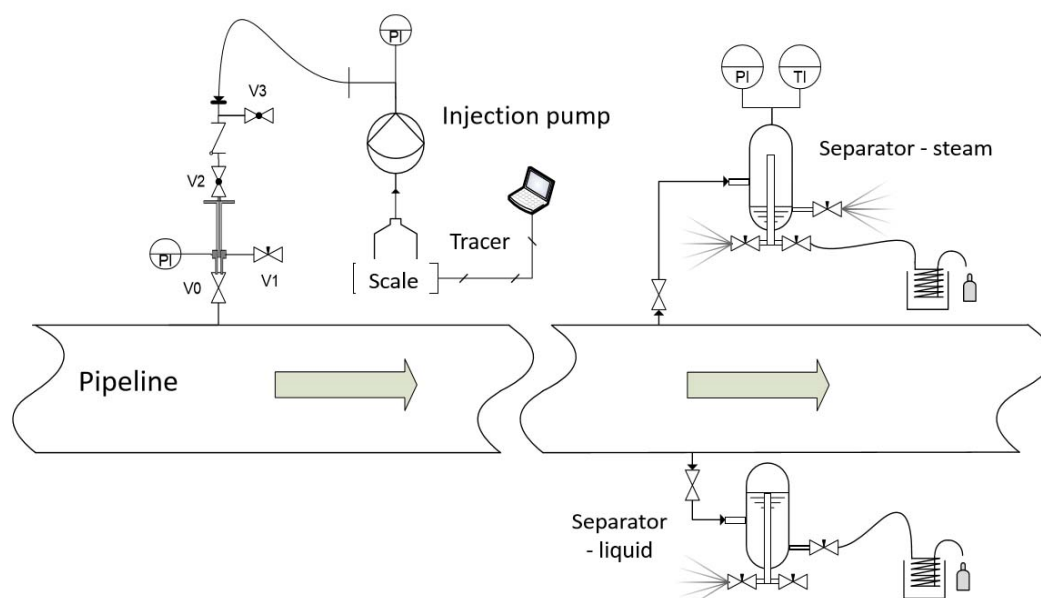


FIGURE 4: Schematic representation of chemical tracer methodology (Steingrímsson, 2016)

4. GEOTHERMAL WELL STIMULATION

4.1 Purpose and importance of the well stimulations

Stimulation techniques have the potential to increase formation permeability and remove the damage to the formation which causes a low flow-rate in the well. Low productivity, due to lack of communication with the naturally occurring main conduits for fluid flow, can be improved by cleaning and by thermal and/or hydraulic fracturing of wells, usually applied at the end of drilling. Sometimes it is necessary to treat damage due to mud invasion into open fractures, blocked pores or minor flow channels (Flores et al., 2005).

The design of any stimulation should start with a thorough assessment of the characteristics of the specific system. The type of stimulation is appropriate and the chemical composition of the produced fluid must be determined. Damage formation, resistance to mechanical and thermal stresses of rock, background temperature, and ore mineralogy are analysed (Galindo, 2015).

4.2 Types of stimulations

Geothermal wells can be stimulated in two main ways: hydraulics or acid, which are subdivided according to specifications of each method. The different types of stimulations are shown in Figure 5.

4.2.1 Hydraulics

A geothermal well can be stimulated by creating fractures either by pumping at fluid pressures greater than the fracture pressure or by injecting cold water, which upon contact with the hot rock will have the effect of a thermal shock and rock strength creating conductive channels (Galindo, 2015).

Hydraulic Fracturing: is performed by pumping specially engineered fluids at sufficiently high pressure for a fracture to be opened. Connection of many, pre-existing fractures and flow pathways within the reservoir rock with a larger fracture may be achieved. The final stage of the treatment is the injection of a proppant¹ (usually sand) slurry. This proppant maintains the fracture flow capacity created after relaxation of the hydraulic pressure (Flores et al., 2005).

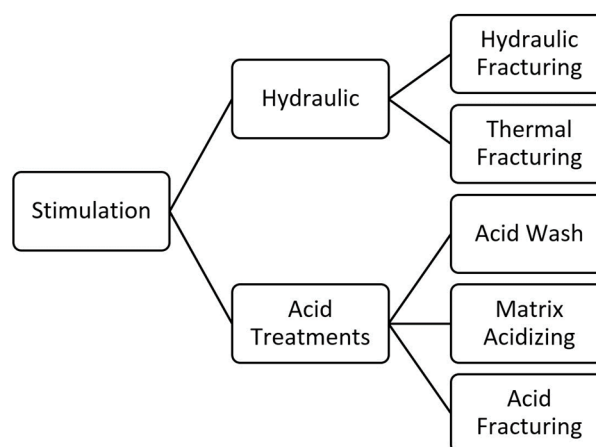


FIGURE 5 : Types of stimulation
(Galindo 2015)

Thermal fracturing: takes place when a fluid (e.g. produced water, seawater, aquifer water or surface water), considerably colder than the hot receiving formation, is injected. Injection of the cooler water leads to thermal contraction of the reservoir rock in the region near the injection well, reducing the stresses. The reservoir can be fractured at a lower pressure than the original in-situ stress would indicate, if there is a large temperature difference between the injected water and the formation (Galindo, 2015).

4.2.2 Acid treatment

Acids have the ability to dissolve formation minerals and foreign material, such as drilling mud, which may be introduced into the formation during well drilling, as well as after precipitated minerals have formed during production. This is the reason for utilizing acids to stimulate geothermal wells, to increase flow production or injection capacity (Galindo, 2015).

Acid cleaning: is employed to remove scale from production lines, discharge lines and the face of the producing formation, and is the oldest stimulation technique still used today. Each geothermal system is subject to different scaling problems, due to the chemical characteristics of the geothermal fluid and pressure and average temperature of the well, and also to the petro-physical properties of the producing formation such as permeability and porosity (Galindo, 2015).

Matrix acidizing: involves injecting acid into the formation of the well at a pressure below the pressure at which a fracture can be opened. On the other hand, acid fracturing requires that acid is injected into the formation at a high enough pressure to fracture the formation or open existing fractures. Acid treatment for sandstones differs significantly from treatment intended for carbonate rocks. Carbonate rocks rapidly dissolve in hydrochloric acid and the reaction products are water soluble. Unlike acidification reactions in carbonate rocks, chemical reactions in siliceous rocks are extremely complex. The sandstones are comprised of quartz grains, different types of clays, feldspar, chert, micas and various carbonate minerals. HCl is not effective in dissolving most components of siliceous rocks. Hydrofluoric acid (HF) combined with hydrochloric acid (HCl), formic acid or acetic acid is commonly used in sandstone acid treatment, and the acid formulation used in any specific case depends on the

¹ A material that prevents the fracture from closing after completion, ending pumping and ensuring a newly created conductive channel.

mineralogy of the formation. Commonly employed solutions are 10% HCl, a mixture of 12% HCl and HF 3%, for dissolving silicates and silica (Galindo, 2015).

Acid fracturing: involves injecting acid into naturally fractured or previously fractured rock. The injection should be carried out at a greater pressure than the formation pressure. It is widely used to stimulate carbonate rocks or formations that are more than 85% acid soluble. This involves first injecting a viscous fluid at a pressure exceeding the fracture pressure of the formation. The following injection increases the length and width of the fracture, and injecting acid sets off a reaction along the fracture to create a channel extending deep into the formation. The key to success is the penetration of acid along the fracture. However, the volume of acid used in fracturing treatment is much larger than that used in the matrix acidification treatment. The effective fracture length depends on the type of acid used, and the reaction rate of acid fluid lost in the formation (Galindo, 2015).

5. DESCRIPTION OF ACTIVITIES DURING PRODUCTION TEST AND STIMULATIONS

Different sub-activities are carried out during production tests (lip pressure and tracers flow test) and stimulations (matrix acidifications), e.g. activities that need to be considered for environmental analysis. The DASI method (dissociation of aspects/ synthesis of impacts) has been used for the identification of environmental (Arévalo and Padilla, 2008) activities and sub-activities identified and shown in Table 2.

TABLE 2: Typical actions or sub-activities realized during productions test and stimulations

Activities	Typical actions/sub-activities
1. Production test (Lip Pressure)	1.1 Transportation and conditioning of equipment 1.2 Measurement equipment installation 1.3 Measurements of steam flow 1.4 Measurements of water flow
2. Production test (TFT)	2.1 Transportation and conditioning of equipment 2.2 Injection of tracers 2.3 Collection of sample
3. Production test with stimulation (Matrix Acidifications)	3.1 Transportation and conditioning of equipment 3.2 Preparation and mixing of chemicals 3.3 Injection of treatment fluids 3.4 Rest or warm up 3.5 Measurements of steam flow 3.6 Measurements of water flow

5.1 Activities during production tests (lip Pressure)

Once a well is stimulated its fluid is directed into the muffler, located on the side of the main platform. Separation to a two-phase fluid is effected by sending steam to the atmosphere and water to the weir box and after this, water is drained to the pipeline and finally injected into a reinjection well.

5.1.1 Transportation of equipment and materials

This stage involves the transportation of equipment that will be used for discharge of steam and water, and the equipment with which the measurements will be made. For example, portable mufflers, weir-box, pipe, pressure gauges, etc.

5.1.2 Measurement equipment installation

At this stage one proceeds to the placement of equipment such as a portable muffler, weir box and piping system to channel water to the reinjection well. In this case it must be ensured that flanges and valves are tightened, the pipeline is anchored and that the water piping system is properly installed.

5.1.3 Measurements of steam flow (discharge steam to atmosphere)

Once the equipment is properly installed, the total flow of water and vapour from the well is passed through a pipe, which discharges it. The steam is discharged to the atmosphere vertically through a muffler for approximately one month (depending on the technical and environmental characteristics of the site where this discharge test takes place) until the pressure is stable. The variables that are monitored are:

- Wellhead pressure
- Lip pressure
- Gas concentrations

5.1.4 Measurements of water flow (injection of waste water)

The muffler is connected to a weir box where flow measurements are made, then the water is conducted through a pipe system to the well where it will be reinjected. The variables that are monitored during this activity are:

- Water flow in weir box
- Temperature of water

5.2 Production test (TFT)

5.2.1 Transportation and conditioning of equipment and materials

This stage involves the transfer of equipment to be used to carry out the tracer flow test. For the transportation it is only necessary to pick up the equipment for the injection of tracers, sampling separators and complementary equipment.

5.2.2 Injection of tracers (SF_6 and KF)

Once the specialized equipment for the tracer flow test has been installed, the tracers are injected, the KF, 1% concentration and injective velocity is $200 \text{ cm}^3/\text{min}$, is used to evaluate the liquid phase, and for the gas phase 1% SF_6 with velocity of flow 20 g/min is used.

5.2.3 Collection of samples (steam and water)

The sampling point is located about 40 meters downstream of the injection point after a bend or valve to provide sufficient mixing. Samples are collected to determine the concentrations of the tracers. Collection of samples starts when the injection has reached equilibrium, usually 10-15 minutes after injection started. Samples are collected from downstream sampling points using sampling separators operating at line pressure (Figure 6). Separated steam and water are passed through condensing coils and collected into screw-cap containers (Lovelock, 2001).

5.3 Activities during stimulation (matrix acidifications)

This part describes one type of stimulation. The procedure for matrix acidification is as described in the following sections.

5.3.1. Transportation of equipment, materials and chemicals

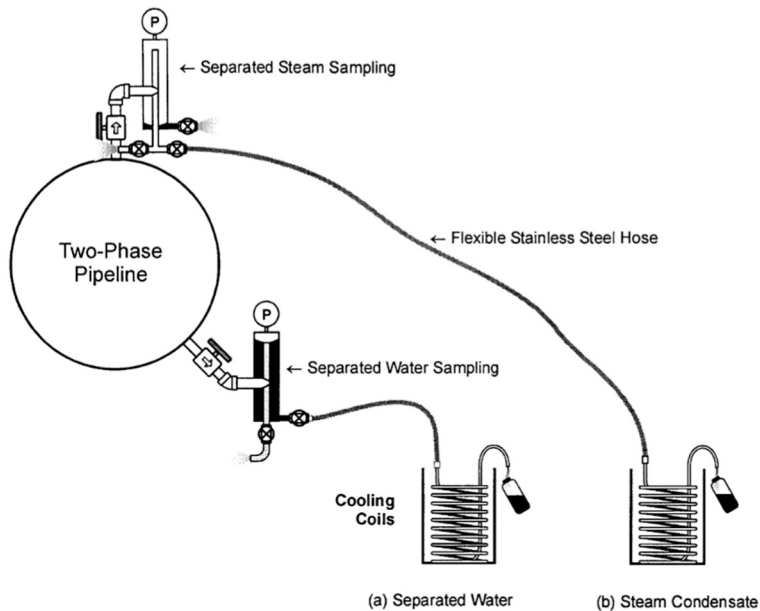


FIGURE 6: Tracer sampling equipment (Lovelock, 2001)

For chemical stimulation piping systems, valves, hoses and tanks are required; and are handled on the platform as follows:

To make the transfer from the tanks it is necessary to use a crane and a truck. When it has reached the work platform, the tanks are put on a layer of sand, the space between individual tanks is 40 cm and 3" valves are installed parallel to facilitate the discharge of the acid mixture into the manifold. Behind the mixing tanks it is necessary to put a set of scaffolds, which will be used for the personnel that carries out the mixing. The water supply system is installed too.

To transfer chemicals and produce agitation, an air supply from a compressor with air at 125 psi and 100 ft³ / min flow rate is installed. The racking system is completed by installing pipes and hoses needed to direct the air to the air pump. Besides, the pump must be close enough to reach with a 1½" hose each of the barrels containing chemical additives and acids, that can be discharged with a hose to all tanks available for the stimulation of a given well. Likewise, the stirring system is complete when air can reach each of the tanks and every one of them can be shaken.

5.3.2 Preparation and mixing of chemicals

The addition totes and ammonium bifluoride bags are transported to the platform trucks, these are packed in specific locations on pallets to avoid ground contact. Similarly, hydrochloric acid is transported to transport tanks.

Before the start of mixing, the proper operation of the equipment, water supply line and mixing tanks is checked by a hydrostatic test. A mixture of primary acids (hydrochloric acid 15% more additives) and the main component (Sandstone acid 6%), is prepared according to formulations depending on the possible damage to the well. Then the manifold is ready to be installed or the flow diverted to the different tanks by means of flexible hoses and the pump.

5.3.3 Injection of treatment fluids

Injection of treatment fluids is the most important process in chemical stimulation and involves a sequential way of cooling, pre-flow injection, main injection of fluid (MUD Acid) and displacement.

Initially, gaskets, screw connections and the operation of each component of the injection circuit are checked. One of the outlets of the main pump manifold is fed with the acid mixture. When ready to

pump, operation of the opening valve starts from the first tank and keeping valves on other tanks closed so that the mixture is downloaded from each of the tanks to the manifold and pumped into the well. The injection is a continuous process lasting from 20 to 23 hours, depending on the progress of the operation. Each of the activities included in the sequential injection process has a specific function, as described below:

- Pre-flow displaces formation water out of the rock matrix to create a potential environment for the reaction of the main mixture (HCl-HF) and is directed specifically to damage treatment without the risk of precipitate formation.
- The main fluid is used to restore the permeability of the damaged area. Permeability damage may occur from drilling, cementing, and/or a critical matrix formed by fluid invasion causing saturation changes or solid migration.
- The primary fluid has the capacity to dissolve all the minerals that are soluble in 15% HCl. Moreover, it will dissolve all siliceous material such as bentonite, clays and other minerals. Chlorides of calcium, magnesium, sodium and potassium brines react with HF to form insoluble precipitates.
- The displacement flow objectives are to move the main acid (mud acid) into the formation to displace the reaction products out of the critical rock matrix, maintaining the pH of spent acid as low as possible, because some of the acid reaction products may form insoluble precipitates as the pH is increased. Therefore, it is always advisable keep the pH of the reaction products low.

5.3.4 Rest or warm up

HCl with ammonium bifluoride reacts completely with sludge, cuts and minerals. When thermal degradation is applied: the additives are completely degraded by the effect of temperature; which reaches about 200°C. Producing wells are opened from 1 to 2 months after injection in order for the fluids to degrade with temperature.

5.3.5 Measurements of steam flow (Discharge steam to atmosphere)

When the measured temperature is higher than 200°C, it is necessary to take measurements during the discharge test usually with the lip pressure methodology.

The variables that are monitored are:

- Wellhead pressure
- Lip pressure
- Gas concentrations

5.3.6 Measurements of water flow (injection of waste water)

When the measured temperature is higher than 200°C during a steam flow measurement, it is necessary to make measurements during the discharge test usually with the lip pressure methodology. The following variables are monitored:

- Water flow in weir box
- Temperature of water
- pH

6. POSSIBLE ENVIRONMENTAL IMPACTS OR EFFECTS DURING PRODUCTION TESTS AND STIMULATION

This section provides an assessment of potential direct environmental effects of a production test (lip pressure and TFT) and stimulation with matrix acidification. Direct environmental effects include potential impacts to air quality, water quality, induced seismicity, and other impacts.

6.1 Specific interaction matrix and identification of possible impacts

This section consists of linking the interaction of each project activity (described in chapter 5) to environmental factors, so that, a relationship between the two is established. This allows positive or negative potential environmental impacts of an activity to be identified, generating a specific interaction matrix for each of the activities analysed (Tables 3-5):

For lip pressure there are 1 positive impacts and 9 negative impacts (Table 3); for TFT 9 negative impacts and 1 positive impact (Table 4); and for stimulation there are 11 negative and 1 positive impacts (Table 5). More detail about matrix interaction is shown in Appendix I. These impacts were evaluated using the Rapid Impact Assessment Method (RIAM).

TABLE 3: Identification of possible impacts for lip pressure

Environmental factors	Results			Possible potential impacts
	+	0	-	
Geology and site stability risk	0	3	1	Microseismicity
Soil quality	0	3	1	Soil pollution
Water quality	0	3	1	Water pollution
Noise	0	2	2	Noise
Air quality. Chemical (odours and gases)	0	3	1	Air pollution
Vegetation cover	0	3	1	Effects on flora
Local traffic	0	3	1	Traffic accidents
Tourism	0	3	1	Effects on tourism
Effective visibility	0	3	1	Change in landscape
Employment	1	3	0	Employment creation

TABLE 4: Identification of possible impacts for tracer flow test

Environmental factors	Results			Possible potential impacts
	+	0	-	
Geology and site stability risk	0	2	1	Microseismicity
Soil quality	0	1	2	Soil pollution
Water quality	0	1	2	Water pollution
Noise	0	1	2	Noise
Air quality Chemical (odours and gases)	0	2	1	Air pollution
Vegetation cover	0	2	1	Effects on flora
Local traffic	0	2	1	Traffic accidents
Tourism	0	2	1	Effects on tourism
Effective visibility	0	2	1	Change in landscape
Employment	1	2	0	Employment creation

TABLE 5: Identification of possible impacts for matrix acidizing

Environmental factors	Results			Possible potential impacts
	+	0	-	
Geology and site stability risk	0	5	1	Microseismicity
Soil quality	0	2	4	Soil pollution
Water amount	0	4	2	Water supply
Water quality	0	1	5	Water pollution
Noise	0	2	4	Noise
Air quality Chemical (odours and gases)	0	3	3	Atmospheric pollution
Vegetation cover	0	3	3	Effects on flora
Wild life	0	5	1	Disturbance of wildlife
Local traffic	0	5	1	Traffic accidents
Tourism	0	5	1	Affectation tourist
Effective visibility	0	5	1	Change landscape
Employment	4	0	2	Employment generation

6.2 Description of possible impacts

6.2.1 Air pollution (chemicals)

During well tests (lip pressure and TFT) some gases such as H₂S, CO₂ and CH₄ contained in the steam are emitted to the atmosphere. The steam composition from well HE-58 during a lip pressure method test of approximately 35 days duration with an average flow 10.81 kg/s, a total steam discharge of 31,840 tons, is shown in Table 6. The behaviour of these in the atmosphere depends on several factors such as the meteorological conditions at the site where discharge is made.

TABLE 6: Amount of gases discharged during production test of well HE-58

Name of gas	Average concentration (ppm)	Average emission (g/s)	Accumulated quantity discharged (ton)
Carbon dioxide (CO ₂)	2944.8	31.1	93.8
Hydrogen sulphide (H ₂ S)	822.6	8.7	26.2
Nitrogen (N ₂)	83.7	0.884	2.7
Hydrogen (H ₂)	24.8	0.262	0.789
Methane (CH ₄)	3.4	0.036	0.108
Oxygen (O ₂)	2.1	0.022	0.067
Argon (Ar)	0.5	0.005	0.016

If a TFT discharge test is applied it is necessary to know the amount of SF₆ (greenhouse gas and its global warming potential is 23900 with respect to CO₂ according to UNFCCC (1995)) discharge to the atmosphere. A flow of 0.005 l/s was injected for 60 min 0.1 l/min at 5% total amount discharge to the atmosphere therefore 0.3 l per TFT measurement. If four TFT measurements are made during a flow test the total SF₆ discharged is about 1.2 l or 943.2 g (equivalent to 22.5 ton CO₂). If a well has been stimulated through the matrix acidizing procedure it is necessary to take into account the possible sub-products resulting from the operational use of HCl, HF, additives.

According to an environmental study, the estimated annual emissions for Hellisheidi power plant are 57,000 tons of CO₂, 11,000 tons of H₂S and 48 tons of CH₄. Compared to these values, the emissions from the discharge test for one month are 0.19% CO₂, 2.9 % H₂S and 2.7 % CH₄ of the total annual emissions from the Hellisheidi power plant.

One effect that is necessary to be considered is that of the weather conditions such as wind speed, direction and amount of precipitation, because it modifies the dispersion of chemicals in the air with the corresponding effect of increase or decrease in the concentration that is received by the receptor.

6.2.2 Water pollution

Water pollution generated can be any spillage during reinjection of wastewater resulting from test discharge. The most important potentially polluting chemicals in the liquid fraction are hydrogen sulphide (H_2S), arsenic (As), boron (B), mercury (Hg) and other heavy metals such as lead (Pb), cadmium (Cd), iron (Fe), zinc (Zn) and manganese (Mn). Lithium (Li), ammonia (NH_3), and aluminium (Al) are also found (Kristmannsdóttir and Ármannsson, 2003). In Table 7 the concentration of some substances in the geothermal water in the Hengill area and a calculated amount from a 35 day flow test of well HE-58 is shown. The arsenic concentration is above the limits in the Icelandic regulation and WHO regulations for drinking water, and the concentration of potassium is above that stipulated in the Icelandic regulation for drinking water only. The concentrations of other substances are below the limits. During the test at well HE-58 the amount of water discharged was 22,692.72 m³ (start date 11/16/2015 12:50 end 12/21/2015 10:00) and the maximum flow around 21.5 l/s compared with a total of 1,100 l/s (Reykjavik Energy, 2005) estimated for the Hellisheidi power plant or 1.95% of the total amount of water injected.

TABLE 7: Water chemical concentration in the Hengill area (Reykjavik Energy, 2015) with a calculated amount from a 35 day flow test of HE-58

Substance	Average concentration (mg/L)	Accumulated Quantity (kg)
Sodium (Na)	160	3630.8352
Potassium (K)	26.8	608.1649
Fluoride (F ⁻)	0.98	22.2389
Boron (B)	0.917	20.8092
Arsenic (As)	0.074	1.6793
Lead (Pb)	0.00369	0.0837
Copper (Cu)	0.00134	0.0304
Barium (Ba)	0.00066	0.0150
Nickel (Ni)	0.00022	0.0050
Cadmium (Cd)	0.0001	0.0023
Chromium (Cr)	0.00006	0.0014
Mercury (Hg)	0.00001	0.0002

During flow tests the impacts of water discharge on water quality of surface and groundwater in the shallow aquifers during production and normal injection were investigated. The fluid from the power plant is, on the other hand, injected into the geothermal reservoir, which is not connected to the groundwater system. However, the local water quality could deteriorate if system failures occur. Accidental spills of liquid geothermal surface drainage could take place if released due to escapes during drilling. Leaking pipes or wellheads, and overflowing sinks can be problems, but the biggest concern is the protection of public drinking water supplies (Noorollahi, 2005). Injection and mixing may cause some leakage of substances used in the process (HCl and ammonium bifluoride).

During flow tests, occasional TFT measurements are commonly performed, usually at different wellhead pressures. Each TFT measurement takes approximately 60 minutes and 30 g/m of KF are used. The total discharge is therefore 1800 g per TFT measurement. If four TFT measurements are carried out during a flow test the total KF discharged is about 7.2 kg.

6.2.3 Soil pollution

Contamination of the ground could be due to spills to faults in the injection system when downloading, and water injection tests (LP and TFT) are carried out during production. In an acid stimulation, tanks where acids or spillage use substances for the formulation are stored, could leak.

6.2.4 Noise

The noise during production tests (LP and TFT) is from monitoring wells connected to the plant system. Noise exposure is small because the duration of the tests is short and the noise generated by the equipment is muffled. However, if wells are discharged for the first time the noise generated can exceed 120 dB if they are not silenced, but if the system is silenced the noise generated can be about 90 dB (Kristmannsdóttir and Ármannsson 2003). These noise levels are generated in the vicinity of the operations. Therefore, it is important that the workers use hearing protection. During stimulation, maximum noise is experienced at the time of injection of fluids and can reach 90 dB, so that hearing protection is required.

6.2.5 Occupational risks

During well discharge tests (TFT and LP) personnel is exposed to certain risks such as burns, inhalation of gases (H_2S), falls and exposure to high noise levels. During acid stimulation, staff may be exposed to harmful substances (HCl, ammonium bifluoride and additives) due to injection and mixing

6.2.6 Traffic accidents

During the test stage of production, transport of pipes, valves and measuring equipment is needed. In the case of Hellisheidi the equipment is transported by a road in good conditions.

In the case of acid stimulations, the impact may be more significant to traffic due to pumping and injection equipment that has to be moved by cranes and trucks. Tanks and substances used in the process of mixing (HCl, ammonium bifluoride and additives) are also transported and therefore special care should be taken, as appropriate permissions for handling and use are needed. The proximity to villages, schools, power lines, routes used by the population etc. should also be taken into account because of possible damages.

6.2.7 Microseismicity

Separated water (geothermal water) and condensate need to be reinjected to protect surface and ground water, and for a good utilization of the geothermal reservoir (Reykjavik Energy, 2015). During 2011 microseismicity was observed in the Hellisheidi area, about 40 earthquakes over 2.5 ML and 8 between ML 3 and 4, (Thorsteinsson, 2016). That year the total amount of disposal water injected was around 1.8 million tons per month as a result of separated water via overflow and the disposal at Gráuhnúkar, Húsmúli areas. Wells HE-13 and HE-40 receive effluent from the Hellisheidi Power Plant.

The work procedure for a large scale reinjection and a temporary shutdown, or when significant changes are made in the reinjection, was revised. In the procedure the pumping increases in stages with lag times in between. The result of this is very little seismic activity during changes of flow in the reinjection wells. In September 2016 a large seismic event took place at the Húsmúli reinjection site. This was not connected to any changes in the reinjection procedure and has to be studied further.

The average flow from HE-58 was 11.6 l/s (Appendix 2) or 30,000 tons of water per month, less than 1% of the total annual amount of water injected during all field operations, so it is not expected to significantly affect the environment.

6.2.8 Effects on flora

During well tests, steam and spray can have an adverse effect on the local vegetation with trees and grass being scalded (Noorollahi, 2005). In the case of Hellisheidi the environment is not very sensitive to such effects since e.g. there is not a lot of vegetation in the vicinity of well HE-58. But analysing chemical stimulation depends on the sensitivity of the medium. To find out whether there can be a significant impact on the vegetation in some areas it is important to take into account whether these areas are near woods or other vegetated areas as there may be deposition of chemical substances on the vegetation.

6.2.9 Disturbance to wildlife

From the analysis of environmental parameters in wells HE-58 and HE-21 these are not considered to present a significant impact on the nature of the area. Analysis of matrix acidizing suggests that wildlife can especially be affected by noise, odours and transport of materials, and equipment.

6.2.10 Effects on tourism

Such impacts are especially harmful in geothermal areas that are much visited by tourists. These may be effected by unloading activities, especially by the use of paths. This impact has been listed as negative but in many tourists' opinion geothermal operations constitute a tourist attraction.

6.2.11 Water consumption

This impact has been considered by evaluation because of the sensitivity of the environment to water availability in the area of indirect influence and the amount of water that the project requires. In this case, acid stimulation is being considered and this impact will be evaluated depending on the sensitivity of the environment to water availability in the area, because a specific area for acidification is not under discussion, but this impact will be considered generally. The production test does not require much water, but for the stimulation it is necessary to use a significant amount of water. For example, it is necessary to use approximately 1000 m³ for matrix acidizing. This could impact consumption, depending on the characteristics of the aquifer and the time of year when the work is carried out, potentially reducing the availability of groundwater

6.2.12 Changes in landscape

When the steam plume is discharged to the atmosphere, a visual effect is created. Occasionally wells being tested are near vehicular access routes and may impair visibility or distract drivers on these roads.

6.3 Prioritization of impacts

In Section 6.1 the impacts of discharge tests (LP and TFT), and discharge test with stimulation (matrix acidizing) are identified. These impacts were subsequently grouped and described in Section 6.2. In this section, the impacts are prioritized by the RIAM method.

The RIAM method is based on the definition of important evaluation criteria and existing environmental considerations in the area where the project will be developed. This method provides a holistic research approach, classified as the environment for evaluation of four environmental components: physico-chemical, biological-ecological, socio-cultural and economic-operational (Arévalo, 2003).

The classification criteria are divided into two groups, A and B, these in turn are subdivided and classified as shown in Table 8.

TABLE 8: Classification criteria

Criterion	Value	Importance of condition
A1	4	Important to national/international interests
	3	Important to regional/national interests
	2	Important to areas immediately outside the local condition
	1	Important only to the local condition
	0	No importance
Criterion	Value	Magnitude of change/effect
A2	3	Major positive benefit
	2	Significant improvement in status quo
	1	Improvement in status quo
	0	No change/status quo
	-1	Negative change to status quo
	-2	Significant negative dis-benefit or change
	-3	Major disadvantage or change
Criterion	Value	Permanence
B1	1	No change/not applicable
	2	Temporary
	3	Permanent
Criterion	Value	Reversibility
B2	1	No change/not applicable
	2	Reversible
	3	Irreversible
Criterion	Value	Cumulative
B3	1	No change/not applicable
	2	Non-cumulative/single
	3	Cumulative/synergistic

Once the impact criteria have been qualified, the environmental scores are calculated (Equation 5).

$$\text{Score ES} = (A_1 \times A_2) \times (B_1 + B_2 + B_3) \quad (5)$$

In Table 9, the impact or effect is categorized according to the corresponding range.

TABLE 9: Significance level impacts

Environmental score (ES)	Range	Description
+72 at +108	+E	Major positive impacts
+36 at +71	+D	Significant positive impacts
+19 at +35	+C	Moderate positive impacts
+10 at +18	+B	Positive impacts
+1 to +9	+A	Lightly positive impacts
0	N	“status quo” or not applicable
-1 to 9	-A	Lightly negative impacts
-10 at -18	-B	Negative impacts
-19 at -35	-C	Moderate negative impacts
-36 at -71	-D	Significant negative impacts
-72 at +108	-E	Major negative impacts

The items in the following matrices have been assessed and quantified using the RIAM method. In Table 10, the impacts from the discharge test using lip pressure and evaluated for HE-58 in Hellisheidi are shown. For this activity 2 moderate negative impacts, 3 negative impacts, 4 lightly negative impacts and 1 positive impact are recorded. This activity was evaluated for a duration of approximately 35 days.

TABLE 10: Prioritization of impacts from discharge test using lip pressure

Environmental Impacts	RIAM					Score ES	Range RV
	A1	A2	B1	B2	B3		
Air pollution (Chemical)	2	-2	2	2	2	-24	-C
Noise	2	-2	2	2	2	-24	-C
Traffic accidents	2	-1	3	2	2	-14	-B
Water pollution	2	-1	2	2	2	-12	-B
Effects on flora	2	-1	2	2	2	-12	-B
Microseismicity	2	-1	2	2	1	-10	-A
Change landscape	2	-1	2	1	1	-8	-A
Effects on tourism	2	-1	2	1	1	-8	-A
Soil pollution	1	-1	2	2	2	-6	-A
Employment creation	3	1	2	1	1	12	+B

The impacts from the discharge test using tracer flow test, evaluated for HE-21 in the Hellisheidi are shown in Table 11. For this activity 2 moderate negative impacts, 3 negative impacts, 4 lightly negative impacts and 1 positive impacts are recorded. This activity was recorded for one day and well (HE-21) was connected to the power plant, but the evaluation method for this activity assumes a duration of approximately 35 days and the well is considered not to be connected to the power plant.

TABLE 11: Prioritization if impacts from discharge test using TFT

Environmental Impacts	RIAM					Score ES	Range RV
	A1	A2	B1	B2	B3		
Air pollution (Chemical)	2	-2	2	2	2	-24	-C
Noise	2	-2	2	2	2	-24	-C
Traffic accidents	2	-1	3	2	2	-14	-B
Water pollution	2	-1	2	2	2	-12	-B
Effects on flora	2	-1	2	2	2	-12	-B
Microseismicity	2	-1	2	2	1	-10	-B
Changes in landscape	2	-1	2	1	1	-8	-A
Effects on tourism	2	-1	2	1	1	-8	-A
Soil pollution	1	-1	2	2	2	-6	-A
Employment creation	3	1	2	1	1	12	+B

The impacts from the discharge test when the well is stimulated (matrix acidification) are shown in Table 12. The duration is assumed to be 2 weeks, and the location of the well that is evaluated is at a normal

TABLE 12: Prioritization of impacts discharge test with stimulation (matrix acidification)

Environmental Impacts	RIAM					Score ES	Range RV
	A1	A2	B1	B2	B3		
Air pollution (Chemical)	2	-2	2	2	2	-24	-C
Noise	2	-2	2	2	2	-24	-C
Water supply	2	-1	3	2	2	-14	-B
Water pollution	2	-1	3	2	2	-14	-B
Effects on flora	1	-2	3	2	2	-14	-B
Traffic accidents	1	-2	3	2	2	-14	-B
Soil pollution	1	-2	2	2	2	-12	-B
Microseismicity	2	-1	2	2	1	-10	-B
Changes in landscape	2	-1	2	1	1	-8	-A
Effects on tourism	2	-1	2	1	1	-8	-A
Employment creation	3	1	2	1	1	12	+B

location in the field. Two moderate negative impacts, 6 negative impacts, 2 lightly negative impacts and 1 positive impacts were obtained.

7. ENVIRONMENTAL AND OCCUPATIONAL SAFETY REGULATIONS

The most relevant regulations to establish a control level for environmental aspects include consideration of air and water quality.

7.1 Air quality

7.1.1 Environmental regulations

Hydrogen sulphide (H₂S) is the gas most people relate to geothermal fields and the utilization of geothermal energy. The levels of H₂S in the atmosphere in geothermal areas are commonly in the range from 0-0.5 ppm. Humans detect smell at very low concentrations (Gunnlaugsson et al., 2010).

In 2010, the Government of Iceland set a health limit in Iceland at 50 µg/m³ for a running 24-hour average. This regulation requires the geothermal industry in Iceland to lower H₂S emissions (Gunnarsson, et al., 2013).

The environmental regulations that can serve as a reference are the air concentration guidelines by the World Health Organisation (WHO) as well as an Icelandic regulation from 2010 on the atmospheric concentration of H₂S. Stricter rules than the WHO guidelines took effect in 2014 (Table 13).

Noise. Guidelines for community noise of the World Health Organization, (WHO, 1999); stipulate that the values have been set at 50 or 55 dBA, representing daytime levels below which the adult population will be protected from becoming moderately or seriously annoyed.

TABLE 13: Environmental guidelines for H₂S air concentration and emissions (Franco, 2010)

Guidelines/regulation	Averaging period	Level (µg/m ³)	Notes
WHO Air quality guidelines, 2nd Edition	30 min 24 hour	7 150	To avoid odour annoyance This guideline was obtained by dividing the threshold for eye irritation of 15,000 µg/m ³ by factor 100
2010 Icelandic regulation on atmospheric H ₂ S concentration	3 hours 24 hours 1 year	150 50 * 5	*Allowed instances of surpassing limit decreased from 5 to 3 times per year in 2014

7.1.2 Occupational safety regulations

Occupational safety guidelines and limits include the American Conference of Governmental Industrial Hygienists (ACGIH), the Occupational Safety and Health Administration (OSHA) and the National Institute for Occupational Safety and Health (NIOSH). These authorities consider different exposure limits, as described below in Table 14. They consider different times of exposure and the activity that is developed.

TABLE 14: Occupational safety guidelines and limits (OSHA, 2012a)

Sustance	Limits values	Agency
Hydrogen sulphide (H ₂ S)	1 ppm, 1.4 mg/m ³ TLV-TWA (8-hour) 5 ppm, 7.0 mg/m ³ TLV-STEL (15 min) 10 ppm, 15 mg/m ³ REL-C (10 min) 20 ppm PEL-C	ACGIH (2010) NIOSH (2005) OSHA (2012b)
Carbon dioxide (CO ₂)	5,000 ppm (9,000 mg/m ³) TLV-TWA 30,000 ppm (54,000 mg/m ³) TLV-STEL 5,000 ppm (9,000 mg/m ³) TWA 30,000 ppm (54,000 mg/m ³) REL-STEL 5,000 ppm (9,000 mg/m ³) PEL-TWA	ACGIH (2001) NIOSH (1978a) OSHA (2012c)
Hydrogen chloride (HCl)	2 ppm (3 mg/m ³) A4 TLV-C 5 ppm (7 mg/m ³) PEL-C 5ppm (7 mg/m ³) C	ACGIH (2003) NIOSH (1978b) OSHA (2012d)
Hydrogen fluoride (HF)	0.5 ppm TWA-TLV 2 ppm TLV-C 3 ppm (2.5 mg/m ³) TWA-REL 6 ppm (5 mg/m ³) (15 minutes) REL-C 3 ppm (2 mg/m ³) TWA-PEL	ACGIH (2005a) NIOSH (1978c) OSHA (2012e)
Sulphur hexafluoride (SF ₆)	1000 ppm TWA-PEL 1000 ppm TWA-REL 1000 ppm PEL	ACGIH (2005b) NIOSH (1978d) OSHA (2012f)

PEL: Permissible Exposure Limits, are regulatory limits on the amount or concentrations of a substance in the air, and they are enforceable.

REL-C: Recommended Exposure Levels-Ceiling: the concentration that should not be exceeded during any part of the working exposure.

STEL: Short Term Exposure Limit: the concentration to which it is believed that workers can be exposed to continuously for a short period of time without suffering from irritation, chronic or irreversible tissue damage, or narcosis.

TVL: Threshold Limit Values are defined as an exposure limit to which it is believed nearly all workers can be exposed day after day for a working lifetime without ill effect,

TWA: Time Weighted Average, the time weighted average concentration for a conventional 8-hour workday and a 40-hour workweek, to which it is believed that nearly all workers, may be repeatedly exposed, day after day, without adverse effect.

Noise. Under OSHA standards, workers are not permitted to be exposed to an 8-hour TWA equal to or greater than 90 dBA. OSHA uses a 5-dBA exchange rate, meaning the noise level doubles with each additional 5 dBA. In Table 15 it is shown for how long time workers are permitted to be exposed to specific noise levels (OSHA, 2016).

TABLE 15: Extended work shifts and action level reduction

Permissible duration (hours per day)	Sound level (dBA, slow response)
16	85
8	90
4	95
2	100
1 ½	102
1	105
½	110
¼ or less	115

7.2 Water quality

For the water quality the guidelines for drinking water quality from WHO (2011) shown in Table 16 have been used. The components listed are expected to be present in geothermal fluids, knowing that this will be related to the reservoir composition, so that the reference will need to be consulted for different components.

7.2.1 Environmental regulations

TABLE 16: Chemical composition of geothermal water in Hellisheidi and guidelines for drinking water quality, 4th edition. WHO (2011)

Substance	Average concentration (mg/L)	Limits WHO	Iceland regulation 1995
Sodium (Na)	160	50	200
Potassium (K)	26.8	N.E	12
Fluoride (F ⁻)	0.98	1.5	1.5
Boron (B)	0.917	2.4	1000
Arsenic (As)	0.074	0.01 (AT)	0.01
Lead (Pb)	0.00369	0.01 (A, T)	0.01
Copper (Cu)	0.00134	2	2
Barium (Ba)	0.00066	0.7	0.7
Nickel (Ni)	0.00022	0.07	0.02
Cadmium (Cd)	0.0001	0.003	0.005
Chromium(Cr)	0.00006	0.05 (P)	0.05
Mercury (Hg)	0.00001	0.006	0.001

NB: A, provisional guideline value as calculated guideline value is below the achievable quantification.

T, provisional guideline value because the calculated guideline value is below the possible level, which can be quantified.

N.E, occurs in drinking-water at concentrations well below those of health concern

8. ENVIRONMENTAL AND OCCUPATIONAL SECURITY CONSIDERATIONS

The most important possible environmental impacts according to the prioritization of impacts are shown in Section 6.4 using lip pressure and TFT methodology for the discharge test and stimulation with matrix acidification. The possible impacts and some considerations grouped according to their environmental effect are selected and shown in

17.

A protocol with guidelines to be followed should be prepared in the development of activities, whose general features take into account the possible impacts set forth below:

8.1 Considerations for atmosphere pollution and noise

8.1.1 Use of a muffler

A silencer to be used during discharge or production tests should be installed. The equipment also separates liquid and vapour. The liquid phase is directed to a landfill where temperature and flow measurements are performed during production tests and the vapour phase ascends through the silencer where it produces a controlled discharge into the atmosphere. This separator allows isenthalpic expansion and reduces the fluid pressure, which attenuates the noise levels at the source and thus reduces the impact on the environment.

TABLE 17: Environmental and occupational security for impacts

Environmental impacts or effects	Environmental and occupational security considerations
Atmospheric pollution	1. Designing and planning a monitoring and control system 2. Mitigation of H ₂ S emissions 3. Use of personal protective equipment (PPE)
Noise	1. Designing and planning a monitoring system 2. Use of a muffler 3. Use of PPE
Water and soil pollution	1. Check of equipment and leakage control 2. Containment barriers
Effects on flora	1. Designing and planning a monitoring and control system 2. Compensation for effects
Water supply	1. Compensation for water consumption can be a social approach or reforestation
Microseismicity	1. Designing and planning a monitoring and control system for injection
Traffic accidents	1. Warning signs and special routes

8.1.2 Mitigating H₂S emissions

Injection using 50% NaOH will be on a stoichiometric scale that allows for the absorption of 80% of the H₂S in the vapour discharged to the atmosphere. The injection system will be known as a "scrubber" and consists of the following components: a diaphragm pump, a 1 m³ tank for storing NaOH and an injection nozzle connected to the expansion nozzle muffler.

This system can be applied during a discharge test (LP and TFT) and with the well stimulated.

8.1.3 Designing and planning a monitoring system

For designing and planning a monitoring system the next steps are the following:

1. The components to be monitored are shown in Table 18, where the relation of different components to the planned activity is shown, the matrix acidification is the activity with most chemical components used. It is important to define locations measurement of the components shown in Table 18. These sites can be classified as emission sources or receivers.

TABLE 18: Identification of components for monitoring

Components monitored	LP	TFT	Matrix acidification
Hydrogen sulphide (H ₂ S)	X	X	X
Carbon dioxide (CO ₂)	X	X	X
Noise	X	X	X
Hydrogen chloride (HCl)			X
Hydrogen fluoride (HF)			X

2. Characterization of the receptor environment and other possible sources of emission. For this the knowledge of certain variables such as other possible natural emission sources (fumaroles, power station), topographic conditions (elevation place activity, elevation where there is a possible receptor such as communities), weather (wind speed, direction and precipitations) and other characteristics such as the state of vegetation etc. is necessary.

3. Baseline monitoring: The concentrations of different gases present in the area before the activity is developed have to be known, so that an environmental baseline can be established. The components to be monitored have to be those in Table 18. Monitoring takes place at the point of baseline establishment.
4. Process for monitoring - discharge test: Once the discharge of the well has started it will be necessary to monitor the concentrations of each component. The components monitored will be the same and from the same location that were determined for the base line for the method used depending of the activity, commonly H₂S and noise.
5. Injection and mixing monitoring (for stimulation only): For the injection and mixing, it is necessary to monitor for occupational security. In this case, the control level the health of workers should be accounted for, and the most important components to monitor are: noise, HCl, and HF.

For monitoring process the following is required to have in mind:

1. Equipment for monitoring: The equipment below is used in LaGeo El Salvador for monitoring during discharge test: for noise soundProud DL I/3, for CO₂ AIQ Surveyor II and for short time H₂S monitoring Jerome 631 and Jerome j605, for long time monitoring ODA log low range an H₂S logger. For more detail see Appendix III.
2. Control levels: A system of control levels needs to be established and these may differ according to the H₂S concentration needed to activate the alarm system. In the ACGIH it is 1 ppm, but this level may be increased.

8.1.4 Use of personal protective equipment (PPE)

For exposure to gas the workers need use a mask and to HCl a mask and protective clothing. Protection against noise is also necessary.

8.2 Considerations for water and soil pollution

8.2.1 Check of equipment and leakage control

When LP or TFT is operating it is necessary to check if the storage tanks are properly prepared to receive all geothermal water that later will be reinjected. This includes a check that there is no structural damage that can produce a leakage. The reinjection system has to be checked to verify that there is no risk of water contamination. Storage tanks for temporary storage shall be constantly checked during any test to prevent that the level goes above 90% of tank capacity. If this level is reached the test has to be stopped.

Prior to well opening it is necessary to check whether there is any leakage in storage tanks and all the components of the piping system that discharge all the chemicals that will be injected for the stimulation. The storage tanks have to be located above a uniform surface to prevent any damage to them.

8.2.2 Designing and planning a monitoring and control system

If there is any suspicion of aquifer contamination with reinjection water during or after well testing, analysis for the suspected contaminating components, principally components identified in Table 16 is suggested, followed by actions to be taken in case of contamination.

Negative impacts to surface water may be avoided by introducing strict discharge criteria and appropriate means to bring water quality and temperature to acceptable standards.

For matrix stimulation it is necessary to manage the concentration of HCl, and other chemicals used especially with regard to storage and transportation, using protective barriers to contain possible spills.

8.3 Considerations for effects on flora

Prior to any activity, the surrounding vegetation has to be identified to establish a baseline, and after that it will be necessary to monitor to find out if there has been any change in vegetation that could be caused by well testing. If the results of the monitoring show that vegetation has been affected by the test it will be necessary to implement a compensation plan for the effects in line with the national regulations.

8.4 Considerations for water supply

After the test it will be necessary to quantify how much water has been used during the test, and if it has been a significant quantity that can affect the surroundings. This will need to be compensated for through reforestation or rain collection and infiltration.

8.5 Considerations of microseismicity

Considering that seismicity can be induced by reinjection, this has to be monitored during a test and if seismic activity starts on a scale between 2 and 3 (Richter scale) it will be necessary to set an alarm. If the quakes observed are between 3 and 4 the reinjection has to be reduced to a level of seismicity previously observed. If the seismicity is greater 4 the test has to be stopped immediately.

8.6 Considerations for traffic accidents, prevention signs and special routes

To prevent any accident on the platform, the “weir-box”, the muffler area or the route, it will be necessary to place the correct signs that inform occupants, visitors or neighbours about the risks or equipment in use.

9. CONCLUSIONS

The most important impacts identified for the three activities (LP, TFT and Matrix Acidification) were air and noise pollution. Monitoring is especially important for air quality because it is essential to keep such activities under control and not exceed either environmental or occupational limits.

According to the environmental evaluation, a well discharge that has been stimulated requires special attention to the chemicals that are injected. Because the products of the stimulation are unknown, unlike those from unstimulated wells, several components have to be monitored. Characterization of the emissions are recommended due to their possible effects on the environment but depending on the sensitivity of the environment, where they are emitted, they may present a different degree of importance or magnitude from an environmental point of view, for example considering activities that take place near inhabited areas. It is recommended to strengthen the relationship with the communities through various actions in order to build trust, commitment and collaboration from the communities when such activities are performed.

Simulation using a dispersion model for all wells and for each chemical species identified for a discharge test using software such as AERMOD or CALLPUFF is recommended because it can help in places where no information is available.

Impacts that initially were believed to be significant such as water consumption and pollution and seismicity were found to be insignificant because the quantity of water injected during well testing is less than 1% of the quantity of water injected by the power plant. Nonetheless, the effects of reinjection on seismicity and groundwater quality should be monitored to be able to prevent any impact.

ACKNOWLEDGEMENTS

I express my sincere gratitude to my employer, LaGeo S.A. de C.V and United Nations University Geothermal Training Programme for giving me the opportunity to participate in the six months training in Iceland, especially to Rosa Escobar, Luis Franco, Ana Silvia Arévalo and Jorge Castillo for believing in my abilities and help in the process. My sincere gratitude to the UNU-GTP staff: Mr. Lúdvík S. Georgsson, Mr. Markús, A. G. Wilde, Ms. Thórhildur Ísberg, Mr. Ingimar G. Haraldsson and Ms. Málfríður Ómarsdóttir for your help and support during my stay in Iceland. I want to give special thanks to my supervisors, Mr. Halldór Ármannsson and Einar Gunnlaugsson, for their support and guidance while working on this geothermal report.

I thank my colleagues in LaGeo for advice and technical support staff and especially Luis Franco, Luz Barrios and my colleagues in the environmental field.

And of course I thank God and my family, especially my dears sisters for always being aware of me at all times, and my boyfriend, for their unconditional support during my stay, both in my project work and for giving me their recommendations and advice.

REFERENCES

ACGIH, 2001: *Documentation of the Threshold Limit Values (TLVs) and Biological Exposure Indices (BEIs) - carbon dioxide*. American Conference of Governmental Industrial, ACGIH.

ACGIH, 2003: *Documentation of the Threshold Limit Values (TLVs) and Biological Exposure Indices (BEIs) - hydrogen chloride*. American Conference of Governmental Industrial Hygienists, ACGIH.

ACGIH, 2005a: *Documentation of the Threshold Limit Values (TLVs) and Biological Exposure Indices (BEIs) - hydrogen fluoride*. American Conference of Governmental Industrial Hygienists, ACGIH

ACGIH, 2005b: *Threshold Limit Value (TLV), sulphur hexafluoride*. American Conference of Governmental Industrial Hygienists, ACGIH.

ACGIH, 2010: *Threshold Limit Value (TLV); Hygienists - hydrogen sulphide*. American Conference of Governmental Industrial, ACGIH.

Arévalo, A.S., 2003: Rapid environmental assessment tool for the extended Berlin geothermal field project. *Proceedings of the International Geothermal Conference IGC-2003 "Multiple Integrated Uses of Geothermal Resources"*, Reykjavik, Session 12, 81-87.

Arévalo, A.S, and Padilla, E.K., 2008: An innovative environmental impact assessment applied to the Chinameca deep exploration project. *30th Anniversary Workshop*, UNU-GTP, Iceland, <http://www.unugtp.is>.

Axelsson, G., 2013: Geothermal well testing. *Presented at "Short Course V on Conceptual Modelling of Geothermal Systems"*, organized by UNU-GTP and LaGeo, Santa Tecla, El Salvador, 30 pp.

Axelsson G. and Franzson H., 2012: Geothermal drilling targets and well siting. *Presented at "Short Course on Geothermal Development and Geothermal Wells"*, organized by UNU-GTP and LaGeo, Santa Tecla, El Salvador, 16 pp.

Earlougher, R.C., Jr. 1977: *Advances in well test analysis*. SPE, New York, Dallas.

Elmi, H.D., 2008: *Geothermal resource assessment through well testing and production response modelling*. University of Iceland, MSc Thesis, UNU-GTP, Iceland, report 1, 73 pp.

Flores, M., Davies D., Couples, G., and Pálsson, B., 2005: Stimulation of geothermal wells, can we afford it? *Proceedings of the World Geothermal Congress 2005, Antalya, Turkey*, 8 pp.

Franco, L.A., 2010: Hydrogen sulphide abatement during discharge of geothermal steam from well pads: A case study of well pad TR-18, El Salvador. Report 13 in: *Geothermal training in Iceland 2010*. UNU-GTP, Iceland, 183-212.

Galindo, A.V., 2015: *Acid and hydraulic stimulation in geothermal wells*. National Autonomous University of Mexico, Mexico, 107 pp.

Grant, M.A., Donaldson, I.G., and Bixley, P.F., 1982: *Geothermal reservoir engineering*. Academic Press Ltd., New York, 369 pp.

Gunnarsson, I., Aradóttir, E.S., Sigfússon, B., Gunnlaugsson, E., Júlíusson, B.M., 2013: Geothermal gas emission from Hellisheidi and Nesjavellir power plants, Iceland. *Geothermal Resources Council, Transactions*, 37, 785-789 pp

Gunnlaugsson, E., 2012: The Hellisheidi geothermal project. Financial aspects of geothermal development. Presented at "Short Course on Geothermal Development and Geothermal Wells", organized by UNU-GTP and LaGeo, Santa Tecla, El Salvador, 9 pp, UNU-GTP SC-14, 9 pp.

Gunnlaugsson, E., Leifsson, H., Hrólfsón, I., and Geirsson, S.B., 2010: Environmental issues related to the building of new power plants in the Hengill area. *Proceedings of the World Geothermal Congress 2010, Bali, Indonesia*, 5 pp.

James, R., 1962: Steam-water critical flow through pipes. *Inst. Mech. Engrs. Proc.*, 176, 741-745.

Kristmannsdóttir, H., and Ármannsson, H., 2003: Environmental aspects of geothermal energy utilization. *Geothermics*, 32, 451-461.

Lovelock, B.G., 2001: Steam flow measurement using alcohol tracers, *Geothermics*, 30, 641-654.

Muffler, P., and Cataldi, R., 1978: Methods for regional assessment of geothermal resources. *Geothermics*, 7, 53-89.

NIOSH 1978a: *Occupational Health Guideline for Carbon Dioxide*. National Institute for Occupational Safety and Health, NIOSH, U.S. Department, NIOSH, 4 pp.

NIOSH 1978b: *Occupational health guideline for hydrogen chloride*. National Institute for Occupational Safety and Health, NIOSH, U.S. Department, NIOSH, 5 pp.

NIOSH 1978c: *Occupational health guideline for hydrogen fluoride*. National Institute for Occupational Safety and Health NIOSH, U.S. Department, 6 pp.

NIOSH 1978d: *Recommended Exposure Limit (REL) - sulphur hexafluoride*. National Institute for Occupational Safety and Health, NIOSH, U.S. Department, NIOSH.

NIOSH 2005: *Immediately dangerous to life or health concentration (IDLH) - hydrogen sulphide*. National Institute for Occupational Safety and Health, NIOSH, U.S. Department, website: <http://www.cdc.gov/niosh/topics/chemical.html>

Noorollahi, Y., 2005: *Application of GIS and remote sensing in exploration and environmental management of Námafjall area, N-Iceland*. University of Iceland, MSc thesis, UNU-GTP, Iceland, report 1, 124 pp.

OSHA, 2012a: *Chemical sampling information*. US Department of Labor, Occupational Safety and Health Administration - OSHA, website: www.osha.gov/dts/chemicalsampling/toc/chmn_C.html

OSHA, 2012b: *Permissible Exposure Limit (PEL): general industry: 29 CFR 1910.1000, Table Z-2-hydrogen sulphide*, US Department of Labor, Occupational Safety and Health Administration, OSHA, website: www.osha.gov/dts/chemicalsampling/data/CH_246800.html.

OSHA, 2012c: *Permissible Exposure Limit (PEL), general industry 29 CFR 1910.1000 Table Z-1-carbon dioxide*. US Department of Labor, Occupational Safety and Health Administration, OSHA, website: www.osha.gov/dts/chemicalsampling/data/CH_225400.html.

OSHA, 2012d: *Permissible Exposure Limit (PEL) - general industry, 29 CFR 1910.1000 Table Z-1 - hydrogen chloride*. US Department of Labor, Occupational Safety and Health Administration, OSHA, website: www.osha.gov/dts/chemicalsampling/data/CH_246300.html.

OSHA, 2012e: *Permissible Exposure Limit (PEL) - general industry, 29 CFR 1910.1000 Table Z-2-hydrogen fluoride*. US Department of Labor, Occupational Safety and Health Administration, OSHA, website: www.osha.gov/dts/chemicalsampling/data/CH_246500.html.

OSHA, 2012f: *Permissible Exposure Limit (PEL) general industry - sulphur hexafluoride*. US Department of Labor, Occupational Safety and Health Administration, OSHA, website: www.osha.gov/dts/chemicalsampling/data/CH_268600.html.

OSHA, 2016: *OSHA technical manual, section III: Chapter 5*. US Department of Labor, Occupational Safety and Health Administration - OSHA, website: www.osha.gov/dts/osta/otm/new_noise/index.html

Reykjavik Energy, 2005: *Environmental impact assessment extension of Hellisheidi*. Reykjavik Energy, Reykjavík, report, 162 pp.

Reykjavik Energy 2015: *Environmental report 2015*. Reykjavik Energy, Reykjavík, report, website: www.or.is/sites/or.is/files/or_environmental_report_2015.pdf

Steingrímsson, B, 2016: *Discharge measurement and injection tests*. UNU-GTP, Iceland, unpublished lecture notes, 64 pp.

Thorsteinsson, H., 2016: *Reinjection and induced seismicity. Paper presented at the International Geothermal Conference IGC2016, Reykjavík*, 15 pp.

UNFCCC, 1995: *The science of climate change*. UNFCCC, Contribution of working group to the 2nd assessment report of the intergovernmental panel on climate change, report 1, 588 pp.

WHO, 1999: *Guidelines for community noise*. World Health Organization, Geneva, 140 pp.

WHO, 2011: *Guidelines for drinking-water quality* (4th ed.). World Health Organization, Geneva, 564 pp.

APPENDIX I: Matrix interactions

<div><div>1</div>Positive environmental impacts</div> <div><div>-6</div>Negative environmental impacts</div>		ACTIVITIES				TOTAL			
		Production test (Lip Pressure)							
		1.1Transportation of equipment and conditioning	1.2.Installation Equipment Measurements	1.3.Measurements of steam flow (Discharge steam to at	1.4.Measurements of water flow (Injection waste water)	Frequency of positive impacts by factors	Frequency of negative impacts by actions	Indifferent frequency impacts factors	
ENVIRONMENTAL COMPONENTS		ENVIRONMENTAL FACTORS							
PHISYCAL-CHEMICAL	LAND- GEOLOGY	Land use	0	0	0	0	0	0	4
		Organic soil	0	0	0	0	0	0	4
		Drains	0	0	0	0	0	0	4
		Soil permeability	0	0	0	0	0	0	4
		Geology and site stability risk	0	0	0	-8	0	1	3
		Subsidence and disturbance	0	0	0	0	0	0	4
	WATER	soil quality	0	0	0	-9	0	1	3
		Water amount	0	0	0	0	0	0	4
		Water quality	0	0	0	-10	0	1	3
AIR	Air quality Physica (Noise)	-1	0	-3	0	0	2	2	
	Air quality Chemical (odors and gases)	0	0	-4	0	0	1	3	
BIOLOGICAL-ECOLOGICAL	FLORA	Vegetal cover	0	0	0	-11	0	1	3
	FAUNA	Wild life	0	0	0	0	0	0	4
		Habitats	0	0	0	0	0	0	4
SOCIAL - CULTURAL	POPULATION	Local traffic	-2	0	0	0	0	1	3
		Quality life	0	0	0	0	0	0	4
		Tourist	0	0	-5	0	0	1	3
	LANSCAPE	Effective visibility	0	0	-6	0	0	1	3
ECONOMIC - OPERATIONAL	ECONOMY	Local economy	0	0	0	0	0	0	4
		National economy	0	0	0	0	0	0	4
		Employment	0	0	7	0	1	0	3
		Taxes	0	0	0	0	0	0	0
TOTAL	Frequency of positive impacts by actions		1	1	1	1	1		
	Frequency of negative impacts by actions		2	1	3	4		10	
	Indifferent frequency impacts actions		18	19	17	16			73

FIGURE 1: Matrix interactions for lip pressure

			<div> <div>1</div> Positive environmental impacts </div> <div> <div>-6</div> Negative environmental impacts </div>								
			ACTIVITIES			TOTAL					
			Production test (TFT)								
			2.1Transportation of equipment and conditioning	2.2 Injection tracers (SF6 and KF)	2.3 Sampling (steam and water)	Frequency of positive impacts by factors	Frequency of negative impacts by actions				
ENVIRONMENTAL COMPONENTS			ENVIRONMENTAL FACTORS								
PHYSICAL-CHEMICAL	LAND- GEOLOGY	Land use	0	0	0	0	0	0	3		
		Organic soil	0	0	0	0	0	0	3		
		Drains	0	0	0	0	0	0	3		
		Soil permeability	0	0	0	0	0	0	3		
		Geology and site stability risk	0	0	-6	0	1	2			
		Subsidence and disturbance	0	0	0	0	0	0	3		
	WATER	soil quality	0	-3	-7	0	2	1			
		Water amount	0	0	0	0	0	3			
		Water quality	0	-4	-8	0	2	1			
	AIR	Air quality Physical (Noise)	-1	0	-9	0	2	1			
		Air quality Chemical (odors and gases)	0	0	-10	0	1	2			
BIOLOGICAL- ECOLOGICAL	FLORA	Vegetal cover	0	0	-11	0	1	2			
	FAUNA	Wild life	0	0	0	0	0	3			
		Habitats	0	0	0	0	0	3			
SOCIAL - CULTURAL	POPULATION	Local traffic	-2	0	0	0	1	2			
		Quality life	0	0	0	0	0	3			
		Tourist	0	0	-12	0	1	2			
	LANDSCAPE	Effective visibility	0	0	-13	0	1	2			
ECONOMIC - OPERATIONAL	ECONOMY	Local economy	0	0	0	0	0	3			
		National economy	0	0	0	0	0	3			
		Employment	0	5	14	1	0	0			
		Taxes	0	0	0	0	0	3			
TOTAL	Frequency of positive impacts by actions		1	1	1	1					
	Frequency of negative impacts by actions		2	4	5		12				
	Indifferent frequency impacts actions		18	16	15						51

FIGURE 2: Matrix interactions for tracer flow test





			ACTIVITIES									TOTAL				
			Stimulations (Matrix Acidifications)													
			ENVIRONMENTAL COMPONENTS			ENVIRONMENTAL FACTORS			3.1.Transportation and conditioning of equipment	3.2 Preparation and Mixing Chemicals	3.3 Injection of treatment fluids	3.4.Rest or warm up	3.5. Measurements of steam flow (Discharge steam to atmosphere	3.6 Measurements of water flow (Injection waste water)	Frequency of positive impacts by factors	Frequency of negative impacts by actions
PHISYCAL-CHEMICAL	LAND- GEOLOGY	Land use	0	0	0	0	0	0	0	0	0	0	0	0	0	6
		Organic soil	0	0	0	0	0	0	0	0	0	0	0	0	0	6
		Drains	0	0	0	0	0	0	0	0	0	0	0	0	0	6
		Soil permeability	0	0	0	0	0	0	0	0	0	0	0	0	0	6
		Geology and site stability risk	0	0	0	0	0	0	-28	0	1	5				
		Subsidence and disturbance	0	0	0	0	0	0	0	0	0	6				
	WATER	soil quality	0	-3	-10	-16	0	-29	0	4	2					
		Water amount	0	-4	0	0	0	-30	0	2	4					
		Water quiality	0	-5	-11	-17	-18	-31	0	5	1					
		AIR	Air quality Physica (Noise)	-1	-6	-12	0	-19	0	0	4	2				
Air quiality Chemical (odors and gases)	0		-7	-13	0	-20	0	0	3	3						
BIOLOGICAL-ECOLOGICAL	FLORA	Vegetal cover	0	-8	-14	0	-21	0	0	3	3					
	FAUNA	Wild life	0	0	0	0	-22	0	0	1	5					
		Habitats	0	0	0	0	0	0	0	0	6					
SOCIAL - CULTURAL	POPULATION	Local trafic	0	0	0	0	-23	0	0	1	5					
		Quality life	0	0	0	0	0	0	0	0	6					
		Tourist	0	0	0	0	-24	0	0	1	5					
	LANSCAPE	Effective visibility	0	0	0	0	-25	0	0	1	5					
ECONOMIC - OPERATIONAL	ECONOMY	Local economy	0	0	0	0	0	0	0	0	6					
		National economy	0	0	0	0	0	0	0	0	6					
		Employment	2	9	15	0	26	0	4	0	2					
		Taxes	0	0	0	0	0	0	0	0	6					
TOTAL	Frequency of positive impacts by actions		1	1	1	1	1	1	4	22	102					
	Frequency of negative impacts by actions		1	6	5	2	5	3								
	Indifferent frequency impacts actions		19	14	15	18	15	17								

FIGURE 3: Matrix interactions for matrix acidizing

APPENDIX II: Water flow in discharge test (Lip pressure)

Date / Time	Water flow
16.11.2015 12:50	21.5
16.11.2015 13:20	21.5
16.11.2015 14:47	21.5
16.11.2015 16:22	21.5
17.11.2015 12:00	17.5
18.11.2015 12:30	16.3
19.11.2015 11:00	18.8
20.11.2015 16:00	16.3
23.11.2015 11:00	11.0
23.11.2015 14:40	11.0
23.11.2015 15:25	8.4
23.11.2015 15:00	11.0
24.11.2015 11:00	11.0
24.11.2015 13:00	11.0
24.11.2015 13:00	11.0
24.11.2015 15:00	11.0
25.11.2015 08:00	10.1
25.11.2015 09:00	11.0
25.11.2015 15:00	10.1
25.11.2015 15:25	10.1
30.11.2015 10:24	5.6
2.12.2015 11:00	4.4
2.12.2015 11:00	4.4
3.12.2015 14:04	3.9
4.12.2015 10:50	5.6
7.12.2015 11:45	5.0
11.12.2015 13:30	4.4
18.12.2015 09:40	3.4
21.12.2015 10:00	2.5

APPENDIX III: Equipment use for monitoring in discharge test

Component to monitoring	Technical description	Figure
Noise	<u>Equipment for noise monitoring</u> Brand: Quest Technologies Model: SoundPro DL 1/3 Range: 12.5 Hz to 20,000 Hz Permissible sound level: 55 dB(A)	
CO ₂	<u>Equipment for CO₂ monitoring</u> Brand: GrayWolf Model: IQA Surveyor II Range: 0 to 5,000 ppm Permissible exposure limit: 5,000 ppm	
H ₂ S Short term monitoring	<u>Equipment for H₂S monitoring- Short term monitoring</u> Brand: Arizona Instrument LLC Model: Jerome 631 Range: 0.003 to 50 ppm Resolution: 0.001 ppm Brand: Arizona Instrument Model: Jerome j605 Range: 0.003 to 10 ppm Resolution: 0.00002 ppm	
H ₂ S Long term monitoring	<u>Equipment for H₂S monitoring- Long term monitoring</u> Brand: App Tek International Model: OdaLog Low Range H ₂ S Logger Range: 0.003 to 10 ppm Memory Capacity: 30,000 data points Permissible exposure limit: 0.102 ppm in 24 hours	



UNITED NATIONS
UNIVERSITY

UNU-GTP

Geothermal Training Programme

Orkustofnun, Grensasvegur 9,
IS-108 Reykjavik, Iceland

Reports 2016
Number 11

GEOHERMAL DISTRICT HEATING MODELLING FOR TYPICAL HUNGARIAN RESIDENTIAL BUILDINGS IN DEBRECEN

Zoltán Békés

Ministry of National Development

49. 8/48. Lebstock M. Str.

1042 Budapest

HUNGARY

zoltan.bekes@nfm.gov.hu, vipbekes@gmail.com

ABSTRACT

The most important aim of this paper is to examine the technical possibilities to replace natural gas fired district heating system in Debrecen, E-Hungary, with geothermal energy. In order to present these challenges in a comparable way, the existing common residential buildings were grouped into seven subcategories and linked together theoretically, representing a system with diverse conditions. It has been established that hot geothermal water is able to replace a natural gas boiler in the range of 97-98% of the energy consumption, saving 91,000-111,000 m³ of natural gas yearly. The calculation identified, that the radiator system and the heat loss parameters of the residential buildings are the most crucial elements of the system. According to the presented scenario-B, which assumes only radiator replacement in more than half of the heat market, representing 325,000 net m², a decrease in total energy consumption is experienced in the range of 8-10%. On the other hand, scenario-C, which is assuming complex reconstructions for out-dated buildings, results in a significant 17-19% energy consumption savings, compared to Scenario-A (original case). In this regard, it is worth considering improvement to out-dated buildings within the heat market before starting geothermal energy development, to get an efficient, well-constructed system.

1. INTRODUCTION

The main aim of this paper is to investigate the replacement of the existing natural gas fired district heating system for geothermal energy in Debrecen city. This paper works out a mathematical model to design a purposeful project, linking together residential buildings from seven defined subcategories which describe well the building structure in Debrecen and also Hungary. To demonstrate the differences between these residential buildings in a comparable way, each major building category (1-family houses, 2-prefabricated concrete panel block buildings and 3-new apartment buildings) was balanced to consume roughly the same quantity of heat in design condition. It was essential to analyse the current heat market and explore what are the technical barriers and bottlenecks of a similar geothermal district heating project in Hungary. The theoretical model shows the importance of energy efficiency and also heating system refurbishment, before deciding on any geothermal district heating development. The final results of the report, aiming at replacing the natural gas boiler, were drawn up as three different proposals (scenario-A: "Status quo"; scenario-B: "radiator replacement"; scenario-C:

“complex refurbishment”) to optimize the energy consumption of this theoretical system. During the design progress, it should be considered that the temperature level of the geothermal water is limited in Hungary, in order to get a realistic, reliable result about the possibilities.

2. THE ENERGY SECTOR IN HUNGARY

2.1 Energy overview for Hungary

Hungary is a relatively poor country in conventional energy sources, therefore most of the time in the past, energy import had a significant role. Regarding the production side, in 2013 the most dominant energy source was nuclear, with a 50.83% gross electricity production share, solid fuels had 20.79% share (mostly coal), and natural gas had 18.48% share (European Commission, 2015). Heating production is less diverse than electricity production, because natural gas plays the main role in several forms of cogeneration and also direct heat supply by gas boilers, furthermore individual gas boilers are also very prevalent. Statistical data suggests that natural gas has the biggest influence within the Hungarian energy sector, adding that it is mainly imported. In 2011, the heat consumption of the building sector had a 38.6% share of the Hungarian primary energy consumption, representing 403 PJ (ÉMI Non-Profit Llc., 2015).

Hungary has a long tradition of low-temperature geothermal utilisation. In 2014, there were 672 active thermal wells, producing almost 80 million m³ hot water per year. Almost the half of the utilization was used for balneology purposes (Tóth, 2015). Also in 2014, the country had the fifth largest annual geothermal use in the world with 9573 TJ (excluding heat pumps) (Lund and Boyd, 2015). The main fields of direct utilization are the greenhouse sector, more specifically plastic-tent heating. The biggest agricultural producers are in Szentés, Szeged, Csongrád and Szegvár. The estimated geothermal use of agriculture was around 2800 TJ in 2011. Space heating is also an important part of the utilization; in 2013 more than 2000 TJ was consumed for this purpose. There are 23 geothermal district heating systems in Hungary, located mainly close to the Great Hungarian Plain (Nádor et al., 2013). The country has still no geothermal power generation, however the implementation of the first 2.7 MW unit just started in the town of Tura in June of 2016. This project was a unexpected result of an exploration, finding unusual geothermal conditions in that area.

2.2 Geological details

Hungary is situated in the Carpathian Basin bordered with Alpine, Carpathian and Dinaric mountains with mostly sedimentary formations, which are derived from the Miocene through Quaternary in age (Horváth et al., 2013). Regarding the characteristic geologic formation, Hungary does not have any active volcanic areas, most of the reservoirs been considered relatively low-temperature fields (excepting some unusual geologic anomalies). For instance, in the southeast part of the country, the Békes basin has a 90–100°C temperature reservoir conditions (Hotváth et al., 2013) in average at 2000 m depth, which is one of the most promising geothermal areas in Hungary. It is also notable that the maximum depth of thermal water yield allowed by the sedimentary formations is around 3000 m (Kozák and Mikó, 2004). For geothermal district heating, it is crucial to find not only high enough temperature, but as well sufficient yield. For summary, the possibilities of finding geothermal water above 90°C below 2000–2500 m with sufficient mass flow is better than average condition. Tura example suggests that very often the role of luck is very important, even more than strongly established geological exploration.

2.3 Basic details of Hungarian district heating sector

The history of the Hungarian district heating application started in the early 1950s and 1960s. Initially this began with industrial consumers, however, since that time residential space heating has played the main role, as shown in Figure 1. Considering the energy policy aspects and the most easily exploitable resources with the available technologies for each time, all of the district heating system were designed for natural gas and coal. These district heating systems are a kind of heritage for Hungary, as well as for other ex-communist countries of the Eastern Bloc. District heating systems had a spectacular improvement until 1989 (GKI - Energy Research and Consulting Ltd., 2005) but at that time the political system changed significantly; Hungary escaped from the Eastern Bloc, which has had a serious impact on the energy policy framework. The expanding role of district heating systems was closely related with the residential block house building strategy implementation, which was discontinued at that time, which also hindered the district heating improvement. Therefore, these, often old, thermal power stations were oversized to account for a planned higher heat market. This has led to the thermal power stations (or cogeneration power plants) still having a surplus of heat generation. The industrial district heating demand decreased significantly between 1985 and 1999, or more than fifty per cent.

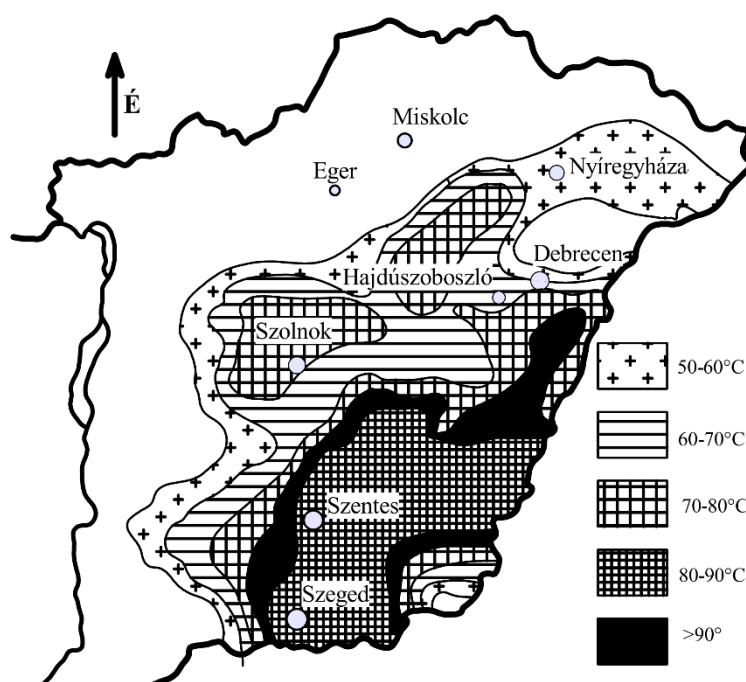


FIGURE 1: Estimated reservoir temperature data in East-Hungary (Kozák and Mikó, 2004)

In 2014, district heating facilities are available in 94 settlement, comprising 219 district heating systems. Most of the consumption or 76.4% is from households, which consist of space heating and hot water. There are no significant changes in the number of flats supplied with district heating; in 2014 the total was 648,329, almost the same number as in 1990, shown in Figure 2. More than 90% of those are also supplied with heat for hot tap water (MEKH, 2014). There are 168 power plant units in operation in Hungary, with more than 8000 MW installed capacity, providing district heating facilities. Thirty units are operating as a cogeneration power plant (with gas engine generator set

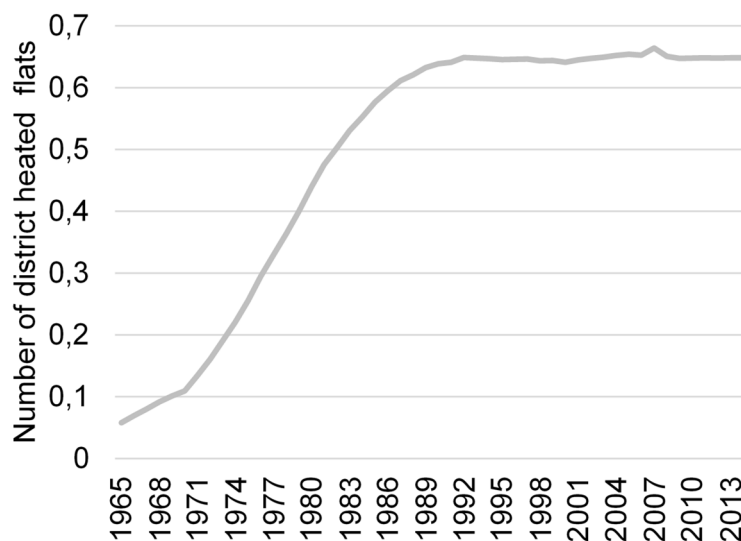


FIGURE 2: Number of district heated flats in Hungary between 1965 and 2014 (Hegedűs, 2005; MEKH, 2014)

and boiler to supply direct heat, representing more than 1800 MW installed capacity), producing electricity and using heat for district heating, however 62 power plants (representing 1371 MW) produce only hot water for direct heat supply by boilers. This paper focuses on the most common power plants, having the highest number. Besides there are, however, many different systems existing which are less common.

There are three power plant units in Debrecen, situated next to each other roughly in the central part of the city. The three power plant units are owned by three different companies: Tiszántúli Hőtermelő Kft., E.ON Energiatermelő Kft. and Debreceni Kombinált Ciklusú Erőmű Kft. The first unit is a gas engine generator set combined with a natural gas boiler (29 MW), the second unit is the same as the first unit, but includes a back-pressure steam turbine generator set (349 MW), and the third unit is a combined cycle power plant unit (90 MW). The available thermal capacity of these units, all together, is 468 MW. These units operate together for the district heating supply. They are, however, also able to run separately, which will be very important according to the final goal of this theoretical project.

2.4 Meteorological conditions

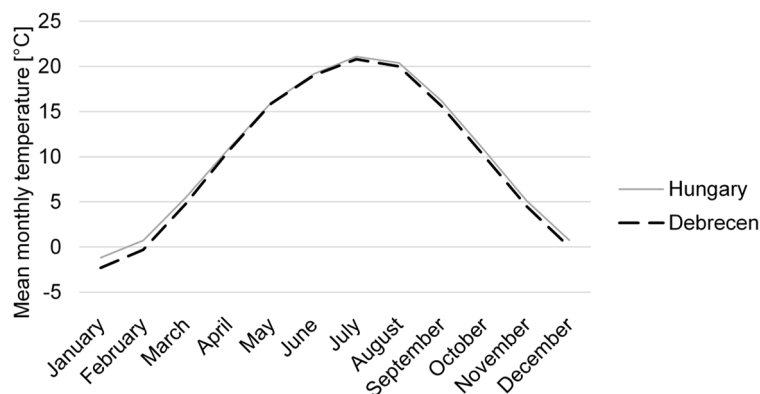


FIGURE 3: Mean monthly temperature in Debrecen and Hungary (data sample 1900-2010) (OMSZ, 2016)

Hungary is located between the 45°45' and 48°35' latitude in the middle of Central Europe in the Pannonian Basin. The country has basically a continental climate, however, different surrounding climates have modification effects. In this regard, the temperature and general weather conditions are changeable during the whole year. The Hungarian annual mean temperature is around 9.5-11°C, calculated data from 1900-2010 (OMSZ, 2016), (Figure 3). Temperature conditions in winter and summer can be very far from this

average value, which is important for heating system design. During the heating system design, it is essential to take into account the coldest (possible) temperature conditions of the analysed location. Before the heating system design, the most crucial task is to analyse all of the available meteorological data about the measured mean daily outdoor temperature history. Outdoor design temperature is one of the most important chosen elements of the model, which serves as a basis to estimate the volume of the necessary heat consumption of the heat market.

Hungarian Meteorological Service (OMSZ) has reported temperature and other essential meteorological data for five Hungarian cities; Budapest, Debrecen, Pécs, Szeged and Szombathely from 1900 to 2010, shown in Table 1. Between 1901 and 1965 the daily mean temperature was calculated with the measured 7 am, 2 pm and 9 pm average, where the 9 pm measurement was weighted twice. Since 1965, the calculation method of the daily temperature consists of the 7 am, 1 pm, 7 pm and 1 am recordings with a simple arithmetic average in equal weight for each measurement (Baumann, 2012). On the other hand, according to the Hungarian Standard (MSZ-04-140/3-87, see Appendix I) which defines the required design outdoor temperature in the function of the location (Zsebik, 2004), the minimum designed temperature is:

- 1) Southwest Hungary: -11°C;
- 2) Northeast Hungary: -15°C;
- 3) Central Hungary (lies between 1 and 2): -13°C.

TABLE 1: Used flats in the function of building material and floor area
(Hungarian Central Statistical Office, 2013)

Building material	≤ 49 [m ²]	50–99 [m ²]	≥ 100 [m ²]	Total	Average floor area [m ²]
Brick, stone	363,670	1,342,978	777,359	2,484,007	84
Prefabricated concrete panel block building	196,446	539,491	41,326	777,263	62
Adobe, slob	53,986	422,126	107,377	583,489	77
Wooden, other	7,874	37,575	22,221	67,670	84
Total	621,976	2,342,170	948,283	3,912,429	78

This is a relatively old standard (28 years old) however it is still in use. Experience has shown, that the heating activity is necessary if the mean daily temperature is below 12°C (this is the marginal heating temperature). In case it happens more than three times continuously, the district heating companies should have to start the system operation, regardless of the date. Officially, the heating season in Hungary is between 15th of October and 15th of April. Furthermore, if the temperature conditions require; the customers also have the right to ask the heating service to operate outside of the heating season (Zsebik, 2004).

2.5 Temperatures records

Considering the long-term history temperatures, the north-eastern part of the country is the coldest. This study will relate to the coldest part of Hungary and will focus on the town of Debrecen. The measurement history of Debrecen in the last half-century (1960-2010) is shown in Figure 4. There were only 16 cooling days (Hungarian Meteorology Service, 2016), when the mean daily temperature was lower than the commonly used -15°C design temperature (Hungarian Standard, MSZ-04-140/3-87 – Appendix I). This statistical sample of about 51 years consisting of 18,627 days (altogether with leap years), shown in Figure 4 (see also table in Appendix II), with only 16 extremely cold days below this designed temperature, means that, on average, there is only one cold day in every three years; which is an acceptable rate (OMSZ, 2016).

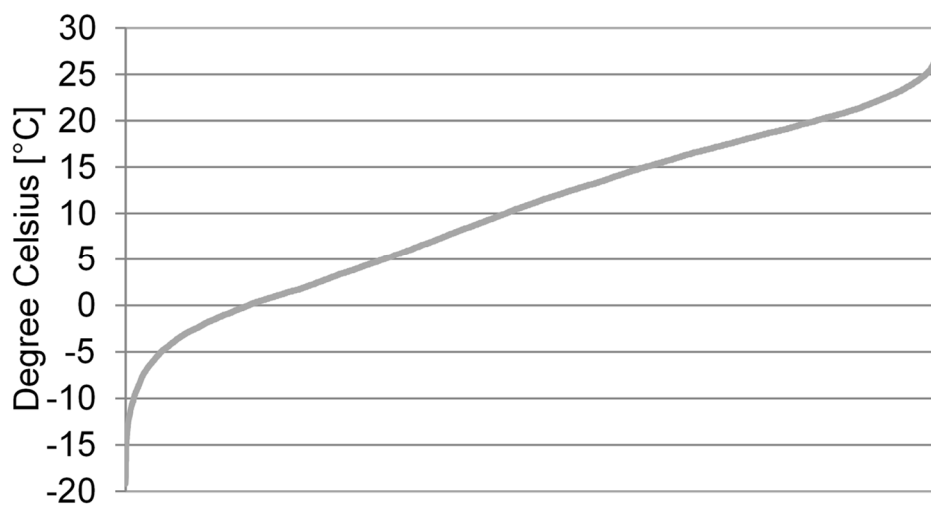


FIGURE 4: Outdoor temperature duration curve for Debrecen (1961-2010) (OMSZ, 2016)

For a heating engine, it is necessary to calculate the number of degree days, it is therefore the first element of the calculation to estimate the length of the heating season. Within this statistic sample, there were 9917 days when the outdoor mean temperature was lower than 12°C (N_T days), and 8710 when it

was higher. Dividing with 365.25 (considering leap years as well) gives the average number of heating season within a year as 194.4 days. This result is very close to the widely used heating design practice; with district heating companies usually expecting to cope with 190-200 days long heating seasons. Also necessary to know, is the average mean outdoor temperature for N_T days (N_{mT}), which is 3.14°C in this case (Karlsson, 1982). Degree days for “T” period are given by Equation 1:

$$DD_{(T)} = N_T(T - N_{mT}) \quad (1)$$

where $DD_{(T)}$ = Annual degree days, for the desired indoor temperature (T);

N_T = Number of days when the outdoor temperature is below T, through the whole year;

N_{mT} = The mean outdoor temperature for N_T days ($^\circ\text{C}$).

Regarding the calculation above, the average degree days in Debrecen are around 3280. The same formula is used to calculate degree hours depending on what is the exactness requirement. This result bears out the degree days map (see Baumann, 2012 – Appendix III).

Meteorological calculation basis is a very important element of the district heating design progress, to avoid under or overdesign. If the system is under-designed it will not be able to keep the desired indoor temperature, therefore cannot fulfil the heating requirements. Also, if the system is overdesigned it will cause unnecessary thermal capacity, increasing the investment and operational costs which makes the system economically ineffective. Furthermore, heat loss parameters about the building structure are also a crucial part of the designing progress.

2.6 Building structure details

The following section will provide an overall summary and detailed information about Hungarian private apartments. The most important data source is the population census from 2011 (Hungarian Central Statistical Office, 2013). The total number of the counted flat units was 4,381,976 in 2011. This paper takes into account only the dwellings, which was 3,904,103. Brick is the most common building material in Hungary (shown in Table 2), with almost 2.5 million dwellings. Also, an important condition is that more than 2.2 million buildings are detached houses, which are mostly built from brick according to the general experiences. Houses which are made from adobe or slob also have a significant share with almost 0.6 million detached houses. Almost 80% of these houses are located in the eastern part of the country and surrounding Budapest. Also, a significant segment are the panel and concrete buildings; 95% of which are located in cities of various size. Wood and other building materials have a very low share within dwellings, and are negligible.

2.7 Heating system details

In most cases the building material and the location of the building determines the applicable heating resource and also the type of heating system. Natural gas is the main energy resource in Hungary (see Section 2.1), and is widely used for district heating, for individual convector heating, for circulating hot water heating, and also for central gas boiler heating. More than 2.4 million dwellings have central heating system and almost 1.5 million flats heating have individual heating systems (shown in Table 2). The share and role of individual heating is reducing year by year. Between 2001 and 2011 the number of individually heated flats decreased by -12%. The share of district heating has also decreased in this period, however less than individual heating, or by -3%. The most commonly used heating system in Hungary is the central heating solutions, including the newly built apartment buildings as well. District heating applications are mostly used for heating prefabricated concrete panel block buildings (for the further text it will be called: “block building”) in Hungary, and almost nowhere used for family house heating. These block buildings were constructed without extra insulation, with relatively small radiators designed for 90/70 systems. The lack of heating control possibility is also a serious problem. These facts were evaluated and district heating got a very negative image, however, this is not evidence.

TABLE 2: The share of different kind of heating systems in Hungary
(Hungarian Central Statistical Office, 2013)

Type of heating system		2001	2011	Change compared to 2001
District heating (incl. pipeline from heating-station)	Central heating	625,333	607,578	97.16%
One or more flat heated w. central heating (house central heating, circulating hot water heating/individual central heating) boiler, or other equipment	Central heating	1,395,917	1,829,459	131.06%
Individual room heating	Individual heating	1,669,523	1,475,392	88.37%
Total		3,690,773	3,912,429	106.01%

Single pipe free-flow system (Figure 5A) is a serial connected secondary circle, which was widely used mostly between 1970 and 1980. According to the Hungarian architectural policy of that time, this was the obligatory applied heating system. The difficulties of this system is that there is no possibility to control the indoor temperature, it is only balanced from the heat source which takes a long time, furthermore inhabitants usually “control” the temperature by opening windows. Accordingly, over- or under heating is very common in the system, and therefore the system is not able to work efficiently and sufficiently. Today, the opinion is that this is not a development that people want to continue. Single-cross pipe system with individual valve (Figure 5B) is a developed single-pipe flow system, inserting an individual valve. However, these heating systems development of (Figure 5A and B) are not the best option, but became a very commonly used practise as it requires low investment costs. Double pipe systems (Figure 5C) are the latest version of secondary heating circles which provide the best option (of these common types) to control heating system individually (MIHŐ, Ltd., 2016).

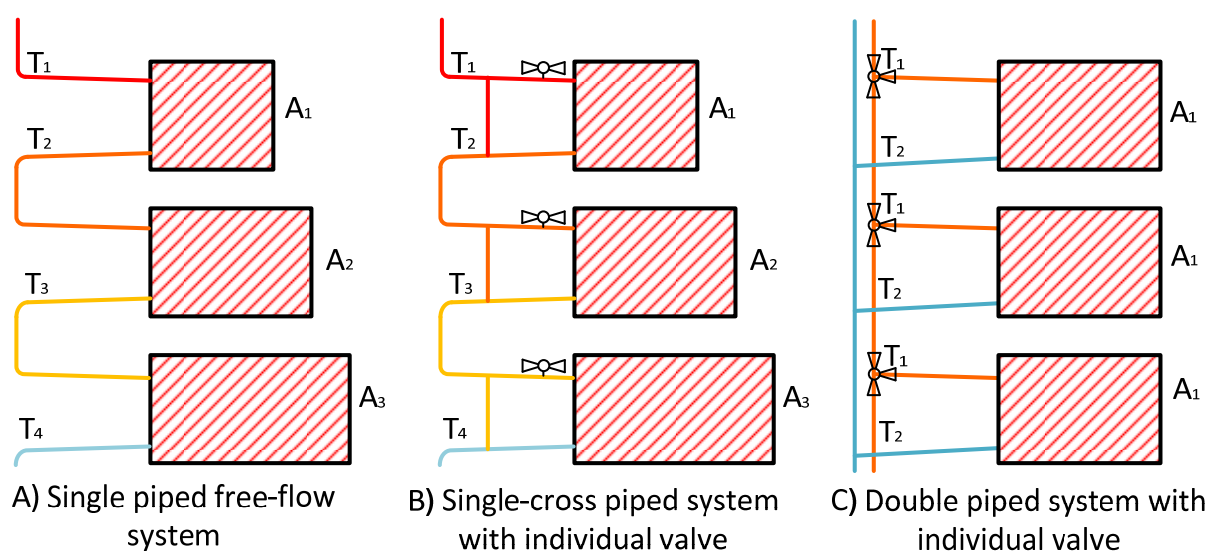


FIGURE 5: Different types of radiator heating circles in Hungary
(drawing based on MIHŐ, Ltd., 2016)

3. HEAT MARKET ANALYSIS

3.1 Debrecen city

To explain the challenges of the design process of a geothermal district heating system, this study will present a mathematical model for an invented development project. In this regard, it is necessary to choose a concrete location for this purpose. The main focus of this study will be in Debrecen city, which is situated in the eastern part of Hungary, one of the major cities of the Great Hungarian Plain. Debrecen is the second most populated city in Hungary with around 200,000 inhabitants (Hungarian Central Statistical Office, 2013). The following important aspects were taken into account on the selected settlement. It should:

- Consist of several types of residential buildings (located close to each other);
- Already have an existing fossil fuel fired district heating system;
- Be located relatively close to the explored geothermal fields (Hajdúszoboszló, Nagyvárad);
- Be one of the coldest parts of the country;
- Have significant agricultural production for further cascaded use.





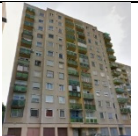
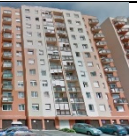

In 2011 there were 94,708 dwelling units in Debrecen, which increased to 95,772 in 2014. The number of unoccupied dwellings in Debrecen was 9,458 (Hungarian Central Statistical Office, 2013), but it is important to emphasise that this phenomenon is not common in the central area of the city where the examined heat market is located. In this regard, the model will not account for it. To get a realistic and applicable result of the study, it is also necessary to set out typical building groups, for simplification.

3.2 Building groups

It is important to emphasize, that this study is not an already planned project. This is only a simulation, based on mainly the available geothermal utilization experiences of Miskolc, regarding the geothermal wells. The main goal of the model is to represent proportionally and properly the existing building structure, which is typical in Debrecen, and also for Hungary. It is suitable to represent the conditions and parameters of the different types of buildings in one system. The floor area and the shape of the buildings give only an example for the calculation. The mathematical model is also applicable for other settlements. To demonstrate these differences in a comparable way; each major building category (1-family houses, 2-block buildings, 3-new apartment buildings - Appendix IV) will require roughly the same quantity of heat in the design conditions, around 10 MW. In this regard, the heat market will represent around 30 MW heat consumption in design condition. This quantity, however, does not include the system losses such as distribution heat loss. The full size of the heat market was estimated with the help of calculated heat loss data for the different building types, based on the already district heated block buildings.

According to the aim of the theoretical project, the system will mostly be based on the geothermal energy resource, considering that the temperature of the geothermal water is usually the bottleneck within the implementation. The temperature and the yield of the geothermal water in this area is able to provide a constant base load, but above that level gas boiler is necessary to provide enough heat supply in the peak periods. Each of the selected building categories are relatively widespread in Debrecen, but this limited geothermal heat supply allows only smaller parts to link to the theoretical system. To use a realistic heat loss coefficient (U) value (shown in Table 3) for each building of the model, calculations were based on a very detailed literature, National Typology of Residential Buildings in Hungary (Csoknyai et al., 2014).

TABLE 3: Heat loss coefficient values of the defined building groups

	Group-1: Family house		Group-2: Prefabricated concrete panel block buildings				Group 3: New apartm. houses
Building element	Building type 1	Building type 2	Building type 3	Building type 4	Building type 5	Building type 6	Building type 7
All parameters in $\left[\frac{W}{m^2 K} \right]$							
Wall + insulation	1.50	0.17	0.8	0.19	0.8	0.19	0.21
Roof	1.50	0.14	0.91	0.14	0.91	0.14	0.17
Slab	1.30	0.14	-	-	-	-	-
Floor above ground	0.98	0.98	0.55	0.15	0.55	0.15	0.26
Windows	3.00	1.30	1.15/3.30	1.00	1.15/3.30	1.00	1.15
Doors	3.00	1.30	1.15/3.30	1.00	1.15/3.30	1.00	1.15

Furthermore, it is also important to estimate the typical number of inhabitants for each sort of building type. The available statistics from the population census (2011) provide a good basis to estimate these values. Accordingly, the average number of inhabitants in Debrecen from the mentioned statistics are:

- $\leq 79 \text{ m}^2$: 2-3 inhabitants / unit;
- $\geq 80 \text{ m}^2$: 3-4 inhabitants / unit (regardless of the building material of the building).

$79\text{-}80 \text{ m}^2$ is the border value between the categories, because most block building flats are smaller than 79 m^2 , and most family houses are bigger than 80 m^2 . Block buildings have a very complex structure regarding flat sizes. Appendix V shows the copy of ground plans for type P100 of prefabricated concrete block building (Csoknyai et al., 2014), while Appendix VI represents the original ground plans for type MOT I. 58-264/76-K C-1. Therefore, all net floor sizes are known, allowing estimation of the number of inhabitants based on the building types (Appendix IV).

3.2.1 Family houses

The first category consists of family houses. There are almost 2.5 million family houses in Hungary, most of them (1.8 million) were built earlier than 1979. The bigger part of them have never been reconstructed, therefore these houses have already become out-dated. More than 50% of the existing buildings in Debrecen were built earlier than 1979, representing 53,929 flats altogether; mostly family houses. Obviously there were built several different sort of dwellings during that time, but to simplify this group, two commonly built subcategories will be taken into account: 1) “*Old Hungarian cube house*” (or also called “*Kádár cube house*”) and 2) “*Refurbished family house*”.

Old Hungarian cube houses were commonly built between 1945 and 1979 (Csoknyai et al., 2014), and even nowadays are quite widespread. These houses were built from solid brick, without any additional insulation, with only a plaster layer added for both sides. Typical U values (shown in Table 3) of the walls are between 1.36 and $1.77 \text{ W/m}^2\text{K}$, depending on thickness. In the mathematical model an average will be considered, using $1.5 \text{ W/m}^2\text{K}$ as the heat transmission coefficient value. The average floor area

of these houses is approximately 90-110 m². Generally, the roof does not serve as a dwelling area, as it is only used for storage during the year. These houses were built without cellar, with one floor, including 2 or 3 bedrooms. The most common heating system is (constant temperature non-condensing) gas boilers or firewood stoves. The wooden windows and doors are not well insulated, and most of these houses are poorly maintained, out-dated, and do not satisfy the basic thermoeconomic requirements. These are the most wasteful type of residential buildings in Hungary; heat consumption is two times higher than for the reconstructed, well insulated family houses. Almost all family houses are heated with individual gas boilers or firewood stoves in Hungary (Hungarian Central Statistical Office, 2013). Most of these houses are situated at the borders of the central area or outside them, in poor districts and usually owned by poor people and/or senior citizens. Commonly, full reconstruction would be more expensive than the value of the house and the site itself.

The second category was mainly built later, and until around 2000. These houses were refurbished and/or extended to nearly 200 m². The most important difference between the two categories, is that the second type of houses were developed with a 10-20 cm thick insulation and new plastic made insulated windows, resulting in significantly lower heat loss parameters. The most frequent heating system is constant temperature non-condensing gas boilers, but in ambitious refurbishments, condensing gas boilers are used (Csoknyai et al., 2014). Full renovation generally requires large amounts of money; therefore, very often it is implemented in more affluent areas than the first category. As a result of these developments, the heat loss values have decreased significantly.

3.2.2 Prefabricated concrete panel block buildings

This building category represents a very common type of building in Debrecen and also in Hungary. Roughly 7-8% of the Hungarian population are living in this type of buildings, representing 777,263 inhabitants (Hungarian Central Statistical Office, 2013). Also in Debrecen, a significant part of the population is living in block buildings, with several thousands of flats being built between 1957 and 1990. It is known that the number of district heated flats was 30,895 in Debrecen in 2011 (Hungarian Central Statistical Office, 2013), and also known that 99% (EMI Non-Profit, Llc., 2015) of the district heated flats are prefabricated concrete block buildings, meaning that this number is very close to the total number of block buildings in Debrecen. In the last decade, the Hungarian Government through financial programmes, started to support the refurbishment of these buildings, resulting in the number of refurbished block buildings starting to increase. These refurbishments generally result in significantly lower heat loss parameters. This was also considered, as well as windows and balcony doors being also replaced in buildings, which are still in original condition. The ratio between the “new” and “old” window/balcony equipped flats was estimated by Google Maps.

3.2.3 New buildings

This category includes all the buildings which were recently built (or will be potentially built in the future) and have low heat loss parameters (Table 3). In fact, these houses are generally operating with house central heating based on a gas boiler. In the model, it was assumed that these buildings are constructed with district heating systems. An example of a floor map of a newly planned building is shown in Appendix VII (from Hatvan street 62, Debrecen).

3.2.4 Tap water

It is difficult to estimate the tap water consumption with accuracy. The number of inhabitants is estimated according to the statistics; however, the estimate is highly dependent on personal behaviours, the standard of living, the average staying time at home and so on. Consequently, the estimate of the tap water heat consumption was calculated based on the type-7 building radiator heat consumption divided by the number of inhabitants. This methodology gives a 0.147 kW / inhabitant value as a constant which is very close to widely used estimation; which predict tap water heat consumption as 8-10% of the building radiator heat consumption (Zsebik, 2004).

3.3 Exact location of the theoretical project

The model will be using three different types of building groups and seven subcategories described in detail in Appendix IV. Considering the concrete location of these typical Hungarian buildings the selected location is in the northern part of the city, located at a 2-3 km distance from the main square of Debrecen (Appendix VII). This is an ideal place for this analysis because all of the building categories can be found next to each other (except type-7, which is not existing).

The left side of the map (Appendix VIII) is basically an area covered with family houses, shown with a red rectangular. The exact location of the area shows that it borders with the Szabó Lőrinc - József Attila - Böszörményi and Akademia streets. It is around 0.25 km², mostly covered with buildings of type-1 and type-2. It should be emphasized that district heating access is not provided here, as these houses are usually running with individual gas boilers. In model calculation, it is assumed that new district heating connection and refurbished radiator heating facilities will already be provided for these houses. The new pipeline thermal efficiency is considered to be 96% (0.96) (Appendix IV). The model will assume that 280 type-1 and 440 type-2 buildings will be linked to the system. It is also assumed according to the statistical data (Hungarian Central Statistical Office, 2013) that three people live in building type-1 and four people live in building type-2 on average. This is altogether 720 family houses representing 116,000 m² net heated floor area, with 2600 inhabitants. This part of the heat market needs 9.97 MW thermal capacity based on design conditions.

The biggest housing estate area is situated in the central part of Debrecen, only 2-3 km distance from the city centre, shown with yellow rectangular in the right side of the location map (Appendix VIII). The Újkert housing estate area was built in 1970, representing around 20,000 inhabitants. These buildings are heated by the local district heating system, hence the distribution system and radiator heating facilities are already arranged. This fact was the major reason to select this area for the theoretical model. The location of this area shows that its borders are along Doberdó – Böszörményi – Füredi – Nádor -Thomas Mann – Mikszáth - Békeffy and Kartács streets. The area is around 0.78 km², mostly covered with buildings of type-3, type-4, type-5 and type-6. The supply pipeline was built more than 40 years ago, therefore it is assumed that some part of it has been reconstructed since that time, so the existing pipeline is considered with an estimated 92% (0.92) thermal efficiency value. There are several types of block buildings in this area, but the most common types in the examined area are the fifteen-storey (type P-100) and a ten-storey (MOT I. 58-260/76-K C-1) block buildings (Appendices V and VI). From the bordered area, nine P-100 buildings and 29 refurbished block buildings will be linked to the theoretical model. Of the P-100 buildings there are two buildings already refurbished, but seven buildings are in the original state without complex development. From the C-1 block buildings, 29 buildings will be linked to the system theoretically (24 refurbished, five in out-dated conditions). This is altogether 38 block buildings, representing 209,329 m² net heated floor area, with 8388 inhabitants. This part of the heat market needs 10.35 MW thermal capacity in design condition.

The selection of newly built apartment buildings is more flexible than the two previously mentioned categories, because currently it does not exist. At two streets in a north direction from the family houses and also next to block buildings there is a 0.26 km² green field, shown with blue rectangular in Appendix VIII, which is theoretically suitable for building type-7. This is, however, only an example for the location. The exact location of this area is bordered by Károli Gáspár - Tessedik Sámuel - Böszörményi and Vezér streets. As a result of this, it is assumed that for new houses with a new district heating pipeline, the thermal efficiency is considered to be 98% (0.98). This means that theoretically, additional 130 new buildings will be linked to the system, representing 214,760 m² net heated floor area, with 7280 inhabitants. This part of the heat market needs 10.03 MW thermal capacity in design condition.

4. DESCRIPTION OF THE THEORETICAL MODELLING

One of the main goal of this project to design a geothermal district heating system which uses as much geothermal energy as possible (respecting sustainability aspects) to reduce natural gas boiler usage. Regarding to the 51 years statistical sample of weather measurements, and also considering the related Hungarian standard (Appendix I), the minimum outdoor design temperature of the systems in Debrecen is -15°C . This is one of the most important fixed parameter of the district heat system; each further step of the design process will be based on this value. The second important parameter is the designed (desired) indoor temperature. This parameter depends on the individual expectations, and is a strict parameter with large influence on the installed thermal capacity of the power plant. For indoor design temperature, 20°C is the widely used value in Hungary. Therefore, this value will be used for the current modelling (during the heating season). This project assumes that a significant part of the heat consumption could be provided by the geothermal resource for the assigned building groups, therefore the gas boilers will only be used for back-up.

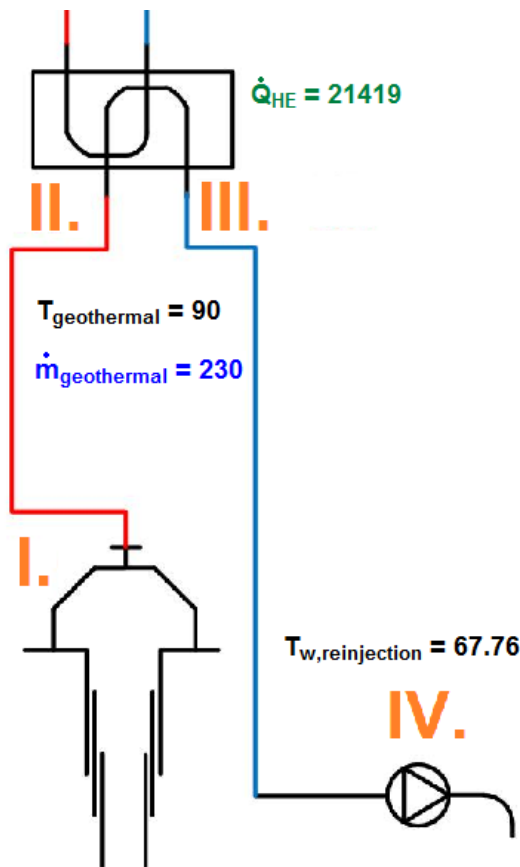


FIGURE 6: Schematic drawing of the primary circle of the designed district heating system

4.1 Primary circle

The most important role of the primary circle is to heat up the return water using the geothermal energy, transferring heat to the secondary circle through a heat exchanger and keep the desired temperature conditions of the system, shown in Figure 6. The theoretical model assumes only one heat exchanger between the primary circle and the heat market which is not common in the existing Hungarian district heating systems. Therefore, this requires a modification, mainly regarding the existing block buildings. The primary circle consists of the geothermal well(s), the heat exchanger (between the primary and secondary circle) and the reinjection well(s). The theoretical project assumes two geothermal production wells and two reinjection wells with the technical parameters of the system found in the table in Appendix IV. This estimate is based on the technical parameters of a similar existing geothermal project implemented in Miskolc, which is around 85-90 km from Debrecen. It is also assumed, that the heat exchanger is operating 4.5°C pinch (on the return side) and 5°C pinch (in the intermediate side) during the energy transfer. According to Table 4, the geothermal fluid mass flow is expected to be 230 l/s with a 90°C constant temperature.

TABLE 4: The most important parameters of the assumed geothermal wells for the theoretical project (based on Miskolc-Mályi geothermal system conditions)

Type of well	Mass flow of geothermal water [l/s]	Temperature of geothermal water [$^{\circ}\text{C}$]	Depth [m]
I. Production well	100	90	1500-2500
II. Production well	130	90	1500-2500
I. Reinjection well	90	-	800-1800
II. Reinjection well	100	-	800-1800

One of the biggest problems for geothermal utilization in Hungary is that the heating season length is around 200 days and the heat markets do not need any space heating during the remaining 165 days. Because of this, geothermal wells are commonly closed out of the heating season. Consequently, the model has to follow this practise.

4.2 Secondary circle

The most important role of the secondary circle to heat up the intermediate water temperature using the natural gas boiler, if the temperature is not high enough to cover the heat market needs. Therefore, it is important to emphasize that the gas boiler is not used at all most of the time, unless it is necessary. Nevertheless, the gas boiler is also able to replace geothermal wells if the geothermal system requires unexpected maintenance work or when the daily mean temperature is below the outdoor design temperature, $t_{od\ des}$. The intermediate water temperature is 81.035°C in design condition and considering the size and conditions of the heat market, the necessary system supply temperature should be 95°C . This is the “worth” case, when the outdoor temperature is -15°C . It means that considering the examined system parameters, the maximum Δt required with gas boiler is $95 - 81.035 = 13.965^{\circ}\text{C}$, as shown in Figure 7. The system is operating with mass flow control according to the actual heat consumption of the system. In this regard, the mass flow and intermediate water temperature are the two important variables of the designed system to satisfy the heat market needs. The water circulation is provided by circulation pumps.

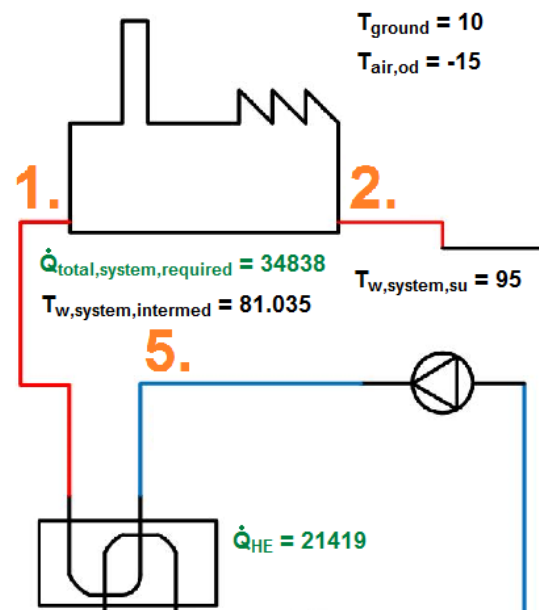


FIGURE 7: Schematic drawing of the boiler station and intermediate stage of the designed district heating system

4.3 The mathematical model for district heating

4.3.1 Tap water heat consumption

The level of hot water consumption is roughly the same during the whole year for residential consumers. Actually, the consumed heat is higher during the heating season and usually lower in summer time, but this difference is not significant. To simplify this factor, the model will assume that the heat consumption is constant during the year. This simplification means that the result of the boiler load in design condition could be a little higher in real conditions. Slovakian experience has shown that the supplied heat quantity used for hot water heating (per capita) is roughly equal with the heat loss of a modern building in 13°C outdoor temperature (per capita). According to the heat loss calculation for tap water heat, a constant $0.147\text{ kW/inhabitant}$ value will be used for all types of building. It is also very important to estimate realistically the number of inhabitants/ m^2 (Hungarian Central Statistical Office, 2013), because tap water consumption is highly dependent on the number of users.

4.3.2 Space heating – heat loss calculation

The necessary heat consumption should always be a bigger value than the total heat losses, because of the several forms of heat losses (pinch in the heat exchange, heat loss of the distribution system, heat loss from the houses, etc.). The major task is to provide sufficient quantity of heat for the heat market. Considering that, the first important task is to calculate the total heat loss of the building. There are

several elements in a building, which are able to modify the volume of the total heat loss considerably. The most crucial elements are the windows, doors, and the quality of the additional insulation. To avoid the over-, or under-design, the first task is to calculate the heat loss value (Q_T) for the heated unit (building/house) using a fixed design temperature. From the respect of the building, there are three values to consider in calculating the heat balance, 1) heat loss, 2) heat equity and 3) heat surplus. Heat

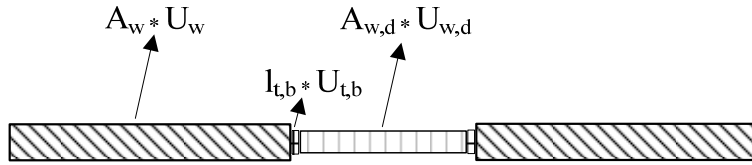


FIGURE 8: Calculation methodology of different types of transmission heat losses

loss is the usual heat transfer during the heating season caused by transmission and filtration. To simplify the heat loss calculation; the transmission (Q_{tr}) and filtration heat loss (Q_{fr}) will be considered almost as 100% of the building heat loss, other sort of heat losses are negligible (such as other complex energy transfers within the building, wind cooling effect etc.), as demonstrated in Figure 8. For the current purpose, it is not necessary to calculate in more detailed heat losses. Equation 2 defines the total heat loss for a building:

$$Q_T = Q_{tr} + Q_{fr} \quad (2)$$

where Q_T = Total heat loss of the building [kW];
 Q_{tr} = Transmission heat loss [kW]; and
 Q_{fr} = Filtration heat loss (caused by infiltration and ventilation) [kW].

Transmission heat loss (Q_{tr})

To quantify transmission and filtration heat losses, it is necessary to know the geometrical data for all types of buildings. For this purpose, floor maps could provide sufficient information (Appendices V, VI and VII) about the shape of buildings, surface and building material of the walls and windows/doors, etc. This simple modelling simulation used a contracted U value for doors and windows, including a thermal bridge coefficient as well. Transmission heat loss was calculated from Equation 3 used for all type of buildings:

$$Q_{tr} = \left(\sum A_{w,d} * U_{w,d} + \sum A_w * U_w + \sum (l_{tb} * U_{tb}) * (t_{id} - t_{od}) \right) \quad (3)$$

where $A_{w,d}$ = Surface covered by windows or doors [m^2];
 $U_{w,d}$ = Coefficient of heat transmission for windows or doors [W/m^2K];
 A_w = Wall surface [m^2];
 U_w = Coefficient of heat transmission for walls [W/m^2K];
 l_{tb} = Length of thermal bridge [m^2];
 U_{tb} = Coefficient of heat transmission for thermal bridge [W/m^2K];
 t_{id} = Indoor temperature [$^{\circ}C$];
 t_{od} = Outdoor temperature [$^{\circ}C$].

For calculation, it is sufficient and important to take into account the exact shape of the buildings, not only the value of floor area, because it does not determinate the surface area of the borders (which is highly related to the heat loss). To set the usual number of windows for each building category, Google Street View software was used for building types 1, 2, 3 and 4 as a sufficient estimation, considering these buildings are not completely similar. For the rest of the building types (5, 6 and 7) floor maps were available, which provided more exact basis for estimation (Appendices V, VI and VII). For the calculation of the buildings volumetric data it is important to divide the gross floor area and net floor in the case of complex buildings. This was considered in all types of buildings except building of type 1 and 2, because in these cases, gross and net floor areas are equal. For instance, garages, staircases and caloric centres do not need any heat or only a lower quantity. This is a significant difference, as calculated in Appendix VIII, meaning that the net floor is only 75-85% of the total floor area depending on the building type.

Transmission heat loss would be the only significant heat loss if the heated unit would be perfectly isolated all the time and all of the windows/doors would be closed constantly (without causing any air leaks), but in real life it is not true at all. Obviously air exchange is essential for everyday life and so in this respect it is necessary to take into account the filtration heat loss (z) (consists of infiltration and ventilation factor) caused by opening doors, windows, operating ventilation system, air condition, etc. Evidently, this factor is highly based on the number of inhabitants/dwellings, from other individual habits, and also from the quality of doors and windows. In order to get a proper value, it is possible to estimate this factor according to the heat engine experiences and also from usually applied standards. Filtration heat loss (Q_{fr}) given by Equation 4:

$$Q_{fr} = z * c_a * \rho_a * (t_{id} - t_{od}) \quad (4)$$

where z = Infiltration and ventilation factor [1/h];
 c_a = Specific heat of the air [kJ/kg K].

The difference between infiltration and ventilation is that ventilation is a purposeful, human controlled air exchange process but infiltration cannot be controlled directly, as it is caused by air leakages and other faults of the building. Infiltration and ventilation factor has a crucial role in filtration heat loss, because this factor determinates the value of the final heat consumption, especially in large buildings (types 3, 4, 5 and 6). To quantify this factor, it is usually given in estimated values, which are based on several measurements and experiences. Considering that 0.75 1/h value will be considered for building types 1, 3 and 5; 0.6 1/h for building types 2, 4 and 6, and 0.5 1/h for building type 7, according to the quality of the building materials (Soltész, 2008). The results of the heat loss calculations give significant differences between the examined buildings types. It is remarkable, that the refurbished block buildings had the best results regarding the heat consumption per inhabitant and also the heat consumption per square metre, shown in Figure 9. Newly built apartment buildings have a similar good value, however these buildings usually consist of larger flats in which case the number of inhabitants is lower and the specific energy consumption is larger.

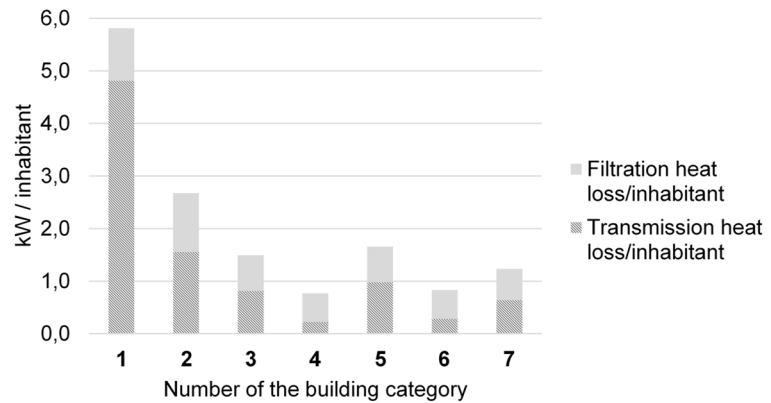


FIGURE 9: Heat consumption values per inhabitant, weighted with the net floor area for 7 different types of examined building

After the heat loss calculation, all data is known to calculate how much thermal energy is needed for the whole system in design condition. Before, it was explained how many buildings will be linked together in the theoretical model to keep the balanced ratio between the different types of buildings within the system.

According to the previously calculated heat loss values, all the parameters are known to calculate the overall heat transfer coefficient number for all type of buildings (K_l value) for design condition, shown in Appendix IV. This parameter is a specific value to describe the building heat loss conditions, representing how much heat is consumed by the building while the outdoor temperature decreases by 1°C:

$$K_l = \frac{Q_{T_des}}{(t_{id_des} - t_{od_des})} \quad (5)$$

where K_l = Overall heat transfer coefficient [kW/°C].

According to the parameters above, for the next step it is necessary to calculate the heat consumption of the building for each case of varying outdoor temperature by:

$$Q = Kl * (t_{id} - t_{od}) \quad (6)$$

where Q = Heat consumption [W].

All of the Kl values related to each building type are listed in Appendix IV.

4.3.3 Heat consumption by the radiator

Most of the district heating systems are using hot water in order to provide heat transfer from the power plant to the heated area. Evidently, total heat loss of the building has to be equal with maximum heat load of the radiators. One of the most important parameters of the system is to calculate the return water temperature from the radiators in design condition. This result describes the quality of the heat market, and determines how much energy is required to keep the heating system circulation. It is also necessary to estimate the volume of the mass flow required for the system. The surface temperature of the radiator is different in each point, as shown in the thermal photo in Figure 10, but for the quantification, it is necessary to assume a fixed value to for further calculations. Equation 7 is used for calculating logarithmic temperature difference on the radiator surface:

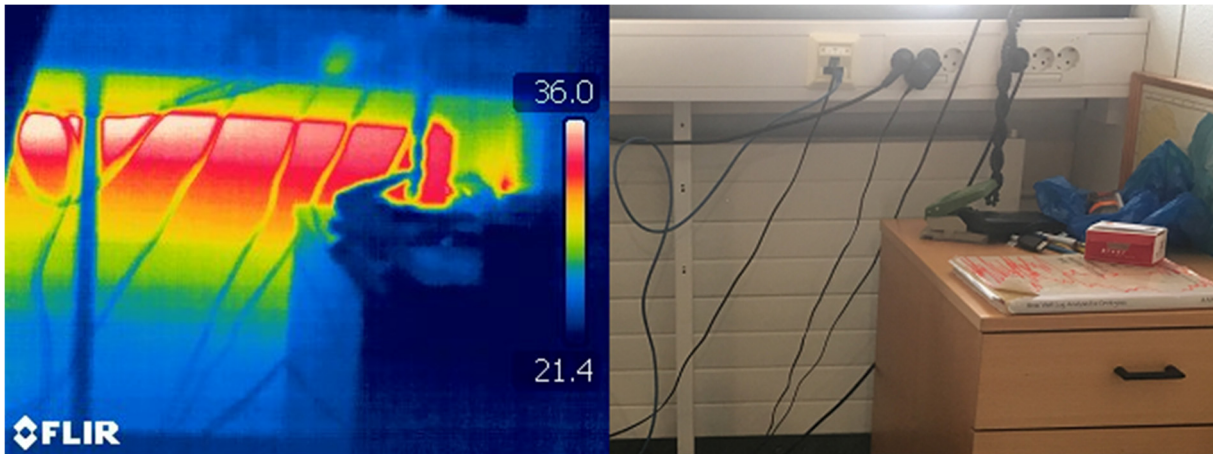


FIGURE 10: Heat consumption values per inhabitant, weighted with the net floor area for 7 different types of examined building (photo taken by Gunnlaugur M. Einarsson, 29/09/2016, ÍSOR, Iceland)

$$\log (\Delta t_{rad_des}) = \frac{(t_{w_su_des} - t_{w_re_des})}{\ln \left[\frac{(t_{w_su_des} - t_{id})}{(t_{w_re_des} - t_{id})} \right]} \quad (7)$$

Total heat consumption consists of not only heat consumed by radiators, tap water heating is also considered as a part of the heat consumption. With the help of Equation 7, radiator heat consumption is known for design conditions for the whole system for each building type (Valdimarsson and Tryggvason, 2005).

Relative heat load of the radiator is calculated according to Equation 8:

$$\frac{\dot{Q}_R}{\dot{Q}_{R-0}} = \left(\frac{\log(\Delta T_{RAD})}{\log(\Delta T_{RAD-0})} \right)^{\frac{4}{3}} \quad (8)$$

where Δt_{RAD-0} = Radiator temperature difference between the supply and return water

Figure 11 shows the temperature of the return water in the function of different building types. The supply temperature was assumed with a constant level for each building (see Figure 14 later). However, building types 2 and 7 have a modern 80/40 and 75/32 heating system, which provides the possibility to utilize better available heat to a lower level. The existing Hungarian district heating systems has a 90°C supply and 70°C return temperature radiators in design conditions, which requires a higher temperature. In that case, the return water is warmer than 60°C in design condition, which makes the system inefficient, furthermore reinjection temperature is also very high, 67.76 °C.

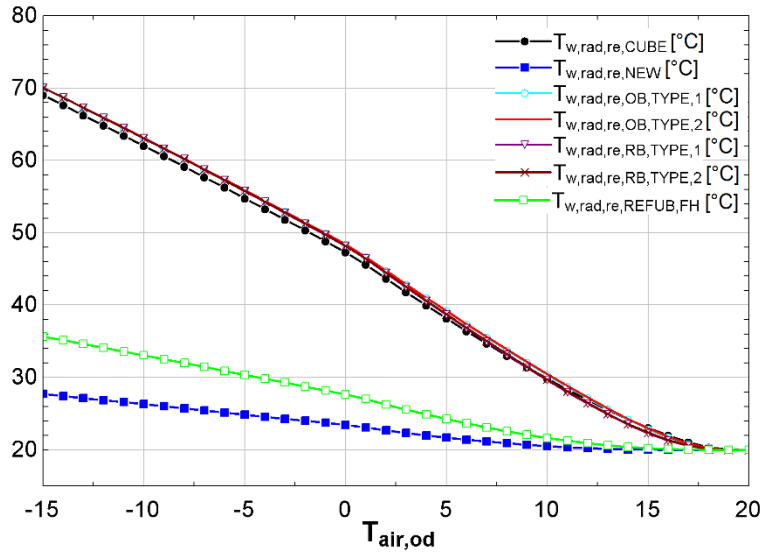


FIGURE 11: Return water temperature from the radiators as a function of different building types in the designed district heating system

In Figure 7, it was shown that the system intermediate, is the temperature, which is available from the geothermal field, considering the heat exchanger, while the system supply is the temperature, which is required by the heat market. The fact of the higher requirement, shown in Figure 12, is simply caused by outdated buildings and secondary circles. To decrease the system supply temperature, two possible scenarios are considered in the further part of this study.

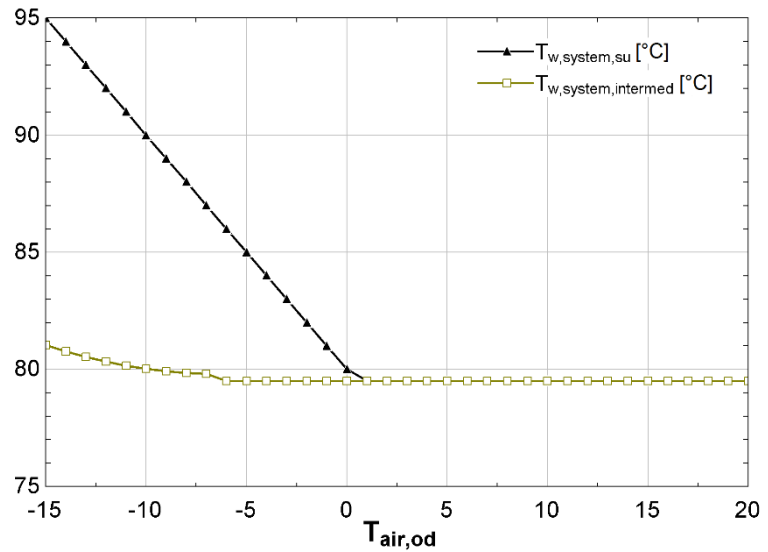


FIGURE 12: Supply and intermediate water temperature of the designed district heating system

4.3.4 Mass flow calculation

Mass flow in the primary circle coming from the geothermal well is assumed at a constant level with 230 l/s, as shown in Figure 13.

In the secondary circle, mass flow is depending on the heat requirements due to the outdoor temperature. Eventually mass flow in the secondary side is also related with conditions of the radiator system. The mass flow is given by Equation 9.

$$\dot{m}_{des} = \frac{\frac{Q_{rad,des}}{cp_w}}{(t_{w,su,des} - t_{w,re,des})} \quad (9)$$

where $\dot{m}_{rad,des}$ = Radiator mass flow (secondary circle) in design condition [kg/s];
 $Q_{rad,des}$ = Heat consumption in design condition [kW];
 cp_w = Specific heat of the water [kJ/kg K];
 $t_{w,su,des}$ = Supply water temperature of the secondary system in design condition [°C];
 $t_{w,re,des}$ = Return water temperature of the secondary system in design condition [°C].

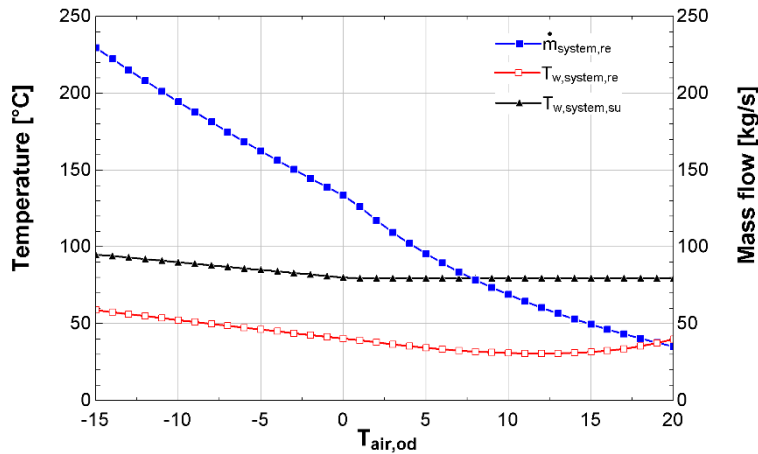


FIGURE 13: Return and supply water temperature as a function of mass flow for designed district heating system

It is also important to take into account the heat loss caused by transmission pipelines. To describe this quality of pipeline, the tau value (τ_{des}) gives a proper value between 0-1, where 1 means a totally insulated pipeline and 0 is a pipe which loses all the heat content of the heating fluid. This parameter of the pipeline bears on the supply and return temperature of the system. If the pipeline heat losses are too high, the system requires higher and higher heat consumption (Valdimarsson and Tryggvason, 2005), as shown through Equation 10:

$$\tau = \tau_{des} \left(\frac{\dot{m}_{rad_des} + \dot{m}_{tap_des}}{\dot{m}_{rad} + \dot{m}_{tap}} \right)^{\frac{4}{3}} \quad (10)$$

- where τ = Heat loss coefficient for a district heating pipeline [%];
 τ_{des} = Heat loss coefficient for district heating pipeline in design condition [%];
 \dot{m}_{rad} = Radiator mass flow (in secondary circle) [kg/s];
 \dot{m}_{tap} = Mass flow for tap water heat (in secondary circle) [kg/S].

Figure 14 shows a schematic drawing of the designed district heating system. Pipeline heat loss was considered only between points 2 and 3/b in Figure 14. The pipeline between the power plant and block building exists, therefore it was assumed with 0.94 pipeline coefficient value (Appendix VIII). In the cases for the rest of the building connections, it was assumed that the existing pipeline has to be extended to link together family houses and new buildings (Appendix VIII) with a 0.96 pipeline coefficient value considering that this is a newly built pipeline, for only a few hundred metres' distance.

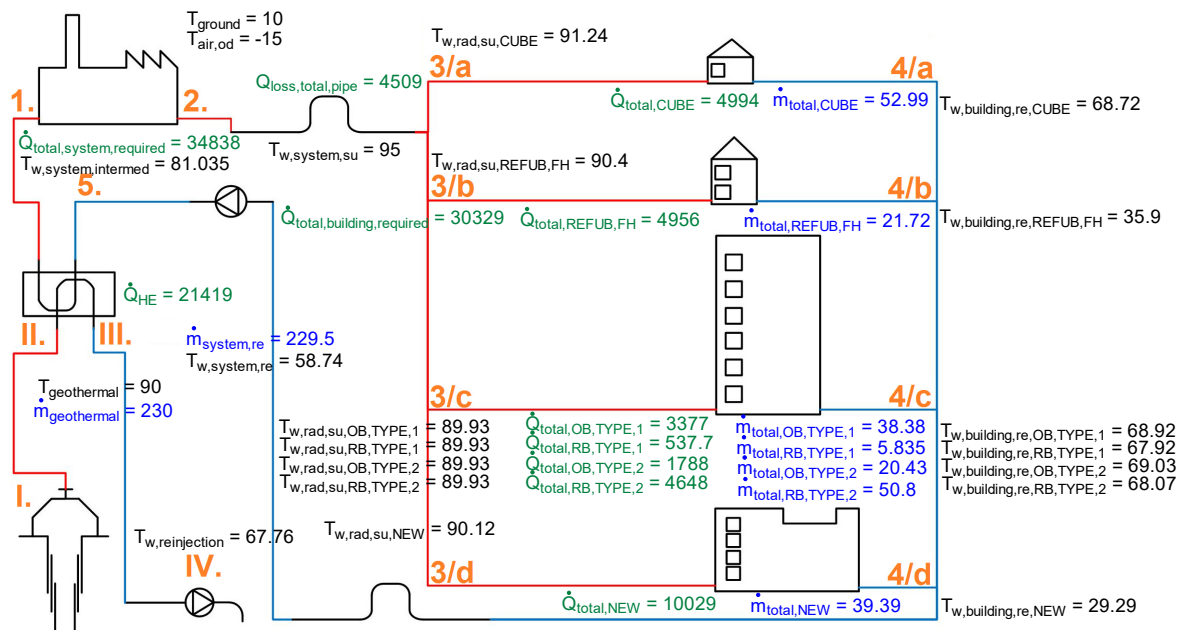


FIGURE 14: Schematic drawing about the designed district heating system

5. RESULTS

The most important result of the examination is that the natural gas boiler could be replaced most of the time within the heating season and it is possible to reduce the total heat consumption of the boiler to 12854 GJ/year. In Figures 15-17, an orange colour triangle shows the necessary heat consumption provided by the boiler within a year. Obviously, tap water heat consumption is considered as a base load during the whole year, according to the usage 0.147 kW/inhabitant, therefore out of the heating season this is the only heat need for the buildings. Return water temperature is 58.74°C and reinjection temperature is also high; 67.76°C. Considering this result, it is possible to design a more efficient system.

Scenario A: “Status quo”

A significant part of the heat market (building types 1, 3 and 5) is badly equipped with high temperature radiators (90/70), which have a relatively small surface. The only assumed modification here is the radiator system work up in building types 1 and 2 because these buildings are not connected to the district heating system now and are usually equipped with a firewood stove. The calculations find that the gas boiler can be replaced in a range of 127-139 days within the heating season, when the outdoor temperature is colder than 0 or -1°C. It means that the geothermal water reduced the usage of the natural gas boiler on average to 55-67 day a year. The system requires a 435.6 TJ thermal output, however, the gas boiler has to run for two months, but 97.05 % of the thermal output provided by geothermal. The utilization provided by the gas boiler is marked with an orange colour triangle (shown in Figure 15). This scenario is mainly a theoretical solution (Figure 15), because the significant number of out-dated buildings (such as types 1, 3 and 5) makes the system inefficient.

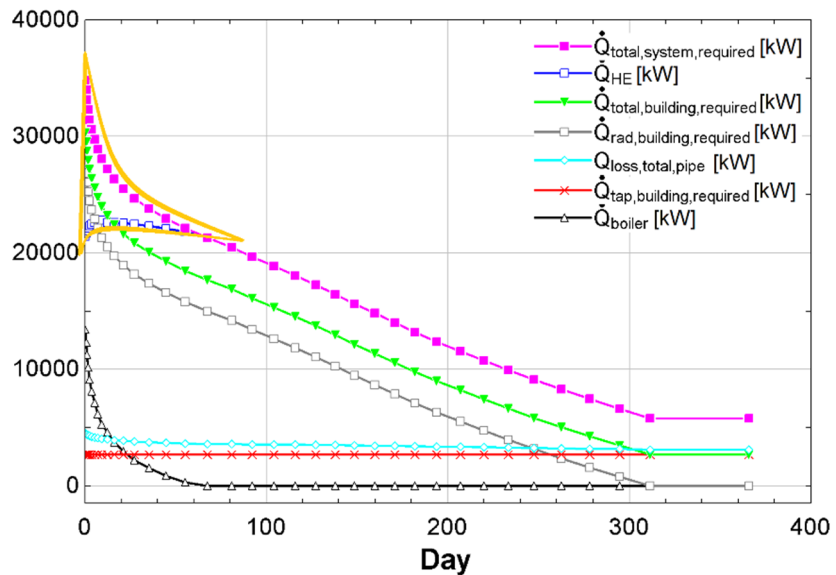


FIGURE 15: The most important heat consumption results of the designed district heating system in case of Scenario A

Scenario B: “Radiator replacement”

According to previous calculations, it was seen that the size of the radiator is the crucial element of the system. In the second case it is assumed that only the radiators will be replaced in out-dated buildings (building types 1, 3, and 5), and also in refurbished block buildings (building types 4 and 6) by installing 80/40 radiators with a bigger surface. In that case, the system requires only 391.2 TJ thermal output, with a very similar renewable/fossil fuel ratio as Scenario A assumes, or 97.98% geothermal and 2.02% natural gas usage. Gas boiler usage is marked with orange colour triangle (see Figure 16.), representing a lower area than in the case of Scenario A. This case assumes that the natural gas boiler is necessary for only 44 days in a year. This reconstruction requires a relatively low expenditure and manpower, considering that the recorded total energy consumption it saves is around 8-10%.

Scenario C: “Complex refurbishment”

This alternative assumes full refurbishment, including additional insulation, replacement of the windows, doors, radiators and reconstruction of the roof area. More specifically; building type 1 is developed similarly to type 2, building type 3 is developed similarly to type 4, and type 5 is developed similarly to type 6. It requires refurbishing 280 houses from building type 1, seven buildings from type 3 and five buildings from type 5, which represents almost the half of the heat market (104,087 net m²) in floor area. In this case (Figure 17), the system requires only 345.8 TJ thermal output, which is significant 17-19% savings compared with Scenario A (in system level). The ratio between renewable and fossil fuel is very similar to the previous two cases; 97.93% geothermal and 2.07% natural gas usage.

According to the final results (shown in Table 5) in my opinion, Scenario-C is the most perspective way to design an efficient geothermal district heating system in Debrecen with the existing block buildings to replace a significant part from the currently used natural gas resource.

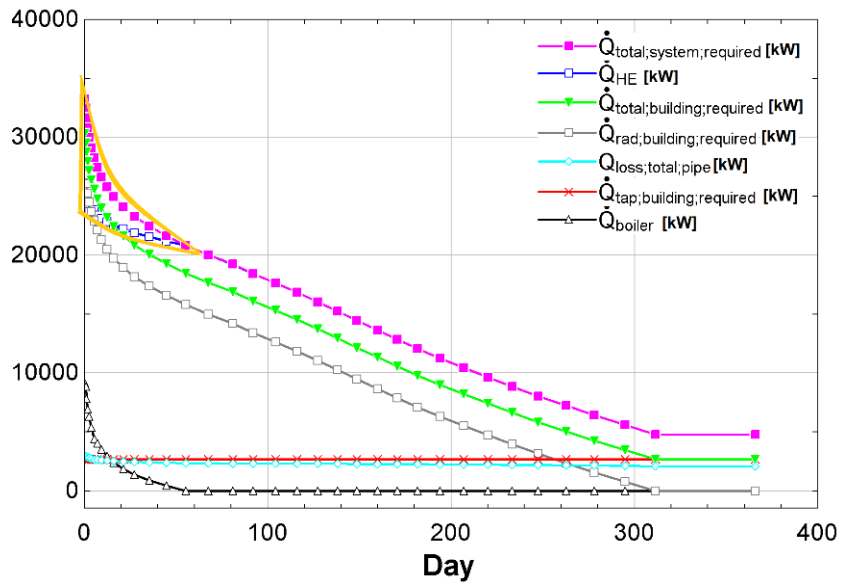


FIGURE 16: The most important heat consumption results of the designed district heating system in case of Scenario-B

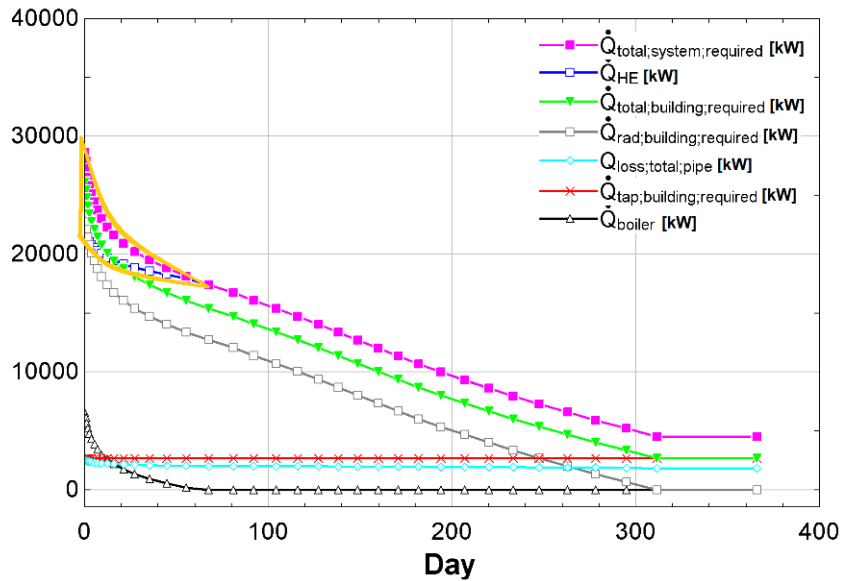


FIGURE 17: The most important heat consumption results of the designed district heating system in case of Scenario-C

TABLE 5: Comparison of the final results for the possible contribution of geothermal energy

	Geothermal energy			Gas boiler		Total system consumption
	[TJ]	[%]	Saved natural gas [m ³]	[TJ]	[%]	[TJ]
Scenario A	422.8	97.05	111,252	12.854	2.95	435.6
Scenario B	391.2	97.98	102,957	8.068	2.02	399.3
Scenario C	345.8	97.93	91,007	7.324	2.07	353.1

6. CONCLUSION

1. It has been established that the potentially available, relatively low-temperature geothermal water is more than enough to replace a significant part of the installed thermal capacity of the natural gas fired district heating power plant.
2. The limited possibilities of using geothermal water with high temperatures require paying special attention to the heat market facilities to organise an effective system.
3. Only the replacement of the old radiators could decrease the system heat consumption itself. Larger radiators do not require a high supply water temperature, which is not common in Hungary.
4. Complex building rehabilitation is the best way to combine with geothermal energy, which causes significantly lower heat consumption and a lower radiator supply temperature.
5. Considering the current energy production running with natural gas cogeneration in Debrecen, the replacement of the thermal capacity could cause a significantly lower efficiency of natural gas based electricity production. It is worth considering to replace all the fossil fuel based energy production (thermal and electricity production as well), not only the thermal output part.

ACKNOWLEDGEMENTS

I would like to express my gratitude to my supervisor Prof. Dr. Páll Valdimarsson to provide a professional guidance during the project period. Special thanks to my employer to the Ministry of National Development for granting me the opportunity to be a fellow in this excellent programme.

Last but not least, I would also like to extend my deeply grateful to the Government of Iceland, all of the staff of United Nations University Geothermal Training Programme, and especially to Mr. Lúdvík S. Georgsson who has spent unbelievable work to this program and become the “father” of the UNU-GTP family in the last decades.

REFERENCES

- Baumann, M., 2012: *Building energy*. Széchenyi Terv and Edutus College, European Union Project TAMOP-4.1.2.A/2-10/1 (in Hungarian), 178 pp.
- Csoknyai, T., Hrabovszky-Horváth, S., Seprődi-Egeresi, M., and Szendrő, G., 2014: *National typology of residential buildings in Hungary*. EU Episcopo / Tabula report, 90 pp.
- European Commission, 2015: *EU energy in figures. Statistical pocketbook 2015*. Publications Office of the European Union, 268 pp.
- ÉMI Non-Profit Ltd., 2015: *National building energy performance strategy*. Commissioned by the Ministry of National Development, Hungary, 96 pp.
- Hegedűs, M. (ed), 2005: *The Hungarian district heating sector*. GKI Energy Research and Consulting Ltd., Budapest, Hungary, 54 pp.
- Horváth, F., Musitz, B., Balázs, A., Végh, A., Uhrine, A., Nádor, A., Koroknai, B., Pap, N., Tóth, T., and Wórum, G., 2013: Evolution of the Pannonian basin and its geothermal resources. *Geothermics*, 53, 328-352.

Hrabovszky-Horváth, S., 2015: *The climate strategy aspects of the energy efficient refurbishment of precast concrete buildings*. Budapest University of Technology and Economics, Depmt. of Building Constructions, English summary of PhD thesis, 15 pp.

Hungarian Central Statistical Office, 2013: *Population census 2011. Country wide data*. Hungarian Central Statistical Office, Budapest, Hungary, 276 pp.

MEKH, 2014: *Statistical data of the Hungarian district heated sector*. Hungarian Energy and Public Utility Regulatory Authority (MEKH).

OMSZ, 2016: *Climate data 1901-2010*. OMSZ - Hungarian Meteorology Service, webpage: www.met.hu/eghajlat/magyarorszag_eghajlata/eghajlati_adatsorok/

Karlsson, Th., 1982: *Geothermal district heating. The Iceland experience*. UNU-GTP, Iceland, report 4, 116 pp.

Kozák, M., and Mikó, L., 2004: Possibilities of utilising geothermal energy in eastern Hungary. In: Cirsí, A., and Baros, Z. (ed.), *Researching and utilising renewable energy in the North Hungarian Plain region*. Hungarian Wind Energy Association, publication no. 2 (in Hungarian), 11-19.

Lund, J.W., and Boyd, T.L., 2015: Direct utilization of geothermal energy 2015. Worldwide review. *Proceedings of the World Geothermal Congress 2015, Melbourne, Australia*, 31 pp.

MIHŐ, Ltd., 2016: *District heating explanation*. Miskolci Hőszolgáltató, Ltd., Miskolc City, Hungary, webpage: www.miho.hu/tavfutesi-rendszer-mukodese-0.

Szirmai, R., 1976: *Prefabricated concrete panel block residential buildings specific catalogue*. Ministry of Construction and Urban Development, Budapest, Hungary, Chapter 3 (in Hungarian), 23.

Nádor, A., Tóth, A.N., Kujbus, A., and Ádam, B., 2013: Geothermal energy use, country update for Hungary. *European Geothermal Congress 2013, Pisa, Italy*, 12 pp.

Soltész, I., 2008: *Detailed methodological guidance for building elements audit*. Ministry of National Development and Economy, Budapest, Hungary, 14 pp.

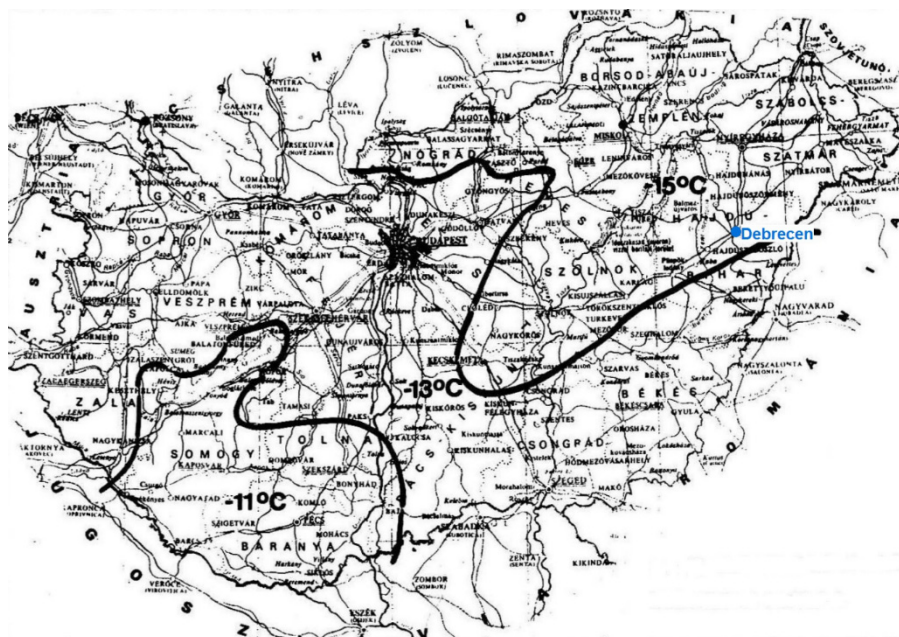
Tóth, A.N., 2015: Hungarian country update 2010-2014. *Proceedings of the World Geothermal Congress 2015, Melbourne, Australia*, 8 pp.

Új Lakás Debrecen, 2016: *Newly built apartments in the centre of Debrecen, a 22 unit condominium – First floor plan*. Webpage: ujlakasdebrecen.hu/belvarosi-22-lakasos-uj-epitesu-tarsashaz/

Valdimarsson, P., and Tryggvason, G., 2005: Influence of cogeneration on the efficiency of geothermal utilization. *Proceedings of Geothermal Practice Symposium Rheinland-Pfalz, Ministry of Economics, Transport, Agriculture And Viticulture of Rheinland-Pfalz, Mainz, Germany*, 16 pp.

Zsebik, A., 2004: *Network energy resources - district heating. University guidebook*. Budapest University of Technology and Economics, Budapest, Hungary, 71 pp.

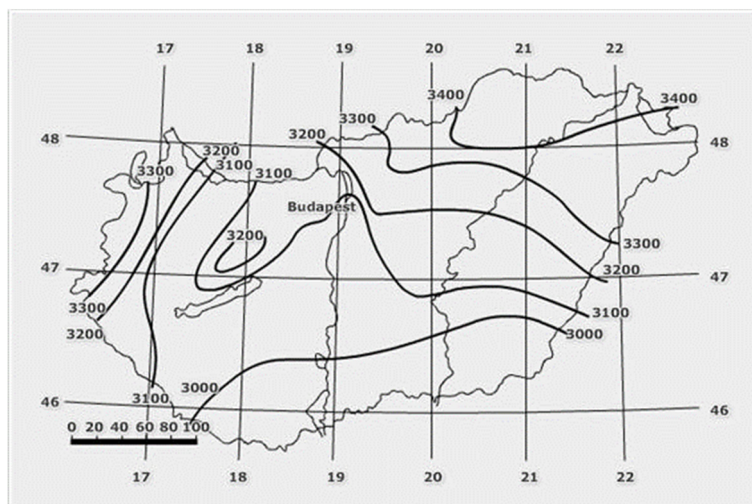
**APPENDIX I: Hungarian standard on regional required outdoor design temperature
(Standard Number: MSZ-04-140/3-87)**



**APPENDIX II: Lowest mean daily temperature records of Debrecen (1960-2010)
(OMSZ, 2016)**

Mean daily temperature [°C]		Date			Mean daily temperature [°C]		Date		
-15.1	17	January	1964		-17.0	19	January	1964	
-15.2	8	January	1985		-17.1	22	January	1964	
-15.4	10	February	2005		-17.2	19	January	1982	
-15.5	12	February	1985		-17.5	13	January	1987	
-15.8	17	January	1982		-17.5	21	January	1964	
-16.4	24	January	1963		-17.9	17	January	1963	
-16.7	18	January	1982		-18.4	18	January	1963	
-16.8	14	January	1982		-19.2	13	January	1964	

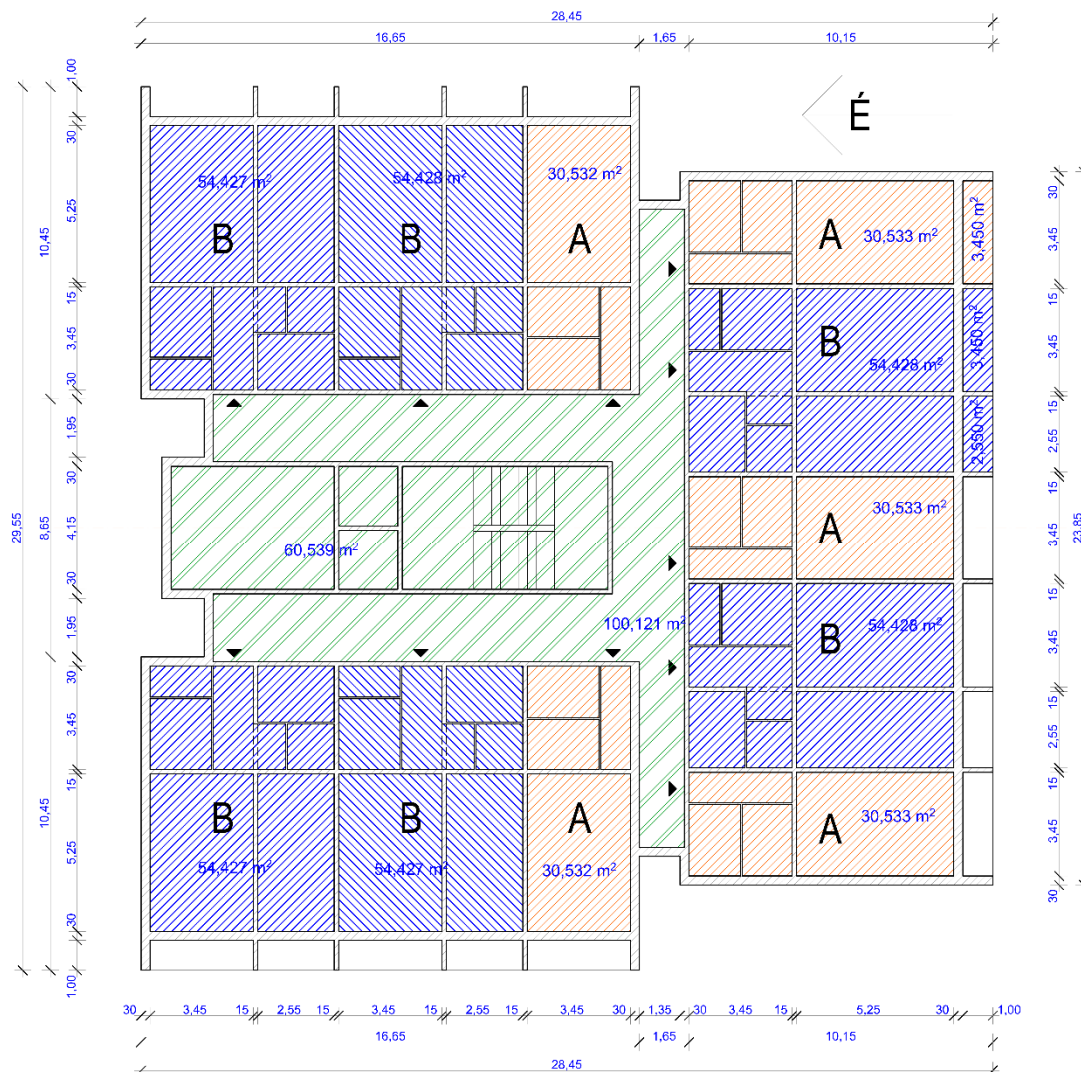
APPENDIX III: Degree days curves of Hungary (Baumann, 2012)



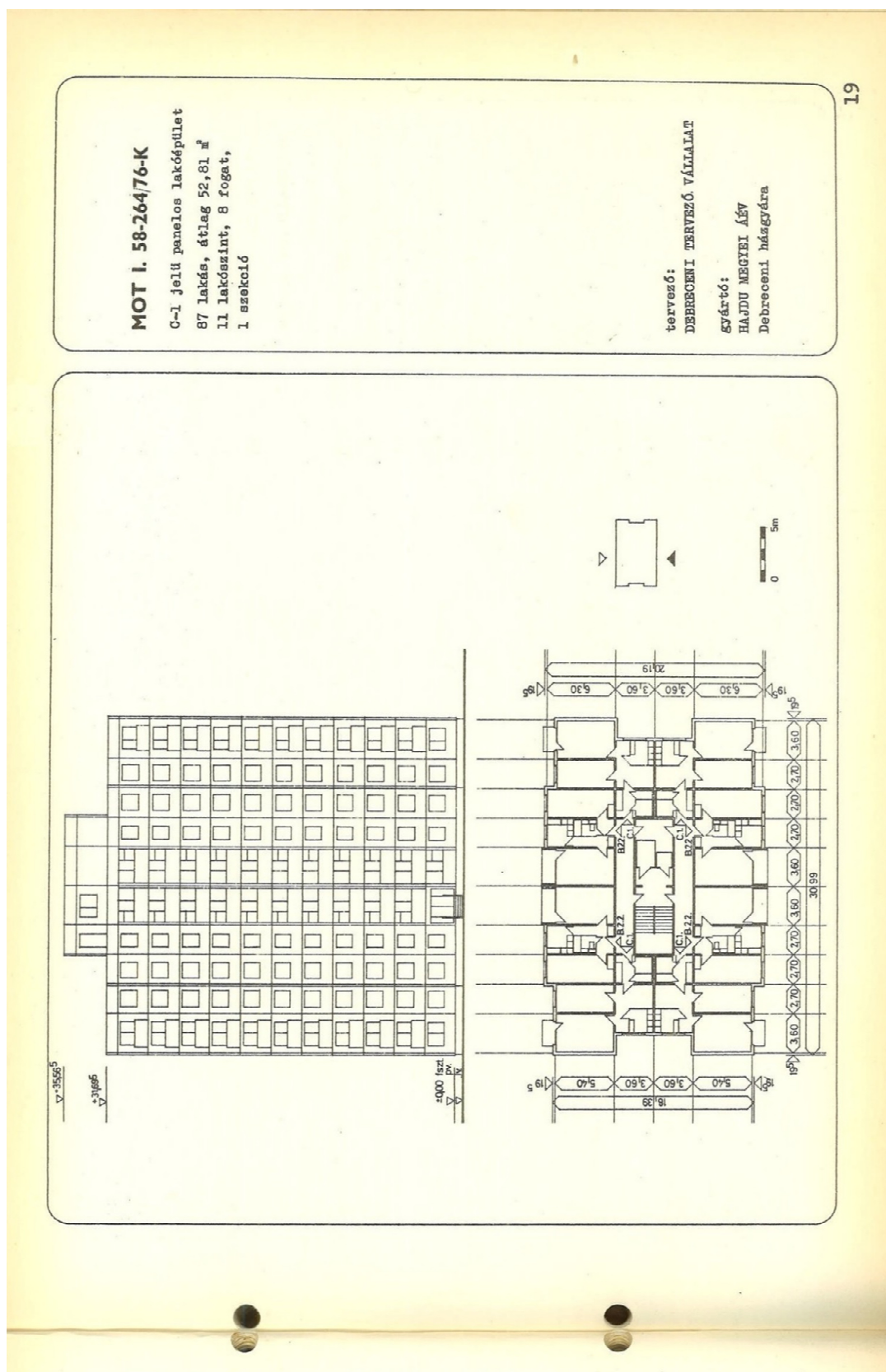
APPENDIX IV: Summary table for the most important parameters and results for different building types

	Parameter	1. Old Hungarian "Cube" house	2. Refurbished family house	3. Old block building type P100	4. Refur. block build. type P100	5. Old block building, type C-1	6. Refur. block building, type C-1	7. New apartment house
0	Pipeline heatloss coefficient	0.96	0.96	0.94	0.94	0.94	0.94	0.96
1	Gross area [m2]	100	200	9750	9750	6366	6366	1928
2	Net area [m2]	100	200	7341	7341	4940	4940	1652
3	Inhabitant/unit	3	4	294	294	198	198	56
4	K1 value [kW]	0.4978	0.3055	12.547	6.446	9.384	4.702	1.969
5	Transmission heat loss/unit	14.461	6.234	240.153	66.435	194.61	57.518	35.693
6	Transmission heat loss/inhabitant	4.820	1.559	0.817	0.226	0.983	0.290	0.637
7	Filtration heat loss/unit	2.964	4.458	198.982	159.185	133.836	107.068	33.21
8	Filtration heat loss/inhabitant	0.988	1.115	0.677	0.541	0.676	0.541	0.593
9	Radiator design consumption/unit [kW]	17.425	10.692	439.135	225.62	328.446	164.586	68.903
10	Tap water consumption/ unit [kW]	0.441	0.588	43.218	43.218	29.106	29.106	8.232
11	Tap water constant/inhabitant [kW]	0.147	0.147	0.147	0.147	0.147	0.147	0.147
12	10+11 [kW]	17.87	11.28	482.35	268.84	357.55	193.69	77.14
13	Heating system design parameters [°C]	90/70	80/40	90/70	90/70	90/70	90/70	75/32
14	Heat consumption in design condition/ person [kW]	5.96	2.82	1.64	0.91	1.81	0.98	1.38
15	Heat consumption in design condition/square metre [kW]	0.179	0.056	0.066	0.037	0.072	0.039	0.047
16	Number of inhabitants in the system	840	1760	2058	588	990	4752	7280
17	Heat consumption of the building group in design consumption [MW]	5.002	4.963	3.376	0.538	1.788	4.649	10.028
18	Number of buildings in linked to the system	280	440	7	2	5	24	130
19	K 1 value / m ²	4.98	1.53	1.71	0.88	1.90	0.95	1.19
20	Size of system [MW]	9.97		10.35				10.03
21	Heated floor area [m2]	116000		209329				214760
22	Number of inhabitants	2600		8388				7280

APPENDIX V: Floor map of type P100 prefabricated concrete panel block building
(Hrabovszky-Horváth, 2015)



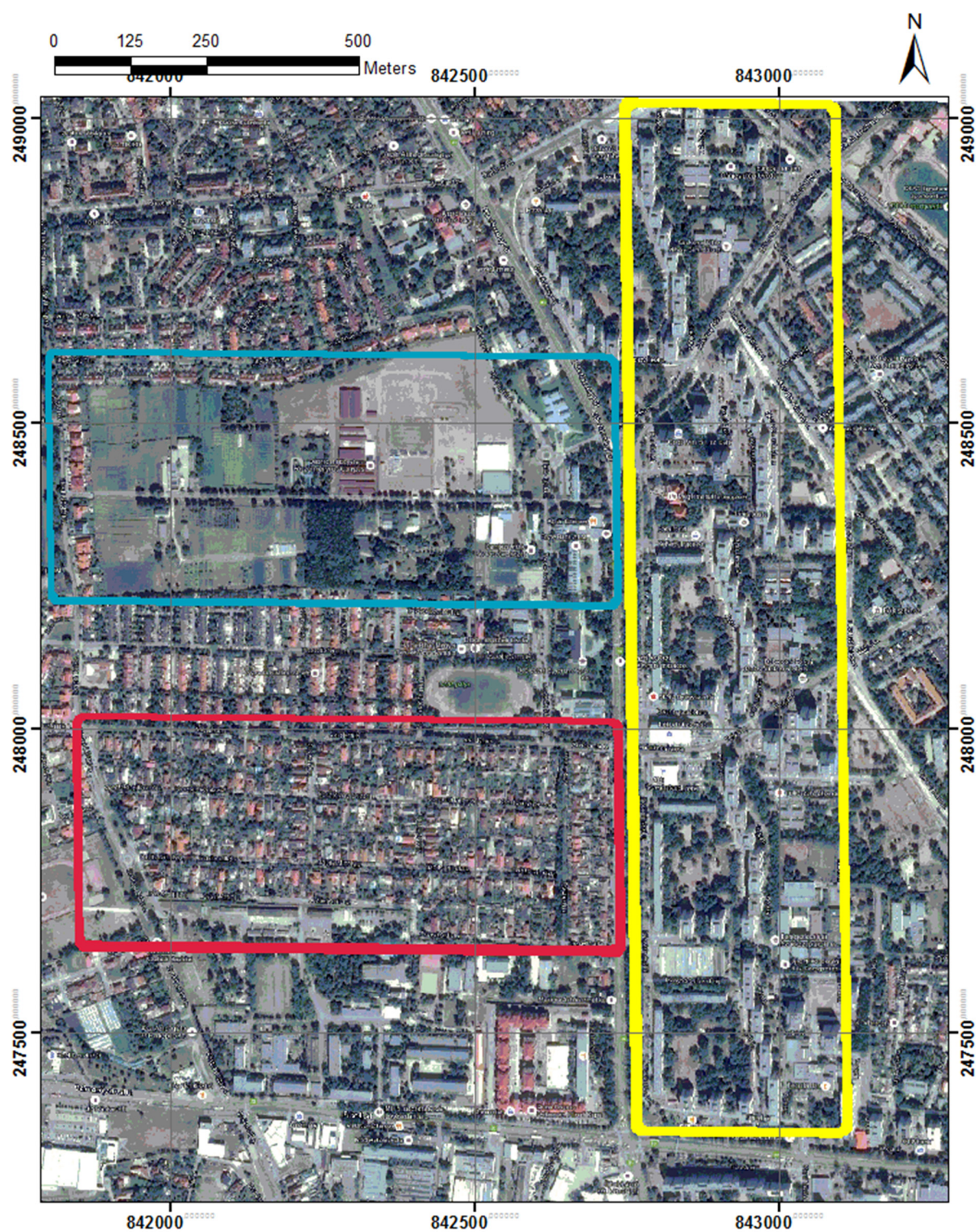
APPENDIX VI: Floor map of type MOT I. 58-264/76-K C-1 prefabricated concrete panel block building (Szirmai, 1976)



**APPENDIX VII: Floor map of newly designed apartment building in Hatvan street 62,
Debrecen (Új Lakás Debrecen, 2016)**



APPENDIX VIII: Location map for the examined area in Debrecen
drawn with background from Google Earth (2016)





UNITED NATIONS
UNIVERSITY

UNU-GTP

Geothermal Training Programme

Orkustofnun, Grensasvegur 9,
IS-108 Reykjavik, Iceland

Reports 2016
Number 12

FOSTERING GEOTHERMAL DEVELOPMENT IN HUNGARY: OPPORTUNITIES AND BOTTLENECKS

Kristof Boda

Ministry of National Development
Department of Renewable Energy
Fő Street 44-50
Budapest 1011
HUNGARY
kristofboda@gmail.com

ABSTRACT

Hungary has very good geothermal prospects and the use of geothermal energy has a long history in district heating, agricultural and balneology utilizations. After Turkey, Iceland and Italy, the country was ranked in 4th place regarding installed geothermal direct use in Europe in 2015. Geothermal resources are providing constant energy output, which is independent from weather conditions and time, utilize safe technology, which does not endanger human life and evades the possibility of huge human and environmental catastrophes, as well as having a lower carbon footprint than most other renewable energy utilizations. Therefore, geothermal energy is suitable for reaching various environmental and energy efficiency aims, energy policy targets, and also to reduce fossil energy dependency.

Hungary has very ambitious geothermal energy utilization targets to fulfil the country's EU 2020 aims, which require fast and effective development of geothermal utilization policies and projects. There are several EU and nationally supported projects, however private investors seem to be waiting to enter the Hungarian geothermal market and the number of new project inquiries has been decreasing since 2011. Therefore, strengthening of geothermal energy policy and related procedures could be a useful asset and toolkit for better enabling new investors to enter the market and help fulfilling the 2020 geothermal energy targets. Support for geothermal exploration and revision of the legislative, financial and policy interfaces and interplay of the institutional, legislative and business environment of geothermal projects in order to remove bottlenecks can have a crucial role in strengthening exiting opportunities and in reducing the barriers of future geothermal development.

In this report, current status of the Hungarian institutional, legislative and business environments related to geothermal energy utilization are analysed and evaluated from the investor perspective. Relevant good international practices are incorporated, as well as practical experiences of the first geothermal electricity-producing project of Hungary, which is expected to be online in July 2017. This should provide development recommendations and enable better geothermal development in Hungary. The report draws conclusions concerning the policy and regulatory framework, which is essential and needed to promote geothermal development.

1. INTRODUCTION

Hungary has very good geothermal prospects and internationally famous geothermal resources. The utilization of geothermal energy has a long history and several spas, medicinal waters, balneology and agricultural and district heating facilities are in use, reflecting the mostly low-temperature geothermal resources. Geothermal energy utilization has accelerated since the political transformation of 1989 mainly by spa and district heating projects and in 2015 Hungary was ranked 4th in Europe among countries utilizing most geothermal heat, after Turkey, Iceland and Italy. Geothermal development is part of Hungary's *National Renewable Energy Strategy* and has a share in fulfilling the country's 2020 EU development aims. Geothermal development is backed up by the European Economic Area (EEA), EU and national supporting schemes. During last decade, large-scale district heating systems were built and old ones were reconstructed, as well as a new EGS project being started. The year 2017 is expected to be a milestone in the history of geothermal development in Hungary, as the first geothermal energy power plant, which is also to produce electricity besides heat, will go online in July 2017.

The number of inquiries to launch new geothermal projects has increased steadily during the last decades, even during the time of the economic crisis in 2008. Hungary has no specific geothermal development strategy, but geothermal is included into the country's energy policy targets and there is a significant amount of regulations and legislation governing geothermal utilizations. Separate energy- and network operators, as well as mining-, water- and environmental authorities are responsible for permitting and licensing geothermal energy utilization projects. The number of new geothermal project inquiries has, however, been decreasing since 2013, state concessions for the utilization of deep geothermal (below 2500 m) are not advertised and not expected to start soon. Most of the geothermal projects to be implemented are either EU demonstration projects or highly subsidized projects, supported by EU or other grants. Private or public investors seem to be waiting and collecting information to introduce new projects. The institutional, legal and regulatory frameworks addressing geothermal development is constructed from a complicated set of rules that developers must follow through the development of their projects. These laws and regulations may present themselves as barriers or enabling factors to development (Kujbus, 2016; Tóth, 2010).

This research aims to provide a picture of the current status of geothermal energy production and utilization in Hungary and also to explore how Hungarian geothermal development environment can be developed and recommendations provided to better enable and foster geothermal development based on the experiences of international geothermal development facilities. The research target is reached by analysing international good practices and examples of geothermal development and apply this practice to the current Hungarian geothermal development environment. The goal is to learn from the outcomes and experience of the implementation of the first geothermal electricity power plant project of Hungary. Therefore, based on international and current Hungarian geothermal policy practices and the first Hungarian geothermal electricity and heat power plant project, this research will point out the bottlenecks and enabling factors of geothermal development in Hungary. This will be done through analysing the policy interfaces between the financial, institutional and legislative environments and creating a set of recommendations for policy and decision makers, which are responsible for geothermal development, in order to foster geothermal energy development in Hungary.

2. GEOTHERMAL DEVELOPMENT ENVIRONMENT – INTERNATIONAL EXPERIENCES AND GOOD PRACTICES

For most investments, including geothermal energy development projects, the main deciding factors about where and when to invest are the credibility, transparency, consistency and simplicity of relevant legislations. To this can be added existing institutional policies and practices, the availability of project related information, technical and financial support schemes, risk mitigation tools for project

development support, the amount of time needed for project implementation, which depends on many multiple factors, and the possible profitability of the investment.

Geothermal energy resources have been identified in over 90 countries and are utilized in 78 (Lund and Boyd, 2015) and geothermal electricity is generated in 24 countries (Bertani, 2015). Most countries utilizing geothermal resources have ambitious and specialized agendas for further geothermal energy development. Kenya plans to increase its electricity production from geothermal resources, from 590 MWe in 2015 to 5000 MWe until 2030 through its Kenya Vision 2030 strategy. Many other countries in East Africa and Europe (Iceland, Turkey, Germany, Italy, Austria, Netherlands, Switzerland, France, Slovakia, Slovenia, Croatia and Hungary) are planning increased geothermal development (Georgsson, 2016; Micale et al, 2015; Transenergy, 2011; Nádor, 2013). For European Union member states, the EU requires a certain increase in both renewable energy production and consumption and the introduction of related policies and planning (National Energy Efficiency Action Plans – NREAPs) in order to fulfil the policy aims of the Renewable Energy Directive (RED).

National agendas for geothermal development usually consist of various elements including geothermal resource related research and development. This includes supportive policies towards geothermal field development, institutional, legislative and regulatory framework, licensing and permitting procedures, commercially available financial sources or international and national financial supporting schemes and loans, sometimes even with state endorsement, insurance, risk mitigation tools and technical assistance as well as transparent, competitive and non-discriminatory procedures. Together these form a country specific development environment for geothermal projects and at the same time also become the main measures and tools for policy making to better enable geothermal development.

There are significant differences in the approach and practice of countries towards applying these elements in practice. These differences originate from and reflect the specific geothermal properties and country specific needs. However, there are some conditions that most countries successful in geothermal development have in common, such as:

- Clear cut, streamlined and specialized legislation: a single geothermal law, establishing the basis of geothermal developments and creation of a legislative framework reflecting geothermal needs but also ensuring environmental perspectives, the ownership and possible interference of reservoirs;
- Straightforward licensing procedures;
- One agency or institution responsible for licensing and permitting the investment and for geothermal development – an energy agency;
- Available public geothermal subsurface datasets;
- Effective financing and risk mitigation schemes: financing and insurance schemes reflecting the special needs of geothermal investments;
- Strong interaction between geothermal research, financial schemes and policymaking;
- Continuous transfer of knowledge and information between the various state actors and strong institutional capacity building;
- Available geothermal information for the public, awareness raising;
- Thoughtful and consistent national geothermal policy for the creation of legislative and institutional frameworks.

2.1 Geothermal legislation

Governments can provide support to geothermal project developers in various ways. This can be done through policies, programmes and legislation, institutional structures and streamlined administrative procedures, increasing the consistency of legislations, providing geothermal data and financial support, financial and risk insurance schemes or technical assistance.

2.1.1 Complexity of legislation

Geothermal energy utilizations are usually regulated by a set of legislations. The consistency, emphasis and simplicity of these legislations are crucial factors in the implementation of geothermal development. A supportive and enabling legislation, which is concise, simple and does not have numerous additional regulations, is a key factor for creating a solid foundation for geothermal development, thus encouraging greatly development.

In numerous countries (Germany, France, Hungary, Romania, Switzerland), geothermal energy is regulated by several separate legislations, mining law, water management law, environmental law, concession law and other related regulations and additional rules (France – Decree 77-620 – Low temperature geothermal deposits, Rybach. 2003; Transenergy 2011, Geothermal ERANET, 2013). These legislative areas are targeted for their respective areas, so a mining law is more focused on utilization of underground resources, while the water management law is more focused on preservation of surface and underground waters. The different scopes of these legislative areas often result in contradictions between each other and cause inconsistency in licensing and other procedures related to project implementation. Also, the separate legislative areas then usually belong to different administrative bodies or authorities, which will have different views and interests, as well as separate and independent procedures. This might cause inconsistencies in licensing and permitting procedures, resulting in loss of time and the need to cooperate with multiple authorities (Geothermal ERANET, 2013, Fraser / Geoelec 2013).

In numerous countries, a specific geothermal law or complete legislation has been introduced such as in Iceland, many African and Central Asian countries and in the US. The aim of these regulations are to provide one concise framework for the regulation, licensing, permitting and all other bureaucratic procedures, related conditions, deadlines, participating authorities, which then serves as the legal basis and guideline for all stakeholders of the development to evade time consuming and repeated procedures.

Haraldsson (2012) states that there is a great diversity of definitions of geothermal resources and geothermal energy between different countries. Several international studies show that these definitions are the underpinnings of legislative and regulatory frameworks for geothermal development (Geothermal ERANET 2013, Transenergy 2011, Haraldsson 2012). It is of primary importance that they are clearly cut. The diversity of legislative aspects may be seen as a barrier for national or international geothermal developers who need to get acquainted with the different legislative frameworks. According to Haraldsson (2012), regulatory frameworks of various countries should be consistent, so developers do not have to adjust to new legislations when operating in different countries.

Another aspect of consistency of legislative frameworks is that legislations are made of several rules, procedures and laws of a certain country. As developers must follow the legislations of the country they operate in, the consistency within the national frameworks and the complexity of regulations are also influencing factors. The importance of consistency and clearness within a single regulatory framework and between administrative procedures cannot be underestimated as a concise and optimised set of legislation and transparent procedures can make the difference if a certain development can start.

In some countries, geothermal development has its separate legislation, which is often a single geothermal act. This legislative structure certainly has its advantages for collecting all related information and regulations about the conditions of a geothermal development. So investors or administrative bodies have a reference point and can act accordingly, which creates a business situation where decision-making can be more efficient, providing crucial benefits for launching and monitoring geothermal projects (Fraser, 2013).

Appendix I presents an excerpt from the Transenergy (2011) research, showing the number of laws and regulations related to geothermal energy in Hungary and Slovakia for comparison.

2.1.2 Resource and reservoir ownership

An important element of legislation and institutional practice is how the ownership of a geothermal reservoir is regulated and how it is ensured that new projects do not interfere with or endanger the productivity of other projects in the same area. In most countries, geothermal energy belongs to the state. This is the case in Germany, France, Netherlands, Slovakia, Slovenia, Austria, Romania, Hungary (Rybach, 2003, Transenergy 2011, Századvég Gazdaságkutató Zrt, 2013) as well as on most other continents, even if the utilization area is owned by a private entity. After the state and the owner or the investor, who made a contract with the landowner, has started geothermal energy production, it is of crucial importance that other new geothermal projects do not influence the existing ones. A straightforward and clear definition of the reservoir and a regulation for entering new users creates an opportunity for the prevention of cross influence or interference between projects. This is crucial when initiating new projects and highlights the need for straightforward definition of the reservoir and legal guarantees, as the land owned does not necessarily cover the area of the reservoir.

It is important that the definition of resource ownership and the role of relevant geothermal institutions be efficient and capable. The legislative and administrative practices of most EU countries show that this question is either not or only partially solved. According to the general practice (Geothermal ERANET, 2013), the new investor needs to prove by an Environmental Impact Study and reservoir model of the new investment that it is not interfering with other projects. This methodology passes the main responsibility to the firm preparing the EIA and relies on the knowledge and information of the permitting authority, as the authority has to check and accept the results and grant the permissions for the new project. If any actor makes a mistake causing interference, the question will arise of who has to bear the responsibility for the damages.

One possible solution to prevent and resolve conflicts between projects is the development of institutional capacity, so decision makers are able to evaluate geothermal data, which is backed up by reliable geothermal information. This needs to be backed up by a straightforward definition of resource ownership and clearly defined reservoir boundaries. A unique solution to this question was implemented in Iceland. The territory of the country was divided into five bigger areas, which have been awarded to single investors (energy companies) to carry out research, exploration and utilization of energy. ÍSOR - Iceland GeoSurvey had prepared 3D models of the areas, which served dual purpose: by using the 3D models, it was possible to estimate the productivity of the geothermal fields, which was needed to effectively advertise the concessions, and also to make it possible to prevent interference of projects (Orkustofnun, 2016). Therefore, geothermal developers have useful and reliable information about the prospects of the planned investment (possible energy output) as well as being ensured that new projects do not interfere with the old ones.

2.2 Institutional arrangements

The institutional frameworks for development of geothermal resources show a great diversity across countries. However, two main paths can be identified, with different levels of complexity or clarity.

In some countries' policies (Germany, France, Netherlands, Austria, Slovakia), licensing procedures, permitting and financial support related to geothermal utilization are overseen by several different institutions or authorities, such as the mining office, environmental authority, water directorates, building authorities and municipalities. For this approach to work, responsibilities and knowledge of the different institutions must be ensured by very transparent and concise legislation and bureaucratic procedures. In order to overcome the challenge of multiple authorizing entities, in many states a national authority for energy or specifically for geothermal energy development, either a company or a single institution, has been appointed or founded ("a champion"). Thus, geothermal development related issues are brought together and supervised by one institution. In many countries, among them the USA (EPA), Iceland (Orkustofnun) and El Salvador (LaGeo), this authority, agency or ministry is the only authority

in charge of geothermal energy development. It evaluates applications for geothermal utilizations, issues licenses and permissions and their experts also oversee the conduction of works. Ethiopia, the US, Iceland, Germany, Austria are a few of the countries where either a National Energy Agencies was founded and put in charge of researching, licensing and permitting geothermal facilities, or dedicated geothermal authorities were created (Geothermal ERANET, 2013; Fraser / Geoelec, 2013; Orkustofnun, 2016; Nador, 2013; and Montalvo, 2014).

By this methodology and division between institutions, the legislative, regulatory, permitting, licensing, utilization and operational/energy production rules are kept in one house, so the flow of information and knowledge for shaping the legislation is not fragmented and individual institutional interests have less influence on the procedures. Consequently, the fulfilment of other overall development aims such as protection of the environment could be endangered. But this is prevented as environmental impacts, procurements, tendering and many other development aspects are strictly regulated by national laws that are applied to energy development and the geothermal authority has to act accordingly as is being done in the US, Iceland or the Philippines (Gehring and Loksha, 2012; Orkustofnun, 2016).

If such an institution or national authority is responsible for all energy related development, the knowhow and good practices of various renewable energy solutions are more likely to be transferred between different institutional departments and more knowledge can be collected to form suitable legislations and administrative procedures. The quality of decisions will be increased so that failures or administrative hurdles are reduced.

A unique example of institutional cohesion and clear cut regulatory framework can be observed in Iceland, where Orkustofnun - the National Energy Agency has been appointed as the leader of energy development, as described in Section 2.2.1. The building where Orkustofnun is located also hosts other geothermal energy related institutions, such as ÍSOR – Iceland GeoSurvey and the United Nations University Geothermal Training Programme (UNU-GTP), ensuring the continuous flow of information and know-how between the geothermal actors.

In countries where legislations and institutions are fractured, the areas of responsibilities and procedures are more complex to adjust and the flow of information is more limited. The developers often need to negotiate with several institutional partners at different locations, which all represent their individual interests and have their own way of bureaucratic procedures as they have their own sets of laws. This proposes an additional challenge to both the investor and the legislators as they constantly need to monitor and comply with a huge set of, often contradictory, laws.

2.2.1 Orkustofnun – the National Energy Authority of Iceland – in practice

Orkustofnun (National Energy Authority of Iceland) is a central hub of licensing and permitting procedures. In the current Icelandic institutional system, Orkustofnun is overseen by the Ministry of Industries and Innovation, which works in close cooperation with the Ministry for Environment and Natural Resources. The legislations governing the two ministries are closely related. The Ministry for Environment and Natural Resources is responsible for EIA and SEA legislations, for municipal planning and nature conservation. The Ministry of Industries and Innovation formed the Electricity Act, Energy and Mineral Resources Act, Water and Hydrocarbons Acts as well as the Act regulating the functions of Orkustofnun. Orkustofnun cooperates with both ministries and follows their legislations during its activities in order to ensure the aims of both legislations and ministries. Orkustofnun also considers regulations related to the Planning and Building Act.

The general activities of Orkustofnun include issuing research, utilisation and power plant licenses as well as considering transmission, distribution and municipal planning and building regulations. Therefore, the whole spectrum of licenses needed from exploration phase until energy production is the responsibility of this single agency. In 2012, the Parliament of Iceland further extended the licensing powers of Orkustofnun, which became fully independent in its decision-making (Orkustofnun, 2016).

Another unique aspect of the Icelandic institutional system is that decisions of Orkustofnun, such as issued licenses and permits, can be revised by the two ministries. Therefore, in case of any issues, there is an option for investors or for locals to have decisions of Orkustofnun revised either by the ministries, or the Committee for Environmental and Resource Matters. First stage issues stay within the bureaucracy, and the administration has simple methods for controlling and protecting local interests, while, as both Orkustofnun and Ngugi (2014) suggest, investors account this as a favourable condition for development. According to Ngugi (2014), all investments will inherently result in various business transaction and contractual relationships. Potentially, all these transactions and relationships could give rise to disputes necessitating arbitration or court adjudication. Therefore, investors and financiers would be concerned whether justice will be served and enforced by evaluating institutions and national policies. Ngugi's argument is also valid for bureaucratic and tendering procedures, licensing, permitting and reservoir ownership conflicts. For this case, a national champion for energy development or a legal and administrative reform can provide a solution.

This institutional system is also in place in numerous other countries besides Iceland. Several countries have appointed a single institution for geothermal energy development, such as the Geothermal Development Company - GDC in Kenya, and in Tanzania, the Geothermal Development Office in Djibouti, Environmental Protection Agency (USA), Energy Development Corporation (Philippines) and CFE – the state power company in Mexico (Gehring and Loksha, 2012).

2.3 Geothermal research and capacity

Available information about prospective areas and geothermal resources is the first key element of supporting projects during their development as available and relevant information is a key factor in development decisions. Governments play an important role in providing resource related surface and underground information such as seismic, deep drilling and ground water data for project development. This requires surface and subsurface explorations financed by the governments. In Iceland, a governmental agency is responsible for these works (ÍSOR). According to the ESMAP Handbook (Gehring and Loksha, 2012), in an ideal scenario this information is formulated into 3D reservoir models. The collected information should be available for geothermal project developers, providing information and reducing time for development.

In case of the Philippines, an inventory of prospective geothermal areas and initial surface investigation results are available from the Bureau of Energy Development (BED) of the Department of Energy (Dolor, 2005; 2006). In Iceland, Orkustofnun makes this information available.

Governments should facilitate data and information sharing between public agencies and fee-paying private developers with a specialized data system to reduce exploration risks. In the short term, such a system can attract potential investors as they have basic data about geothermal opportunities, while long term, the database can help preventing possible reservoir overlaps and legal disputes about ownership (Micale and Padraig, 2015).

2.3.1 Institutional capacity building and transfer of know-how

The available information, experience, knowledge and know-how is of high importance for all stakeholders, participating institutions and authorities in case of a geothermal utilization. Education, training and technical assistance, the transfer of know-how and capacity building is essential for smooth operation of institutions, authorities and also for project owners. Geothermal knowledge and knowledge transfer play a crucial role in establishing capable geothermal institutions and authorities, by better enabling streamlined procedures, simplified, clear-cut legislation and faster, more efficient and less contradictory bureaucratic procedures by better informed decision makers and policy personnel. As geothermal energy cannot be utilized in all countries of the world, the related experience and education is limited to the utilizing countries. Specific geothermal education programmes exist only in few

countries such as the USA and Iceland, who is leading in this field, however, in Hungary, El Salvador, Kenya and Japan there are several postgraduate or certification programmes as well (Tóth, 2013).

The best known geothermal education program, benefitting from more than 80 years of geothermal experience in Iceland, is the United Nations University Geothermal Training Program (UNU-GTP), which has been in operation in Iceland since 1979. UNU-GTP receives its basic funding from the Icelandic Government, but its organization is through the United Nations University and Orkustofnun. It also receives funding from other sources. The six-month training programme is aiming at assisting experts of developing and EEA program participant countries with significant geothermal potential in building up expertise in most areas of geothermal utilizations. There are eight lines of study, including: Geothermal Geology, Geophysical Exploration, Reservoir Engineering and Borehole Geography, Chemistry of Thermal Fluids, Environmental Science, Geothermal Utilization, Drilling Technology and Project Management and Finances, which represent nearly all aspects of a geothermal exploration and development. These are the areas needed by institutions, which are responsible for geothermal development, to increase their geothermal know-how. In cooperation with the University of Iceland (UI) (since 2000) and the Reykjavik University (RU) (since 2013), UNU-GTP fellows can extend their studies to MSc and PhD levels (Georgsson et al., 2015a).

The UNU-GTP can also offer short courses about geothermal utilizations in interested countries within the framework of the UN Millennium Development Goals – now modified into the UN Sustainable Development Goals. The annual short courses series were started in Kenya in 2005, and in El Salvador in 2006. Since then participation has been extended to many East-African and Latin American countries. The latest capacity building service of the UNU-GTP are customer-designed short courses or trainings on offer for partner countries, which was started in 2010. The customer specifies the outline of the programme, while the contents are defined in detail and guaranteed by UNU-GTP. This form of education was introduced for countries planning fast geothermal development and their need for training and capacity building, which at the same time had the necessary financial resources (Georgsson et al., 2015b).

Capacity building and transfer of information is also ensured through one of the most relevant open-access geothermal knowledge and publications database, prepared and maintained by the UNU-GTP. Since the early 2000s, the older and current publications of workshops and short courses, reports of 6-month programme fellows and other experts have been published in open access pdf-versions at the UNU-GTP website (www.unugtp.is) (Georgsson et al., 2015a).

2.4 Financing geothermal projects

Within the ESMAP handbook (Gehring and Loksha, 2012), eight different models are described for state participation in geothermal development projects. The two extremes of the model are that a single national entity is realizing the project, the other extreme is that the complete investment is outsourced or tendered to a private company. The main difference between the two extremes and the other forms in between is the entity or entities participating, and who has to bear and in what proportion the risks associated with geothermal development as well as the total cost of the investment. The possible formulas for state participation include various versions of public-private partnerships or involvement of multiple national entities. Another possible approach is that the state participates only before or after a certain stage of project development such as build-operate-transfer (BOT).

According to ESMAP, energy developers naturally prefer support through state participation, when high initial risks and financial needs are associated with exploration and collection of data at early project stages, but with independent power producers (IPPs) performing the middle and later stages.

2.4.1 Investments and financing

Geothermal energy utilizations require different financing methods and tools compared to other renewable energy sources, as there is a limited amount of information from surface exploration measurements about the properties of the geothermal reservoir and its energy production capabilities available before making the expensive investments related to subsurface researches and exploration drilling. Therefore, the size of the investment or the power plant cannot be fixed at the beginning of the investment. As investors, at this stage, cannot describe a totally valid business plan, it is less likely that the project can attract outside investors (Kreuter, 2008; Gehringer and Loksha, 2012). From the investor perspective, the most crucial information are the availability, quality, amount, flow rate and temperature of the geothermal fluid, as these provide the basis for the estimations of final energy output and therefore profitability of the project. In case of geothermal utilization, this information becomes available and reliable only when the majority of surface and underground exploration works are finished and some exploration and production wells have been drilled and approximately up to 30-40% of the total investment costs are spent (Gehringer and Loksha, 2012; Micale and Padraig, 2015). Therefore, a huge initial investment has to be made, before the results are fully ensured, and the feasibility of the project is not known. Before the exploration phase is completed, the bankability of the project is low as there is no reliable information about how much energy can possibly be produced. In most cases, this requires the investor to take all related financial risks as finding appropriate public or private financial resources, loans, supports or grants represents a unique challenge. Therefore, financial supporting schemes should reflect the unique properties of geothermal development by providing early stage financing (Hólm, 2016).

Providing geothermal information can be used as a financial tool for geothermal development as the presence of good geothermal surface and subsurface data greatly reduces the risk, time and cost of project planning, thus creating more favourable conditions for development. Therefore, the availability of previous geographical information is of significant importance for reducing exploration costs and attracting outside investors.

Regarding financial support schemes, two types of financing instruments are widely used for energy related development, which can also be further differentiated. One is *investment support*, which includes loans, insurance and investment support programmes and aims at reducing the initial risk. The other scheme is *operational support*, which consists mostly of tax incentives or exemptions and Feed-in-Tariff systems provided for operational projects. Its goal is to increase feasibility downstream and thereby to increase risk willingness through a better risk-reward profile for the project.

Rybach (2010) and Haraldsson (2014) recommend that governments should finance the exploratory and preferably also the pre-feasibility phases of geothermal development. At later stages of the investment, investors should bear the risks. It is easier for them to receive financing for a project that is backed up by relevant information after the exploration drillings. This methodology is also in line with the past approach of the Icelandic government, which funded geothermal exploration activities for decades for the benefit of the public (Rybach, 2010; Haraldsson, 2012). This practice reflects the need of geothermal development and provides effective tools to deal with the high initial costs and the late appearance of reliable information about the possible size of the power output and development.

Investment support can be provided in numerous ways. A basic difference between various types of investment support, is in who bears the financial risks of a failure. In case of loans or grants, the investors or project owners are responsible for financial damages in case of a failure, which is followed by various possible difficulties and naturally has a negative effect on investments. Insurances or loan guarantees for loans overcome this challenge but still require the investment to be made by the investor or project owners. In case of a failure, the insurance can cover the losses, which is beneficial for both the investor and financial provider, as insurances require less financial resources. Therefore, overall policy costs can be reduced compared to grant programmes only.

Regarding policymaking, grant and insurance programmes play important roles and they have to be applied if necessary, preferably providing both.

Providing funding and insurance for the early stages of project development is the practice by both public and private re-insurance companies in Germany such as Axa, Swiss Re, Gothaer, R&V, Marsh & Willis and Munich RE (Münich Reinsurance Company) which have expertise in financing and insurance for geothermal projects. The German company provides geothermal risk insurance specialized for each stage of geothermal projects, mostly in Germany and Turkey. The insurance schemes usually cover up to 70-80% of the investment costs and it is possible to insure only certain parts of the investment, creating favourable conditions for geothermal investors (Münich RE, 2015; Századvég Gazdaságkutató Zrt, 201; Kreuter and Schrage, 2009).

Regarding insurance, another example of the market based geothermal project financing offered by a state owned and governed re-insurance company is the KfW Entwicklungsbank (German Development Bank) and its subsidiary, Deutsche Investitions- und Entwicklungsgesellschaft (DEG), which are owned by the German Federal Government and primarily the Federal Ministry for Economic Cooperation and Development. The KfW partially financed the Olkaria Geothermal Power Plant in Kenya and many projects in Germany. Re-insurance offered by KfW is based on direct or indirect public involvement, e.g. through funding of facilities or ownership of institutions (Századvég Gazdaságkutató Zrt, 2013; Haraldsson, 2014; Micale et al., 2015 and KfW, 2016).

In Germany, France, the Netherlands and Switzerland public and private insurances are both available for geothermal investors. In Germany, where geothermal risk insurance has a relatively long history, the grants, loans, insurances and fees are adjusted individually for projects. All drilling and exploration related works can be supported. The financing is adjusted according to the planned capacity and output of the projects and it is possible to decrease the funding according to the final production capacity if that would be lower than was planned. If the project is only a partial success, the rates of financing, fees and insurance coverage and refunded amount are adjusted accordingly (Századvég Gazdaságkutató Zrt, 2013; Rybach, 2010; Kreuter, 2008; 2009).

The practice of providing both loans and insurance or the two combined is also a practice used by some international public development finance institutions (DFIs) and agencies. These include the Climate Investment Funds, EU-Africa Infrastructure Fund or the Japanese International Cooperation Agency, Geothermal Risk Mitigation Facility, which is active in Africa and Latin-America (; Micale et al., 2015; and GRMF, 2016). Besides these private loans and insurance examples, in many cases the state itself can take the leading role and create a loan and/or insurance fund or is participating in multilateral agreements and institutions in order to provide loans and insurance through international investment banks, multilateral development banks (MDBs) or specialized development funds. Here can be mentioned the Clean Technology Fund (CTF), the Scaling –up Renewable Energy Program (SREP), GeoFund or ARGeo (Gehringer and Loksha, 2012).

The Icelandic Energy Fund was set up to provide low-interest loans to municipalities, firms or individuals for geothermal drilling, to share the risk of drilling with developers. The loans normally cover 60% of drilling costs and can be converted into grants if the development of a new geothermal field proves unsuccessful, thus also functioning as insurance for the developer (Haraldsson, 2014). Loan programmes are also in place and accessible within the United States from the federal government. The Geothermal Loan Guarantee Program grants loans for up to 75 percent of project costs since 1974 with the federal government guaranteeing the full amount. Besides, various loan programmes are available at federal and state levels. In Germany, a drilling insurance programme was introduced in 2010, where a premium is paid on a loan which is converted into a grant in the case of drilling failure. A governmental risk coverage system has been in place in France since 1981 where a short-term risk guarantee covers all or part of an investment in case of drilling failure and a long-term risk guarantee covers the risk of resource decline for up to 25 years. A risk guarantee system was also established in Switzerland in 1987. The provided guarantee extends to 50% of drilling and testing costs and in specific cases up to 80%. A

new governmental risk coverage system was introduced in 2008 in which the maximum guarantee is 50% of the subsurface exploration costs (Századvég Gazdaságkutató Zrt, 2013).

The European Economic Area Grants and the Norway Grants (EEA, 2016) are supporting programmes jointly financed by Iceland, Liechtenstein and Norway for EU member states. Among other aims, the EEA and Norway Grants are supporting development of renewable energy sources by providing funding for various energy projects from environmental awareness raising to drilling costs. The EEA recognized the special needs of geothermal development; therefore, it is possible to receive support only for parts of a larger project (EEA, 2016).

The European Union and the European Investment Bank are funding several scientific research programmes and mechanisms that support geothermal research and development, such as FP7, H2020, Intelligent Energy Europe, Structural- and Cohesion Funds, European Fund for Strategic Investments (EFSI) Connecting Europe Facility (CEF) or NER300 and 400 (Századvég Gazdaságkutató Zrt, 2013; EIB, 2015; 2016).

The Geothermal Technologies Program in the US was launched in 2009 with USD 400 million funding for a broad portfolio of projects including demonstration projects, research and development, innovative exploration techniques, national geothermal data system, resource assessment and classification system and ground source heat pumps (Wall, 2009).

The Global Environmental Facility (GEF), administered by the World Bank and UNEP, is financing geothermal investments in Europe and central Asia, from which, among others, a geothermal project of the MOL oil group in Armenia received an insurance grant (Gehring and Loksha, 2012; GeoFund, 2016).

As the success rate of exploration drillings is 68% (Gehring and Loksha, 2012), the insurance for exploration phase geothermal projects seems to be advantageous both for public and private insurance or loan providers and investors. Goodman et al. (2010) and Fraser (2013) suggest that geothermal risk insurance should extend to the whole EU. A common European Geothermal Risk Insurance Fund (EGRIF) could be a great asset in mediating geothermal financing conflicts (Haraldsson, 2012; Fraser, 2013).

Micale and Pádraig (2015) state that with the right policies and financial measures, governments can drive investments that deliver the same amount of geothermal energy while providing only 15-35% of the national resources, which would have been spent if the projects had been built and operated by themselves.

Preferably, after a successful investment support and if the power plant is operational and production has started, operational support can be provided. Feed-in tariffs for geothermal electricity are currently in place in 20 countries world-wide (REN21, 2014), including Austria, Hungary, Croatia, Czech Republic, Ecuador, France, Germany, Greece, Indonesia, Italy, Japan, Kenya, Serbia, Slovakia, Slovenia, Spain, Switzerland, Turkey, Uganda and the United Kingdom (Haraldsson, 2012). However, within the EU, according to the current practice, geothermal electricity is supported but geothermal heat production is usually not, except in France (Orkustofnun, 2016).

2.4.2 Development strategies

In case of geothermal development implementation two major approaches, conventional and stepwise development strategies can be distinguished. According to the conventional development methodology, geothermal resources and production capacity are estimated by exploration and planning of the power plant and all related administrative procedures are started. During the development of the project, if something does not go according to plan, e.g. the energy output is not as expected, there is less space for adjustments as all financials and licenses are according to the original plan.

The stepwise development strategy involves starting the development at a smaller scale. When the resources are partly in use, it is possible to collect more relevant information and plan further utilization. An example of the stepwise development is the development of the Nesjavellir geothermal field operated by Reykjavik Energy in Iceland. The development started in 1982, initially as a hot water production project. A 100 MW thermal power plant was constructed in 1990 and when the reservoir was further explored and more data had been collected, electricity production was gradually added and the hot water production was extended to 150 MW and later to 290 MW (Steingrímsson, 2009). This methodology creates favourable conditions for adjustments during implementation, as development can be evaluated and adjusted according to the output capacity of the reservoir. As the amount of relevant information about the investment and the possible output increases, the investor is able to provide relevant information for collecting financial sources.

The stepwise development approach also provides additional benefits in case of low-temperature geothermal resources. By aiming for moderate utilization levels during the first phase of development instead of the possible maximum output of the reservoir, there is more space for adjustment if the temperature is lower or output of the geothermal resource is less than previously anticipated and utilization can be changed from electricity generation to direct use.

Stepwise development can also add to the sustainable use of the reservoirs by preventing over-exploitation of the resource.

Stepwise development can also be suitable for smaller investments at local levels. Smaller projects can be presented in the form of a programme or portfolio and developed accordingly. The European Union supports numerous energy related large scale demonstration projects through various programmes, such as European Fund for Strategic Investments (EFSI), Connecting Europe Facility (CEF) or NER300 and 400. While these developments are necessary, geothermal development can also be fostered at a smaller scale, especially in low-enthalpy reservoirs such as the Pannonian-basin, which could be an area for national or local governments to act. Small scale, local district heating, electricity systems and heat pumps could be also supported, promoting local improvements and keeping the benefits of the investment in the local communities. Small-scale geothermal projects (0.5-5 MW according to ESMAP (Gehring and Loksha, 2012)) could be suitable to provide a reliable base load power or heat, which is constantly available. Geothermal energy can also be successfully combined with other renewables, which have stronger environmental footprints. In such cases, the electricity does not need to be transferred over long distances by national networks, evading some of the transmission development costs.

The idea of stepwise development and methodology should also be considered, for development of existing projects. In case of existing utilizations, careful planning of further development should be carried out to avoid unnecessary capacities.

2.4.3 Tax incentives and fees

Another area of possible state support for geothermal development are tax incentives. The international practice is mostly aiming to ease the tariff duties on imported machinery and equipment for geothermal power plants or provide accelerated depreciation. In El Salvador and the Philippines, the governments supported geothermal investments extensively using these tools (Haraldsson, 2014). In some EU states such as in Hungary, large companies will be able to receive corporate tax incentives or reductions starting in 2017, if a company makes energy efficiency investments related to its own facilities (Soltész, 2016). The Philippine Renewable Energy Act of 2008 provides various fiscal and non-fiscal incentives for renewable energy developers. These include income tax holiday for the first 7 years of commercial operation of renewable energy facilities, special realty tax rates on equipment and machinery, net operating loss carry-over, accelerated depreciation, 0% VAT rate for the sale of renewable power, tax exemption of carbon credit sales, and tax credit on domestic capital equipment and services (Haraldsson, 2012).

Geothermal energy projects are also required to pay license fees and mining royalties for the use of geothermal energy or for the extraction of hot water. By reduced fees and royalties, governments can also effectively support sustainable geothermal investments. However, tax incentives are not considered as efficient for speeding up geothermal development as risk mitigation schemes (Gehring and Loksha, 2012).

3. GEOTHERMAL ENERGY PROSPECTS IN HUNGARY

3.1 Geology

Hungary is located in Central Europe (Figure 1), the area is 93,000 km² and its population is 10 million. Hungary's excellent geothermal potential is well-known and the country has a long history and tradition of utilization of thermal waters for direct heat supply. The country is most famous for its low-temperature utilizations, which are mostly internationally recognized thermal baths and spas and district heating systems.

Hungary lies in the Pannonian Basin, which is encircled by the Carpathian Mountains. The crust below Hungary is relatively thin (approx. 25 km) due to sub-crustal erosion. This thinned crust has sunk isostatically. The basin that formed is filled mostly by multi-layered tertiary sediments, which are composed of sandy, shaly and silty beds. Lower Pannonian sediments are mostly impermeable. The upper Pannonian and Quaternary formations contain vast porous, permeable sand and sandstone beds. The thickness of the individual sandy layers varies between 1 and 30 m and most of them are

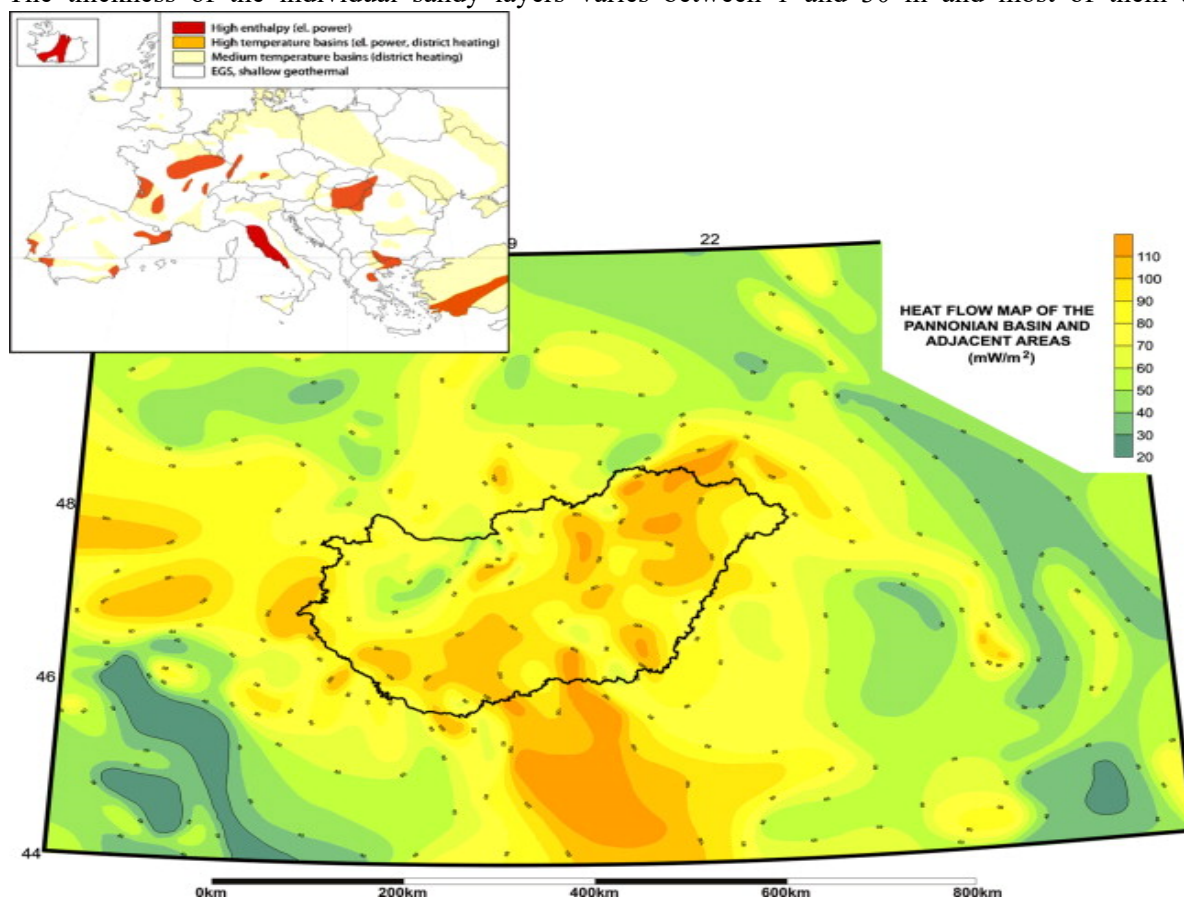


FIGURE 1: Heat flow map of the Pannonian basin and adjacent areas, based on Dövényi et al. (2002); inset (top left) is a geothermal thematic map of Europe, based on Antics and Sanner (2007) and Szanyi and Kovacs (2010)

interconnected. These form the upper Pannonian aquifer, which is the most important thermal water resource in Hungary. This aquifer has an area of 40,000 km², an average thickness of 200-300 m, a bulk porosity of 20-30%, and a permeability of 500-1,500 mD. Another type of geothermal reservoir is found in the carbonate rocks from the Triassic, which have secondary porosity. These can be fractured or karstified rock masses with continuous recharge and important convection. About 20% of the Hungarian geothermal wells draw fluids from such carbonate rock formations, mainly in the western part of the country (Tóth, 2015).

The underground natural conditions in Hungary are very favourable for low- and medium-enthalpy geothermal energy production and utilization. The sedimentary layers provide heat insulation for the permeable sandstone layers below. The surrounding mountains and fractured structures provide substantial supply and flow of water. The main areas of good geothermal prospects are located on the western and southeastern side of the country, but the anomalously high terrestrial heat flow (~ 0.09 W/m²) and the high geothermal gradient ($\sim 0.05^\circ\text{C}/\text{m}$) also provide good prospects for low- and medium-enthalpy utilizations. This applies to most of the country, except for the mountainous areas ranging from the west part of the country to the north-east areas (Tóth, 2015). Individual and relatively small fracture zones and other anomalies can be found in various parts of the country, such as at the town of Tura in central east Hungary, Fábánsebestyén in southeast Hungary and Miskolc-Mályi (northeast Hungary) which are providing much higher than average temperatures and flow of geothermal fluids.

3.2 Short history and current status of geothermal utilization

The history of geothermal utilization dates back to the Roman Empire when spas and public baths were built. During the medieval times, this development was continued by the Hungarian Kings and by invading regimes. These utilizations made use of the existing geothermal surface manifestations. Exploration of geothermal resources began in 1877, when the deepest well in Europe at that time (971 m) was drilled in Budapest overseen by the drilling engineer V. Zsigmondy (Geothermal ERANET, 2013). Between the two World Wars, exploration for oil and gas was begun. However, in most cases only huge thermal water reservoirs were discovered. District heating developments were started at the Budapest Zoo and some surrounding apartments, as the nearby Széchenyi Spa could provide excess water. After World War II, during the 1950s and 1960s, hundreds of geothermal wells were drilled, mostly for balneology, greenhouses and for other agricultural purposes (Tóth, 2010).

In the late 1950s, district heating projects were started in southeast Hungary in Hódmezővásárhely, Szeged, Szentes, Makó and Kistelek. The technical level of these geothermal heating systems was varying. In some cases, there are well-designed and well-controlled sophisticated systems, where dozens of geothermal wells could supply a cascade of sub-systems with greenhouses, plastic tunnels and soil heating all connected in series (e.g. Hódmezővásárhely), while in other cases, a single well provided thermal water directly to greenhouses. The peak of geothermal activity was in the late 70's when a total of 525 geothermal wells were registered and the thirty best wells had a production temperature exceeding 90°C. Total thermal power capacity of these wells was 1,540 MWt, but utilization was seasonal and the efficiency was rather low (Tóth, 2010; Ádok, 2016, Kurunczi, M., and Ádám, B., 2016).

Since the 1980s, hundreds of the agricultural wells have been shut down, mostly due to the political transformation of 1989. Since then, a continuous but slow development and research of geothermal resources is ongoing. In 2014, 672 wells produced thermal water warmer than 30°C. However, 179 wells are abandoned and 220 are temporarily closed (MFGI, 2013).

Since the 1990s and onwards, the development of geothermal energy sources has been slow but continuous. In many cases the former agricultural wells became private property or are owned by agricultural investors. Geothermal development since then is characterized by three main development domains. One is the development of the spa industry, the second is agricultural use and the third is heat production.

Spa development has taken place at several locations during the last decades. It has been financed either by private funds or EU development projects, such as Zalakaros, Sárvár, Hévíz, Bük, Budapest, Visegrád, Baja, Szeged, Eger, Miskolc-Tapolca, Hódmezővásárhely, Hajdúszoboszló, Gyula and additional places. Altogether 295 thermal wells and 132 natural springs produce water for sport and therapeutic purposes. The outflow temperature typically ranges from 30 to 50°C. These wells mostly discharge the porous sedimentary sandstone reservoirs, which lie at an average depth of 500-1500 m. About 50 wells have higher outflow temperature than 60°C, many of them discharging the fractured basement aquifers. The hottest ones are at Zalakaros (SW-Hungary, 99°C) and at Gyula (SE-Hungary, at the Romanian border, 91°C). The estimated amount of thermal water used for bathing and swimming is about 41.18 million m³, or 352 MWt / resp. 3,912 TJ/year (Tóth, 2015).

Agricultural use is another major area of geothermal energy utilization. Various vegetables are grown on more than 70 ha. in greenhouses and on more than 250 ha. in soil-heated plastic tents. Heat and water are supplied by 181 operating thermal wells, which produce 10.97 million m³ of thermal water (Tóth, 2015). Further, more than 50 farms utilize geothermal energy for animal husbandry. The major agricultural users are the Árpád-Agrár Zrt. in Szentes and Flóratom, Bauforg Ltd.-s. in Szeged, Bokrosi Ltd. in Csongrád, Primőr-Profit Ltd. in Szegvár and many smaller users, especially in SE-Hungary. Fish ponds near Szarvas and Győr are also heated with low-temperature geothermal water. In 2013, the total installed capacity in the agriculture sector was 306 MWt and the estimated annual use was 3,414 TJ. National and EU funds also support development of these areas.

The development of existing independent small district heating projects is also ongoing, as well as several new projects that were also started in recent years. Mayor reconstruction and development of geothermal heating systems were performed at Hódmezővásárhely, Miskolc-Mályi, Eger, Makó and other places. The technical level of development of these geothermal heating systems is varying. Some are very sophisticated and well-controlled systems such as in Hódmezővásárhely, where large number of wells (12) supply a cascade of sub-systems, and excess heat utilized for greenhouses. In other cases, a single well provides thermal water directly to greenhouses with the excess heat not utilized and water not reinjected, sometimes causing environmental problems. In 2013, individual space and district heating capacity was 186.58 MWt and actual use was 2,026 TJ/y for all of Hungary. Hódmezővásárhely is the city with the most developed geothermal district heating system with a capacity of 21 MWt (Tóth, 2015).

The mayor geothermal heat developments in Hungary are often joint projects of local governments or assemblies of neighbouring towns. The investments are funded by various supporting programmes, some of them in collaboration with Iceland within the framework of the EEA and Norwegian financial mechanisms (EEA, 2016), the EEA FM (Geothermal ERANET, 2013) and various EU grants, such as the NER300 and NER400 initiatives. Others are financed by various national supporting programmes such as Environment and Energy Operative Programme and the latter Environment and Energy Efficiency Operative Program and their sub-programmes and predecessor-programmes since EU accession in 2004. These programmes provided funding for direct utilization, but also for exploration and cooperation regarding geothermal energy utilization. As funding was available for scientific and exploration projects as well, several research and exploration projects took place both on national and international (Hungary and its neighbours) levels. However, the majority of current geothermal development has become dependent on and characterized by EU grants, as local governments are lacking funding and the existence and involvement of private investors are rare.

Between 2010 and 2014, about 24 deep geothermal projects received EU and/or national support with grants totalling 27.2 million Euros. The Szolnok hospital, the Szeged heating system, and the Gyopárosfürdő Thermal Bath are three main examples. In addition, two large district heating projects were begun in 2010 by Pannergy Ltd., in Szentlőrinc and in Miskolc-Mályi, and finished in 2013 (Pannergy, 2013; 2016). Many other projects are also currently underway which are focusing on geothermal power plants, CHP, district heating and GSHP incentives, for example in Mosonmagyaróvár, Szolnok, Győr, Battonya and Tura.

Hungary's largest geothermal based district heating system is in Miskolc, which is the first large scale district heating project in Hungary. The aim of the project is to heat the several hundreds of apartments at „Avas” housing estate at Miskolc, the second largest city in Hungary. The project was started in 2013 when the first phase of the system began operation and the development has been continuous since then. Heat is supplied by the unique high-temperature wells in Miskolc-Mályi, where a total of 5 wells were drilled. Two production wells went to a depth of 2,305 and 1,514 m, respectively, yielding 6,600-9,000 l/min flow with a temperature between 90 and 105°C from a karstified-fractured Triassic limestone reservoir (Tóth, 2015). Three reinjection wells were also drilled and a 22 km long pipeline constructed. The planned heat capacity is 55 MWt and the heat demand is 695,000-1,100,000 GJ. To use the run-off water in a future project, 10 ha. of greenhouses are under development. Another project is planned in Szentlőrinc, where the town's heating system is planned to become 100% geothermal energy based. Both projects are supported by the EU and/or national grants and owned by PannErgy PLC, which is a private investor. As reported by the investment firm, the investment cost was 25 million EUR of which the EU support was more than 5 million EUR. In both projects, the contracted off-take partners are local government-owned companies (PannErgy, 2013; 2016). Some other private investment firms, such as CBA and EUFIRE, have become involved in geothermal energy production and utilization. Such firms have signed contracts with local governments, e.g. in Mosonmagyaróvár, Kecskemét and Eger, to create geothermal district heating systems.

Hungary is about to make a significant step forward in geothermal based electricity production which is not yet existing in Hungary. The first geothermal energy based electricity power plant is expected to be operational in the middle of 2017 with 2.7 MWt capacity at Tura, central E-Hungary, the project will be described in detail later in this report. Another project for geothermal based electricity production is on the way at Jászberény, Central-Hungary, where a 2.5 MW power plant is to be built.

Crucial development regarding high-enthalpy reservoirs are also on the way. Recent national and EU funded surface and underground studies have proven the existence of deep high enthalpy geothermal reservoirs, most of them located in SE-Hungary. The obtained undisturbed temperature of the rock is 252°C at 6,000 m depth. These areas have good prospects for high-enthalpy utilizations and are targets for future EGS development projects. They also provide the basis for geothermal electricity production, as there is no geothermal electricity production in Hungary yet. The first EGS power plant in Hungary is to be launched at the end of 2019 according to the project developer (EU-FIRE, 2016a; 2016b).

The European Commission has awarded over 1.2 billion Euros to 23 highly innovative renewable energy projects all over the EU in 2013 through the NER300 Programme. This program provides support for Hungary's first Enhanced Geothermal System (EGS) project, run by EU-FIRE and Mannvit Ltd, at Battonya, Hungary. The project, which was awarded almost 40 million Euros of the NER300 funding, has an estimated total investment cost of €116 million and an expected capacity of 11.8 MWt. Other institutional and private investors will fund the project's remaining costs (Kovács, 2013; Energiainfo.hu, 2012; Askjaenergy.com, 2013).

Ground source heat pumps (GHPs) or shallow geothermal heat utilization have increased from 2000 to 2010, but the economic crisis in 2008-2009 caused a setback. In order to foster development, the installation of a shallow heat pump no longer needs formal permission (since 2013) and does not even require a notification before drilling (Kujbus, 2016; Nádor, 2013; Haehnlein et al., 2010). The estimated installed capacity of GHPs is about 40 MWt. The actual number of installed units is more than 4,200, the average obtained COP is 4.0, but the relevant data is incomplete because installed devices do not have to be reported. The biggest Hungarian heat pump systems (around or over 1 MW capacity) are significant in the European market. Many international companies operating in Hungary made major investments in heat-pump systems in the recent years (e.g. Telenor Office at Törökbálint, central Hungary and TESCO). The average size of individual units ranges from 10 kW to 14 kW for residential use. In many cities and towns with good geothermal prospects, new investments for condominiums and apartment houses are commonly planned for GHP heating only, or GHP is used as additional source of heat additional to natural gas due to financial, environmental and energy efficiency constraints (Tóth,

2015). The installed capacity and annual energy use for the various geothermal energy applications in Hungary are (Lund and Boyd, 2015):

- 33.02 MWt or 326.05 TJ/yr, for individual space heating;
- 153.56 MWt or 1,700.26 TJ/yr, for district heating;
- 271 MWt or 3,024.12 TJ/yr, for greenhouse heating;
- 6 MWt or 61.51 TJ/yr, for fish farming;
- 4 MWt or 31.34 TJ/yr, for animal farming;
- 25 MWt or 297.13 TJ/yr, for agricultural drying;
- 19 MWt or 220.62 TJ/yr, for industrial process heat;
- 352 MWt or 3,912.03 TJ/yr, for bathing and swimming;
- 42 MWt or 695 TJ/yr, for geothermal heat pumps.

The total installed geothermal energy capacity and annual energy use in Hungary are 905.58 MWt and 10,268.06 TJ/yr, respectively (Tóth, 2015; Lund and Boyd, 2015).

After Turkey, Iceland and Italy, Hungary is ranked at 4th place regarding installed geothermal direct use in Europe (Geothermal ERANET, 2013; Lund and Boyd, 2015).

4. GEOTHERMAL DEVELOPMENT ENVIRONMENT IN HUNGARY

4.1 Current energy and geothermal policy development

The current renewable energy development are backed up by the country's renewable energy targets, which are based on the EU 2020 and 2030 renewable energy goals. The National Energy Strategy 2030 was introduced in 2011 and the measures are aiming at the security of energy supply, competitiveness and environmental protection and integration to the common European structures as well as the creation of decentralised energy systems and fostering renewable energy production in Hungary (National Energy Strategy 2030, 2010). The strategy also states, that such policy and institutional reforms have to be introduced that result in a predictable investment climate in order to increase supply security and also to avoid the lack of essential energy investments, such as reduction of bureaucracy, opening up the space for decisionmakers to act in favour of renewable energy sources, including geothermal. The strategic environmental assessment of the National Energy Strategy 2030 emphasizes the importance of geothermal electricity and heat utilizations (Pálvölgyi et al., 2011; MND, 2011).

According to the Hungarian National Energy Strategy 2030, the proportion of renewable energy resources of the energy consumption should reach 14.65% of the gross annual energy production in 2020 (National Energy Strategy, 2010). The total share of renewable energy sources was 9.61% within the GFCoE in 2014 and 5,2 PJ out of 65 PJ of the annual renewable energy consumption comes from geothermal resources (MEKH, 2015).

The aims and commitments of the National Energy Strategy 2030 are supported by the National Renewable Energy Action Plan 2010-2020 (NREAP) of Hungary (MND, 2010; NREAP, 2013). According to the renewable energy development path described in the NREAP, electricity production from geothermal resources should be increased from none in 2010 to 57 MW (2015) and to 410 GWh of the gross energy consumption until 2020. Heating and cooling from geothermal resources should grow 3,5 times between 2010 and 2020, from 101 kTOE to 357 kTOE, as well as the total geothermal energy utilized that should be increased 3.8 times from 4.23 PJ in 2010 to 16.43 PJ in 2020 (NREAP, 2010; Geothermal ERANET, 2013).

In 2010, geothermal energy was responsible for 8% of the gross annual renewable energy production (55.25 PJ) of Hungary. According to the NREAP, until 2020 the amount of geothermal energy will provide 14% of the gross annual RES production (120.57 PJ) (Fancsik, 2013) (Figure 2).

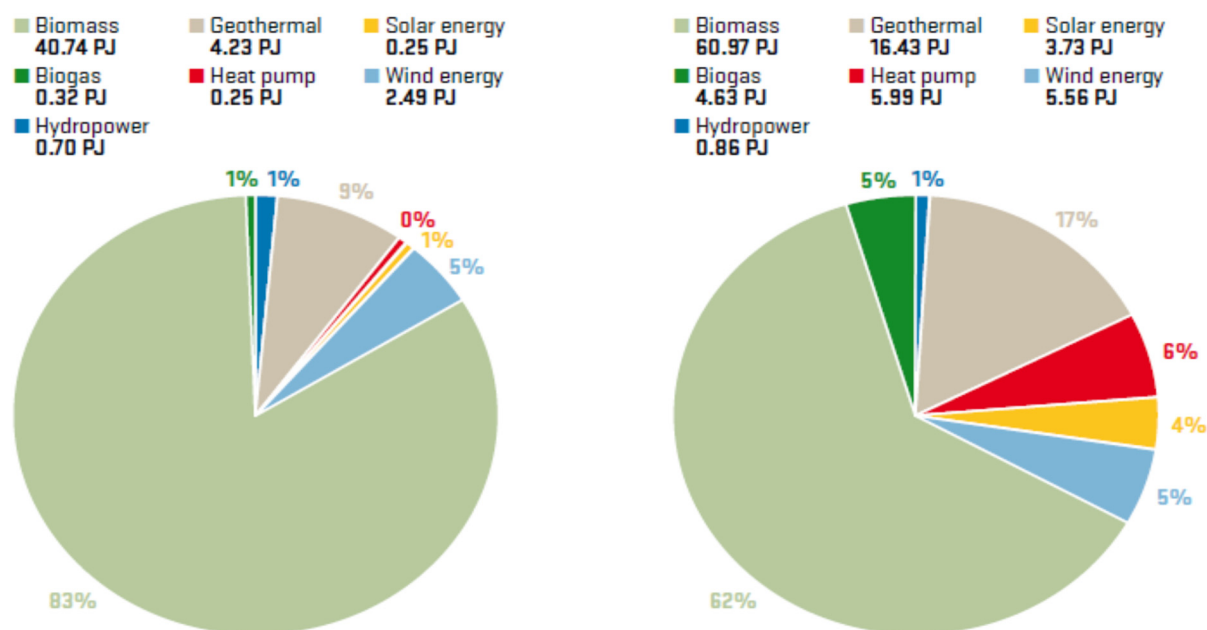


FIGURE 2: Distribution of renewable energy sources used in the electricity, heating and cooling sectors (2010 and 2020) in the NREAP of Hungary

Despite the ambitious geothermal targets of the NREAP of Hungary and the new development, the overall number of geothermal energy utilization permits issued by the relevant authorities have been decreasing continuously since 2008, from 15 to 20 new permits per year, to 2 to 6 permits. According to Attila Kujbus (2016), the current development and the ongoing projects are at least partially if not fully supported and fuelled by the EU or other international sources. Private investors and local governments tend to stay in the background due to the economic crisis and because of the lack of own resources, but most of all, as EU projects are usually providing support for complete projects, not for certain phases of geothermal development. They also have only a 1 or 2 years' timeframe, which is not enough to plan and complete a new geothermal investment. Therefore, current EU and nationally supported projects have the leading role in showing the path and initiate new projects. However, the introduction of new national and international supporting schemes, geothermal research and updated legislation should be enhanced to push development to the next level (Kujbus, 2016).

Both the National Energy Strategy 2030 and the National Renewable Energy Action Plan 2010-2020 are general strategies that describe the country's energy and renewable energy development priorities and provide a roadmap of development and production of energy until 2030 and 2020, respectively. Geothermal energy development aims are represented by the planned amount of geothermal electricity and heat produced between 2010 and 2020, but no specific geothermal strategy or policy recommendations are described.

The Mineral Resources and Resource Utilization Action Plan of 2013 is aiming at fostering mining and the mining based industries in Hungary including geothermal. The Action Plan contains the estimation of energy potentials of mining industries including geothermal potential. It states, that the increasing geothermal energy utilization is key to decreasing energy dependency and enforces the measures of related to geothermal energy development (Jávor, 2016, MFGI, 2016.)

Related to the renewable energy aims of Hungary, large companies that are performing energy efficiency related investments in order to optimize their production procedures or reduce their energy consumption, are eligible for corporate tax reduction for a certain period after their investments had been finalized. The regulation is expected to come into force in 2017 (Soltész, 2016).

Besides the EU and national energy targets, there are some other unique geographical conditions and properties of Hungary, which are also influencing the future geothermal development and policy. One is that the Pannonian reservoir extends beyond the state borders, therefore interstate agreements, the common policies, planning of development and monitoring of the cross-border reservoirs should be enhanced, as neighbouring countries such as Slovenia, Croatia, Romania and Slovakia are showing a growing interest in geothermal energy utilization (Transenergy, 2011). The existing transboundary agreements with all neighbours of Hungary should be further developed regarding future geothermal development. The other is that nearly all of the rivers and other surface waters in Hungary, which are one of the main sources of subsurface geothermal reservoirs, are originating from neighbouring countries. Therefore, the cooperation with our neighbours for the prevention of pollution of reservoirs and interference between projects, the preservation of good quality of the natural resources and reservoirs and the future public and private projects have a crucial role in maintaining the long term sustainability of the Pannonian reservoir.

4.2 Legislation related to geothermal energy

Utilization of geothermal energy and licensing procedures for geothermal investments in Hungary are regulated by the Mining Act. However, when water extraction is involved, provisions of the environmental and water management legislation should also be considered (Tóth, 2015). No single geothermal legislation or geothermal act exists. The only activity related to geothermal energy utilization, which does not require a permit or license, is surface exploration work, as for this only an agreement with the owner of the land is needed, while the mining authority should be informed 30 days in advance about the start of exploration (Dumas et al., 2013). Besides surface exploration works, the regulation applied for geothermal investments is dependent on two main factors:

1. The depth of the targeted geothermal resource;
2. Whether geothermal exploitation requires water extraction.

The legislation and authorities involved in procedures, depend on if the resource is found in an open area (at a depth from 20-30 to 2500 m), and if groundwater extraction is involved or not (Nádor, 2013). If no groundwater extraction is involved, the Regional Mining Inspectorate is competent to issue an exploration license and a license for the exploitation and utilization of geothermal energy, including construction and setup of related underground and surface facilities. On the other hand, if groundwater extraction is involved, which is usually the case, the Regional Directorates for Environment, Nature and Water are the competent authorities to issue a license for the utilization of thermal groundwater found between 30 and 2500 m ('water permit'). Simultaneously, this is considered a license for prospection, exploitation and utilization of geothermal energy and the Regional Mining Inspectorate intervenes in the procedure as a co-authority, notably by delivering a technical-safety license for drilling. However, the National Directorate General for Disaster Management (NDGDM) is also involved in giving permission to construct energy production facilities (Dumas et al., 2013).

The relevant legislative framework governing geothermal development in Hungary is made up by three different legislative areas: energetics, mining, and environment and water. These three areas cover an exceptionally big area of legislations consisting altogether of more than 118 regulations that relate to geothermal energy utilization. As Mádlné (2008) states, this amount of regulation is not transparent for investors and project owners. Different institutions are also responsible for the separate areas, so contradictions and legal gaps are frequent.

A good example of contradictory regulations are the Mining Act and the Ministerial Decrees related to water management (Ministerial Decree 101/2007 (XII. 23) and 96/2005 (XI. 4)). Each of the regulations give different values for the depth that acts as division line for determining if the drilling requires a permit or not. The Mining Act does not define any depth in connection with permit requirements. One Ministerial Decree set the depth to 20 m, the other to 30 m (Transenergy, 2011). Another possible example for contradictions could be that the necessary documents for handing in geothermal license inquiries and building permits for water facilities are not well defined and the Environmental Authority and the Land Use Office are partially free regarding what kind of documents they require. Therefore, it can happen that one authority is requiring the permission of the other authority, which requires the permission of the first authority to issue the permit to be granted by itself (Mannvit, August 2016, personal communication).

The legislation is also unbalanced and often contradictory. For example, the Mining Law states, “Geothermal energy exploited with thermal water is not geothermal energy, because it entails thermal water production”. Therefore, it is not subject to the Mining Law, but is subject to the Water Management Law, which does not include the terms of geothermal energy and its utilization (Rybach, 2003).

The Act on Water Management 2005 establishes a ranking for geothermal resource utilization, and energetic utilization is ranked low. The Water Management Act also states that waters extracted for geothermal energy only need to be reinjected, however, this differs depending on the circumstances according to Ministerial Decree 101/2007. Also, geothermal energy is subject both to mining and water resource fees, however agricultural use is only subject to water resource fee (Tóth, 2015).

The overall aims of the three legislative areas are also different. The Water Management Act is aiming at water protection, while the Mining Law aims at responsible use of geothermal resources.

In April 1st 2015, the Act VI of 2015 came into force, targeting more efficient state administration. The Regional Mining Inspectorates and the Regional Directorates for Environment, Nature and Water were integrated into a new national administrative system and into a new institutional structure (Kormanyhivatal.hu, 2016). The aims of the reform was to simplify administrative procedures. However, the reorganization of licensing authorities and relocations, in practice means one address to communicate with (the Regional Governmental Offices), but with the same legislation applied. Hence, multiple licenses are still required for geothermal utilizations, and while the authorities are unchanged, the investors still need to negotiate with each involved authority, separately.

Legislative and expert questions can arise if the reorganization of the authorities related to geothermal development is challenged concerning know-how and capacities of the new institutions. An example from Hungary is that the construction permits related to some of the power plant buildings and equipment are to be granted by the National Directorate General for Disaster Management, Ministry of the Interior (NDGDM). This authority has the task to protect the lives and properties of the population living in Hungary, ensuring the safe operation of the national economy, and protecting the elements of the critical infrastructure by preventing disasters. This is done by carrying out rescue operations in civil emergencies, organizing and controlling protection activities, eliminating the negative consequences of emergencies and performing reconstruction and rehabilitation. These are highly important public safety tasks and not geothermal energy utilization specific, which raises the question of capable institutions and smooth administrative and permitting procedures.

In Hungary, different legislations are applied for geothermal energy utilizations targeting geothermal resources above or below 2500 m depth. If the resource is above this depth (open area), a licensing procedure is applied, but if the resource is below 2500 m depth, then utilization can only be enabled by a state concession procedure and licensing. Currently there is no area in Hungary, which has been tendered out for geothermal concession (Dumas et al., 2013) and according to Kujbus (2016), none is in planning yet. Only one EU EGS project has been started, an EU demonstration project, where

exceptional rules are applied and no concession was involved (Pannergy, 2016). As there is no concession contract or call for proposals yet, exploration and development of geothermal energy in more than 2500 m depth or licensing procedure for exploration cannot be started (Table 1).

TABLE 1: Legislative distinction according to depth and main actors in licensing procedures and participating authorities in Hungary for geothermal projects

Depth (m)	Area	Energy extraction	Licensing authority	Consulting/licensing co-authorities	
0-20	No licensing, but the well should be reported.				
20-2,500	Open area	Closed loop, no water production (GSHP)	Regional Mining Inspectorates		The Hungarian Energy and Public Utility Regulatory Authority (electricity production, FIT)
		Extraction of thermal water	Regional governmental offices (environmental concerns)	Regional mining Inspectorates (implementation of deep-drilling)	The Hungarian Energy and Public Utility Regulatory Authority (electricity production, FIT)
Below 2,500	Closed area (concession procedure)	Extstraction of thermal water	- Regional Mining Inspectorates (concessional procedures) - Regional Governmental Offices (environmental concerns)		The Hungarian Energy and Public Utility Regulatory Authority (electricity production, FIT)
		Extraction of thermal water (EGS)	Regional Mining Inspectorates (concessional procedures)	Regional Governmental Offices (EIA)	The Hungarian Energy and Public Utility Regulatory Authority (electricity production, FIT)

4.2.1 Reservoir ownership

The ownership of the reservoir and the limitations for competitors to prevent the simultaneous exploitation of the same reservoir is not guaranteed by the current legislation. Several competitors and projects can use the same reservoir (Fraser, 2013). The legislation about the *Intervention into underground reservoirs and the requirements for drilling of wells* (Kvvm 101/2007 3 § (4) states, that during the planning of the drillings and wells, the connecting of separate underground waters or reservoirs is prohibited, but if there is no danger of cross-pollution, the Environmental Authority may grant an exception. Also, according to 5 § (2), the Environmental Authority may grant an exception from geophysical measurements if the design engineer of the project provides a statement that there is enough data available for relevant measurements.

Therefore, the exclusive usage of a reservoir is not guaranteed (Transenergy, 2011). The new investor can get a license if he provides a study proving that the new drilling will not interfere with the other utilizations and the authority grants the exception. This has happened in West-Hungary (Sipos, 2011), where a new well was drilled between two other wells, which were several kilometre from each other, but the utilization of the third well reduced the flowrate, temperatures and recharge of all three wells. This should be prevented by capable institutions and personnel at the authorities because separate

projects utilizing the same reservoir can change the reservoir and well properties, which highly influences the success of both projects and creates a barrier for investors.

Reservoir ownership causes another problem related to the sustainable use of reservoirs in Hungary. Many of the reservoirs are located on country borders and there are well-documented cases of independent geothermal utilization projects in Hungary and its neighbours that are influencing each other and can cause reduction of production capabilities on both sides of the border. This had happened both in East- and West-Hungary (Oradea (RO) – Gyula (HU), Lutzmannsburg (A) – Bük (HU)) (Sipos, 2011) which clearly points out the importance of trans-national solutions.

4.2.2 Reinjection

Reinjection is a sensitive topic in the Hungarian geothermal industry. According to the relevant legislation, which was modified in 2013, reinjection is not compulsory for balneology and agricultural uses, but for energy related utilizations. However, the Environmental Authority can grant an exception (Geothermal ERANET, 2013). Consequently, energy related projects are less competitive compared to the agricultural utilizations, and higher initial investment is needed.

Reinjection is essential for sustainable use of the reservoirs and therefore in the interest of the project owner as the Geoelec project suggests. Considering the structure of the Pannonian basin and the recharge of the reservoirs, the Geological and Geophysical Institute of Hungary has found that the duration of the water cycle of the reservoirs is approximately 10,000 years (Sipos, 2011), making sustainable use essential.

According to the relevant legislation, reinjection is only possible if the produced water is not polluted in any way during its utilization. Practically, this means that only the heat content of the thermal fluids can be utilized. As the majority of the produced thermal waters is used for balneology, most of the thermal waters cannot be reinjected. This results in the continuous decrease of fluids in certain reservoirs as only 2% of the produced thermal waters are reinjected (Kujbus, 2012a; 2012b). The low rate of reinjection highlights the need for more efficient utilizations and the need for reconstruction of old geothermal systems.

Reinjection in Hungary is challenging as most reservoirs consist of porous sedimentary rock and sandstone. Experiences show that reinjection into these reservoirs often causes the degradation of the reservoir as changes in fluid directions and new fractures cause a lot of floating particles, which decrease the permeability and finally the production capacity of the reservoir. This problem has been realized by well owners and geothermal companies. Scientific research projects have been started within the Economic Development and Innovation Operational Programme of Hungary to develop an efficient and sustainable reinjection methodology to avoid the permeability decrease (GEOSZ, 2016). Therefore, it would be important to provide more support for the development of new geothermal technologies and research projects to avoid technical challenges and reduce environmental effects (Jávor, 2016). Research and development also provide new jobs, which are of high value.

4.2.3 Environmental Impact Assessment

As a general rule, an Environmental Impact Assessment (EIA) has to be prepared and submitted as a part of the application package for the water license if groundwater abstraction is exceeding 5 million m³/year or reinjection is more than 3 million m³/year for the generation of electricity or direct heat. Same applies in all cases where groundwater exploitation from karstic aquifers exceeds 500 m³/day or 2000 m³/day from porous aquifers. Also, if energy production of more than 20 MW is aimed at or the project location is within the protection zone of mineral, medicinal or drinking water resources or on nature protection areas, an EIA should always be prepared (Nádor, 2013).

The EIA is evaluated and checked by the Regional Inspectorate for Environment, Nature and Water, which issues the environmental license for the applicant (Nádor, 2013). Based on the legislation and the current practice, an EIA should be prepared for nearly all utilizations.

As a part of the EIA, environmental monitoring and reporting of well data are compulsory for the well owners. The regulation (101/2007) related to the planning, construction and utilization of geothermal wells describes the necessary expertise, appropriate planning, usage, monitoring and reporting of the wells. Furthermore, the project owner has to report about water usage and well monitoring data under the Mining Act and Water Management Act (Fraser, 2013).

4. 3. Institutional arrangements and licensing

Hungary introduced the single administrative points, which are governmental offices with universal authorizations. Geothermal developers have to hand in inquiries and documents at these offices. However, the experts and decisions makers are still at the authorities, which had been formally put under the guidance of the governmental offices (Kormanyhivatal.hu, 2015).

Due to the separate legislative areas, responsibilities related to geothermal utilizations are distributed among separate authorities, namely the Mining Office and the Water and Environmental Directorate. If energy or heat production is involved, investors need to negotiate with the local service providers, the national distributor and balance circle manager as well as the office for Hungarian Energy and Public Utility Regulatory Authority. The construction of buildings, if a power plant is built, is overseen by the National Directorate General for Disaster Management, Ministry of the Interior (NDGDM), which is a public safety authority, as well as by local authorities and land use offices, which might lack the necessary geothermal knowledge for permitting. The grid connection and for participation of the FiT Systems, the permission and agreement of the balance circle manager (MAVIR Zrt.), the grid operator, the renewable electricity market (HUPIX) and the local service provider are all required.

In case of *open area projects*, the most crucial permits are the three types of water permits, namely the planning (preliminary) permit, the construction permit and the operation permit. During the permitting procedure, production and reinjection wells have to be handled separately.

In general, application for water permits (planning, construction and operation) has to be submitted to the Regional Inspectorate for Environment, Nature and Water. The planning permit issued by the water and environmental authority describes the general water management objectives and basic technical parameters of the planned activity and determines the amount of water to be used in the future but it does not authorize the drilling of wells or any kind of water utilization (Fraser, 2013). The drillings are licensed by the Mining Authority.

Among other documents and plans, the application for a water planning permit shall include the aim of the planned water use, the quality and quantity of the water to be abstracted, the time schedule, the planned methods for water treatment, the technology of the acquisition and the results of preliminary investigations if available. Furthermore, it should include a location map of the area affected by the well and other water uses in the vicinity. Most of these factors are unclear at the planning phase of a geothermal project, therefore continuous cooperation between the project owner and licensing authorities during project preparation could be essential, instead of a not fully funded permit, which needs modifications later.

The construction permit is the one necessary for drilling, reconstruction or abandonment of a well. The application for a water construction permit shall notably include the documentation relating to the property rights, information on the category of water use (public, private), the utilization purpose, the type of the targeted aquifer and the groundwater temperature. Furthermore, it should include the exact location of the drilling, technical parameters of the operation, technical parameters of the well, a

geological description of the location, a hydrogeological model, potential contamination sources and measures of protection (Fraser, 2013).

The water operation permit is the one, which authorizes the execution of water use within a given period of time. The application for an operation permit shall notably include the name of the operator, results of testing, the conditions, rights and obligations of operation and a hydrogeological report.

If the energy or heat produced is to be sold through the national networks or local heat systems, legislations, licenses and permissions related to the construction of buildings, grid connection and sales of electricity and heat are also required. These licenses are not directly related to geothermal energy but rather to general construction, environmental, safety hazard and sales of electricity. The authorities involved in the process are also focused on these areas and not on the specialties of geothermal utilizations.

If energy production and sales of electricity are involved in the project, a set of licenses, permissions and contracts related to energy production, participation in the Feed in Tariff system, electricity off-take to the local and national grids are also required. The procedures to obtain these permits can start simultaneously with the construction of the power plant. The most crucial procedures are to obtain the permission to sell electricity to the national grid, which is assessed by the Hungarian Energy and Public Utility Regulatory Authority (MEKH) and to establish a contract with the local service provider for the electricity offtake to the local grid. Due to the limitations of the electricity grid capacity to adjust the production to the demand, these negotiations are usually expected to last between 3 months up to 1.5 years, which can possibly cause a delay of projects. The fulfilment of all the requirements of the legislation and rules to be applied for energy production and the FIT System can be challenging due to the high number of regulations and amount of time needed to work out the agreement. Therefore, the investor needs to apply for various licenses and permits, in some cases to authorities, which are lacking specific geothermal knowledge for granting a well-funded permit or license. This might cause delays and inconsistencies between the separate administrative procedures of those involved and separate licensing authorities, causing an increase of time and financing for projects. The institutions and authorities have a crucial role in removing these kind of barriers for developments, by introducing specific legislation (geothermal law) and reducing the interface between the investor and the authorities by creating an energy authority acting as the only interface.

4.4 Financing geothermal projects

4.4.1 Fees related to geothermal utilization

Geothermal energy production requires both a mining and a water resource fee, while abstraction of water for balneology, medicinal or water supply only requires a water fee (Geothermal ERANET, 2013; Transenergy, 2011). This multiple taxation disadvantages energy utilizations over other uses.

4.4.2 Project financing

Regarding available public financial resources, geothermal investments in Hungary can be supported from numerous EU, other international and national supporting schemes. Best-known are the GeoFund Geothermal Energy Development Program, the European Economic Area (EEA) Grants, EU Funds and the Environment and Energy Efficiency Operative Programme, which already provided support for some projects. Most of these supporting schemes are aiming at supporting complete projects, such as construction of a complete geothermal district heating system. Also, due to the financial requirements and general project guidelines of EU Funds, usually supported projects are to be implemented in a relatively short period, 1 or 2 years. These two constraints, support of complete projects and the short time for which support is available, limit the support opportunities for new geothermal investments. This has to do with them having long implementation timeframes, because planning, licensing, exploration,

drilling and testing of the wells can take up to 10 to 12 years (Icelandic Generic Plan of 1982) and designing, permitting and the construction of the power plant and its facilities takes up to 2-5 additional years (Steingrímsson, 2009). Therefore, providing financial support to implement complete projects in 1 or 2 years' time does not meet the requirements of geothermal project financing, especially not of new projects. On the contrary, it only fulfils the requirements of certain reconstructions of existing systems. In order to better enable the initiation of new geothermal projects, these EU and national state governed supporting schemes need to be able to reflect the unique necessities of geothermal project financing, and also provide an effective tool for supporting geothermal development by providing financing for certain project phases instead of complete projects.

There are good examples of implemented geothermal projects, which present a possible solution. One is the GeoFund – Geothermal Energy Development Program, which is funded by the GEF trust fund and the International Geothermal Association (IGA) and is administered by the World Bank GeoFund coordination office. Implementation is done by the IFC. The fund aims at removing barriers to geothermal energy use in Central Asia and Europe. It provides low cost loans, contingent and outright grants as well as short and long term cover geological risk insurance (GRI) for project developers. The fund also provides technical assistance for developers. GeoFund supported and provided insurance for one Hungarian project in 2006, the drilling of a new well at Iklódbördöce, Zala county, SW-Hungary, operated by the MOL Hungarian Oil and Gas plc.. The GRI grant covered 85% of the drilling costs (USD 3.72 million), provided technical assistance and related technical assistance grants of USD 810.000. MOL signed an agreement with the World Bank with the endorsement of the Hungarian Government (GeoFund, 2016).

Another good example is the Economic Development and Innovation Programme (EDIP/GINOP), which supports geothermal research projects with short timeline (development of reinjection to porous reservoirs) and the EEA Grant, which supported EUFIRE Ltd. in their geothermal district heating project at Kiskunhalas, Hungary. In this project, the planning and drilling of the first well and related well tests are financed. These were only parts of a larger investment and had a shorter (1 or 2 years) timeframe, and not the complete geothermal development project. The support of the project for drilling the first well and testing is 34% of the total cost, so the financial risks of the investor are significantly reduced (EUFIRE, 2015; 2016a) by providing support for certain parts of a geothermal investment instead of complete projects (Nádor, 2013).

Only some of the international public or private development funds are accessible in Hungary due to its economic status. These funds are the GeoFund, EU development funds, World Bank loans and EBRD loans as well as several international renewable energy investments funds and bank associations that are providing loans for geothermal investments. The Hungarian state itself currently does not provide geothermal development loans or supports, bank guarantee, endorsements etc. For receiving international development funds, the government would need to participate and bear some of the financial risks.

The availability of traditional capital markets is limited for geothermal project developers (Münich RE, 2015). Private loans or bank loans for geothermal energy investments are also limited. Banks in Hungary do not have geothermal institutional practices and specific knowledge about geothermal investments, therefore, external expertise is needed for decision making which creates additional costs and prolongs the time for business negotiations. According to Munich RE (2015), the geothermal risk insurance (GRI) is effective in reducing financial risks of a project by providing backup in case of a failure. Therefore, it provides an advantage for obtaining other loans (Münich RE, 2015).

4.4.3 Availability of geothermal surface and subsurface data

Providing geothermal data for prospective investors also supports investors by reducing the pre-feasibility cost. The creation and maintenance of public geothermal databases can also help in ensuring

the continuous development of institutional capacity. The Geological and Geophysical Institute of Hungary has participated in international projects to develop a database of geothermal wells in Hungary (MFGI GeoBank, 2016). The map provides a lot of data about the wells, however in case of private wells or waters that are not used for energy, the data is provided on a voluntary basis and it is not monitored by an independent entity. The database also contains only limited amount of information such as depth of wells but no production rates or ground water levels. Therefore, the data is not accurate enough to decide about a geothermal development, meaning that no concise public database exists (Nádor, 2013). Private investors and geothermal companies are preparing their own databases that they do not share for obvious reasons. Here the state needs to interfere by conducting research and collect geothermal data in order to be able to provide this information to all investors to achieve better results from geothermal concessions.

5. TURA GEOTHERMAL PROJECT: THE FIRST GEOTHERMAL POWER PLANT IN HUNGARY PRODUCING ELECTRICITY

The geothermal power plant at Tura will be the first power plant utilizing geothermal energy for electricity production in Hungary, as geothermal resources are currently used only for heat production and other conventional utilizations. Due to its pioneering role in geothermal electricity generation, the Tura geothermal project represents a high value in terms of the experience and know-how collected which could be utilized by the relevant institutions, decision makers or investors. Being the first of its kind in Hungary, the project also has a unique interface with the country's geothermal development environment, which is also to be explored by this research.

5.1 Short history of the Tura geothermal project

The Tura geothermal project aims at developing and operating a geothermal heat and electricity production plant in the town Tura in Pest county, 30 km east of Budapest. Tura is well-connected through a motorway close by and the national train network. It is developing rapidly with 8,000 inhabitants. The main source of income at Tura originates from agricultural activities, but spa development is also on the way, utilizing the geothermal resources near the town of Tura.

The first geothermal well of the area (TU-4) has been in production since 1969. Since 2002, the project area has been under continuous development and 3 other wells have been drilled with very good results. Based on this new resource with unexpectedly high temperature, the overall aim of the Tura geothermal project became the building of a geothermal „Organic Rankine Cycle” (ORC) power plant with a capacity to produce 2.7 MW of electricity, and to utilize the cooled fluid from the power plant in surrounding greenhouses as a secondary heat consumer. The operation and sale of electricity is planned to start in the middle of 2017. If the project can keep its timeline, this will be the first example of electricity production from geothermal resources in Hungary. Therefore, it might be useful to collect and analyse the major factors influencing and enabling the success of this development.

The geothermal resource in Tura has been well known for decades. The geothermal reservoir rock is fractured limestone of Triassic age. There are several tectonic structures in the vicinity of Tura area. The primary reservoir rock is 700-1000 m thick, but together with the overlying and underlying carbonate rocks the theoretical thickness of all subsequent carbonate rocks might exceed 3 km. The geothermal gradient in the overlying sediments varies between 50 and 53°C/km. In the project area one well was drilled in 1963 as an agricultural well of the collective farm. The water gained was used for balneological purposes as the area of Tura is mostly an agricultural area, supplying vegetables for the neighbouring towns and Budapest. Following the political changes of 1989, the collective farm as an agricultural enterprise was outdated and the land became private property. This was the time when the municipality of Tura became the owner of some of the agricultural areas and the geothermal wells on them.

The area/property where the well is located is owned by the municipality of Tura. The municipality formed a legal firm, Tura-Therm Ltd., to utilize the wells and the heat of the geothermal waters by building a 2-5 ha. of greenhouses to grow cherry-tomatoes. The municipality needed an investor to bring in know-how, deal with the risks and cover the investment costs of this development. In 2002, the municipality found the investor, Turawell Ltd. As a result of the business negotiations, the ownership rights of the wells were held by the original owner, Tura-Therm Ltd., while the production rights were given to the new investor. Turawell Ltd. had attained 80% of Tura-Therm Ltd. (the original investor) while 20% is still owned by the municipality of Tura. Turawell Ltd. (the new investor) is a Hungarian firm and its majority owner is Mr. László Miszori, while the minority is owned by his colleague, Mr. László Szántó. As a result of the business transaction, Turawell Ltd. bought the majority of Tura-Therm Ltd. and the lands needed in Tura to execute a greenhouse project to grow cherry-tomatoes. The greenhouse project was launched by drilling two reinjection wells in 2011, as reinjection was compulsory according to the relevant legislation. The testing of the two new wells provided much better results than previously anticipated. In well V-1, 126°C hot geothermal water of 91 l/s flow rate was found, which was later verified by well tests. Therefore, the TU-4 well, which was scheduled to be a reinjection well, was turned into a production well. With these new and promising results, the project scope was changed significantly and the target became building of a power plant to produce electricity for the national network and heat for the greenhouses.

The first well, TU-4, drilled in 1963, was used for agricultural purposes and became the basis of the greenhouse development in the area, when a workover was carried out in 2000. Two new wells, T-1 and V-1, were drilled in 2011. T-1 is located close to the old TU-4 well and was originally planned as a production well of the greenhouse project, while the other new well, V-1, located 1.0 km to the southwest from the other two, was originally planned as a reinjection well. The two areas are connected by a 1.1 km long pipeline. Results of the drilling indicated that well V-1 has better outflow parameters than expected and even better than the other two wells, as 126°C hot water with a flow rate of 91 l/s was produced from 1400 m depth. Therefore, the project scope was significantly changed from heat production to heat and electricity production. The licenses of the wells have been modified to allow production from V-1 and reinjection into T-1 and TU-4. Besides these three wells, a standard shallow, cold water production well (HV-1) was also drilled at the power plant site to supply cold water for the cooling tower. The production index of the well is up to 8 l/s for 2 bar drawdown. The arrangement of the project area and the location of the four wells utilized by the project is shown in Figure 3.



FIGURE 3: Overview of the area of the Tura geothermal project

Tura-Therm Ltd. was not a power production company, therefore in order to start the development of the project, a new investor was needed who had the necessary experience and know-how to implement such a new kind of investment in Hungary where only partial technical, licensing, permitting, legislative and policy experience was available for a geothermal based electricity power plant. In 2012, KS Orka Singapore Ltd. purchased the majority of Tura-Therm Ltd. and became the investor and majority owner of the project. KS Orka Singapore is well-known in the geothermal industry and has significant experience in geothermal power plant constructions and related technology. KS Orka is a joint venture between Hugar Orka ehf, an Icelandic company, and Zhejiang Kaishan Compressor Co., Ltd. (Kaishan), which is listed on the China Shenzhen stock exchange. KS Orka combines Hugar Orka's geothermal and project development expertise with Kaishan's power plant technology and manufacturing expertise to form a vertically integrated geothermal and waste energy company, KS Orka, in 2016. Mannvit Budapest Office is providing the project management, specific local knowledge and technical assistance for the project implementation (Mannvit Budapest Office, 2016).

In 2012, the new project was launched, called Tura geothermal project. KS Orka, which bought a 51% stake in the Tura geothermal project, will be building the power plant at an estimated cost of HUF 3.4 billion (USD 11.9 million) with an additional preparation cost of HUF 2.1 billion (USD 7.3 million) (KS Orka, 2016). Figure 4 shows the schematic plan of the scheduled Tura power plant.

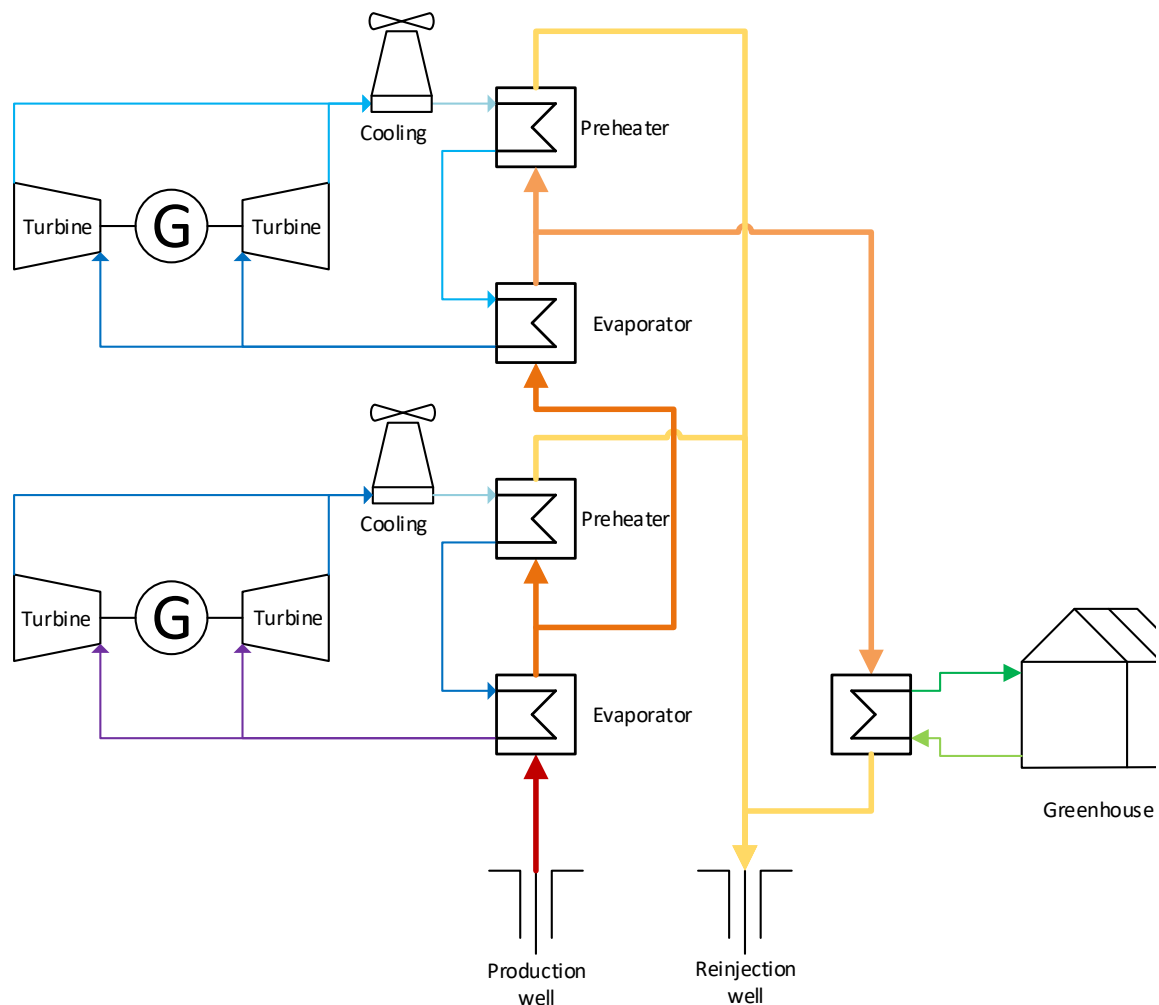


FIGURE 4: Schematic plan of the planned geothermal power plant at Tura

The design temperature of the power plant system is 125°C with 91 l/s (86 kg/s) outflow rate. The total production capacity is 2.7 MW. The excess water of the power plant is 75/78°C hot water, which will be utilized by a greenhouses covering 5-7 ha. The greenhouses will later be extended to 11 ha. and a total annual production capacity of 6300 tons of cherry-tomatoes.

Since 2012 until 2016, the project team of the Tura geothermal project has been working on the modification of existing licenses, permissions, reworking of the wells, the power plant design and construction and electricity and heat production.

On July 15th 2016, at a ceremony in Tura, KS Orka and its partners officially kicked-off the Tura geothermal project and the foundation stone of the first geothermal power plant in Hungary was laid at the project site. The construction of the power plant will be finished and all licenses and permissions have to be obtained by the middle of 2017, when the power plant will go online and production will start (Think GeoEnergy, 2016, Mannvit, 2016).

When this report is written, the construction of the power plant has started and most of the licenses, permissions for the wells and pipelines are in place and the land ownership rights are settled as well. Most licenses and permissions affected by change of project scope and electricity production have been obtained but modifications of these and the final permissions have to be obtained during and after the construction has finished. Simultaneously, new negotiations and licensing procedures need to take place due to electricity production. Permissions and agreements are needed to establish the connection to the electricity grid and related to the sales of electricity, including participation in the Feed in Tariff System have to be obtained. The experiences of this period is explored in detail in this research.

5.2 Advantages and bottlenecks of the project implementation

The project was well developed in many aspects, providing the new investors with a good base to start with. This provided multiple advantages for the investor and for project generation and implementation from various planning, preoperational, financial and management perspectives.

The resource was known and tested. The geothermal capacity of the area had been known since 1963, when the first well of the area was drilled. Also there was no need for extensive and time consuming surface exploration and other tests, previous geographical and other geothermal data was available. In addition, information on the structure of the town and land ownership questions had been solved.

Tura-Therm, Ltd. covered initial project cost, such as exploration and drilling cost of two new wells in 2011. This eliminated most of the initial financial risks of the new investor with the high-temperature resource having been discovered through these drillings, creating favourable conditions for project development. This is a crucial point for any investor in geothermal project development because geothermal development, compared to other renewable energy sources, have high initial costs due to surface exploration, land purchase costs, drilling costs and well testing costs. These costs have to be covered before the actual productivity of the resource can be established and with it the profitability and size of the power plant determined. This makes geothermal projects cost intensive and high risk until the resource size is finally determined. It can be hard to find financial sources willing to cope with this risk. Naturally the investor needs to cover all other costs emerging after becoming owner. However, this could be done by utilization of its own financial resources, therefore the need for further investors or national or EU support had also been evaded.

According to Steingrímsson (2009), market opportunity, knowledge and technical skills, time, financing and luck are the main factors, which will determine the success of a geothermal project. At the beginning of a project, important and costly decisions have to be made, when the resource and expected profitability of the project is not yet known. The original project owner had definitely benefited from

this factor in 2011 when the decision was made to drill two wells for reinjection purposes and the productivity of the new wells exceeded the original production well. When this unique geothermal resource was found, the project could be extended to electricity production in addition to the heat production. In this case, luck proved to be essential for the development of the Tura project.

The area of drilling and the power plant site was also owned by the original investor, Tura-Therm Ltd., therefore, no ownership questions emerged with the land owned by the project company proving suitable for the execution of the project.

Regarding the reservoir ownership, the project is in an advantageous position. According to the relevant Hungarian legislation, the ownership of a geothermal reservoir is not consistently regulated. According to the mining law, reservoirs have an underground volume of 2 km³ size which is covered by the owner's license for utilization. However, in practice reservoirs tend to extend, at least partially, beyond this volume. In order to avoid two projects influencing the productivity of each other, the Mining Authority performs a licensing procedure which includes the estimation and testing of the reservoir by the new project. If this study shows that the new project will not affect the older one and the Mining Authority does accept this argument, the new project can be started. If later the findings of the study are shown to be wrong and production is affected, no responsibility can be established as it can be argued that the results of the exploration were misleading.

Due to its location, the Tura geothermal project is currently not and probably will not be endangered by other projects. The Tura area consists of small size agricultural lands with several owners and families, and inhabited town areas, so there is no space for other energy production geothermal development. However, development of spas has started in the area.

Many of the licenses and permits for wells and pipelines were already in place when the new investor joined the project. However, modifications were needed for many of these licenses and permits at later stages, during the power plant development due to the change of project scope and to adjust to new and previously unknown circumstances. For example, the construction of a geothermal pipeline was needed to connect the wells and the power plant. The original investor had prepared plans and obtained a preliminary permission for construction in order to make the project more advantageous for finding an investor. When the new investor revised the project and the permit for the geothermal pipeline, it became obvious that at numerous locations the pipeline would be crossing roads and other underground installations such as other pipelines and cables. Therefore, the whole permitting procedure had to be restarted and new permitting documentation and plans were needed. This issue highlights the importance of capable geothermal institutions and authorities. If the authority responsible for granting the preliminary permission for the pipeline had noticed that the documentation for the permit was insufficient, the project implementation could have been more efficient.

Local municipalities and their population are also supporting the project, as it is expected to create between 50 and 60 job opportunities. The project and the power plant were designed taking environmental and sustainability aims into account, as the power plant outlay and design were prepared after the relevant regulations and decades long experience of the investor, considering both social and environmental aims. Reinjection and sustainable use of the reservoir are also ensured, minimizing the effect on the environment.

Time is a very important factor in project implementation and profitability of an investment. The Tura geothermal project has an advantage in that respect that no previous surface and underground exploration was needed, neither test nor exploration drillings. Besides enormous cost savings (up to 45% of the total investment), this also saved a lot of time. Typically, a geothermal development from the initial idea until the power plant is online takes usually between 7 to 10 years or even 10 to 12 years (Steingrímsson, 2009; Steingrímsson et al., 2005; Ármannsson et al., 2014). The drillings of the wells

usually take place after the surface exploration and initial environmental impact study and feasibility studies had been prepared and evaluated. Drilling usually takes 3-4 months per well. It is interesting to calculate how long it takes to implement the Tura geothermal project. The period between the original investor purchasing the area and onset of development was 8 years (2002-2010). The drilling of the wells, including receiving permissions, took 2 years from 2009 to 2011. Then the project scope was changed and the new investor started the development in 2012. The power plant is expected to be online in 2017. Hence, the development period lasted from 2011 to 2017, even though no exploration and drillings of wells was necessary.

Licenses needed for the construction of the original project, the greenhouse heated with geothermal energy without the electricity production, are in place. However, with the significant change in the project scope, with the power plant being added to the originally planned greenhouse, a series of modified or new permissions were needed and other legal steps to be performed in order to launch and implement the project. These changes are due to the changes in the size of the greenhouses and the completely new power plant for electricity production:

- The necessary licensing for the construction of the pipeline to connect the wells and the power plant is in place and the extent of that license is expected to be appropriate for the construction. However, there is some risk that the construction license for the pipeline has to be modified due to unknown prescriptions of potentially affected local utilities operators, and unclear status of agreements with land owners which may be affected by the pipeline construction.
- Operation licenses for water facilities can be requested only after the construction of the complete system (i.e. wells and pipeline).
- Construction license for the building of the power plant is already obtained. However, if the design of the power plant is to be changed a licensing modification will be needed.
- The most critical group of the licenses are the permits for the electric network connection. Due to the planned capacity increase, the licensing process including negotiations with the local system operator (ÉMÁSZ) has to be re-started. This could be a relatively long process (from 3 months up to 1.5 years).
- The licenses of the planned technology are already in place, due to the unique rules of procedures, with the license having to be changed only after instalment of modified equipment.

Concerning the water permit of the geothermal pipeline between the project sites, the issuing authority (Environmental and Water Authority) requires the verification of the property rights and the right of way for the project owner for issuing the water construction permit. This means that the investor has possibly to pay all affected landowners a fee before the granting of the water construction permit. The property rights and the right of way have to be issued by the Land Registry Authority, which requires the water construction permit as verification of reason, before the property rights and the right of way can be issued. This contradictory situation between the two authorities and legislations can cause significant delays for the investor and the project until the authorities and the project owner can settle the ownership questions and licenses. As land ownership and property rights are challenging, and are usually time consuming to settle, a legislation is needed to better enable project owners to obtain and keep permits for a longer time to settle challenging situations and avoid delays (Mannvit, 2016).

It should be mentioned that a water construction permit is valid for 2 years, meaning that the construction should be finished within 2 years. However, in case of building constructions in which water is not involved, the local authorities issue the building permit, which is valid for 5 years, leaving more space and time for the investor to start the construction (Mannvit, 2016).

The construction of the geothermal power plant, pipelines, cooling tower, grid connection and all other facilities requires a regular construction permit, which generally is issued by the local municipality.

However, the National Master Builder Office (part of the Ministry of Internal Affairs) intervenes if the aim of the project is the sales of energy.

The National Directorate General for Disaster Management (NDGDM) intervenes in the process of issuing the construction permit of the power plant facilities and some of the machinery and equipment related to power production (heat exchangers). As the original mission of NDGDM is to provide physical help and rescue for people in case of natural disasters and catastrophes, the question of institutional capacity arises if a decision is needed about a specific construction and safety solutions of a power plant when the processes and equipment to be used are related to thermal waters.

Besides network capacity issues, the experience of the Tura project also shows, that institutional capacity and knowledge on geothermal electricity utilization is crucial, both for authorities and investors. In case of the Tura geothermal project, the capacity (3 MW) of the generators and transformers that are installed and connected to the local grid, exceeds the maximum possible production capacity of the production well and the power plant (2.7 MW), as the supplier does not produce this equipment with less than 3 MW capacity. The local service provider and the permitting authority questioned the installation of the planned generator and transformer setup on the basis of that their capacity exceeding the amount that is to be loaded to the grid according to the application of the investor for electricity production and this is may endanger the grid and distribution systems. This is of course impossible to happen because the resource itself is unable to deliver that much energy for electricity and the electricity output of the systems is adjustable. Such a case highlights the need for capable institutions, where know-how and expertise can benefit the institution itself by making well-funded decisions and also shorten the time for the investor to obtain the licenses (Mannvit, 2016).

5.3 Licensing procedures and involved authorities in the Tura geothermal project

The Hungarian licensing environment for almost every constructing activity is divided into to the three main phases:

- I. Licenses for preparation phase;
- II. Licenses for construction phase;
- III. Licenses for operational phase.

During the licensing phases several areas have to be evaluated. The main ones are as follows:

- Environment;
- Water management;
- Buildings;
- Transport of electric energy;
- Power plant technology.

During the licensing process there are a few main authorities who have to approve and issue the necessary permits. These main authorities are however to a certain extent dependent on the opinion of involving/special authorities. Table 2 introduces the procedure, including relevant special permits (indicated with italic style fonts) which are prerequisites of the main licenses and the competent authorities and main steps of the licensing procedure (Mannvit, 2016).

TABLE 2: Summary of the main permitting procedures of the Tura geothermal project

	License/permit/prerequisite	Licensing authority	Scope of license
Preparation	Environmental license (Preliminary environmental assessment)	Environmental and Nature Conservation Authority	Assessment of potential environmental effects of the construction and operation of the complete system
Construction phase	Water legal license for construction	Directorate for Disaster Management of the Capital	Construction license for <ul style="list-style-type: none"> • production well, • injection well, • water pipeline.
	<i>Plant and soil protection plan</i>	<i>Capital and Pest County Government Office Plant and Soil Protection Directorate</i>	<i>Saving of fertile soil on the affected land</i>
	<i>Change of land usage type</i>	<i>Land Registry Office</i>	<i>Change the current agricultural usage type to industrial</i>
	Construction permit	Hungarian Trade Licensing Office (MKEH)	Construction of buildings <ul style="list-style-type: none"> • power plant • transformer
	Electric cable license	Hungarian Trade Licensing Office (MKEH)	Construction of electric transmission lines
	<i>Contract with local electric network operator</i>	<i>ÉMÁSZ Hálózati Kft.</i>	<i>Connection with existing electric network system, takeover of produced electric power</i>
	Consolidated permit for small power plants	Hungarian Energy and Public Utility Regulatory Authority (MEKH)	Construct power plant technology
Operation phase	Water legal license for operation	Directorate for Disaster Management of the Capital	Operation license for <ul style="list-style-type: none"> • production well • injection well • water pipeline
	License of commission	Hungarian Trade Licensing Office (MKEH)	Commission of the buildings <ul style="list-style-type: none"> • power plant • transformer
	Electric cable operation license	Hungarian Trade Licensing Office (MKEH)	Operation of electric transmission lines
	Consolidated permit for small power plants	Hungarian Energy and Public Utility Regulatory Authority (MEKH)	Operation of power plant

6. CONCLUSIONS AND GEOTHERMAL POLICY RECOMMENDATIONS

Although the existing geothermal policy frameworks and licensing systems for geothermal projects show a great diversity, it may be noted that they also share strong similarities. These similarities allow the identification of the broad outlines of a geothermal licensing system, towards which all European countries shall progress (Fraser, 2013).

Effective, clear and concise geothermal legislation or preferably a single geothermal act, streamlined administrative procedures, dedicated and capable institutional system and effective financial support schemes are essential elements to remove administrative and financial barriers of geothermal development, as we can see in case of the Tura geothermal project. There, it can be stated that there would have been no project without the EU Funds and luck with the private investor.

A good policy framework for effective geothermal development is required to reflect the unique needs of geothermal energy compared to other renewable energy sources. The long time span from surface exploration until energy production, the high initial costs and high risks must be reflected and remedied by a capable supporting system. In addition, institutional framework, legislative, legal and administrative constraints are bottlenecks that limit development, should be explored and mended by a specific legislation. Therefore, it is crucial, that a policy framework is proactive and enabling rather than restrictive.

Besides the essential existence of a geothermal resource, the ESMAP handbook (Gehring and Loksha, 2012) identified four key elements that are inevitable in supporting geothermal development:

1. Availability of sufficient geothermal resource data and other relevant information and related research;
2. Effective, dedicated and specialized institution or energy authority;
3. Supportive policies and regulations, and preferably a single geothermal act; and
4. Access to suitable financing for the project developer, including risk mitigation.

The ESMAP handbook (Gehring and Loksha, 2012) handbook states based on the experience of successful countries of geothermal development, that all share the following:

- Dedicated national exploration and development organization, capable of managing large scale infrastructure projects;
- Committed and adequately staffed ministry or similar governmental department;
- Committed and adequately staffed national power utility; and
- Capable regulator.

As the GeoDH study suggests, developing geothermal energy requires an enabling framework starting with clear and consistent national/regional strategies of public authorities. From the project developer's point of view, realising a geothermal project requires several authorizations and the compliance with a number of national and local regulations and legal and financial safeguards. Regulatory barriers and long-administrative procedures can result in additional costs. It is therefore crucial that a fair, transparent and not too burdensome regulatory framework for geothermal and district heating is in place, which not only protects the environment and other aims but also enables development by removing burdens and barriers to development and creates a legislation that is concise and not contradictory (GeoDH, 2016).

The current Hungarian legal, institutional and policy frameworks for geothermal energy use are rather complicated and need to be simplified. The administrative procedures related to mining, energy, environmental protection, water management, disaster management directorates and the authorities responsible for regulations and licensing procedures should be streamlined. The majority of international studies have shown that legal contradictions and time-consuming licensing procedures are still in place (Dumas et al., 2013; GeoDH, 2016; Kujbus, 2012b; Transenergy, 2011; Fraser, 2013; GeoFund, 2016;

Geothermal ERANET, 2013; Rybach, 2003; 2010; Nádor, 2013). Experts agree that reforms have been started but there will always be an area that can be further developed and optimized.

In order to strengthen future geothermal development, the question of reservoir ownership and limitations of use should be addressed and the needed institutional preventive measures and capacity building should be fostered. The main advantage of this would be the prevention of interference between projects, which is a basic deciding factor for geothermal investments. Due to the specific situation of Hungary where numerous cross-border reservoirs are existing, this issue should also be further discussed with its neighbours beyond the existing international agreements.

According to recommendations from various experts of geothermal energy development for the fulfilment of the targets of the NREAP of Hungary, a state funded supporting and risk-mediating mechanism would be a great asset. International experience indicates that public support is needed to reduce the very high upfront risk and cost elements in geothermal for starting geothermal development (Gehring and Loksha, 2012; Századvég Gazdaságkutató Zrt, 2013; Jávora, 2016; and Hólm, 2016). When designing such supporting programmes it has to be ensured that the support is granted for the exploration and drilling phase and not for the complete project, in order to reduce initial risk and evade one of the biggest obstacle of geothermal development (Hólm, 2016).

The experience of the EEA and Economic Development and Innovation Programme previous or ongoing geothermal energy related research projects shows that geothermal research and development can play an essential role in supporting Hungarian geothermal industry and it creates related jobs of high value. Therefore, more emphasis on research and development to support the geothermal industry in developing new geothermal technologies together with a geothermal specific insurance and support scheme could better enable geothermal development.

The examples of financial factors and administrative hurdles and bottlenecks at the Tura geothermal project, as well as the international studies mentioned in this report, seem to be pointing to the need for an adjustment of the Hungarian geothermal development framework in order to foster new development and to increase the annual number of new geothermal energy project inquiries.

Geothermal industry actors and experts agree that the acceleration of geothermal energy development processes is crucial to reach the renewable energy targets of the NREAP. The National Energy Strategy 2030 and the government's determination for the simplification of administrative procedures opened up the opportunity to introduce supporting changes and restructuring of all geothermal energy related areas that the state can enhance. The experiences and measures of other countries, which are successful in geothermal development, should serve as a basis for further development of the Hungarian geothermal policy framework.

ACKNOWLEDGEMENTS

I would like to express my gratitude to my supervisor, Mr. Engilbert Gudmundsson for providing me useful materials, ideas and his work for advising me during the preparation of this report. The Mannvit Budapest Office provided me with essential information and experiences about the Tura geothermal project. I also would like to express my gratitude for Mr. Lúdvík S. Georgsson and the rest of the UNU-GTP staff and lecturers for the possibility to participate in the programme and to gain geothermal project management knowledge and skills. Lastly, but not least, I would like to thank my colleagues and supervisors at the Ministry of National Development, Budapest, Hungary.

REFERENCES

- Ádok, J., 2016: The geothermal heating system in Hódmezővásárhelyi (in Hungarian). Fókusz, website: geotermia.lapunk.hu/tarhely/geotermia/dokumentumok/adokjanos_cikk_hodmezovasarhelyi_geot_fut_rendszer.pdf
- Antics, M., and Sanner, B., 2007: Status of geothermal energy use and resources in Europe. *Proceedings of the European Geothermal Congress 2007, Unterhaching, Germany*, 8 pp.
- Ármanncsson, H., Steingrímsson, B., Gudmundsson, Á., 2014: Planning of geothermal projects in Iceland. *Presented at "Short Course IX on Exploration for Geothermal Resources", organized by UNU-GTP, GDC and KenGen, at Lake Bogoria and Lake Naivasha, Kenya*, 10 pp.
- Askjaenergy.com, 2013: *Mannvit Engineering awarded EU energy funding*. Askjaenergy, website: askjaenergy.com/2013/02/04/mannvit-engineering-eu-funding/_NER300.
- Bertani, R., 2015: Geothermal power generation in the world, 2010-2014 update report. *Proceedings of the World Geothermal Congress 2015, Melbourne, Australia*, 19 pp.
- Dolor, F.M., 2005: Phases of geothermal development in the Philippines. *Paper presented at "Workshop for Decision Makers on Geothermal Projects and Management", organized by UNU-GTP and KenGen in Naivasha, Kenya*, 10 pp.
- Dolor, F.M., 2006: Ownership, financing and licensing of geothermal projects in the Philippines. *Presented at "Workshop for Decision Makers on Geothermal Projects in Central America", organized by UNU-GTP and LaGeo in San Salvador, El Salvador*, 17 pp.
- Dövényi, P., Horvath, F., Drahos, D., et al., 2002: Atlas of geothermal resources in Europe. In: Hurter, S., Haenel, R. (Eds.), *Atlas of geothermal resources in Europe*. European Commission, Office for Official Publications of the European Communities, Luxembourg, Publication No. 17811.
- Dumas, P., Serdjuk, M., Kutschick, R., Fraser, S., Reith, S., and Koelbel, T., 2013: *GEOELEC deliverable 4.1 – report presenting proposals for improving the regulatory framework for geothermal electricity, final draft v. 4, Report on geothermal regulations*. GEOELEC, website: www.geoelec.eu/wp-content/uploads/2011/09/4.1.pdf.
- EEA, 2016: *Programme areas 2009-2014 – Brochure*. EEA Grants, website: eeagrants.org/Results-data/Documents/Publications/Brochures/Programme-Areas-2009-2014-brochure.
- EIB, 2015: *Investment plan for Europe to support renewable energy and strategic infrastructure projects*. European Investment Bank, website: www.eib.org/infocentre/press/releases/all/2015/2015-104-investment-plan-for-europe-to-support-renewable-energy-and-strategic-infrastructure-projects.htm.
- EIB, 2016: What is the “European Fund for Strategic Investments” (EFSI). European Investment Bank, website: bei.europa.eu/efsi/what-is-efsi/index.htm.
- Energiainfo.hu, 2012: *The EGS Hungary Consortium won 11 billion HUF for the establishment of a connected geothermal power plant in Hungary*. Energiainfo.hu, website: energiainfo.hu/cikk/tizenegymilliard_forint_geotermikus_eromure.28844.html,_NER300.
- EU-FIRE, 2015: *Geothermal heating system in Kiskunhalasi* (in Hungarian). EU-FIRE, website: eu-fire.hu/pages/kiskunhalas.

EU-FIRE, 2016a: *Our projects* (in Hungarian). EU-FIRE, website: eu-fire.hu/pages/projektek

EU-FIRE, 2016b: *EGS geothermal power plant in Hungary* (in Hungarian). EU-FIRE, website: eu-fire.hu/pages/egs-hungary.

Fancsik, T., 2013: *Transenergy, the role of geothermal energy in the energy policy of the EU and Hungary*. Transenergy, 11 pp, website: transenergy-eu.geologie.ac.at/Downloads/Events/Public_Event/HU/energetika_FT.pdf

Fraser, S., / GEOELEC, 2013: *A prospective study on the geothermal potential in the EU. GEOELEC, deliverable 4.1, Appendix I – Overview of national rules of licensing for geothermal*. GEOELEC, website: www.geoelec.eu/wp-content/uploads/2011/09/D4.1-A.1-Overview-of-National-Rules-of-Licensing.pdf.

Gehring, M. and Loksha, V., 2012: *Geothermal handbook: planning and financing power generation*. Energy Sector Management Assistance Program (ESMAP), technical report 002/12, 150 pp.

GeoDH, 2016: *Geothermal district heating*. GeoDH, website: geodh.eu.

GeoFund, 2016: *Case study 10: Hungary*. GeoFund, website: documents.worldbank.org/curated/en/255021468030285546/pdf/761080BRI0P07500Box374367B00PUBLIC0.pdf.

Georgsson, L.S., 2016: *Geothermal energy in the world – present status and future predictions*. UNU-GTP, Iceland, unpublished lecture notes.

Georgsson, L.S., Fridleifsson, I.B., Haraldsson, I.G., Ómarsdóttir, M., Ísberg, Th., and Gudjónsdóttir, M.S., 2015a: *UNU Geothermal Training Programme in Iceland: Capacity building for geothermal energy development for 36 years. Proceedings of the World Geothermal Congress 2015, Melbourne, Australia*, 11 pp.

Georgsson, L.S., Haraldsson, I.G., Ómarsdóttir, M., and Ísberg, Th., 2015b: *The UNU Geothermal Training Programme: Training activities offered on-site in developing countries. Proceedings of the World Geothermal Congress 2015, Melbourne, Australia*, 12 pp.

GEOSZ, 2016: *Presentation of the project "Technological development of deployment of deep geothermal systems"* (in Hungarian). GEOSZ, website: geosz.hu/index.php/kf-projektrol.

Geothermal ERANET, 2013: *Geothermal energy status and policy review, Part A, Analysis*. Geothermal ERANET, website: www.geothermaleranet.is/media/publications-2015/Geothermal-ERA-NET-D2_1-Geothermal-energy-status-and-policy-review-NTs.pdf

Goodman, R., Pasquali, R., Dumas, P., Háamor, T., Jaudin, F., Kepinska, B., Reay, D., Rueter, H., Sanner, B., Van Heekeren, V., Bussmann, W., and Jones, G., 2010: *GTR-H – geothermal legislation in Europe. Proceedings of the World Geothermal Congress 2010, Bali, Indonesia*, 5 pp.

GRMF, 2016: *Geothermal risk mitigation facility for East Africa*. GRMF, website: <http://www.grmf-east africa.org/about>

Haehnlein, S., Bayer, P., and Blum, P., 2010: *International legal status of the use of shallow geothermal energy. Renewable and Sustainable Energy Reviews*, 14-9, 2611–2625.

Haraldsson, I.G., 2012: *Legal and regulatory framework – Barrier or motivation for geothermal development? Paper presented at "Short Course on Geothermal Development and Geothermal Wells", organized by UNU-GTP and LaGeo, Santa Tecla, El Salvador*, 24 pp.

Haraldsson, I.G., 2014: Government incentives and international support for geothermal project development. *Paper presented at "Short Course VI on Utilization of Low- and Medium-Enthalpy Geothermal Resources and Financial Aspects of Utilization"*, organized by UNU-GTP and LaGeo, in Santa Tecla, El Salvador, 12 pp.

Hólm, S.L., 2016: *Geothermal development - a private company's experience*. Unpublished presentation, Mannvit Budapest Office.

Jávör, B. (ed.), 2016: *Alternative and sustainable energy scenarios for Hungary* (in Hungarian). Green Hungarian Foundation, Budapest, website: zma.hu/sites/default/files/ASES_hun_20161102.pdf.

KfW, 2016: *Our tasks and goals*. KfW, website: www.kfw-entwicklungsbank.de/International-financing/KfW-Development-Bank/Tasks-and-goals/.

Kormanyhivatal.hu, 2015: "Simpler administration, faster decision making - a unified government office system is created" (in Hungarian). Governmental offices, website: www.kormanyhivatal.hu/hu/csongrad/hirek/egyszerubb-ugyintezes-gyorsabb-donteshozatal-egyseg-kormanyhivatali-rendszer-jon-letre.

Kovacs, I., 2013: *A new opportunity for geothermal energy in Hungary: a picture of a EGS project* (in Hungarian). Geothermia, website: geotermia.lapunk.hu/tarhely/geotermia/dokumentumok/kovacsimredr_eu_fire_eloadasa_20131030.pdf.

Kreuter, H., 2008: Risk mitigation in deep geothermal projects - experience in Germany. *Workshop on Geological Risk Insurance, World Bank Geothermal Energy Development Program (GEOFUND)*, Karlsruhe, Germany, 4 pp.

Kreuter, H., and Schrage, C., 2009: Geothermal market based insurance schemes. *Paper presented at GeoFund – IGA Geothermal Workshop "Turkey 2009"*, Istanbul, Turkey, 4 pp.

KS Orka, 2016: *Tura geothermal project*. KS Orka, website: ksorka.com.

Kujbus, A., 2012a: *Current and future status of the Hungarian geothermal energy production* (in Hungarian). RETS EU project International Conference, Vescs, Hungary, website: www.rets-project.eu/UserFiles/File/pdf/Vecses%20Seminar%20September%202012/2012-09-25-Semin-Hungary-present-and-future-of-geothermal-energy-production-Attila-kujbus_HU.pdf

Kujbus, A., 2012b: *National Environmental and Energy Center (NEEC) non-profit co., and action plan for publicity of low-enthalpy geothermal energy in Hungary till 2020*. Interreg IVC, GeoPower Project, 17-22, website: geopower-i4c.eu/docs/Action%20Plan_final_hungary.pdf.

Kujbus, A., 2016: *Presentation and personal communication at the Ministry of National Development*. MND, March 29th, 2016, Budapest.

Kurunczi, M., and Ádám, B., 2016: *Hódmezővásárhely geothermal heating system: Geothermal water as an alternative energy source* (in Hungarian). Website: <http://www.hoszisz.hu/tanulmanyok/24-a-geotermikus-energia-termalviz-es-foeldh-mint-alternativ-energiaforras>, visited on 04. October 2016.

Lund, J.W., and Boyd, T.L., 2015: Direct utilization of geothermal energy 2015, worldwide review. *Proceedings of the World Geothermal Congress 2015 Melbourne, Australia*, 31 pp.

Mádlné, S.J. (ed.), 2008: *Geothermal energy utilization in international and domestic status and future opportunities in Hungary: Recommendations of governmental steps in support* (in Hungarian). Report

to the Hungarian Academy of Sciences, Budapest, website: www.geotermika.hu/portal/files/mta-geotermika.pdf.

Mannvit, 2016: *Turawell geothermal project underway*. Mannvit, website: www.mannvit.com/news/turawell-geothermal-project-underway/.

Mannvit Budapest Office, 2016: *Parts of the Tura diligence report*. Mannvit, Budapest.

MEKH, 2015: *Report on the use of renewable energy in Hungary 2004-2014* (in Hungarian). Hungarian Energy and Public Utility Regulatory Authority – MEKH, website: www.mekh.hu/download/3/f3/20000/beszamolo_a_magyarorszagi_megujuloenergia_felhasznalas_2004_2014_evi_alakulasarol.pdf

MFGEI, 2013: *Mineral resources and resource utilization action plan of 2013* (in Hungarian). MFGEI, website: www.mfgei.hu/hu/node/703.

MFGEI, 2016: *Public maps and databases for geothermal energy in Hungary*. MFGEI, website: map.mfgei.hu/furas/.

MFGEI GeoBank, 2016: A geological and drilling database for Hungary. MFGEI, website: www.mfgei.hu/hu/node/79.

Micale, V., and Padraig, O., 2015: *Lessons on the role of public finance in deploying geothermal energy in developing countries*. Climate Investment Fund – CIF, website: climatepolicyinitiative.org/wp-content/uploads/2015/08/Lessons-on-the-Role-of-Public-Finance-in-Deploying-Geothermal-Energy-in-Developing-Countries-Full-Report.pdf.

Micale, V., Trabacchi, C., and Boni, L., 2015: *Using public finance to Attract Private Investment in Geothermal: Olkaria III: case study, Kenya*. Climate Investment Fund - CIF, website: climatepolicyinitiative.org/publication/using-public-finance-to-attract-private-investment-in-geothermal-olkaria-iii-case-study-kenya/

MND, 2010: *Renewable energy, Republic of Hungary, National renewable energy action plan 2010-2020*. Ministry of National Development, website: www.kormany.hu/download/6/b9/30000/RENEWABLE%20ENERGY_REPUBLIC%20OF%20HUNGARY%20NATIONAL%20RENEWABLE%20ENERGY%20ACTION%20PLAN%202010_2020.pdf

MND, 2011: *National energy strategy of Hungary*. Ministry of National Development, website: www.kormany.hu/en/ministry-of-national-development/news/national-energy-strategy-2030-published.

Montalvo E., F., 2014: Regional geothermal office for Central America. *Paper presented at “Short Course VI on Utilization of Low- and Medium-Enthalpy Geothermal Resources and Financial Aspects of Utilization”*, organized by UNU-GTP and LaGeo, in Santa Tecla, El Salvador, 10 pp.

Münich RE, 2015: *Exploration risk insurance – Munich RE’s experience in Turkey*. Munich RE & IRENA, website: www.irena.org/EventDocs/S3.4GeothermalExplorationInsuranceTurkey-MunichRE.pdf.

Nádor, A., 2013: *List of legal and economic deficiencies, non-technical barriers of geothermal development*. TransEnergy, website: transenergy-eu.geologie.ac.at/Downloads/outputs/Summary%20report%20of%20the%20supra-regional%20hydrogeological%20model/WP6/2CE124P36PR_WP6C_6.2.3_%20List%20of%20legal%20and%20economic%20deficiencies.pdf

Nádor, A., Tóth, A.N., Kujbus, A., and Ádam, B., 2013: Geothermal energy use, country update for Hungary. *European Geothermal Congress, Pisa, Italy*, 12 pp.

Ngugi, P.K., 2014: Risks and risk mitigation in geothermal development. *Paper presented at “Short Course VI on Utilization of Low- and Medium-Enthalpy Geothermal Resources and Financial Aspects of Utilization”*, organized by UNU-GTP and LaGeo, in Santa Tecla, El Salvador, 11 pp.

NREAP, 2013: “Hungary’s National Renewable Energy Action Plan” (in Hungarian). NREAP website: www.kormany.hu/download/d/61/10000/Magyarorsz%C3%A1g%20Meg%C3%BAjul%C3%B3%20Energia%20Hasznos%C3%ADt%C3%A1si%20Cselekv%C3%A9si%20Terve.pdf.

Orkustofnun, 2016: Geothermal policy options and instruments for Ukraine. Orkustofnun – National Energy Authority, report prepared for the Ministry for Foreign Affairs, Iceland, 132 pp.

Pálvölgyi, T. (ed.), Dönsz-Kovács, T., Kukely, G., Mészáros, G., and Enikő, E.S., 2011: Environmental assessment for the national energy strategy until, 2030, with outlook until 2050 for the strategic environmental assessment (in Hungarian). Ministry of National Development – MND, website: www.fataj.hu/2011/06/236/ESTRAT2030-Kornyezeti-Hataselemzes-20110513.pdf

PannErgy, 2013: *PannErgy Plc., preliminary information concerning business operations 2013*. PannErgy, Plc., website: pannergym.com/wp-content/uploads/2014/02/2013q4_v5_1_9_en.pdf

PannErgy, 2016: *Projektjeink*. PannErgy, Plc., website: pannergym.com/projektek/

Ren21, 2015: Renewables 2015 global status report. Ren21, website: www.ren21.net/wp-content/uploads/2015/07/REN12-GSR2015_Onlinebook_low1.pdf

Rybach, L., 2003: Regulatory framework for geothermal in Europe – with special reference to Germany, France, Hungary, Romania, and Switzerland. *Lectures on the sustainable use and operating policy for geothermal resources - Proceedings of short course for IGC2003, Sept., UNU-GTP, publicat. 1, Reykjavik*, 43-52.

Rybach, L., 2010: Legal and regulatory environment favourable for geothermal development investors. *Proceedings of the World Geothermal Congress 2010, Bali, Indonesia*, 7 pp.

Sipos, G., 2011: *Geothermal power at deep levels in Hungary* (in Hungarian). Origo, website: www.origo.hu/idojaras/20110928-geotermikus-energia-tavfutes-furdes-visszasajtolas-csak-a-fold-melyen-szomit.html

Soltész, I., 2016: *Energy efficiency investments supported by tax incentives* (in Hungarian). TERC, website: www.terc.hu/cikk/adokedvezmennyel-tamogatott-energiahatekonysagi-beruhazasok.

Steingrímsson, B., 2009: Geothermal exploration and development from a hot spring to utilization. *Paper presented at “Short course on Surface Exploration for Geothermal Resources”*, organized by UNU-GTP and LaGeo, in Ahuachapán and Santa Tecla, El Salvador, 8 pp.

Steingrímsson, B., Ármannsson, H., and Gudmundsson, Á., 2005: Phases of geothermal development in Iceland. *Paper presented at Workshop for Decision Makers on Geothermal Projects and Management*, organized by UNU-GTP and KengGen in Naivasha, Kenya, 11 pp.

Szanyi, J., and Kovács, B., 2010: Utilization of geothermal systems in southeast Hungary. *Geothermics* 39-4, 357-364.

Századvég Gazdaságkutató Zrt, 2013: *Recommendations for designing a risk mitigation framework for geothermal investments* (in Hungarian). Századvég Gazdaságkutató Zrt, Website: tasz.hu/files/szazadvég-tanulmányok/NFM_201312/NFM02_TANSZ_201312_EN_free.pdf.

ThinkGeoenergy, 2016: *Official kick-off for Turawell geothermal project in Hungary*. Think GeoEnergy, website: www.thinkgeoenergy.com/official-kick-off-for-turawell-geothermal-project-in-hungary/

Tóth, A.N., 2010: Hungary country update 2005-2009. *Proceedings of the World Geothermal Congress 2010, Bali, Indonesia*, 8 pp.

Tóth A.N., 2013: Hungarian-American cooperation in geothermal e-learning. *European Geothermal Congress, 2013, Pisa, Italy*.

Tóth, A.N., 2015: Hungarian country update 2010-2014. *Proceedings of the World Geothermal Congress 2015, Melbourne, Australia*, 8 pp.

Transenergy, 2011: *Transenergy - Transboundary geothermal energy resources of Slovenia, Austria, Hungary and Slovakia - overview of EU, national and regional legislation*. Transenergy, website: transenergy-eu.geologie.ac.at/Downloads/2CE124P3_4PR_WP3%203.3.1_Overview%20of%20EU%20national%20and%20regional%20legislation.pdf.

Wall, E., 2009: Recovers act funding for geothermal technologies. GRC - Department of Energy Update, website: www.geothermal.org/PDFs/Articles/09MayJune21.pdf.

**APPENDIX I: Excerpt from Transenergy (2011) research.
Overview of laws and regulations related to geothermal energy in Hungary and Slovakia -
regulations related to grid connection, building permits
and participation in FiT are not included**

HUNGARY

Regulations related to mining:

1. Act XVI of 1991 on concession.
2. Act XLVIII of 1993 on mining.
3. Governmental Decree 203/1998 (XII.19.) on the execution of Act XLVIII of 1993 on mining.
4. Governmental Decree 267/2006 (XII.20.) on the Hungarian Office for Mining and Geology.
5. Governmental Decree 54/2008 (III.20) on the determination of the specific value of mineral resources and geothermal energy and the method of value calculation.
6. Governmental Decree 103/2011 (VI.29.) on the complex vulnerability and impact assessment of the natural occurrences of mineral resources and geothermal energy.

Regulations related to energetics:

7. Act LXXXVIII of 2003 on energy tax.
8. Act XVIII of 2005 on district heating.
9. Governmental Decree 157/2005 (VIII.15.) on the execution of Act XVIII of 2005 on district heating.
10. Act LXXXVI of 2007 on electric energy.

11. Governmental Decree 273/2007 (X.19.) on the execution of certain regulations of Act LXXXVI of 2007 on electric energy.
12. Governmental Decree 389/2007 (XII.23.) on the compulsory acceptance system and feed-in tariffs of electricity produced by energy gained from renewable energy resources and waste, as well as the co-generated electricity.
13. GKM/Ministerial Decree 110/2007 (XII.23.) on the calculation method to determine the quantity of the useful heat and the co-generated electricity.

Regulations related to environmental protection:

14. Act LIII of 1995 on the general rules of environmental protection.
15. Act XLIII of 2000 on waste management.
16. Governmental Decree 219/2004 (VII.21.) on the protection of groundwaters.
17. Governmental Decree 220/2004 (VII. 21.) on the protection of surface waters.
18. Governmental Decree 221/2004 (VII.21.) on certain rules of river basin management.
19. KvVM /Ministerial Decree 28/2004. (XII. 25.) on the threshold values of water contaminating materials and on certain rules of their application.
20. KvVM /Ministerial Decree 30/2004 (XII.30.) on certain rules of examination of groundwaters.
21. KvVM /Ministerial Decree 33/2005 (XII.27.) on the administrative service fees of environment, nature protection and water authorities.
22. Governmental Decree 314/2005 (XII.25.) on the licensing process of environmental impact assessment.

Regulations related to water management:

23. Act LVII of 1995 on water management.
24. KHVM / Ministerial Decree 18/1996 (VI.13) on the contents of the application form and its annexes to be submitted for granting the water permits.
25. Governmental Decree 72/1996 (V.22.) on the implementation of authority powers in water management.
26. Governmental Decree 121/1996 (VII.24.) on the establishment and utilization of public baths.
27. KHVM /Ministerial Decree 12/1997 (VIII.29.) on the degassing of the produced and supplied waters.
28. Governmental Decree 123/1997 (VII.8.) on the protection of water resources, potential water resources and water establishments supplying drinking water.
29. KHVM /Ministerial Decree 23/1998 (XI.6.) on the water management register of the water inspectorates.
30. KHVM /Ministerial Decree 43/1999 (XII.26.) on the calculation of the water resource fee.
31. EüM/ Ministerial Decree 74/1999 (XII.25.) on the natural medicinal factors.
32. KvVM /Ministerial Decree 24/2007 ((VII.3.) on the Water Safety Regulations.
33. KvVM /Ministerial Decree 101/2007 (XII.23.) on the professional requirements about the intervention into the groundwater reserves and water well drilling.
34. KvVM /Ministerial Decree 30/2008 (XII.31.) on the technical regulations related to the activities and establishments serving the utilization, protection and mitigation of damages of waters.
35. Governmental Decree 147/2010 (IV.29.) on the general regulations related to the activities and establishments serving the utilization, protection and mitigation of damages of waters.
36. Governmental Decision 1002/2012 (I.11.) on the exemption of re-injection of thermal water used for energetic purposes in agriculture.

Regulations related to heat pumps:

37. Governmental Decree 264/2004 (IX.23.) on the taking back of waste deriving from electric and electronic gadgets.
38. KTM /Ministerial Decree 10/1995 (IX.28.) on the environmental protection product fee and the execution of Act LVI of 1995 on the environmental protection product fee of certain products.
39. GKM /Ministerial Decree 96/2005 (XI.4.) on the regulations of certain building processes concerning special buildings falling within the competence of the mining inspectorates.
40. TNM /Ministerial Decree 7/2006 (V.24.) on the determination of energetic features of buildings.

SLOVAKIA**National legislation in relation to geothermal energy exploration and exploitation:**

1. Constitution of the Slovak Republic, Constitutional Act. 460/1992 Coll. as subsequently amended.
2. Civil Code, Act. 40/1964 Coll., as amended.
3. Water Act. 364/2004 Z.z. on waters as amended and amending Law No.. 372/1990 Coll. on offences, as amended.
4. Geological Act. 569/2007 Z.z. on geological works, as amended.
5. Mining Act. 44/1988 Coll., protection and utilization of mineral resources, as amended.
6. Act. 92/1991 Coll. on the transfer of state property to other persons, as amended.
7. Commercial Code Act. 513/1991 Coll., as amended.
8. Trades Act. 455/1991 Coll. on trades, as amended.
9. Building Act. 50/1976 Coll., the Planning and Building Order (Building Act) as amended.
10. Slovak Republic Government Order no. 755/2004 Coll., laying down the amount of nonregulated payments, fees and details related to charging for water use.
11. Ministry of the Environment Regulation no. 51/2008 Coll. that administers Geological Act, as amended.
12. Act. 309/2009 Coll. the promotion of renewable energy and high-efficiency cogeneration and amending certain laws.
13. Act. 656/2004 Coll., on energy and amending certain laws.
14. Decree of the Regulatory Office for Network Industries 225/2011 Coll. establishing price regulation in the electricity energy.
15. Act 657/2004 Coll. of thermal energy and amending certain laws.
16. Decree of the Regulatory Office for Network Industries no. 219/2011 Coll. establishing price controls on thermal energy.
17. Act. 24/2006 Coll. Assessment of environmental impact (Environmental Impact Assessment) and amending certain laws.
18. Government Order no. 269/2010 Coll., laying down the requirements for achieving good water status.
19. Ministry of Agriculture, Environment and Regional Development of the Slovak Republic no. 418/2010 Coll. for implementing certain provisions of the Water Act.

MAIN HUNGARIAN LAWS AND REGULATIONS REFERRED IN THE REPORT:

Mining Law Act: XLVIII of 1993 of Hungary.

Website: njt.hu/cgi_bin/njt_doc.cgi?docid=19243.328105

Water Management Act: LVII of 1995 of Hungary.

Website: njt.hu/cgi_bin/njt_doc.cgi?docid=23855.328110

Governmental Decree 103/2011. (VI.29.) on the Complex Vulnerability and Impact Assessment.

Governmental Decree 219/2004 (VII.21.) on the protection of ground waters.

Website: njt.hu/cgi_bin/njt_doc.cgi?docid=86354.332598

Governmental Decree 221/2004 (VII.21.) on certain rules of river basin management.

Website: njt.hu/cgi_bin/njt_doc.cgi?docid=86359.298018

Act XVI of 1991 on Concession.

Website: njt.hu/cgi_bin/njt_doc.cgi?docid=15165.330720

Ministerial Decree 101/2007 (XII.23.) rules of intervention to groundwater resources and guidelines to the drilling of wells. Website: njt.hu/cgi_bin/njt_doc.cgi?docid=111083.291366

Governmental Decree 314/2005 (XII.25.) on environmental impact assessment.

Website: njt.hu/cgi_bin/njt_doc.cgi?docid=96394.330273.



UNITED NATIONS
UNIVERSITY

UNU-GTP

Geothermal Training Programme

Orkustofnun, Grensasvegur 9,
IS-108 Reykjavik, Iceland

Reports 2016
Number 13

ANALYSIS OF WELL TESTING, TEMPERATURE AND PRESSURE IN HIGH-TEMPERATURE WELLS OF ALUTO-LANGANO, ETHIOPIA

Mesay Fekadu Biru

Ethiopian Electric Power – EEP

Kirkos Kifle Ketema, Wereda 07, House No. 944/05

Meba Building, P.O. Box 15881

Addis Ababa

ETHIOPIA

abushmech@gmail.com

ABSTRACT

Drilling in Aluto-Langano geothermal field started in 1981 with the aim of harnessing steam for electricity power production. Eight wells were drilled between 1981 and 1986, thereof four productive, one reinjection and three non-productive wells. Recently, between 2013 and 2015, two directional wells were drilled and they are still undergoing different measurements and tests. Measurements from the wells, LA-9D and LA-10D, as well as from an older one, LA-3, were analysed and are presented in this report. Results from analyses of injection tests for wells LA-3 and LA-10D are characterized by having fairly good transmissivity and storativity values and the injectivity indices are rather low. The evaluated fluid enthalpy for wells LA-9D and LA-10D is in the range of 1600-2200 kJ/kg, with steam flow ranging from 5 to 9 kg/s with separation pressure of 1 bar-a as well as with separation pressure of 5 bar-a of Aluto-Langano pilot power plant.

Formation temperatures of wells LA-9D and LA-10D were estimated by extrapolation of temperature logs from their warm up periods. The results suggest that the reservoir temperature is in the range of 300-315°C and reservoir pressure in the range of 85-100 bar for both wells.

1. INTRODUCTION

Ethiopia is one of the East African countries with the most significant geothermal resources. Exploration of the resources started in 1969 and they have been investigated gradually. A total of 10 wells have already been drilled in one of the most promising fields, the Aluto-Langano geothermal field, but the field has only been utilized to a small extent.

In this report the results of analyses conducted on measurements from the Aluto-Langano geothermal field are introduced. From this area, wells LA-3, LA-9D and LA-10D were selected for studying. Different types of analyses were performed including simulations of injection tests from the end of drilling of LA-3 and LA-10D, as well as estimation of formation temperature, initial pressure and analysis of discharge testing from directionally drilled wells LA-9D and LA-10D.

The injection test simulation was made by using Welltester software, based on non-linear regression

(Júlíusson et al., 2008; Marteinnsson, 2016). The injectivity index is the first parameter analysed and is a simple relationship between change in flow and change in pressure, reflecting the capacity of a well or how open it is to the surroundings, which is useful for determining whether a well is sufficiently open to be a successful producer, if it should be stimulated or if drilling should possibly be continued to look for better feed zones at deeper levels.

Formation temperature estimations were obtained by using the Berghiti software developed at ISOR – Iceland GeoSurvey (Helgason, 1993; Marteinnsson, personal communication). Formation temperature estimation is important to increase the knowledge about a geothermal system for decision making when selecting new sites and for developing conceptual models. The initial pressure is also obtained by using Predyp from ICEBOX software (Arason et al., 2004). Discharge test analysis is obtained by using Lip from ICEBOX software.

Discharge data from LA-9D and LA-10D were analysed at different wellhead pressures.

A short description of Aluto-Langano geothermal system is given in Section 2. Injection tests from two wells were analysed and discussed in Section 3. Temperature and pressure profiles during warm up period were analysed to determine the formation temperature and initial pressure and the process and results are introduced in Section 4 and, finally, the result of discharge testing is analysed followed by discussion and conclusion in Sections 5 and 6.

1.1 Geothermal system

Geothermal resources are distributed throughout the planet. Even though most geothermal systems and the greatest concentration of geothermal energy are associated with the Earth's plate boundaries, geothermal energy can be found in most countries. It is highly concentrated in volcanic regions, but can also be found as warm groundwater in sedimentary formations worldwide as low-temperature systems (Axelsson, 2012). Geothermal systems are governed by the surface and subsurface hydrological pattern, heat source and surface activity associated with the geothermal resource. While the term geothermal field is considered to refer to the area of geothermal activity on surface, intended as a geographic description, it is regarded as a component of the geothermal system. The geothermal reservoir is the section in the geothermal system that can be economically exploited for energy utilization.

Geothermal systems exist in different forms and are classified on the basis of reservoir temperature, enthalpy, physical state, geological settings and nature (Axelsson, 2012). Low-temperature systems ($<150^{\circ}\text{C}$), are referred to as low-enthalpy systems ($<800\text{ kJ/kg}$). This type of geothermal systems exists e.g. in sedimentary basins with permeability at great depth and is classified as liquid-dominated geothermal systems. High-temperature systems ($>200^{\circ}\text{C}$) may also be described as high-enthalpy systems ($>800\text{ kJ/kg}$). They are mostly characterised by active volcanism, the heat source being shallow magma, intrusions or dykes.

1.2 Geothermal wells

Geothermal wells play a key role in research and development of geothermal systems. Geothermal wells provide access for direct testing and measurements of the systems. They are vital components in both geothermal research and utilization, since they provide essential access for both energy extraction and information collection (Axelsson, 2013). Geothermal wells can be classified as low-temperature or high-temperature wells. A low-temperature (liquid-dominated) well produces liquid water at wellhead while a high-temperature well in which the flow from feed zone(s) is liquid or two-phase produces either a two-phase or dry steam at wellhead (Grant and Bixely, 2011).

There are many types of geothermal wells, some of them are described in the following. Temperature gradient wells are designed as slim and shallow, typically less than 100 m in depth, drilled in the early stage of geothermal research. Their main purpose is to determine the temperature gradient near surface at shallow depth. Another type are the exploration wells which are drilled during the exploration phase, usually deeper than gradient wells to hit the geothermal reservoir with the purpose of exploring its conditions. The production wells have the main purpose of facilitating the geothermal energy extraction from the reservoir but are also used for gaining further information about the reservoir. The step-up wells are drilled to extend the confirmation of a particular geothermal reservoir while the make-up wells are used to make up for either damaged production wells due to scaling or collapse or regular declining output of production wells with time. The injection wells are used for injecting water back into the geothermal system which helps maintaining production capacity, for environmental management and decreasing pressure drops. The monitoring wells are used for management purposes, i.e. for monitoring how the geothermal system reacts to the production (Axelsson, 2013).

2. ALUTO-LANGANO GEOTHERMAL SYSTEM

2.1 Location and geological setting of Aluto-Langano

Ethiopia is one of the East African countries with the most significant geothermal resources, and launched a long-term geothermal exploration in 1969. Over the years a good inventory of the potential target areas has been built up and more than 23 prospects are judged as having potential for electricity production (Teklemariam, 1996; Teklemariam et al., 1996).

The geothermal resources are present in the main Ethiopian Rift System and in the Afar depression, which are parts of the Great East Africa Rift System. More than sixteen geothermal prospects are located along this rift that are believed to have the potential for electricity production. Aluto-Langano, Tendaho, Corbetti, Abaya, Tulumoye-Gedemsa, Dofan and Fantale (Figure 1) are few of the prospect areas in which detailed exploration study and drilling have started due to their expected potential and their strategic location relative to the national electric grid (Worku Sisay, 2016).

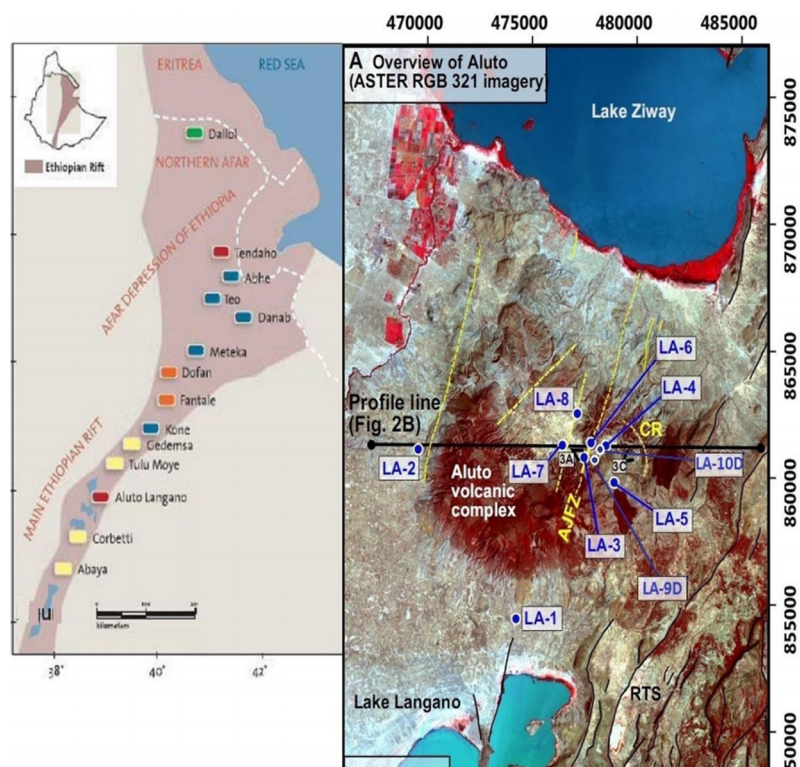


FIGURE 1: Main Ethiopian rift valley to the left and Aluto volcanic complex to the right (Hutchison et al., 2015)

2.2 Surface geology of Aluto-Langano

Aluto volcanic complex covers an area of about 100 km² between lakes Langano and Ziway (Figures 1 and 2) and rises to elevation of 690 m above the surrounding Adami-Tullu plain which has an elevation

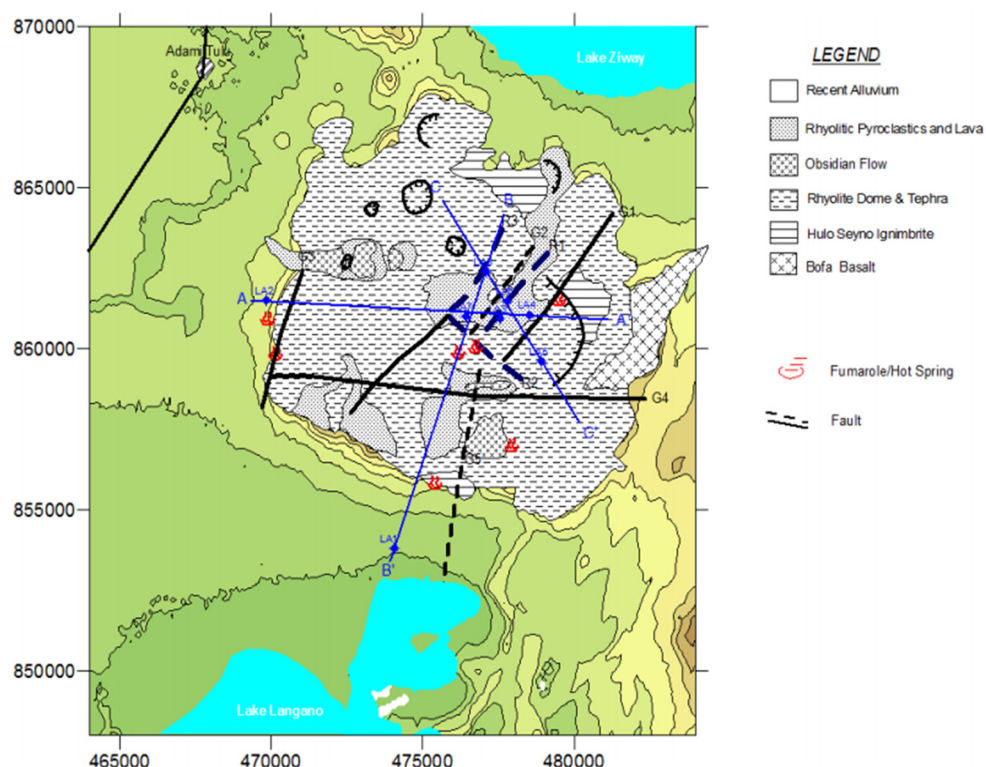


FIGURE 2: Geological map of Aluto-Langano geothermal field and the Wonji Fault Belt (Hutchison et al., 2015)

of about 1600 m a.s.l. The broad truncated base and a summit caldera are 6 km by 9 km (with an area of 37 km²) elongated in a WNW direction have formed a basin of internal drainage (Worku Sisay, 2016). Volcanic activity at the Aluto volcanic centre mostly occurred in the Quaternary with earlier sub-lacustrine eruptions. The activity is initiated with a rhyolite dome building phase intervened by explosive pyroclastic pumice eruptions and a major caldera forming pyroclastic eruption. The ignimbrite is now exposed on the flanks of the Aluto volcanic massif as pumices ignimbrites and sub-aqueous pumices tuff with minor intercalations of lacustrine sediments. Post-caldera collapse rhyolite flows, domes with minor pyroclastic products formed along the NE-SE segment of the Aluto Caldera rim on a basement of pumices ignimbrites and older rhyolite. Predominantly rhyolite post-caldera lava and pyroclastic have erupted from numerous craters with all vents showing a clear control by either the caldera ring fracture or the NNE trending faults of the Wonji Fault Belt (WFB). The northern segment of the centre is characterised by large rhyolite domes and flows, which do not show a marked structural control. Minor basaltic lavas have erupted from the north-northeast trending faults east of Aluto massif. The Aluto caldera is covered by alluvial sediments (Teklemariam and Beyene, 2000).

2.3 Exploration drilling

Aluto-Langano is the first geothermal field in Ethiopia to be exploited. In this area, eight deep exploration wells (LA-1 to LA-8) (Figure 3) were drilled from 1981 to 1986 with a maximum depth of 2500 m, reaching temperatures of up to 335°C (Teklemariam and Beyene, 2000). Wells LA-1 and LA-2 were drilled at the southern and western flanks of Aluto Volcanic Complex (AVC), respectively (Figure 3), and are characterized by low temperature and permeability. Wells LA-3 to LA-8 were sited on top of Aluto-Langano in the south-eastern part of the area. LA-3 and LA-6 were drilled in the most active fault system, Wonji Fault Belt (WFB) (Figure 2), trending in north-northeast direction, and where maximum temperature recorded were 315 and 335°C, respectively (UNDP, 1986). LA-4 and LA-5 were drilled in the eastern part of Wonji Fault Belt and LA-7 and LA-8 in the western part (Figure 3).

The first 7.2 MWe pilot power plant was installed in the Aluto-Langano field by the Ethiopian Electric Power Corporation and connected to the national power grid in May 1998. It was started by connecting four production wells, LA-3, LA-4, LA-6 and LA-8, and one reinjection well, LA-7 (Teklemariam and Beyene, 2000). The expected capacity of this geothermal field was 30 MWe for 30 years. The pilot power plant has not been in full operation due to problems related to the production wells (e.g. decline of well pressures, scaling and wellhead valve problems) and problems related to the power plant involving cooling tower fan breakdowns, pentane leakage from the heat exchangers and so on. According to Kebede (2012), the plant has been partially renewed and started to produce 4 MWe in 2007. Recently, two exploration wells have been drilled, LA-9D and LA-10D, using a rig owned by the Geological Survey of Ethiopia. LA-9D and LA-10D are the first directional wells in Ethiopia and both wells are in testing phase.

Information about wells LA-3 to LA-10D is given in Table 1.

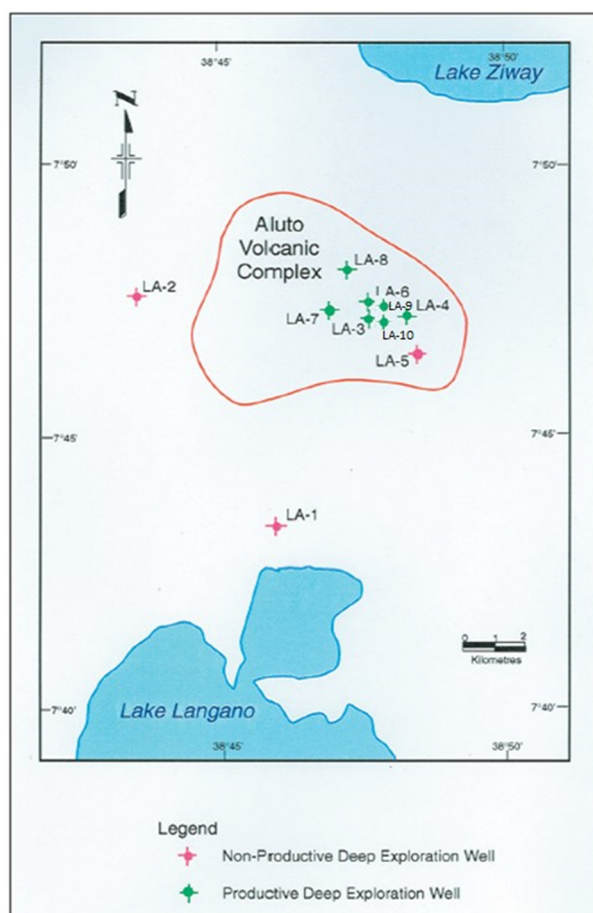


FIGURE 3: Wells LA-1 to LA-10D located in Aluto-Langano geothermal field

TABLE 1: Information about exploration wells in Aluto-Langano geothermal field (P: Productive; NP: Non productive; RW: Reinjection well)

Well	LA-3	LA-4	LA-5	LA-6	LA-7	LA-8	LA-9D	LA-10D
Drilled depth (m)	2114	2062	1867	2203	2448	2500	1921	1950
Elevation (m a.s.l.)	1921	1956	2037	1962	1891	1895	1963	1960
Permeable zones (m)	2000-2121	1445-1800	-	2000-2200	2100-2300	2300-2500	760-1350	920-1760
Maximum T (°C)	322	240	210	335	228	284	308	310
Status of the well	P	P	NP	P	RW	P	P	P
Time of drilling	21/1/83-13/6/83	6/7/83-23/10/83	15/11/83-11/3/84	24/3/84-2/7/84	12/7/84-21/10/84	26/10/84-13/5/84	12/11/13-01/02/15	25/06/15-02/10/15

3. INJECTION WELL TESTING

3.1 Introduction of pressure transient analysis

Immediately after completion of geothermal well drilling, well testing is conducted in order to assess the conditions of a well and the properties of the reservoir intersected by the well, by subjecting it to injection or production. During an injection test, the response of a reservoir to changing injection rate is monitored. A change in flow rate usually results in changes in pressure which can be measured. Examples of parameters that control the reservoir response are storativity, transmissivity (permeability),

wellbore storage, wellbore skin, fracture properties and reservoir boundaries. A mathematical model is commonly set up to simulate the pressure transient response in the well and the reservoir caused by an instantaneous step change in injection or production. The mathematical model depends on values selected for properties characterising the reservoir and by iterating these values such that the modeled response fits the observed data though one can infer the characteristic properties of the reservoir (Horne, 1995). Pressure diffusion equation is the basis of all models in well testing theory or pressure transient analysis.

The pressure diffusion equation is used to calculate the pressure (p) in the reservoir at a certain distance (r) after a given time (t) of an injection (or production) well receiving or producing fluid at specific rate (Q), starting at time $t = 0$. The pressure diffusion equation is derived by combining the conservation of mass law, Darcy's law and the equation of state of the fluid.

The following assumptions are made before the equation is derived (Horne, 1995; Haraldsdóttir, 2016):

- Horizontal radial flow;
- Darcy's law applies;
- Homogeneous and isotropic reservoir;
- Isothermal conditions;
- Uniform thickness of reservoir, h ;
- Single-phase flow;
- Small pressure gradients;
- Small and constant compressibility, c_i ;
- Constant porosity, ϕ ;
- Constant fluid viscosity, μ ;
- Constant permeability, k .

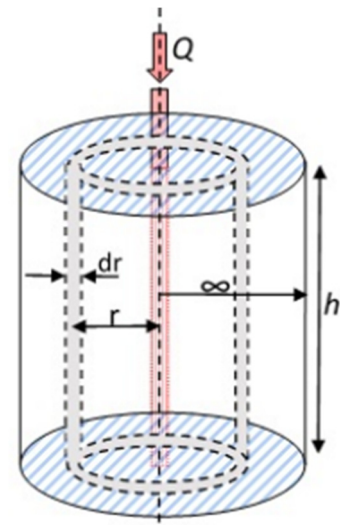


FIGURE 4: Radial flow through a cylindrical shell around a well (Haraldsdóttir, 2016)

The law of conservation of mass says that mass flow in minus mass flow out equals mass rate of change within the control volume. Consider the flow through a cylindrical shell of thickness dr situated at a distance r from the centre of the cylinder in Figure 4.

Then applying the law of conservation of mass leads to:

$$\left(\rho Q + \frac{\delta(\rho Q)}{\delta r} dr \right) - \rho Q = 2\pi r \frac{\delta(\phi \rho h)}{\delta t} dr \quad \text{or}$$

$$\frac{\delta(\rho Q)}{\delta r} = 2\pi r \frac{\delta(\phi \rho h)}{\delta t} \quad (1)$$

where ρ = Density (kg/m^3);
 ϕ = Porosity (ratio $0 < \phi < 1$);
 Q = Volumetric flow rate (m^3/s);
 r = Radial distance (m) from the well;
 t = Time (s);
 h = Reservoir thickness (m).

Darcy's law or law of conservation of momentum in radial form is:

$$Q = \frac{2\pi r h k}{\mu} \frac{\delta p}{\delta r} \quad (2)$$

where p = Pressure (Pa);
 μ = Dynamic viscosity (Pa. s);
 k = Formation permeability (m^2).

The equation of state (compressibility at constant temperature) can be expressed as:

$$c_t = c_w \phi + (1 - \phi)c_r \text{ where } c_w = \frac{1}{\rho} \frac{\delta \rho}{\delta p} \text{ and } c_r = \frac{1}{1 - \phi} \frac{\delta \phi}{\delta p} \quad (3)$$

where c_w = Fluid compressibility (Pa⁻¹)
 c_r = Rock or formation compressibility (Pa⁻¹)
 c_t = Total compressibility (Pa⁻¹)

By combining Equations 1, 2, and 3, we obtain the pressure diffusion equation:

$$\frac{1}{r} \frac{\partial}{\partial r} \left(r \frac{\partial p(r, t)}{\partial r} \right) = \frac{\mu c_t}{k} \frac{\partial p(r, t)}{\partial t} = \frac{S}{T} \frac{\partial p(r, t)}{\partial t} \quad (4)$$

$$\frac{\partial^2 p}{\partial r^2} + \frac{1}{r} \left(\frac{\partial p(r, t)}{\partial r} \right) = \frac{\mu c_t}{k} \frac{\partial p(r, t)}{\partial t} = \frac{S}{T} \frac{\partial p(r, t)}{\partial t}$$

Equation 4 is the basic equation for well testing. Solutions for this equation can be obtained for different regimes depending on the initial and boundary conditions but that is beyond the scope of this project.

3.2 Injection well test process and analysis

An injection test is done by lowering a pressure tool to a selected depth near to a major permeable zone in the well. Water is pumped into the well at different pumping rates. In some cases constant injection rate is applied for a while before starting the test, allowing the pressure to stabilize, but in other cases there is no injection until the step test starts, e.g. in the injection tests from Aluto-Langano. The first pumping rate in the test is held constant to allow the pressure to stabilize. The pumping rate is then changed stepwise with the duration of each step long enough to allow the pressure in the well to stabilize again. This process is repeated for several pumping rates. In some countries the pump is turned off at the end of the well test and the well is monitored and allowed to return to its natural pressure, which is the so called fall-off test. During all this process, the well pressure is recorded as a function of time.

The analysis of the injection test is done using the software Welltester vers. 2 (WT) (Marteinsson, 2016) to handle data manipulation, to analyse well tests (mainly multi-step injection tests) and to present the results both graphically and in tables. The software works like this: (Haraldsdóttir, 2016; Marteinnsson, 2016).

- Initial parameters: The reservoir temperature, rock type and porosity are fed into the program and the initial pressure is deduced by WT. These values are used to calculate approximate values of the dynamic viscosity of the reservoir fluid and the total compressibility of the rock matrix and the fluid. The wellbore radius which is the average radius of the well below the production casing to reservoir depth is also fed into the program.
- Set steps: The initiation time of injection steps is selected on the graph.
- Modify: This step is designed to clean, correct and resample the data.
- Model: In this step, the most appropriate model for the reservoir being investigated is selected. To achieve this, the derivative plot is used along with the pressure data as a function of time on graphs with log-log scale as well as linear and log-linear scale.

The main parameters deduced from the Welltester simulation are explained in the manuals of WellTester and Welltester V2 (Júliússon et al., 2008; Marteinnsson, 2016) as follows:

Transmissivity, T, describes the ability of the reservoir to transmit fluid, hence largely affecting the pressure gradient between the well and the reservoir. Its physical formulation is kh/μ , where k is the effective permeability of the reservoir, h is the reservoir thickness and μ is the dynamic viscosity of the active reservoir fluid.

Storativity, S , defines the volume of fluid stored in the reservoir per unit area per unit increase in pressure [$\text{m}^3/(\text{Pa m}^2)$ or m/Pa]. How fast the pressure can travel within the reservoir depends on the storativity of the reservoir. Storativity depends on fluid compressibility, or $S = c_r h$. It varies greatly between reservoir types, i.e. liquid dominated vs. two phase or dry steam. Common values for liquid-dominated geothermal reservoirs are around $10^{-8} \text{ m}^3/(\text{Pa m}^2)$ and $10^{-5} \text{ m}^3/(\text{Pa m}^2)$ for two-phase reservoirs.

The skin factor, s , is a variable used to quantify the permeability of the volume immediately surrounding the well. This volume is often affected by drilling operations, being either damaged (e.g. because of drill cuttings clogging the fractures) or stimulated (e.g. due to erosion or extensive fracturing around the well). For damaged wells the skin factor is positive and for stimulated wells it is negative.

The injectivity index, II , is often used as a rough estimate of the connectivity of the well to the surrounding reservoir. Mathematically, injectivity is defined as the change in the injection flow divided by the change in the stabilized reservoir pressure and its unit is $[(\text{L/s})/\text{bar}]$.

Wellbore storage, C , is defined as the difference between the wellhead flow rate and the sand face flow rate (i.e. the flow into or out of the actual formation). Wellbore storage effects can occur in several ways, but most commonly by changing the liquid level and fluid expansion. In injection testing the most dominant cause for wellbore storage is changing liquid level.

The radius of investigation, r_e is the approximate distance at which the pressure response from the well becomes undetectable, although the value of the parameter should be viewed more qualitatively.

Statistical parameters, e.g. the coefficient of variation CV , are defined as the ratio between the standard deviation σ and the mean value μ for the particular parameter in the model. The lower the value of CV the better is the modelling.

3.3 Injection well tests in Aluto-Langano

Injection step tests from LA-3 and LA-10D were simulated. Recordings were scarce from the test in LA-3 which was done in the 1980's but abundant from LA-10D which was done recently in a technically much better way. Yet it was possible to simulate the data from both of the wells with WT with some extra data manipulation. Tables 2 and 3 show the selected initial parameters and the selected model for the Welltester analysis of the injection tests of both wells.

TABLE 2: Initial parameters used in the well test analysis of LA-3 and LA-10D where those marked with * and are inserted by the user as well as the type of rock.

Parameters and units	LA-3	LA-10D
Estimated reservoir temperature [$^{\circ}\text{C}$] *	300	300
Estimated reservoir pressure [bar-g]	97	91.45
Wellbore radius r [m] *	0.11	0.11
Porosity ϕ *	0.1	0.1
Dynamic viscosity of reservoir fluid μ , [Pa.s]	8.962×10^{-5}	8.6×10^{-5}
Compressibility of reservoir fluid c_w , [Pa^{-1}]	2.4413×10^{-9}	3.14×10^{-9}
Compressibility of rock matrix c_r , [Pa^{-1}]	2.44×10^{-11}	2.44×10^{-11}
Total compressibility C_t , [Pa^{-1}]	2.66×10^{-10}	3.36×10^{-10}

TABLE 3: Model selected for injection tests in wells LA-3 and LA-10D

Reservoir	Homogeneous
Boundary	Constant pressure
Well	Constant skin
Wellbore	Wellbore storage

3.4 LA-3

The third deep exploration well of the Aluto-Langano geothermal field, LA-3 was drilled between 21 January and 13 June 1983. The well was completed at 2143.9 m and the maximum measured temperature was 309°C at 1834 m after 132 hrs of warm up period. Loss of circulation encountered up to 10.5 L/s below 1890 m and complete loss of up to 29.2 L/s occurred between 2117 and 2143.9 m (Bödvarsson, 1986). The injection test in LA-3, consisted of three injection steps (9.7, 19.7 and 28.2 L/s) with increasing injection rates, followed by a falloff period as step no. 4. In Bödvarsson's report (1986), Figure 5 shows the injection/falloff data in a graph for well LA-3 (ELC, 1986). More points were added to injection steps of Figure 5 by reading off the graph because it was not possible to simulate the well with what was provided numerically for this project and clearly this had been done previously.

The reservoir parameters for all steps are shown in Table 4 and step four (the fall-off step) was selected as the best model, having lower CV values (Júlíusson et al., 2008) than the other steps. Clearly the modelling of step nr. 2 does not show good results with high CV in general. There the skin factor is positive but negative between -2.3 and -3.2 in the other steps so the closest surroundings of the well have higher permeability than the reservoir, having the effect that well acts as if its radius is larger than the real radius. The transmissivity is rather low and the storativity is relatively good. Figure 6 shows the results of the analysis of pressure against time in logarithmic scale (A) and log-log scale (B) for step 4 in the injection test. The log-log scale graph of pressure and time shows the derivative of pressure response multiplied by the time passed since the beginning of the steps. Derivative plots are helpful in determining the best reservoir model. As we can see from Figure 6 the model fits the collected data fairly well.

TABLE 4: Reservoir parameters from nonlinear regression model for well LA-3

Parameter	Step 1	CV %	Step 2	CV %	Step 3	CV %	Step 4	CV %
Transmissivity T ($\text{m}^3/(\text{Pa}\cdot\text{s})$)	2.7×10^{-9}	5.5	1.1×10^{-8}	35.2	2.8×10^{-9}	14.9	5.7×10^{-9}	0.4
Storativity S ($\text{m}^3/(\text{m}^2\text{Pa})$)	7.6×10^{-8}	3.4	1×10^{-8}	381.8	6×10^{-8}	12.8	5.5×10^{-8}	1.2
Radius of investigation r_e (m)	10	3	10	319.3	17	13.6	104	2.7
Skin factor s	-2.9	-	3	-	-3.2	-	-2.3	-
Wellbore storage C (m^3/Pa)	3.1×10^{-6}	1.7	5.7×10^{-6}	1.9	2.5×10^{-6}	11.4	4.8×10^{-6}	0.5
Reservoir thickness h (m)	284		23		227		206	
Permeability k (m^2)	9×10^{-16}		4.3×10^{-14}		1.1×10^{-15}		2.5×10^{-15}	
Injectivity index II ($(\text{L/s})/\text{bar}$)	1.1		1.0		1		1	
Porosity ϕ	0.1		0.1		0.1		0.1	

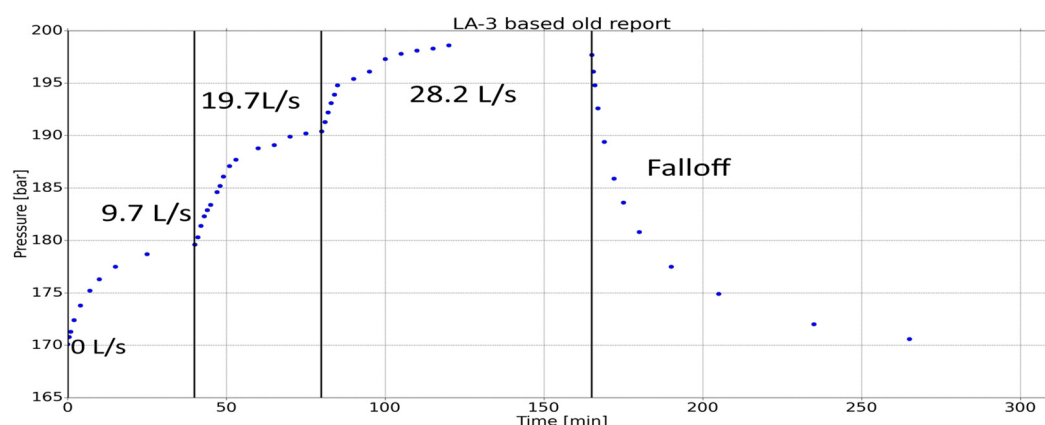


FIGURE 5: LA-3 pressure response and injection rate as a function of time in four injection steps with a total duration of 5.2 hours (based on data in ELC, 1986)

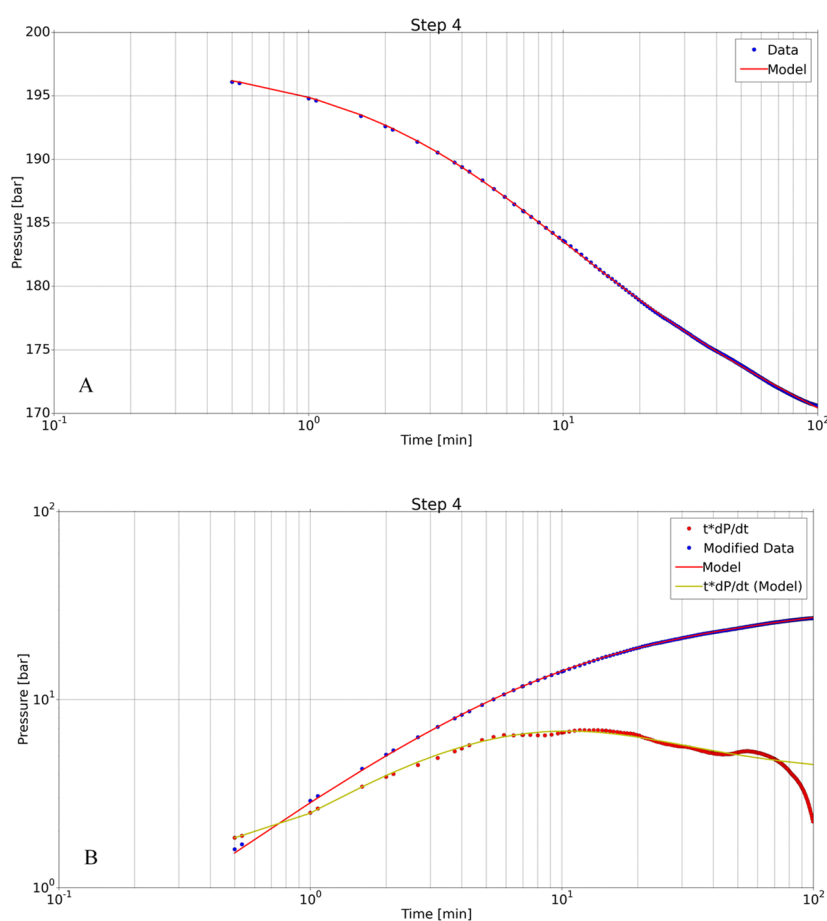


FIGURE 6: LA-3 model results and recorded pressure for step 4 using a logarithmic time scale (A) and log-log scale including the derivative ($t*dp/dt$) (B)

3.5 LA-10D

This is the second directional well drilled in Aluto-Langano geothermal project. It is the 10th deep well and was completed in October 2015. The well is drilled to the maximum measured depth of 1940 m in the direction of N43°W with an inclination of 28° and with a maximum measured temperature of 310°C at the bottom of well. The directional drilling kick off point (KOP) is at 450 m depth. The pressure temperature spinner (PTS) tool was set at 551 m depth and the water injection rate increased from 0 L/s to 14.9 L/s. After that, the injection rate was increased to 17, 19.3 and 21.7 L/s in the following steps and the pressure in the well was recorded (Figure 7). The injection rate of each step was stable for one hour.

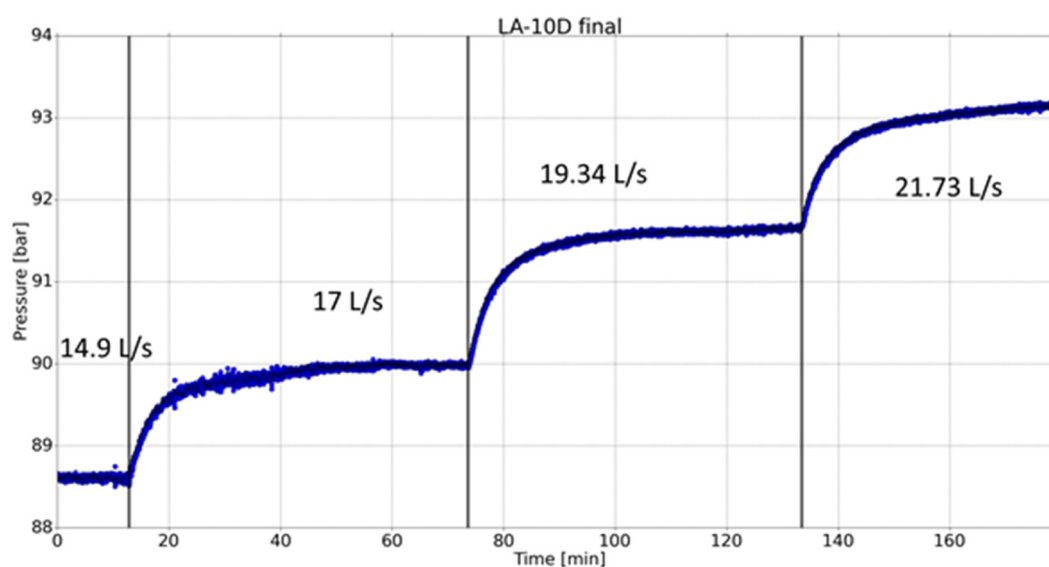


FIGURE 7: LA-10D pressure response and injection rate as a function of time in three injection steps with a total duration of 3 hours

The resulting reservoir parameters from the model for all steps are shown in Table 5 and the results of step three were selected as the best ones, having lower CV values than the other steps (Júlíusson et al., 2008). The results show relatively good transmissivity and storativity but the skin factor is not so good.

TABLE 5: Reservoir parameters from nonlinear regression model for well LA-10D

Parameter	Step 1	CV %	Step 2	CV %	Step 3	CV%
Transmissivity T ($\text{m}^3/(\text{Pa}\cdot\text{s})$)	1.3×10^{-8}	0.7	2×10^{-8}	0.7	1.3×10^{-8}	0.4
Storativity S ($\text{m}^3/(\text{m}^2\text{Pa})$)	5.1×10^{-8}	2.2	3×10^{-8}	3.4	5.7×10^{-8}	2.1
Radius of investigation r_e (m)	122	5.6	62	2.4	119	4.8
Skin factor s	0.07	-	3.1	-	-0.3	-
Wellbore storage C (m^3/Pa)	3.1×10^{-6}	0.68	4.1×10^{-6}	0.24	4.3×10^{-6}	0.3
Reservoir thickness h (m)	152		87		168	
Permeability k (m^2)	7.1×10^{-15}		1.9×10^{-14}		6.8×10^{-15}	
Injectivity index II ($(\text{l/s})/\text{bar}$)	1.4		1.4		1.6	
Porosity ϕ	0.1		0.1		0.1	

Figure 8 shows the result of the analysis of pressure as a function of time on logarithmic scale (A) and log-log scale (B). The log-log scale graph of pressure and time shows the derivative of pressure response multiplied by the time passed since the beginning of the steps. Derivative plots are helpful for determining the best reservoir model. As we can see from the Figure 8 the model fits fairly well the collected data.

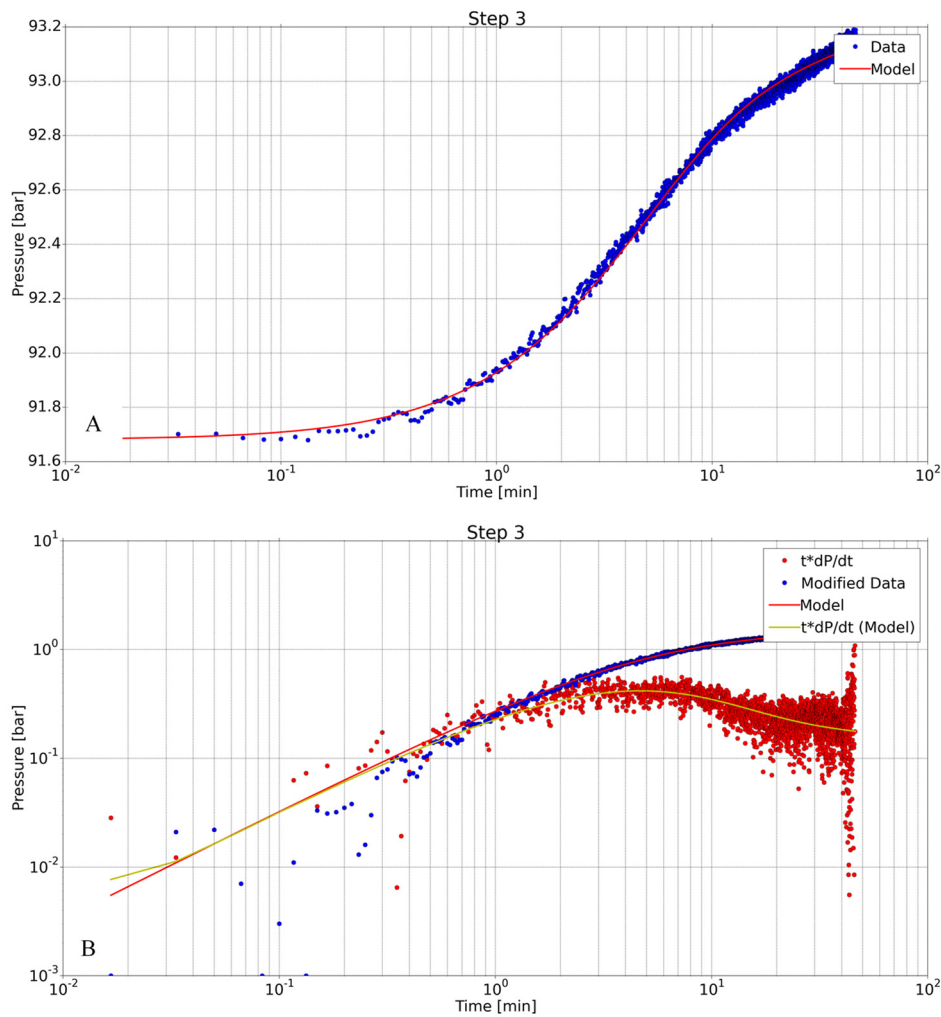


FIGURE 8: LA-10D model results and recorded pressure for step 3 using a logarithmic time scale (A) and log-log scale including the derivative ($t \cdot dp/dt$) (B)

3.5.1 Modelling of step 3

Injection well test analyses done for wells LA-3 and LA-10D gave the best result for step number 4 and 3, respectively (Table 6) using a model assuming homogenous reservoir and constant boundary pressure. The skin factor values for the selected model steps are negative in both wells, which indicates that the nearest surroundings of the wells have higher permeability than the surrounding reservoir. The results (Tables 4 and 5) generally show better transmissivity in LA-10D than in well LA-3 and relatively good storativity as in LA-3. The skin factor on the other hand is not particularly good in LA-10D and not as good as in well LA-3.

TABLE 6: Estimated reservoir parameters of LA-3 and LA-10D from the best model and best step

Parameter	LA-3		LA-10D	
	Step 4	CV %	Step 3	CV %
Transmissivity, T ($\text{m}^3/(\text{Pa}\cdot\text{s})$)	5.7×10^{-9}	0.4	1.3×10^{-8}	0.4
Storativity, S ($\text{m}^3/(\text{m}^2\text{Pa})$)	5.5×10^{-8}	1.2	5.7×10^{-8}	2.1
Radius of investigation, r_e (m)	104	2.7	119	4.8
Skin factor, s	-2.3	-	-0.3	-
Wellbore storage, C (m^3/Pa)	4.8×10^{-6}	0.4	4.1×10^{-6}	0.3
Reservoir thickness, h (m)	206		168	
Permeability, k (m^2)	2.5×10^{-15}		6.8×10^{-15}	
Injectivity index, II ($(\text{L/s})/\text{bar}$)	1.0		1.6	
Porosity, ϕ	0.1		0.1	

The injectivity indices are rather low in both of the wells, but higher in the new well LA-10D than in LA-3. Both wells LA-3 and LA-10D produce from a liquid-dominated reservoir.

4. ANALYSIS OF FORMATION TEMPERATURE AND INITIAL PRESSURE PROFILES

4.1 Introduction

Temperature and pressure logs are used extensively in geothermal exploration and development. The temperature and pressure logs are measured during drilling of wells, during heating up, after drilling and during flow tests as well as for monitoring. During drilling, the well temperatures are highly disturbed by drilling fluid circulations with cold water being injected into the well. During drilling the temperature logs provide valuable information on the location of aquifers (feed zones) and their relative sizes (permeability). Internal flow often exists in very permeable wells with multiple feed zones. This flow is clearly seen in temperature logs as constant temperature in the depth interval between feed points in the well, and sometimes the internal flow rate can be estimated based on temperature transients (Steingrímsson, 2013).

In geothermal investigation, temperature and pressure logging is important in determining formation temperature and reservoir pressures. The temperature and pressure disturbances that occur in a well during drilling will fade away gradually after the drilling stops. The wells will heat up and reach thermal equilibrium with the surroundings within several weeks or months and the well pressures will also recover after drilling and reach equilibrium with the permeable feed zones of the well. Temperature and pressure logs during the recovery period after drilling are the most important data to estimate formation temperatures and reservoir pressure (Steingrímsson, 2013).

Conditions inside the well during logging are not the same as in the surrounding formation or as undisturbed conditions in the reservoir before drilling. Different methods are used to estimate the formation temperature and pressure. Formation temperature can be estimated by extrapolation of a short

term temperature data from the well logs during warm up at selected depth for each estimation using Horner plot method (Steingrímsson, 2013).

The Horner plot method is a simple analytical technique used for analysing temperatures to determine the formation temperature (Helgason, 1993). The basic criterion for the technique is the linear relationship between measurements of temperatures at the selected depth and $\ln(\tau)$:

$$\tau = \frac{\Delta t}{\Delta t + t_0} \quad (5)$$

where τ = Horner time;
 Δt = Time passed since circulation stopped (s);
 t_0 = Circulation time (s).

By using the equation above one can plot the wellbore temperature at the selected depth from logs during the warm up as a function of $\ln(\tau)$ and then plot a straight line through the data. Extrapolation to $\ln(\tau) = 0$ gives an estimate of the formation temperature (Helgason, 1993). A computer software from the ICEBOX package, BERGHITI, is used for estimation of formation temperatures (Arason et al., 2004; Marteinsson, personal communication).

The reservoir pressure is estimated from data obtained during the recovery period. It is determined with the help of another software called PREDYP from ICEBOX (Arason et al., 2004) using the obtained formation temperature as a function of vertical depth and known initial wellhead pressure or water level as input. The warm up pressure profiles are plotted to determine their intersection with each other, known as pivot point, which shows the depth and pressure at the best zone in the borehole and can be considered as the actual pressure value in the reservoir. The water level is changed in PREDYP until the pressure at the depth of the pivot point matches the pressure in the logs.

In Sections 4.2 and 4.3, the temperature and pressure profiles are analysed to determine the formation temperatures and estimate the initial reservoir pressure for Aluto-Langano wells LA-9D and LA-10D. The temperature and pressure measurements in these wells were performed during injection and warm up of the wells, but only logs during warm up can be utilized to find the formation temperature. Figure 9 shows an example of results from BERGHITI.

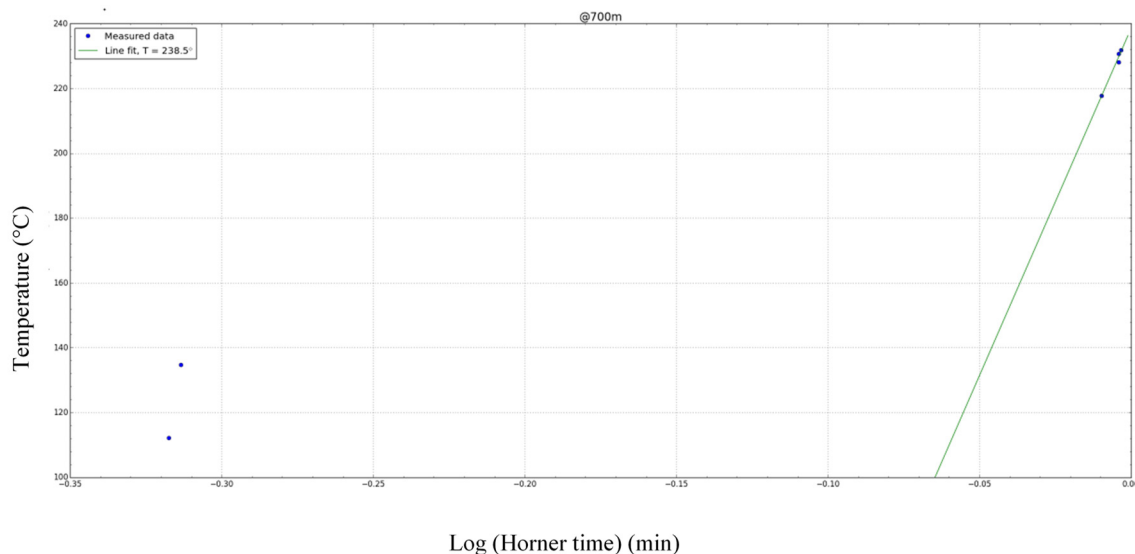


FIGURE 9: Formation temperature at 700 m in well LA-9D estimated with the Horner method

4.2 Well LA-9D

Drilling of well LA-9D started on November 12, 2013. Drilling of this well was interrupted due to repeated loss of circulation and insufficient water supply system to continue drilling blind. After procurement of water supply pumps and equipment, drilling was re-started on February 1, 2015 and was completed on April 30, 2015. The directional drilling kick off (KOP) is at 700 m where the well turns to a direction of N70°W with 51° maximum inclinations. Table 7 shows its depths and casing depths.

TABLE 7: Depths and casing depths in LA-9D with respect to ground surface and casings information

Depth (m)	Vertical depth (m)	Bit size (")	Casing diameter (")	Casing depth (m) from ground surface
60	60	26	20	56.7
210	210	17 ½	13 ¾	207.9
608	608	12 ¼	9 ⅝	605
1920	1785	8 ½	7	1915

In well LA-9D seven small feed zones were located at 760, 830, 940, 1000, 1136, 1585 and 1707 m vertical depth, while a large feed zone was encountered at 1333 m vertical depth. The feed zones were identified from logs during injection and warm up logs and with the help of loss of circulation data sets.

The water injection into the well was stopped at 00:00 on 7 May 2015 and the temperature recovery was monitored. The logging during the warm up period was done with a PTS (pressure, temperature, spinner) tool on the 7th, 8th and 9th of May. Additional measurements were carried out on 1 of June to check the well temperature conditions and PTS measurements were carried out on 5 May. However, due to problems at the spinner part of the tool, only pressure and temperature were obtained (WJEC, 2015).

The temperature recovered steadily and the temperature below 1870 m depth exceeded 250°C during the log on 7 May. The logging survey on 9 May recorded more than 280°C around the well bottom of about 1900 m depth. On 1 June the temperature had recovered slightly more than during the first warm up logs. Focusing on the production zone of the well, the measured temperature is 192°C, at casing shoe (605 m) and 306°C at the maximum logging depth (1911 m) in the log from 1st June (Figure 10).

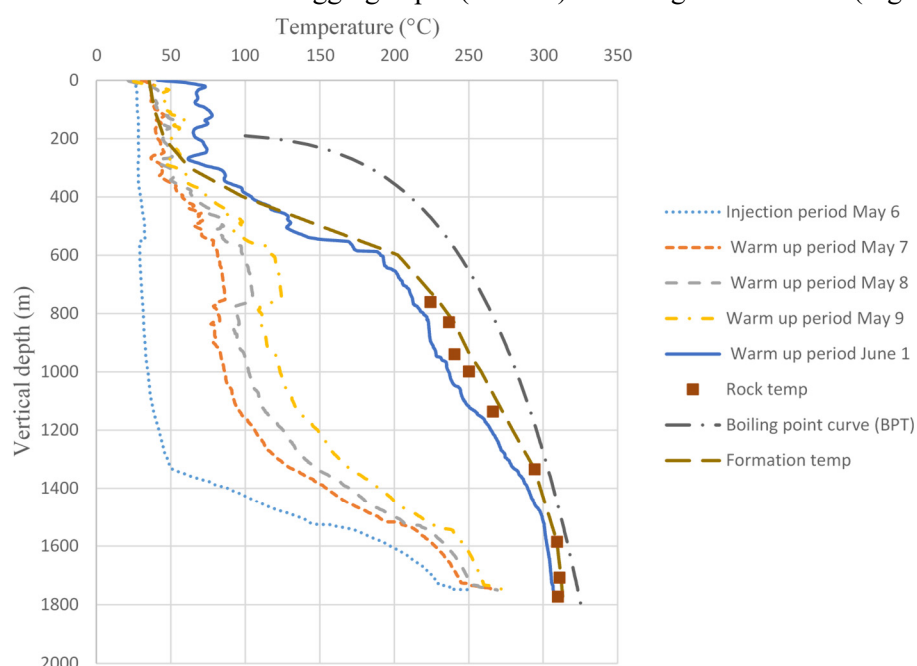


FIGURE 10: Temperature logs with injection, during warm up, boiling point curve (BPT) and estimated formation temperature of LA-9D

The formation temperature was estimated from the data set obtained during the temperature recovery of the well. The estimated formation temperature increases with depth and reaches about 309°C at the well bottom. The data points to be used in the BERGHITI program were selected from the temperature logs at the depth of the feed zones, their estimated formation temperatures were determined and then plotted in Figure 10 with the temperature logs as a function of vertical depth. The formation temperature of the well was estimated from these points. The formation temperature increases with depth in the production part of the well to 300-311°C.

To calculate the initial pressure, the estimated formation temperature profile from Figure 10 was used as input to the PREDYP program. The water level was adjusted in the calculations until the calculated profile matched the pivot point pressure. The pressure match was achieved with water levels at approximately 200 m vertical depth. The pressure profile obtained during the warm up period and the initial pressure profile are shown in Figure 11 as a function of vertical depth. The pivot point of LA-9D is located at 1100 m vertical depth where pressure of 85 bar has been measured in the 4 relevant logs.

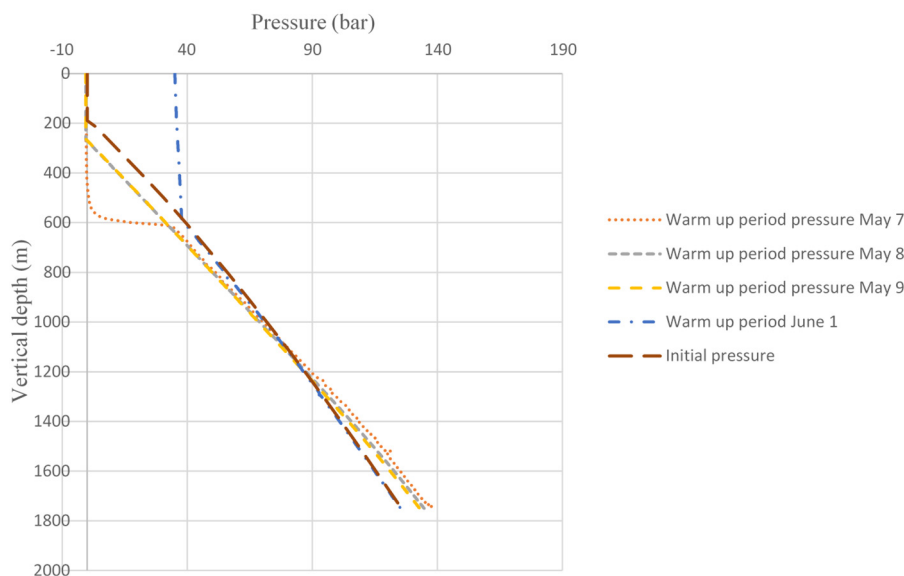


FIGURE 11: Pressure logs during warm up period and estimated initial pressure of LA-9D

4.3 Well LA-10D

Drilling of well LA-10D started on 25 June, 2015 and was completed on 2 October, 2015. The directional drilling kick off point (KOP) is at 450 m depth where it turns to a direction of N43°W with a maximum inclination of 28°. Table 8 shows its depths and casing depths.

In well LA-10D six small feed zones were located at 909, 1244, 1260, 1519 and 1642 m, vertical depth, while a large feed zone had been encountered at 699 m vertical depth (circulation loss zone).

The water injection into the well was stopped at 00:00 on 5 October 2015 and the temperature recovery was monitored. The monitoring logs were carried out after 12 hours and 24 hours, on October 6 and on October 24, 2015. Additional measurements were carried out on 18 November and 19 November 2015 to check the well temperature conditions but are not used in this study since the data recovered were of very poor quality.

The temperature recovered steadily and the temperature below 1700 m depth exceeded 250°C in the first log after 6 hours warm up. In the logging survey on 24 October, temperatures of more than 300°C were recorded around the well bottom at about 1800 m depth. Focusing on the production zone of the

well, the measured temperature is more than 200°C at casing shoe depth (807 m) and more than 300°C at maximum logging depth (1800 m) (Figure 12).

The formation temperature was estimated from the temperature well logs during warm up on 6 and 24 October (12 hours and 24 hours), respectively. Frequent temperature logging during warm up is strongly advised since too few temperature logs from that period increase the uncertainty of the estimated formation temperature. The estimated formation temperature increases with depth and reaches about 305°C at the well bottom at 1800 m depth (Figure 12).

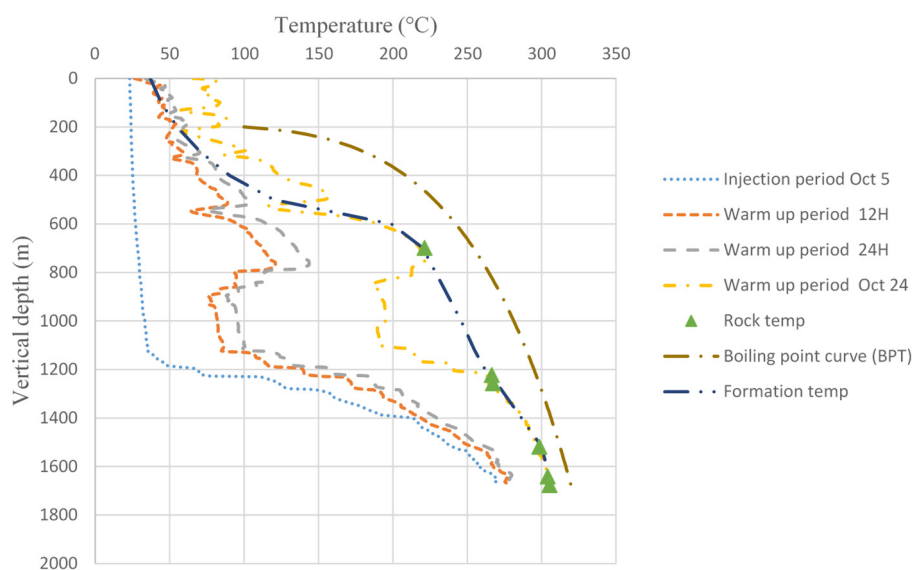


FIGURE 12: Temperature logs with injection, during warm up, boiling point curve (BPT) and estimated formation temperature of LA-10D

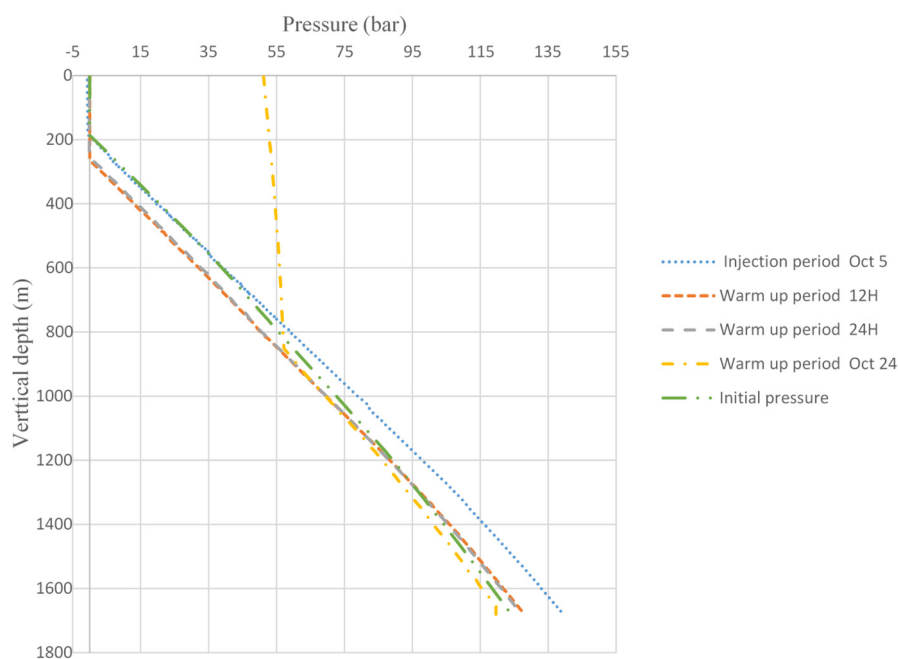


FIGURE 13: Pressure logs during warm up period and estimated initial pressure of LA-10D

The data points to be used in the Berghiti program were selected from the temperature logs at the depth of selected feed zones. Their estimated formation temperature was determined and plotted with the well logs in Figure 12 as a function of vertical depth.

The pivot point of LA-10D is located at 1200 m vertical depth where pressures of 92 bar were measured. To calculate the initial pressure, the estimated formation temperature profile from Figure 12 was used as input to the PREDYP program. The water level was adjusted in the calculations until the calculated profile matched the pivot point pressure. The pressure match was achieved with water levels at approximately 200 m depth. The pressure profiles obtained during the warm up period and the initial pressure profile are shown in Figure 13 as a function of vertical depth.

5. DISCHARGE TESTING

5.1 Introduction

Discharge testing is performed after a well has been allowed to warm up and recover its temperature. As the temperature of the fluid increases during the warm up period, in a high temperature geothermal field wellhead pressure sometimes builds up. The first step in flow testing is starting the well discharge. For most wells this is not difficult, since they naturally develop sufficient pressure, either cold gas or steam, so that opening the control valve will initiate flow. But in some wells it can be difficult to start fluid flow. Even after waiting for weeks for the well to heat up, no pressure develops at the wellhead, and when the valve is opened there is no flow. This is most common in wellbores that have cold sections in the upper part of the well (Grant and Bixley, 2011). Different methods like gas lift, steam injection and work overs are used to stimulate geothermal wells.

During the warm-up period, the water level in the well will gradually rise and eventually build a wellhead pressure above atmospheric pressure if the well is artesian. When the wellhead pressure has built up sufficiently, a discharge test can be conducted by flowing the well through an orifice (Böðvarsson and Witherspoon, 1989). Measurements can be performed to evaluate the total flow rate and enthalpy of the fluid. The lip pressure method (James, 1970) or often called Russel James method, can be used to determine the total flow rate and enthalpy with a simple weir being used to measure liquid flow. By repeating these flow tests with different sized orifices, the well productivity as a function of wellhead pressure can be determined. That is one of the so called characteristic curves for the well that can be used in selecting operating conditions for the turbines in the power plant (Böðvarsson and Witherspoon, 1989).

If environmental conditions permit, a short term discharge test can be used applying the lip pressure method to get a first estimate of the longer term production potential and to determine the most suitable equipment for longer term testing. The discharge can also help to clear debris from the well (Grant and Bixely, 2011). Russel James lip pressure method is used to determine the flow characteristics and production capacity of both wells LA-9D and LA-10D during discharge testing.

5.2 Russel James lip pressure method

The lip pressure method is a convenient means of measuring the flow of many geothermal wells. It is based on an empirical equation developed by Russell James (1970) and is considered to be the most versatile method for testing all medium-enthalpy wells. Grant and Bixely (2011) stated: “To use this method, the steam-water mixture is discharged through an appropriately sized pipe into a silencer or some other device to separate the steam and water phases at atmospheric pressure (Figure 14). The lip pressure is measured at the extreme end of the discharge pipe using a liquid-filled gauge to damp out pressure fluctuations. Water flow from the silencer is measured using a sharp-edged weir near the silencer outlet.”

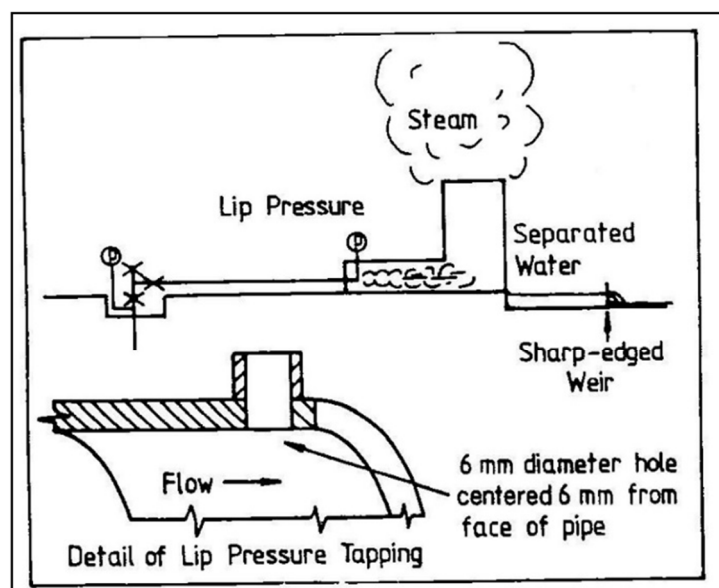


FIGURE 14: Flow measurement by lip pressure and silencer (Grant et al., 1982)

Grant and Bixely (2011) said: “James’s formula, relates mass flow, discharge pipe area, enthalpy, and lip pressure”. The empirical formula can be presented as:

$$Q = \frac{184 p_{lip}^{0.96} A}{H_t^{1.102}} \quad (6)$$

where Q = Total flow rate (kg/s);
 p_{lip} = Lip pressure (bar-a);
 A = Cross-sectional area of the discharge pipe (cm²); and
 H_t = Total enthalpy (kJ/kg).

According to Grant and Bixley (2011) Equation 7 is used when the flow is measured in tonnes per hour.

$$Q = \frac{663 p_{lip}^{0.96} A}{H_t^{1.102}} \quad (7)$$

The total mass flow rate obtained from Russel James lip pressure method can be related to water flow rate measured at the silencer after flashing:

$$Q = \frac{H_s - H_w}{H_s - H_t} Q_w \quad (8)$$

where Q_w = Water flow rate measured at the silencer after flashing (kg/s);
 H_s & H_w = Saturated steam and saturated water enthalpies at the separation pressure measured in kJ/kg.

If we combine Equations 6 and 8 we obtain:

$$\frac{Q_w}{A p^{0.96}} = \frac{184}{H^{1.102}} \frac{H_s - H_t}{H_s - H_w} \quad (9)$$

The steam mass fraction X can be calculated as:

$$X = \frac{H_t - H_w}{H_s - H_w} \quad (10)$$

By measuring the lip pressure, water flow rate and cross-sectional area of the pipe then the total enthalpy can be obtained numerically. The enthalpies of steam and water can be obtained with the help of steam tables from their corresponding temperatures and pressures.

With the help of the LIP program from the ICEBOX software package (Arason et al, 2004; Marteinsson, 2016), the enthalpies and flow rates are calculated considering weir properties corresponding to a standard 90° V-notch weir box.

5.3 Discharge testing of well LA-9D

Figure 15 shows recordings during two flow test in well LA-9D. The one-month long discharge test of well LA-9D was started on 4 November 2015 by opening the master valve and the discharged geothermal fluid was sent to a silencer. The mass flow data was measured every one hour during the testing period. The different sizes of discharge pipe with diameter of 3", 4", 5" and 6" were used to obtain the stable discharge mass flow data at different wellhead pressure. The lip pressure was monitored as well as the wellhead pressure (WHP) and the height of the liquid in the weir-box. Fluid sampling was also carried out for chemical analysis. The well was closed on 4 December 2015 to finish the one-month single-well discharge test (Table 9).

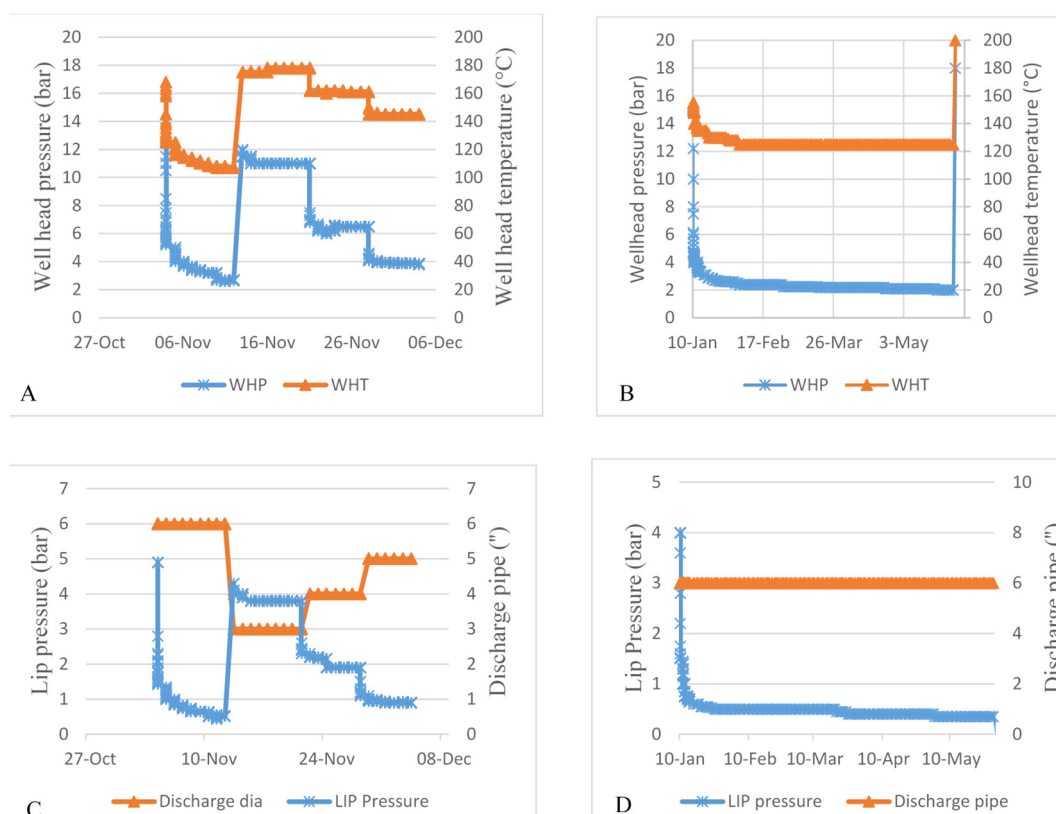


FIGURE 15: First (A and C) and second (B and D) discharge test data of well LA-9D, showing wellhead pressure and temperature (A and B), lip pressure and discharge pipe diameter (C and D)

Then well LA-9D was discharged again on 10 January 2016 (Table 9) which was during the period when well LA-10D was discharging continuously. The two wells were discharged simultaneously until well LA-10D was closed on 1 June 2016. The PTS logging (flowing survey) was carried out on 18 March 2016 to obtain the data on flow conditions in the wellbore. The master valve of LA-9D was closed gradually from 27 May and completely shut off on 1 June 2016. The fluid was discharged through a 6" discharge pipe and the wellhead pressure and the total mass flow rate was 2.25 bar-g and about 10.61 kg/s, respectively. Figure 15 shows wellhead temperature, wellhead pressure (A and B), lip pressure and discharge pipe (C and D) of the first and second discharge for well LA-9D.

TABLE 9: Measurements and results for well LA-9D from the Russel James lip pressure method with separation pressure of 1 bar-a

No.	Date	P ₀ (bar)	P _c (bar)	D _p (")	W _{height} (cm)	H (kJ/kg)	Q _t (kg/s)	Q _w (kg/s)	Q _s (kg/s)	X
1	2015-11-12	2.7	0.5	6	8	2152.8	10.7	2.7	8	0.7
2	2015-11-20	11	3.8	3	8.5	1949.3	9	3.1	5.9	0.7
3	2015-11-27	6.5	1.9	4	8.3	2025.1	9.4	2.9	6.5	0.7
4	2015-12-04	3.8	0.9	5	8	2087.3	9.5	2.7	6.8	0.7
5	2016-05-27	2.3	0.5	6	8	2147.6	10.6	2.7	7.9	0.7

The calculated water, steam, total mass flow rate and fluid enthalpy of the first and second discharge test of LA-9D are shown in Figure 16. At the beginning of the test and at the time of discharge pipe replacement the flow rate is relatively higher but stabilizes with time, even stabilized flow rate data were obtained with different discharge pipe sizes.

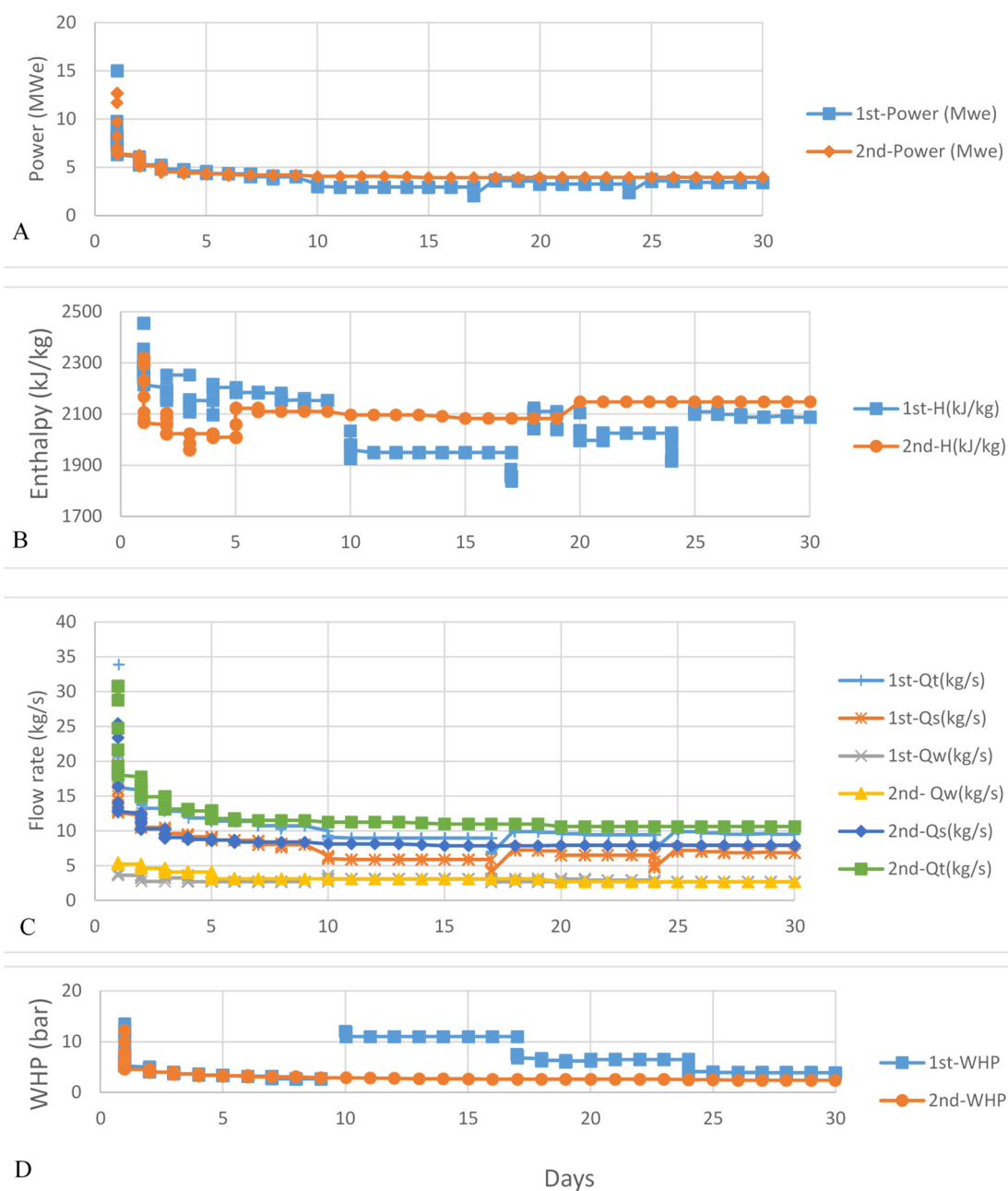


FIGURE 16: Results of the first 30 days of LA-9D long term discharge test, after which it was constant (see Figure 15 B and D), showing power (A); enthalpy (B); flow rate (C); and well head pressure (D) in the two flow tests (1st and 2nd)

The analysis of the measurements from the single well discharge (first discharge) test of well LA-9D gives an estimate of steam flow in the range of 5.9-8.0 kg/s at the separation pressure of 1 bar-a (Table 9) which is equivalent to 2.4-5.6 MW of electric power output assuming 2 kg/s of steam flow convert to 1 MW_e. The steam flow rate at the wellhead of 6.5 bar-g was 6.49 kg/s which is equivalent to 3.2 MW_e. Table 10 shows the results with a separation pressure of 5 bar-a, as in the Aluto-Langano pilot power plant.

TABLE 10: Measurements and results for well LA-9D from Russel James lip pressure method with separation pressure of 5 bar-a, as in the Aluto-Langano pilot power plant

D _p (in)	Q _w (kg/s)	Q _s (kg/s)	X
6	3.1	7.6	0.6
3	3.5	5.5	0.4
4	3.3	6.1	0.5
5	3.1	6.5	0.5
6	3.1	7.5	0.6

5.3.1 Flow characteristics

Geothermal wells can be characterized by their mass flow and enthalpy of the steam-water mixture produced at various wellhead pressures. By plotting these characteristics, the general processes occurring in the reservoir can be inferred.

The well characteristic curves of LA-9D are shown in Figure 17, as entities of the relationship between wellhead pressure and steam, water, total mass flow rate and fluid enthalpy were extracted from the well. These were calculated and plotted using relatively stable data at different wellhead pressures. The wellhead pressure of LA-9D was 2.25 bar-g using the 6-inch discharge pipe. It rose up to 11 bar-g when the 3-inch discharge pipe was used. Enthalpy increases when wellhead pressure decreases, at 11 bar it is 1950 kJ/kg and reaches 2153 kJ/kg at 2.65 bar. The steam flow rate is around 5.9-8.0 kg/s for separation pressure of 1 bar but 5.5-7.6 kg/s with separation pressure of 5 bar. The steam flow rate at 11 bar is around 6 kg/s and 8 kg/s at 2.65 bar. The flow data show that the fluid enthalpy decreases when the wellhead pressure is lowered. This is rather unusual but suggests that the feed zones of the well produce fluid of different enthalpies and the contribution of the lower enthalpy feed zones becomes larger than that of the higher enthalpy feed zones when the wellhead pressure is lowered.

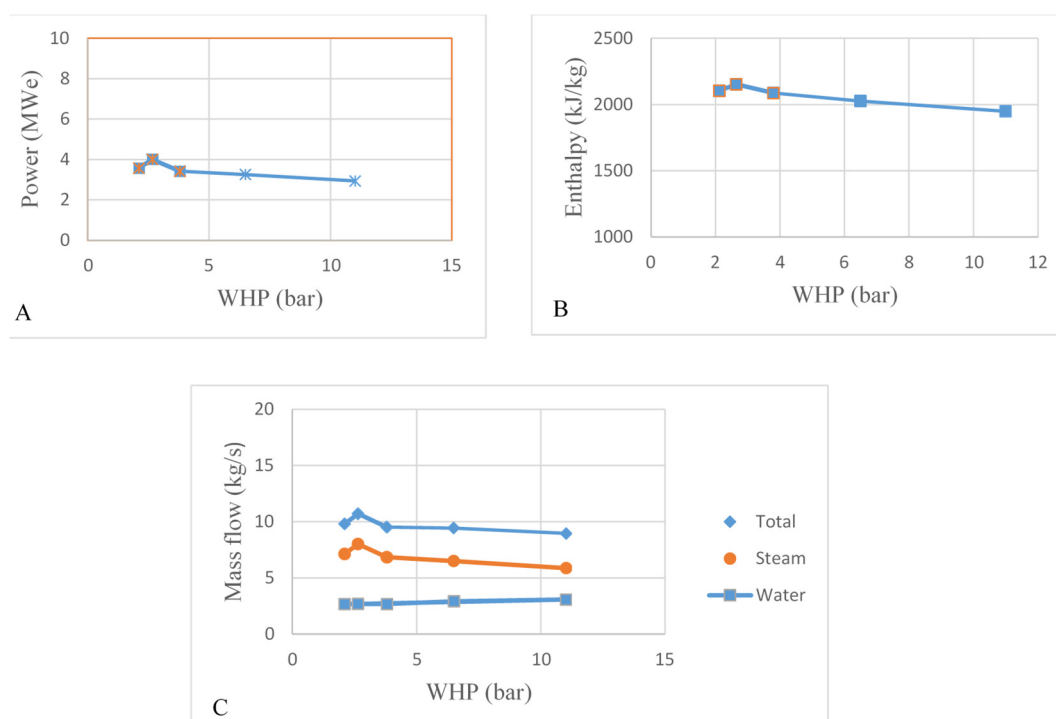


FIGURE 17: Characteristic curves of LA-9D showing power (A), enthalpy (B) and mass flow rate (C) as a function of well head pressure (WHP)

Figure 17 shows that the flow rate does not increase much when the wellhead pressure decreases. This behaviour is typical for two-phase wells where boiling starts in the formation and water and steam enter the well. The main pressure drop during flow occurs then in the formation, not in the well. Often a pressure drop >100 -150 bar is seen in two-phase wells and 90% of the drop is before the two-phase fluid enters the well. A change in the wellhead pressure of 5-10 bar is then a relatively small change of the total drawdown and does not change the flow much. The flat section of a deliverability curve formation indicates formation controlled flow or formation choked flow. Steep deliverability curves, which are typical for single-phase liquid inflow wells, indicate that the wellbore is controlling the flow from the well.

5.4 Discharge testing of well LA-10D

Figure 18 shows measurements during two flow tests in well LA-10D. The first long term discharge test of LA-10D was started on 8 December 2015. The mass flow data was measured every one hour during the testing period. Different sizes of discharge pipe with diameter of 3", 4", 5" and 6" were used to obtain stable discharge mass flow data at different wellhead pressures. The single well discharge test of LA-10D was completed on 9 January 2016. The PTS logging was carried out on 21 March 2016 to obtain data on flow conditions in the wellbore. On 24 May, LA-10D was discharged again and the discharge was completed on 15 June 2016.

The PTS logging was attempted on 14 and 15 of March 2016 at LA-10D while the well was discharging though a 6" discharge pipe. However, the tool could not go deeper than 1040 m and 1113 m, respectively. On 21 March 2016 the sinker bar (weight bar) was connected to the tool and then the tool could reach close the well bottom. The wellhead pressure was 3.25 bar-g and the total mass flow rate was 12.8 kg/s

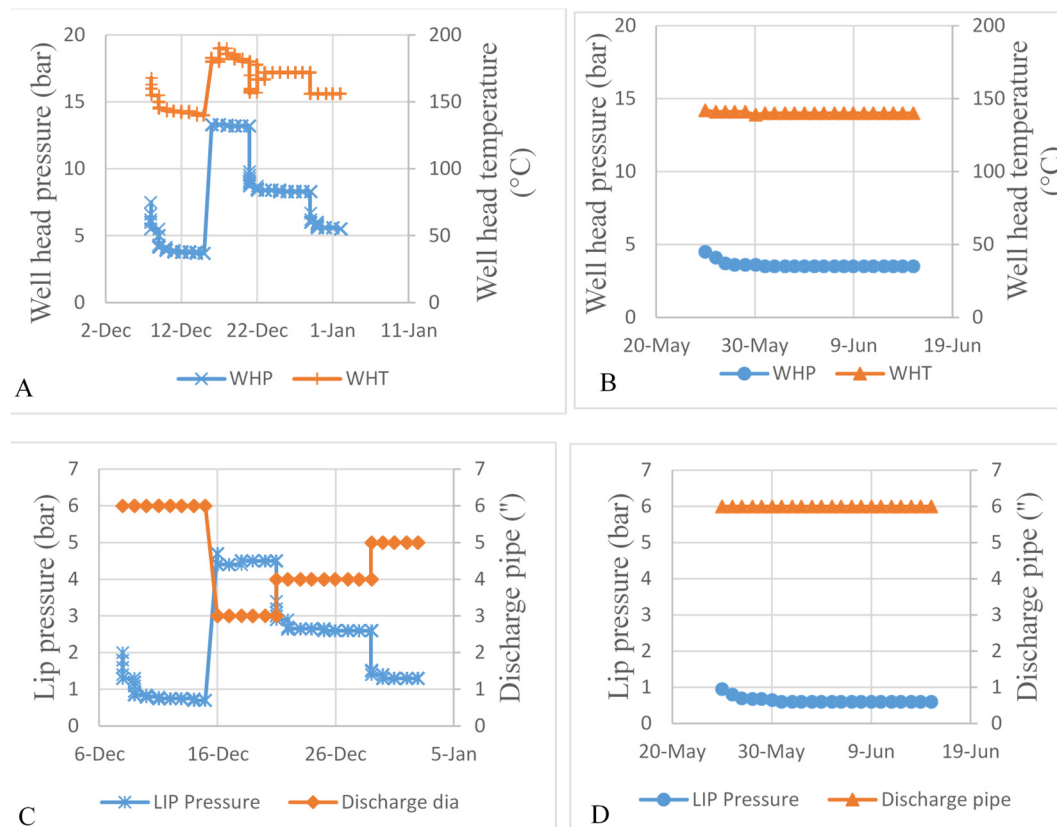


FIGURE 18: First (A and C) and second (B and D) discharge test data of well LA-10D, showing wellhead pressure and temperature (A and B); and lip pressure and discharge pipe diameter (C and D)

during the survey. The pressure, temperature, and spinner rotation data in the well were continuously measured and recorded from wellhead to close to the well bottom with the PTS tool.

The calculated water, steam, total mass flow rate and fluid enthalpy of the first and second discharge test of LA-10D are shown in Table 11 and Figure 19. The first month is the period of single well discharge test and the rest is the period of multi well discharge test together with well LA-9D. Different discharge pipe sizes were used in the test and almost stable flow rates at each condition were obtained.

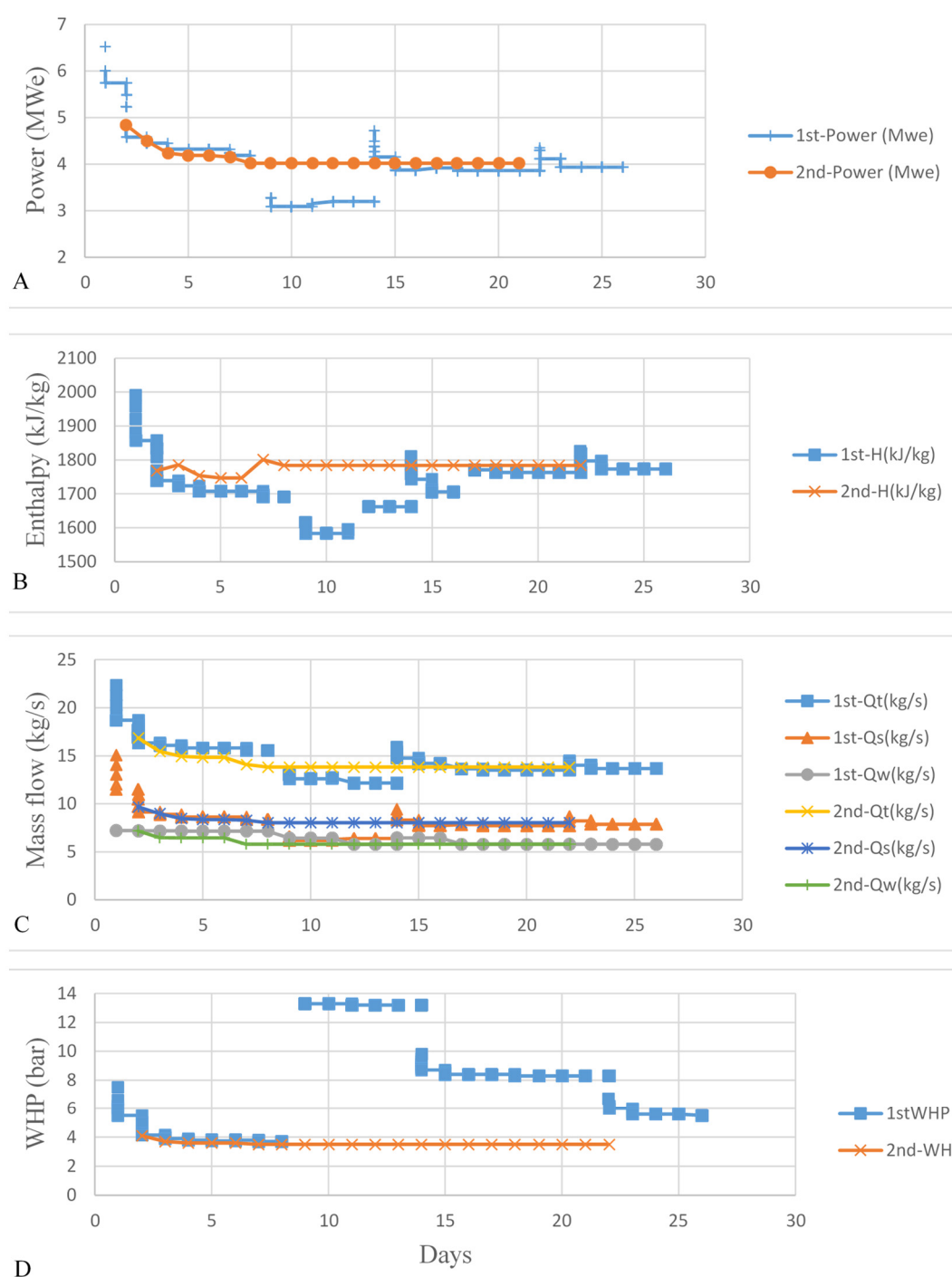


FIGURE 19: Results of first 30 days of LA-10D long term discharge test, after which it was constant (see Figure 18 B and D), showing power (A), enthalpy (B), flow rate (C), and well head pressure (D), and in two flow tests (1st and 2nd)

TABLE 11: Measurements and results for well LA-10D from the Russel James lip pressure method with separation pressure of 1 bar-a

No.	Date	P ₀ (bar)	P _c (bar)	D _p (inch)	W _{height} (cm)	H (kJ/kg)	Q _t (kg/s)	Q _w (kg/s)	Q _s (kg/s)	X
1	2015-12-15	3.7	0.7	6	12	1691.3	15.6	7.2	8.4	0.6
2	2015-12-21	13.2	4.5	3	11	1662.2	12.2	5.8	6.4	0.6
3	2015-12-29	8.3	2.6	4	11	1763.1	13.5	5.8	7.7	0.6
4	2016-01-05	5.6	1.3	5	11	1773.6	13.7	5.8	7.9	0.6
5	2016-04-01	3.3	0.5	6	10.5	1815.1	12.8	5.8	7.6	0.6
6	2016-06-15	3.5	0.6	6	11	1784.3	13.8	5.8	8.1	0.6

The analysis of the measurements from the single well discharge test of well LA-10D gives an estimate of steam flow in the range of 6.4-8.4 kg/s at the separation pressure of 1 bar-a which is equivalent to 3.2-5.7 MW electric power assuming 2 kg/s of steam flow converts to 1 MW_e. The steam flow rate at the wellhead pressure of 8.3 bar-g is 7.74 kg/s and 7.87 kg/s at wellhead pressure of 5.6 bar-g. This is equivalent to 3.8-3.9 MW_e.

The 6-inch discharge pipe was used during the second test. The flow conditions became stable and the wellhead pressure and the total mass flow rate were constant at 3.5 bar-g and 13.83 kg/s. The steam flow rate and steam fraction are summarized in Table 12 and the equivalence of power (MW_e) for 5 bar-a separation pressure is in the range of 2.9-3.8 MW_e.

TABLE 12: Measurements and results for well LA-10D from the Russel James lip pressure method with separation pressure of 5 bar-a as in the Aluto-Langano pilot power plant

D _p (")	Q _w (kg/s)	Q _s (kg/s)	X
6	7.9	7.6	0.5
3	6.4	5.8	0.5
4	6.4	7.1	0.5
5	6.4	7.2	
6	5.8	7	
6	6.5	7.4	0.5

The well characteristic curves of LA-10D (Figure 20) shows the relationship between wellhead pressure and steam, water, total mass flow rate and fluid enthalpy extracted from the well, plotted using relatively

stable data at different wellhead pressures. The wellhead pressure of LA-10D was 3.25-3.7 bar-g while using the 6-inch discharge pipe. It rose up to 13.2 bar-g when the 3-inch discharge pipe was used. The steam flow rate is around 6-8 kg/s. The fluid enthalpy is 1662-1815 kJ/kg. The curves are relatively flat and the change of mass flow rate as a function of wellhead pressure is not large. At the end of the first long term discharge test, the wellhead pressure was 3.25 bar-g and the steam flow rate was 7.6 kg/s when using the 6" discharge pipe. The stabilized wellhead pressure and steam flow rate were 3.5 bar-g and 8.1 kg/s, respectively, during the second discharge.

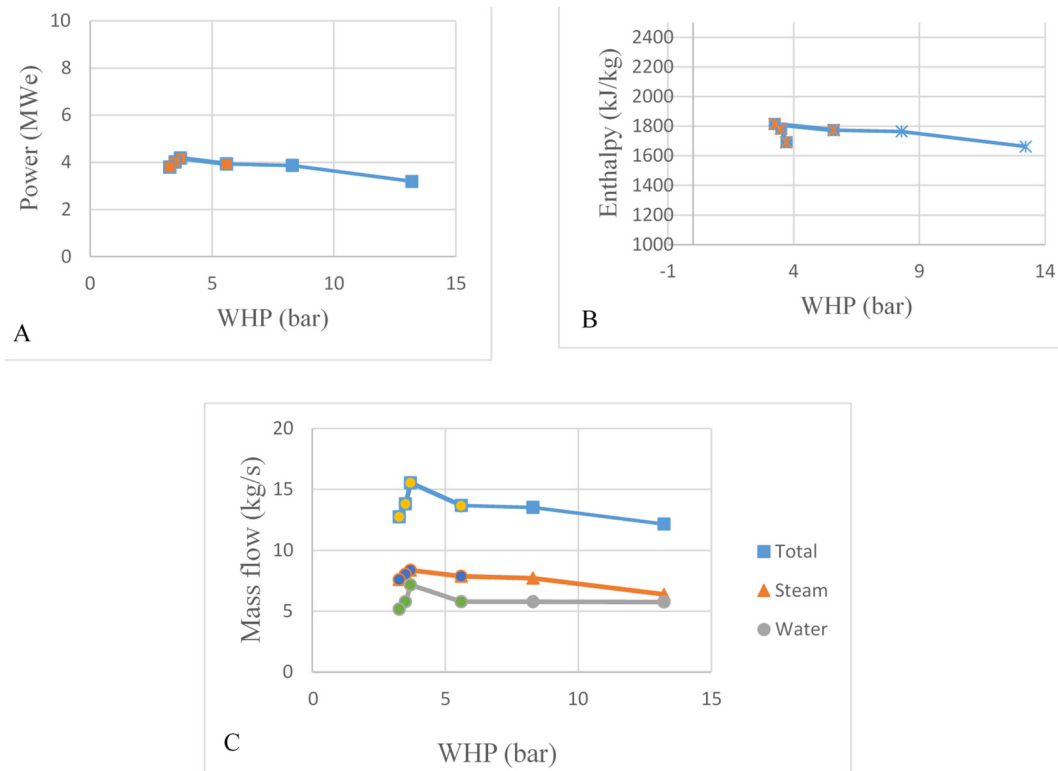


FIGURE 20: Characteristic curves of LA-10D showing power (A), enthalpy (B) and mass flow rate (C) as a function of well head pressure (WHP)

6. DISCUSSION AND CONCLUSION

The selected model for simulating the injection step tests in wells LA-3 and LA-10D assumed a homogenous reservoir and constant boundary pressure. The results show in general better transmissivity in LA-10D than in well LA-3 and a relatively good storativity in both of the wells. The transmissivity values were on the order of 10^{-9} [$\text{m}^3/(\text{Pa}\cdot\text{s})$] and 10^{-8} [$\text{m}^3/(\text{Pa}\cdot\text{s})$] for well LA-3 and LA-10D, respectively, and the storativity values in the order of 10^{-8} [$\text{m}^3/(\text{Pa}\cdot\text{m}^2)$ or m/Pa], the wells are classified as producers from a liquid-dominated geothermal reservoir.

The results for LA-3 for the skin factor for the best step show that it is -2.3 but in the range of -2.3 to -3.2 in the steps which had good simulations (CV criteria). These values indicate that the well has higher permeability in its closest surroundings than farther away and its effective radius is therefore larger than its real radius. The skin factor in the best step in LA-10D was on the other hand only -0.3 and in one step it was as high as 3.1, i.e. a positive skin factor, which means worse permeability in the close surroundings than farther away from the well.

The injectivity index is often used as a rough estimate of the connectivity of a well to the surrounding reservoir. Injectivity indices are fairly low for both wells with 1.1 (l/s/bar) for LA-3 and 1.6 (l/s/bar) for LA-10D.

Temperature and pressure data from LA-9D and LA-10D in the Aluto-Langano geothermal field were interpreted with the help of Horner plot method to estimate formation temperature. The corresponding initial pressure of the reservoir was found using the PREDYP in the ICEBOX software. Results from LA-9D and LA-10D show an estimated formation temperature ranging from 300 to 311°C and from 300 to 305°C, respectively, in the bottom of the wells. The pivot point of LA-9D is located at 1100 m vertical

depth with pressure of 85 bar. The pivot point of LA-10D is located at 1200 m vertical depth with pressure of 92 bar. The Horner plot method did not prove equally useful in the interpretation of LA-10D as it did in the interpretation of LA-9D. Only three warm up logs were available for LA-10D with the first two only 12 hours apart, making the results from the interpretation more uncertain than in the case of LA-9D.

The analysis of the measurements from the single well discharge (first discharge) test of well LA-9D gives an estimate of steam flow in the range of 5.4-7.6 kg/s at the separation pressure of 5 bar-a in Aluto-Langano pilot power plant which is equivalent to 2.7-3.8 MWe of electric power output assuming that 2 kg/s of steam flow convert to 1 MWe.

The analysis of the measurements from the single well discharge test of well LA-10D gives an estimate of steam flow in the range of 5.8-7.6 kg/s at the separation pressure of 5 bar-a in Aluto-Langano pilot power plant which is equivalent to 2.9-3.8 MWe electric power assuming that 2 kg/s of steam flow convert to 1 MWe.

7. RECOMMENDATIONS

A major problem with the injection tests and all of the other injection tests performed on the Aluto-Langano wells lies in the test design. The time period for each of the steps is only about one hour. A better design could be to let each injection step last at least three hours. In cases where the water supply is a problem, it is preferable to reduce the number of injection steps rather than their duration. One or two steps of sufficient duration provide more useful results than ten steps that are too short. If the steps are long enough, they can all be analysed and produce good estimates.

It is important in new wells to measure temperature and pressure frequently during warm up, especially in the beginning of the warm up period for better interpretation of the formation temperature and initial pressure.

The importance of monitoring the wells through their lifetime should never be underestimated to be able to follow the evolution of the geothermal reservoir and the wells themselves.

ACKNOWLEDGMENTS

I want to express my deepest gratitude to the United Nations University, the Government of Iceland and the Ethiopian Electric Power (EEP) for allowing me to attend this training. I want to thank Mr. Lúdvik S. Georgsson, director of the UNU geothermal training program and Mr. Ingimar G. Haraldsson, deputy director for allowing me to study reservoir engineering, Ms. Thórhildur Ísberg, school manager, Mr. Markús A. G. Wilde, service manager and Ms. Málfríður Ómarsdóttir, environmental scientist and all staff of ÍSOR for the teachings and dedication to make us well educated.

My special thanks go to my supervisors, Dr. Svanbjörg H. Haraldsdóttir and Ms. Saeunn Halldórsdóttir, for sharing their great knowledge and experience, for their patience and support during this project as well as Mr. Benedikt Steingrímsson, for his valuable comments. I would also like to thank Mr. Kjartan Marteinsson for his support and guidance to the use of softwares developed at ÍSOR. Finally, I want to thank former geothermal project manager of EEP Mr. Mulugeta Asaye for believing in me and recommending me for studies in this study area.

Finally, I would like to thank my lovely wife Sofia Midaso for having Sena, my new born baby girl while I was doing this project.

REFERENCES

- Arason, Th., Björnsson, G., Axelsson, G., Bjarnason, J.Ö., and Helgason, P., 2004: *The geothermal reservoir engineering software package ICEBOX, user's manual*. Iceland GeoSurvey - ÍSOR, Reykjavík, report ISOR-2004/014, 80 pp.
- Axelsson, G., 2012: The physics of geothermal energy. In: Saying, A., (ed.), *Comprehensive Renewable Energy*, 7, 3-50.
- Axelsson, G., 2013: Geothermal well testing. *Paper presented at "Short Course V on Conceptual Modelling of Geothermal Systems", UNU-GTP and LaGeo, Santa Tecla, El Salvador, UNU-GTP, SC-17*, 30 pp.
- Bödvarsson, G.S., and Witherspoon, P.A., 1989: Geothermal reservoir engineering, part 1. *Geotherm. Scie & Tech*, 2-1, 1-68.
- Bödvarsson, G.S., 1986: *Independent review of reservoir engineering work at the Aluto-Langano geothermal field, Ethiopia*. Lawrence Berkeley Lab., US, for UN Department of Technological Cooperation for Development, NY, 59 pp.
- ELC, 1986: *Exploitation of Langano-Aluto geothermal resources, feasibility report*. Electroconsult – ELC, Milan Italy, report.
- Grant, M.A., and Bixley, P.F., 2011: *Geothermal reservoir engineering* (2nd ed.). Academic Press, Burlington, USA, 359 pp.
- Grant, M.A., Donaldson, I.G., and Bixley, P.F., 1982: *Geothermal reservoir engineering*. Academic Press, NY, 369 pp.
- Haraldsdóttir S.H., 2016: *Well testing theory - injection*. UNU-GTP Iceland, unpublished lecture notes.
- Helgason, P., 1993: Step by step guide to BERGHITI. User's guide. In: Arason, Th., Björnsson, G., Axelsson, G., Bjarnason, J.Ö., and Helgason, P., 2004: *ICEBOX – Geothermal reservoir engineering software for Windows, a user's manual*. Iceland GeoSurvey - ÍSOR, Reykjavík, report ISOR-2004/014, 80 pp.
- Horne, R.N., 1995: *Modern well test analysis, a computer aided approach* (2nd ed.). Petroway Inc., USA, 257 pp.
- Hutchison, W., Mather, T.A., Pyle, D.M., Biggs, J., and Yirgu, G., 2015: Structural controls on fluid pathways in an active rift system: a case study of the Aluto volcanic complex. *Geosphere*, 11-3, 542-562.
- James R., 1970: Factors controlling borehole performance. *Geothermics, Sp. issue*, 2-2, 1502-1515.
- Júlíusson, E., Grétarsson, G.J., and Jónsson, P., 2008: *WellTester 1.0b, user's guide*. Iceland GeoSurvey - ÍSOR, Reykjavík, 27 pp.
- Kebede, S., 2012: Geothermal exploration and development in Ethiopia: Status and future plan. *Paper presented at "Short Course VII on Exploration for Geothermal Resources", organized by UNU-GTP, KenGen and GDC, in Naivasha, Kenya, UNU-GTP SC-15*, 16 pp.
- Marteinsson, K., 2016: *Well Tester User Manual. Version 2*. ÍSOR-. – Iceland GeoSurvey, Reykjavik, report in publication.

Steingrímsson, B., 2013: Geothermal well logging: Temperature and pressure logs. *Paper presented at "Short Course V on Conceptual Modelling of Geothermal Systems", UNU-GTP and LaGeo, Santa Tecla, El Salvador*, UNU-GTP, SC-17, 16 pp.

Teklemariam, M., 1996: *Water-rock interaction processes in the Aluto-Langano geothermal field, Ethiopia*. University of Pisa, Department of Earth Sciences, PhD thesis, 295 pp.

Teklemariam, M., Battaglia, S., Gianelli, G., and Ruggieri, G., 1996: Hydrothermal alteration in the Aluto-Langano geothermal field, Ethiopia. *Geothermics*, 25-6, 679-702.

Teklemariam, M., and Beyene, K., 2000: *Geochemical monitoring of the Aluto-Langano geothermal field, Ethiopia*. Geological Survey of Ethiopia, Addis Ababa, report., 141 pp.

UNDP, 1986: *Development of geothermal resources Ethiopia*. UNDP, report, 283 pp.

WJEC, 2015: *LA-9D well drilling report*. West Japan Engineering Consultants, Inc, Tokyo Japan, report, 39 pp.

Worku Sisay, S., 2016: *Sub-surface geology, hydrothermal alteration and 3D modelling of wells LA-9D and LA-10D in the Aluto-Langano geothermal field, Ethiopia*. University of Iceland, Reykjavík, MSc thesis, UNU-GTP, report 7, 83 pp.



UNITED NATIONS
UNIVERSITY

UNU-GTP

Geothermal Training Programme

Orkustofnun, Grensasvegur 9,
IS-108 Reykjavik, Iceland

Reports 2016
Number 14

GEOHERMAL DEVELOPMENT OPPORTUNITIES IN ORADEA

Adrian George Foghiş

Oradea Metropolitan Area

Piata Unirii 1-3

P.O. Box 410100, Oradea

ROMANIA

adifoghis@gmail.com

ABSTRACT

Located in an area of sedimentary basins with low-enthalpy geothermal resources, Oradea city in Romania has a tradition of geothermal research and exploitation. Considering the objectives of the local public administration to develop further the utilization of geothermal resources, the report presents potential geothermal development opportunities in the area.

The necessity of a more efficient use of the existing resources and infrastructure is underlined, plus the need for a strategic orientation towards the increase in geothermal exploitation opportunities. Optimization with sustainability as a key goal in the utilization of the geothermal resource in Oradea is of importance, as well as improving air quality by reducing burning of fossil fuels, lowering the heating cost for the population and improving energy safety by increasing usage of a local energy source. This can help Romania to fulfil the 20-20-20 goal of the EU, which can improve the local development of the area. The report presents a proposal of a geothermal road map to 2030, with 3 phases of development at metropolitan level.

1. INTRODUCTION

The main topic of the report relates to geothermal development opportunities, as it considers the geothermal resource being one of the most important future inputs for energetic mix independence in the Oradea region. This implies also actions towards a more extensive use of geothermal energy.

The general literature review about the benefits of geothermal power and energy shows, that geothermal resources are a cheap form of renewable energy, with many advantages proven over time. No energy storage is necessary and it is reliable as it is season and weather independent. It is green energy and can be utilized in a sustainable way, with natural recharge or maintained through injection.

The utilization forms of geothermal resources with temperatures over 150°C include electricity production as the most important utilization form, while the medium- to low-temperature resources (<150°C) are suited for many different types of applications for heating, industry, agriculture, aquaculture, spas etc. (Lindal, 1973). For an improved utilization of geothermal resources, the Lindal diagram shows the cascading utilization and combined uses as an instrument for improved feasibility of geothermal projects. Although the temperature factor can limit some options, other applications can be developed (Gudmundsson, 1988).

The paper will review the existing geothermal characteristics and infrastructure, as a starting point to identify steps for improved efficiency and development opportunities of the geothermal resource in the area, and its impact in the local community.

1.1 Oradea metropolitan area

The city of Oradea is located in the western part of Romania, close to the Hungarian border (Figure 1). Capital city of Bihor County, Oradea is also the leading local economy driver of the county, with a population of approx. 200,000 inhabitants. The surrounding metropolitan area further develops an urban pole of around 250,000 inhabitants (Table 1 and Figure 2).



FIGURE 1: Romania, location of Oradea (modified from Infoturism.ro, 2016)

TABLE 1: Oradea statistical data: population and surface (INS, 2016)

Statistical data	Population	Surface (km ²)
Romania	20,121,000	238,391
Bihor county	600,223	7,544
Oradea metropolitan area	251,000	792
Oradea city	201,000	116

The most significant economic activities in Oradea are related to trade, manufacturing industry, transport and storage, construction, and professional, scientific and technical activities.

In 2007, the Municipality of Oradea created the Oradea metropolitan area, an association of Oradea city and the surrounding communities for common joint approach for more efficient development. The main

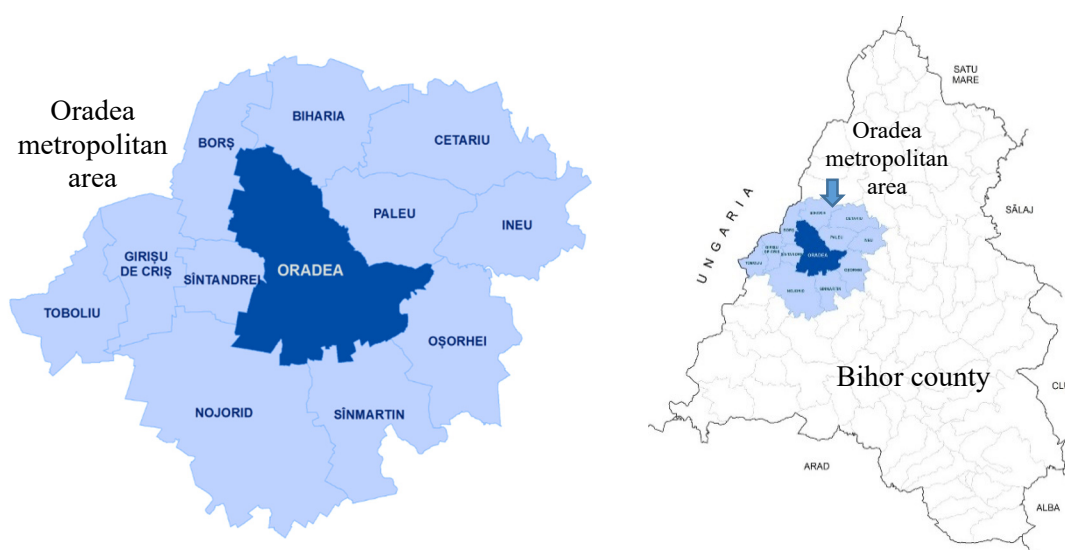


FIGURE 2: Bihor county and the location of the Oradea metropolitan area (Oradea, 2016)

objective was to share the resources and the efforts for a common development of the urban pole of Oradea. This association is generating specific common approaches for coherent planning and also projects for the geothermal development in the metropolitan area.

Regarding the weather in Oradea, the annual average air temperature is 10.6°C, with the highest value recorded in 2014, 12.8°C, and the lowest value in 1985, 9.0°C, which gives a thermal amplitude of 3.8°C. The monthly minimum is recorded in January, with an average of -0.7°C, and the maximum in July, when it reaches 21.3°C (Pereş and Köteles, 2015).

1.2 National Agency for Mineral Resources (NAMR)

According to the official website of NAMR (2016) and according to the law *Decision no. 1419 / 18.11.2009, amended by GD no.550 / 2013* regarding the organization and functions of NAMR, its main tasks are as follows:

General provisions of NAMR:

- It is organized and operates as a specialized body of the central public administration, with legal personality, subordinated to the Government and coordinated Prime Minister by a state councillor;
- It is governed by a president with the rank of Secretary of State;
- The funding comes from the General Secretariat of the Government, through a tertiary credit;
- It is the competent authority empowered to apply the provisions of the Mining Law no. 85/2003, as amended and supplemented, and the Petroleum Law no. 238/2004 modified and supplemented.

Main duties of NAMR:

- Manages resources of hydrocarbons (oil and gas) and mineral resources as public property, defined by Law no. 85/2003, as amended and supplemented, and Law no. 238/2004, modified and supplemented;
- Organizes the National Geological Fund – the resources / reserves, confirms, verifies, records and draws movement resources or reserves;
- Does concede with other state authorities, negotiate and conclude agreements on behalf of the state oil mining concession licenses and operating permits;
- Issues regulatory acts, rules, instructions, orders and regulations;
- Checks on holders of petroleum agreements and provisions of licenses or permits;

- Manages the national pipeline transport of oil and gas and regulates its operating activities through the system concession agreements concluded with domestic commercial companies nominated by the Government;
- Cancels acts of concession / administration; fees, taxes and tariffs;
- Establishes, under the law, the reference price for oil extracted in Romania to establish appropriate fee;
- Establishes national tariffs to exploit oil transport system;
- Sets tariffs for documents issued in the exercise of this or consultation and for use of documents and information concerning mineral resources;
- Follows the production of hydrocarbons and mineral resources in order to determine and correct receipt of the fee, opinions and other:
- Approves documentation on execution of prospecting, exploration or exploitation, mining and oil and documentation terminating the operations of oil and mining activities;
- Approves the annual exploitation;
- Develops and approves regulations and specific technical prescriptions;
- Follows established environmental protection measures during and after the oil and mining operations;
- Sets the safety parameters for hydrothermal mineral deposits, sludge and peat therapeutic and approves the establishment of sanitary protection perimeters;
- Develops and keeps oil books, books on mining and mining regulations;
- Collaborates with the regional authorities of water management, environmental protection and labour protection in the exercise of inspection;
- Certifies professional competence of individuals and businesses who undertake work and documentation;
- Guards and punishes offenders to the Petroleum Law and the Mining Law;
- Other duties established by law.

1.3 The Oradea geothermal system

The Oradea geothermal system is found within a fractured carbonated formation (Figures 3 and 4). According to Antics and Rosca (2003), the reservoir is located in Triassic limestone and dolomites at depths of 2,200-3,200 m in an area of about 75 km² mostly within the Oradea City limits. The water is about 20,000 years old, of calcium sulphate-bicarbonate type, with no dissolved gases, and mineralisation lower than 0.9-1.2 g/l. The reservoir is part of an active natural flow with the recharge

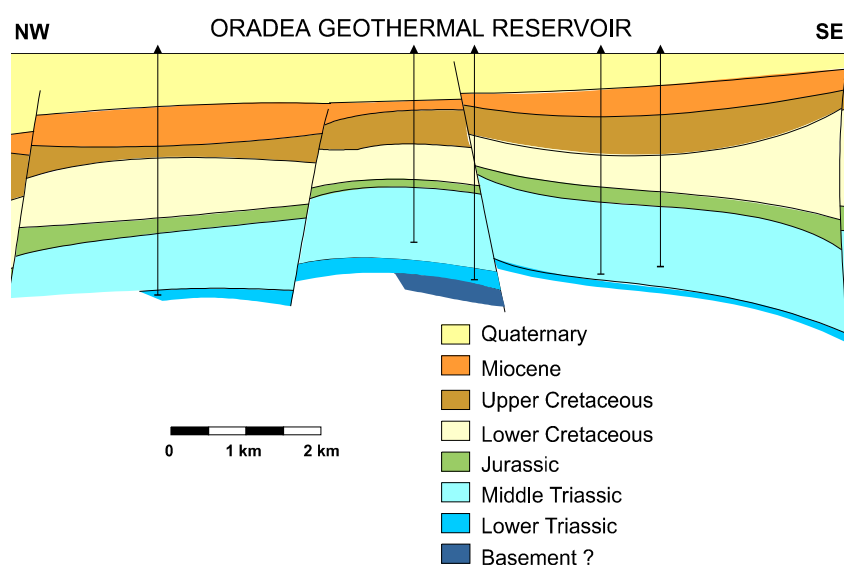


FIGURE 3: Cross-section through the Oradea reservoir (Rosca et al., 2016)

coming from the northern edge of the Padurea Craiului Mountains and the Borod Basin (Antics and Rosca, 2003). Studies indicate that exploitation in excess of an average annual total flow rate of about 300 l/s generates excessive pressure draw down in the system, thus exceeding the natural recharge. The current utilization permit, issued by NAMR, states that the maximum annual average utilization flow rate must not exceed 90 l/s without re-injection.

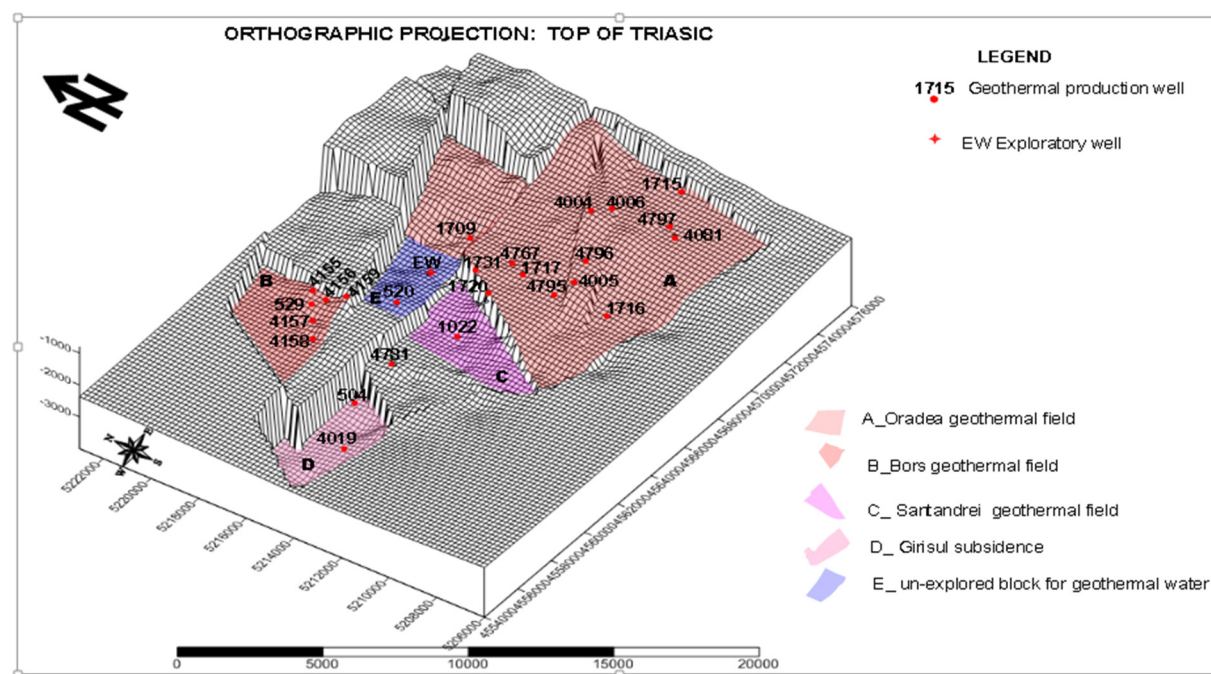


FIGURE 4: Top of the Triassic formation in Oradea and surrounding perimeters (Transgex, 2016)

1.4 Geothermal utilization in Oradea perimeter

The low-enthalpy geothermal energy is used mostly for heating purposes (including residential areas and industrial spaces), warm water preparation for the centralised district heating, industrial processes, greenhouse heating, but also for balneology, pools and spas, fish farming and aquaculture.

In the Oradea perimeter, there are currently 14 wells, 12 of which are production wells and 2 re-injection wells. Current annual average flow rate is about 60 l/s. The total installed capacity is about 21.5 MWth for the approved flow rate of 90 l/s. The current annual heat production is about 430 TJ/year with an average capacity factor of 63% (Rosca et al., 2013).

The estimated exploitation potential of the reservoir is around 250 GWh/year, but only 44% are utilised at present, giving a geothermal production in Oradea around 110 GWh/year. The development throughout the last 15 years of utilization shows no major changes. Table 2 shows geothermal utilization in Oradea.

TABLE 2: Utilization of the Oradea geothermal resource in 2013 (Vasiu, 2014)

	GWh/year
Thermal energy provided by the cogeneration plant	730
Geothermal potential	250
Geothermal production	110
Geothermal district heating production	55
Expected future potential of geothermal	52

In 2013, the geothermal resource in Oradea provided 55 GWh/year for district heating, about 7% of the overall thermal demand by the end users. Due to the relatively low geothermal temperature, the main utilization is supplying heat energy for the central district heating system. The geothermal energy is included in the energy mix for the district heating system, supplying the primary heating agent to some existing and updated substations of the old district heating system (Bendea et al., 2015). Geothermal heating energy is delivered to the district heating system by Transgex, from the 12 existing wells. Three main geothermal stations are used, mainly for preparing hot household water (HTW - hot tap water) as secondary agent for space heating, using additional heat, based on natural gas (Table 3).

TABLE 3: Characteristics of geothermal stations providing district heating in Oradea (Vasiu, 2014)

Oradea Geothermal Stations in 2013	Well parameters		Geothermal fluid temp. at the outlet of the installation	Thermal power capacity	Secondary thermal stations connected	Number of dwellings supplied	
	Temperature at the well outlet	Flow rate				Hot water	Space heating
	(°C)	(l/s)	(°C)	(MW _{th})	-	-	-
Nufarul	74	45	32	6	7	6,000	-
Iosia Nord	105	30	38	12	3	3,400	3,400
Calea Aradului	92	10	30	3	2	1,200	-
Total		85		21	12	10,600	

According to current data (Termoficare, 2016) the energy mix for the district heating system is mostly covered by SC Termoficare Oradea SA (publicly owned) that operates the cogeneration fossil fuel plant, plus the geothermal energy provided by the 3 geothermal plants owned and operated by the Transgex company, the local geothermal power private producer. The district heating system of Oradea uses 50% (around 55 GWh/year) of the total geothermal energy production, which makes it the main consumer of geothermal energy in the area. Reported to national level, this consumption corresponds to almost 35% of the total geothermal heat produced in Romania (Rosca et al., 2016). The following lists some short facts on the geothermal utilization in Oradea:

Tradition

- Spas attested during the Roman Empire times;
- First well drilled in 1885 in Felix Spa (depth 51 m, flow rate 195 l/s, temp. 49°C) – still in use.

Exploitation

- 14 wells in Oradea + 20 wells in the metropolitan area (30 km radius);
- District heating covering 70% of population;
- The district heating system of Oradea currently uses 6% geothermal input, which means around 35% of the total geothermal heat produced in Romania.

Research

- National Centre for Geothermal Research (1992) – Oradea State University;
- Romanian Association of Geothermal (1994);
- First geothermal power generation unit in Romania (2012);
- Study case for a hybrid project: electric energy production plant using geothermal + photovoltaic panels (2014);
- Pilot centre for studying geothermal exploitation (2014);
- First reinjection well in the last 20 years drilled in Romania (2016).

2. FURTHER OPPORTUNITIES FOR GEOTHERMAL DEVELOPMENT IN ORADEA

In the context of increased natural gas prices, the renewable geothermal energy is the solution for sustainable development. A more intensive exploitation of the potential geothermal resources in Oradea and its metropolitan area, can provide a clean, safe and cheap energy. Considering the existing situation regarding the geothermal resources and exploitation in the Oradea area, this research project is divided into two parts:

- Considerations regarding an improved efficiency utilization of the existing geothermal resources and infrastructure in Oradea;
- Identifying development opportunities for geothermal exploitation and utilization in Oradea and metropolitan area.

The geothermal development opportunities will link development tools over different potential utilization forms of geothermal resources in Oradea area, related to the specific conditions of the national and regional level (geothermal reservoir and exploitation capacity, electricity and thermal energy market, specific development of the area and available resources, business opportunities and sources of funding, etc.). Figure 5 shows a version of the Lindal diagram with potential utilization of geothermal energy in the agriculture and agro-industry sectors.

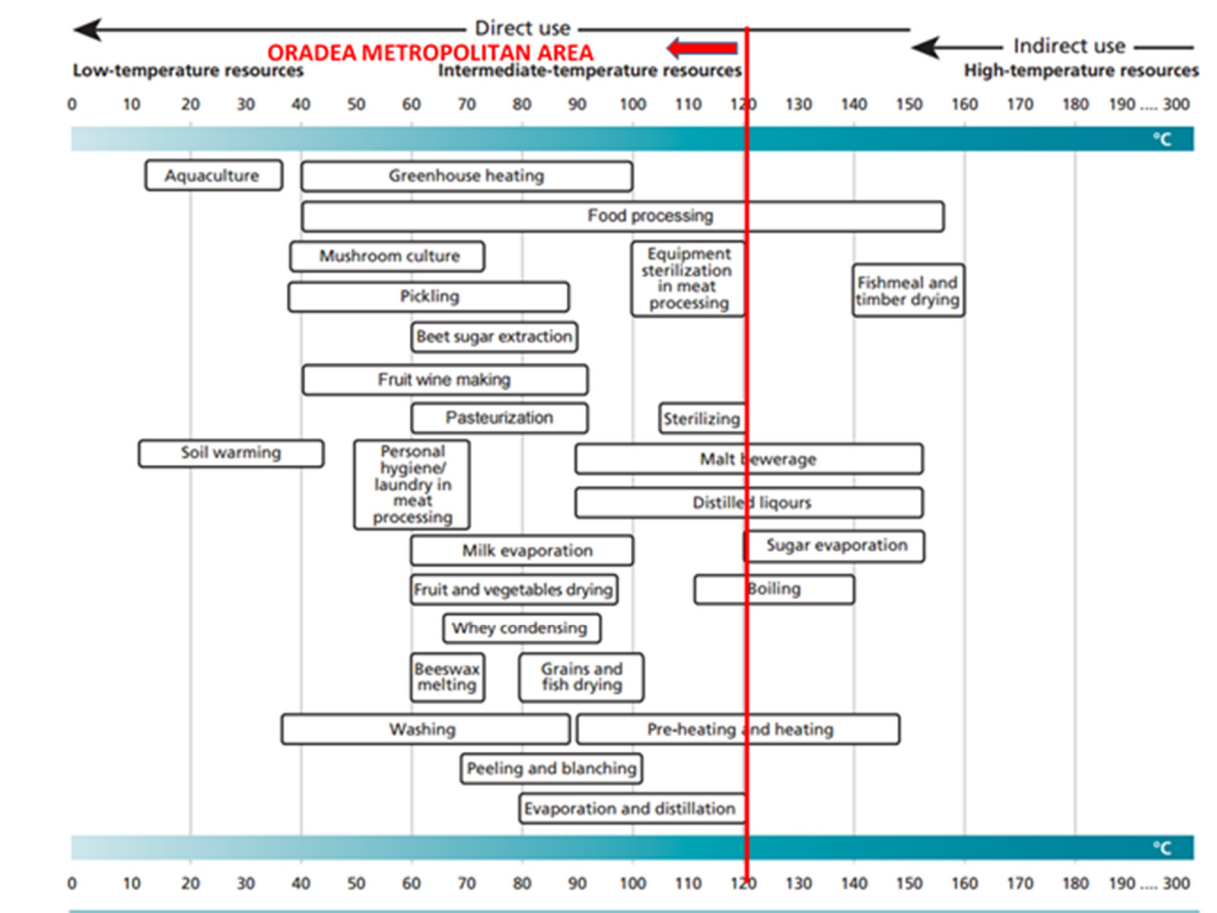


FIGURE 5: Lindal diagram for potential uses of geothermal energy in the agriculture and agro-industry sectors (modified from Van Nguyen et al., 2015)

2.1. Utilization of the existing geothermal resources and infrastructure in Oradea

It is necessary to create a large scale, commercially viable system for Oradea, which will optimise the value stream of lower temperature resources through systems based on cascaded use of geothermal. In

addition to electricity generation this could include direct heating and cooling, industrial and commercial applications, and agricultural uses. This way, the geothermal resources can be utilized for our own advantage and benefit of the environment.

Currently, the low-enthalpy geothermal energy exploited in the Oradea area is used directly, mainly for heating, industrial processes, greenhouses, balneology, spas, fish farming and aquaculture. The target is to develop the Oradea geothermal reservoir, so that it can be utilized up to its maximum potential. Research needs to identify the optimal conditions of efficient and profitable geothermal exploitation (gas fuelled plant vs. geothermal plants), energy mix etc. A cascaded system is a good example for increasing the energy utilization factor from the available flow rate of the geothermal water. The objective is to use the waste thermal water from the district heating system and create added value by more forms of utilization. A good example is the model from the Iosia geothermal plant where the waste geothermal water from the district heating is used for swimming pools in the area. The proposed model (Figure 6) can include: Power plant - 100°C, district heating & greenhouse - 50°C, spas, swimming pools and fish farms - 20°C, and return water going to water company.

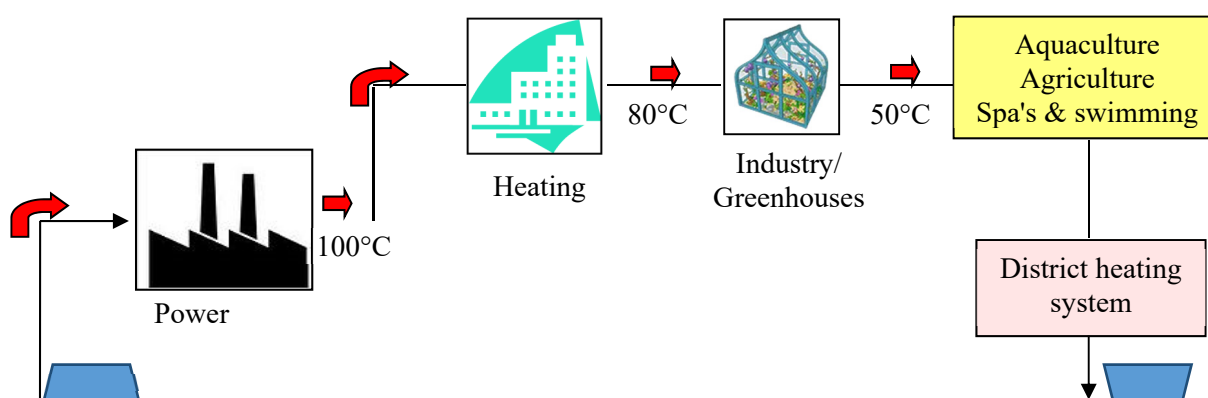


FIGURE 6: Geothermal cascaded utilization model for Oradea

2.1.1 Geothermal power production – Transgex Iosia geothermal plant

The public company Termoficare is producing electricity from the fossil-fuelled fired cogeneration plant. Until 2016 it coal was used as heating media. In April 2016 a new 50 MW gas cogeneration plant replaced it, producing now 43 MWe. The gas-generated electricity is sold on the national grid, with additional incomes available due to the special royalties offered by the Romanian government as a bonus for the high efficiency cogeneration electricity generated by the gas turbine, and green certificates (GC) for low impact on the environment. For the Oradea public cogeneration electricity producer, the Regulatory Authority for Energy (ANRE) in Romania stipulates, in the ANRE decision no. 2810 from 17.12.2014, that for the year 2015, the royalties shown in Table 4 are applicable (ANRE, 2016).

TABLE 4: Royalties for high efficiency cogenerated electricity (gas)

	Euro/MWh
Bonus for high efficiency electricity produced in cogeneration	37.35
Cogenerated electricity sold from the grid (no VAT)	32.74
Heating	21.63
Hot water	22.43

The system is fragile and political changes can affect the economic viability of the new cogeneration gas plant, such as through law changes, which can cancel the royalties and subsidies, low price of electricity in the national grid, increasing price of gas from the market, etc. Appendix I shows the monthly consumption of thermal energy (Gcal) in the Oradea DH system in 2015.

Termoficare does not use geothermal energy for the production of electricity. On the other hand, the private company Transgex is operating a 50 kW model of geothermal power unit in Iosia geothermal station, with the comment that it is not economically viable in the existing context. According to the existing legislation for electricity produced from geothermal energy there are no state subsidies or special royalties, not even green certificates. This is due to an unclear legislation that is not mentioning geothermal as a protected and supported resource by the state for power generation. The lack of special royalties, state subsidies or green certificates in the Romanian market, plus the low price for electricity in the national grid, was decisive in the geothermal power generation module from Oradea not being considered an economically viable project.

Due to the low enthalpy of the fluids in the sedimentary basin, geothermal fluid is not considered suitable for a cogeneration process based on a thermodynamic cycle, for simultaneously obtaining thermal and electrical energy (Vasiu, 2014). A financial analysis from the functioning period and considering the consumption of heat to produce electrical energy and revenues generated by this, showed that currently it is preferable for Transgex to concentrate on thermal energy district heating at the Iosia geothermal plant (personal communication with Transgex staff members), as seen by the following:

$$\text{Revenues from 1 Gcal/h thermal energy} = 8 \text{ MWe/h electricity}$$

Further development regarding geothermal power production has to be correlated with an initiative for legislation change in order to promote geothermal resources as a state-supported option for the energy grid mix in Romania.

2.1.2 Geothermal energy - Oradea district heating system

The main consumer of geothermal resources from the Oradea perimeter is the district heating system (Figure 7). In order to increase the efficient utilization of the geothermal resources, it is necessary to analyse and improve the functioning model of the district heating system and the geothermal exploitation rate. As mentioned above, for the reference period of the year 2015, the main heat source was the

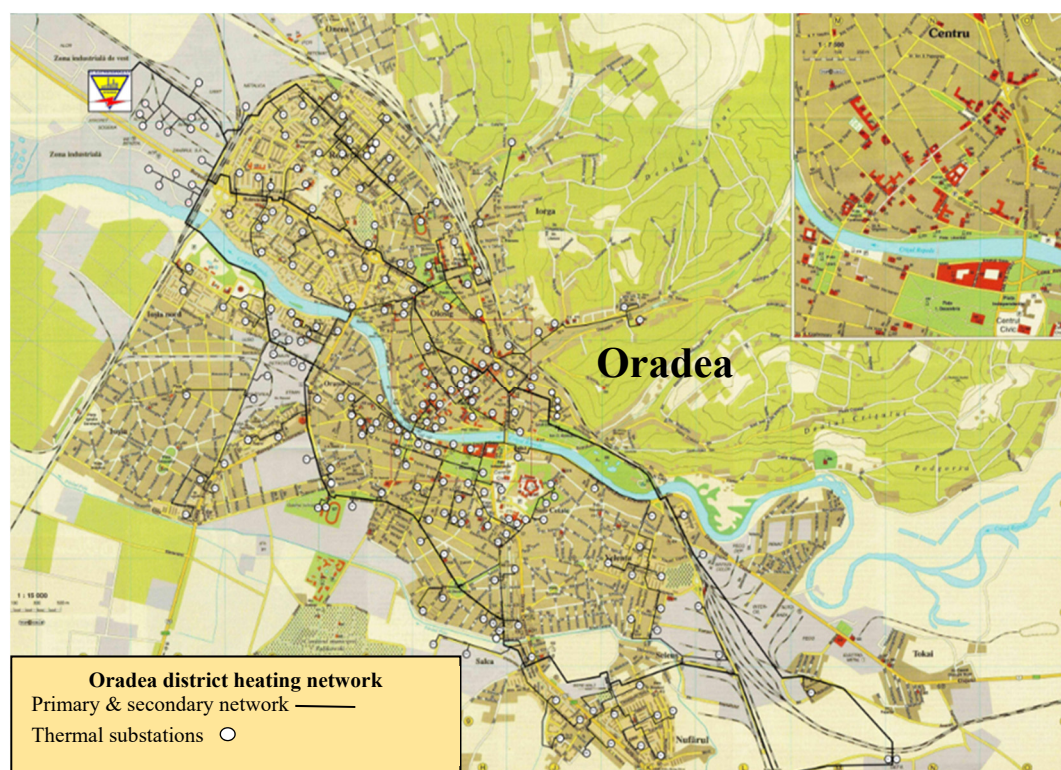


FIGURE 7: Oradea district heating system network (SC Termoficare SA, 2016)

cogeneration coal based plant, but today the Oradea district heating system main heat source is the 50 MW gas fuelled cogeneration plant, commissioned in 2016 by the local administration. The local transport network and district heating in Oradea is operated by SC Termoficare Oradea S.A. which manages a thermal network 219.5 km long (77 km primary and 142.5 km secondary and a total of 149 substations). It serves approximately 61,344 flats, 226 public institutions (schools, colleges, kindergartens and municipality) and a total of 1937 economic entities (banks, manufacturing facilities, etc.).

The water, which goes through the heat exchangers, is heated up to 90-110°C and returned at 35-40°C. The temperature of the geothermal water from the wells is suitable for hot tap water or industrial processes. An increasing or surplus of demand of space heating is provided through combined use of natural gas and heat pumps (Vasiu, 2014). According to the data (Termoficare, 2016; Vasiu, 2014) on the share of the geothermal resources vs. the fossil fuels used in the Oradea district heating thermal energy mix, the situation is as shown in Figure 8.

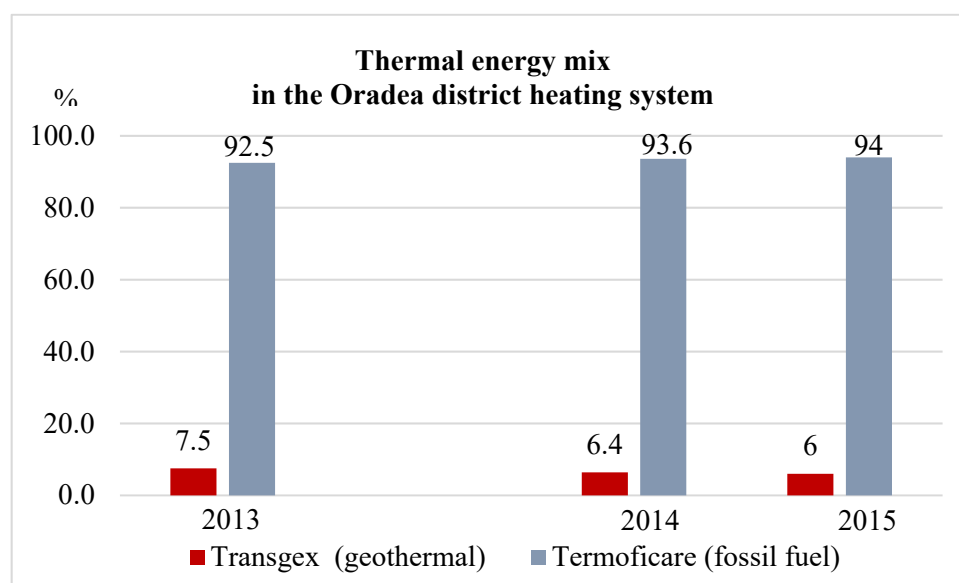


FIGURE 8: Thermal energy production analysis from the last 3 years in Oradea (comparison is made with the old cogeneration plant based on coal)

In order to identify the opportunities for potential development for the existing infrastructure, it is necessary to analyse the district heating efficiency in terms of production, sales and pricing policy for the end users (population and private companies). The year 2015 is the reference period for the analysis (Table 5). The potential exploitation level of the existing 11 production wells operated by Transgex in the Oradea perimeter is around 200,000 Gcal/year at approx. 25 Gcal/h (personal communication with Transgex staff members), which includes the rising level of injection as well. The hypothesis is that the share of geothermal energy in the total energy mix can be increased from the existing infrastructure (wells and geothermal stations), and that it can generate important savings for the local heating company (reducing the costs of thermal energy vs. fossil fuel) and for the local administration (reducing the subsidies per Gcal unit for population). Appendix II shows data on import prices for natural gas for EU.

TABLE 5: Total thermal energy production and sales in Oradea district heating (Termoficare, 2016)

Year	Production (Gcal/year)			Sales (Gcal/year)			Losses/ year
	Total	Fossil fuel	Geothermal	Total	Fossil fuel	Geothermal	
2014	823,705	790,053	33,652	482,637	451,809	30,828	41%
2015	892,635	853,613	39,022	558,772	525,027	33,745	37%

The average heat losses for EU district heating systems are around 10% (Nussbaumer and Verenum, 2014). In 2015, the production increased 8.4% from the previous year, while the sales increased with 15.8%. The reason was that the winter in 2015 had lower temperatures and the cold season was fully present from October to April. If the characteristics of last year (2015) for district heating are analysed, the situation is as shown in Table 6 and summarized in Figure 9.

TABLE 6: Total sales of Gcal/h units in the Oradea district heating system in 2015
(space heating + hot water)

2015 (Gcal/ h)	Total sales	%	Fossil fuel	%	Geothermal	%
Space heating	450,390	80.6%	432,630	96.1%	17,760	3.9%
Hot tap water	108,382	19.4%	92,397	85.3%	15,985	14.7%
Total	558,772	100	525,027	94.0%	33,745	6.0%

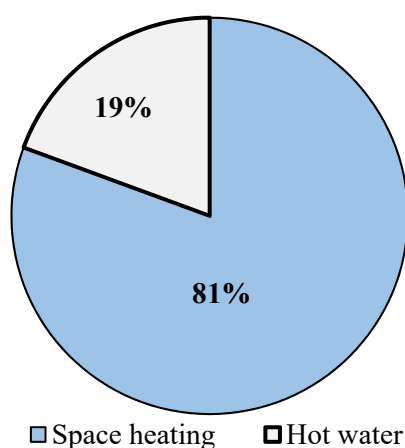


FIGURE 9 : Proportion of thermal energy consumption in Oradea in 2015

The data in Table 6 were processed from the information obtained from Termoficare in September 2016. It shows that main part of thermal energy for users is needed for space heating, which is operated an average period of 6 months, between the months of October-April. As expected, the geothermal input is mainly used for the hot water production (14.7% of the total Gcal units produced are used for hot water production) (see Figure 10). Based on this, a proposed option is, that during the summer period (May-

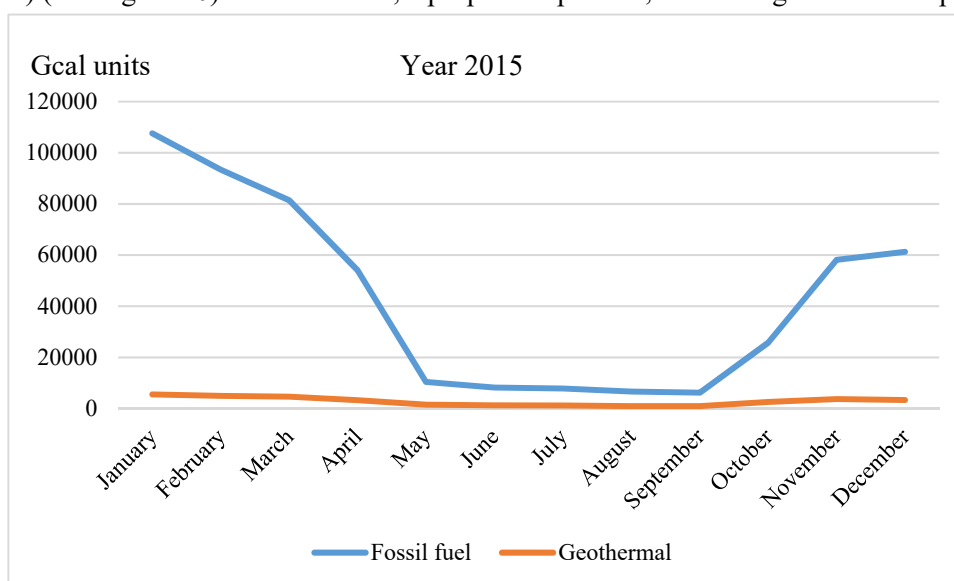


FIGURE 10: Monthly thermal energy sales in ORADEA district heating system

September), geothermal input in Oradea is increased to fully cover the needs of the system for hot water production, as there is a potential to increase the exploitation to 200,000 Gcal/year (personal communication with Transgex staff members). This means a considerably increased share of the geothermal energy in the total thermal energy mix.

In 2015, the data analysis on the monthly thermal energy consumption in the Oradea district heating (Appendix 1 – table with Gcal units consumption), reveals the heavy consumption due to the cold winter experienced (October-April). Figure 11 shows the consumption and the sources of thermal energy during the cold year of 2015 for the Oradea district heating system.

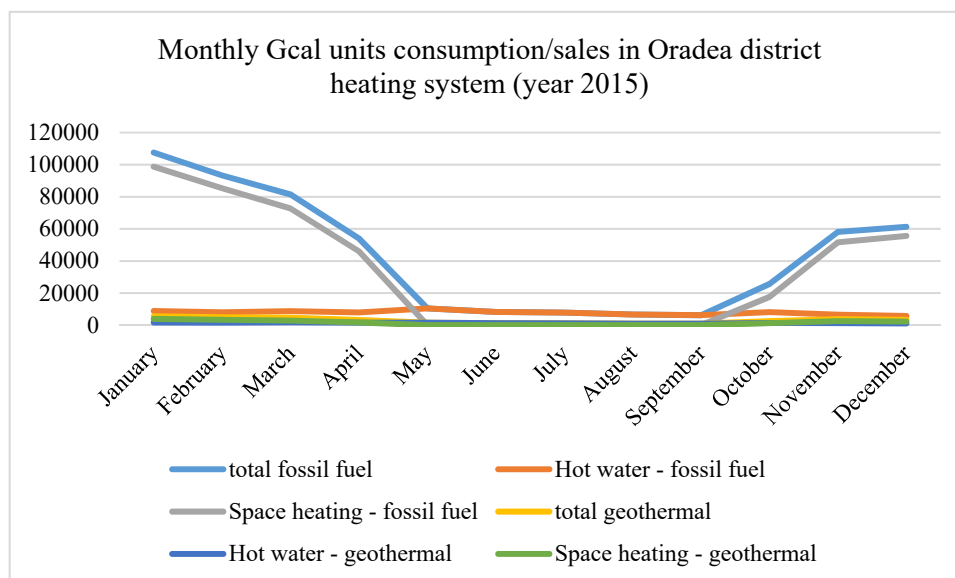


FIGURE 11: Consumption and sources for the thermal energy use in the Oradea district heating system during the year of 2015

A further review, reveals the high space heating demand, especially during the critical 3 months of January, February and March, covered by the cogeneration plant from fossil fuel. The geothermal energy is mainly providing for the hot water part, maintaining a stable delivery system for the district heating.

When discussing the thermal energy price policy in Oradea, it must be considered that Termoficare Company is producing the fossil fuel energy, but purchases the produced geothermal energy from Transgex, an independent private operator under state control. The total thermal energy is sold to the local district heating market at a weighted average price (final unique selling price on the market) of 260.7 RON/Gcal (Termoficare, 2015), which is converted to 57.9 €/Gcal (24% VAT included), at the currency rate of the Romanian National Bank for September 2016 (1 Euro = 4.45 RON). The continued calculations are based on this currency conversion, showing the market price and sales of thermal energy in Oradea. Table 7 shows the total Gcal thermal energy sales registered by Termoficare during 2015. It underlines the pricing policy and the total sales.

TABLE 7: Market prices and sales of Gcal units in Oradea in 2015

Year 2015	Price Euro/Gcal (VAT included)	% of total price	Sales (Gcal)	Sales (Mil. Euro)
Thermal energy sale price / Gcal	58.6	100	558,772	32.7
Local price billing/ Gcal	53.9	92.1%	-	30.1
Local subsidy / unit	4.7	7.9%	-	2.6

The final local thermal energy market price/Gcal is benefiting from the local subsidy policy (7.9%) from the Oradea municipality, in order to reduce the heat cost for the citizens. This local subsidy is not granted for business entities; they have to pay the full price of 58.6 €/Gcal (VAT included).

The registered losses from the thermal energy distribution and transportation network (Termoficare, 2016) reveal an annual loss of approx. 37.6% from the total Gcal production (approx. 1.5 M€). The huge losses put a constant pressure on the Gcal/unit cost on the local thermal energy market. This underlines the urgent need for the district heating distribution and transport network rehabilitation, revealing the urgency and importance for solving this problem. Even if these losses were not sold on the market, based on a stable demand on thermal energy, the production could slow down and reduce the costs for the extra production, distribution and transportation.

Losses from the system represent opportunity costs. In the near future, correlated to the declared rate of losses in the system of 34% for the year 2016, the production will lower as it does not have to cover so many losses, and can better adapt to the local economy trend regarding the thermal energy demand for district heating. The impact of low price geothermal in Gcal/unit on the thermal energy market is given in Table 8.

TABLE 8: Price analysis of Gcal thermal units (fossil fuel vs. geothermal):

Year 2015	Euro/ Gcal	% of total price
Geothermal Gcal price sold to DH	19.18	33.1%
DH Gcal price – mostly gas based	57.9	-
Final consumer price / Weighted average price	57.9	-

The data from the table underlines the fact that the selling price of geothermal energy/Gcal from Transgex towards Termoficare, is 3 times lower than the thermal energy/Gcal produced by fossil fuels. It is though important to note that for the final market price for of Gcal towards the end users, this comparison does not include the additional cost of distribution and transportation of the geothermal Gcal to the end user. A more detailed analysis to this aspect will be further developed in the next calculations, considering the production price as the reference point for an appropriate comparison between fossil fuel vs. geothermal feasibility analysis.

After processing the financial report of the public companies managing the district heating (Termoficare, 2015) the correlated data reveals the price structure, according to the Romanian legislation. The structure of the price and percentages of the total price were calculated (Tables 9 and 10).

TABLE 9: Thermal energy market price structure analysis – year 2015

Euro/Gcal	Fossil fuel		Geothermal
	Electrocentrale	Termoficare	Transgex
Production price	26.4	0	14.6
Transport tariff	0	8.2	4.6
Distribution tariff	0	14.1	0
Weighted average price = final price local market	58.6		19.2
Legal framework	ANRSC decision no. 3514/27.11.2013	ANRSC approval no. 114434/02.10.2013	ANRSC approval no. 215075/16.07.2014

TABLE 10: Gcal production prices - structure and sources analysis – year 2015

Gcal production prices in 2015 – structure & sources			
Thermal energy resource	Customers	Price Euro/Gcal	% of consumer Gcal price
Fossil fuel	Population	26.4	45.0%
	Economic entities	27.4	46.7%
Geothermal	Population	14.6	24.8%
	Economic entities		

The analysis of the thermal energy production prices from the fossil fuel vs. geothermal resources, considers that the distribution and transport tariff for the primary and secondary distribution and transportation network of the district heating will also have to be added, no matter what the energy source is. It could be added as an extra cost only for the geothermal fluid transport cost to the thermal stations. The geothermal Gcal distribution price is 75.9% of the total selling price of geothermal Gcal towards the district heating system (Table 11 and Figure 12). Reported as the weighted average price of Gcal on the local market, the production price is 24.8% of the final price.

TABLE 11: Average price break down structure in the local DH thermal energy mix in Oradea – 2015

Price structure	Euro/Gcal	% of final price
Production	26.4	45.0%
Distribution	14.1	24.1%
Transport	8.2	14.0%
Others	9.9	16.9%
Total	58.6	100

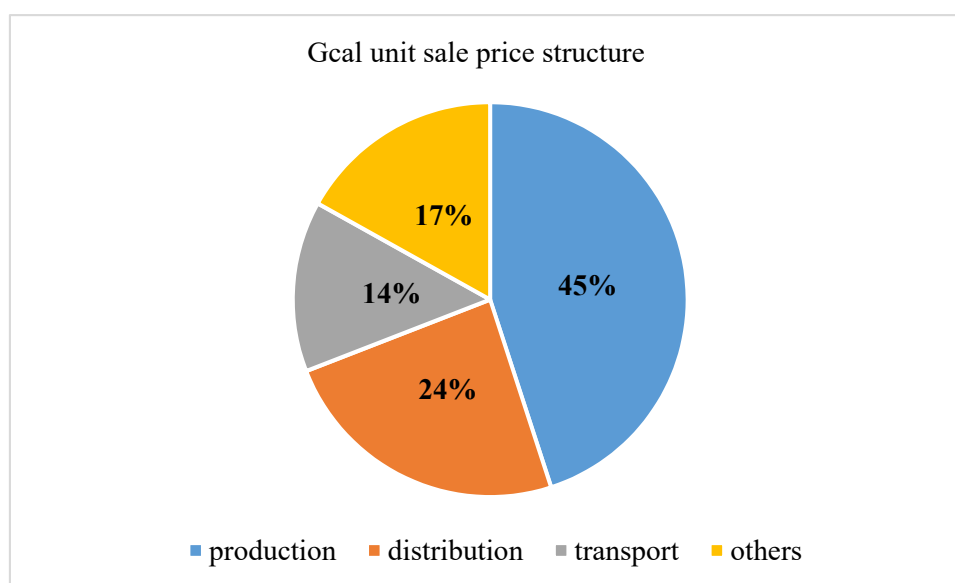


FIGURE 12: Average price structure in the local thermal energy mix

It is clear that the production price is the most important component of the final Gcal price on the market for a gas-based operation. For a clear comparison between the final thermal energy selling price of the fossil fuel Gcal vs. the geothermal Gcal, one has to consider that for the geothermal Gcal, the selling price is actually the selling cost towards the district company, without the extra costs for the distribution and transportation in the district heating network to the final users. For a clearer and close to reality comparison, it is better to compare the production prices of both (Table 12).

TABLE 12: Unit production prices (Euro/Gcal) – fossil fuel vs. geothermal – year 2015

Production price	Fossil fuel	Geothermal
	26.4	14.6

In terms of production prices of thermal energy in the Oradea district heating system, the geothermal Gcal unit feed-in price is 1.8 times less than the fossil fuel production Gcal unit:

$$1 \text{ Gcal geothermal production price} = 0,56 \times \text{Gcal fossil fuel production price}$$

As a main result regarding the 2015 geothermal energy production and sale analysis, related to the existing situation of geothermal utilization in the Oradea district heating and the comparison vs. the fossil fuelled thermal energy, the important data is emphasized in Table 13.

TABLE 13: Geothermal energy input and results in the thermal energy mix of 2015

Geothermal Gcal units production sales	% from total thermal energy mix sales	Savings (%)	Savings (Euro)
33,745	6%	4.5%	242,964

2.2 Intermediary conclusions

In order to improve the utilization efficiency of the geothermal resources based on the existing infrastructure and context in Oradea, the following conclusions have to be considered:

- The current exploitation rate of the Oradea geothermal reservoir is around 44%, with an average production of 60,000 Gcal/year, most of which is used for supplying approx. 6% of the total energy mix of the Oradea district heating system. The rest is sold by Transgex on the local energy market (to users which are not connected to the district heating system).
- The geothermal energy production from the Oradea perimeter can be improved with the existing infrastructure up to a production of 200,000 Gcal/year.
- Geothermal power production is not considered by the local geothermal operator (Transgex) as a viable approach for exploitation, due to low temperature of the Oradea geothermal reservoir. Its most efficient usage is producing thermal energy (due to malfunctioning legislation, low electricity price on the market, no state subsidies or green certificates).
- Geothermal energy in Oradea is mainly used for the district heating purposes, as it provides thermal energy for 70% from the population:
 - Geothermal energy mainly serves the market demand for hot tap water (14.7% of total mixed production of Gcal units)
 - Increasing the geothermal resource input in the thermal energy mix of the district heating to the full potential of the existing wells and geothermal stations (around 200,000 Gcal/year which would generate 35.8% in the total yearly thermal energy mix) will generate 8.3% savings related to the production prices of approx. 1.2 M€/year.
 - This will also reduce the DH energy costs (the production price of 1 unit geothermal Gcal is 1.8 times cheaper than the fossil fuelled Gcal/unit) for the population and economic entities. It will also reduce the local subsidy offered by the local municipality to support the population.
 - Actions are needed to reduce the losses of the district heating distribution and transportation network (approx. 1.5 M€/year) for a more feasible economic model of the district heating.
 - Improvements and extensions in infrastructure are needed for increased access and utilization of the geothermal fluid in the district heating system.
 - Furthermore, maintaining and boosting of the thermal energy market demand are needed in the area by supporting dedicated areas for district heating consumers and preparing new

development areas (Industrial Parks, Sport Centre, Ceyrat residential area, total geothermal coverage in Sinmartin area).

- Other utilization forms of geothermal energy in Oradea are limited and at a very low rate. The existing infrastructure and location of the geothermal source do not encourage reuse of the geothermal spent water for other utilization forms due to lack of infrastructure (except in the area of the Iosia geothermal plant, with cascaded utilization in the outdoor swimming pools nearby).

The above-mentioned points have to be included in the local and metropolitan development strategy, for a more efficient and sustainable approach. An improved policy for geothermal energy efficiency utilization must be based on the following main principles:

- Increase in heat exchanger efficiency in DH substations;
- Use of geothermal heat mainly for hot tap water production;
- Increased use of geothermal energy in the local DH thermal energy mix;
- Reducing the losses from the district heating distribution and transportation network.

3. FURTHER DEVELOPMENT OPPORTUNITIES FOR GEOTHERMAL EXPLOITATION AND UTILIZATION IN ORADEA AND THE METROPOLITAN AREA

3.1 Short facts on the geothermal development opportunities in Oradea

The potential

- 56% reservoir capacity exploitation is still available in the Oradea perimeter;
- There are 14 existing wells and geothermal stations plus additional wells from the metropolitan area (existing wells and potential projects for drilling of new wells in Oradea, Bors, Girisu de Cris, Toboliu);
- Increased heat demand request has been identified for the district heating (Oradea, Sanmartin) which can be covered by the existing infrastructure up to the full potential capacity of the Oradea reservoir and the wells from Bors and Santandrei.

Opportunities

- Local and national economy trends require renewable and cheaper energy;
- EU funding sources are available for geothermal development investments or related activities in the cascaded utilization line (PNDR, POIM, ROHU, EEA Grants, etc.);
- *Oradea Geothermal City* – in April 2016, the local administration management publicly accepted the idea of obtaining the license for exploration and drilling for geothermal resources – this is included in the Local Development Strategy of Oradea 2014-2025;
- *Oradea Geothermal Cluster* – based on the existing geothermal traditions and infrastructure in Oradea, a regional association platform should be created to lobby, promote and support legislation change in favour of geothermal development in Romania. This includes financing, state subsidies, green certificates, changing of the Mine law and reconsidering geothermal as a renewable energy as well as putting it under a different legislation – water, energy. Separate law is needed for geothermal resources.

Challenges

- National legislation (geothermal = renewable resource, green certificates, state support etc.);
- Coherent development strategy (national, regional and at local level);
- Funding (EU grants eligibility, World Bank, European Bank of Investments, public and private partnerships, etc.);

3.2 Energy price levels

Analysing the European Union natural gas import price historical data (YCHARTS, 2016 – Appendix II), it is clear that the actual price is at an historical lower level (Figure 13). The utilization of the geothermal energy resources has been delayed due to the high investment costs and the very low price of the hydrocarbons. However, with the current international market prices of fossil fuels, and the dramatic decrease of the domestic oil and gas production, the geothermal development has favourable conditions.

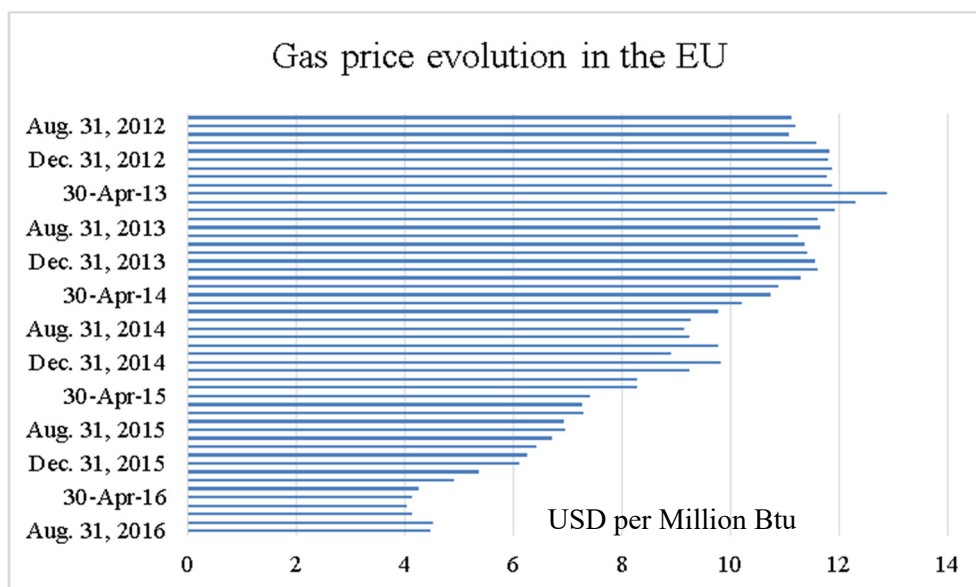


FIGURE 13: Natural gas price history (YCHARTS, 2016)

The risk analysis related to the increasing price of the natural gas on the international market, will directly determine the increasing final price of the Gcal unit in the Oradea district heating system. The sensitivity and risk analysis data regarding the natural gas price evolution underlines the disaster that can happen, and the need to further develop the geothermal system as an alternative in Oradea thermal energy market. Projections related to the year 2015 indicators (production, price, sales) are set as a reference point in order to generate different scenarios for development of the geothermal input and can be divided into 3 phases. The timeline of implementation of these development phases also takes into consideration the 5-year sustainability period of the EU funded gas cogeneration plant, after which it is possible to propose a major change in the local thermal energy mix in favour of the geothermal resources.

3.3 Oradea geothermal supply and demand market – further development plans

A short analysis of the existing infrastructure in Oradea (Figure 14) and the geothermal development opportunities from the technical side emphasizes some specific potentials (Transgex, 2016; Termoficare, 2016; personal communication with staff members) highlights the following:

- *Iosia geothermal station* is connected to the M2 primary network, including the heat stations PT 510 and PT 511. Well 1731 was connected to the Iosia geothermal power plant to provide the thermal energy for the *Andrei Saguna* and *Traian Vuia* high schools. Deep well line shaft pump was installed in well 1717 and connected to Iosia geothermal station to provide geothermal heat to sub-stations PT 510 and PT 511.
- A new updated project for a geothermal plant in Nufarul for harnessing geothermal energy in combination with heat pumps and natural gas to produce thermal energy for heating and hot water

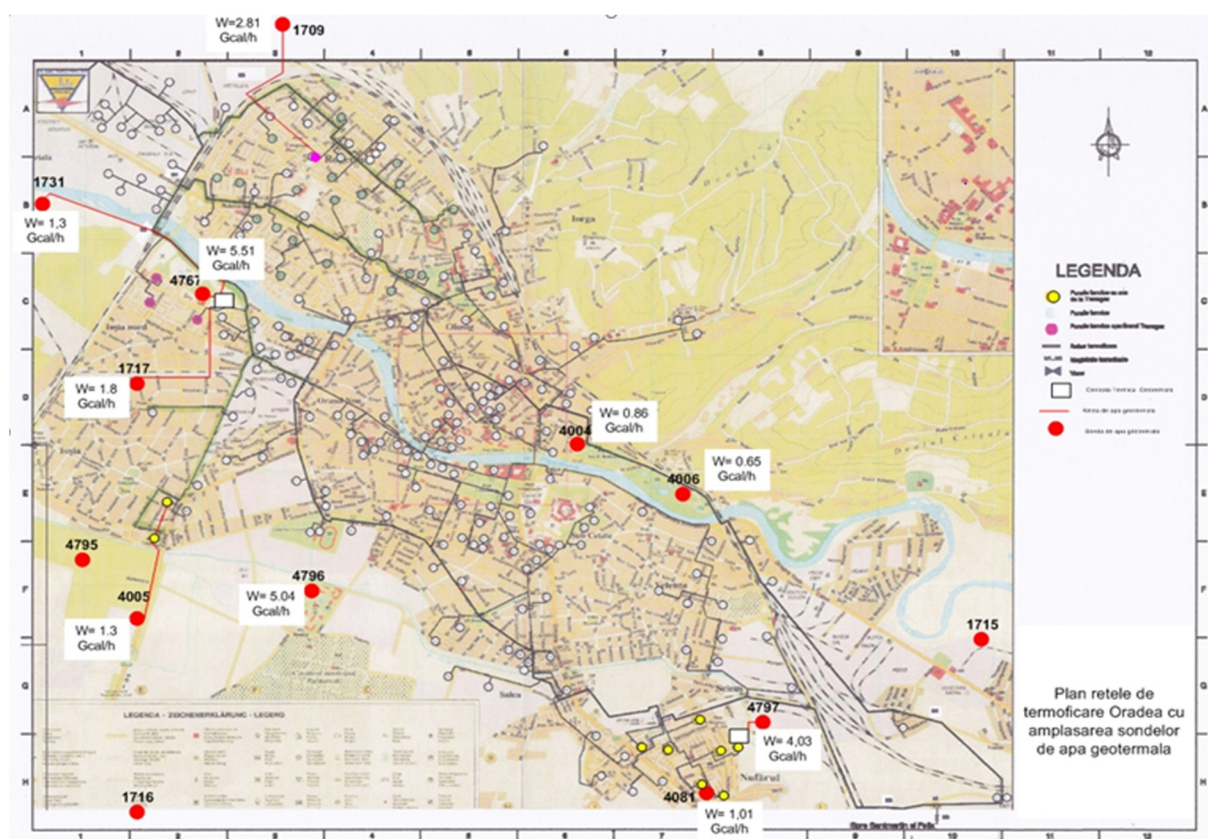


FIGURE 14: Heating networks in Oradea with the wells location and geothermal energy potential (Transgex 2016)

consumption to consumers in Oradea I Nufarul district.

- *Geothermal system for the Felix + Sinmartin areas*, either from existing sources or by updating the Nufarul I project with a new geothermal plan that can cover this special area (geothermal for Sinmartin / Felix). This project involves rethinking and updating the technical documentation for the Nufarul I geothermal plant, by converting the plant and replacing the heat pumps with pumps that provide geothermal energy (for hot water and space heating) towards Felix-Sanmartin area for the summer.
- Connection of new consumers to the geothermal pipeline from well 4796 to thermal unit PT 902 with new heat exchangers. The flow rate of well 4796 is high enough to allow for new consumers, which could include: Bihor County Library, building of Cadastral Office, Economy High School, the new Sports Centre, etc.
- Connection of well 1715 in Velenţa district to thermal unit PT 836, including thermal units from Dragos Voda district, and/or PT 864 with the block flats from the Moreni street, Ioan Slavici School and other economic entities.
- A new residential geothermal plant for customers in the Ceyrat residential area and the Polivalenta Hall, through thermal units PT 850 and PT 834.
- The main strategy for the district heating should be to assure hot water production from geothermal sources. The geothermal water will be transported from the wells located in the southwest section of the city, towards the DH plant where the hot water / primary heating energy is produced. In this option, Termoficare public company remains the official producer of domestic hot water, only changing from gas to geothermal fluid for the production of hot water for consumption. Transgex Company will remain the provider of the geothermal water.

Figure 15 shows the various types of utilization of geothermal energy in the Oradea metropolitan area. Appendix III lists geothermal projects that are believed to be in the pipelines in the Oradea area.

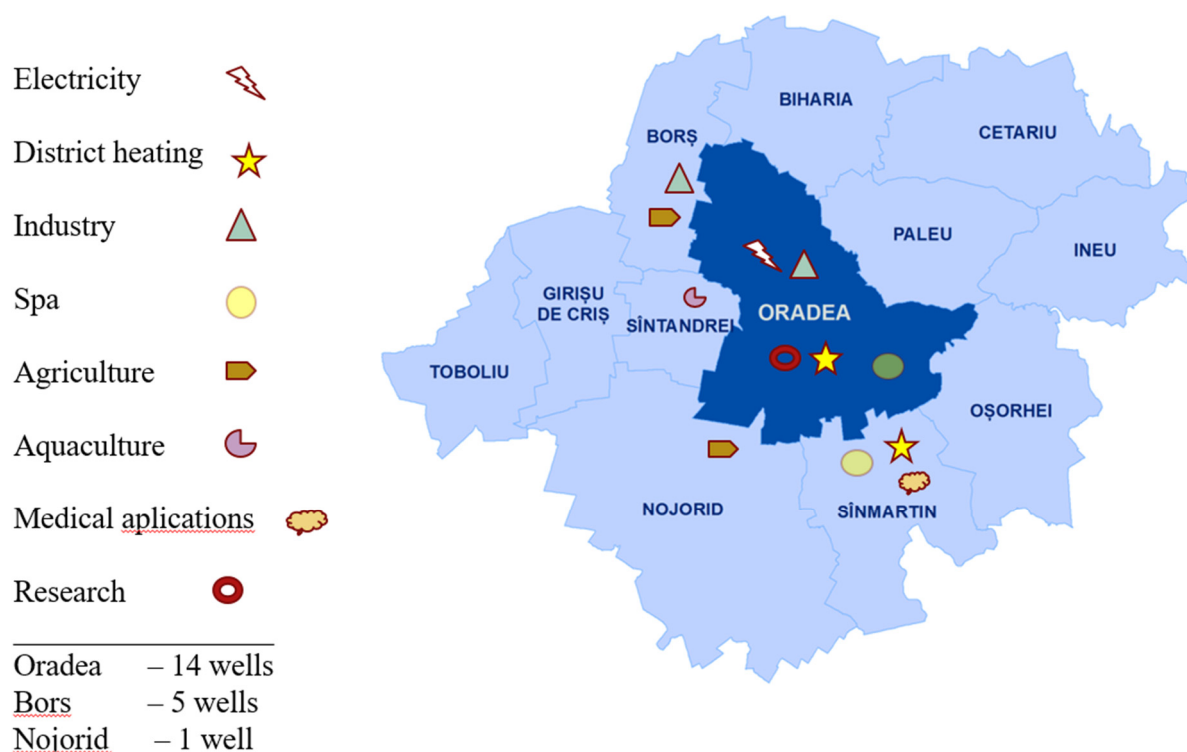


FIGURE 15: Various types of utilization of geothermal energy in the Oradea metropolitan area

3.4 Geothermal Road Map 2030 for the Oradea metropolitan area

For further geothermal development in Oradea metropolitan area, a *Road Map 2030* scenario is presented as a guideline model for planning the extended use of geothermal energy and to increase its efficiency. Starting point of the model is the need of a more efficient approach regarding the existing infrastructure, increasing the geothermal input into the district heating thermal energy mix and also extending it to the surrounding communities where existing wells can be used and directed towards the main consumers in Oradea. Based on the existing geothermal project pipeline, drilling of new wells is proposed in Oradea (3 wells), and more in Girisu de Cris, Toboliu.

The roadmap includes 3 phases aimed at increasing exploitation to 90% through reinjection, up to 500,000 geothermal Gcal units; and drilling of 3 new wells in Oradea and 2 new wells at Girisu de Cris and Toboliu. The areas (Figure 16) to be developed and the timeline are the following:

Area 1 – Oradea (2017): Electricity, district heating, industry, thermal bathing, research, medical.

Area 2 – Oradea, Bors, Sinmartin, Santandrei (2020): Electricity, district heating, industry, thermal bathing, agriculture, aquaculture, research, medical.

Area 3 – Girisu de Cris, Toboliu, Nojorid (2030): 1 + 2 + Electricity, agriculture, aquaculture.

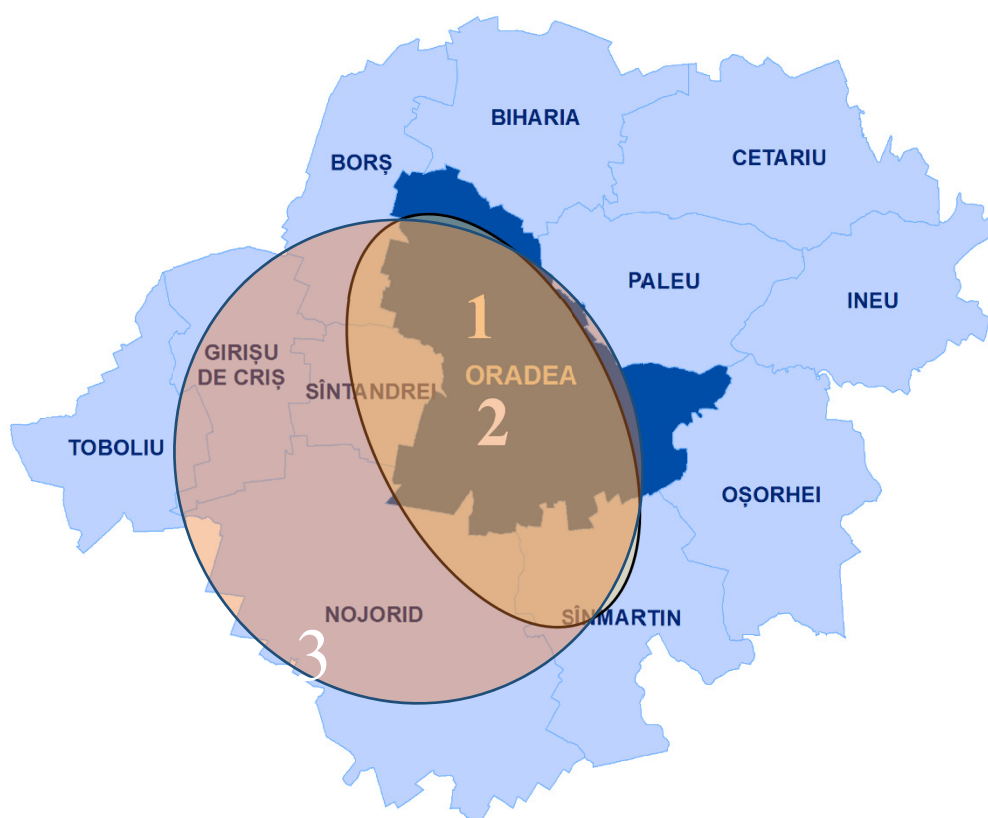


FIGURE 16: The 3-phase geothermal development model for Oradea

3.4.1 Phase 1 – current maximum geothermal production exploitation from the Oradea reservoir

The first phase is based on a more efficient model for the current utilization of the existing geothermal resources, and includes the following (see also Table 14 and Figure 17):

- Timeline: 2016/2017.
- Total production: 200,000 Gcal/year from the Oradea perimeter.
- Geothermal input in the thermal energy mix: 35.8 %.
- Necessary investments in the access infrastructure of the district heating system for the geothermal fluid.
- Geothermal energy used mainly for hot water production in the district heating system.

TABLE 14: Gcal unit sales projections in the Oradea district heating for the period 2016/2017 using the maximum geothermal input (200,000 Gcal/year) in the total thermal energy mix:

Thermal energy sales projection (Gcal/year) Comparison 2015 – future projection with 200,000 Gcal geothermal input			
Year	Total	Fossil fuel	Geothermal
Reference period – production 2015 (Gcal)	558,772	525,027	33,745
% input in total thermal energy mix		94.0%	6.0%
Scenario 2016/2017 (Gcal/year)	558,772	358,772	200,000
% input in total thermal energy mix		64.2%	35.8%
Market production price (Euro/Gcal)		26.4	19.2
Production price sales 2015 (Euro)	14,508,617	13,860,713	647,904
Production price sales estimates 2016/2017 (Euro)	13,311,581	9,471,581	3,840,000
Savings/year for 2016/2017 (Euro)	1,197,036	4,389,132	-3,192,096
Savings/year for 2016/2017 (%)	8.3%		

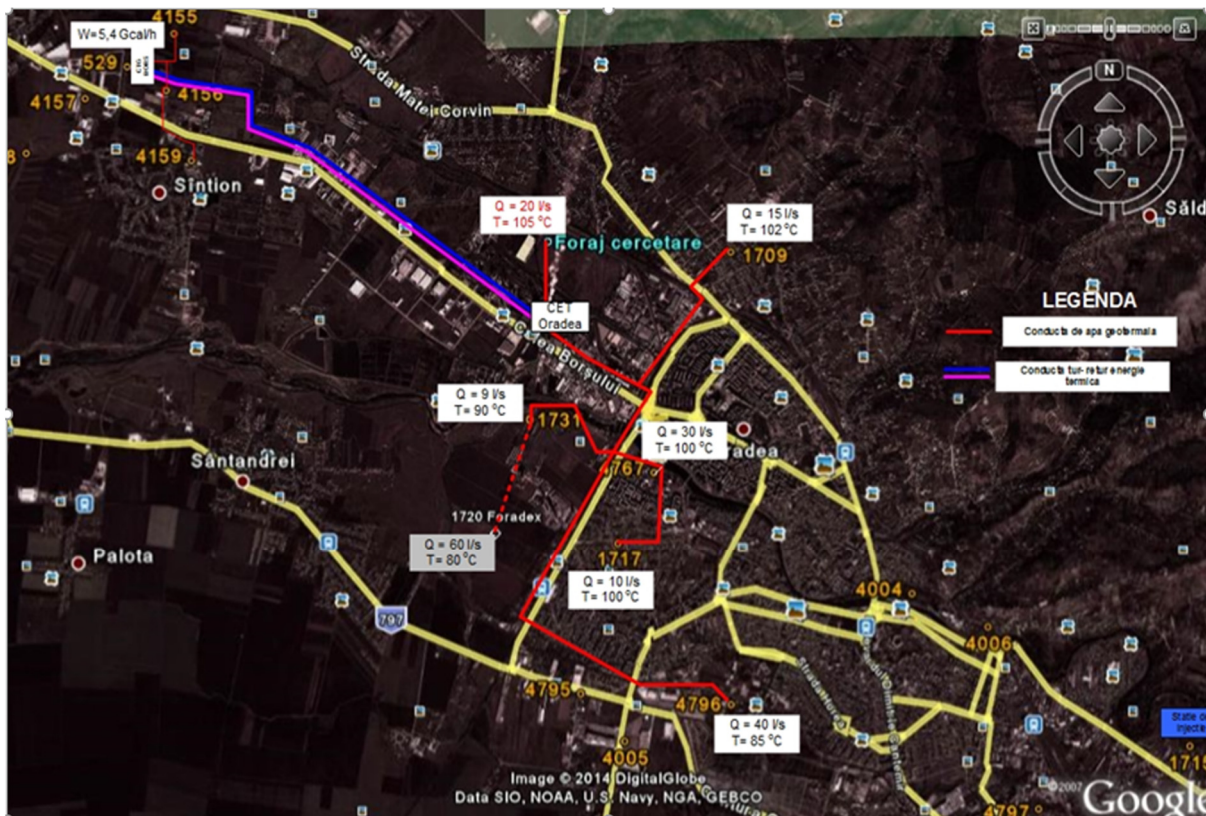


FIGURE 17: Geothermal wells that will be in service for CET Oradea (Transgex, 2016)

The projection model starts with the 200,000 Gcal units input in the total thermal energy mix as the maximum limit of geothermal exploitation results input from the Oradea reservoir (Transgex staff members, personal communication), in terms of infrastructure capacity (wells, temperature and pressure, geothermal stations etc.). The projection is based on a future period of 2016/2017 taking the data values from the year 2015 as a reference point for the total production of Gcal sold on the market. This generates a change in the thermal energy mix of the Oradea district heating system, as the geothermal resource input is up to 35.8% in the total yearly thermal energy mix, generating 8.3% savings related to the production prices of approx. 1,2 million Euro's/year. The values were compared in terms of production price sales (the only common dimension for comparison available at this point).

It is important to mention that for this goal, some investment is necessary for the improved access and more efficient utilization of geothermal energy in the Oradea district heating systems (equipment's, connections, system modifications and adaptations, geothermal substations, etc.). But this investment can be recovered in medium term from the generated savings based on the production price reduction. The injection rate has to increase as well, considering the legal binding level of 90 l/s natural recharge rate. This adds extra costs for the increased geothermal input in the total thermal energy mix of the district heating.

There is an element, which can affect this comparison. Fossil fuel thermal energy benefits from the cogeneration bonus and state subsidy, which is an extra advantage. But due to the fact that this aid scheme is only going to run for the next 5 years, the projections did not take it into consideration in the long run.

Presently, 50% from the total geothermal energy produced by Transgex goes to the Oradea district heating, while the rest has been sold to private and economic beneficiaries in Oradea. For the scenario presented above, it is assumed that all the geothermal energy is going straight to the district heating system. This would mean that former separate clients of Transgex need to move to the centralised system of the municipality.

3.4.2. Phase 2 = Phase 1 + new geothermal energy input from Oradea, Bors and Santandrei

The second phase is based on extended metropolitan model of usage of the existing geothermal resources (Figure 18 and Table 15):

- It considers Phase 1 as implemented, and continues the trend of increased geothermal input in the thermal energy mix of the Oradea district heating.
- Timeline: 2017/2020.
- Metropolitan approach (surrounding wells used for the district heating system).
- Total production: 360,000 Gcal/year = 200,000 Gcal/year from the Oradea perimeter + 100,000 Gcal/year from the Bors wells and 60,000 Gcal/year from the Santandrei well 1720.
- Geothermal input in the thermal energy mix: 36 %.
- The main consumption will go to the Oradea district heating system, plus the cascaded utilization model proposed in Santandrei (heating, hospital, aquaculture, greenhouse, bathing).
- Investments are necessary in the access infrastructure of the district heating system for the geothermal fluid from Bors and Santandrei to the Oradea thermal units and distribution and transportation network.
- Geothermal energy is mainly utilized for hot water production in the district heating system.



FIGURE 18: Phase 2 = Oradea + Bors + Santandrei (2020)

Bors geothermal reservoir is located in Triassic limestone and dolomite, at depths of 2,000-3,000 m, with an area of approximately 12 km², about 6 km northwest of Oradea. It is a closed reservoir with no natural recharge. The wellhead temperatures are about 120°C. Mineralization is 13 g/l with scaling prevented by downhole chemical inhibition and keeping CO₂ in solution (Transgex, 2016, staff members, personal communication).

Five geothermal wells have already been drilled, out of which 3 wells can produce up to 50 l/s (artesian) and 2 wells are used for reinjection. The cold water from shallow wells is injected into all 5 wells during the summer to build up reservoir pressure. The transport of thermal energy from the Bors perimeter to the cogeneration plant in Oradea to be used for preheating its make-up water. The main beneficiary of the potential thermal energy from Bors perimeter will be the cogeneration plant run by SC Termoficare S.A. The expected production potential of geothermal energy from Bors area is around 100,000 Gcal/year.

The Santandrei well 1720: According to data provided by the private owner company (Foradex, 2016), it has to artesian flow rate of 50 l/s with a temperature of 80°C. The plans are to increase the utilization of geothermal heat in the Oradea district heating system (space heating and hot preparation) for connected buildings in the Iosia district, and for future projects in the area (hospital, greenhouse, swimming pool/spas). For this purpose, it is expected to install a shaft pump into the well with the capacity of 60 l/s. The expected production of geothermal Gcal units from the area is around 60,000 Gcal/year. Also investment is necessary in the access infrastructure of the district heating system for the geothermal fluid.

Bors and Santandrei are considered input geothermal energy sources for the Oradea district heating system. Hence, the total expected production will be 360,000 Gcal/year, from which a total of 200,000 Gcal/year comes from the Oradea perimeter, 100,000 Gcal/year from the Bors wells and 60,000 Gcal/year from the Santandrei well 1720.

TABLE 15: District heating energy production projections in Oradea for the period 2020 using 360,000 Gcal/year geothermal input in the total thermal energy mix:

Thermal energy sales projection (Gcal/year)			
Comparison 2020 / future projection with 360,000 Gcal/year geothermal input			
Year	Total	Fossil fuel	Geothermal
Annual production, ref. 2015 (Gcal/yr)	558,772	525,027	33,745
2015 % input of energy source		94%	6%
Scenario 2020 (Gcal/yr)	558,772	198,772	360,000
2020 % input of energy source		35%	64%
Production prices (Euro/Gcal)		26.4	19.2
Annual production cost 2015 (Euro/yr)	14,508,617	13,860,713	647,904
Annual production cost estimate 2020 (Euro/yr)	12,159,581	5,247,581	6,912,000
Savings/year for 2020 (Euro)	2,349,036	8,613,132	-6,264,096
Savings/year for 2020 (%)	16.2%		

The projection model starts with the 360,000 Gcal units input in the total thermal energy mix, considering that Phase 1 is already implemented, and other opportunities are still exploited. The projection is for the future period of 2016/2017 assuming the consumption of district heating energy in Oradea has not changed from the values of the year 2015. This is most likely an over estimate since by 2020 the enormous heat and water losses in the old distribution system, see chapter 2.1.2, will have been reduced to a normal rate through the annual ongoing rehabilitation projects.

This generates a change in the thermal energy production mix of the Oradea district heating system as the geothermal resource share is up from 6 to 36%. This leads to 16.2% savings in production cost for the Oradea district heating company (DH), or approx. 2.3 million Euro/year. It is important to be aware of that for this scenario, considerable investment is necessary for the improved access and more efficient utilization of the geothermal energy in the DH (new wells, down hole pumps, inter-connections and heat exchangers, etc., heat substations etc.). For simplicity and due to lack of detailed data, this calculation assumes that the feed-in price for the geothermal heat energy can be maintained at the same level as current price. It also assumes that the production cost of heat energy from the gas fired co-generation plant has not changed.

3.4.3 Phase 3 = Phase 1 + Phase 2 + new drilling projects for geothermal energy input from new wells in Oradea, Bors, Girisu de Cris and Toboliu

The third phase is based on an extended metropolitan model for utilization of the existing geothermal resources (Figure 19 and Table 16):

- Considers phase 2 as already implemented, and continues the trend of increased geothermal input in the thermal energy mix of the Oradea district heating.
- New wells are scheduled to be drilled and exploited in Oradea (3), Bors (1) and for other forms of cascaded utilization in Girisu de Cris (1) and Toboliu (1).
- Timeline: 2020/2030.
- Total production: 360,000 Gcal/year from the Oradea perimeter.
- Geothermal input in the thermal energy mix: 64 %.
- Necessary investments in the access infrastructure of the district heating system for the geothermal fluid.

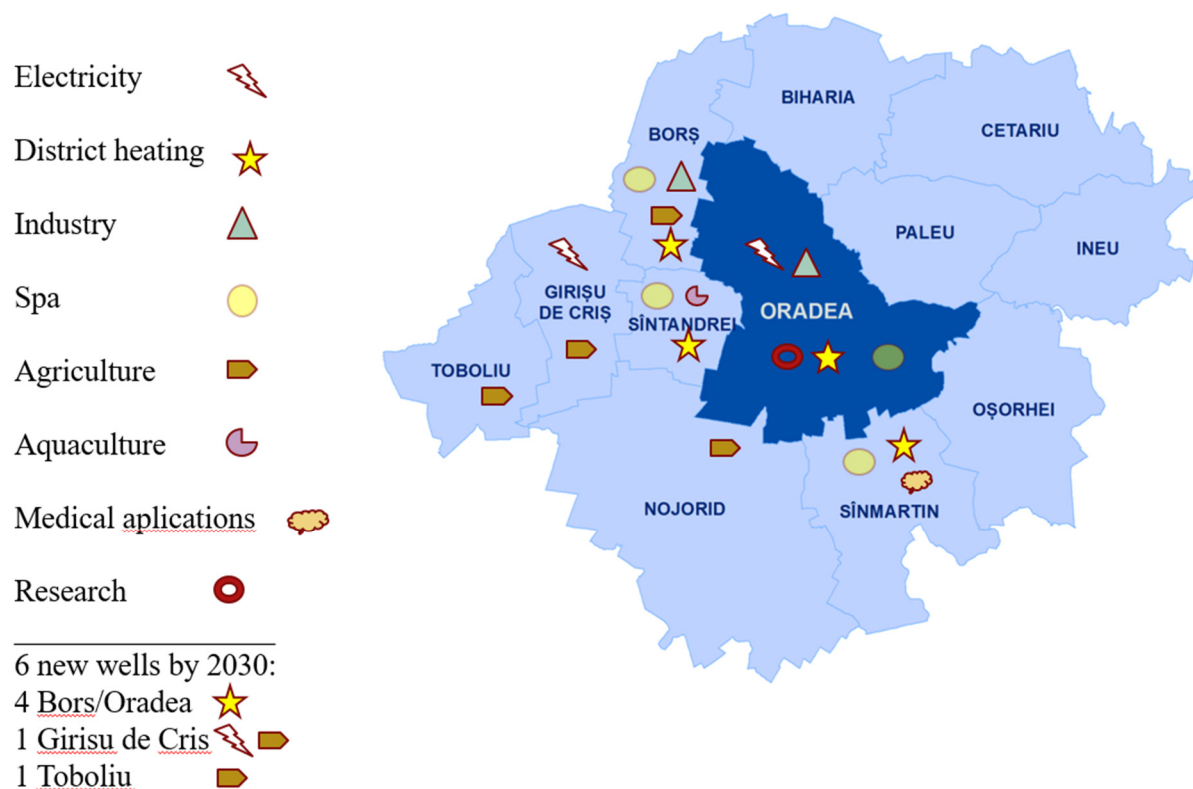


FIGURE 19: Phase 3 Oradea Metropolitan Area (2030)

The projection model starts with the 500,000 Gcal units input in the total thermal energy mix, considering that phase 2 is already implemented, but other opportunities are still unused. The projection is based on a future period of 2030 taking the data values from the year 2015 as a reference point for the total production of Gcal sold on the market. This generates a change in the thermal energy mix of the Oradea district heating system, as the geothermal resource input is up to 64% from total yearly thermal energy mix, generating 16.2% savings related to the production prices of approx. 3,3 million Euro's/year. The values were compared in terms of production price sales (the only common dimension for comparison available at this point).

It is important to mention that for this goal, considerable investment is necessary for the improved access and more efficient utilization of geothermal energy in the Oradea district heating systems (equipment's connections, system modifications and adaptations, geothermal substations, etc.). However, this

investment can be recovered in medium term from the generated savings based on the production price reduction.

Phase 3 contains the investment project for drilling of 3 new wells and exploitation equipment in Oradea DH, at Oradea Fortress, Industrial Park, Tancodrom, at Termoficare, close to the cogeneration plant. It also includes investment for other applications in the surrounding area as Girisu de Cris, Toboliu, Bors (heating, industry, medical, aquaculture, agriculture, spas):

- Drilling of a new well in Girisu de Cris is proposed for geothermal power production, heating and 20 ha greenhouses.
- Drilling of the new well in Toboliu is proposed mainly for agriculture (greenhouses) and aquaculture.
- The 3 new wells proposed for drilling in Oradea for the district heating are at the following points: Oradea Fortress, Industrial Park – Tancodrom, and at Termoficare, close to the cogeneration plant.

TABLE 16: Gcal unit sales projections in the Oradea district heating for the period 2030 using the maximum geothermal input (500,000 Gcal/year) in the total thermal energy mix

Thermal energy sales projection (Gcal/year)			
Comparison 2030 /future projection with 500,000 geothermal input			
Year	Total	Fossil fuel	Geothermal
Reference period production 2015 (Gcal)	558,772	525,027	33,745
% input in total thermal energy mix		94.0%	6.0%
Scenario 2030 (Gcal/year)	558,772	58,772	500,000
% input in total thermal energy mix		10%	90%
Market production price (Euro/Gcal)		26.4	19.2
Production price sales 2015 (Euro)	14,508,617	13,860,713	647,904
Production price sales estimation 2030 (Euro)	11,151,581	1,551,581	9,600,000
Savings/year for 2030 (Euro)	3,357,036	12,309,132	-8,952,096
Savings/year for 2030 (%)	30%		

3.4.4 Results

The main target of this project is to maximise the utilization of the geothermal energy sources available in the Oradea metropolitan area. The proposed projects should also find solutions for optimizing the supply to all types of consumers in the City of Oradea, with possibilities to expand it to the entire Oradea Metropolitan Area, considering also medium to long-term strategic development. It should also present solutions for increasing the energy efficiency for all types of consumers.

The model generated with this stepwise increase in the geothermal production, also enlarges the thermal energy production source. Adding the district heating distribution and transportation costs, it creates the scenario presented in Table 17.

Starting from the 2015 reference point (production prices, energy produced, quantities/sales, prices), the projection model for the 2017-2030 shows that if implemented, the third Phase strategy model can generate savings in production sales prices of the Gcal unit used in the Oradea district heating as follows:

- 2015-2017: The geothermal input of 6% in the thermal energy mix generates savings of approx. 486 k€;
- 2017-2020: A geothermal input of 36% in the thermal energy mix will generate savings of approx. 3.6 m€;
- 2020-2030: A geothermal input of 90% in the thermal energy mix will generate savings of approx. 23.5 m€.

TABLE 17: Conclusions regarding projections of *input* (geothermal Gcal) and *results* for Oradea district heating system

Geothermal energy input & results projections in the thermal energy mix 3-PHASE strategy – main dashboard				
	Estimated geothermal Gcal units production sales/year	%/year from total thermal energy mix sales	Estimated savings/year %	Estimated savings/year Euro
2015	33,745	6%	4.5%	242,964
Phase 1 - 2016/2017	200,000	36%	8.3%	1,197,036
Phase 2 – 2020	360,000	64%	16.0%	2,349,036
Phase 3 – 2030	500,000	90%	30%	3,357,036

In the case of implementing Phase 3, geothermal strategy scenario for the Oradea district heating system, the model estimates a generation of total savings in the Gcal unit production price of approx. 27.6 m€ until year 2019. Onward from 2020 it is recommended to move to the expanded approach of 90% geothermal utilization, that will generate an extra 3.4 m€/year. It is assumed that changes in the market will mean that proportions of structure will be kept.

4. CONCLUSIONS

The EU's Renewable Energy Directive sets a binding target of 20% final energy consumption from renewable sources by 2020. Renewables will continue to play a key role in helping the EU meet its energy needs beyond 2020. EU countries have already agreed on a new renewable energy target of at least 27% of final energy consumption in the EU as a whole by 2030. This target is part of the EU's energy and climate goals for 2030. The National Renewable Energy Action Plan (NREAP) in Romania assumed this targets for Romania also.

In this context, for Romania in general and Oradea metropolitan area in particular, there is an urgent need for an updated geothermal strategy development. This can be done immediately by starting the initial steps:

- a) Improve and optimize the existing geothermal utilization;
- b) Separate geothermal resources from the Mining law;
- c) Gathering and evaluation of existing data about geothermal (update, process and correlation);
- d) Assess the geothermal reservoir potential for sustainable utilization based on more than 4 decades of exploitation, mostly in artesian mode;
- e) Identifying potential projects – maps of geothermal potential and local applications;
- f) Update and expand the surface exploration and exploration drilling aide programme in Romania (the state should not drill, old system thought);
- g) A coherent geothermal development concept and project pipeline;
- h) Projects initiation and implementation.

Considering the previous geothermal input analysis and the situation regarding the geothermal utilization in Oradea, mainly for the local centralised district heating system, correlated with the current energy market situation and thermal energy demand, the main starting points for further development in Oradea are:

- Natural gas prices are increasing;
- The market demand for heat energy is growing – (residential and industrial development);
- There are other known geothermal reservoirs in the area, which can be harnessed more efficiently in the local and metropolitan energy market;

- It is more feasible to increase the efficiency and volume of the geothermal energy in the local thermal energy mix of district heating (socio-economic feasibility, energy mix security);
- Highest efficiency in low-temperature geothermal utilization is to use it for hot tap water production in the DH system;
- Reducing the heat and water losses in the district heating distribution and transportation network;
- Adding value for the geothermal resource by implementing a cascaded utilization system, creating a connecting system to reutilize the spent (return) geothermal water for other applications;
- Geothermal power production is present but not at full potential;
- Oradea geothermal producer – it is an option considered by the local administration;
- Oradea Geothermal Cluster – a platform for geothermal R & D in Romania, national policy of state support for exploration & drilling, green certificates);
- Legislation and financing issues have to be solved (geothermal resource = renewable resource, state support subsidies for geothermal development, allocation of green certificate MWth, etc.).

Oradea has a tradition for geothermal utilization and research in Romania. The main target is to develop the utilization of the Oradea geothermal reservoir and metropolitan area up to its maximum potential.

Why should the development of geothermal energy be furthered in the Oradea metropolitan area?

- The resource is there and not fully exploited;
- Geothermal input from the metropolitan area (Phase 3 of model) can supply 90% of the needs of thermal energy in the district heating system;
- Based on the model of Phase 3, it can generate heat production cost savings, of approx. 27.5 million Euros;
- There is an increased market demand for thermal energy - not all buildings in the city are connected to the DH system and the city population is growing;
- It is cheaper than fossil fuel and more environmentally friendly, reducing air pollution;
- It increases energy supply safety by using a local energy source;
- Geothermal input generates savings that can reduce the DH energy prices;
- Oradea Geothermal City – a cluster assumed by the local administration to be a part of its development strategy and an Oradea city brand.

How should the development of geothermal be carried out?

- Through more efficient use of the existing infrastructure and adding further development projects;
- Through further improvements to the district heating system connections for the geothermal fluid;
- By preparation of a coherent geothermal strategy, project pipeline and an investment plan;
- With added value through cascaded utilization models;
- With metropolitan approach (common management of geothermal resources in the metropolitan area).

ACKNOWLEDGEMENTS

Special thanks towards my supervisor, Mr. Árni Gunnarsson, for the opportunity to share knowledge and work together; to the decision makers and colleagues from my organisation that supported my participation; and gratitude towards Mr. Lúdvík S. Georgsson and the entire UNU-GTP staff who made possible our training in Iceland.

The author acknowledges the important contribution to this paper of Mr. Marcel Rosca from the Oradea University; of Mr. Miron Sferle from Transgex Company; of Mr. Mihail Smarandescu from Foradex company; and, not least, the colleagues from Termoficare company and Oradea Municipality, who provided or confirmed part of the information presented here.

The author also acknowledges that relevant local data was received in September 2016 by personal communication (interviews, meetings, e-mails, letters) from the following relevant organisations operating in Oradea metropolitan area and related to geothermal exploitation in Oradea: SC Transgex SA; SC Foradex SA; SC Termoficare SA; Oradea Municipality (dept. for geothermal development projects for district heating system); and University of Oradea (R&D Geothermal Centre in Romania).

REFERENCES

- ANRE, 2016: *Royalties for high efficiency cogenerated electricity*. ANRE – Regulatory Authority for Energy in Romania, website: www.anre.ro/
- Antics M., and Rosca, M., 2003: Geothermal development in Romania. *Presented at International Workshop on the Future of Geothermal Energy, International Geothermal Association – IGA*, 9 pp, webpage: www.geothermal-energy.org/pdf/IGAstandard/EGC/szeged/I-4-03.pdf.
- Bendea, C., Rosca, M.G., Iacobescu, A., and Bendea, G. 2015: Cascaded uses of geothermal water in Iosia District, Oradea, Romania. *Proceedings of the World Geothermal Congress 2015, Melbourne, Australia*, 10 pp.
- Foradex, 2016: *Data on the Santandrei well 1720*. Foradex S.A., database.
- Gudmundsson, J.S., 1988: The elements of direct uses. *Geothermics*, 17, 119-136.
- INS, 2016: *Population data*. National Statistical Institute of Romania – INS, webpage: www.insse.ro/cms/oradea.
- Lindal, B., 1973: Industrial and other applications of geothermal energy. In: Armstead, H.C.H. (ed.), *Geothermal energy*, UNESCO, Paris, 135-148.
- NAMR, 2016: *Main tasks and operations*. National Agency for Mineral Resources – NAMR, webpage: www.namr.ro/prezentare-anrm/atributii.
- Nussbaumer, T., and Verenum, S.T., 2014: *Status report on district heating systems in IEA Countries*. International Energy Agency, Bioenergy Task 32 and Swiss Federal Office of Energy, Zürich, 5 pp.
- Infoturism.ro, 2016: *Map of Romania and Oradea*. Infoturism.ro, webpage: harta.infoturism.ro/Europa/Romania/harta
- Oradea, 2016: Map of the Oradea metropolitan area. Oradea Metropolitan Area, webpage: zmo.ro/en/index.php/components-zmo.
- Pereş A.C., and Köteles N. 2015: *The monthly and annual air temperature regimes in the area of Oradea*. Analele Universităţii din Oradea, Fascicula Protecţia Mediului Vol. XXV, webpage: protmed.uoradea.ro/facultate/publicatii/protectia_mediului/2015B/im/16.%20Peres%20Ana%20Cornelia%201.pdf
- Roşca, M., Bendea, C., and Cucuţeanu, D., 2013: Geothermal energy use, country update for Romania. *Proceedings of the European Geothermal Congress 2013, Pisa, Italy*.
- Rosca, M., Gavriluc, R., Polizu, R., and Cucuţeanu, D., 2016: Geothermal energy use, country update for Romania. *Proceedings of the European Geothermal Congress 2016, Strasbourg, France*.
- Termoficare, 2016: *Energy mix in district heating systems*. SC Termoficare S.A., webpage: termoficareoradea.ro.
- Transgex, 2016: *Top of the Triassic formation in Oradea*. SC Transgex S.A., webpage: www.transgex.ro

Vasiu I., 2014: The geothermal energy contribution for heating supply in city of Oradea. *J. Sustainable Energy*, 5-1, 3-5.

Van Nguyen, M., Arason, S., Gissurarson, M., and Pálsson, P.G., 2015: *Uses of geothermal energy in food and agriculture – Opportunities for developing countries*. FAO, Rome, 62 pp.

YCHARTS, 2016: *Graphic image created from data on natural gas price history in the EU*. YCHARTS, September 2016, website: ycharts.com/indicators/europe_natural_gas_price.

APPENDIX I: Monthly consumption of thermal energy (Gcal) in the Oradea DH system in 2015 (Termoficare, 2016)

2015 - Gcal	Jan.	Feb.	March	April	May	June	July	Aug.	Sept.	Oct.	Nov.	Dec.
<i>Termoficare, fossil fuel</i>												
Total	107,607	93,361	81,429	53,993	10,411	8,202	7,815	6,671	6,193	25,731	58,134	61,261
Hot water	8,835	7,989	8,737	7,943	10,411	8,202	7,815	6,671	6,193	8,123	6,515	5,680
Space heating	98,772	85,372	72,692	46,050	0	0	0	0	0	17,608	51,619	55,581
<i>Transgex, geothermal</i>												
Total	5,523	4,926	4,610	3,236	1,527	1,229	1,171	953	949	2,566	3,719	3,336
Hot water	1,624	1,551	1,791	1,572	1,527	1,229	1,171	953	949	1,345	1,214	1,049
Space heating	3,899	3,375	2,819	1,664	0	0	0	0	0	1,221	2,505	2,287
Total / month	113,130	98,287	86,039	57,229	11,938	9,431	8,986	7,624	7,142	28,297	61,853	64,597

APPENDIX II: Historical data on import price for natural gas for European Union in USD per Million Btu (YCHARTS, 2016)

Period	Price	Period	Price
31-Aug-16	4.47	31-Jul-14	9.27
31-Jul-16	4.51	30-Jun-14	9.77
30-Jun-16	4.13	31-May-14	10.2
31-May-16	4.04	30-Apr-14	10.73
30-Apr-16	4.13	31-Mar-14	10.88
31-Mar-16	4.26	28-Feb-14	11.3
29-Feb-16	4.9	31-Jan-14	11.59
31-Jan-16	5.35	31-Dec-13	11.55
31-Dec-15	6.1	30-Nov-13	11.42
30-Nov-15	6.24	31-Oct-13	11.37
31-Oct-15	6.43	30-Sep-13	11.25
30-Sep-15	6.71	31-Aug-13	11.64
31-Aug-15	6.95	31-Jul-13	11.6
31-Jul-15	6.93	30-Jun-13	11.92
30-Jun-15	7.29	31-May-13	12.29
31-May-15	7.27	30-Apr-13	12.88
30-Apr-15	7.42	31-Mar-13	11.87
31-Mar-15	8.27	28-Feb-13	11.77
28-Feb-15	8.27	31-Jan-13	11.87
31-Jan-15	9.25	31-Dec-12	11.79
31-Dec-14	9.83	30-Nov-12	11.83
30-Nov-14	8.9	31-Oct-12	11.58
31-Oct-14	9.77	30-Sep-12	11.08
30-Sep-14	9.24	31-Aug-12	11.18
31-Aug-14	9.14	31-Jul-12	11.13

APPENDIX III: Oradea metropolitan area - geothermal projects in the pipeline
(based on discussion/interviews with local administrators in Oradea metropolitan area,
September, 2016)

Year	Location	Projects in pipeline	Investment	Budget M Euro	Financing source
2017	Oradea	Rehabilitation of distribution system	10 km primary and 20 km secondary distribution network	4	EU grants
2020	Oradea/Bors	Well drilling (prod. & reinject.), geothermal plant, thermal station, distribution network	Electricity, district heating	8	National funds
2020	Nufarul	Well drilling (prod. & reinject.), geothermal plant, thermal station, distribution network	District heating for Nufarul & Sanmartin (Baile Felix)	14	EU Grants
2025	Santandrei	Exploitation of existing well	Geothermal plant, district heating industry, agriculture spa, medical research	11	EU Grants
2030	Girisu de Cris	Well drilling (production & reinjection) 60 l/s, T = 170°C.	Electricity plant 3 MWe 20 ha. greenhouses	50	EU Grants
Total				87	



UNITED NATIONS
UNIVERSITY

UNU-GTP

Geothermal Training Programme

Orkustofnun, Grensasvegur 9,
IS-108 Reykjavik, Iceland

Reports 2016
Number 15

MODEL ORGANIC RANKINE CYCLE FOR BRINE AT OLKARIA GEOTHERMAL FIELD, KENYA

Gideon Gitonga Gitobu

Kenya Electricity Generating Company Ltd. - KenGen
P.O. BOX 785 – 20117, Naivasha
KENYA

ggitonga@kengen.co.ke, eng_gitobugideon@yahoo.com

ABSTRACT

A mix of conventional and wellhead power plants is used to generate geothermal power at Olkaria. All these plants utilize only the steam phase of the geothermal fluid flashing process. As a result, huge volumes of brine are left behind which if utilized can extend the exploitable potential of the field. This is possible using organic Rankine cycle (ORC) power plants that have been used successfully all over the world as bottoming units for conventional geothermal power plants. Every installation of organic Rankine cycle power plant requires a custom design tailored to suit the particular conditions of the source fluid and ambient climatic conditions. This paper models a suitable power plant for installation at the combined brine stream from separator stations SD2 and SD3 in Olkaria IV field bound for reinjection to well OW-911. The scope covered here is the design and sizing of major plant components from which it has been estimated that an ORC plant running on n-pentane as the working fluid installed on this brine stream will have a gross capacity of 4.6 MW and cost about 2,202 USD/kW. The cost is low because the installation of a bottoming ORC plant usually comes at such a time when the major geothermal development cost has been assigned to the conventional power plants. Therefore, it is the key finding of this paper that in a well-developed geothermal field like Olkaria, bottoming ORC plants can generate extra power at an economically competitive cost.

1. INTRODUCTION

1.1 Current geothermal development status

Commercial geothermal operation started in Olkaria in 1981. Since then the installed capacity has increased and currently KenGen owns and operates 4 conventional power plants and 15 wellhead units in Olkaria with a total installed capacity of 505 MW. All of these power plants utilize the single flash steam cycle technology. The principle here is to flash the geothermal fluid in a separator to harness steam that goes to the power plant for power production while brine is re-injected into the reservoir. The total separated brine is 2729 t/hr (Table 1) and could be used to produce power using organic Rankine cycle (ORC) plants. The steam field systems serving different power plants are not exactly similar and due to this the separated brine has different properties. These properties affect the relative feasibilities of utilization of the separated brine. An internal report from KenGen's Board of Consultants

in April, 2016 recommended that consideration should be given to the installation of bottoming cycle generation at those power plants where brine temperature remains high after separation (KenGen, 2016). This forms the basis of this project which is to explore how to optimally utilize brine for power generation in Olkaria. Preliminarily, an overall status of all separated brine in Olkaria field will be reviewed. Then the centre piece of this paper will be to model an ORC plant on the location with the best combination of factors such as availability of sufficient brine, ease of power evacuation, minimal environmental impact and existing road network.

1.2 Project justification

As explained above, KenGen currently uses a mix of conventional power plants and wellhead power plants for power production. The designed operating conditions for these plants are different for each one because it is important to match the plant design to the reservoir properties from which the geothermal fluids are tapped. Secondary design optimizations have continuously been pursued and adopted in a bid to bring down overall project costs and keep environmental effects to a minimum. Owing to this, plants are designed differently and besides that the design of pioneer geothermal plants is quite different from the modern ones due to technological advancements. As a result, for instance each plant in Olkaria has a distinct steam gathering system with different layouts and different operating conditions. The main features for Olkaria I and II power plants are that they have one main separator for each well and the separation pressure is about 6.0 bar-a. The new power plants Olkaria IV and Olkaria I additional units 4 and 5 have central separator stations and the separation pressure is about 12 bar-a. The wellhead plants are modular installations mostly fed by one well although in some cases one powerful well can serve two units. The separation pressure for the wellheads is about 15 bar-a. The separated brine is summarized in Table 1 below according to plants.

TABLE 1: Brine mass flows and properties

Plant	Brine (t/hr)	Separation pressure (bar-a)	Brine temperature (°C)
Olkaria I	235	6	158.9
Olkaria II	566	6	158.9
Olkaria IAU	524	12	188
Olkaria IV	815	12	188
Wellheads	589	15	198.3

In principle, it is possible to use all the separated brine for power generation. However, distinct conditions for each field cause the brine which is available to have different utilization potentials. Olkaria I has a partial reinjection scheme that encompasses a hot reinjection system and an open disposal to a lagoon from where it is pumped and used for drilling. Since the brine reinjection system for Olkaria I field is not much integrated, the cost of consolidating the brine together for power generation hugely undermines the economic feasibility of such an undertaking. The scattered nature of the wellheads and the possibility that they can be moved to a new location on a need basis discounts the prospect of having a bottoming cycle on them. Another factor that has to be taken into consideration is that KenGen is licensed to carry out exploitation and development in Olkaria geothermal field that cover about 204 km² and a part of this area lies within the Hells Gate National park. The National park plays a major role in the tourism industry which is a key economic booster in the area. Geothermal development activities and wildlife conflicts have always been kept to a minimum. Olkaria II and Olkaria IAU have well integrated steamfield systems with large brine flows at particular locations but lie within the game park. This paper does not conclude that it is difficult to install an ORC plant anywhere within Olkaria geothermal field. But it recognizes that one of the most ideal places for installation of an ORC plant is Olkaria IV field, the brine stream to reinjection well OW-911. This is the brine stream with the largest mass flow (499.5 t/hr) at a temperature of 188°C and it receives brine from separators stations SD2 and SD3 in Olkaria IV field (Figure 1). An ORC power plant for installation on this brine stream will be modelled here.

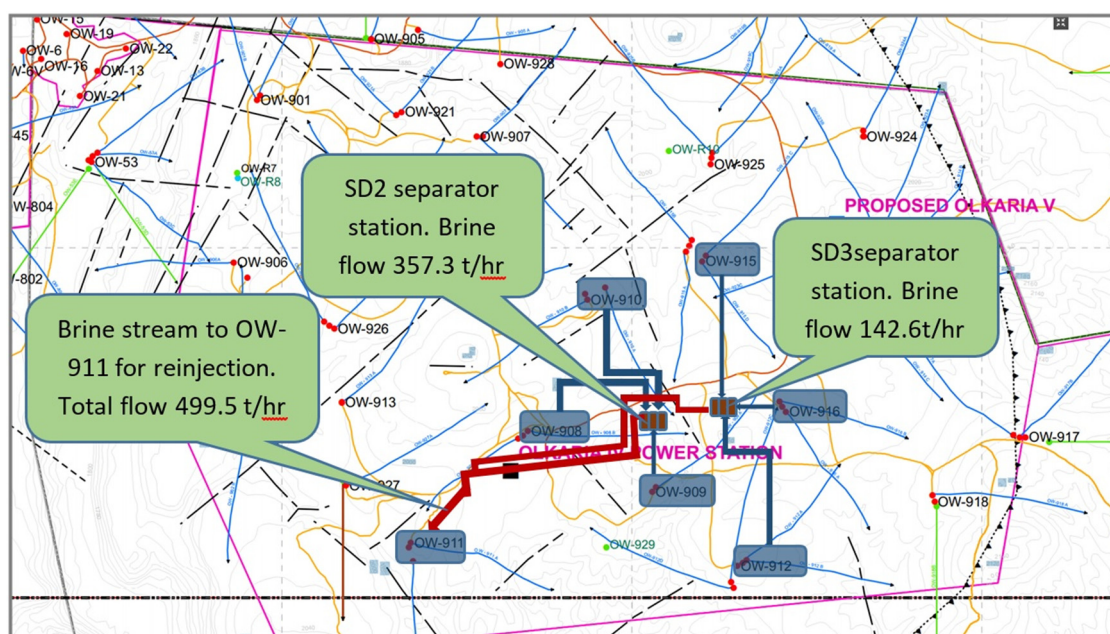


FIGURE 1: Location of separator stations SD2 and SD3 and hot reinjection well OW-911

1.3 Project scope

The scope of the project involves process design and sizing of major system components which then will give a reasonable clue to the expected project cost. In its basic form, a binary power plant under consideration here follows the schematic shown in Figure 2 below.

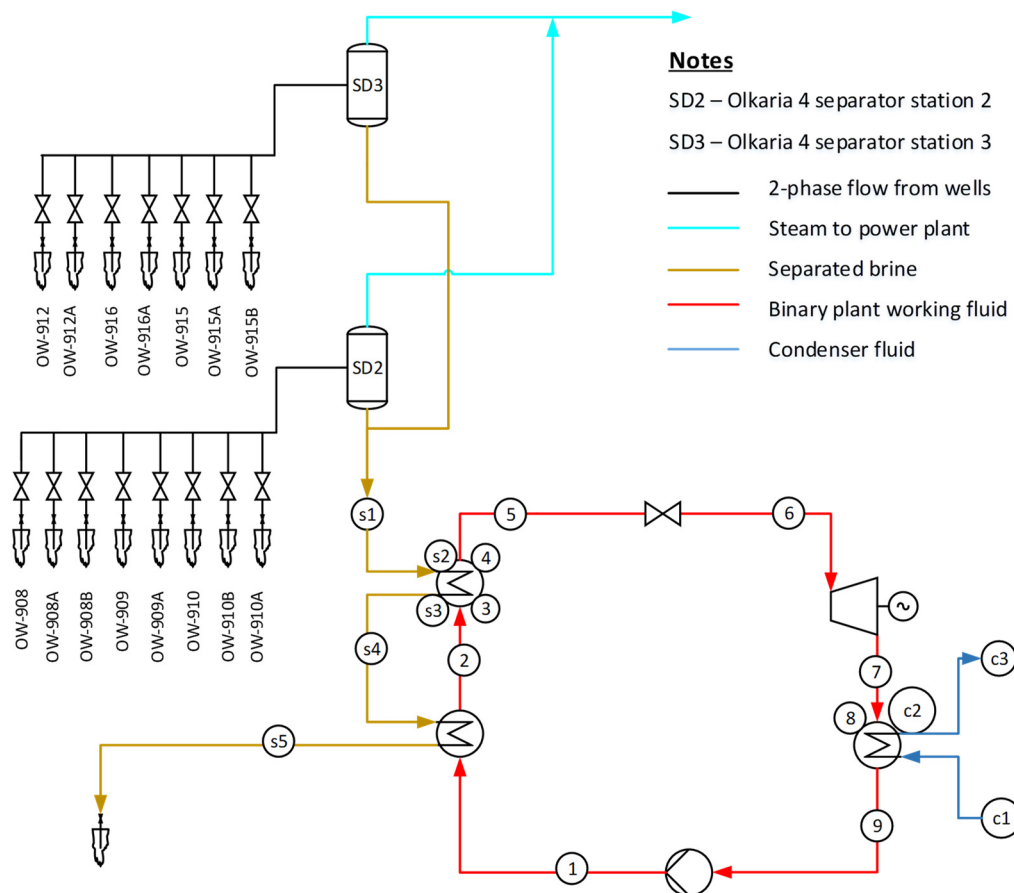
2. REVIEW OF RELATED LITERATURE

2.1 Thermodynamic cycle analysis

Process description in this section will refer to Figure 2. An organic Rankine cycle plant can basically be divided into three technical subsystems: the geothermal fluid or brine in this case, the power conversion cycle and the cooling system for the removal of heat (Frick et al., 2015). In a good design the three subsystems should interact reliably, efficiently and economically. In regard to the three subsystems, the basic theory of an ORC plant is that a working fluid chosen for its appropriate thermodynamic properties is fed to the heat exchanger where it receives heat from the geothermal fluid, expands through the turbine, condenses and then is fed back to the heat exchangers by a feed pump. ORC is a closed loop system and to have sequential description of the system this paper will describe the cycle the working fluid undergoes from the feed pump until it comes back to the same point again. DiPippo (2007) provided the basis of this description of the ORC system alongside the equations to be used in the analysis. It is assumed that the cycle runs in a steady state condition with no system pressure drop except across the turbine inlet valve and negligible kinetic and potential energies.

2.1.1 Feed pump

The enthalpy increase due to pressure differences across the pump and the pumping power can be obtained by Equations 1 and 2, respectively.



$$(h_1 - h_9) = v(P_1 - P_9) \quad (1)$$

$$\dot{W}_p = \dot{M}_{\text{wf}}(h_1 - h_9) = \dot{M}_{\text{wf}}(h_{1s} - h_9)/\eta_p \quad (2)$$

where h_1 and h_9 are the working fluid enthalpy at the feed pump outlet and at the inlet respectively, v is the specific volume, P_1 and P_9 refers to the pressure at the pump outlet and inlet respectively, h_{1s} is the working fluid enthalpy at the pump outlet assuming an isentropic process and η_p is the isentropic pump efficiency.

Eastop and MacConkey (1993) showed that for a liquid that is assumed to be incompressible (i.e. $v = \text{constant}$), the enthalpy change due to isentropic compression is given by:

$$dh = v dP \quad (3)$$

2.1.2 Heat exchanger

The heat exchanger is composed of the preheater and the evaporator. The design of heat exchangers requires examination of the temperature - heat transfer (T-q) diagram shown in Figure 3.

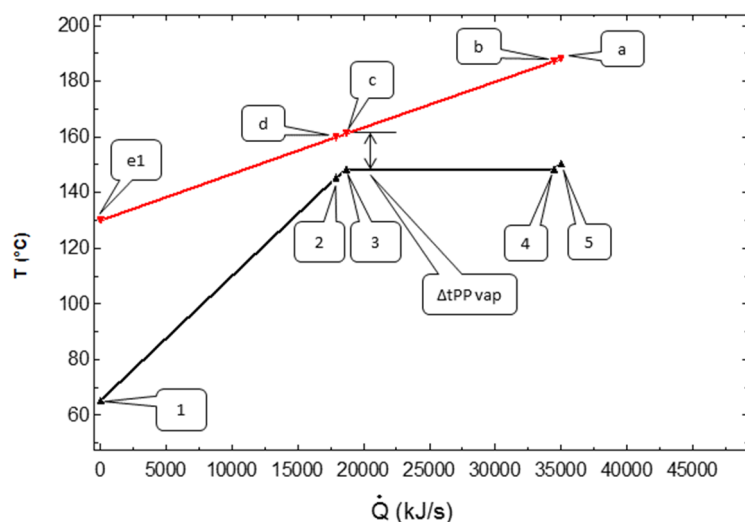


FIGURE 3: Preheater and evaporator T-q diagram

The brine transfers heat to the working fluid in a process that can be described as follows.

Preheater

In the preheater, the working fluid flows in the shell while the brine flows in the tubes. The movement of the working fluid in the shell is guided by baffles. The preheater heats up the working fluid to almost boiling point. That small margin to the boiling temperature in the preheater ensures that vapour doesn't form and gets locked in the baffles. Heat transfer process in the preheater is governed by this heat mass balance equation:

$$\dot{M}_b(h_d - h_e) = \dot{M}_{wf}(h_2 - h_1) \quad (4)$$

where h_d and h_e refers to the brine enthalpy as it enters and leaves the preheater respectively while h_1 and h_2 refers to the working fluid enthalpy as it enters and leaves the preheater respectively.

Evaporator

In the evaporator, the working fluid receives sensible heat up to the boiling point (bubble point), then latent heat up to vapour saturation (dew point) and additional heat up to 2°C superheat. Therefore, the heat duty of the evaporator is the sum of those three heat components whose mass balance equations are explained below:

- Sensible heat required to raise fluid temperature from the preheater outlet temperature up to its boiling point:

$$\dot{M}_b(h_c - h_d) = \dot{M}_{wf}(h_3 - h_2) \quad (5)$$

where h_c and h_d refer to the brine enthalpy at the evaporator bubble point and exit point respectively while h_2 and h_3 refer to the working fluid enthalpy at the evaporator entry and bubble point respectively.

- Latent heat required to vaporize the working fluid from the boiling point to vapour saturation point:

$$\dot{M}_b(h_b - h_c) = \dot{M}_{wf}(h_4 - h_3) \quad (6)$$

where h_b and h_c refer to the brine enthalpy at the evaporator dew point and bubble point respectively while h_3 and h_4 refer to the working fluid enthalpy at the evaporator bubble point and evaporator dew point respectively.

- Heat required to superheat the working fluid to 2°C:

$$\dot{M}_b(h_a - h_b) = \dot{M}_{wf}(h_5 - h_4) \quad (7)$$

where h_a and h_b refer to the brine enthalpy at the evaporator entry and dew point while h_4 and h_5 refer to the working fluid enthalpy at the evaporator dew point and evaporator exit point respectively.

2.1.3 Turbine

The turbine extracts energy from the working fluid. One thing to note here is that there is a pressure drop across the turbine inlet valve estimated at 0.3 bar. This throttling process is isenthalpic and so the turbine inlet enthalpy is the same as the enthalpy at the evaporator outlet. There will however be a slight drop in working fluid temperature between state point 5 and 6 as will be shown in Figures 8 and 9 due to this reduction in pressure.

The turbine power is given by:

$$\dot{W}_t = \dot{M}_{wf}(h_6 - h_7) = \dot{M}_{wf}\eta_t(h_6 - h_{7s}) \quad (8)$$

where h_6 is the vapour enthalpy at turbine inlet, h_7 is the actual vapor enthalpy at the turbine outlet, η_t is the turbine efficiency and h_{7s} is the vapor enthalpy at the turbine outlet assuming isentropic process.

The turbine efficiency is given by the manufacturer and it is the ratio between the real enthalpy change through the turbine to the largest possible (isentropic) enthalpy change (Valdimarsson, 2011).

2.1.4 Condenser

This is where the heat is rejected from the working fluid to the cooling medium which is air in this case. If a dry working fluid is used it exits the turbine in a superheated state. Condensation then is in two stages according to the T-q diagram (Figure 4). The first stage is to de-superheat the fluid to its dew point and the second stage is to remove the latent heat up to liquid saturation.

The heat which is rejected in the condenser to de-superheat the working fluid to its dew point is given by:

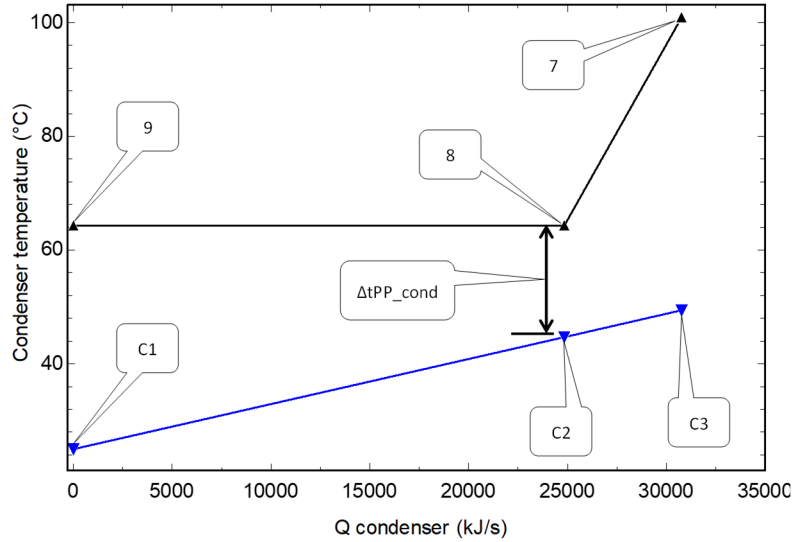


FIGURE 4: Condenser T-q diagram

$$\dot{M}_{wf}(h_7 - h_8) = \dot{M}_{cond_air} C_{air} (T_{c3} - T_{c2}) \quad (9)$$

Where h_7 is the working fluid enthalpy at the turbine outlet, h_8 is the working fluid enthalpy at condenser dew point, \dot{M}_{cond_air} is the cooling air mass flow rate, C_{air} is the constant specific heat of air while T_{c2} and T_{c3} refer to the cooling air temperature at the condenser dew-point and exit point respectively.

The latent heat which is rejected by the working fluid to condense it from dew point to liquid saturation is given by:

$$\dot{M}_{wf}(h_8 - h_9) = \dot{M}_{cond_air} C_{air} (T_{c2} - T_{c1}) \quad (10)$$

Where h_9 is the working fluid enthalpy at condenser outlet and T_{c1} refers to the cooling air temperature as it enters the condenser, which is the same as ambient air temperature. The other parameters are as described in Equation 9 above.

2.2 Heat transfer area calculation

In the preheater and evaporator heat is transferred to the working fluid over a surface area. The same principle applies in the condenser where cooling air draws heat from the working fluid over a surface and cools it as a result. The heat transfer area between two fluids is determined by the following heat transfer equation:

$$\dot{Q}_E = \bar{U} \cdot A \cdot LMTD \quad (11)$$

where \bar{U} is the overall heat transfer coefficient (Table 2 below shows assumed values for this model), A is the heat transfer area and $LMTD$ is the log mean temperature difference which is obtained from the formula below:

$$LMTD = \frac{(\Delta T_A) - (\Delta T_B)}{\ln \left[\frac{(\Delta T_A)}{(\Delta T_B)} \right]} \quad (12)$$

where ΔT_A is the temperature difference between the two streams at end A and ΔT_B is the temperature difference between the two streams at end B (Wikipedia, 2016a).

In the preheater, the working fluid temperature is raised linearly so the heat transfer area calculation is a straightforward application of equations 11 and 12. However in the evaporator, the working fluid temperature increase is non-linear since there is a heat component that heats the fluid to boiling point, another heat component heats the fluid up to the dew point and finally some heat is required to superheat the fluid (Figure 3). This means the LMTD and therefore heat transfer area is calculated separately for these three parts and summed up to get the total evaporator heat transfer area.

TABLE 2: Heat transfer coefficients (Fernando, 2013)

Component	\bar{U} (KW/m ² °C)
Preheater	1
Evaporator	1.6
Air condenser	0.8

In the condenser, the working fluid temperature decreases in a non-linear manner as shown in the T-q diagram (Figure 4). This is because there is a component of heat that is removed from the fluid to de-superheat it to condenser dew point and then latent heat must be extracted to cool it to liquid saturation point. Therefore, the LMTD and heat transfer area is calculated separately for these two parts and summed up to get the total condenser heat transfer area.

The evaporator and the condenser have pinch points where the temperature difference between the two fluids' exchanging heats is minimum. The choice of the pinch affects the overall performance and cost of the plant and therefore its choice is the result of economic optimization. A small pinch increases the performance of the heat exchanger and the condenser but it is costlier. A large pinch corresponds to the smaller and less costly heat exchanger and condenser but with reduced thermal performance.

2.3 Calculation of the parasitic load

The two components that consume the bulk of the auxiliary power are the feed pump and the condenser cooling fans. Feed pump power consumption has been explained in Equation 2. Due to the scarcity of water around the project area an air-cooled condenser is considered here. According to Wolverine (2016) the fan power required to move air through the heat exchanger is:

$$\dot{W} = \frac{GA_{min}\Delta P}{\rho} \quad (13)$$

where G is the mass flux at minimum flow cross section area, A_{min} which is given by $G = \frac{W}{A_{min}}$, W being mass flowrate of air and ΔP is the cooling air pressure drop across the heat exchanger while ρ is the density of air.

The ratio of mass to density is the same as volume. With that, Equation 13 can be rewritten as follows:

$$\dot{W} = \frac{\dot{V} \Delta P}{\eta_{fan}} \quad (14)$$

where η_{fan} is the efficiency of the cooling tower fan.

3. SELECTION OF THE WORKING FLUID

Appropriate selection of a working fluid is an important matter because it has great implications on the performance of a binary power plant. There is a variety of choices available for working fluids but each has its own advantages and drawbacks. The constraints that aid in the selection of a suitable working fluid relate to the thermodynamic properties of the fluids, considerations of health, safety and environmental friendliness (DiPippo, 2007).

3.1 Thermodynamic properties

3.1.1 Types of working fluids

Firstly, the suitability of the fluid is linked to the classification of the fluid as either wet fluid, dry fluid or isentropic fluid. This classification is based on the slope of the expansion process on the T-S saturation curve. Wet fluid expansion in a turbine results in droplets at the later stages which would then impinge on the turbine blades and cause erosion. As a result, isentropic and dry fluids are suggested for Organic Rankine Cycle plants (Chen et al., 2010).

3.1.2 Influence of latent heat, density and specific heat

A fluid with high latent heat and high density are preferable as a working fluid since they absorb more energy from the source in the evaporator and thus reduces the required flow rate, the size of the facility and the pump consumption. Another point to consider is the condensation temperature of the working fluids which should be above the ambient temperature to avoid challenges in condensing. Likewise, the freezing point of the fluid must be below the lowest operating temperature in the cycle (Chen et al., 2010).

3.1.3 Saturation volume and saturation pressure

The specific volume of saturated vapour of a given fluid gives an indication of condenser size, hence it is related to the system initial cost. Working fluids with low specific volumes require smaller condensing equipment which in turn is less costly.

These thermodynamic properties of fluids play out well when matching the working fluid to the geothermal fluid characteristics. The EES modelling tool makes this work easier as will be explained later with the aid of Figure 5.

3.1.4 Stability of the fluid and compatibility with the materials in contact

The working fluid selected should be chemically stable at the maximum operating temperature. It should also be non-corrosive and compatible with the turbine materials and lubricating oil.

3.2 Health, safety and environmental aspects

The major health and safety concerns are toxicity and flammability of the working fluid. In some cases, the toxicity risk is lowered by having an open to air ORC plant installation and so in the event of a leakage the concentrations are not too high. All hydrocarbon working fluids are known to be flammable and therefore would require more onsite investment on firefighting equipment beyond what is essential for ordinary power plants.

The main environmental concerns include the Ozone Depletion Potential (ODP), the Global Warming Potential (GWP), and the Atmospheric Lifetime (ALT). Due to environmental concerns, some working fluids have been phased out such as R-11, R-12, R-113, R-114, and R-115 while others will be phased out by 2020 or 2030 such as R-21, R-22, R-123, R-124, R141b and R-142b (Chen et al., 2010).

Table 3 below is not exhaustive but shows some of the fluids that have been screened and found suitable for use as working fluids in this ORC plant model. Wet fluids are not included in the table due to aforementioned reasons. Similarly, fluids that have been phased out or are in the process of being phased out are not included in this table.

TABLE 3: Properties of working fluids
(data from Chen et al., 2010; Habibzadeh and Rahsid, 2010; Wikipedia, 2016b)

ASHRAE number	Name	Type of fluid	Molecular weight (g/mol)	T _c (K)	P _c (MPa)
R-245fa	1,1,1,2,3,3,3 - pentafluoropropane	Isentropic	134.05	427.2	3.64
R-600	Butane	Dry	58.12	425.13	3.8
R-600a	Iso-butane	Dry	58.12	407.81	3.63
R-601	Pentane	Dry	72.15	469.7	3.37
R-601a	Iso-pentane	Dry	72.1	187.8	3.38

Currently, there is no ideal working fluid with the right combination of thermodynamic properties, influence of latent heat, density and specific heat, low toxicity and non-combustion properties. However, selection of the working fluid that matches the source fluid is made a lot easier by the EES software. For a fixed input parameter range of the source fluids, EES software is able to plot and overlay the performance curves for different working fluids which simplify their performance comparison and the selection of the most suitable fluid. Figure 5 will demonstrate that n-pentane and isopentane are suitable working fluids if brine reinjection temperature is limited to not less than 130°C as it is the case for this project.

4. ORGANIC CYCLE PLANT MODELING

4.1 Modeling software – Engineering Equation Solver (EES)

The program used to model this ORC system is EES. It is a very useful program for thermodynamic modelling of systems. It has inbuilt property functions for fluids of thermodynamic interest such as water, organic refrigerants and hydrocarbons. Any thermodynamic property of those fluids can be obtained from an inbuilt function call in terms of any other two properties. EES is particularly handy when it is of interest to find out how one or more independent variables affect related dependent variables. The program provides this capability with its parametric table. The user chooses the independent parameters and EES calculates the values of the dependent variables (Kopunicova, 2009).

The plot function enables the results of the parametric table to be presented in a visual manner. Different plots can be displayed simultaneously using the overlay function which makes performance evaluation of different options a lot easier.

4.2 EES model description

To build up an EES model of the system some input parameters must be known. The brine pressure and temperature are controlled by the design requirements of the convectional power plants. The brine separation pressures for Olkaria IV range between 11 bar-a to 12 bar-a depending on how far the separator is located from the main power station and the brine temperature at this pressure is about 188°C. The brine exiting from the heat exchangers is limited by its chemistry. The silica concentrations govern the range of temperature through which the brine can be cooled down at the heat exchangers of the ORC plant. The silica concentration for the brine stream considered here is 700 ppm and it is possible to cool it down to 130°C before scaling becomes an issue (West Jec, 2014). That explains how some input parameters turn out to be fixed. Some other input variables like pinch point temperature difference (Δt_{PP}) for the evaporator and condenser are not known conclusively when building up the EES model. They are assigned some reasonable starting values based on desktop studies. Once a working EES model is complete, optimization is done by testing the flexible values over a range to find out the value that yields low plant cost and high power output which is then picked as the final design point.

A complete model will give the sizes of the major components like preheater, evaporator, turbine, condenser, feed pump and cooling fan motors. The cost of these major plant components can then be approximated based on their price tag per unit size as shown in Table 4.

Preheater, evaporator and condenser costs are from Monroy Parada (2013), turbine and feed pump costs are estimates from people familiar with the industry.

TABLE 4: Main equipment costs per unit

Component	Unit	Cost (USD/Unit)
Preheater	Area (M ²)	450
Evaporator	Area (M ²)	500
Turbine	kW	450
Condenser	Area (M ²)	600
Feed pump	kW	450
Cooling fan	kW	450

In addition to the main component cost the total plant cost will be including the cost of the control system, back up installations, SCADA monitoring system, firefighting system and other plant accessories. A general estimate is that the total plant cost is twice the cost of the main components. Then finally the overall project cost must take account of the additional cost of the following activities whose cost estimates are shown in Table 5.

- Civil/site preparation which will include site clearance, terrain levelling, setting of drainage channels, perimeter fencing and casting of cement bases for placing the main equipment.
- Brine gathering and reinjection system which will include pipes, fittings, control valves and pipe supports.
- Transmission and substation cost.

Based on KenGen internal report by West Jec (KenGen, 2014) a binary plant installed at the proposed location could evacuate power through an 11 kV switch gear and 11/220 kV transformer that is supposed to be set up at well pad OW-914. The two sites are 3 km apart and this evacuation system would include an 11/33 kV step up transformer at the binary plant site, a 33 kV transmission line and a 33/11 kV step down transformer.

- Environmental cost that will be incurred to restore the biodiversity on disturbed areas and to undertake general landscaping works and soil erosion control.

TABLE 5: Additional project costs

Activity	Cost (USD)	Cost (KES)
Civil\Site preparation	77,000	7,700,000
Gathering\Reinjection	274,000	27,400,000
Transmission\Substation	616,300	61,630,000
Environmental cost	17,000	1,700,000
Total additional cost	984,300	98,430,000

From the list above the project cost can be approximated from the total of the plant cost and other additional costs. These approximations should give an insight on how to financially prepare for such a project. However, it is rational to anticipate variations from those estimates when actual quotations are sought from manufacturers or contractors.

5. RESULTS AND DISCUSSION

As explained previously, one advantage of EES is its ability to relate how one variable might affect another dependent variable. This is important to have an optimal design solution that satisfies the limits imposed by the source fluid. The plot in Figure 5 shows the variation of turbine output with respect to brine reinjection temperature when different working fluids are considered.

From Figure 5 it is clear that the net turbine power output increases as the brine reinjection temperature $T_{s[5]}$ decreases. However through geochemical analysis it has been established that the brine cannot be cooled to less than 130°C. Therefore, other plant parameters will have to be optimized around this constraint. It is also apparent that the two choices of fluids suitable for application here are isopentane and n-pentane. As a result of this any further discussion in this paper is limited to these two options of working fluids.

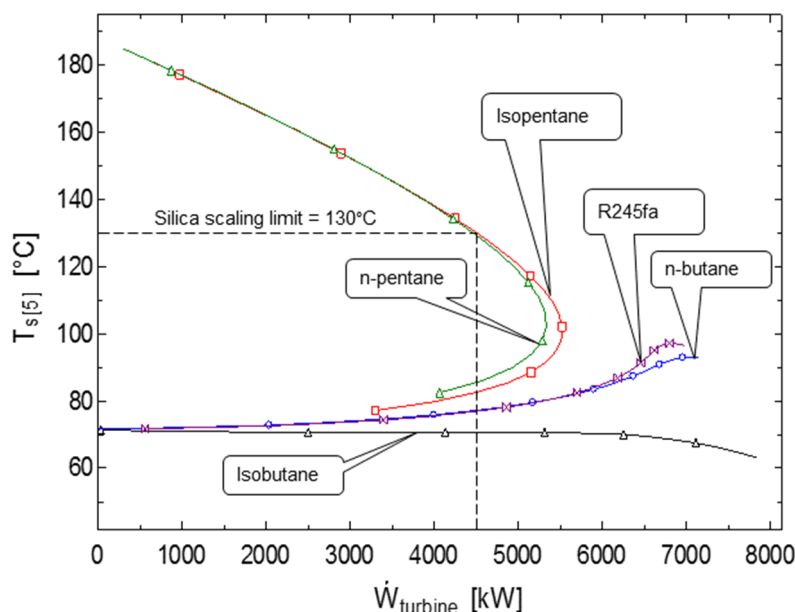


FIGURE 5: Working fluid selection based on brine reinjection temperature

The working fluid recirculates in a closed thermodynamic cycle which can be visualized with the aid of a T-S diagram. Figure 6

and Figure 7 show the T-S diagrams for isopentane and n-pentane power cycles respectively. Since the two fluids are of the dry type it can be seen that they exit the turbine at superheat conditions.

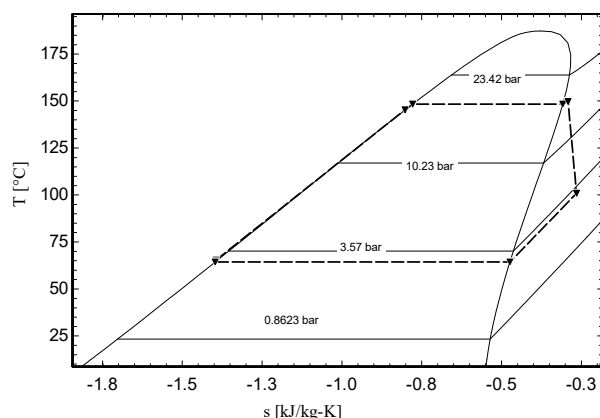


FIGURE 6: Isopentane T-S diagram

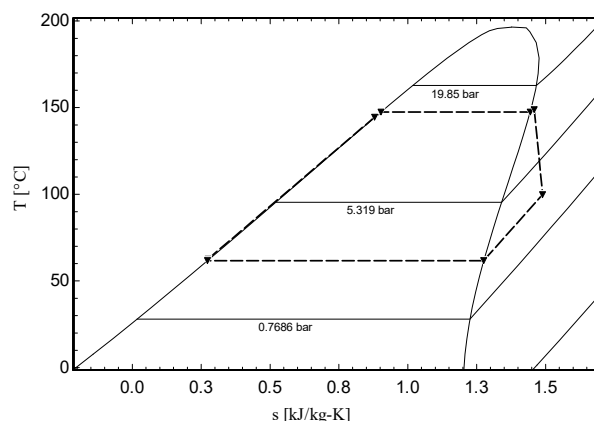


FIGURE 7: n-pentane T-S diagram

It has been explained that some design parameters are known and fixed in advance while for others the final selection is an outcome of both technical requirements and economic considerations. For this project work a complete EES plant model was built and optimized for low specific plant cost per kW. The flexible design parameters that coincided with this low specific plant are recommended as design values and are shown in Table 6. The effect of deviating from these optimal design points is explained briefly later.

TABLE 6: The design parameters at economic optimal point

Design parameter	Turbine inlet pressure	ΔT_{PP} evaporator	ΔT_{PP} condenser	A condenser	A evaporator	A preheater	\dot{W} turbine	\dot{W} pump	\dot{W} fan	\dot{M}_{air}	\dot{M}_{wf}	dT_cooling air
	bar-a	°C	°C	m ²	m ²	m ²	kW	kW	kW	kg/s	kg/s	°C
Isopentane plant	17.8	12.9	19.6	2113	658	665.7	4515	279.9	229.6	1261	79.7	24.4
n-pentane plant	14.9	12.1	22.65	2013	694.2	623.9	4643	220.2	323.5	1776	74.32	17.2

A good ORC plant is one in which all the subsystems interact reliably, efficiently and economically. The model optimization process here has aimed to satisfy that criterion. Figures 8 and 9 show a schematic description of an optimal plant design featuring isopentane and n-pentane as the working fluids respectively. More details on the design parameters and EES model are in Appendices I and II.

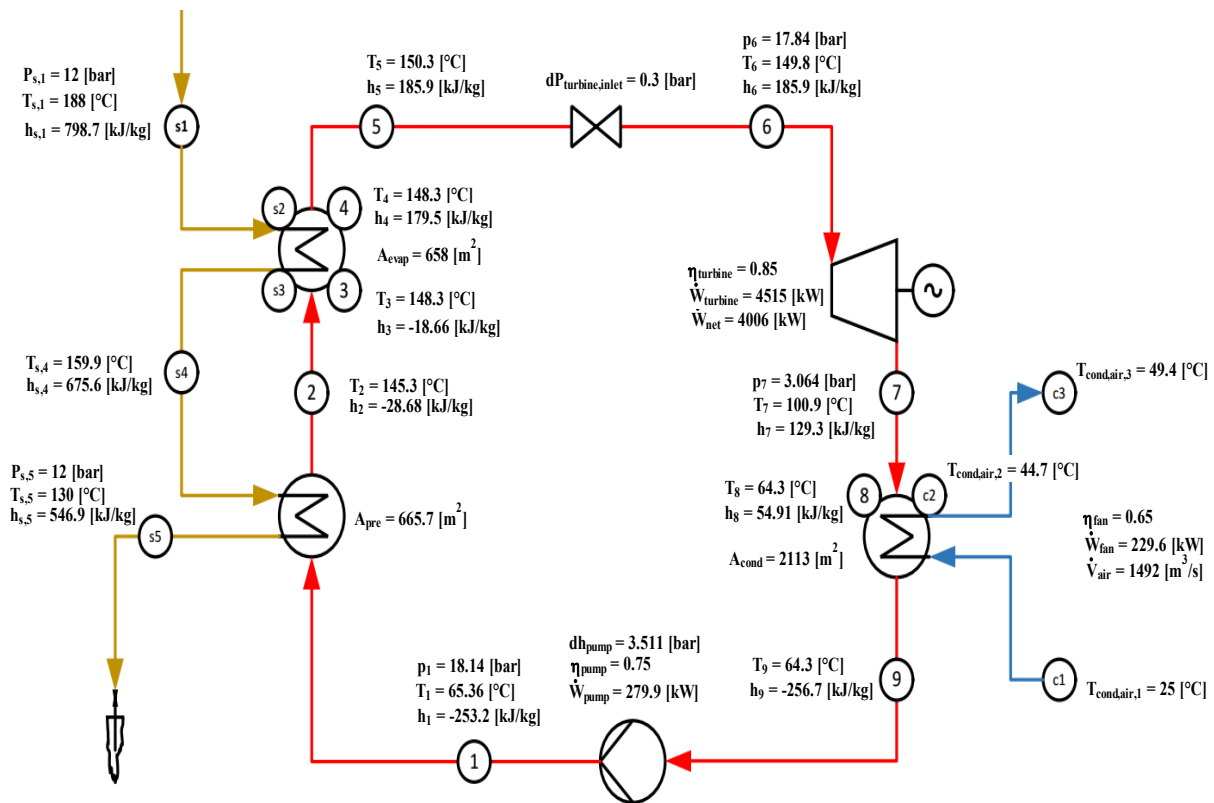


FIGURE 8 : Optimal ORC plant using isopentane as working fluid

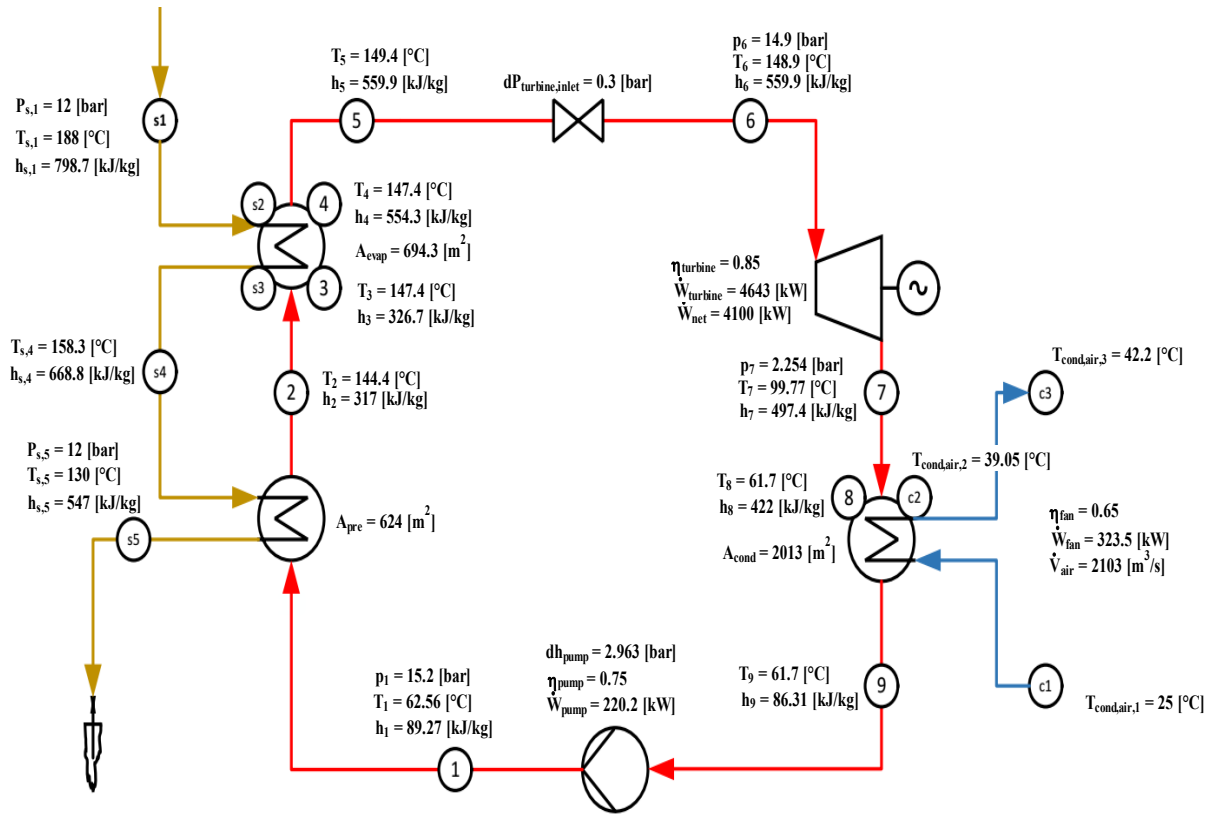


FIGURE 9 : Optimal ORC plant using n-pentane as working fluid

6. FINANCIAL ANALYSIS

An optimized EES model provides the required sizes of major components like feed pump, preheater, evaporator, turbine and condenser. From their sizes one can estimate their costs. A rule of thumb is that the cost of these major components account for 50% of the plant cost. As explained earlier the other cost factors are the control system, SCADA system, back up installation, firefighting and other plant accessories. Then there is also some additional cost of civil works, power evacuation and environmental rehabilitation.

The complete cost of implementing an optimal ORC plant using isopentane or n-pentane would then add up as shown in Table 7 below.

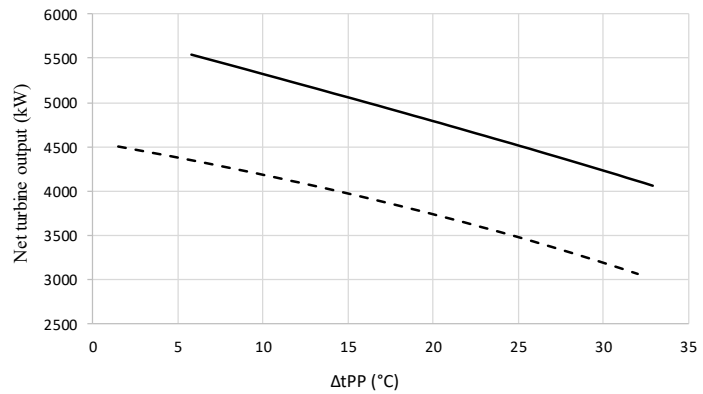
6.1 Effect of choice of the pinch points on the project cost and net turbine output

Variation of flexible parameters has an effect on the plant performance and cost. In the design of the cooling system it needs to be considered that low condensation temperatures which lead to a higher output can only be achieved with high fan power and/or large cooling system sizes (Frick et al., 2015). The $\Delta t_{\text{PP evap}}$ and $\Delta t_{\text{PP cond}}$ is linked to their sizes, cost and overall plant performance. A small pinch increases the performance of the evaporator but it is costlier because it requires a larger heat transfer area. A large pinch corresponds to a smaller and less costly evaporator and condenser but with reduced thermal performance. Figures 11 and 12 illustrate how deviation from the optimal pinch points affects the size and cost of these components for a plant running on n-pentane working fluid. A similar behaviour would be expected for the isopentane plant as well.

TABLE 7: Summary cost of a plant using either isopentane or n-pentane

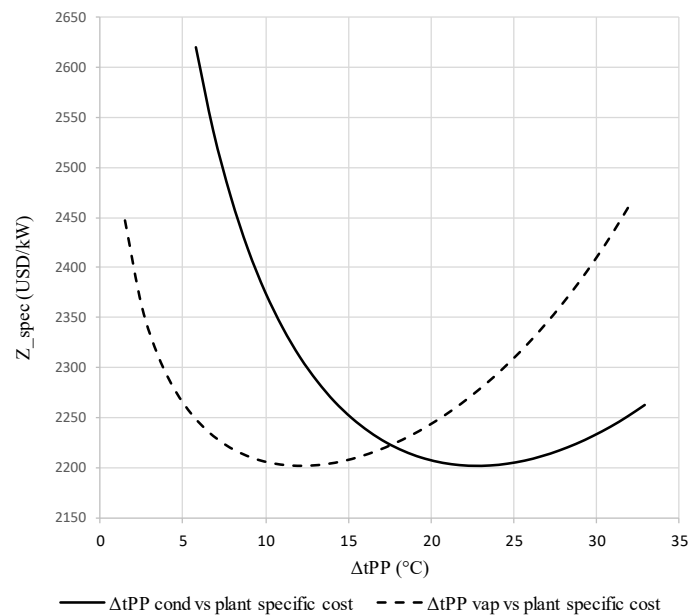
Component	Isopentane		n-pentane	
	Size	Cost (USD)	Size	Cost (USD)
Preheater(m ²)	665.7	332,855.00	623.9	311,965.00
Evaporator (m ²)	658	296,099.00	694.2	312,404.00
Turbine (kW)	4515	2,032,000.00	4643	2,089,000.00
Condenser (m ²)	2113	1,268,000.00	2013	1,208,000.00
Feed pump (kW)	279.9	125,937.00	220.2	99,103.00
Cooling tower fan motor (kW) cost included in the condensor	229.6		323.5	
Plant cost related to controls, SCADA and backup installations		4,054,891.00		4,020,472.00
Civil, mechanical, evacuation and environmental costs from Table 5		984,300.00		984,300.00
Total cost of the plant (USD)		9,094,082.00		9,025,244.00
Net power from the plant (kW)	4006		4099	
Specific cost of the plant (Plant cost/netpower) USD/kW		2,270.10		2,201.80

The optimal pinches for the evaporator and condenser may seem large, but the reason for this is that the cost of the wells and the supply system is already apportioned to the existing flash plant. The effect of this is that the optimum pinch for the evaporator and condenser shifts upward from what is expected in a plant with high upfront cost.

FIGURE 10: Variation of net power against Δt_{PP}

7. CONCLUSIONS

This paper has looked at the details of generating additional power using combined brine stream from separator stations SD2 and SD3 in Olkaria Domes field. The mode of power generation examined here is the ORC plants which is a widely tested and proven technology operating reliably in many countries. Isopentane and n-pentane have been found appropriate for use as working fluids but there is a slight economic advantage in using the latter. One unique advantage of installing bottoming ORC plants in a developed field like Olkaria is that most of the major upfront costs like the field exploration and drilling, steam field systems and road networks are already assigned to the conventional power plants. The key cost associated with an ORC plant would be the cost of the plant

FIGURE 11: Variation of plant cost against Δt_{PP}

itself which is normally delivered as a modular unit on an EPC contract basis. The other costs are minimal like civil, mechanical, electrical and environmental costs. Thus, this paper concludes and recommends that installation of an ORC plant on this brine stream is viable and a quick win for the company.

ACKNOWLEDGEMENTS

First and foremost, I want to pay my gratitude to my employer Kenya Electricity Generating Company (KenGen) and the United Nations University Geothermal Training Program (UNU-GTP) for granting me the chance to attend this course. I cannot describe adequately the unwavering support I got from Mr. Lúdvík S. Georgsson, Mr. Ingimar G. Haraldsson, Mr. Markús A.G. Wilde, Ms. Thórhildur Ísberg and Ms. Málfríður Ómarsdóttir but I will forever be grateful.

I did this project under supervision of Dr. Páll Valdimarsson. He was a good teacher to me and I could always count on him when stuck. The research and compilation of this project report has taken a lot of advantage of his wealth of experience in ORC power plants.

I also want to acknowledge that I was immensely privileged to be with the UNU-GTP group of 2016 and we had a lot in common. I will specifically carry home the memories of the football we played, the mountains we hiked and the jogging we did together. Zsófia Unyi and Adrian Foghis, you have my best regards for inspiring me to run the Reykjavik Marathon.

Finally a special thanks goes to my family who kept on checking on me regularly and ultimately honor and glory belongs to God for strengthening and protecting me all the time.

NOMENCLATURE

A	=	Area (m ²)
cond	=	Condensor
dT _C	=	Cooling air temperature difference at inlet and outlet of the condenser (°C)
evap	=	Evaporator
EES	=	Engineering Equation Solver
h	=	Enthalpy (kJ/kg)
KenGen	=	Kenya Electricity Generating Company LTD
kV	=	Kilovolts
kW	=	Kilowatts
LMTD	=	Log mean temperature difference (°C)
\dot{M}	=	Mass flow rate (kg/s)
ORC	=	Organic Rankine cycle
P	=	Pressure (bar _a)
Pre	=	Preheater
S	=	Entropy (kJ/kgK)
T	=	Temperature (°C)
Turb	=	Turbine
Turb ip	=	Turbine inlet pressure
\dot{V}	=	Volumetric flow rate (m ³ /S)
\dot{w}	=	Power (kW)
West Jec	=	West Japan Engineering Consultants Inc
wf	=	Working fluid
Δt_{PP}	=	Pinch point temperature difference (°C)
η	=	Efficiency

REFERENCES

- Chen, H., Goswami, D.Y., and Stefanakos, E.K., 2010: A review of thermodynamic cycles and working fluids for the conversion of low grade heat. *Renewable & Sustainable Energy Reviews*, 14, 3059-3067.
- DiPippo, R., 2007: *Geothermal power plants. Principles, applications, case studies and environmental impact* (2nd ed.). Butterworth Heineman, Elsevier, Kidlington, United Kingdom, 493 pp.
- Eastop, T.D., and MacConkey, A., 1993: *Applied thermodynamics for engineering technologist*. Longman, England, United Kingdom, 715 pp.
- Frick, S., Saadat, A., Surana, T., Siahaan, E.E., Kupfermann, G.A., Erbas, K., Huenges, E., Gani, M.A., 2015: Geothermal binary power plant for Lahendong, Indonesia: A German-Indonesian collaboration project. *Proceedings of the World Geothermal Congress 2015, Melbourne, Australia*, 5 pp.
- Habibzadeh, A., and Rahsid, M.M., 2016: Thermodynamic analysis of different working fluids used in organic Rankine cycle for recovering waste heat from GT-MHR. *J. Eng. Science and Technology*, 11-1, 121-135.
- KenGen, 2014: *Feasibility study for geothermal power generation for brine at Olkaria*. West Jec report for Kenya Electricity Generating Company Ltd., unpublished internal report.
- KenGen, 2016: *Final report of the 3rd Board of Consultants*. Kenya Electricity Generating Company Ltd., unpublished report.
- Kopunicova, M., 2009: *Feasibility study of binary geothermal power plants in Eastern Slovakia - Analysis of ORC and Kalina power plants*. University of Iceland and University of Akureyri, The School of Renewable Energy Science, MSc thesis, 73 pp.
- Monroy Parada, A.F., 2013: Geothermal binary cycle power plant principles, operation and maintenance. Report 15 in: *Geothermal training in Iceland 2013*. United Nations University Geothermal Training Programme, Iceland, 443-476.
- Valdimarsson, P., 2011: Geothermal power plant cycles and main components. *Paper presented at "Short Course on Geothermal Drilling, Resource Development and Power Plants", organized by UNU-GTP and LaGeo, in Santa Tecla, El Salvador*, 24 pp.
- Wikipedia, 2016a: *Logarithmic mean temperature difference*. Wikipedia, website: en.wikipedia.org/wiki/Logarithmic_mean_temperature_difference.
- Wikipedia, 2016b: *List of refrigerants*. Wikipedia, website: en.wikipedia.org/wiki/List_of_refrigerants.
- Wolverine, 2016: *Heat transfer to air-cooled heat exchangers*. Wolverine Tube Inc., website: www.wlv.com/wp-content/uploads/2014/06/data/db3ch6.pdf.

APPENDIX I: Detailed thermodynamic cycle state points

Isopentane plant cycle details

Power conversion cycle						Geothermal fluid (brine) cycle					Cooling system cycle		
State point	h [kJ/kg]	T [°C]	p [bar]	v [m ³ /kg]	s kJ/kgK	State point	P [bar]	T [°C]	h [kJ/kg]	Q kJ/s	State point	T [°C]	Q kJ/s
1	-253.2	65.36	18.14	0.001741	-1.395	S1	12	188	798.7	0	C1	25	0
2	-28.68	145.3	18.14	0.002187	-0.802	S2	12	187.2	795	17893	C2	44.7	24836
3	-18.66	148.3	18.14	0.002221	-0.778	S3	12	161.2	681.3	18692	C3	49.4	30766
4	179.5	148.3	18.14	0.01746	-0.308	S4	12	159.9	675.6	34486			
5	185.9	150.3	18.14	0.01784		S5	12	130	546.9	35001			
6	185.9	149.8	17.84	0.01829	-0.292								
7	129.3	100.9	3.064	0.1315	-0.265								
8	54.91	64.3	3.064	0.1145	-0.474								
9	-256.7	64.3	3.064	0.001747	-1.397								

n-pentane cycle details

Power conversion cycle						Geothermal fluid (brine) cycle					Cooling system cycle		
State point	h [kJ/kg]	T [°C]	p [bar]	v [m ³ /kg]	s kJ/kgK	State point	P [bar]	T [°C]	h [kJ/kg]	Q kJ/s	State point	T [°C]	Q kJ/s
1	89.27	62.56	15.2	0.001712	0.275	S1	12	188	798.7	0	C1	25	0
2	317	144.4	15.2	0.002123	0.879	S2	12	187.3	795.7	16927	C2	39.05	24952
3	326.7	147.4	15.2	0.002151	0.902	S3	12	159.5	674	17644	C3	42.2	30556
4	554.3	147.4	15.2	0.0223	1.444	S4	12	158.3	668.8	34565			
5	559.9	149.4	15.2	0.02266		S5	12	130	547	34980			
6	559.9	148.9	14.9	0.0233	1.459								
7	497.4	99.77	2.254	0.1807	1.488								
8	422	61.7	2.254	0.158	1.275								
9	86.31	61.7	2.254	0.001716	0.273								

APPENDIX II: EES code

```

{Fluid$ = 'Isobutane'}
{Fluid$ = 'n-butane'}
Fluid$ = 'Isopentane'
{Fluid$ = 'n-pentane'}
{ Fluid$ = 'R245fa'}

```

```
T_air = 25
```

```
{P_turbine_inlet = 14.91}
```

```
dP_turbine_inlet = 0.3
```

```
eta_pump = 0.75
```

```
T_boiling_margin = 3
```

```
T_superheat = 2
```

```
eta_turbine = 0.85
```

```
T_source_in = 188
```

```
P_source_in = 12
```

```
m_dot_source = 139
```

```
Cp_air = 1.00
```

```
{T_pinch_vap = 12.2}
```

```
{T_pinch_cond_fake = 18.75}
```

```
{dT_c = 17.27}
```

```
T_air_out = T_air + dT_c
```

```
T_condensation = T_air_out + T_pinch_cond_fake
```

```
s_in = 1
```

```
s_dew = 2
```

```
s_bubble = 3
```

```
s_vap_out = 4
```

```
s_pre_in = 4
```

```
s_pre_out = 5
```

```
s_plant_out = 5
```

```
pump_out = 1
```

```
pre_in = 1
```

```
pre_out = 2
```

```
vap_in = 2
```

```
vap_bubble = 3
```

```
vap_dew = 4
```

```
vap_out = 5
```

```
turb_in = 6
```

```
turb_out = 7
```

```
cond_in = 7
```

```
cond_dew = 8
```

```
cond_out = 9
```

```
pump_in = 9
```

```
p_vap = 450
p_pre = 500
p_cond = 600
p_turb = 450
p_pump = 450
```

{Pump inlet - condenser hot well}

```
T[pump_in] = T_condensation
h[pump_in] = enthalpy(Fluid$, T=T[pump_in],
x=0)
p[pump_in] = pressure(Fluid$, T=T[pump_in],
x=0)
v[pump_in] = volume(Fluid$, T=T[pump_in], x=0)
```

{System pressures}

```
p[cond_dew] = p[cond_out]
p[cond_in] = p[cond_dew]
p[turb_in] = P_turbine_inlet
p[vap_out] = p[turb_in] + dP_turbine_inlet
p[vap_dew] = p[vap_out]
p[vap_bubble] = p[vap_dew]
p[vap_in] = p[vap_bubble]
p[pre_in] = p[pre_out]
```

{Pump outlet}

```
dh_pump = v[pump_in]*(p[pump_out]-
p[pump_in])*100/eta_pump
h[pump_out] = h[pump_in] + dh_pump
T[pump_out] = temperature(Fluid$,
P=p[pump_out], h=h[pump_out])
s[pump_out] = entropy(Fluid$, P=p[pump_out],
h=h[pump_out])
v[pump_out] = volume(Fluid$, P=p[pump_out],
h=h[pump_out])
```

{Preheater outlet}

```
T[pre_out] = temperature(Fluid$, p= p[pre_out],
x=0) - T_boiling_margin
h[pre_out] = enthalpy( Fluid$, p=
p[pre_out],T=T[pre_out])
s[pre_out] = entropy( Fluid$, p=
p[pre_out],T=T[pre_out])
v[pre_out] = volume( Fluid$, p=
p[pre_out],T=T[pre_out])
```

{Vaporizer bubble point}

```
h[vap_bubble] = enthalpy(Fluid$, p=
p[vap_bubble], x=0)
T[vap_bubble] = temperature(Fluid$, p=
p[vap_bubble], x=0)
s[vap_bubble] = entropy(Fluid$, p= p[vap_bubble],
x=0)
v[vap_bubble] = volume(Fluid$, p= p[vap_bubble],
x=0)
```

{Vaporizer dew point}

```
h[vap_dew] = enthalpy(Fluid$, p= p[vap_dew],
x=1)
T[vap_dew] = temperature(Fluid$, p= p[vap_dew],
x=1)
s[vap_dew] = entropy(Fluid$, p= p[vap_dew], x=1)
v[vap_dew] = volume(Fluid$, p= p[vap_dew],
x=1)
```

{Vaporizer Outlet}

```
T[vap_out] = T[vap_dew] + T_superheat
h[vap_out] = enthalpy(Fluid$, p= p[vap_out],
T=T[vap_out])
v[vap_out] = volume(Fluid$, p= p[vap_out],
T=T[vap_out])
```

{Turbine inlet}

```
h[turb_in] = h[vap_out]
T[turb_in] = temperature(Fluid$, p= p[turb_in],
h=h[turb_in])
s[turb_in] = entropy(Fluid$, p= p[turb_in],
h=h[turb_in])
v[turb_in] = volume(Fluid$, p= p[turb_in],
h=h[turb_in])
```

{Turbine outlet}

```
h_s_turb_out = enthalpy(Fluid$, p= p[turb_out],
s=s[turb_in])
h[turb_out] = h[turb_in] - (h[turb_in] -
h_s_turb_out)*eta_turbine
T[turb_out] = temperature(Fluid$, p= p[turb_out],
h=h[turb_out])
s[turb_out] = entropy(Fluid$, p= p[turb_out],
h=h[turb_out])
v[turb_out] = volume(Fluid$, p= p[turb_out],
h=h[turb_out])
```

{Condenser dew point}

```
h[cond_dew] = enthalpy(Fluid$, p= p[cond_dew],
x=1)
T[cond_dew] = temperature(Fluid$, p=
p[cond_dew], x=1)
s[cond_dew] = entropy(Fluid$, p= p[cond_dew],
x=1)
v[cond_dew] = volume(Fluid$, p= p[cond_dew],
x=1)
```

{Condenser outlet}

```
{h[cond_out] = enthalpy(Fluid$, p= p[cond_dew],
x=0)}
{T[cond_out] = enthalpy(Fluid$, p= p[cond_dew],
x=0)}
s[cond_out] = entropy(Fluid$, p= p[cond_dew],
x=0)
{v[cond_out] = volume(Fluid$, p= p[cond_dew],
x=0) }
```

{Source fluid pressure}

```
P_s[s_in] = P_source_in
```



```
P_s[s_dew] = P_s[s_in]
P_s[s_bubble] = P_s[s_dew]
P_s[s_vap_out] = P_s[s_bubble]
P_s[s_pre_out] = P_s[s_pre_in]
```

```
{Mass flow calculation}
```

```
{T_s[s_in] = T_source_in}
```

```
T_s[s_in] = temperature(Water, P=P_s[s_in], x = 0)
h_s[s_in] = enthalpy(Water, P=P_s[s_in], x = 0)
T_s[s_bubble] = T[vap_bubble] + T_pinch_vap
h_s[s_bubble] = enthalpy(Water, P=P_s[s_in],
T=T_s[s_bubble])
```

```
Q_dot_rhs = m_dot_source*(h_s[s_in] -
h_s[s_bubble])
m_dot_wf = Q_dot_rhs / (h[vap_out] -
h[vap_bubble])
```

```
Q_dot_superheat = m_dot_wf*(h[vap_out] -
h[vap_dew])
h_s[s_dew] = h_s[s_in] - Q_dot_superheat
/m_dot_source
T_s[s_dew] = temperature(Water, h= h_s[s_dew] ,
P=P_s[s_dew])
Q_dot_pre_vap = m_dot_wf* (h[vap_bubble] -
h[pre_out])
h_s[s_vap_out] = h_s[s_bubble] - Q_dot_pre_vap/
m_dot_source
T_s[s_vap_out] = temperature(Water, h=
h_s[s_vap_out] , P=P_s[s_vap_out])
```

```
Q_dot_preheater = m_dot_wf*(h[pre_out]-
h[pre_in])
h_s[s_Pre_out] = h_s[s_Pre_in] -
Q_dot_preheater/m_dot_source
T_s[s_Pre_out] = temperature(Water,
P=P_s[s_pre_out] , h=h_s[s_Pre_out])
```

```
W_dot_turbine = m_dot_wf * (h[turb_in]-
h[turb_out])
W_dot_pump = m_dot_wf * (h[pump_out]-
h[pump_in])
```

```
W_dot_net = W_dot_turbine - W_dot_pump -
Work_dot_fan
```

```
{T-q modelling}
```

```
{Preheater}
```

```
{Point 1 - pump outlet/preheater inlet}
```

```
Q_dot[1] = 0
T_cold[1] = T[pump_out]
T_hot[1] = T_s[s_Pre_out]
```

```
{Point 2 preheater outlet / vapourizer inlet}
```

```
Q_dot[2] = Q_dot[1] + Q_dot_preheater
T_cold[2] = T[pre_out]
T_hot[2] = T_s[s_vap_out]
```

```
{Point 3 - vaporizer bubble point}
```

```
Q_dot[3] = Q_dot[2] + Q_dot_pre_vap
T_cold[3] = T[vap_bubble]
T_hot[3] = T_s[s_bubble]
```

```
{Point 4 - vaporizer dew point}
```

```
Q_dot[4] = Q_dot[3] +(Q_dot_rhs -
Q_dot_superheat)
T_cold[4] = T[vap_dew]
T_hot[4] = T_s[s_dew]
```

```
{Point 5 - vaporizer outlet}
```

```
Q_dot[5] = Q_dot[4] + Q_dot_superheat
T_cold[5] = T[vap_out]
T_hot[5] = T_s[s_in]
```

```
{Condensor heat exchanger model}
```

```
Q_turb_in_turbout = m_dot_wf * (h[turb_in]-
h[turb_out])
Q_turbout_conddew = m_dot_wf * (h[turb_out] -
h[cond_dew] )
Q_conddew_condout = m_dot_wf * ( h[cond_dew]
- h[pump_in] )
```

```
{T-q model for condensor}
```

```
{Condensor inlet}
```

```
Q_cond[1] = 0 {Q_dot[5] - Q_turb_in_turbout}
T_cond_w[3] = t[turb_out]
T_cond_air[1] = T_air
```

```
{Condensor dewpoint}
```

```
Q_cond[2] = Q_conddew_condout {Q_cond[1] -
Q_turbout_conddew }
T_cond_w[2] = T[cond_dew]
```

```
{Condensor outlet}
```

```
{Pinch point of 5deg C assumed at condensor
outlet}
```

```
Q_cond[3] = {Q_cond[2] - Q_conddew_condout
}Q_turbout_conddew + Q_conddew_condout
T_cond_w[1] = T[pump_in]
T_cond_air[3] = {T[pump_in] -
T_pinch_cond_fake} T_air_out
```

```
{Mass flow of air needed and T_air_dew analysis}
```

```
M_cond_air * Cp_air * (T_cond_air[3] -
T_cond_air[2]) = {Q_conddew_condout
}Q_turbout_conddew
M_cond_air * Cp_air * (T_cond_air[2] - T_air) =
{Q_turbout_conddew}Q_conddew_condout
V_dot_air = M_cond_air * density(Air, T=T_air,
P=1.013)
```

```
{Heat exchanger area analysis}
```

```
{Preheater exchange area analysis}
```

```
LMTD_pre = ((T_s[s_vap_out] - T[pre_out]) -
(T_s[s_Pre_out] - T[pump_out])) /
```

$\ln((T_{s_vap_out} - T_{pre_out}) / (T_{s_Pre_out} - T_{pump_out}))$
 $U_{pre} = 0.8$
 $A_{pre} = Q_{dot_preheater} / (U_{pre} * LMTD_{pre})$

{Evaporator exchange analysis}

{Area required to heat fluid up to boiling point}

$LMTD_{Preout_vapbubble} = ((T_{s_bubble} - T_{vap_bubble}) - (T_{s_vap_out} - T_{pre_out})) / \ln((T_{s_bubble} - T_{vap_bubble}) / (T_{s_vap_out} - T_{pre_out}))$
 $U_{preout_vapbubble} = 0.8$
 $A_{preout_vapbubble} =$
 $Q_{dot_pre_vap} / (U_{preout_vapbubble} * LMTD_{Preout_vapbubble})$

{Area required to heat fluid up to vapour saturation point}

$LMTD_{vapbubble_vapdew} = ((T_{s_dew} - T_{vap_dew}) - (T_{s_bubble} - T_{vap_bubble})) / \ln((T_{s_dew} - T_{vap_dew}) / (T_{s_bubble} - T_{vap_bubble}))$
 $U_{vapbubble_vapdew} = 1.2$
 $A_{vapbubble_vapdew} = (Q_{dot_rhs} - Q_{dot_superheat}) / (U_{vapbubble_vapdew} * LMTD_{vapbubble_vapdew})$

{Area required to superheat the fluid to 2deg C}

$LMTD_{vapdew_vapsheat} = ((T_{s_in} - T_{s_vap_out}) - (T_{s_dew} - T_{vap_dew})) / \ln((T_{s_in} - T_{s_vap_out}) / (T_{s_dew} - T_{vap_dew}))$
 $U_{vapdew_superheat} = 0.6$
 $A_{vapdew_superheat} =$
 $Q_{dot_superheat} / (U_{vapdew_superheat} * LMTD_{vapdew_vapsheat})$

{Air cooled condenser area required}

{Area required to bring turbine exhaust vapour to dewpoint}

$LMTD_{turbout_cond dew} = ((T_{turb_out} - T_{cond_air[3]}) - (T_{cond_dew} - T_{cond_air[2]})) / \ln((T_{turb_out} - T_{cond_air[3]}) / (T_{cond_dew} - T_{cond_air[2]}))$
 $U_{turbout_cond dew} = 0.5$
 $A_{turbout_cond dew} =$
 $Q_{turbout_cond dew} / (U_{turbout_cond dew} * LMTD_{turbout_cond dew})$

{Area required to cool fluid from dewpoint to liquid saturation (pump inlet) point}

$LMTD_{cond dew_condout} = ((T_{cond_dew} - T_{cond_air[2]}) - (T_{pump_in} - T_{cond_air[1]})) / \ln((T_{cond_dew} - T_{cond_air[2]}) / (T_{pump_in} - T_{cond_air[1]}))$
 $U_{cond dew_condout} = 0.5$
 $A_{cond dew_condout} =$
 $Q_{cond dew_condout} / (U_{cond dew_condout} * LMTD_{cond dew_condout})$

{Total evaporator area required}

$A_{evap} =$
 $((A_{preout_vapbubble}) + (A_{vapbubble_vapdew}) + (A_{vapdew_superheat}))$

{Total condensor area required}

$A_{cond} =$
 $((A_{turbout_cond dew}) + (A_{cond dew_condout}))$
 $T_{pinch_cond_calc} = T_{cond_w[2]} - T_{cond_air[2]}$

{Fan power}

$dP_{cond_air} = 0.001$
 $\eta_{fan} = 0.65$
 $Work_{dot_fan} = (V_{dot_air} * dP_{cond_air} * 100) / \eta_{fan}$

$Z_{vap} = p_{vap} * A_{evap}$

$Z_{pre} = p_{pre} * A_{pre}$

$Z_{cond} = p_{cond} * A_{cond}$

$Z_{turb} = p_{turb} * W_{dot_turbine}$

$Z_{pump} = p_{pump} * W_{dot_pump}$

$Z_{mc} = Z_{vap} + Z_{pre} + Z_{cond} + Z_{turb} + Z_{pump}$

{Z_{plant} = 5000000}

$Z_{plant} = Z_{mc}$

$Z_{source} = 984300$

$Z_{total} = Z_{mc} + Z_{plant} + Z_{source}$

$z_{spec_mc} = Z_{mc} / W_{dot_net}$

$z_{spec} = Z_{total} / W_{dot_net}$

$P_{vap_junk} = P_{turbine_inlet} * 130 / T_{s[5]}$



UNITED NATIONS
UNIVERSITY

UNU-GTP

Geothermal Training Programme

Orkustofnun, Grensasvegur 9,
IS-108 Reykjavik, Iceland

Reports 2016
Number 16

MONITORING MICRO-EARTHQUAKES IN A GEOTHERMAL FIELD

Fahman Hassan Abdallah

Djiboutian Development Office of Geothermal Energy – ODDEG

P.O. Box 1279

Djibouti

REPUBLIC OF DJIBOUTI

fahman.abdallah@gmail.com

ABSTRACT

Passive seismic technique is one of several geophysical methods used to understand structures in subsurface geology. This technique can be used in geothermal exploration to delineate faults in areas of geothermal activity, and to locate permeable zones within the geothermal system. During the exploitation of a geothermal system, measurements of microseismicity are useful to monitor the response of the system to fluid injection and production. Injection can increase the level of microseismicity in an area by increasing the pore pressure, and thereby reducing the effective stress.

In this study, the discussion is mainly based on monitoring of microearthquakes in the Hellisheidi geothermal system, located in the Hengill volcanic system. The area is located at the triple junction of two spreading zones and a transform zone and is therefore both tectonically and seismically active. The data set used in this report is a part of a larger dataset recorded by a local seismic network operated in the Hengill area by the Iceland GeoSurvey (ÍSOR), Uppsala University, MIT, Reykjavik University, and the Iceland Meteorological Office (IMO) from 2009-2013. In this report, data from a small swarm on April 25th, 2012, were analysed using SeisComp3.

A brief overview of microseismic surveys undertaken in the Hanle-Gaggade area in Djibouti is presented, describing the relationship between microearthquakes and signs of geothermal activity in the area. Earthquakes concentrated near the fault systems are observed, confirming that the area is seismically active and a local seismic network would be recommended for monitoring.

1. INTRODUCTION

Geophysical methods are one of the geoscientific disciplines that allow us to understand subsurface structures. For geothermal exploration, they are divided into direct methods and indirect methods. Direct methods include thermal and electrical methods that measure physical properties like temperature and resistivity directly in subsurface layers. The layers can be affected by alteration or salinity caused by underground natural resources like oil, water or geothermal fluid. Indirect methods or structural methods

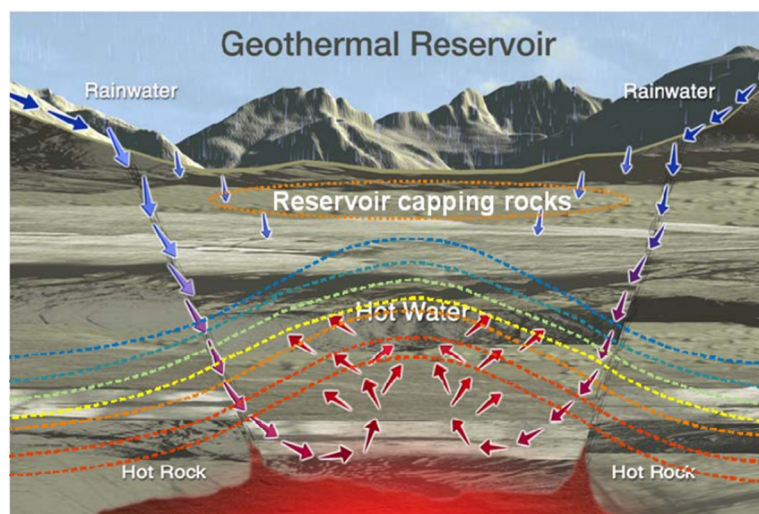


FIGURE 1: Components of a geothermal system: differently shaded/coloured dotted lines show different temperatures as the water heats up with depth (Geothermal Education Office, 2007)

include seismic, gravity and magnetic methods which detect anomalies associated with geological formations or structures (e.g. fault, dykes, or intrusions). In geothermal exploration these methods play an important role in locating and or assessing a geothermal system.

Geothermal systems are characterized by three basic components: a heat source, a reservoir, and conduits or pathways to allow circulation of fluid (Wanjohi, 2007). Where impermeable cap rock is present the geothermal system can be pressurized (Figure 1).

Geothermal areas are often associated with microearthquake activity (Foulger and Julien, 2009), making seismic methods a valuable exploration tool for the general understanding and monitoring of geothermal fields. In this report, the discussion is mainly based on monitoring microearthquakes in geothermal fields using passive seismic techniques. This technique is based on vibrations from natural earthquakes and its aim is to determine the hypocentre of earthquakes in order to image seismically active faults or locate fracture systems in the subsurface.

2. BACKGROUND OF STUDY AREAS

2.1 Geology and geothermal activity

Hellisheidi is one of the high-temperature geothermal fields found in SW-Iceland, located in the southern part of the Hengill volcanic system (Björnsson et al., 1986). This active volcanic system is characterized by a 40-60 km long NNE-SSW trending fissure swarm with normal faults, fissures, frequent magma intrusions, and a central volcano (Figure 2).

The Hengill-Hellisheidi field (Figure 3) is expressed by numerous hydrothermal manifestations. Many explorations with different geoscientific disciplines have been carried out in this area. Resistivity surveys have revealed a large low-resistivity area, which can be interpreted as a layer dominated by smectite alterations representing temperatures between 100 and 200°C. This area is underlain by higher resistivity, which has been interpreted as formations including resistive high-temperature alteration such as chlorite and epidote (Árnason, 1993; Árnason et al., 2000). The presence of chlorite and epidote indicates a temperature of 220-340°C. The Hellisheidi power plant is one of the biggest geothermal power plants in the world producing about 300 MW of electricity and hot water with a thermal capacity of 133 MW for district heating. Hellisheidi has two re-injection zones. The power company is required to inject all wastewater fluid back into the reservoir. The reason for this is twofold, firstly the wastewater must be injected below the groundwater table for environmental reasons and secondly it recharges the system. But this operation has three major challenges: The productivity of the injection decreases with time, the permeability depends on the temperature of the reinjected water and it can increase the level of seismicity.

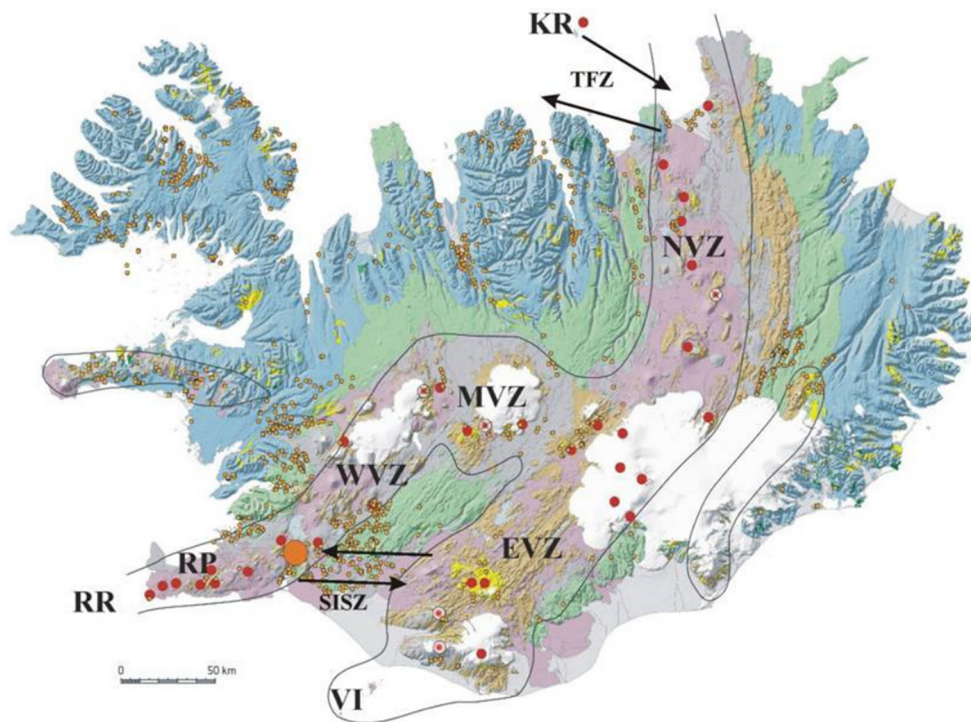


FIGURE 2: Geological map of Iceland showing the location of active volcanic zones and transform faults. RR = Reykjanes Ridge; RP = Reykjanes Peninsula; WVZ = Western Volcanic Zone; MVZ = Mid-Iceland Volcanic Zone; NVZ = Northern Volcanic Zone; EVZ = Eastern Volcanic Zone; VI = Vestmanna Islands; SISZ = South Iceland Seismic Zone; TFZ = Tjörnes Fracture Zone. Red dots indicate high-temperature areas. Orange circle represents the approximate location of the Hengill volcanic system (Hardarson et al., 2010)

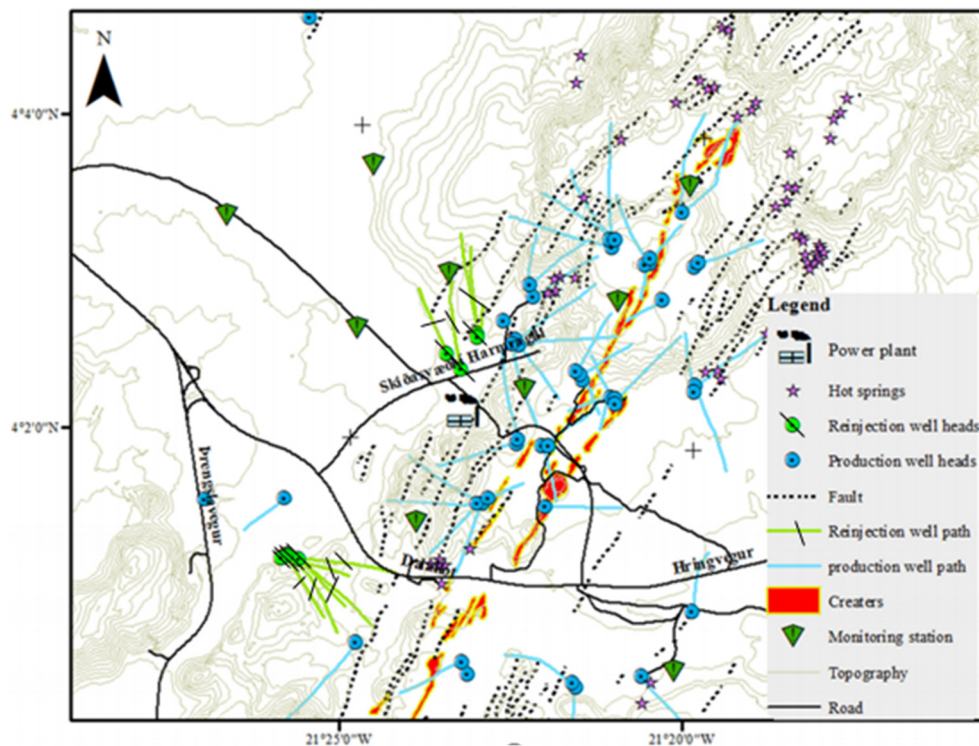


FIGURE 3: Topographical map of the Hellisheidi geothermal field with related faults, craters, surface manifestations, production wells, injection wells and seismic monitoring stations (Samaranayake, 2015)

2.2 Seismic activity

Mostly, the seismic activity in Hellisheidi is due to its location at a triple junction of a rather complex pattern of three tectonically active zones, the Reykjanes Peninsula, the Western Volcanic Zone and the South Iceland Seismic Zone (Figure 2). The two injection sites, Gráuhnjúkar and Húsmúli, in use at the Hellisheidi power plant have both been seismically active. After reinjection started at Gráuhnjúkar some events were recorded on the regional seismic network operated by the IMO, the largest magnitude registering at around 2.0 (Flóvenz et al., 2015). Seven injection wells have been drilled in the Húsmúli area. During the drilling of the last one in February 2011, intense induced seismicity repeatedly occurred, probably related to circulation loss (Ágústsson et al., 2015). It was monitored by a temporary local network operated by ÍSOR.

3. THEORY

3.1 Elastic seismic waves

Earthquakes are vibrations of the Earth caused by large releases of energy that accompany movements of the Earth's crust and upper mantle, usually near tectonic plate boundaries, or associated with volcanic eruptions. There are different kinds of seismic waves such as body waves, which can travel through the

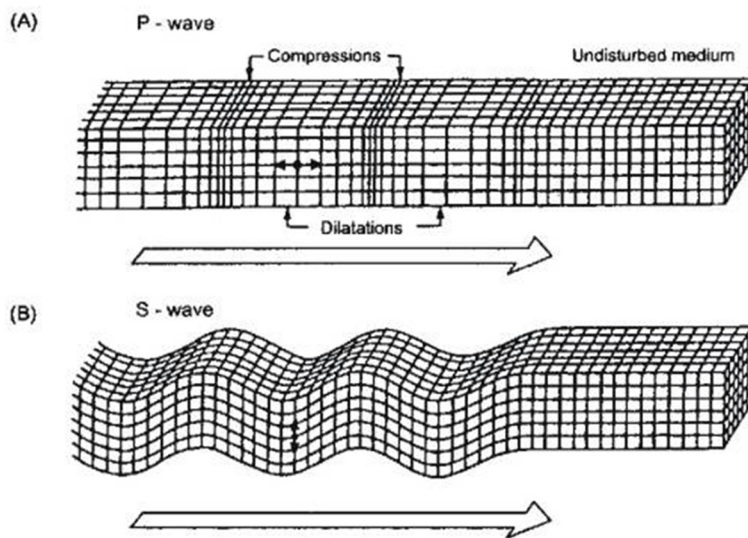


FIGURE 4: a) P wave travels through a medium by means of compression and dilation; b) S wave travels through a medium by means of shearing

Earth's interior, and surface waves, which can only move along the surface. There are two kinds of body waves, called P waves and S waves. P waves involve compressional motion and volumetric changes as the wave disturbances pass through the continuum, but S waves involve shearing motions without volume change (Figure 4).

To describe the behaviour of seismic waves we connect Hooke's law (linking stress and deformation) to Newton's law (connecting force and acceleration). Hooke's law gives us the relationship between the stress and strain. In the case of a linear deformation in one direction (x axis) we get the following equation:

$$S_{xx} = \frac{E\delta u}{\delta x}$$

$$\text{or } S_{xx} = E \epsilon_{xx} \quad (1)$$

giving:

$$\epsilon_{xx} = \frac{\delta u}{\delta x}$$

where E is called the Young's modulus, $\frac{\delta u}{\delta x}$ is the small displacement in the direction x, ϵ_{xx} is the strain and S_{xx} the stress.

For a body of three dimensions (Figure 5) this relationship is more complex because it takes into account both elongation along the x axis (ϵ_{xx}) and the contractions along the y and z axes (ϵ_{yy} and ϵ_{zz}) that are smaller than (ϵ_{xx}), and they are related by the same proportionality constant called Poisson's ratio, $\sigma = \frac{\epsilon_{yy}}{\epsilon_{xx}}$. Hence we get:

$$S_{xx} = \frac{E\delta u}{\delta x} - \sigma S_{xx} = \frac{E\delta v}{\delta y} - \sigma S_{xx} = \frac{E\delta w}{\delta z} \quad (2)$$

with

$$\epsilon_{xx} = \frac{\delta u}{\delta x} \quad \epsilon_{yy} = \frac{\delta v}{\delta y} \quad \epsilon_{zz} = \frac{\delta w}{\delta z}$$

σ is between 0.2 and 0.3 for crystalline rocks and it is between 0.02 and 0.05 for sedimentary rocks. It can be expressed in terms of Young's modulus E , and the Lamé constant λ , where:

$$\lambda = \frac{E\sigma}{(1 + \sigma)(1 - 2\sigma)} \quad (3)$$

Now, if we consider the relation between deformation and shear stress we get:

$$S_{xy} = S_{yx} = \mu \epsilon_{xy} = \mu \left(\frac{\delta u}{\delta y} + \frac{\delta v}{\delta x} \right) \quad (4)$$

μ is called shear modulus and varies between 0.1 and 0.7 Mbar for the most part of the rock. It can be expressed in terms of Young's modulus and Poisson's ratio:

$$\mu = \frac{E}{2(1 + \sigma)} \quad (5)$$

Using the Lamé constant λ defined in Equation 3 and from (Dix, 1952, p. 303-305) we write

$$S_{xx} = \frac{2\mu\delta u}{\delta x} + \lambda \left(\frac{\delta u}{\delta x} + \frac{\delta v}{\delta y} + \frac{\delta w}{\delta z} \right) \quad (6)$$

From the above Equations 1, 4 and 6 we get the Hooke's relations that connect strains and stresses for solid ideals:

$$\begin{aligned} S_{xx} &= \frac{2\mu\delta u}{\delta x} + \lambda \theta \quad S_{xy} = S_{yx} = \mu \left(\frac{\delta u}{\delta y} + \frac{\delta v}{\delta x} \right) \\ S_{yy} &= \frac{2\mu\delta v}{\delta y} + \lambda \theta \quad S_{zx} = S_{xz} = \mu \left(\frac{\delta u}{\delta z} + \frac{\delta w}{\delta x} \right) \\ S_{zz} &= \frac{2\mu\delta w}{\delta z} + \lambda \theta \quad S_{yz} = S_{zy} = \mu \left(\frac{\delta v}{\delta z} + \frac{\delta w}{\delta y} \right) \end{aligned} \quad (7)$$

where $\theta = \epsilon_{xx} + \epsilon_{yy} + \epsilon_{zz}$

Now we connect the Hooke's relation (Equation 7) to Newton's second law to get the velocities of the P wave and S wave (Equation 8):

$$\sum F = ma \quad (8)$$

The large \sum represents the vector sum of all the forces, the other side of the equation can be written as follows:

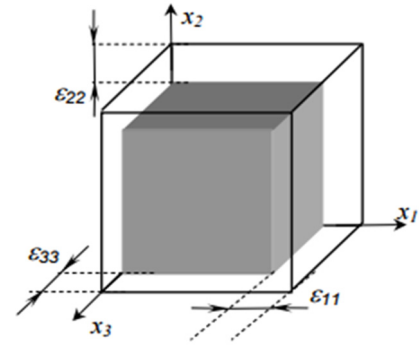


FIGURE 5: The relative change in volume of a cubic element subjected to a strain tensor ϵ

$$\rho dx dA \frac{d^2 u}{dt^2} = ma \quad (9)$$

where ρ is the density and dA is the area of the section (Figure 6). Considering a small element dx is subjected to stress $S(x)$, the force applied is $S(x) \cdot dA$. Hence the net force is $[S(x+dx) - S(x)]dA$ which is also equal to ma (mass times acceleration). Using Equation 9 we get as follows:

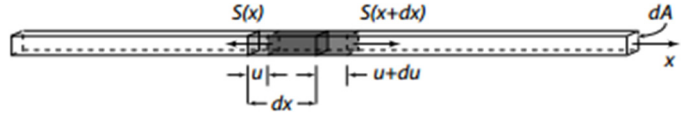


FIGURE 6: A small element dx subjected to a strain caused by a wave P

$$[S(x+dx) - S(x)]dA = \rho dx dA \frac{d^2 u}{dt^2} \quad (10)$$

If $dx \rightarrow 0$, we can write as follows:

$$S(x+dx) - S(x) = \frac{dS}{dx} dx \quad (11)$$

Using Equation 1 and deriving we get:

$$\frac{dS}{dx} = \frac{Ed^2 u}{dx^2}$$

so Equation 10 can be written as:

$$\frac{Ed^2 u}{dx^2} dx dA = \rho dx dA \frac{d^2 u}{dt^2} \quad (12)$$

After simplifying, we get:

$$\frac{d^2 u}{dx^2} = \left(\frac{\rho}{E}\right) \frac{d^2 u}{dt^2} \quad (13)$$

So the classic form of the wave equation in 1D is:

$$\frac{d^2 u}{dx^2} = \left(\frac{1}{V^2}\right) \frac{d^2 u}{dt^2} \quad (14)$$

where V is the wave velocity.

From Equations 13 and 14 we can deduce that:

$$V = \sqrt{\frac{E}{\rho}} \quad (15)$$

or, the wave velocity depends only on the Young's modulus and density.

If we consider the 3D case we get the solution for a compressional wave:

$$\frac{\delta^2 \theta}{\delta x^2} + \frac{\delta^2 \theta}{\delta y^2} + \frac{\delta^2 \theta}{\delta z^2} = \frac{\rho}{\mu + \lambda} \frac{\delta^2 \theta}{\delta t^2} \quad (16)$$

where $\frac{\rho}{\mu + \lambda} = \frac{\rho(1-2\sigma)(1+\sigma)}{E(1-\sigma)}$
 λ is the second Lamé constant.

For a shear wave we get:

$$\frac{\delta^2 \theta_x}{\delta x^2} + \frac{\delta^2 \theta_x}{\delta y^2} + \frac{\delta^2 \theta_x}{\delta z^2} = \frac{\rho}{\mu} \frac{\delta^2 \theta}{\delta t^2} \quad (17)$$

where $\theta_x = \left(\frac{\delta w}{\delta y} - \frac{\delta v}{\delta z} \right)$.

Comparing Equations 16 and 17 with Equation 14 we get:

$$V_p = \sqrt{\frac{\lambda + 2\mu}{\rho}} \quad (18)$$

$$V_s = \sqrt{\frac{\mu}{\rho}} \quad (19)$$

From Equations 18 and 19, we can deduce the following:

- V_p is greater than V_s , meaning that the P wave arrives earlier than the S wave to recording stations on the surface.
- Since shear deformation is not possible in liquid ($\mu = 0$), shear waves do not propagate in liquid ($V_s = 0$).

3.2 Locating earthquakes

The main objective of observational seismology is to locate seismic sources. This involves determining two parameters, the hypocentre and the source origin-time. To solve these parameters requires the identification of seismic phases, measuring their arrival times, and knowledge of the velocity structure between the hypocentre and the seismic station. The data can either be processed with forward or inverse modelling procedures, which are used for interpreting seismic data as well as other geophysical data.

3.2.1 Hypocentre, epicentre and origin time

Hypocentre of an earthquake is the point where the rock starts to fracture, with the vibrating waves travelling away from this point in all directions. The epicentre is the point on land directly above the hypocentre. Origin time is the time when the earthquake started from hypocentre. It can be determined with a very simple graphical technique called a Wadati diagram (Figure 7). In this diagram the difference in arrival time for the S and P wave ($t_s - t_p$) is plotted against the absolute arrival time of the P wave. Since $t_s - t_p$ goes to zero at the hypocentre, a straight-line fit on the Wadati diagram gives the approximate origin time at the intercept with the P arrival time axis.

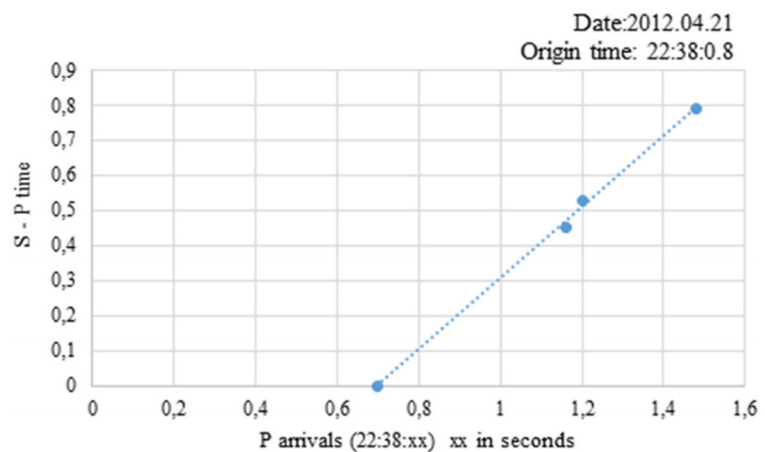


FIGURE 7: An example of a Wadati diagram used for determining the origin time; the intersection with the P wave arrival time axis gives the origin time (Samaranayake, 2015)

Once the origin time (OT) has been estimated, the epicentre distance for the i -th station can be estimated by tracking the travel time of the P wave and multiplying it by an estimate for the average P velocity α as follows:

$$D_i = (t_p^i - OT) \times \alpha \quad (20)$$

The epicentre must lie on a hemisphere of radius D_i centred on the i -th station. The epicentre should be located at the intersection of circles drawn for each station. The focal depth, D_{focal} , can be determined by taking the square root of the difference between the squares of propagation distance, D_i , and the distance along the surface to the epicentre, Δ , as follows:

$$D_{focal} = \sqrt{D_i^2 - \Delta^2} \quad (21)$$

3.2.2 Forward and inverse modelling

Forward models generate results that can be compared to observations. When we find a forward model that closely approximates the observations, we declare that the model sufficiently describes the earthquake location for the given model assumptions. Mathematically, we can think of this as a series of equations:

$$t_{ipredicted} = f(x_i, y_i, z_i, v) = t_{iobserved} \quad (22)$$

where v is the velocity, and f is a function which calculates the travel time, $t_{ipredicted}$, given (x_i, y_i, z_i) location of the earthquake and v .

If we have n stations at which we have actually measured arrival times, we can think of $t_{iobserved}$ as the i -th component of a data vector \mathbf{d} that has n components, which we write as $\mathbf{d} = (t_1, t_2, \dots, t_n)$. We can also consider the model parameters as a vector \mathbf{m} that has four components for the spatial and temporal coordinates of the earthquake:

$$\mathbf{m} = (x, y, z, t_{ipredicted}) \quad (23)$$

Equation (22) can then be written as:

$$\mathbf{F}(\mathbf{m}) = \mathbf{d} \quad (24)$$

where \mathbf{F} is a matrix called the data Kernel; x, y, z and t are the elements of the model vector \mathbf{m} and \mathbf{d} is a data vector where the output is the observation data $t_{iobservation}$.

If we could rearrange the term in Equation 24, such that we could divide \mathbf{d} by some operator \mathbf{F}^{-1} to give \mathbf{m} directly, we would be solving an inverse problem. To develop how an inverse problem is done, consider an earthquake location in a homogenous material with velocity v . Then the i -th observed arrival time can be written as:

$$t_i = \frac{t_0 + \sqrt{(x_i - x)^2 + (y_i - y)^2 + (z_i - z)^2}}{v} \quad (25)$$

$(i = 1, 2, 3, \dots, N)$

where (x_i, y_i, z_i) = The location of the i -th station;
 t_0 = The common time origin;
 (x, y, z) = The event location; and
 N = Number of observations.

\mathbf{F} is an operator and nonlinear, so we must linearize the problem and establish an estimate of \mathbf{m} and \mathbf{d} :

$$\mathbf{m} = \mathbf{m}_0 + \delta\mathbf{m} \quad (26)$$

$$\delta\mathbf{d} = \mathbf{d} - \mathbf{d}_0 \quad (27)$$

where $\delta\mathbf{d}$, $\delta\mathbf{m}$ are the incremental variation of the observed data and model parameter respectively.

Substituting both Equation 26 and 27 into Equation 24, and rewriting gives:

$$\delta\mathbf{d} = \mathbf{d} - \mathbf{d}_0 = \mathbf{F}(\mathbf{m}_0 + \delta\mathbf{m}) - \mathbf{F}(\mathbf{m}_0) \quad (28)$$

Then to get linearization, we use only the first term of a truncated Taylor series as follows:

$$\mathbf{F}(\mathbf{m}_0 + \delta\mathbf{m}) = \mathbf{F}(\mathbf{m}_0) + \left(\frac{\delta\mathbf{F}(\mathbf{m})}{\delta\mathbf{m}}\right)_{\mathbf{m}_0} \delta\mathbf{m} + \mathcal{O}(\delta\mathbf{m}^2) \quad (29)$$

So we can rewrite Equation 28 as:

$$\delta\mathbf{d} = \mathbf{F}(\mathbf{m}_0 + \delta\mathbf{m}) - \mathbf{F}(\mathbf{m}_0) = \left(\frac{\delta\mathbf{F}(\mathbf{m})}{\delta\mathbf{m}}\right)_{\mathbf{m}_0} \delta\mathbf{m} \quad (30)$$

$$\delta\mathbf{d} = \mathbf{G} \delta\mathbf{m} \quad (31)$$

where $\mathbf{G} = \left(\frac{\delta\mathbf{F}(\mathbf{m})}{\delta\mathbf{m}}\right)_{\mathbf{m}_0}$

Then we can rewrite Equation 31 as:

$$\Delta\mathbf{d} = \mathbf{G} \Delta\mathbf{m} \text{ or } \mathbf{d} = \mathbf{G} \mathbf{m} \quad (32)$$

This is the linearized form of the problem. If we have 4 stations we have $n = m$ type problem and Gaussian elimination can be used to solve it. Once δx , δy , δz and δt are calculated, we can modify the parameters using Equation 27. This iterative process can be continued until $\Delta\mathbf{d}$ becomes acceptably small. This method is known as Geiger's method. Its disadvantages are that the final model totally depends on the initial guess and the process does not guarantee convergence (Lay and Wallace, 1995).

Equation 32 relates a data vector of dimension n (number of observations) to a model vector of dimension m (number of model parameters). With many observations ($n > m$), as in the case of earthquake location problems, we can obtain an overdetermined solution, which is the best fit to an average of the data.

3.3 Induced seismicity in geothermal fields

It is well known that geothermal systems are generally located in areas of tectonic activity, where earthquakes can take place. Evidence from earthquake studies indicate that the seismicity in geothermal areas is strongly influenced by the regional structures (Mulyadi, 1986). But earthquakes can also be induced by physical processes such as temperature, pressure, and stress changes associated with geothermal energy production; observable surface deformation associated with reservoir compaction around geothermal plants, and injection of liquid carbon dioxide at carbon sequestration plants (see Figure 8). Some of the major mechanisms of induced seismicity in geothermal environments are categorized as follows (Majer et al., 2007):

Pore pressure increase

Pore fluids are fluids that occupy pore spaces in soil or rock and play an important role in the stress field around earthquake faults. Increased fluid pressure in the pore of the rock or in the fault zone reduces the

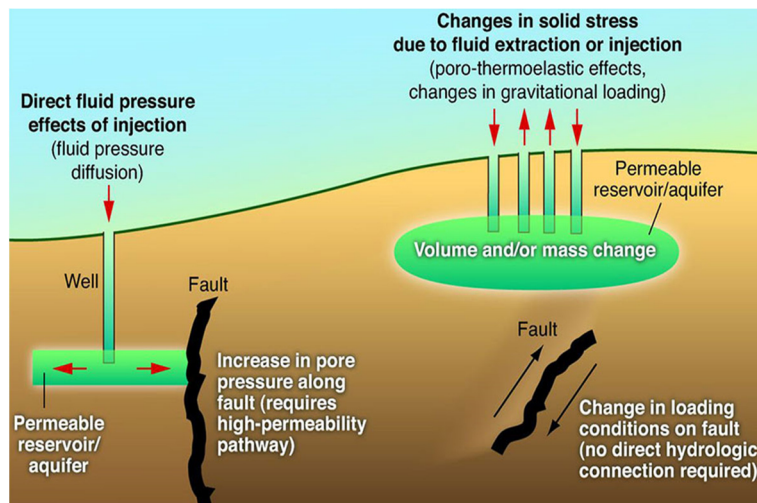


FIGURE 8: Schematic diagram of mechanisms for inducing earthquakes. Earthquakes may be induced by increasing the pore pressure acting on a fault (left) or by changing the shear and normal stress acting on the fault (right) (Ellsworth, 2013)

frictional strength of the fault or rock. Variation in fluid pressure may affect the timing of earthquakes (Miller, 1996).

Temperature decrease

Injection of cool fluids into the subsurface of geothermal areas allows cold fluid to interact with the hot rock and can cause contraction of fracture surfaces, in a process known as thermoelastic strain. Alternatively, cool fluid-hot rock interactions can create new fractures and seismicity directly related to thermal contraction of the rock matrix.

Volume change due to mass extraction and reinjection

As fluid is produced from (or injected into) an underground

resource, the reservoir rock may compact or be stressed. These volume changes cause a perturbation in local stress conditions, which are already close to failure (geothermal systems are typically located within faulted regions under high states of stress). This situation can lead to seismic slip within or around the reservoir.

Chemical alteration of fracture surfaces

Injecting non-native fluid into the formation may cause geochemical alteration of fracture surfaces which cause a change in the coefficient of friction on those surfaces. This change of the coefficient of friction can cause microearthquakes.

4. DATA ACQUISITION AND PROCESSING

4.1 Setting up an earthquake monitoring network

To monitor earthquake activity in a particular area we need to install a seismic network, which has at least four stations, ideally in a Y-shaped configuration. The central station of the Y plays an important role to accurately get the depth of the earthquake and the three outer stations should be evenly spaced around the radius of the area of interest (Figure 9). A seismic monitoring system is made up of several parts: a seismograph, a power source, a data telemetry system, a data reception system, and data analysis software.

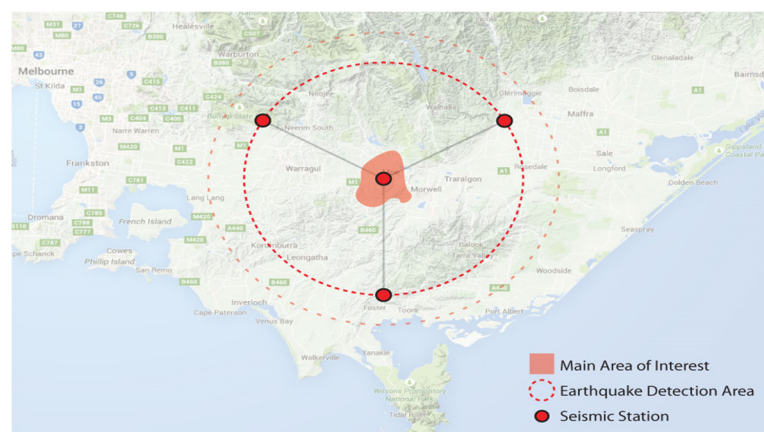


FIGURE 9: Installation of an earthquake monitoring network (Pascal, 2015)

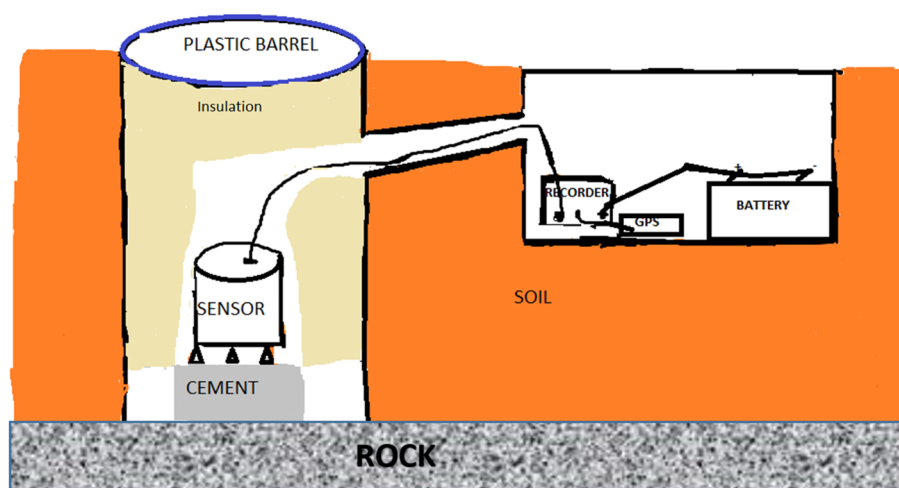


FIGURE 10: Seismometer installation

Seismographs are generally composed of two major components, a seismometer which is a sensor of ground motion and a recording system (Figure 10). Seismometers consist of three components, two of them measuring the horizontal motion along N-S and E-W and one along the vertical direction (Up-Down). Moreover, there are many different kinds of seismometers depending on the range of vibration frequencies that they can detect. Distinction is made between long period and short period seismometers which have become standards for global earthquake analyses, and broadband seismometers which can detect ground motions over a wide range of frequencies (Figure 11).

Usually the seismic station is deployed for a few months in the field, requiring a power source, such as a solar cell, a wind generator, direct connection to a landline and /or high capacity batteries. Obviously, the capacity of the batteries will determine how long the station will keep running. There are many ways in collecting data from the stations, either through a flash disk of high capacity set within the station, or to telemeter all the data continuously to the office.

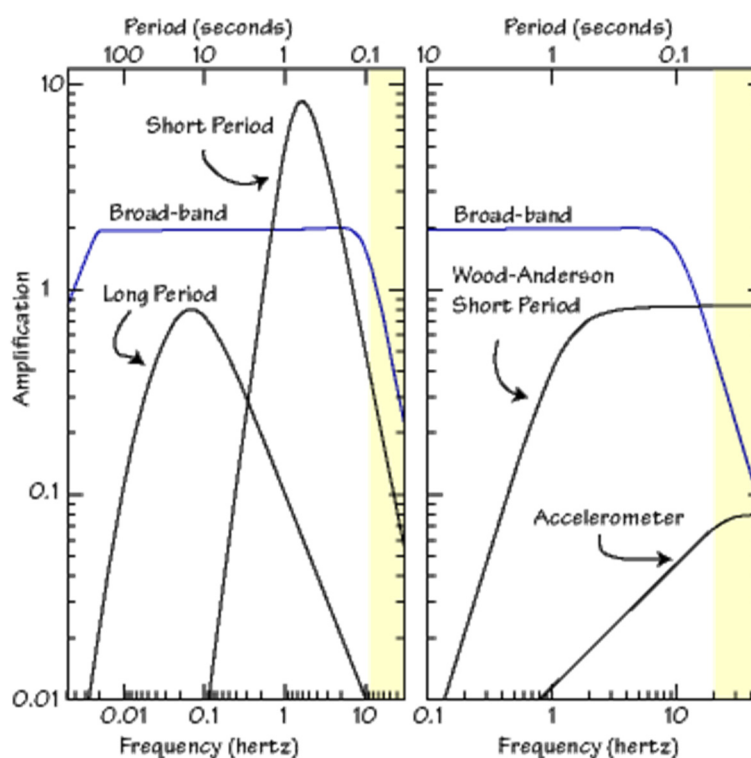


FIGURE 11: The broadband instrument senses most frequencies equally well; the long period and short period instruments are called “narrow” band and the yellow region is the low end of the frequency range audible to most humans (20 – 20000 Hz) (Department of Geoscience, 2016)

Today there are more modern recorders using internet streaming to get the data sent in real time, and a software package can be set on the desktop computer to display the data on a screen, and to archive the data into manageable files. Then a data reception system can be set to analyse and to transfer the recorded data to the preliminary processing system. Detailed analysis of the earthquake is then undertaken using

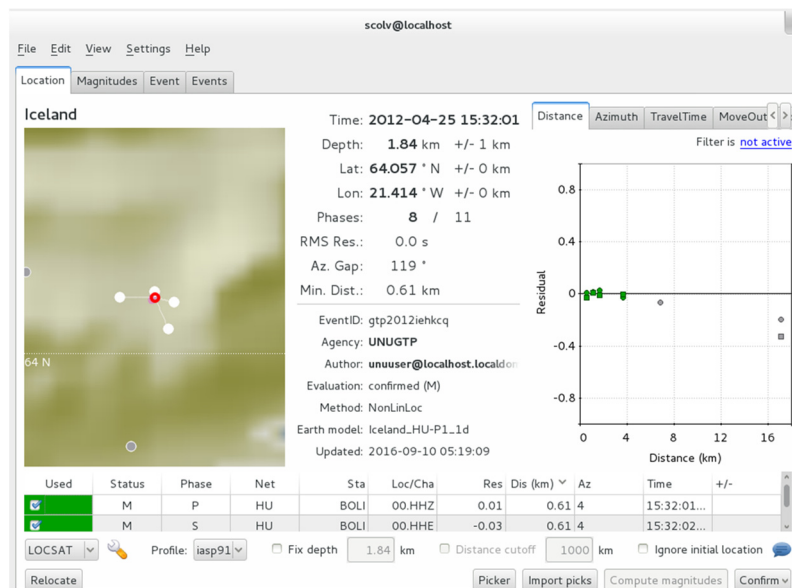


FIGURE 12: Front page view of the SeisComp3 software

Figure 12 shows the front page view of the software. The different steps used to process data in this project are as following:

- Enter the location of the interest area and the origin time through **Location** window;
- Go to **Picker** window;
- Change band pass filter to enhance the signal, in this case 4-50 Hz bandpass filter is used;
- Pick P and S wave arrival times for all the stations (Figure 13);
- Return to the main window and select nonlinear location method and velocity model to relocate the earthquake (Figure 14).

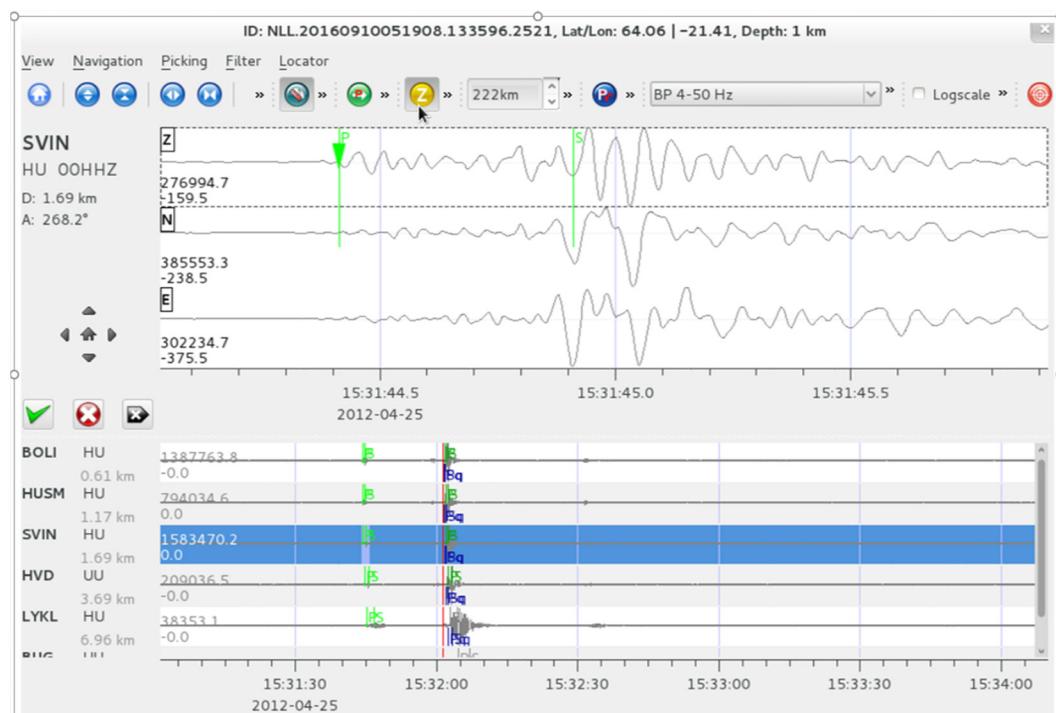


FIGURE 13: Picker window in the SeisComp3 software showing P and S waves from an event in Hellisheidi

analysis and modelling software and the earthquake information stored into a database to form a permanent historical record of seismic activity. In this project, a software called SeisComp3 (2016) (Seismological Communication Processor) is used, which was developed for the GEOPHON program, and is maintained by GEOPHON software development group at GFZ Potsdam. SeisComp3 can be download for free from the internet (www.seiscomp3.com) and consists of acquisition, picking and analysing facilities and it is able to accurately determine an earthquake's location as well as its magnitude.

4.2 Seismic noise

As for any measurement of physical properties, seismic data contains undesired components of ground motion called seismic noise. It is caused by several sources, which can be divided into coherent noise or incoherent noise.

- Coherent noise includes surfaces waves, reflections or reflected refractions from near surface structures such as fault planes or buried stream channels, refractions carried by high-velocity stringers, noise caused by vehicular traffic or farm tractors, multiples, etc. All of the preceding except multiples travel essentially horizontally.

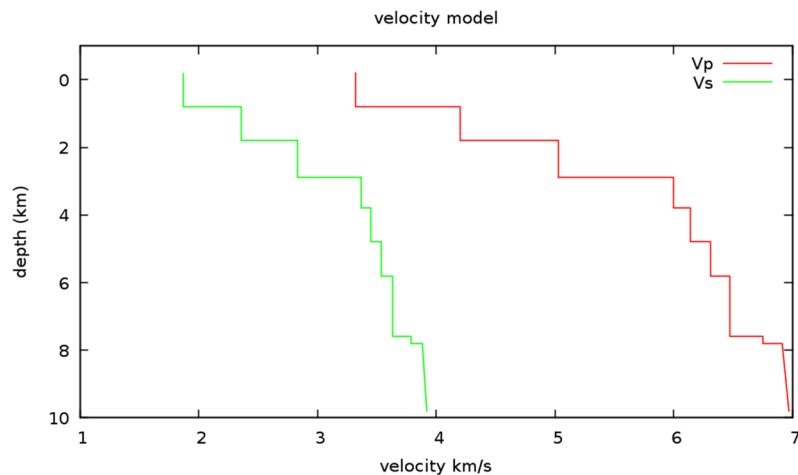


FIGURE 14: Velocity model used for the seismic data processing (Vogfjörð and Hjaltadóttir, 2007)

There are several techniques to reduce the noise and to enhance the seismic signal such as:

- Frequency filtering can be used to advantage (very low frequency components may be filtered out during the initial recording provided the low frequencies are sufficiently separated from the reflection frequencies).
- Protection from environmental noise such as temperature fluctuation, turbulent air flow around walls and human activity at the station.

5. RESULTS AND DISCUSSION

5.1 Hellisheidi area

Hellisheidi area has two reinjection zones, Gráuhnjúkar and Húsmúli. Gráuhnjúkar area is situated on the southern edge of the field. The temperature at depth in this area is higher than 300°C and could be ideal for production. Húsmúli is located in the northwestern part of the field. Seven reinjection wells have been drilled there, the last one in February 2011. Several earthquakes were recorded on a local network during the drilling of the injection wells. They seemed to be related to loss in drilling fluid during drilling operations (Ágústsson et al., 2015). When the reinjection of the waste water of the Hellisheidi power plant started in September 2011, a large number of induced earthquakes were recorded in the Húsmúli area by the Icelandic Meteorological office (IMO). During the period from 2011 to 2012 thousands of earthquakes were located (Figure 15). Four earthquakes with magnitude above 3.0 were observed, and felt in neighbouring

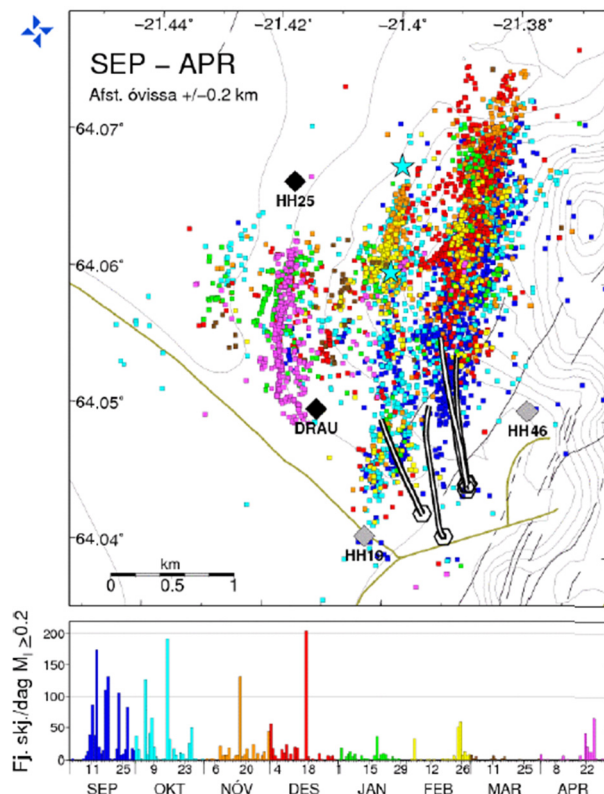


FIGURE 15: Induced seismicity in the Húsmúli area during 2011-2012 (Bessason et al., 2012)

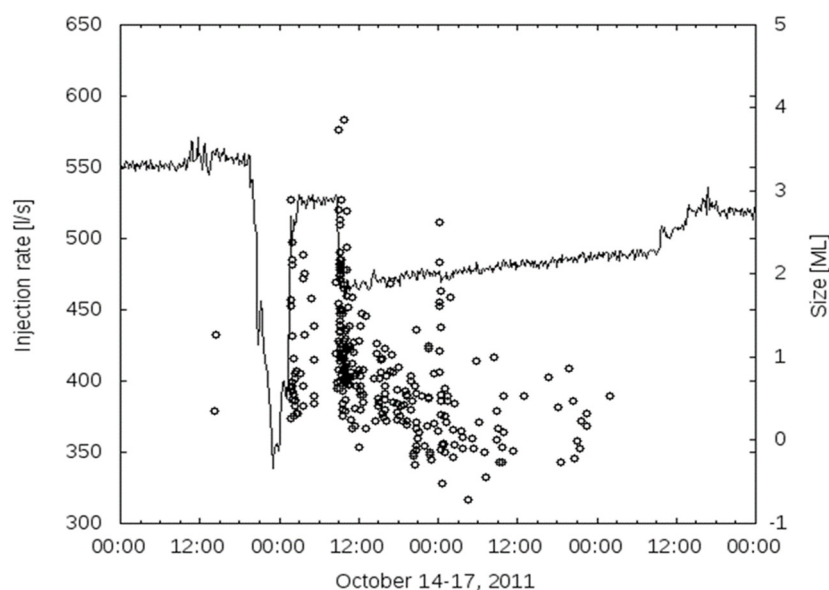


FIGURE 16: Relationship between injection and seismicity
(Kristjánsdóttir, S., personal communication)

municipalities, closest of which is ~ 8 km from the epicentre. Over time the built-up stress in the area was released, leading to a decrease in the seismicity. A link has been found between rapid changes in the reinjection rate and seismicity (Figure 16), therefore injection rate is kept as steady as possible in order to minimize induced seismic activity. Figure 15 also shows that the seismicity is characterized by several swarms, which delineate north-south striking faults, with the activity moving from east to west as time progresses.

In this report, data from of a swarm from April 25th, 2012, was analysed using the SeiscompP3 seismological software, developed by Helmholtz Centre Potsdam, GFZ German Research Centre for Geosciences in collaboration with GEMPA GmbH (2016). In all, 168 earthquakes were picked and located. Figure 17 shows the locations of the earthquakes on different views and the distributions of the magnitude of the recorded events. The detection threshold of the network is around 0.5. This means that events with magnitude below 0.5 are not all detected. A map view of the swarm shows a concentration of earthquakes in the Húsmúli area. They seem to delineate a N-S striking fault, which is vertically dipping (see cross-section). The activity is limited to a depth of 1.5-2.5 km although the uncertainty could be up to ± 1.0 km.

5.2 Overview and discussion on micro-seismic survey in Hanle Gaggade

The Republic of Djibouti is one of the East African countries, which has an exceptional geodynamic situation. It is located at the triple junction of the Red Sea, Gulf of Aden, and East African rifts where volcanic and tectonic activity has been taking place for 30 My (Jalludin, 2014). A recent reconnaissance study done by JICA (Japan International Cooperation Agency) in the whole region of the Republic of Djibouti, identified thirteen potential geothermal fields. Our discussion focuses on a microseismic survey undertaken in the Hanle–Gaggade area (one of the potential geothermal fields) from January 29, 2016 until May 3, 2016.

5.2.1 Geology of Hanle Gaggade

Hanle-Gaggade is located in the south-western region of the country where stratoid basalts circumscribe a succession of high plateaus and sedimentary plains between Lake Abhe and Lake Asal (Figure 18). Within this wide zone, fumaroles and hot springs are identified in the Lake Abhe area, the Galafi plain, on the eastern side of the rhyolitic Baba Alou Mountain and along the northern border of the Gaggade plain. Temperatures of the hot springs can exceed 60°C (Jalludin, 2014).

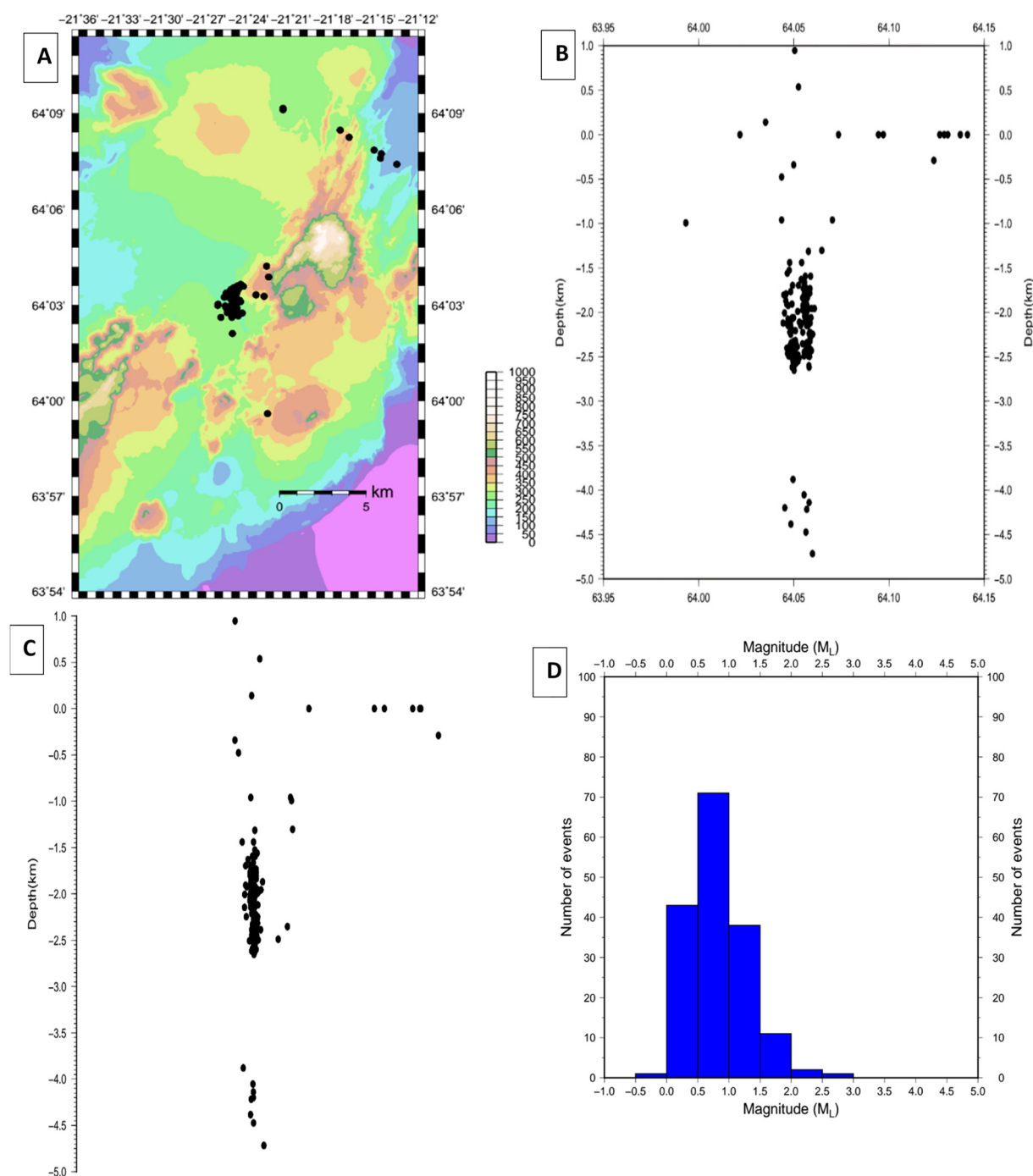


FIGURE 17: Location of the seismic activities a) on top of a topographic map (view from above); b) view from east; c) view from south; and d) magnitude distribution of the recorded events

Recently, the new Djiboutian Office of Geothermal Development (ODDEG) with support from JICA carried out a huge geophysical survey combining several methods such as identifying geothermal fluid movement and the brittle-ductile transition zone, gravity survey for consideration of geological structure in connection with geothermal reservoir system, and MT/TDEM survey to study the underground resistivity structure of the target field. An environmental and social impact assessment is ongoing in parallel. The final report was finalized in July 2016 in order to trigger the next step: the test well drillings.

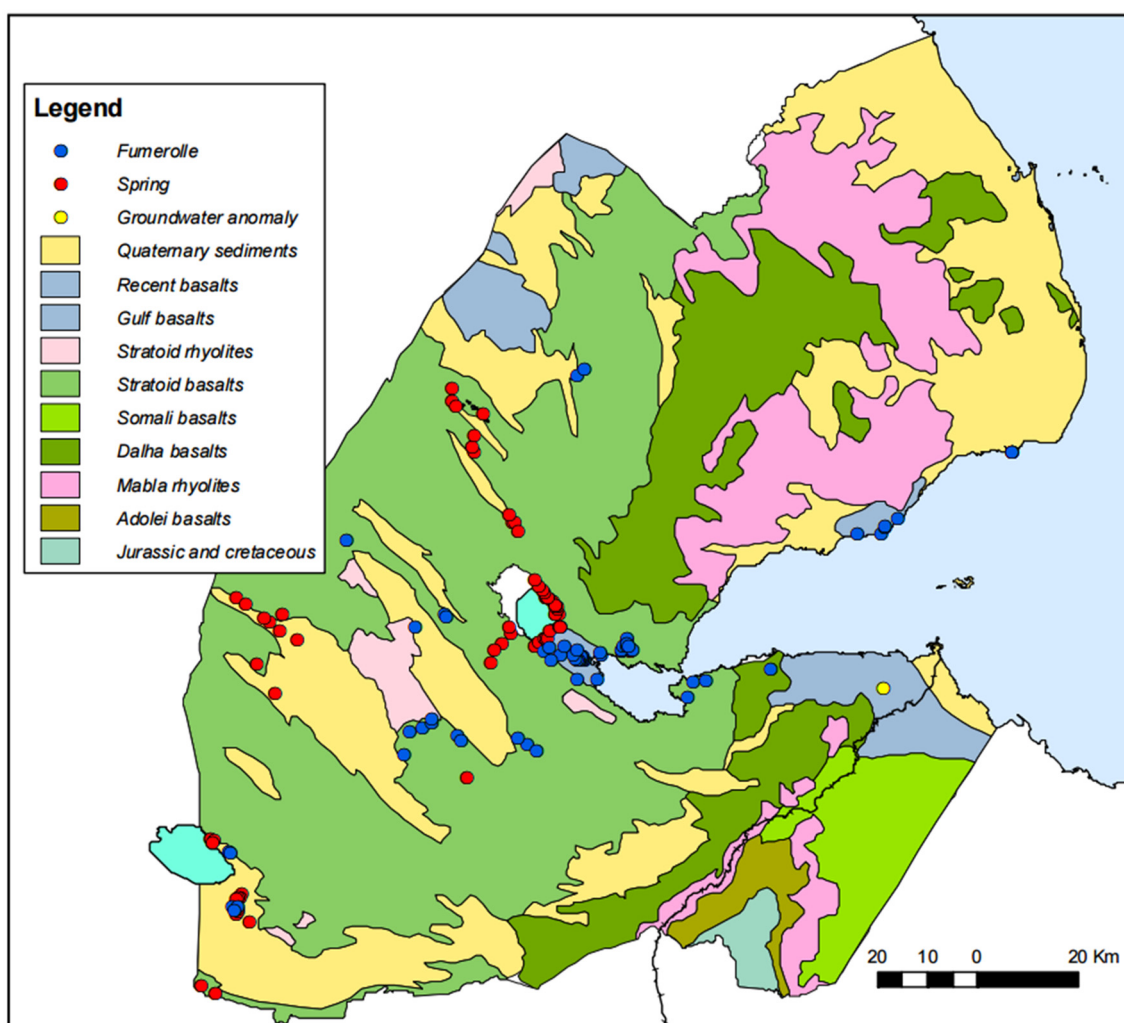


FIGURE 18: Geology and hydrothermal activity in the Republic of Djibouti (Jalludin, 2014)

5.2.2 Micro-seismic surveys

Following the MT/TEM and gravity surveys, a microseismic survey was conducted in August 2016 by ODDEG, covering approximately the same area as the geophysical surveys (MT/TEM, gravity). Velocity-type seismometers consisting of 3 components (N-S, E-W, Up-Down) were installed and collected data for about three months at five different locations. The purpose of this micro-earthquake survey was to understand areas with signs of geothermal activity, and to confirm fault structures and the positions of fault systems.

Figure 19 shows the locations of earthquakes recorded in the study area during the observation period. Most events are located on the lava plateau. A swarm of earthquakes was concentrated on the northwest part of the study area where the rhyolites are more dominant than the lower basalt rock but they were scattered outside of the station network. Distribution of epicentres seems to be concentrated near some faults, which could mean that those faults are active. More accurate locations, such as with relative relocation methods, are necessary to confirm this. In light of the recorded seismic activity, a local seismic network is recommended to monitor microseismic activity in this area during the exploitation of the geothermal field.

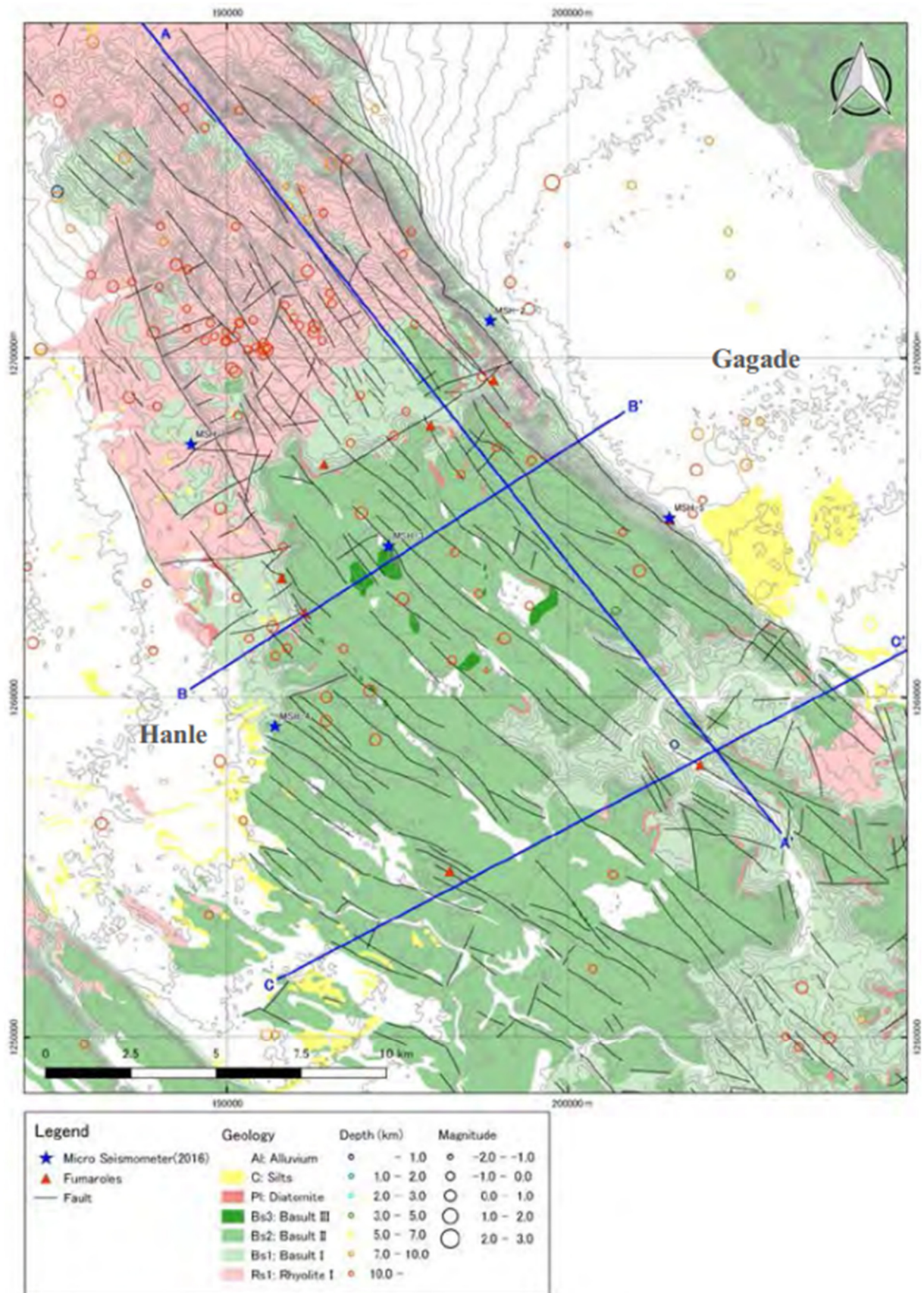


FIGURE 19: Distribution of epicentres in the study area (ODDEG, 2016)

6. CONCLUSION

It is important to minimize negative impacts of induced seismicity and increase the positive aspects for the sustainable use of resources. It is observed, also from microearthquake surveys done in Hanle Gaggade area, that this technique is a helpful tool in the exploration of a geothermal field in order to locate the brittle ductile zone and to map the active faults in a geothermal system. To be able to do that a continuous dataset recording both natural and induced seismicity needs to be analysed.

ACKNOWLEDGEMENTS

First and foremost, I am grateful to Mr. Abdou-Houmed and Mr. Lúdvík S. Georgsson for giving me the opportunity to participate in the UNU Geothermal Training Programme in Iceland.

I am grateful to my supervisor Ms. Sigríður Kristjánsdóttir. I am deeply indebted to her whole-hearted supervision to me during the project period. Her valuable suggestions and guidelines helped me a lot to prepare the report in a well-organized manner.

I would like to thank Mr. Gylfi Páll Hersir and Ms. Ásdís Benediktsdóttir for their constant advice, encouragement and their helping hand to complete my report successfully. I wish also to thank Ingimar, Frída, Thórhildur and Markús, the staff of UNU-GTP who rendered their help during this training programme.

I would also like to thank all the 2016 UNU-fellows for their friendship and fellow feeling.

Finally, I would like to express my deepest gratitude to almighty Allah for giving me the strength and the composure to complete this report.

REFERENCES

Ágústsson, K., Kristjánsdóttir, S., Flóvenz, Ó.G., Gudmundsson, Ó., 2015: Induced seismic activity during drill of injection well at the Hellisheidi power plant, SW Iceland. *Proceedings of the World Geothermal Congress 2015, Melbourne, Australia*, 10 pp.

Árnason, K., 1993: *Relation between resistivity and geothermal activity in basaltic rocks*. English translation of a chapter in: Geothermal activity at the Ölkelduháls field, resistivity soundings in 1991 and 1992. Orkustofnun, Reykjavík, report OS-93037/JHD-10 (in Icelandic), 82 pp.

Árnason, K., Karlsdóttir, R., Eysteinnsson, H., Flóvenz, Ó.G., and Gudlaugsson, S.Th., 2000: The resistivity structure of high-temperature geothermal systems in Iceland. *Proceedings of the World Geothermal Congress 2000, Kyushu-Tohoku, Japan*, 923-928.

Bessason, B., Ólafsson, E.H., Gunnarsson, G., Flóvenz, Ó.G., Jakobsdóttir, S.S., Björnsson, S., and Árnadóttir, Th., 2012: *Working procedures due to induced seismicity in geothermal systems*. Reykjavík Energy, Reykjavík, internal report (in Icelandic), 10 pp.

Björnsson, A., Hersir, G.P., and Björnsson, G., 1986: The Hengill high-temperature area, SW-Iceland: Regional geophysical survey. *Geothermal Resources Council, Transactions*, 10, 205-210.

Department of Geosciences, 2016: *Wave, seismograms and seismometers*. PennState, College of Earth and Mineral Sciences, Department of Geosciences, website: eqseis.geosc.psu.edu/~cammon/HTML/Classes/IntroQuakes/Notes/seismometers.html#seismic_networks.

Dix, C.H., 1952: *Seismic prospecting for oil*. Harper & Brothers, NY, 414 pp.

Ellsworth, W.L., 2013: Injection-induced earthquakes. *Science*, 341-6142.

Flóvenz, Ó.G., Ágústsson, K., Gudnason, E.Á., Kristjánsdóttir, S., 2015: Reinjection and induced seismicity in geothermal fields in Iceland. *Proceedings of the World Geothermal Congress 2015, Melbourne, Australia*, 15 pp.

Foulger, G.R., and Julien, B.R., 2009: *Applied microearthquake techniques for geothermal resource development*. Durham University, Durham, UK, website: community.dur.ac.uk.

Geothermal Education Office, 2007: *Geothermal reservoir*. Geothermal Education Office, website: geothermaleducation.org/GEOpresentation/sld012.htm.

Hardarson B.S., Einarsson, G.M., Gunnarsson, G., Helgadóttir H.M., Franzson, H., Árnason K., Ágústsson, K. and Gunnlaugsson E., 2010: Geothermal Reinjection at the Hengill Triple Junction, SW Iceland. *Proceedings of the World Geothermal Congress 2010, Bali, Indonesia*, 7 pp.

Jalludin. M., 2014: State of knowledge of the geothermal provinces of the Republic of Djibouti. *Paper presented at „Short Course IX on Exploration for Geothermal Resources”, organized by UNU-GTP, GDC and KenGen in Lake Bogoria and Lake Naivasha, Kenya*, UNU-GTP SC-19, 17 pp.

Lay, T., and Wallace, T.C., 1995: *Modern global seismology*. Academic Press, San Diego, CA, 521 pp.

Majer, E.L., Baria, R., Stark, M., Oates, S., Bommer, J., Smith, B., and Asanuma, H., 2007: Induced seismicity associated with enhanced geothermal systems. *Geothermics*, 36-3, 185-222.

Miller, S.A., 1996: Fluid-mediated influence of adjacent thrusting on the seismic cycle at Parkfield. *Nature*, 382, 799-802.

Mulyadi, 1986: *Applications of resistivity methods and micro-earthquake monitoring in geothermal exploration*. UNU-GTP, Iceland, report 6, 52 pp.

ODDEG, 2016: *Micro-seismic survey in Hanle Gaggade*. ODDEG – Djiboutian Development Office of Geothermal Energy, Workshop, Djibouti, August.

Pascale, A., 2015: *Setting up an earthquake monitoring network*. Seismology Research Centre, website: www.src.com.au.

Samaranyake, S.A., 2015: Seismic monitoring of geothermal fields: a case study of Hellisheidi geothermal field, Iceland. Report 32 in: *Geothermal training in Iceland 2015*. UNU-GTP, Iceland, 727-754.

SeisComp3, 2016: *Seiscomp3 software*. Seismological Communication Processor, website: www.seiscomp3.org/.

Vogfjörð, K.S., and Hjaltadóttir, S., 2007: *Mapping of seismic activity at Hverahlíð in Hellisheidi in February 2006*. Icelandic Meteorological Office, Reykjavík, report 07010 (in Icelandic), 20 pp.

Wanjohi, A.W., 2007: Monitoring of micro earthquakes and acoustic emissions within the Hengill-Hellisheidi geothermal reservoirs, June-August 2007. Report 23 in: *Geothermal training in Iceland 2007*. UNU-GTP, Iceland, 555-580.

APPENDIX I: Temporary seismic networks operated in the Hellisheidi area

Number	Station name	Latitude	Longitude	Height
1	BIT	64.05730	-21.25770	0.390
2	GUD	64.01973	-21.18845	0.104
3	HVH	64.00967	-21.33558	0.380
4	LHA	64.02406	-21.04883	0.119
5	IND	64.06153	-21.33585	0.470
6	SHR	64.02401	-21.50160	0.367
7	SKD	64.10792	-21.29883	0.344
8	BJA	63.94590	-21.30258	0.057
9	HEI	64.19978	-21.23603	0.162
10	KAS	64.02290	-21.85200	0.108
11	KRO	64.09806	-21.11976	0.147
12	SAN	64.05602	-21.57013	0.208
13	SOL	63.96230	-20.94357	0.030
14	VOS	63.85279	-21.70357	0.008
15	BUG	63.90450	-21.43760	0.034
16	ENG	64.08783	-21.41047	0.267
17	GEI	63.94818	-21.53068	0.278
18	HVD	64.02451	-21.39945	0.328
19	HVV	64.11147	-21.21532	0.181
20	LHL	63.97915	-21.83195	0.192
21	LME	63.97420	-21.42910	0.255
22	LSK	64.03495	-21.29603	0.367
23	NUP	63.99884	-21.25361	0.300
24	SEL	64.13364	-21.23823	0.169
25	SOG	63.99224	-21.14963	0.065
26	SVH	63.87788	-21.55152	0.150
27	TRH	64.06075	-21.17984	0.342

APPENDIX II: Seismic events recorded during April 24, 2012

Latitude	Longitude	Depth (km)	Origin time	Magnitude
64.05039	-21.43574	-0.948	00:01:01.374	0.53
64.05461	-21.38147	2.352	00:04:04.737	0.5
64.05602	-21.41534	1.973	00:07:14.009	0.34
64.05461	-21.41923	1.836	00:09:31.808	0.53
64.04987	-21.43610	0.341	00:12:04.940	0.3
64.05769	-21.41609	2.412	00:14:48.368	0.96
64.05681	-21.41802	2.343	00:15:52.870	0.77
64.03510	-21.41875	-0.141	00:21:21.584	0.51
64.04829	-21.42029	1.767	00:25:21.466	0.28
64.05839	-21.41454	2.326	00:27:24.682	0.82
63.99327	-21.37744	0.994	00:28:50.351	0.66
64.05479	-21.42367	1.922	00:30:42.845	0.14
64.05707	-21.41623	2.352	00:32:12.078	0.69
64.05532	-21.41688	1.973	00:33:59.260	0.5
64.06463	-21.37629	1.303	00:38:24.406	0.39
64.05496	-21.41846	1.836	00:44:58.868	0.46
64.05250	-21.41021	-0.536	00:56:22.544	0.15
64.05602	-21.41775	1.595	01:07:05.944	0.45
64.05154	-21.41716	2.480	01:08:13.668	0.74
64.05075	-21.41327	2.317	01:11:08.397	0.77
64.05224	-21.41521	2.549	01:15:33.498	1.41
64.05136	-21.41554	2.566	01:18:59.361	0.84
64.05224	-21.41722	2.480	01:23:07.437	1.45
64.05136	-21.41554	2.480	01:37:45.620	1.7
64.05066	-21.41507	2.446	01:57:23.877	0.99
64.04899	-21.41875	2.077	02:01:07.916	0.5
64.04978	-21.41781	2.326	02:02:59.213	1.15
64.05110	-21.41571	2.352	02:04:05.690	1.04
64.05892	-21.41258	2.274	02:12:21.010	1.37
64.05277	-21.41405	2.515	02:15:03.533	2.07
64.05769	-21.41528	1.312	02:16:56.625	1.22
64.05804	-21.41370	2.395	02:19:09.647	1.81
64.05356	-21.41673	2.145	02:42:00.416	0.93
64.05083	-21.41589	2.205	02:45:43.733	1.14
64.04635	-21.41812	2.128	02:49:26.701	0.37
64.04732	-21.41479	2.463	02:50:06.308	1.13
64.04723	-21.41538	2.489	02:53:45.857	0.54
64.04864	-21.41791	2.180	02:55:21.177	0.49
64.04662	-21.41392	2.463	02:56:40.107	1.4
64.05409	-21.42843	1.441	03:07:17.681	0.84
64.04354	-21.43233	0.478	03:10:22.043	0.33
64.05532	-21.41608	1.802	03:14:58.730	0.95
64.04952	-21.42723	3.881	03:15:56.180	1.49

Latitude	Longitude	Depth (km)	Origin time	Magnitude
64.05496	-21.41846	1.733	03:17:53.046	0.89
64.04697	-21.41957	2.120	03:19:55.486	1.24
64.05540	-21.41870	2.446	03:22:15.201	1.06
64.05989	-21.41326	2.248	03:29:13.046	1.22
64.05532	-21.41769	1.939	03:31:04.326	0.64
64.04934	-21.41878	1.698	03:35:43.417	0.53
64.05286	-21.41667	2.111	03:44:31.154	0.66
64.05066	-21.41668	2.584	03:48:45.482	1.05
64.05013	-21.41623	2.652	03:50:12.372	0.8
64.04960	-21.41860	2.618	03:53:05.099	0.43
64.04837	-21.41327	2.446	03:57:38.389	1.37
64.05637	-21.42582	2.008	04:00:26.671	0.24
64.04618	-21.42493	1.905	04:05:15.367	0.84
64.04829	-21.42592	2.145	04:05:47.962	0.87
64.04512	-21.42002	2.008	04:06:57.909	0.39
64.04433	-21.41212	2.120	04:10:54.016	1.58
64.04960	-21.41699	2.549	04:17:02.186	1.15
64.04996	-21.41702	2.498	04:19:18.711	0.97
64.05628	-21.41717	2.412	04:53:07.633	1.21
64.05365	-21.41533	2.120	05:01:50.572	1.5
64.04996	-21.41582	2.343	05:05:45.791	1.1
64.04829	-21.42431	2.248	05:08:21.832	1.06
64.04908	-21.41735	2.618	05:09:54.441	1.29
64.05804	-21.41491	2.618	05:13:24.325	1.24
64.05470	-21.41462	2.223	05:16:05.877	1.32
64.04969	-21.41800	2.592	05:21:31.048	0.47
64.04785	-21.41363	2.377	05:29:13.339	1.3
64.05532	-21.41929	1.870	05:30:45.356	0.59
64.04688	-21.41615	2.077	05:32:50.992	0.63
64.05787	-21.41409	2.601	05:35:06.343	1.01
64.04802	-21.41525	2.395	05:40:34.748	1.34
64.04855	-21.41569	2.343	05:56:54.411	2.75
64.04837	-21.41447	2.498	06:00:15.192	0.97
64.05857	-21.41656	2.120	06:03:42.073	1.52
64.05734	-21.41726	2.120	06:06:55.391	1.46
64.05839	-21.41695	2.223	06:08:08.427	1.5
64.04916	-21.41836	2.059	06:12:39.273	0.54
64.06077	-21.40892	1.956	06:16:12.227	0.2
64.05180	-21.40935	2.386	06:18:06.591	1.19
64.05602	-21.41936	2.077	06:21:22.675	0.59
64.04987	-21.41842	2.059	06:28:16.428	0.28
64.05532	-21.39117	2.489	06:29:58.087	0.54
64.04354	-21.41948	0.959	06:33:12.016	0.49
64.04899	-21.41875	2.386	06:34:25.449	0.4

Latitude	Longitude	Depth (km)	Origin time	Magnitude
64.04635	-21.41812	2.403	06:37:56.728	0.27
64.09447	-21.18683	0	06:40:05.878	0.6
64.13749	-21.28121	0	06:41:31.530	0.45
64.02166	-21.60935	0	06:55:53.353	0.47
64.09705	-21.17714	0	06:57:24.259	0.87
64.07349	-21.17723	0	06:59:33.385	0.75
64.04839	-21.41968	4.384	07:01:34.142	0.73
64.04952	-21.42080	2.506	07:05:09.319	0.28
64.05672	-21.41942	1.733	07:08:31.953	0.02
64.05250	-21.41985	1.698	07:09:58.986	0.57
64.05532	-21.41849	1.733	07:17:45.620	0.52
64.04864	-21.41872	2.214	07:26:29.942	0.49
64.05830	-21.41594	1.784	07:34:24.254	0.28
64.05690	-21.41582	2.059	07:38:14.499	0.8
64.07026	-21.37838	0.959	07:40:35.424	0.21
64.04653	-21.41291	1.561	07:45:35.488	0.58
64.04591	-21.41788	1.793	07:47:22.870	0.93
64.05567	-21.41691	1.664	07:51:06.623	0.25
64.05532	-21.42492	1.698	07:53:40.586	0.59
64.05690	-21.41903	1.922	07:54:43.199	0.72
64.05198	-21.41218	1.991	07:57:15.357	0.46
64.04899	-21.41634	1.905	08:01:47.858	0.29
64.05672	-21.41540	1.802	08:02:50.265	0.45
64.05936	-21.41201	1.956	08:04:40.308	0.22
64.05532	-21.42010	1.905	08:18:28.517	0.22
64.04477	-21.41677	1.802	08:28:13.650	-0.44
64.04811	-21.41425	2.231	08:35:15.217	0.54
64.04758	-21.41541	1.527	08:37:33.244	0.49
64.04582	-21.40723	1.870	08:41:49.805	0.52
64.05883	-21.41237	2.248	08:44:09.388	0.95
64.05461	-21.41923	1.973	08:58:40.357	0.5
64.05602	-21.42016	1.802	09:04:36.952	0.36
64.05602	-21.41936	2.111	09:17:28.010	0.4
64.05602	-21.41855	2.042	09:28:36.118	0.88
64.05813	-21.42034	2.077	09:32:39.830	0.32
64.04688	-21.41696	2.145	09:34:10.639	0.5
64.04705	-21.41496	1.922	09:35:33.125	0.44
64.04776	-21.41663	1.441	09:40:26.166	0.27
64.05760	-21.41588	2.334	09:43:27.848	0.59
64.05637	-21.41778	2.111	09:47:44.274	0.58
64.05848	-21.41234	2.317	09:51:32.478	0.9
64.05672	-21.41942	2.145	09:54:51.399	0.49
64.05567	-21.42013	2.042	10:04:09.181	0.47
64.05743	-21.41626	2.489	10:09:16.336	0.21

Latitude	Longitude	Depth (km)	Origin time	Magnitude
64.05804	-21.41531	2.240	10:10:43.386	0.95
64.05672	-21.41942	1.905	10:12:06.468	0.46
64.05743	-21.41546	2.145	10:14:26.104	0.78
64.15268	-21.35937	0	10:21:01.390	0.64
64.13087	-21.25178	0	10:23:37.597	1.14
64.12352	-21.22503	0.289	10:33:42.242	0.76
64.05975	-21.40598	4.716	10:52:37.177	1.3
64.04523	-21.41698	4.199	10:58:44.022	0.94
64.15182	-21.35936	0	11:02:41.077	0.5
64.14123	-21.29166	0	11:17:33.040	0.92
64.05537	-21.41743	4.054	11:29:39.168	1.66
64.12901	-21.24327	0	11:43:44.881	0.96
64.12663	-21.24445	0	11:54:20.371	1.01
64.05638	-21.41666	4.472	12:06:47.717	1.12
64.05680	-21.41915	4.216	12:32:55.137	1.23
64.05797	-21.41696	4.140	12:38:50.362	1.21
64.05927	-21.41502	2.429	12:40:22.783	1.55
64.05672	-21.41861	1.939	12:41:27.940	0.94
64.05883	-21.41397	2.420	12:48:30.971	0.98
64.05690	-21.41903	1.991	12:57:32.303	0.94
64.05857	-21.41656	2.274	13:14:23.458	1.57
64.04785	-21.41443	2.223	14:15:09.112	1.09
64.05901	-21.41761	2.059	14:19:11.410	1.62
64.05822	-21.41171	2.498	14:21:18.230	1.24
64.05672	-21.41379	1.802	14:24:44.079	0.78
64.05848	-21.41394	1.733	14:28:56.966	0.62
64.04864	-21.41550	2.455	14:31:08.509	0.68
64.05883	-21.41478	1.595	14:39:10.128	0.59
64.05646	-21.41477	2.016	14:44:02.796	1.52
64.05391	-21.42239	1.630	14:45:15.177	0.7
64.04829	-21.41949	2.145	15:03:53.408	0.71
64.05672	-21.41701	2.042	15:08:30.978	1.17
64.05602	-21.41695	1.733	15:15:13.394	1.26
64.05637	-21.41376	1.767	15:21:59.871	0.61
64.05496	-21.41525	1.973	15:24:22.139	1.03
64.05707	-21.41382	1.836	15:32:01.253	2.27



UNITED NATIONS
UNIVERSITY

UNU-GTP

Geothermal Training Programme

Orkustofnun, Grensasvegur 9,
IS-108 Reykjavik, Iceland

Reports 2016
Number 17

GEOCHEMICAL INTERPRETATION OF THERMAL WATER AND GAS SAMPLES FROM LAKE ABBE, DJIBOUTI

Rokiya Houssein Hassan

Djiboutian Development Office of Geothermal Energy – ODDEG

P.O. Box 1279

DJIBOUTI

missroky@hotmail.fr

ABSTRACT

The Lake Abbe geothermal area field is located in the south-western region of the Republic of Djibouti, on the border with Ethiopia. This area is dominated by stratoid basaltic rock and is marked by hydrothermal activities which are manifested by hot springs with surface temperatures of more than 90°C; fumaroles and travertines are also found in this area. Hot springs and fumaroles were sampled and analysed and geochemical data is interpreted in this report to estimate the reservoir temperatures and properties. The different geothermometers estimate the temperature of the reservoir to be in the range of 120-160°C. Hydrothermal data shows that the thermal waters have a high concentration of Cl which classifies them as volcanic waters and that these waters are equilibrated with the rock. The stable isotopic composition and Cl/B ratio were used to determine the origin of the water. The thermal waters are local meteoric waters from the same source and they are not mixed with Lake Abbe's water. The presence of the travertines shows that calcite deposition has occurred in the reservoir during geothermal production. The estimated reservoir temperatures suggest that the Lake Abbe geothermal area is a low-temperature geothermal system.

1. INTRODUCTION

The purpose of this report is to interpret the chemical data of thermal waters and gas from Lake Abbe, Djibouti. The Republic of Djibouti is located in the Horn of Africa in the East Africa rift system where the geology is also influenced by the Red Sea ridges and Gulf of Aden ridges. It is bordered by Eritrea to the north, Ethiopia to the west and south, and Somalia to the southeast. Djibouti has thirteen geothermal areas of interest, including the study area, which has been identified as being sufficiently promising in terms of potential electricity generation utilising geothermal fluids.

The Lake Abbe zone is located in the south western region of the country, at the border of Ethiopia. It lies in the Afar depression and the lake is connected to the Awash River. Fumaroles and hot springs, mainly alkaline chloride, are visible in a large area of more than 100 km² in size with the surface temperatures of more than 90°C, and many spots with temperatures of 100-105°C. This observation suggests that in the Lake Abbe zone, an important thermal anomaly exist, representing a potential geothermal reservoir.

The main objectives of the present study are to interpret the water and gas geochemistry by classifying the thermal waters using the ternary diagram, to estimate the reservoir temperature with geothermometers (quartz, cation and gas) and to determine the origin by interpreting the chloride and boron ratio and the stable isotopic composition (oxygen and deuterium).

2. METHODS

2.1 Field sampling

2.1.1 Sampling of springs

When collecting samples from hot springs it is good if the water is free-flowing from the sampling spot. If not, a sampling pump is needed. The water temperature and discharge is recorded. An untreated sample is collected in an air-tight bottle for pH, CO₂, H₂S and conductivity measurements. If the subsurface temperature is assumed to be high, the sample is diluted with distilled and deionised water for analysis of SiO₂ to have an ideal concentration of 30 to 100 ppm. A filtered sample is collected for anions and a filtered and acidified sample is collected for cation analysis. The filter and the acid used have a 0.45 µm pore size membrane and suprapur acid HNO₃. To analyse SO₄, the sample is filtered and sulphide precipitated with zinc acetate; Zn(CH₃COO)₂. For the analyses of stable isotopes, the sample is filtered and collected to an airtight 60 mL glass bottle. The various sub-samples collected are described in detail in Table 1.

TABLE 1: Sample treatment and analytical methods for geothermal water and gas

Phase	Treatment	Specification	To determine	Analytical method
Liquid	None, amber glass bottle with airtight stopper	Ru	pH, conductivity, CO ₂ , H ₂ S (<i>In situ</i>)	Potentiometry, Titrimetry
	Dilution; 50 mL of sample + 50 mL of distilled, deionized water	Rd (1 :1)	SiO ₂ if > 100 ppm	Spectroscopy with ammonium molybdate
	Filtration	Fu	F, Cl, Br, SO ₄ , B	Ion chromatography, Spectroscopy
	Filtration; 0.8 mL of HNO ₃ added to 200 mL sample	Fa	Na, K, Mg, Ca, Fe	Atomic absorption spectroscopy
	Filtration; 2 mL of 0.2 M ZnAc ₂ + 98 mL of sample	Fp	SO ₄	Ion chromatography
	Filtration	Fu	² H, ¹⁸ O	Mass spectrometry
Vapour	None; amber glass bottle	Ru	² H, ¹⁸ O	Mass spectrometry
	None	Ru	Anions	Ion chromatography
	0.4 mL conc. HNO ₃ (suprapur) added to 100 mL sample	Ra	Cations	Atomic absorption spectroscopy
	Added to 50 mL 40% NaOH in evacuated double port bottle	Gas sample	H ₂ , CH ₄ , N ₂ , O ₂ , Ar CO ₂ , H ₂ S in NaOH	Gas chromatography, Titrimetry

2.1.2 Sampling of fumaroles

The selection of fumaroles for sampling is not as straight forward as that of hot springs. It is generally best to sample small outlets which discharge steam at a considerable flow-rate in areas of the most intense acid surface alteration. Before the sampling, a NaOH solution should be prepared in the laboratory and put in a double port bottle which is then evacuated. The CO₂ and H₂S present in the steam dissolve quantitatively in the alkaline solution whereas the other gases remain in the head-space of the bottle. Samples of condensed steam are also collected. An untreated fraction is collected for Cl, B and Na analyses and a fraction for analyses of stable isotopes of oxygen and hydrogen is collected in an airtight amber glass bottle (Table 1).

2.2 Chemical analysis

Parameters like conductivity and temperature of the water are measured in situ while the pH and concentration of CO₂ and H₂S in samples are analysed in a field laboratory the same day. The major chemical constituents in water samples are analysed in the geochemical laboratory using the analytical methods shown in Table 1.

3. GEOCHEMICAL METHODS IN GEOTHERMAL EXPLORATION: DIFFERENT GEOTHERMOMETERS

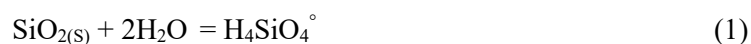
The application of chemical techniques has become an integral part of any geothermal exploration, especially in the early, pre-drilling stages (Giggenbach, 1991). Geochemical methods include sampling and analysis of water, gas and hydrothermal deposition. These methods are relatively inexpensive and can provide valuable information on the source of geothermal fluid and an estimation of temperature conditions in the geothermal reservoir using geothermometers. The soil gas measurements used around geothermal manifestations can allow estimation of the boundaries of the geothermal area and location of faults.

3.1 Geothermometry

The most commonly used “classic” solute geothermometers are the silica geothermometers (Fournier, 1977), Na/K geothermometers (White, 1965; Ellis, 1969; Fournier and Truesdell, 1973; Truesdell, 1975; Fournier, 1979), Na-K-Ca geothermometers (Fournier and Truesdell, 1973). The methods of chemical geothermometer allow, from the analysis of waters from the hot sources, to calculate the temperature at which they reached equilibrium with the host minerals. Various processes which can affect the chemical composition of deep hot waters, during their ascent and during their cooling since the geothermal reservoir towards the surface, the chemical geothermometers must be treated with caution according to the geologic environment where they are applied and according to the estimated ranges of temperature.

3.1.1 Silica geothermometers

The various silica phases (quartz, chalcedony and amorphous silica etc.) dissolve in water to reach equilibrium with aqueous H₄SiO₄.



The reaction of dissolution is independent of the pH and the ionic strength, thus the equilibrium state is essentially a function of temperature. Indeed, experimental results show that different solid phases of

silica (quartz, chalcedony and amorphous silica, etc.) have a solubility curve which varies with temperature (Fournier and Rowe, 1962).

The quasi-independence of the solubility of silica with regard to the ionic strength and the pH makes it possible to use the concentration of silica like geothermometer in the geothermic systems (Arnórsson, 1975; Truesdell, 1975). For higher temperature in the contents out of silica is generally controlled by quartz (Arnórsson, 1975). Between 120 and 180°C in fact the quartz or the chalcedony determines the solubility of silica; below 120°C only chalcedony.

It was reported that geothermal water boils in the process of rising towards the surface if the temperature of the reservoir exceeds 100°C (D'Amore and Arnórsson, 2000). This could cause inter alia an increase in the pH of thermal water because the dissolved acid gases (CO₂ and H₂S) are partitioned into the vapour phase during their ascent to the surface.

The silica geothermometers equations used to calculate subsurface temperatures are in Table 2.

TABLE 2: Temperature equations for silica geothermometers

No. of equation	Geothermometer	Equation	Range (°C)	Reference
1	Quartz-no steam loss	$T=1309 / (5.19 - \log S) - 273.15$	25-250	Fournier (1977)
2	Quartz ^a	$T=1522 / (5.75 - \log S) - 273.15$	25-250	Fournier (1977)
3	Quartz	$T=42.198 + 0.28831S - 3.6686 \times 10^{-4} S^2 + 3.1665 \times 10^{-7} S^3 + 77.034 \log S$	25-900	Fournier and Potter (1982)
4	Quartz ^a	$T=-53.5 + 0.11236S - 0.5559 \times 10^{-4} S^2 + 0.1772 \times 10^{-7} S^3 + 88.390 \log S$		Fournier and Potter (1982)
5	Quartz	$T=-55.3 + 0.3659S - 5.3954 \times 10^{-4} S^2 + 5.5132 \times 10^{-7} S^3 + 74.360 \log S$	0-350	Arnórsson et al (1998)
6	Quartz ^a	$T=-66.9 + 0.1378S - 4.9727 \times 10^{-5} S^2 + 1.0468 \times 10^{-8} S^3 + 87.841 \log S$	0-350	Arnórsson (2000)
7	Chalcedony	$T=1032 / (4.69 - \log S) - 273.15$	0-250	Fournier (1977)
8	Chalcedony	$T=1112 / (4.91 - \log S) - 273.15$		Arnórsson (2000)

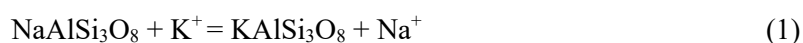
S represents silica concentration as SiO₂ in mg/kg.

^a Silica concentrations in water initially in equilibrium with quartz after adiabatic boiling to 100°C

3.1.2 Na/K geothermometers

It has been shown that the ratio between activity of sodium and potassium in a thermal solution is controlled by the chemical potential of these elements in silicates (Ellis and Mahon 1967).

The Na/K geothermometers are based on the equilibrium between a plagioclase and the K-feldspar. White (1965) and Ellis (1969; 1970) were the first to present the relationship between Na/K ratio and the temperature. They set related this with the equilibrium:



This relationship has, thereafter, been formulated in form of a thermometric relationship by Fournier and Truesdell (1973) and Fournier and Potter (1979) for temperatures above 120°C. Table 3 gives the Na/K geothermometers equations.

At lower temperatures, calcium usually compensates for significant fraction of cations and the Na/K geothermometers give to high temperature estimates for waters rich in calcium. Due of that, the Na-K-Ca geothermometer has been developed to estimate the temperature of those waters (Fournier and Truesdell, 1973).

TABLE 3: Temperature equations for Na/K geothermometers

No. of equation	Geothermometer	Equation	Range (°C)	Reference
9	Na/K	$T = [856 / (0.857 + \log(\text{Na/K}))] - 273.15$	100-275	(Truesdell, 1976)
10	Na/K	$T = [1217 / (1.483 + \log(\text{Na/K}))] - 273.15$		(Fournier, 1979)
11	Na/K	$T = [833 / (0.857 + \log(\text{Na/K}))] - 273.15$		(Tonani, 1980)
12	Na/K	$T = [933 / (0.857 + \log(\text{Na/K}))] - 273.15$	25-250	(Arnórsson et al., 1983)
13	Na/K	$T = [1319 / (1.483 + \log(\text{Na/K}))] - 273.15$	250-350	(Arnórsson et al., 1983)
14	Na/K	$T = [1178 / (1.470 + \log(\text{Na/K}))] - 273.15$		(Nieva and Nieva, 1987)
15	Na/K	$T = [1390 / (1.750 + \log(\text{Na/K}))] - 273.15$		(Giggenbach et al., 1988)
16	Na/K	$T = 733.6 - 770.551Y + 378.189Y^2 - 95.753Y^3 + 9.544Y^4$	0-350	(Arnórsson et al., 1998)

Na and K concentrations are given in mg/kg.

3.1.3 Na-K-Ca geothermometer

Fournier and Truesdell (1973) developed the Na-K-Ca geothermometers for application to waters with high concentrations of calcium. The cation geothermometers include the empirical Na-K-Ca geothermometer by Fournier (1981), which has been found to be consistent with measured well temperatures. This is an empirical geothermometer and theoretical constraints include equilibrium between Na-K feldspars plus conversion of calcium aluminosilicate minerals (e.g. Plagioclase) to calcite.

The main advantage of the Na-K-Ca geothermometer in comparison with the quartz geothermometer, and especially the Na/K geothermometer, is that it does not give high and misleading results for cold and slightly thermal, non-equilibrated waters.

The following considerations apply in application of this geothermometer:

$$T^{\circ}\text{C} = (1647 / (2.24 + \log(\text{Na/K}) + \beta * \log(\text{Ca}^{1/2}/\text{Na}))) - 273.15 \quad (2)$$

The methodology for the application of the Na-K-Ca geothermometer is as follows: Calculate the temperature using $\beta=4/3$ and cation concentrations expressed as mg/kg. If that calculated temperature is $< 100^{\circ}\text{C}$ or $[\log(\text{Ca}^{1/2}/\text{Na}) + 2.06]$ is negative, use $\beta=1/3$ to calculate the temperature (Arnórsson, 2000). Obviously, the Na-K-Ca geothermometer is applicable to a larger temperature range of thermal fluids than the Na/K geothermometer because the Na-K-Ca geothermometer appears to give excellent results for most waters above about 200°C , but erratic results are obtained for waters from reservoirs at less than 200°C . These erratic results appear to come from effects of high partial pressures of CO_2 and exchange reactions involving Na^+ , K^+ , or Ca^+ with additional ions (particularly Mg) (D'Amore, 1991). These are more or less the same limitations as for the Na-K geothermometer; it is also very good above 200°C (or 180°C) but often gives erratic results at lower temperatures. This geothermometer is affected by boiling and dilution.

3.1.4 Gas geothermometers

CO₂ in geothermal gas is mainly produced by volcanic activity while CH₄ is produced by two mechanisms: reduction of CO₂ but also the breakdown of organic matter by bacterial activity. H₂S is of magmatic origin but at very low concentrations and for H₂ some authors (D'Amore, 1991; Glover, 1970) propose an electrochemical origin of this gas (H⁺), produced by oxidation of sulphide. Chemical reactions in the steam due to oxidative contact with atmospheric gases, or the lowering of temperature may change the gas composition, hence it is necessary to sample the highest temperature fumaroles which guarantees the composition which is most likely to be representative of the source of the geothermal reservoir gas.

The gas geothermometers are often used to estimate deep temperatures in early exploration. Gas-gas or gas-mineral equilibrium is assumed to exist at the source (Óskarsson and Ármannsson, 2015), and they have the disadvantage of being more prone to errors than fluid geothermometers due to secondary processes. (Óskarsson, 2016). N₂ and Ar concentration are assumed to be source-controlled rather than equilibrium controlled, but CO₂, H₂S, H₂ and CH₄ are assumed to be controlled by equilibrium. The main gas geothermometers applied in this report can be seen in Table 4:

TABLE 4: Temperature equations for gas geothermometers

Geothermometer	Temperature equations	Remarks
CO ₂	$t^{\circ}\text{C} = 44.1 + 269.25Q - 76.88 Q^2 + 9.52 Q^3$	All waters
H ₂ S	$t^{\circ}\text{C} = 246.7 + 44.8Q$	All waters above 300°C
H ₂ S	$t^{\circ}\text{C} = 173.2 + 65.04Q$	Arnórsson and Gunnlaugsson 1985
CH ₄ /CO ₂	$t^{\circ}\text{C} = [4625/(10.4 + \log(\text{CH}_4/\text{CO}_2))] - 273.15$	Giggenbach 1991
CO ₂	$t^{\circ}\text{C} = 4.724 Q^3 - 11.068 Q^2 + 72.012 Q + 121.8$	Arnórsson et al. 1998
H ₂ S	$t^{\circ}\text{C} = 4.811 Q^2 + 66.152 Q + 177.6$	Arnórsson et al. 1998
CO ₂ /N ₂	$t^{\circ}\text{C} = 1.739 Q^3 + 7.599 Q^2 + 48.751 Q + 173.2$	Arnórsson et al. 1998
H ₂ S/Ar	$t^{\circ}\text{C} = 4.108 Q^2 + 42.265 Q + 137.6$	Arnórsson et al. 1998

Q = log mmol/kg of gas

3.2 Classification and plots

Giggenbach (1991) proposed a SO₄-Cl-HCO₃ ternary diagram (Figure 1) for the initial classification of geothermal solutions to identify whether the geothermometers are applicable for the given water sample, as geothermometry assumes an equilibrium between fluid and rock at depth. A hot spring with significant chloride, moderate bicarbonate and minimal sulphate is consistent with outflow from a geothermal reservoir. It will be much more likely to provide reliable cation geothermometry than a spring that contains mainly bicarbonate or sulphate. When the fluid rises to the surface, the decrease of pressure can produce the evolution of a vapour phase which coexists with the liquid phase in the hydrothermal system. Then this vapour can either condense or dissolve in superficial ground water. To distinguish

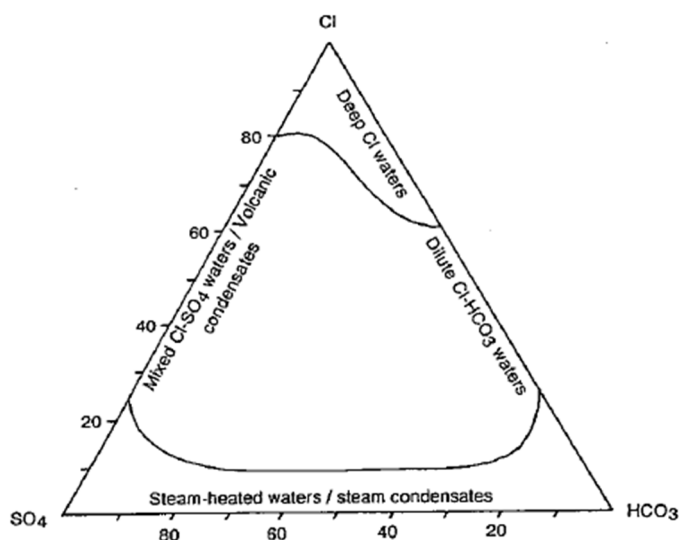


FIGURE 1: Ternary diagram Cl-SO₄-HCO₃

between those different types of fluids, a ternary diagram representing the proportion of chloride, sulphate and bicarbonate is used.

The interpretation of geothermal water chemistry is best carried out on the basis of an initial classification in terms of their major anions Cl, SO₄ and HCO₃. The position of a data point in such a triangular diagram (Giggenbach, 1991) is obtained by first calculating the sum S of the concentrations of all three constituents involved, which is in the present case:

$$S = C_{\text{Cl}} + C_{\text{SO}_4} + C_{\text{HCO}_3} \quad (4)$$

The next step consists the evaluation of %-Cl, %-SO₄ and %-HCO₃ according to the following equation:

$$\% \text{-Cl} = 100C_{\text{Cl}}/S; \% \text{-SO}_4 = 100C_{\text{SO}_4}/S; \% \text{-HCO}_3 = 100C_{\text{HCO}_3}/S \quad (5)$$

4. APPLICATION OF THE CHEMICAL PROGRAM WATCH

The computer program WATCH (Arnórsson et al., 1982; Bjarnason, 2010) is used to calculate aqueous speciation in natural waters. Its primary area of application are geothermal fluids, but it is useful for non-thermal waters as well. The program reads chemical analyses of water, gas, and steam condensate samples collected at the surface and computes the chemical composition of downhole, aquifer or fluids at some suitably chosen reference temperature. WATCH is available for both Linux and Windows operating systems. A companion program, WAIN, is used to create input data files. The concentrations of the species considered in the program are expressed in terms of the component concentrations by mass balance equations. The chemical equilibria between the species are also expressed as mass action equations. The program contains provisions for 69 different aqueous species which are treated separately.

The output from the program lists the component and species concentrations in the deep fluid at the reference temperature as well as the activity coefficients. Finally, the ion activity products log Q and solubility products log K of selected minerals are computed and printed. From these, it is straightforward to compute the corresponding saturation indices log Q/K.

In this study, the WATCH program is used to estimate and evaluate the state of saturation of common scale forming minerals. This saturation index is useful in the study of scaling.

5. LAKE ABBE GEOTHERMAL FIELD, DJIBOUTI

5.1 Geology of the country

The Republic of Djibouti is located within the Afar depression, which is a big crustal zone resulting from the separation of the Arabian and African plates. This zone establishes the connection between the current oceanic ridge in the Red Sea and the Gulf of Aden system, which evolved into laterally intra-continental rifts. The geology of the country is affected by the junction of the Aden gulf, the Red Sea oceanic ridge, and also by the East African rifting system which constitute the triple junction system (McKenzie et al., 1970) (Figure 2). Almost all of the Afar depression is covered by stratoid basalts, which are partially hidden and were created in the early stages of rifting (Barbéri et Varet, 1975).

The republic of Djibouti has been the place of a major tectonic activity since the Oligo-Miocene period until today. All stages of rifting have occurred there which were followed by the formation of the Afar depression. This is why all the different geological formations can be found in the Republic of Djibouti.

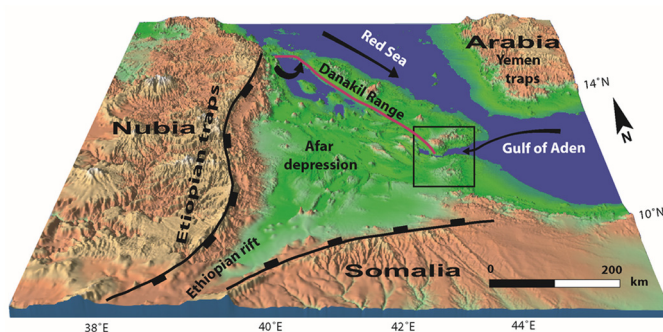


FIGURE 2: The rifting system and Afar depression

Almost all the rocks in the country are of basaltic composition (Figure 3) and Quaternary sediments are found in the north of the country. In Figure 3, surface manifestations are shown by dots which are located mainly on the rift stream bed (SW-NE trend). About thirteen geothermal provinces have been identified in the country according to the location of surface manifestations. The study area is one of them: Lake Abbe, the red circle in the Figure 3.

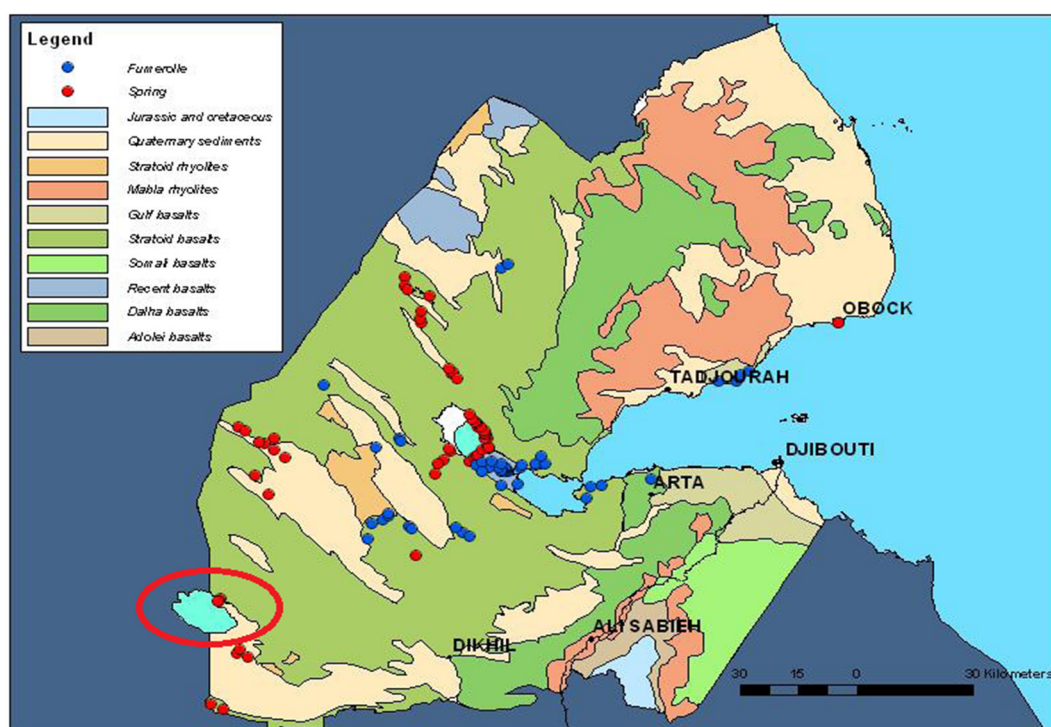


FIGURE 3: Geological Maps of Djibouti (CERD). The red circle shows Lake Abbe

5.2 Regional geology: Lake Abbe

The Lake Abbe site is located in the south-western region of the Republic of Djibouti near the Ethiopian border. It is the western end of the Goba'ad plain and the eastern end of the downstream valley of the Awash River from the Ethiopian plateau. Its surface covers an area of about 150 km² and trends to 240 m of altitude. The Lake Abbe is the remainder of an old lake from 6000 years ago surrounded by volcanoes and is marked out by its calcium chimney edified on fractures related to the collapse of the region. The travertines were formed under water. The highest is about 60 m (Figure 4). These travertines are formed inside the lake where hot springs with high calcium concentration rise up through fractures and it mixes with the cold lake water. This causes precipitation and deposition of calcite throughout the orifice of the outflow. Thus, the travertines were formed in some thousands of years (Pantecost and Viles, 1994). The most characteristic feature of the Lake Abbe region is the presence of a linear chain of travertine chimneys and the temperature of resurgence of the hot springs being generally higher than 90°C. The area is still in formation due to the ongoing movement of the divergent plate boundary.

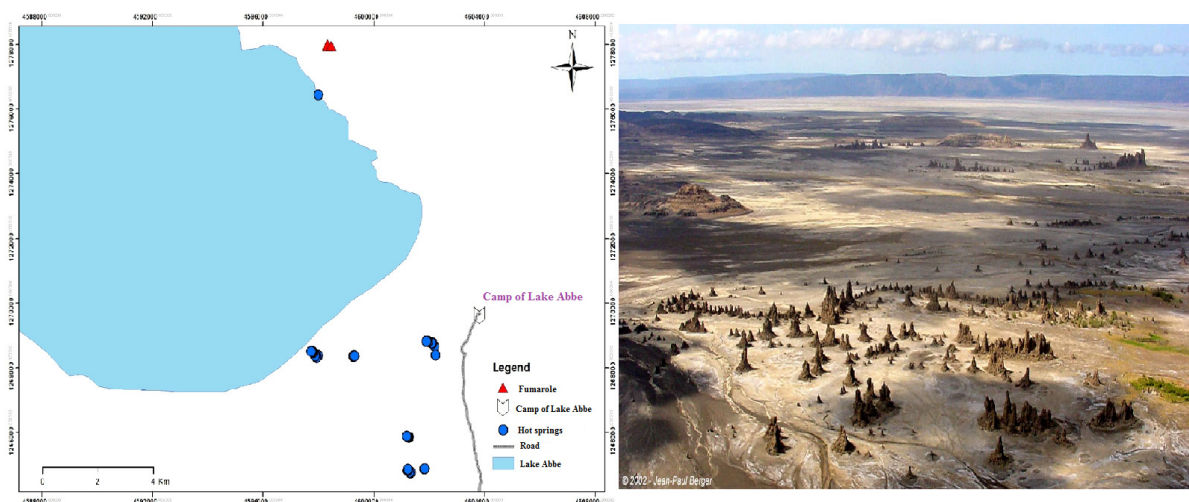


FIGURE 4: Location map of geothermal manifestations (left). Travertine chimneys (right)

Stratoid basalt (3.5-1 Ma) and recent cinder cones dominate the site, which lies at the eastern coast of Lake Abbe, the Goba'ad basin and the north-eastern horst (240 to 560 m high). Several rhyolitic intrusions-pyroclastic are distributed along the south-eastern margin. Lacustrine, calcareous and salty sediments fill every small polygonal depressions and the basin (Sabkha) up to salty Lake Abbe. Major WNW fracture systems are parallel to graben and horst structures, while minor transversal NNE trend fractures are also recognized. Recent cinder cone distributions seem to be controlled by intersection positioning of the two fracture systems. Scattered acidic alteration spots or small mounds (sinter cones) are common in the recent pyroclastic cone foothill and rhyolite related alteration is scarce at this site.

6. RESULTS AND DISCUSSIONS

In this study, samples from eight hot springs, one cold groundwater spring and one fumarole were collected (Fig 4) and analysed. The major, minor and trace elements of these waters are reported in Appendix II. The temperature of the geothermal water samples of Lake Abbe ranged from 94.2 to 99.8°C. The conductivity of these waters ranges between 3140-7210 $\mu\text{S}/\text{cm}/^\circ\text{C}$.

6.1 $\text{Cl}-\text{SO}_4-\text{HCO}_3$ ternary diagram

This diagram classifies geothermal waters using the major anion concentrations (chlorides, sulphates and bicarbonates) (Giggenbach, 1988) and also helps distinguishing the waters as mature, peripheral, volcanic or steam-heated waters. On the triangular diagram $\text{Cl}-\text{SO}_4-\text{HCO}_3$ in Figure 5, thermal waters are near to the chloride corner but not in the field of mature geothermal waters. This part of the diagram represents waters of volcanic origin. From this diagram, it can be interpreted that these thermal waters are probably volcanic waters while groundwater is cold water and its location in this figure indicates that this water is mixed water.

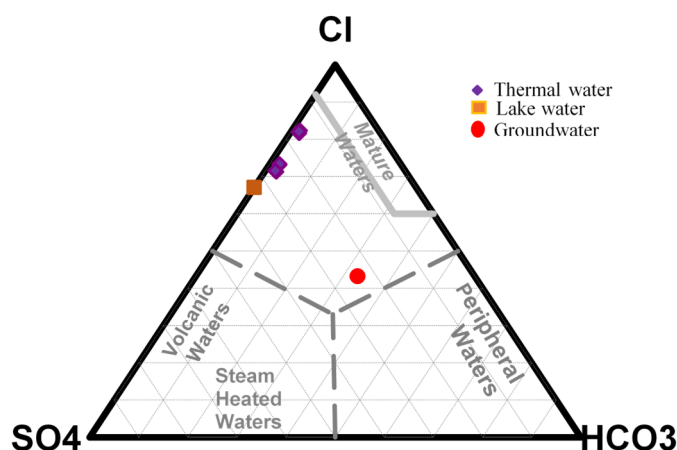


FIGURE 5: $\text{Cl}-\text{SO}_4-\text{HCO}_3$ Ternary diagram

6.2 Na-K-Mg ternary diagram

The ternary diagram of Na-K-Mg shown in Figure 6 was developed by Giggenbach (1988). It is used to estimate the reservoir temperature and to select the waters most suitable for geothermometry by recognizing the fluid maturity of waters which have attained equilibrium with the host rock. Fournier (1990) states that the diagram is most useful for determining which waters are most suitable for geothermometry. Data points that plot on the full equilibrium in the diagram indicate that water-rock equilibrium has been attained. Plotting on the partial equilibrium indicates either a mineral that has dissolved but has not attained equilibrium or geothermal water that has mixed with dilute unequilibrated cold water. Immature water indicates initial dissolution of minerals before equilibrium reaction begins.

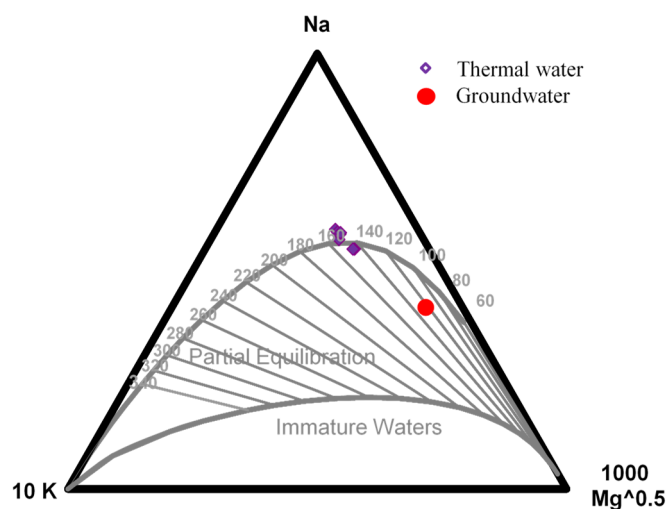


FIGURE 6: Na-K-Mg ternary diagram for Lake Abbe water samples

Figure 6 shows that the samples from thermal water are fully equilibrated or close to equilibration, whereas the groundwater sample is only partly equilibrated. It is normal that this water is not at equilibrium because at low temperatures the reactions between the water and the rock are very slow. The thermal water appears to be well equilibrated at temperatures of 140-160°C according to the Na-K-Mg ternary diagram.

6.3 Geothermometers of Lake Abbe

6.3.1 Silica and cation geothermometers

In this paper, nine geothermometers equations were used (Table 5): three for quartz, three for Na-K, two for chalcedony, and Na-K-Ca. Among the six quartz geothermometers, three are chosen because the samples were collected at the surface, thus the geothermal fluid has boiled down to 100°C: equations 2, 4 and 6 (Table 2). For the Na/K geothermometer also three equations were chosen: equations 12, 14 and 16 (Table 3). They are applied to predict subsurface temperatures of the geothermal water from Lake Abbe. All the thermal water samples lie in the temperature range 121-145°C for quartz, 107-125°C for chalcedony, 91-124°C for Na-K and 84-115°C for Na-K-Ca. The average temperature calculated was 133°C, 114°C, 109°C and 97°C for quartz, chalcedony, Na-K and Na-K-Ca respectively. The Na-K geothermometer temperatures were high while the Na-K-Ca geothermometer gave low temperatures.

Figure 7 shows comparison plots of calculated temperature results obtained from nine different equations of geothermometers for Lake Abbe. In this area, the silica geothermometers yield temperatures less than about 180°C. Thus, chalcedony appears to control dissolved silica concentrations in the Lake Abbe area. The equilibrium between dissolved silica and quartz is very slow at low temperature. The low value of Na-K-Ca geothermometer (Abbe-04, Abbe-05, Abbe-06 and Abbe-07) is due to the calcium loss (see Appendix II for the Ca values) caused by boiling of water which leads the precipitation of aragonite confirmed by the travertine deposit. The low temperature reservoir may be explained by greater meteoric recharge or greater heat conduction due to shallow reservoir depths.

TABLE 5: Calculated values for 9 equations for solute geothermometers temperatures (in °C) for Lake Abbe, Djibouti

	Quartz			Na-K			Chalcedony		Na-K-Ca
Name	T _{qz, 2}	T _{qz, 4}	T _{qz, 6}	T _{Na-K, 12}	T _{Na-K, 14}	T _{Na-K, 16}	T _{ch, 7}	T _{ch, 8}	T _{Na-K-Ca}
Abbe-01	141	142	131	97	120	119	121	119	106
Abbe-02	141	143	132	102	124	123	122	120	110
Abbe-03	135	136	124	91	115	114	113	111	115
Abbe-04	133	134	122	93	116	115	110	109	85
Abbe-05	131	133	121	93	116	115	109	107	85
Abbe-06	133	134	122	93	116	116	110	109	85
Abbe-07	134	135	124	93	116	115	112	111	84
Abbe-12	143	145	134	91	114	114	125	122	103
Abbe-14	94	93	80	67	93	94	62	64	239

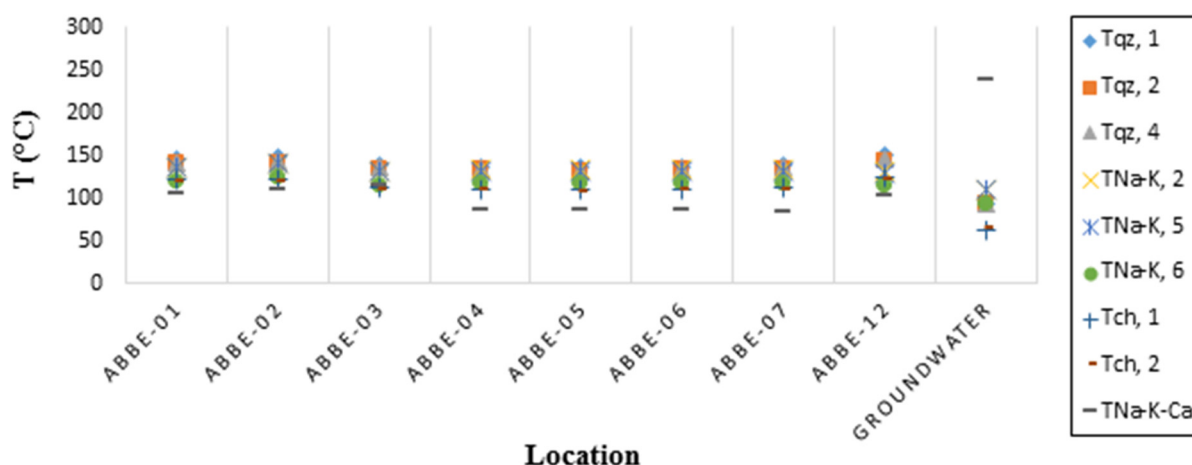


FIGURE 7: Calculated temperature results obtained with silica, Na-K and Na-K-Ca geothermometers

6.3.2 Gas geothermometers

The following gases are invariably present in geothermal discharges from both natural features and wells: CO₂, H₂S, N₂, H₂, CH₄, NH₃. So it is important to know the behaviour of these geothermal gases (Appendix I).

In this area, only one sample was collected from a fumarole. Gas geothermometers (Table 4) were applied to the results of chemical analysis. Gas geothermometer temperature ranges (Table 6) are very large (20-250°C) and that is not a good sign. Because of the fact that there is only one sample, we cannot know if it is characteristic of the area and there is also no smell of H₂S indicating a high-temperature system. The sample is probably air contaminated, the significant values of O₂, N₂ and Ar (Appendix I) allow the assumption that these gases were added to magmatic gas by atmospheric contamination because soil air contains oxygen, nitrogen and other trace atmospheric gases and these can be entrained in the steam discharge as it passes through the soil profile. These contaminations can also be added to a sample during the sampling process. Contamination of air, whatever the source is, changes the chemical composition of the sample and renders the gas geothermometers useless unless the contamination can be quantified. This fumarole cannot provide information about the area.

TABLE 6: Calculated values for gas geothermometers temperatures (in °C) for Lake Abbe, Djibouti

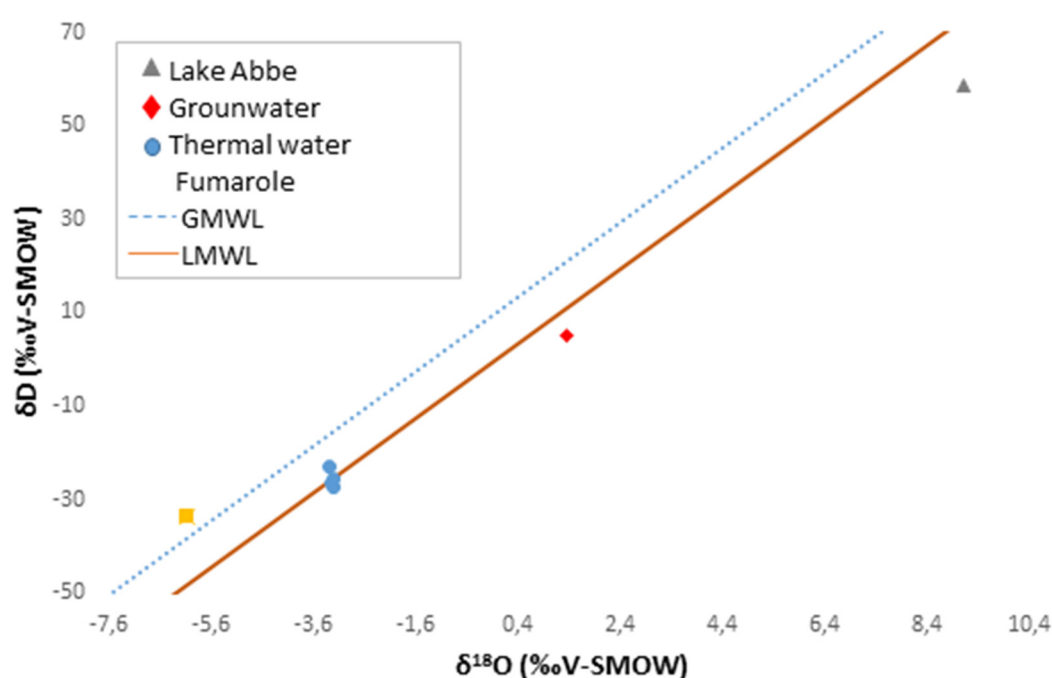
	T	Source	Range
CO ₂	148	Arnórsson and Gunnlaugsson 1985	All waters
H ₂ S	141	Arnórsson and Gunnlaugsson 1985	All waters above 300°C
H ₂ S	20	Arnórsson and Gunnlaugsson 1985	All waters below 200°C
CH ₄ /CO ₂	250	Giggenbach (1991)	
CO ₂	183	Arnórsson et al. 1998	> 100°C, basaltic rock
H ₂ S	48	Arnórsson et al. 1998	> 150°C, basaltic rock
CO ₂ /N ₂	182	Arnórsson et al. 1998	If Ar and N ₂ conc. in reservoir water are equal to those in air saturated water at 5°C
H ₂ S/Ar	87	Arnórsson et al. 1998	

6.4 Origin of the water

6.4.1 Isotopes

The isotopic ratios correspond generally to small values and it is not easy to measure absolute isotopic ratios (Arnórsson, 2000). For this reason, isotopic concentrations are conveniently expressed in delta notation (δ) as parts per thousand. $\delta^{18}\text{O}$ and δD are related by the Global Meteoric Line water (GMWL) developed by Craig (1961) and this GMWL is a result of climatic and geographic factors. There is also a Local Meteoric Water Line for Djibouti (LMWL; Fontes et al., 1980) which is derived from precipitation collected from local sites.

Stable $\delta^{18}\text{O}$ and δD isotopic analyses were used to determine the origin of thermal waters and the geothermal reservoir recharge area (Figure 8). The δD and $\delta^{18}\text{O}$ values of meteoric waters at any locality is dependent upon latitude, altitude and distance from the ocean. In this study area, the oxygen and hydrogen isotopes are plotted and compared to the global meteoric line (GMWL) and local meteoric line (LMWL). The equations of GMWL defined by Craig (1961) and LMWL defined by Fontes et al. (1980) are respectively: $\delta\text{D} = 8 \cdot \delta^{18}\text{O} + 10$ and $\delta\text{D} = 8 \cdot \delta^{18}\text{O} + 0$.

FIGURE 8: Plot of $\delta^{18}\text{O}$ - δD of the thermal waters and fumarole from Lake Abbe

The thermal water is probably of local origin, plotting on the LMWL. The fumarole sample is more depleted in deuterium and oxygen-18, most likely due to boiling. It is probably from the same source as the thermal waters but it is very hard to say exactly because the fumarole is located very far away from the thermal water (approx. 12 km, see coordinates in Appendix II). The cold groundwater comes from different source than thermal water because the difference in hydrogen isotopes is more than 30‰ indicating a different source. Lake Abbe water is much evaporated so it is normal to have higher values of 9.12‰ and 58.63‰ for $\delta^{18}\text{O}$ and δD respectively.

6.4.2 Ratio Cl/B

The B and Cl contents of geothermal waters have been used to obtain information on the origin of these waters (White, 1957a, b; White et al., 1963; Truesdell, 1976) to evaluate mixing of hot and cold water in the upflow zones of geothermal systems and to assess other characteristics of such systems (Ellis, 1970; White, 1970; Fournier, 1977, 1979; Arnórsson, 1985; Janik et al, 1991; Truesdell, 1991).

In the Figure 9, the rock ratio was assumed 30 because the study area is basaltic. The concentration of Cl in thermal water lies in the range of 835-2170 ppm and that of B in the range of 0.95-1.57 ppm. Their Cl/B ratio is on the range of 879-1151. This ratio is significantly higher than the Cl/B ratio in most analysed basalts. The concentrations of B and Cl of thermal waters are somewhat higher than in groundwater and these are due probably to water rock interaction. These thermal waters are from the same source which is shown by the fact that they are all in the same line (Figure 9) while the concentration of B and Cl in groundwater are 2.25 ppm and 1040 ppm and it has the same Cl/B ratio as Lake Abbe. It is possible that the groundwater is related to Lake Abbe. The location of groundwater in Figure 9 indicates that it is probably comes from different source than thermal water. The concentration of B and Cl in Lake Abbe is very high (Appendix II) and the Cl/B ratio is lower than thermal water. Due to the very different Cl/B ratios despite the high Cl and B concentrations in Lake Abbe, it seems very likely that the thermal waters have a different origin than lake water.

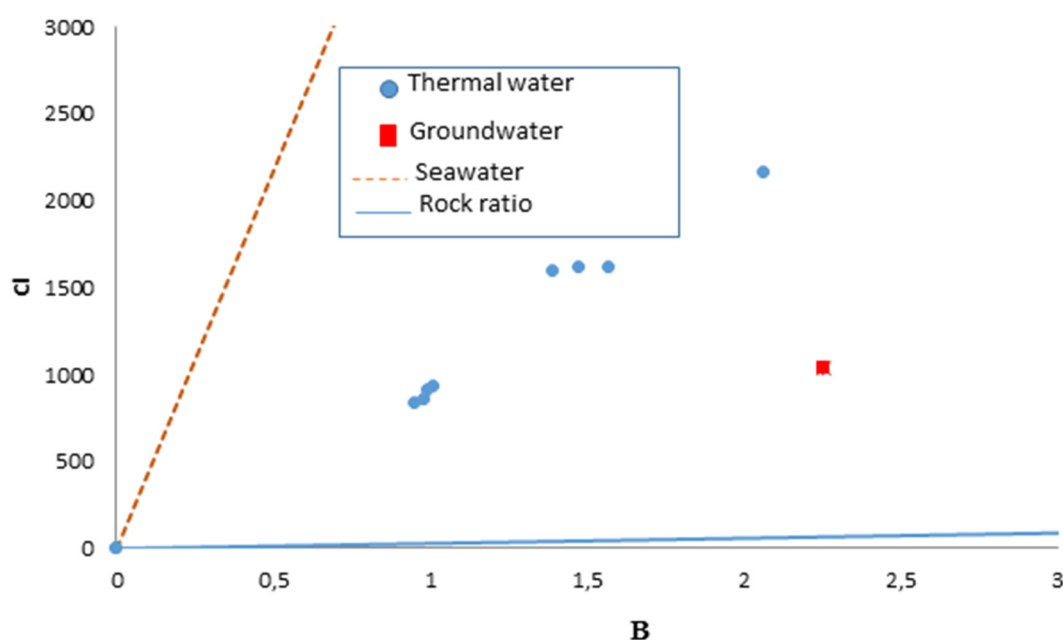


FIGURE 9: Distribution of Cl and B in thermal waters and groundwater in Lake Abbe area

6.5 Mineral saturation index

One of the most common production problems in geothermal fields is scaling deposition and corrosion. For that mineral equilibrium calculations are used to predict the presence of reactive minerals and to estimate mineral reactivity in a groundwater system. The saturation index was calculated for some

minerals (calcite, quartz, chalcedony and anhydrite) using a chemical speciation model, the WATCH program (Table 7). Available chemical analyses were entered into the WATCH program and the ion activity product (log Q) and solubility product (log K) of these minerals were computed, using the boiling springs model. The reference temperature used is measured temperature.

TABLE 7: Saturation index of the thermal waters from the study area

	Calcite	Quartz	Anhydrite	Chalcedony	T
ABB1	0.568	0.398	-0.143	0.133	96.9
ABB2	0.579	0.384	-0.131	0.123	99.6
ABB3	0.718	0.315	-0.024	0.054	99.8
ABB4	0.742	0.284	-0.117	0.023	99.8
ABB5	0.738	0.317	-0.194	0.048	94.2
ABB6	0.788	0.318	-0.183	0.051	95.8
ABB7	0.807	0.289	-0.162	0.028	99.5
ABB12	0.493	0.404	-0.128	0.143	99.5
GW	0.507	0.583	-2.352	0.234	34

All thermal waters of the study area are undersaturated with respect to anhydrite (CaSO_4) at sampling conditions but might be saturated at reservoir temperatures. The silica minerals (quartz, chalcedony) were found to be oversaturated and near equilibrium state. It is normal for the silica minerals to be in equilibrium, their reactions are pretty fast (at least for chalcedony at this temperature) and if they were not in equilibrium we could not use the silica geothermometers. Silica minerals are most likely to precipitate as scales from the geothermal waters during geothermal production. Regarding calcite scaling, all thermal waters are oversaturated and the saturation index (SI) is between 0.493 and 0.807. If the SI is higher than 0.38, the potential for calcite scaling exists (Bai, 1991). This is the case of the study area and it is shown by the presence of calcite travertines in Lake Abbe area.

7. CONCLUSIONS

Analyses of geochemical data of thermal waters from hot springs and gas from fumaroles was carried out in order to estimate the subsurface reservoir temperatures and to investigate the origin of the waters. The thermal waters from the vicinity of Lake Abbe were found to be volcanic waters due to high concentrations of Cl and SO_4 and low concentration of CO_2 . The Na-K-Mg ternary diagram indicates attainment of water-rock equilibrium. The reservoir temperatures were estimated using various solute geothermometers (silica, cation) which were found to be in the range of 120-160°C. This is in accordance with the Na-K-Mg ternary diagram which gives a similar range of temperature. Regarding the stable isotopic composition (oxygen and hydrogen), the thermal waters are meteoric water and have a different origin than the lake. The Cl/B ratios also suggest that these thermal waters are not derived from the lake. Saturation index of the thermal waters at the measured temperatures suggest that the thermal water in the study area is undersaturated with respect to anhydrite and supersaturated with respect to quartz, chalcedony and calcite. The calcite deposits can be even observed and the hypothesis is made that the formation of travertines was due to the precipitation of calcite.

The reservoir temperature was calculated also using gas geothermometers. The temperature range obtained is very large (20-250°C) which indicates that the sample was probably air contaminated during sampling or was mixed with soil air that contains oxygen. This sampling was only from one fumarole so it does not give information about the whole area.

Finally, geochemical studies and field observations suggest that the study area is a low temperature geothermal system, which has to be confirmed by drilling. The others fumaroles found have to be sampled by other method than the classic one.

ACKNOWLEDGEMENTS

I would like to express my gratitude to Mr. Lúdvik S. Georgsson, director, for giving me the chance to attend this training for six months. My thanks also go to Mr. Ingimar G. Haraldson for his help and for taking his time to guide us. I would like to thank Ms. Málfríður Ómarsdóttir, Mr. Markús A. G. Wilde and Ms. Thórhildur Ísberg for having us facilitated all our sejour and for the great learning experience during the six months. Remembering of course to thank all the lecturers of UNU-GTP for sharing their knowledge. How could I forget to thank Ms. Rósa S. Jónsdóttir for spending time to find for us all the papers we needed. I am going also to thank the UNU class of 2016 fellows for their friendliness, their help and the sharing of their experience during the six months.

I give the biggest thanks to my supervisor Ms. Ester Inga Eyjólfsson for her patience, her efforts and for sharing her knowledge with me. Also I would like give thanks Finnogi Óskarsson for reviewing the report. Finally, my biggest set of thanks must go all to my parents, sisters and brothers, whose support has been spectacular during these six months.

REFERENCES

- Arnórsson, S. (ed.), 2000: *Isotopic and chemical techniques in geothermal exploration, development and use. Sampling methods, data handling, interpretation*. International Atomic Energy Agency, Vienna, 351 pp.
- Arnórsson, S., Andrésdóttir, A., Gunnarsson, I., and Stefánsson, A., 1998: New calibration for the quartz and Na/K geothermometers – valid in the range 0-350°C (in Icelandic). *Proceedings of the Geoscience Society of Iceland Annual Meeting, April*, 42-43.
- Arnórsson, S., and Gunnlaugsson, E., 1985: New gas geothermometers for geothermal exploration – calibration and application, *Geochim. Cosmochim. Acta*, 49, 1307-1325.
- Arnórsson, S., Gunnlaugsson, E., and Svavarsson, H., 1983: The chemistry of geothermal waters in Iceland III. Chemical geothermometry in geothermal investigations. *Geochim. Cosmochim. Acta*, 47, 567-577.
- Arnórsson, S., Sigurdsson, S. and Svavarsson, H., 1982: The chemistry of geothermal waters in Iceland I. Calculation of aqueous speciation from 0°C to 370°C. *Geochim. Cosmochim. Acta*, 46, 1513-1532.
- Arnórsson, S., and Stefánsson, A., 1999: Assessment of feldspar solubility constants in water in the range 0-350°C at P_{sat}. *Am. J. Sci.*, 299, 173-209.
- Arnórsson, S., and Svavarsson, H., 1985: Application of chemical geothermometry to geothermal exploration and development. *Geoth. Res. Council, Transactions*, 9-1, 293-298.
- Bai Liping, 1991: *Chemical modelling programs for predicting calcite scaling, applied to low-temperature geothermal waters in Iceland*. UNU-GTP, Iceland, report 3, 45 pp.
- Barbéri, F., Ferrara, G., Santacrose, R. and Varet, J. 1975: Structural evolution of the Afar triple junction. In: Pilger, A., Rösler, A. (eds.) *Depression of Ethiopia*. Schweizerbart, Stuttgart, 1, 38-54.
- Craig, H., 1961: Isotopic variations in meteoric water. *Science*, 133, 1702-1703.
- D'Amore, F., 1991: Gas geochemistry as a link between geothermal exploration and exploitation. In: D'Amore, F. (coordinator), *Application of geochemistry in geothermal reservoir development* UNITAR/UNDP publication, Rome, 93-117.
- Ellis, A.J., 1969: Present-day hydrothermal systems and mineral deposition. *Proceedings of the 9th Commonwealth Mining and Metal Congress, Inst. Min. Metall., London*, 1-30.

- Ellis, A.J., 1970: Quantitative interpretation of chemical characteristics of hydrothermal systems. *Geothermics*, 2, 516-527.
- Ellis, A.J., and Mahon, W.A.J., 1967: Natural hydrothermal systems and experimental hot water/rock interactions (part II). *Geochim. Cosmochim. Acta*, 31, 519-538.
- Fontes, J.C., Pouchon, P., Saliege, J.F. and Zuppi, G.M., 1980: Environmental isotope study of groundwater systems in the Republic of Djibouti. In: *Arid-zone hydrology: investigations with isotope techniques*. IAEA, Vienna, 237-262.
- Fournier, R.O., 1977: Chemical geothermometers and mixing model for geothermal systems. *Geothermics*, 5, 41-50.
- Fournier, R.O., 1981: Application of water chemistry to geothermal exploration and reservoir engineering. In: Rybach, L., and Muffler, L.J.P. (editors), *Geothermal system: Principles and case histories*. John Wiley and Sons Ltd., Chichester, 109-143.
- Fournier, R.O., 1990: The interpretation of Na-K-Mg relations in geothermal waters. *Geothermal Resources Council, Transactions 14*, 1421-1425.
- Fournier, R.O., 1991: Water geothermometers applied to geothermal energy. In: D'Amore, F. (coordinator), *Application of Geochemistry in Geothermal Reservoir Development*. UNITAR/UNDP publication, Rome, 37-69.
- Fournier, R.O., and Potter, R.W. II, 1979: Magnesium correction to the Na-K-Ca geothermometer. *Geochim. Cosmochim. Acta*, 43, 1543-1550.
- Fournier, R.O., and Potter, R.W. II, 1982: A revised and expanded silica (quartz) geothermometer. *Geoth. Res. Council Bull.*, 11-10, 3-12.
- Fournier, R.O., and Rowe, J.J., 1962: The solubility of cristobalite along the three-phase curve, gas plus liquid plus cristobalite. *Am. Mineralogist*, 47, 897-902.
- Fournier, R.O., and Truesdell, A.H., 1973: An empirical Na-K-Ca geothermometer for natural waters. *Geochim. Cosmochim. Acta*, 37, 1255-1275.
- Giggenbach, W.F., 1988: Geothermal solute equilibria. Derivation of Na-K-Mg-Ca geoindicators. *Geochim. Cosmochim. Acta*, 52, 2749-2765.
- Giggenbach, W.F., 1991: Chemical techniques in geothermal exploration. In: D'Amore, F. (coordinator), *Application of geochemistry in geothermal reservoir development*. UNITAR/UNDP publication, Rome, 119-144.
- Glover, R.B., 1970: Geochemical investigations of the Ahuachapán geothermal fields. In: *Survey of geothermal resources in El Salvador*. United Nations Development Programme, unpublished report.
- Gunnarsson, I., and Arnórsson S., 2000: Amorphous silica solubility and the thermodynamic properties of $\text{H}_4\text{SiO}_4^\circ$ in the range of 0° to 350°C at P_{sat} . *Geochim. Cosmochim. Acta*, 64, 2295-2307.
- Janik, C.J., Truesdell, A.H., Goff, F., Shevenell, L., Stallard, M.L., Trujillo, P.E. and Counce, D., 1991: A geochemical model for the Platanares geothermal systems, Honduras. *J. Volcanol. Geothermal Research*, 45, 125- 146.
- McKenzie, D.P., Davies, D. and Molnar, P. 1970: Plate tectonics of the Red Sea and East Africa. *Nature*, 226, 243-248.
- Morey, G.W., Fournier, R.O. and Rowe, J.J., 1962: The solubility of quartz in water in the temperature interval from 29 to 300°C. *Geochim. Cosmochim. Acta*, 26, 1029-1043.
- Nieva, D., and Nieva, R., 1987: Developments in geothermal energy in Mexico, part 12-A: Cationic composition geothermometer for prospection of geothermal resources. *Heat Recovery Systems and CHP*, 7, 243-258.

Óskarsson, F., 2016: *Chemistry of thermal fluids*. UNU-GTP, unpublished lecture notes.

Óskarsson, F. and Ármannsson, H., 2015: Geochemical methods in geothermal surface exploration. *Presented at Short Course X on Exploration for Geothermal Resources, organized by UNU-GTP, KenGen and GDC, at Lake Bogoria and Lake Naivasha, Kenya*, UNU-GTP SC-21.

Pantecost, A. and Viles, H., 1994: A review and reassessment of travertine classification. *Geographie physique et quaternaire*, vol. 48, n°3, p.305-314.

Tonani, F., 1980: Some remarks on the application of geochemical techniques in geothermal exploration. *Proceedings, Adv. Eur. Geoth. Res., 2nd Symposium, Strasbourg*, 428-443.

Truesdell, A.H., 1976: Summary of section III - geochemical techniques in exploration. *Proceedings of the 2nd U.N. Symposium on the Development and Use of Geothermal Resources, San Francisco, I*, liii-lxxix.

Truesdell, A.H., 1991: Effects of physical processes on geothermal fluids. In: D'Amore, F. (coordinator), *Application of geochemistry in geothermal reservoir development*. UNITAR/UNDP publication, Rome, 71-92.

White, D.E., 1957a: Thermal waters of volcanic origin. *Bull. Geol. Soc. Amer.*, 68, 1637-1658.

White, D.E., 1957b: Magmatic, connate and metamorphic waters. *Bull. Geol. Soc. Amer.* 68, 1659-1682.

White, D.E., 1965: Saline waters of sedimentary rocks. *Proceedings of the Symposium „Fluids in Subsurface Environments“*. *Amer. Assoc. Petrol. Geol., Mem.*, 4, 352-366.

White, D.E., 1970: Geochemistry applied to the discovery, evaluation, and exploration of geothermal energy resources. *Geothermics, Sp. issue, 2-1*, 58-80.

White, D.E., Hem, J.D., and Waring, G.A., 1963: *Chemical composition of sub-surface waters*. In: Fleischer, M. (ed.), *Data of Geochemistry* (6th ed.), US Geol. Survey, Prof. Paper 440F.

APPENDIX I: Chemical composition of fumarole in Lake Abbe geothermal area

Location name		Fumarole
Temperature	(°C)	99
Coordinates	Northern	N11.22886
	Eastern	E41.85441
Gas phase		
Ar	% Volume	1.76
CH ₄	% Volume	3.81
H ₂	% Volume	0
N ₂	% Volume	93.11
O ₂	% Volume	1.32
CO ₂	mg/kg condensate	380
H ₂ S	mg/kg condensate	0.15
Condensate phase		
B	mg/kg	0.03
Cl	mg/kg	0.13
Na	mg/kg	0.60
δD	‰ VSMOW	-33.55
δ ¹⁸ O	‰ VSMOW	-6.08
L gas / kg condensate		0.1534

APPENDIX II: Chemical data of springs in Lake Abbe geothermal area

location name	Abbe-01	Abbe-02	Abbe-03	Abbe-04	Abbe-05	Abbe-06	Abbe-07	Abbe-12	Groundwater	Lake Abbe
Coordinates	N11.14745 E41.88131	N11.14851 E41.87919	N11.14631 E41.84077	N11.12268 E41.87017	N11.14502 E41.89090	N11.11385 E41.87503	N11.11298 E41.86997	N11.14483 E41.88167	N11.12764 E41.89419	-
Temperature (°C)	96.9	99.6	99.8	99.8	94.2	95.8	99.5	99.5	34	-
Conductivity	5580/34.1	5360/34.9	7210/30.1	3580/38.3	3380/38.4	3180/32.9	3140/32.8	5410/34.4	5190/32.3	100
B	1.47	1.39	2.06	1.01	0.99	0.98	0.95	1.57	2.25	209
Br	7.21	7.16	9.62	4.51	4.38	4.26	4.03	7.38	5.26	-
Ca	225	217	262	177	173	161	157	223	3.87	39200
Cl	1620	1600	2170	935	912	863	835	1620	1040	-
CO ₂	20.8	25.1	29.2	18	16.5	20.5	17.6	22.4	572	138
F	0.94	1.15	0.97	0.85	0.82	0.83	0.84	1.21	5.26	-
Fe	0.03	0.03	0.04	0.03	0.02	0.03	0.02	0.04	0.05	-
H ₂ S	0.02	0.01	0.03	0.03	0.03	0.02	0.04	0.03	0.04	-
K	28.3	30.5	35.4	15.7	15.5	15	14.7	25.8	22.8	-
Mg	0.18	0.38	0.51	0.06	0.05	0.05	0.08	0.17	2.45	-
Na	950	950	1310	567	558	537	527	960	1280	-
SiO ₂	118	120	104	100	97	100	103	125	40.5	-
SO ₄	328	325	426	319	308	319	308	322	573	19300
UE	3570	3630	4660	2370	2320	2200	2170	3550	3470	-
HCO ₃	28.84	34.80	40.48	24.95	22.88	28.42	24.40	31.05	793.00	-
δD	-	-25.55	-23.1	-27.29	-	-	-26.62	-	4.94	58.63
δ ¹⁸ O	-	-3.17	-3.26	-3.2	-	-	-3.22	-	1.38	9.12



UNITED NATIONS
UNIVERSITY

UNU-GTP

Geothermal Training Programme

Orkustofnun, Grensasvegur 9,
IS-108 Reykjavik, Iceland

Reports 2016
Number 18

GEOTHERMOMETRY AND QUANTIFYING OF MIXING AND WATER-ROCK INTERACTIONS IN THE NGOZI GEOTHERMAL FIELD, SW-TANZANIA

Sadock Josephat

Tanzania Geothermal Development Company

P. O Box 14801, Dar es Salaam

TANZANIA

sadockz16@gmail.com

ABSTRACT

Ngozi geothermal field is located at the southern triple junction of the East African Rift System (EARS) where the Rukwa-Tanganyika basin, the Ruaha-Mtera-Usangu segment and the Karonga-Malawi rift branches meet. Being at the triple junction the area is characterized by complex tectonic forces leading to development of structures trending in the NW, NE and NS directions. The area is characterized by the Ngozi volcano, which is one of the four volcanoes in the Mporoto-Rungwe volcanic province. Surface geology is characterized by pyroclastic ash cover while outcrops of basalts, trachy-andesite, phonolitic trachyte, alluvial sediments and sandstones occur in some parts. Geothermal surface manifestations in the area include thermal springs and altered ground and gas vents. The surface water consists of rivers, cold and warm springs, hot springs and a lake. The waters are mostly dilute (<100 ppm Cl) with the exception of the lake water that is more saline (~1500 ppm Cl) and have discharge temperatures of 30-82°C. Based on geothermometry, the maximum reservoir temperatures for the springs are ~120-130°C. Mixing model reveals that the surface thermal waters are a mixture of non-thermal water (rivers), reservoir thermal fluid, and saline lake water. Some thermal and non-thermal water show elevated CO₂ concentrations considered to originate from deep source(s). The chemistry of thermal waters shows that the concentration of main rock forming elements are controlled by water-rock interaction.

1. INTRODUCTION

Ngozi geothermal field is located in the southwest Tanzania, partly in the Mporoto Ridge Forest Reserve, which act as a hydrological divide in the area. The ridge also controls the climate of the area. The northern part of it is sparsely vegetated and warm most times of the year while the southern part has dense vegetation, rainfall and is cooler. The area is characterized by fertile soils, which have attracted intense human activities ranging from settlement, pastoralism to farming of different crops.

The area is characterized by tropical climate where dry and cold months are June to October while other months are warmer and associated with rainfall of varying quantities. High abundance of rainfall has encouraged thick vegetation in some of the prospect areas as seen in Figure 1. There is high temperature fluctuation in the area between day and nights with temperature ranging from 5 to 29°C. According to

Delalande et al. (2015), specific meteorological conditions occur within the Ngozi caldera where average annual air temperature above Lake Ngozi was 18°C with seasonal variation of $\pm 1^\circ\text{C}$ while the annual average temperature for the region is 17°C. Lake Ngozi is almost permanently covered by clouds which reduce the rate of evaporation on the lake surface.

Ngozi geothermal field has been studied by a number of academicians and researchers at different times and has been proven to have a significant geothermal resource (Kalberkamp et al., 2010; Kraml et al., 2010; Ochmann, and Garofalo, 2013; TGDC and GDC, 2015). The contribution of the present study to geoscientific knowledge of the area includes an estimation of subsurface temperatures for thermal springs around the Ngozi volcano, modelling of mixing trends of different water types in the area (lake, thermal springs and river waters) and quantification of the water-rock interactions in the area.

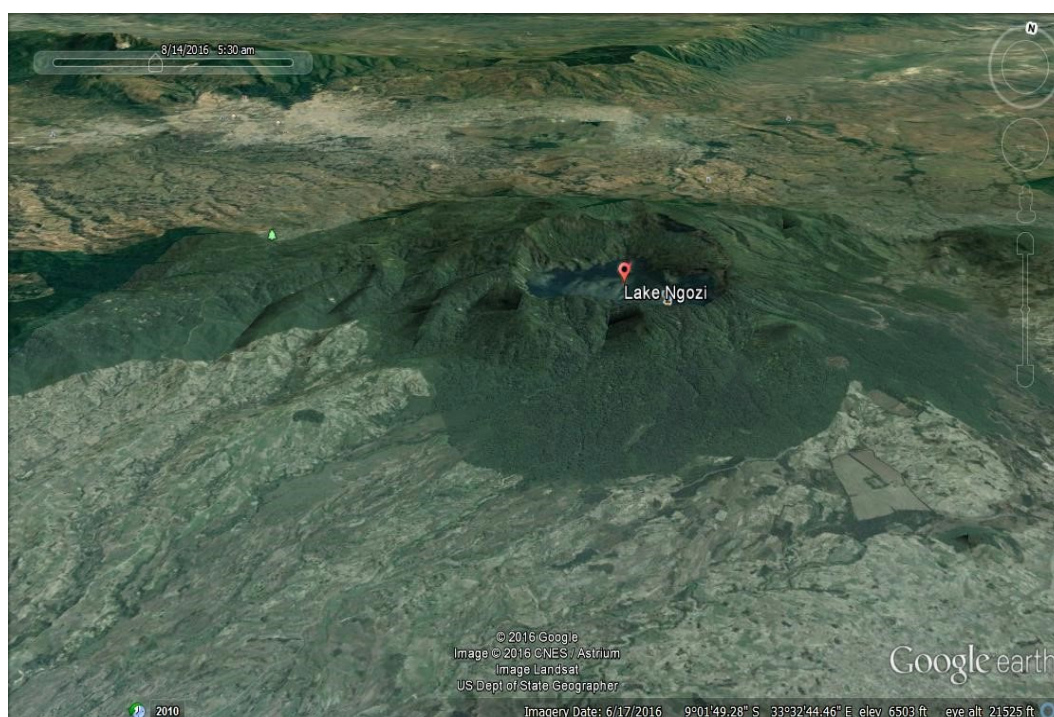


FIGURE 1: Google earth image showing topography around Lake Ngozi

2. DESCRIPTION OF THE STUDY AREA

2.1 Topography and evolution of Ngozi caldera

The topography in the Ngozi geothermal field appears to have been largely influenced by its geological setting with generally mountainous and hilly appearance, most of which are volcanic cones, domes and eruption craters (Figure 1). The Ngozi volcano marks the highest elevation in the area with the caldera rims standing at 2,260 m a.s.l. Being 2.5 km long, 1.6 km wide with a surface of about 3.1 km² and depth of 74 m, Lake Ngozi is considered the second largest Crater Lake in the East African Rift and Africa and it drains a watershed of 4.6 km² (Delalande et al., 2015).

Lake Ngozi is located inside a collapsed caldera of late Quaternary to Holocene age inside the Mporoto-Rugwe volcanic province (Fontijn et al., 2012; Delalande et al., 2015). The caldera is characterized by vertical rims, which have been collapsing over time. Landslides, soil creeping and denudation are common around the caldera rims especially on the faulted blocks (Delalande et al., 2015). The sides of the caldera are dominated by tuffs and some bands of lava all of phonolitic-trachytic and other basaltic

Surface geology at Ngozi is characterized by volcanic rocks of Plio-pleistocene to Holocene age, local low elevation areas are however filled with recent alluvial sediments. Using the Source Parameter Imaging (SPI) technique, the thickness of pyroclastic material in the area has been estimated to be at average 1000 m. This material probably forms the cap rock for the geothermal system in the area.

The heat source for the Ngozi geothermal system may be the trachytic magma chamber that was replenished during the Holocene (Kraml et al., 2010) and the event is possibly associated with the fault controlling the location of the volcano (Fontijn et al., 2010a). The geophysical survey conducted by Kalberkamp et al. (2010) concluded that the geothermal reservoir is on the NW of lake Ngozi and could be accessed by drilling 2,200 m deep wells. This is also supported by a negative Bouguer gravity anomaly correlating with the volcanic eruption centres which suggests that the heat source is located near the Usangu-Karonga accommodation zone at relatively shallow depth (Ebinger et al., 1989).

Mapping of structures in the area has been a challenge due to a thick cover of pyroclastic materials. However, several structures were mapped using remotes sensing techniques (Fontijn et al., 2010a) and field observations. The mapped structures can be grouped as lineaments, inferred faults, observed faults and alignment of eruption centres. The lineaments mapped, largely agree with the strike of regional tectonic structures in the area (Fontijn et al., 2010a) which exhibit NNE, NNW and NE trends. The NNE trending lineaments mapped east of the volcano are mimicking old basement structures (TGDC & GDC., 2015). The NW and NE lineaments appear to be following the current stress regime that reactivated NW and NE faults (Fontijn et al., 2010a) and are therefore younger. This kind of movement is expected in a region where several stresses intersect and this is true for Ngozi located at the triple junction of the regional mobile belts. The inferred faults on the east and southeast of the volcano, strike NE and NW forming several intersections with each other (Figure 3). They are inferred based on the alignment of the eruption centres from field observation. The observed faults occur to the northwest and southwest of the volcano. The downthrows of these faults are to the southeast and northeast creating a basin that pre-dates the Ngozi volcanic activity (TGDC & GDC, 2015). They are therefore bounding faults to the Ngozi geothermal system limiting the possibility of its connection with the Songwe geothermal system.

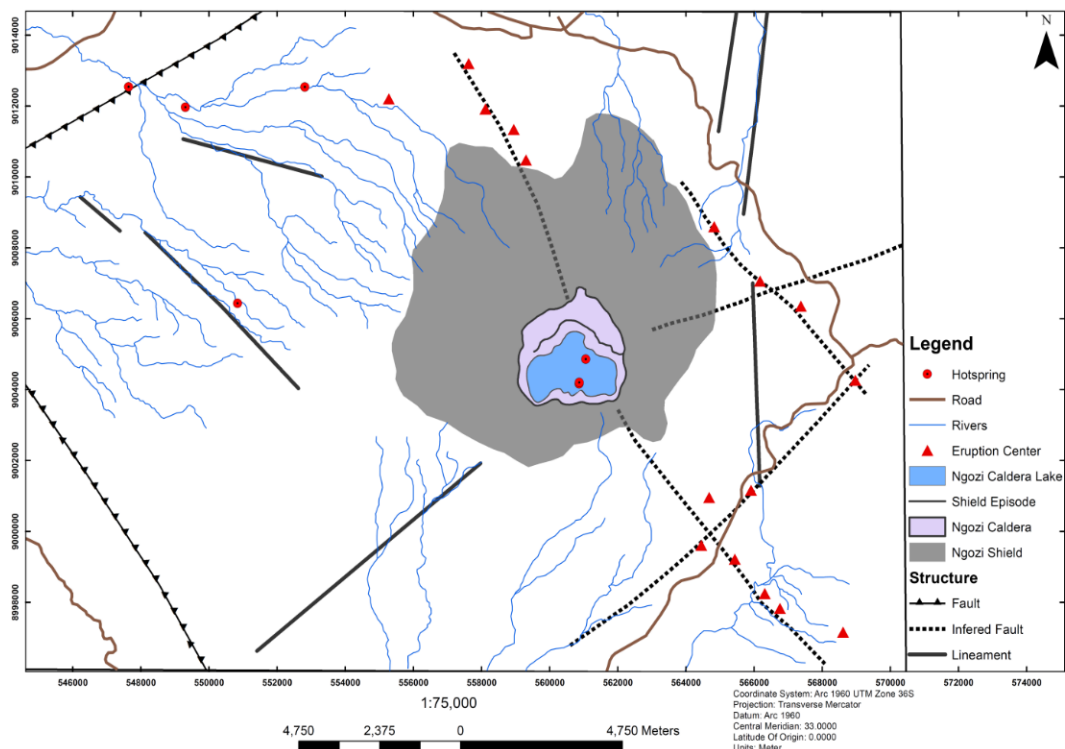


FIGURE 3: The map showing geological structures, drainage pattern and geothermal surface manifestations in the Ngozi geothermal field (TGDC & GDC, 2015)

2.3 Tectonic setting

Ngozi geothermal field is located at the triple junction of the Rukwa-Tanganyika, Usangu and Karonga-Malawi rift branches of the East African Rift System (EARS) where the Nyasa Rift split into the eastern and western branches around the stable Tanzanian Craton (Fontijn et al., 2012; Delalande et al., 2015). The western branch of the EARS in the south of Tanzania is made up by Lake Rukwa and Lake Tanganyika Rifts while the eastern branch is evidenced by the Usangu basin which trends in NE direction. The NE trending segment is poorly defined, it is punctuated by the Mtera, Ruaha and Usangu depression, but the study area is precisely located between the NW trending Rukwa-Tanganyika basin, N-S Karonga-Malawi rift basin and NE trending Usangu basin of the Ruaha-Mtera-Usangu segment (Fontijn et al., 2010a) as shown in Figure 4. The current stress regime has been interpreted by Fontijn et al. (2010a) as NE-SW compression along the NNW-SSE to N-S trending strike-slip faults.

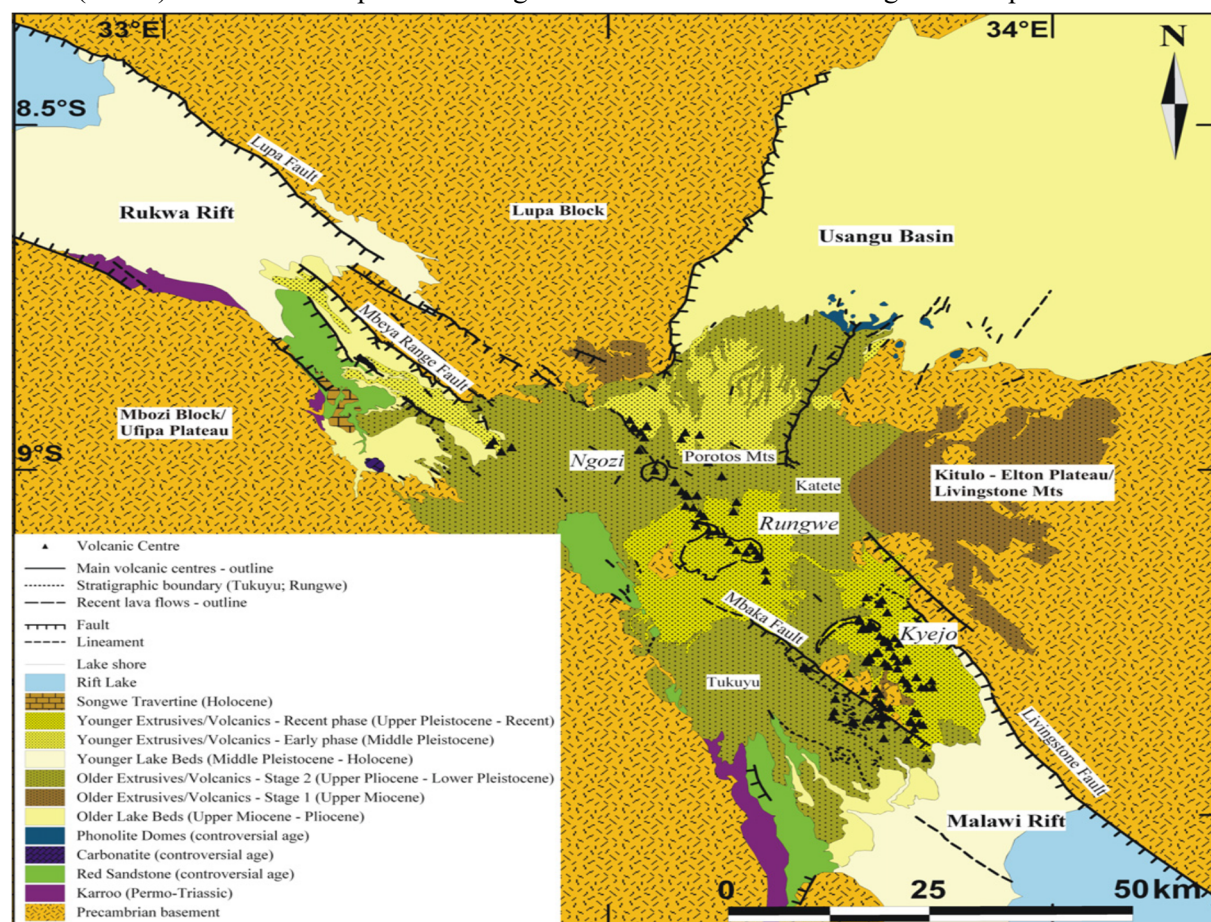


FIGURE 4: Location of the study area at the southern triple junction of the East Africa Rift System. Map taken from Fontijn et al. (2012)

The location of volcanic centres including the main volcano in the study area (Ngozi volcano) is tectonically controlled (Fontijn et al., 2010a). The Ngozi volcano is located at the intersection of active faults especially faults associated with the Usangu basin. A narrow NW-SE elongated zone of vents passes through the volcano summit and is consistent with the major NW-SE buried rift fault intersecting with NNE-SSW faults (Fontijn et al., 2012).

2.4 Hydrology

The drainage pattern of the area shows that the Mporoto ridge hosting the Ngozi caldera lake acts as a hydrological divide in the area. This is evidenced by multiple rivers draining radially away from the

volcano (Figure 3). The flow of these rivers is structurally controlled according to observation by Delvaux et al. (2010). Meteorological data shows that in the area there is more rainfall than in the other low-lying areas within the Mbeya region. Most of the rainfall at Ngozi volcano is infiltrated into the ground recharging the ground water reservoir and the deeper geothermal system (TGDC and GDC, 2015). The infiltration rates are high because evaporation and surface runoff are minimal due to the thick vegetation cover. The pyroclastic from younger eruptions ensures suitable aquifers in terms of permeability and storability below the area.

Considering the elevation of Lake Ngozi which is higher than all the nearby surroundings, recharge of the geothermal system has been considered to be local recharge by precipitation. Due to peculiar features of Lake Ngozi, it was proposed that it receives water from the geothermal reservoir below (Delalande et al., 2015). This is in agreement with the bathymetry survey results described in the next section.

2.5 Geothermal activities in the area

Geothermal activity in the area appears to be related to volcanic and plate tectonic activities which pave the way for heat, volatile and deep water uprising (Delvaux et al., 2010; Delalande et al., 2015). The hot and warm springs in the study area mainly occur in the NW and far to the SE of the Ngozi volcano and are attributed to the ascent of magmatic fluids (Delalande et al., 2011). Most thermal springs are aligned along the major NW-SE rift trend controlled by the development of the Rukwa and North Nyasa rift basins (Delvaux et al., 2010).

Geothermal surface manifestations are limited in the area, the visible surface manifestations include hot and warm springs, CO₂ vents and young volcanic eruption centres including calderas (Njue, 2015). Surface manifestations are believed to have been masked by a thick volcanic ash cover hence Ngozi can be described as an almost blind geothermal system. This volcanic ash cover is the result of plinian-style volcanic eruption that affected the area during the Holocene (Fontijn et al., 2012). The hot and warm springs of temperatures up to 30 - 82.4°C occur in low elevation, NW of Ngozi volcano. The cold CO₂ vents in the area includes the Shiwaga crater in the southeast of Ngozi volcano and CO₂ vent bubbling into Shiwaga River in the southwest of the Ngozi volcano. Fontijn et al. (2012) proposed that these gas vents imply the presence of magma at depth. Gas chemistry determination has proved that the helium and CO₂ characterizing the area are of mantle origin (de Moor et al., 2012). Due to limited geothermal surface manifestations, efforts have been employed to search for geothermal indicators that may not be directly visible at the surface. Here discussed are a bathymetry survey and sampling of rocks and lithics of the volcanic cones, crater and marls. Bathymetric survey was conducted by the Federal Institute of Geosciences and Natural Resources of Germany (BGR) in collaboration with expertise of the Ministry of Energy and Minerals of Tanzania, the Geological Survey of Tanzania and Tanzania Electric Supply Company. The survey results revealed three hot spring feeding the Ngozi caldera lake from below.

According to Ochmann and Garofalo (2013), two hot springs discharging 78°C and 89°C hot water exist south of the lake while one hot spring discharging 66°C hot water is on the north bank of the lake. These hot springs are aligned on a N-S trending line, implying that their locations is structurally controlled (TGDC & GDC, 2015). During January 2016, fieldwork samples of rocks fragments and lithics were collected from different eruption centres including volcanic cones, domes and marls for XRD and microscopic analysis. XRD analysis identified different type of clay including illite, smectite and kaolinite. The presence of illite indicates that the samples were once in the reservoir environment at temperature >200°C, also this assemblage of secondary minerals indicate hydrothermal alterations in the area. Petrographic analysis identified secondary minerals like calcite, clays, epidotes, quartz, and zeolites. These secondary minerals suggest that the sampled rocks has been in reservoir conditions.

3. METHODOLOGY

3.1 Water sampling and analysis

Sampling and analysis were conducted in the course of studies that took place in the Ngozi geothermal field at different times. For the lake water samples were collected on the lake surface and measurements for temperature, pH, EC and TDS were made along vertical profiles. In the recent geochemical study, carried out by TGDC in collaboration and GDC and UNEP in January 2016, samples collection and treatment was done according to the procedures described by Nicholson (1993). Samples for determination of pH, TDS, conductivity and total carbonate were not treated. Samples for anions analysis were only filtered using 0.45 μm filter membrane, samples for analysis of cations were filtered and acidified by 1 ml HCl. Samples for SiO_2 analysis were diluted to avoid silica polymerization while 1 ml of 0.2 M Zn-acetate was added to samples for SO_4 analysis in order to precipitate sulphur as zinc sulphide (ZnS).

Analysis of H_2S was done on site by titration using 0.1M HCl and 0.001M mercuric acetate ($\text{C}_4\text{H}_6\text{O}_4\text{Hg}$), also measurement of pH, TDS and EC were done in the field using a pH/TDS/conductivity meter. Laboratory analysis of samples was conducted in the GDC laboratory. Analysis of B, SiO_2 and SO_4 was done with the spectrophotometry method using UV-Vis, analysis of Na, K, Ca, F and NH_4 was done with the electrochemical method using ISE while analyses of Mg, Cl and TCC- CO_2 were done by using EDTA, Mohr's titration and autotitrator respectively. A total number of 70 water analyses from the lake, thermal springs and rivers were considered for this study.

3.2 Speciation, ionic balance calculations and water-rock interaction

Speciation, ionic balance also referred to as charge balance calculation and calculation of reaction quotient (Q) and equilibrium constants (K) values used for evaluation of water-rock interaction was done by using the WATCH 2.4 computer program (Bjarnason, 2010). Ionic balance was calculated in order to check the quality of data before proceeding to data processing and interpretation. Although it was applied here, CBE has received some critiques including that it takes into account the major charged ions leaving behind the neutral species and trace components (Nicholson, 1993; Arnórsson, 2000).

Data with ionic/charge balance of -10% to 10% (Figure 5), which are considered good (Arnórsson, 2000), were only 44 hence further processed in this study.

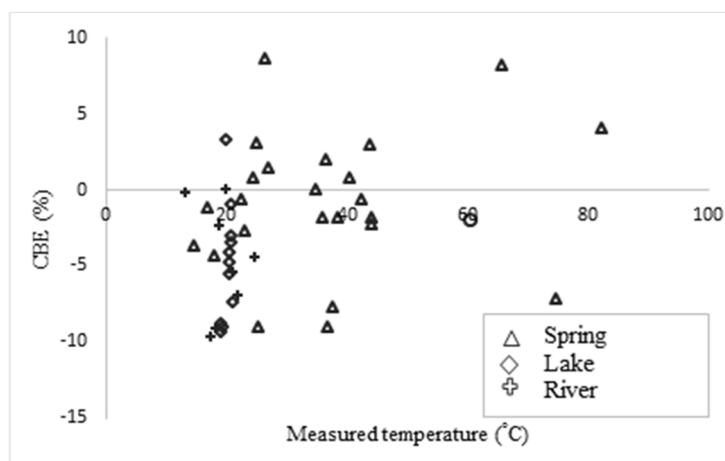


FIGURE 5: Ionic balance for the data used in this study

The log Q and log K values were used to calculate the saturation indices (SI) of the waters in respect to secondary minerals using equation 1. This calculation was performed using excel and the minerals selected were analcime, chalcedony, laumontite, Na-montmorillonite, K-montmorillonite and Ca-montmorillonite. The SI values were then used to assess if waters under investigation were under saturated, saturated or super saturated in respect to the secondary minerals.

$$SI = \log Q - \log K \quad (1)$$

where Q is the reaction quotient and K is the reaction equilibrium constant.

3.3 Geothermometry calculation

Geothermometry refers to the use of chemical composition of thermal fluids to estimate the subsurface (reservoir) temperature. There are different Geothermometry techniques used, among others solute, gas, isotope and multiple equilibrium geothermometry. Solute geothermometers are based on temperature dependent mineral-fluid equilibria. Solute geothermometers includes SiO_2 , Na/K, Na-K-Ca, Na-K-Ca (Mg-correction), Na/Li, K/Mg, Li/Mg, Na-K-Mg, Ca/Mg and SO_4/F (Fournier and Potter, 1979; Marini et al., 1986; Nicholson, 1993).

In this study, multiple equilibrium geothermometry technique was adopted to constrain the aquifer temperatures for thermal springs around the Ngozi volcano. Four thermal springs (Inyala, Ikumbi, Shongo and Ilamba) were selected for geothermometry calculation. This technique was adopted because it provides good temperature estimates and it does not involve assumption of particular fluid-mineral equilibria to exist in the subsurface as it is the case for other conventional geothermometers (Reed and Spycher, 1983; 1984). This technique involves to simultaneously look at the saturation state of different minerals and to find the mineral suites that are likely to equilibrate with water (Reed and Spycher, 1984).

The estimation of aquifer temperatures involves plotting of $\log(Q/K)$, which is the saturation index, as a function of temperature and assessment of the intersection of the curves. The saturation states of different minerals were calculated using the PHREEQC Version 3 computer program (Parkhurst and Appelo, 2015). For comparison purposes, other solute geothermometers were also used to estimate the subsurface temperature for Inyala, Ikumbi, Shongo, and Ilamba thermal springs. The geothermometers used are quartz, chalcedony, Na-K-Ca (Mg-correction) and K/Mg and their equations are presented in Table 1.

TABLE 1: Solute geothermometry equations used in this study

Geothermometers	Equation	Source
Quartz	$t(^{\circ}\text{C}) = C_1 + C_2S + C_3S^2 + C_4S^3 + C_5\log S$	Fournier and Potter, 1982
Chalcedony	$t(^{\circ}\text{C}) = \frac{1032}{4.69 - \log S} - 273.15$	Fournier, 1977
Na-K-Ca (Mg correction)	$t(^{\circ}\text{C}) = \frac{C_{Mg}}{C_{Mg} + 0.6C_{Ca} + 0.31C_K} \times 100$	Fournier and Potter, 1979
K/Mg	$t(^{\circ}\text{C}) = \frac{4410}{13.95 - L_{km}} - 273.2$	Giggenbach, 1986

$$C_1 = -4.2198 \times 10^1, C_2 = 2.8831 \times 10^{-1}, C_3 = -3.6686 \times 10^{-4}, C_4 = 3.1665 \times 10^{-7}, \\ C_5 = 7.7034 \times 10^1, S = \text{Concentration of } \text{SiO}_2, C = \text{Concentration}, L_{km} = \log C_{K^2+} / C_{Mg^{2+}}$$

3.4 Modelling of mixing

The process of quantifying mixing in this study was based on the chloride-enthalpy mixing model developed and described by Björke et al. (2015) and Stefánsson et al. (2016). The only modification made to this model in order to fit the current study is that temperature was replaced by SiO_2 concentration. The end members water types defined for quantifying mixing in this study are lake water (lk), thermal spring waters (spr) and river waters (riv). The sample with highest chloride among the analyses of lake water was chosen to represent lake water, Inyala was chosen to represent thermal springs and the Mbalizi River was chosen to represent rivers as non-thermal waters in this study. Results of mixing calculations presented in Table 2 were done using the factor D defined by the mathematical equations presented below by applying Cramer's rule.

TABLE 2: Percentage mixing between lake, thermal spring and non-thermal waters in Ngozi geothermal field

Sample location	X^{lk}	X^{spr}	X^{riv}
Thermal springs waters			
Ilamba	0.000*	0.236	0.766
Manyogopa	0.000*	0.065	0.935
Mbete	0.000*	0.005	0.995
Ivumwe	0.002	0.434	0.570
Mwasanga	0.006	0.125	0.878
Hombo	0.001	0.186	0.816
Ibayi	0.074	0.382	0.655
Songwe	0.129	0.250	0.812
Udindilwa	0.053	0.289	0.738
Songwe	0.130	0.254	0.809
Aqua Afia	0.000*	0.852	0.155
Aqua Afia	0.000*	0.947	0.061
Ikumbi	0.000*	0.873	0.134
Ikumbi	0.000	0.862	0.145
Inyala	0.000	1.000	0.008
Iyela	0.002	0.915	0.094
Shimilaa	0.003	0.431	0.574
Shongo	0.000*	0.895	0.111
Swaya	0.005	0.470	0.536
Swaya	0.005	0.485	0.521
Inyala	0.004	0.980	0.030
Shongo	0.000	0.869	0.139
Lake water			
Ngozi	0.941	0.000*	0.059 [#]
Ngozi	0.952	0.000*	0.048 [#]
Ngozi	0.977	0.000*	0.023 [#]
Ngozi	0.967	0.000*	0.033 [#]
Ngozi	0.981	0.000*	0.019 [#]
Ngozi	1.000	0.000	0.000 [#]
Ngozi	0.984	0.013	0.003 [#]
Ngozi	0.975	0.005	0.020 [#]
Ngozi	0.970	0.019	0.012 [#]
Ngozi	0.966	0.013	0.021 [#]
Ngozi	0.988	0.000*	0.012 [#]
Ngozi	0.973	0.000*	0.027 [#]
River waters			
Mchewe	0.000	0.000*	1.000 [#]
Igogwe	0.165	0.321	0.514 [#]
Songwe	0.000	0.051	0.949
Shiwaga	0.000	0.139	0.862
Gogozimba	0.018	0.288	0.723
Itembele	0.000	0.254	0.748
Kiwira	0.026	0.186	0.827
Kwamana	0.015	0.253	0.756
Mbalizi	0.000	0.000	1.000
Shiwaga	0.001	0.149	0.852

* Negative values assigned to be zero

[#] corrected values assuming $x^{lk} + x^{spr} + x^{riv} = 1$

$$D = m_{cl}^{lk}(SiO_2^{spr} - SiO_2^{riv}) - SiO_2^{lk}(m_{cl}^{spr} - m_{cl}^{riv}) + (m_{cl}^{spr} SiO_2^{riv} - m_{cl}^{riv} SiO_2^{spr}) \quad (2)$$

$$D^{lk} = m_{cl}^m(SiO_2^{spr} - SiO_2^{riv}) - SiO_2^m(m_{cl}^{spr} - m_{cl}^{riv}) + (m_{cl}^{spr} SiO_2^{riv} - m_{cl}^{riv} SiO_2^{spr}) \quad (3)$$

$$D^{spr} = m_{cl}^{lk}(SiO_2^m - SiO_2^{riv}) - SiO_2^{lk}(m_{cl}^m - m_{cl}^{riv}) + (m_{cl}^m SiO_2^{riv} - m_{cl}^{riv} SiO_2^m) \quad (4)$$

$$D^{riv} = m_{cl}^{lk}(SiO_2^{spr} - SiO_2^m) - SiO_2^{lk}(m_{cl}^{spr} - m_{cl}^m) + (m_{cl}^{spr} SiO_2^m - m_{cl}^m SiO_2^{spr}) \quad (5)$$

It follows then:

$$X^{lk} = D^{lk} / D \quad (6)$$

$$X^{spr} = D^{spr} / D \quad (7)$$

$$X^{riv} = D^{riv} / D \quad (8)$$

where m_{cl} stands for chloride concentration, SiO_2 for silica concentration, m for measured value and X for fraction composition.

The Grapher 12 computer program and Excel were used to make the ternary plots showing the mixing percentages for lake, thermal spring and river waters.

4. RESULTS AND DISCUSSION

4.1 Analytical results

Ionic balance calculation results were used to select good data used in this study. Chemical relationships between the lake, thermal spring, and river waters were assessed using plots of concentration versus measured temperature for selected chemical species (Figure 6). As listed in Table 3, springs have discharge temperatures ranging from 17 to 82°C, pH from 5.82 to 6.7 and E.C from 78 to 3700 $\mu S/cm$. River waters have temperatures from 13.3 to 23°C, pH from 5.24 to 8.4 and E.C from 168 to 1350 $\mu S/cm$. Lake water has temperatures from 19.2 to 21°C, pH of 6.4 to 7.15 and E.C of 4490 to 5300 $\mu S/cm$. Lake water displays highest chloride concentration of 1505 mg/kg, high SO_4 and low CO_2 compared to most springs. Others are significantly high SiO_2 , high sodium and highest potassium compared to most springs and river waters (Figure 6). The low content of SiO_2 could be a result of dilution of geothermal water by the cold lake water, low CO_2 could be a result of steam loss and high SO_4 could be a result of H_2S and/or SO_2 oxidation at the near surface when thermal water mixes with lake water while lowest magnesium could indicated little input of local ground water into the lake.

Thermal spring waters are characterized by variable characteristics (Figures 6) but are generally low in chloride, high in CO_2 and SiO_2 , have moderate to high sodium, potassium varies from low to high, calcium is low, magnesium is high and sulphate content of significant to high concentrations. High magnesium levels can be a result of mixing with ground water while sulphate can be a result of reactions in the near surface to surface environment.

River waters generally display the following chemical properties (Figures 6); low chloride, sodium and potassium, low CO_2 except Shiwaga River which is associated with a cold gas vent, significant content of SiO_2 and low calcium, magnesium and sulphate. The Igogwe River displays significant amounts of both chloride and CO_2 , while it has low sodium and potassium concentration because these minerals have probably reacted on the way from the lake and thermal springs to the sampling point. Other rivers display insignificant amount of lake water. Presence of lake water in the rivers was thought to be the evidence that these rivers drain the lake Ngozi water in the subsurface.

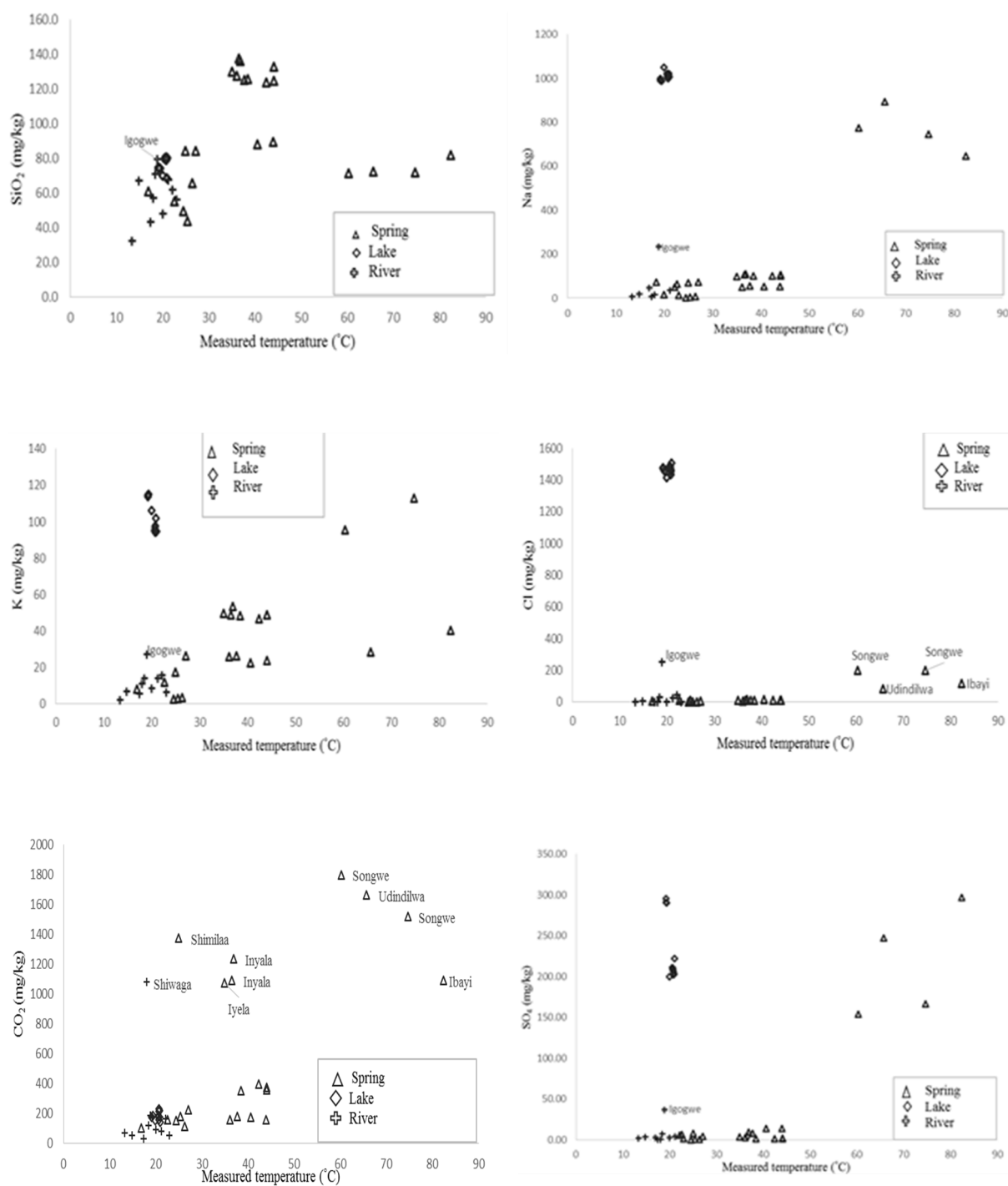


FIGURE 6: Relationship between the waters in the study area using selected chemical constituents

TABLE 3: Major chemical composition of waters in the Ngozi geothermal field, temperature (°C), EC (µS/cm), concentration in mg/kg and isotopes in ‰

		Concentrations												Isotopes	
Location	T	EC	pH	SiO ₂	B	Na	K	Ca	Mg	Cl	CO ₂	SO ₄	F	δ ² H	δ ¹⁸ O
Spring water															
Ilamba	26	239	7.2	65.7	n.a	6.3	3.4	22.2	11.9	0.72	110	0.7	0.2	-22	-4
Manyogopa	25	78	5.8	49.5	n.a	2.5	2.5	5.5	4.1	0.02	149	<dl	0.1	-23	-4.1
Mbete	25	94	5.8	43.9	n.a	4.3	2.8	5.1	4.8	0.4	178	0.3	0.12	-27	-4.5
Ivumwe	27	440	6.90	84.6	0.01	71.4	26.5	5.6	4.0	7.8	223	4.2	1.95	-35.2	-6.1
Mwasanga	23	200	7.00	55.5	0.01	64.2	11.7	3.1	1.9	10.8	156	6.3	1.5	-36.8	-6.4
Hombo	17	200	8.20	61.1	0.02	47.9	8.0	2.3	1.1	4.6	100	2.8	1.2	-37.9	-6.6
Ibayi	82	2640	6.80	82.3	1.63	646.0	40.3	12.0	2.3	116	1089	297.0	<dl	-37.9	-6.1
Songwe	60	3700	6.70	71.8	0.61	775.0	95.4	30.3	15.6	197	1796	154.0	<dl	-37.1	-6.4
Udindilwa	66	3400	7.00	72.7	0.30	893.0	28.5	13.4	3.9	82.4	1659	247.0	<dl	-41.1	-6.7
Songwe	75	3580	7.2	72.2	0.17	745.4	113.0	20.9	15.6	199	1517	166.4	7.7	n.a	n.a
Aqua Afia	42	650	6.70	124.0	n.a	100.0	46.9	15.5	5.8	8.2	393	1.0	1.05	-39.6	-5.7
Aqua Afia	44	640	6.90	133.0	0.01	106.0	48.7	12.1	4.5	9	358	1.7	0.83	-38.9	-5.8
Ikumbi	39	670	7.00	126.0	n.a	102.0	48.3	15.5	5.7	8.3	351	0.9	1.08	-39.9	-5.9
Ikumbi	44	670	6.80	125.0	n.a	102.0	48.7	13.5	4.9	8.7	374	1.4	0.83	-39.4	-5.7
Inyala	37	1000	6.10	138.0	0.01	107.0	48.9	50.7	26.8	9.5	1089	4.0	0.56	-37	-6.3
Iyela	35	980	6.10	130.0	0.02	99.2	49.8	50.9	26.2	11.9	1075	3.4	0.66	-37.8	-6.6
Shimilaa	25	380	5.40	84.3	0.00	68.9	17.4	4.7	2.2	9.5	1370	8.2	0.86	-35.9	-6.3
Shongo	36	340	7.40	128.0	n.a	49.0	26.0	9.0	2.9	4.4	158	2.5	0.39	-35.4	-5.8
Swaya	41	380	6.80	88.1	0.00	51.7	22.4	11.3	4.6	12.8	175	13.9	0.46	-32.5	-5.9
Swaya	44	360	7.20	89.5	0.01	52.1	23.8	13.1	4.8	12.5	154	14.0	0.43	n.a	n.a
Inyala	37	975	6	136.3	0.40	109.0	53.4	43.9	13.3	14.7	1231	9.0	0.56	n.a	n.a
Shongo	38	325	7.1	125.6	0.70	54.9	26.2	7.7	1.1	8.8	176	8.1	0.28	n.a	n.a
Lake water															
Ngozi	20	4820	7.15	70.1	1.40	1050	106	4.2	0.9	1416	149	200.00	<dl	n.a	n.a
Ngozi	21	5300	6.70	68.7	1.41	1020	102	3.8	0.9	1433	178	203.00	6.49	-10.7	-1.4
Ngozi	19	4670	6.7	75.1	n.a	991	115	3.9	1	1470	178	291.00	8	-11	-1.4
Ngozi	19	4690	6.7	74.2	n.a	987	115	3.8	0.9	1456	184	290.00	7	-11	-1.3
Ngozi	19	4690	6.7	74.2	n.a	1000	114	3.9	0.9	1477	172	295.00	7	-12	-1.3
Ngozi	21	4510	6.8	80.2	n.a	1008	94.8	3.9	0.9	1505	138	222.30	12.4	-10	-1.2
Ngozi	21	4500	6.5	80.9	n.a	1018	96.2	3.9	0.9	1481	156	16.68	12.0	-11	-1.4
Ngozi	21	4500	6.4	79.8	n.a	1009	94.4	3.9	0.9	1468	226	16.46	11.9	-10	-1.3
Ngozi	21	4490	6.4	80.9	n.a	1021	94.5	3.9	0.9	1460	217	203.20	11.5	-11	-1.2
Ngozi	21	4490	6.4	80.2	n.a	1000	95.2	3.9	0.9	1455	179	16.55	11.8	-12	-1.4
Ngozi	21	4510	6.4	79.6	n.a	1022	95.1	4	0.9	1487	195	16.42	12.1	-10	-1.4
Ngozi	21	4510	6.4	79.2	n.a	1015	97.6	34	0.9	1464	209	202.30	12.1	-10	-1.4
River water															
Mchewe	13	168	8.40	32.4	<dl	8.2	2.0	16.2	5.9	0.4	72	1.6	0.18	-37.5	-6.4
Igogwe	19	1350	8.20	79.9	0.24	234.0	27.3	12.8	9.6	252	186	36.5	9.05	-28.7	-5.1
Songwe	20	200	8.00	48.3	0.02	16.6	8.6	14.4	6.4	1.9	91	2.7	0.49	-33.1	-5.4
Shiwaga	23	200	6.90	56.6	0.00	14.1	6.5	3.3	1.3	2.3	55	1.0	0.35	-30.6	-5.6
Gogozimba	18	358	7.9	71.3	n.a	73.0	13.8	2.1	1.1	30	118	7.0	9.05	-34	-5.5
Itembele	15	109	7.5	67.5	n.a	18.7	6.8	5.0	1.3	3.08	53	3.1	0.73	-35	-5.6
Kiwira	22	334	6.4	62.0	n.a	49.6	15.6	3.8	3.0	42	164	5.6	1.93	-33	-5.5
Kwamana	21	184	8.1	67.9	n.a	35.0	14.0	7.0	3.9	26	80	4.4	0.56	-38	-6
Mbalizi	17	55	7.4	43.4	n.a	7.7	5.3	1.9	0.8	0.8	29	0.5	0.24	-39	-6.1
Shiwaga	18	110	5.2	57.5	n.a	14.8	10.9	9.3	3.8	3	1082	0.8	0.2	-29	-5.6

n.a = not analysed

<dl= below detection limit

4.2 Classification of waters

In this study classification of waters was done using the Cl-SO₄-HCO₃ and Na+K-Ca-Mg ternary diagrams. The Cl-SO₄-HCO₃ ternary diagram classify the geothermal waters on the basis of the abundance of major anions. In Figure 7, Lake Ngozi water plots close to the field of mature water (Cl vertex) while the thermal springs plot close to the field of peripheral water (HCO₃ vertex).

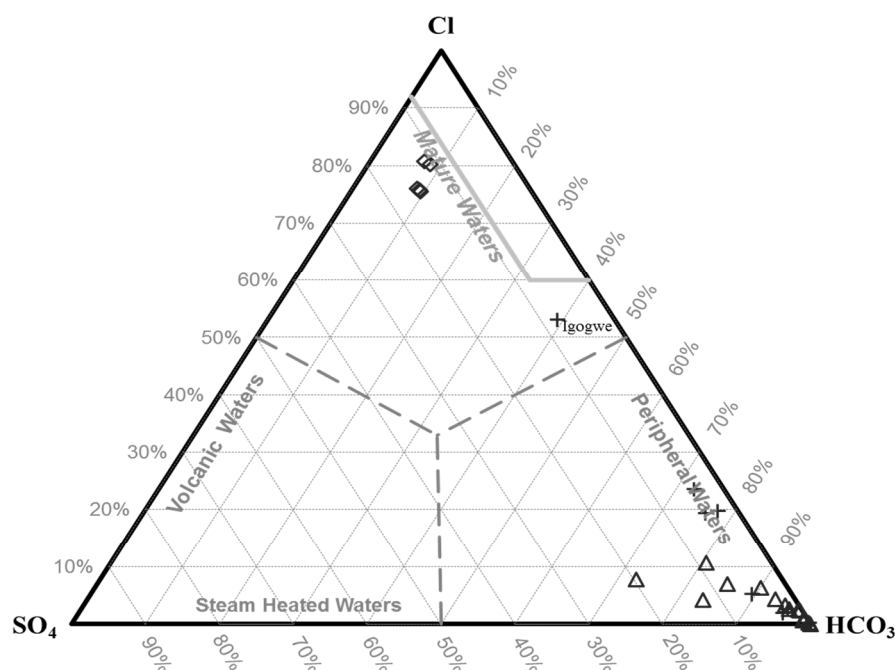


FIGURE 7: A Cl-SO₄-HCO₃ ternary plot showing classification of waters in the Ngozi geothermal field. Diamond shapes represent lake water, triangles thermal spring waters and crosses river waters

The chemistry of river waters depends on the mixing of lake and thermal spring waters. Most rivers plot in the HCO₃ field which can be interpreted as a result of heavy mixing with thermal spring waters. The Igogwe River has a significant amount of Lake Ngozi water hence it plots close to the lake water.

In Figure 8, Lake Ngozi water plots at the Na + K vertex, most thermal springs plot close to the Na + K vertex while three thermal spring plot in the Ca-Mg field. River waters also plot close to the Na + K vertex as they are mixed with lake and thermal spring waters.

From this classification, it can be concluded that lake waters are of Na - Cl type and thermal spring waters are of Na - HCO₃ type. Ilamba, Manyogopa and Mbete springs are heavily mixed with non-thermal ground waters hence display Ca (Mg) - HCO₃ composition.

The geothermal brine feeding Lake Ngozi could come from the deep geothermal reservoir which is associated with magmatic gases like Cl, H₂S, SO₂ and CO₂ from a deep degassing magmatic body. This brine was not studied in detail in this work. The HCO₃ waters of thermal springs can be a result of a degassing magmatic body from where CO₂ find its way to the surface through the deep structures and mix with thermal waters. In springs fed by shallow circulation of meteoric water, HCO₃ can be a result of dissolution of carbonate bearing rocks in the area.

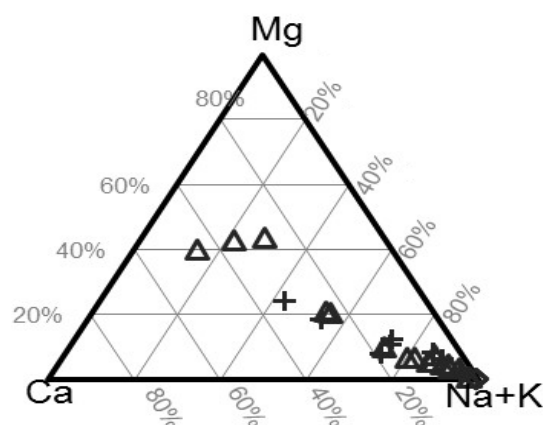


FIGURE 8: The Na+K-Mg-Ca ternary diagram showing classification of waters in the Ngozi geothermal field. Diamond shapes represent lake water, triangles thermal spring waters and crosses river waters

4.3 Geothermometry

In this study, four thermal springs namely Inyala, Ikumbi, Shongo and Ilamba were selected from the Ngozi geothermal field based on their chemistry and their subsurface temperatures were estimated. The $\log (Q/K)$ versus temperature plots that were used to estimate the subsurface temperatures for these thermal springs are presented in Figures 9-12. According to Reed and Spycher (1983), the temperature

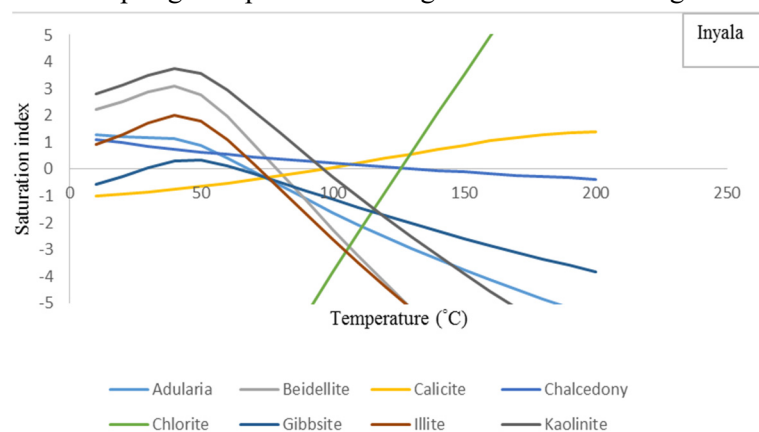


FIGURE 9: Multiple equilibrium geothermometry plot for Inyala thermal spring

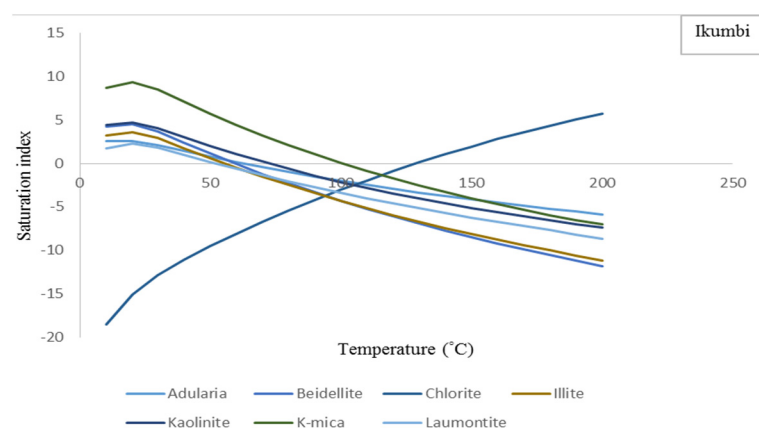


FIGURE 10: Multiple equilibrium geothermometry for Ikumbi thermal spring

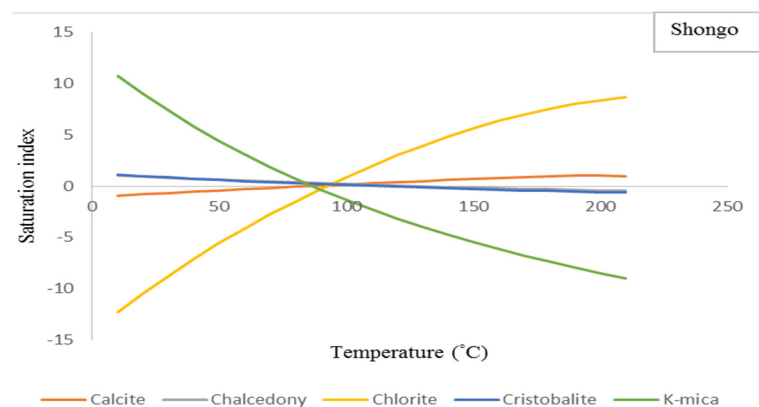


FIGURE 11: Multiple equilibrium geothermometry plot for Shongo thermal spring

at which the $\log (Q/K)$ curves intersect each other at a saturation index ($SI=0$) is the equilibration temperature. Reed and Spycher (1984) described that the characteristic convergence of $\log (Q/K)$ curves for the equilibrium assemblage to zero at the temperature of equilibration establishes the basis for determining a mineral assemblage and temperature of equilibration of natural geothermal waters, fluid inclusions, hot spring waters etc. from analysis of water alone. Reed and Spycher (1984) also point out that the plots of $\log (Q/K)$ behaviour can be used to assess boiling, mixing and lack of equilibrium.

For Inyala thermal spring there is no single convergent temperature as can be seen on Figure 9, the curves for adularia, beidellite, gibbsite and illite intersect the equilibrium line at the lowest temperature of about 70-80°C, calcite and kaolinite curves intersect the equilibrium line at 100°C and chalcedony and chlorite curves intersect the equilibrium line at about 125°C. Therefore, the subsurface temperature for Inyala spring can be estimated to be 70-125°C. For Ikumbi thermal spring (Figure 10), adularia, beidellite, illite, kaolinite and laumontite curves converge at 60-80°C, K-mica and chlorite intersect the equilibrium curve at 100°C and 130°C respectively, the subsurface temperature can therefore be estimated in the range of 60°C to 130°C. For Shongo spring Figure 11, K-mica, chlorite, cristobalite, chalcedony and calcite converge and intersect the equilibrium line at 85-100°C. For Ilamba spring (Figure 12) calcite, chalcedony, gibbsite and

illite converge and intersect the equilibrium line at 70-80°C. In this plot calcite has two intersections, it also converges and intersects with kaolinite and quartz at 100°C hence the temperature for Ilamba spring can be estimated to be 70-100°C.

As pointed out earlier, in multiple equilibrium geothermometry technique the temperature at which the log (Q/K) curves converge and intersect the equilibrium line (SI=0) is the subsurface temperature, but most of the springs studied have no single convergence temperature. As

seen from Figures 9, 10, 11 and 12, only Shongo spring display a small range of convergence temperatures, others shows a wide range of temperature which limit the probability of estimating the true temperature because the distinct clustering of the curves for many minerals in a short temperature range gives high probability that the estimated temperature is correct (Reed and Spycher, 1984). The dispersion and broadness of the log (Q/K) curves has been explained by Reed and Spycher (1984) as a possible result of water and/or CO₂ loss and/or mixing, resulting in changes concentration of components and pH changes. The convergence points for the springs has also moved down the equilibrium line which has also been explained by Reed and Spycher (1984) to be a result of mixing with near surface waters. Therefore, it was necessary to quantify the mixing processes affecting the thermal springs in the study area.

However, lack of single convergence temperature can also be a consequence of other issues like poor water analysis, poor thermodynamic data and lack of equilibrium for a particular spring (Reed and Spycher, 1984). Analysis of the geothermometry plots also reveal that different mineral curves have different slopes, this can be interpreted as a consequence of difference in temperature sensitivity of minerals. The minerals with high slope are highly sensitive to temperature changes while the minerals with low slopes are less sensitive to temperature changes.

For comparison, other solute thermometers were also used to estimate the subsurface temperatures for the selected thermal springs and the results are presented in Table 4. Chalcedony, K/Mg and Na-K-Ca with Mg correction give fairly comparable temperatures to the multiple equilibrium geothermometry results while quartz geothermometer gives generally temperatures of about 20°C higher.

TABLE 4: Temperature estimated by different geothermometry techniques for selected springs around the Ngozi volcano in the Ngozi geothermal field

Spring	Multiple equilibrium geothermometers (Reed and Spycher, 1983 and 1984)	T_chalcedony (Fournier, 1977)	T_quartz (Fournier and Potter, 1982)	T_K/Mg (Giggenbach, 1986)	T_Na-K-Ca (Mg corr) Fournier and Potter, 1979
	(°C)	(°C)	(°C)	(°C)	(°C)
Inyala	80-120	132	156	116	125
Shongo	70-110	126	151	100	98
Ikumbi	70-140	125	151	120	139
Ilamba	80-100	86	115	81	62

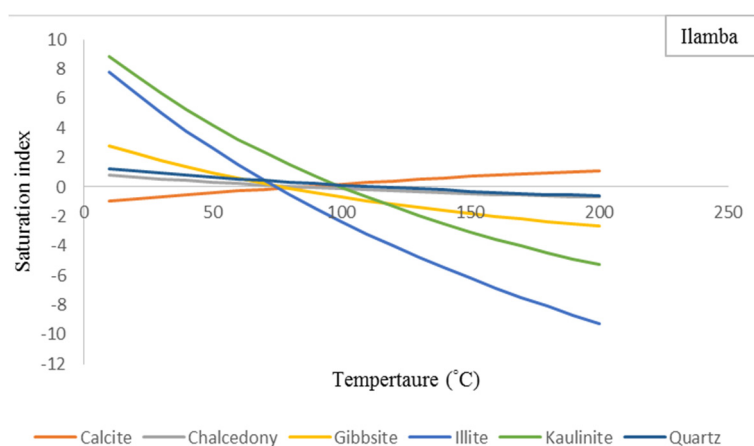


FIGURE 12: Multiple equilibrium geothermometry plot for Ilamba thermal spring

4.4 Mixing

The composition and temperature of geothermal fluids does not remain unchanged as it ascends from the geothermal reservoir to the surface, the changes can be a result of depressurization boiling, conductive heat loss and/or mixing with cold near surface or surface water (Fournier, 1977; Reed and Spycher, 1984; Arnórsson, 1985; Arnórsson, 2000; Björke et al., 2015; Stefánsson, 2016). On ascent to the surface waters can re-equilibrate, depending on different factor like flow rate, the flow path, initial reservoir temperature and kinetics of chemical reactions taking place (Fournier, 1977). Mixing which is the subject of this section occurs when the ascending geothermal fluids meet the shallow ground or surface water sometimes referred to as dilution (Arnórsson, 1985; Arnórsson, 2000). Evaluation of mixing and reactions occurring in the up flow is important in order to understand the subsurface conditions, evaluate potential geothermal utilization and assess the environmental impacts that can arise upon extraction of geothermal fluids (Truesdell and Fournier, 1977; Arnórsson, 1985; Stefánsson et al., 2016).

The thermal springs in the study area are characterized by relatively high silica concentrations compared to discharge temperature, low pH and high total carbonate. This situation has been described by Arnórsson (1985) as a chemical evidence of mixing. According to Arnórsson, the chemistry of mixed waters tends to be under-saturated with respect to calcite and is also characterized by lack of equilibrium with secondary minerals which is a characteristic feature of geothermal water. Looking at Figure 13, it is evident that thermal springs in the study area have been affected by mixing.

The modification to the model described by Björke et al. (2015) and Stefánsson et al. (2016) was made because some of the thermal spring with low discharge temperature indicate higher SiO_2 concentration (Figure 6) and chalcedony geothermometry temperature (Figure 14) than springs with higher discharge temperature. This was thought to be the result of cooling upon mixing with cold non-thermal waters because the concentration of SiO_2 is directly proportional to temperature.

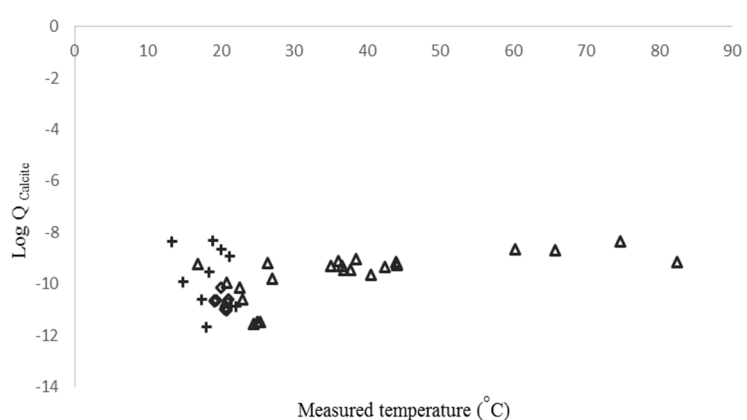


FIGURE 13: The state of calcite saturation relative to sampling temperatures in the Ngozi geothermal field.

Diamond shapes represent lake water, triangles spring water and crosses river water

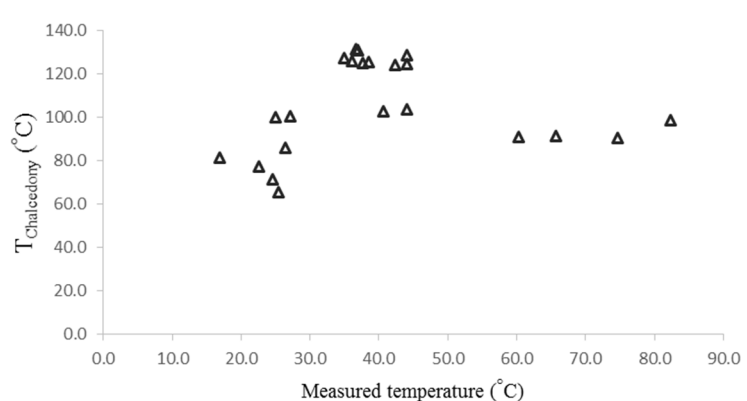


FIGURE 14: Chalcedony geothermometry relative to measured temperature for thermal spring waters in the study area

According to Fournier (1977) and Arnórsson (2000) the dissolved silica in most natural waters is not affected by common ion effect, formation of complexes and loss of volatile components. For this reason, silica can be regarded as a conservative upon mixing and chloride has also been considered to be non-

reactive upon mixing and tend to remain in solution and do not enter into the secondary minerals structure (Mahon, 1970; Stefánsson et al., 2016).

The mixing modelling results (Table 2) indicate that thermal springs close to the Ngozi volcano are generally not mixed with lake water. Songwe spring shows about 13% mixing with lake water however the structural setting in the area limits this possibility due to the presence of bounding fault between two described in section 2.2 of this study. Therefore, its slight similarity with lake water can be explained by an interaction with rocks with similar chemistry. Ibayi and Udindilwa springs display about 7% and 5% mixing with lake water respectively and are the only thermal springs in the area that can be postulated to have a relationship with the lake. However thermal springs display varying degrees of dilution by non-thermal waters in the area where most springs are heavily mixed while some are moderately mixed. Only Inyala, Iyela and Aqua-Afia springs show insignificant mixing with non-thermal waters.

Most rivers also do not show mixing with lake water. However, Igogwe, Kiwira, Gogozimba and Kwamana rivers display about 16.5%, 2.6%, 1.8% and 1.5% mixing with lake water, respectively. This implies that these rivers are draining Lake Ngozi water in the subsurface because the lake has no surface outlet. In the Ngozi geothermal field most rivers show mixing with thermal springs water in the area of varying degrees (Table 2; Figure 15 and 16). Only Mbalizi and Mchewe rivers shows no mixing with thermal spring waters while Songwe River shows insignificant mixing with thermal spring waters.

4.5 Water-rock interactions

The chemistry of geothermal water is not only modified by mixing, depressurization boiling or conductive heat loss during ascent to the surface, but also by water rock interaction (Björke et al., 2015, Stefánsson et al., 2016). Water-rock interaction leads to alteration of rock, hence formation of alteration mineralogy, as well as to increased concentration of rock forming elements in geothermal water especially when the flow rate of the spring is not high enough. Auko (2014) pointed out that water-rock interaction can be viewed as an acid-base reaction where water containing dissolved gasses act as acid while the rock forming minerals act as base and they react to a stable or metastable secondary minerals. As seen in Table 3 and Figure 6, most of the thermal springs are enriched with rock forming elements like SiO₂, Na, K, Ca and Mg. In the study area, there are few alteration minerals identified as discussed in section 2.5 of this study probably due to thick cover of pyroclastic ash as discussed in section 2.2 of this study. However, the intensity of surface activities like alteration can be limited by mixing described in the section 4.4 above and limited residence time of fluids.

From Figure 17, it can be noted that the waters have been interacting with Na-Al silicates and Ca-Al silicates, which belong to the zeolites group of minerals, with Na-Ca-Al-Mg silicates belonging to smectite group of minerals and with silica bearing rocks. Because most of the thermal spring waters are super saturated with respect to Na-Al mineral analcime, all the waters are super saturated with respect to chalcedony. Lake water is saturated with respect to Ca-Al minerals and montmorillonites while thermal springs and rivers are generally super saturated with respect to Ca-Al minerals and montmorillonites. The observation that waters in the study area have been interacting with zeolites, minerals of the smectite-group and silica bearing rocks is in agreement with secondary mineral assemblage identified in the area as described in part 2.5 of this study.

Some river waters in the study area which are considered non-thermal waters are enriched with rock forming elements and hence saturated and/or super saturated with respect to the secondary minerals. This is in agreement with the mixing calculation which shows that most rivers are significantly mixed with thermal spring waters hence it can be concluded that the concentration of rock forming elements like Si, Na, K, Ca and Mg is controlled by water-rock interaction.

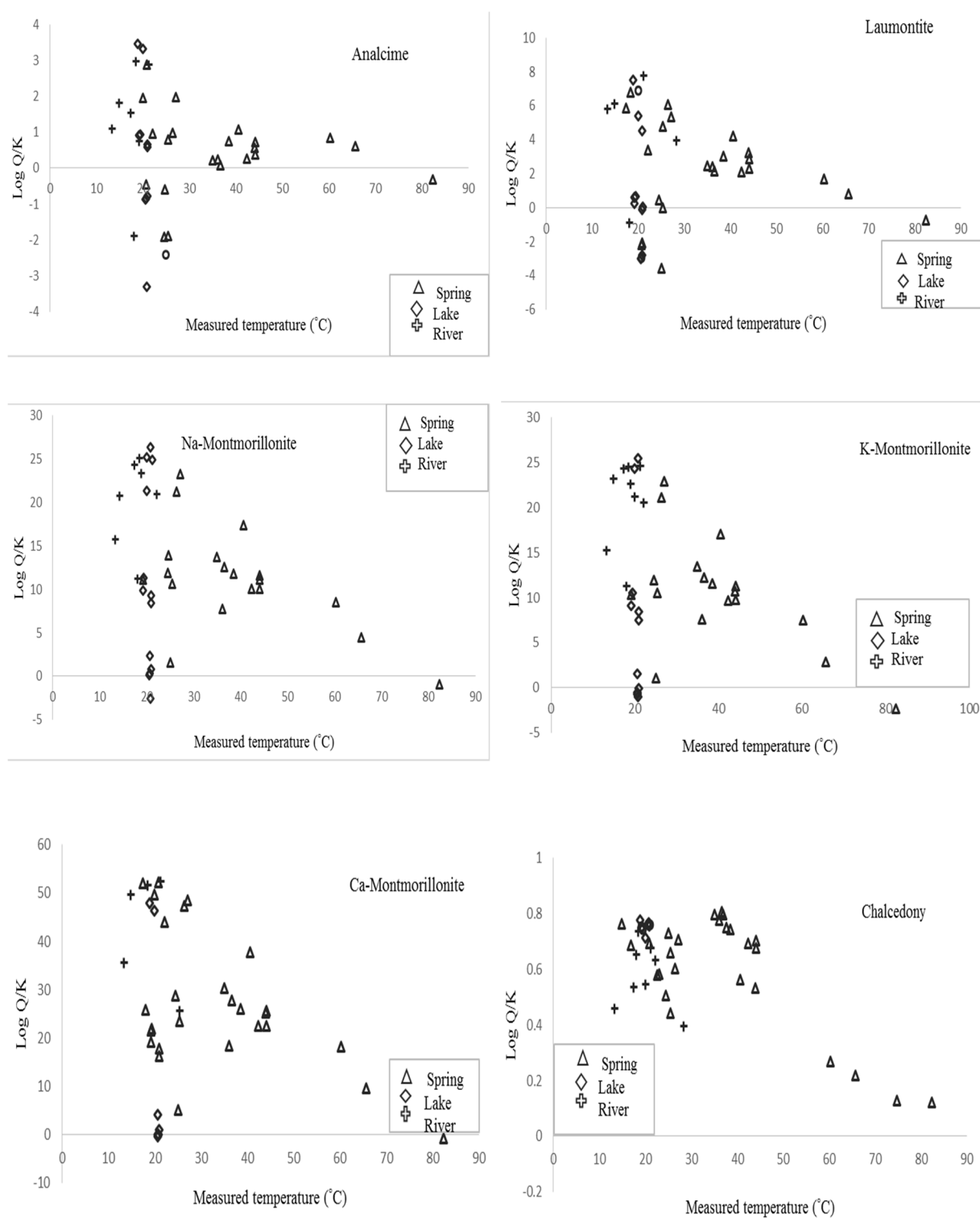


FIGURE 17: Saturation state of waters in the Ngozi geothermal field with respect to secondary minerals

5. CONCLUSIONS

The waters of different types (thermal springs, rivers and lake waters) in the Ngozi geothermal field were studied. Geothermometry temperatures for selected springs were estimated using the multiple equilibrium technique and other solute geothermometers. The results of geothermometry shows that the maximum temperatures to be expected in the subsurface of thermal springs around Ngozi volcano is 120-130°C. From these results, it can be concluded that the thermal springs around the Ngozi volcano maybe fed by meteoric water percolating to the subsurface through permeable structures and get heated up. After attaining reasonable temperatures and becoming less dense, the water rises to the surface as thermal springs in the fairly shallow circulation (Figure 18).

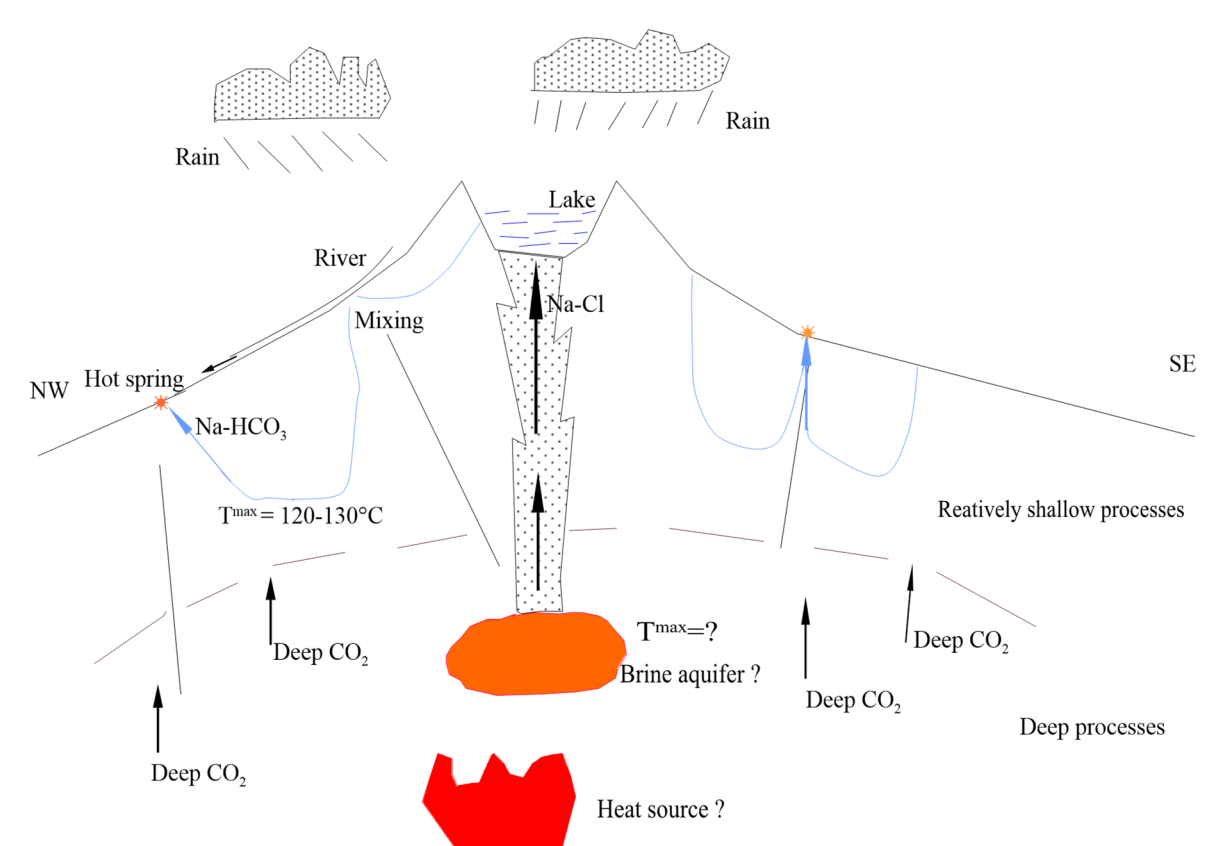


FIGURE 18: Conceptual model of the processes controlling water chemistry in the Ngozi geothermal field

Considering the EC values of the springs it can be concluded that the springs have had relatively low residence time that was not enough to dissolve much ions from the rocks. The idea of shallow circulation is also supported by very low concentration of volcanic gases like HCl and H₂S in some of the studied springs. For these springs, the source of HCO₃ fluids can be explained as a result of dissolution of carbonate bearing rocks in the shallow depth as evidenced by Ilamba, Manyogopa and Mbete springs which are characterized by Ca (Mg) - HCO₃ composition which was thought to be a result of calcite dissolution.

Mixing between the lake, thermal springs and river waters was quantified based on the model developed and described by Björke (2015) and Stefánsson (2016) with little modification. The results show that some rivers including Igogwe, Kiwira, Gogozimba and Kwamana contain lake water in the order of 16.5%, 2.6%, 1.8% and 1.5% respectively while other rivers do not show mixing with lake water. However, most rivers show mixing with thermal spring waters. On the other hand, thermal springs show insignificant to no mixing with lake water but significant mixing with non-thermal water. The chemistry

of thermal spring waters and rivers mixed with thermal spring waters shows that the concentration of main rock forming elements are controlled by water-rock interaction and these waters have been interacting with zeolites, smectite and silica bearing minerals.

The cold gas vents in the area can be interpreted as a result of deep degassing and transport to surface. Why this gas is cold can be explained in two ways: firstly, the gas cools by expansion when leaving the magma body towards the surface, and the second possibility is that this gas interacts on its ascent with groundwater aquifers and cools before reaching the surface.

ACKNOWLEDGEMENTS

I would like to thank the UNU-GTP and the government of Iceland at large for giving me the opportunity to attend the six months course in Chemistry of Thermal Fluids. My gratitude also goes to my company, Tanzania Geothermal Development Company Limited for granting me time to attend this course.

My appreciation also goes to all staffs of UNU-GTP; Mr. Lúdvík S. Georgsson, Mr. Ingimar G. Haraldsson, Ms. Þórhildur Ísberg, Mr. Markús A. G Wilde and Ms. Málfríður Ómarsdóttir for their generous support and care they have been providing when needed throughout the training. Staff of ÍSOR and all lecturers are appreciated for their support and/or transferring their knowledge and experience during lectures and other meetings also Ms. Rósa S. Jónsdóttir for proving the references whenever required. UNU Fellows for the year 2016 are also appreciated for their various support. My landlady during my time in Iceland Ms. Þórkatla Jónsdóttir is also appreciated.

I am also thankful to my final project supervisor Prof. Andri Stefánsson of Faculty of Earth Sciences, University of Iceland, for his patience and guidance throughout preparation of this work. The knowledge gained from him is highly appreciated and will help me further in my career. Mr. Finnþogi Óskarsson and Halldór Ármannsson are also appreciated for always having time for discussion whenever requested.

I also thank Almighty God for his grace and mercy that kept me safe and healthy throughout the training. Last but not least, my heart felt gratitude is to my lovely wife and my family who have been supporting me in different ways throughout the course.

REFERENCES

Arnórsson, S., 1985: The use of mixing models and chemical geothermometers for estimating underground temperature in geothermal systems. *J. Volc. Geotherm. Res.*, 23, 299-335.

Arnórsson, S. (ed.), 2000: *Isotopic and chemical techniques in geothermal exploration, development and use. Sampling methods, data handling, interpretation*. International Atomic Energy Agency, Vienna, 351 pp.

Auko, L.O., 2014: Evaluation of fluid-mineral interaction in the Menengai geothermal syatem, Central Rift, Kenya. Report 8 in: *Geothermal training in Iceland 2014*. UNU-GTP, Iceland, 39-64.

Bjarnason, J.Ö., 2010: *The chemical speciation program WATCH, version 2.4*. ÍSOR – Iceland GeoSurvey, Reykjavik, website: www.geothermal.is/software.

Björke, J. K., Stefánsson, A. and Arnórsson, S., 2015: Surface water chemistry at Torfajökull, Iceland – Quantification of boiling, mixing, oxidation and water-rock interaction and reconstruction of reservoir fluid composition. *Geothermics*, 58, 75-86.

de Moor, J.M., Fischer, T.P., Sharp, Z. D., Hilton, D.R., Barry, P.H., Mangasini, F., and Ramirez C., 2012: Gas chemistry and nitrogen isotope compositions of cold mantle gases from Rungwe Volcanic Province, southern Tanzania. *Chemical Geology*, 339, 30-42.

Delalande, M.M., Bergonzini, L., Gherardi, F., Guidi, M., Andre, L., Abdallah, I. and Williamson, D., 2011: Fluid geochemistry of natural manifestations from the southern Poroto-Rungwe hydrothermal system (Tanzania): Preliminary conceptual model. *J. Volc. Geotherm. Res.*, 199, 127-141

Delalande, M.M., Gherardi, F., Williamson, D., Kajula, S., Kraml, M., Noret, A., Abdallah, I., Mwandapile, E., Massault, M., Majule, A., and Bergonzini, L., 2015: Hydrogeochemical features of Lake Ngozi (SW Tanzania). *J. African Earth Sciences*, 103, 153-167.

Delvaux, D., Kraml, M., Sierralta, M., Wittenberg, A., Mayalla, J. W., Kabaka, K., Makene, C and GEOTHERM working group, 2010: Surface exploration of a viable geothermal resource in Mbeya area, SW-Tanzania. Part I: Geology of the Ngozi –Songwe geothermal system. *Proceedings of the World Geothermal Congress 2010. Bali, Indonesia*, 7 pp.

Ebinger, C.J., Deino, A.L., Drake, R.E and Tesha, A.L., 1989: Chronology of volcanism and rift basin propagation: Rungwe Volcanic province, East Africa. *J. Geophys. Res.*, 94 15,785-15,803.

Fontijn, K., Delvaux, D., Ernst, G.G.J., Kervyn, M., Mbede, E., and Jacobs, P., 2010a: Tectonic control over active volcanism at a range of scales: Case of the Rungwe volcanic province, SW Tanzania; and hazard implications. *J. African Earth Sciences*, 58, 764-777.

Fontijn, K., Ernst, G.G.J., Elburg, M.A., Williamson, D., Abdallah, E., Kwelwa, S., Mbede, E., and Jacobs, P., 2010b: Holocene explosive eruption in the Rungwe volcanic province, Tanzania. *J. Volc. Geoth. Res.*, 196, 91-110.

Fontijn, K., Williamson, D., Mbede, E. and Ernst, G.G.J., 2012: The Rungwe volcanic province, Tanzania – a review. *J. African Earth Sciences*, 63, 12-31.

Fournier, R.O., 1977: Chemical geothermometers and mixing model for geothermal systems. *Geothermics*, 5, 41-50.

Fournier, R.O., and Potter, R.W. II, 1979: Magnesium correction to the Na-K-Ca geothermometer. *Geochim. Cosmochim. Acta*, 43, 1543-1550.

Fournier, R.O., and Potter, R.W. II, 1982: A revised and expanded silica (quartz) geothermometer. *Geoth. Res. Council Bull.*, 11-10, 3-12.

Giggenbach, W.F., 1986: Graphical techniques for the evaluated water/rock equilibration conditions by use of Na, K, Mg and Ca contents of discharge water. *Proceedings of the 8th New Zealand Geothermal Workshop, Auckland, NZ*, 37-43.

Kalberkamp, U., Schaumann, G., Ndonde, P.B., Chiragwile, S.A., Mwano, J.M and GEOTHERM Working Group, 2010: Surface exploration of a viable geothermal resource in Mbeya area, SW Tanzania. Part III: Geophysics. *Proceedings of the World Geothermal Congress 2010. Bali, Indonesia*, 6 pp.

Kraml, M., Mnjokava, T.T., Mayalla, J.W., Kabaka, K., and GEOTHERM Working Group., 2010: Surface exploration of a viable geothermal resource in Mbeya area, SW Tanzania. Part II: Geochemistry. *Proceedings of the World Geothermal Congress 2010. Bali, Indonesia*, 8 pp.

Mahon, W.A.J., 1970: Chemistry in the exploration and exploitation of hydrothermal systems. *Geothermics, Sp. issue 2-2*, 1310-1322.

Marini, L., Chiadini, G., and Cioci, R., 1986: New geothermometers for carbonate-evaporite geothermal reservoir. *Geothermics, 15-1*, 77-86.

Nicholson, K., 1993: *Geothermal fluids: chemistry and exploration techniques*. Springer-Verlag, Berlin, 268 pp.

Njue, L., 2015: Geothermal manifestations. Presented at “Short Course X on Exploration for Geothermal Resources”, UNU-GTP, KenGen and GDC, Lake Naivasha, Kenya, UNU-GTP SC-21, 17 pp.

Ochmann, N., and Garofalo, K., 2013: *Geothermal energy as an alternative source of energy for Tanzania*. GEOTHERM Project, final technical report, 156 pp.

Parkhurst, D.L., and Appelo, C.A.J., 2015: *Description of input and examples for PHREEQC, version 3 - A computer program for speciation, bath-reaction, one-dimensional transport, and inverse geochemical calculations*. USGS, USA, computer software.

Reed, M.H., and Spycher, N.F., 1983: Calculated pH at high temperature in hydrothermal waters with application to geothermometry. *Paper presented at 4th Internat. Symposium on Water-Rock Interaction, Extended Abstracts*, 401-404.

Reed, M.H., and Spycher, N.F., 1984: Calculation of pH and mineral equilibria in hydrothermal water with application to geothermometry and studies of boiling and dilution. *Geochim. Cosmochim. Acta*, 48, 1479-1490.

Stefánsson, A., Keller, N.S., Robin, J.G., Kaasalainen, H., Björnsdóttir, S., Pétursdóttir, S., Jóhannesson, H., and Hreggvidsson, G.O., 2016: Quantifying mixing, boiling, degassing, oxidation and reactivity of thermal waters at Vonarskard, Iceland. *J. Volcanology and Geothermal Res.*, 309, 53-62.

TGDC and GDC, 2015: *Geological and structural mapping of Ngozi geothermal field*. Tanzania Geothermal Development Company, Ltd., and Geothermal Development Company, Ltd., Kenya, report of field mapping.

Truesdell, A.H., and Fournier, R.O., 1977: Procedure for estimating the temperature of a hot water component in a mixed water using a plot of dissolved silica vs. enthalpy. *US Geol. Survey, J. Res.*, 5, 49-52.



UNITED NATIONS
UNIVERSITY

UNU-GTP

Geothermal Training Programme

Orkustofnun, Grensasvegur 9,
IS-108 Reykjavik, Iceland

Reports 2016
Number 19

FINANCIAL VIABILITY OF DEVELOPING 35 MW OF GEOTHERMAL POWER AT MENENGAI FIELD, KENYA

Moses Kipsang Kachumo

Geothermal Development Company – GDC

P.O BOX 100746-00101

Nairobi

KENYA

mkachumo@gdc.co.ke; kachumo@yahoo.com

ABSTRACT

Developing a geothermal project from the initial stage to the operation stage is difficult, complex, expensive and time consuming. Most investors and independent power producers in the geothermal sector prefer a viability assessment to be undertaken and a decision made based on the assessment's results which include investment advantages and the risks involved in the project.

Currently, the Geothermal Development Company (GDC) is developing a 105 MW (3 x 35 MW) geothermal project in the Menengai geothermal field in Kenya. The purpose of this study is to present a financial viability assessment for the development of a 35 MW single unit at the Menengai geothermal field by using an Excel based profitability model.

The calculated internal rate of return obtained from the model for the total cash flow and net cash flow are more than the total marginal attractive rate of return of 10% and the equity discounting rate of 15%, respectively. That fulfils the criteria that the internal rate of return should be greater than the marginal attractive rate of return. Based on the results of the model, the project is viable and worth investing.

1. INTRODUCTION

1.1 Background

Kenya is endowed with a vast geothermal resource potential. Most of these resources are located along the Kenyan Rift that transects the country from north to south. Studies reveal that the geothermal potential in the country exceeds 10,000 MWe. Detailed surface studies have been done in most of the country's prospects which comprises of Suswa, Longonot, Olkaria, Eburru, Menengai, Bogoria and Baringo-Silali prospects and their geothermal systems identified as summarised by Omenda (2012).

Currently, the country's installed generation capacity adds up to 2,295 MWe, the geothermal share is about 630 MW and is mainly produced from the Olkaria geothermal field which is operated by Kenya Electricity Generating Company (KenGen).

To fast track and accelerate the development of geothermal prospects in the country, the Government of Kenya formed the Geothermal Development Company (GDC). The company has the task to accelerate the development of geothermal energy in the country by prospecting, exploring, assessing, developing and marketing geothermal energy in Kenya and to support the government initiative to raise the requisite development funds.

Through GDC the Government of Kenya has assumed its responsibility to prepare bankable projects that will be eligible to receive financing from financial institutions and also to address the various issues to fulfil the criteria for financial approval.

In the long term, GDC is mandated to develop 5,000 MWe from geothermal resources in accordance to the country's development blueprint, Vision 2030. In the short term, the government has set up an acceleration program to generate over 5,000 MW of electricity from various energy sources in the country. Under this program, the Government of Kenya recognizes geothermal as the lowest cost source of power and has mandated GDC to develop a total of 810 MW from geothermal resources in the country.

1.2 Project objective

The main aim of this study is to analyse and present a financial viability assessment for the development of a 35 MW single flash geothermal power plant unit at the Menengai geothermal field using a Microsoft Excel-based profitability assessment model developed by Jensson (2016). The model is made up of different spreadsheets, each with different specific functions and all the spreadsheets are interconnected. The tasks in the spread sheets in the model include project cost breakdown, summary, investment, operations, cash flows and profitability sheets.

The financial viability assessment model will help determine the following:

- Project investment requirements;
- Working capital requirements;
- Net present value;
- Internal rate of return;
- Risk assessment of the project.

The profitability model will specifically assess whether the project will generate acceptable financial returns. Also, sensitivity impact analysis is done to determine the effects of change on energy sales price, sales quantity, cost of equipment and operation and maintenance cost of the project to the overall project profitability.

1.3 Existing energy policy framework in Kenya

1.3.1 Feed-in-tariff

In January 2010, the Kenyan government published its new feed-in-tariffs (FIT) to provide investment security to renewable electricity generators, reduce administrative and transaction costs, and encourage private investors. The 2010 feed-in-tariff was revised and became effective in 2012 indicating a tariff of 0.0088 USD/kWh for power plants with installed capacity ranging from 35-70 MW. Some of the revisions in the policy include standardization of Power Purchase Agreements (PPAs), connecting small scale renewables and change in feed-in-tariff levels. The policy document addressed the need for a long term PPAs between generators and off-takers (Ministry of Energy, 2012).

1.3.2 Energy act

Kenya's energy policy of 2004 encourages implementation of indigenous renewable energy sources to enhance the country's electricity supply capacity. The policy is implemented through the Energy Act of 2006, which provides for mitigation of climate change through energy efficiency and promotion of renewable energy (Government of Kenya, 2016).

1.3.3 Public Private Partnerships (PPP) Framework

The Government of Kenya recognizes that the required funds that are needed to fully support the country's development agenda and to meet the infrastructure deficit will require involvement of the private sector, hence Public Private Partnerships (PPP). PPP arrangements offer an opportunity for the country to attract enhanced private sector participation in financing, building and operating infrastructure services and facilities (National Council for Law Reporting, 2013).

1.3.4 Least Cost Power Development Plan (LCPDP)

Kenya's power industry generation and transmission system planning is undertaken on the basis of a 20 year rolling Least Cost Power Development Plan (LCPDP) which is updated every year. The plan reviews the load forecast based on changed pertinent parameters, commissioning dates for committed projects, costs of generating plants and transmission system requirements. It incorporates key lessons learnt and the need to incorporate population, urbanization and efficiency gains and technology in undertaking the demand forecast and capturing of potential new demand arising from the vision 2030 flagship projects and other investor projects (Energy Regulatory Commission, 2013).

1.3.5 Land policy

The national land policy was formulated to provide an overall framework and define the key measures required to address the critical issues of land administration, access to land, land use planning, restitution of historical injustices, environmental degradation, conflicts, unplanned proliferation of informal urban settlements, outdated legal framework, institutional framework and information management. It also addresses constitutional issues such as compulsory acquisition and development control as well as tenure (Ministry of Lands, 2009). It recognizes the need for security of tenure for all Kenyans (all socio-economic groups, women, pastoral communities, informal settlement residents and other marginalized groups).

1.3.6 Environmental policy

The goal of the environmental policy is to improve the quality of life for present and future generations through sustainable management and use of the environment and natural resources with the objective of providing a framework for an integrated approach to planning and sustainable management of Kenya's environment and natural resources (Ministry of Environment, Water and Natural Resources, 2013).

1.4 Project location

The Menengai geothermal field is a high temperature field and the third geothermal field to be developed in Kenya after Olkaria and Eburu geothermal fields. Menengai is a large caldera volcano inside a rift valley. The project is located in Nakuru County, about 10 km north of Nakuru town and 180 km from Nairobi, Kenya (Figure 1).

GDC is currently developing the first 105 MW power plant generating geothermal electric power from the Menengai field which is expected to be made of three units of each 35 MW. GDC has already

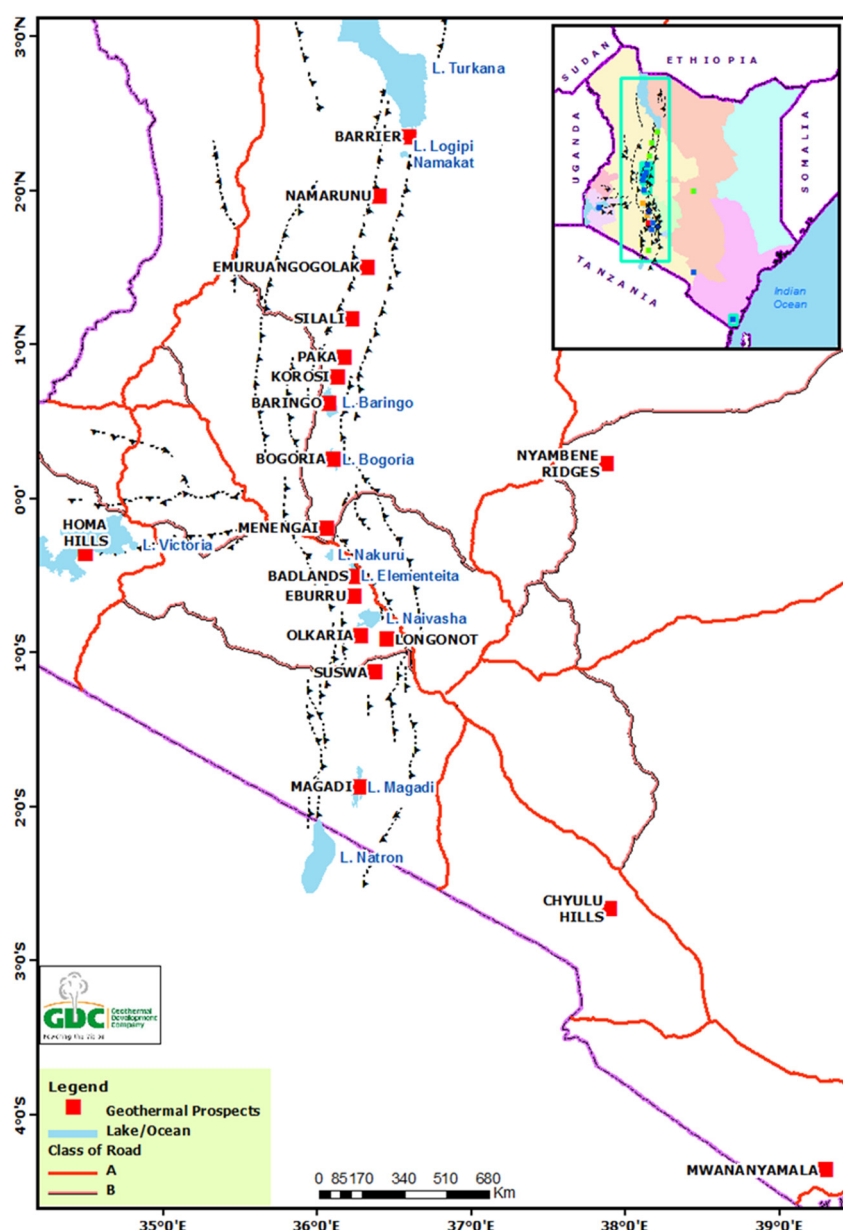


FIGURE 1: Location of Menengai geothermal field

1.5 Project scope and timelines

1.5.1 Project scope

The scope of my study will involve estimating the cost components of each project phase, analyse the investment required and determine financial viability of the project using the profitability model.

Mwangi (2005) describes that a geothermal project consists of successive development phases that aim at locating the resource, confirming the capacity of the reservoir, drilling of wells, construction of the steam gathering system, and building of the power plant and its associated structures.

The 35 MW Menengai project is developed in five main development phases and each phase' activities are described in Table 1.

procured three Independent Power Producers (IPPs) to develop and operate 35 MW modular power plants for a period of 25 years each.

The development of the 105 MW power plant project is guided by Kenya's current institutional and legal framework within the sector. The guidelines include the Vision 2030, Feed in Tariff (FiT), Least Cost Power Development Plan (LCPDP), Kenyan laws and the Public Private Partnerships Framework among other laws.

For the realization and acceleration of geothermal development in Kenya, the Government of Kenya is in the process of developing geothermal prospectors which will act as a guide in determining the development and implementation models for the various undeveloped geothermal fields in the country.

TABLE 1: Project detailed description

Project phase	Detailed description
Reconnaissance	Involves collecting information from previous geological, geochemical or geophysical studies made in an area and which relate to mapping of volcanic activities, hot springs, steam jets, groundwater boreholes and even known traditional utilization of geothermal resources.
Detailed surface exploration	The main purpose of undertaking detailed surface exploration program is to cost-effectively minimize risks related to resource temperature, depth, productivity, and sustainability prior to appraisal drilling. Successful drilling of exploration and appraisal wells would culminate to bankable feasibility study report which is a key document required when seeking project financing.
Infrastructural development	It involves construction of main access roads, establishment of waterline system (pipeline and pump stations), well pads and drilling fluid recirculation pond.
Steam field development	In this stage, three to four exploration wells are drilled to prove the presence of steam. The drilling of the exploration wells is followed by the drilling of appraisal wells after which a feasibility study is carried out. Positive outcomes of the feasibility studies lead to drilling sufficient production wells for the project.
Power plant construction and its auxiliaries	This stage involves design, tendering, manufacturing and installation of the power plant. The steam from the wells will be connected to a 35 MW single flash power plant through a steam gathering system. The power from the 35 MW project will be evacuated through a 132 kV transmission line to the nearest national grid.

2. LITERATURE REVIEW

A viable project is a project that is able to generate income and is in a position to meet its operating and investment costs over its operation lifetime and generate an acceptable rate of return. Most of the investors/Independent Power Producers (IPPs) in the geothermal business prefer project assessment to be done to determine its financial viability and to estimate if the investment advantages outweigh the risks involved in the project before making an investment decision.

Determining project profitability assessment is important for investors, government institution and financiers in the geothermal business in order to make critical project decisions on either to accept or reject a project.

Some previous studies have been done to determine the financial viability of developing geothermal power projects.

Bloomquist (2004) presented a study on economic factors impacting direct use geothermal development viability and indicated that economic factors that ultimately determine the viability of a geothermal project are extremely complex and highly variable. The study proposed that each and every project should be evaluated at every stage based on the results obtained as more and more information becomes available.

Kiptanui (2015) presented a study on financial assessment of commercial extraction of sulphur and carbon dioxide from geothermal gases in Menengai geothermal field in Kenya. The study focussed on the commercial extraction of elemental sulphur and carbon dioxide (CO₂) from non-condensable gases (NCG) and applied an excel based profitability assessment model to determine the profitability of the

project by using gas chemistry data from 11 production wells in Menengai with the main objective of generating an additional stream of revenue to the Geothermal Development Company (GDC) and also eliminate the environmental effects of hydrogen sulphide (H_2S) and CO_2 .

Geirdal (2013) developed a method which is using wellhead technology to generate early revenues during the construction phase of geothermal projects. The study presented the importance of wellhead power plants being utilized at early stages of the development and showed how this can increase the Net Present Value (NPV) of the project and make the project viable and attractive.

Hance (2005) presented a study on factors affecting costs of geothermal development. The study explains how the capital costs of a geothermal project are very site and resource specific. The resource temperature, depth, chemistry and permeability are major factors affecting the cost of the power project. The study showed further how the resource temperature of a geothermal system will determine the power conversion technology (steam vs. binary) as well as the overall efficiency of the power system. Other factors which affect the capital costs include site accessibility and topography, local weather conditions, land type and ownership are additional parameters affecting the cost and time required to bring the power plant online.

3. PROJECT VIABILITY ASSESSMENT

The primary objective of investing in a project is to earn profit. In geothermal project development, profits are normally directly related to the set electricity price per kWh and the quantity of energy sales delivered in comparison with the cost of producing it.

Other factors that influence the cost of production include project financing structure, initial capital investment required and loan costs which are normally directly related to the money interest rate and the length of the repayment period.

Therefore, before investors engage in a geothermal project, a viability assessment is advisable. That means that the capital invested in a project must have a potential to generate an economic return to investors, at least in comparison to other similarly risky investments, i.e. the return on investment needs to be equal or higher.

The financial viability analysis is important because it helps to evaluate the economic viability of an investment and guides investors in making prudent investment decisions. The financial model used in this project is mainly based on the lectures notes of the profitability assessment and financing lectures at the UNU-GTP (Jensson, 2006). The model is used to evaluate financial conditions of project, operating performance of the investment and forecasting its future condition of the investment.

3.1 Methodology and data used

In order to assess project viability, project cost components were broken down according to project phases and factors influencing these costs were considered at each project phase. This study defines the various project phases according to the sequence of development including the various parameters that contribute to its costs. Most of the costs used in the analysis were obtained from existing literature, vendors, geothermal developers/experts, own estimates, and UNU-GTP training notes. The detailed description of the project phases is outlined below.

3.1.1 Exploration costs

Exploration is the initial development phase in any geothermal development. This phase seeks to locate a geothermal resource that can provide sufficient energy to run a geothermal power plant and produce electricity. In order to explore geothermal subsurface resources, several scientific studies have to be done and these include geological, geochemical, and geophysical studies. The scientific studies help to determine the subsurface thermal structure of the geothermal system and use the information obtained to estimate the temperature of the reservoir as well as the source of the fluid and to locate active up flow zones.

The cost of geothermal surface exploration varies considerably from one geothermal field to the other. These variances are attributed to the size of the geothermal area to be explored, geological settings of the field, accessibility of the area, and availability of previous studies.

3.1.2 Number of wells required

To determine the number of wells to generate 35 MW of net electricity, several assumptions were made to fill data gaps and to simplify the analysis. All the assumptions are based on conservative estimates. To do the analysis, a percentage success rate probability was assumed on exploration appraisal and production drilling. The simplified calculated analysis is based on the assumption that each well will yield 5 MW of average net electricity production and well success rate are assumed as shown in Table 2.

TABLE 2: Number of wells required for the project
Author's estimates and assumptions

Activity	Success rate	Well productivity (MW)	No of wells	Power output (MW)
Exploration wells	50%	5	3	8
Appraisal wells	75%	5	3	11
Production wells	80%	5	4	16
Subtotal (MW)				35
Excess steam	10%			3
Total power output				38
Reinjection wells			2	
Total number of wells			12	

As the table above shows, an estimated 10 wells are required for the 35 MW project and 2 additional wells are dedicated to reinjection purposes.

3.1.3 Drilling plan and strategy

The main aim of drilling is to determine geothermal resource availability, hydrothermal capacity and chemical characteristics of the resource. To access the resource, drilling must be done to a certain depth. The costs of drilling vary from one region to the other. This is attributed to some drilling parameters which include hard formation, loss of circulation during drilling, loose formation and changing lithology in the wells at various depths. According to Kipsang (2013), the cost of drilling geothermal wells is estimated to be about 40% of the total investment cost for a new high temperature geothermal field.

To mitigate delays and other challenges in drilling, the following assumptions, strategies, and plans were prepared to keep the drilling program on track during the scheduled drilling period:

Drilling days

- Drilling of one well is expected to take 80 days which includes the moving of the rig.
- A Project Implementation Team (PIT) will be formed to closely supervise drilling operations and monitor the services rendered by drilling contractors to ensure that the drilling operations run smoothly and according to plan.
- There will be technical meetings (weekly, monthly, quarterly and as need arises) between GDC and the service contractor to address drilling challenges/issues.

Drilling costs

- The drilling cost considered per well for this project is GDC's average drilling expenses of 3.5 M USD (Million US Dollars). The assumption is that GDC will use its own rigs. The cost can be higher if hired rigs are used.

Supply of drilling materials

- GDC ensures sufficient provisions of drilling consumables i.e. drilling diesel and cement. The procured hardware goods will be stored in GDC stores, from where the material will be transported to the drill sites when required. This will ensure that the supply contractor has control on the supply to eliminate delays.

Drilling services contractors

- GDC will use its own rigs for the drilling operation of this project.
- In order to mitigate delays in the drilling operations, GDC will hire a contractor which will be responsible for providing the following services:
 - Directional drilling
 - Cementing
 - Fishing
 - Air drilling

3.1.4 Steam pipeline system

The location of the wells determines the length of the steam pipeline system to be constructed. Other parameters which dictate the length of the steam gathering system including site conditions such as environmental conditions, flowing pressure, topography, chemistry of the fluids and pipeline layout greatly affect the selection of a pipeline system.

The costs of the steam gathering system vary depending on the distance from the production and injection wells to the power plant. In the 35 MW Menengai project, most of the wells are located within a radius of approximately 0.5-1 km from the proposed power plant site. A reinjection pump is not required since the flow of brine will be facilitated by gravity.

3.1.5 Power plant

In order to determine the size of the power plant, the reservoir capacity of the field should first be evaluated. This is achieved by undertaking a field feasibility study to obtain information on the resource availability and to estimate if it can sustain the required power generation.

The U.S. Department of Energy (2008) Geothermal Market Report indicates that the cost of geothermal power production is very capital-intensive with high first-cost and risk, with fairly low operating and maintenance costs and a high capacity factor which makes the geothermal energy technology one of the most economical base load power generation options available. The report estimated developmental costs for a typical 50 MWe geothermal power plant at USD1700 per kW. In this study, power plant costs and other project costs were calculated based on the available literature, UNU-GTP training notes, own communication with turbines developers/experts and own estimations.

The power plant technology type considered for the project is a single flash type since Menengai is a high temperature geothermal field. The assumption in the analysis is that GDC will undertake the project development all the way from exploration to power plant construction.

3.1.6 Transmission availability and nearness to the grid

The power generated from the 35 MW Menengai project will be relayed to switchyard using a 132 kV single circuit transmission line network. The switchyard will be interconnected with a switchyard at a bay installed with the controls, protection and supervisory facilities – including communication systems. A substation will be put up for the purpose of boosting power before joining the national pylon grid. The substation will be mounted with equipment such as transformers, circuit breakers, isolators, and switchgears and a transmission line constructed to evacuate from the proposed power station through Rongai to connect to the Olkaria-Lessos transmission line which lies approximately 15 km from the proposed 35 MW Menengai power plant.

3.1.7 Project permitting costs

According to the Ministry of Environment, Water and Natural Resources (2013), geothermal projects have to comply with existing project legislative requirements related to environmental and construction issues. In Kenya, the National Environmental Management Authority (NEMA) was established as the principal institution of government charged with the implementation of all policies relating to the environment, and to exercise general supervision and coordination over all matters relating to the environment. In consultation with the lead agencies, NEMA is empowered to develop regulations, prescribe measures and standards and to issue guidelines for the management and conservation of natural resources and the environment.

The act provides for environmental protection through environmental impact assessment, environmental audit and monitoring, environmental restoration orders, conservation orders and easements. According to NEMA, the cost of an Environmental Impact Assessment (EIA) is prescribed at a fee of the total cost of the project and with no upper capping required for the processing of an EIA license. Apart from an EIA, other project permits include feasibility studies, generation license, and geothermal and land lease which are part of other permitting requirements in geothermal development.

3.2 Project cost breakdown

To estimate and determine the costs of the project, the project phases were further broken down into its related activities and the cost of each activity was computed as in Table 3.

In order to use the costs estimates above in the model, the cost breakdown is divided into three main project components which are buildings, equipment and others costs:

- i. Buildings: Access roads, well pads and wells, water storage tanks and supply system, and resettlement;
- ii. Equipment: Power plant, steam gathering system and transmission line and substation;
- iii. Others: Detailed surface studies, environmental studies, feasibility study and other permits and licenses.

The calculations indicated the average cost of developing 35 MW to be **USD3,865/Kw**, this includes connection to the grid. The percentage cost breakdown of the project per phase is as shown in Figure 2.

TABLE 3: Project cost breakdown

	Activities	Units	Unit Price (USD)	Total Price (USD)	USD/kW	%
1	Preparation Work:					
	Access roads	20	40,000	800,000		
	Well pad site preparation	12	90,000	1,080,000		
	Water pipeline system (approx. 20 km)	20	60,000	1,200,000		
	Water pump station and storage tanks	1	380,000	940,000		
	Subtotal:			4,020,000		
	Engineering, supervision and commissioning	10%		402,000		
	Contracting and other fees	15%		663,300		
	General contingency	10%		508,530		
	Total Preparation Cost			5,593,830	160	4%
2	Drilling					
	Exploration wells	3	3,500,000	10,500,000		
	Appraisal wells	3	3,500,000	10,500,000		
	Production wells	4	3,500,000	14,000,000		
	Re-injection wells	2	3,500,000	7,000,000		
	Total Drilling Cost			42,000,000	1,200	31%
3	Steam pipeline system:					
	Piping (12*500 m)	6,000	1,000	6,000,000		
	Separator and vent stations (piping, vessels, earthworks and foundation)	1	3,500,000	3,500,000		
	Electrical and control equipment for well field	1	100,000	100,000		
	Reinjection System:					
	Piping system	1000	700	700,000		
	Reinjection pumping	0	800,000			
	Subtotal:			10,300,000		
	Engineering, supervision and commissioning	10%		1,030,000		
	Contracting and other fees	15%		1,699,500		
	General contingency	10%		1,302,950		
	Total pipeline cost			14,332,450	409	11%
4	Power plant:					
	Mechanical:					
	Turbine-generator, incl. lube oil unit, control etc.	1	16,000,000	16,000,000		
	Mechanical balance of plant	1	12,000,000	12,000,000		
	Compressed air system, cranes, platforms etc.	1	600,000	600,000		
	Electrical & Control					
	Main transformer and aux transformers	1	3,000,000	3,000,000		
	Local connection to the grid	15	250,000	3,750,000		
	Control & Instrumentation	1	1,800,000	1,800,000		

	Activities	Units	Unit Price (USD)	Total Price (USD)	USD/kW	%
5	Electrical balance of plant	1	7,000,000	7,000,000	2,014	52%
	Civil works					
	Earthworks	1	1,500,000	1,500,000		
	Buildings and building services	1	5,000,000	5,000,000		
	Subtotal:			50,650,000		
	Engineering, supervision and commissioning	10%		5,065,000		
	Contracting and other fees	15%		8,357,250		
	General contingency	10%		6,407,225		
	Total Power Plant Costs			70,479,475		
	Other Permitting Cost				82	2%
	Generation license	1	2,000	2,000		
	Feasibility study	1	1,000,000	1,000,000		
	Resettlements	20	25,000	500,000		
	Detailed surface studies	1	1,000,000	1,000,000		
	ESIA licenses for drilling and power plant	2	200,000	400,000		
	Total			2,902,000	82	2%
	TOTAL PROJECT COST			135,307,755	3,865	100%

In order to obtain total cost of project activities, some other additional costs were calculated in Table 3 and calculated as shown below:

- Engineering: 10% of the total cost
- Contracting fees: 15% of (total cost + engineering)
- Contingency: 10% of (total cost + engineering + contracting fees)

3.3 Operation and maintenance (O&M) costs

Operation costs include all the expenses related to the operation of the power plant, steam gathering, and transmission line.

Maintenance costs are related to labour costs and all expenses related to the maintenance of all the equipment i.e. steam gathering system pipes, pumps, turbines, vehicles, buildings, etc. Therefore, operation and maintenance costs of a geothermal power plant correspond to all expenses needed to keep the power system in good working condition. According to Paul Ngugi (2012), the rate of operation and maintenance is fairly low for geothermal, given the operation and maintenance costs are 0.00763 USD per kWh in other Kenyan power plants. Therefore, the cost of O&M considered for this project is calculated based on the country's Least Cost Development Plan.

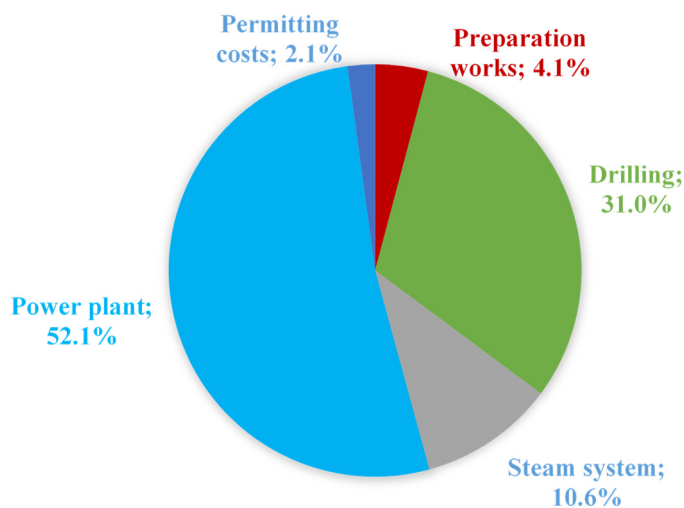


FIGURE 2: Project cost representation

3.4 Market factors, such as electricity sell price, raw material and drilling material costs

According to the Power Africa (2015) report, Kenya's economy has been growing at a rate of approximately 5.1% per year over the last 10 years with 2,295 MW of installed capacity (March 2015). The country's economic growth however has been constrained by an insufficient supply of electricity. In order to increase the current power capacity in the country, the Kenyan electricity sector investment framework was set up. The framework offered an investment enabling environment to investors/IPPs by providing protections and fiscal incentives:

- The Feed-In-Tariff projects guarantees a FIT (USD/kWh) that eliminates pricing risk;
- A priority purchase obligation by Kenya Power and guaranteed access to the national grid;
- A 20 year FIT, providing an amortization period sufficient to raise long-term project financing;
- An obligation for Kenya Power to enter into a Power Purchase Agreement (PPA) with the project company to meet the criteria required by the FIT program.

3.5 Rationale for assessment

Before an investment decision is made in a project, it is prudent to determine whether or not the planned investment idea is feasible and viable. This is only achieved by carrying out a financial assessment to determine whether the project is worth investing. The analysis is a critical and important step in the project decision-making process.

The assessment considers all project costs development parameters in the entire phases of the project i.e. from initial surface exploration to power plant construction and commissioning stages. The assessment will also help to determine the project investment requirements and assess the project profitability.

3.6 Project assumptions

This study based some of the costs and results on actual costs obtained from surface exploration studies, exploration, appraisal and production drilling by GDC in the Menengai geothermal field. Other costs were based on the current market prices and literature as well as experts' opinions.

In order to use the profitability model to determine the financial viability of the project, economic, technical and financial inputs assumptions have to be determined and accepted as true so as to be used in the model while others assumptions vary from one country to another i.e. income tax rate. The project assumptions used for this project are as shown in Table 4.

3.7 Project financing

Geothermal project financing varies from one project to the other depending on the type of the investment, the risk level of the investment, and the credit rating of the project owner. Lenders would normally require an equity percentage to ensure the sponsor's or project owner's continued commitment. In this case, the 35 MW projects financing arrangement will assume financing arrangement of 30% from equity and 70% debt.

TABLE 4: Other project assumptions

Project Parameter	Unit
The power plant type	Single flash
Net electricity output	35 MW
Capacity factor	95%
Construction time	8 years
Planning horizon (operations)	25 years
Loans	70%
Loan interest rate (no inflation)	6%
Income tax rate	30% of profit
Loan repayment	20 years
Operating & maintenance costs	2.3 MUSD
Electricity price	0.088 USD/kWh (FIT)
Sales quantity	291.3 (MWh/yr)
Depreciation buildings	4%
Depreciation equipment	15%
Depreciation other	10%
Loan management fee	0.8%
Discounting rate (MARR) total	10%
Discounting rate (MARR) equity	15%

3.8 Revenue estimation

To calculate estimate revenues from net power output, the power output results are converted to energy produced during one year using a capacity factor as follows:

$$\text{Revenue Per Year} = 365 * 24 * \text{NPO} * \text{C. F.} * \text{E. P.} \quad (1)$$

where 365 = Days in a year;
 24 = Hours in a day;
 NPO = Net Power Output;
 C.F. = Capacity Factor; the capacity factor considered for this study is 95%;
 E.L. = Electricity Price; the electricity price is considered 0.088 USD/kWh (as given by the FIT policy).

4. MAIN RESULTS OF THE PROFITABILITY MODEL

In this section, the main focus is to analyse the results obtained from the profitability model. Based on the results from the model, an indication of the financial conditions of the investments, capital investment requirements of the project, the net present value, internal rate of return, and forecast future performance of the investment is determined as described in the subsequent sections.

4.1 Marginal Attractive Rate of Return (MARR)

According to Salas (2012), the Marginal Attractive Rate of Return (MARR) is the discount rate that an investor or project owner most appreciates compared to other financial investment of an equivalent risk. It is the rate of return which provides the most preferred investment alternatives. Usually, MARR for

equity is the same as investors cost of capital. According to Paul Ngugi (2012), the rate of return on equity (ROE) in Kenya is 15% and above. The Government requires a ROE of 15% while private investors would normally charge between 18% and 23% but sometimes this can be higher.

In this project, the minimum acceptable rate of return on the total and equity project is 10% and 15%, respectively.

4.2 Net cash flows

As shown from Figure 3, the cash flow in the first 8 years shows a negative trend, resulting from the outflow of cash during the construction of the project. At this stage most of the high costs are related to drilling operations, construction of the steam pipeline system and power plant construction.

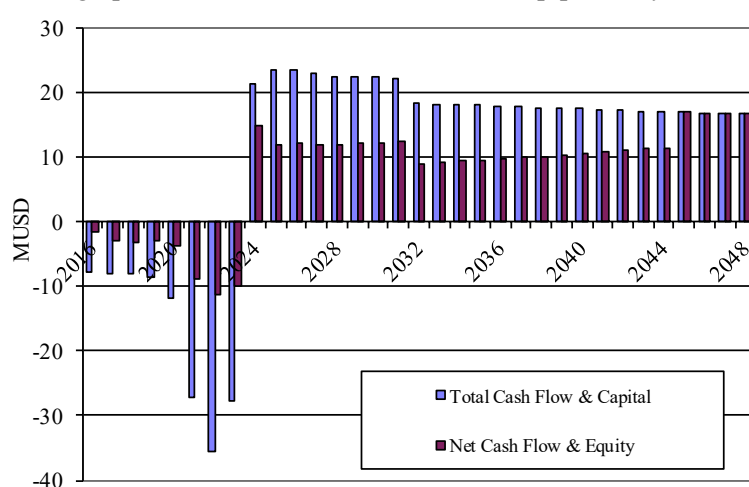


FIGURE 3: Cash flow

The cash flow becomes positive in 2024, this is when the power plant begins commercial production of electricity and cash flow is generated from electricity energy sales.

The difference between the total cash flow, capital, the net cash flow and equity in the first 8 years (project construction period) is the loan part of the capital requirement while the difference after 2024 (the positive part) is the loan repayment and the interest rate. Also, it can be observed that after 20 years the total cash flow and capital is equal to the

net cash flow and equity. This is because the loan repayments and interests have been concluded.

4.3 Net Present Value

The Net Present Value is defined as the value of future cash flows minus the present value of the cost of investment. Investments require initial capital. The initial capital go into cash outflow payments for the project at the initial stage of development which is followed by cash inflows in form of revenue during the operation stage of development.

The Net Present Value is a tool used for the evaluation of an investment and represents the sum of all the years discounted cash flows. For a project to be attractive and to generate returns on an investment, the NPV should be positive. In order to determine the profitability of this project, the Net Present Value was calculated and compared with regard to the future cash flows resulting from the investment to other investment alternatives. Therefore, the NPV is calculated using the following formula (Salas, 2012):

$$NPV = \sum_{i=0}^k \left(\frac{C_i}{(1+r)^i} \right) \quad (2)$$

where

- r = The discounting rate;
- i = The time of the cash flows, i.e. the return that could be earned per unit of time on an investment with similar risk;
- C_i = The net cash flows, i.e. cash inflow – cash outflow, at time i ;
- k = The service life of the project.

- When the project Net Present Value is greater than zero, accept the project.
- When the project Net Present Value is less than zero, reject the project.

As can be seen in Figure 4, the accumulated NPV for the total capital with discounting rate of 10% is 7 M USD while the accumulated NPV for equity with discounting rate of 15% is 5 M USD. The accumulated NPV for the net cash flows turns positive after 11 years of operation while the accumulated NPV for the total cash flows turns positive after 17 years of operation. Given that the NPV turns positive, the project is therefore profitable and economically viable.

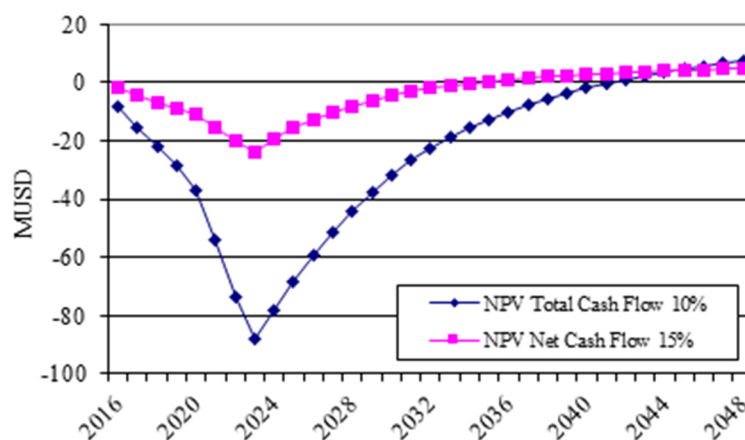


FIGURE 4: Accumulated net present value

4.4 Internal Rate of Return

To determine the profitability of an investment, the internal rate of return (IRR) is calculated to evaluate the profitability potential of an investment. Internal rate of return is a discount rate that makes the net present value (NPV) of all cash flows from a particular project equal to zero. It is a measure to determine the level of annual return (profitability) over the life span of an investment.

According to Salas (2012), the IRR is defined as the compound rate of return r that makes the NPV equals to zero and it is expressed as:

$$\sum_{i=0}^k \left(\frac{C_i}{(1+r)^i} \right) = 0 \quad (3)$$

For a decision to be made either to go on with the project or not, the basic investment rule can thus be described as:

- When the project IRR is greater than MARR, accept the project.
- When the project IRR is less than MARR, reject the project.

As shown in Figure 5, the model indicates that the internal rate of return of total cash flow is 11% while the internal rate of return of net cash flow (equity) is 17% which is more than the total discounting rate (MARR) of 10% and equity discounting rate (MARR) of 15%, respectively. This analysis meets the criteria that for a project to be viable, IRR should be greater than ($>$) MARR as shown in Equation 3. Based on the analysis above, the project is financially viable and worth investing.

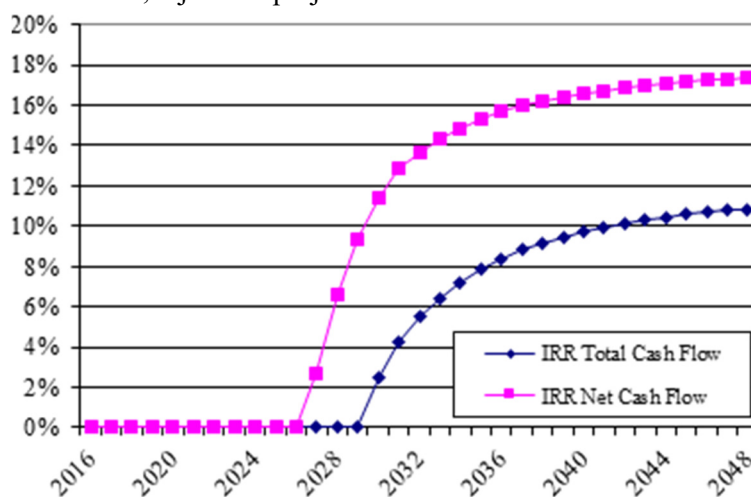


FIGURE 5: Internal rate of return

4.5 Debt service coverage ratio

The debt service coverage ratio refers to the amount of cash that is available to meet annual interest and principle payment on debt and is therefore used to calculate the debt service ratio. This is calculated by dividing the net operating income (NOI) by the annual debt as expressed in the formula below (Jensson, 2006):

$$\text{DSCR} = \frac{\text{Net operating income}}{\text{Total debt service (Principal \& Interest payments)}} \quad (4)$$

The debt service coverage represents the amount of the project's free cash flow that is expected to be available for debt service over the loan repayment period.

The project's debt service coverage ratio rises from 0.9 in 2023 to 3 in 2044. For a project to meet its debt obligation, the debt service ratio should be greater than the minimum critical value of 1.5.

As shown in Figure 6, the lowest debt service coverage ratio realized during the operation period of the plant is 1.9. This shows that the project's cash flow is sufficient to meet its debt service obligations over the plant operation lifetime.

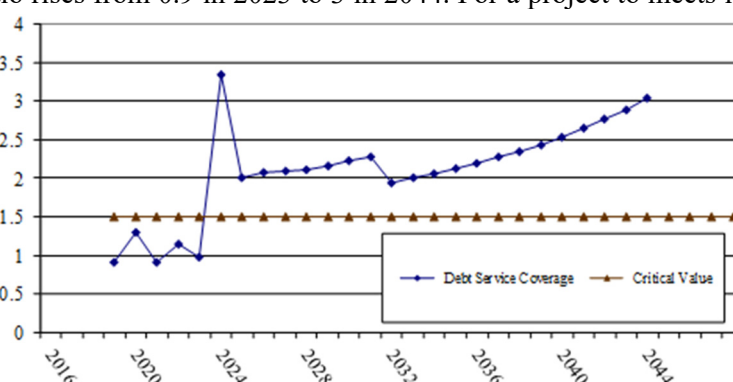


FIGURE 6: Debt service coverage ratio

4.6 Risk assessment analysis

The purpose of performing sensitivity analysis is to help to identify key variables which influences the project cost and benefit of stream of the project. It includes electricity sales price, sales quantity and operation and maintenance costs of the project.

Therefore, sensitivity analysis is conducted by determining how much the IRR changes relative to a given change in input parameters i.e. electricity price, sales quantity and operation and maintenance costs. Firstly, a base case is defined from the most likely values for each variable (pessimistic, most likely and optimistic). One variable at a time is changed by a specified percentage. In this case, we have used values from -50% to +50% while other variables are held constant at the base case value. The output is then calculated for the new value. In this case the output is the IRR of equity and the results are shown in Table 5.

TABLE 5: Impact analysis

		Price		Sales quantity		Equipment		O & M
		17%		17%		17%		17%
-50%	50%	2%	50%	4%	50%	23%	50%	18%
-40%	60%	6%	60%	7%	60%	22%	60%	18%
-30%	70%	9%	70%	10%	70%	21%	70%	18%
-20%	80%	12%	80%	13%	80%	19%	80%	18%
-10%	90%	15%	90%	15%	90%	18%	90%	18%
0%	100%	17%	100%	17%	100%	17%	100%	17%
10%	110%	19%	110%	19%	110%	16%	110%	17%
20%	120%	21%	120%	21%	120%	15%	120%	17%
30%	130%	23%	130%	22%	130%	14%	130%	17%
40%	140%	25%	140%	24%	140%	13%	140%	17%
50%	150%	26%	150%	25%	150%	12%	150%	16%

Based on Table 5, the project sensitivity assessment indicates that increasing the electricity price and sales quantity of the project increases the IRR, hence making the project more profitable while decrease in sales price and quantity by more than 10% will make the project unprofitable.

5. CONCLUSIONS AND RECOMMENDATIONS

To determine geothermal project viability, it is important to take into consideration all the necessary parameters that enable the successful development of the project. Some of these parameters include the country's existing supporting policy framework on geothermal development, development of a bankable project document, and project financing structure.

It is important to note that in all the cost components such as engineering, supervision and commissioning, general contingency and contracting fees were added in order to cover for unforeseen costs in the project. In this study, it is assumed that GDC will use its own rigs which ultimately reduced the cost of drilling, ultimately reducing the cost of the project. The costs can be higher if hired rigs are used.

The analysis of the result obtained from the profitability model, considering the data used and the assumptions made in the project, leads to the following conclusions:

- The planning horizon considered in the viability assessment of the project is 25 years.
- The calculated IRR obtained from the model for the total cash flow and net cash flow are more than the total discounting rate (MARR) of 10% and equity discounting rate (MARR) of 15%, respectively, which meets the criteria that the IRR should be greater than ($>$) the MARR. That indicates that, based on the analysis above, the project is viable and worth investing.
- The project debt service coverage ratio analysis shows that the minimum DSCR ratio obtained is 1.9 which is more than the critical value of 1.5 (Figure 6). Therefore, the project cash flow is sufficient to meet its debt service obligations over the lifetime of the project.
- It is advisable to undertake Project financial viability studies at early stages of project development in order to reduce risks involved in the project before making financial commitment.

ACKNOWLEDGEMENTS

My sincere gratitude goes to Mr. Lúdvík S. Georgsson, the Director of the UNU Geothermal Training Programme for providing me with the opportunity to take part in the 6 months training programme, the Deputy Director, Mr. Ingimar Gudni Haraldsson, Ms. Thórhildur Ísberg, Mr. Markús A. G. Wilde, Ms. Málfríður Ómarsdóttir and my fellow UNU fellows for their great support during my study here in Iceland.

Special thanks to my supervisor, Professor Páll Jensson for assisting and guiding me during my research project.

Special thankfulness to my employer, Geothermal Development Company (GDC), for granting me this special opportunity to attend the training.

Thanks to my wonderful wife Beatrice for her love and encouragement and taking care of the family while I was away; to my children; Joy Jemator, Billy Ruto and Tracy Jelagat for their great moral support and praying for me.

Finally, I thank God for His sufficient grace that made the programme possible.

REFERENCES

- Bloomquist, R.G., 2004: Economic factors impacting direct use geothermal development viability. *Proceedings of the International Geothermal Days Poland 2004, International Summer School, Polish Geothermal Association, Krakow and Skopje*, 203-210.
- Energy Regulatory Commission, 2013: *Least cost power development plan, final report*. Energy Regulatory Commission, Kenya, 203 pp, website: www.erc.go.ke/index.php?searchword=LCPDP&searchphrase=all&Itemid=606&option=com_search
- Geirdal, C.A.C., 2013: *Economic comparison between a well-head geothermal power plant and a traditional geothermal power plant*. Reykjavik University, Reykjavik, MSc thesis, 100 pp.
- Government of Kenya, 2016: *The Energy Act*. Government of Kenya, 120 pp, webpage: www.eisourcebook.org/cms/Kenya%20Energy%20Act,2006.pdf
- Hance, C.N., 2005: *Factors affecting costs of geothermal power development*. Geothermal Energy Association, publication for the US Department of Energy”.
- Jensson, P., 2006: *Profitability Assessment Models*. In: Workshop on Fisheries and Aquaculture in Southern Africa: Development and Management. Windhoek, Namibia. ICEIDA and UNU-FTP, August 21-24 2006.
- Kipsang, C., 2013: Cost model for geothermal wells. Report 11 in: *Geothermal training in Iceland 2013*. UNU-GTP, Iceland, 177-199.
- Kiptanui, S.K., 2015: Financial assessment of commercial extraction of sulphur and carbon dioxide from geothermal gases in Menengai, Kenya. Report 17 in: *Geothermal training in Iceland 2015*. UNU-GTP, Iceland, 329-355.
- Ministry of Energy, 2012: Feed-in-tariffs policy – On wind, biomass, small-hydro, geothermal, biogas and solar resource generated electricity. MoE, Kenya, 17 pp, webpage: www.renewableenergy.go.ke/downloads/policy-docs/Feed_in_Tariff_Policy_2012.pdf
- Ministry of Environment, Water and Natural Resources, 2013: *National environment policy, 2013*. MEWNR, GoK, Kenya, 70 pp, webpage: faolex.fao.org/docs/pdf/ken147906.pdf
- Ministry of Lands, 2009: *National land policy*. Ministry of Lands, Kenya, Sessional paper No. 3, 73 pp. www1.uneca.org/Portals/lpi/CrossArticle/1/Land%20Policy%20Documents/Sessional-paper-on-Kenya-National-Land-Policy.pdf
- Mwangi, M.N., 2005: Phases of geothermal development in Kenya. *Paper presented at Workshop for Decision Makers on Geothermal Projects and Management, organized by UNU-GTP and KenGen in Naivasha, Kenya*, UNU-GTP SC-01, 11 pp.
- National Council for Law Reporting (Kenya Law), 2013: *Public private partnerships act*. NCLR, webpage: www.kenyalaw.org/lex//actview.xql?actid=NO.%2015%20OF%202013.
- Ngugi, P.K., 2012: What does geothermal cost? - The Kenya experience. *Paper presented at “Short Course on Geothermal Development and Geothermal Wells”, organized by UNU-GTP and LaGeo, in Santa Tecla, El Salvador*. UNU-GTP, SC14, 13 pp.
- Omenda, P.A., 2012: *Geothermal development in Kenya: a country update*. Geothermal Development Company - GDC, Kenya, report, 5 pp.
- Power Africa, 2015: *Investment brief for the electricity sector in Kenya*. Power Africa, US AID, 6 pp, webpage: www.usaid.gov/sites/default/files/documents/1860/Kenya%20_IG_2015_05_03.pdf
- Salas, R.J.E., 2012: *Geothermal power plant projects in Central America: technical and financial feasibility assessment model*. University of Iceland, Reykjavik, MSc thesis, 108 pp.
- U.S. Department of Energy, 2008: *Geothermal technologies market report*. US DoE, report, 19 pp, website: www.nrel.gov/docs/fy09osti/46022.pdf.

Appendix III: Operation

		Operations																																		
		2016	2017	2018	2019	2020	2021	2022	2023	2024	2025	2026	2027	2028	2029	2030	2031	2032	2033	2034	2035	2036	2037	2038	2039	2040	2041	2042	2043	2044	2045	2046	2047	2048	Total	
Operations Statement																																				
	Sales	0	0	0	0	0	0	0	291.3	291.3	291.3	291.3	291.3	291.3	291.3	291.3	291.3	291.3	291.3	291.3	291.3	291.3	291.3	291.3	291.3	291.3	291.3	291.3	291.3	291.3	291.3	291.3	291.3	291.3	7283	
	Price	0	0	0	0	0	0	0	0.088	0.088	0.088	0.088	0.088	0.088	0.088	0.088	0.088	0.088	0.088	0.088	0.088	0.088	0.088	0.088	0.088	0.088	0.088	0.088	0.088	0.088	0.088	0.088	0.088	0.088	0.088	
	Revenue	0	0	0	0	0	0	0	25.63	25.63	25.63	25.63	25.63	25.63	25.63	25.63	25.63	25.63	25.63	25.63	25.63	25.63	25.63	25.63	25.63	25.63	25.63	25.63	25.63	25.63	25.63	25.63	25.63	25.63	641	
	Variable Cost	0	0	0	0	0	0	0	0	0	0	0	0	0	0	0	0	0	0	0	0	0	0	0	0	0	0	0	0	0	0	0	0	0		
	&M Costs	2	0	0	0	0	0	0	2	2	2	2	2	2	2	2	2	2	2	2	2	2	2	2	2	2	2	2	2	2	2	2	2	2	68	
	Diverse Taxes																																			
	Operating Surplus (EBITDA)	0	0	0	0	0	0	0	0	23	23	23	23	23	23	23	23	23	23	23	23	23	23	23	23	23	23	23	23	23	23	23	23	23	593	
	Inventry Movement																																			
	Depreciation	0	0	0	0	0	0	0	0	13	12	10	9	9	9	9	9	9	9	9	9	9	9	9	9	9	9	9	9	9	9	9	9	9	123	
	Operating Gain/Loss (EBIT)	0	0	0	0	0	0	0	0	13	12	10	9	9	9	9	9	9	9	9	9	9	9	9	9	9	9	9	9	9	9	9	9	9	459	
	Financial Costs	0.0	0.4	-0.76	1.1	1.5	-2.2	-3.5	5.1	6.3	6.0	5.7	5.4	5.1	4.7	4.4	4.1	3.8	3.5	3.2	2.8	2.5	2.2	1.9	1.6	1.3	0.9	0.6	0.3	0.0	0.0	0.0	0.0	0.0	0.0	
	Profit before Tax	0.0	-0.4	-0.76	-1.1	-1.5	-2.2	-3.5	-5.1	6.6	5.6	4.0	3.7	3.4	3.7	4.0	17.4	17.7	18.0	18.3	18.6	19.2	19.5	19.9	20.2	20.5	20.8	21.1	21.4	21.8	21.8	21.8	21.8	21.8	372	
	Tax Transfer	0	-0.0	-1.22	-2.3	-3.9	-6.1	-9.6	-14.7	-8.1	-2.5	0.0	0.0	0.0	0.0	0.0	0.0	0.0	0.0	0.0	0.0	0.0	0.0	0.0	0.0	0.0	0.0	0.0	0.0	0.0	0.0	0.0	0.0	0.0	0.0	
	Taxable Profit	0.0	0.0	0.0	0.0	0.0	0.0	0.0	0.0	1.5	3.1	3.4	3.7	4.0	17.0	17.4	17.7	18.0	18.3	18.6	19.2	19.5	19.9	20.2	20.5	20.8	21.1	21.4	21.8	21.8	21.8	21.8	21.8	21.8	21.8	
	Income Tax	0.0	0.0	0.0	0.0	0.0	0.0	0.0	0.0	0.0	0.0	0.0	0.0	0.0	0.0	0.0	1.2	5.1	5.2	5.3	5.4	5.5	5.6	5.8	5.9	6.0	6.1	6.1	6.2	6.3	6.4	6.5	6.5	6.5	112	
	Profit after Tax	0.0	-0.4	-0.76	-1.1	-1.5	-2.2	-3.5	-5.1	6.6	5.6	3.5	2.1	2.4	2.6	2.8	11.9	12.1	12.4	12.6	12.8	13.0	13.5	13.7	13.9	14.1	14.3	14.6	14.8	15.0	15.2	15.2	15.2	15.2	261	
	Dividend	0.0	0.0	0.0	0.0	0.0	0.0	0.0	0.0	0.0	0.0	0.0	0.0	0.0	0.0	0.0	0.0	0.0	0.0	0.0	0.0	0.0	0.0	0.0	0.0	0.0	0.0	0.0	0.0	0.0	0.0	0.0	0.0	0.0	0.0	
	Net Profit/Loss	0.0	-0.4	-0.76	-1.1	-1.5	-2.2	-3.5	-5.1	6.6	5.6	3.5	2.1	2.4	2.6	2.8	11.9	12.1	12.4	12.6	12.8	13.0	13.5	13.7	13.9	14.1	14.3	14.6	14.8	15.0	15.2	15.2	15.2	15.2	261	

Appendix IV: Cash flows

Cash Flow																																																																																																																																																																																																																																																																																																																																																																																																																																																																																																																																																																																																																																																		
	2016	2017	2018	2019	2020	2021	2022	2023	2024	2025	2026	2027	2028	2029	2030	2031	2032	2033	2034	2035	2036	2037	2038	2039	2040	2041	2042	2043	2044	2045	2046	2047	2048	Total																																																																																																																																																																																																																																																																																																																																																																																																																																																																																																																																																																																																																
Cash Flow																																																																																																																																																																																																																																																																																																																																																																																																																																																																																																																																																																																																																																																		
Operating Surplus (EBITDA)	0	0.00	0	0	0	0	0	0	0	23.3	23.3	23.3	23.3	23.3	23.3	23.3	23.3	23.3	23.3	23.3	23.3	23.3	23.3	23.3	23.3	23.3	23.3	23.3	23.3	23.3	23.3	23.3	583																																																																																																																																																																																																																																																																																																																																																																																																																																																																																																																																																																																																																	
Debtors	0	0.00	0	0	0	0	0	0	0	2.1	2.1	2.1	2.1	2.1	2.1	2.1	2.1	2.1	2.1	2.1	2.1	2.1	2.1	2.1	2.1	2.1	2.1	2.1	2.1	2.1	2.1	2.1	2.1	2.1																																																																																																																																																																																																																																																																																																																																																																																																																																																																																																																																																																																																																
Debtor Changes	0	0.00	0	0	0	0	0	0	-2.1	0	0	0	0	0	0	0	0	0	0	0	0	0	0	0	0	0	0	0	0	0	0	0	0	-2																																																																																																																																																																																																																																																																																																																																																																																																																																																																																																																																																																																																																
Creditors	0	0.00	0	0	0	0	0	0	0	0	0	0	0	0	0	0	0	0	0	0	0	0	0	0	0	0	0	0	0	0	0	0	0	0																																																																																																																																																																																																																																																																																																																																																																																																																																																																																																																																																																																																																
Creditor Changes	0	0.00	0	0	0	0	0	0	0	0	0	0	0	0	0	0	0	0	0	0	0	0	0	0	0	0	0	0	0	0	0	0	0	0																																																																																																																																																																																																																																																																																																																																																																																																																																																																																																																																																																																																																
Financing	1	1.00	0	0	0	0	0	0	0	0	0	0	0	0	0	0	0	0	0	0	0	0	0	0	0	0	0	0	0	0	0	0	0	0																																																																																																																																																																																																																																																																																																																																																																																																																																																																																																																																																																																																																
Financing Expenditure	2	2	2	2	2	2	4	5	21	23	23	23	23	23	23	23	23	23	23	23	23	23	23	23	23	23	23	23	23	23	23	23	23	595																																																																																																																																																																																																																																																																																																																																																																																																																																																																																																																																																																																																																
Cash Flow before Tax		1.00	0	0	1	2	2	4	5	21	23	23	23	23	23	23	23	23	23	23	23	23	23	23	23	23	23	23	23	23	23	23	23	23																																																																																																																																																																																																																																																																																																																																																																																																																																																																																																																																																																																																																
Paid Taxes		0.00	0	0	0	0	0	0	0	0	0	0	0	0	0	0	0	0	0	0	0	0	0	0	0	0	0	0	0	0	0	0	0	0																																																																																																																																																																																																																																																																																																																																																																																																																																																																																																																																																																																																																
Cash Flow after Tax		1.00	0	0	1	2	2	4	5	21.17	23.3	23.3	22.86	22.39	22.29	22.2	22.1	18.1	18.1	17.91	17.81	17.72	17.54	17.44	17.35	17.25	17.16	16.97	16.87	16.78	16.78	16.78	16.78	16.78	16.78	16.78	16.78	16.78	16.78	16.78	16.78	16.78	16.78	16.78	16.78	16.78	16.78	16.78	16.78	16.78	16.78	16.78	16.78	16.78	16.78	16.78	16.78	16.78	16.78	16.78	16.78	16.78	16.78	16.78	16.78	16.78	16.78	16.78	16.78	16.78	16.78	16.78	16.78	16.78	16.78	16.78	16.78	16.78	16.78	16.78	16.78	16.78	16.78	16.78	16.78	16.78	16.78	16.78	16.78	16.78	16.78	16.78	16.78	16.78	16.78	16.78	16.78	16.78	16.78	16.78	16.78	16.78	16.78	16.78	16.78	16.78	16.78	16.78	16.78	16.78	16.78	16.78	16.78	16.78	16.78	16.78	16.78	16.78	16.78	16.78	16.78	16.78	16.78	16.78	16.78	16.78	16.78	16.78	16.78	16.78	16.78	16.78	16.78	16.78	16.78	16.78	16.78	16.78	16.78	16.78	16.78	16.78	16.78	16.78	16.78	16.78	16.78	16.78	16.78	16.78	16.78	16.78	16.78	16.78	16.78	16.78	16.78	16.78	16.78	16.78	16.78	16.78	16.78	16.78	16.78	16.78	16.78	16.78	16.78	16.78	16.78	16.78	16.78	16.78	16.78	16.78	16.78	16.78	16.78	16.78	16.78	16.78	16.78	16.78	16.78	16.78	16.78	16.78	16.78	16.78	16.78	16.78	16.78	16.78	16.78	16.78	16.78	16.78	16.78	16.78	16.78	16.78	16.78	16.78	16.78	16.78	16.78	16.78	16.78	16.78	16.78	16.78	16.78	16.78	16.78	16.78	16.78	16.78	16.78	16.78	16.78	16.78	16.78	16.78	16.78	16.78	16.78	16.78	16.78	16.78	16.78	16.78	16.78	16.78	16.78	16.78	16.78	16.78	16.78	16.78	16.78	16.78	16.78	16.78	16.78	16.78	16.78	16.78	16.78	16.78	16.78	16.78	16.78	16.78	16.78	16.78	16.78	16.78	16.78	16.78	16.78	16.78	16.78	16.78	16.78	16.78	16.78	16.78	16.78	16.78	16.78	16.78	16.78	16.78	16.78	16.78	16.78	16.78	16.78	16.78	16.78	16.78	16.78	16.78	16.78	16.78	16.78	16.78	16.78	16.78	16.78	16.78	16.78	16.78	16.78	16.78	16.78	16.78	16.78	16.78	16.78	16.78	16.78	16.78	16.78	16.78	16.78	16.78	16.78	16.78	16.78	16.78	16.78	16.78	16.78	16.78	16.78	16.78	16.78	16.78	16.78	16.78	16.78	16.78	16.78	16.78	16.78	16.78	16.78	16.78	16.78	16.78	16.78	16.78	16.78	16.78	16.78	16.78	16.78	16.78	16.78	16.78	16.78	16.78	16.78	16.78	16.78	16.78	16.78	16.78	16.78	16.78	16.78	16.78	16.78	16.78	16.78	16.78	16.78	16.78	16.78	16.78	16.78	16.78	16.78	16.78	16.78	16.78	16.78	16.78	16.78	16.78	16.78	16.78	16.78	16.78	16.78	16.78	16.78	16.78	16.78	16.78	16.78	16.78	16.78	16.78	16.78	16.78	16.78	16.78	16.78	16.78	16.78	16.78	16.78	16.78	16.78	16.78	16.78	16.78	16.78	16.78	16.78	16.78	16.78	16.78	16.78	16.78	16.78	16.78	16.78	16.78	16.78	16.78	16.78	16.78	16.78	16.78	16.78	16.78	16.78	16.78	16.78	16.78	16.78	16.78	16.78	16.78	16.78	16.78	16.78	16.78	16.78	16.78	16.78	16.78	16.78	16.78	16.78	16.78	16.78	16.78	16.78	16.78	16.78	16.78	16.78	16.78	16.78	16.78	16.78	16.78	16.78	16.78	16.78	16.78	16.78	16.78	16.78	16.78	16.78	16.78	16.78	16.78	16.78	16.78	16.78	16.78	16.78	16.78	16.78	16.78	16.78	16.78	16.78	16.78	16.78	16.78	16.78	16.78	16.78	16.78	16.78	16.78	16.78	16.78	16.78	16.78	16.78	16.78	16.78	16.78	16.78	16.78	16.78	16.78	16.78	16.78	16.78	16.78	16.78	16.78	16.78	16.78	16.78	16.78	16.78	16.78	16.78	16.78	16.78	16.78	16.78	16.78	16.78	16.78	16.78	16.78	16.78	16.78	16.78	16.78	16.78	16.78	16.78	16.78	16.78	16.78	16.78	16.78	16.78	16.78	16.78	16.78	16.78	16.78	16.78	16.78	16.78	16.78	16.78	16.78	16.78	16.78	16.78	16.78	16.78	16.78	16.78	16.78	16.78	16.78	16.78	16.78	16.78	16.78	16.78	16.78	16.78	16.78	16.78	16.78	16.78	16.78	16.78	16.78	16.78	16.78	16.78	16.78	16.78	16.78	16.78	16.78	16.78	16.78	16.78	16.78	16.78	16.78	16.78	16.78	16.78	16.78	16.78	16.78	16.78	16.78	16.78	16.78	16.78	16.78	16.78	16.78	16.78	16.78	16.78	16.78	16.78	16.78	16.78	16.78	16.78	16.78	16.78	16.78	16.78	16.78	16.78	16.78	16.78	16.78	16.78	16.78	16.78	16.78	16.78	16.78	16.78	16.78	16.78	16.78	16.78	16.78	16.78	16.78</

Appendix VI: Profitability

[illegible]



UNITED NATIONS
UNIVERSITY

UNU-GTP

Geothermal Training Programme

Orkustofnun, Grensasvegur 9,
IS-108 Reykjavik, Iceland

Reports 2016
Number 20

CHALLENGES OF DIRECTIONAL WELL DRILLING IN KENYA: CASE STUDY OF OLKARIA, KENYA AND THEISTAREYKIR, ICELAND GEOTHERMAL FIELDS

James Karanja Kahutu

Kenya Electricity Generating Company, Ltd. - KenGen

P.O Box 785-20117

Naivasha

KENYA

jkahutu@kengen.co.ke

ABSTRACT

Directional drilling in Olkaria geothermal field started in the year 2007. This was necessitated by the need to drill high productivity geothermal wells by intercepting multiple fractures as well as taking advantage of the benefits associated with directional drilling. These advantages include the ability to exploit geothermal resources in an area that would be difficult to access, the ability to drill multiple wells from the same well pad, thereby minimizing surface disturbance among others. Since then, over 100 directional wells have been drilled successfully. All the directional wells in Olkaria employ the build and hold (J shape) design with a target angle of inclination set at 20°. The kick-off point for the wells ranges from 300 to 600 mRKB. Kick-off is achieved by the use of a mud motor to build the required angle after which an angle holding BHA composed of two stabilizers is used to hold the angle to the total depth. Drilling of the wells is done using water based mud for the upper section of the wellbore down to 300 mRKB and then aerated drilling is employed for the remaining section. Directional drilling in Olkaria is facing a number of challenges. This report focusses on the different challenges with emphasis on the BHA design related challenges. Proper BHA design for directional wells is important as it ensures that the wellbore trajectory is contained within the acceptable dog-leg severity. Excessive dog-legs in drilling results in drill string problems such as fatigue failure and worn out tool joints due to excessive torque and drag. A comparison of the different BHA designs and their performance for two wells drilled in Olkaria, Kenya and two wells drilled in Theistareykir, Iceland is used to highlight these challenges and explore how some of them can be addressed.

1. INTRODUCTION

Directional drilling involves a technique of deviating a wellbore intentionally along a predetermined path to reach a given target (Vieira, 2009). Directional drilling can be done through various techniques that include the use sophisticated technologies like a mud motor with bent sub, measurement while drilling (MWD) integrated with in-field referencing, real time multi survey measurement, analysis that ensure that the target is reached accurately, use of steerable assemblies, logging while drilling (LWD)

and finally the use of older drilling methods like the use of whipstocks, rotary assemblies and jetting techniques (Economides et al., 1998).

Currently, there are over 200 geothermal wells that have been drilled in Olkaria Geothermal Field with at least 100 of these being directional wells. While directional drilling offers numerous advantages, drilling of directional wells in Olkaria has been facing two main challenges which are formation related challenges and BHA (bottom hole assembly) design challenges. With the huge number of wells in the field, it is important to ensure that the directional wells plan is followed properly to ensure that wells do not target the same resource area. For this reason, there is need to ensure that the BHA design and formation related challenges are properly addressed to meet this objective efficiently and economically.

2. LITERATURE REVIEW

2.1 Directional drilling methodology

Directional drilling is a process that involves intentionally deviating a wellbore along a predetermined path to a target or location normally given by lateral distance and true vertical depths (TVD) from an originally known point (Bourgoyne et al, 1986). Historically, wells were drilled in vertical direction only, and this continued until 1934 when wellbore deviation became acceptable in the drilling industry after it was used to drill a directional relief well in Texas. With the adoption of directional drilling techniques, it became possible to drill multiple wells targeting different directions from the same well pad. Over the years there has been a tremendous improvement on how directional drilling is being conducted to improve the efficiency and accuracy with which the targets are hit. The use of measurement while drilling (MWD) tools, steerable mud motors and logging while drilling (LWD) tools has had the biggest impact on drilling of directional wells. When used together, these tools have made it possible to follow complex 3D well profiles without bottom hole assembly (BHA) change, and to measure the inclination and the direction of the well without running the wireline to log or survey (Economides et al., 1998). In addition to the sophisticated technology, older drilling practices such as the mud motors with bent subs, rotary assemblies, jetting technique, whipstocks and wireline steering tools to orient and survey are still being used for drilling directional wells.

2.2 Terminologies used in directional drilling

There are different terminologies used in directional drilling with reference to the well that has been drilled or is being drilled. These terminologies are important as they help identify the wellbore direction, wellbore trajectory and well design characteristics. The major terminologies used are listed below (Aadnoy et al., 2009):

- a) Azimuth - The angle (in degrees) of a wellbore on a horizontal plane measured clockwise with reference to North. Azimuth can be referenced using magnetic North, grid North or true North. In directional drilling survey coordinates are normally represented with reference to true or grid North.
- b) Kick off Point (KOP) - Any point below the surface where the initial deflection of the wellbore from vertical starts. KOP for many geothermal wells lie in 300 m - 600 m depth what is mainly dependent on the geometry of the wellbore, geological conditions and the location of the adjacent wells.
- c) Build up Rate (BUR) - This refers to the rate with which the angle of inclination increases with depth, normally expressed in degrees/100 ft or degrees/30 m.
- d) Drop off Rate - Rate with which the inclination angle is returned towards vertical, expressed in degrees per feet.
- e) Inclination - The angle between the vertical line and the tangent line at a given point in a wellbore.

- f) Hold - Tendency of maintaining a constant azimuth and inclination of a wellbore.
- g) True Vertical Depth (TVD) - This is the vertical distance (meter or feet) measured from the rotary Kelly bushing (RKB) to the current or final depth of a wellbore.
- h) Measured Depth (MD) - Depth of the wellbore measured along the well path from one known point to another. It is expressed in meters or feet.
- i) Dog leg - Sudden change in angle or direction of a wellbore.

2.3 Application of directional drilling in geothermal wells

Adoption of directional drilling technology in the geothermal industry has made it possible to achieve a number of objectives as shown in Figure 1:

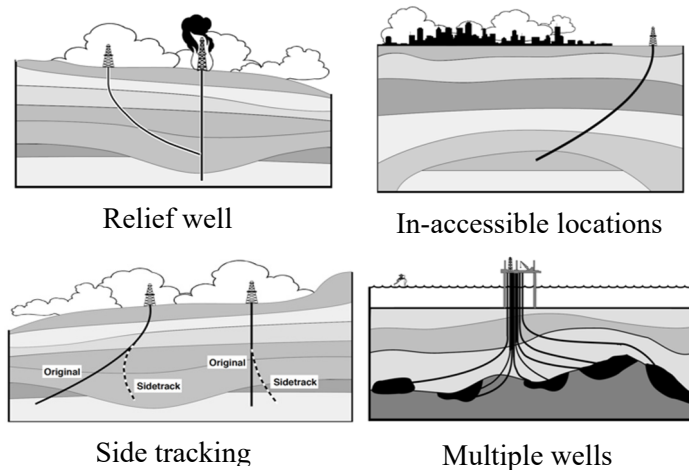


FIGURE 1: Applications of directional drilling
(Baker Hughes INTEQ, 1995)

- a) Accessing inaccessible locations - In geothermal drilling, it is possible that some of the target zones are located beneath areas with severe topographic features such as mountains where rigging up would be impossible. This means that the target resource can only be accessed by drilling a directional well (Devereux, 1998).
- b) Drilling multiple wells from a single well pad - Traditionally, one well pad could only accommodate one well but with the adoption of directional drilling, it is possible to have multi-wells in a single platform. This is not only economical but also helps conserving the environment as it causes less disturbance on the surface both in drilling phase and steam gathering phase as less land is required to achieve both (Speith, 2015).
- c) Side tracking - This involves deviating from the original well trajectory to avoid an obstruction such as a twisted off drill string that cannot be fished out. It is different from other types of directional drilling applications as it lacks a predetermined target and therefore cannot be defined as controlled drilling.
- d) Targeting several faults - Directional drilling is employed in an effort to intersect as many faults as possible to improve productivity of a well.
- e) Drilling a relief well - Directional drilling technology is used in drilling a directional well to relief another well when all the other well control mechanisms have failed and the rig has been damaged. To control the well, another directional well is drilled targeting the well which is out of control, after which high viscosity mud is pumped after intercepting the target (Adams, 1985).
- f) Fault drilling - This involves drilling of a directional well in order to avoid having a vertical well going through an area with steeply inclined fault plane which could slip and shear off casings in case of fault movement.

3. DIRECTIONAL WELL TRAJECTORY PLANNING

In planning of any directional well, there are a number of factors that have to be considered. The first key factor that must be considered is the design of the wellbore trajectory with respect to the set target. The design should propose the different types of wellbore paths that can be drilled in the most economical way possible. The other factor that should be considered is the effectiveness of the desired bottom hole assembly in a given formation type and the influence of other factors on the desired well

trajectory (Bourgoyne et al., 1986). In addition, it is important to consider the angle build up rate to avoid subjecting the drill pipes to fatigue when drilling, avoid key seats and minimize the effects of torque and drags generated when the angle of inclination increases. The wellbore profile selected has a very big influence on the torque and drags subjected to the drill string during drilling as well as the drag that occur when running casings and logs. Highly deviated wells with significant azimuth changes may cause serious problems due to the frictional forces generated. Other factors that should also be considered include the surface coordinates and how they have been defined, adjacent wells in the area, geological sequence of the area, performance of BHAs in adjacent wells and rig information among others (Devereux, 1998).

3.1 Types of wellbore trajectory

There are different types of wellbore path designs can be used in directional drilling. The most popular types include:

- a) Build and hold trajectory/J-profile - It is the most common type of well path design in geothermal well drilling. In this design, the wellbore is kept vertical until a KOP is reached after which the well is deflected off and a desired angle built. When the required angle is acquired, the wellbore is kept straight and made to intersect the target at an angle that is equal to the build-up angle as shown in Figure 2a (Baker Hughes INTEQ, 1995).
- b) Build, hold and drop trajectory/S-profile - For this design the wellbore is drilled just like in the build and hold design but instead of holding the angle to total depth after the tangent section is drilled the angle is then dropped to allow the wellbore intersect the target vertically as shown in Figure 2b.
- c) Build, hold, partial drop and hold trajectory/modified S-profile - As the name suggest the design of this trajectory employs the same principle of the S-profile trajectory with the difference being that the wellbore is designed to intersect the target at an inclination angle which should be less than the maximum angle attained in the hold section.
- d) Horizontal wells trajectory - In this design the well is kept vertical for the first section then the wellbore path inclination angle is allowed to reach 90° or more. Most of these wells are designed

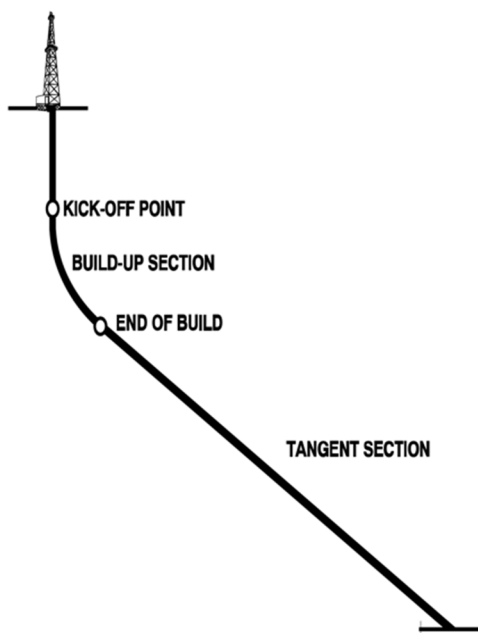


FIGURE 2a: Build and hold (J-type)
(Baker Hughes INTEQ, 1995)

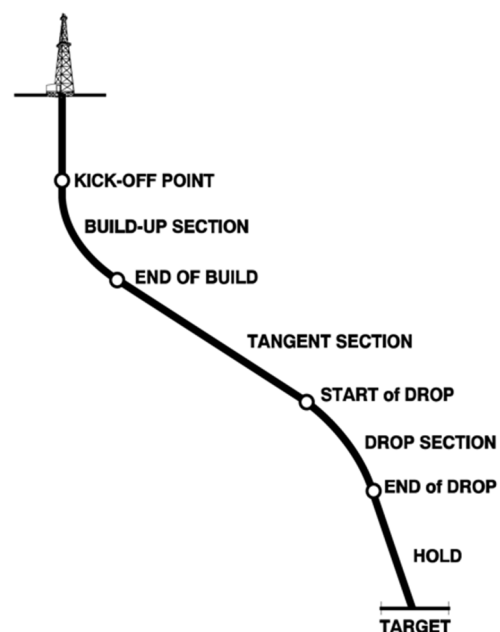


FIGURE 2b: Build, hold and drop
(S-type) (Baker Hughes INTEQ, 1995)

as production wells due to their increased flow rates due to increased reservoir exposure. This design is most popular in oil and gas industry (Economides et al., 1998).

4. TOOLS FOR DIRECTIONAL DRILLING

Drilling of directional wells unlike the vertical wells requires that the well path control be done in the best way possible as it is one of the most complex and important phases of drilling. For this reason, a lot of research has to be done to better understand how different variables affect the BHA behaviour. Such variables include the weight on bit, rate of penetration, geological conditions, rotary speed and hole inclination among others. In order to drill a directional well, the BHA can be manipulated to include different components to achieve the desired results. Currently, there are a number of equipment that have been developed to drill directional wells such as mud motors with bent subs, jetting bits, rotary steerable assemblies and whipstocks among others. The selection of the tool to use for well deflection is a very important exercise as it determines how well the predetermined path can be achieved as discussed below.

4.1 Basic rotary assemblies

The bottom hole assembly is the major portion of the drill string that affects the path of the bit and consequently the trajectory of the wellbore. The assemblies can be designed to either build or drop the angle of inclination or to steer the well either to the right, left or maintain the existing wellbore direction (Devereux, 1999). In directional drilling, the composition of BHAs ranges from a simple one consisting of the bit, collars and the drill pipes (Figure 3a) to a complex one integrating a drill bit, stabilizers, collars, reamers, shock subs, jars, subs, heavy weight drill pipes and the regular drill pipes as shown in Figure 3b.

The tendency of any assembly to cause deviation when drilling is dependent on the flexibility of the drill collars and the forces acting on the BHA causing the drill collars to bend. The design of any BHA for directional drilling is based on principles that involve the active length of the drill collars. The point at which the collars get into contact with the low side of the wellbore is known as the tangent point while the distance from the tangent point to the bit is known as the active length. Active length of any BHA is dependent on the collar size, hole size, weight on bit, hole curvature and hole inclination (Computerlog Drilling Services, 2000). When the active length of the drill collars is short, it results in a fulcrum effect used in angle building and when the length is increased it results in a pendulum effect that is used in angle dropping. When these two principles are combined, they give rise to angle holding. All this can be achieved by placing the stabilizers at different positions. In addition, the directional tendency or behaviour of any bottom hole assembly is governed by a number of factors that include:

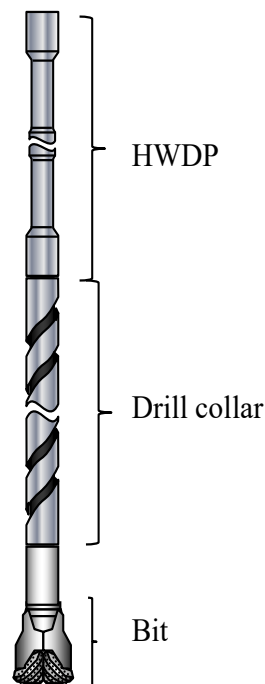


FIGURE 3a: Slick BHA (Simple)

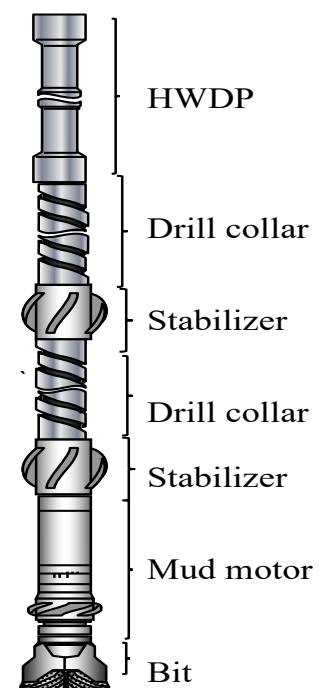


FIGURE 3b: Complex BHA

- Bit tilt
- Diameter and length of drill collars
- Rotary speed/Revolution per minute (RPM)
- Bit type
- Weight on bit (WOB)
- Flow rate
- Rate of penetration
- Bit side force
- Rock type/properties
- Hydraulics
- Formation dip

This report focuses more on the effect of bit side forces as a result of stabilizer placement in rotary assemblies as well as the effect of drilling parameters such as WOB and rotary speed and their impact on directional drilling.

4.1.1 Angle building BHA

The configuration of this BHA utilizes what is known as the fulcrum principle. Typical build assemblies consist of one to three stabilizers. The first one is the near bit stabilizer normally placed 3 to 5 feet from the bit face or connected directly to the bit followed by two to three drill collars and a second string stabilizer as shown in Figure 4. The near bit stabilizer acts like a pivot in the assembly, while the bending of the drill collars between the first and the second stabilizer causes the drill bit to press against the top side of the well bore. At lower inclinations, building assemblies with only one stabilizer are recommended as they generate more side forces (Bourgoyne et al., 1986). The bit side force generated determines the rate of build which can range from 2° to 5°/30 m. This is dependent on the distance between the first and the second stabilizer, increase in distance results in high build rates and vice versa. However, there is a limit with which the build-up rate is influenced by the increase in spacing between the two stabilizers. If the second stabilizer is more than 120 ft from the near-bit stabilizer (depending on the hole size and collar OD), the collars contacts the low side of the hole and any further increase in distance has no effect on the build rate. In addition, the rate of build is also influenced by the weight on bit application and the size of the drill collars in the assembly (Economides et al., 1998). Increase in WOB lowers the tangency point thus increasing the angle build up rate. The rate of build in this case is however not caused so much by the side force but by the bit tilt. Other factors that affect the build assembly include the inclination of the well bore and the rotary speed. If the rotary speed is too high the drill collars tend to be straightened up thus reducing the angle build rate. It is recommended that a rotary speed of 70-100 RPM is used for fulcrum assemblies. Unlike in the past, the build assemblies are currently composed of few drill collars and stabilizers. Heavy walled drill pipes can replace some of the drill collars thus reducing the need to have stabilizers that hold the collars off the walls of the wellbore (Bourgoyne et al., 1986).

4.1.2 Angle holding BHA

This assembly is also known as a packed assembly as it contains three to five stabilizers in close proximity. Normally, it consists of a full gauge near bit stabilizer, drill collar, string stabilizer, drill collar and another stabilizer as shown in Figure 4. Packed assemblies in directional drilling are normally introduced after achieving the required inclination. The series of stabilizers helps guiding the bit to drill straight ahead. Careful selection of the right BHA to be used above the bit should be done to ensure that the drill bit is forced to drill in the direction of an already drilled hole. If done properly, hole angle changes encountered are normally so gradual and wellbore problems like key seat, doglegs, ledges and offsets can be avoided. In addition, packed assemblies have a slight tendency to turn to the right. To compensate this the build section should be completed when it is slight to the left of the required azimuth to the target. In situations where the geology of the area causes a normal holding BHA to drop faster, an under-gauge second stabilizer is introduced in the assembly as it has a positive side force which

results to a building tendency. The advantage of this assembly is that it allows optimum utilization of the drilling parameters like the weight on bit and the rotary speed (120-160+RPM) which have a direct impact on the drilling progress (Devereux, 1999).

Unlike other types of BHAs, holding BHAs are characterized by small changes in side forces as a function of WOB application (Bourgoyne et al., 1986). It should be noted that it is easy to control the direction using rotary assemblies if the angle of inclination is greater than 17° from the vertical (Devereux, 1998). The side forces generated by the BHA are dependent on the angle inclination of the well bore. A four stabilizer holding BHA shown in Figure 4 example D, normally shows the least change in side force as the angle of inclination increases what is the case especially in soft formation (Inglis, 1987). It has been proven that using more than five stabilizers to control deviation has no notable change in the neutrality of the BHA. Five stabilizers add too much torque at higher inclinations when used in rotary systems and that is why the three to four stabilizers BHA's are recommended for use (Bourgoyne et al., 1986). In geothermal drilling, the use of more than two stabilizers is avoided since drilling is normally done in total loss zones and it is too risky to have many stabilizers in the assembly especially because only water and polymer or aerated drilling is used in the production sections where the hold BHA is necessary. The factors listed below should be considered when selecting the BHA to use:

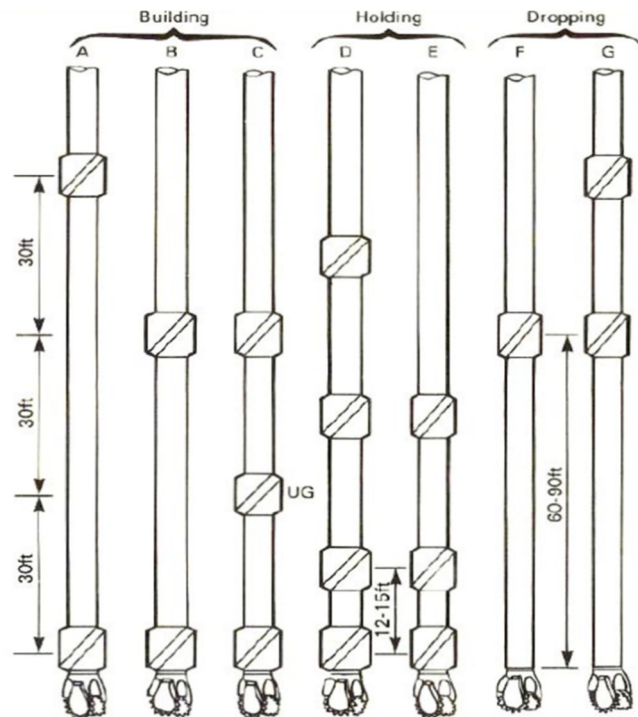


FIGURE 4: Building, holding and dropping assemblies (Economides et al., 1998)

a) *Length of the tool assembly*

This is a very important factor as it determines the ability of an assembly to provide sufficient contact length to guarantee alignment with an already drilled hole. A single stabilizer above the bit cannot be used to maintain a straight path as it acts as a pivot point. It causes the bit to push to one side of the weight being applied, hence building an angle. If another stabilizer is added in the assembly, say 10 m above the bit, it will nullify some of the fulcrum effect experienced in scenario one as it provides another stabilizing point. This will reduce the tendency of the BHA to build angle but two stabilizing points are not enough as they can still follow a curved path. For this reason, a BHA with three stabilizing points is recommended as it forms a stiff assembly which makes it easy to maintain the path of an originally drilled hole. However, other factors like the stability of the well being drilled need to be considered since a packed assembly with many stabilizers poses a lot of challenges should a drill string get stuck.

b) *Stiffness*

The stiffness of the drill collars used in any BHA is a very important factor that should be taken into consideration. It is important to note the relationship between the drill collars diameter and stiffness; it has been found that doubling the diameter of a bar normally increases its stiffness by 16 times. This means that the diameter of a drill collar influences how much it can be deflected. For this reason, maximum diameter of drill collars should be considered for different BHA configurations since large diameter drill collars provide the required stiffness. For example, a $12\frac{1}{4}$ " hole can be drilled using the following sizes of drill collars; $9\frac{1}{2}$ ", 7" and 8". Since the relative stiffness of a drill collar is proportional to the collar radius to the fourth power the $9\frac{1}{2}$ " diameter drill collar for example, will be four times stiffer than 7" drill collars (Smith Services, 2001).

c) *Hole clearance*

Hole clearance plays a major role in determining the effectiveness of BHA in maintaining the required path. For smallest deviation, there should be a minimum clearance between the stabilizers and the walls of the wellbore. Hole enlargement also plays a very big role in determining how well the bottom-hole assembly is aligned in the hole to achieve its intended purpose. Good drilling practices and proper mud design should always be adopted in cases where hole enlargement due to unconsolidated formation is anticipated (Devereux, 1998). In addition, it is important to consider the wear on the contact tools.

d) *Wall support and length of the contact tool*

In order to ensure that the drill bit is stabilized and the drill collars are centralized, the surface area in contact with the bottom hole assembly should be adequate to ensure that the stabilizing tool does not dig into the walls of the hole. If the surface area is not sufficient, the stabilization is lost and the wellbore tend to drift. Formations that are strong, uniform and hard normally provide the best stabilization in comparison to soft and unconsolidated formations which may require the use of a long blade stabilizer to achieve stabilization (Smith Services, 2001).

4.1.3 Angle dropping BHA

The assembly uses the pendulum principle which is derived by removing the near bit stabilizer in the assembly and retaining the stabilizers in the upper section. Normally, a dropping assembly consists of two stabilizers, with the distance between the first stabilizer and the bit being around 30 - 90 ft as shown in Figure 4. With increasing distance between the bit and the first stabilizer, the bit is pulled towards the low side of the wellbore by gravity. This increases the bit tilt and bit side force and hence the angle drop. Hole inclination plays a very important role in determining the rate of drop for different dropping assemblies. Higher hole inclinations result in higher rate of drop and vice versa since the force that causes the dropping tendency is a sine function of the inclination angle (Computerlog Drilling Service, 2000). The dropping assemblies are normally used in S trajectory type wellbores which require planned drop in an angle. In addition, the assembly is used when the angle of inclination goes beyond the intended size and must be dropped to bring the well trajectory back on course.

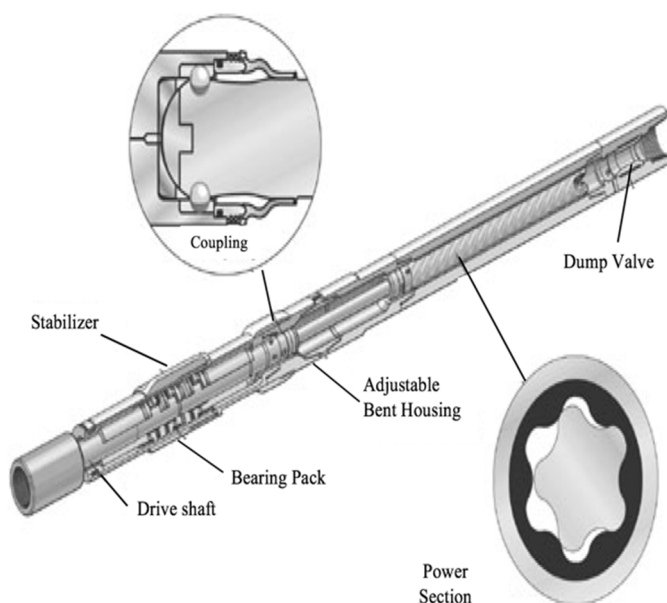


FIGURE 5: PDM assembly (Economides et al., 1998)

4.2 Positive displacement motors (PDM)

PDM refers to downhole mud motors that makes use of the Moineau pump principle to provide motion to the bit without rotating the entire drill string (Economides et al., 1998). Mud motors can be powered using different kinds of drilling fluids such as drilling mud, air and water. In order to deviate a well, PDMs contain a bent housing and if not a bent sub is run above the PDM. Figure 5 shows a PDM assembly which is made of the following four sections:

- i) *Dump valve/by pass valve* - Makes it possible to fill up or drain the drill string during tripping in or out of hole.
- ii) *Motor assembly* - Contains a rubber lined stator which contains a spirally shaped cavity of elliptical cross section. A solid steel shaft which is spiral in shape runs through the stator cavity with the lower end of the shaft fixed to a connecting rod.

- iii) *Connecting rod* - It has a universal joint on both sides to accommodate the eccentric rotation of the rotor and transfer the rotation to the draft shaft.
- iv) *Drive shaft and bearing assembly* - Contains bearings (thrust and radial) which allows free rotation of the drive shaft. The drive shaft is then connected to the bit sub, which is the only rotating external part of the mud motor.

4.3 Jetting technique

This is an old technique developed in 1950s that is used to deviate wellbores in soft formation. This method although not very popular today is still used frequently in some situations as it offers numerous advantages. To achieve the deflection a special jet bit can be used but also standard tri-cone bits with one very large nozzle and two small ones can be used (Baker Hughes INTEQ, 1995). This is however only possible if the formation is soft and can be easily eroded by mud exiting the largest nozzle and if the rig hydraulic horsepower is adequate to provide jetting enough to erode the formation. Figure 6 shows the jetting technique.

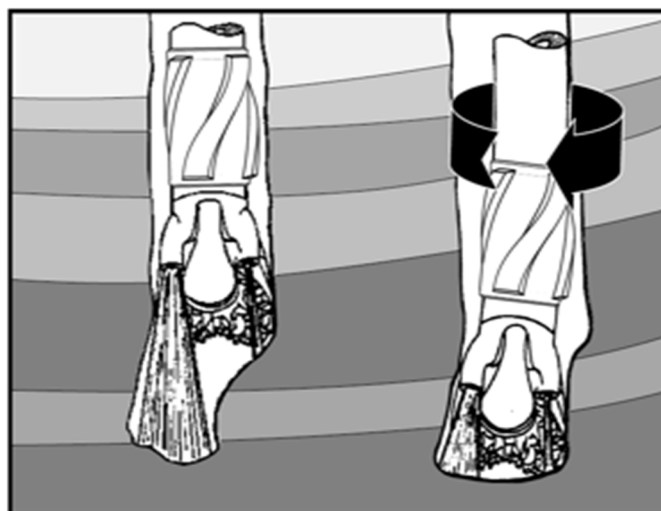


FIGURE 6: Jetting technique
(Baker Hughes INTEQ, 1995)

4.4 Whipstock

A whipstock is a wedge with a concave face which is placed in a well with the face pointed to the direction that the well is meant to go to. These were the main deflection tools between 1930 and 1950. Although rarely used nowadays they are used in some special operations like coiled tubing drilling for work over jobs. There are three types of whipstocks that are used in directional drilling namely; standard removable whipstock which is mainly used for kick off and side-tracking, circulating whipstock and permanent casing whipstock which is designed to stay permanently in the well (Rabia, 2002).

5. DIRECTIONAL DRILLING CHALLENGES IN OLKARIA, KENYA

Directional drilling in Olkaria geothermal field started in the year 2007. This was necessary in order to drill high productivity geothermal wells and take advantage of the other benefits associated with directional drilling as discussed earlier in this report. Over 100 directional wells have been drilled in Olkaria and all of them employ the build and hold (J shape) design with the target angle of inclination being 20° (Munyoki, 2012). As shown in Figure 7, the kick off point for the wells is mostly done at 400 mRKB where the formation is competent or as advised by the geologists. The drilling media for the upper section of the wellbore is water based mud while aerated drilling is introduced from 300 m. Directional drilling in Olkaria poses a number of challenges. This report focuses on the different challenges faced in Olkaria, emphasising the BHA design related challenges. Data for 2 wells drilled in Olkaria, Kenya and 2 wells drilled in Theistareykir, Iceland will be used for analysis and comparison. The challenges discussed in this report represent typical problems faced while drilling directional wells in Olkaria geothermal field.

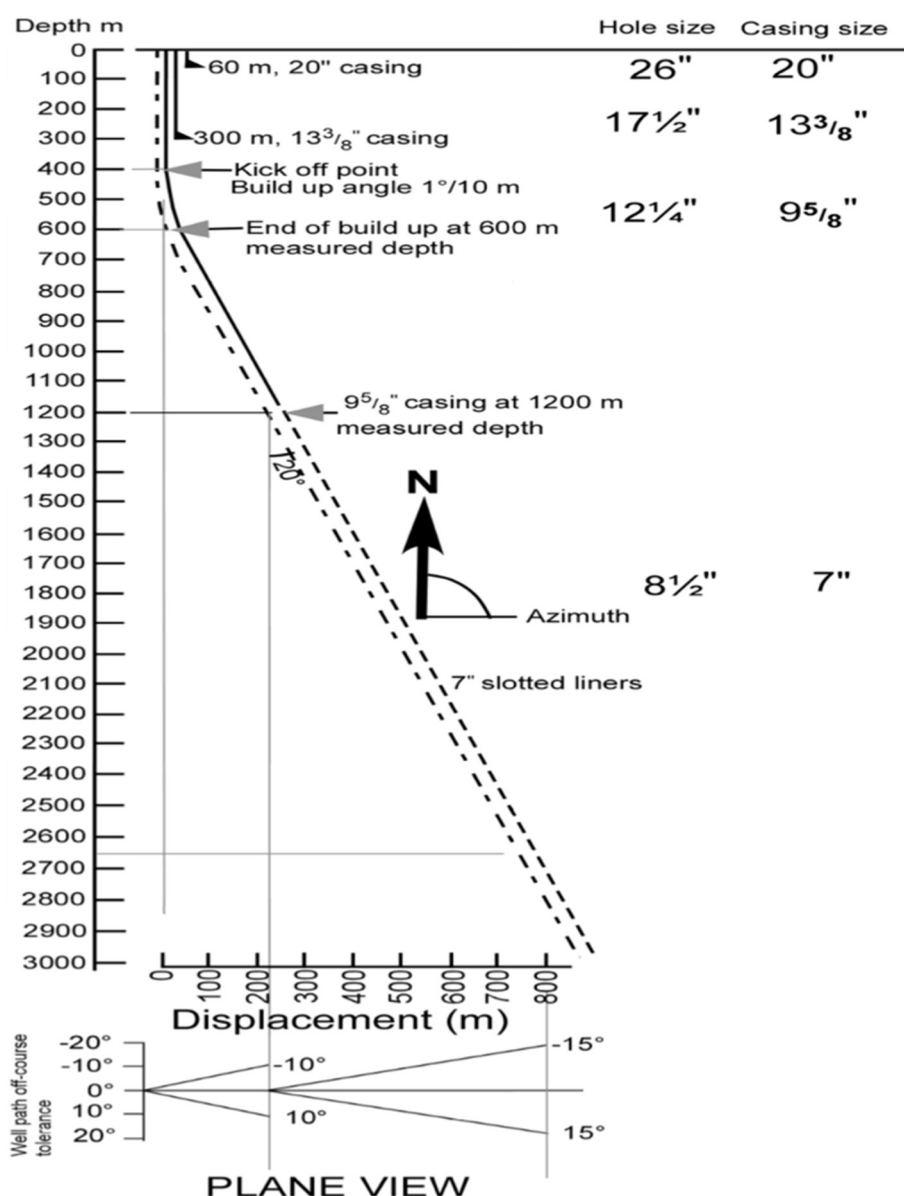


FIGURE 7: Typical Olkaria directional well profile (Munyoki, 2012)

5.1 Formation challenges

Olkaria geothermal field is primarily dominated by loose and unconsolidated rocks that are prone to collapsing or sloughing when drilling using a directional bottom hole assembly. This makes it hard to control the desired trajectory as the BHA tends to lie on the softer side of the wellbore, generating undesirable side forces which makes the drill bit follow a different path. The other danger that is caused by the unconsolidated formation is collapse that lead to hole pack-off which may result in a stuck drill string. The other challenge faced in drilling directional wells is possible poor hole cleaning. The efficiency of directional drilling operation is dependent on how well the hole cleaning is done. Due to numerous losses encountered in Olkaria field, sometimes hole cleaning is not efficient even when using aerated drilling. Poor hole cleaning especially during kick-off often results to low rate of penetrations which overworks the mud motor thus reducing its life time. Interbedded lithology consisting of alternating hard and soft rocks layers present another serious challenge in maintaining the course of a directional well. With this kind of formation, it is hard to optimize bit selection as the bit is made to

drill through formations desired and undesired for its use. This kind of formation normally cause some deflecting forces that may lead to bit walk especially if the bit is damaged from drilling in formations it is not designed for (Devereux, 1998). This may lead to sudden increase or drop in angle of inclination which is not desirable in directional drilling. The other formation challenge is encountered when drilling through aquifer rich formations. Cases like this have been encountered in Olkaria. This normally causes the bottom hole assembly to hang down to vertical thus affecting the angle of inclination adversely. Other formation challenges include drilling in very soft formations which causes the angle of inclination to drop and drilling in clay rich formations which makes it very hard to build an angle by sliding the mud motor in clay.

5.2 Bottom hole assembly design challenges

In Olkaria the main wellbore trajectory design employed is the J-shape type. Drilling of a J-shaped type well is a process of two phases which are building the desired inclination after the kick off, and holding the angle to the target depth. The build section ranges from 400 m to 600 m RKB. Building the angle requires an angle building BHA and holding the angle requires an angle holding BHA. The design of these BHAs has presented some serious challenges in directional drilling as discussed below.

5.2.1 Angle building BHA

The BHA configuration normally consists of a 12¼" drilling bit, a 8" or 7¾" bent-housing mud motor, non-magnetic drill collar (NMDC), 4 drill collars, heavy walled drill pipes and drill pipes. The mud motor has an integral 12¼" stabilizer. The BHA is normally introduced at 400 m RKB or according to the drilling program and is required to build the angle of inclination of 20° at a rate of 3°/30 m. The build section is usually 200 m measured along the actual trajectory of the well. When using the BHA, the following challenges are encountered:

- Failure to achieve the desired results using the same BHA at times for the same geological conditions and hence the need to optimize the drilling parameters or BHA configuration
- Very hard formations lead to lower build up rate especially when sliding. This normally leads to exceeding the working life of the mud motor before the required inclination is achieved. The mud motor operating time is rated at 175 running hours.
- While sliding in alternating hard rocks in the upper sections of the hole, torque is induced in the string and cases of shear breakage on the tool joint of NMDC have been witnessed.
- Drill bit bearing failure has also been noticed while using this BHA especially when drilling through hard formation with consistent string vibrations.

5.2.2 Angle holding BHA

This BHA is normally introduced after achieving the desired angle of inclination and azimuth. It consists of a 12¼" or 8½" bit, a near bit stabilizer and a string stabilizer located after two drill collars. This BHA design has always presented the biggest directional drilling challenge in Olkaria. Due to unconsolidated formations that collapse easily, there is always a very big risk of getting stuck if a third stabilizer is introduced should the formation collapses on this packed BHA. Using two stabilizers in the configuration has given the following results:

- The angle of inclination usually drops.
- The azimuth shifts on either side of the desired path. This is due to bit walk.
- Minor doglegs start to develop and the torque rises. This causes a lot of resistance causing drill string rotation due to friction.
- When correcting the BHA to achieve azimuth, the inclination sudden changes can occur that make it difficult to maintain the intended trajectory.

For this reason, there is a need to optimize the BHA design for the angle holding as well as optimising the relevant drilling parameters such as revolution per minute (RPM), weight on bit (WOB) and pump strokes per minute (SPM) among other factors that may limit the effectiveness of this BHA.

5.2.3 Angle correction BHA

This BHA is used to correct the target direction or angle of inclination by either lowering or increasing based on the survey data. The following challenges are faced when using this BHA:

- BHAs expected to increase the angle can sometimes lead to a decrease in angle and also a noted shift in the azimuth.
- BHAs meant to hold the inclination usually do so for a short interval. The BHA will hold for about 100 m and then start to drop. The BHA may also lead to sudden increase in the inclination.

6. DATA ANALYSIS

In this section, data for the different BHA configurations and drilling parameters used is presented in tables. The tables provide the different BHA configurations used for the four wells which are considered here. The data provided in the tables will be used to analyse the effectiveness and the performance of different BHAs, when subjected to different drilling parameters. The analysis will focus on the BHAs used from the kick-off point to the target depth. The drilling parameters used for the analysis are the WOB and RPM. For the purposes of comparison, the average WOB in each well has been used instead of the instantaneous WOB.

6.1 Case studies – BHA design for directional drilling in Olkaria, Kenya and Theistareykir, Iceland

In this section, the effectiveness of different BHA configurations from kick off point to target depth when subjected to different drilling parameters (WOB and RPM) will be analysed. Data for four wells, two from Kenya and two from Iceland will be used for the analysis.

6.1.1 OW-710B in Olkaria field, Kenya

This well was drilled to cater for additional steam for Olkaria 1, unit IV and V. The KOP for the well was done at 500 m depth as planned and went well until 804 m when the drill string got stuck. Efforts to free it were unsuccessful and a back-off opted. The fish was plugged in hole using cement and a new kick off was initiated at 710 m using a kick off BHA. This BHA was meant to build an inclination angle of not more than 20° at a rate of 3°/30 m with deviation surveys conducted at different intervals as shown in Appendix I. As shown in Table 1, drilling of OW-710B was accompanied by several challenges related to angle holding BHA design.

The second kick off for the well was done successfully using two types of BHAs as shown in Table 1 from 710 m to 1,202 m attaining the required angle of 22.85° and an azimuth of 337.19°N. An average WOB ranging from 5.4 -7 tons and an average rotary speed of 43-50 rpm was used to build the angle of inclination from 5.1° to 22.85° within a measured distance of 376 m. As shown in Table 1, introduction of angle holding BHAs with the provided configuration from a depth of 1,202 m to 1,550 m and 1,856 m to 2,076 m leads to an angle decrease from 22.85° to 17.77° and 22.05° to 17.21° respectively. The angle drop may have been caused by a number of factors such as introduction of a new BHA in a section that had been drilled by a totally different BHA. Before the first holding BHA was introduced a slick BHA without stabilizers had been used to drill out cement and drill 7 m into the formation past the 9½" casing shoe. Normally, introducing a BHA in a section of the hole that has been created by a BHA of a

TABLE 1: OW-710B BHA data performance

BHA Type	Depth (m)		Metres drilled	Inclination (°)		Average angle drop/build (30m)	Av. WOB (tons)	RPM	Desired result	Achieved result
	In	Out		In	Out					
Kick-off BHA (12¼" hole) Bit- MM- O-SUB- NMDC- 3/8"DC-xo-9/5"HWDP	710	826	116	1.55	5.1	0.92	5.4	-	Build angle	Build angle
Angle building BHA Bit- bit sub- STB- NMDC- 1/8"DC- STB- 8/8"DC- Flex joint- jar- xo- 9/5"HWDP	826	1202	376	5.1	22.9	1.42	7	43-50	Build angle	Build angle
Angle holding BHA (8½" hole) Bit- bit sub- STB- xo- short DC- xo- STB- NMDC- xo- 15/6.5"DC- xo- 9/5"HWDP	1202	1550	348	22.9	17.8	-0.44	5.8	47-48	Angle hold	Angle drop
Angle correction Bit- NB- xo- 2/short DC- xo- STB- NMDC- xo- 15/6.5" DC- xo- 9/5"HWDC	1550	1600	50	17.8	14.3	-2.06	5.7	47	Angle correct	Angle drop
Angle correction Bit- bit sub- STB- NMDC- xo- 2/short DC- xo- STB- xo- 15/6.5" DC- xo- 9/5"HWDP	1600	1858	258	14.3	22.1	0.90	6	47-66	Angle correct	Angle correct
Angle holding Bit- bit sub- STB- xo- 2/short DC- xo- STB- NMDC- xo- 15/6.5"- xo- 9/5"HWDP	1858	2076	218	22.1	17.2	-0.67	5.7	47-60	Angle hold	Angle drop
Angle correction Bit- bit sub- STB- NMDC- xo- 15/6.5"-xo-9/5"HWDP	2076	2509	433	17.2	22	0.33	5.2	47-60	Angle correct	Angle correct
Slick BHA due to high torque Bit- bit sub- NMDC- xo- 15/6.5"- xo-9/5"HWDP	2509	3120	611	22	15	-0.34	6.5	45-50		

different configuration, the hole curvature may cause the new BHA to behave in an opposite manner to which it was designed for (Bourgoyne et al., 1986). Secondly, the other factor that may have resulted in the angle drop is the stabilizer placement in the BHA. Holding BHAs by design are meant to minimize the rate at which an angle of inclination builds or drops but they do not maintain the inclination angle entirely. It is difficult to maintain the angle of inclination using these assemblies due to the effects of formation and gravity. To overcome this, the packed assembly should be designed to provide sufficient length of contact to ensure alignment with an already drilled hole as discussed earlier in this report. Normally, three or more stabilizing points are necessary to ensure effectiveness of a packed assembly (Smith Services, 2001). The two angle holding BHAs introduced had only two stabilizing points with the second stabilizer placed 24 and 43 ft from the first stabilizer respectively. This means that there was no sufficient length of contact to hold the angle. Based on their configurations, the BHAs should have built the angle instead of dropping. The WOB application for these two assemblies may not have been sufficient to provide the right tangent length that would have resulted in angle build. In addition, if the stabilizers in the assembly were under gauge the assembly would decrease the angle (Bourgoyne et al., 1986). Other factors listed earlier in this report may have contributed to the angle drop.

To correct for the angle drop, another BHA was introduced at a depth of 1,550 m as shown in Table 1. This BHA was supposed to control the angle drop but instead led to a severe angle drop of 2.06° in only 50 m. This rapid angle drop may have been caused by the factors discussed above.

The angle drops in the two instances were corrected by the use of building BHA composed of just one near bit stabilizer. These BHAs were introduced at a depth of 1,600 m to 1,858 m and 2,076 m to 2,500 m and an average build-up angle of 0.9° and 0.33° per every 30 m respectively was achieved as shown in Table 1. Single stabilizer building assemblies are very effective at low inclinations since they can generate more side force as discussed earlier in this report. Due to high torque generated during drilling of the well, a slick BHA without stabilizer was used to drilling the well to 3,120 m RKB.

6.1.2 OW-49C in Olkaria field, Kenya

The well was drilled to provide steam for 560 MWe. The kick off for the well was done at 480 m RKB using a kick off BHA with a downhole motor. A build-up rate of $2.47^\circ/30$ m was achieved and by 677 m depth the angle of inclination was 17.8° . Drilling of the well was faced by several BHA design challenges just like OW-710B discussed earlier. Some of the challenges encountered are similar to those faced in OW-710B and will only be mentioned but not discussed in details in this case study.

An angle holding BHA shown in Table 2 was introduced after the build-up section. It was supposed to hold the angle but after drilling for only 70 m the angle dropped from 17.8° to 11.9° . Based on the configuration of the BHA, the two stabilizers with only 30 ft between them would have provided sufficient side forces to build the angle instead of dropping. Fulcrum assemblies with such configurations are affected greatly by the WOB application. The drilling parameters used to drill the section were not fully optimized, the WOB and the RPM used were too low as shown and may have contributed to the BHA behaviour. The angle correction was done by introduction of another BHA as shown in Table 2 with two stabilizers which were 60 ft apart. The WOB and RPM were also optimized what resulted in a good response. Other BHAs introduced while drilling the $12\frac{1}{4}$ " hole section responded well based on their configuration and the drilling parameters used. However, to minimize the rate of build from a depth of 995 m, one of the short drill collars should have been removed. The distance from the near-bit stabilizer to the first drill string stabilizer is the main design feature of any fulcrum assembly that affects the build rate (Bourgoyne et al., 1986). This means that if the distance between the near-bit stabilizer and the string stabilizer is reduced from 20 ft to 10 ft by removing one short drill collar, the build rate would have dropped if all other factors would have been kept constant. The longer the fulcrum section, the more the bend which results in higher side forces being generated hence the build rate for the angle increases. In addition, the build rate can have been affected by the hole inclination as discussed earlier in this report.

In drilling of the $8\frac{1}{2}$ " section, similar angle holding challenges were encountered. A combination of pendulum and fulcrum assemblies were used to drill this section. From a depth of 1,372 to 1,872 m a fulcrum assembly consisting of two short drill collars was used. The angle rose steadily at a rate of $0.54^\circ/30$ m and the inclination angle rose from 20.6° to 29.6° . This means that the wellbore at this point was at a tangent point and with the right BHA configuration, it would have been easy to maintain the angle at this point. However, due to the well design requirement, the angle had to be dropped to 21.2° using an angle dropping BHA with the first string stabilizer placed 33 ft from the bit. With this pendulum BHA an angle drop-rate of $2.07^\circ/30$ m was hold for 122 m. The angle holding BHA introduced thereafter resulted in an increase in the angle of inclination from 19.5° to 27° within 248 m and had to be dropped again to 20° using a pendulum BHA. Due to these interchanging drops and increases in the angle of inclination, there was very high torque during drilling and a slick BHA without stabilizers had to be used to drill the wellbore from 2,517 m to 2,960 m. The well was terminated at that depth due to high torque and drag. In Appendix II, the survey data shows clearly that the Dog Leg Severity (DSL) was high at some occasions what possibly led to very high torque during the drilling of the well.

TABLE 2: OW-49C BHA data performance

BHA Type	Depth (m)		Metres drilled	Inclination (°)		Av. angle drop/build (30m)	Av. WOB (tons)	RPM	Desired result	Achieved result
	In	Out		In	Out					
Kick-off BHA (12¼" hole) Bit- MM-O-sub-NMDC- 4/8"DC- xo- 7/HWDP	480	677	197	1.6	17.8	2.5	5		Angle build	Angle build
Angle holding Bit- bit sub- STB- NMDC- STB- 9/8"DC- xo- 12/HWDP	677	747	70	17.8	11.9	-2.5	5.5	35-40	Angle hold	Angle drop
Angle building Bit-NB-NMDC-8"DC- STB-5/8"DC-xo- 15/HWDP	747	995	248	11.9	20.6	1.1	10.5	40-45	Angle build	Angle build
Angle holding Bit- bit sub- STB- 2SDC- STB- NMDC- 6/8"DC- xo-15/HWDP	995	1186	191	20.6	25.3	0.7	7	45-52	Angle hold	Angle build
Angle correction (8½" hole) Bit- bit sub- 2/6.5"DC- STB- NMDC -9/6.5"DC- 15/HWDP	1186	1372	186	25.3	20.6	-0.8	6.6	45-60	Angle correct	Angle correct
Angle holding BHA Bit- STB- 2SDC- STB- NMDC- 12/6.5"DC- 15/HWDP	1372	1840	468	20.6	29.2	0.6	7	55-70	Angle hold	Angle build
Angle correction BHA Bit- bit sub- 6.5"DC- STB- NMDC- DC- Stab- 10/6.5DC- 15/HWDP	1840	1998	158	29.6	21.2	-1.6	6.8	50-60	Angle drop	Angle drop
Angle holding BHA Bit- STB- 2SDC- STB- NMDC- 12/6.5"DC- 15/HWDP	1998	2057	59	21.2	19.5	-0.9	5	55	Angle hold	Angle drop
Angle holding BHA Bit- bit sub- STB- NMDC- STB- 9/6.5"DC- 15/HWDP	2057	2305	248	19.5	27	0.9	5	50-60	Angle hold	Angle build
Angle correction BHA Bit- bit sub-2/6.5"DC- STB- NMDC- 9/6.5"DC- 15/HWDP	2305	2517	212	27	20	-1.0	8	60	Angle correct	angle correct
Slick BHA Bit-bit sub-NMDC-STB- 9/6.5"DC-12HWDP	2517	2960	443	20	12	-0.5	9.2	45-60		

6.1.3 THG-6 in Theistareykir, Iceland

THG-6 well design was based on the information obtained after drilling THG-3. The target azimuth for the well was planned to be $285^{\circ}\text{N} \pm 10^{\circ}$ with the final angle of inclination at TD set at $30^{\circ} \pm 3^{\circ}$. The angle build-up rate for the well was planned to be $2^{\circ}/30\text{ m}$ with the KOP set at 290 m. As planned, the kick off for the well was done at 288 m RKB using a kick off BHA composed of a mud motor and an MWD tool as shown in Table 3. The drilling of the 12¼" section of the well went well without any angle building challenges and by 663 m the angle of inclination was with 25.3° close to the target inclination. This continued until 846 m which was the target production casing depth, the angle of inclination at this depth was 30.5° . Only one BHA was used for drilling this hole section and the average WOB used was 12 tons.

Drilling of the 8½" section was done using the same BHA configuration as the one used for drilling the production section. The tangent section of this wellbore was drilled by a combination of rotation of the drill string and sliding to drill ahead. As shown in Table 3 and Appendix III the angle of inclination was maintained at 30° to a depth of 1,315 m using the angle holding BHA. The drill bit had to be changed at 2,161 m during which the MWD tool was laid down and replaced by a drill collar. With the absence of the MWD tool, it was not possible to monitor the angle change on real time and hence the angle of inclination rose from 31° to 37.9° by the time the target depth of 2,799 m was reached. Despite this, drilling of the main hole was done successfully with no BHA related challenges. An average WOB of 6.3 - 8 tons and an average rotary speed of 60 – 70 rpm was used to drill the production section.

TABLE 3: THG-6 BHA data performance

BHA Type	Depth (m)		Metres drilled	Inclination (°)		Av. angle drop/build (30 m)	Av. WOB (tons)	RPM	Desired result	Achieved result
	In	Out		In	Out					
Kick off BHA (12¼"hole) Bit-bit sub-mud motor-STB-MWD-STB-BT050-3DC-6 other	266	846	580	1	30.9	1.6	12	50-60	Angle build	Angle build
Angle holding BHA (8½" hole) Bit-mudmotor-STB-MWD-STB-5DC-jar-DC-3HWDW-wiper	846	2161	1315	30.9	31	0.0	6.3	50-80	Angle hold	Angle hold
Angle holding BHA Bit-mud motor-STB-DC-STB-5DC-Jar-DC-3HWDW-Wiper	2161	2799	638	31	37.9	0.3	8	60-70	Angle hold	Angle build

6.1.4 THG-07 in Theistareykir, Iceland

This well was drilled in order to study the geothermal reservoir conditions of the resource under Ketill mountain. Drilling the well would provide important data such as the heat condition, permeability and the characteristics of the geothermal fluid in the area as well as confirm the results from the previous studies showing that there is an upward flow in the area. The KOP for the well was done at 294 m RKB as planned in the drilling program. A BHA composed of a 9⅝" mud motor and an MWD tool as shown in Table 4 was used for the kick-off. The kick-off for the well was successful but several plug jobs had to be conducted before reaching a depth of 397 m due to losses and H₂S influx between 345 and 385 m. After the plug job the cement was drilled out using the kick off BHA and an inclination of 7.14° was attained. A fulcrum BHA with just one near bit stabilizer was introduced and used to drill up to 416 m. The WOB used on this BHA was around 11 tons and as discussed earlier, fulcrum assemblies respond highly to WOB application and hence the high build up rate. The earlier BHA used for kick off was then re-introduced and used to build up the angle from 9.03° to 34.94° with a build-up rate of 2.98°/30 m as shown in Table 4. As indicated in Appendix IV, the build-up rate was smooth for this hole section. An average WOB of 7 tons was used.

For the 8½" section, the same BHA configuration as shown in Table 4 was used to hold the angle of inclination from 776 to 1,573 m. Using that configuration, the inclination angle was maintained as required with the dog leg severity kept below 0.6° as shown in Appendix IV. After this the mud motor and the MWD tool were laid down and a fulcrum assembly consisting of two stabilizers placed 30 ft between them was introduced. The introduction of this BHA configuration resulted in angle rise of a total of 15.76° from 33.71° to 49.47° within 657 m with a build-up rate of 0.72°/30 m. This build up may have been the result of use of high ROP and WOB during drilling. The last BHA introduced in the well dropped the angle from 49.47° to 45.67° within 278 m as per the BHA design. The WOB application was also reduced to accelerate the angle drop.

TABLE 4: THG-7 BHA data performance

BHA Type	Depth (m)		Metres drilled	Inclination (°)		Av. angle drop/build (30 m)	Av. WOB (tons)	RPM	Desire d result	Achieved result
	In	Out		In	Out					
Kick off BHA (12¼" hole) Bit -mud motor-STB-MWD-UBHO-STB-4DC-9 other	270	397	127	0.7	7.1	1.5	6.5	50-60	Angle build	Angle build
Bit-STB-4DC-jar-2DC-wiper, 5 other	397	416	19	7.1	9.0	2.9	11	50-60		
Angle building BHA Bit -mud motor-STB-MWD-UBHO-STB-4DC-9 other	416	776	360	9.0	34.9	2.1	7	50-70	Angle build	Angle build
Angle holding BHA (8-1/2" hole) Bit-mudmotor-STB-MWD-STB-4DC-jar-7other	776	1573	797	34.9	33.7	-0.1	5.7	50-80	Angle hold	Angle hold
Angle holding BHA Bit-NBS-DC-STB-5DC-Jar-9other	1573	2230	657	33.7	49.5	0.7	5.3	50-80	Angle hold	Angle build
Angle dropping BHA Bit-BS-PC-STB-PC-DC-STB-3DC-9other	2230	2508	278	49.5	45.7	-0.4	3.8	65-80	Angle drop	Angle drop

7. DISCUSSION

As shown in the two case studies for the Olkaria wells, the fulcrum assembly introduced to build the angle responded very well to WOB application. As discussed earlier in the report, high WOB applications for these assemblies results in high angle build up rates. The major challenges encountered were mainly on angle holding. The angle holding BHA used in the two case studies consisted of two stabilizers. Two stabilizer assemblies can be used especially in areas where the formation is not properly consolidated like it is the case in Olkaria. However, the near bit and the string stabilizer should be full gauge. Should the near bit stabilizer be under gauge, an assembly that is meant to build an angle may cause an angle drop. It is also possible that with two stabilizer BHA configuration that the behaviour changes significantly when they reach a certain depth like shown in the two case studies. A BHA which was supposed to hold inclination may start decreasing the angle. Assuming that the near bit stabilizer is not under gauge, the angle drop may be caused by change in formation, change in formation dip or strike among others (Devereux, 1998). For this reason, it is important to have a very good geological database of the respective area so that such problems can be anticipated earlier and measures taken. In addition, when drilling the tangent (hold) section, the tangent inclination should be greater than 15°. It has been proven that the directional control problems are made worse if the drift angle is less than 15°. This is because a small drift angle increases the tendency of the bit to walk (change in azimuth) (Hole, 2008). Bit walk has been one of the challenges experienced in drilling directional wells in Olkaria and can be minimized by increasing the tangent inclination angle of the hold section.

From the two Olkaria case studies, it is evident that drilling parameters optimization for most BHA configurations is a very important factor. While drilling OW-49C for example, changes in drilling parameters WOB and RPM showed a very big impact on the behaviour of an angle correction BHA consisting of two stabilizers. This means that fewer trips to change the BHA can be made if the response of the BHA to the drilling parameters being used is fully understood. It is advisable to understand these variables as well as taking into account the kind of formation that is being drilled. If these two are combined, some of the challenges experienced could have been avoided or addressed more quickly.

Angle correction in directional drilling should be done sooner rather than later. In the two case studies for the Olkaria wells, in some cases the angle correction was done when it was too late. In OW-49C the BHA introduced at 1,372 m was supposed to hold the angle but it continued building the angle from 20.6° to 29.6° at 504 m before it was changed as shown in Table 2. Correcting the angle at deeper depths is a long process which is hard to control and should therefore be discouraged. In addition, dropping an angle at deeper depths is not recommended as it normally leads to serious drilling challenges. If the circumstances dictate that the angle has to drop, the choice of the BHA to use is very important. In most cases a pendulum assembly is preferred over downhole motors because when the tool face of a downhole motor is aligned to the low side of the hole, the tool normally flips over when reactive force is applied as the bit contacts the bottom. This makes it very hard to hold the motor in its position especially when the well is deep and dipping at a high angle. When using a pendulum assembly to drop an angle, the drilling parameters used should be selected carefully. Low WOB should be applied until the drop trend is established and the second stabilizer in the BHA is in the section of the hole that is dropping. Once this is established, the WOB can be brought up. When this is done, the ROP will improve and the drop rate may increase since the drill collars will be forced to bend outward due to the bend in the hole between the bit and the second stabilizer (Devereux, 1998).

The two case studies for the Icelandic wells drilled in Theistareykir show a different BHA configuration design from that used in Olkaria wells. The BHA used in drilling the two directional wells consists of a downhole motor and an MWD tool for relaying the survey data to the surface as the drilling continues. The down hole motor and the MWD tool are maintained in the BHA as much as possible and only removed if significant losses are encountered when reaching a certain depth. With this combination, it was possible to hold the angle of inclination while maintaining the target azimuth for the well. With mud motor and MWD tool in the assembly it is possible to follow the directional plan more closely since no frequent trips are required to change the BHA and corrections in the slide mode can be done when required. These corrections ensure that the wellbore is kept as close as possible to the planned path (Devereux, 1998). In addition, the use of this kind of BHA configuration for almost the entire well section from KOP to TD minimizes the number of trips to correct the BHA in comparison to when basic rotary assemblies are used as shown in the case studies. When angle or azimuth correction is required, the motor is oriented in the desired direction (tool face angle) and drilling is done in slide mode (without pipe rotation) until the correction is achieved. The change in azimuth or inclination is achieved by the bit tilt derived from bent housing in the motor assembly or from the side force exerted from the stabilizers. Drilling in rotary mode is then continued until another correction is required. In rotary mode, the bit tilt and side forces generated are cancelled out by the rotation of the drill string which causes the assembly to act like a stabilized rotary assembly (Carden and Grace, 2007). In addition, to save trip time, frequent motor corrections normally minimize the problem associated with key seats. Frequent BHA changes when using basic rotary assemblies can result to high dog leg severity if not properly monitored. This normally results in very high torque during drilling which has a direct impact on running of casings as well as the overall drilling progress. The two wells from Olkaria had to be terminated a few meters before reaching the target depth due to excess torque during drilling.

8. CONCLUSIONS AND RECOMMENDATIONS

As shown in the report, BHA design for directional wells plays a very important role for achieving the desired results. In Olkaria, the major BHA related challenges are experienced in the angle holding section. These challenges have led to numerous BHA changes that increase the number of days spent in drilling a well. In OW-710B for example, approximately 6 drilling days were spent on trips to change the BHA. This would have been minimized if the right BHA configuration was adopted for drilling the well. In addition, frequent BHA changes and lack of proper drilling parameters optimization lead to increased torque while drilling, making it impossible to drill to target depth in some wells. For rotary assemblies, stabilizer placement and drilling parameter optimization play a very important role in directional well drilling. The side forces generated by different assemblies determines the behaviour

tendency relative to holding, building or dropping the angle of inclination. In order to benefit fully from BHA design optimization, an understanding of different BHA response to design and operating parameters is necessary. With this knowledge, it is possible to vary the BHA configuration or the drilling parameters to control the directional tendencies appropriately.

In Iceland, BHA related challenges have been minimized by the use of the downhole motor and MWD after the build-up section. Those two make it easy to follow the directional plan more closely and to avoid many trips to change BHA. In addition, it ensures that a smooth trajectory is achieved thus minimizing key seats and severe dog legs that can be brought about by frequent BHA changes. If this is done, the torque values while drilling can be maintained within normal range and hence the well can be successfully drilled to the target depth. In addition, a two stabilizer assembly with a short drill collar between them can be used for the tangent section of a directional well. This BHA has a slight building tendency which can be controlled by optimizing the drilling parameters. The near-bit stabilizer and the string stabilizer should however be full gauge. If the geology of an area is properly understood, a three stabilizer assembly can also be used for drilling the tangent section.

A consideration to increase the tangent inclination angle from 20° to 25-35° should be made. This will minimize bit walks experienced in drilling the tangent section which lead to constant BHA changes to control the azimuth and inclination. In addition, when drilling directional wells, either using rotary assemblies or by downhole motors, a key seat wiper should be included in the BHA. This is very important especially when dog legs are expected. The main purpose of the key seat wiper is to increase the key hole diameter by drilling it out when POOH. To be fully effective, it has to have an outside diameter (OD) that is greater than the OD of any other part of the BHA excluding the stabilizer blades and the bit. The key seat wiper rotates freely and does not have any reaming affect during drilling or when reaming downwards in the well. With a key seat wiper in BHA configuration, torque experienced when drilling due to dog legs is minimized.

ACKNOWLEDGEMENTS

My appreciation goes to the Mr. Lúdvík S. Georgsson, Director UNU-GTP, and Mr. Ingimar G. Haraldsson, Deputy Director for giving me the opportunity to undergo the six-month training program. Many thanks to UNU-GTP staff: Ms. Málfríður Ómarsdóttir, Ms. Thórhildur Ísberg and Mr. Markús A. G. Wilde for supporting me during my stay in Iceland. I wish also to thank my company, KenGen for giving me this opportunity to learn and enhance my skills in geothermal technology.

I am grateful for all the support my supervisor, Mr. Arnar Bjarki Árnason, his fellow engineers at MANNVIT and Mr. Sverrir Thórhallsson gave me. Their encouragement and fruitful ideas kept me going during my project period. I would also like to thank my colleagues at work for providing me with data and support all the time.

My sincere gratitude goes to my family for their support and prayers during my stay in Iceland and Almighty God for protecting me and my family during my absence.

REFERENCES

- Aadnoy., B.S., Cooper, I., Miska, S.Z., Mitchell, R.F., and Payne, M.L. (eds.), 2009: *Advanced drilling and well technology*. Society of Petroleum Engineers, Richardson, TX, 888 pp.
- Adams, N.J., 1985: *Drilling engineering, a complete well planning approach*. Pennwell Books, Tulsa, OK, 849 pp.
- Baker Hughes INTEQ., 1995: *Drilling engineering workbook, a distributed learning course*. Baker Hughes INTEQ Inc., Houston, TX, 410 pp.
- Bourgoyne Jr., A.T., Millheim, K.K., Chenevert, M.E., and Young Jr., F.S., 1986: *Applied drilling engineering*. Society of Petroleum Engineers, SPE Textbook Series, 2, Richardson, TX, 502 pp.
- Carden, R.S. and Grace, R.D., 2007: *Horizontal and directional drilling*. Petroskills, Tulsa, OK, 409 pp.
- Computerlog Drilling Service 2000 (?): *Directional Drilling 1*. Houston, TX: Technology Services Group, 188 pp.
- Devereux, S., 1998: *Practical well planning and drilling manual*. PennWell Corp., Tulsa, OK, 524 pp.
- Devereux, S., 1999: *Drilling technology in nontechnical language*. PennWell, Corp., Tulsa OK, 337 pp.
- Economides, M.J., Watters, L.T., and Dunn-Norman, S., 1998: *Petroleum well construction*. John Wiley & Sons, NY, 622 pp.
- Hole, H., 2008: *Directional drilling of geothermal wells*. Petroleum Engineering Summer School, Workshop 26, Dubrovnik, Croatia, June 2008.
- Inglis T.A., 1987: *Directional drilling, vol. 2*. Graham & Totman Ltd., London, 260 pp.
- Rabia, H., 2002: *Well engineering and construction*. Entrac Consulting, 789 pp.
- Smith Services., 2001: *Drilling assembly handbook*. Smith International, Inc., Houston, TX, 190 pp.
- Speith J.G., 2015: *Handbook of offshore oil and gas operations*. Gulf Professional Publ. WY, USA, 444 pp.
- Vieira, J.L., 2009: *Controlled directional drilling* (4th edition). Petroleum Extension Service, Austin TX, 129-134.

APPENDIX I: OW-710B survey data

KOP Measured Depth (mRKB)	752.0 Depth from KOP	Azimuth Inclination (deg)	337.5 Azimuth					
				TVD	Displacement	North	East	Dog leg severity
739	-13	1.19	79.00	752.00	0.00	0.00	0.00	0.00
758	6	1.55	72.34	739.00	0.27	-0.05	-0.27	-2.79
772	20	1.32	46.03	758.00	-0.24	0.10	0.22	0.63
789	37	1.75	344.78	771.99	-0.57	0.33	0.46	1.50
809	57	3.06	323.63	788.98	-1.09	0.83	0.32	2.88
826	74	5.10	320.72	808.96	-2.15	1.69	-0.31	2.38
838	86	5.27	321.00	825.89	-3.66	2.86	-1.27	3.68
937	185	10.55	330.09	837.84	-4.77	3.72	-1.96	0.44
1071	319	15.78	332.52	935.16	-22.89	19.43	-11.00	1.67
1229	477	22.85	337.19	1064.11	-59.33	51.76	-27.82	1.20
1284	532	21.79	338.66	1209.71	-120.69	108.31	-51.60	1.40
1379	627	20.46	338.18	1260.79	-141.10	127.33	-59.03	0.66
1529	777	17.77	337.19	1349.70	-174.28	158.13	-71.36	0.43
1598	846	15.93	332.21	1492.64	-220.09	200.35	-89.12	0.55
1645	893	14.33	335.27	1558.99	-239.02	217.11	-97.95	1.03
1691	939	14.66	335.90	1604.53	-250.66	227.67	-102.82	1.16
1739	987	16.36	337.09	1649.03	-262.30	238.30	-107.57	0.24
1829	1077	18.76	340.37	1695.08	-275.82	250.75	-112.83	1.10
1920	1168	22.05	345.58	1780.30	-304.76	278.02	-122.56	0.88
2000	1248	22.3	346.6	1864.65	-338.93	311.10	-131.07	1.26
2162	1410	17.21	346.77	1938.66	-369.28	340.63	-138.10	0.17
2229	1477	17.99	348.52	2093.41	-417.22	387.29	-149.07	0.96
2833	2081	16.31	334.51	2157.13	-437.91	407.57	-153.19	0.43
3120	2368	15.03	334.68	2736.83	-607.53	560.68	-226.19	0.22
				3014.01	-681.96	627.96	-258.02	0.14

APPENDIX II: OW-49C survey data

KOP	480.00	Azimuth	225	Planned				
Measured depth	Depth from KOP	Inclination	Azimuth	TVD	Displacement	North	East	Dog leg severity
				480.00	0.00	0.00	0.00	0.00
495.00	15.00	1.80	173.60	494.99	0.47	-0.47	0.05	3.66
514.00	34.00	2.70	172.00	513.97	1.37	-1.35	0.18	1.45
523.00	43.00	2.60	191.60	522.96	1.77	-1.75	0.09	3.07
533.00	53.00	3.80	190.80	532.94	2.44	-2.41	-0.03	3.66
543.00	63.00	4.20	192.50	542.91	3.17	-3.12	-0.19	1.27
552.00	72.00	5.60	195.00	551.87	4.05	-3.97	-0.42	4.80
562.00	82.00	6.80	200.30	561.80	5.23	-5.08	-0.83	4.05
571.00	91.00	8.20	200.10	570.71	6.52	-6.28	-1.27	4.74
581.00	101.00	8.80	207.40	580.59	8.05	-7.64	-1.97	3.76
590.00	110.00	10.00	209.20	589.45	9.61	-9.01	-2.73	4.18
600.00	120.00	10.90	212.00	599.27	11.50	-10.61	-3.74	3.15
610.00	130.00	12.00	216.40	609.05	13.58	-12.28	-4.97	4.28
619.00	139.00	13.70	217.00	617.80	15.71	-13.99	-6.25	5.78
629.00	149.00	15.20	220.60	627.45	18.33	-15.98	-7.96	5.33
638.00	158.00	15.50	224.80	636.12	20.74	-17.68	-9.65	3.90
647.00	167.00	17.10	224.80	644.72	23.38	-19.56	-11.52	5.42
656.00	176.00	17.80	225.60	653.29	26.13	-21.49	-13.48	2.51
677.00	197.00	19.50	226.50	673.09	33.14	-26.31	-18.57	2.50
746.00	266.00	11.90	225.40	740.61	47.37	-36.30	-28.70	3.36
795.00	315.00	11.50	225.90	788.62	57.14	-43.10	-35.71	0.26
804.00	324.00	12.10	227.10	797.42	59.03	-44.38	-37.10	2.20
815.00	335.00	12.60	225.90	808.16	61.43	-46.05	-38.82	1.56
823.00	343.00	12.80	226.90	815.96	63.20	-47.27	-40.11	1.13
842.00	362.00	13.40	229.20	834.44	67.60	-50.14	-43.45	1.28
869.00	389.00	14.70	226.80	860.56	74.45	-54.83	-48.44	1.61
900.00	420.00	16.30	223.60	890.31	83.16	-61.13	-54.44	1.78
928.00	448.00	17.70	231.10	916.99	91.67	-66.48	-61.07	2.83
957.00	477.00	19.00	235.50	944.41	101.11	-71.83	-68.85	2.00
986.00	506.00	20.30	229.80	971.60	111.17	-78.32	-76.53	2.43
995.00	515.00	20.60	230.80	980.03	114.34	-80.32	-78.99	1.56
1031.00	551.00	23.50	232.60	1013.04	128.69	-89.04	-90.39	2.52
1051.00	571.00	23.60	230.30	1031.37	136.70	-94.16	-96.55	1.41
1153.00	673.00	24.80	233.30	1123.96	179.48	-119.73	-130.85	0.51
1190.00	710.00	25.30	225.60	1157.41	195.30	-130.79	-142.15	2.72
1295.00	815.00	28.10	244.40	1250.04	244.75	-152.16	-186.75	2.57
1353.00	873.00	25.00	247.10	1302.60	269.26	-161.70	-209.33	1.75
1372.00	892.00	20.60	217.60	1320.39	275.95	-166.99	-213.41	19.42
1418.00	938.00	22.10	222.20	1363.01	293.26	-179.81	-225.04	1.49
1514.00	1034.00	24.30	231.60	1450.50	332.76	-204.35	-256.00	1.37
1571.00	1091.00	24.70	239.50	1502.29	356.58	-216.44	-276.52	1.76
1725.00	1245.00	26.70	226.20	1639.87	425.77	-264.33	-326.46	1.21
1812.00	1332.00	29.20	224.60	1715.81	468.22	-294.55	-356.26	0.91
1862.00	1382.00	30.40	230.70	1758.94	493.52	-310.58	-375.84	1.99
1896.00	1416.00	29.60	227.10	1788.50	510.31	-322.01	-388.15	1.77
1970.00	1490.00	23.20	232.80	1856.52	539.47	-339.64	-411.37	2.83
2000.00	1520.00	21.20	234.40	1884.49	550.31	-345.95	-420.19	2.12
2022.00	1542.00	19.70	232.90	1905.20	557.73	-350.43	-426.10	2.20
2057.00	1577.00	19.50	231.80	1938.19	569.41	-357.65	-435.28	0.37
2104.00	1624.00	20.50	233.90	1982.21	585.87	-367.35	-448.58	0.80
2195.00	1715.00	23.80	232.10	2065.48	622.60	-389.91	-477.56	1.13
2217.00	1737.00	24.70	230.10	2085.46	631.79	-395.80	-484.61	1.69
2246.00	1766.00	25.30	226.80	2111.68	644.18	-404.29	-493.65	1.60
2290.00	1810.00	27.00	224.10	2150.89	664.16	-418.63	-507.55	1.44
2341.00	1861.00	26.80	227.60	2196.41	687.15	-434.14	-524.53	0.95
2398.00	1918.00	20.70	218.00	2249.73	707.30	-450.02	-536.93	3.85
2432.00	1952.00	19.50	219.30	2281.78	718.65	-458.80	-544.12	1.15
2476.00	1996.00	18.00	215.30	2323.62	732.25	-469.89	-551.98	1.37
2517.00	2037.00	20.10	218.70	2362.13	746.34	-480.89	-560.79	1.77
2698.00	2218.00	13.80	217.40	2537.90	789.51	-515.19	-587.01	1.06
2861.00	2381.00	12.10	222.60	2697.28	823.68	-540.34	-610.14	0.39

APPENDIX III: THG-6 survey data

Depth	Inclination (from Vert)	Grid Azimuth	Closure Direction	True Depth	Coordinates		Dogleg Severity	Closure Distance
					+N/ -S	+E/ -W		
930,0	28,97	293,27		0,00	0,00	0,00		0,00
1300,0	30,22	285,55	289,41	321,72	60,73	-172,35	0,33	182,74
1308,0	29,75	288,78	289,36	328,65	61,91	-176,17	6,30	186,73
1350,0	29,93	287,72	289,25	365,08	68,45	-196,02	0,40	207,63
1400,0	30,23	288,27	289,11	408,35	76,19	-219,85	0,24	232,68
1450,0	30,29	287,41	288,99	451,53	83,91	-243,83	0,26	257,87
1500,0	30,09	288,05	288,88	494,75	91,57	-267,78	0,23	283,00
1550,0	30,27	287,11	288,77	537,98	99,16	-291,74	0,31	308,13
1600,0	30,74	286,98	288,64	581,06	106,60	-316,00	0,28	333,50
1650,0	30,11	289,35	288,61	624,17	114,49	-340,06	0,81	358,81
1700,0	30,33	289,88	288,67	667,38	122,94	-363,76	0,21	383,97
1710,0	30,14	289,20	288,68	676,02	124,62	-368,51	1,18	389,01
1750,0	30,18	287,30	288,66	710,61	130,92	-387,59	0,72	409,11
1800,0	30,21	288,45	288,62	753,82	138,64	-411,53	0,35	434,25
1850,0	30,24	287,08	288,57	797,02	146,32	-435,50	0,41	459,42
1900,0	31,09	285,23	288,44	840,03	153,41	-459,99	0,76	484,90
1950,0	30,44	282,79	288,22	883,00	159,60	-484,80	0,84	510,40
2000,0	29,52	283,76	287,99	926,31	165,34	-509,12	0,62	535,29
2050,0	30,16	284,42	287,82	969,68	171,40	-533,25	0,43	560,12
2100,0	30,26	285,63	287,70	1012,89	177,92	-557,55	0,37	585,25
2150,0	30,97	287,32	287,65	1055,92	185,14	-581,96	0,67	610,70
2200,0	32,19	288,69	287,66	1098,51	193,23	-606,87	0,85	636,89
2250,0	33,21	287,73	287,68	1140,59	201,68	-632,52	0,69	663,90
2300,0	34,40	289,75	287,73	1182,13	210,61	-658,87	0,98	691,71
2350,0	35,83	290,83	287,83	1223,03	220,59	-685,84	0,93	720,44
2400,0	36,79	290,11	287,93	1263,33	230,94	-713,58	0,63	750,02
2450,0	37,76	291,10	288,04	1303,11	241,60	-741,92	0,68	780,26
2500,0	38,84	292,91	288,19	1342,35	253,21	-770,65	0,93	811,18
2550,0	40,01	292,88	288,37	1380,97	265,56	-799,90	0,70	842,83
2600,0	39,87	293,16	288,54	1419,31	278,12	-829,44	0,13	874,83
2650,0	39,14	298,07	288,78	1457,89	291,87	-858,12	1,92	906,40
2700,0	38,68	292,19	289,00	1496,80	305,20	-886,56	2,23	937,62
2750,0	37,98	298,19	289,19	1536,02	318,40	-914,62	2,27	968,46
2770,0	37,87	297,81	289,30	1551,79	324,18	-925,47	0,39	980,61

APPENDIX IV: THG-7 survey data

Survey Type	Meas. Depth	Inc.	Azimuth	TVD	Closure	Vertical Section	Coordinates		D.L.S.
							N-S	E-W	
GMS	300,00	0,793	93,39	299,99	2,08	-0,12	S 0,1	E 2,1	0,079
GMS	330,00	3,619	72,31	329,97	3,19	0,15	N 0,2	E 3,2	2,893
GMS	360,00	6,192	70,63	359,85	5,70	0,98	N 1,0	E 5,6	2,577
GMS	390,00	6,709	65,49	389,66	9,01	2,24	N 2,2	E 8,7	0,775
GMS	420,00	7,134	58,62	419,45	12,55	3,94	N 3,9	E 11,9	0,930
GMS	450,00	9,026	46,55	449,15	16,56	6,53	N 6,5	E 15,2	2,531
GMS	480,00	11,675	40,20	478,66	21,59	10,46	N 10,5	E 18,9	2,880
GMS	510,00	14,801	37,47	507,86	28,06	15,83	N 15,8	E 23,2	3,187
GMS	540,00	18,574	39,61	536,59	36,39	22,55	N 22,5	E 28,6	3,822
GMS	570,00	21,307	40,00	564,79	46,44	30,41	N 30,4	E 35,1	2,736
GMS	600,00	24,265	41,18	592,44	57,96	39,22	N 39,2	E 42,7	2,993
GMS	630,00	27,189	42,65	619,47	70,93	48,91	N 48,9	E 51,4	2,993
GMS	660,00	30,377	44,41	645,76	85,36	59,37	N 59,4	E 61,3	3,298
GMS	690,00	32,920	46,41	671,30	101,10	70,41	N 70,4	E 72,5	2,752
GMS	720,00	34,942	47,77	696,19	117,84	81,81	N 81,8	E 84,8	2,158
GMS	750,00	35,210	48,02	720,74	135,07	93,37	N 93,4	E 97,6	0,307
GMS	780,00	34,914	48,03	745,29	152,30	104,89	N 104,9	E 110,4	0,296
GMS	810,00	34,925	47,88	769,89	169,46	116,40	N 116,4	E 123,2	0,086
GMS	840,00	33,974	48,02	794,63	186,43	127,76	N 127,8	E 135,8	0,954
GMS	870,00	33,930	47,89	819,52	203,18	138,98	N 139,0	E 148,2	0,084
GMS	900,00	34,234	47,12	844,36	219,99	150,34	N 150,3	E 160,6	0,528
GMS	930,00	34,666	46,16	869,10	236,96	161,99	N 162,0	E 172,9	0,693
GMS	960,00	35,224	46,03	893,69	254,14	173,91	N 173,9	E 185,3	0,563
GMS	990,00	34,856	46,08	918,25	271,37	185,86	N 185,9	E 197,7	0,369
GMS	1.020,00	33,866	46,26	943,02	288,30	197,59	N 197,6	E 209,9	0,995
GMS	1.050,00	34,489	46,57	967,84	305,15	209,21	N 209,2	E 222,1	0,647
GMS	1.080,00	34,241	46,92	992,60	322,08	220,81	N 220,8	E 234,5	0,315
GMS	1.110,00	34,374	47,35	1.017,38	338,99	232,31	N 232,3	E 246,9	0,277
GMS	1.140,00	35,122	47,24	1.042,03	356,09	243,91	N 243,9	E 259,4	0,751
GMS	1.170,00	35,759	47,20	1.066,47	373,48	255,72	N 255,7	E 272,2	0,638
GMS	1.200,00	35,411	47,52	1.090,87	390,94	267,55	N 267,5	E 285,0	0,394
GMS	1.230,00	35,147	47,44	1.115,36	408,27	279,26	N 279,3	E 297,8	0,267
GMS	1.260,00	35,035	47,85	1.139,91	425,51	290,88	N 290,9	E 310,6	0,260
GMS	1.290,00	34,930	47,94	1.164,49	442,71	302,41	N 302,4	E 323,3	0,116
GMS	1.320,00	34,832	48,22	1.189,10	459,86	313,87	N 313,9	E 336,1	0,185
GMS	1.350,00	34,769	48,76	1.213,73	476,98	325,22	N 325,2	E 348,9	0,315
GMS	1.380,00	34,871	48,83	1.238,36	494,10	336,51	N 336,5	E 361,8	0,110
GMS	1.410,00	35,176	49,01	1.262,93	511,31	347,82	N 347,8	E 374,8	0,321
GMS	1.440,00	34,817	49,22	1.287,51	528,50	359,08	N 359,1	E 387,8	0,380
GMS	1.470,00	34,802	49,11	1.312,14	545,62	370,28	N 370,3	E 400,7	0,067
GMS	1.500,00	34,923	49,22	1.336,75	562,76	381,49	N 381,5	E 413,7	0,136
GMS	1.530,00	35,137	49,52	1.361,32	579,97	392,71	N 392,7	E 426,8	0,275
GMS	1.560,00	35,745	49,31	1.385,76	597,35	404,03	N 404,0	E 440,0	0,619
GMS	1.590,00	33,711	48,95	1.410,41	614,43	415,21	N 415,2	E 452,9	2,045
GMS	1.620,00	33,927	49,18	1.435,34	631,13	426,15	N 426,1	E 465,5	0,253
GMS	1.650,00	34,260	49,30	1.460,18	647,93	437,13	N 437,1	E 478,3	0,339
GMS	1.680,00	34,997	49,48	1.484,87	664,97	448,22	N 448,2	E 491,2	0,744
GMS	1.710,00	36,009	49,63	1.509,29	682,39	459,53	N 459,5	E 504,5	1,016
GMS	1.740,00	35,927	49,76	1.533,57	700,00	470,92	N 470,9	E 517,9	0,113
GMS	1.770,00	36,811	49,88	1.557,73	717,77	482,40	N 482,4	E 531,5	0,887
GMS	1.800,00	37,507	50,14	1.581,64	735,88	494,05	N 494,0	E 545,4	0,714
GMS	1.830,00	37,820	50,48	1.605,38	754,19	505,75	N 505,8	E 559,5	0,375
GMS	1.860,00	38,733	50,84	1.628,93	772,76	517,53	N 517,5	E 573,9	0,941
GMS	1.890,00	39,671	50,40	1.652,18	791,70	529,56	N 529,6	E 588,5	0,980
GMS	1.920,00	40,607	50,33	1.675,12	811,02	541,90	N 541,9	E 603,4	0,937
GMS	1.950,00	41,362	50,38	1.697,76	830,68	554,46	N 554,5	E 618,6	0,756
GMS	1.980,00	42,104	50,83	1.720,15	850,63	567,13	N 567,1	E 634,0	0,802
GMS	2.010,00	43,088	51,78	1.742,23	870,91	579,82	N 579,8	E 649,8	1,176
GMS	2.040,00	43,716	51,50	1.764,03	891,49	592,61	N 592,6	E 666,0	0,657
GMS	2.070,00	44,880	51,42	1.785,50	912,41	605,67	N 605,7	E 682,4	1,165
GMS	2.100,00	46,025	50,92	1.806,55	933,76	619,07	N 619,1	E 699,0	1,200
GMS	2.130,00	46,884	50,25	1.827,21	955,49	632,88	N 632,9	E 715,8	0,984
GMS	2.160,00	48,091	50,27	1.847,49	977,60	647,01	N 647,0	E 732,8	1,207
GMS	2.190,00	49,050	50,32	1.867,34	1.000,08	661,38	N 661,4	E 750,2	0,960
GMS	2.220,00	50,122	50,78	1.886,79	1.022,91	675,90	N 675,9	E 767,8	1,128
GMS	2.250,00	49,473	50,75	1.906,15	1.045,80	690,39	N 690,4	E 785,5	0,649
GMS	2.280,00	49,121	50,46	1.925,71	1.068,53	704,83	N 704,8	E 803,1	0,417
GMS	2.310,00	48,583	50,50	1.945,45	1.091,11	719,20	N 719,2	E 820,5	0,539
GMS	2.340,00	47,748	49,88	1.965,46	1.113,46	733,51	N 733,5	E 837,7	0,953
GMS	2.370,00	47,786	49,79	1.985,63	1.135,67	747,84	N 747,8	E 854,7	0,077
GMS	2.400,00	47,385	49,86	2.005,86	1.157,81	762,13	N 762,1	E 871,6	0,404
GMS	2.430,00	46,529	49,39	2.026,34	1.179,74	776,33	N 776,3	E 888,3	0,924
GMS	2.460,00	46,314	48,86	2.047,02	1.201,47	790,55	N 790,6	E 904,7	0,436
GMS	2.490,00	45,668	49,33	2.067,86	1.223,04	804,68	N 804,7	E 921,0	0,726



UNITED NATIONS
UNIVERSITY

UNU-GTP

Geothermal Training Programme

Orkustofnun, Grensasvegur 9,
IS-108 Reykjavik, Iceland

Reports 2016
Number 21

BUSINESS CASE OF NGOZI GEOTHERMAL POWER PROJECT, MBEYA, SW-TANZANIA

Chagaka Kalimbia

Tanzania Geothermal Development Company, Ltd.

P.O. Box 14801

Dar es Salaam

TANZANIA

chagaka@hotmail.com

ABSTRACT

The objective of the study is to present a preliminary business case of Ngozi high-temperature geothermal field for power generation. The field is ranked as the topmost promising prospect in the country and stands as a flagship project of Tanzania Geothermal Development Company (TGDC). The Ngozi high-temperature field has undergone copious geo-scientific studies since late 1970s at different level, the most recent one being in March 2016 in collaboration with Geothermal Development Company (GDC) of Kenya. Following the vulnerability to hydrology and adverse impacts of climate changes on the hydroelectric power generation, the Government of Tanzania is currently undertaking strong impetus to diversify the energy mix to attain a more robust and resilient modern energy supply to foster the desired socio-economic transformations. Thus, it intends to move the country closer to achieving middle-income status, as envisioned in the National Development Vision 2025. A number of electricity supply industry policies, reforms and implementation strategies are in place to recognise the mandatory requirement of developing geothermal resources and the power is anticipated to contribute up to 200 MW by 2025.

The preliminary preparation of this business case is therefore a humble attempt to highlight rudimentary issues in the development of Ngozi geothermal power project and will be used as a tool to subsequently make sound financial decisions on the further commitment of funds between 22 and 32 million USD in the exploration drilling phase to meet an attractive return on investment during exploitation of resource. The two risks, geological and financing, were seen to be much more prominent and require further mitigation measures in place prior to the execution of the project. The single-flash technology which is considered the mainstay of the geothermal power industry and by far the most installed power technology, was the chosen work cycle with two scenarios of project implementation strategy, namely directly a 50 MW power plant, or first building a 5 MW modular wellhead plant before building a 50 MW conventional power plant. The overall conclusion on the scenarios realised is that a step wise development of 5 MW modular wellhead plant then a 50 MW plant has lower risks, more technical and environmental benefits and reasonable financial returns. This is realised on the Net Present Value of 6 million USD with Internal Rate of Return of 16% on equity, hence a highly recommended sustainable development alternative.

1. INTRODUCTION

1.1 Overview of geothermal energy, development and utilization

Geothermal is derived from two Greek words ‘*geo*’ meaning earth and ‘*therm*’ meaning heat. Geothermal energy is therefore heat derived from the core of the earth as the result of reactions/decays of radioactive materials. On the surface, geothermal energy is usually manifested by the presence of hot springs, calderas, boiling grounds, fumaroles etc. The heat content of the resource usually dictates the type of geothermal resource utilization. Typically, high-temperature resources with temperature $>200^{\circ}\text{C}$ are used to generate electricity whereas low-temperature resources with temperature $<150^{\circ}\text{C}$ are mainly used for providing direct heat for numerous applications, such as space and district heating, water heating, aquaculture, horticulture and industrial processes, among others. Geothermal energy is considered a renewable resource because it exploits the earth’s interior heat, which is considered abundant, and water, once used and cooled, is then piped back to the reservoir.

The scope of this project will however only be limited to production of electricity whereby several wells are drilled at a typical depth of 2000–3000 m into the reservoirs after comprehensive geoscientific surface studies to create enough steam and depending on the characteristics of the geothermal reservoirs, one of several geothermal electric production technologies is deployed to power turbines. The first geothermal electricity production is traced back to 1904 where an experimental plant installation was built in Larderello, Tuscany, Italy with a capacity of 15 kW (DiPippo, 2012). Now, 112 years later, a total of 24 countries in the world generate electricity from geothermal resources with a total installed capacity 12,635 MW with overall utilization 73,549 GWh/a (Bertani, 2015). The United States of America is by far the world leader in geothermal electricity production with an installed capacity of 3,450 MW while Kenya is the only African country among the world top ten electricity producers and currently holds eighth place with an installed capacity of 594 MW (Bertani, 2015).

Contrary to other renewable power generation technologies, geothermal power plants operate at a consistent base load power production level, twenty-four hours a day regardless of changing weather, seasonal variation and climate change impacts and providing a uniquely reliable and continuous source of clean energy. Geothermal power development is however characterized by a high capital investment for exploration, drilling wells, and plant installation, but operations and maintenance cost is relatively low, which makes the levelized cost of energy of geothermal power considerably lower than for other power generation alternatives. According to studies done and contemporary utilisation technology, geothermal energy has been proved to be a renewable, affordable, reliable and environmentally benign (“green”) electricity supply. The other imperative advantage worth mentioning is the local cultivation of the geothermal resources of which its development brings significant economic advantages to local economies (Kalimbia, 2016).

1.2 Geothermal energy in Tanzania

Tanzania is one of the East African countries with indications of existence of high potential for geothermal energy resources. Most of the prospects are located in the Tanzanian part of the Eastern African Rift System, which has traversed the country in both eastern and western arms. The prospects are identified by their surface manifestations, mainly thermal springs. About fifty geothermal prospects have been identified in the country with a crude estimated potential of above 5,000 MW according to the National Energy Policy, 2015. The geothermal prospects are localized in four zones, these include:

- (i) North-eastern Area: Lake Natron, Lake Manyara and Lake Mason;
- (ii) South-eastern coastal area: Kisaki, Utete, Luhoi and Luhombero;
- (iii) South-western area: Songwe River, Rukwa Trough, Kasumulo and Mampulo; and
- (iv) Rungwe volcanic complex.

Despite this enormous resource base, geothermal energy remains undeveloped to support the desired socio-economic transformation in the country. It is along these lines the Government of Tanzania (GOT), embarked on a strong commitment to increase the country's development and utilization of geothermal power resources to subsequently improve the generation mix and meet increasing power demand through adopting a green growth pathway (Ministry of Energy and Minerals, 2013). In December 2013, GOT through Ministry of Energy and Minerals (MEM) established a 100% state owned agency, Tanzania Geothermal Development Company, Ltd. (TGDC) as a subsidiary company of Tanzania Electric Supply Company (TANESCO) with institutional mandate of expediting geothermal resource development in the country. The company became operational in July 2014. Since its inception, TGDC has acquired a total of eight prospecting licences in the country namely Ngozi, Lushi, Kisiwa, Lake Natron, Mbaka and Kasumulu.

1.3 Late development of geothermal energy in Tanzania

There are many reasons to explain the slow pace of geothermal development in the country. The most significant reason, which is accepted with geothermal experts worldwide, is the high degree of uncertainty at the early stage of exploration, which is accompanied by high upfront costs. Other factors include the previous stable and reliable hydroelectric power generation, which made the country not put emphasis on other renewable energies, discovery of abundant natural gas and later utilization in power generation, inadequate development of human capacity, industry underfunding and long lead times of geothermal power development. In other words, development of a geothermal field from the exploration phase to full conventional power plant operation (excluding wellhead generation) can take time ranging 5 to 9 years, hence doesn't provide a solution to the urgent demand for power. So, the establishment of TGDC has been the most positive initiative towards fast tracking realisation of geothermal development in the country.

2. MEANING OF A BUSINESS CASE

A business case may be defined as a formal, well-structured written document intended to convince a decision maker to approve some kind of action through exploring all feasible approaches to a given problem and enables project owners to select the option that best serves the organization (whatis.com, 2016). It is therefore a fundamental project management decision tool, which weighs all the risks, anticipated commercial benefits and savings to be gained in executing the particular project. The case lastly offers the best recommended option in a pool of alternatives to meet the desired output of the project.

2.1 Usefulness of business case

The usefulness of business case can be categorized in three groups (Pálsson, 2016) namely:

- *For managers and board of directors of the geothermal company* (in this case TGDC) which is typically referred to as business plan and used for internal decision making, prioritizing projects (portfolio management), ensuring that all critical aspects of a project preparation have been fully covered;
- *For financiers*, often referred to as bankable document, to ensure that money put into the geothermal power project is likely to be paid back;
- *For permit providers* (in this case Government of Tanzania), to ensure that the power will be online on time and in the right quantity, and that the resource will be used in a responsible and sustainable way.

2.2 Necessity of business case for TGDC

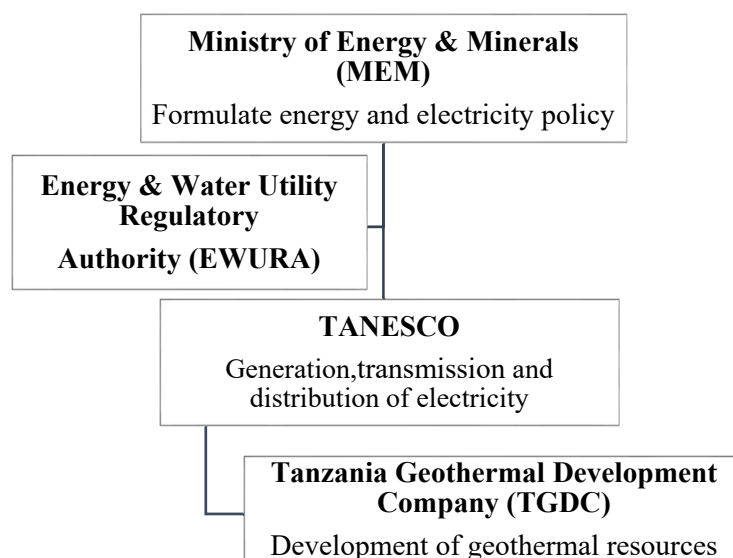
As a new player in the geothermal industry, TGDC is required to properly strategize utilization of its financial resources on the development and exploitation of geothermal energy to minimize the risks associated with exploration, development and utilisation, through analysing all the available options that will justify the feasibility of developing the resources in a particular way.

The development of a rigorous and comprehensive business case is one important step to engender business changes as well as demonstrate confidence and accountability to GOT and financiers on the ability of the company to meet its financial obligations. Therefore, the preliminary preparation of this business case is an important step to highlight the key project issues that will be used to provide the context for investment decisions in the next phase of exploration drilling in the Ngozi geothermal project and on whether to proceed, modify or abandon the project and in what forms.

3. PROJECT DESCRIPTION AND SCOPE

3.1 Project proponent

Project is being developed by TDGC with close collaboration of TANESCO, MEM and EWURA. For the purpose of co-financing arrangements, several external development partners will be involved in different phases of the project. Figure 1 below shows the position of the project owner in the electricity supply industry in the country.



3.2 Ngozi project location and overview

Ngozi geothermal field belongs to Rungwe Volcanic Province (RVP), situated directly south of Mbeya city with a population of 385,279 (National Bureau of Statistics, 2012), in SW-Tanzania at a triple junction of the East African Rift system as shown in Figure 2. The city is furthermore 822 km (tarmac road) northwest of Dar es Salaam, the country's largest commercial city. Mbeya city is also reached by air (1 hr 25 minutes) or TAZARA railway.

The Ngozi geothermal field is located 18 km from the existing Mwakibete substation with 220 kV transmission and 11 km from the proposed Igawilo substation (land acquisition process is going on and is in advanced stages) with transmission lines 400 kV / 220 kV / 33 kV. The site access requires full operation of a 4WD vehicle as the terrain is hilly and the roads are not paved.

FIGURE 1: Position of TGDC in the country's electricity supply

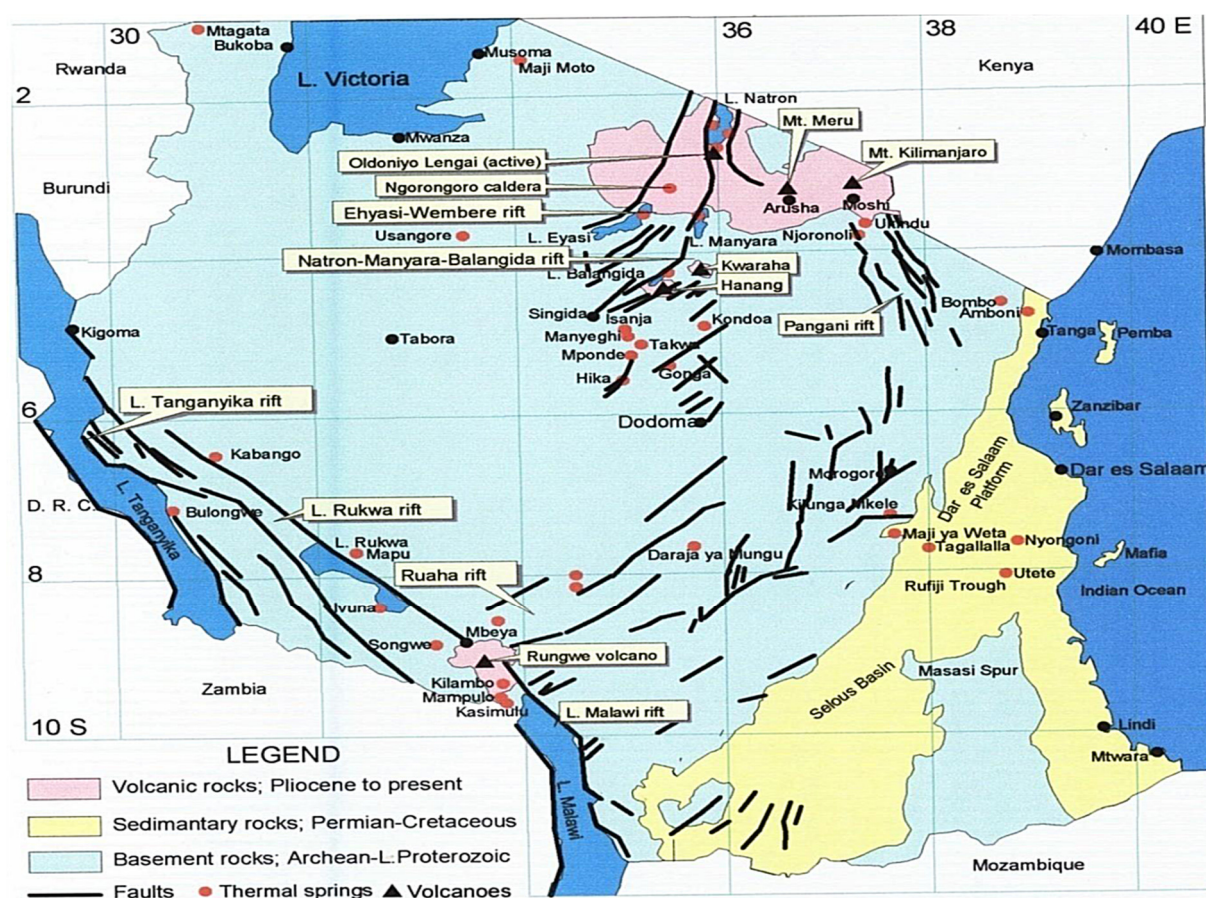


FIGURE 2: Location of Ngozi geothermal field, SW-Tanzania (MEM, 2014a)

3.3 Ngozi topmost geothermal field

Ngozi geothermal field is ranked as the most promising in the country and stands as a flagship project of TGDC. The field, as will be shortly explained below, has undergone copious geo-scientific studies since late 1970s at different levels. The most recent one was in March 2016 in collaboration with Geothermal Development Company (GDC) of Kenya, financed by Icelandic International Development Agency and United Nations Environmental Programme (UNEP).

The preliminary geo-scientific studies have indicated the magma chamber of the Ngozi volcano acting as a heat source for a high-temperature geothermal system with reservoir temperatures of more than 250°C, at >2,000 m depth. The active NW-SE trending faults are responsible for fluid flow in a north-westerly direction and based on fracture permeability. However, based on geology it is suggested that many structures in this region could be covered by the thick pyroclastic material, which is more than 250 m thick, and hence are not expressed on the surface.

Drilling of three exploratory wells is anticipated to start in the last quarter of 2017 and based on the results of flow tests from the exploration wells, the exact potential of the resource will be assessed to fully develop the resource. Table 1 describes competitive advantages of Ngozi geothermal field with respect to other geothermal prospects in the country, hence the *topmost project*.

TABLE 1: Ngozi geothermal field competitive advantages

S/N	Reason	Advantage
1.	Presence of adequate geo-scientific information from numerous previous studies.	Provide a baseline to commence detailed surface studies at medium cost.
2.	Geologically located in volcanic setting.	Possibly a high-temperature resource.
3.	Adequate source of drilling waters.	Easier drilling operations.
4.	Located close to the existing Mwakibete substation with 220kV transmission.	Low power evacuation cost.
5.	Presence of excellent infrastructure system, i.e. roads, airport, railway.	Easy to transport equipment and materials.
6.	Proximity of the prospect to Mbeya city.	Easy to access support services.
7.	Positive social acceptance of geothermal energy.	Slightly high level of awareness of geothermal energy development.
8.	Cold climatic conditions.	Suitable for numerous direct utilisations of geothermal heat.

3.4 Previous geoscientific studies

Ngozi geothermal prospect, like many other prospects in the country, has been actively subjected to preliminary reconnaissance and multidisciplinary surface exploration studies from different government agencies, development partners and private companies to precisely establish its geothermal potential. All of the studies carried out indicated the presence of a scientifically viable resource with additional recommendation of various geoscientific studies. The following are some of the documented exploration studies done in the prospect;

- a) Swedish consultant group (SWECO) between 1976 and 79 in collaboration with VIRKIR, Iceland carried out geothermal exploration under financial support from the Swedish International Development Cooperation Agency (SIDA). The objective of the study was finding possibilities of exploiting geothermal recourses in Tanzania. The results were favourable, indicating good possibility of encountering high-temperature resources. However, the studies recommended further studies (Ministry of Energy and Minerals, 2014a).
- b) Between 2004 and 2005, Tanzanian Rural Electrification Study (TRES) was conducted by the German company Deutsche Energie-Consult Ingenieurgesellschaft mbH (DECON), SWECO and InterConsult. Tanzania Electric Supply Company (TANESCO) was the implementing institution on the client's side. The African Development Bank (ADB) was the funding organisation of TRES. The study involved geophysical surveying (magnetic, gravity and resistivity surveys). In the study, geothermal energy, among others, was regarded as an indigenous, renewable energy source suitable for future electricity supply in Tanzania and recommended detailed assessment of Ngozi prospect in Mbeya (Mjokava, 2008).
- c) GEOTHERM (Phase I, 2009 and Phase II, 2013) conducted a project titled "Geothermal as an alternative Source of Energy for Tanzania" in Ngozi prospect, Mbeya with the overall objective of locating geothermal areas favourable for development and to locate the drilling site. The project is part of GEOTHERM programme, which is a technical cooperation programme of the German government. The field campaign to Lake Ngozi-Songwe prospect involved geological mapping as well as geochemical and geophysical surveys. Based on the combined data evaluation from geological, geochemical and geophysical findings, locations of three temperature gradient wells were identified. The intention of these wells was to acquire better understanding the hydrothermal characteristics of the resource. However, the wells were not drilled.
- d) Geothermal Power Tanzania (GPT), Ltd., a private company registered in 2012 in Tanzania, among others was licensed to explore and develop Ngozi geothermal resources. GPT was 70% owned by Geothermal Power Limited (GPL – registered in Mauritius), Interstate Mining & Minerals, Ltd. (Interstate, 25%) and National Development Corporation (NDC, 5%) (Geothermal Power, 2016).

Based on the previous GEOTHERM programme phase I and II, GPT planned supplementary fieldwork mainly for finding the best located and accessible drill sites and subsequently producing power depending on reservoir characteristics. However, the prospecting licenses were revoked one year later. In the eyes of the licensing authority, the license holder was found in default as the result of failing to meet obligations as stipulated in the country's Mining Act 2010.

- e) Japan International Cooperation Agency (JICA) conducted reconnaissance satellite-based geothermal resource characterization study meant to assist in identifying promising geothermal sites to obtain fundamental information to consider the future contribution by JICA to geothermal development in Tanzania. Through utilisation of Monte Carlo analysis with 50% probability, the Ngozi geothermal resource potential was estimated to be 359 MW (JICA, 2014).

3.5 Ngozi preliminary resource assessment

The numerous previous geoscientific works had established preliminary resource capacity of the field, however, the most recent resource potential of 270 MW using the simple power density method within the delineated area of 18 km² northwest of the field has been established as shown in the Figure 3. The northwest area has been studied in detail and is so far considered as the most suitable area for exploration drilling and three wells were sited. On the other hand, little has been done on the southeast part of the field which provides the greater confidence of enlarging the resource of the field upon full completion of the detailed surface studies. Upon completion of drilling and obtaining results of flow tests from the exploration wells, the comprehensive characteristics of the reservoir and final estimate will be established.

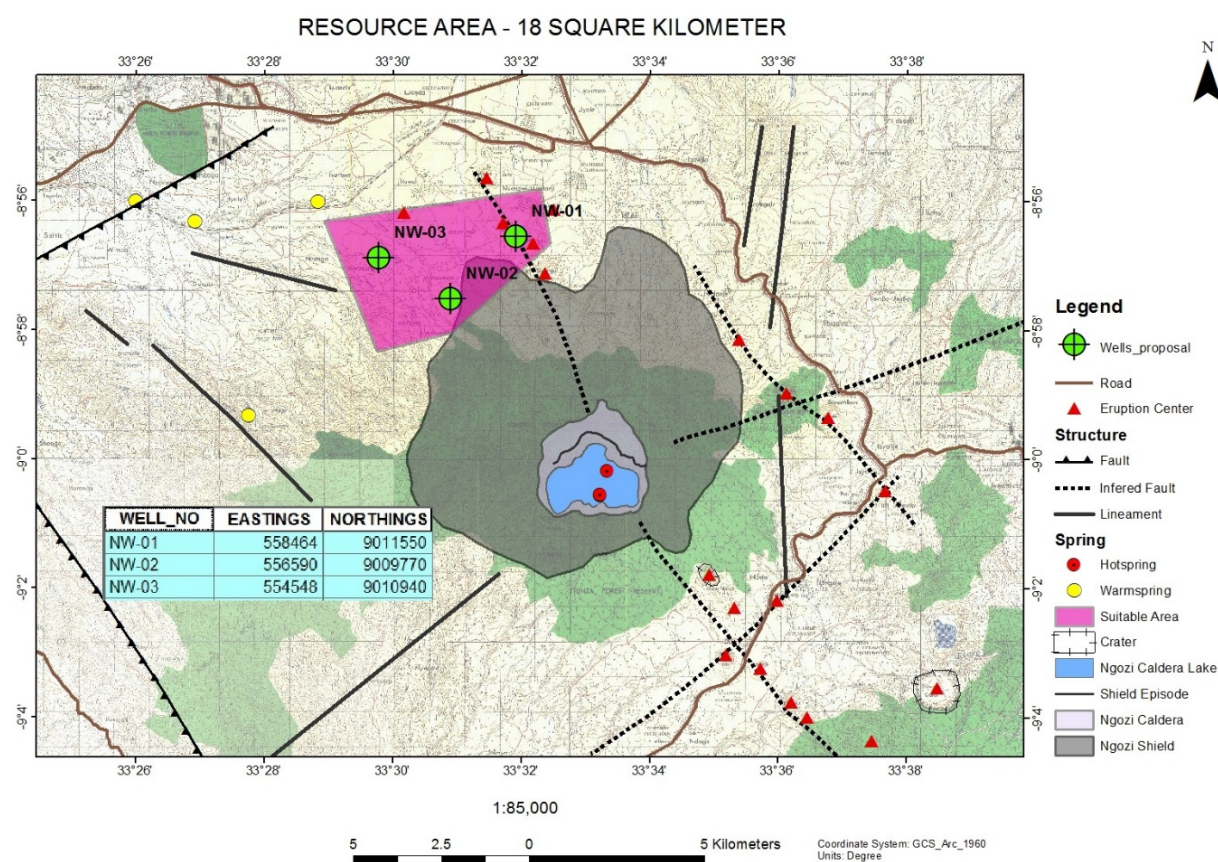


FIGURE 3: Resource estimates and preliminary drilling sites

3.6 Scope of the study

The scope of this project will be comprised of the technical, economic, financial and environmental viability of the project while assessing and managing potential risks associated with power development of Ngozi geothermal project. For the simplicity of this business case, single-flash power plant technology will be utilised under the following development scenarios:

- *Scenario 1* - building of a 50 MW power plant;
- *Scenario 2* - installation of a 5 MW modular wellhead plant, and thereafter building of 50 MW conventional power plant.

4. BUSINESS OUTCOME

Ngozi geothermal power project is aligned with a number of key social and economic governmental issues as well as the electricity supply industry policies that are expected to radically increase power demand in the country, which is also in parallel with the intention of embracing green energy growth and hence promoting environmental protection. The business outcomes are categorised into the groups and discussed below;

4.1 Key country issues and rationales

4.1.1 Social-economic issues

Tanzania has a total land area of about 945,203 km², with a total estimated population of 44.9 million. The current rate of population growth is 2.9% per year and it is estimated to reach 64 million by 2025 and 83 million by 2035 (National Bureau of Statistics, 2012). Today, about three quarters of Tanzanians live in rural areas, by 2035 it is projected that urban population will have increased, although rural residents will still constitute the majority of population. Along those lines, the government has put in place an action plan to accelerate access to electricity in rural areas implemented by both Tanzania Electric Supply Company (TANESCO) and the Rural Energy Agency (REA). These plans will significantly record a fast growth in demand of electricity in the rural areas. The country has furthermore registered a significant development in harnessing mineral resources amongst other planned developments, the move will contribute significantly to economic growth and increased energy demand.

4.1.2 Tanzania Development Vision (TDV) 2025

The TDV 2025 came into effect in 1999 with the aim of transforming Tanzania into a globally competitive, newly industrialized, prosperous and middle-income country with an economy achieving an annual per capita income of at least US\$3,000 by 2025, from an income per capita of USD 640 (2014). It furthermore seeks to ensure a high quality of life to all citizens in a clean and secure environment by 2025. The vision recognises access to modern energy as the one fundamental prerequisite for proper functioning of the economy and other social settings. Socio-economic transformation can only be realised under the presence of adequate, affordable, reliable and environmentally friendly electricity supply.

4.1.3 The National Energy Policy, 2015 (NEP, 2015)

The policy provides a comprehensive legal and regulatory framework and institutional set up aimed at improving energy sector governance and performance. The policy recognises the fundamental role that the huge potential of renewable energy in the country can play. Among others, the policy has set an objective of enhancing geothermal resources governance and mitigating exploration and development

risks. Among other things, the Government has guaranteed to establish institutional, legal and regulatory frameworks for geothermal development, encourage private sector investment in geothermal development, facilitate the availability of infrastructure for deployment of geothermal and develop a mechanism for public-private partnership in geothermal development.

4.1.4 International initiative for green energy

Presence of many initiatives from various development partners and international organisations in the world of green energy. Tanzania is not left behind on this, geothermal, being one of the environmentally friendly energy types, plays a greater role in demonstrating the country commitment in moving to this direction. The United Nations Sustainable Development Goal 7 (SDG7) is designed to ensure access to affordable, reliable, sustainable and modern energy for all. Developing the geothermal energy in the country is aligned with this goal and demonstrates the strong commitment of the Government of Tanzania towards turning the goal into reality. The presence of international financing windows to finance the risk party of geothermal industry in forms of grants and concessional loans and in-kind support provides an outstanding opportunity to accelerate development of the resource.

4.1.5 Electricity sector issues

- *Traditional dependence on hydropower, not healthy for achieving the desired socio-economic transformations:*

As of May 2014, the grid installed capacity was 1583 MW composed of hydro 561 MW (35%), natural gas power plants of 527 MW (34%) and liquid fuel power plants of 495 MW (31%). TANESCO also imports power from Uganda (10 MW), Zambia (5 MW) and Kenya (1 MW) (Ministry of Energy and Minerals, 2014b). In the past two decades, the country has observed a dramatic disturbance in traditional hydropower generation caused by persistent and frequent droughts, hence extensive load shedding in the whole country. The situation forced TANESCO to enter into short term contracts with diesel based generation emergency power producers (EPPs) which have relatively rapid installation time, however are accompanied with a higher tariff per kWh and are environmentally unfriendly, hence bad for the country's economy. For instance, in 2013, TANESCO contracted EPPs which in total installed 317 MW capacity at a cost of 30-35 US\$/kWh. The power crisis has accentuated the high risk of reliance on hydropower and consequently the fundamental need of diversifying power generation sources to mitigate the results of climate change.

- *Electricity supply and demand:*

At present, only 24% of the Tanzanian population are connected to electricity whereby only about 11% of the rural population are connected to electricity services. Under this situation, the energy balance in Tanzania is dominated by traditional use of biomass in the form of charcoal and firewood. The government plans to increase the connectivity level to 50% by 2025 and at least 75% by 2033. On average, demand for electricity is growing at 10-15% per annum. The current peak demand is 935 MW which occurred on 12th December 2014 and it is projected to grow to 7,644.8 MW by the year 2025 according to the Power System Master Plan (2012 update). The low accessibility and affordable energy services is consistently identified as a major constraint in achieving desired socio-economic transformation in Tanzania, hence to foster the desired socio-economic transformation, universal access to modern energy services in an affordable, reliable, sustainable and environmentally-friendly manner is inevitable.

4.2 Strategic alignment

TGDC in close collaboration with the Government of Tanzania and TANESCO has made sectorial plans and reforms to develop geothermal power to meet the targets mentioned in Section 4.1 of this report. TGDC aims at developing geothermal projects and Ngozi has been prioritised as the first project. The company has furthermore aimed at strengthening the institution and building strong capacity in science,

engineering, social and environmental know-how, and for that purpose, step wise phase development is preferred. The following are the two strategic alignments in developing the Ngozi project;

4.2.1 Additional 200 MW of geothermal power by 2025

As of June 2014, Ministry of Energy and Minerals (MEM) has developed the Electricity Supply Industry (ESI) reform strategy and roadmap, which proposes a rationale and a framework for the reform of Tanzania's electricity sub-sector in governance and performance for supporting the desired economic transformation, while protecting the environment. It aims at meeting the current and future demand for electricity, reducing public expenditure on ESI for operational activities, attracting private capital, and increasing electricity connection and access levels. The reform highlighted the optimistic commitment and deliberate move towards increasing the installed power capacity from 1,583 MW (April 2014) to at least 10,000 MW by 2025 as shown in Table 2 below, while the transmission and distribution systems are to be expanded. Renewable energy, geothermal of particular interest, has to inject 200 MW of geothermal power by 2025. Ngozi geothermal power project is anticipated to inject up to 100 MW.

TABLE 2: Present and projected installed capacity by year 2025
(Ministry of Energy and Minerals, 2014b)

Source	Current capacity	Additional capacity (2015 -25)	Capacity by 2025
Hydro (MW)	561	1,529.00	2,090.84
Natural Gas (MW)	527	3,968.00	4,469.00
HFO/GO/diesel (MW)	495	-	438.40
Coal (MW)	-	2,900.00	2,900.00
Wind (MW)	-	200.00	200.00
Solar (MW)	-	100.00	100.00
Geothermal (MW)	-	200.00	200.00
Interconnector (MW)	-	400.00	400.00
Total (MW)	1,583	9,297.00	10,798.24

4.2.2 Power System Master Plan (PSMP), 2012 update

TANESCO in collaboration with the Ministry of Energy and Minerals (MEM) is currently undertaking review of the PMSP 2012, among other reasons to tentatively reflect the future power demand and supply while considering all the available options to generate electricity in the country and moreover to increase the share of renewable energy in the national energy mix. Ngozi geothermal power project was the first power project to be considered in the plan to meet the future power demand in the country.

5. PROJECT PLANNING AND EXECUTION STRATEGY (HIGH LEVEL)

5.1 Project milestones

Tanzania Geothermal Development Company Limited (TGDC) in collaboration with geothermal exploration experts around the world is currently carrying out additional geo-scientific studies to fill in the gaps that remain so far. Upon results of the studies, the exploratory drilling decision to intersect the geothermal reservoir will be made. Drilling is expected to start in the last quarter of 2017. Based on the power production strategy, a power plant will be constructed and the timeline will be established. An overview of the proposed timeframe for project phases and major decision points are shown in Table 3 (mainly for scenario 2).

TABLE 3: Timeframe for each phase of the project

Project phase	Commencement	Completion	Remarks/status
Project preparation (surface studies & land acquisition)	July, 2014	May, 2017	On -going
Environment.& Social Impact Assessment (ESIA) study	May, 2014	June,2017	On -going
Major decision point			
Exploration drilling - mobilisation, site preparation, well construction, drilling and well testing	Q4, 2017	Q2, 2018	Projected (Scenario 2)
Major decision point			
Installation of well head power plant	Q2, 2018	Q4, 2018	Projected (Scenario 2)
Major decision point			
Additional surface exploration and reservoir study	Q1, 2019	Q4, 2019	Projected (Scenario 2)
Appraisal drilling and well testing	Q1,2020	Q4,2023	Projected (Scenario 2)
Feasibility study - evaluate geothermal resource	Q1, 2022	Q1,2023	Projected (Scenario 2)
Major decision point			
Steam gathering system construction	Q1, 2023	Q1, 2025	Projected (Scenario 2)
Power plant development construction	Q1, 2022	Q1, 2025	Projected (Scenario 2)
Power plant operation and maintenance	Q1, 2026	Q4, 2050	Projected (Scenario 2)

5.2 Project dependencies

Ngozi prospect is located in a very mountainous area with heavy rainfalls and slippery ground. It is, therefore anticipated that drilling will start during the dry season of the year i.e. from September 2017.

5.3 Project team

Apart from utilizing in-house experts, TGDC will deploy various experienced consultancies in the geothermal industry in the areas of surface studies. These include drilling supervision consultancies and drilling contractors, who will undertake drilling and testing of the wells, as well as Engineering, Procurement and Construction (EPC) contractor in power plant construction activities. Figure 4 shows the anticipated Ngozi project organogram for the drilling programme.

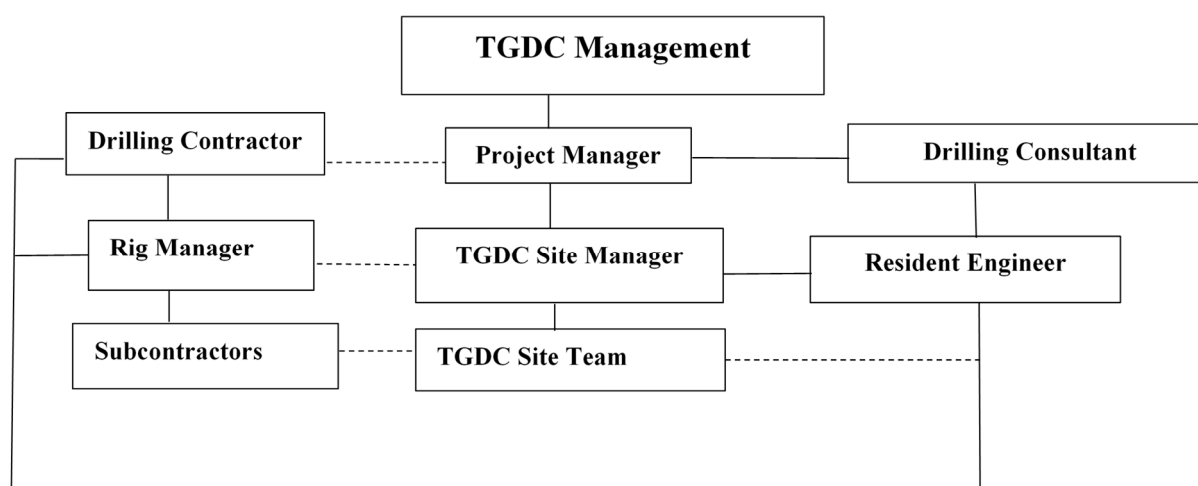


FIGURE 4: Proposed Ngozi organogram for the drilling phase

6. RESOURCE ASSESSMENT

6.1 Exploration strategy

TGDC in collaboration with consultancies undertook a review of available geophysical, geochemical and geological data and focused on analysing the quality of previous work and reports. The review report was then used as a baseline for additional survey plans for Ngozi geothermal prospect.

Following the completion of the above, TGDC has carried out additional studies to appraise the site and precisely locate the drilling sites. A combination of geo-scientific methods (geological, geochemical and geophysical) will be employed to gather information on the subsurface for better understanding the prerequisite characteristic of geothermal system (i.e. heat source, permeability, recharge mechanism and cap-rock). TGDC in collaboration with consultants will carry out additional studies in the following areas:

- **Geophysical studies**
Additional geophysical studies with Transient Electromagnetic (TEM) and magnetotelluric (MT) methods to further reveal the existence of hidden structures and sub-surface resistivity anomalies. Both MT and TEM soundings are carried out at the same locality for static shift correction at shallow depth.
- **Geochemistry studies**
Geochemical studies carried out involve the measurement of ground radon (Rn) and carbon dioxide (CO₂) radioactivity in numerous areas in the prospect. It will be furthermore include sampling of steam and gaseous discharge from geothermal manifestations, analysis of chemical parameters, rare earth elements (REEs) and isotopes. The analytical and isotopic results will be used to improve details of the underlying geothermal reservoirs.
- **Geological studies**
Geological studies include additional lithological and stratigraphic studies, the volcanological evolutions, structural mapping, mapping of the manifestations and hydrogeological surveys.
- **Environmental and social baseline studies**
An environmental social and impact assessment study shall be conducted to collect baseline information and assess potential environmental impacts and suggest mitigation measures that may arise from geothermal development.

6.2 Anticipated cost

Following the available data and previous geoscientific exploration, the anticipated cost of the activities is estimated to be 2 million USD. The cost has taken into consideration both previous level of geoscientific studies and ongoing studies.

7. DEVELOPMENT STRATEGY

7.1 Geothermal business model assumption

This is an approach on how the geothermal development can be undertaken and primarily involves deciding at which stage if suitable the private sector is engaged. There are numerous geothermal development models in the world, all variants lying between purely state-owned model, purely private owned or the participation of both parts under a Public-Private Partnership (PPP) or Joint Venturing (JV) arrangements. Options are not mutually exclusive, the decision is based on a balance of many factors including, but not limited to (i) development speed; (ii) price, cost and risk allocation; (iii)

availability of funding; (iv) public entity development capability; (v) public entity cost recovery compared with risk profile; (vi) and the available private sector incentives (EAGER, 2015).

TGDC has not yet acquired a geothermal development business model, however, for the purpose of developing this business case, it is assumed that the company will be the power producer, that is to say, TGDC will undertake whole geothermal development value chain phases from reconnaissance to power plant construction and operation, hence carrying all resource risk. TGDC will have the entire control of the resource with the obligation of committing the large investment required to have the power online. The GOT anticipate to co-finance the project components in collaboration with development partners and other financing windows under which TGDC is eligible.

7.2 Power plant technology

There are mainly three types of power plant technology (work cycles) that are applied in electricity production in geothermal power plants. The work cycles are referred to as condensing (single-flash), back-pressure (atmospheric exhaust) and binary or twin-fluid system (organic Rankin cycle - ORC). For all suggested technologies, the spent geothermal fluid geothermal liquid is assumed to be reinjected into the reservoir through reinjection wells. However, out of the three work cycles, two technologies are the most common, namely, condensing cycle which utilises fluid from reservoirs with temperatures in the range of 200–320°C, and binary cycle which utilises fluid with temperatures as low as 120°C (Eliasson et al., 2011).

For development of this business case, the single-flash technology power plant technology, as shown in Figure 5, was considered in the development of two scenarios. The choice was merely due to two reasons, one being within the range of Ngozi anticipated reservoir temperature and secondly being by far the most common geothermal power plant work cycle employed in the world, as of 2015 a total installed capacity of 5079 MW has been observed (Bertani, 2015).

The technology is furthermore the most economical choice for high-enthalpy liquid-dominated resources. The single-flash technology is essentially

thermodynamic improvement on the back-pressure design where before the steam from the turbine is being discharged to the atmosphere, it is discharged to a condensing chamber (Hudson, 2003). The two-phase flow of a geothermal fluid (a mixture of steam and liquid) is piped from the production well to the separator, where the fluid is separated from the steam. The liquid is disposed of into the reservoir through a reinjection well, the steam flows from the separator through a turbine and electrical power is generated in the generator, coupled to the turbine. The steam then enters the condenser, where it is condensed at sub atmospheric pressure. This condenser provides cooling with cooling water circulating through a cooling tower. The condensate is used as make-up water for the cooling tower to make up for losses due to evaporation and blowdown.

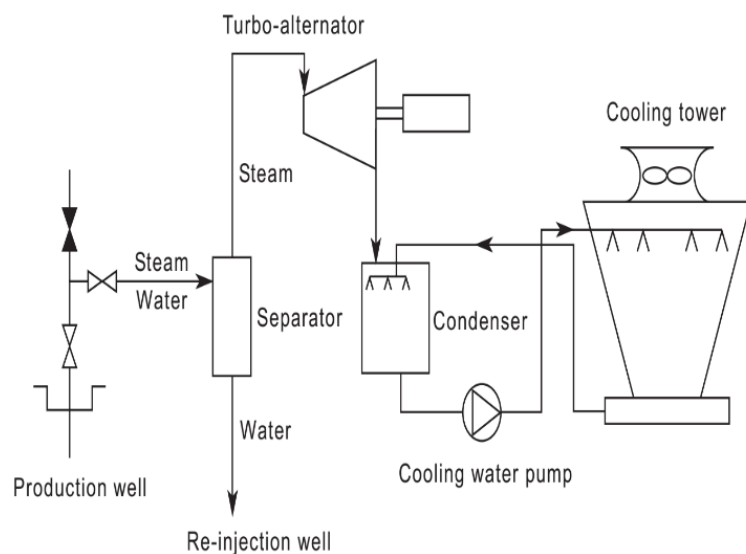


FIGURE 5: Simplified schematic diagram of single flash power plant (Hudson, 2003)

7.3 Power development strategy

Stepwise exploitation of a geothermal resource has proven to be a successful model of development in various part of the world. Power plants as small as a few tens of megawatts can be economically built and provide substantial understanding of the resource, hence sustainable extraction. Ngozi geothermal field is still not a very well-known site as no wells have been drilled. It is along these lines, the following stepwise power generation methodologies can be deployed.

7.3.1 Scenario 1 – a direct 50 MW power plant

This is the long term solution of power generation, upon successful drilling and testing of the first three exploration wells, drilling of appraisal wells shall be done followed by feasibility studies. A positive feasibility study will lead to drilling of production and reinjection wells to supply enough steam to generate 50 MW. A total of 15 wells are anticipated to be drilled and later a steam gathering system is to be constructed where the costs for the construction on a turnkey basis are estimated to be 0.4 million USD per MW (confidential communication). Under this scenario, the project is scheduled to commence operations in 2023. The power plant capital cost (excluding the wells) under EPC contractor ranges between 1.8 and 2.5 million USD per MW (Hallgrímsdóttir and Gudmundsson, 2016).

7.3.2 Scenario 2 – First a 5 MW wellhead plant then a 50 MW conventional power plant

This is the hybrid strategy made to generate early revenue from a wellhead unit before the construction of a 50 MW conventional power plant. The revenue will be directly reinvested during the construction period of the large plant. The wellhead units are positioned next to a production well pad and are supplied with steam from one the production wells. The units are installed after each well is drilled and tested. For TGDC to comprehend early power generation and first unlock the geothermal potential in the country, wellhead generation is anticipated to be one of the options as the plant can be installed in a matter of months, providing early return on investment and relieve the company from the long wait for the large conventional power plant development period.

Upon a successful drilling of full sized exploration wells and testing, a 5 MW portable wellhead unit will be installed. This will involve utilising one production well (one of the exploration wells), one reinjection well and utilization of single-flash technology to generate electricity. The steam gathering system shall be designed so that the well will be connected to the large power plant in the future. For a standard size power plant, a fixed price EPC turnkey budgetary pricing excluding wells is estimated to be 1.75 – 2.4 million USD per MW (Hallgrímsdóttir and Gudmundsson, 2016). Under this scenario, the project is scheduled to commence operations in 2019 with regards to the well head unit and thereafter the 50 MW power plant is anticipated to be online in the year 2026 hence totalling 55 MW of electricity.

8. ENVIRONMENTAL AND SOCIAL IMPACT ASSESSMENT

8.1 Potential environmental impacts in geothermal development

Geothermal power projects compared to other conventional power generation projects has proven to have less impacts on the environment. However, the phases of exploration and production drilling as well as power production may result in possible physical impact on the environment that surrounds the resource area, hence requiring mitigation measures. The impacts during drilling phase include flora, fauna, ecosystems and biodiversity disturbance – as a result of clearing vegetation, levelling of land surface, excavated materials and drainage requirements. During power production the main registered impacts are observed due to emission of greenhouse gases (GHG) together with other minor rare possible impacts, including subsidence and induced seismicity. The established global weighted average of GHG for geothermal power plant is 122 g/kWh, which is still significantly lower than from fossil fuel

plants (ESMAP, 2016). The implementation will furthermore have a significant social impact due to land acquisition, which will result in loss of ownership of agricultural land and relocation of people.

8.1.1 Overview of environment acts and requirements

Tanzania Environmental Management Act (2004) and the Environmental Impact Assessment and Audit Regulations of 2005 require mandatory EIA before the implementation of any development project. The regulation defines Environmental Impact Assessment (EIA) as a systematic examination conducted to determine, whether or not, a programme, activity or project will have any adverse impacts on the environment. In accordance with the law, Ngozi geothermal project falls under the projects, which require a full Environmental and Social Impact Assessment study.

The geothermal power development falls under clause 7 and 16 of energy and extractive industry, respectively, and requires mandatory undertaking of EIA studies. It furthermore requires TGDC as a project developer to undertake EIA at their own cost prior to major decisions and commitments on the financing of project or actual project execution in two phases of exploration and production drilling as well as power plant construction. National Environment Management Council (NEMC) is the main EIA authority in the country with institutional mandate to undertake the review, monitoring, enforcement and compliance activities for EIA and facilitates public participation. The environmental impact assessment and audit regulation has highlighted key steps to embark on and satisfy the awarding of an environmental certificate. TGDC shall in the first place register the project to NEMC for screening, undertake scoping exercises, and conduct impact analysis and finally implementation of mitigation and impact management. Upon finishing, the comprehensive report is submitted to NEMC for decision.

8.1.2 Overview of land acquisition and resettlement

Project development will involve a significant amount of land for operations, therefore resettlement will be necessary and hence compensation will be involved. The entire process is guided by Tanzania Land Acquisition Act 1967 and Land Act number 4 & 5 of 1999.

8.2 Current status on Ngozi environmental impact assessment

As per law requirements, TGDC has initiated a process to acquire the EIA certificate to successfully undertake exploratory drilling at the last quarter of 2017. NEMC registered Ngozi geothermal project with number 4711. The hired local contractor in collaboration with TGDC technical, environmental and social experts undertook the scoping exercise and the comprehensive report was submitted to NEMC. The report a.o.t. provides decision makers with useful information towards predicting the impact severity and determines the level of ESIA required. Upon reviewing NEMC recommended further Environmental and Social Impact Assessment, which is anticipated to take place as soon as precise final drilling sites locations have been established. The environmental certificate will enable TDGC to proceed with drilling of exploratory wells and further the construction of power plants.

9. STAKEHOLDERS AND COMMUNICATIONS

Geothermal energy is not among the more known sources of energy in Tanzania, despite significant economic and environmental benefits from developing geothermal energy, a low level of awareness of industry is observed across all stakeholders. It is along these lines, that TGDC is obliged to map all the project stakeholders to comprehensively understand their connections and interest to the project, hence helping in identification of the key objectives of engagement or communication to raise awareness of geothermal energy exploration, development, utilisation as well as environmental benefit of the energy. This is important as the implementation of the project will be associated with direct social impacts on

indigenous people, such as acquisition of their agricultural land and resettlement of some communities. The proper handling of project stakeholders will have reputational risk for TGDC, financiers and development partners.

9.1 Geothermal stakeholder analysis

Geothermal projects, like many other energy projects, crosscut a number of interested parties. The diverse range of stakeholders include people, groups, or organizations interested in the performance and/or success of the project, or who are constrained by the project or perceive to be affected by the project. Stakeholders are typically classified into two groups of primary and secondary stakeholders. Primary are project members executing the project while secondary stakeholders are generally outside of the project, they usually receive the project information provided from the project team or through indirect information. Table 4 below shows the compiled preliminary mapping up of stakeholders as well as the scale of the power or influence and interest in the Ngozi geothermal project.

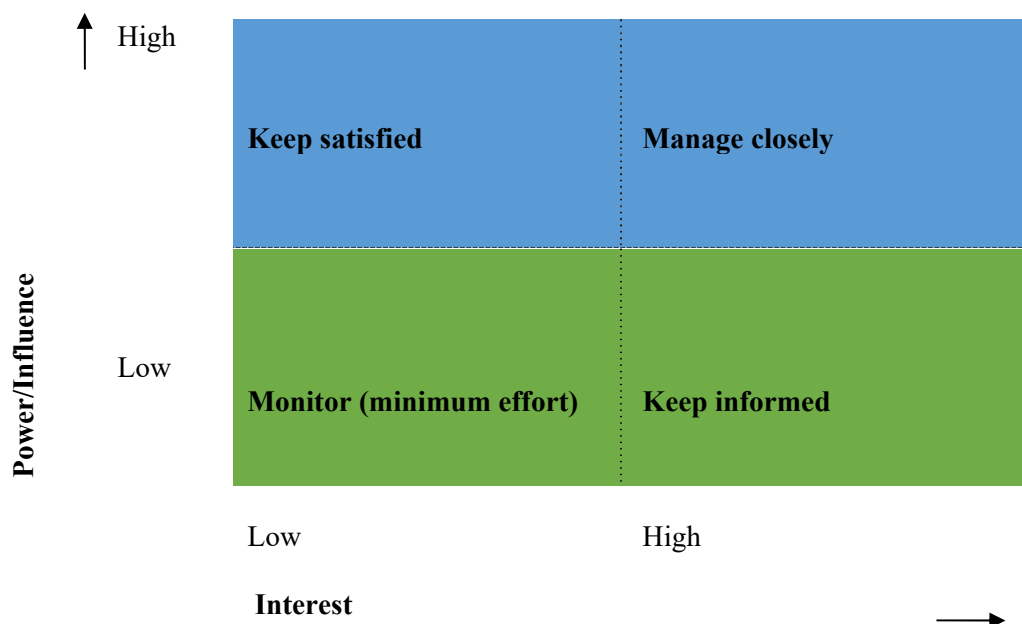
TABLE 4: Stakeholder mapping

S/N	Group	Category	Power/Influence	Interest
1.	TGDC	Primary	Low	High
2.	Project team members - EPC contractors, sub-contractors advisors and others working in the project	Primary	Low	High
3.	TANESCO	Primary	Low	High
4.	MEM and EWURA	Primary	Low	High
5.	Financiers - lenders and investors	Primary	High	Low
6.	Local community	Secondary	High	Low
7.	Politicians	Secondary	High	Low
8.	International communities	Secondary	Low	Low
9.	Development partners	Secondary	Low	Low
10.	Public at large (Tanzanian community)	Secondary	Low	Low
11.	Competitors	Secondary	Low	High
12.	Suppliers	Primary	Low	High
13.	Perceived to be stakeholders	Secondary	High	High

9.2 Communication plan

The communication plan was developed depending on scale of power, influence and interest in the project. This was deliberately made to ensure that stakeholders receive the precise level of information on the understanding of the project and its benefits at the right time and from the right source and the right quantity. Table 5 shows the developed grid of power/interest for stakeholder prioritization and communication strategy.

TABLE 5: Grid of power/interest



From the above grid, the communication strategy to the stakeholders can be made under the following guidelines;

- High influence, highly interested people/groups: The group shall be fully engaged and make the greatest efforts to satisfy, e.g. perceived to be stakeholders;
- High influence, less interested people/groups: The group shall be provided with sufficient information to ensure that they are up to date but not overwhelmed with information, e.g. local communities;
- Low influence, interested people/group: The group shall be adequately informed to ensure that no major issues arise. This group can often be very helpful with the detail of the project, e.g. project team members;
- Low influence, less interested people/group: The group shall be monitored, providing them with minimal communication to prevent boredom, e.g. public at large (Tanzanian community).

The forms of communication ranges from public meetings, internal and external presentations and local media visits. TGDC has so far made deliberate efforts to reach all interested and affected parties of a project, including but not limited to local people closer to the project, region and district leaders, politicians, local community leaders and the general public. From July 2015, TGDC undertook a geothermal awareness campaign in Mbeya region, particularly to the areas surrounding Ngozi geothermal prospect to raise awareness, prepare the community and win their acceptance of the proposed project. The strategy was mainly dissemination of the benefits of geothermal energy as a clean, renewable, reliable and affordable source of energy. Among many concerns of the stakeholders was land compensations and project employment policy.

During power plant operation, TGDC will establish programs to promote corporate social responsibility, which will provide additional benefits for project affected persons and other residents of the project area with the purpose of uplifting the lives of people through providing better education, health, water and electricity supply along with a cleaner environment.

10. RISKS ASSESSMENT AND MANAGEMENT

Geothermal development like many other power investments, is associated with numerous risks. These range from exploration to power plant operations. The greener the field, the more the risk. Ngozi field being virgin and first of its kind in the country is anticipated to weigh much higher compared to brown fields in other parts of the world. The upfront activities, particularly exploratory drilling, bears greater risk and is the second largest investment after the power plant construction. The risk magnitude goes down as the project reaches operations phases. The intention of this case is to highlight and analyse both resource and non-resource risks in detail, examining threats and opportunities that could prevent the project from realising its objectives in terms of sustainability, schedule, cost, quality and performance. The content of this business case will involve highlighting key project risks, and its management will be utilising a probability impact matrix as a qualitative risk analysis method and finally providing risk reporting and control.

10.1 Risks identification

The recognition of potential geothermal power project risks was done based on various geothermal power projects and author experience through observing all the stages and phases of a project life cycle. Predominantly, the risk profile varies depending on the existing development phase of the project, development setup and social and environment concerns. The development risk factors of Ngozi geothermal power development are summarized below.

10.1.1 Resource risks

- *Exploration risks/geological risk*

This is explained as the probability of the prospect not yielding the anticipated resource production characteristics. Geothermal development depends on two factors which both define the amount of energy that can be extracted from the subsurface, namely temperature and flow rate. Prior to drilling, there is very little knowledge on the resource characteristics, such as the existence of adequate flow rate, temperature, system inherent permeability, the chemical components of the geothermal fluids and size of resource. The geological risk is reduced with every well drilled and with the time they flow but it is still present during all phases of the geothermal project development and throughout the lifetime of the power plant;

- *Operational risks*

The risks are observed during actual power production phase of a project, often happen when the field is not well maintained as per set standards. The involved risks comprise reservoir depletion, mechanical failure or plant breakdown, industrial and environmental accidents, plant and equipment chemical scaling from geothermal fluids, corrosion, earthquakes during reinjection, delays in drilling and connecting make-up wells, unexpected shortages or increases in the costs of consumables and spare parts.

10.1.2 Non-resource risks

- *Legal and regulatory risk*

Geothermal power development in Tanzania falls under Mining Act 2010, Energy and Water Utilities Regulatory Authority (EWURA) Act of 2001 (2006), Environmental Management Act 2004, Rural Energy Agency and Rural Energy Fund Act No.8 of 2005, Electricity Act No. 10 of 2008 and Petroleum Act No.10 of 2008. These provide conducive environment for independent power producers to invest in the energy sector. However, most of these regulations and others are not well coordinated as there exists no geothermal policy, legislation or regulatory framework that can link together all the existing structure. For example, the mining law does not communicate with the EWURA and electricity acts. This is one of the major risks to the

development of Ngozi geothermal project as it will not only repel the participation of private developers, but also will increase hardship in securing financing for power development.

- *Drilling delays and cost overrun*

The project has set average number of days a rig has to spend drilling one well. However, during drilling operation, there is a risk of spending more days than anticipated. The delays tend to have a multiplying effect on other phases of the project, and would therefore lead to cost overrun. For example, each day in geothermal drilling typically costs \$25,000-\$50,000 so a 30-day delay due to e.g. permits, road, drill pad or water supply not being ready or delay in delivery of casing, wellhead valve, etc., could cost around \$1 million.

- *Health and safety issues*

Drilling operations, construction and power plant operation area are associated with complex processes and therefore pose great risk to the health and safety of personnel and equipment.

- *Environmental and social risk*

This is a critical risk that may lead to delay or cancellation of the project as a result of non-attendance of social and environmental issues, and hence a delay/denial of financing from the government or possible financiers. Ngozi project area is partly surrounded with environmentally sensitive areas such as Poroto Ridge Forest Reserve, Itunza Forest Reserve and other miner forests. The project is furthermore located in small and medium scale agricultural areas, the implementation of the project in the above settings might raise concerns if little consultation is done, lack of direct benefits as well as land acquisitions problems.

- *TGDC capability risk*

TGDC, being a new company with an operational history of less than 2 years, might suffer through inadequate experienced geothermal professionals providing expertise in executing various phases of the project.

- *Economic risk*

These include overall economic conditions, movements in interest, inflation rates, currency exchange rates as well as expansion or increase in taxes and royalties after the power purchase agreement. These might have an adverse effect on the exploration, development and production activities.

- *Financing risk*

Deficiency or unavailability of funds from the government and other financing partners will subsequently lead to delay in executing the project.

- *Development and construction delay risk*

There is a risk of delay during construction of the steam gathering systems, power plant and power evacuation facilities that is always caused by incoordination of the construction activities.

- *Change in political regime*

The geothermal development phases as well as the economical conventional power plant life are subject to various political regimes change (Ngugi, 2012). Within the time range, the government energy policies might change the focus on geothermal power development and concentrate on other forms of energy or other investment priorities. These policies may have a material impact on the development of Ngozi power project.

10.2 Risk analysis and assessment

The above registered potential risks require a comprehensive risk management plan, which assesses the vulnerability of critical assets to specific threats, determines the risk (expected likelihood and consequences of specific attacks on specific assets) and identify ways to reduce risk and prioritize risk reduction measures based on strategy. This is done by establishing a risk matrix, which is also referred to as a probability and impact matrix. The content of this business case will involve highlighting a

theoretical form of the key project risks and its management will be utilising the probability impact matrix as a qualitative risk analysis method.

Probability impact matrix

The method involves defining risks in a two dimensional approach, namely uncertainty occurrence (probability) and the outcome effect (impact) of risk chance likelihood and risk impact consequence. Likelihood is derived from uncertainty of risk occurrence and the impact is the effect of the contingency. Potential event of loss designating risk (R) is translated in mathematical terms as a result of the product of the size of the impact (I) and likelihood of (P) (Dumbravă and Iacob, 2013):

$$R = I * P$$

The project probability of risk occurrence was set between 1 and 6, while the impacts on a scale of 1 to 4 were established as shown in Tables 6 and 7, respectively. Moreover, the risk exposure was calculated as shown in Table 8 below.

TABLE 6: Likelihood score risk

Score	1	2	3	4	5	6
Likelihood level	Almost impossible	Unlikely	Remote	Occasional	Moderate	Frequent

TABLE 7: Impact analysis

Score	1	2	3	4
Magnitude of impact	Minor	Moderate	Critical	Catastrophic

TABLE 8: Calculation of the exposure risk score

Likelihood					Severity
6	6	12	18	24	
5	5	10	15	20	
4	4	8	12	16	
3	3	6	9	12	
2	2	4	6	8	
1	1	2	3	4	
	1	2	3	4	

The project probability impact matrix was developed in Table 9, with risk categorised. The details of the risk are found in Appendix I.

TABLE 9: Probability impact matrix

Likelihood					
6	6	12	18	24	
5	5	10	15	20	
4	4	8	12	16	
3	3	6	9	12	
2	2	4	6	8	
1	1	2	3	4	
	1	2	3	4	Severity

	High risk
	Critical risk
	Low risk
	Marginal risk

10.3 Risk escalation and reporting

Table 10 below shows the risk escalation and reporting. It defines who must be informed and has the authority to accept risk based on its magnitude.

TABLE 10: Risk escalation and reporting

	Risk escalation and reporting levels for each level of risk
High risk	TGDC board members
Critical risk	TGDC Chief Executive office
Low risk	Project team senior leadership
Marginal risk	Project manager

10.4 Risk treatment and control

Several risk mitigation measures were put in place to minimize the severity of the key risks as shown in Appendix I. Despite the risk treatment and control measures in place, the exploration and financing risks were seen as dominant and requiring further measures.

11. PROJECT FINANCING

This explains a range of funding arrangements available to execute the project and therefore stands as the most critical part of the project development. Geothermal resource development, like many other power development projects, is critically dependent on access to financing under attractive conditions to earn a return commensurate with the risk at that particular phase of the project (NREL, 2011).

Regardless of the significant technical competitive advantages of geothermal power to other forms of energy technologies, securing funds for geothermal power projects has proven to be a great challenge in the early stages of exploration as most financiers have limited appetite for geologically risky projects, especially on green fields. The substantial initial investment is related to the drilling cost and to the need to cover the geological risk at the beginning of the exploration.

However, TGDC has ensured the access of adequate funding to successfully implement various phases of the project. In this case, TGDC has to secure loans, then the Government of Tanzania will be the borrower and Ministry of Energy and Minerals will serve as a beneficiary executing agency and beneficiary of the proposed loan, and TGDC will serve as the implementing agency. For the development of this case, the following financing windows are considered in the development of Ngozi geothermal power project.

11.1 Financing of surface exploration

For development of this case, TGDC is anticipated to finance the surface exploration to precisely locate the drilling sites. This is currently done through funding from GOT and the available financing windows both in monetary and in-kind forms, e.g. Geothermal Risk Mitigation Facility (GRMF) grant, The United Nations Environment Programme (UNEP), Iceland Directorate for International Development Cooperation (ICEIDA), Japan International Cooperation Agency (JICA), etc.

11.2 Financing of exploration and appraisal drilling

As stated above, drilling is the highest risk development phase for geothermal projects and requires a substantial amount of funding, hence it is the most difficult phase to mobilise capital as well as the greatest uncertainty to meet the return on the investment. TGDC might utilize the available financing sources at this phase including GOT, public support investment climate funds and geothermal risk mitigation facility grants. This includes GRMF grant, Scaling-up renewable energy programme (SREP), grant part of the Climate Fund Framework, SREP grant and loan through World Bank etc.

11.3 Financing of power plant construction

Depending on the development strategy in this case, GOT with the available partners will fund the wellhead units plant while the conventional power plant and associated infrastructure will be co-financed with other international agencies and institutional lenders. The possible financing windows include, but are not limited to, JICA, African Development Bank, European Investment Bank, World Bank, Agence Française de Développement (AFD), SREP grant, TOSHIBA (MoU with TGDC), etc.

12. PROJECT ECONOMICS

To fully understand the financial and economic analysis of various options, the field development costs shall be assessed on a green field basis, that is taking into account all costs incurred from initial surface exploration, exploration and development drilling, steam field and power plant development, construction and commissioning, operation and maintenance. The cost estimates were done based on the ESMAP 2012 handbook (Gehring and Lokhsa, 2012), unpublished lecture notes as developed by (Pálsson, 2016) and presentation from Hallgrímsdóttir and Gudmundsson (2016) as well as considerations of Ngozi site specific factors.

12.1 Assumptions

The assumptions are shown in Table 11 for general project assumptions, Table 12 for specific cost assumptions and Table 13 for financial assumptions that were used to assess the financial viability of project;

TABLE 11: General project assumptions

Parameter	Unit	Value
Average well output	MW	5
Exploration drilling success rate	%	50%
Appraisal wells drilling success rate	%	75%
Production drilling success rate	%	90%
Ratio of reinjection to production wells	Ratio	1/5
Well drilling days	Days	90

TABLE 12: Specific cost assumptions

Item	Unit	Amount (M USD)
Well drilling (hired rigs)	USD/Well	4
Drilling materials	USD/Well	1
Steam gathering system	USD/MW	0.4

TABLE 13: Financial assumptions

Parameter	Value
Plant capacity factor	95%
Planning horizon (operations)	25 years
Equity share in cap. ex	30%
Loans	70%
Loan interest rate (no inflation)	5%
Electricity price	100 \$/MWh
Loan management fee	1%
Income tax rate	30% of profit
Loan repayment	20 years
Depreciation buildings	20%
Depreciation equipment	25%
Depreciation other	20%

12.2 Financial viability

The net present value (NPV), internal rate of return (IRR) and discounted payback period (PB) methods are the three most popular decision rules used to assess the viability of many investment planning problems. The financial viability was done using a modified Microsoft Excel-based profitability assessment model developed by (Jensson, 2016) which is made up of different spread sheets including investment, operations, cash flows and profitability. The three methods will be used in this case to conclude the profitability of the chosen project scenarios. Appendix II shows screenshots from the probability model.

12.2.1 The Net Present Value (NPV)

The net present value (NPV) of a project is the sum of the present value of all its cash flows in each year of the project's implementation, both inflows and outflows, discounted at a rate consistent with the project. Mathematically, NPV is presented as:

$$NPV(i) = \frac{A_0}{(1+i)^0} + \frac{A_1}{(1+i)^1} + \dots + \frac{A_N}{(1+i)^N}$$

$$= \sum_{n=0}^N \frac{A_n}{(1+i)^n}$$

where A_n = Net cash flow at the end of period n ;
 i = MARR (Minimal Attractive Rate of Return);
 N = Service life of the project.

If the $NPV(i)$ is positive for a single project, the project should be accepted, since a positive NPV means that the project has greater equivalent value of inflows than outflows and therefore makes a profit. According to the decision rule for NPV:

If $NPV(i) > 0$	Accept the investment;
If $NPV(i) = 0$	Remain indifferent to the investment;
If $NPV(i) < 0$	Reject the investment.

12.2.2 Internal Rate of Return (IRR)

An internal rate of return (or IRR) for an investment is typically defined as a discount rate that makes the net present value of the investment cash flows equal to zero. The IRR is equal to the rate of return for which the following function is zero:

$$NPV(i^*) = \sum_{n=0}^N \frac{A_n}{(1+i^*)^n} = 0$$

Investors usually want to do better than breaking even in their investments. Their investment policy usually defines a MARR (Minimal Attractive Rate of Return), in which case the IRR and the MARR can be used to decide whether a project is feasible or not. The decision rule for a simple project is as follows:

If $IRR > MARR$	Accept the project;
If $IRR = MARR$	Remain indifferent;
If $IRR < MARR$	Reject the project.

12.2.3 Discounted Payback Period (PB)

The discounted payback period of a project shows the time it takes the project to recover investment outlays. The project with discounted payback period in the desired time frame is considered feasible. However, the method does not measure profitability, as it only measures the time it takes to recover the initial investment outlay but not the profit that is made after paying back the initial investment. Hence, it doesn't allow for the possible advantages of a project with a longer economic life.

12.3 Sensitivity analysis

This is the process of determining to what extent the project financial viability results can be affected with changes in the input parameters. The values of input parameters are often associated with a degree of uncertainty; it is therefore crucial to examine the project's financial viability results given a change in these parameters. The business case has determined how much IRR and NPV change relative to a given change in input parameters of sales price, sales quantity, and investment cost of equipment and operation and maintenance expenses.

12.4 Discussion on project economics in Scenario 1

12.4.1 Project assumptions

The assumptions on the financial feasibility analysis of Scenario 1:

- Three exploration wells will be drilled with 50% success rate, 4 appraisal wells at 75% success rate and 9 production wells at 90% success rate to supply steam to power the turbine. Upon careful reservoir study, some of the unsuccessful wells will be used as reinjection wells, however, one reinjection well will be drilled.
- TGDC/GOT will partly finance the project's total investment at the arrangement of 30% equity and 70% loan at an interest of 5%.

12.4.2 Project cost estimates

The investment cost items are classified as:

- Buildings-power plants cost (EPC package), workshop (electrical, mechanical and carpentry), civil works, access road construction, water supply infrastructures and power evacuation facilities (transmission line and substation). The total investment cost for the 7 years of construction period was 149 million USD.
- Equipment-exploration drilling, appraisal drilling, production drilling, rig mobilisation and demobilisation, transfer of rig between pads, project management drilling consultant. The total investment cost for the 7 years of construction period was estimated to be 91 million USD.
- Other-detailed surface studies, environmental studies, feasibility study, water and environmental project permit, state concession fee, land purchase and resettlement. The total investment cost for the 7 years of construction period was estimated to be 9 million USD.
- The project will require a total working capital of 18 million USD.

12.4.3 Summary of results

From the three financial viability analysis methods and sensitivity analysis, the following results were observed:

- *The Net Present Value (NPV)*
The NPV at 15% MARR for the total equity of 80 million USD at the 25th year of operation was calculated to be 15 million USD, while the NPV at 10% MARR for the total project investment of 266 million USD was calculated to be 5 million USD. Since the NPV in both cases > 0, the project is considered feasible. The accumulated NPV graph is as shown in Figure 6.
- *Internal Rate of Return (IRR)*
The IRR at was calculated to be 20% for the total equity of 80 MUSD at the 25th year of operation, while the IRR for the total project investment of 266 million USD was calculated to be 10%. Since the IRR>MARR for the equity, then project is accepted meanwhile the MARR = IRR for the total project investment, then the project viability decision becomes indifferent. The IRR graph is as shown in the Figure 7.
- *Discounted Payback Period (PB)*
The PB period of the project is reached at the 8th year of project operation for equity, i.e. 2029/2030, while in the 22nd year for the total project, i.e. 2044. This can be read from the NPV graph in Figure 6.
- *Sensitivity analysis*
The sensitivity analysis was done to find out how sensitive the NPV and IRR are against the cost of equipment, price of electricity, sales quantity of electricity, loan interest and operation and maintenance. From Figure 8, the four parameters of equipment, price of electricity, sales quantity

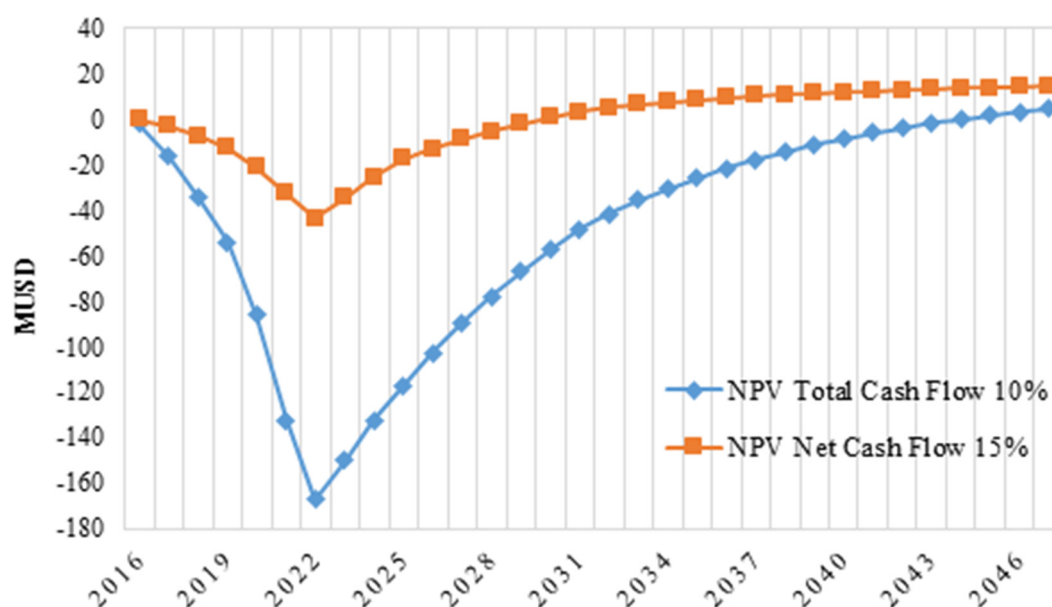


FIGURE 6: Accumulated Net Present Value

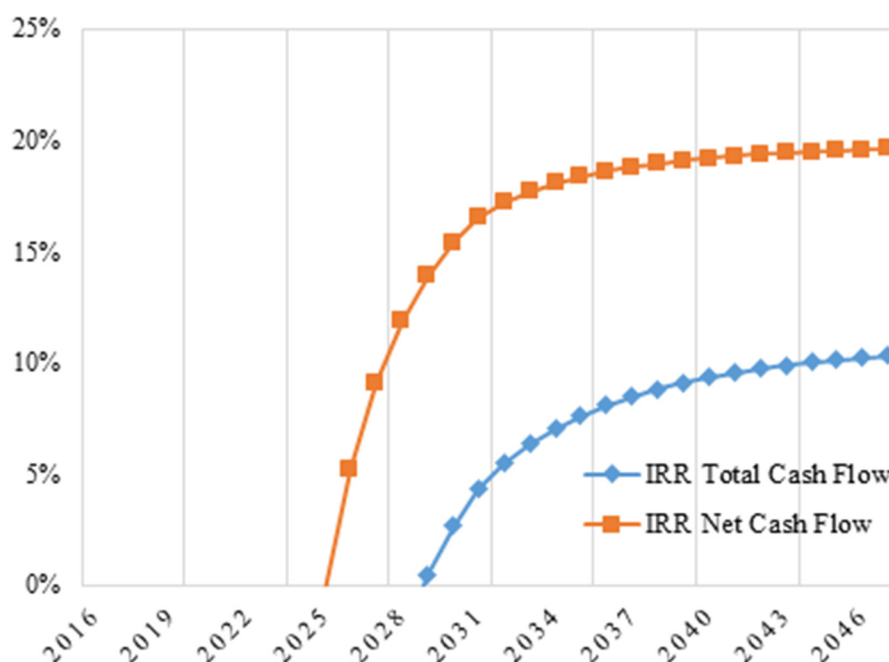


FIGURE 7: Internal Rate of Return (IRR)

of electricity and loan interest were very sensitive on the NPV of Equity. For example, a 20% decrease in price and quantity of electricity to be sold will make the project not feasible while a 50% increase in the price of equipment will make the project not viable. The other parameters of loan interest, operation and maintenance cost as well as the cost of others will have no significant impact on the NPV of the equity. For example, the 50% increase of all costs will still make the project feasible.

The same parameters were checked on the IRR of the equity, from Figure 9. The analysis showed that with the decrease of the price and sales quantity of electricity by 10% the project becomes not feasible as the IRR becomes 13%, less than the MARR of 15%, whereas a 60% increase of the cost of equipment and loan interest will still make the project feasible. The cost operation and

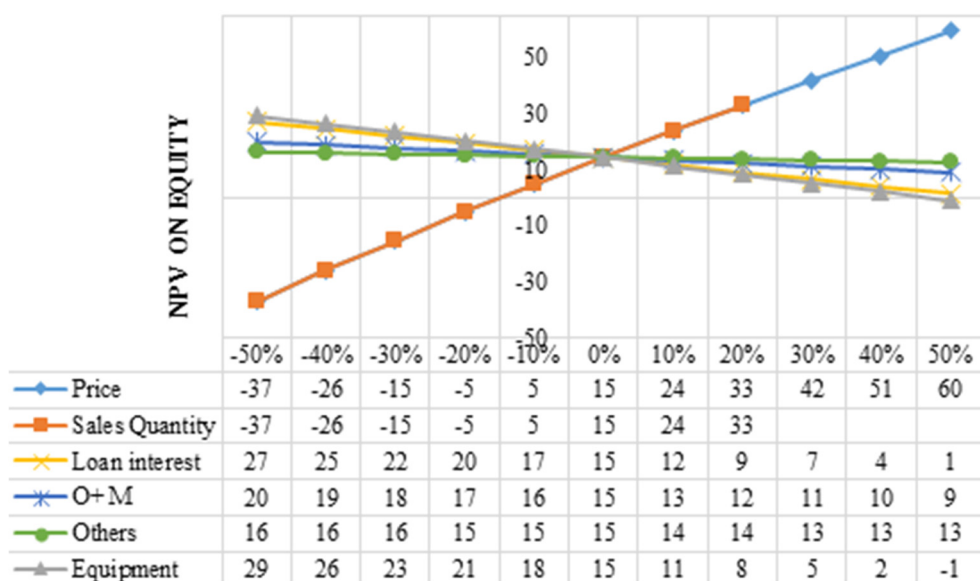


FIGURE 8: Sensitivity analysis on the NPV of equity

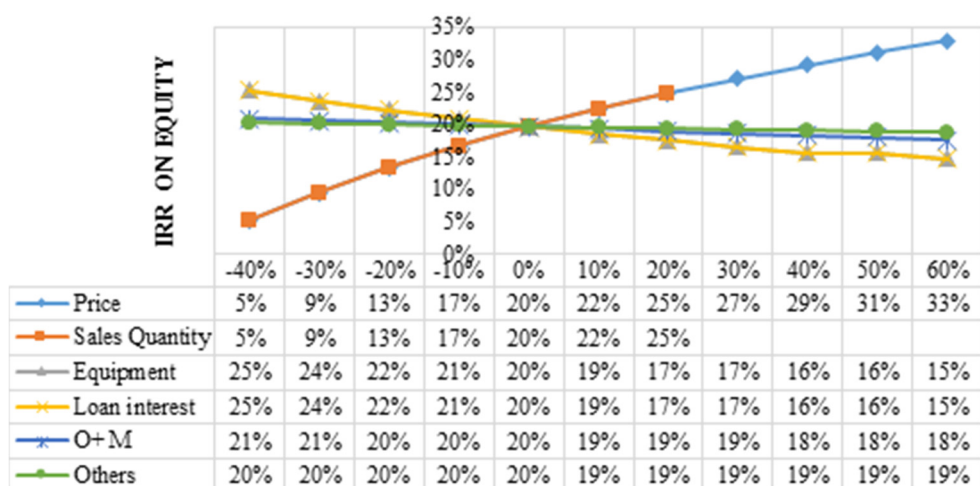


FIGURE 9: Sensitivity analysis on the IRR of equity

maintenance as well as the cost of others will have no significant effect on the changes on the IRR of the equity.

12.5 Discussion on project economics on Scenario 2

12.5.1 Project assumption

The assumptions on the financial feasibility analysis of Scenario 2:

- Three exploration wells will be drilled with 50% success rate and one of the wells will be used to supply steam to power the turbine in the wellhead unit. The unsuccessful wells will be used as reinjection wells.
- GOT will finance the exploration drilling and installation of 5 a MW well head unit.
- Following the successful installation of a wellhead unit, the 50 MW power plant field development activities will be undertaken i.e. surface studies, drilling of appraisal, production and reinjection wells.

12.5.2 Project cost estimates

The investment cost items are classified as shown below:

- *Buildings standard size wellhead power plants cost (EPC package)*, workshop (electrical and mechanical and carpentry), civil works, access road construction, water supply infrastructures and power evacuation facilities (transmission line and substation). The total investment cost for the 3 years of construction period was estimated to be 12 million USD.
- *Equipment* – exploration drilling, rig mobilisation and demobilisation, transfer of rig between pads, wellheads, well silencers and connections to steam system, project management drilling consultant. The total investment cost for the 3 years of construction period was estimated to be 16 million USD.
- *Other-detailed surface studies*, environmental studies, feasibility study, water and environmental project permit, state concession fee and land purchase and resettlement. The total investment cost for the 3 years of construction period was estimated to be 3 million USD.
- *This scenario* utilised same cost estimates as in 50 MW power plant above with exclusion of the field development costs that were previously covered from the 5 MW plant. The total investment cost for the large power plant was estimated to be 214 million USD.

12.5.3 Summary of results

From the three financial viability analysis methods and sensitivity analysis, the following results were observed:

- *The net present value (NPV)*
The NPV at 15% MARR for the total equity of 94 MUSD at the 35th year of operation was calculated to be 6 MUSD. Since the NPV > 0, the project is feasible meanwhile the NPV at 10% MARR the total project was calculated to be 24 MUSD at the 35th year of operation with a total investment of 240 MUSD. Since the NPV > 0, the project is feasible. The accumulated NPV graph is as shown in the Figure 10.

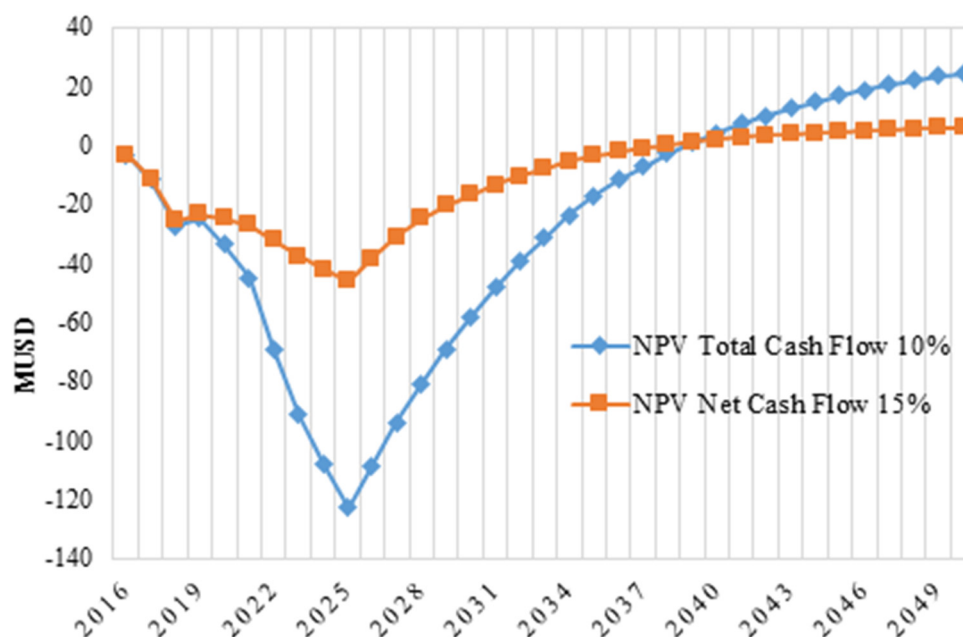


FIGURE 10: Accumulated Net Present Value

- *Internal Rate of Return (IRR)*
The IRR was calculated to be 16% for the total equity of 94 MUSD at the 35th year of operation, since the IRR > MARR then the project is accepted. The IRR for the total project was calculated

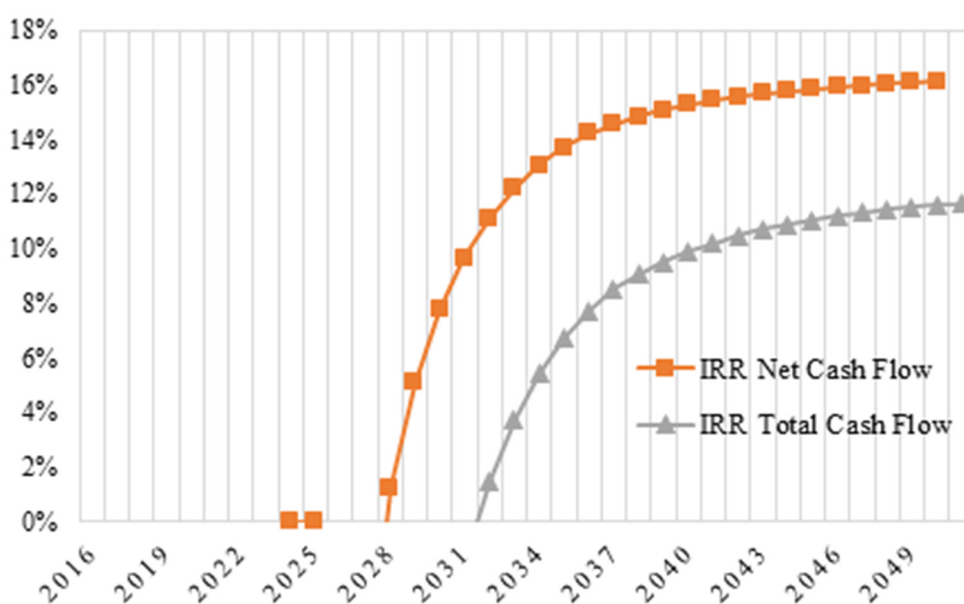


FIGURE 11: Internal Rate of Return (IRR)

to be 12%. Since the $IRR > MARR$ then the project is accepted. The IRR graph is as shown in Figure 11.

- *Discounted Payback Period (PB)*

The discounted PB of the project was attained at the 22nd year of project operation, i.e. 2038/2039 for both equity and the total project. This can be read from the NPV graph in Figure 10.

- *Sensitivity analysis*

The sensitivity analysis was done to find out how sensitive the NPV and IRR are against the equipment, price of electricity, sales quantity of electricity, loan interest and operation and maintenance. From Figure 12, the three parameters of equipment, price of electricity and sales quantity of electricity sales were very sensitive for the NPV of Equity. For example, a 10% decrease of price of electricity and quantity of electricity to be sold will make the project not feasible while a 20% increase in the price of equipment will make the project not feasible. The loan interest has little significance as 40% increase in the loan interest will make the project still feasible. The operation and maintenance costs will have no significant impact on the NPV of the equity. For example, a 50% increase in the operation and maintenance costs will still make the project feasible.

The same parameters were checked on the IRR and the equity, however the IRR of the equity is not adversely affected by any of the parameters, Figure 13 shows that even with a decrease of the price and sales quantity of electricity of 50% the project becomes feasible. The same is seen on the cost of equipment and operation and maintenance, the increase of these factors by 50% will still make the project feasible.

12.3 Overall summary of results

Both scenarios were sensitive to the price of electricity, sale quantity and the cost of equipment. A significant sensitivity was also observed on the loan interest in Scenario 1, as the slight increase in loan interest could make the project not viable, this is explained by the large amount of loans needed to develop this scenario. Again, Scenario 2 provides a substantial amount of revenue from the wellhead unit, or close to 29 million in 7 years of operations with the initial investment of close to 15 million USD (for well head unit), hence saving the company from requesting working capital from the financier.

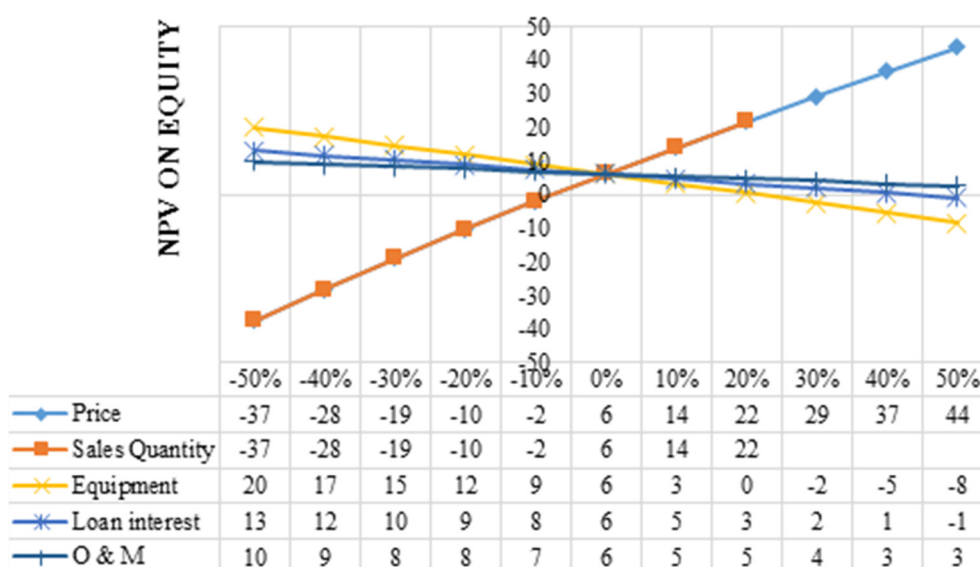


FIGURE 12: Sensitivity analysis of the NPV on equity

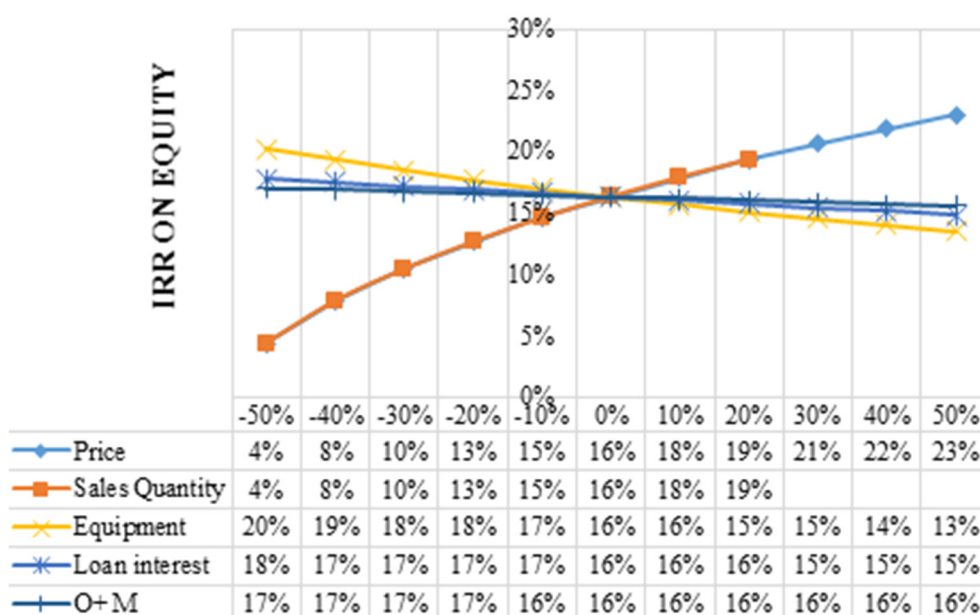


FIGURE 13: Sensitivity analysis of the IRR on equity

13. CONCLUSIONS AND BUSINESS RECOMMENDATIONS

The preliminary build-up of this business case is one crucial step for various interested parties to provide justifications for the investment in the exploratory wells drilling in Ngozi geothermal field and, subsequently, the installation of the first geothermal power plant in the country. The case has covered all the essential social-economical project benefits, identified key project risks, identified possible project financing arrangements, project implementation scenarios, project social and environmental issues, stakeholder management and communication plan and, finally, financial viability analysis. Table 14 shows a snapshot of the business case parameters with the two project implementation scenarios.

TABLE 14: Snapshot of the two options of business cases

Factors	50 MW flash plant	5 MW WH unit + 50 MW flash plant
Strategic alignment	Aggressive approach towards including geothermal as a part of Tanzania's energy mix.	Careful approach in developing local skills and experience in utilising geothermal resources in Tanzania.
Environmental	The scenarios will attract significant environmental impacts to the area, particularly during drilling and operation phase.	Limited impacts will be produced from this strategy, if there are to occur, the 5 MW wellhead unit will be an excellent prototype to properly mitigate the problems for the 50 MW power plant.
Stakeholder impact	Significant number of stakeholders will be involved hence a large impact.	The 5 MW plant will attract few stakeholders at first hence it is easier to properly map the number of interested parties during the construction and operation of the large power plant.
<i>Risk:</i>		
Resource risk	The risk is higher due to little understanding of the reservoir.	Stepwise development of the 5 MW unit will offer the best knowledge of the reservoir and reduce the risk.
Operation. risk	May require significant support from outside Tanzania for the start-up of a 50 MW unit.	More experience in handling geothermal wells and turbines when starting operation of a 50 MW unit.
Risk of cost overrun	In case of risk of cost overrun, the risk will be much pronounced as it involves drilling of many wells at the beginning.	Few wells will be drilled, the risk will not be significant.
ESIA risk	Large area will be covered hence significant social and environmental shock.	The 5 MW WHP will occupy a small area, providing room for community acceptance and understanding on response to the environment. The latter 50 MW plant will utilize both environmental and social concerns raised during the 5 MW unit construction and operation.
Financing	More difficult to finance a 50 MW power plant with limited understanding of the reservoir as well as limited institutional capacity.	Easier to finance a 5 MW wellhead unit and also to finance the 50 MW plant with multidisciplinary experience gained from the 7 years of experience in exploration and exploitation of the reservoir from the 5 MW plant.
<i>Economy:</i>		
Cost	266 Million USD	245 Million USD
NPV	15 Million USD	6 Million USD
IRR	20%	16%
Pay-back period	15 years	23 years

The financial viability of the two scenarios indicate a positive financial viability on equity, whereby Scenario 1 yielded a NPV of 15 million USD with IRR of 20% while Scenario 2 generated a NPV of 6 million USD with IRR of 16%,. Under financial rationalization, Scenario 2 seems to be more profitable. However, the strategy is associated with a large investment close to 80 million USD, higher degree of uncertainty following the limited technical understanding of the Ngozi geothermal reservoir and limited TGDC capability. Scenario 2 is less profitable but associated with a significantly lower risk profile, the strategy of installing a wellhead unit after successful drilling and testing of exploration wells reduces both technical and financial risks as only 31 million USD will be spent. The strategy will generate early revenue for the company, which will be reinvested in development of a large 50 MW power plant and reduces bulky project financing obligations as well as building a strong capacity in the TGDC workforce on the geoscientific, social, environmental and technical expertise on development and exploitation of geothermal resources. It is along these lines, that Scenario 2 is recommended as the best strategy to undertake for the project.

ACKNOWLEDGEMENTS

I would like to express my sincere gratitude to The Government of Iceland through the United Nations University Geothermal Training Programme (UNU-GTP) for awarding me a fellowship opportunity to undertake the six months training in the specialized course of Project Management and Finances. I would also like to extend my heartfelt appreciation to the management of Tanzania Geothermal Development Company, Ltd. for allowing me to attend the training.

I am indebted to my supervisor, Dr. Bjarni Pálsson from the Iceland National Power Company – Landsvirkjun for his dedicated time, excellent guidance and detailed review during the entire preparation of this business case. I furthermore thank Professor Páll Jensson, from School of Science and Engineering, Reykjavik University for his useful lectures on building up profitability models and guidance during the actual preparation of the project financial viability analysis.

My appreciation goes to the UNU-GTP Director, Mr. Lúdvík S. Georgsson, the Deputy Director, Mr. Ingimar G. Haraldsson, Environmental Scientist/Editor, Ms. Málfríður Ómarsdóttir, School Manager, Ms. Thórhildur Ísberg and Service Manager, Mr. Markús A. G. Wilde, for their noble support, encouragements and endless help for my entire six month stay in Iceland. Appreciations also goes to entire 2016 group of UNU fellows.

Finally, I take this opportunity to express the profound gratitude from the core of my heart to my most treasured fiancée *Ester Raphael* for her enduring patience during the most difficult time of our live, she managed to stand firm and survive during the time she needed me most. Thanks more to my parents for their love and continuous support – both spiritually and materially. I feel honoured and blessed to have you both in my life.

Last but not least important, I am grateful to God, the Almighty for his unparalleled grace, continuous blessings, superior protection and guidance during the entire six-month period in Iceland. Lord, I am very thankful.

REFERENCES

- Bertani, R., 2015: Geothermal power generation in the world 2010-2014 update report. *Proceedings of the World Geothermal Congress 2015, Melbourne, Australia*, 19 pp.
- DiPippo, R., 2012: *Geothermal power plants. Principles, applications, case studies and environmental impact* (3rd ed.). Butterworth Heineman, Elsevier, Kidlington, UK, 587 pp.
- Dumbravă, V. and Iacob, V.S., 2013: Using probability–impact matrix in analysis and risk assessment projects, *J. Knowledge Management, Economics and Information Technology, Spec. Issue*, 76-99.
- EAGER, 2015: “*TGDC business models workshop*”. TGDC, internal training document.
- Eliasson, E.T., Thórhallsson, S., and Steingrímsson B., 2011: Geothermal power plants. *Presented at “Short Course on Geothermal Drilling, Resource Development and Power Plants”, organized by UNU-GTP and LaGeo, in Santa Tecla, El Salvador*, 16 pp.
- ESMAP, 2016: *Greenhouse gases from geothermal power production*. ESMAP, The World Bank Group, Washington DC, USA, 52 pp.
- Gehring, M. and Loksha, V., 2012: *Geothermal handbook: planning and financing power generation*. Energy Sector Management Assistance Program (ESMAP), technical report 002/12, 150 pp.

Geothermal Power, 2016: *Geothermal Power, Ltd.*, website: www.gpl-international.com/

Hallgrímsdóttir, E., and Guðmundsson, Y., 2016: Well head power plants. *Paper presented at the 3rd Iceland Geothermal Conference 2016, Reykjavík*, 18 pp.

Hudson, R.B., 2003: Electricity generation. In: Dickson, M.H., and Fanelli, M., *Geothermal energy: utilization and technology*. UNESCO Renewable Energy Series, 47-221.

Jensson, P., 2016: *A model for profitability assessment*. UNU-GTP, Iceland, unpubl.lecture notes 18 pp.

JICA, 2014: *Data collection survey on geothermal energy development in East Africa - Final report Tanzania*. JICA, website: open_jicareport.jica.go.jp/pdf/12147823.pdf.

Kalimbia, C., 2016: TZ can learn from Iceland geothermal energy strides. *The Citizen*, 23 August, 05, webpage: www.thecitizen.co.tz/News/1840340-3357372-k5ryl4z/index.html.

Ministry of Energy and Minerals, 2013: *Scaling-up renewable energy programme (SREP): Investment Plan for Tanzania*. Ministry of Energy and Minerals - MEM, Dar es Salaam, 146 pp.

Ministry of Energy and Minerals, 2014a: Tanzania energy statistical yearbook 2012. MEM, Dar es Salaam, 52 pp.

Ministry of Energy and Minerals, 2014b: The electricity supply industry (ESI) reform strategy and roadmap. MEM, Dar es Salaam, 52 pp.

Mjokava, T.T., 2012: Geothermal development in Tanzania – a country update. *Proceedings of the 4th ARGeo Conference, Nairobi, Kenya*, 5 pp.

National Bureau of Statistics, 2012: *2012 PHC: Tanzania regional profiles*. NBS, webpage: www.nbs.go.tz/nbs/takwimu/census2012/RegProfiles/12_Mbeya_Regional_Profile.zip

Ngugi, P.K., 2012: What does geothermal cost? - the Kenya experience. *Paper presented at “Short Course on Geothermal Development and Geothermal Wells”, organized by UNU-GTP and LaGeo, in Santa Tecla, El Salvador*. UNU-GTP, SC14, 13 pp.

NREL 2011: *Guidebook to geothermal power finance*. National Renewable Energy Laboratory, US Department of Energy, Colorado, USA, 61 pp.

Pálsson, B., 2016: *The geothermal business case*. UNU-GTP, Iceland, unpubl. lecture notes, 107 pp.

whatis.com, 2016: *Business case*. whatis.com, webpage: whatis.techtarget.com/definition/business-case

APPENDIX I: Risk identification, treatment and control

Ref.	Risk category	Risk and description	Risk chance likelihood	Risk Impact consequence	Risk priority (initial)	Risk treatment plan	Risk owner	Due	Risk chance likelihood	Risk impact consequence	Residual risk
1	Exploration /Geological	Unfavourable characteristics of reservoir such existence of inadequate flow rate, low temperature, poor system inherent permeability and the chemical components of the geothermal fluids hence hitting dry wells	3	4	12	Comprehensive geoscientific studies to precisely establish the drilling targets	TGDC	10.10.2016	2	2	4
2	Operational and Maintenance	Reservoir depletion, mechanical failure or plant breakdown, environmental accidents, plant and equipment chemical scaling from geothermal fluids, corrosion, earth quake during reinjection, delays in drilling and connecting make-up wells, unexpected shortages or increases in the costs of consumables, spare parts.	2	3	6	Periodic maintained of power plant and associated infrastructures as per set standards	TGDC	10.10.2016	1	2	2
3	Legal and regulatory	Miscommunication of existing legal and regulatory framework in relation to geothermal development	3	2	6	Establishment of geothermal policy, legislation and regulatory framework to link with available framework.	GOT	10.10.2016	2	1	2
4	Environmental and Social	Flora, fauna, ecosystems and biodiversity disturbance, GHG emission as well as land acquisition and resettlement area may cause rejection of project	2	4	8	Undertaking detailed ESIA study,prepare strategic and time plans to mitigate the challenges	TGDC	10.10.2016	2	1	2
5	Drilling delays and cost overrun	Geological formation, mechanical problems and unforeseen problems may lead to the delays and cost overrun	2	2	4	Comprehensive geological studies to establish the formation parameters as well as having the cost contingency.	TGDC	10.10.2016	1	1	1
6	Economic	Higher return on investment,unclear tax incentives, High interest rate, Delay in PPA	2	3	6	Early preparation of Business case outlying all the possible economic sensitive factors	TGDC	10.10.2016	1	2	2
7	Financing	Non-availability or insufficient funds from GOT and the project counterpart	3	4	12	Early preparation and submission request of project financing plan to the possible project financier	TGDC	10.10.2016	2	2	4
8	Development and Construction Delay	Delay during construction of steam gathering systems, power plant and power evacuation facilities	2	3	6	Undertaking detailed feasibility study while outlying various options	TGDC	10.10.2016	1	1	1
9	Political	Shift in project political support due to change in government regime	2	2	4	Comprehensive awareness campaign to publicize the importance of geothermal energy as renewable, reliable and environmentally friendly source of electricity generation.	TGDC, GOT	10.10.2016	1	1	1
10	Healthy and Safety	Drilling, construction and power plant operation pose great risks to health and safety of personnel and equipment's	2	3	6	Preparation of healthy and safety plan prior the commencement of activities as well as strict implementation strategy	TGDC, Contractors	10.10.2016	1	2	2
11	TGDC Capability	TGDC is new company with limited geothermal experts	3	2	6	Engaging geothermal experienced implementation consultancies and contractors in various phases of the project	TGDC	10.10.2016	1	1	1

FIGURE 1: Identification of risks, treatment and control measures

APPENDIX II: Screen shots from profitability model

	Assumptions and Results						MARR	Equity	15%	Planning Horizo				25	years		
Assumptions:							MARR	Project	10%								
Investment:	MUSD	2016	2017	2018	2019	2020	2021	2022	2023	2024	2025	2026	2027	2028	Total USD		
Buildings	100%	0	9	0	1	25	58	57	0	0	0	0	0	0	149		
Equipment	100%	0	6	21	21	21	17	5	0	0	0	0	0	0	91		
Other	100%	2	1	0	5	0	0	0	0	0	0	0	0	0	9		
Total Investment		2	16	21	27	46	75	62	0	0	0	0	0	0	248		
Financing:																	
Working Capital		1	2	2	3	3	6	1	0	0	0	0	0	0	18		
Total Financing		3	18	23	30	49	81	63	0	0	0	0	0	0	266		
Equity	100%	30 years															
Loan Repayments	100%			20													
Loan Interest	100%	5%															
Operations:																	
Sales Quantity	100%	0.0	0.0	0.0	0.0	0.0	0.0	0.0	0.4	0.4	0.4	0.4	0.4	0.4	MWh/year		
Sales Price	100%	0.0	0.0	0.0	0.0	0.0	0.0	0.0	100.0	100.0	100.0	100.0	100.0	100.0	100\$/MWh		
Variable Cost	100%	0	MUSD/MW														
Operation and Maintenance	100%	5	MUSD/year														
Inventory Build-up																	
Other Assumptions:																	
Debtors	1/12	of turnover (revenue)		Total Cap.						Equity							
Creditors	1/12	of variable cost		NPV of Cash Flow						5		15					
Dividend	0%	of profit		Internal Rate						10%		20%					
Income Tax	30%	of taxable profit															
Depreciation Buildings	20%	Tanzania Investment Act, 1997			Internal Value of Shares				6								
Depreciation Equipment	25%	Tanzania Investment Act, 1997			After 25 Years												
Depreciation Other	20%	Tanzania Investment Act, 1997															
Loan Management Fee	1%																
Main Results:																	
								Total Cap.		Equity							
								NPV of Cash Flow		5		15					
								Internal Rate		10%		20%					
								Internal Value of Shares		6							
								After 25 Years									

FIGURE 1: Assumptions and results for Scenario 1

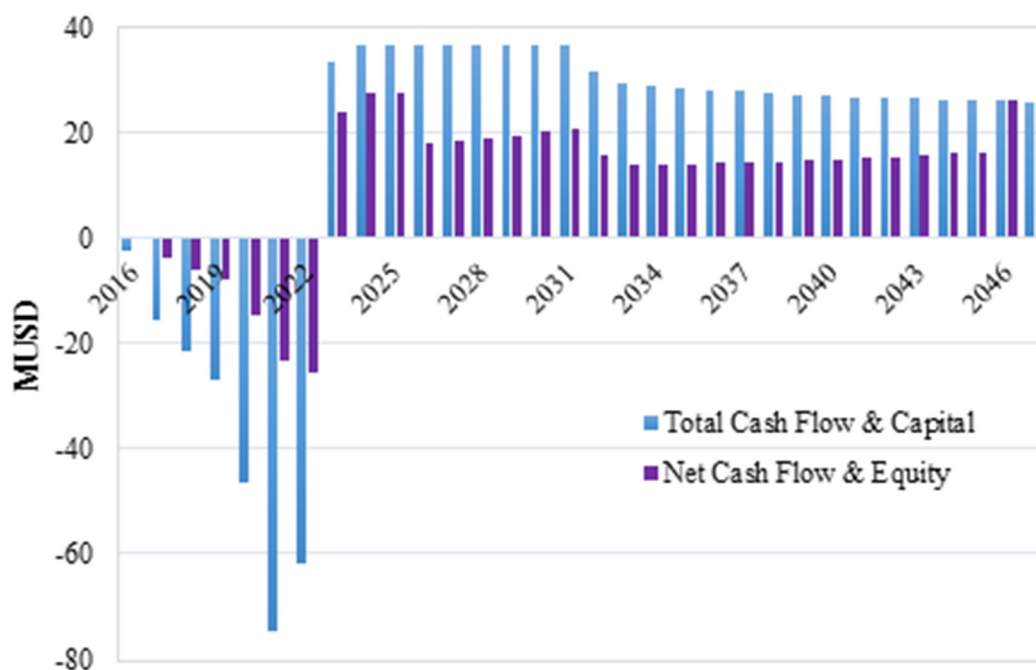


FIGURE 2: Cash flow to be generated from Scenario 1

Assumptions and Results													MARR (Equity)	15%	Planning Horizon	7	5 MW
Assumptions:													MARR (Project)	10%	Planning Horizon	25	50 MW
		2016	2017	2018	2019	2020	2021	2022	2023	2024	2025	2026	2027	2028			
Investment:	MUSD																
Buildings	100%	0	2	10	0	0	0	22	35	39	39	0	0	0			
Equipment	100%	1	6	9	1	15	20	20	16	0	0	0	0	0			
Other	100%	3	1	0	1	0	0	3	1	0	0	0	0	0			
Total Investment		3	9	19	2	16	21	45	52	39	39	0	0	0			
Financing:																	
Working Capital		0	0	0	0	0	0	0	0	0	0	0	0	0			
Total Financing		3	9	19	2	16	21	45	52	39	39	0	0	0			
		5 MW	50 MW														
Equity	100%	100%	30.0%														
Loan Repayments	100%	0	20	years													
Loan Interest	100%	0%	5%														
Operations:		2016	2017	2018	2019	2020	2021	2022	2023	2024	2025	2026	2027	2028			
Sales Quantity	100%	0.0	0.0	0.0	0.04	0.04	0.04	0.04	0.04	0.04	0.04	0.46	0.46	0.46			
Sales Price	100%	0.0	0.0	0.0	100.0	100.0	100.0	100.0	100.0	100.0	100.0	100.0	100.0	100.0			
Variable Cost - 5 MW	100%	0.0	MUSD/MWh/year														
Variable Cost - 50 MW	100%	0.0	MUSD/MWh/year														
Operation & Maintenance - 5 MW	100%	0.3	MUSD/MWh/year														
Operation & Maintenance - 50 MW	100%	5	MUSD/MWh/year														
Inventory Build-up	100%	0	0	0	0	0	0	0	0	0	0	0	0	0			
Other Assumptions:																	
Debtors	1/12	of turnover (revenue)															
Creditors	1/12	of variable cost															
Dividend	0%	of profit															
Income Tax	30%	of taxable profit															
Depreciation Buildings	20%	Tanzania Investment Act, 1997															
Depreciation Equipment	25%	Tanzania Investment Act, 1997															
Depreciation Other	20%	Tanzania Investment Act, 1997															
Loan Management Fee	1%																

FIGURE 3: Assumptions and results for Scenario 2

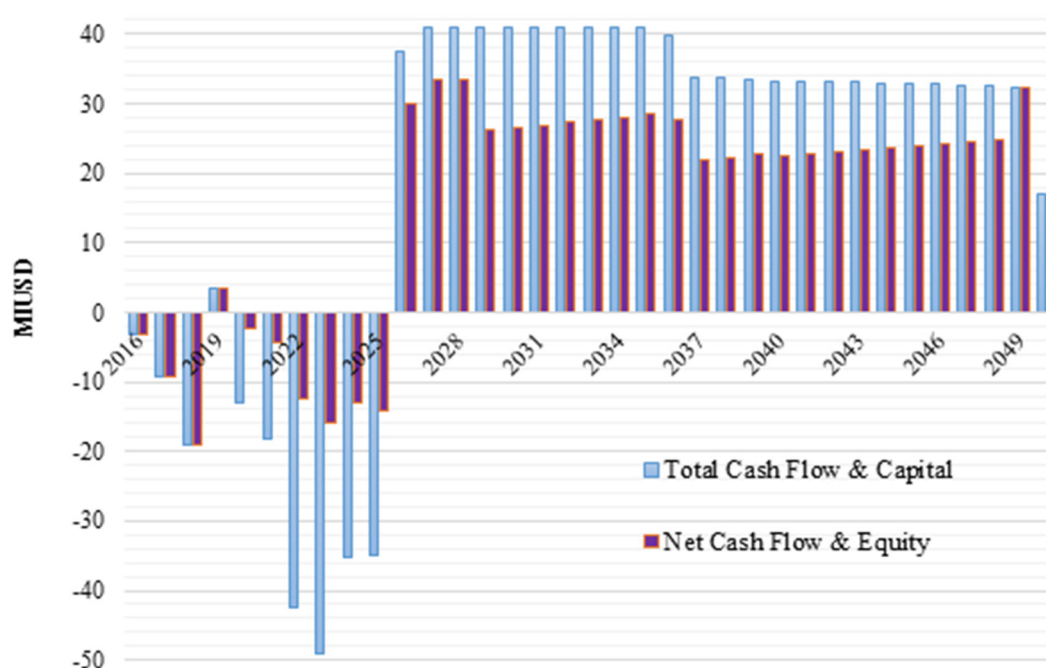


FIGURE 4: Cash flow to be generated from Scenario 2



UNITED NATIONS
UNIVERSITY

UNU-GTP

Geothermal Training Programme

Orkustofnun, Grensasvegur 9,
IS-108 Reykjavik, Iceland

Reports 2016
Number 22

METHODOLOGY FOR OPTIMIZING PIPELINE ROUTE SELECTION, SEPARATOR AND POWER PLANT PLACEMENT IN GEOTHERMAL PROJECTS – CASE OF OLKARIA IV IN KENYA

Harrison Kiplimo Keter

Kenya Electricity Generating Company, Ltd. - KenGen

P.O. Box 785-20117

Naivasha

KENYA

kketer@kengen.co.ke

ABSTRACT

The objective of this study is to create a tool and develop a methodology for optimizing pipeline route selection, placement of separators and power plants in geothermal projects. The process usually faces a number of constraining challenges including environmental protection issues, land use policies and technical requirements. Among the technical constraints considered are pressure drop along the pipeline, flow regimes, pipeline diameter, thickness and length, maximum allowable gradients and associated costs for each component. The pipe diameter, thickness and overall length have a great bearing on the total pipeline cost. An optimized route and pipe diameter will directly lead to an optimized project cost that is the drive for this study.

Variable topography distance transform (VTDT) method was used to define the routes and weighted variable topography distance transform (WVTDT) to find best location for the separators and the power plant. Application of constraints was used to optimize the pipe network and flow in each pipe. VTDT is based on the chamfer metric distance transform algorithm which works with the digital elevation matrix (DEM) to get height values for each cell. For this study the DEM and field data for Olkaria IV geothermal field were used to test the model. The study has shown that good results are obtained with VTDT for route selection, separator and plant location optimization. The study also proposes a sequence of optimization steps where the separator location is first optimized taking into account the location of production wells and hot reinjection wells. Cold reinjection wells are not considered since the pipes are usually made of polyethylene whose price is much lower compared to the price of steel used for other pipelines. The length of the routes from each well to the separator is then determined. This is followed by optimizing the plant location considering the already optimized separator locations. In this study, the use of WVTDT shows that the length of the pipeline can be shortened by 1542 m. It is, however, important to conduct a detailed survey of the area to map out all the coordinates of the no-go zones as defined by human, technical or environmental constraints for inclusion in the program as constraints.

1. BACKGROUND

1.1 Geothermal energy in Kenya

Geothermal resources in Kenya are mainly found along the Kenyan Rift Valley with the exception of a few areas outside of the rift having been mapped that contain geothermal resources. Some of the areas mapped out of the rift system are Masa Mukye located in the coast region and around Homa Hills in the Nyanza province in the west of the country. Figure 1 shows the geothermal areas of Kenya which have been mapped. The rift system is characterized by striking structural and topography features trending in north-south direction through central Kenya (Riaroh and Okoth, 1994). Various studies which have been conducted indicate the presence of near surface heat sources. The Kenyan government has prioritized the exploitation of the geothermal resource as a main source of energy. The greater Olkaria geothermal field is located in the Kenya Rift Valley, about 120 kilometres northwest of Nairobi, covering more than 200 square kilometres. It is the largest exploited geothermal field in Africa with over 600 megawatts

(MWe) of developed power (August 2016). The field is home to Olkaria I, II, III and IV power plants and fifteen wellhead plants developed and operated by Kenya Electricity Generating Company (KenGen). The wellhead or modular plants together generate a total of 81.1 MW. According to KenGen internal reports in 2012, the development of Olkaria V and VI power plants are at advanced stages with planned operational timelines of 2017 and 2018, respectively (Mannvit, 2012). There are intentions to further develop Olkaria VII, VIII, IX and X within the Olkaria field. Olkaria V and VI each require a total of 45 wells to avail required steam. In June 2016, 43 and 41 wells had been drilled in Olkaria V and VI respectively. The next stage will include steam field development and power plant construction. The Olkaria field is surrounded by further geothermal prospects such as Suswa and Longonot.

In order to fast track geothermal development, the government of Kenya has created a conducive policy framework that encourage private sector investments. This has resulted in three private developers being granted licences to develop geothermal energy in Olkaria, Akiira and Longonot fields. Drilling in Longonot and Akiira is on-going and the plans for development very alive. This study considers a case study of Olkaria IV geothermal field. However, the results can be used to inform planning and decision making processes for development in other areas.

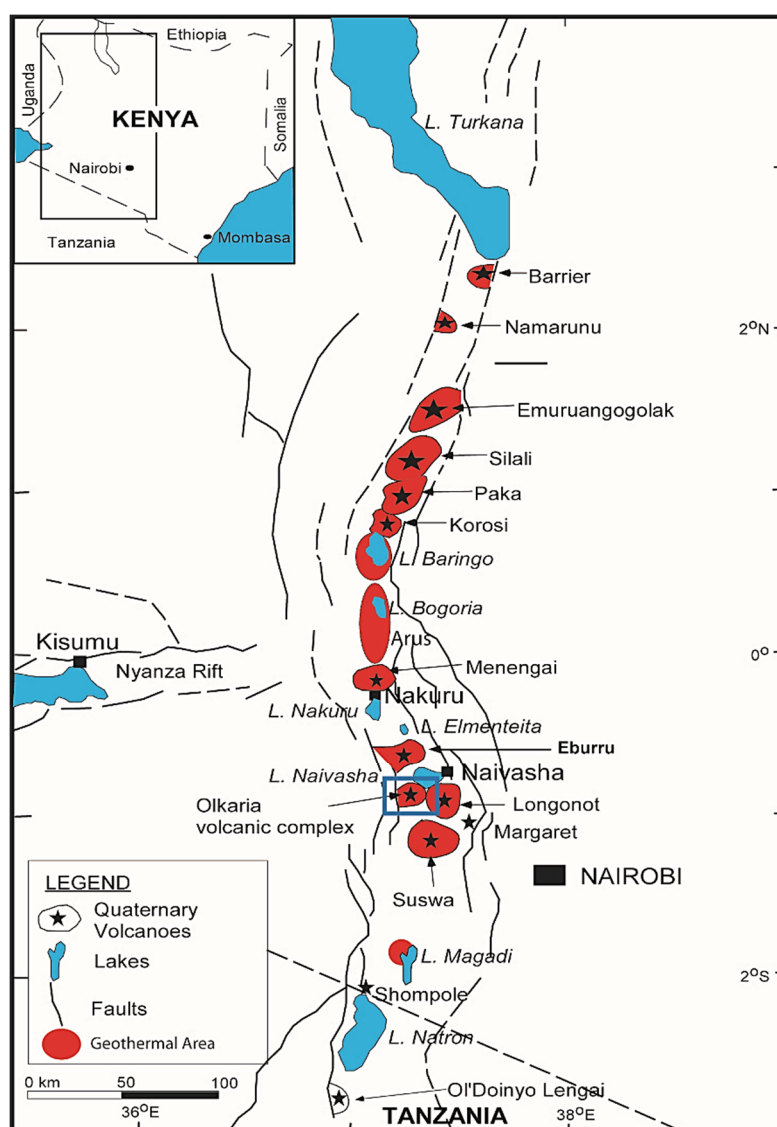


FIGURE 1: Geothermal prospects in the Kenyan rift (Mwawongo, 2013)

1.1.1 General layout of Olkaria IV geothermal field

The Olkaria IV geothermal field is part of the greater Olkaria geothermal field in Kenya. It covers an area of approximately 25 square kilometres. The field has been developed and Olkaria IV power plant in this field currently produces 140 MWe. The field has a total of 30 wells drilled, 21 of which are production wells, while 7 are hot re-injection wells and two are cold reinjection wells. A total of 4 separator stations are used in the field. Figure 2 shows a schematic diagram of the location of various systems in the Olkaria IV field. The study has used data from this field to test the model.

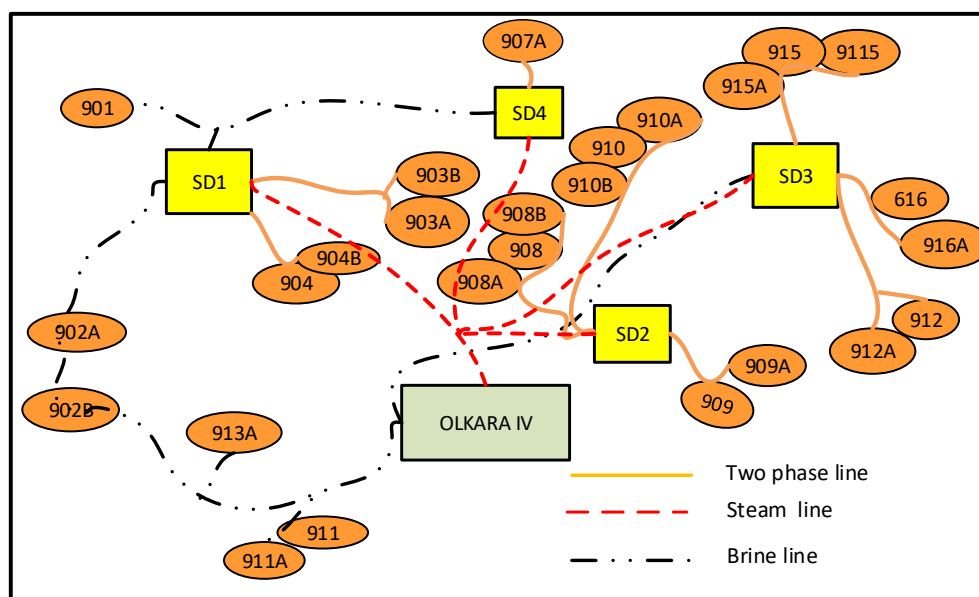


FIGURE 2: Schematic drawing of Olkaria IV geothermal field

1.2 Motivation

Geothermal energy is fast taking a leading role in the generation of electricity in Kenya. In the future plan Vision 2030, the government has set the target of 5000 MWe by the year 2030 out of which over 2000 MWe will come from geothermal energy (GoK, 2014). Among other companies in the energy sector in the country, KenGen has the obligation of generating 700 MWe. The company has generated additional 300 MWe in the last two years (2014-2015) in Olkaria geothermal field and has an ambitious plan for more power production in the same field. In March 2016, wells providing steam for about 280 MWe had already been drilled and more drilling work continues. The steam system forms part of the critical sections of the geothermal power generation, contributing about 10% of the overall cost of geothermal field development (Onyango, 2015). The optimization of pipeline routes, separator and power plant placement is essential for managing the steam gathering system cost. In order to achieve this, a tool is required to guide the company in designing and sizing such systems. Current practice is to propose preliminary routes and separator stations by experienced staff before engaging consultants. This can be subjective depending on individual's judgement. Therefore there is need for a structured way of doing this kind of work, which forms the basis of this study. The objective of the study presented is to develop a decision making tool to be used to optimize pipeline routes, separator and power plant placement. The initial inputs for the model include the digital elevation matrix (DEM), location of wells using global positioning system (GPS), mass output from wells and plant location. In this project the model is tested with data from Olkaria IV geothermal field in Kenya and with improvements it can be used to guide designs and for budgetary planning purposes within Olkaria fields and any other new geothermal fields.

1.3 Objectives of the study

The main objective of this study is to develop a tool for route selection, placement of separators and power plant in order to optimize the steam system. Specifically, the tool will be used for the following:

- I. Define the route of a pipeline using weighted variable topography distance transform (WVTDT) - using Olkaria IV as an example;
- II. Determine the best location for the separators;
- III. Determine the best location of the power plant and compare with the existing location;
- IV. Dimensional design of the pipeline and separators; and
- V. Determine the preliminary cost for the various systems.

1.4 Scope of the study

This study covers development of an optimization tool for pipeline route selection, design and placement of separator stations and location of power plant. Data from Olkaria IV geothermal field in Kenya is used for the case study to analyse and compare results. The steam field system considered in this design is equipped with pipelines connecting eight production wells currently serving separation station (SD2) and a steam pipeline that runs from the separation station (SD2) to the power plant. The separated brine pipeline from the separator station (SD2) to the hot re-injection wells and steam lines from all separators to the optimized plant location are also considered. For the reinjection system, only hot reinjection wells serving SD2 are considered. The works done include selection and optimization of pipeline routes, pipeline and separator design. The cost of the steam system is determined based on Olkaria IV field data presented. Mechanical stress analysis and thermal analysis, while important, are not considered in this report.

2. LITERATURE REVIEW

2.1 Geothermal power plants

In geothermal power production, vapour is required to drive turbines for generating electricity. This vapour is derived directly from naturally occurring vapour which derives its energy from the natural heat of the earth's crust. Geothermal power plants can be broadly categorized into steam power plants mostly located in fields with high enthalpies and binary plants largely found in fields with low enthalpies. High temperature fields with bad chemistry can also be used to feed binary plants. In some areas however, very high temperatures have been found but no fluids are present to transport the heat, instead they have hot dry rocks with very high temperatures. In such areas, the rocks can be fractured and fluids are pumped down to pick up the heat and then pumped up again. These systems are referred to as enhanced geothermal systems and have not been widely developed.

Steam power plants can further be grouped into *direct steam plants* and *flash steam plants* and they can be single flash, double flash or triple flash systems. Dry (direct) steam power plants are built in vapour dominated reservoirs which are characterized by dry saturated or superheated steam. The pressures are constant and above atmospheric, largely controlled by the predominantly continuous steam phase.

In the flash power plants steam is separated from two-phase geothermal fluid in one or several separators depending on the type of plant. Fluids in single flash plants undergo a separation process after which the separated steam is sent to the turbine while the separated brine is directed to a reinjection well. In the double flash cycle systems on the other hand, there is high pressure and low pressure separation. Generally, flash power plants are similar to fossil fuel power plants except for the characteristic that

steam is at saturated state when entering the turbine. Fossil plants may have superheated steam up to temperatures imposed by turbine blades material limits (Nag, 2008).

Binary cycles are installed for temperatures below 180°C and they make use of a secondary working fluid with a low boiling point in a closed power generation cycle. A heat exchanger is used to transfer heat from the geothermal fluid to the working fluid, and the cooled brine is then rejected to the environment or re-injected. The Organic Rankine Cycle (ORC) is commonly used in binary cycle plants and examples are of use of the Kalina cycle. The decision on which type of plant to build in a particular location is depended on the nature of the resource and its properties. In all the cases, a steam line must be constructed between the well and the plant. The design of the pipelines and separation stations is critical to minimize losses along the line and to ensure high efficiencies.

2.2 Geothermal steam gathering system

The steam gathering system in a geothermal power plant is used for collection and transportation of steam from the well head and delivering it to the turbine inlet in the desired condition. It comprises of the following major components: the well, silencers, steam delivery pipeline and expansion loops, flashers, valves, separator stations, gas ejectors and associated auxiliaries. The pipelines can be single-phase or two-phase fluid pipelines depending on the geofluid conditions and designs in place.

Separator stations can be located near the well head or close to the turbine, both possibilities have their merits and demerits. They can also be separate for each well head or centrally placed to serve a number of well heads combined. The selection of separator pressure is very critical for a power plant. If the well head pressure is low, boiling may occur in the formation around the well, which may lead to scaling within the cracks and thus narrow flow passages in the formation. This will lead to short well life. Higher separation pressure means that better steam is available for the turbine (higher enthalpy), but the amount will be less, dictated by separator energy balance as well as productivity due to higher wellhead pressure. This may also influence the separation of non-condensable gases from the geothermal fluid (Valdimarsson, 2010).

Therefore, the selection of the separator pressure is an optimization process. According to DiPippo (2007) the best choice will be determined by the economics taking into account site-specific conditions including temperature, pressure and chemical nature of geofluid, well distribution (both production and reinjection wells) relative to the powerhouse location, topography of the site, and method of fluid disposal, including any required scale control technique. Generally, the efficiency of the entire gathering system will be determined by careful placement and design of all parts.

2.3 Geothermal steam system optimization

Steam system optimization implies the selection of steam routes and placement of separator stations and auxiliary equipment to ensure delivery of steam in the right quality to the turbine with minimal pressure drop and cost of the system. The shortest route usually should be the cheapest. However, large diameters and other constraints along the route may make the route expensive or not practical. The optimal route therefore takes into consideration all the constraints in the field like technical issues, environmental or even administrative restrictions. Different approaches have been developed for route selection and optimization for different applications like transportation routes. De Smith (2004) shows that Distance Transforms (DTs) can be modified and used to solve optimization problems involving location theory, path determination, planning and decision support. Distance transforms can be combined and weighted to generate alternatives which can be used to solve problems in spatial decision making. These weighted distance transforms are referred to as multiple weighted distance transforms (MWDT). Another modification is the variable topography distance transforms (VTDTs) which allows determination of shortest paths across physical landscapes. This can be used to optimize the route

selection and placement of separators and power plants. The third extension to distance transforms introduces cost dimension. Under certain circumstances, shorter routes may be more expensive. Also the route may cause a longer travelling time to reach a point of interest due to certain challenges. To address this problem distance transforms can be modified to capture such interests and are referred to as least cost distance transforms (LCDT).

2.3.1 Separator and power plant placement

The location of a separator is always a very challenging exercise for steam field designers. The argument is whether to locate satellite separators close to well heads with longer steam pipelines running to power stations or have them centralized for many wells and close to the power station. Many authors have researched and written about this subject. Satellite separators located close to well heads will result in good scrubbing of solid minerals from separator carry over as well as good moisture removal of condensates through drain pots along the long pipeline (Lee, 1982). It will also reduce the need for using large scrubbers and steam demisters or vortex separators (Lee, 1995) near the power stations. On the other hand, centralized separators located close to the power station will result in shorter steam pipelines to the power station that are easy to control, have lower pressure drop and are cheaper. However, it is necessary to have large scrubbers and demisters near the power stations to improve the purity and quality of the steam entering the turbine. Entry of steam condensate to the turbine can also be minimized by having the power station at higher elevation than the steam field. According to Watson et al. (1996), separator location should be chosen in a way that it prevents flashing in the separated water (brine) pipelines.

The location of a separator needs to balance all the conditions and is an optimization problem. From experience in the Olkaria field (author's experience), optimal separator location tends to be central one where a separator can handle a group of wells from either the same pad or from different pads. For this study, the optimal separator location is obtained using weighted distances in the VTDT algorithm. Topology considerations and design restrictions are also considered. In the event of individual wells which are found to be inappropriately situated from the optimal location, consideration should be made for placement of individual separator in an appropriate location.

Power plant placement is done taking into account separator stations, the environmental issues, accessibility and operational issues. It is important for instance to locate the power plant in such a way that entry of steam condensate to the turbine is avoided. This may be achieved by locating the plant in higher elevation compared to supply steam lines from separator stations. In the distance transform algorithm, this is achieved by imposing a gradient constraint between delivery lines and desired location.

2.4 Cost issues in geothermal steam system

The cost of geothermal steam system development consisting of piping costs and separator costs is a critical component of the overall cost of geothermal projects. Several estimates have been put forward to quantify the actual value with regard to the total cost of the project. Oyango (2015) reports that the steam gathering system contributes about 10% of the overall cost of the geothermal field development. However, the process of cost determination is a highly secretive venture as information required is often held classified by the suppliers for competition reasons.

The main components of cost in a steam system are piping and separator material cost, installation cost, cost of fittings, welding costs, bends and bend installation cost. The cost of access roads and civil works can be treated separately under infrastructure costs. The piping installation cost is made up of material (30%), fittings (10%), installation labour (25%), installation equipment (10%), supports (15%) and P&G (10%). The total cost can vary from US\$ 600 to US\$ 1200 per meter, depending on pipe diameter, slope of the terrain, cross-country or well pad piping (Henriquez and Aguirre, 2011).

In this report, the piping and separator material cost is evaluated as it forms the bulk of the steam system cost. Depending on the temperature of the fluid both metallic and non-metallic piping can be used in geothermal application. Steel is the most widely used material due to its ability to handle high temperatures and longer service life. Thus, the cost of steel greatly influences the cost of the pipes. Similarly, the costs for equipment, installation, bending and bend installation and welding increase with increasing pipe nominal diameter (Kalinci et al., 2008).

3. METHODOLOGY

This chapter describes the procedure carried out in this study. It involves determination of optimum location for separator station with respect to production wells, hot reinjection wells and the power plant. The first step is to optimize the location of separator stations and the second step involves optimal placement of the power plant with respect to optimized separator locations. Each optimization step also defines the route and total distance of the route. The study employs the use of distance transforms to determine the path to the proposed optimal locations, specifically a modified form of distance transform, which involves weighting of variable topography distance transform (VTDT) to become weighted variable topography distance transform (WVTDT).

3.1 Distance transforms (DTs)

The central function in the distance transform algorithm is given by the Bellman's Equation 1 expressed as (de Smith, 2004):

$$d_{i,j} = \min(d_{i+m,j+n} + c_{m,n}, d_{i,j}) \quad (1)$$

where $d_{i,j}$ is the value of the distance matrix at the central point of the chamfer mask, $d_{i+m,j+n}$ is the value of the distance matrix at the same location from the central point as $c_{m,n}$ is placed in the chamfer matrix. The algorithm involved is in the order of Mn^2 computations where n is the maximum dimension of the lattice, and M is the number of cells used in the neighbourhood computation.

In the above distance transform algorithm, the objective function works with a two-pass scan (forward and backward) of a square or rectangular lattice data set. Each pass involves adding values in a divide form of the adjacency matrix or mask to cell in the underlying lattice as shown in Figure 3. The value in mask position of the transformed lattice is then set to the minimum of the calculated sums.

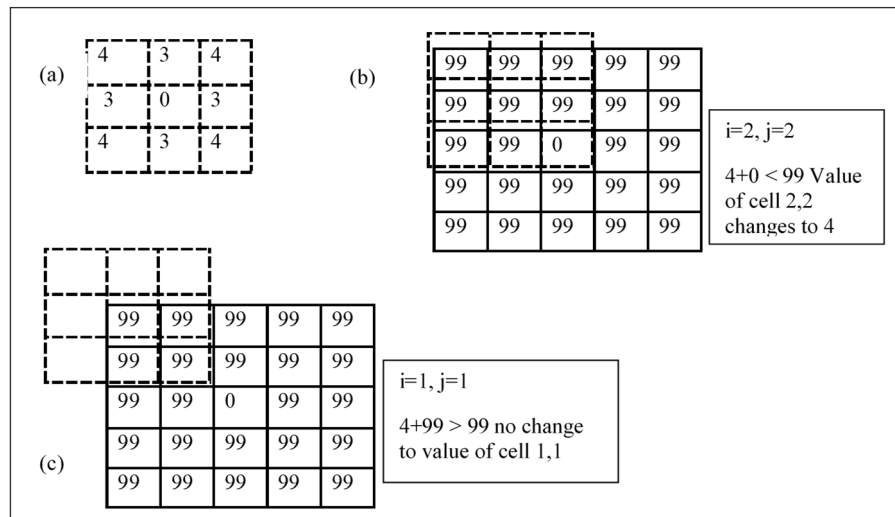


FIGURE 3: (a) 3 x 3 integer chamfer masks for distance transformation; (b) and (c) are forward scans (Jónsson, 2016a)

3.1.1 Variable topography distance transform (VTDT)

The variable topography distance transform (VTDT) works with the digital elevation matrix (DEM). Basically, DEM is a digital representation of real-world ground topography where the rectangular lattice

of points or cells has allocated elevation values. VTDT is a chamfer distance metric with each point having latitude, longitude and altitude (height) values assigned. In this case therefore, the chamfer matrix and distance transform is extended to a 3D model. The value in the cell represents the elevation value at that particular point, hence, given two points the gradient can be evaluated. In route selection therefore, the gradient phenomenon is added to the distance transform algorithm as a constraint. The resultant function is a modified function incorporating the gradient given by Equation 2:

$$\begin{aligned} & \text{if } \{([d_{i+m,j+n} + c_{m,n}] < d_{i,j}) \text{ and } (|S| < Smax)\} \\ & \text{then } d_{i+m,j+n} + c_{m,n} \end{aligned} \quad (2)$$

where maximum allowable slope, ($Smax$), is the constraint value and slope (S) is the magnitude of the path gradient.

This function is referred to as the gradient constrained transform (GCDT) and can be applied to other target points or lines like existing roads for exclusion in the route design. Solving the equation by iteration of the GCDT scanning algorithm results in optimal paths selected with small differences in the total surface path length. However, by modification of the maximum gradient constraint over a range of values above or below the target, it is possible to determine a series of solution paths with further iterations.

The solutions of the path lengths obtained can further be subjected to a cost constrained. If a generalized cost field is introduced and can be defined over the rows (r) and columns (c) of the lattice as $COST(r, c)$, then the central distance transform function can be modified to incorporate cost as in Equation 3:

$$d_{i,j} = \min (d_{i+m,j+n} + c_{m,n} * [COST(r, c)], d_{i,j}) \quad (3)$$

By evaluating the equation above for every alternative path, one can compare the cost of each path and the optimal path is the one with minimum cost.

3.1.2 Multiple weighted distance transforms (MWDT)

As MWDT involves alternative routes, the general equation involves obtaining a weighted sum z of multiple transforms. If we denote distance transform of type k applied to an object set $\{A_i\}$ as $DT_k\{A_i\}$, then the weighted sum of MWDT can be deduced from Equation 4 as:

$$z = \sum_i w_i DT_k\{A_i\} \quad (4)$$

This is a composite surface or set of values with one or more minima. In this kind of problem, it is possible to find one point that can minimize the sum of the distances as a function of each of the vertices. According to de Smith (2004), MWDT fails to accurately locate the point. The introduction of WVTDT in this project addresses the shortcoming in MWDT.

3.2 Route selection, separator and power plant placement and optimization

The aim of route selection is to identify the shortest path that avoids restricted areas like park reserve sites, unnecessary crossing of roads and rivers and excessively steep slopes which would make construction work difficult or push costs up. Generally, this includes consideration of environmental effects and public safety. In this study, variable topography transform (VTDT) is used to find the shortest distance.

A 2-D matrix is used in the DEM model, where every element ($H_{i,j}$) represents the height of allocation on the surface with coordinates (i,j). The slope is then calculated from the altitudes of the cells obtained from the DEM and a maximum gradient constraint (S_{max}) is applied. The normal distance transform equation is modified to Equation 5:

$$S = \frac{(H_{i+m,j+n} - H_{i,j})}{c_{m,n}} \quad (5)$$

Hence if the slope is S and maximum allowable slope is S_{max} , then:

$$\begin{aligned} & \text{if}(d_{i+m,j+n} + c_{m,n} < d_{i,j} \text{ and } S < S_{max}); \\ & \text{then } d_{i,j} = d_{i+m,j+n} + c_{m,n} \end{aligned} \quad (6)$$

If Equation 6 returns untrue, no route can lie between the two cells in question. The equation therefore ensures that the gradient of the “shortest route” is within the desired value, whereby the gradient constraint is implemented in the condition in Equation 7 and 8:

$$\begin{aligned} & \text{If } (H_{i+m,j+n} - H_{i,j} < \Delta H_c \text{ and } S_{i+m,j+n} < S_c) \\ & \text{then } d_{i,j} = \min(d_{i+m,j+n} + c_{m,n}, d_{ij}); \text{ else } d_{i,j} = d_{i,j} \end{aligned} \quad (7)$$

where $H_{i+m,j+n}$ and $S_{i+m,j+n}$ are height and slope respectively, both calculated from the altitudes of the particular cells from the DEM. The constraints, critical height ΔH_c and critical slope S_c , are user defined.

The way to define the critical values was proposed by Kristinsson (2005), where the altitude values of the cells representing constraints are set to either Not a Number (NaN) or a very high number. In this case, the excessively high resultant gradients will fail the maximum height test.

3.3 Topology design and pipeline design criteria

The standard pipeline design process involves (Jónsson, 2016b):

1. Topology and route selection;
2. Demand and flow analysis;
3. Pipe diameter optimization (minimum cost due to head loss);
4. Thickness and pressure class design;
5. Thermal stress analysis (anchors, expansion loops and expansion units); and
6. Pump sizing and arrangement.

However, this study is limited to pipe diameter optimization and thickness and pressure class designs. The topology design optimizes the distances between the production wells and separator stations and from the separator stations to the re-injection wells and the power plant. This is done by organizing the output from the distance transform in the route selection above into a distance table. Flow in the different pipeline options can be optimized in excel using the Solver ad-in program.

3.4 Pipe diameter optimization

The selection of the correct pipe diameter is very important in hydraulic calculation as this would ensure smooth flow of fluid which can be devoid during pulsing operation of the pipeline. The pipe diameter also has a critical influence on pressure drop in the pipeline together with other parameters like bends or irregularities in the pipe layout. It is also necessary to have pipe thicknesses of the right structural

strength that can withstand pressure as well as other external loads like wind and earthquakes. The main optimization goal is to minimize cost and reach acceptable pressure drop along the pipeline. Optimization of pipe diameters for brine flow, steam flow and two-phase flow is done separately due to different conditions in the different fluid pipelines. The process is done by considering single-phase flows first, then the two-phase flow.

3.5 Single-phase pressure drop

This is where the fluid in the pipe is in one phase, either liquid or steam. In this study the brine leaving the separator to the turbine is saturated. Similarly, the brine coming from the turbine for reinjection is saturated. Generally, the primary variables in single-phase flow are velocity, pressure, enthalpy and density.

Single-phase pressure drop is calculated from the Darcy-Weisbach Equation (Equation 8). The two main controlling pressure drops are the frictional and static pressure drops. Friction pressure loss is influenced by fluid velocity, pipe internal diameter, pipe roughness and Reynolds number while the static loss is basically the difference in elevation between the start and end of the pipe.

$$\frac{dp}{L} = f \frac{\rho v^2}{2D_i} \quad (8)$$

where dp is the pressure drop (Pa), L the length of pipe (m), f the friction factor, ρ fluid density (kg/m^3), v flow velocity (m/s) and D_i the internal pipe diameter (m).

The pressure drop can also be rewritten in terms of head loss (dh) given by Equations 9 and 10:

$$dp = \rho g dh \quad (9)$$

Hence,

$$\frac{dh}{L} = f \frac{v^2}{2gD_i} \quad (10)$$

The Reynolds number Re is then calculated using Equation 11 below:

$$Re = \frac{\rho v D_i}{\mu} \quad (11)$$

where μ is the dynamic viscosity of the fluid in SI units (Pa s).

The Colebrook-White equation (approximated in Equation 12) is then used to calculate the friction factor, f :

$$f = \frac{0.25}{\left(\log_{10} \left(\frac{\epsilon}{3.7 D_i} + \frac{5.74}{Re^{0.5}} \right) \right)^2} \quad (12)$$

where ϵ is the pipe roughness. The Moody diagram can also be used to approximate the friction factor.

3.6 Two-phase flow pressure drop models

Two-phase flow involves flow of both steam and water in the same pipe at same time. However, in geothermal fluid flow, there exist non-condensable gases in the mix but this is usually a very small proportion of the total flow hence disregarded in calculations. Two-phase flows can be classified into

different flow regimes using flow regime maps. Some regimes like slug and plug are not desirable as they often lead to damage of pipelines resulting in high maintenance costs. The selection of optimum diameter for a two-phase flow pipe aims to avoid such regimes. Two critical parameters involved are reasonable pressure drop and maximum steam velocity which is recommended to be at a range of 25 to 40 m/s. Generally, a smaller diameter is preferred due to cost but pressure drop must be within acceptable limits.

There exist many models that have been used to predict the pressure drop in two-phase flow. In broad terms they are commonly classified as homogenous flow models and separated flow models (Pálsson et al., 2006).

3.6.1 Pressure drop in homogenous flow model

In homogeneous flow, the two phases are treated as a single fluid, with the two phases uniformly distributed over the flow cross-section area with the same flow direction and velocity. The thermodynamic and hydrodynamic properties can therefore be assumed to be defined by the mean values of properties of the two phases. The homogeneous void fraction derived from averaging the properties of the two phases is used. The void fraction is the term used for the ratio of area occupied by the steam to the pipe cross-sectional area. The total pressure drop in a homogeneous flow model is given by the sum of static pressure drop (elevation head), momentum pressure drop (acceleration), and frictional pressure drop (h_f). The homogeneous flow void fraction (α), which is given by Equation 13, can be used to estimate the cross-sectional areas occupied by the gas and the liquid phases:

$$\alpha = \frac{1}{1 + \left(\frac{1-x}{x}\right) * \frac{\rho_g}{\rho_l}} \quad (13)$$

The other critical parameters in the estimation of friction pressure drop, $dp_{friction}$, are two-phase viscosity, homogeneous density, homogenous Reynolds number and two-phase friction factor which are calculated using the respective equations below. Two-phase viscosity is calculated by Equation 14:

$$\mu_{tp} = x\mu_g + (1-x)\mu_l \quad (14)$$

where x is the quality (the gas mass flow fraction).

Homogenous Reynolds number and homogeneous density are given by Equation 15 and 16, respectively:

$$Re = \frac{D_{in} * \dot{m}_{total}}{\mu_{tp}} \quad (15)$$

$$\rho_{tp} = \alpha\rho_g + (1-\alpha)\rho_l \quad (16)$$

where α is the area averaged local void fraction of the gas, ρ_g and ρ_l are the densities of the gas and the liquid.

Two-phase friction factor for homogenous flow is given by Equation 17:

$$f = \frac{0.079}{Re^{0.25}} \quad (17)$$

Hence, the homogenous friction pressure drop can be calculated by optimizing the inner pipe diameter by restricting the velocity of the two phases to 40 m/s. Equation 18 thus applies:

$$\Delta p_{friction} = \frac{2f\dot{m}_{total}^2}{d_{in}\rho_{tp}} \quad (18)$$

The momentum pressure gradient per unit length for homogenous flow is given by Equation 19:

$$\left(\frac{dp}{dz}\right)_{\text{momentum}} = d \frac{\left(\frac{\dot{m}_{\text{total}}}{\rho_{tp}}\right)}{dz} \quad (19)$$

The static pressure drop is given by Equation 20:

$$\Delta p_{\text{static}} = \rho_{tp} g \Delta H \quad (20)$$

The total two-phase pressure drop for homogenous model in this study considered the static and friction pressure drop calculated from Equation 21:

$$\Delta p_{\text{total}} = \Delta p_{\text{static}} + \Delta p_{\text{friction}} \quad (21)$$

3.6.2 Pressure drop in separated flow models

Separated flow models assume that the gas and the liquid phases flow separately with distinct mean properties for each phase. Interactions within the phases, between the phases, and between phases and channel walls are evaluated separately in order to find a suitable correlation for predicting pressure drop.

Separated flow model mimics two distinct pipelines each carrying the equivalent of a single-phase fluid with each fluid occupying a certain percentage of the cross-sectional area in the pipeline and having distinct mean properties for each phase. To estimate the pressure drop in separated flow, knowledge of the void fraction is a mandatory requirement. The total pressure drop is the sum of four different pressure loss terms for each fluid which are friction, dynamic, acceleration and elevation pressure losses. Correlations describing pressure drop in two-phase flow revolve around two main approaches: conservation of momentum and conservation of energy. Several correlations have been developed for calculating void fraction in separated flows and can be classified as either analytical or empirical models

a) Analytical void fraction models

In this category, the Zivi kinetic energy model for annular flow and the Levi momentum model are mostly used. Zivi derived two models, one for liquid entrainment in gas phase and the other assumes no liquid entrainment in the gas phase. The Levi correlation on the other hand assumes that momentum is exchanged constantly between the two phases as the fluid properties vary and the flow tends to maintain a value which is equal to the sum of frictional and static head losses in each phase. Neither correlation is used in this study.

b) Empirical void fraction models

Several empirical correlations for void fraction exist together with recommendations on how to apply for best results. In this section, some of the most recommended are described.

Harrison (1975) correlation method

This correlation is derived from the analysis of two-phase flow velocity distribution using the Seventh Power Law which is given in Equation 22:

$$\frac{1 - \alpha}{\alpha^{7/8}} = \left[\left(\frac{1 - x}{x} \right) \left(\frac{\rho_g}{\rho_l} \right) \left(\frac{\mu_l}{\mu_g} \right) \right]^{7/8} \quad (22)$$

This method is recommended for large diameter pipes (Zhao et al., 2000). The gaseous-phase volume flow rate \dot{v}_g from the seventh power law is applied to two-phase flow velocity distribution that results in Equation 23:

$$\dot{v}_g = \frac{49}{60} U_g \pi R^2 \alpha \quad (23)$$

where U_g is the gaseous phase centreline velocity.

And the gaseous mass flow rate \dot{m}_g is calculated from Equation 24:

$$\dot{m}_g = \frac{49}{60} \rho_g U_g \pi R^2 \alpha \quad (24)$$

The velocity distribution for the gaseous phase is given by Equation 25:

$$\bar{u} = \bar{u}_{ip} + U_g \left(1 - \frac{r}{\sqrt{\alpha}R}\right)^{\frac{1}{7}} \quad (25)$$

where \bar{u} is velocity at radius r , \bar{u}_{ip} is the interphase velocity, U_g is the gaseous-phase centre velocity and R is the pipe radius.

Similarly for the liquid phase, the seventh power law yields the following Equations 26 and 27 for liquid volume flow rate (\dot{v}_f) and liquid mass flow rate (\dot{m}_f) respectively:

$$\dot{v}_f = \frac{49}{60} U_f \pi R^2 (1 - \sqrt{\alpha})^{\frac{8}{7}} (1 + \frac{8}{7} \sqrt{\alpha}) \quad (26)$$

$$\dot{m}_f = \rho_f \dot{v}_f \quad (27)$$

Now the average liquid-phase film velocity is calculated from Equation 28:

$$\bar{v}_f = \frac{\dot{v}_f}{A_f} = \frac{49}{60} U_f \frac{(1 - \sqrt{\alpha})^{\frac{8}{7}} (1 + \frac{8}{7} \sqrt{\alpha})}{(1 - \alpha)} \quad (28)$$

while the average velocity of the equivalent single-phase flow is defined by Equation 29:

$$\bar{v}_{eq} = \frac{\int_0^R U_f (1 - \frac{r}{R})^{1/7} 2\pi r dr}{\pi R^2} = \frac{49}{60} U_f \quad (29)$$

Velocity ratio ($\frac{\bar{v}_f}{\bar{v}_{eq}}$) is used in predicting pressure drop and is calculated from Equation 30:

$$\frac{\bar{v}_f}{\bar{v}_{eq}} = \frac{(1 - \sqrt{\alpha})^{\frac{8}{7}} (1 + \frac{8}{7} \sqrt{\alpha})}{(1 - \alpha)} \quad (30)$$

Lockhart Martinelli correlation

The Lockhart-Martinelli correlation makes use of the friction multiplier (also known as two-phase multiplier) approach for predicting two-phase pressure drop. This approach relates the two-phase frictional pressure gradient in terms of frictional multipliers both for gas (ϕ_g^2) and for liquid (ϕ_l^2) which are assumed to flow independently inside the pipe. The two multipliers for gas and liquid are defined in Equations 32 and 33, respectively, as:

$$\phi_g^2 = \frac{\left(\frac{dp}{dz}\right)_{f_{tp}}}{\left(\frac{dp}{dz}\right)_{fg}} \quad (32)$$

$$\phi_l^2 = \frac{\left(\frac{dp}{dz}\right)_{f_{tp}}}{\left(\frac{dp}{dz}\right)_{fl}} \quad (33)$$

where $\left(\frac{dp}{dz}\right)_{ftp}$ is the two-phase pressure gradient and $\left(\frac{dp}{dz}\right)_{fg}$ and $\left(\frac{dp}{dz}\right)_{fl}$ are the pressure gradients for gaseous phase and liquid phase flowing alone in the pipe.

Then Lockhart-Martinelli parameter or pressure drop ratio (X) is defined as given by Equation 33:

$$X^2 = \frac{\left(\frac{dp}{dz}\right)_{fl}}{\left(\frac{dp}{dz}\right)_{fg}} = \left(\frac{1-x}{x}\right)^{1.8} \left(\frac{\rho_g}{\rho_l}\right) \left(\frac{\mu_l}{\mu_g}\right)^{0.2} \quad (33)$$

By relating the two-phase frictional pressure gradient to the gradient for the steam phase, the single-phase pressure drop for steam can be calculated from the standard Equation 34 below:

$$\left(\frac{dp}{dz}\right)_{fg} = f \left(\frac{L}{D}\right) \frac{1}{2} \rho_g V_g^2 \quad (34)$$

Consequently, the two-phase pressure drop can be derived using Equation 35:

$$\left(\frac{dp}{dz}\right)_{fTP} = \phi^2 f \left(\frac{L}{D}\right) \frac{1}{2} \rho_g V_g^2 \quad (35)$$

where dp is the two-phase pressure drop (N/m^2) while ϕ^2 is the two-phase multiplier (dimensionless), f is the friction coefficient, L the effective length, D is the inside diameter of pipe, while ρ_g is the density of steam (kg/m^3) and V_g^2 is the velocity of steam if it was flowing alone in the pipe (m/s).

The velocity of steam can be found from Equation 36:

$$V_g = \frac{4 m x}{\rho_g \pi D^2} \quad (36)$$

Hence, the two-phase pressure drop due to friction can be calculated using Equation 37:

$$\Delta p = \frac{8}{\pi^2} \phi^2 \frac{L f (m x)}{D^5 \rho_g} \quad (37)$$

The friction coefficient f is a function of Reynolds number Re and pipe wall roughness factor is ϵ . The Reynolds number of the steam phase is given by Equation 38:

$$Re_g = \frac{\rho_g V_g D}{\mu_g} \quad (38)$$

where μ_g is the dynamic viscosity for the steam phase (kg/ms). The friction coefficient f for rough pipes is calculated from the Colebrook and White relation (Equation 39).

$$f = 1.74 - 2 \log \left(\frac{2\epsilon}{D} + \frac{18.7}{Re \sqrt{f}} \right) \quad (39)$$

However, for $Re > 4 \cdot 10^4$ the friction factor can be approximated by Equation 13 (Jónsson, 2016b).

Friedel correlation

The Friedel correlation relates the two-phase frictional pressure gradient to the frictional pressure gradient for a single-phase flow at the same total mass velocity but with the physical properties of the liquid phase, namely $\left(\frac{dp}{dz}\right)_{flo}$. In this case, the two-phase frictional multiplier ϕ is defined by Equation 40:

$$\phi_{lo}^2 = \frac{\left(\frac{dp}{dz}\right)_{ftp}}{\left(\frac{dp}{dz}\right)_{flo}} \quad (40)$$

The Friedel correlation for the vertical upward flow and horizontal flow is defined as Equation 41:

$$\phi_{lo}^2 = E + \frac{(3.24FH)}{Fr^{0.045}We^{0.035}} \quad (41)$$

where the Froude number Fr , Weber number We , and parameters H , E and F are defined by Equations 42-46, respectively:

$$Fr = \frac{m^2}{gD\rho_{tp}^2} \quad (42)$$

$$We = \frac{m^2 D}{\rho_{tp} \sigma} \quad (43)$$

$$H = \left(\frac{\rho_l}{\rho_g}\right)^{0.91} \left(\frac{\mu_g}{\mu_l}\right)^{0.19} \left(1 - \frac{\mu_g}{\mu_l}\right)^{0.7} \quad (44)$$

$$E = (1 - x)^2 + x^2 \left(\frac{\rho_l f_{go}}{\rho_g f_{lo}}\right) \quad (45)$$

$$F = x^{0.78}(1 - x)^{0.24} \quad (46)$$

In the above set of equations, μ_l is the dynamic viscosity for liquid measured in kg/ms, σ is the surface tension in N/m while f_{go} and f_{lo} are the friction factors calculated as if the liquid and the gas respectively were flowing alone in the pipe.

For this particular correlation, ρ_{tp} is given by Equation 47:

$$\rho_{tp} = \left[\frac{x}{\rho_g} + \frac{(1 - x)}{\rho_l} \right]^{-1} \quad (47)$$

According to Hewitt (1982), the following recommendations are made for use with the above correlations:

- I. For $\frac{\mu_l}{\mu_g} < 1000$, the Friedel correlation should be used;
- II. For $\frac{\mu_l}{\mu_g} > 1000$, and $m > 100$, the Chisholm correlation (Hewitt, 1982) should be used; and
- III. For $\frac{\mu_l}{\mu_g} > 1000$, and $m < 100$, the Martinelli correlation should be used.

c) Pressure drop in bends

Calculation of pressure drop in bends and fittings is done by using the equivalent length technique. Ouma (1992) reports that increasing the pipe length by 15% can compensate for pressure losses in bends and fittings. Since this study has same pipeline properties as the one in Ouma's case, similar assumption would be made.

3.7 Pipe thickness, pressure class and mechanical stress analysis

3.7.1 Pipe thickness and pressure class

The structural analysis of the pipes takes into consideration the design code ASME B31.1 (ASME, 2007) which outlines the equations for pipe stress analysis. The wall thickness T_m is determined by Equation 48:

$$T_m = \frac{pD_o}{2(SE + Py)} + A \quad (48)$$

where T_m is wall thickness (mm), p is the design pressure (kPa), the pipe outside diameter D_o is given in millimetres, SE is the allowable stress (kPa), y is a constant based on temperature range and steel type and A is the corrosion and erosion allowance. In most geothermal applications y is 0.4 while A is 3 mm.

The operating pressure for individual wells has to be optimized to result in maximum flow. However, when wells in the same fields have different well head pressure, it is difficult to optimize. In this case, the design pressure is set by considering the highest pressure of the wells in question and adding a margin of safety.

3.7.2 Mechanical stress analysis, bending moments and length of supports

According to Henriquez and Aguirre (2011), stress analysis should be carried out for the following load cases in piping design: sustained loads, occasional loads, operational loads and thermal loads. Also bending moments and pipe support designs have to be investigated, this is however not included in the scope of this report

3.8 Separator dimensional design and cost estimation

The separator considered is the vertical cyclone separator which is the most common in the Olkaria field. The separator works more or less as a centrifuge that creates a vortex that pushes the heavier liquid phase to the walls of the vessel while the lighter gaseous phase remains in the middle. The liquid will move down along the walls of the vessel and is collected at the bottom while the lighter steam will move up and will be directed into the centrally placed delivery tube downwards to leave the vessel through the bottom pipe as shown in Figure 4. The critical parameters controlling the size of the separator are separation pressure, flow enthalpy and total mass flow in the separator.

The first step in designing the separator is to determine the terminal velocity v_t as a function of liquid density ρ_l and vapour density ρ_g . Equation 49 below defines this relationship:

$$v_t = K' \left[\frac{\rho_l - \rho_g}{\rho_g} \right]^{1/2} \quad (49)$$

where K' is a constant based on gravity, droplet diameter and drag coefficient of a liquid particle.

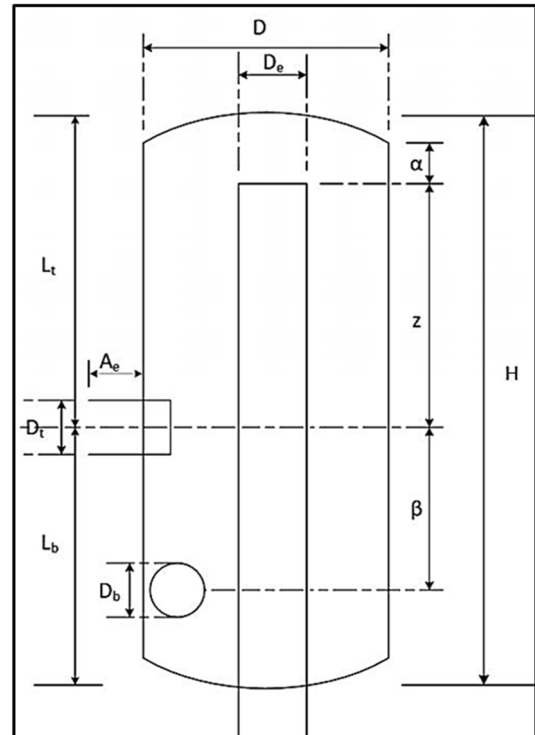


FIGURE 4: Vertical cyclone separator

For most systems, the constant K' ranges between 0.012 and 0.030, however a recommended value of 0.069 m/s is to be used except where special considerations are required (Gerunda, 1981).

The inlet size pipe diameter D_t , is calculated from the relationship given below in Equation 50:

$$D_t = \left[\frac{4A_i}{\pi} \right]^{1/2} \quad (50)$$

where A_i is the cross-sectional area of inlet pipe expressed in terms of volumetric steam flow.

Q_{vg} , is given in Equation 51:

$$A_i = \frac{Q_{vg}}{v_t} \quad (51)$$

The general guidelines recommended for cyclone separator design are summarised in Table 1 (DiPippo, 2007).

TABLE 1: Cyclone separator design guideline (DiPippo, 2007)

Parameter	Separator speed
Maximum steam velocity at 2-phase inlet pipe	45 m/s
Recommended range of steam velocity at 2-phase inlet pipe	25 - 40 m/s
Maximum upward steam velocity inside separator	4.5 m/s
Recommended range of upward annular steam velocity inside cyclone separator	2.5 - 4.0 m/s

Several studies have been done on separator dimensions determination. In this study approaches by Bangma (1961) and Lazalde-Crabtree (1984), together with the spiral inlet guidelines for separator sizing proposed by Purnanto et al. (2012), as shown in Table 2 below, will be considered. All three approaches determine the various dimensions of the separator as a function of separator inlet pipe diameter.

The thickness of the separator will be determined in the same way as pipe wall thickness to satisfy the condition that it should be sufficient to withstand the pressure of the separator in working condition. The pipe thickness (Equation 48) as per ASME shall apply. The performance of the separator is measured by comparing the proportion of brine to the mass flow rate of water entering the separator. This ratio gives the separator efficiency. Field experience with operation of separators indicates that 100% efficiency is not practical. Typical separator efficiencies of between 99.5% and 99.9% have been reported by some studies (Onyango, 2015). However, efficiency measurement is out of the scope of this report.

TABLE 2: Vertical separator design guidelines
(Purnanto et al., 2012)

Parameter	Bangma design	Lazalde-Crabtree design	Spiral-inlet design
D	$3D_t$	$3.3D_t$	$2.95D_t$
D_e	$0.8D_t$	$1D_t$	$1D_t$
D_b	$1D_t$	$1D_t$	$0.7D_t$
α	$3.25D_t$	$0.15D_t$	$0.28D_t$
β	$3D_t$	$3.5D_t$	$3.2D_t$
Z	$3D_t$	$5.5D_t$	$5.8D_t$
L_T	$7D_t$	$6.475D_t$	$6.8D_t$
L_B	$4.5D_t$	$4.975D_t$	$4.9D_t$

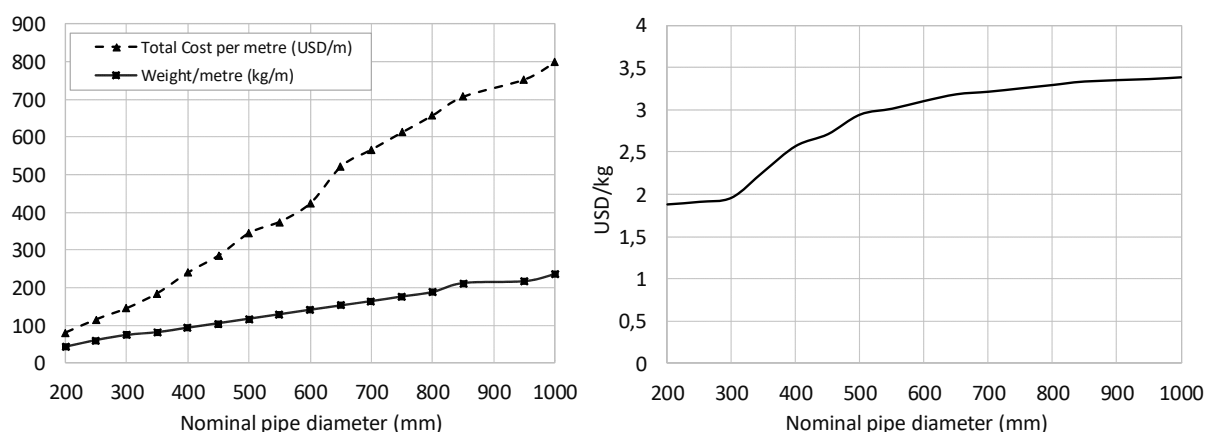


FIGURE 5: Graphs of a) Nominal pipe diameter vs cost per metre and weight per metre; and b) Nominal pipe diameter vs cost per kilogram

3.8.1 Cost estimation

Pipes are manufactured in different grades and schedules depending on the application, and prices will therefore vary from one grade to another and between schedules and diameter sizes. Separators on the other hand are non-standard equipment which are produced according to the client requirements and application. A good way of estimating a generalized initial cost of such equipment will be to find the total weight of material required to make the equipment and then determine cost of material per unit weight. This procedure is used in this study. The cost values used are derived from cost variation values presented by Kalinci et al. (2008) and summarized in Table 3 below. Using Excel, the values are interpolated to cover pipe diameters not included in Kalinci's report.

TABLE 3: Values of different cost elements for different nominal pipe diameter (Kalinci, 2008)

Nominal pipe diameter	Total cost per metre (USD/m)	Pipe installation cost (USD/m)	Pipe bend cost (USD/bend)	Bend installation cost (USD/m)
0.20	50	30	150	25
0.25	70	45	300	50
0.30	90	55	450	100
0.35	115	79	700	225
0.40	150	90	950	275
0.45	175	110	1350	375
0.50	215	130	1750	403

A graph of nominal diameter as a function of each of the cost elements and the total pipe cost is illustrated in Figure 5. The cost of pipe per unit weight for each pipe nominal diameter can be evaluated. The values for the data provided in the report by Kalinci et al. (2008) and after interpolation is presented in Table 4 below.

The cost of steel material per metre is evaluated by comparing total cost per metre from Kalinci (2008) data and the pipe chart from Tiago pipe supplies (Tioga, 2014), which is given in Appendix I per metre of steel pipe for different pipe diameters.

TABLE 4: Variation of pipe cost per kilogram with nominal diameter

Nominal pipe diameter (mm)	Total cost per length (USD/m)	Weight per length (kg/m)	Cost per weight (USD/kg)
0.20	80.0	42.5	1.88
0.25	115.0	60.29	1.91
0.30	145.0	73.86	1.96
0.35	185.0	81.33	2.27
0.40	240.0	93.27	2.57
0.45	285.0	105.17	2.71
0.50	345.0	117.15	2.94
0.55	374.9	129.14	3.01
0.60	424.4	141.12	3.10
0.65	522.1	152.88	3.18
0.70	567.0	164.40	3.21
0.75	613.1	176.68	3.25
0.80	658.1	188.83	3.29
0.85	707.7	212.57	3.33
0.95	753.6	217.57	3.36
1.00	799.4	236.62	3.38

4. RESULTS AND DISCUSSIONS - CASE STUDY OLKARIA IV FIELD

4.1 Field data

Appendix II shows some properties of the wells in the Olkaria IV field serving separator SD2 while Table 5 contains details of all four separators in the field.

TABLE 5: Olkaria IV field separators data

Separator	Northing (m)	Easting (m)	Elevation (m)	Separator capacity (MW)	Steam flow (kg/s)
SD1	202340	9899980	1985	24.2	36.4
SD2	203160	9900630	1960.4	8.0	134.7
SD3	203650	9898900	2010	74.0	124.2
SD4	204510	9899170	2029	67.7	12.5

In the current status, separator station SD2 has three separators SD2A, SD2B and SD2C. The test data for wells serving each separator are presented in Table 6.

Some observations and assumptions made in the process of this study include:

1. The well parameters are used as per results of well test data and separation pressure is predetermined.
2. Separation pressures for all separators are predetermined as 12 bars.
3. For separator placement exercise, only separator SD2 will be considered for optimization illustration and new coordinates obtained. An assumption is made for the remaining three, current locations are used as optimized locations.
4. Power plant placement will be done taking into account all the separators. In this case, distances from production and reinjection wells have been taken care of during separator placement. The cold reinjection wells are not considered since they are made of low budget plastic (HDPE) making its cost negligible compared to the price of steel piping for the other pipelines.

TABLE 6: Olkaria IV SD2 separator station well test data

Separator	Wells	Well head pressure	Separator pressure	Two-phase mass flow (t/h)	Enthalpy (kJ/kg)	Steam flow (t/h)	Steam flow (kg/s)	Brine flow- (t/h)	Power (MWe)
SD2A	908	14.9	12	30	2200	21.2	5.9	8.8	4.0
	908A	17.5	12	115	14200	36.1	10.0	78.9	6.0
	908B	14.7	12	87	2050	54.9	15.3	32.1	8.8
	910	18.3	12	60	1950	34.8 (147)	9.7	25.2 (145)	4.6
SD2B	910A	18.1	12	110	2250	80.5	22.4	29.5	13.0
	910B	18.6	12	210	2000	127.3 (207.8)	35.4	82.7 (112.2)	14.9
SD2C	909	12.9	12	130	2000	78.8	15.3	51.2	12.5
	909A	12.4	12	100	1820	51.5 (130.3)		48.5 (99.7)	10.2
Total				842		485	134.7	357	74.0
Average			12		1941				

5. The steel prices used are estimates from previous studies and not actual prices.
6. SI units are used in all calculations.
7. For the pipeline cost, only the cost of material and installation are considered.
8. Upward flow for the two-phase flow is restricted to a specified slope for each case.

4.2 Route selection and separator SD2 placement

In this study, coordinates of the point that is optimized (separator location) is treated as a sample point identified as separators, while the well coordinates are defined as endpoints.

This is a two-step process. The first step is to find the best place to locate the separator with respect to all production wells leading to it, all hot reinjection wells from the separator and the power plant. The reference point of interest (separator) is a sample (S) point while all wells (production and hot reinjection) and power plant are endpoints (E). The coordinates of the sample and end points are inputs to the VTDISTRA program. The constraints included are maximum height difference, maximum slope

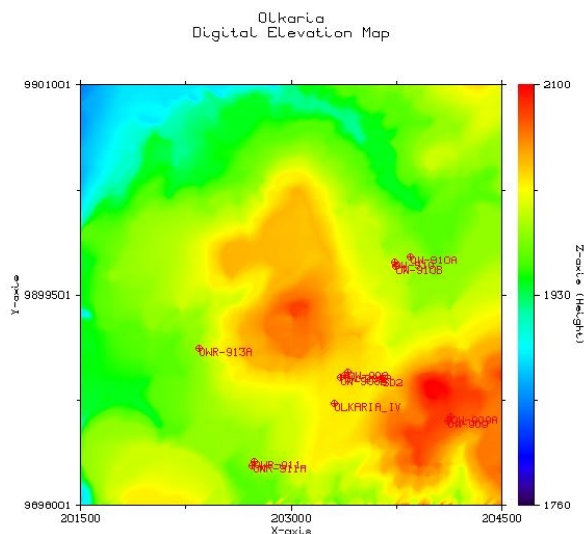


FIGURE 6: Olkaria IV distance map

and route weight as indicated in sample input file (Appendix III). The output results of the program include a digital elevation map (Figure 6), distance maps and weighted distance maps of the area in question showing positions of all input points and relative distances from the initial location of the separator. The routes and distances from each end point to the current location of the separator is shown in the maps and the best location of the separator is given. An output file shown in Appendix IV also captures the coordinates of the optimized separator location, total distance to each end point and coordinates of the route sampled with one metre intervals.

The second step utilises the new optimized separator coordinates as sample point and a second run gives optimized distances of all end points to the optimized location of the separator. Depending

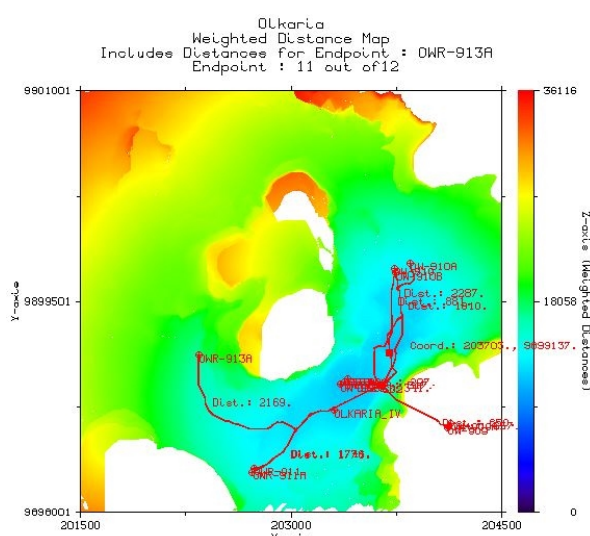


FIGURE 7: Distance map with new SD2 coordinates and distances to all routes

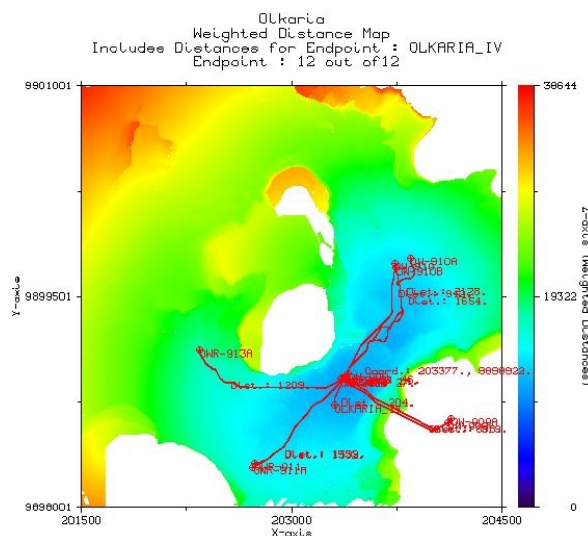


FIGURE 8: Olkaria IV distance map with modified route to OW913A, new SD2 coordinates and distances to all routes

on the number of separators in the field, the same procedure is repeated for all separators. An optimized location to place each separator is obtained and the route to each production, hot reinjection well and to the power plant is defined (Figure 7).

The digital maps generated as output are very interactive and allow one to make a decision whether there is still room for further optimization or not. As Figure 7 shows, the route to OW-913A can be further improved as indicated by the available blue coloured region in the weighted distance map. The route could still be optimized by allowing a little more slope difference and the results change as shown in Figure 8.

The final optimized routes and the location of power plant is achieved and results recorded in an output file. Table 7 summarizes the results. From the results it is clear that using this approach to locate the

TABLE 7: Results for pipeline route selection and separator location optimization

Wells/power plant	Distance from initial location separator - SD2 (m)	Distance from optimized location separator - SD2 (m)
908	297.40	45.76
908A	316.69	13.52
908B	341.11	26.82
909	649.90	897.92
909A	656.90	919.37
910	881.15	942.43
910A	2286.64	2127.65
910B	1810.46	1654.46
911	1743.72	1499.28
911A	1776.40	1531.96
913A	2168.85	1924.40
OLKARIA_IV	400.56	203.53
Total length	13329.78	11787.1
New optimized separator SD2 location coordinates		
Easting (X)	Northing (Y)	Elevation (m a.s.l.)
203375.00	9898916.00	2024.57

power plant leads to a reduction of pipeline length to 11,787.1 m compared to the initial length of 13,329.8 m. This result, while being correct, may not be entirely true as other parameters which were not considered in this optimization may have led to the current route being an option. However, given all constraints, this optimization approach could give accurate results.

4.3 Power plant placement and optimization

The inputs in this step take into account only the optimized coordinates of all separators as end points. The initial plant location then becomes the sample point. The necessary slope, height and weight constraints are then defined in the VTDISTRA. The input to the program is configured to accept plant given name as sample point without starting with initials, S_Name of plant as shown in Appendix III. The output is a weighted distance map (Figure 9) and weighted distance maps from each end point to

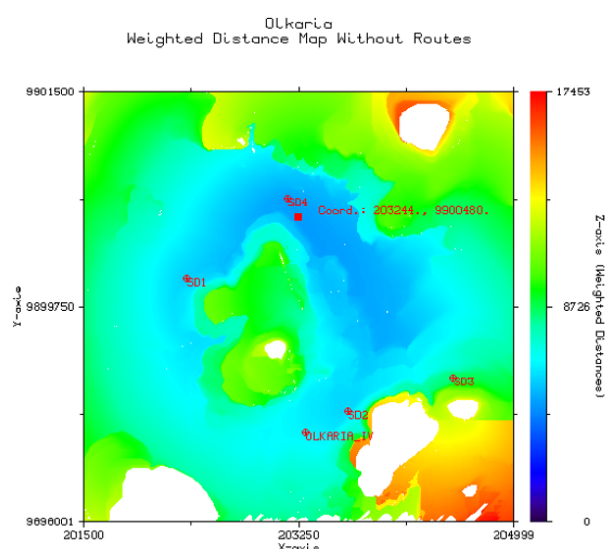


FIGURE 9: Olkaria 4 weighted distance map with optimized separators and current plant locations

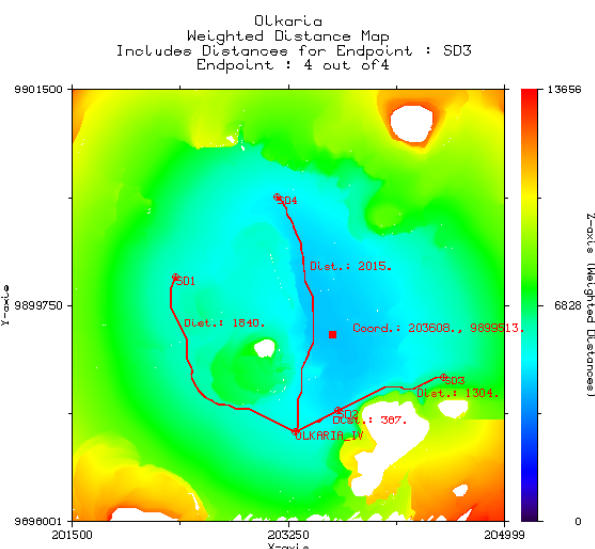


FIGURE 10: Olkaria 4 weighted distance map with routes to all separators and new coordinates for plant location

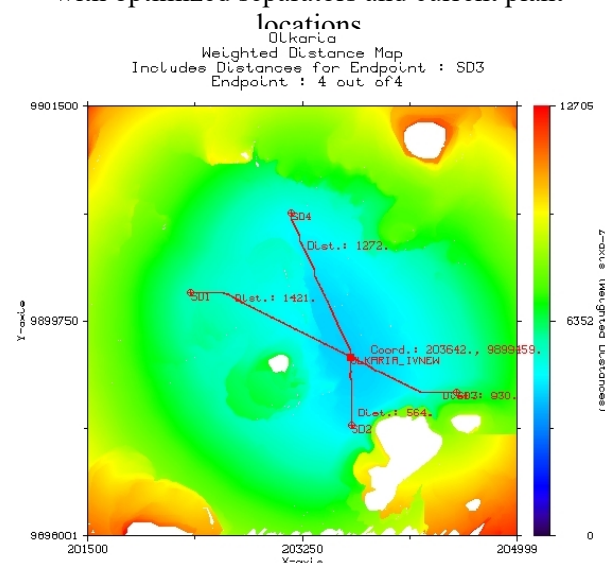


FIGURE 11: Olkaria 4 weighted distance map with routes to all separators and new coordinates for plant location

the sample point complete with routes and their distances. New optimized coordinates for the plant and distances to separators are displayed in the weighted distance map shown in Figure 10. Now using the new plant coordinates as the sample point and separator station coordinates as endpoints, VTDISTRA is run again to obtain the routes and distances to each of the endpoints. The output is captured in form of distance maps, weighted distance maps and an output file which captures the power plant optimized location coordinates and those of all routes sampled with one metre intervals. The new distances from each separator to the optimized power plant location and the coordinates for the optimized location are presented in Table 8. Figure 11 illustrates the graphical outcome of the plant location optimization.

TABLE 8: Results for power plant location optimization

Separators	Run 1 (m)	Run 2 (m)	Run 3 (m)	Run 4 (m)	Run 5 (m)
SD1	2681.67	2681.67	1840.00	1704.00	1420.92
SD2	386.74	386.74	386.74	386.74	563.55
SD3	No route	1303.00	1304.00	1296.00	929.51
SD4	4463.00	2014.95	2015.00	1923.00	1271.67
TOTAL		6386.36	5545.74	5310.00	4185.65
New optimized power plant coordinates					
Easting (X)		Northing (Y)		Height (m a.s.l.)	
203642.00		9899459.00		2008.72	

4.4 Separator and pipeline dimensional design and cost estimation

4.4.1 Separator dimensions

Separator dimensions are designed using the guidelines by Purnanto et al. (2012). The recommended velocity is selected as 40 m/s and results recorded are listed in Table 9.

Using the results from Spiral-inlet design formulas in Table 9, the separator thickness was evaluated. An attempt was made to calculate the separator thickness as if it was one unit and also a design for three separators was considered individually. Each possible layout of well combination serving each separator was followed and the cost of each separator was estimated. The results are presented in Table 10.

The full design results are found in Appendix V (a-d) together with separator design worksheets which show all parameters calculated including diameters and thicknesses.

TABLE 9: Results for separator design

Parameter	Bangma design	Lazalde-Crabtree design	Spiral-inlet design
D	2.90	3.19	2.8
D _e	0.77	0.97	1.00
D _b	0.97	0.97	0.70
α	3.14	0.14	0.3
β	2.90	3.38	3.10
Z	2.90	5.31	5.60
L _T	6.76	6.25	2.00
L _B	4.35	4.80	4.70

TABLE 10: Results for separator thickness and cost estimation

Separator unit	No. of wells	Steam mass flow rate (kg/s)	Thickness T (mm)	Weight (kg)	Cost (USD)
SD2 (1 unit)	8	134.70	23	3566	12056
SD2A	4	40.83	7	548	1609
SD2B	2	57.72	16	2063	6209
SD2C	2	36.19	13	1548	4196

4.4.2 Results of pipeline design, optimization and cost

Pipeline dimensions are calculated separately for single-phase and two-phase flow pipes. Summary design results are presented in Table 11 while the full design results are presented in Appendix VI including a pipeline design worksheet.

TABLE 11: Calculated results of pipelines design and cost estimation

Pipeline	Total length (m)	Diameter D (mm)	Thickness (mm)	Weight (kg)	Cost (USD)
908-SD2A	45.76	200	15.09	3,474	6,531
908A-SD2B	14.00	250	18.26	1,551	2,963
908B-SD2C	26.82	300	31.44	6,082	11,920
909 & 909A-SD2	1654.00	450	29.37	512,752	1,389,558
910-SD2	898.00	250	18.26	103,038	196,802
910A-SD2	919.00	350	23.83	179,278	406,961
910B-SD2	942.00	450	29.37	292,079	791,534
SD2-911&	45.76	100	11.53	1,277	2,400
SD2-911A	46.76	400	30.96	133,323	34,017
SD2-913	47.76	300	21.44	7,638	15,032
SD1-OLK4	1420.90	350	6.35	70,662	160,403
SD2-OLK4	563.55	350	6.35	28,046	63,665
SD3-OLK4	929.51	350	6.35	46,246	10,4979
SD4-OLK4	1271.67	350	6.35	63,253	143,584
					(3,330,349)

5. CONCLUSIONS

A tool for optimizing route selection, separator and power plant placement has been developed. The tool was tested using data from Olkaria geothermal field and the best location of the separator and power plant were obtained together with the optimum pipeline route and total length of each route.

The study proposes a methodology where first the separator location is obtained using coordinates of all production and hot reinjection wells and an initial proposed power plant location. Using VTDT, a new optimized separator location and distance from each well to the plant is obtained. This process is repeated for all separators. The second process step involves plant location where only the optimized separator locations and any constrained areas are used as input in the VTDT program. The result is an optimized location of the plant coordinates and distances from the plant to each separator.

The use of WVTDT for route selection, separator and power plant location gives very good results that can be used to optimize steam systems in geothermal projects. The model developed can be modified to include further constraints to achieve a more acceptable or compromised route.

Using data for Olkaria IV geothermal field, the overall pipeline length reduced by 1542 m. This goes a long way in reducing cost of the pipeline. Accurate results can be achieved in any field by first carrying out a study including all the sensitive areas like protected wildlife breeding grounds and migratory routes, existing buildings and excessively harsh terrains which can then be excluded by introducing their coordinates as constraints.

This model and methodology can be useful in designing preliminary pipeline routes and locations for separators and power plants before detailed survey of the area and consideration of constraints is done. This can help in project planning and cost estimation.

While pipeline diameter and thickness were optimized in this study, it is important in a real case to always go an extra mile and calculate other pipeline design parameters like bending moments, length between pipe supports pipeline anchors and expansion loops which were not considered in this study.

ACKNOWLEDGEMENTS

Firstly, I would like to express my sincere gratitude to my project supervisor Professor Magnús Thór Jónsson for the continuous support, patience, and immense knowledge. Your availability and guidance helped me all the time. To my project mate Dan, thank you so much for your assistance.

I thank UNU-GTP and in particular the director, Lúdvík for giving me a chance to pursue this program in Iceland. To all the staff of UNU-GTP and ÍSOR you made me feel at home away from home. I thank my company KenGen, through the Geothermal Development Director, Eng. Abel Rotich for nominating and according me time of duty to study this course.

I would like to thank my colleagues of UNU-GTP 2016 for their wonderful collaboration and special moments shared. You were all always willing to help me. I trust that the contacts and network we have made will last through our future engagements. To the football team thank you so much for your time. To my housemates James and Gideon, the wonderful evenings we chatted, the 'Fiskur' and 'Jakuzi' experience were all moments to reckon. And to our landlord, Jóhann and family, thank you for allowing us to use the facilities in your apartment that made our stay in Sogavegur memorable.

To my dear wife Nelly and my lovely daughter Angela, those evening calls always rejuvenated my spirits and ensured I had a peaceful sleep every day! Thank you for your understanding and encouragement.

Last but not least I thank God for my life and good health and for blessing me with a beautiful family.

REFERENCES

ASME, 2007: *ASME B31.1-2007. Power piping*. The American Society of Mechanical Engineers, New York, NY, United States, 336 pp.

Bangma, P., 1961: The development and performance of a steam – water separator for use on geothermal bores. *Proceedings of the UN Conference on New Sources of Energy, Vol. 2, Geothermal Energy Agenda, item II.A.2*, 60-77.

de Smith, M.J., 2004: Distance transforms as a new tool in spatial analysis, urban planning, and GIS. *Environment and Planning, B: Planning and design*, 31, 85-104.

DiPippo, R., 2007: *Geothermal power plants. Principles, applications, case studies and environmental impact* (2nd ed.). Butterworth Heineman, Elsevier, 493 pp.

Gerunda, A., 1981: How to size liquid-vapour separators. *Chemical Engineering*, 88, 81-84.

GoK, 2014: *10-year power sector expansion plan 2014-2024*. Government of Kenya, report, 68 pp.

Henriquez M., J.L. and Aguirre A., L., 2011: Piping design, the fundamentals. *Paper presented at "Short Course on Geothermal Drilling, Resource Development and Power Plants", organized by UNU-GTP and LaGeo, in Santa Tecla, El Salvador*, 15 pp.

Hewitt, G.F., 1982: Pressure drop. In: Hetsroni, G. (ed.), *Handbook of multiphase systems*. Hemisphere, McGraw Hill, NY, United States, 2.44-2.75.

Kalinci, Y., Hepbasli, A., and Tavman, I., 2008: Determination of optimum pipe diameter along with energetic and exergetic evaluation of geothermal district heating systems: Modeling and application. *Energy and Buildings*, 40, 742–755.

Kristinsson, H., 2005: *Pipe route design using variable topography distance transforms*. University of

Iceland, Reykjavík, Iceland, 28 pp.

Jónsson, M.Th., 2016a: *Mechanical design of geothermal power plants and district heating systems*. UNU-GTP, Iceland, unpublished lecture notes, 79 pp.

Jónsson, M.Th., 2016b: *Design and optimization – distance transforms*. UNU-GTP, Iceland, unpublished lecture notes.

Lazalde-Crabtree, H., 1984: Design approach of steam-water separators and steam dryers for geothermal applications. *Geothermal Resource Council Bulletin, September 1984*, 11-20.

Lee, K.C., 1982: Performance tests of the condensate drain pots at Wairakei. *Proceedings of the Pacific Geothermal Conference, Wairakei, New Zealand*, 123–129.

Lee, K.C., 1995: Performance of a model in-line vortex separator: *Proceedings of the World Geothermal Congress 1995, Florence, Italy*, 2075-2079.

Mannvit, 2012: *Proposed field development plan for Greater Olkaria geothermal field*. Mannvit Consortium – consultancy services for geothermal resource optimisation study of Greater Olkaria geothermal fields, report 8, Kenya Electricity Generating Company Ltd. – KenGen, internal report, 59 pp.

Mwawongo, G.M, 2013: Geothermal mapping using temperature measurements. *Presented at “Short Course VIII on Exploration for Geothermal Resources”, organized by UNU-GTP, GDC and KenGen, at Lake Bogoria and Lake Naivasha, Kenya*, 13 pp.

Nag, P.K., 2008: *Power plant engineering* (3rd ed.). Tata, McGraw Hill, New Delhi, India, 478-539.

Onyango, S.O., 2015: *Design of steam gathering system for Menengai geothermal field, Kenya*. University of Iceland, MSc thesis, UNU-GTP report 1-2015, 71 pp.

Ouma, P.A, 1992: *Steam gathering system for NE-Olkaria geothermal field, Kenya – preliminary design*. United Nations University Geothermal Training Programme, Reykjavík, Iceland, report 9, 46 pp.

Pálsson, H., Bergthórsson E.S., and Pálsson O.P., 2006: Estimation and validation of models of two phase flow from geothermal wells. *Paper presented at 10th International Symposium on District Heating and Cooling, Hanover, Germany*, 11 pp.

Purnanto, M.H., Zarrouk, S.J., and Cater, J.E., 2012: CFD modelling of two-phase flows inside geothermal steam-water separators. *Proceedings of the 34th New Zealand Geothermal Workshop, University of Auckland, Auckland, New Zealand*, 9 pp.

Riaroh, D. and Okoth, W., 1996: The geothermal fields of the Kenya rift. *Tectonophysics*, 236, 117-130.

Tioga Pipe, 2014: *Pipe thicknesses*. Tioga Pipe – pipe supply company, PH, USA, website: www.tiogapipe.com.

Valdimarsson, P., 2010: Production of electricity from a geothermal source. In: *Geothermal Energy*. Macedonian Geothermal Association (MAGA), Skopje, 150-176 pp.

Watson, A., Brodie, A.J., and Lory, P.J., 1996: The process design of steam fields pipeline systems for transient operation from liquid dominated reservoirs. *Proceedings of the 18th New Zealand Geothermal Workshop, Auckland, New Zealand*, 53-58.

Zhao, H., Lee, K., and Freeston, D., 2000: Geothermal two-phase flow in horizontal pipes. *Proceedings of the World Geothermal Congress, 2000, Kyushu-Tohoku, Japan*, 3349-3353.

APPENDIX I: Pipe thicknesses and costs (Tioga, 2014)



Philadelphia Regional Center
2450 Wheatseaf Lane
Philadelphia, PA 19137
O 215-831-0700
F 215-533-1645
E sales@tiogapipe.com

Houston Regional Center
616 FM 1960 W, Suite 700
Houston, TX 77090
O 713-433-2111
F 281-397-0132
E sales@tiogapipe.com

Chattanooga Regional Center
1301 Riverfront Parkway, Suite 108
Chattanooga, TN 37402
O 423-899-3398
F 423-899-9695
E sales@tiogapipe.com

PIPE DIMENSIONS AND WEIGHTS

Available in commercial and nuclear 

U.S./METRIC

NOMINAL PIPE SIZE	OD	SCHEDULE DESIGNATIONS				WALL THICKNESS		WEIGHT			ID	
INCH MM	INCH MM			ASME	INCH	MM	LBS/ FOOT	KG/ METER	INCH	MM		
1/8 6	0.405 10.3	10 STD XS	40 40S	80 80S	0.049	1.24	0.19	0.28	0.307	7.82		
					0.068	1.73	0.24	0.37	0.269	6.84		
					0.095	2.41	0.31	0.47	0.215	5.84		
1/4 8	0.540 13.7	10 STD XS	40 40S	80 80S	0.065	1.65	0.33	0.49	0.410	10.40		
					0.088	2.24	0.43	0.63	0.364	9.22		
					0.119	3.02	0.54	0.80	0.302	7.66		
3/8 10	0.675 17.1	10 STD XS	40 40S	80 80S	0.065	1.65	0.42	0.63	0.545	13.80		
					0.091	2.31	0.57	0.84	0.493	12.48		
					0.126	3.20	0.74	1.10	0.423	10.70		
1/2 15	0.840 21.3	5 10 STD XS	40 40S	80 80S	0.065	1.65	0.54	0.80	0.710	18.00		
					0.083	2.11	0.67	1.00	0.674	17.08		
					0.109	2.77	0.85	1.27	0.622	15.76		
3/4 20	1.050 26.7	5 10 STD XS	40 40S	80 80S	0.147	3.73	1.09	1.62	0.546	13.84		
					0.188	4.78	1.31	1.95	0.464	11.74		
					0.294	7.47	1.72	2.55	0.252	6.36		
1 25	1.315 33.4	5 10 STD XS	40 40S	80 80S	0.065	1.65	0.87	1.29	1.185	30.10		
					0.109	2.77	1.41	2.09	1.097	27.86		
					0.133	3.38	1.68	2.50	1.049	26.64		
1-1/4 32	1.660 42.2	5 10 STD XS	40 40S	80 80S	0.179	4.55	2.17	3.24	0.957	24.30		
					0.250	6.35	2.85	4.24	0.815	20.70		
					0.358	9.09	3.66	5.45	0.599	15.22		
1-1/2 40	1.900 48.3	5 10 STD XS	40 40S	80 80S	0.065	1.65	1.11	1.65	1.530	38.90		
					0.109	2.77	1.81	2.69	1.442	36.66		
					0.140	3.56	2.27	3.39	1.380	35.08		
2 50	2.375 60.3	5 10 STD XS	40 40S	80 80S	0.191	4.85	3.00	4.47	1.278	32.50		
					0.250	6.35	3.77	5.61	1.160	29.50		
					0.382	9.70	5.22	7.77	0.896	22.80		
2-1/2 65	2.875 73.0	5 10 STD XS	40 40S	80 80S	0.140	3.56	2.27	3.39	1.380	35.08		
					0.191	4.85	3.00	4.47	1.278	32.50		
					0.250	6.35	3.77	5.61	1.160	29.50		
3 80	3.500 88.9	5 10 STD XS	40 40S	80 80S	0.382	9.70	5.22	7.77	0.896	22.80		
					0.400	10.15	6.41	9.55	1.100	28.00		
					0.400	10.15	6.41	9.55	1.100	28.00		
3-1/2 90	4.000 101.6	5 10 STD XS	40 40S	80 80S	0.065	1.65	1.28	1.90	1.770	45.00		
					0.109	2.77	2.09	3.11	1.682	42.76		
					0.145	3.68	2.72	4.05	1.610	40.94		
4 100	4.500 114.3	5 10 STD XS	40 40S	80 80S	0.200	5.08	3.63	5.41	1.500	38.14		
					0.281	7.14	4.86	7.25	1.338	34.02		
					0.400	10.15	6.41	9.55	1.100	28.00		
4-1/2 115	5.000 127.0	5 10 STD XS	40 40S	80 80S	0.065	1.65	1.61	2.39	2.245	57.00		
					0.109	2.77	2.64	3.93	2.157	54.76		
					0.154	3.91	3.66	5.44	2.067	52.48		
5 125	5.550 141.3	5 10 STD XS	40 40S	80 80S	0.218	5.54	5.03	7.48	1.939	49.22		
					0.344	8.74	7.47	11.11	1.687	42.82		
					0.436	11.07	9.04	13.44	1.503	38.16		
5-1/2 140	6.000 152.4	5 10 STD XS	40 40S	80 80S	0.083	2.11	2.48	3.69	2.709	68.78		
					0.120	3.05	3.53	5.26	2.635	66.90		
					0.203	5.16	5.80	8.63	2.469	62.68		
6 150	6.625 168.3	5 10 STD XS	40 40S	80 80S	0.276	7.01	7.67	11.41	2.323	58.98		
					0.375	9.53	10.02	14.92	2.125	53.94		
					0.552	14.02	13.71	20.39	1.771	44.96		
6-1/2 160	7.000 177.8	5 10 STD XS	40 40S	80 80S	0.083	2.11	3.03	4.52	3.334	84.68		
					0.120	3.05	4.34	6.46	3.260	82.80		
					0.216	5.49	7.58	11.29	3.068	77.92		
7 180	7.625 194.0	5 10 STD XS	40 40S	80 80S	0.300	7.62	10.26	15.27	2.900	73.66		
					0.438	11.13	14.34	21.35	2.624	66.64		
					0.600	15.24	18.60	27.68	2.300	58.42		
7-1/2 190	8.125 206.7	5 10 STD XS	40 40S	80 80S	0.083	2.11	3.48	5.18	3.834	97.38		
					0.120	3.05	4.98	7.41	3.760	95.50		
					0.226	5.74	9.12	13.57	3.548	90.12		
8 200	8.625 219.1	5 10 STD XS	40 40S	80 80S	0.318	8.08	12.52	18.64	3.364	85.44		
					0.636	16.15	22.87	34.03	2.728	69.30		
					0.636	16.15	22.87	34.03	2.728	69.30		
8-1/2 210	9.125 231.8	5 10 STD XS	40 40S	80 80S	0.083	2.11	3.92	5.84	4.334	110.08		
					0.120	3.05	5.62	8.37	4.260	108.20		
					0.156	3.96	7.24	10.78	4.188	106.38		
9 225	9.750 248.3	5 10 STD XS	40 40S	80 80S	0.188	4.78	8.67	12.91	4.124	104.74		
					0.237	6.02	10.80	16.08	4.026	102.26		
					0.337	8.56	15.00	22.32	3.826	97.18		
9-1/2 240	10.375 266.7	5 10 STD XS	40 40S	80 80S	0.438	11.13	19.02	28.32	3.624	92.04		
					0.531	13.49	22.53	33.54	3.438	87.32		
					0.674	17.12	27.57	41.03	3.152	80.06		
10 250	11.000 279.4	5 10 STD XS	40 40S	80 80S	0.083	2.11	4.58	6.75	4.506	114.46		
					0.120	3.05	6.35	9.27	4.290	108.96		
					0.180	4.57	9.14	13.27	3.990	99.06		
10-1/2 260	11.625 295.7	5 10 STD XS	40 40S	80 80S	0.210	5.33	11.56	16.81	3.770	96.86		
					0.270	6.86	14.53	21.04	3.530	91.26		
					0.340	8.64	18.48	26.44	3.290	84.50		
11 280	12.375 316.8	5 10 STD XS	40 40S	80 80S	0.438	11.13	19.02	28.32	3.624	92.04		
					0.531	13.49	22.53	33.54	3.438	87.32		
					0.674	17.12	27.57	41.03	3.152	80.06		
11-1/2 290	13.125 338.0	5 10 STD XS	40 40S	80 80S	0.083	2.11	5.18	7.58	4.506	114.46		
					0.120	3.05	7.24	10.78	4.260	108.20		
					0.156	3.96	9.14	13.27	3.990	99.06		
12 300	13.875 352.3	5 10 STD XS	40 40S	80 80S	0.188	4.78	10.80	16.08	4.026	102.26		
					0.237	6.02	12.52	18.64	3.826	97.18		
					0.337	8.56	15.00	22.32	3.624	92.04		
12-1/2 315	14.625 371.9	5 10 STD XS	40 40S	80 80S	0.438	11.13	19.02	28.32	3.624	92.04		
					0.531	13.49	22.53	33.54	3.438	87.32		
					0.674	17.12	27.57	41.03	3.152	80.06		
13 330	15.375 393.1	5 10 STD XS	40 40S	80 80S	0.083	2.11	5.78	8.37	4.506	114.46		
					0.120	3.05	7.87	11.41	4.260	108.20		
					0.156	3.96	10.44	15.07	3.990	99.06		
13-1/2 345	16.125 412.7	5 10 STD XS	40 40S	80 80S	0.188	4.78	11.56	16.81	4.026	102.26		
					0.237	6.02	12.52	18.64	3.826	97.18		
					0.337	8.56	15.00	22.32	3.624	92.04		
14 360	16.875 431.9	5 10 STD XS	40 40S	80 80S	0.438	11.13	19.02	28.32	3.624	92.04		
					0.531	13.49	22.53	33.54	3.438	87.32		
					0.674	17.12	27.57	41.03	3.152	80.06		
14-1/2 375	17.625 450.5	5 10 STD XS	40 40S	80 80S	0.083	2.11	6.38	9.14	4.506	114.46		
					0.120	3.05	8.64	12.57	4.260	108.20		
					0.156	3.96	10.44	15.07	3.990	99.06		
15 390	18.375 468.3	5 10 STD XS	40 40S	80 80S	0.188	4.78	11.56	16.81	4.026	102.26		
					0.237	6.02	12.52	18.64	3.826	97.18		
					0.337	8.56	15.00	22.32	3.624	92.04		
15-1/2 405	19.125 486.1	5 10 STD XS	40 40S	80 80S	0.438	11.13	19.02	28.32	3.624	92.04		
					0.531	13.49	22.53	33.54	3.438	87.32		
					0.674	17.12	27.57	41.03	3.152	80.06		
16 420	20.000 508.0	5 10 STD XS	40 40S	80 80S	0.083	2.11	6.98	10.16	4.506	114.46		
					0.120	3.05	9.14	13.27	4.260	108.20		
					0.156	3.96	10.44	15.07	3.990	99.06		
16-1/2 435	20.875 528.7	5 10 STD XS	40 40S	80 80S	0.188	4.78	11.56	16.81	4.026	102.26		
					0.237	6.02	12.52	18.64	3.826	97.18		
					0.337	8.56	15.00	22.32	3.624	92.04		
17 450	21.750 554.2	5 10 STD XS	40 40S	80 80S	0.438	11.13	19.02	28.32	3.624	92.04		
					0.531	13.49	22.53	33.54	3.438	87.32		
					0.674	17.12	27.57	41.03	3.152	80.06		
17-1/2 465	22.625 577.9	5 10 STD XS	40 40S	80 80S	0.083	2.11	7.58	11.07	4.506	114.46		
					0.120	3.05	9.74	14.13	4.260	108.20		
					0.156	3.96	10.44	15.07	3.990	99.06		
18 480	23.500 600.3	5 10 STD XS	40 40S	80 80S	0.188	4.78	11.56	16.81	4.026	102.26		
					0.237	6.02	12.52	18.64	3.826	97.18		
					0.337	8.56	15.00	22.32	3.624	92.04		
18-1/2 495	24.375 621.5	5 10 STD XS	40 40S	80 8								

NOMINAL PIPE SIZE	OD	SCHEDULE DESIGNATIONS			WALL THICKNESS		WEIGHT		ID	
INCH MM	INCH MM	ASME			INCH	MM	LBS/ FOOT	KG/ METER	INCH	MM
5 125	5.563 141.3	5		5S	0.109	2.77	6.36	9.46	5.345	135.76
		10		10S	0.134	3.40	7.78	11.56	5.295	134.50
		STD		40S	0.258	6.55	14.63	21.77	5.047	128.20
		XS		80S	0.375	9.53	20.80	30.97	4.813	122.24
		120			0.500	12.70	27.06	40.28	4.563	115.90
		160			0.625	15.88	32.99	49.12	4.313	109.54
		XX			0.750	19.05	38.59	57.43	4.063	103.20
6 150	6.625 168.3	5		5S	0.109	2.77	7.59	11.31	6.407	162.76
		10		10S	0.134	3.40	9.30	13.83	6.357	161.56
					0.188	4.78	12.94	19.28	6.249	158.77
		STD		40S	0.280	7.11	18.99	28.26	6.065	154.08
		XS		80S	0.432	10.97	28.60	42.56	5.761	146.36
		120			0.562	14.27	36.43	54.21	5.501	139.76
		160			0.719	18.26	45.39	67.57	5.187	131.78
XX			0.864	21.95	53.21	79.22	4.897	124.40		
7 175	7.625 193.7	STD		40S	0.301	7.65	23.57	35.10	7.023	178.40
		XS		80S	0.500	12.70	38.08	56.69	6.625	168.30
		XX			0.875	22.23	63.14	94.00	5.875	149.24
8 200	8.625 219.1			5S	0.109	2.77	9.92	14.78	8.407	213.56
				10S	0.148	3.76	13.41	19.97	8.329	211.58
		10			0.250	6.35	22.38	33.32	8.125	206.40
		20			0.277	7.04	24.72	36.82	8.071	205.02
		STD		40S	0.322	8.18	28.58	42.55	7.981	202.74
		60			0.406	10.31	35.67	53.09	7.813	198.48
		XS		80S	0.500	12.70	43.43	64.64	7.625	193.70
		100			0.594	15.09	51.00	75.92	7.437	188.92
		120			0.719	18.26	60.77	90.44	7.187	182.58
		140			0.812	20.62	67.82	100.93	7.001	177.86
		XX			0.875	22.23	72.49	107.93	6.875	174.64
		160			0.906	23.01	74.76	111.27	6.813	173.08
9 225	9.625 244.5	STD	40	40S	0.342	8.69	33.94	50.54	8.941	227.12
		XS	80	80S	0.500	12.70	48.77	72.60	8.625	219.10
		XX			0.875	22.23	81.85	121.85	7.875	200.04
10 250	10.750 273.0			5S	0.134	3.40	15.21	22.61	10.482	266.20
				10S	0.165	4.19	18.67	27.78	10.420	264.62
					0.188	4.78	21.23	31.62	10.374	263.44
					0.250	6.35	28.06	41.76	10.250	260.30
		20			0.307	7.80	34.27	51.01	10.136	257.40
		STD			0.365	9.27	40.52	60.29	10.020	254.46
		XS		40	0.500	12.70	54.79	81.53	9.750	247.60
		80			0.594	15.09	64.49	95.98	9.562	242.82
		100			0.719	18.26	77.10	114.71	9.312	236.48
		120			0.844	21.44	89.38	133.01	9.062	230.12
		140			1.000	25.40	104.23	155.10	8.750	222.20
		160		XX	1.125	28.58	115.75	172.27	8.500	215.84
11 275	11.750 298.5	STD	40	40S	0.375	9.53	45.60	67.91	11.000	279.44
		XS	80	80S	0.500	12.70	60.13	89.51	10.750	273.10
		XX			0.875	22.23	101.72	151.46	10.000	254.04
12 300	12.750 323.8			5S	0.156	3.96	21.00	31.24	12.438	315.88
				10S	0.180	4.57	24.19	35.98	12.390	314.66
					0.188	4.78	25.25	37.61	12.374	314.24
					0.250	6.35	33.41	49.71	12.250	311.10
		20			0.330	8.38	43.81	65.19	12.090	307.04
		STD			0.375	9.53	49.61	73.86	12.000	304.74
		30			0.406	10.31	53.57	79.71	11.938	303.18
		XS		40S	0.500	12.70	65.48	97.44	11.750	298.40
		60			0.562	14.27	73.22	108.93	11.626	295.26
		80			0.688	17.48	88.71	132.05	11.374	288.84
		100			0.844	21.44	107.42	159.87	11.062	280.92
		120		XX	1.000	25.40	125.61	186.92	10.750	273.00
140			1.125	28.58	139.81	208.08	10.500	266.64		
160			1.312	33.32	160.42	238.69	10.126	257.16		
14 350	14.000 355.6			10S	0.188	4.78	27.76	41.36	13.624	346.04
					0.250	6.35	36.75	54.69	13.500	342.90
		10			0.312	7.92	45.65	67.91	13.376	339.76
		STD		40S	0.375	9.53	54.62	81.33	13.250	336.54
		40			0.438	11.13	63.50	94.55	13.124	333.34
		XS		80S	0.500	12.70	72.16	107.40	13.000	330.20
		60			0.594	15.09	85.13	126.72	12.812	325.42
		80			0.750	19.05	106.23	158.11	12.500	317.50
		100			0.938	23.83	130.98	194.98	12.124	307.94
		120			1.094	27.79	150.93	224.66	11.812	300.02
		140			1.250	31.75	170.37	253.58	11.500	292.10
		160			1.406	35.71	189.29	281.72	11.188	284.18

NOMINAL PIPE SIZE	OD	SCHEDULE DESIGNATIONS		WALL THICKNESS		WEIGHT		ID		
INCH MM	INCH MM	ASME		INCH	MM	LBS/ FOOT	KG/ METER	INCH	MM	
16 400	16.000 406.4	10S		0.188	4.78	31.78	47.34	15.624	396.84	
				0.250	6.35	42.09	62.65	15.500	393.70	
		40S	30	0.312	7.92	52.32	77.83	15.376	390.56	
				0.375	9.53	62.64	93.27	15.250	387.34	
		80S	40	0.500	12.70	82.85	123.31	15.000	381.00	
				0.656	16.66	107.60	160.13	14.688	373.08	
			60	0.844	21.44	136.74	203.54	14.312	363.52	
				1.031	26.19	164.98	245.57	13.938	354.02	
			100	1.219	30.96	192.61	286.66	13.562	344.48	
				1.438	36.53	223.85	333.21	13.124	333.34	
	120	1.594	40.49	245.48	365.38	12.812	325.42			
18 450	18.000 457	10S		0.188	4.78	35.80	53.31	17.624	447.44	
				0.250	6.35	47.44	70.57	17.500	444.30	
		40S	20	0.312	7.92	58.99	87.71	17.376	441.16	
				0.375	9.53	70.65	105.17	17.250	437.94	
		80S	30	0.438	11.13	82.23	122.38	17.124	434.74	
				0.500	12.70	93.54	139.16	17.000	431.60	
			40	0.562	14.27	104.76	155.81	16.876	428.46	
				0.750	19.05	138.30	205.75	16.500	418.90	
			60	0.938	23.83	171.08	254.57	16.124	409.34	
				1.156	29.36	208.15	309.64	15.688	398.28	
			100	1.375	34.93	244.37	363.58	15.250	387.14	
				1.562	39.67	274.48	408.28	14.876	377.66	
			120	1.781	45.24	308.79	459.39	14.438	366.52	
20 500	20.000 508	10S		0.218	5.54	46.10	68.61	19.564	496.92	
				0.250	6.35	52.78	78.56	19.500	495.30	
		40S	20	0.375	9.53	78.67	117.15	19.250	488.94	
				0.500	12.70	104.23	155.13	19.000	482.60	
		80S	30	0.594	15.09	123.23	183.43	18.812	477.82	
				0.812	20.62	166.56	247.84	18.376	466.76	
			40	1.031	26.19	209.06	311.19	17.938	455.62	
				1.281	32.54	256.34	381.55	17.438	442.92	
			100	1.500	38.10	296.65	441.52	17.000	431.80	
				1.750	44.45	341.41	508.15	16.500	419.10	
			120	1.969	50.01	379.53	564.85	16.062	407.98	
22 550	22.000 559	10S		0.218	5.54	50.76	75.55	21.564	547.92	
				0.250	6.35	58.13	86.55	21.500	546.30	
		40S	20	0.375	9.53	86.69	129.14	21.250	539.94	
				0.500	12.70	114.92	171.10	21.000	533.60	
		80S	30	0.875	22.23	197.60	294.27	20.250	514.54	
				1.125	28.58	251.05	373.85	19.750	501.84	
			40	1.375	34.93	303.16	451.45	19.250	489.14	
				1.625	41.28	353.94	527.05	18.750	476.44	
			100	1.875	47.63	403.38	600.67	18.250	463.74	
				2.125	53.98	451.49	672.30	17.750	451.04	
			120							
			140							
	160									

PIPING • TUBING • FITTINGS FLANGES • RELATED PRODUCTS

Type	Seamless & Welded
Commodity	Chrome • Stainless • Carbon • Low Temperature
Specifications	A/SA335 • A/SA312 • A/SA213 • A/SA106 • A/SA53/API5L • A/SA333
Sizes (O.D.)	1/8" (3.175mm) - 60" (1524mm) (Larger ODs Available)
Grades	Chrome: P1 • P5 • P9 • P11 • P22 • P91 Stainless: 304 • 304H • 304L • 316 • 316H • 316L • 316LN • 321 • 321H • 347 • 347H • 310 • 310s • 309 • Alloy 20 Low Temp: Grade 1/6 • Grade 3 Carbon: Grade B • Grade C • Galvanized

MILITARY SPEC PIPE & TUBING

Program	MIL-I-45208A Quality Program • Approved Level 1 Supplier
Contact Tioga for	U.S. Navy Specifications • Navy Nuclear • MIC Level 1 • Ultrasonic Testing
Fittings & Flanges	All Fittings & Flanges to Match the Pipe

NUCLEAR MATERIALS

Program	ASME Section III - ASME QSC 467
Specifications	10CFR50 Appendix B • N45.2 • NQA-1 • U.S. Navy Nuclear Specifications
Products	Pipe • Tubing • Fittings • Flanges • Structural • Fasteners • Forgings • Castings • Weld Rod • Plate
Grades	Carbon • Stainless • Chrome Moly • Nickel Alloys • Duplex • 6 Moly Alloys • Low Temperature • Special Melts • Copper • Titanium

NOMINAL PIPE SIZE	OD	SCHEDULE DESIGNATIONS		WALL THICKNESS		WEIGHT		ID	
INCH MM	INCH MM	ASME		INCH	MM	LBS/ FOOT	KG/ METER	INCH	MM
24 600	24.000 610	10 STD	20 40S	0.250	6.35	63.47	94.53	23.500	597.30
				0.375	9.53	94.71	141.12	23.250	590.94
		XS	80S	0.500	12.70	125.61	187.07	23.000	584.60
				0.562	14.27	140.81	209.65	22.876	581.46
		40	60	0.688	17.48	171.45	255.43	22.624	575.04
				0.969	24.61	238.57	355.28	22.062	560.78
		80	100	1.219	30.96	296.86	442.11	21.562	548.08
				1.531	38.89	367.74	547.74	20.938	532.22
		120	140	1.812	46.02	429.79	640.07	20.376	517.96
				2.062	52.37	483.57	720.19	19.876	505.26
		2.344	59.54	542.64	808.27	19.312	490.92		
26 650	26.000 660	10 STD XS	40S 80S	0.312	7.92	85.68	127.36	25.376	644.16
				0.375	9.53	102.72	152.88	25.250	640.94
				0.500	12.70	136.30	202.74	25.000	634.60
28 700	28.000 711	10 STD XS	40S 20 80S 30	0.312	7.92	92.35	137.32	27.376	695.16
				0.375	9.53	110.74	164.86	27.250	691.94
				0.500	12.70	146.99	218.71	27.000	685.60
				0.625	15.88	182.90	272.23	26.750	679.24
30 750	30.000 762	10 STD XS	40S 20 80S 30	0.312	7.92	99.02	147.29	29.376	746.16
				0.375	9.53	118.76	176.85	29.250	742.94
				0.500	12.70	157.68	234.68	29.000	736.60
				0.625	15.88	196.26	292.20	28.750	730.24
32 800	32.000 813	10 STD XS	40S 20 30 40	0.312	7.92	105.69	157.25	31.376	797.16
				0.375	9.53	126.78	188.83	31.250	793.94
				0.500	12.70	168.37	250.65	31.000	787.60
				0.625	15.88	209.62	312.17	30.750	781.24
				0.688	17.48	230.29	342.94	30.624	778.04
34 850	34.000 864	10 STD XS	40S 20 30 40	0.312	7.92	112.36	167.21	33.376	848.16
				0.375	9.53	134.79	200.82	33.250	844.94
				0.500	12.70	179.06	266.63	33.000	838.60
				0.625	15.88	222.99	332.14	32.750	832.24
				0.688	17.48	245.00	364.92	32.624	829.04
36 900	36.000 914	10 STD XS	40S	0.312	7.92	119.03	176.97	35.376	898.16
				0.375	9.53	142.81	212.57	35.250	894.94
				0.500	12.70	189.75	282.29	35.000	888.60
42 1050	42.000 1067	STD XS	40S	0.375	9.53	166.86	248.53	41.250	1047.94
				0.500	12.70	221.82	330.21	41.000	1041.60
				0.625	15.88	276.44	411.64	40.750	1035.24
				0.750	19.05	330.72	492.33	40.500	1028.90
48 1200	48.000 1219	STD XS	40S	0.375	9.53	190.92	284.25	47.250	1199.94
				0.500	12.70	253.89	377.81	47.000	1193.60

SPECIALTY ALLOYS

Type	Seamless & Welded
Commodity	Nickel • Duplex & Titanium
Specifications & Grades	Alloy 800 • Alloy 825 • Alloy 600 • Alloy 625 • Alloy 400 • 6% Moly Grades • Duplex A790 UNS 31803 • 316LN
Sizes (O.D.)	1/8" (3.175mm) - 8" (203.2mm)
Wall Dimensions	0.035" (.889mm) - 0.875" (22.23mm)

TIOGA SPECIALTIES

<ul style="list-style-type: none"> Project Management 24/7 Emergency Service Just-In-Time Programs Inventory in Stock All Schedule Walls Special Heavy Walls to 4" (101.6mm) Header Pipe to 4" Wall (101.6mm) Special Intermediate Walls Average & Minimum Walls Saw Cut up to 40" (101.6mm) Cutting: Square & Miter Custom Lengths and OD's End Preps-Variou Hard to Find Metals & Sizes Se Habla Español Exceptional Mill/Sourcing Relations 	<ul style="list-style-type: none"> Dedicated Project Solution Teams Vendor Managed Inventory Programs Mobile On-Site Inventory Programs Quick Response Programs Low Total Cost Solutions International Export & Packaging EN PED 97/23/EC ISO 9001:2008 MIC Level 1 Supplier In-House Testing Destructive Examination Non-Destructive Examination In-House Hydrostatic Testing Full EDI Capabilities Customized e-business Solutions Emergency Forged and Butt-weld Fittings
--	--

Note: Actual dimensions can vary from the figures based on specifications/manufacturing tolerances. The Data for weight is based on the following calculation for wrought steel pipe:
 LB/foot = (Outside diameter [in.] - Wall Thickness [in.]) x (Wall Thickness [in.] x (10.69)
 KG/Meter = (Outside diameter [mm] - Wall Thickness [mm]) x (Wall Thickness [mm]) x (0.0246615)

Equal Opportunity Employer © Tioga Pipe, Inc. 12/2013

When it has to be right.™

Call the center of your choice for our 24-hour emergency service
 tiogapipe.com



APPENDIX II: Summary data for wells serving separator SD2

Well ID / Type	Northing (m)	Easting (m)	Elevation (m)	Rated output MW
Production				
OW-903A	202839.139	9899769.92	2042.982	4.5
OW-903B	202923.868	9899823.513	2046.225	4.0
OW-904	202472.42	9899973.375	2004.042	5.2
OW-904A	202481.75	9900131.597	1988.862	5.5
OW-904B	202506.899	9899988.952	2003.995	5.0
OW-907A	203113.003	9900635.792	1973.286	8.0
OW-908	203404.234	9898951	2013.65	4.0
OW-908A	203378.169	9898929.201	2013.475	6.0
OW-908B	203348.999	9898911.173	2013.181	8.8
OW-909	204115.88	9898603.874	2088.06	12.5
OW-909A	204138.056	9898631.681	2088.194	10.2
OW-910	203733.158	9899737.594	1994.956	4.6
OW-910A	203847.998	9799774.438	1986.917	13.0
OW-910B	203745.908	9899703.351	1994.977	14.9
OW-912	204602.369	9898181.674	2073.471	5.1
OW-912A	204634.343	9898198.266	2073.497	7.9
OW-915	204327.366	9900010.083	1980.541	7.5
OW-915A	204308.619	9899978.968	1980.584	13.0
OW-915B	204342.441	9900093.36	1980.53	10.5
OW-916	204858.848	9899094.309	2035.621	16.0
OW-916A	204879.446	9899063.912	2035.637	7.7
Hot reinjection	Northing (m)	Easting (m)	Elevation (m)	Injection capacity (t/h)
OW-901	201857.61	9900842.957	1891.762	300
OW-902	201681.992	9899012.784	1951.568	
OW-906	201803	9899830	1974.8	645
OW-906A	201724.686	9899916.941	1964.14	308
OW-911	202736.133	9898315.193	1979.506	
OW-911A	202725.67	9898287.453	1979.519	
OW-913A	202341.87	9899117.509	1980.837	
Cold reinjection	Northing (m)	Easting (m)	Elevation (m)	Injection capacity (t/h)
OW-902A	201788.014	9899062.327	1953.873	900
OW-902B	201801.32	9899032.181	1953.891	420

Note: Well OW906 has been earmarked for conversion from reinjection to production, hence it will not be considered in this study during optimization.

APPENDIX III: Sample input file for the VTDISTRA software

The file left behind has a .inp extension, and we cannot open it. The appendix should preferably not be longer than 1 page.

Title: Olkaria;

Output Device, Monitor/Gif/WMF/PDF (0/1/2/3): 1;
Color for marks, lines (0 Black/1 Red) (0/1): 1;
Draw Digital Elevation Map (0/1): 1;
Draw Distance Map (DM) Without Routes (0/1): 1;
Draw DM, each with Route from nearest Endpoint (0/1): 1;
Draw DM with Routes from nearest Endpoint (0/1): 1;
Draw DM with Routes to CP from Each Endpoint (0/1): 1;
Draw Weighted Distance Map Without Routes (0/1): 1;
Draw Weighted DM with Routes from Each Endpoint(0/1): 1;
Print Result File (0/1): 1;

Max height differences: 0.15;
Max allowable slope upward (ratio): 0.04;

Coordinates for Area Under Consideration A_Name:xmin;ymin;xmax;ymax
A_Olkaria IV: 201500.0; 9799000.0; 204500.0; 9902500.0;

Digital Elevation Matrix: Olkaria.dem;

Result file: Okaria.out;

Coordinates for Constraint Area C_Name:xmin;ymin;xmax;ymax
XC_A1: 201500.0; 9898500.0; 202000.0; 9899000.0;

Coordinates for Endpoints E_Name:X;Y;Z;w;maxh;maxs;
E_OW-908: 203404.234; 9898951.000; 2013.650;
E_OW-908A: 203378.169; 9898929.201; 2013.475;
E_OW-908B: 203348.999; 9898911.173; 2013.181;
E_OW-909: 204115.880; 9898603.874; 2088.060;
E_OW-909A: 204138.056; 9898631.681; 2088.194;
E_OW-910: 203733.158; 9899737.594; 1994.956; 1.0; 0.2; 0.1;
E_OW-910A: 203847.998; 9899774.438; 1986.917;
E_OW-910B: 203745.908; 9899703.351; 1994.977;
E_OWR-911: 202736.133; 9898315.193; 1979.506;
E_OWR-911A: 202725.67; 9898287.453; 1979.519;
E_OWR-913A: 202341.87; 9899117.509; 1980.837; 1.0; 0.2; 0.1;
E_OLKARIA_IV: 203306.0; 9898726.0; 1500.0;

Coordinates for Sample Points S_Name:X;Y;Z; (Separators, Powerplant)
§_SD2NEW: 203375.00; 9898916.00; 20224.57;

APPENDIX IV: Sample output file for the VTDISTRA software

The file left behind has a .out extension. When opened in Notepad and copied to Word, the information spreads over 83 pgs. Perhaps it is enough to show a sample? The appendix should preferably not be longer than 1 page, so this needs to be edited or opened differently.

Title: Olkaria

Matrix size (nx ny):	3001	3001	
Area dim xmi xma dx:	201500.00	204500.00	1.00
Area dim ymi yma dy:	9898001.00	9901001.00	1.00
Height (Hmin Hmax):	1760.00	2100.00	
Crit. Height Slope :	0.150	0.040	
Coord. heighest poin	203957.00	9898854.00	2100.00
Coord. s. weigh dist	203377.00	9898922.00	2024.74

Route coordinates for shortest dist. Form To:

Number of places To :	1
Number of places From :	12
Route number :	1 1

Route from: OW-908

Route to : SD2NEW

Distance : 45.76

No. points: 28

2	203375.00	9898916.00	2024.57
3	203376.00	9898917.00	2024.61
4	203377.00	9898918.00	2024.64
5	203378.00	9898919.00	2024.68
6	203379.00	9898920.00	2024.71
7	203380.00	9898921.00	2024.74
8	203381.00	9898922.00	2024.78
9	203382.00	9898923.00	2024.81
10	203383.00	9898924.00	2024.84
11	203385.00	9898926.00	2024.91
12	203386.00	9898927.00	2024.94
13	203387.00	9898928.00	2024.98
14	203388.00	9898929.00	2025.01
15	203389.00	9898930.00	2025.04
16	203390.00	9898931.00	2025.08
17	203391.00	9898932.00	2025.11
18	203392.00	9898933.00	2025.14
19	203393.00	9898934.00	2025.18
20	203394.00	9898935.00	2025.08
21	203395.00	9898936.00	2025.11
22	203397.00	9898938.00	2025.18
23	203398.00	9898939.00	2025.21
24	203399.00	9898941.00	2025.27
25	203400.00	9898943.00	2025.33
26	203401.00	9898945.00	2025.39
27	203402.00	9898947.00	2025.45
28	203403.00	9898949.00	2025.50
29	203404.00	9898951.00	2025.56

APPENDIX V: Design results for the separator dimensions

Appendix Va - Separator Design Work Sheet				
Case of combined separator SD2				
Separation Pressure	1,2	mPa		
Steam Density@12bar	6,13	kg/m ³		
Water Density@12bar	878,4	kg/m ³		
Design Pressure CL150	2,0	mPa	Design pressure for Class 150 = 20 bar	
Mass flow rate steam, m	134,7	kg/s		
Volumetric flow rate, Qvs	21,97	m ³ /s		
Steam velocity (outlet)	40	m/s		
Flow Area, A	0,549	m ²		
Diameter, Dt	0,836	m	Selected diameter DN850	
	Bangma	Lazalde - Crabtree	Spiral Inlet	
D	2,51	2,76	2,5	m
D_e	0,67	0,84	0,8	m
D_b	0,84	0,84	0,6	m
α	2,72	0,13	0,2	m
β	2,51	2,93	2,7	m
Z	2,51	4,60	4,9	m
L_T	5,85	5,41	2,0	m
L_B	3,76	4,16	4,1	m
Separator Wall Thickness				
Allowable Stress, S	122	mPa	17.7 ksi	(1 ksi = 6.895 mPa)
Welding Factor, E	1			
Temperature coefficient, y	0,4			
Corrosion Allowance, A	0,003			m
	Bangma	Lazalde - Crabtree	Spiral Inlet	
Minimum thickness, tm	0,023	0,025	0,023	m
Nominal Thickness 12.7mm MAX AS PER STEEL SCHEDULES				
Overall height, H	9,62	9,58	6,14	m
Ellipse short radius, b	0,63	0,69	-3,04	m
Ellipse long radius, a	1,25	1,38	1,23	m
Ellipse Surface Area	2,47	2,99	-11,80	m ²
Cylinder Surface Area	75,81	83,03	47,58	m ²
Total Surface Area	78,28	86,02	35,78	m ²
Volume of Steel, V	0,99	1,09	0,45	m ³
Density of steel	7850			kg/m ³
Weight of steel (rhoX volume)	7804,33	8575,72	3566,72	kg
Cost/kg	3,38			USD/kg
Total Cost	26378,62	28985,94	12055,50	USD

Appendix Vb				
Separator Design Work Sheet - Case of SD2c unit				
Separation Pressure	1,2	mPa		
Steam Density@12bar	6,13	kg/m3		
Water Density@12bar	878,4	kg/m3		
Design Pressure CL150	2,0	mPa	Design pressure for Class 150 = 20 bar	
Mass flow rate steam, m	5,9	kg/s		
Volumetric flow rate, Qvs	0,96	m3/s		
Steam velocity (outlet)	40	m/s		
Flow Area, A	0,024	m3		
Diameter, Dt	0,175	m	Selected diameter DN200	
	Bangma	Lazalde - Crabtree	Spiral Inlet	
D	0,53	0,58	0,5	m
D_e	0,14	0,18	0,2	m
D_b	0,18	0,18	0,1	m
α	0,57	0,03	0,0	m
β	0,53	0,61	0,6	m
Z	0,53	0,96	1,0	m
L_T	1,23	1,13	2,0	m
L_B	0,79	0,87	0,9	m
Separator Wall Thickness				
Allowable Stress, S	122	mPa	17.7 ksi	(1 ksi = 6.895 mPa)
Welding Factor, E	1			
Temperature coefficient, y	0,4			
Corrosion Allowance, A	0,003			
	Bangma	Lazalde - Crabtree	Spiral Inlet	
Minimum thickness, tm	0,007	0,008	0,007	m
Overall height, H	2,01	2,00	2,90	m
Ellipse short radius, b	0,13	0,14	0,98	m
Ellipse long radius, a	0,26	0,29	0,26	m
Ellipse Surface Area	0,11	0,13	0,79	m2
Cylinder Surface Area	3,32	3,64	4,70	m2
Total Surface Area	3,43	3,77	5,49	m2
Volume of Steel, V	0,04	0,05	0,07	m3
Density of steel	7850			kg/m3
Weight of steel (rhoX volume)	341,84	375,63	547,55	kg
Cost/kg	2,94			USD/kg
Total Cost	1005,00	1104,34	1609,79	USD

Appendix Vc				
Separator Design Work Sheet - Case of SD2B unit				
Separation Pressure	1,2	mPa		
Steam Density@12bar	6,13	kg/m ³		
Water Density@12bar	878,4	kg/m ³		
Design Pressure CL150	2,0	mPa	(Design pressure for Class 150 = 20 bar)	
Mass flow rate steam, m	57,72	kg/s		
Volumetric flow rate, Qvs	9,42	m ³ /s		
Steam velocity (outlet)	40	m/s		
Flow Area, A	0,235	m ²		
Diameter, Dt	0,547	m	Selected diameter DN550	
	Bangma	Lazalde - Crabtree	Spiral Inlet	
D	1,64	1,81	1,6	m
D_e	0,44	0,55	0,5	m
D_b	0,55	0,55	0,4	m
α	1,78	0,08	0,2	m
β	1,64	1,92	1,8	m
Z	1,64	3,01	3,2	m
L_T	3,83	3,54	2,0	m
L_B	2,46	2,72	2,7	m
Separator Wall Thickness				
Allowable Stress, S	122	mPa	17.7 ksi	(1 ksi = 6.895 mPa)
Welding Factor, E	1			
Temperature coefficient, y	0,4			
Corrosion Allowance, A	0,003			
	Bangma	Lazalde - Crabtree	Spiral Inlet	
Minimum thickness, tm	0,016	0,018	0,016	m
Overall height, H	6,30	6,27	4,72	m
Ellipse short radius, b	0,41	0,45	-1,29	m
Ellipse long radius, a	0,82	0,90	0,81	m
Ellipse Surface Area	1,06	1,28	-3,27	m ²
Cylinder Surface Area	32,49	35,58	23,96	m ²
Total Surface Area	33,54	36,86	20,69	m ²
Volume of Steel, V	0,43	0,47	0,26	m ³
Density of steel	7850			kg/m ³
Weight of steel (rhoX volume)	3344,21	3674,76	2063,01	kg
Cost/kg	3,01			USD/kg
Total Cost	10066,09	11061,04	6209,67	USD

Appendix Vd				
Separator Design Work Sheet - Case of SD2c unit				
Separation Pressure	1,2	mPa		
Steam Density@12bar	6,13	kg/m3		
Water Density@12bar	878,4	kg/m3		
Design Pressure CL150	2,0	mPa	Design pressure for Class 150 = 20 bar	
Mass flow rate steam, m	36,19	kg/s		
Volumetric flow rate, Qvs	5,90	m3/s		
Steam velocity (outlet)	40	m/s		
Flow Area, A	0,148	m3		
Diameter, Dt	0,433	m	Selected diameter DN450	
	Bangma	Lazalde - Crabtree	Spiral Inlet	
D	1,30	1,43	1,3	m
D_e	0,35	0,43	0,4	m
D_b	0,43	0,43	0,3	m
α	1,41	0,07	0,1	m
β	1,30	1,52	1,4	m
Z	1,30	2,38	2,5	m
L_T	3,03	2,81	2,0	m
L_B	1,95	2,16	2,1	m
Separator Wall Thickness				
Allowable Stress, S	122	mPa	17.7 ksi	(1 ksi = 6.895 mPa)
Welding Factor, E	1			
Temperature coefficient, y	0,4			
Corrosion Allowance, A	0,003			
	Bangma	Lazalde - Crabtree	Spiral Inlet	
Minimum thickness, tm	0,014	0,015	0,013	m
Overall height, H	4,98	4,96	4,16	m
Ellipse short radius, b	0,33	0,36	-0,60	m
Ellipse long radius, a	0,65	0,72	0,64	m
Ellipse Surface Area	0,66	0,80	-1,20	m2
Cylinder Surface Area	20,37	22,31	16,73	m2
Total Surface Area	21,03	23,11	15,53	m2
Volume of Steel, V	0,27	0,29	0,20	m3
Density of steel	7850			kg/m3
Weight of steel (rho * volume)	2096,80	2304,05	1548,65	kg
Cost/kg	2,71			USD/kg
Total Cost	5682,32	6243,97	4196,84	USD

APPENDIX VI: Design results for the pipelines – both single-phase and two-phase flow pipes

Appendix VI - Pipeline Design Work Sheet								
Pipe diameter								
Well	908	908A	908B	910	910A	910B	909&909A	
Separation Pressure	1,2	1,2	1,2	1,2	1,2	1,2	1,2	mPa
Steam Density@12bar	6,13	6,13	6,13	6,13	6,13	6,13	6,13	kg/m ³
Water Density@12bar	878,4	878,4	878,4	878,4	878,4	878,4	878,4	kg/m ³
Design Pressure CL150	2,0	2,0	2,0	2,0	2,0	2,0	2,0	mPa
(Design pressure for Class 150 = 20 bar =2.0 mpa)								
Mass flow rate steam, m	5,9	10	15,25	9,66	22,36	35,36	36,16	kg/s
Volumetric flow rate, Qvs	0,9625	1,6313	2,49	1,5759	3,6476	5,7684	5,8989	m ³ /s
Steam velocity (outlet)	40	40	40	40	40	40	40	m/s
Flow Area, A	0,0241	0,0408	0,0622	0,0394	0,0912	0,1442	0,1475	m ²
Diameter, Dt	0,1750	0,2279	0,2814	0,2240	0,3407	0,4285	0,4333	m
Selected diameter(Do)	DN200	DN250	DN300	DN250	DN350	DN450	DN450	
Pipe Thickness Work Sheet								
1. Two-phase pipes	908-SD2	908A-SD2	908B-SD2	910-SD2	910A-SD2	910B-SD2	909&909A-SD2	
CL900 - 150 bar to take care of master valve P								
Design Pressure	15	15	15	15	15	15	15	mPa
Pipe Outer Diameter, D	0,2	0,25	0,3	0,25	0,35	0,45	0,45	m
Allowable Stress, S	122,00	122,00	122,00	122,00	122,00	122,00	122,00	mPa
Welding Factor, E	1	1	1	1	1	1	1	
Temperature coefficient, y	0,4	0,4	0,4	0,4	0,4	0,4	0,4	
Corrosion Allowance, A	0,003	0,003	0,003	0,003	0,003	0,003	0,003	m
Minimum Thickness, t (m)	0,0147	0,0176	0,0206	0,0176	0,0235	0,0294	0,0294	m
Minimum Thickness, t (mm)	14,72	17,65	20,58	17,65	23,51	29,37	29,37	mm
Selected Thickness (mm)	15,09	18,26	31,44	18,26	23,83	29,37	29,37	mm
Pipe OD (mm)	219,08	273,05	323,85	273,05	355,6	457,2	457,2	mm
Pipe ID (mm)	188,90	236,53	260,97	236,53	307,94	398,46	398,46	mm
Pipe OD (m)	0,21908	0,27305	0,32385	0,27305	0,3556	0,4572	0,4572	m
Pipe ID (m)	0,18890	0,23653	0,26097	0,23653	0,30794	0,39846	0,39846	m
Cost calculation								
Two phase pipe length	45,76	13,52	26,82	897,92	919,37	942,43	1654,46	m
Two-phase pipe steel volume	0,4426	0,1976	0,7747	13,1258	22,8380	37,2075	65,3187	m ³
Steel Density	7850	7850	7850	7850	7850	7850	7850	kg/m ³
Steel Mass (kg)	3474,2	1551,4	6081,5	103037,8	179278,1	292078,9	512751,9	kg
Cost per kilogram (USD/Kg)	1,88	1,91	1,96	1,91	2,27	2,71	2,71	USD
Total cost/pipe line (USD)	6.531	2.963	11.920	196.802	406.961	791.534	1.389.558	USD
Total two-phase pipeline cost							2.806.269	

2. Single-phase pipes Steam	SD2-OLK4	SD1-OLK4	SD3-OLK4	SD4-OLK4			
CL150 - 20 bar std steam class							
Design Pressure	2	15	15	15	mPa		
Pipe Outer Diameter, D	0,32	0,32	0,323	0,323	m		
Allowable Stress, S	122,00	122,00	122	122	mPa		
Welding Factor, E	1	1	1	1			
Temperature coefficient, y	0,4	0,40	0,4	0,4			
Corrosion Allowance. A	0,003	0,003	0,003	0,003	m		
Minimum Thickness, t (m)	0,00563	0,02193	0,02193	0,02193	m		
Minimum Thickness, t (mm)	5,63	21,93	21,93	21,93	mm		
Selected Thickness (mm)	6,35	6,35	6,35	6,35	mm		
Pipe OD (mm)	323,85	323,85	323,85	323,85	mm		
Pipe ID (mm)	311,15	311,15	311,15	311,15	mm		
Pipe OD (m)	0,32385	0,32385	0,32385	0,32385	mm		
Pipe ID (m)	0,31115	0,31115	0,31115	0,31115	m		
Brine Pipe length (m)	564	1421	930	1272	m		
Brine pipe steel volume	3,573	9,002	5,891	8,058	m3		
Steel Density	7850	7850	7850	7850	kg/m3		
Steel Mass (kg)	28046,09471	70662,2351	46246,22	63252,89446	kg		
Cost per kilogram (USD/Kg)	2,27	2,27	2,27	2,27	USD/kg		
Total cost/pipe line (USD)	63664,635	160403,274	104978,919	143584,0704	USD		
Total steam line cost				408966,2635	USD		
3. Single-phase pipes brine							
CL900 - 150 bar std steam class	SD2-911	SD2-911A	SD2-913				
Design Pressure	15	15	15	mPa			
Pipe Outer Diameter, (Db)	0,10	0,4	0,3	m			
Allowable Stress, S	122,00	122,00	122,00	mPa			
Welding Factor, E	1	1	1				
Temperature coefficient, y	0,4	0,4	0,4				
Corrosion Allowance. A	0,003	0,003	0,003	m			
Minimum Thickness, t (m)	0,00886	0,02644	0,02058	m			
Minimum Thickness, t (mm)	8,86	26,44	20,58	mm			
Selected Thickness (mm)	11,53	30,96	21,44	mm			
Pipe OD (mm)	114	406,04	323,8	mm			
Pipe ID (mm)	92,04	344,48	280,92	mm			
Pipe OD (m)	0,114	0,40604	0,3238	m			
Pipe ID (m)	0,09204	0,34448	0,28092	m			
Brine Pipe length (m)	45,76	46,76	47,76	m			
Brine pipe steel volume	0,162636	1,696999	0,972791	m3			
Steel Density	7850	7851	7852	kg/m3			
Steel Mass (kg)	1276,7	13323,1	7638,4	kg			
Cost per kilogram (USD/Kg)	1,88	2,56	1,968	USD/kg			
Total cost/pipe line (USD)	2.400	34.107	15.032	USD			
Total Brine line cost			51.540	USD			



UNITED NATIONS
UNIVERSITY

UNU-GTP

Geothermal Training Programme

Orkustofnun, Grensasvegur 9,
IS-108 Reykjavik, Iceland

Reports 2016
Number 23

ELECTROMAGNETIC EXPLORATION OF THE EYJAFJÖRDUR LOW-TEMPERATURE GEOTHERMAL AREA, N-ICELAND

András Kovács

Eötvös Lóránd University
Tolnay Károly str. 3
1163 Budapest
HUNGARY
bandee.k@gmail.com

ABSTRACT

This report discusses a resistivity survey, which was carried out in North Iceland, within the southern part of Eyjafjörður in 2012 and 2013 by Iceland GeoSurvey, ÍSOR. The dataset consists of TEM and MT measurements from the area, which are processed, 1D inverted and discussed. The methodology is shown, from data acquisition to the resulting resistivity model. In this study the relationship between the present work and former studies is discussed. Furthermore, a possible interpretation is evaluated on an enigmatic deep-seated resistivity anomaly, based on older magnetotelluric measurements as well as, recent structural geological and tectonic studies.

1. INTRODUCTION

Iceland's second most inhabited region is the Eyjafjörður area, where approximately twenty thousand people live and where one of the biggest city in the country, Akureyri is located. Around the fjord, six independent district heating systems serve the local municipalities. The most remarkable supplier is the Nordurorka, which owns four of these systems and operates around Akureyri. During the second part of the 20th century the increasing demand for hot water usage in the district heating system required new reservoir discoveries. In order to achieve reasonable success, DC resistivity soundings were carried out in the mid-seventies. As a result of this exploration a low-resistivity anomaly was found towards the south end of the fjord at the field Laugaland. This field was drilled into in 1975 and resulted in around 100 L/s of free flowing 96°C hot water. Another huge discovery was made in the early years of the 21st century, on the western coast of the fjord and north of Akureyri. A significant thermal anomaly was recognized in the vicinity of the village of Hjalteyri, which resulted in the discovery of a reservoir capable of serving 200 L/s of hot water (Flóvenz et al., 2010). In order to create realistic conceptual models and detailed numerical models, an improved picture of the reservoirs is needed, hence TEM and MT resistivity soundings were carried out at the beginning of the 21st century in the valley south of the fjord, where the Laugaland and Botn fields are located. This work presents the methodology and some results from these detailed studies.

2. GEOLOGICAL OVERVIEW OF THE EYJAFJÖRDUR AREA

Eyjafjörður is one of the longest fjords in Iceland with its 70 km. The fjord got its name from the island Hrísey in its central part. The fjords in Iceland were formed during the Quaternary Ice Age, as a result of the outlet of the glacier domes from the middle of the island. The glaciers flooded into the ocean at geographically predefined places, in trenches and valleys (Gudmundsson, 2015). The geology of the Eyjafjörður area has been summarized by e.g. Flóvenz et al., 2010 and Flóvenz and Karlsdóttir, 2000. The geological formations of the study area are mostly tertiary flood basalts with an age around 6 to 9 Ma. These sequences are built up of several layers of tholeiitic lavas, interbedded with scoria and inter-eruptional sediments, olivine tholeiites and porphyritic basalts (see details in Figure 1). While the lava piles are deeply glacially eroded, the bedrock at sea level belongs to the mesolite/scolecite alteration zone, the laumontite zone starts at 500 m depth and the epidote zone is at 3000 m depth. The sediment fill in the valley is mostly alluvial. The general dip of the compound lava layers fits well with the trend throughout the whole island, that is the dip points to the rift zone from which the lavas originated, because the bending of the weak crust due to loading of the lava pile. Here this process manifests in a 3-6° dip towards the south, but southwards along the fjord, the dip is to the east. The matrix permeability of the lava formations is negligible, except for the inter-eruptional sediments, so the groundwater flow is fracture-controlled in these formations. However, in the valley fill, the horizontally layered sediments could have some matrix permeability, leading to horizontal groundwater flow. The fractures and faults

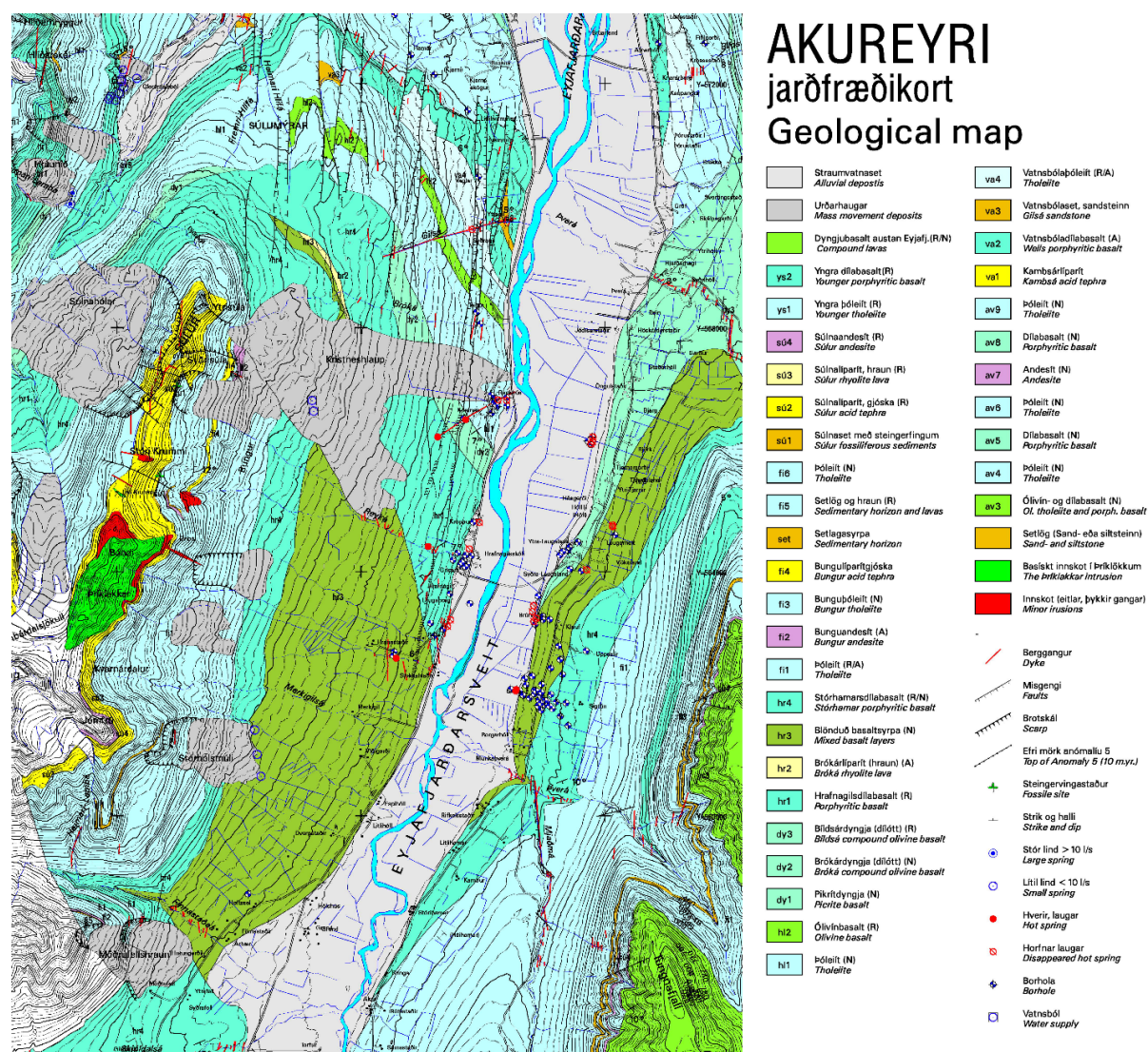


FIGURE 1: Geological map of the Eyjafjörður (Hjartarson and Jónsdóttir, 2004)

are mainly caused by recent tectonic activity at the Tjörnes fracture zone, north of the study area, which is a right lateral transform fault system in the North Atlantic Ocean. The other possible mechanism causing recent tectonic activity might be the glacial isostatic rebound in the area. The geological features in the area that influence ground water flow are near vertical dykes and normal faults. The geothermal temperature gradient in the area is 40-60°C/km which is to be expected as Eyjafjörður is located 100 km west of the active rift zone. Because of the low heat flow the geothermal fields of Eyjafjörður are low-temperature fields with reservoir temperature ranging from 50 to 100°C (Flóvenz and Karlsdóttir, 2000). Within the formations, two heat transfer mechanisms could be present: - heat conduction in the uneroded lava piles and convective cells in the fractures (Flóvenz and Saemundsson, 1993).

3. ELECTROMAGNETIC GEOPHYSICAL METHODS – THEORY AND APPLICATION

Resistivity methods are geophysical methods widely used in geothermal exploration, where the investigated geological formations are distinguished by their electrical properties, because in geothermal fields, the fluid content and the alteration mineralogy can lead to sharp resistivity contrasts compared to the generally resistive rocks. This statement applies especially in fracture-dominated areas like Eyjafjörður, where the convection of the hot fluid gives rise to a low-resistivity anomaly. Early on, the methods applied were based on the injection of direct current into the ground through two electrodes, with the potential field measured between other two electrodes. To reach reasonable penetration depths a few kilometres of cables have to be used. Therefore, this method is fairly slow to use and requires a lot of field work, if reasonable amount of data is to be collected. In addition, at places where the uppermost layer has high resistivity, for example lava fields, it is nearly impossible to inject enough current into the ground, to reach good depth of penetration. The data processing is though relatively easy for these measurements. To overcome these difficulties new techniques were needed. The solution to this was implementation of electromagnetic methods. In Iceland, these methods were implemented in the mid-1980s and proved very successful in geothermal exploration.

The common principle in resistivity sounding methods is to induce currents in the ground and measure the response. In DC methods the electrical field is built up by injecting currents into the ground, while in the case of electromagnetic methods discussed here, the currents in the ground are induced by a time varying magnetic field. This time varying magnetic field could have two types of sources; in the case of naturally varying field we speak about the magnetotelluric method (MT), while if the magnetic field is artificial the method usually referred to is the Transient Electromagnetic Method (TEM). The natural sources of the magnetic field of the MT method are the daily varying ionospheric and magnetospheric currents, with these processes giving low-frequency variation, whereas the high-frequency variations are induced by thunderstorm activity around the equator. Although, this high frequency signal is stronger at low latitudes, it can be measured at higher latitudes too, because the electrical signal created by the thunderstorm, travels as a guided wave between the earth and the ionosphere to higher latitudes. Between the two frequency ranges a band is present where the intensity of the signal is considerably lower, it is called the MT-dead band and ranges from 0.5 to 5 Hz. In contrast with this, the TEM measurements use a controlled source to build up time varying magnetic field created by transmitting current into a loop. When the current is turned off, currents are induced in the ground giving rise to decaying magnetic field which decay rate is measured by induction in a receiver coil.

3.1 Conductivity of rock formations - consequences of the temperature of a geothermal system

The resistivity methods are fundamentally important in geothermal prospecting, because they measure properties of rocks, which are strongly related to the fluid content and temperature of the reservoir. These parameters determine the quality of a geothermal reservoir. Therefore, resistivity methods give valuable information about the reservoir itself. In most rocks in low-temperature areas the main electrical conduction mechanism is the electrolytic conduction in aqueous solutions flow in the pore

space of the rocks, while the rock matrix is an insulator. The electrical resistivity of rocks depends on several factors: porosity and pore structure, water saturation, ion content of the water, temperature, phase of the fluid and the water rock interaction. Although the above mentioned factors determine mainly the resistivity of rocks, different rock types can have different resistivity as shown in Table 1 (Hersir and Björnsson, 1991). Since high-temperature geothermal fields are usually in volcanic areas, the relationship between the formations at these areas and the resistivity structure is fundamental. The resistivity structure in high-temperature geothermal areas is not correlated with the lithology, but with the alteration mineralogy. These altered formations are created by the high-temperature fluid flow in the surrounding rocks. As the substantial majority of the rock formations in Iceland, the compound lavas of Eyjafjörður were formed along the rift system under high-temperature conditions, so these rocks are altered too. A general alteration structure in a high-temperature area starts with the smectite-zeolite zone with resistivity values ranging from 5 to 10 Ωm , below the unaltered rocks. These clay zones act as a low-permeability cap rock of the system. This zone is followed by the high-resistivity core with the chlorite and chlorite-epidote zoning. The grade of the alteration depends primarily on the temperature of the fluid. Therefore, the resistivity structure is a first approximation for the formation temperature. However, this only applies if the geothermal system is in temperature equilibrium. In the case of an old or young system the temperature deduced from the alteration mineralogy can differ from the actual formation temperature (Flóvenz et al., 2012).

TABLE 1: Resistivity of Icelandic rocks (Hersir and Björnsson, 1991)

Formation	Resistivity (Ωm)
Recent lava flows, above groundwater table	5,000-50,000
Dense intrusives (gabbro, dolerite)	10,000-15,000
Recent lava flows, below groundwater table	100-3,000
Basalts, rather dense	100-300
Palagonite	20-100
Low-temperature areas in basalt formation	30-100
Low-temperature areas in hyaloclastite formation	10-50
Rocks with brine	5-15
High-temperature areas, fresh water	1-5
High-temperature areas, brine areas	1-4

3.2 Electromagnetic theory for MT measurements

In this section the basic electromagnetic theory for the magnetotelluric method will be discussed. It is based on the response of the subsurface conductors to incoming waves of time varying magnetic fields. Therefore, Maxwell equations describe the problem:

$$\nabla \times \mathbf{H} = \sigma \mathbf{E} + \varepsilon \frac{\partial \mathbf{E}}{\partial t} \quad (1)$$

$$\nabla \times \mathbf{E} = -\frac{\partial \mathbf{B}}{\partial t} \quad (2)$$

$$\nabla \cdot \mathbf{B} = 0 \quad (3)$$

$$\nabla \cdot \mathbf{E} = \frac{1}{\varepsilon} \eta \quad (4)$$

where \mathbf{E} is the electric field in V/m, \mathbf{H} is the magnetizing field vector in A/m, \mathbf{B} is the magnetic flux density vector in T, ε is the electrical permittivity in As/Vm, η is the electrical charge density in C/m³ and the relationship between \mathbf{H} and \mathbf{B} is the following: $\mathbf{B} = \mu \mathbf{H}$ where μ is the magnetic permeability.

Considering the assumption, that there is no charge density and after some algebraic transformation, we get the following equations:

$$\nabla^2 \mathbf{E} - \mu\sigma \frac{\partial}{\partial t} \mathbf{E} - \mu\epsilon \frac{\partial^2}{\partial t^2} \mathbf{E} = 0 \quad (5)$$

$$\nabla^2 \mathbf{H} - \mu\sigma \frac{\partial}{\partial t} \mathbf{H} - \mu\epsilon \frac{\partial^2}{\partial t^2} \mathbf{H} = 0 \quad (6)$$

If $\sigma \simeq 0$ (a non-conductive medium) these equations are wave equations, if σ is non-zero these equations are diffusion equations. For the easier discussion it is worth to introduce a vector \mathbf{A} where the expression is the same for the electric and magnetic field, later it will be used instead of the separate notation of \mathbf{E} and \mathbf{H} . If the fields vary harmonically in time (as $e^{i\omega t}$) the following forms can be used:

$$\nabla^2 \mathbf{A} + k^2 \mathbf{A} = 0 \quad (7)$$

With the complex number, k^2 :

$$k^2 = \mu\epsilon\omega^2 - i\mu\sigma\omega \quad (8)$$

The differential equation (Equation 7) has a plane wave solution. Consider the solution where the wave propagates in the direction of \mathbf{u} :

$$\mathbf{A}(\mathbf{x}, t) = \mathbf{A}^+ e^{-\beta \mathbf{u} \cdot \mathbf{x}} e^{-i(\alpha \mathbf{u} \cdot \mathbf{x} - \omega t)} \quad (9)$$

which is a wave propagating with the velocity:

$$v = \frac{\omega}{\alpha} \quad (10)$$

where α and β are equal to the following expressions:

$$\alpha = \sqrt{\epsilon\mu\omega} \sqrt{\frac{1}{2} \left(\sqrt{1 + \left(\frac{\sigma}{\epsilon\omega}\right)^2} + 1 \right)} \quad (11)$$

$$\beta = \sqrt{\epsilon\mu\omega} \sqrt{\frac{1}{2} \left(\sqrt{1 + \left(\frac{\sigma}{\epsilon\omega}\right)^2} - 1 \right)} \quad (12)$$

After expressing the components of k and considering the assumption based on the values of the conductivity, the electrical permittivity and the angular frequency, it can be shown that:

$$\frac{\sigma}{\epsilon\omega} \gg 1 \quad (13)$$

By using this approximation (called the quasi-stationary approximation) in Equations 11 and 12 the following relationship appears for α and β :

$$\alpha \simeq \beta \simeq \sqrt{\frac{\mu\omega\sigma}{2}} \quad (14)$$

Equation 14 can be written as:

$$\frac{1}{\beta} = \delta = \sqrt{\frac{2}{\mu\omega\sigma}} \quad (15)$$

which is the depth where the amplitude has decreased to e^{-1} of its surface value, known as the skin depth (penetration depth).

The penetration depth depends on the frequency of the wave and the conductivity of the medium. Suppose the wave propagates in the direction of \mathbf{u} with the wave vector $\mathbf{k} = k\mathbf{u}$ from. From Equation 9 we get the following wave equation:

$$\mathbf{A}(\mathbf{x}, t) = \mathbf{A}_0 e^{-i(\mathbf{k}\mathbf{x} - \omega t)} \quad (16)$$

From Equations 3 and 4 and from the condition that the charge density is zero, it is seen that:

$$k \cdot \mathbf{E} = k \cdot \mathbf{u} \cdot \mathbf{E} = 0 \quad (17)$$

$$k \cdot \mathbf{H} = k \cdot \mathbf{u} \cdot \mathbf{H} = 0 \quad (18)$$

Therefore, the electrical and magnetic field is perpendicular to the propagation direction. After putting Equation 16 into Equation 1, and changing back \mathbf{A} to the adequate notation and assuming that \mathbf{u} is parallel to the z-axis the following expressions add up:

$$E_x = \frac{\mu\omega}{k} H_y \quad (19)$$

$$E_y = -\frac{\mu\omega}{k} H_x \quad (20)$$

Or, in matrix notation:

$$\begin{pmatrix} E_x \\ E_y \end{pmatrix} = \begin{pmatrix} Z_{xx} & Z_{xy} \\ Z_{yx} & Z_{yy} \end{pmatrix} \begin{pmatrix} H_x \\ H_y \end{pmatrix} \quad (21)$$

where the \mathbf{Z} tensor is the complex impedance tensor, which contains information on the subsurface resistivity distribution.

While the \mathbf{Z} tensor in Equation 21 is antisymmetric, in case of homogenously layered Earth and a steady-state approximation the resistivity can be expressed as:

$$\rho = \frac{1}{\sigma} = \frac{1}{\mu\omega} \left| \frac{E_x}{H_y} \right|^2 = \frac{1}{\mu\omega} \left| \frac{E_y}{H_x} \right|^2 \quad (22)$$

An additional parameter is calculated, the phase:

$$\theta = \arg(Z) \quad (23)$$

The measured values are the time varying E_x , E_y and H_x , H_y and H_z values, of which the apparent resistivity can be calculated depending on the measuring frequency after Kaufman and Keller, 1983.

3.3 Static shift problem

The MT method, as any other resistivity method, where the electric field is measured on the surface is affected by the telluric or static shift problem. It is manifested as an unknown multiplier of the apparent resistivity. This unknown multiplier is independent of frequency, which means the effect of the surface is seen in the long period data reflecting the resistivity structure at great depth. This phenomenon can be caused by near surface resistivity inhomogeneities or significant topography around the station. According to Árnason (2015) two types of near-surface resistivity inhomogeneity exist: 1) electric field distortion due to the dependency of the electric field on the resistivity of the material where the voltage difference is measured and 2) current distortion, when the current is channelled or repelled by a resistivity inhomogeneity. If we consider a section under the measuring site, where a lower resistivity section is surrounded by higher resistivity, the measured electric field in the low resistivity is lower,

giving too low apparent resistivity. Current channelling happens when current is flowing in the ground within a localised resistivity anomaly and the current lines are deflected. If the anomaly has lower resistivity than its environment the current lines are deflected into the anomaly, if the anomaly has higher resistivity the current lines are repelled from it. If the resistivity inhomogeneity is close enough to the surface, this will affect the current density at the surface and hence the electric field and apparent resistivity.

The effect of the topography can also lead to a static shift, manifesting in current distortion. The laterally flowing current density is spread out in the vicinity of local highs but concentrated in topographic lows. Compared with a constant resistive earth, it leads to apparent resistivity lower than the actual resistivity on topographic highs and higher apparent resistivity in topographic lows. Because these processes affect our results the amount of the static shift has to be determined. The solution is brought by Transient ElectroMagnetic measurements - TEM, which is affected only at early times by the above mentioned phenomena. The resistivity values calculated from the late times are comparable to the values measured by MT at the same periods. Hence the ratio between the two values give the value of the static shift multiplier and this value can be used to correct the whole resistivity curve measured by MT, since the shift multiplier is independent of the frequency.

3.4 Magnetotelluric and Transient ElectroMagnetic data collection

In both methods time varying potential fields are measured, so the recorded data are time series data. Since for the MT method long wavelength information is needed, the data collection takes usually about one day. For TEM the data collection is much shorter, so the instrument is not left in the field for one day, as the data collection only takes a few tens of minutes. In the following section, the data collection process for each method will be discussed.

A typical MT sounding station is shown in Figure 2. In pursuance of MT measurements five channels are recorded. Two perpendicular electrical components parallel to the surface are measured by electrodes and three magnetic components in orthogonal directions are measured by magnetic coils. The direction of the setup is aimed to the magnetic north direction, such that the E_x component points to the magnetic north, and the E_y component is in the magnetic east direction. The two horizontal magnetic coils are parallel to the electrical directions, and the third component is the vertical component of the magnetic field measured perpendicular to the surface. The dipole length between the electrodes is usually 50 m. A remote reference station is set up with only the surface-parallel magnetic coils far from any cultural noise and far from the measuring station in order to decrease the noise in the dataset. This is done so the uncorrelated noise can be extracted from the dataset. There are several practical ways to reduce the noise in the measured data; for better contact with the ground, bentonite and water is applied in the holes where the electrodes are put into, in order to increase the contact with the Earth. As with seismic data collections, the wind noise can be seen in the dataset, small currents are induced in any of the long cables by the wind, which makes the dataset noisy. Therefore, these cables should be covered.

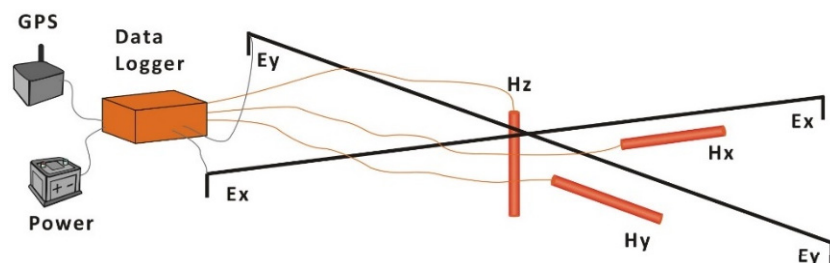


FIGURE 2: A typical layout of an MT measurement (Flóvenz et al., 2012)

The direction of the setup is aimed to the magnetic north direction, such that the E_x component points to the magnetic north, and the E_y component is in the magnetic east direction. The two horizontal magnetic coils are parallel to the electrical directions, and the third component is the vertical component of the magnetic field measured perpendicular to the surface. The dipole length between the electrodes is usually 50 m. A remote reference station is set up with only the surface-parallel magnetic coils far from any cultural noise and far from the measuring station in order to decrease the noise in the dataset. This is done so the uncorrelated noise can be extracted from the dataset. There are several practical ways to reduce the noise in the measured data; for better contact with the ground, bentonite and water is applied in the holes where the electrodes are put into, in order to increase the contact with the Earth. As with seismic data collections, the wind noise can be seen in the dataset, small currents are induced in any of the long cables by the wind, which makes the dataset noisy. Therefore, these cables should be covered.

In the case of central-loop TEM measurements, loops are applied to measure and to induce electrical field in the ground. Each coil is laid down around the centre of the station, the bigger loop is the source, usually a rectangular loop with the effective area around 40,000 m², while the receiver loops are smaller

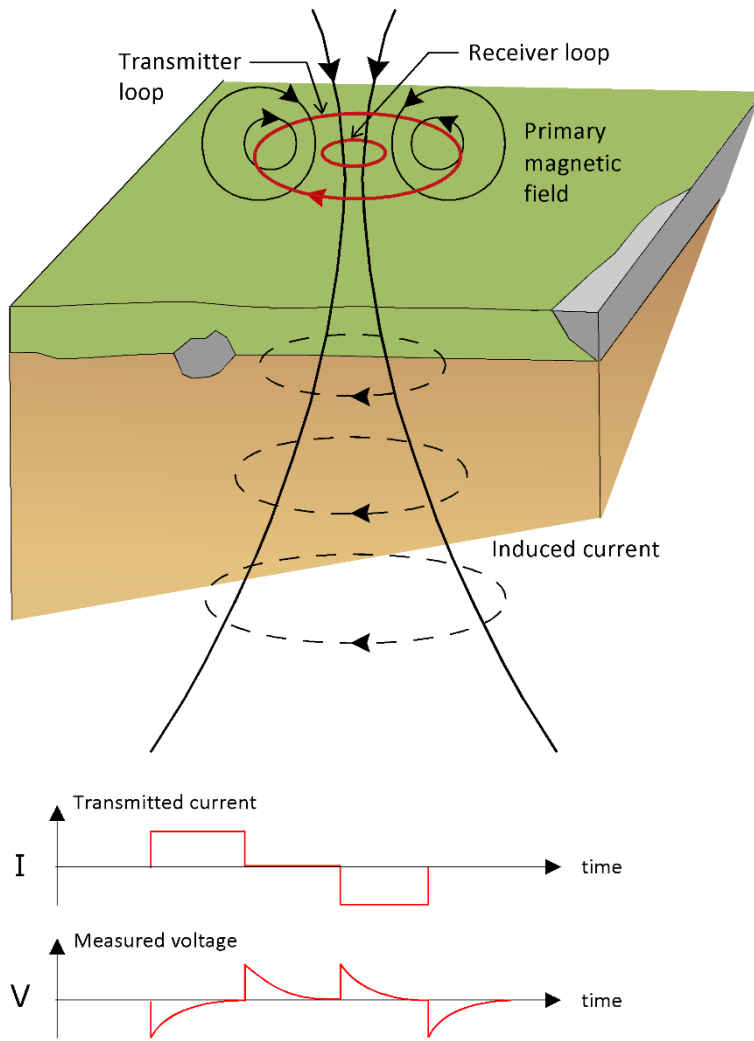


FIGURE 3: Typical layout of a TEM measurement (Flóvenz et al., 2012)

ones with the effective area about 100 m^2 and $5,700 \text{ m}^2$ in the centre of the source loop. The current frequency varies for the different receiver loop, it is either 2.5 Hz or 25 Hz . Into the source loop, a half-duty square wave is transmitted, after turning off the current in the source loop, the decay rate of the magnetic field is measured in the receiver coil, by recording the induced voltage in the receiver loop. As it is impossible to turn of the voltage instantaneously the transmitters turn off the current linearly during a short but finite time, the so called turn-off time. Therefore, the measurements are done in the receiver loop according to the time when the current in the source loop becomes zero. It means that the receiver has to know the turn-off time. In order to reduce the electro-magnetic noise in the signal, the recorded transients are stacked over a number of cycles before storing. The depth of penetration depends on the time after the current is turned off, the longer the elapsed time, the deeper the penetration depth. The resulting dataset consists of voltages at the time gates for the selected frequency, selected gain and the effective area of the receiver loop (Árnason, 2006a). The schematic layout and the transmitted and

induced current curves of a TEM sounding are shown in Figure 3.

A complete discussion of the central loop TEM problem is not the purpose of this work, only the forward problem is shown here. The complete discussion of the central-loop TEM problem can be found in Árnason (1989). The induced voltage $V(t, r)$ for a central loop configuration in a homogenous half space is given by the following expression:

$$V(t, r) = I_0 \cdot \frac{C(\mu_0 \sigma r^2)^{2/3}}{10\pi^{1/2} t^{5/2}} \quad (24)$$

where C :

$$C = A_r n_r A_s n_s \frac{\mu_0}{2\pi r^3} \quad (25)$$

is a constant, containing the properties of the coils, A is the areas for the receiver and source loops, respectively, and n is the number of turns in the coils. In Equation 24, I_0 is the current in the source loop, μ_0 is the magnetic permeability in vacuum in H/m , σ is the conductivity of the media in S/m , r is the radius of transmitter loop, t is the elapsed time after the transmitter current is turned off.

Equation 24 is used as the forward problem in the TEM inversion. However, from this equation the apparent resistivity is expressible, as the following relationship:

$$\rho_a = \frac{\mu_0}{4\pi} \left(\frac{2\mu_0 I_0 A_r n_r A_s n_s}{5t^{5/2} V(t, r)} \right)^{2/3} \quad (26)$$

3.5 Joint interpretation of TEM and MT resistivity soundings

3.5.1 TEM and MT data processing

The outputs of an MT measurement are time series data of the three components of the magnetic field and the two components of the electrical field. The processing of the dataset is done in a software developed by Phoenix Geophysics. The first step is to make sure that the five different components and the remote reference station are synchronized so the further processing uses the appropriate dataset. It is done via editing the table files, from which the program reads out the proper association of the data. When it is done the next step is to define the processing parameters for the Fourier transformation. The data are in the time domain but in Equation 22 the data must be in the frequency domain, therefore the Fourier transformation is a crucial step during the processing. For each frequency value there are 5 different corresponding magnetic and electrical values, from which the apparent resistivity and the phase (from Equation 23) can be calculated. The next step is the graphical editing of the apparent resistivity and phase curves in the MTeditor program, from Phoenix Geophysics. Next, the results of the processing are exported as edi files. The last step is converting these files into a Unix compatible format, which is the input for the inversion. An example of the result of the MT processing is shown in Figure 4.

For the processing of the TEM data a Unix based software is used, which was developed by Knútur Árnason at ÍSOR (Árnason, 2006a). In

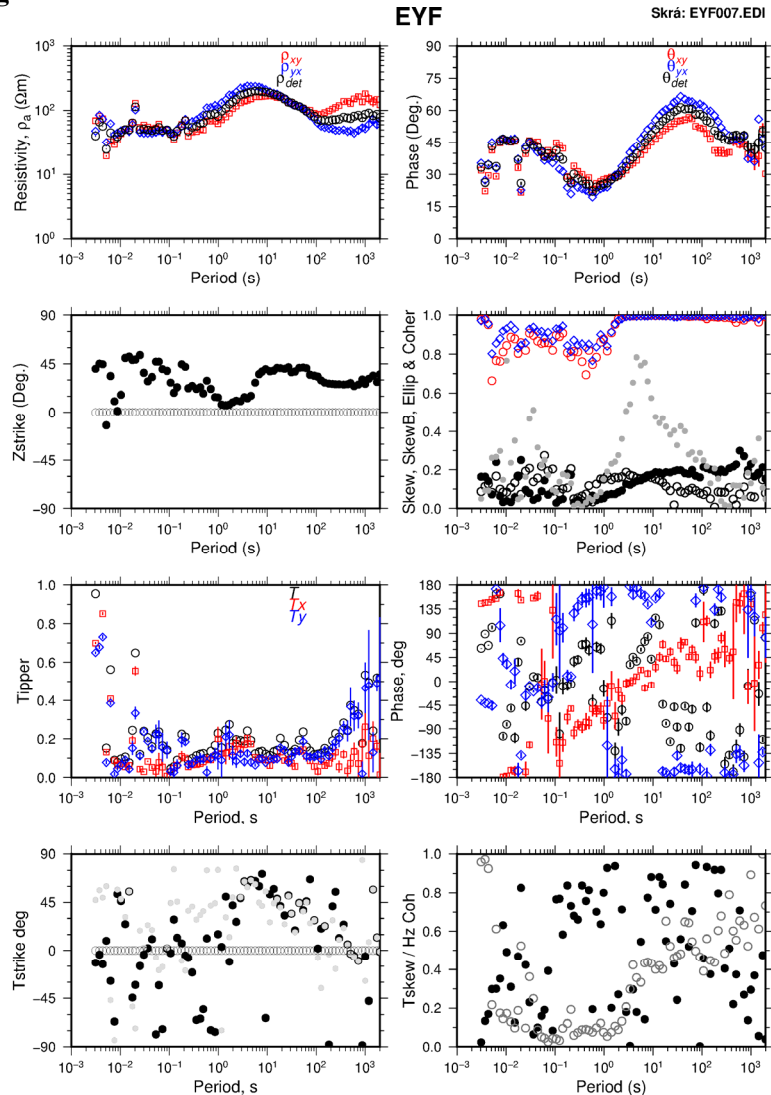


FIGURE 4: On the upper left panel the resistivity values are plotted, as a function of period in both directions as well as the resistivity value calculated from the determinant of the impedance tensor. On the top right panel the three associated phases are plotted. On the other panels additional parameters are plotted, which will not be discussed in detail. It has to be remarked that in the coherency plot (blue and red circles in the second uppermost right panel) the MT dead band appears as a low coherency

this program, through a graphical interface, the data are edited, so the outliers are omitted and the parts of the apparent resistivity curves, which were measured with different current frequencies are linked. The resulting file contains apparent resistivity values as a function of time after current turn off.

3.5.2 Joint inversion of MT and TEM data

Because, both methods have their limitation, a joint interpretation of the datasets is necessary in order to get the best results. As the MT measurement are affected by the above discussed static shift problem, the measurements have to be corrected by adjusting them to the TEM measurements, which are not affected by the static shift. However, the TEM cannot be used by itself because it has limited depth of penetration depending on the parameters of the loop. The inversion process is made in two steps: at first MT measurements are inverted with a constant resistivity model as the starting model. The output of this inversion is the starting model for the joint inversion, where the static shift is calculated. For the inversion, Occam (minimum structure) inversion was used. An Occam model is built up of many equally thick layers on a logarithmic scale. The inversion software is also Unix based and called TEMTD, it was developed by Knútur Árnason in 2006 at ÍSOR (Árnason, 2006b). In the appendices report (Kovács, 2016), the results of the TEM and MT processing for all the soundings, the joint 1D inversion for all the sounding pairs as well as all the resistivity cross-sections and depth slices are shown.

4. THE TEM AND MT DATASET FROM THE EYJAFJÖRDUR AREA – RESULTS

The following topographical map (Figure 5) shows the location of the TEM and MT stations in the vicinity of the main southern geothermal fields of the Eyjafjörður area. The map also contains the

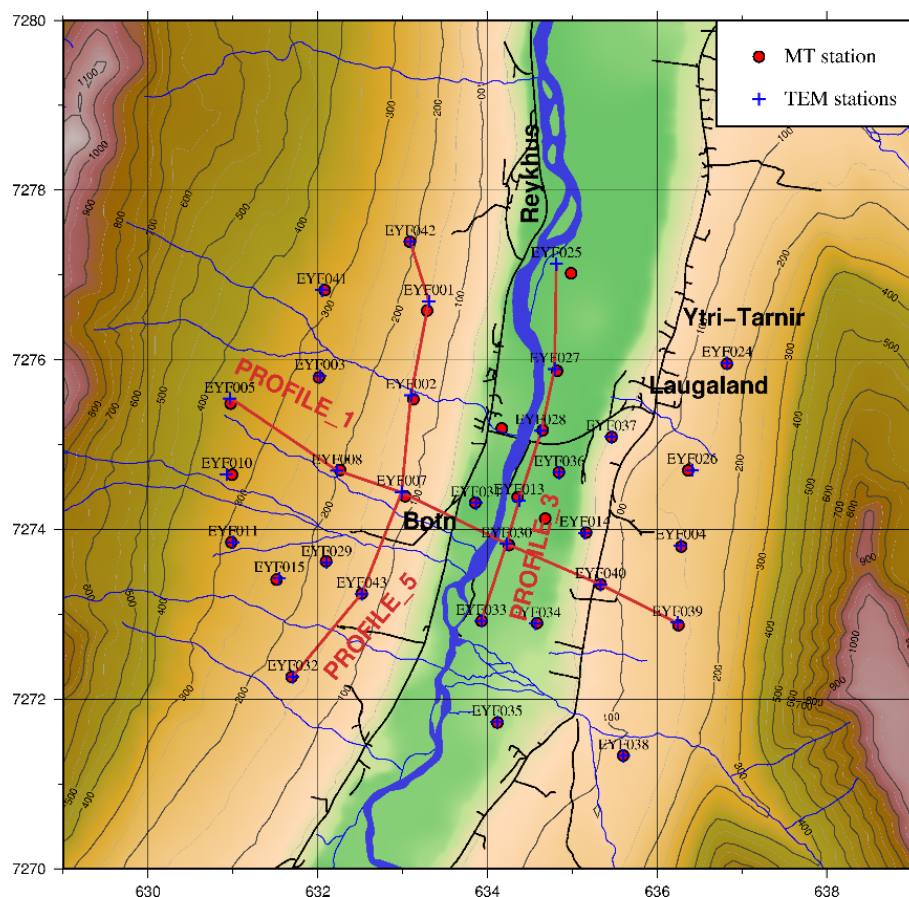


FIGURE 5: Topographical map of the survey area with stations locations; the profiles are shown as red lines

location of the resistivity cross-sections presented. Since the N-S geometry of the valley fundamentally determines the expected resistivity pattern, the orientation of the cross-sections was chosen to be parallel and perpendicular to this main direction. The location of the stations extends from the western part of the valley to the eastern part, covering the bottom of the valley. This dataset extends to the south from the older dataset from the seventies, which was the basis of the discovery of the Laugaland field. The station network covers the Botn field completely, which enables the possibility to compare the results from this study to the work of Flóvenz and Karlsdóttir (2000). During the inversion of the data it was observed that the stations from the valley (EYF027 station in Figure 6) gave much higher misfit than those situated on the mountainside (EYF043 station in Figure 6). This phenomenon was due to the great resistivity variation of the shallow part. Certainly, the uppermost high-resistivity layer is the part which is above the water table, the low-resistivity part is the water saturated sediments and the following high-resistivity part is the bedrock of the valley. It is fundamentally important to distinguish these two types of soundings, because of the flat and horizontally layered geometrical assumption in the inversion. The TEM soundings over conductive sediments see the flanking resistive bedrock of the valley, and cannot be fitted by horizontally-layered model. An example is shown in Figure 6 for both resistivity structures.

5. INTERPRETATION

It is known from the results of Flóvenz and Karlsdóttir (2000) that the Botn field is a fracture-controlled geothermal system, where the strike of the fault is NE-SW, as is expected from the orientation of the valley. In the above-mentioned work, the authors reached the conclusion that this fracture is sealed by secondary mineralization, which acts as an aquifuge. A permeable layer conducts the water flow to the north where it ascends to the surface along dikes and fractures as shown in the N-S cross-section in Figure 7 from the same work. In Figure 8 the resistivity image of the southernmost 5 km of the resistivity model is shown.

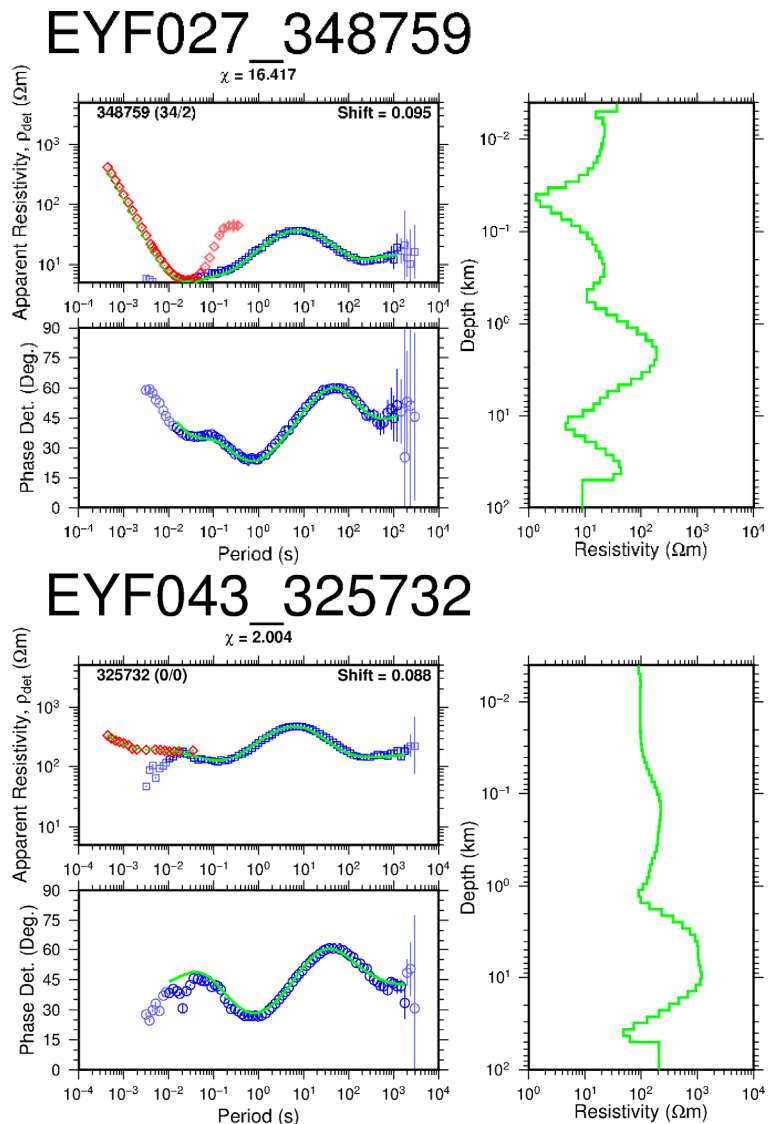


FIGURE 6: On the upper left panels the red dots show the measured apparent resistivity from the TEM data, the blue dots show the measured apparent resistivity from the MT data, the lower left panel shows the measured phase. On the right panel the calculated Occam resistivity is plotted. The green curve on the left side panels is the calculated response of the model

FIGURE 6: On the upper left panels the red dots show the measured apparent resistivity from the TEM data, the blue dots show the measured apparent resistivity from the MT data, the lower left panel shows the measured phase. On the right panel the calculated Occam resistivity is plotted. The green curve on the left side panels is the calculated response of the model

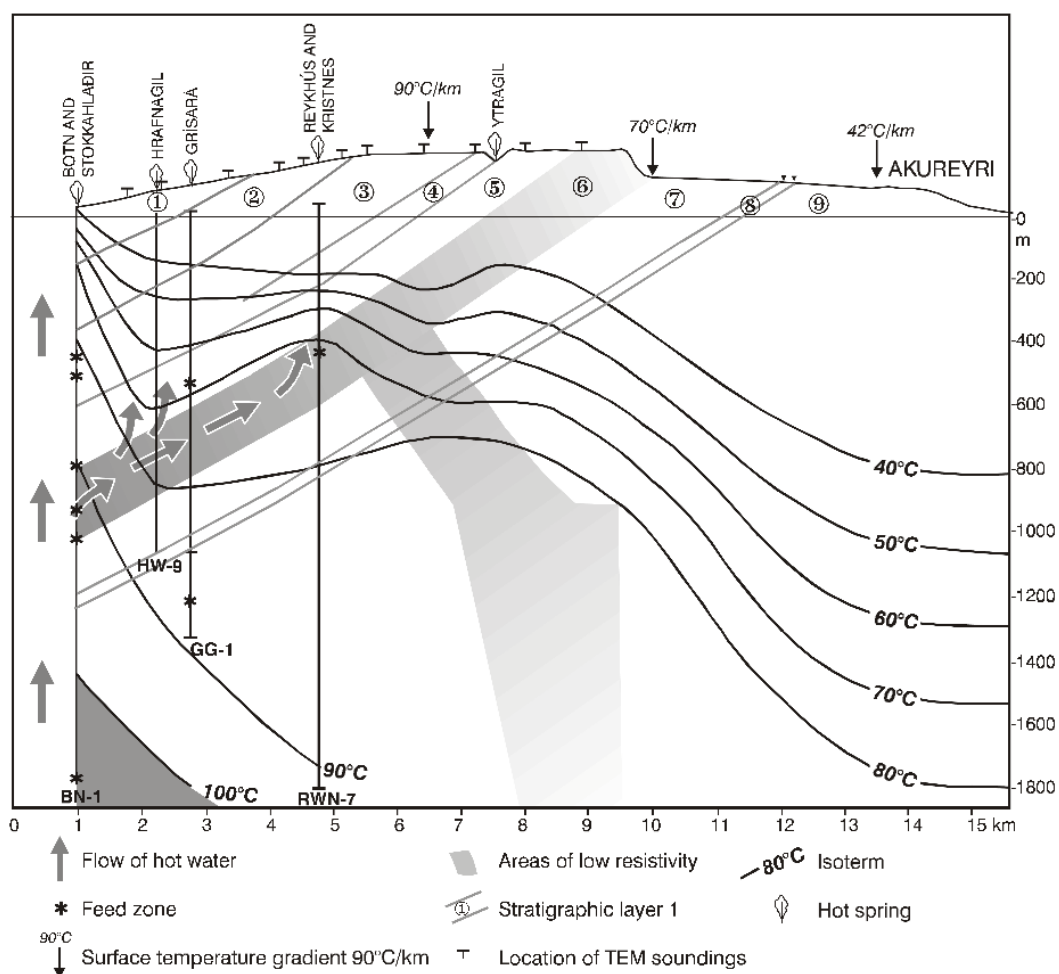


FIGURE 7: Conceptual model of the Botn field (Flóvenz and Karlsdóttir, 2000)

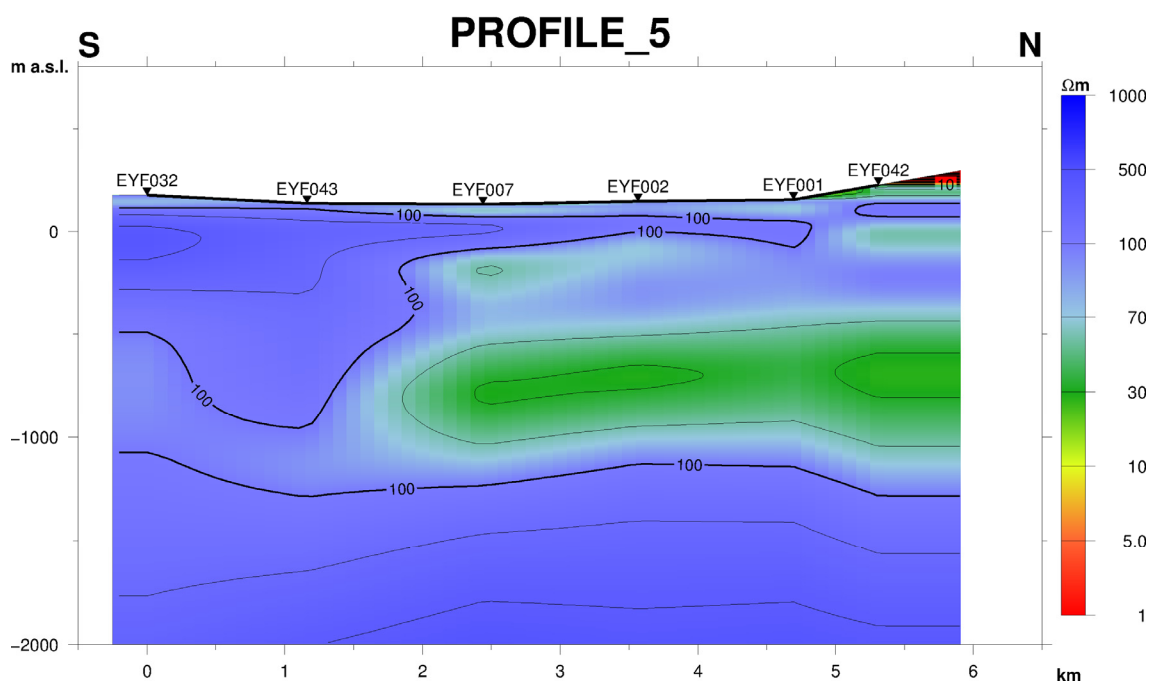


FIGURE 8: Resistivity profile showing the southernmost part of the conceptual model from Flóvenz and Karlsdóttir (2000); black triangles show the location of the MT soundings; location of the profile is given in Figure 5

It is apparent that a near-horizontal low-resistivity layer is mapped pretty well, at around 1 km in Profile_5. This corresponds to the southernmost 5 km of the dipping water flow discussed in the above mentioned work. However, the ascending part of the water-flow was not mapped by this resistivity survey, but it is probably along a near-vertical dike or fault. It is seen clearly on the resistivity depth slices in Appendix V (Kovács, 2016), that this anomaly extends further to the east. According to the resistivity structure in Profile_5, and in order to understand better the behaviour of the reservoir, a perpendicular cross-section was drawn, which crosses the valley itself (Figure 9). The low-resistivity anomaly on this cross-section shows the extent of the field in the valley. However, the resistivity structure is very similar to the concluded resistivity distribution in Flóvenz et al. (1985), for Quaternary formations. It is the author's opinion, that this low-resistivity anomaly is the same structure as discovered in the seventies, leading to the discovery of the deep Laugaland system (Flóvenz et al., 2010).

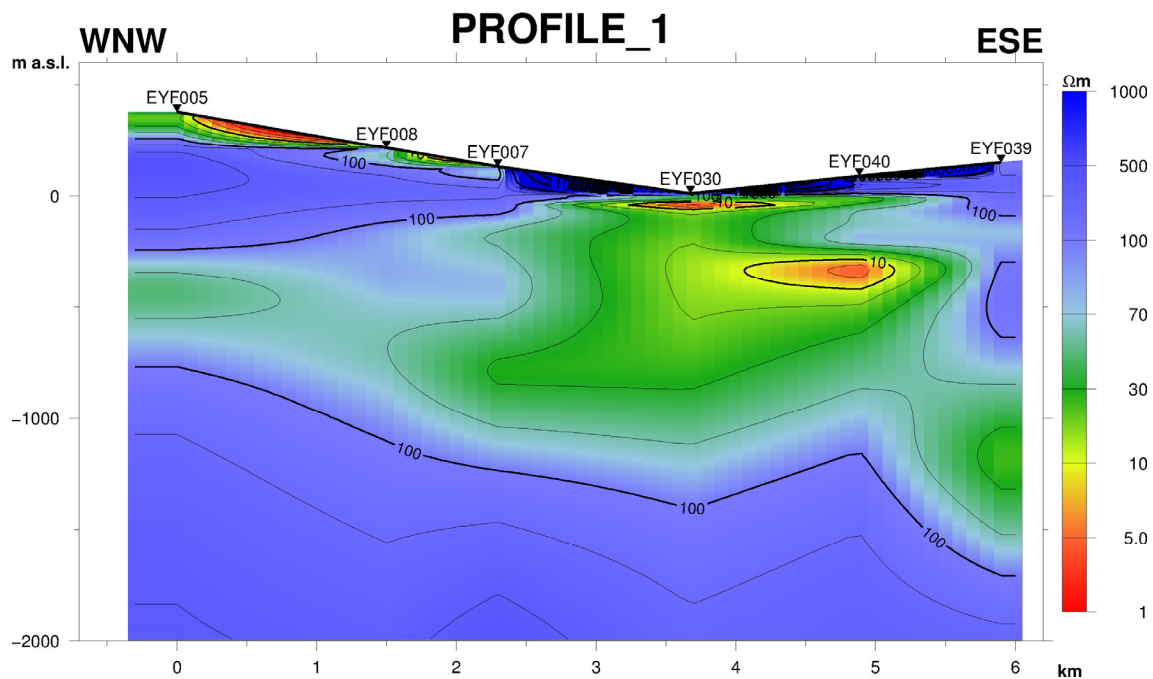


FIGURE 9: The shallow valley crossing resistivity profile; black triangles show the location of the MT soundings; location of the profile is given in Figure 5

For the proper usage of a geothermal field, it is necessary to understand the whole system, with its key elements such as its geometrical characteristics and of course the heat source. Therefore, a deeper version of Profile_1 is presented in Figure 10. In this cross-section, a pronounced low-resistivity anomaly is seen from 7 km depth down to the bottom of the plot. It is also seen in the deeper lying depth slices in Appendix V (Kovács, 2016) that this low-resistivity anomaly extends further down, its direction, coinciding with the direction of the valley. It raises the question, what is the cause of such a deep-seated low-resistivity anomaly. It cannot be a huge fluid saturated reservoir at such a depth, because pore spaces and fractures are mostly closed under high lithostatic pressure. Also, it cannot be a highly altered zone, because the highly altered formations are not far away from the surface, due to glacial erosion. Hersir et al. (1984) described such a deep-seated, low-resistivity anomaly, where they suggested, that the low-resistivity anomaly was caused by enrichment in basaltic melt, which has lower resistivity than ultramafic rocks. This deep-seated enigmatic low-resistivity anomaly is seen below most of Iceland, based on data from numerous surveys. If it was a partially melted body, then these anomalies should cause seismic S-wave attenuation, although these anomalies are not seen. Árnason et al. (2010) proposed similar resistivity anomalies based on data in the Hengill area, which might reflect sheeted dike complex. These basaltic dikes and intrusions are ductile, while the underlying gabbro formations are more brittle. It is known from a recent structural geological study (Proett, 2015), that the deformation styles show sinistral strike-slip and normal faulting in the area. As a result of the normal faulting and

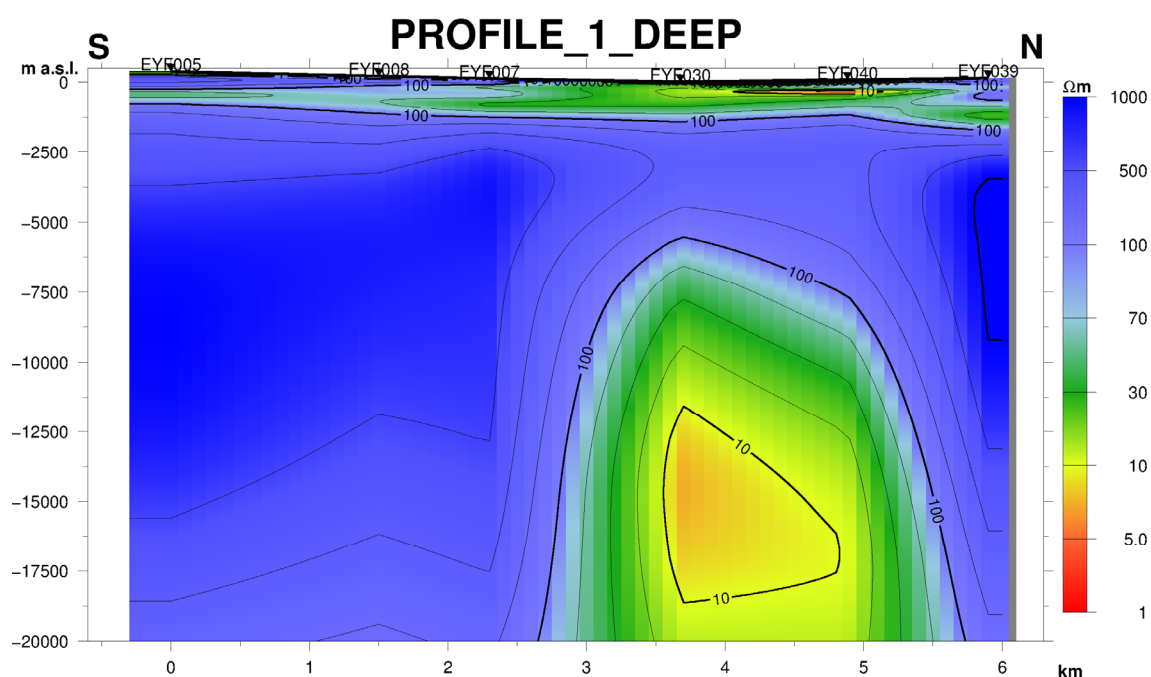


FIGURE 10: The deep valley crossing profile; black triangles show the location of the MT soundings: the location of the profile is given in Figure 5

the extensional component of the sinistral strike-slip faulting, a space could be developed, where the intrusives could be pushed into.

6. DISCUSSION

In this study the methodology of the electromagnetic method was described, concentrating on the Magnetotelluric method (MT) and the Transient Electromagnetic method (TEM). A dataset from Eyjafjörður was processed and interpreted. As a result, the low-resistivity anomaly caused by warm groundwater flow was confirmed from former studies. A proposal for the interpretation was made for an enigmatic and highly debated resistivity structure.

The methods discussed here seem to be a powerful tool to detect shallow resistivity structures, which coincide with formerly confirmed geothermal reservoirs. The MT method can be used to detect deep seated inhomogeneities, although it cannot give a clear picture of these formations on its own. Therefore, further studies are required in order to understand the described phenomena.

ACKNOWLEDGEMENTS

I would like to thank Mr. Lúdvík S. Georgsson and his colleagues for their devoted work, which resulted as an unforgettable and immensely precious six months. A special thank must be said to Mr. Gylfi Páll Hersir for showing me the geophysical methods, which are used successfully in geothermal research. I thank Mr. Knútur Árnason for showing me the example of how a physicist could contribute in geophysical work, and of course I must thank him for introducing me to the new world of Unix. I have to thank Ms. Ásdís Benediktsdóttir for her always helping advices. And naturally all UNU fellows, who showed me a beautiful world through their personality. Nordurorka is acknowledged for allowing the use of the resistivity data from the Eyjafjörður area for this project.

And I must say thanks to my family who helped me to get into this nice profession, with their suggestions and the stable base. I must say thanks to my girlfriend who helped me get through the lonesome moments during last year. And my beloved grandfather, whom I lost during this period, köszönöm Papa.

REFERENCES

- Árnason, K., 1989: *Central loop transient electromagnetic sounding over a horizontally layered earth*. Orkustofnun, Reykjavík, report OS-89032/JHD-06, 129 pp.
- Árnason, K., 2006a: *TemX, a graphically interactive program for processing central-loop TEM data – A short manual*. ÍSOR – Iceland GeoSurvey, Reykjavík, internal report, 17 pp.
- Árnason, K., 2006b: *TEMTD, a programme for 1D inversion of central-loop TEM and MT data – A short manual*. ÍSOR – Iceland GeoSurvey, Reykjavík, short manual, 16 pp.
- Árnason, K., 2015: The static shift problem in MT soundings. *Proceedings of the World Geothermal Conference 2015, Melbourne, Australia*, 12 pp.
- Árnason, K., Eysteinnsson, H. and Hersir, G.P., 2010: Joint 1D inversion of TEM and MT data and 3D inversion of MT data in the Hengill area, SW Iceland. *Geothermics*, 39, 13-34.
- Flóvenz, Ó.G., Árnason, F., Gautason, B., Axelsson, G., Egilson, T., Steindórsson, S.H., and Gunnarsson, H.S., 2010: Geothermal district heating in Eyjafjörður, N-Iceland: Eighty years of problems, solutions and success. *Proceedings of the World Geothermal Conference 2010, Bali, Indonesia*, 8 pp.
- Flóvenz, Ó.G., Georgsson, L.S., and Árnason, K., 1985: Resistivity structure of the upper crust in Iceland. *J. Geophysical Research*, 90-B12, 10,136-10,150.
- Flóvenz, Ó.G., Hersir, G.P., Saemundsson, K., Ármannsson, H., and Fridriksson, Th., 2012: Geothermal energy exploration techniques. In: Sayigh, A. (ed.), *Comprehensive Renewable Energy*, 7. Elsevier, Oxford, UK, 51-95.
- Flóvenz, Ó.G., and Karlsdóttir R., 2000: TEM-resistivity image of a geothermal field in N-Iceland and the relation of the resistivity with lithology and temperature. *Proceedings of the World Geothermal Conference 2000, Kyushu – Tohoku, Japan*, 1127-1132.
- Flóvenz, Ó.G., and Saemundsson, K., 1993: *Heat flow and geothermal processes in Iceland*. *Tectonophysics*, 225, 123-138.
- Gudmundsson, A.T., 2015: *Living earth – outline of the geology of Iceland*. Mál og menning, Reykjavík, 260-263.
- Hersir, G.P., and Björnsson, A., 1991: *Geophysical exploration for geothermal resources principles and application*. UNU-GTP, Iceland, Report 15, 94 pp.
- Hersir, G.P., Björnsson, A., and Pedersen, L.B., 1984: Magnetotelluric survey across the active spreading zone in southwest Iceland. *J. Volcanology & Geothermal Research*, 20, 253-265.
- Hjartarson, Á., and Jónsdóttir, H.E., 2004: *Akureyri, geological map* (2nd ed.). ÍSOR – Iceland GeoSurvey, Reykjavík.

Kaufman, A., and Keller, G.V., 1983: *Frequency and transient sounding. Methods in geochemistry and geophysics, vol. 16*. Elsevier Scientific Publishing Co., Amsterdam, the Netherlands, 685 pp.

Kovács, A., 2016: *Appendices to the report “Electromagnetic exploration of the Eyjafjörður low-temperature geothermal area”*. UNU-GTP, Iceland, report 23 appendices, 72 pp.

Proett, J.A., 2015: *Enigmatic rift-parallel, strike-slip faults around Eyjafjörður, Northern Iceland*. Syracuse University, surface, MSc thesis, 57 pp.



UNITED NATIONS
UNIVERSITY

UNU-GTP

Geothermal Training Programme

Orkustofnun, Grensasvegur 9,
IS-108 Reykjavik, Iceland

Reports 2016
Number 24

MODELLING THE GEOCHEMICAL EFFECTS OF GEOTHERMAL FLUID INJECTION IN THE OLKARIA GEOTHERMAL FIELD, KENYA

Catherine Ndinda Leech

Kenya Electricity Generating Company Ltd. - KenGen

P.O. Box 785-20117

Naivasha

KENYA

cnl@unugtp.is; cndinda@kengen.co.ke

ABSTRACT

Reinjection of used geothermal waters has become an integral part for sustainable geothermal utilization in the Olkaria geothermal field. The location of the field inside the Hell's Gate National Park requires an environmentally friendly way of disposing of separated brine and condensate. Additionally, increased production capacity has been proceeded over the years with increased reinjection. Despite the benefits mentioned, one of the major issues associated with reinjection is the possible loss of permeability due to scaling. In this study, the potential for scale formation in several hot reinjection wells in the Olkaria geothermal field was evaluated. The first approach assessed the potential of scale formation in reinjection wells prior to production using the WATCH speciation program to obtain the baseline data. The second approach using the PHREEQC geochemical model, simulated mixing of injected fluids and aquifer fluids to assess the scaling potential of the mixed fluid. The results from the two approaches were then compared for calcite, amorphous silica and anhydrite saturation in the geothermal fluid. The saturation state of the injected fluid with respect to calcite, amorphous silica and anhydrite at the temperature of reinjection was also assessed in the PHREEQC program using different databases. The results from this study did not only show both positive and negative geochemical effects of fluid injection in the Olkaria geothermal field, but they also showed some inconsistencies in the mineral thermodynamics properties in different PHREEQC databases. Despite these limitations, the confidence level for using the PHREEQC program in geothermal fluids was identified.

1. INTRODUCTION

In recent years, reinjection of used geothermal waters has become an integral part of sustainable geothermal utilization projects in the world (Kaya et al., 2011). The notable benefits associated with reinjection include: (1) provision of an environmentally friendly method of disposing separated geothermal brine and steam condensate, (2) recharging of the reservoir and providing the necessary pressure support. Pressure decline due to long term exploitation of the geothermal resource is a common observation in geothermal production wells (Axelsson, 2008). Despite these benefits, scale formation is the most problematic process associated with the reinjection and may result in loss of well

FIGURE 2: Map of the Greater Olkaria complex showing major tectonic structures (Otieno, 2016)

Upper Olkaria Volcanics. The Olkaria field can further be divided into two units with reference to the formations: (1) the western sector which is characterized by the Mau tuffs and (2) the area east of the Olkaria hill, which has the plateau trachytes and Olkaria basalts as its signatures. The occurrences of different hydrothermal alteration minerals have been used to predict reservoir temperatures, fluid chemistry, permeability, and the evolutionary stage of the system. Omenda (1998) and Lagat (2010) summarized the common secondary minerals which occur in the Olkaria geothermal field. They include; calcium silicates, clays, oxides, silica minerals, zeolites, pyrite, fluorite, calcite, and albite. Further studies by Mibei (2012), identified four alteration zones in the Olkaria geothermal area. This was after correlating hydrothermal mineral assembles from three wells each belonging to three subfields: Olkaria East field, Olkaria North-East field, and the Olkaria Domes field.

2.2 Structural geology

The Eburru-Olkaria alignment was noted by Riaroh and Okoth (1994) as one of the three major alignments in the Kenyan Rift. A further examination revealed that the alignment does not always follow the general orientation of the Rift Valley, especially in sections where there is a change in direction. Studies on the structural pattern of the Olkaria geothermal area support the existence of several fault trends (Figure 2). These trends which include: NS, NW-SE, NNW-SSE, and ENE-WSW control the bulk fluid movement in the region (Omenda, 1998). The NS faults and fractures, which represent the latest tectonic event, are common in the axial region of the rift floor with vertical permeability indicated by strong fumarole activity. The most prominent is the Ololbutot fracture zone. The NW-SE trending faults on the other hand have been inferred from the alignment of the volcanic centres. The Suswa fault intersects the NNW rift faults whereas the ENE-WSW trending Olkaria fault has been interpreted as an old geothermal rejuvenated structure that cut through the geothermal field.

2.3 The history of utilization and the current status

The first research at the Olkaria geothermal field started between 1955 and 1959 when two exploratory wells, X-1 and X-2, were drilled, but failed to discharge. In the mid-1960s, the Olkaria area was considered as a promising geothermal prospect area after geophysical surveys had been carried out between Lake Bogoria (Figure 1) and Olkaria area. Funding from the United Nations Development Program (UNDP) supported more extensive geoscientific survey, which started in 1970. The geothermal resources were further confirmed by six exploratory wells, which were drilled between 1973 and 1976 (KPC, 1994). By 1981, the first 15MWe unit was commissioned in the Olkaria East field. Two more units were commissioned in 1983 and 1986 and the current installed capacity for Olkaria I is 45 MWe. Extensive exploration led to the discovery of additional resources in the Olkaria geothermal area. The Greater Olkaria geothermal area (GOGA) is divided into several fields based on the characteristics and location. These are; Olkaria East field, North-East field, Olkaria Domes, Olkaria South-East field, Olkaria Central field, Olkaria North-West field and Olkaria West field (Figure 3). The latter is owned by OrPower Inc, an independent power producer (IPP). With the exception of the Olkaria North-West Field, the other fields are operated by the mostly state owned Kenya Electricity Generating Company (KenGen). The Olkaria II power plant in the North-East Field was built in two stages; the first two units were built in 2003 with a capacity of 70 MWe and the third unit in 2010 with a capacity of 35 MWe.

The most recent additions to the Olkaria geothermal field were done in 2014 when two power plants, each with 140 MWe capacity, were commissioned. The first power plant is the Olkaria I addition unit (AU) also in the Olkaria East field and the other one is in the Olkaria Domes where Olkaria IV power plant is located. Apart from the convection flash power plants, KenGen also generates electricity using wellhead technology. This technology allows the wells to be utilized and generate revenues in the short term. Usually in the construction of the conventional power plant those wells would be set to idle and would only be used to supply steam to the power plant once it has been commissioned.

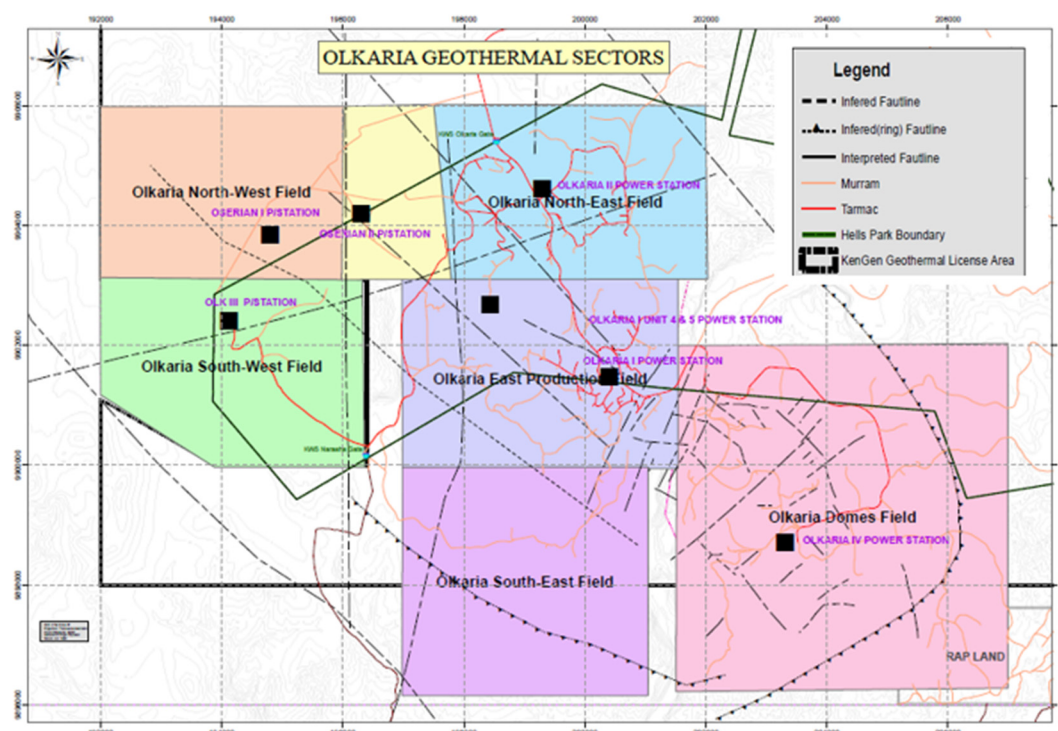


FIGURE 3: Map showing the Olkaria geothermal sectors (KenGen Database, 2016)

2.4 Reinjection in the Olkaria geothermal field

Extensive geoscientific data has been obtained over the years in the Olkaria geothermal area. This data has revealed that the Olkaria geothermal field can sustain further production and therefore future expansion plans are ongoing. In order to be able to sustain future expansion, resource management programmes started in the mid-90s. As a result, a six-month injection and tracer test was carried out in the Olkaria East production field (Ambusso, 1994). The purpose of this test was to determine the effect of the injection on the production wells performance and to evaluate the possibility of implementing long term injection programmes in the field. This experiment was carried out after substantial pressure drawdown which was measured in the wells supplying steam to the Olkaria I power plant, ten years after commercial operations had started. The conclusion from this test was that commencement of reinjection prior to the onset of large drawdown in the reservoir leads to greater sustenance of well production.

The initial practise for disposal of used geothermal waters in the Olkaria Field was surface disposal, where geothermal brine was disposed of in surface ponds and left to percolate into the ground. However, due to environmental effects of such disposal and the need for geothermal resource management, a reinjection strategy was adopted in Olkaria. Currently both hot and cold reinjection is carried out in different sectors of the field. Cold reinjection is used to dispose of cooling tower condensate. Hot reinjection is preferred to minimize cooling of production wells and scaling process (Mariaria, 2011). Several hot reinjection wells are used at different sectors of the Olkaria geothermal field. In this study, the following hot reinjection wells will be considered in the modelling approach: the OW- 703 and OW-708, (located in the North East Field), OW-R3 (located in a buffer zone between the North-East Field and the East Field) and OW-911 (located in the Domes Field) (Figure 4). Apart from well OW-911 which was commissioned as a reinjection well in 2014, the other three wells have been used since 2003 when the Olkaria II power plant came online. The recent addition of the 140 MWe in the Olkaria East Field has seen a change in the reinjection regime such that the separated brine from wells with different chemical compositions is also being directed to the existing reinjection wells. The data considered for this study is prior to these changes which took place in 2014.

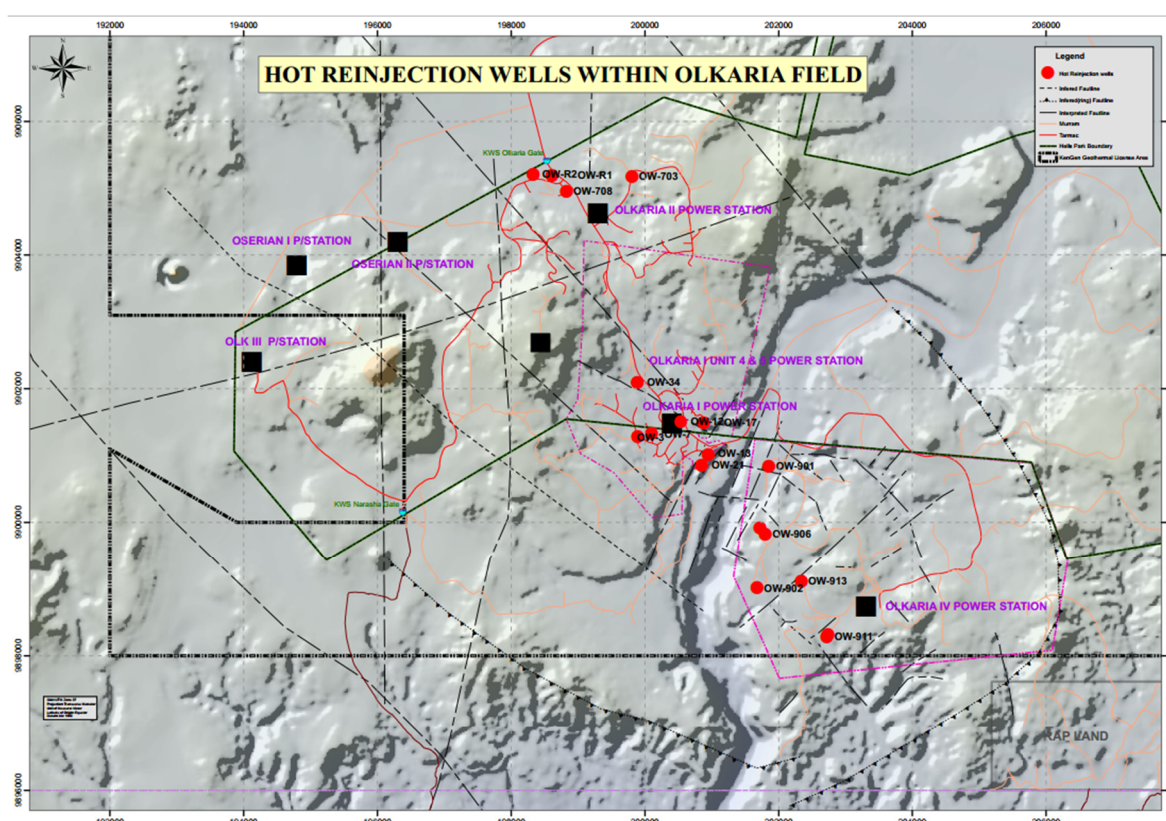


FIGURE 4: Location of hot reinjection wells in Olkaria (arrows show wells investigated during this study)

3. CHEMISTRY OF THE THERMAL FLUIDS IN THE OLKARIA GEOTHERMAL FIELD

3.1 Fluid classification

The chemical composition of the fluids in the Olkaria geothermal area have been routinely sampled and analysed at the Olkaria Geochemistry Laboratories over the years. The main purpose of those analyses is to understand the physical and chemical properties of the fluid, estimate subsurface temperatures, locate recharge zones and identify other reservoir processes such as mixing, boiling and cooling. The chemical composition of the discharge fluids is distinct between fields and also varies between wells located in the same field (Wambugu, 1996). This variability is attributed to the extent of water-rock interaction, boiling processes during the ascent of the geothermal fluid to the surface and possible mixing with colder fluids (Arnórsson et al., 2007).

The Cl-SO₄-HCO₃ diagram as specified by Giggenbach (1981) is based on the relative concentration of three major anions (Cl⁻, SO₄²⁻, CO₃²⁻). This diagram not only aids in classification of the geothermal waters, it also provides a good indication of mixing processes and helps isolate unsuitable fluids for application of geo-thermometry. The fluids in the Olkaria geothermal field can be classified as sodium chloride, sodium bicarbonate or a mixture of all those waters (Figure 5). The wells in the Olkaria East and North East Production fields have a near neutral sodium chloride water type whereas those derived from the central part of the field and in the Domes area are a mixture of chloride and bicarbonate endmembers with alkaline pH. The fluids from the Olkaria west part are predominantly bicarbonate rich. According to Ouma (2007), the Olkaria reservoir is a two phase liquid dominated reservoir which is overlain by a thin, steam dominated zone that is widest in the south and thinnest in the north. The top of the reservoir is further marked by impermeable basalts which act as the cap rock for the system.

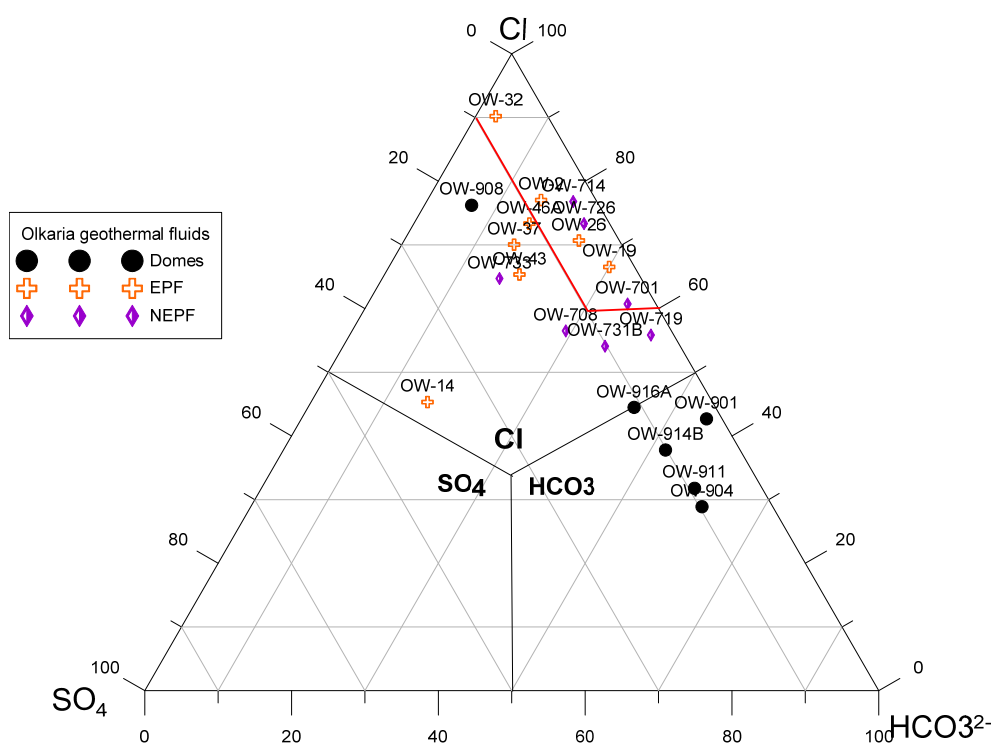


FIGURE 5: The $\text{Cl-SO}_4\text{-HCO}_3^{2-}$ ternary diagram for fluid classification in the Olkaria field

3.2 The geothermometry

The chemical composition of geothermal fluids is useful for estimating the subsurface reservoir temperatures. Several geothermometers can be used depending on the applications. One of the main assumptions when calculating the temperature using geothermometers is that the temperature dependent chemical equilibria prevails in the source aquifer (D'Amore and Arnórsson, 2000). This assumption does not always hold. However, studies of mineral equilibria in geothermal aquifers indicate that quartz and alkali feldspar equilibria prevail in geothermal fluids with temperatures above 150-180°C. Therefore, the temperatures estimations based on quartz and Na-K geothermometers in high temperature reservoirs are valid. The application of the Na/K solute geothermometer as proposed by Fournier and Potter (1982) in the Olkaria geothermal field (Figure 6), indicates temperatures between 250 and 290°C for the East production field, while the Northeast production field indicates

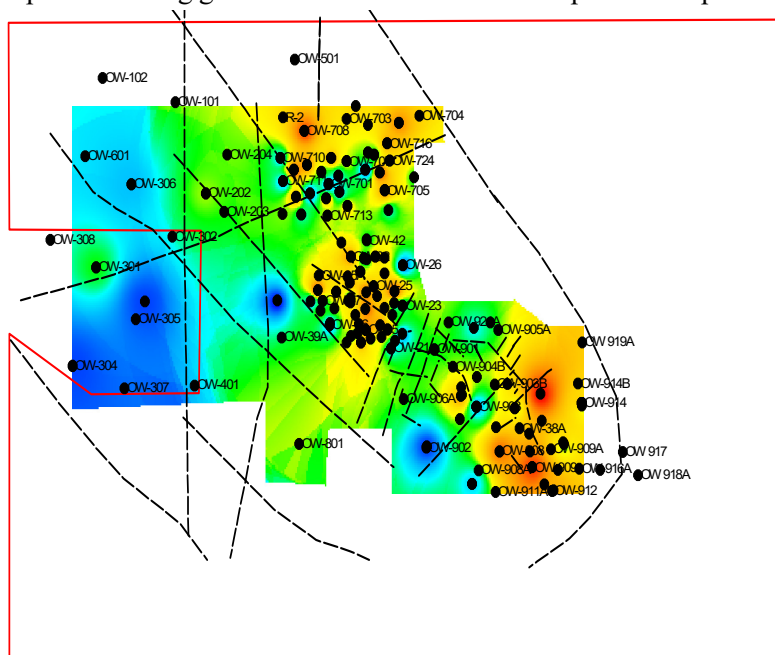


FIGURE 6: Temperature distribution map in the Olkaria geothermal area calculated using Na/K geothermometers (Fournier and Potter, 1982)

temperatures slightly higher than the East production field. The Domes Production field waters show temperatures above 270°C for most of the wells. This information is comparable to the temperature estimates based on enthalpy chloride diagrams for the wells in Olkaria, which indicate a deep upwelling of fluid at 320-340°C, its cooling to 280°C before the onset of boiling and mixing in the North East and East production fields. In the Domes area, subsurface temperatures are closer to 330°C with reservoir boiling starting at this temperature without initial cooling.

4. THE DATABASE AND DATA HANDLING

4.1 Databases

4.1.1 Sampling and analysis

Samples discussed in this report have been classified into two: well discharge data (Table 1) and injected fluid data (Table 2). The well discharge data samples (Figure 7) were collected based on high-temperature sampling protocol described by Ármannsson and Ólafsson (2006). A Webre separator was connected along the two phase line and was used to sample liquid and steam phases. Sampling of the individual phases is made possible by adjusting the water level inside the Webre separator. A high water level is maintained during sampling the water phase and a low water level when sampling the steam phase. The recommended sampling pressure is usually close to the wellhead pressure. Both the sampling pressure and temperatures were recorded to be used in calculating the steam fraction.

TABLE 1: Chemical analysis for injected fluids (in mg/kg)

Well	OW-703	OW-708	OW-R3
TDS	1430	1870	1930
pH/T (°C)	9.34/20	9.72/20	9.56/20
B	2.73	1.81	2.3
SO ₄	21	38.8	39.2
Cl	621.6	585.04	658.17
CO ₂	252.34	209.44	196.02
F	26.76	73.03	67.17
H ₂ S	64.6	31.45	21.25
SiO ₂	774	836	854
Ca	0.077	0.348	0.176
Li	1.52	1.39	1.376
Na	528.1	538.3	523.5
K	106.7	112.2	95.7
Mg	0.036	0.019	0.04

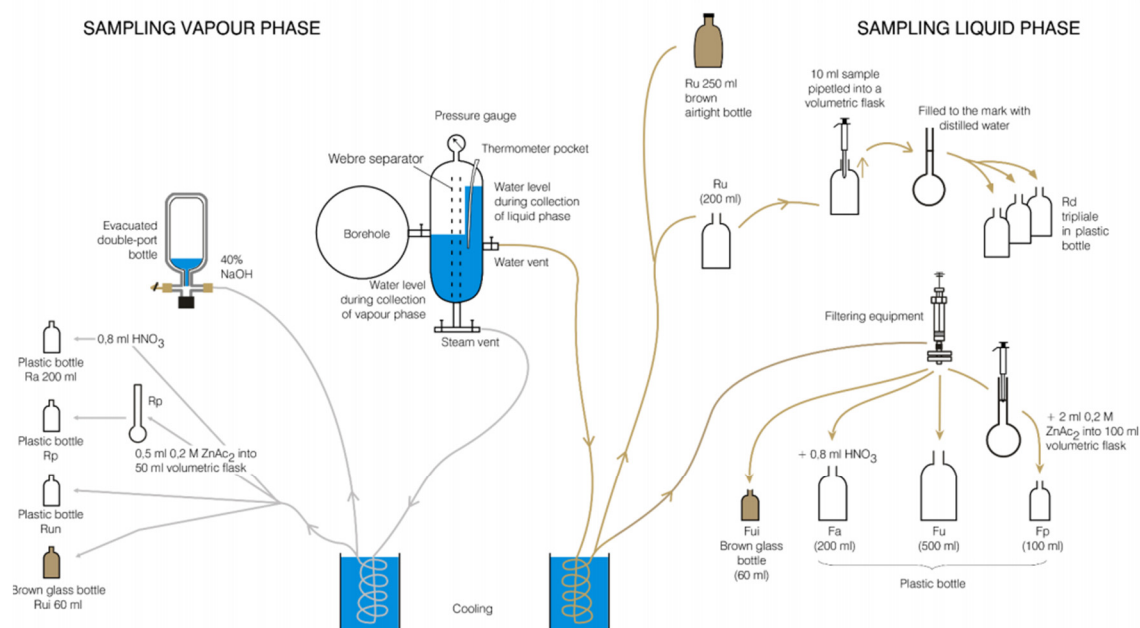


FIGURE 7: Two phase sampling of high temperature geothermal wells (Ármannsson and Ólafsson, 2006)

TABLE 2: Sample preservation methods for geothermal fluids samples
(modified from Ármannsson and Ólafsson, 2006)

Type	Method	Purpose	Sample type	Specification
physical	Filtration	Prevent interaction with suspended matter	Anions, cations	
	Airtight container	Prevent interaction with atmospheric air	Volatiles	Ru-raw untreated samples
	On-site analysis	Prevent reactions of reactive constituents	Reactive constituents	
Chemical	Base addition	Absorption of acid gases	CO ₂ , H ₂ S in steam	
	Acidification	Prevent adsorption on walls of containers	Cations	Fa- filtered acidified samples 0.8ml conc. HNO ₃ mixed with 200ml filtered sample
	Precipitation	Prevent a constituent from reaction to change the concentration of another	Sulphide to preserve sulphate	2 ml 0.2 M ZnAc ₂ added to sample in 100 ml volumetric glass flask and 10 ml to 500 ml bottle containing 25 mg SO ₄ to precipitate sulphide
	Dilution	Prevent polymerization and precipitation	Silica	Rd (1:10) 10ml of sample mixed with 90ml distilled water

Several liquid phase samples were collected in different sampling bottles for the analysis of various components. Different methods of sample preservations were also used (Table 2). Steam samples on the other hand were collected using an evacuated double port glass flask containing 50 ml of 40% sodium hydroxide. The caustic solution dissolves the acidic gases (CO₂ and H₂S) while the residual gases fill up the head space in the gas flask.

The second dataset, which includes the chemical composition of samples from injected fluids, was sampled in a similar manner to one phase wells, however, the Webre separator was not used here. A cooling coil and appropriate sample preservation treatment was used. Sample preservation methods for both two phase fluids and liquid only phase are the same for all high-temperature wells described in this study.

4.1.2 Analysis and results

Results of chemical analyses of water, steam and (condensate) wells' samples are presented in Table 3. Sampling and analysis of those samples were performed according protocol described by Ármannsson and Ólafsson (2006).

TABLE 3: Water and gas analysis of discharge wells

Well	OW-703	OW-708	OW-911
WHP bar-g	8.39	2.41	4
SSP bar-g	4.94	0.69	2.2
Enthalpy (KJ/kg)	1257	1323	1484
Tref (OC)	271	246	226
TDS	2642	1165	1120
pH @20°C	9.2	9.31	9.4
B	1.2	2.6	1.14
SO ₄	24	129	69.2
Cl	884	507	239.5
CO ₂	216.5	261	444.36
F	83	33	70.28
H ₂ S	1.42	0.26	13.6
SiO ₂	886	379	618.5
Ca	0.2	0.04	1.32
Li	1.51	1.5	1.358
Na	710	505	461.5
K	176	79	64.47
Mg	0.1	0.2	0.225

gas values in mmoles/100moles H ₂ O			
CO ₂	246.2	314	360.4
H ₂ S	4.3	0.3	2.6
CH ₄	2.7	0	0.9
H ₂	18.3	0	0.2
N ₂	4.5	15.1	10.7
O ₂	0	0	0.6

The atomic absorption spectrometer (AAS) was used for analysis of major and minor cations (Na, K, Li, Ca, and Mg). Silica and boron analysis were carried out using spectrophotometric methods while fluoride was determined using ion selective electrode. The titration method with pH adjustment from 8.2 to 3.8 using 0.1 N HCl was used to obtain the concentrations of the total inorganic carbon (DIC) in the analysed water and steam. The H₂S concentration in water and steam was determined by titration using mercury acetate titrant and dithizone as a colour reagent. For determination of chloride, titration with silver nitrate and potassium chromate indicator was used. The liquid phase component values were reported in parts per million (ppm). The residual gases (CH₄, H₂, N₂ and O₂) in the steam were determined by gas chromatography. The gas concentration values are reported in mmoles per 100 moles steam for each gas component (Table 3).

4.2 Data handling

The first step in data handling involved using the analytical results from the separated water and gas samples from well OW-703, OW-708 and OW-911 to calculate the aquifer deep fluid composition using the WATCH speciation program version 2.4 (Bjarnason, 2010). The conductive cooling and adiabatic boiling simulations calculated the mineral

saturation indices of anhydrite, calcite, and silica. They were considered as the baseline data prior to reinjection. The reference temperature used for simulation was the measured downhole temperature. The degassing coefficient representing the completeness of degassing when the fluid boils was 1, 0.5 and 0.1 with 1 representing equilibrium degassing while 0.1 indicating little degassing

The second step involved mixing of reinjected fluid with the aquifer fluid. This mixing simulation was done using the geochemical model PHREEQC version 3.7 (Parkhurst and Appelo, 2013). The output from the mixing simulation was then used as an input for boiling simulation using the WATCH speciation program. Results of this simulation revealed the scaling potential of the minerals assessed in the first step. The saturation state of the injected fluid with respect to calcite, anhydrite and amorphous silica was also assessed using the same version of the PHREEQC geochemical program.

4.2.1 Calculation of aquifer fluid composition

The computation of the aquifer deep fluid composition was done using the WATCH speciation program version 2.4 (Bjarnason, 2010) and discharge data (samples' pressure, temperature, pH, and chemical composition) obtained at the surface (Table 4). The basic assumption

TABLE 4: Variation in log K value for different minerals in different databases in the PHREEQC program

LOG K VALUES IN DIFFERENT DATABASES			
	PHREEQC.DAT	MINTEQ.V4.DAT	PITZER.DAT
Calcite	-8.48	-8.48	-8.406
Anhydrite	-4.36	-4.36	-4.362
SiO ₂ (a)	-2.71	-2.74	-2.71
Chalcedony	-3.55	-3.55	-3.55
Quartz	-3.98	-4	-3.98

when performing those calculations is the conservation of mass and enthalpy.

The enthalpy conservation is described by:

$$h^t = Xh^v + (1 - X)h^l \quad (1)$$

where h^t is the total enthalpy of the fluid, h^v and h^l are the enthalpies of the vapour and liquid phases respectively and X is the steam fraction which is obtained by:

$$X = \frac{h^t - h^l}{h^v - h^l} \quad (2)$$

The conservation of mass for the i -th component is defined as:

$$m_i^t = Xm_i^v + (1 - X)m_i^l \quad (3)$$

where m_i^t is the total concentration of the i -th component in the total fluid, m_i^v and m_i^l are the i -th component in the vapour and liquid phases, respectively.

For non-volatile components which do not go into the vapour phase, the Xm_i^v is equivalent to zero, hence the concentration of such components in the total aquifer fluid is defined by:

$$m_i^t = (1 - X)m_i^l \quad (4)$$

For components such as hydrogen and methane, which partition completely into the vapour phase, their concentration in the total aquifer fluid is derived using:

$$m_i^t = Xm_i^v \quad (5)$$

4.2.2 Simulation of mixing using the PHREEQC program

The PHREEQC program is a hydro-geochemical tool used for simulation of a variety of reactions and processes in natural waters and also in laboratory experiments. The PHREEQC is a speciation program that can be used to calculate saturation indices, the distribution of aqueous species, and the density and specific conductance of a specified solution composition. In order to simulate mixing in the program, specific KEYWORDS such as solution and mix are used. They allow data to be inserted into the input and database files.

The first step for the mixing of injected fluid with aquifer fluid involved defining the aqueous composition of the solution. For instance, SOLUTION 1, represented the injected fluid composition and SOLUTION 2, the aquifer fluid composition. The keyword MIX was used to assess the effects of mixing, between the injected fluid and aquifer fluid, on speciation and mineral saturation state. Various mixing ratios between injected and aquifer fluid were used. These were 1:1, 0.3:0.7 and 0.7:0.3. Those ratios were chosen to simulate how mixing of different amounts of solutions will affect the final mixture concentrations.

5. MINERAL SATURATION STATES

In order to determine the state of equilibrium of specific minerals in the aquifer fluid composition at a reference temperature, it becomes important to calculate the aqueous speciation for the same. The WATCH speciation program allows for the calculation of individual aqueous activities. From these activities, the reaction quotient, Q , for individual minerals can be obtained. In thermodynamics terms, the activity describes the behaviour of aqueous species. A comparison between the reaction quotient, Q ,

and the equilibrium constant, K , allows for the determination of the mineral state of equilibrium in a system.

The relationship between the logarithm ratio of the reaction quotient, Q , to the equilibrium constant, K , gives the saturation index (SI) of a particular mineral, and is expressed by the equation below

$$SI = \log \left(\frac{Q}{K} \right) \quad (6)$$

Hence, the determination of mineral saturation states is based on activities of various aqueous species and their mineral solubility. $SI = 0$ implies a state of equilibrium, while, $SI < 0$ and $SI > 0$ denotes water undersaturation and supersaturation with respect to minerals, respectively.

As previously mentioned, only three minerals were considered for assessing the mineral saturation states. These are 1) anhydrite, 2) calcite 3) amorphous silica. The choice for these minerals was mostly governed by the chemical analysis data available, which did not include chemical data for aluminium and iron. It was therefore not possible to establish the level of saturation in the geothermal fluid with respect to pyrite, despite the fact that it is a common alteration mineral observed during borehole logging. Amorphous silica on the other hand has occasionally shown signs of being problematic within the Olkaria field especially on surface installations such as steam pipelines, hence the consideration. Anhydrite has not been known to pose a threat with reinjection. However, there was a need to confirm this fact.

5.1.1 Anhydrite and calcite saturation

Mineral deposition from boiling fluid largely occurs as a response of cooling and degassing (Arnórsson et al., 2007). Unlike amorphous silica, which has prograde solubility, the solubility of anhydrite and calcite decrease with increasing temperatures (retrograde solubility). This means that undersaturation occurs during cooling. Calcite is known to have a pH dependent solubility, which decreases with increasing pH.

The dissolution of calcite is defined by:



whereas the reaction quotient Q , is given as,

$$Q = aCa^{2+} aCO_3^{2-} \quad (8)$$

The dissolution of anhydrite is given as,



whereas the reaction quotient is defined as,

$$Q = aCa^{2+} aSO_4^{2-} \quad (10)$$

Results of the WATCH adiabatic boiling of the aquifer fluid from OW-703 shows that the fluids in the well are saturated with respect to calcite at temperatures of about 180°C and above (using a degassing coefficient of 1). The highest saturation level is attained at temperatures of 250°C after which there is a substantial decrease to undersaturation at temperatures below 180°C. (Figure 8). The onset of boiling either in the wellbore or in the feeding aquifer may be taken to be the cause of this sharp rise in the saturation state. Upon boiling, the fluid pH will rise as a result of degassing and eventually increase the solubility of calcite which is reflected in the saturation state (from the supersaturated state until it reaches an undersaturated state). Similar findings were reported by Wambugu (1996) where the saturation peak

indicates the first level of boiling, which further implies that effective boiling in the well would take place in the feeding aquifer.

Wells OW-708 and OW-911 reflect a different picture when compared to well OW-703. Fluids in well OW-708 (Figure 9) are undersaturated with respect to calcite from the reservoir temperatures all the way to atmospheric conditions. It can therefore be said, that calcite scaling prior to reinjection in this well does not seem to pose a risk. Fluids in well OW-911 (Figure 10) on the other hand, are supersaturated with respect to calcite throughout the boiling process from the aquifer temperatures of 226°C. At temperatures of around 200-240°C the solubility of carbon dioxide is relatively low and the degassing is rapid. Stratigraphy data for this well indicates a presence of calcite. The presence of platy calcite has been documented in well OW-911A (Njathi, 2012) and is indicative of a boiling system similar to well OW-911. Calcite scaling in the Olkaria field has been well documented for well OW-202 in the Olkaria Central field (Opondo, 2015).

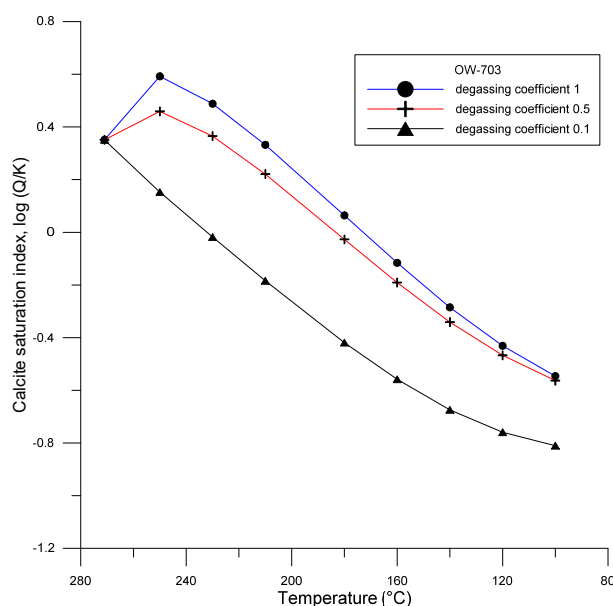


FIGURE 8: Calcite saturation curve for fluids from well OW-703

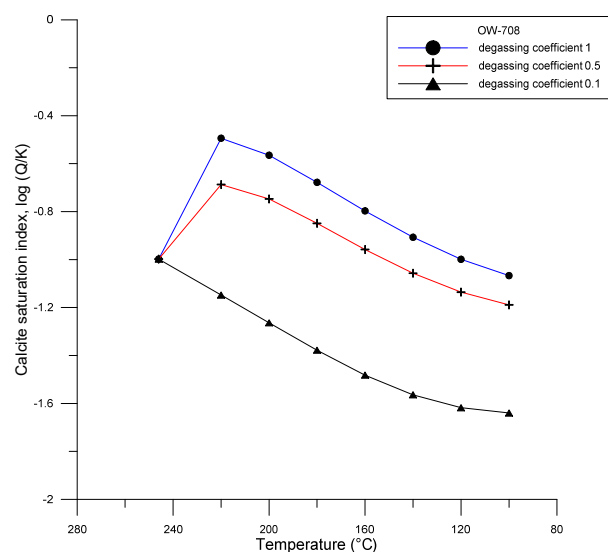


FIGURE 9: Calcite saturation curve for fluids from well OW-708 after adiabatic boiling

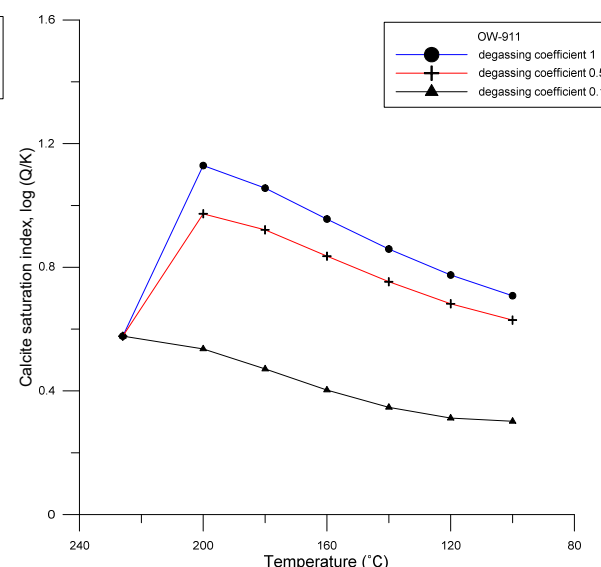


FIGURE 10: Calcite saturation curve of fluids from well OW-911 after adiabatic boiling

Anhydrite scaling in geothermal fields may also pose problems in production wells and is thought to be as a result of mixing of deeper high calcium brines with shallower sulphate rich fluids (Brown, 2013). The fluids in all the three wells under consideration are undersaturated with respect to anhydrite.

5.1.2 Silica saturation

Silica exists in a variety of forms such as quartz, amorphous silica, and chalcedony. Quartz is the most stable and common form of silica in geothermal systems. The solubility of quartz in geothermal reservoir conditions determines the concentrations of dissolved silica in the brines. The difference in solubility between quartz and amorphous silica allows for the exploitation of geothermal systems

limiting silica scaling (Brown, 2013). The deep fluid is saturated with respect to quartz and under-saturated with respect to amorphous silica. Adiabatic boiling of the reservoir fluid has two effects; 1) it increases concentration of silica due to steam loss, 2) lowers solubility of silica due to a drop in temperature as the pressure decreases. The dissolution of solid silica is given as:



The reaction quotient is given as:

$$Q = a_{\text{H}_4\text{SiO}_{4(aq)}} \quad (12)$$

The pH dependence of silica solubility can play an important role in determining the temperature of injecting fluids. The solubility of amorphous silica increases with increased pH as silicic acid becomes dissociated.

The first order dissociation of weak silicic acid can be expressed as:

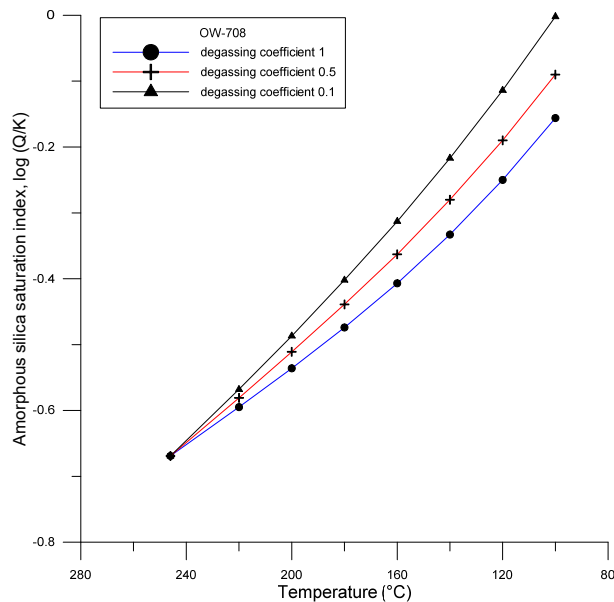


FIGURE 11: Amorphous silica saturation curve for fluids from well OW-708

For most dilute geothermal fluids, the pH value of the residual flashed waters is alkaline (1-2.5 pH units above neutral) and in this pH range the solubility of silica is strongly dependent on pH (Henley, 1983). This would further imply that flashed waters from 250-290°C reservoirs may not reach saturation as is the situation in well OW-708. (Figure 11), where the fluid is undersaturated with respect to amorphous silica.

The pH of geothermal water following steam separation in wellhead separators is a function of composition and temperature and is strongly dependent on the gas removal during single stage and multistage steam separator (Henley, 1983).

The current practice in the operation of production wells in the Olkaria geothermal field is to operate them at temperatures higher than that of amorphous silica saturation to minimize the risk of scaling. With this in mind, both wells OW-703 and OW-911, which are at potential risk of

scaling need to be operated at temperatures no lower than 150 and 160°C, respectively (Figures 12 and 13). This approach, however, limits the amount of energy than can be extracted from the geothermal fluid upon reaching the surface.

5.2 Effects of fluids mixing

Simulations for mixing was done using the PHREEQC program as discussed earlier. Prior to simulating the effect of mixing of injected fluid with aquifer fluid, the chemical composition of the injected fluid at 158°C was obtained using the PHREEQC program. The input data was the chemical analysis results acquired during sampling of injection fluid at the point of reinjection. The results based on the three different databases are comparable, except for the concentration of carbon dioxide. The reason for this variation can be attributed to inconsistencies in the mineral thermodynamics properties in different PHREEQC databases. (Table 4). This variation also affects the pH values (Table 5). Additionally, the

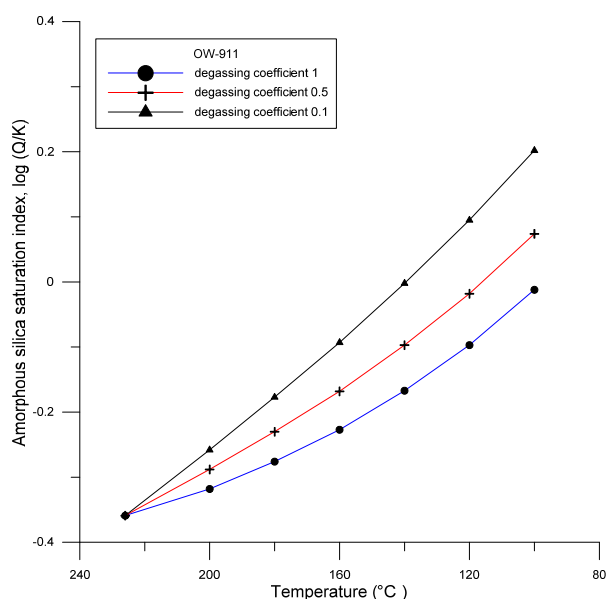


FIGURE 12: Amorphous silica saturation curve for fluids from well OW-911

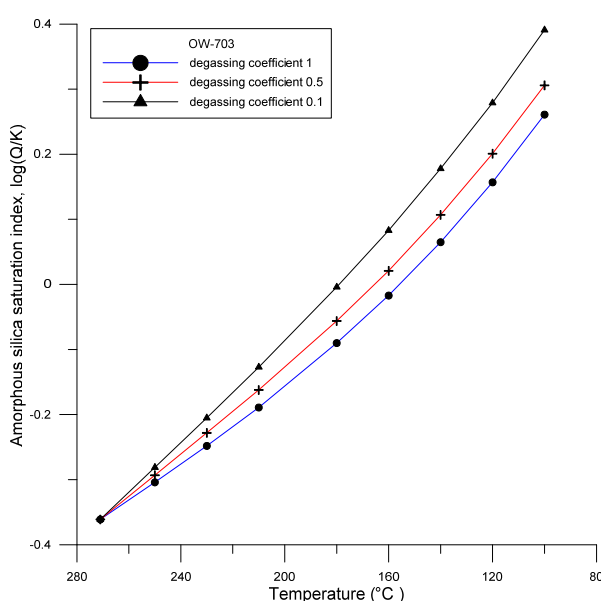


FIGURE 13: Amorphous silica saturation curve for well fluids from well OW-703

state of mineral saturation for calcite, anhydrite and amorphous silica at the point of injection was assessed using the three databases used (Table 6).

It is important to emphasize that the limitations in the number of phases, components, and species contained in the pitzer.dat and phreeqc.dat databases could not allow comparison of the saturation level for amorphous silica with the minteq.v4.dat, without modifications of the database, which was not done during this study.

For the simulation of mixing, three different mixing ratios were assumed between the injected fluid and the aquifer fluid: 1) 1:1 ratio, 2) 0.3:0.7 ratio, and 3) 0.7:0.3 ratio.

TABLE 5: Injected fluid chemistry after simulation in PHREEQC using a reaction temperature of 158°C

Component	OW-703	OW-708	OW-R3
pH/°C in different databases			
pitzer.dat	8.31	8.59	8.46
minteq.v4.dat	7.83	8.19	8.07
phreeqc.dat		8.44	
Ca	0.08	0.38	0.18
Cl	622.86	586.34	659.37
F	26.81	73.19	67.32
K	106.90	112.41	95.91
Li	1.52	1.39	1.38
Mg	0.04	0.02	0.04
Na	529.23	539.35	524.63
SO ₄	21.02	38.85	39.25
SiO ₂	361.44	390.36	398.76
CO ₂	252-257	209-213	196-199

The results for the mixed fluid composition obtained from PHREEQC program was then used as an input in the WATCH speciation program and adiabatically boiled using the downhole measured temperatures as the reference temperature.

Results obtained after adiabatic boiling show that mixing of injected fluid with aquifer fluid in the Olkaria geothermal field has an effect on the saturation state of the fluids with respect to calcite, amorphous silica and anhydrite. The fluids however remain undersaturated with respect to anhydrite.

TABLE 6: Saturation states for injection fluids for calcite, anhydrite and amorphous silica at the point of injection

wells	databases	calcite	anhydrite	Amorphous silica
OW-703	1) pitzer.dat 2) Minteq.v4.dat	undersaturated	undersaturated	N/A supersaturated
OW-708	1) pitzer.dat 2) phreeqc.dat 3) Minteq.v4.dat	supersaturated ~ equilibrium undersaturated	undersaturated	N/A N/A undersaturated
OW-R3	1) pitzer.dat 2) Minteq.v4.dat	~ equilibrium undersaturated	undersaturated	N/A undersaturated

N/A implies that this phase was absent in the chosen database during simulation

The mixing ratio affects the saturation state of the mixed fluid. Fluids in well OW-703 display a slight departure of calcite saturation compared with the initial aquifer saturation state (Figure 14). The mixing causes an increase in the saturation state of calcite with 0.7:0.3 ratio being nearest to that of the aquifer. The effect of mixing of fluids in well OW-703 with respect to amorphous silica, shows that mixing lowers the saturation state of the fluids to a point where it is not seen as a risk during production (Figure 15).

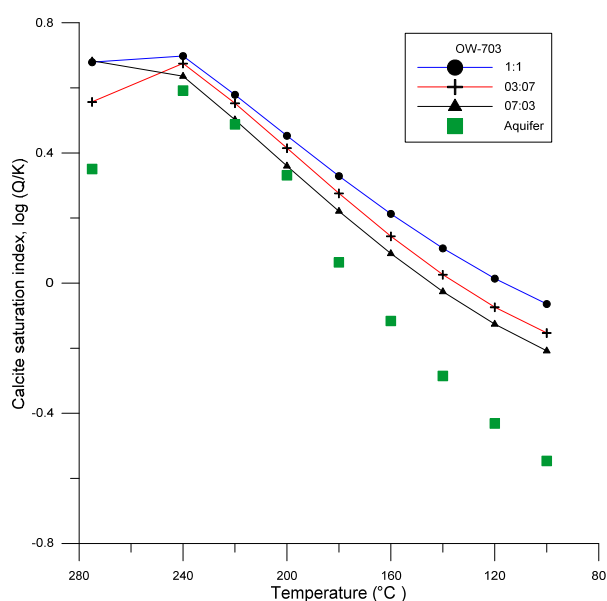


FIGURE 14: Calcite saturation curve for mixed fluids in well OW-703 after adiabatic boiling

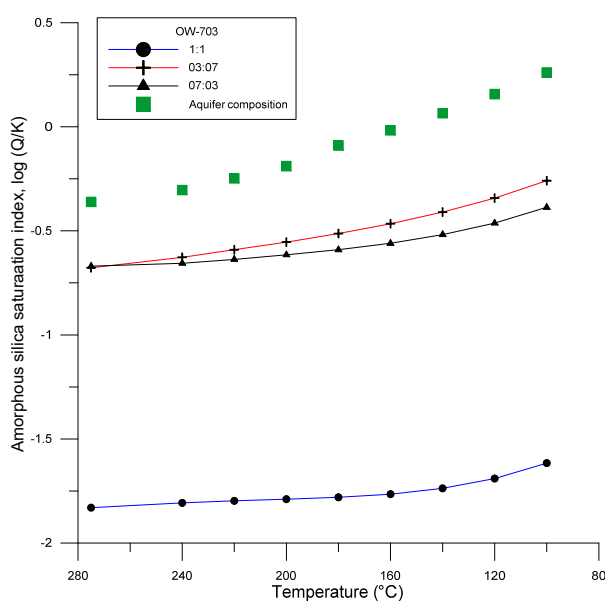


FIGURE 15: Amorphous silica saturation curve after adiabatic boiling of mixed fluids in well OW-703

A similar scenario is seen in fluids in wells OW-708 (Figure 16 and 17) and OW-R3 (Figure 18 and 19). The reason for these changes can be attributed to the change in pH. The injected fluid, which is alkaline with pH values above 9, has both a positive and negative effect on mixing with the dilute neutral aquifer fluid. An increase in the pH value at the aquifer increases solubility of silica whereas the pH dependence solubility of calcite is favoured at low pH values. This would cause the increased solubility of calcite.

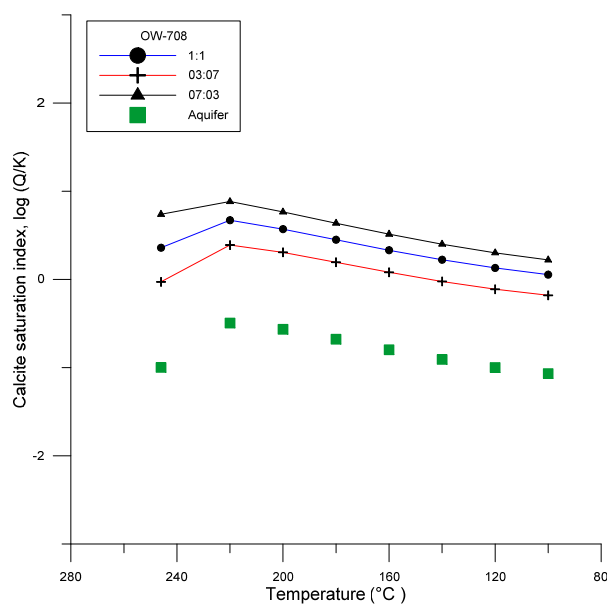


FIGURE 16: Calcite saturation curve after adiabatic boiling of mixed fluids in well OW-708

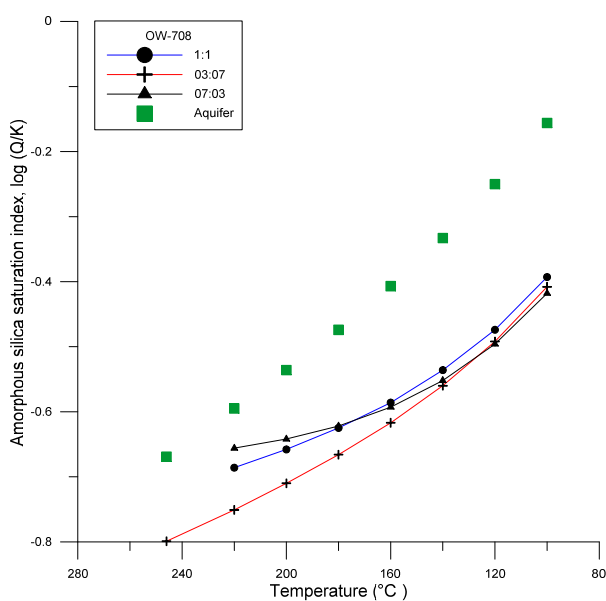


FIGURE 17: Amorphous silica saturation curve after adiabatic boiling of mixed fluids in well OW-708

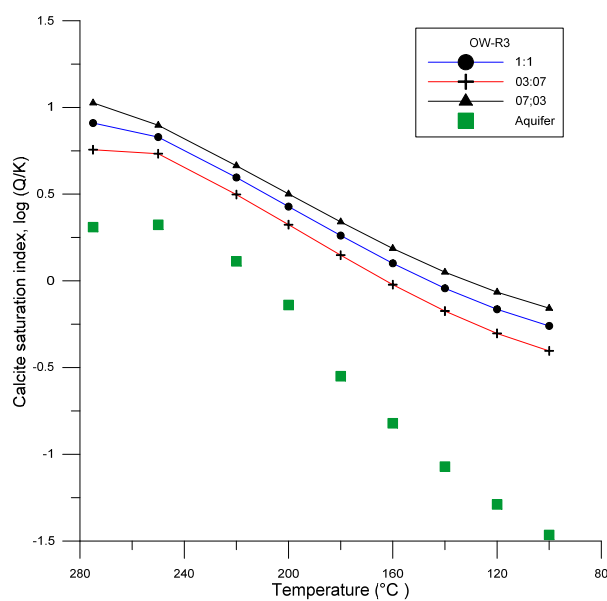


FIGURE 18: Calcite saturation curve after adiabatic boiling of mixed fluids in well OW-R3

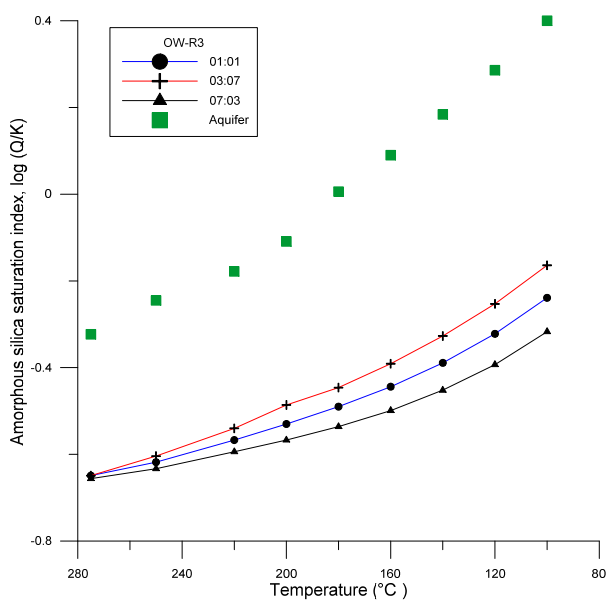


FIGURE 19: Amorphous silica saturation curve after adiabatic boiling of mixed fluids in well OW-R3

6. CONCLUSIONS

The assessment for potential scale formation in hot reinjection wells OW-708, OW-703 and OW-911 in the Olfaria field prior to production show that the fluids from the three wells are undersaturated with respect to anhydrite. Furthermore, fluids from well OW-708 are undersaturated with respect to both calcite and amorphous silica. Fluids from well OW-911, on the other hand, are supersaturated with respect to calcite and the well has a higher risk of scaling compared to well OW-703, which reaches

supersaturation at temperatures above 160°C. The current practice to minimize silica scaling is to operate them at temperatures above that of amorphous silica saturation. With this in mind, well OW-703 and OW-911 need to be operated at temperatures above 150°C and 160°C respectively.

Comparison of the saturation states prior to injection and as a result of mixing of injected fluid with aquifer fluid confirm that mixing of fluids as a result of reinjection in the Olkaria geothermal field has both positive and potentially negative impacts. However, since only mixing of injected fluid and aquifer fluid was simulated in this study, additional of other equilibrium phases to the model may change the outcome, especially when incorporated with residence time of the fluid in the aquifer. Consideration of mixing with other fluids recharging the system may equally change the outcome of the model.

Based on the study, the following recommendations should be considered:

- The limitations in the databases within the PHREEQC program may require comparison with other geochemical modelling programs, which can incorporate the high-temperature conditions common in geothermal reservoirs.
- The practise of converting production wells with low production capacities to reinjection wells should be done with caution and should additionally incorporate thermodynamic information from geochemistry to aid in decision making.
- Well OW-911 should be closely monitored as it poses a risk of calcite scaling problems.
- The absence of aluminium and iron chemical analysis data from the sampled fluids excluded the assessment of possible formation of metal scales such as pyrite, which is a common alteration mineral in the Olkaria geothermal field. Therefore, it will be prudent to routinely analyse the fluids for these components together with other trace elements.
- More studies on how mixing of reinjected fluids with other fluids can modify the mineral saturation indices in the reinjection well and receiving aquifer should be carried out in the Olkaria geothermal field. These studies should also include both thermodynamics and kinetics studies to be able to complement reservoir data on reinjection and also build up the information database, which is helpful when carrying out numerical models.

ACKNOWLEDGEMENTS

My sincere gratitude goes to Mr. Lúdvík S. Georgsson, Director of UNU-GTP, for granting me the opportunity to participate in the UNU-GTP 2016 program. The Kenya Electricity Generating Company for allowing me the six-month study leave. Warmest regards to Mr. Ingimar G. Haraldsson, Mr. Markús A.G. Wilde, Ms. Thórhildur Ísberg, Ms. Málfríður Ómarsdóttir and the UNU 2016 fellows for making my stay in Iceland memorable. To Ms. Rósa S. Jónsdóttir, thank you for always honouring my numerous requests for reading material in time. Special gratitude to my supervisor, Iwona Monika Galeczka, for the guidance, patience and brilliance during the course of my project work. It has been an honour working with you.

Sincere gratitude goes to Mr. Kizito Opondo for supporting this study together with the entire geochemistry section team in Olkaria for the wonderful work they do.

Lastly, my heartfelt gratitude to the people I am honoured to call my family; my mum, Terry, my husband Maj, Mark, the Oworis and the Mbithis together with the wonderful friends whom I consider family, Edwin, Carol, Essy and Irene, for taking time to check on me, for the encouragement and most importantly for taking care of my daughter, Kayla, for the last six months. I can never repay your kindness. With humility, I also thank God for all his blessings and for this journey in my life

REFERENCES

- Ambusso, W.J., 1994: Results of injection and tracer tests in Olkaria-East geothermal field. *Proceedings of the 19th Workshop on Geothermal Reservoir Engineering, Stanford University, California*, 155-160.
- Ármansson, H. and Ólafsson, M., 2006: *Collection of geothermal fluids for chemical analysis*. ÍSOR – Iceland GeoSurvey, Reykjavík, report ISOR-2006/016, 17 pp.
- Arnórsson, S., 2000: Injection of waste geothermal fluids: chemical aspects. *Proceedings of the World Geothermal Congress, 2000, Kyushu-Tohoku, Japan*, 3021-3024
- Arnórsson, S., Stefánsson, A., and Bjarnason, J.Ö., 2007: Fluid-fluid interaction in geothermal systems. *Reviews in Mineralogy & Geochemistry*, 65, 229-312.
- Axelsson, G., 2008: Production capacity of geothermal systems. In: Fridleifsson, I.B., Holm, D.H., Wang Kun and Zhang Baiming (eds.), *Workshop for Decision Makers on Direct Heating Use of Geothermal Resources in Asia, Tianjin, China*. UNU-GTP, TBLRREM and TBGMED, CD, 14 pp.
- Axelsson, G., Arnaldsson, A., Ármannsson, H., Árnason, K., Einarsson, G., Franzson, H., Fridriksson, T., Gudmundsson, G., Gylfadóttir, S.S., Halldórsdóttir, S., Hersir, G.P., Mortensen, A.K., Thordarson, S., Jóhannesson, S., Bore, C., Karingithi, C., Koech, V., Mbithi, U., Muchemi, G., Mwarania, F., Kizito, O., and Ouma, P., 2013: Updated conceptual model and capacity estimates for the Greater Olkaria geothermal system, Kenya. *Proceedings of the 38th Workshop on Geothermal Reservoir Engineering, Stanford University, CA*, 16 pp.
- Bjarnason, J.Ö., 2010: *The chemical speciation program WATCH, version 2.4*. ÍSOR – Iceland GeoSurvey, Reykjavík, website: www.geothermal.is/software.
- Brown, K., 2013: *Mineral scaling in geothermal power production*. UNU-GTP, Iceland, report 39, 30 pp
- Chorowicz, J., 2005: The East African Rift System. *J. African Earth Sciences*, 43, 379-410.
- D'Amore, F., and Arnórsson, S., 2000: Geothermometry. In: Arnórsson, S (ed.), *Isotopic and chemical techniques in geothermal exploration, development and use. Sampling methods, data handling, interpretation*. International Atomic Energy Agency, Vienna, 152-199.
- Fournier, R.O., and Potter, R.W., 1982: An equation correlating the solubility of quartz in water from 25° to 900°C at pressures up to 10,000 bars. *Geochim. Cosmochim. Acta*, 46, 1969-1973.
- Giggenbach, W.F., 1981: Geothermal mineral equilibria. *Geochim. Cosmochim. Acta*, 45, 393-410.
- Henley, R.W., 1983: pH and silica scaling control in geothermal field development. *Geothermics*, 12, 307-321.
- Kaya, E., and Zarrouk, S.J., and O'Sullivan M.J., 2011: Reinjection in geothermal fields: A review of worldwide experience. *Renewable and Sustainable Energy Reviews*, 15, 47–68.
- KenGen Database, 2016: *Unpublished internal data*. KenGen, Kenya.
- KPC, 1994: *Brief of geothermal energy development at Olkaria Kenya. Status as in March*. Kenya Power Co., Kenya, unpubl. report.
- Lagat, J.K., 2004: *Geology, hydrothermal alteration and fluid inclusion studies of the Olkaria Domes geothermal field, Kenya*. University of Iceland, MSc thesis, UNU-GTP, Iceland, report 1, 79 pp.
- Lagat, J.K., 2010: Hydrothermal alteration mineralogy in geothermal fields with case examples from Olkaria Domes geothermal field, Kenya. *Presented at "Short Course V on Surface Exploration for*

Geothermal Resources”, UNU-GTP, KenGen and GDC, Lake Naivasha, Kenya, UNU-GTP SC-10, 24 pp.

Macdonald, R., and Scaillet, B., 2006: The central Kenya peralkaline province: Insights into the evolution of peralkaline salic magmas. *Lithos*, 91, 59-73.

Mariaria, J., 2011: Hot and cold reinjection: Olkaria experience. *Proceedings of the Kenya Geothermal Conference 2011, Nairobi*, 12 pp.

Mibei, G.K., 2012: *Application of alteration minerals and thermal fluid geochemistry in geothermal conceptual modeling, case study of Olkaria geothermal field in Kenya*. University of Nairobi, Kenya, MSc thesis, 90 pp.

Mwangi, M.N., 2000: Country update report for Kenya 1995-1999. *Proceedings of the World Geothermal Congress 2000, Kyoto-Tohoku, Japan*, 327-333.

Mwawongo, G.M., 2005: Kenya's geothermal prospects outside Olkaria: Status of exploration and development. Lecture 4 in: Mwangi, M.N. (lecturer), *Lectures on the geothermal in Kenya and Africa*. UNU-GTP, Iceland, Report 4, 41-50.

Naylor, W.I., 1972: *Geology of the Eburru and Olkaria prospects*. U.N. Geothermal Exploration Project, report.

Njathi, D.W., 2012: Borehole geology and hydrothermal mineralisation of well OW-911A, Olkaria Domes geothermal field, Central Kenya Rift Valley. Report 25 in: *Geothermal training in Iceland 2012*. UNU-GTP, Iceland, 573-600.

Odongo, M.E.O., 1993: A geological review of Olkaria geothermal reservoir based on structure. *Proceedings of the 15th New Zealand Geothermal Workshop, Auckland, NZ*, 169-173.

Ofwona, C.O., 2002: *A reservoir study of the Olkaria East geothermal system, Kenya*. University of Iceland, MSc thesis, UNU-GTP, Iceland, report 1, 74 pp.

Omenda, P.A., 1998: The geology and structural controls of the Olkaria geothermal system, Kenya. *Geothermics*, 27-1, 55-74.

Opondo, K.O., 2015: Carbonate scale formed in well OW-202 in Olkaria central field, Kenya *Proceedings of the World Geothermal Congress 2015, Melbourne, Australia*, 10 pp.

Otieno, V.O., 2016: *Borehole geology and sub-surface petrochemistry of the Domes area, Olkaria geothermal field, Kenya, in relation to well OW-922*. University of Iceland, MSc thesis, UNU-GTP, Iceland, Report 2, 94 pp.

Ouma, P.A., 2007: Geothermal exploration and development of the Olkaria geothermal field. *Paper presented at "Short Course II on Surface Exploration for Geothermal Resources"*, UNU-GTP, KenGen and GDC, Lake Naivasha, Kenya, UNU-GTP SC-05, 17 pp.

Parkhurst, D.L., and Appelo, C.A.J., 2013: *Description of input and examples for PHREEQC (vs. 3) - A computer program for speciation, batch-reaction, one-dimensional transport, and inverse geochemical calculations*. US Geological Survey, Techniques and Methods, Book 6, A43, 497 pp.

Riaroh, D., and Okoth, W., 1994: The geothermal fields of the Kenya rift. *Tectonophysics*, 236, 117-130.

Serpen, U., and Aksoy N., 2005: Reinjection problems in overpressured geothermal reservoirs. *Proceedings of the 30th Workshop on Geothermal Reservoir Engineering, Stanford University Stanford, CA*, 8 pp.

Wambugu, J.M., 1996: Assessment of Olkaria-Northeast geothermal reservoir, Kenya based on well discharge chemistry. Report 20 in: *Geothermal training in Iceland 1996*. UNU-GTP, Iceland, 481-509.



UNITED NATIONS
UNIVERSITY

UNU-GTP

Geothermal Training Programme

Orkustofnun, Grensasvegur 9,
IS-108 Reykjavik, Iceland

Reports 2016
Number 25

RESISTIVITY SURVEYING IN GEOTHERMAL EXPLORATION WITH AN APPLICATION TO THE EYJAFJÖRDUR LOW-TEMPERATURE AREA, N-ICELAND

Sarantsetseg Lkhagvasuren

Institute of Astronomy and Geophysics

Mongolian Academy of Science

P.O. Box 152, Ulaanbaatar

MONGOLIA

sarantsetseg@iag.ac.mn

ABSTRACT

Geothermal exploration involves geology, geochemistry and geophysics. In geophysical exploration, resistivity surveying plays the most important role in delineating the reservoir. The parameters that control the geothermal system show a strong response to electrical resistivity. The resistivity methods that are mostly used in geothermal exploration in Iceland are TEM (Transient ElectroMagnetics) and MT (MagnetoTellurics). The application of these methods is discussed in this report together with an example from the Eyjafjörður low-temperature area in N-Iceland. The resulting resistivity cross-sections and resistivity depth slices show a shallow lying low-resistivity layer and a deep lying low-resistivity anomaly towards the end of the cross-sections. The result of this work has been compared with results from Flóvenz and Karlsdóttir (2000) which interpreted TEM data from the same area. The results are also compared with borehole data and stratigraphy.

1. INTRODUCTION

Geothermal manifestations are commonly seen along plate boundaries and faults. A good example is Iceland, which is sliced or crossed by the North America and Eurasian plate's boundary. Geothermal systems are controlled by temperature, pressure, porosity, permeability and chemical composition of the fluid. These parameters give a response to electrical resistivity. Because of this, resistivity methods are the most powerful method used to find and delineate geothermal areas. The resistivity model of the Eyjafjörður low-temperature geothermal area is presented through 1D joint inversion of the MT (magnetotelluric) and TEM (transient electromagnetic) data. This work includes the two parts. Firstly, the intention is to give a short introduction to geophysical exploration methods that are widely used in geothermal exploration. This might be useful for future geothermal exploration in Mongolia. Secondly, resistivity of rocks is discussed and why resistivity methods are the most beneficial ones in geophysical exploration. The main part of this project work is the application of the MT and TEM methods in exploration of low-temperature geothermal areas. In TEM, an electrical current is injected into a source loop and then turned off abruptly. Afterwards, voltage is registered in a receiver loop as a function of time. MT uses natural fluctuations of the Earth's electromagnetic field – the electric and magnetic fields are registered in orthogonal directions. Data processing gives an apparent resistivity curve and a

resistivity model of the subsurface is obtained from an inversion process. Finally, the model is used for geothermal interpretation. These methods have been used effectively in geothermal exploration in Iceland for decades. Finally, the theory and application of the MT and TEM methods, respectively, are explained.

2. GEOPHYSICAL METHODS IN GEOTHERMAL EXPLORATION

According to the origin of field source, geophysical methods are divided into two groups that are called natural field and artificial field (controlled source) methods or passive and active methods. The natural field methods utilize the gravitational, magnetic and electromagnetic field of the Earth, searching for local perturbations of these naturally occurring fields that may be caused by concealed geological features of economic or other interest (Kearey et al., 2002). Geophysical methods are often used in combination. The objective of geophysics is to locate or detect the presence of subsurface structures or bodies and determine their size, shape, depth and physical properties (density, velocity, porosity and so on).

2.1 Seismic surveying

Seismic waves transfer energy through the ground. There are two types of seismic waves, body waves and surface waves. According to the polarization of particles, body waves are classified into primary (P) waves and secondary (S) waves. Surface waves are called Rayleigh (R) waves and Love (L) waves. Seismic waves travel through the earth's interior and indicate different elastic properties of the rock and composition of the rock with different density through their velocities. Equations 1 and 2 show their relationship with density and elastic coefficients of the rock.

$$V_P = \sqrt{\frac{\lambda + 2\mu}{\rho}} = \sqrt{\frac{K + \frac{4}{3}\mu}{\rho}}; V_S = \sqrt{\frac{\mu}{\rho}} \quad (1)$$

where K = Bulk modulus (modulus of incompressibility), ratio of pressure change to relative volume change;
 μ = Shear modulus (modulus of rigidity), equal to 0 for molten rocks;
 ρ = Density (kg/m³);
 λ = Lamé parameter.

The V_P/V_S ratio can be expressed as a function of the Poisson's ratio (σ). Poisson's ratio can be measured from seismic wave arrivals:

$$\frac{V_P}{V_S} = \sqrt{\frac{2(1 - \sigma)}{1 - 2\sigma}} \quad (2)$$

In geothermal environment, Poisson's ratio is typically in the range of 0.25 to 0.3 for normally saturated rock (Hersir and Björnsson, 1991).

2.1.1 Active seismic surveying

Seismic surveying has developed within oil and gas exploration, coupled with development of advanced electronic and data technology. According to the source of the energy, seismic surveying is divided into two methods, active and passive seismics. According to the wave propagation path, they may be classified into reflection and refraction methods (Lucius et al., 2006). Except for oil and mineral exploration, seismic methods are used to determine the depth and lateral extent of layers, thickness and

volume of deposits, and thickness of overburden. Seismic surveys record the ground motion caused by a known source in a known location (Kearey et al., 2002) and also with known magnitude. In active seismic surveying, seismic waves are caused by a controlled source, explosion, drop hitter, hammer or air guns and propagate through the subsurface. In a homogeneous earth, energy transmits by seismic waves from the source in all directions. Gradually, the seismic wave attenuates. In a heterogeneous and layered earth, seismic waves refract, reflect, diffract, convert and transmit between rock layers. Seismic traces are recorded in geophones mostly at the surface. Geophones are detectors of the seismic waves and usually laid out on the ground along a straight line. The electrical signal from the geophones is converted into digital values using modular 12-, 24- or 48-channel, high resolution, signal-enhancement seismographs. Seismographs are often linked together to increase the number of geophones. Portable computers record seismic waveforms (Lucius et al., 2006). Using the travel times of the seismic waves, a velocity model of the subsurface is obtained.

Generally, seismic surveying is divided into refraction methods, which give good information about stratigraphy, faults, intrusions and geological structure (Hersir and Björnsson, 1991) and reflection method, which is the main exploration tool in oil and gas exploration and very well suited to detect in details the interior of the sedimentary basins. However, in volcanic areas, the reflection method is expensive and not properly used because of the lack of reflector boundary and scattering due to chaotic structures. If a geothermal system is emplaced in a sedimentary basin, it is applicable (Flóvenz et al., 2012).

2.1.2 Passive seismic surveying – Seismological methods

Seismology is the science that studies earthquakes and seismic waves that travel through and around the earth. Earthquakes are mighty manifestations of abrupt releases of strain energy accumulated during extensive time intervals in the upper part of the earth. Various types of seismic waves radiate from the earthquake to all directions through the earth's interior and are recorded at large distances by sensitive instruments placed on or near the earth's surface (Kulhanek, 1988). An earthquake is classified into tectonic earthquake, volcanic earthquake, etc. Earthquakes happen along plate boundaries, faults and fissures. Volcanic earthquakes frequently happen in a volcanically active zone. A volcanically active zone is certainly found in Iceland where many volcanic eruptions happen. Some of the volcanoes are still active while others are dormant. Seismic stations are installed around the island and in study areas. Time series data are recorded at the stations and transmitted to a data centre, where locations of earthquakes are determined automatically or manually.

The main parameters of the earthquake are the origin time (t_0), epicentre (φ, λ) which is the end point of the vertical line starting from the hypocentre, depth (h) and the magnitude which is the amount of energy that is released by the earthquake. The seismic velocity provides information on the physical properties and compositions of the earth's layers and discontinuities.

The P-wave velocity is always considerably higher than the S-wave velocity. In seismic surveying, compressional waves are mostly used (Burger et al., 2006). Passive seismic surveying is used to investigate the earth's internal structure and monitor the seismic activity in the area. Earthquakes are induced during geothermal exploitation. Effects of exploitation of a geothermal reservoir can be monitored through micro-seismic activity (Mariita, 2011). Sometimes it is hard to say what causes an earthquake. Was it natural or induced? Passive seismic methods are widely used in geothermal exploration and monitoring (Samaranayake, 2015).

2.2 Gravity surveying

The basic theory of gravity surveying is governed by the law of gravitation. According to Newton's law of gravitation, the gravity force is directly related to the masses, m_1 and m_2 and reversely related to the distance squared, r^2 between the two bodies as expressed in Equation 3:

$$F = G \frac{m_1 m_2}{r^2} \quad (3)$$

where G = The universal gravitational constant $G = 6.67 \cdot 10^{-11} \text{ [Nm}^2\text{/kg}^2\text{]}$.

In gravity surveys, the gravitational acceleration $[\text{m/s}^2]$ is measured. The average gravitational acceleration (gravity) at the surface of the earth is $g \approx 9.81 \text{ m/s}^2$. Gravity varies by rock density, elevation and the earth's movement. Gravity, g is same for all bodies at a given place on Earth. It is expressed by Equation 4 given by Galileo:

$$g = \frac{F}{m} = \frac{G M_{\text{earth}}}{r^2} \quad (4)$$

Density varies for different types of rocks in the earth (Hersir and Björnsson, 1991). Lateral density variations in the subsurface cause gravity anomalies (Kearey et al., 2002). Gravity is measured at one place relative to a reference base station. In order to obtain useful information from the observed data that shows subsurface density variations at each gravity station, the following corrections have to be applied on the gravity readings before interpretation:

- *Tidal correction* (g_M) – measured gravity has to be corrected for the tidal effects (attraction of moon and sun) and drift in the gravimeter.
- *Free air correction* (C_{FA}) – reduces the gravity field from the altitude of the measuring site to sea level. Most on-land surveys are done above sea level, therefore this correction increases the gravity reading.
- *Bouguer correction* (C_B) – removes the effect of the rock mass between the measuring site and sea level. This correction decreases the gravity reading.
- *Terrain correction* (C_T) – topography variations (mountains or valleys) near each station affect gravity. The correction is carried out by estimating the differences between the elevation of the station and its surrounding. Terrain correction always reduces the gravity reading: mass excess above the station (mountains) decreases the gravity reading and mass deficiencies below (valleys) lead to overcorrection in the Bouguer correction and must be corrected for in the terrain correction. Thus, terrain corrected reading will always be higher than the measured values.
- *Latitude correction* (g_N) – correction that accounts for Earth's elliptical shape and rotation. Remember the gravity increases when moving towards the poles.

Having done all these corrections, the corrected gravity anomaly is called Bouguer anomaly, Δg_B , and expressed as:

$$\Delta g_B = g_M + C_{FA} - C_B + C_T - g_N \quad (5)$$

These corrections are discussed e.g. in Kearey et al., 2002; Hersir and Björnsson, 1991; Lichoro, 2014. Gravity anomalies are created by the lateral density contrasts between a body of rock and its surroundings. Density $\Delta\rho$ is given in Equation 6:

$$\Delta\rho = \rho_1 - \rho_2 \quad (6)$$

In Bouguer and terrain corrections and interpretation of the gravity anomaly, knowledge of rock density plays an important role. Rock density depends on its composition and porosity (Kearey et al., 2002).

Gravity measurements are a typical structural method that is used to detect geological formations with different densities in geothermal areas (Hersir and Björnsson, 1991). In gravity surveying, subsurface geological investigation is carried out on the basis of variations in the earth's gravitational field generated by differences of density between subsurface rocks. Since, gravity decreases as elevation increases, the elevation of each station has to be measured with an error of not more than about 10 cm. Differential GPS provides sufficient accuracy of the elevation evaluation.

2.3 Magnetic surveying

The magnetic field of the earth is imagined like a field from a large bar magnet located near the centre of the earth, a dipole field. The magnetic field is created by fluid currents in the conductive outer core. The magnetic lines are almost vertical close to the poles and horizontal near the equator (Figure 1). The earth's magnetic field is not a pure dipole field but contains higher order pole component (80% dipole, 20% higher order poles). The magnetic field vectors around the earth are defined to point in the direction from south to north. Magnetic properties are different for the different rock types. The magnetic field B_0 can induce a magnetic field B_M (magnetization field) in a material, which is proportional to the undisturbed external field B_0 ($B_M = kB_0$):

$$B = B_M + B_0 = (1 + k)B_0 = \mu B_0 \quad (7)$$

where, $\mu = 1 + k$ is the magnetic permeability, which is the relative ability of a material to create a local magnetic field while k is the magnetic susceptibility.

Minerals are divided into paramagnetic ($0 < k < 10^{-5}$), diamagnetic where the susceptibility is smaller and has a negative value, ferrimagnetic ($k \approx 1-4$) and ferromagnetic ($k \approx 10^1-10^6$). The magnetic field at any point on the earth's surface is a vector quantity defined by its total intensity and direction. The total field vector, \mathbf{B} , is defined by its intensity, its inclination I , which is the angle the vector makes with a horizontal plane, and its declination D , which is the angle the horizontal component \mathbf{H} of the total-field vector makes with geographic north. This is demonstrated in Figure 1.

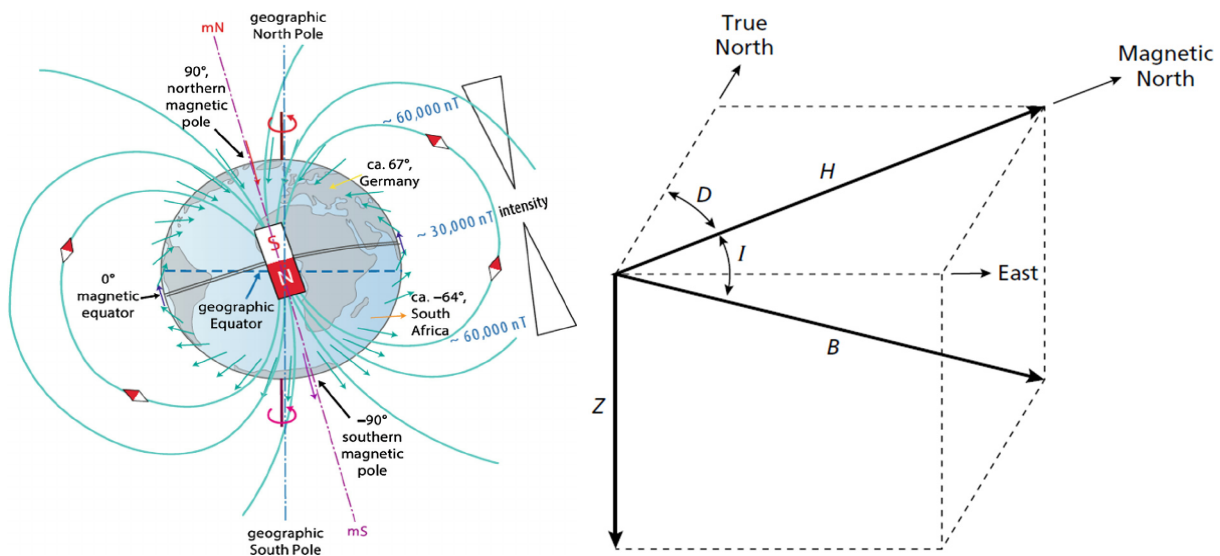


FIGURE 1: The elements of the earth's magnetic field: \mathbf{B} = total-field vector, \mathbf{H} = horizontal component, Z = vertical component, D = declination, and I = inclination (Kearey et al., 2002)

\mathbf{B} can be resolved into a vertical component Z and a horizontal component \mathbf{H} . The vertical plane containing \mathbf{F} , Z and \mathbf{H} is a magnetic meridian. \mathbf{H} can also be resolved into horizontal components directed toward geographic north H_x and geographic east H_y . Magnetic data collected at any points on the earth's surface can be displayed on a map of the world as contours of \mathbf{B} , I and D . Observations show that values of each element of the earth's magnetic field are permanently changing from hour to hour and from year to year. Magnetic surveying is an indirect method or structural method. Magnetics can be carried out on the ground and as aeromagnetics. Generally, magnetic methods are used to investigate regional geological structures.

Numerous aeromagnetic surveys have been completed over geothermal areas. Magnetic lows can be due to hydrothermal alteration of the geothermal system as confirmed by the surveys. Rocks lose their

magnetic properties at temperatures above Curie temperature (demagnetization). Detailed ground-magnetic surveys are used in Iceland to trace narrow linear features like dykes and faults where the basement is covered with soil (Hersir and Björnsson, 1991). Ground magnetic surveys are usually performed over relatively small and previously defined areas (Kearey et al., 2002).

2.4 Thermal methods

Thermal methods measure directly the temperature or heat of the geothermal system. There are basically the following four methods (Hersir and Björnsson, 1991):

- Temperature measurement; direct interpretation, mapping;
- Geothermal gradient that shows vertical variation of the temperature measured in soil or in shallow drillholes;
- Heat flow, that is calculated from the temperature gradient and thermal conductivity;
- Heat budget, that is done by measurement of spring flow and steam output and/or integrating areal heat flow.

The main heat exchange mechanisms are conduction and convection. Radiation in the earth does not play an important role for geothermal systems.

Conduction heat transfer is expressed by Equation 8:

$$Q_{cond} = -k \cdot \frac{\Delta T}{\Delta Z} \quad (8)$$

where k = Thermal conductivity (W/m °C), a constant of each material;
 $\Delta T/\Delta Z$ = Thermal gradient, defining temperature variations with depth, its distribution is very important to achieve an understanding and to delineate the geothermal resource on a regional and local scale.

Convection is heat transfer by motion of the mass, for example, natural circulation of hot water which is driven by a density gradient in the fluid.

2.5 Electrical resistivity of rocks - resistivity methods

2.5.1 Resistivity of rocks

The specific resistivity is defined by Ohm's law:

$$\mathbf{E} = \rho \mathbf{j} \quad (9)$$

where ρ = Resistivity (Ωm);
 \mathbf{E} = Electric field magnitude (V/m);
 \mathbf{j} = Current density (A/m^2).

The reciprocal value of resistivity is called conductivity $\sigma = 1/\rho$ (S/m or $1/\Omega\text{m}$).

Specific resistivity can also be defined as the ratio of the potential difference ΔV (V) to the current I (A), across a material which has a cross-sectional area of 1 m^2 and is 1 m long, or:

$$\rho = \frac{\Delta V A}{I L} = R \frac{A}{L} \quad (10)$$

where A = Cross-sectional area (m^2);
 L = Length (m).

Electrical conductivity in minerals takes place by the movement of electrons and ions. Conduction of electricity is mostly through groundwater present inside the pores of the rocks and along surface layers at the contact of rocks and solution (Hersir and Arnason, 2009).

2.5.2 Main factors affecting resistivity of water-bearing rocks

The specific resistivity of rocks is controlled by important parameters of the geothermal system like temperature, fluid type and salinity, porosity, the composition of the rocks, and the presence of alteration minerals.

Temperature plays a key role in altering the bulk resistivity of rock material. An aqueous environment present in the rock matrix contributes to this effect. The conductivity of pore fluid varies according to the formula given by Dakhnov (1962):

$$\sigma_w = \sigma_{wo}(1 + \alpha(T - T_0)) \quad (11)$$

where σ_w = Conductivity of the pore fluid (S/m) at temperature of T (°C);
 σ_{wo} = Conductivity of the pore fluid (S/m) at reference temperature of T_0 (°C);
 T = Temperature (°C);
 α = Temperature coefficient of resistivity, i.e. $\alpha = 0.023/^\circ\text{C}$ for $T_0 = 25^\circ\text{C}$.

Equation 11 is valid only for a temperature range of 0-200°C, the trend starts to reverse as the temperature increases further (Flóvenz et al., 2012).

Porosity and permeability: The fractional porosity ϕ_t of a material is defined as the ratio of the pore volume and the total volume of the material. There are primarily three types of porosity in rocks. Intergranular – pores are formed like spaces between particles in sediments and volcanic ash; joints - fractures – pores are formed by a net of fine fissures caused by tectonics or cooling of the rock; and vugular porosity – big and irregular pores have been formed because of the dissolution of material, especially in limestone (Flóvenz et al., 2012). The fractional porosity of rock is given in Equation 12:

$$\phi_t = \frac{V_\varphi}{V} \quad (12)$$

where ϕ_t = Fractional porosity;
 V_φ = Volume of the voids;
 V = Total volume of the material.

The porosity of the rock matrix and its pore connectivity or effective porosity has a large effect on resistivity. Porosity is described as primary where interstices are originally present in the rock matrix and secondary where void spaces are created as a result of external factors such as pressure and erosion (Todd and Mays, 2005). At this point, it is noteworthy to include Archie's law (Archie, 1942) which is an empirical law relating bulk resistivity to pore fluid resistivity and porosity as expressed in Equation 13:

$$\rho = \rho_w a \phi_t^{-n} \quad (13)$$

where ρ = Bulk (measured) resistivity (Ωm);
 ρ_w = Resistivity of the pore fluid (Ωm);
 a = An empirical parameter depending on porosity type, usually around 1;
 ϕ_t = Porosity in proportions of total volume;
 n = Cementing factor which is empirically determined; usually around 1-2.

Equation 13 may be simplified and expressed as shown in Equation 14:

$$\rho = \rho_w F \quad (14)$$

where F = The formation factor.

Permeability depends on porosity type and its connection. For example, a rock might be highly porous but the pores are isolated, then the rock would have no permeability and it will have high resistivity. The degree of interconnected pores within the rock is described as effective porosity. The characteristics of the host material, the viscosity and pressure of the fluid also affect the rate at which the fluid will flow (Lee et al., 2006).

Salinity is a measure of ions (salts) dissolved in water. The salinity in the groundwater varies and it affects the resistivity of the subsurface. The bulk resistivity of rocks in low-temperature geothermal areas is mostly controlled by the resistivity of the pore fluid, which is dependent on the salinity of the fluid. As the amount of dissolved solids in the pore fluid increases, the conductivity increases. The conductivity σ of a solution is a function of the salinity (the concentration of the ions) and the mobility of the ions in the solution. This is shown in Equation 15:

$$\sigma = \frac{1}{\rho} = F \cdot (c_1 q_1 m_1 + c_2 q_2 m_2 + \dots) \quad (15)$$

where σ = Conductivity (S/m);
 F = Faraday's number ($9.649 \cdot 10^4$ C/mole);
 c_i = Concentration of ions;
 q_i = Valence of ions;
 m_i = Mobility of the different ions.

2.5.3 DC methods

In the DC (direct current) resistivity method, a constant current I is injected into the earth through a pair of electrodes at the surface while the potential difference is measured at two receiver electrodes. The current creates a potential field which depends on the resistivity of the earth which can be inferred from the measured electric field (potential difference between the two electrodes) and the injected current. The most common DC methods are Schlumberger soundings, Head-on profiling, dipole soundings and profiling (Georgsson, 2009). Resistivity measurements are used to delineate geothermal systems, locate aquifers and sometimes to estimate porosity and physical conditions within the geothermal system. Electrical sounding methods reveal resistivity of the subsurface as a function of depth at a fixed location. Electrical profiling method can show lateral resistivity changes along a profile.

Schlumberger sounding: One type of electrode configuration of the DC method is the Schlumberger sounding, a conventional DC method which has been used widely (Georgsson and Karlsdóttir, 2007). In the Schlumberger configuration, two potential electrodes (M and N) and two current electrodes (A and B) are located along a straight line and connected to the voltage receiver and current transmitter, respectively. The distance between the A and B electrodes is symmetrically extended from the midpoint O (Hersir and Björnsson, 1991) to achieve greater depth of penetration. The setup of a Schlumberger sounding is illustrated in the Figure 2.

A current I is injected into the ground through electrode A, and the circuit is closed at electrode B. As the current travels through different conductivity media (Figure 2), the potential difference between the M and N electrodes is measured in the receiver. Apparent resistivity of the ground ρ_a is computed through Equation 16. Here is $AO = OB = S$ and $MO = ON = P$.

$$\rho_a = \frac{\pi S^2 - P^2}{2P} \frac{\Delta V}{I} \quad (16)$$

where ΔV = Potential difference;
 I = Injected current;
 $K = \frac{\pi S^2 - P^2}{2P}$ is a geometrical factor.

The apparent resistivity ρ_a is an average resistivity of the ground layers through which the current passes. The depth of penetration increases with increasing distance between the current electrodes and higher current must be injected. When the distance increases, potential difference decreases. The apparent resistivity is interpreted as specific resistivity and becomes a function of depth only applying 1D interpretation. If resistivity changes in one horizontal direction as well, 2D interpretation is needed.

The head-on profiling method can detect narrow near-vertical resistivity structures like faults, dykes and fractures. These structures are often correlated to upflow of geothermal fluid. The setup is the same as for Schlumberger soundings but it has an additional current electrode C placed far away from the A and B electrodes. A current is injected into the ground three times closing the circuit AC, BC and AB. The potential difference between M and N is measured in each case. Instead of increasing the current electrode spacing, like in Schlumberger soundings, all electrodes except C are moved along the profile. Resistivity values are calculated at each point for the three cases. The head-on profiling method is described by Flóvenz (1984).

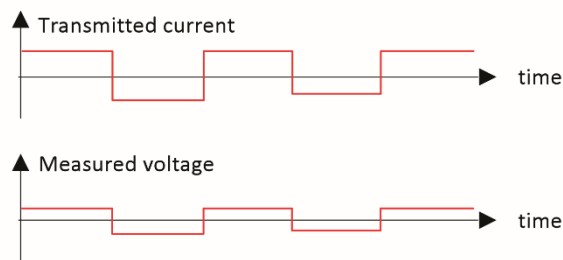
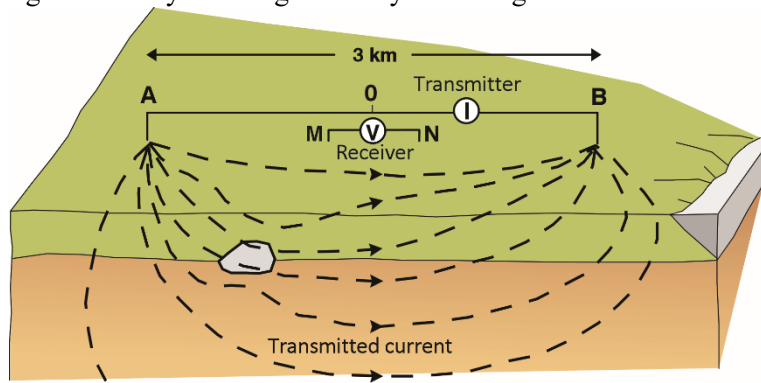


FIGURE 2: The setup of a Schlumberger sounding measurement (Flóvenz et al., 2012)

2.5.4 EM-methods

MT and AMT are natural source electromagnetic methods. AMT (audio-electromagnetics) refers to audio frequencies between 100 and 10 kHz. TEM is a controlled-source electromagnetic method (central loop and grounded dipole).

TEM (transient electromagnetic) method.

The TEM method is an active method used widely in geothermal exploration in Iceland. A constant current is injected into a transmitter loop from a transmitter that is fed by a generator or batteries. According to Biot-Savart's law, a constant magnetic field of known strength is created (Figure 3).

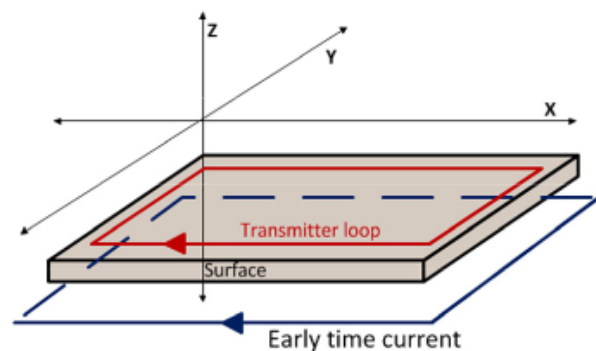


FIGURE 3: Current propagation at early times (from Badilla, 2011; modified from Rowland, 2002)

A receiver loop (big flexible loop or small coil) is connected to the receiver and placed at the centre of the transmitter loop. Then the current is abruptly turned off. The current and magnetic field decrease downwards and outwards and the magnetic field induces a current in the ground simultaneously in the resistive media that the current travels through at late times. (Figure 4).

After the turn off (the current turns off linearly) measurements start. During the decay of the magnetic field, a current is induced in the ground. According to Faraday's law, induced voltage in the receiver coil creates a decaying secondary magnetic field. The rate and magnitude of the decaying secondary magnetic field depends on the resistivity of the ground. Resistivity of the ground can be estimated by measuring the voltage that is registered in the receiver coil. Measurements are done in the big flexible loop (effective area of 57,000 m²) and a small loop (effective area of 100 m²) using a frequency of 2.5 and 25 Hz, respectively. The current and frequency are fed by the operator into the equipment. The turn off time is written down in the field book together with other information. Generally, the source loop is 200 × 200 m square and the transmitted current is 20-25 A.

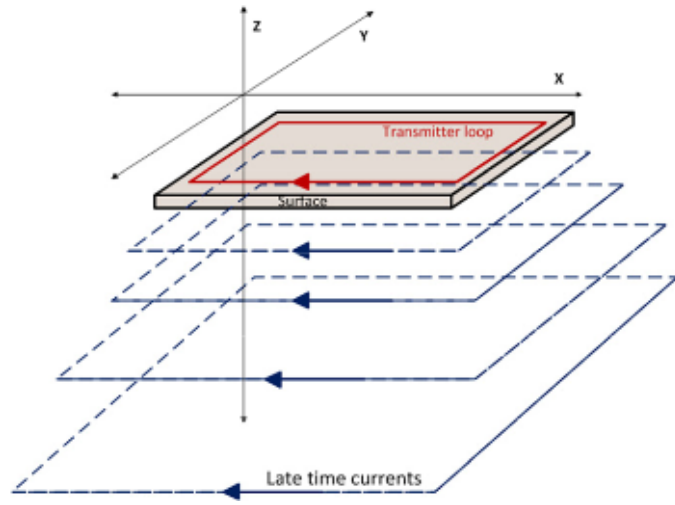


FIGURE 4: Current propagation at late times (from Badilla, 2011; modified from Rowland, 2002)

The depth of penetration of the TEM method depends on the resistivity beneath the sounding as well as on the setup geometry, the generated current and its frequency. The depth of penetration increases with time after the current turn-off (Flóvenz et al., 2012). The depth of penetration in the central loop TEM sounding depends on how long the induction in the receiver coil can be traced before it is drowned in noise. The induced voltage in the receiver coil in a homogeneous half space of conductivity σ at late time is given as (Árnason, 1989):

$$V(t, r) = I_0 \frac{C (\mu_0 \sigma r^2)^{3/2}}{10\pi^{1/2} t^{5/2}} \quad (17)$$

where, $C = A_r n_r A_s n_s \frac{\mu_0}{2\pi r^3}$;

- n_r = Number of windings in the receiver coil;
- A_s = Area of the transmitting loop (m²);
- A_r = Area of the receiver coil (m²);
- n_s = Number of windings in transmitting loop;
- t = Time elapsed after the current in the transmitter is turned off (s);
- μ_0 = Magnetic permeability in vacuum (Henry/m);
- $V(t, r)$ = Induced voltage (V);
- r = Radius of the transmitter loop (m);
- I_0 = Current in the transmitting loop (A).

The apparent resistivity can be derived from Equation 17:

$$\rho_a = \frac{\mu_0}{4\pi} \left[\frac{2I_0 \mu_0 A_r A_s n_r n_s}{5t^{\frac{5}{2}} V(t, r)} \right]^{\frac{2}{3}} \quad (18)$$

Using Equation 18, the apparent resistivity curve is calculated as a function of time after the current is turned off.

MT (magnetotelluric) method

MT is a passive electromagnetic method that uses the natural magnetic field which provides a broad range of frequency between 10⁻⁴ and 10³ Hz. The magnetic field changes with time and a corresponding

electric field changes in the surface of the ground is measured to reveal subsurface resistivity distribution for great depth ranges. The signal sources are natural fluctuations of the Earth's magnetic field. Those fluctuations or primary magnetic field (H_p) induce a current in the ground (Kearey et al., 2002). A local conductive structure effects the density and distribution of the eddy currents. The current induces a secondary magnetic field (H_s). The resulting magnetic field $H = (H_p + H_s)$ is measured with induction coils in horizontal and orthogonal directions (H_x , H_y and H_z). The accompanied electric field (E_x and E_y) using a voltmeter as a potential difference ΔU between pairs of electrodes at distance L at the surface $E = \Delta U/L$. The small amplitude geomagnetic time variations of the Earth's field contain a wide spectrum, generated by two different sources. One is a low frequency signal (< 1 Hz, long period) which is created from ionospheric and magnetospheric currents caused by solar winds radiating from the sun and interacting with the earth's magnetic field known as micropulsations. This is used for deep crustal and upper mantle structure investigations. The other one is high frequency (> 1 Hz, short period) signal that is generated by thunderstorm activity near the equator, used for shallow crustal structure study. The magnetic \mathbf{H} and electric field \mathbf{E} are measured at the surface and reveal the apparent resistivity ρ_a as a function of ω ($2\pi/T$).

$$\mathbf{E}(\omega) = \mathbf{Z}(\omega)\mathbf{H}(\omega) \quad (19)$$

where \mathbf{Z} is a tensor that depends on the resistivity structure of the ground and ω is the angular frequency (Hz) (Hersir and Björnsson, 1991).

The tensor equation can be written as:

$$\begin{bmatrix} E_x \\ E_y \end{bmatrix} = \begin{bmatrix} Z_{xx} & Z_{xy} \\ Z_{yx} & Z_{yy} \end{bmatrix} \begin{bmatrix} H_x \\ H_y \end{bmatrix} \quad (20)$$

For a 1D earth, conductivity changes with depth only. Therefore, the diagonal elements of the impedance tensors, Z_{xx} and Z_{yy} , are equal to zero, while the off-diagonal components are equal in magnitude, but have opposite signs:

$$Z_{xy} = -Z_{yx} \quad (21)$$

From the impedances, the apparent resistivity of the earth ρ_a and phase θ_a for each period T are calculated by the following relationships:

$$\begin{aligned} \rho_{xy}(T) &= 0.2T|Z_{xy}|^2 = 0.2T \left| \frac{E_x}{H_y} \right|^2; \\ \theta_{xy} &= \arg(Z_{xy}) \end{aligned} \quad (22)$$

$$\begin{aligned} \rho_{yx}(T) &= 0.2T|Z_{yx}|^2 = 0.2T \left| \frac{E_y}{H_x} \right|^2; \\ \theta_{yx} &= \arg(Z_{yx}) \end{aligned} \quad (23)$$

As mentioned above, $Z_{xy} = -Z_{yx}$, for a homogeneous and 1D Earth as well as $\rho_{xy} = \rho_{yx}$ (Flóvenz et al., 2012). In the 1D inversion in this work, the determinant of the impedance tensor, which is rotationally invariant (the value of the resistivity does not change with rotation) are used. The determinant value is calculated by the following equation:

$$\rho_{det} = \frac{1}{\omega\mu_0} |Z_{det}|^2 = \frac{1}{\omega\mu_0} \left| \sqrt{Z_{xx}Z_{yy} - Z_{xy}Z_{yx}} \right|^2; \quad \theta_{det} = \arg(Z_{det}) \quad (24)$$

The determinant of the impedance tensor is like an average value of the apparent resistivity (see Figure 10).

Skin depth is determined as a depth where the electromagnetic fields have been reduced to e^{-1} of their original value at the surface. It is used like a scale length for the time changing field or an estimate of how deep such a wave penetrates into the earth.

$$\delta = 500\sqrt{\rho T} \quad (25)$$

where δ = Skin depth (m);
 T = Period (s);
 ρ = Resistivity (Ωm).

The skin depth depends on the resistivity and the period. Consequently, a low frequency signal penetrates deeper into the earth than the high frequency signal (Hersir and Björnsson, 1991).

Static shift. All resistivity methods that measure the electric field on the surface suffer the static shift or telluric shift problem that is manifested as an unknown multiplier of the apparent resistivity. In MT, the electrical field ($E = \rho j$) is measured at the surface. It is affected by current distortion and topography. When voltage difference is registered on the surface and there is a high-resistivity body in the layer, the current always flows through the low-resistivity part. It causes a distortion of current, assuming that the current flows along the horizontal layers. Because of the shape of the topography, at high elevation, current density is low and the curve is shifted downwards but at the low elevation, it would be high and it is shifted upwards.

Static shift problems of MT are fixed by comparing the MT data with a nearby TEM resistivity curve when doing joint inversion. The TEM method is only sensitive to the near-surface resistivity structure and topography at early times. On the other hand the TEM data collected are measured during late times.

3. TEM AND MT DATA ACQUISITION

3.1 TEM data acquisition

In central loop TEM soundings, the transmitter is fed by a generator or batteries and connected with a transmitter loop, which is usually a square with a variable effective area of 40,000-90,000 m² (but rarely less than 10,000 m², except for shallower probing). Around 20–25 A current is injected from the transmitter into the transmitter loop. Additionally, even if the current is less than 10 A, one can get data with lower signal-to-noise ratio (SNR). The receiver is connected with the receiver loop that is a 10 × 10 m square loop with several windings and a circular loop of 1 m² with 100 windings (effective area is 100 m²), respectively. Those receiver loops are used at 2.5 Hz while a small loop is used at 25 Hz or even higher frequency. The receiver loop is placed at the centre of the transmitter loop.

Initially, the TEM receiver instrument is calibrated using a known signal source. Geonics PROTEM digital receiver can do its calibration automatically (Geonics, 1999). Time synchronization between the receiver and transmitter must be done precisely before the measurements are carried out because TEM works with very rapid signal transition. There are two ways to do synchronization, either through a reference cable or crystal clocks, which were used in this case.

3.2 MT data acquisition

In MT measurement, two lines are placed perpendicular to each other for the purpose of measuring the electric field (E_x and E_y) oriented N-S and E-W. The lines are connected to a data logger and an electrode that is usually composed of lead-chloride with a porous ceramic bottom for measuring telluric currents. The electrode must be in good contact with the ground. Magnetic coils are used to measure the magnetic field in three orthogonal directions (H_x , H_y and H_z). MT measurement setup is sketched in Figure 5.

For a homogeneous or layered earth, the electrical field is induced by its orthogonal source magnetic field (E_x correlates with H_y and E_y with H_x) (Hersir et al., 2013). In order to prevent noise from random or unnecessary movements, the coils are embedded into the ground. The polarity of the coils must be taken into account (Phoenix Geophysics, 2009). After the setup is completed, one should write down the direction of the setup and the coils used for each line and the distance between electrodes, as this information is needed for later data processing. The data logger is configured to record at least for one day. During night time the signal strength is stronger than during day time (Simpson and Bahr, 2005). Before the operator downloads the data from the MT units for processing, an MT data quality check has to be carried out at the site location. Example of time series data is shown in Figure 6. Data in Figure 6 are from the study presented here. The time series data are viewed by time series viewer.

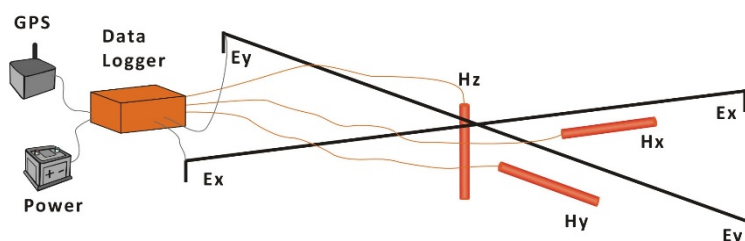


FIGURE 5: The setup of an MT sounding: Electrodes for measuring the electric field, coils for the magnetic field, acquisition unit for digital recording and GPS for synchronizing the data (Flóvenz et al., 2012)

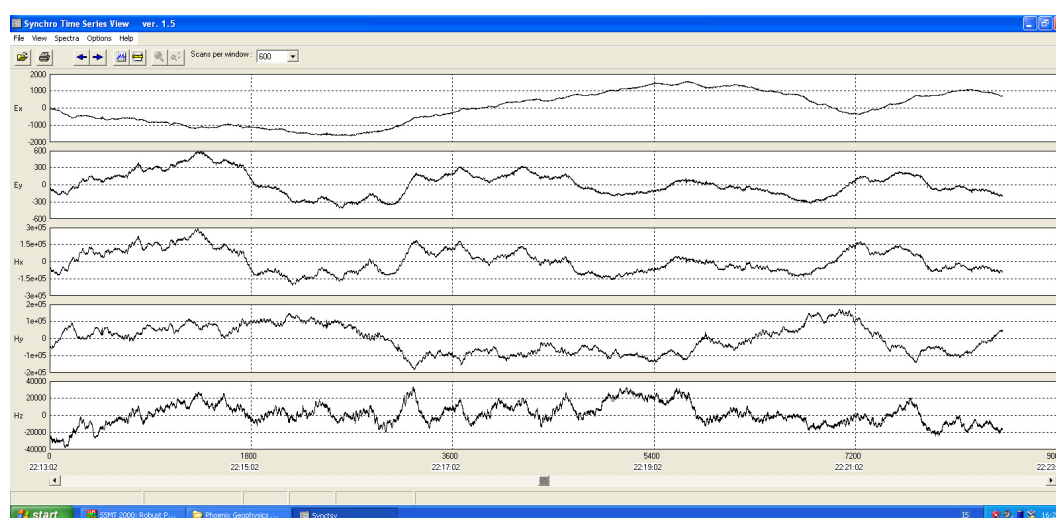


FIGURE 6: Time series data recording

4. PROCESSING OF TEM AND MT DATA

4.1 TEM data processing

TEM raw data are (extension .fru) files, which contain the induced voltage values measured during the late times in 20 gates (Figure 7) in the TEM receiver for different frequencies (25 Hz and 2.5 Hz). The raw data are an input for TemX (Árnason, 2006a) which is a Linux-based software. It supports stacking of the measured values and excludes outliers. The format of the output file is a text file (extension .inv) that includes the apparent resistivity. During one period one can measure 2 times and for the 25 Hz frequency one will have 50 measurements that are stacked in the program and for 2.5 Hz frequency, 5 measurements are stacked.

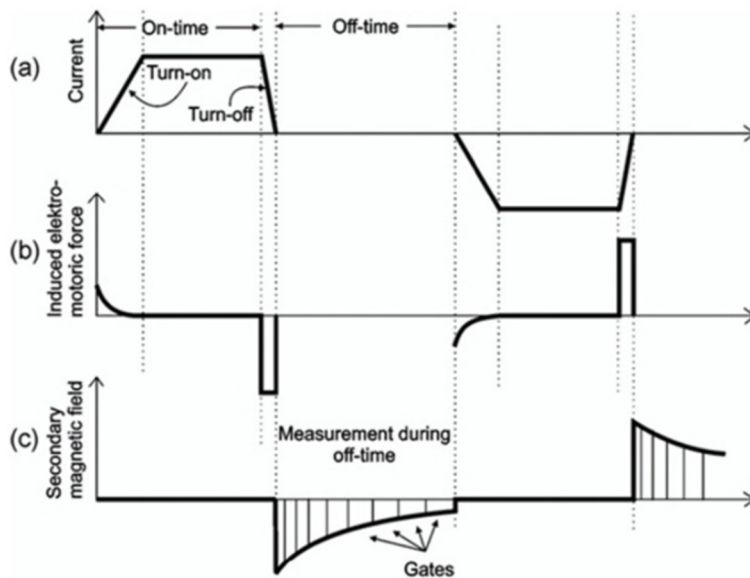


FIGURE 7: Time gates (Gichira, 2012)

MTEditor is used for iterative weighting of residuals to identify and exclude data points. Finally, the resistivity and phase curves are plotted. Now we have data that is Fourier transformed and with misfit minimized. Then, there are some parameters of the plot files, which are displayed such as tipper magnitude, coherency between channels, and strike direction (shown in Figure 12 later). These files are converted into industry-standard Electrical Data Interchange (edi) format (SEG, 1991) for the TEMTD (Árnason, 2006b).

4.2 MT data processing

Raw MT data are time series data that contain two electric and three magnetic field readings. Data processing is completed by SSMT2000 software provided by Phoenix Geophysics in Canada. The Fourier transform in its various forms, decomposes a time series data into its frequency components. In MT, raw time series data are processed using calibration and site parameter files. The Fourier coefficients are calculated and then reprocessed with data from base stations, using robust routines. The output MT plot file contains multiple cross powers for each of the frequencies analysed (Africa, 2013).

5. INVERSION OF THE DATA

The inversion problem consists of obtaining physical parameters that can explain the measured values. Modelling of resistivity soundings is achieved using forward modelling and, thereafter, an inversion process. In forward modelling, an apparent resistivity curve is calculated from a guessed initial model by the geophysicist. After the forward calculation, the measured and the calculated data are compared. Then, the model is changed and the process repeated until the best solution is found. Inversion works with data and the initial model to calculate the best solution of the forward calculation. The initial model is gradually enhanced through an iterative process by calculating adjustments to the model from the difference between the measured data and the response of the model (Figure 8), until a satisfactory fit is reached.

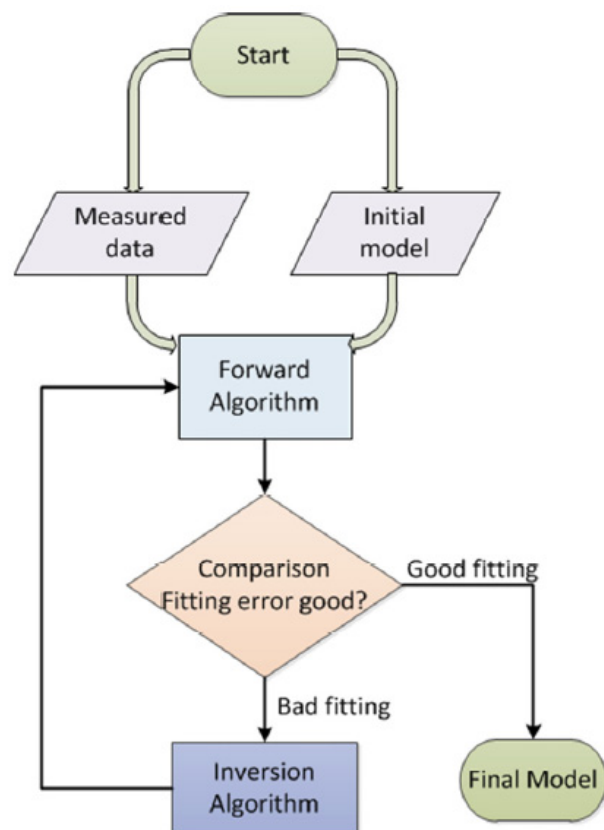


FIGURE 8: The inversion process

6. CASE EXAMPLE – EYJAFJÖRDUR LOW-TEMPERATURE AREA, N-ICELAND

6.1 The study area

Iceland lies at the intersection of the Mid-Atlantic Ridge and the Wyville-Thomson Ridge, a seismically inactive transverse ridge crossing most of the north-eastern branch of the North Atlantic between East Greenland and the Faroe Islands. The North America and Eurasian plate boundary crosses Iceland from southwest to northeast. Active volcanoes and earthquakes are signs of the plate boundaries in Iceland, showing where active plate movement is taking place. Productivity of volcanic material has been shown to be anomalously high on this part of the mid-oceanic ridge system (Vogt, 1971).

Eyjafjörður is the longest fjord in Iceland. It is located in the central north of the country (Flóvenz and Karlsdóttir, 2000). This is the second most populous area of Iceland with the town of Akureyri in its centre with almost 20,000 inhabitants. The mountains of Eyjafjörður are built of 3-10 m.y. old Tertiary volcanic formations. The rocks are mainly basaltic lavas with thin scoraceous and sedimentary inter-layers. The lava pile dips about 4-7°C to the south and southeast. Thick sedimentary beds are found locally. At least three extinct central volcanoes are buried in the basaltic lava pile around Eyjafjörður (see Figure 9). Map of the Eyjafjörður area is presented in Figure 10 with locations of the TEM and MT soundings.

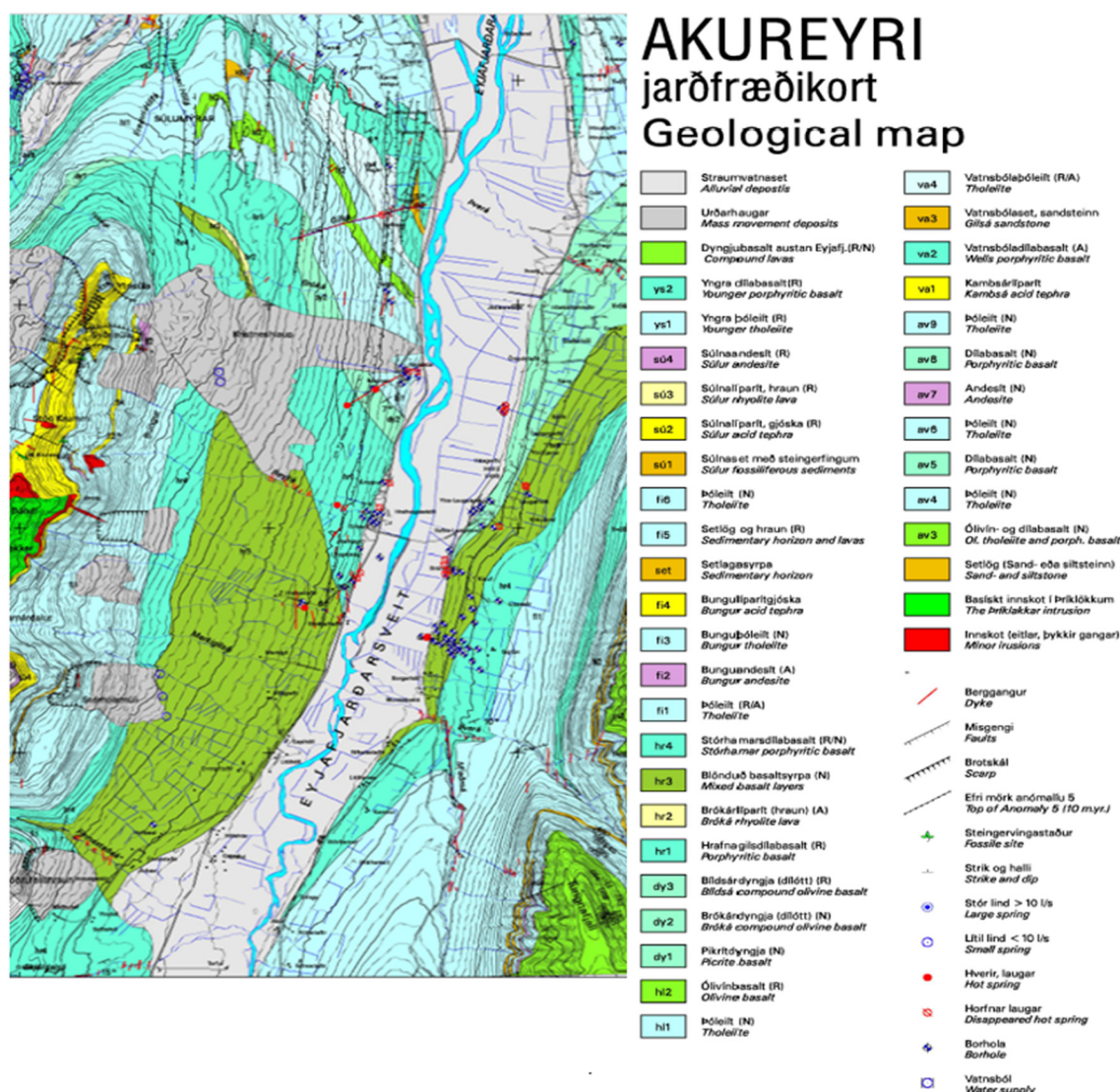


FIGURE 9: Geological map of the Eyjafjörður area (Hjartarson and Jónsdóttir, 2004)

6.2 TEM and MT soundings – data collection and processing

In framework of this work, 38 TEM soundings and 25 MT soundings are processed and inverted separately. Twenty-three of them are used here for the joint inversion (Figure 10). The stretched 2 lines shown in Figure 10 are locations of the resistivity cross-sections which were drawn down to different depths (see further Section 7.1).

6.2.1 1D inversion of TEM data

Input files for the inversion program, TEMTD (Árnason, 2006b) are .inv files that contain the apparent resistivity and a guessed model of resistivity and layer-thickness values using a layered model. The purpose of the inversion is to obtain the true resistivity for each layer. The output file includes resistivity changes with depth (Figure 11). The inversion algorithm that is used in the program is the non-linear least-squares inversion of the Levenberg-Marquardt type (Árnason, 2006b). The misfit function is the root-mean-square difference between measured and calculated values, weighted by the standard deviation of the measured values. In Occam inversion, which is used here in the inversion, layer thicknesses are kept fixed, equally spaced on a log scale, and the conductivity distribution is forced to be smooth by adjusting damping parameters. Appendix I shows the TEM data and the associated 1D models (Lkhagvasuren, 2016).

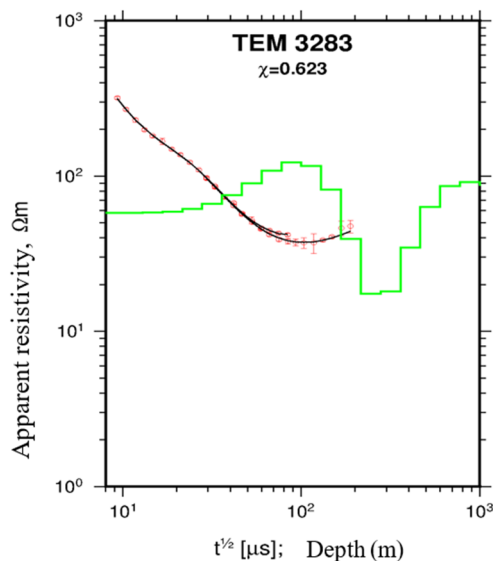


FIGURE 11: Inversion of TEM sounding 3283

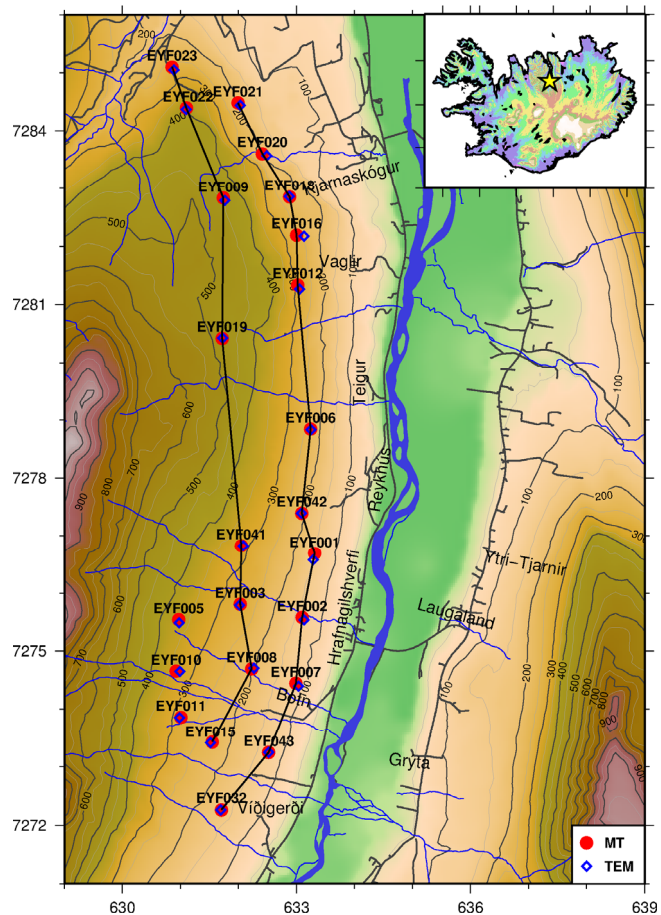


FIGURE 10: Location map for the TEM and MT soundings in Eyjafjörður. The yellow star on the Icelandic map on the right top corner of the figure shows the location of Eyjafjörður low-temperature geothermal area; locations of two cross-sections are shown as black lines

6.2.2 1D inversion of MT data

The magnetotelluric sounding method for the determination of subsurface electrical conductivity was first proposed by Cagniard (1953). For an an-isotropic or laterally inhomogeneous earth, the impedance becomes a tensor quantity. For the inversion program, the input is .edi-files from the MT soundings that include impedances or apparent resistivity and phase values. In the 1D case, only the determinant of the impedance tensor is used which is rotationally invariant. Figure 12 presents the apparent resistivity and phase derived from the xy (red) and yx (blue) components of the impedance tensor and the determinant invariant (black), the Z-strike or Swift angle (black dots), and multiple coherency of xy (red) and yx (blue) and ellipticity (gray dots). Appendix II shows the MT data and the associated 1D models (Lkhagvasuren, 2016).

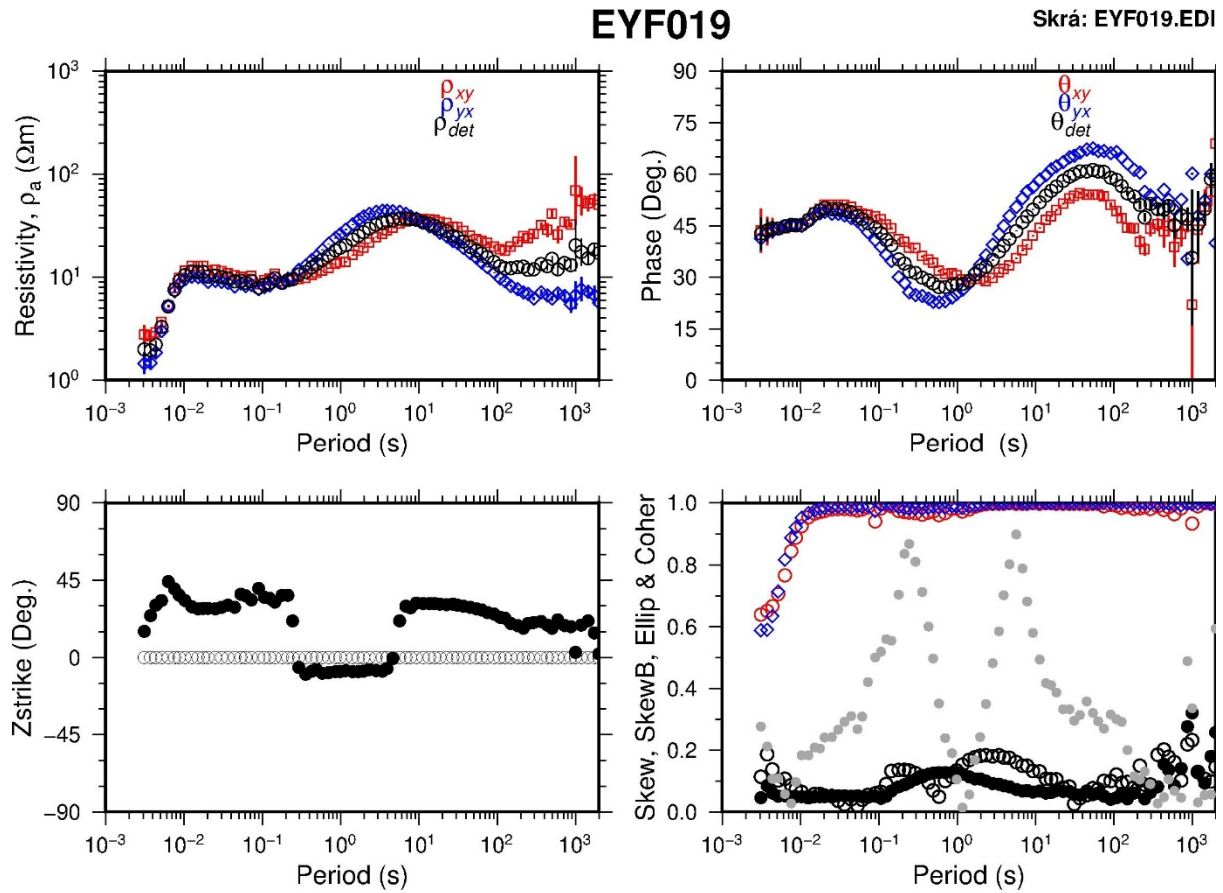


FIGURE 12: Processed data for MT sounding 019 from the Eyjafjörður low-temperature geothermal area, North Iceland

6.3 Joint 1D inversion of TEM and MT data

For the joint inversion, the input is .inv files for the TEM data and .edi files for the MT data. Joint inversion of TEM and MT data is executed using the TEMTD program. For 1D inversion of TEM data the program inverts for time, voltage and the apparent resistivity. The software is used to invert for the MT apparent resistivity and phase obtained from the rotationally invariant determinant of the tensor elements.

TEM soundings play an important role in correcting for static shift problem of MT data by jointly inverting both TEM and MT data. An example of the result of the jointly inverted TEM and MT data is presented in Figure 13.

Appendix III shows the 1D models of the joint inversion for all of the TEM and MT data (Lkhagvasuren, 2016).

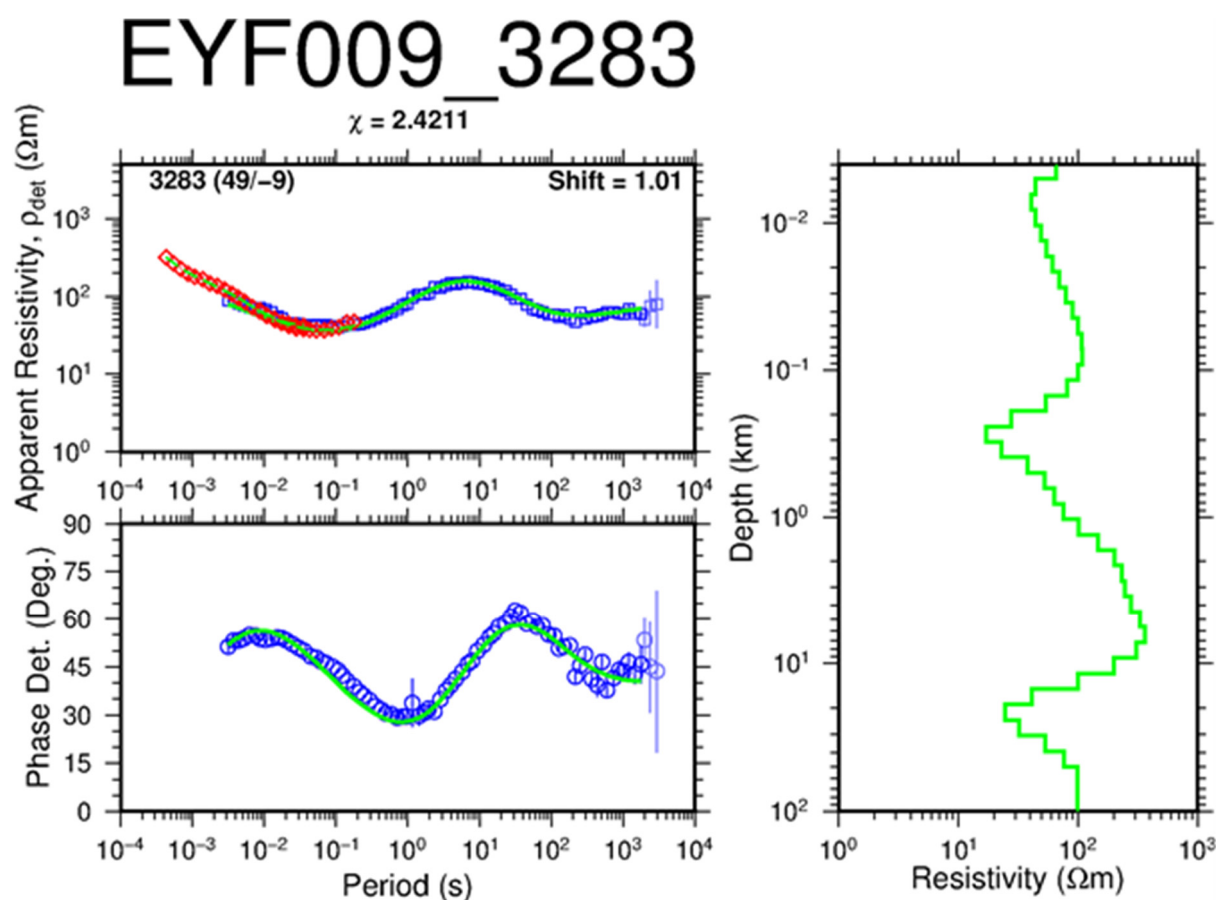


FIGURE 13: 1D joint inversion result of TEM sounding (3283) and MT sounding (EYF009); here, red diamonds are TEM apparent resistivity points, blue squares are MT apparent resistivity and blue circles are MT apparent phase points which are derived from the determinant of MT impedance tensor, green lines on the right represent the 1D joint inversion model. On top of the figure are the names of the MT and TEM soundings that are located close to each other and the misfit value. The shift value executed to MT data in order to fit the TEM data is 1.01

7. RESULTS

7.1 Resistivity cross-sections and resistivity depth slices

Figures 14 and 15 show two resistivity cross-sections reaching down to different depths in the Eyjafjörður area, based on the 1D joint inversion of the TEM and MT data. Additional cross-sections (down to different depths) are presented in Appendix 4 (Lkhagvasuren, 2016). Their location is given in Figure 10. A total of 8 resistivity depth slices are shown in Figures 16 and 17. Additional depth slices are shown in Appendix 4 (Lkhagvasuren, 2016).

The resistivity cross-sections show a shallow low-resistivity anomaly extending from the surface down to a depth of around 1,000 m. The low-resistivity is dipping upwards towards the north. At greater depths of several km, another low-resistivity body is seen in both cross-sections doming up in the northern part of the sections. These resistivity structures are even more visible in the depth slices. The deep lying conductive body is seen in one sounding only in the northwest part of the survey area at 7,000 and 10,000 m b.s.l. but extends over the northern part of the area at 15,000 m b.s.l. and in particular at 20,000 m b.s.l.

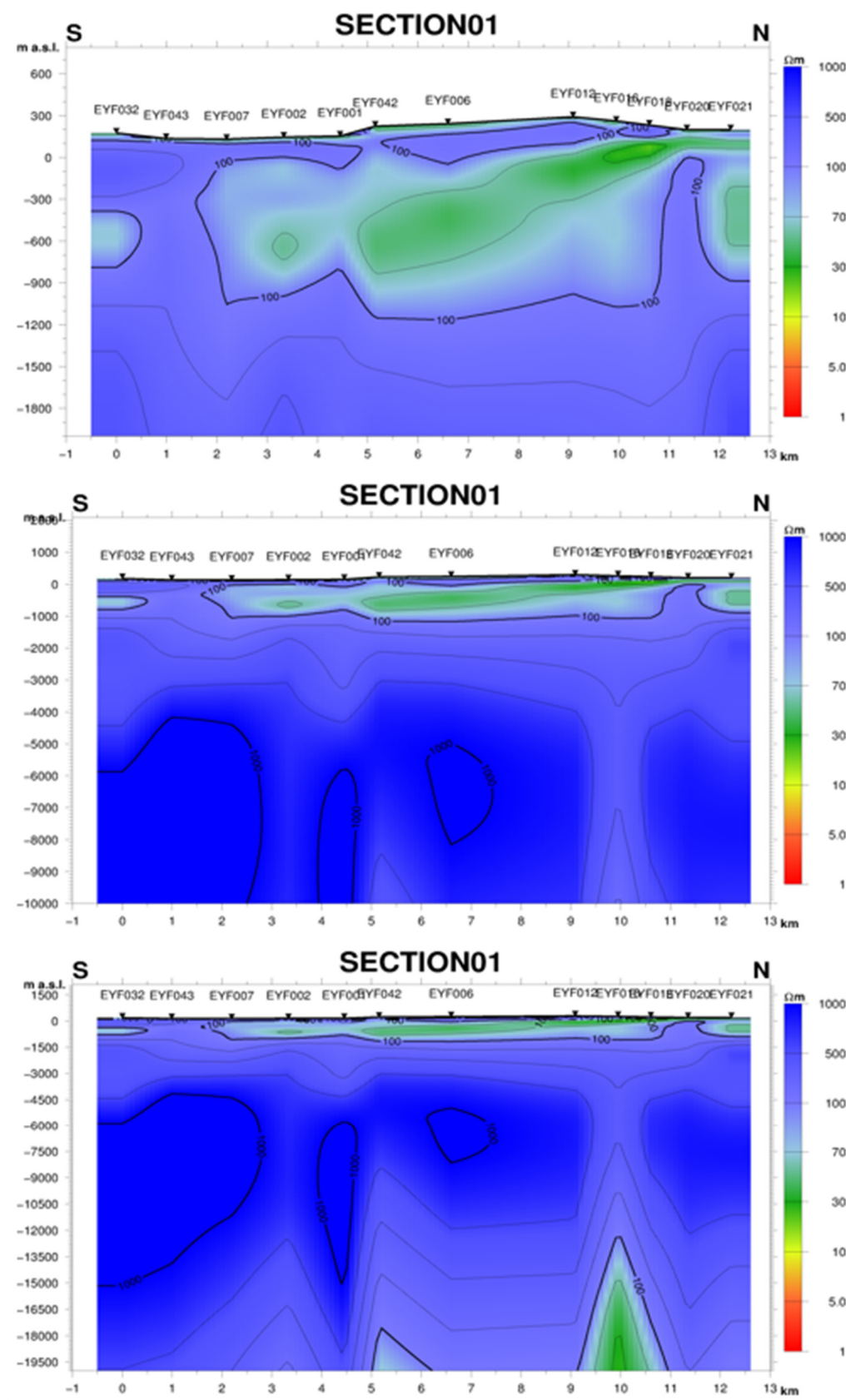


FIGURE 14: Resistivity cross-section N01 down to three depth levels, 2,000, 10,000 and 20,000 m b.s.l.; black triangles show the location of the MT soundings; the location of the cross-section is given in Figure 10

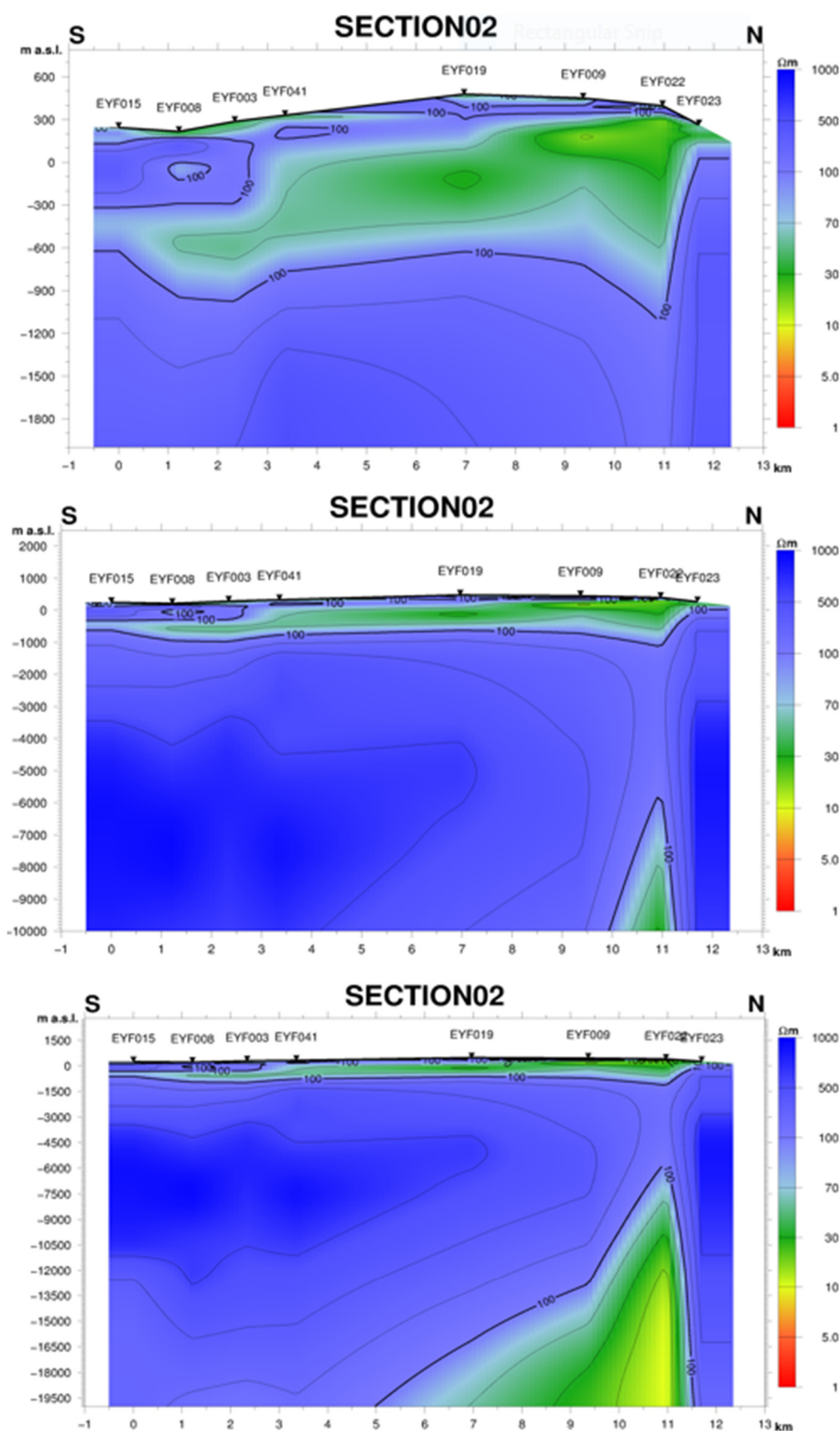


FIGURE 15: Resistivity cross-section N02 down to three depth levels, 2,000, 10,000 and 20,000 m b.s.l.; black triangles show the location of the MT soundings; the location of the cross-section is given in Figure 10

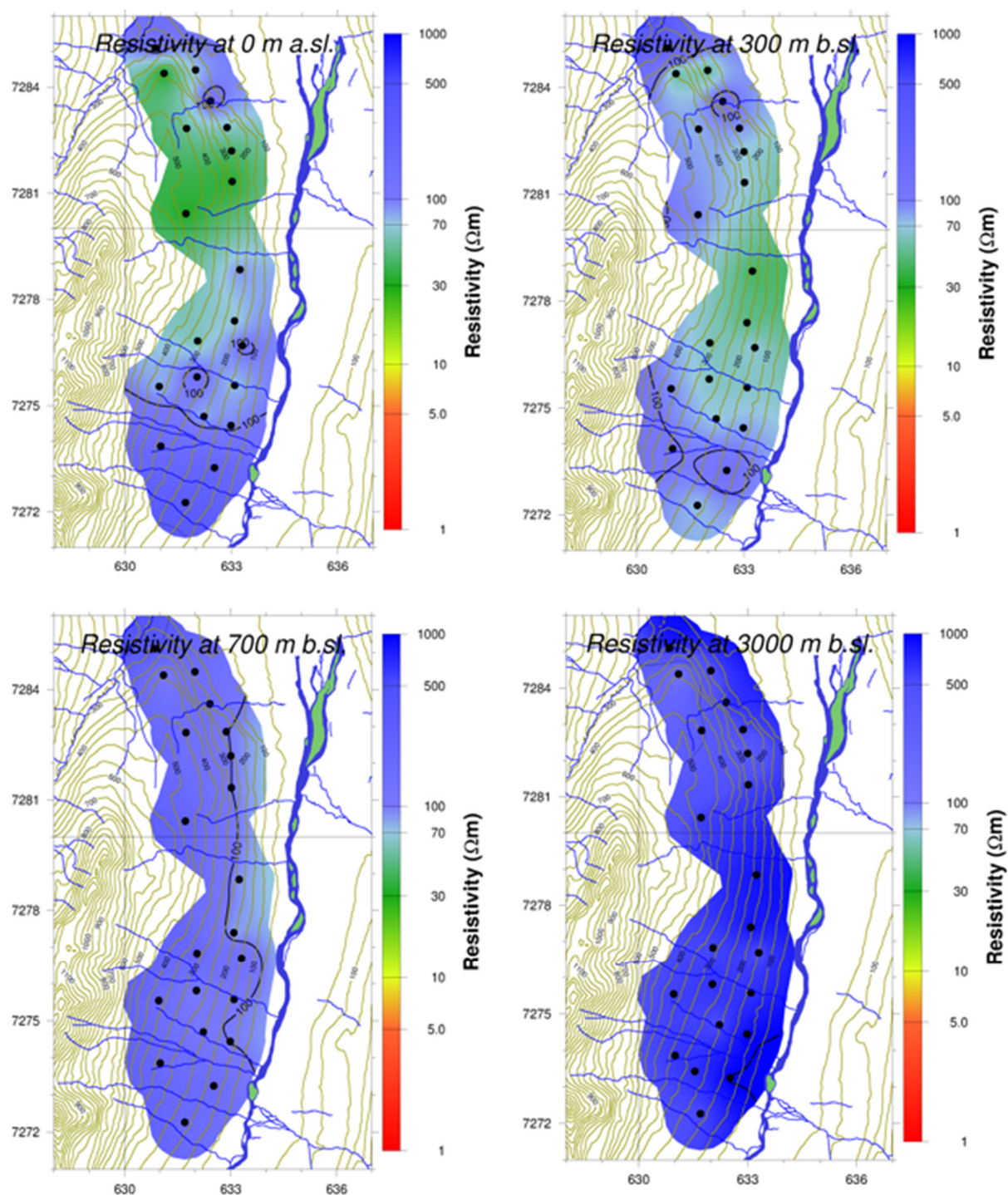


FIGURE 16: Resistivity depth slices at sea-level and at depths of 300, 700 and 3000 m b.s.l.; black dots show locations of MT soundings

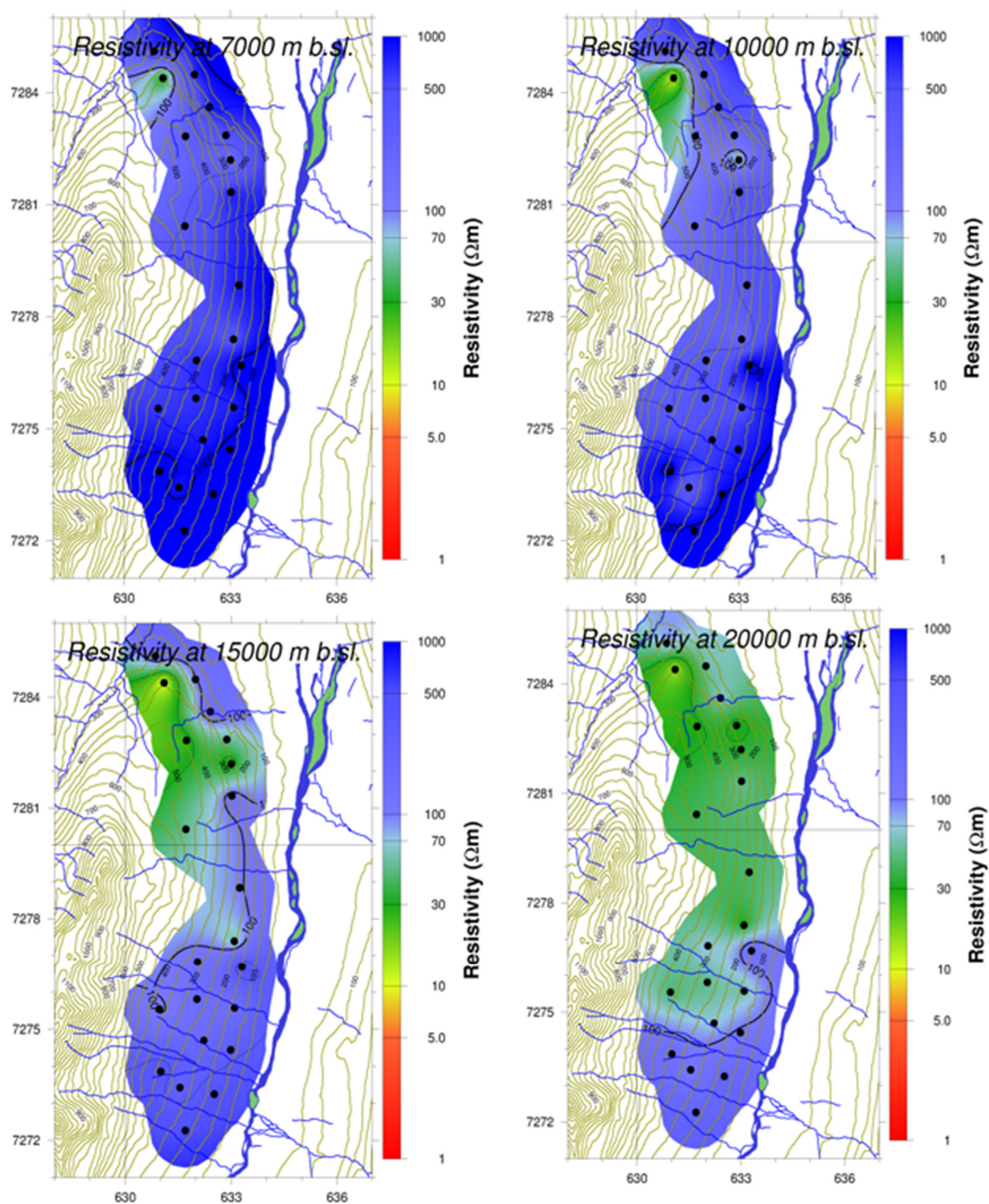


FIGURE 17: Resistivity depth slices at depths of 7,000, 10,000, 15,000 and 20,000 m b.s.l.; black dots show locations of MT soundings

8. CONCLUSIONS

Geophysical methods are mostly used in combination with other investigations. Here, a case study was done in Eyjafjörður low- temperature geothermal field where TEM and MT methods were applied. The TEM and MT data have been processed and 1D inverted. The 1D joint inversion of TEM and MT data was performed using the TEMTD inversion program. The resistivity depth slices and cross-sections have been mapped from the results of the joint inversion.

A resistivity cross-section along the same N-S profile has been done previously by Flóvenz and Karlsdóttir (2000) and compared with isotherms from deep boreholes in the south part of the cross-section (Figure 18). From a depth of around 300-800 m, a low-resistivity layer extends up to the surface along the dipping lava pile layers. To the left, a shallow lying low-resistivity anomaly is coinciding with a phorphyritic and tholeiitic lava interbedded with sedimentary layers, a higher-resistivity layer coincides with a series of compound tholeiitic lavas. The low-resistivity anomaly observed in this work coincides with the temperature anomaly, which is interpreted as the main up flow zone of the geothermal activity according to Flóvenz and Karlsdóttir (2000). From the resistivity cross-sections and depth slices, a low-resistivity layer is seen extend upwards in a northerly direction. It reaches the surface at 11.5 km in cross-section 02 at 200 m a.s.l. (Figure 15).

A deep laying low resistivity is seen in cross-section 02 at 6,000 m b.s.l. and at 12,000 m in cross-section 01. It is seen in the subsurface in Eyjafjörður low-temperature area as in most of Iceland. It is presumably somehow connected to the heat source. According to Flóvenz and Karlsdóttir (2000), the heat source is

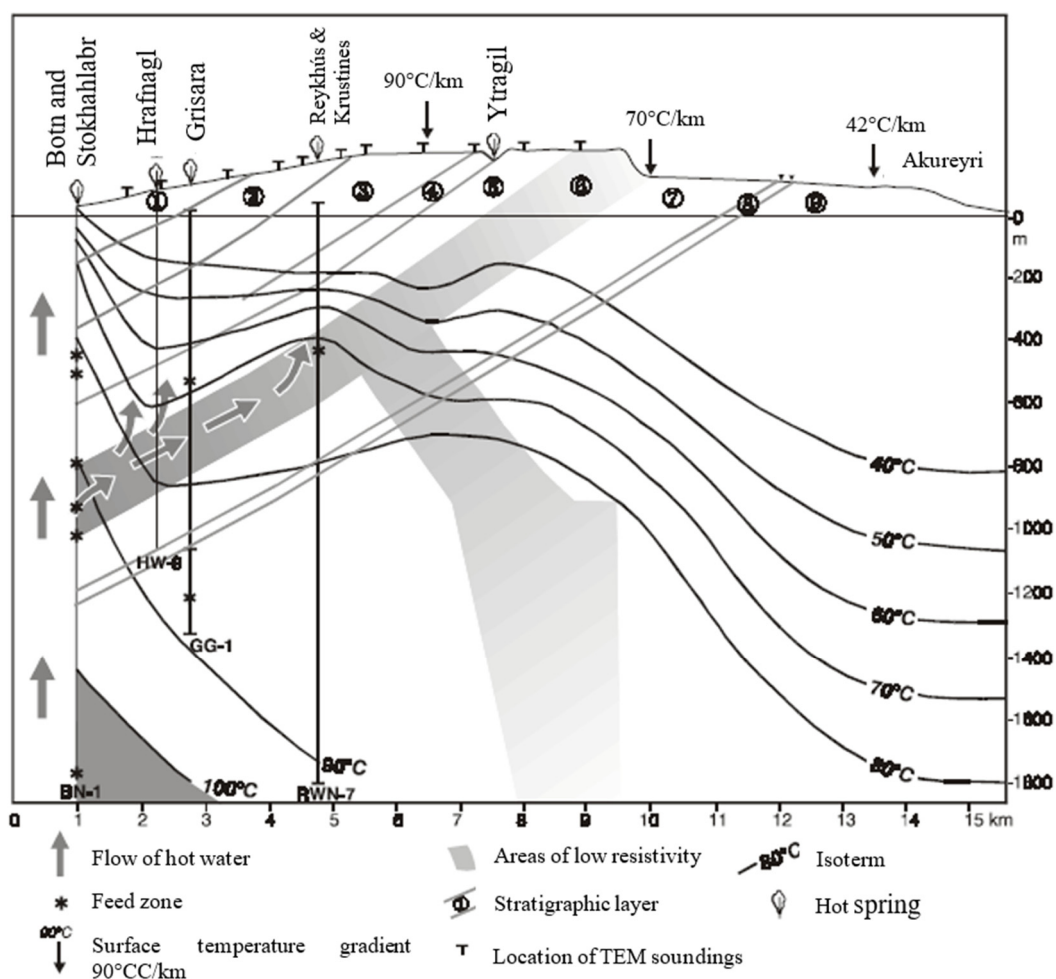


FIGURE 18: Geothermal interpretation of the Eyjafjörður low-temperature geothermal area (Flóvenz and Karlsdóttir, 2000)

around Botn area, close to MT soundings 007 and 008 (see Figure 10). When the results of this study are compared with those from Flóvenz and Karlsdóttir (2000), they are quite similar.

The low-resistivity anomaly is composed of porphyritic lavas, which temperature measurement analyses have shown to be the main up flow zone of the geothermal activity. The higher-resistivity host rock is presumably composed of a series of compound basaltic lavas.

Using resistivity surveying methods, the resistivity structure of the subsurface of the Earth is mapped as a function of depth. In geothermal areas, resistivity is prone to the parameters that can reveal the character of the geothermal reservoir. Resistivity surveying on the surface can directly probe deep structures in the subsurface of the Earth. It has many attributes for predicting the conditions of the geothermal reservoir. The main significance of resistivity surveying is diagnostic of geothermal activity and it adds to the understanding of geothermal reality in the subsurface.

ACKNOWLEDGEMENTS

I would like to appreciate my supervisors Mr. Gylfi Páll Hersir and Mr. Knútur Árnason for their support, kind discussions, direct advice and for revising the report. Also, I would like to express my gratitude to the UNU-GTP staff for their assistance and guidance during the past 6 months. I learned a lot of things during the 6 months of the geothermal training programme.

Thank you, dear international friends. I did not have time to get bored with you around. We were learning a lot, running, swimming, hiking and travelling to new places around Iceland where it is magnificent and peaceful.

I extend my appreciation to Demberel S (Director of Institute of Astronomy and Geophysics in Mongolia) for this big opportunity to learn and to my colleagues for their assistance and encouragement. I thank my whole family for taking care of our boys. It was obviously a big support for the study and work not to have to worry about the kids.

Also I want to express my appreciation to ÍSOR staff for their kind help.

REFERENCES

Africa, J.R., 2013: 1D inversion of MT and TEM data with application of soundings from Krýsuvík, SW-Iceland and a review of MT/TEM data from Bacman geothermal project, Central Philippines. Report 5 in: *Geothermal training in Iceland 2013*. UNU-GTP, Iceland, 1-34.

Archie, G.E., 1942: The electrical resistivity log as an aid in determining some reservoir characteristics. *Trans. AIME*, 146, 54-67.

Árnason, K., 1989: *Central-loop transient electromagnetic sounding over a horizontally layered earth*. Orkustofnun, Reykjavík, report OS-89032/JHD-06, 129 pp.

Árnason, K., 2006a: *TemX short manual*. ÍSOR – Iceland GeoSurvey, Reykjavík, report, 17 pp.

Árnason, K., 2006b: *TEMTD (Program for 1D inversion of central-loop TEM and MT data)*. ISOR – Iceland GeoSurvey, Reykjavík, short manual 16 pp.

Badilla E., D., 2011: Resistivity imaging of the Santa Maria sector and the Northern zone of Las Pailas geothermal area, Costa Rica, using joint 1D inversion of TDEM and MT data. Report 8 in: *Geothermal training in Iceland 2011*. UNU-GTP, Iceland, 85-118.

Burger, H.R., Sheehan, A.F., and Jones, C.H., 2006: *Introduction to applied geophysics*. W.W. Norton & Company, Inc., NY, 614 pp.

Cagniard, L., 1953: Basic theory of the magneto-telluric method of geophysical prospecting. *Geophysics*, 18, 605-635.

Dakhnov, V.N., 1962: Geophysical well logging. *Q. Colorado Sch. Mines*, 57-2, 445 pp.

Flóvenz, Ó.G., 1984: Application of the head-on resistivity profiling method in geothermal exploration. *Geothermal Resources Council. Transactions*, 8, 493-498.

Flóvenz, Ó.G., Hersir, G.P., Saemundsson, K., Ármannsson, H., and Fridriksson Th., 2012: Geothermal energy exploration techniques. In: Sayigh, A. (ed.), *Comprehensive renewable energy*, vol. 7. Elsevier, Oxford, 51-95.

Flóvenz Ó.G., and Karlsdóttir, R., 2000: TEM-resistivity image of a geothermal field in N-Iceland and the relation of the resistivity with lithology and temperature. *Proceedings of the World Geothermal Conference 2000, Kyushu – Tohoku, Japan*, 1127-1132.

Geonics, Ltd., 1999: *Operating manual for PROTEM 67 D*. Geonics Ltd, Ontario, 58 pp.

Georgsson, L.S., 2009: Geophysical methods used in geothermal exploration. *Presented at Short Course IV on Exploration for Geothermal Resources, organized by UNU-GTP, KenGen and GDC, at Lake Naivasha, Kenya*, UNU-GTP, SC-10, 16 pp.

Georgsson, L.S., and Karlsdóttir, R., 2007: Resistivity methods – DC and TEM with examples and comparison from the Reykjanes peninsula and Öxarfjörður, Iceland. *Paper presented at “Short Course II on Surface Exploration for Geothermal Resources”, organized by UNU-GTP and KenGen, at Lake Naivasha, Kenya*, UNU-GTP SC-5, 14 pp.

Gichira, J.M., 2012: Joint 1D inversion of MT and TEM data from Menengai geothermal field, Kenya. Report 11 in: *Geothermal training in Iceland 2012*. UNU-GTP, Iceland, 137-167.

Hersir, G.P., and Árnason K., 2009: Resistivity of rocks. *Paper presented at “Short Course on Surface Exploration for Geothermal Resources”, organized by UNU-GTP and LaGeo, Santa Tecla, El Salvador*, UNU-GTP SC-09, 8 pp.

Hersir, G.P., and Björnsson, A., 1991: *Geophysical exploration for geothermal resources. Principles and applications*. UNU-GTP, Iceland, report 15, 94 pp.

Hersir, G.P., Vilhjálmsson, A.M., and Árnason K., 2013: 3D inversion of magnetotelluric (MT) resistivity data from Krýsuvík high temperature geothermal area in SW Iceland. *Proceedings of the 38th Workshop on Geothermal Reservoir Engineering, Stanford University, Stanford, CA*, 14 pp.

Hjartarson, Á., and Jónsdóttir, H.E., 2004: *Akureyri, geological map* (2. ed.). ÍSOR – Iceland GeoSurvey, Reykjavík.

Kearey, P., Brooks, M., and Hill, I., 2002: *An introduction to geophysical exploration*. Blackwell Scientific Publications, Oxford, 254 pp.

Kulhanek, O., 1988: *Anatomy of seismogram*. Elsevier, Amsterdam, 178 pp.

Lee L., K., Lerner, B.W., and Cengage, G., 2006: *Porosity and permeability*. World of Earth Science, webpage: www.enotes.com/earth-science/.

Lichoro, C.M., 2014: Gravity and magnetic methods. *Presented at Short Course IX on Exploration for Geothermal Resources, organized by UNU-GTP, GDC and KenGen, at Lake Bogoria and Lake Naivasha, Kenya*, UNU-GTP SC-19, 8 pp.

Lkhagvasuren, S., 2016: *Appendices to the report "Resistivity surveying in geothermal exploration with an application to the Eyjafjörður low-temperature area, N-Iceland"*. UNU-GTP, Iceland, report 25 appendices, 41 pp.

Lucius, J.E., Langer, W.H., and Ellefsen, K.J., 2006: *An introduction to using surface geophysics to characterize sand and gravel deposits*. US Geological Survey, Reston, VI, open-file report 2006-1257, 55 pp.

Mariita N.O., 2011: Application of geophysical methods to geothermal energy exploration in Kenya. *Presented at Short Course VI on Exploration for Geothermal Resources, organized by UNU-GTP, GDC and KenGen, at Lake Bogoria and Lake Naivasha, Kenya*, UNU-GTP SC-13, 9 pp.

Phoenix Geophysics, 2009: *Data processing. User's guide*. Phoenix Geophysics, Ltd., Toronto.

Rowland, B.F., 2002: *Time-domain electromagnetic exploration*. Northwest Geophysical Associates, Inc., report, 6 pp.

Samaranayake, S.A., 2015: Seismic monitoring of geothermal fields: A case study of Hellisheidi geothermal field. Report 32 in: *Geothermal training in Iceland 2015*. UNU-GTP, Iceland, 727-754.

SEG, 1991: *MT/EMAP data interchange standard*. Society of Exploration Geophysicists, 112 pp.

Simpson, F., and Bahr, K., 2005: *Practical magnetotellurics*. Cambridge University Press, Cambridge, UK, 254 pp.

Todd, D.K., and Mays, L.W., 2005: *Groundwater hydrology* (3rd ed.). John Wiley & Sons, Inc., NY, 636 pp.

Vogt, P.R., 1971: Asthenosphere motion recorded by the ocean floor south of Iceland. *Earth Planet. Sci. Lett.*, 13, 153-160.



UNITED NATIONS
UNIVERSITY

UNU-GTP

Geothermal Training Programme

Orkustofnun, Grensasvegur 9,
IS-108 Reykjavik, Iceland

Reports 2016
Number 26

BOREHOLE GEOLOGY, HYDROTHERMAL ALTERATION AND STRUCTURE OF WELL SV-26 IN THE SVARTSENGI AREA, SW-ICELAND

Andrei Eugen Lup

SC Daflog SRL

Mediaş, str. Nicolae Titulescu nr. 3
ROMANIA

ABSTRACT

This report describes the stratigraphic sequence and alteration in drill hole SV- 26 in the Svartsengi high-temperature field, SW-Iceland. Well SV-26 is a make-up and exploration well for the Svartsengi power plant. It is a directional well deviated to the east towards the southern part of Mt. Sýlingarfell to explore and extend the southeastern part of the Svartsengi production field. The stratigraphy of well SV-26 is characterized by basaltic lava flows and different hyaloclastite formations. Drill cuttings in the uppermost part of the well are characterized by a high degree of oxidation. Three alteration zones were observed: Unaltered zone (0-112 m), smectite-zeolite zone (112-622 m) and chlorite-epidote zone (622-1394 m). No drill cuttings were available for analysis below 1394 m due to total loss of circulation within the well. Aquifers in this well were located based on borehole measurements and records of circulation losses. It is important to note that the temperature loggings and mineral sequences of SV-26 do not show any evidence of temperature reversal which implies that the Svartsengi geothermal system could extend further to the east than previously believed.

1. INTRODUCTION

1.1 Geology of Iceland

Geographically, Iceland is in the northern part of the Mid-Atlantic Ridge between Greenland and Norway at 63 °23'N to 66 °30'N. Iceland has an area of 103,106 km² and an average altitude of 500 m making it the third largest island located in the Atlantic Ocean (Jakobsson, 1979; Saemundsson, 1979). The subaerial part represents about 30% the Iceland Basalt Plateau, which rises more than 3,000 m above the surrounding sea floor and covers about 350,000 km² (Thórdarson, 2012). Geologically, Iceland is a very young land mass that started to form in Early Miocene, about 25 million years ago but the oldest rocks that can be found exposed on the surface belong to the Tertiary period around 16 million years ago (Hardarson et al., 1997). The construction of Iceland is a consequence of a stationary plume and the spreading of two tectonic plates: American and Eurasian, which move apart at an average rate of 1 cm per year in each direction. This spreading started about 70 million years ago and the plate boundary is delineated by series of faults and volcanoes, which together form a distinguishing ridge-like structure in the middle of the ocean. Iceland resides on a mantle plume, which has been active for

the last 65 million years and has caused significant volcanic activity. These eruptions are effusions of basaltic lava from fissures or shield volcanoes. Volcanism, sedimentation and erosion are more active in Iceland than in other places, changing the surface radically in a relatively short time. Iceland is the only place where the active spreading and plate growth of the Mid-Atlantic Ridge can be seen because this is the only section of the plate boundary exposed above the sea level. The narrow belts of active faulting and volcanism spreading from Reykjanes in the southwest, which zig-zag across Iceland all the way to the north and into the Arctic Ocean, represent the surface expressions of this plate boundary (Thórdarson, 2012).

The three main geological formations in Iceland are shown in Figure 1. The oldest are successions of lava that generally dip gently towards the volcanic zones and belong to the Tertiary formation (3- 16 my). The second formation is of Quaternary, Plio-Pleistocene age (0.7-3 m.y.). The succession is comprised of alternating sequences of lavas and hyaloclastites. The lavas were formed during interglacial periods while the hyaloclastites were created as a result of subglacial eruptions during ice ages. The third and youngest formation is contained within the neovolcanic zone and is composed of Upper-Pleistocene and Postglacial formations (< 0.7 m.y.) (Saemundsson, 1979; Rodas, 1996).

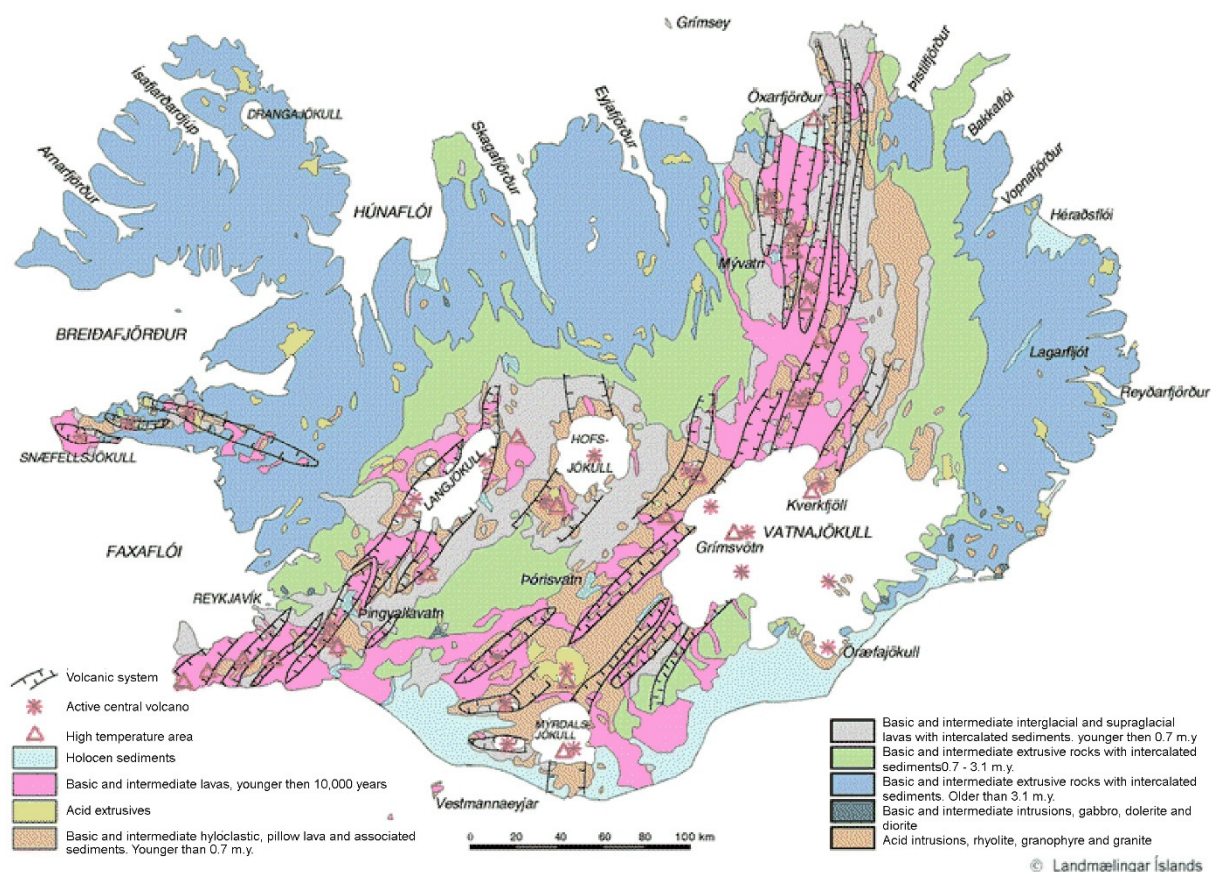


FIGURE 1: Geological map of Iceland showing oldest Tertiary rocks, older Plio-Pleistocene eruptives, Holocene rocks plus other young formations; volcanic systems follow the oceanic ridge (based on Jóhannesson and Saemundsson, 1999)

Due to intense volcanism and very active tectonics, Iceland is rich in geothermal resources. The geothermal areas in Iceland are classified as high or low in temperature, based on the geological setting and temperature information collected from loggings in the areas. Most of the high-temperature areas are within the active volcanic belts, but most of the low-temperature areas occur in Quaternary and Tertiary formations.

In the high-temperature areas, the underground temperature reaches 200°C within 1,000 m depth and the heat source is generally shallow magma intrusions (Björnsson et al., 2010). These areas are confined to the active volcanic zones (Figure 2). The surface manifestations are mostly steam vents because the topography and the high bedrock permeability of these very young rocks results in a deeper groundwater table.

Most of the low-temperature areas can be found flanking the active zone, and the largest of these can be found in southwest of the country. There are about 250 low-temperature areas, which do not exceed 150°C in the uppermost 1,000 m (Figure 2). The common surface manifestations are hot or boiling springs and to date, and over 600 hot springs (temperature over 20°C) have been located (Worku, 2012).

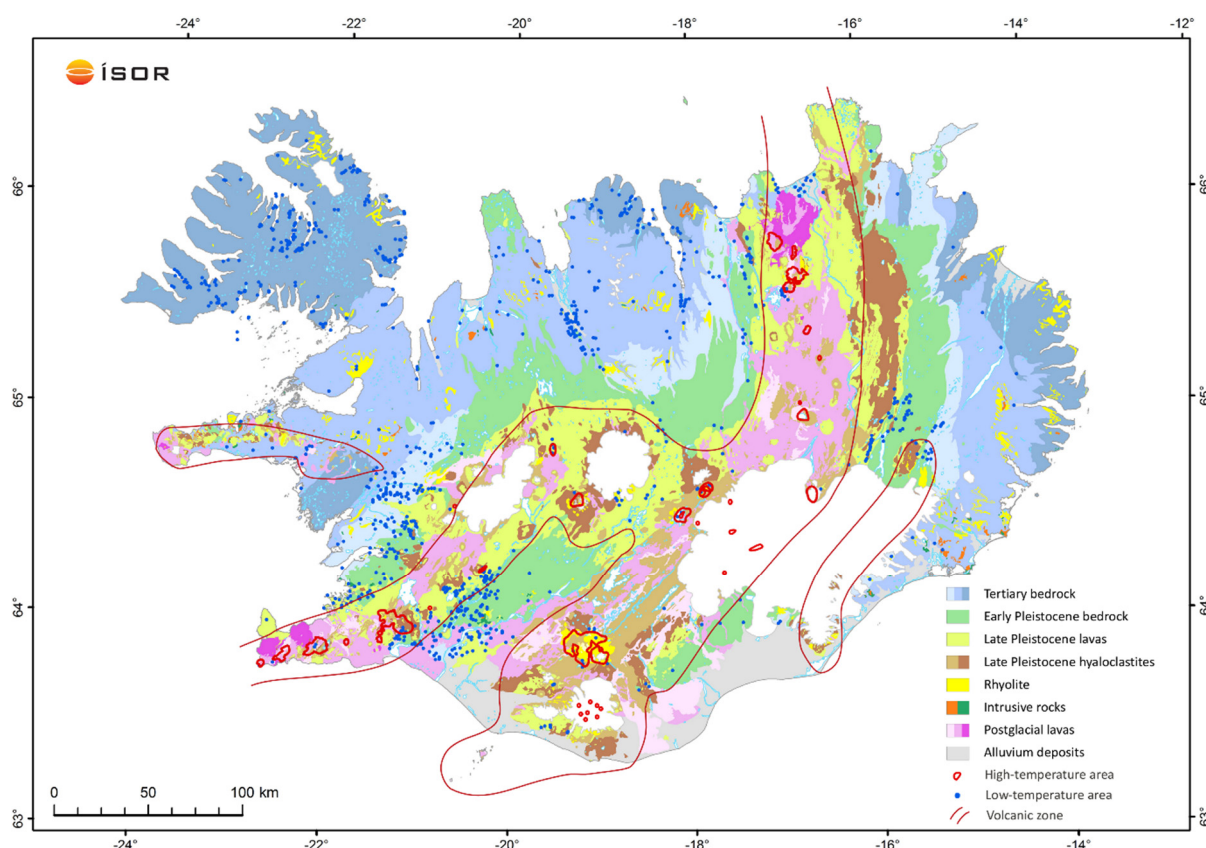


FIGURE 2: Geological map of Iceland showing high-temperature and low-temperature areas (Hjartarson and Saemundsson, 2014)

1.2 Local geology

In southwest of Iceland, the geology spans over the last 3.2 million years, since the very last stages of the Pliocene across the Quaternary to the present day. Outcrops of the oldest rocks can be found in and around Mt. Esja (Figure 3) in the north, and the succession gradually becomes younger towards the south. The submarine Reykjanes Ridge and the West Volcanic Zone are connected by the axis of the Reykjanes Volcanic Belt along which the youngest rocks outcrop (Figure 3). From east to west, the belt comprises four volcanic systems: the Hengill, Brennisteinsfjöll, Trölladyngja, and Reykjanes systems. The systems have a north-easterly strike and extend across the peninsula (Thórdarson, 2012).

The Svartsengi area is located on the Reykjanes Peninsula, approximately 50 km southwest of the capital Reykjavik, and covers the Svartsengi geothermal field, the lava fields surrounding it, and the pillow lava piles of Hagafell, Lagafell and Thorbjarnarfell and the table mountain of Svartsengisfell. An active

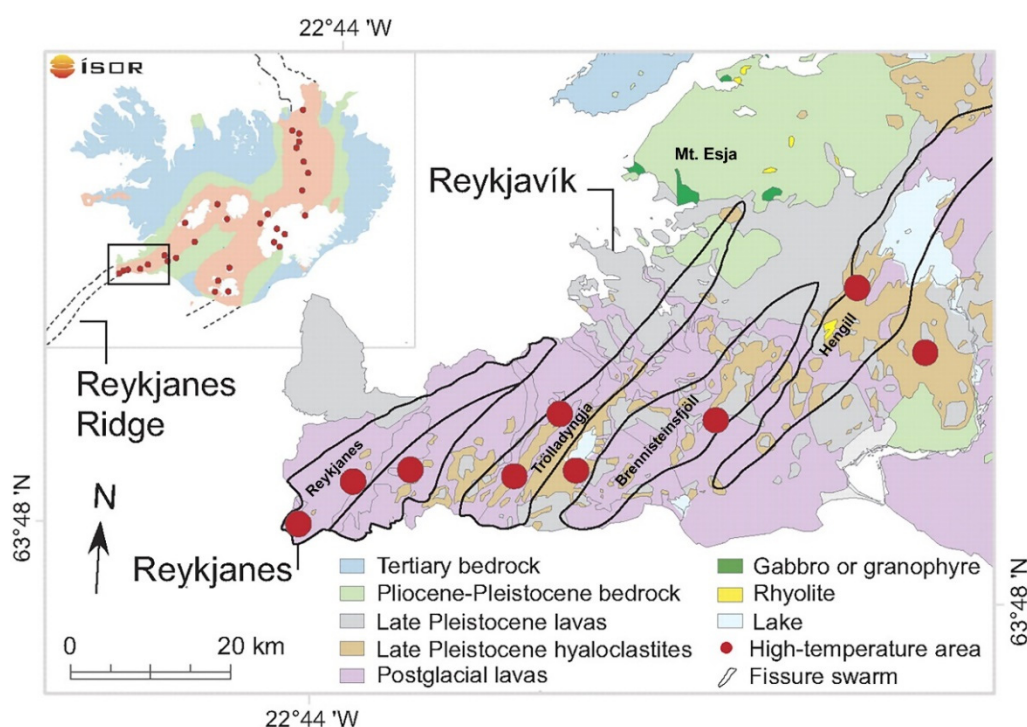


FIGURE 3: The main geological features of the Reykjanes Peninsula

fissure swarm cutting across the field causes the geothermal field to have a very high degree of faulting, but surface manifestations are scarce and surface alteration is relatively small (Rodas, 1996).

Fissure swarms are described in the geological literature of Iceland as being part of a volcanic system with anomalous volcanic accumulation rates, especially in its central part. The elevation of the lava plain at Svartsengi only rises about 30 m above sea level, and there is no indication of an anomalous volcanic production linked with the central part of the fissure swarm which could denote a central “volcano activity”. A central underlying heat source, in the form of a magma chamber, for the geothermal system may therefore be unlikely (Franzson, 2017).

The Svartsengi high-temperature field lies within the Grindavík fissure swarm, which is the second west most fissure swarm on the Reykjanes Peninsula (Figure 3). About 30 eruptions are believed to have occurred within the swarm during Holocene age (Postglacial) and are mostly fissure eruptions (Jakobsson et al., 1978). The oldest rock formations outcrop at Mt. Thorbjörn and Svartsengisfell mountains, consist, to a large extent, of pillow lavas and some hyaloclastites. The second main geological surface formation comprises both aa and pahoehoe lava types. These lavas are postglacial flows (< 12 ka) and cover the entire high-temperature area. At the northern foot of Mt. Thorbjörn there are two small lava craters. The lavas released from the two small craters that can be found at the northern foot of Mt. Thorbjörn are likely to be found underlying the topmost lava to the north and east. The Svartsengi area is mainly covered by the two youngest lavas, the northern one originated from an approximately 10 km long fissure to the east of Svartsengisfell, and the lava flow to the south derived from a short fissure west of Mt. Thorbjörn. These lavas are mostly of aa type (Rodas, 1996).

1.3 Tectonic setting

The main tectonic faults and fissures shown in Figure 4 are dominantly NE-SW aligned and are a part of the Reykjanes-Svartsengi NE-SW fissure swarm. A few N-S structural features are shown mainly in Svartsengisfell and to the south from there. As expected in an area of continuous seismic activity, the tectonic structures are more pronounced in the oldest formations but sporadic in the most recent formations. The most noticeable faults are those forming the ca. 200 m wide graben in Mt Thorbjörn.

The throw of these faults, however, are most pronounced in the centre of the mountain but decreases rapidly in both directions, indicating a topographic effect on the dimension of the throw (Franzson, 2017).

In order to clarify further faults, fractures and geothermal manifestations in and around Svartsengi, a separate tectonic study was made, mainly based on aerial photographs (Franzson, 1990). As previously mentioned, the tectonic and volcanic features are most noticeable in the older formations, while largely absent in the youngest lavas. The main tectonic lineation in Thorbjörn hyaloclastite formation is NE-SW and a relatively strong northerly trend is observed in Selhåls, south of Svartsengi. These have been confirmed by a ground study where the northerly fracture directions are obvious in the southern part of the Svartsengisfell hyaloclastite formation. This fracture trend extends towards the Svartsengi well field in the north and probably carpeted there by the young Illahraun fissure lava (Franzson, 2017).

1.4 Previous studies at the Svartsengi area

Previous work done in the area consists of geological mapping by Kuthan (1943), Jónsson (1978), Sigurdsson (1985) and Jóhannesson (1989). Hjalti Franzson (1990) mapped the surface alteration and structural lineation of the geothermal field. According to the degree of surface alteration intensity, three alteration zones have been defined: high, medium and low. High-intensity alteration is found where widespread formations of clay occur; medium intensity alteration is characterized by extensive deposition of silica, in the form of opal crusts, and/or aragonite, and low-intensity alteration is characteristic of slight deposition of silica, also in the form of opal crusts. Active manifestations are depicted by hot soil and steaming ground (Franzson, 1990; Rodas, 1996).

The area from Svartsengi to the Reykjanes high-temperature field has been investigated using resistivity surveys, ranging from the original dipole, Schlumberger, TEM, MT and an integrated TEM-MT survey, which can detect anomalies to more than 10 km depth. Figure 5 shows the 4 Ohm low resistivity anomalies at 200, 400 and 600 m depths within the Svartsengi drill field, which indicate the top of the geothermal system from an early TEM survey (Georgsson, 1984). The resistivity structures show an overall NE-SW alignment around the Svartsengi field, however there is a clear structural trend that is slightly west of north within the central of the field, and which appears to extend towards Selhåls in the south. No apparent anomaly is observed around the steam cap in the north or below the hydrothermal alteration at the northern end of Svartsengisfell, which may indicate that that area there is at the outer periphery of the reservoir (Franzson, 2017).

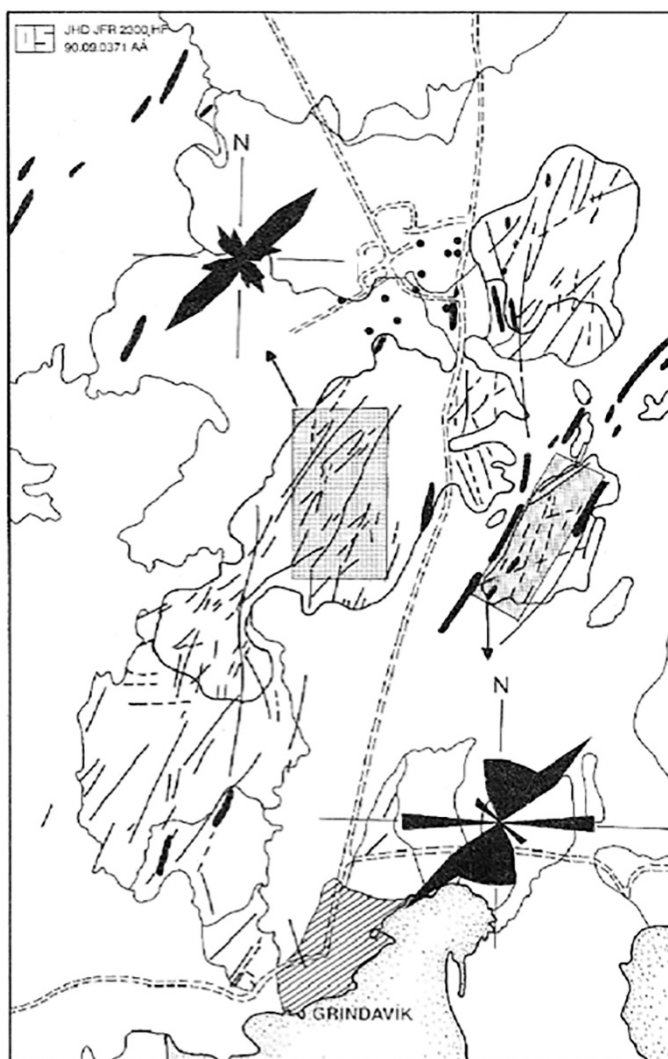


FIGURE 4: Tectonic lineaments around Svartsengi along with rose diagrams of fracture orientation deduced from ground study (Franzson, 1990; 1995)

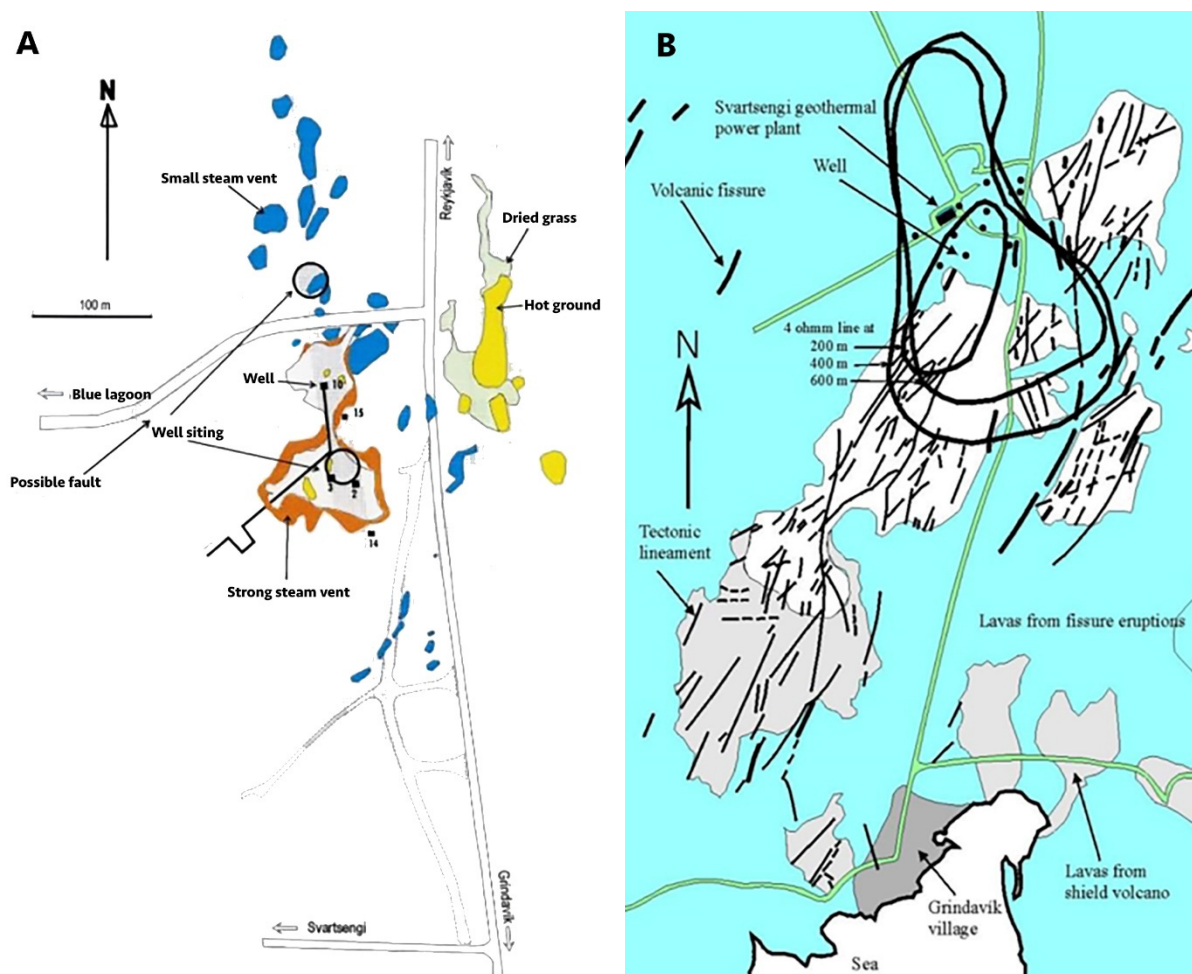


FIGURE 5: A) A sketch showing the surface features of the steam zone and the probable underlying tectonic lineaments that control the steam flow. B) Simplified geological map, tectonic lineaments and the shape of the shallow resistivity anomalies (Georgsson, 1984)

2. BOREHOLE GEOLOGY

2.1 Drilling well SV-26

Well SV-26 is a make-up and exploration well for the Svartsengi power plant (Figure 6). It was drilled from the same platform as SV-18. The well is located southeast of the power plant in Svartsengi. The planned depth of SV-26 was 2500 m or more. The final depth, however, was 2537 m. The location of well SV-26 and the well path is shown in Figure 6. Well head coordinates are: X = 331589.767 Y = 379078.146 Z = 24.6 m a.s.l. Drilling was planned towards the east to explore if the geothermal resource had an eastward extension. The aim was to drill a directional well through known faults within the southern part of Mt. Sýlingarfell in order to penetrate feed points to obtain maximum productivity in the well.

The planned design of well SV-26 and the division of the drilling into sections was as follows (Sigurdsson and Fridleifsson, 2015):

- Phase 0: Pre-drilling for surface casing with 26" bit to 100 m, cased with 22½".
- Phase 1: Drilling for anchor casing with 21" bit to 340 m, cased with 18¾".

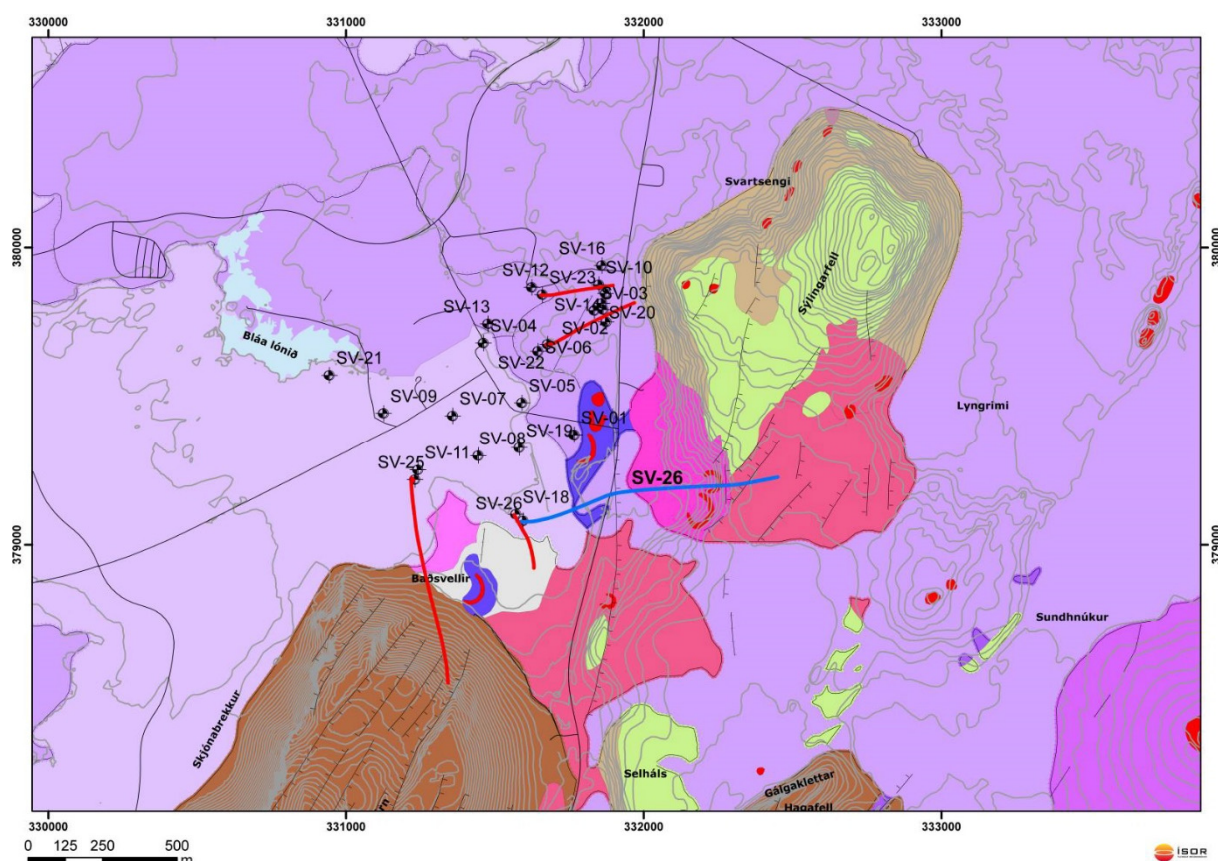


FIGURE 6: Geological map of the Svartsengi field (Saemundsson, 2015).
It shows the trajectory path (solid blue line) of well SV-26

- Phase 2: Drilling for production casing with 17½" bit to 1000 m, cased with 13⅜".
- Phase 3: Drilling of the production part with 12¼" bit to about 2500 m, cased with 9⅝" perforated liner (Weisenberger et al., 2016).

The actual well as drilled deviates from the planned well design by an additional hanging casing as seen in Table 1. The well was drilled in 5 phases (0–4). An overview of the drilling phases and details of the casing depths are shown in Table 1. Figure 7 shows the drilling progress of well SV-26.

TABLE 1: Drilling and casing depths in well SV-26. All drilling and casing depths are measured from the rig floor (RF) of the Thor rig, 9.0 m above the ground level, except for the pre-drilling phase where depths are measured from the rig floor of Saga, 2.0 m above ground level

Drill-rig	Phase	Depth (m)	Depth reference	Bit Size	Casing type	Casing depth (m)	Casing depth reference
Saga	Pre-drilling	100.6	Saga RF	26"	22½"	99.8 m	Saga-RF
Thor	1. phase	352	Thor RF	21"	18⅝"	351	RF
Thor	2. phase	886	Thor RF	17½"	13⅜"	873.5	RF
Thor	3. phase	1250	Thor RF	12¼"	9⅝"	805.8-1247.5	RF
Thor	4. phase	2536.6	Thor RF	8"	7" (liner)	1203-2532.2	RF

Drill rig Saga was ready for drilling of the pre-drilling (phase 0) on the 4th of July, 2015. Drilling with a 26" air hammer into formation commenced the same morning. The drilling went slowly due to collapses in the well, causing seven cement jobs during drilling. Drilling, casing, and cementing of phase 0 were completed on July 15th and the drill rig Saga was ready for transportation, after a total of

SV-26 - Drilling Progress

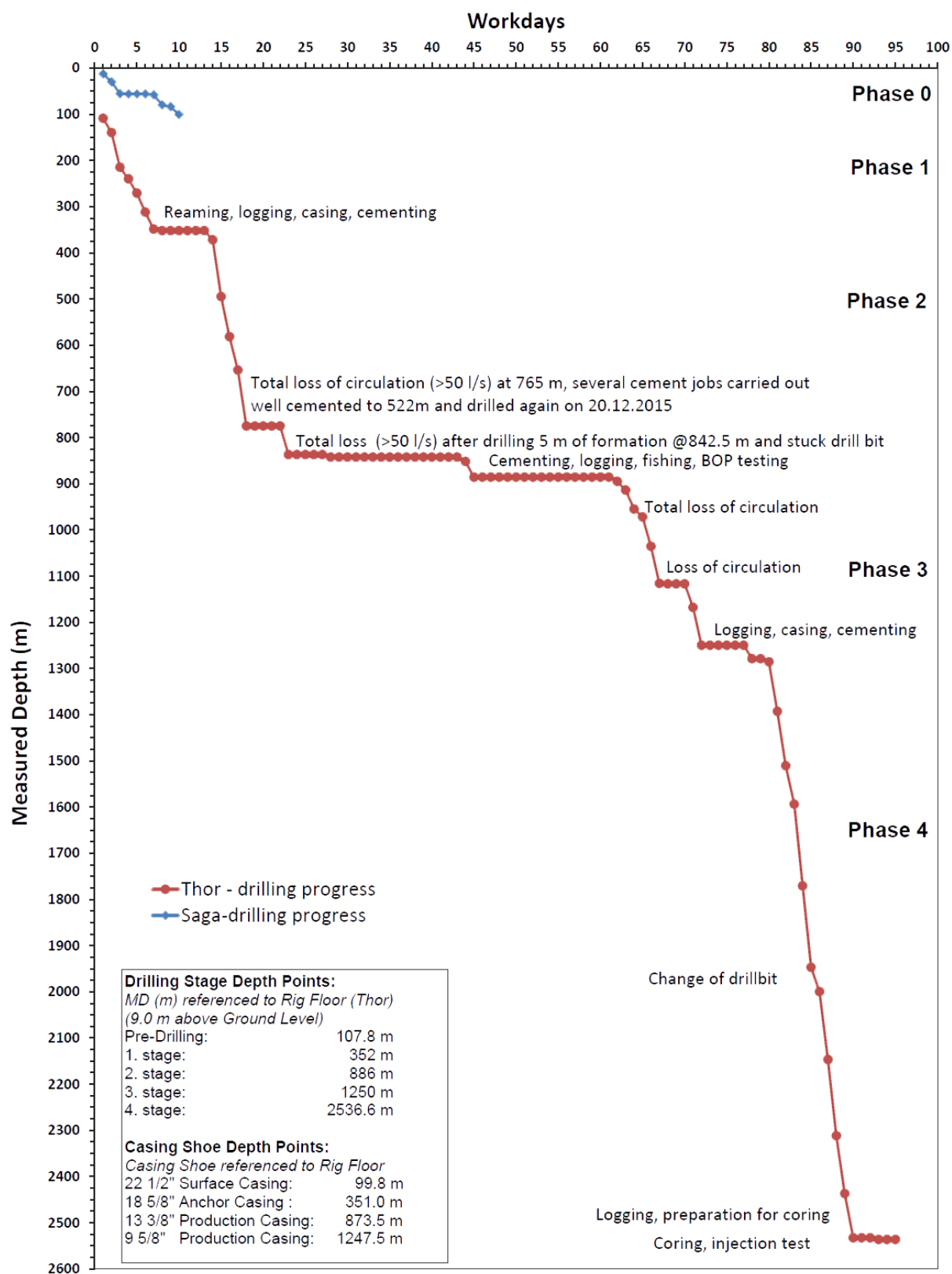


FIGURE 7: Drilling progress of well SV-26. Workdays of rigs Thor (red line) and Saga (blue line)

12 working days. At this point the well was 100.6 m deep from the rig floor of Saga, which corresponds to 107.8 m depth from the rig floor of Thor.

Preparation for the drilling of phase 1 with the drill-rig Thor started on November 29th with testing of the blow-out preventers. Drilling into a formation started the next day at 108 m. Phase 1 was finished on December 11th (workday 13 of Thor). An 18 $\frac{3}{8}$ " anchor casing was run down to 351 m depth with reference to the rig floor.

Drilling of phase 2 started on December 12th (workday 14), with testing of the blow-out preventers, and finished on January 16th (workday 49). Complications occurred during drilling of phase 2 due to repeated circulation losses in the well, resulting in 13 cement jobs. At a depth of 842.5 m the drill string got stuck on December 26th. It took 11 days to release the drill string, which occurred on January 5th. The well was drilled down to 886 m using rotary mud drilling method with a 17 $\frac{1}{2}$ " tri-cone drill bit and a 13 $\frac{3}{8}$ " production casing was run down to 873.5 m MD with reference to the rig floor of Thor. Cementing of the production casing was successful with total of 95.3 m³ cement slurry used.

Rig operations of phase 3 started on January 17th 2016 (workday 50). After the installation and testing of the blow-out preventers the drilling crew was ready to run in the bottom hole assembly (BHA) with a 12 $\frac{1}{4}$ " drill bit, motor and MWD. In the early morning on the 18th of January the elevator sprang open and parts of the BHA were lost in hole. The fishing procedures lasted for 8 days (January 18th to January 26th). Drilling into formation commenced on January 29th and was delayed by 2 total losses of circulations but drilling of phase 3 was completed on February 15th (workday 79) at a depth of 1250 m. A 9 $\frac{5}{8}$ " hanging casing was installed from 805.8 to 1247.5 m.

Rig operations on phase 4 started on February 16th 2016 (workday 80), with setting up and testing of the blow-out preventers. Drilling of phase 4 was finished on March 2nd (workday 95). The well was drilled down to a measured depth of 2534 m (with reference to the rig floor) using an 8 $\frac{1}{2}$ " drill bit. A total loss of circulation occurred at 1346 m and no cuttings were retrieved after 1394 m.

An attempt was made to drill a core on February 29th. However, coring had to be stopped after 3 meters of drilling at a depth of 2537 m, which is the final depth of the well but no core was retrieved from the core barrel. After the coring attempt, a liner was lowered into the well with the top of the liner being at 1203 m and bottom at 2532 m depth as measured from the rig floor.

2.2 Analytical methods

Binocular microscope

Rock cuttings at well SV-26 were sampled at an interval of 2 m. An Olympus binocular microscope was used to identify lithology, analyse grain size, oxidation, alteration minerals, veins, vein fillings and primary minerals. The analysis in the binocular microscope was done on wet samples to have clear visibility of any obscured features in the cuttings and acid was used to identify carbonates. An initial binocular microscope analysis was carried out at the drill-site but further detailed analyses were carried out at the ÍSOR labs in Reykjavík.

Petrographic microscope

The petrographic analyses are more accurate in determining the mineral assemblage of each stratigraphic unit and alteration mineralogy and was based on 11 thin sections selected from different depths. These were used to confirm rock type, texture, porosity, alteration minerals, alteration sequences and to identify additional minerals not seen in the binocular microscope. The petrographic analyses were also very helpful in identifying the alteration of primary minerals.

XRD analysis

The XRD analysis is a technique used to study crystallized materials based on the scattering of X-rays according to the crystal type of the material. The X-ray diffractometer analyses were carried out to

differentiate between various clay minerals. Each clay mineral group is characterized by a particular type of layer structure and interlayer material. Samples from SV-26 were collected and XRD analysed at ÍSOR XRD lab. The equipment used is a Bruker AXS D8 Focus, producing Cu α radiation with 1.54 Å wavelength at 40 kV and 40 mA. The detector used is a NaI scintillation counter. The samples are washed with distilled water to remove all dust or mud. After, about 2 g are put in a glass test-tube nearly filled with distilled water and put in a mechanical shaker for about four hours to separate the clay from the rock matrix. The suspended clay-slurry is left to settle for about 10 minutes and then transferred onto a glass-slide, using a pipette. The sample is left to dry in ambient temperature and humidity. Each sample undergoes three different treatments. First the sample is measured after complete drying (UNT, untreated). After the first measurement the sample undergoes a special glycol treatment inside a closed desiccator where it is left in the ethylene-glycol fume for 24 hours to see if the clay can swell or not, and then it is measured again (GLY, glycolated). Lastly, the sample is heated in a furnace for about 1 hour in 550°C and after cooling, measured again (HIT, heated). The set of three measurements is then viewed superimposed using special software for X-ray diffraction data display (Bruker, Diffra-Eva). Such analyses are useful in determining the alteration zones along with other index minerals found in binocular and petrographic analysis. The XRD analyses of clay minerals in well SV-26 are found in Appendix III.

Fluid inclusion analysis

The analysis offers direct information on the temperature during the formation of the hydrothermal minerals and was used in this report (along with the temperature of first appearance of alteration minerals and the formation temperature) for the interpretation of the thermal condition of the geothermal system. The examination is conducted by gradually heating up the sample using micro thermometry, to the homogenization temperature of the fluid inclusions, so that the bubble inside the fluid inclusions, trapped during crystallisation, disappears. Fluid inclusions were identified from specific depths and mostly quartz was selected for the fluid inclusion studies.

Interpretation of geophysical logs

Neutron logs: The physical basis of measurements of neutron logs is the scattering and capture of neutrons; the main purpose is to estimate the formation porosity (Steingrímsson, 2011). This is useful in the identification of intrusions, which are usually compact compared to the intruded rock formations.

Calliper log measures the diameter of the well as a function of depth using a logging probe with arms placed symmetrically around it (Steingrímsson, 2011). Indications of wider areas in the well can point to the locations of soft formations or fractured areas where the walls of the well are easily broken.

Resistivity logs: The specific resistivity of the reservoir rock is the result of two different contributions, the resistivity of the rock matrix and the formation fluid. An igneous rock matrix is generally a poor electrical conductor at geothermal temperatures (Mostaghel, 1999). Therefore, an igneous rock with considerable porosity or fluid filled vesicles will show rather low resistivity. The resistivity graph will show lower resistivity in the aquifer zones.

Gamma log measures the natural gamma radiation, used to determine the clay content in rocks. Investigations in Iceland show, however, that the gamma ray activity in volcanic rocks is related to the SiO₂ content of the rock and can, consequently, be used to identify rocks of evolved compositions (Mostaghel, 1999).

2.3 Stratigraphy of well SV-26

The lithology of well SV-26 corresponds well with the lithology model made by Franzson (2017). The model is based on cutting analysis from older wells in the Svartsengi area and shows how interglacial lava series are intersected by hyaloclastite horizons, including pillow basalt, breccia, tuffs and reworked tuffs. Due to total loss of circulation in well SV-26, no drill cuttings were retrieved below 1394 m. In addition, several gaps of cutting retrievals existed at shallower depths, due to loss of circulation during

drilling. Geological information below 1394 m depths is exclusively based on the geophysical logs and the drilling parameters. These correlate fairly well with Weisenberger et al. (2016). An overview of the lithology, alteration and alteration mineral distribution is shown in Figure 8.

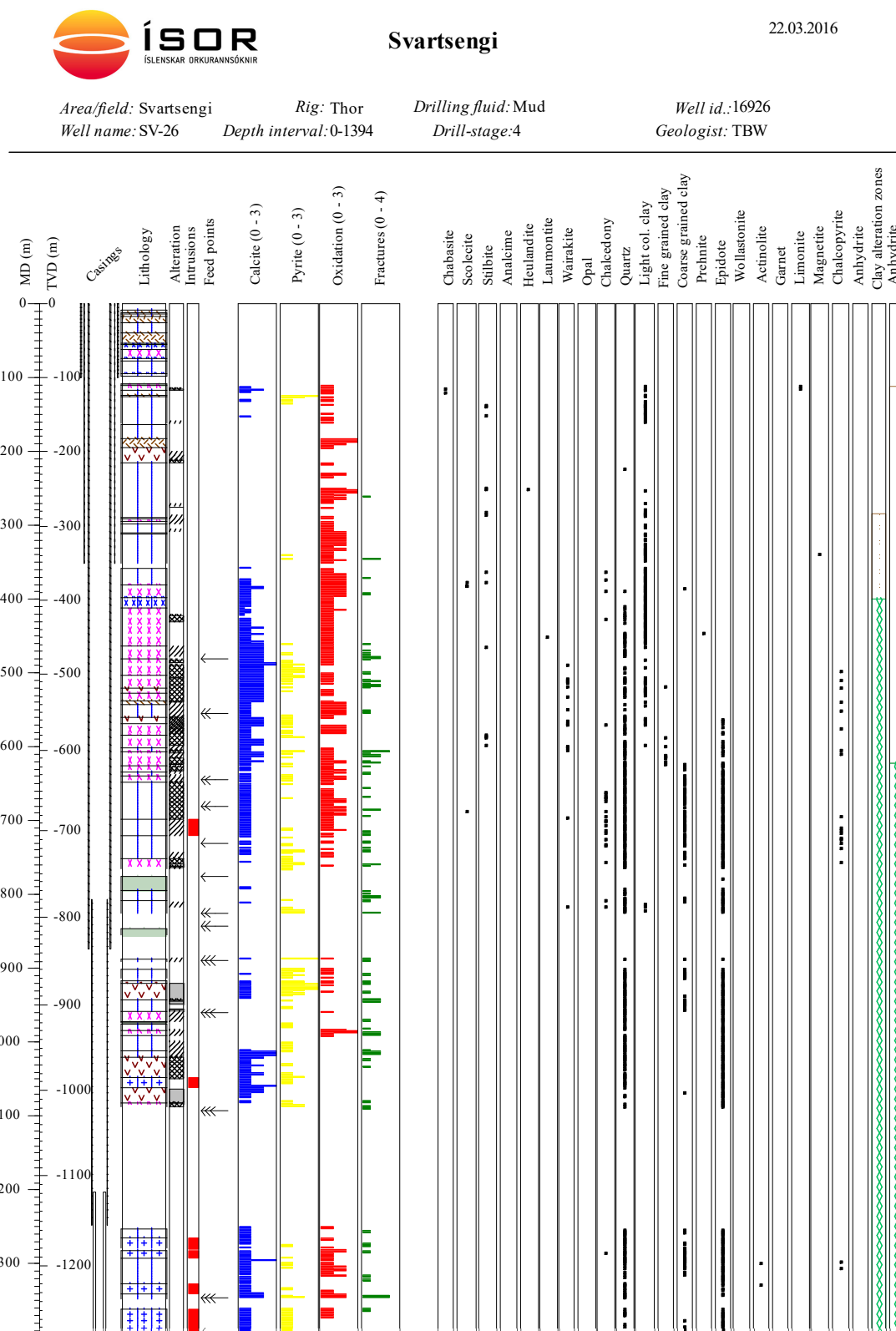


FIGURE 8: An overview of alteration and lithology in well SV-26 from 0–1394 m measured depth. Please include further explanation

8–10 m: Lava

Fine- to medium-grained well crystallized basalt. Occasional plagioclase micro-phenocrysts are seen. Grains are dark in colour, dense and fresh. Red scoria fragments are mixed in.

*10–12 m: No cuttings**12–14 m: Scoria*

Lava boundary. Mostly red and foam-like scoria grains observed. Tuff mixed in and broken plagioclase crystals.

14–18 m: Lava

Red scoria and tuff fragments with occasional light grey and fine-grained basalt.

18–26 m: Scoria

Scoria mixed with crystallized basalt grains.

26–40 m: Lava

Fine- to medium-grained light grey coloured and dense basalt grains. Few plagioclase and clinopyroxene micro-phenocrysts. Abundance of grains are crystallized and oxidized.

40–54 m: Scoria

Red and foam-like scoria. Crystallized basalt grains mixed in along with few tuff grains. Large plagioclase micro-phenocrysts.

*54–56 m: No cuttings**56–62 m: Pillow basalt*

Scoria and orange coloured grains mixed with cement.

62–74 m: Basalt breccia

Breccia formation. Increase in black, fresh tuff grains. Basaltic grains are very fine-grained and poorly crystallized. Occasional plagioclase micro-phenocrysts occur.

74–78 m: Pillow basalt

Less tuff grains than previous.

78–94 m: Lava

Abundance of euhedral pyrite crystals. Dark grey, medium-grained and plagioclase-rich basaltic grains. Some grains are somewhat porous and also green grains can be found. These are mixed with oxidized grains.

94–98 m: Pillow basalt

Glassy and porous grains containing green and yellow fillings. Fine-grained clay noticed and abundance of calcite. Cuttings are with occasional well-crystallized basaltic grains. Highly altered olivine micro-phenocrysts are noticed.

108–110 m: No cuttings

Only cement

110–118 m: Breccia

Basaltic breccia. Cement fragments are still present. Secondary minerals like calcite and limonite are found within pores. Fragments are slightly oxidized.

118–124 m: Lava

Fine-grained basaltic lava with olivine. Alteration minerals found inside pores include clays, thomsonite, and calcite. Upper part of the unit is slightly oxidized.

124–126 m: Scoria

Basaltic scoria. Highly oxidized, pores contain very fine-grained subhedral pyrite crystals.

126–162 m: Lava

Fine-grained plagioclase porphyritic basalt. Very vesicular and partially oxidized. Secondary pore filling minerals are few and including calcite, clays and stilbite. The lithology does not show any sign of alteration.

*162–164 m: No cuttings**164–182 m: Lava*

Fine-grained plagioclase porphyritic, slightly oxidized basalt. Limited amounts of secondary pore filling minerals are noticed. No signs of alteration.

182–194 m: Scoria

Basaltic scoria with foam-like texture. Highly oxidized.

194–216 m: Tuff

Greenish basaltic tuff. Shallower samples are mixed with scoria. The upper tuff units are unaltered, in contrast to the lower unit which shows signs of low to medium alteration.

216–290 m: Lava

Fine- to medium-grained basalt with very limited appearance of vesicles. Few secondary minerals are observed, including quartz, clay, zeolites (stilbite, scolecite). The middle part of the basalt formation shows strong oxidation (possibly 2 lava flows).

290–292 m: Breccia

Basaltic breccia, slightly altered.

292–294 m Lava

Fine- to medium-grained basalt. It is slightly altered and oxidized.

294–298 m: Breccia

Basaltic breccia, slightly altered and oxidized.

298–310 m Lava

Fine- to medium-grained basal. It is fresh and slightly vesicular. Vesicles are coated with clays.

310–312 m: Breccia

Basaltic breccia. Slightly altered and oxidized.

312–352 m: Lava

Fine- to medium-grained olivine-bearing basalt. It shows strong, grain selective oxidation. Alteration minerals are mostly clays which replace the olivine. Some pyrite is observed.

*352–358 m: No cuttings**358–380 m: Lava*

Fine- to medium-grained (sometimes almost glassy) basalt. It is quite dense. Olivine crystals are mostly oxidized or altered to clay. Oxidation is also prevalent in the groundmass. The main alteration minerals

are calcite and clay but stilbite and other zeolites are also found.

380–398 m: Breccia

Fragments with a variety of crystallinity, mostly porous tuff and fine-grained basalt. Increased alteration due to higher glass content. Variety of clays, unidentified zeolites, calcite and aragonite in few places.

398–412 m: Glassy basalt

Increase in crystallinity, more homogeneous and less porous and oxidized than above. Dark grey with few secondary minerals.

412–464 m: Breccia

Porous tuff, glassy basalt and fine-grained basalt. Quartz is often found below 410 m and in every sample below 448 m.

464–480 m: Breccia

A mixture of blue-green tuff and light-grey basalt. The tuff fragments have been partially oxidized and the pores and fractures are mostly filled with alteration minerals such as calcite, clay and quartz. The small pores in the basalt are mostly filled with dark green clay.

480–504 m: Breccia

There is an increase in the amount of tuff that appears to be white due to alteration. Rich in secondary minerals, but mostly calcite and quartz. Wairakite is found in fractures below 490 m. Minor fine-grained dark, plagioclase porphyritic basalt fragments are mixed in. The plagioclase phenocrysts show signs of alteration.

504–520 m: Breccia

Colourful, tuff-rich breccia, green, white and oxidized. Minor black, dense, fine-grained basalt.

520–528 m: Tuff

Greenish tuff cemented together, mostly with calcite.

528–538 m: Breccia

Same tuff as above mixed with dark grey dense, plagioclase porphyritic, fine-grained basalt that is slightly oxidized.

538–542 m: Scoria

Oxidized and porous glassy, scoria. Top of lava.

542–560 m: Lava

Grey, fine-grained rather dense and fresh basalt. Small amounts of alteration minerals. The cuttings have much sharper edges.

560–568 m: Tuff

Greenish tuff with white secondary minerals. Mainly calcite, quartz and possible wairakite. Green fine-grained clay is found in pores. Pyrite is observed in small amounts. Epidote appears for the first time at a depth of 564 m.

568–582 m: Breccia

Greenish tuff with light-grey and dark fine-grained basalt. Some of the fine-grained basalt fragments are oxidized. Some zeolites are found in pores but other are being transformed into other higher temperature alteration minerals.

584–602 m: Breccia

Basaltic breccia. Fine-grained breccia that consists of dark-brownish fine-grained basalts and greenish

altered tuff fragments. Rich in secondary minerals (calcite, stilbite, clays, zeolites).

602–606 m: Lava

Fine-grained basalt. Fine-grained basalt with lots of vesicles, which appears to be partially glassy. The cuttings are coarser grained than previous samples. Minor greenish altered tuff is mixed in. It is rich in secondary minerals, which include zeolites and quartz (euhedral). Several small fracture fills are observed.

606–626 m: Breccia

Very heterogeneous basaltic breccia. Fine-grained breccia that consists of dark-brownish fine-grained basalt that often are highly vesicular and greenish altered tuff fragments. Fragments are slightly altered and oxidized. Olivine phenocrysts are altered to clay minerals. Secondary minerals include calcite, zeolites, quartz, clays, pyrite, and epidote. Rich in fractures filled with secondary minerals.

626–634 m: Breccia

Very heterogeneous basaltic breccia. Fine-grained breccia that consists of dark-brownish fine-grained basalt which often are highly vesicular, greenish altered tuff fragments, and light coloured small- to medium-grained crystalline olivine-bearing rock fragments.

634–640 m: Lava

Fine-grained basalt. Plagioclases porphyritic in places, vesicular and slightly oxidized, pores are filled with secondary white minerals. Small amount of light coloured fine-grained fragments that contain plagioclase and olivine phenocrysts of variable alteration degrees. White secondary pore filling minerals and epidote.

640–648 m: Breccia

Very heterogeneous basaltic breccia. Fine-grained breccia that consist of dark-brownish, fine-grained basalts that often are highly vesicular, greenish altered tuff fragments, and light coloured fine- to medium-grained crystalline rock fragments, that contain fresh to altered olivine.

648–698 m: Lava

Fine-grained basaltic lava. Medium- to strongly-altered, light-dark, slightly reddish, very fine-grained olivine-bearing basalt. In parts plagioclase porphyritic. Appears to be massive, but vesicles and pore space appear irregular in higher quantities. Low-degree of oxidation is observed throughout the unit, whilst the oxidation is patchy and not homogenously distributed within the rock. Very rich in epidote (present in every sample). Additional secondary minerals include calcite, quartz (including euhedral quartz) and clays.

698–720 m: Lava

Fine- to medium-grained basaltic lava. Similar lava fragments as within the lava unit above, but mixed with minor, non-altered medium-grained dark basalt fragments. Rich in epidote and quartz (both euhedral and anhedral).

720–752 m: Lava

Unaltered fine- to medium-grained basalt. Lava unit is coarser-grained than previous unit. Basalt fragments are dark and unaltered. Only limited pore space, but most of the pores are lined with epidote and quartz. Epidote also occurs as replacement phase of primary minerals. Additionally, pyrite, chalcopryrite and chlorite occur. At a depth of 732m, large (1 cm) quartz aggregate with disseminated pyrite are observed.

752–765 m: Breccia

Mixture of quartz aggregates with disseminated pyrite (euhedral and anhedral), highly altered basalt and fine- to medium-grained fresh basalt fragments. Cuttings are large (up to 5 mm) and individual fragments are semi-rounded. At 765 m a total loss of circulation happened.

765–766 m: *No cuttings*
Loss of circulation.

776–794 m: *No cuttings*
Cement only.

794–808 m: *Lava*
Fine-grained basalt: dark fine-grained basaltic lava. Relatively massive with only limited pore space. Epidote is the dominant secondary mineral, with minor quartz and pyrite. Several small mineralized fractures.

808–826m: *Lava*
Fine- to medium-grained basalt. It is coarser-grained than previous lava unit. Epidote is the dominant secondary mineral. Additional quartz and pyrite appear in the deeper parts of the unit in larger quantities. Several small mineralized fractures.

826–888 m: *No cuttings*
Loss of circulation.

888–890 m: *Lava*
Fine-to medium-grained basalt. The slightly greyish cuttings are slightly altered and oxidized. They contain a large amount of pyrite. Olivine phenocrysts are altered to clays/chlorite. Additional secondary minerals are quartz, epidote, chlorite, and calcite. Thereby pyrite and quartz are associated as disseminated pyrite in quartz. One quartz fracture was detected.

890–902 m: *No cuttings*
Loss of circulation

902–914 m: *Lava*
Fine-to medium-grained basalt. The slightly greyish cuttings show a slight sign of alteration and oxidation. Olivine, which occurs sparsely, is altered to chlorite. The unit contains a high content of pyrite, whereas pyrite is often disseminated within whitish quartz fragments. Additional secondary minerals are epidote, chlorite and calcite. One fracture fill with epidote was detected at 908 m. Cutting fragments get finer with increasing depth.

914–917 m: *No cuttings*

917–920 m: *Lava*
Fine-to medium-grained basalt. The slightly greyish cuttings are slightly altered. Secondary minerals include quartz, pyrite and epidote.

920–942 m: *Tuff*
Highly altered whitish to slightly greenish hyaloclastite. It contains a very high amount of quartz fragments that are disseminated with pyrite. In addition, minor massive pyrite aggregates are found. Some minor oxidized grains occur within the upper part of the stratigraphic unit. Upper cutting samples of this unit are mixed with fine- to medium-grained basalt, whereas the basalt content decreases with depth. Secondary minerals include quartz, pyrite, epidote, and minor calcite.

942–958 m: *Lava*
Fine-to medium-grained basalt. Sharp contact with the previous basaltic tuff unit. The slightly greyish to brownish cuttings are slightly altered on top of the stratigraphic unit. Cutting samples contain a high content of epidote. Additional secondary minerals are minor quartz, pyrite, and chlorite. Hyaloclastite grains are mixed in variable concentrations.

958–974 m: Breccia

Basaltic breccia. Fine-grained cuttings that consist of similar proportions of fine-grained basalt and basaltic tuff fragments. The whitish basaltic tuff is highly altered, whereas the brownish to reddish basalt fragments are only slightly altered. It contains a high content of epidote. Additional quartz and chlorite are present.

974–976 m: No cuttings

Only cement

976–984 m: Lava

Fine-grained basalt. It is slightly altered and grains are slightly reddish in colour. Some grains are highly vesicular and vesicles are in general totally filled with secondary minerals. Epidote is the dominant alteration mineral. In addition, quartz occurs in variable quantities. Pyrite is found in the upper part of the unit. Minor amount of altered basaltic tuff fragments is found.

984–990 m: Breccia

Highly oxidized basaltic breccia. Very heterogeneous unit that is composed of reddish fine-grained and altered components, darkish only slightly altered fine-grained basalt fragments that are sometimes vesicular. Epidote is found in minor amounts.

990–1012 m: Lava

Fine- to medium-grained basalt. The crystalline and massive basalt fragments which are slightly altered are very bright and greyish and whitish in colour. With depth the cutting colour is getting darker. Rich in epidote and quartz, which is also found as fracture fill. Additionally, pyrite is found in minor amounts. Small amounts of oxidized fragments are mixed in. Sample at 1008 m has a high content of epidote and quartz.

1012–1020 m: Lava

Fine- to medium-grained basalt. Similar to the unit above. But in addition it contains a high content of whitish mono-mineral calcite.

1020–1048 m: Hyaloclastite

Whitish to greenish basaltic tuff. Glass fragments are greenish and are only slightly altered. Glass fragments are semi-rounded and sit within a whitish matrix. It contains a high content of secondary minerals, including epidote (euhedral in places), quartz, and calcite. In addition, pyrite occurs in small amounts. Minor amount of basaltic lava fragments is mixed in.

1048–1062 m: Intrusion/dike

Medium-grained basalt. Fresh, crystalline basalt that is black in colour. Minor amounts of secondary minerals, including epidote, quartz, calcite and pyrite.

1062–1082 m: Hyaloclastite

Basaltic tuff. Whitish to slightly greenish basaltic tuff. In contrast to the previous basaltic tuff, the cuttings are finer-grained and the fragments are highly altered. It contains a high content of secondary minerals, including epidote (euhedral in places), quartz, calcite, and chlorite.

1082–1088 m: Breccia

Basaltic breccia that consists of basaltic tuff fragments and slightly reddish fine-grained basalt fragments. Fragments are in general altered and epidote occurs frequently as a major alteration product. Additional pyrite (incl. euhedral pyrite) is found in higher quantities. Cuttings are coarser-grained than hyaloclastite unit above.

1088–1252 m: No cuttings

Loss of circulation

1252–1564 m: Lava

Fine to medium-grained fresh basaltic lava. Fresh holocrystalline and massive basalt, which is slightly reddish to greyish in colour. It contains some minor amounts of oxidized grains. Upper part of the unit is mixed with cement fragments. Epidote and quartz occur in large quantities, and euhedral crystals are also common. Additional chlorite aggregates are found and minor calcite.

1264–1279 m: Possible intrusion/dike

Medium-grained fresh basalt. Fresh holocrystalline and massive basalt, which is very dark (blackish with a reddish tint) in colour that marks a sharp colour contact with the previous lava unit. Oxidized grains are found sporadically and particularly in the deeper part of the unit. Minor cement fragments are present. Upper part of the unit is mixed with cement fragments. Epidote and quartz are the dominant secondary minerals, but occur in much lower amounts.

1279–1282 m: No cuttings

Only cement

1282–1292 m: Possible intrusion/dike

Medium-grained fresh basalt. Holocrystalline, massive basalt, which is grey in colour and has a reddish tint. It is fresh but shows a higher degree of oxidation, whereas the oxidation decreases with increasing depth. Minor cement fragments are present. Epidote, quartz and chlorite are the dominant secondary minerals with minor calcite being present. Within the lower part of the unit, minor large (> 3 mm) whitish aggregates are observed, which contain black inclusions that show a preferred orientation.

1292–1326 m: Lava

Fine- to medium-grained fresh basalt. Massive basalt with minor vesicles within the upper part of the unit, and occasionally vesicles are observed in samples within the lower unit. It is dark-greyish and the individual depth intervals are slightly oxidized. Epidote, quartz and chlorite are the dominant secondary minerals with minor calcite. In the sample at 1298 m a dark, slightly greenish secondary fibrous mineral is found that forms a radiating aggregate around quartz (possible actinolite). Occasionally minor pyrite is observed. The content of secondary minerals decreases with increasing depth. Minor large (> 3 mm) whitish aggregates are observed, which contain black inclusions that show a preferred orientation.

1326–1340 m: Possible intrusion/dike

Medium-grained fresh basalt. Holocrystalline, massive basalt, which is dark-greyish to black in colour. Very limited content of secondary minerals that includes epidote, quartz, and calcite. Chlorite is the dominant secondary mineral with minor calcite being present. Minor large (>3 mm) whitish aggregates are observed, which contain black inclusions (actinolite?) that show a preferred orientation.

1340–1348 m: Lava

Fine- to medium-grained basalt. The fresh basalt is dark-greyish in colour and contains numerous deep-red totally oxidized fragments, where the dark-greyish fragments do not show any sign of oxidation. Secondary minerals include epidote, quartz, calcite and pyrite.

1348–1362 m: No cuttings

Total loss of circulation

1362–1394 m: Possible intrusion/dike

Medium-grained basalt. The fresh and massive holocrystalline basalt is dark-grey in colour, whereas minor variations (greenish and reddish) are observed. Small amounts of fine-grained basalt fragments are present in variable proportions. Secondary minerals included epidote, quartz, calcite, and pyrite. Minor large (mm—size) whitish aggregates are observed within the upper part of the lithological unit, which contains black inclusions that show a preferred orientation.

1394–2537 m: No cuttings

Total loss of circulation

2.4 Intrusions

Intrusions are emplacements of magma into pre-existing rocks. As the subterranean magma slowly cools it gives time for the crystals to grow thus, they usually show relatively coarser textures compared to the host rock. Intrusive rocks are characterized by their massive, compact nature and appear fresh in comparison to the surrounding lithology, and are sometimes marked by oxidation near their margins (Worku, 2012).

No intrusions were observed above 1000 m depth in well SV-26, except at the depth interval between 698 and 720 m where a lava unit contained fresh medium-grained basalt fragments, which may indicate the presence of dikes/feeder-dikes. In contrast, several possible intrusions and/or dikes have been detected in deeper parts of the well (1048–1062, 1264–1279, 1282–1292, 1326–1340, and 1362–1394 m). This approximately coincides with the depth interval from 1100 to 1300 m that is well known for high amounts of intrusions within the Svartsengi geothermal field (Franzson, 1990). However, a lack of drill cuttings below 1300 m from most wells in Svartsengi, results in limited knowledge of locations of intrusions at greater depths (Gudjónsdóttir et al., 2015).

Spikes in the gamma log which often also show in the neutron and resistivity logs can be markers of possible intrusions. This are indicative for evolved rocks that are low in porosity. This is noticed at following depth intervals: 1420–1440, 1540, 1560–1580, 1740, 1755, 1780, 2120–2140, 2180–2235, and 2310–2400 m.

2.5 Geophysical logs

Geophysical logs (Weisenberger et al., 2016) for each phase can be found in Appendix I (Figures 1-4).

Phase 1

Temperature log. Maximum temperature measured was about 60°C and as no loss of circulation had been reported and no indication of feed zones is noted in the temperature log.

XY-calliper log. The log shows a cave from 200–215 m depth which is associated with the tuff horizon at similar depth.

Resistivity log. The small peaks in resistivity at 215–250 m correlate with a fresh, massive basalt lava formation.

Neutron-neutron log. Is rather flat and does not reveal any details in a well of this wide diameter and full of thick mud.

Phase 2

Temperature log. Shows a small step in temperature at 480 m and larger step at 550 m. Both steps indicate an inflow into the well. The water table is located at shallower depth (430 m), as indicated by the neutron and gamma logs as well as the resistivity log. A small pivot point appears at 640 and coincides with a previously reported feed point, but a large amount of the injection (and the inflow) flows towards the bottom of the well and flows out of the well at 860–870 m depth.

XY-calliper log. Shows large variations of well diameter along the depth interval. In general, it seems that the washout is higher within the hyaloclastite formations than in the lava formations. A large caving is located between 550 and 590 m. This coincides to a hyaloclastite formation with thin lava formations both above and below the hyaloclastite. A possible intrusion was logged at around 700 m. The calliper log shows a resistant unit at similar depth and as well as small caving structure below and above the intrusion. Within the lowest part of the well the calliper log shows a sharp contraction at 850 m within

a clear washout zone above from 825 to 850 m. At similar depth a loss of circulation occurred and the drill bit got stuck several times.

Neutron-neutron log. Can be divided in a shallower interval down to about 600 m and a deep interval below. The transition is marked by a sharp increase in neutron count rate at 600 m, indicating lower porosity rocks. Above 600 the lithology is characterized by a hyaloclastite formation and higher porosity. Small spikes in the neutron log within the hyaloclastite formation are probably associated with brecciated layers and/or basaltic dikes within hyaloclastite. A sharp peak neutron log at 540 m that coincides with the upper contact zone of an intercalated lava flow within the hyaloclastite formation. The abrupt increase in the neutron log at 600 m is not directly associated with a significant change in lithology according to the drill cuttings. The formation boundary of the hyaloclastite and lava formations is at 648 m. However, the lower part of the hyaloclastite formation (> 600 m) contains intercalated lava units. This transition zone from the hyaloclastite to the lava formation is possibly associated with the sharp increase in the neutron log. Below 750 m the neutron logs shows a large scattering, which may reflect the brittle formations within the graben structure.

Gamma log. Shows an increase at 650 m and coincides with a postulated change in alteration to the epidote alteration zone.

Resistivity log. Shows a low-resistivity cap within the shallow depths down to about 640 m. The increase in resistivity at 650 m coincides with the appearance of epidote, which starts to occur in every sample below 634 m. The appearance of epidote and the increase in resistivity are an indication for the transition of the mixed layer clay alteration to the chlorite-epidote alteration zone at the depth around 640 m.

Phase 3

Temperature log. The logging program started with a pumping rate of $Q = -15$ L/s. The flow screened the feed zones at 900 and 950 and a good feed zone is clearly seen at s 1090–1100 m. The well is relatively tight below 1100 m but the temperature log shows a minor down flow in the well towards feed zones at 1235 m. Maximum temperature showed about 110°C at 1245 m. At 1090 m depth a total loss of circulation occurred. This took place in a basaltic breccia formation where epidote occurs frequently as a major alteration product, in addition to quartz, calcite, and chlorite. Abundance of pyrite was also found in the cuttings just before the loss.

XY-calliper log. It shows wash-out, even caving, below the casing which was set at 873.5 m depth. The well was rather elliptic down to about 985 m, but less elliptical from there on and down hole. However, at about 1090 m a clear, moderately narrow, yet substantial wash-out is observed, correlating to the fracture causing the total circulation loss observed at this depth and quite possibly a fault zone, indicated by the abundance of high-temperature alteration minerals and pyrite/calcite.

Neutron-neutron, gamma and resistivity logs. NN and gamma logging was measured to a depth of 1235 m. The gamma log shows clearly that the rock formations so far penetrated are of a basaltic geochemical composition. The NN and resistivity correlate fairly well, for example at the interval between 940–980 m, which consists mostly of basaltic lavas and some breccia, followed by highly oxidized breccia, which again is followed by lava down to about 1020 m and subsequently hyaloclastite rocks. From 1090 m depth no cuttings are available and it is hardly possible to interpret the geophysical logs according to rock formation. However, there do not appear to be any intrusive rocks from 1090–1235 m depth.

Phase 4

Temperature log. Shows major inflow at 1346 m depth, same depth as the TLC happened and minor inflow at 1450 m. The log shows some flow out of the well at 2120 and 2250 m, but the main outflow is at 2430 m about 100 m above the bottom. At this depth the drilling parameters indicate the penetration of a fault. The temperature profile indicates that practically no down flow continues past the feed zone at 2428 m indicated by the temperature rise from ~50°C at 2400 to ~150 at 2500 m.

The XY-calliper. A major cave is at 2060 m depth but there is no sign of a feed zone at this depth according to temperature logs. Additional small caves are identified at 1346, 1550, 1580, 1650, 1900, 2210, 2380, 2428 m depth.

Gamma log. Shows only limited variations. Gamma peaks appear at depth of 1420, 1440, 1540, 1560, 1580, 1740, 1755, 1780, 2120–2140, 2180–2235 and 2310–2400 m and may indicate lithological units with higher gamma radiation and may reflect higher fractionated dikes or intrusions.

Neutron-neutron log. Shows only minor variations. Notable is the high neutron count in the depth interval from 2235 to 2310 m, which may reflect a lower porosity layer in between the dike/intrusions above and below this depth interval. Further small peaks within the neutron log are observed, which often coincide with peaks of the resistivity logs and may reflect thin, low porosity layers.

Resistivity log. The resistivity curves show a gradual increase with increasing depth from about 10 Ωm to about 60 Ωm for the 64'' log. The oscillation of the resistivity logs and the location of observed peaks (e.g. at depth of 1320, 1540, 1580, 1870, 2250 and 2350 m) mimic peaks observed also in the neutron log.

2.6 Hydrothermal alteration

A summary of the distribution of alteration minerals in well SV-26 is presented in Figure 8. A regular progressive hydrothermal alteration with increasing depth was noticed from the alteration mineral assembly in well SV-26 (Table 2). Such depth and temperature controlled mineral alteration zoning is well known in Icelandic hydrothermal systems (Kristmannsdóttir and Tómasson, 1978; Franzson 1998; Weisenberger and Selbekk, 2009). Low-temperature minerals, like fine-grained clay and zeolites occur at shallower levels, whereas high-temperature minerals, like epidote and coarse-grained clay appear at deeper levels in the well. The production casing is located at 1250 m and based on the mineral assembly, the production casing was extended well into the geothermal reservoir, with abundance of epidote (> 230–250°C) noticed in cutting samples at that depth. Epidote was first observed at 564 m depth, whereas below 626 m epidote was frequently observed in the majority of the cutting samples. In samples at 1298 m and 1328 m, a fibrous dark greenish mineral has been observed, but due to the very small grain size there is still unclear whether it is actinolite or not. No drill cuttings were available for analysis below 1394 m depth due to total loss of circulation.

TABLE 2. An overview of the depth of occurrence of alteration minerals in SV-26

Alteration mineral	SV-26 (m)
Calcite	112
Zeolites appear	116
Quartz	390 (224)
Wairakite	490
Epidote	564
Low-T zeolites disappear	584
Actinolite*	1298
*uncertain	

The upper boundary of cap-rock of the geothermal reservoir is found at about 380 m in well SV-26. This is at about the same depth as in well SV-25 (360 m) (Gudjónsdóttir et al., 2015). However, the shallower cap-rock formation does not show any sign of alteration but alteration suddenly appears at a depth of about 465 m. Increased calcite content is observed at depths below 380 m (Figure 8). High oxidation was noticed in the drill cuttings from SV-26. The oxidation was especially noticed in the upper 700 m of the well, associated with lava formations, breccia and pillow basalts (Figure 8). Within

the depth interval between 700 and 1100 m, only limited oxidation was observed. However, at the depth interval between 1280 and 1370 m the lithological units show a high degree of oxidation again.

2.6.1 Primary rock minerals in SV-26

Primary minerals are rock forming minerals that form during rock crystallization. The minerals form in a sequence or in sequential groups as detected by the chemistry and physical conditions under which the magma solidifies and it is essential for the classification of the rock. Primary minerals tend to alter and form secondary minerals at conditions of high temperatures, high permeability and fluid activity in a hydrothermal environment (Franzson, 1998; Gebrehiwot, 2010). Hyaloclastite and basaltic lavas are the main rock types throughout well SV-26, and they are mostly composed of volcanic glass, olivine, plagioclase, pyroxene and opaques as the primary minerals.

Volcanic glass is an amorphous (uncrystallised) product formed during the quenching of magma. Glass has low resistance to alteration compared to primary minerals. In well SV-26, clay, smectite and calcite are the common alteration minerals of glass.

Olivine is formed in basaltic rocks. It is the second most vulnerable to alteration after glass. In thin section it is distinguished by its high birefringence, distinctive irregular fracture pattern, lack of cleavage, and its parallel extinction. Along its fractures, the alteration products are usually clay, calcite and chlorite.

Plagioclase is the most abundant primary mineral in igneous rocks. It is easily identified in thin section by its low relief, maximum interference colours are usually first-order grey or white, and twinning distinguishes plagioclase from most other minerals. (Mnzava, 2014). As temperature increases it is progressively altered to clay, calcite, albite, quartz, wairakite, chlorite and epidote.

Pyroxene minerals are significant components of many intermediate and most mafic igneous rocks. Pyroxene is black or dark green in colour and forms prismatic crystals with vitreous lustre and perfect cleavage. Extinction at an inclined angle distinguishes it from olivine as well as its apparent cleavage and light brown colour in plain polarized light.

Opaque minerals do not transmit light in transmitted light microscopes. They are usually magnetite (oxide mineral) in basalt. These minerals were hardly altered throughout the well although often there were signs of oxidation on their edges.

2.6.2 Hydrothermal alteration minerals

Hydrothermal alteration is very informative on various aspects of the geothermal system. It designates the reaction between the reservoir rock and the circulating geothermal fluid, resulting in compositional changes of both the solid and fluid phase as the interaction between rock and fluid usually involves additional and/or removal of major rock-forming components. The factors that usually control alteration in geothermal systems are temperature, rock type, permeability, fluid composition and the duration of fluid-rock interactions (Browne, 1978).

Phase 1

Within the shallow zone of drilling phase 1 (108–352 m) the alteration is very limited and where it appears, it is associated with formation boundaries. Secondary minerals are observed predominantly in the vesicle-rich units. Thereby, clays and various zeolites (stilbite, scolecite, thomsonite) are dominant secondary minerals, with minor calcite, limonite and pyrite, which only occur at limited depth intervals.

Phase 2

Within drilling phase 2 (352–886 m) the secondary mineral inventory is in general higher, but the content depends on the availability of primary pore space. In general, calcite appears throughout the

entire section of drilling phase 2. Zeolites, such as stilbite and scolecite, are found in the lava sequence (< 380 m). They become less frequent in the hyaloclastite formation below the lava formation, which is the cap-rock of the hydrothermal system. Quartz is first detected at a depth of 390 m (beside a single appearance at a shallower depth of 224 m), (Table 2) and implies an alteration temperature increase with depth (180°C). Other secondary minerals include clays, both as fine-grained clay lining in pores and bright-green coarse-grained clay in pores and chalcedony. Zeolites are still found at 458 m but they seem to be overgrown by calcite and quartz. The secondary minerals change with increasing depth and therefore higher formation temperatures can be expected during formation of the secondary minerals. Low-temperature zeolites are rarely seen apart from around 570–584 m, where stilbite seems to be transforming into another secondary mineral, possibly quartz. Wairakite was first spotted at 490 m depth which suggests a formation temperature of about 200°C. In the same sample, big plagioclase phenocrysts showed some alteration. This is the exact same depth at which plagioclase alteration was first observed in well SV-18 (Richter et al., 1999). Below 600 m clays and quartz (including euhedral quartz) occur in variable contents. In addition, pyrite disseminated within quartz was observed at depths of 614 and 622 m. The occurrence of disseminated pyrite within quartz is most likely associated with a fracture zone, and may be associated with the appearance of fault A (Figure 9). Epidote (230-250°C) was first observed at a depth of 564 m and below 634 m epidote is found in more or less every sample within drilling phase 2 and throughout the entire section below, where cuttings were retrieved (< 1394 m). Below 600 m, clays appear coarse-grained. However, the clay content seems to be highly variable. The occurrence of disseminated pyrite within quartz that is found at around 750 and 820 m in large quantities is noticeable. At both depths drilling subsequently resulted in a total loss of circulation. This indicates that the fracture zones are located at these depths.

Phase 3

Within drilling phase 3 cuttings were only received between 886 and 1088 m, due to a total loss of circulation. The inspection of alteration minerals indicates that epidote is the dominant alteration mineral. Calcite and chlorite appear in minor quantities. In addition, disseminated pyrite within quartz is observed often at discrete depth intervals (e.g. between 920 and 942 m) and may indicate the penetration of a larger fault during drilling. However, particularly in the depth interval between 700 and 950 m, pyrite is quite common, whereas a significant decrease is observed below 950 m.

Phase 4

The alteration mineralogy is dominated by the high amount of epidote and quartz. Thereby, the content of both minerals is higher in the lava flow unit than in the possible intrusion/dike. Minor amount of chlorite and calcite is found. At a depth of 1278 m some sulphide minerals are observed. In sample 1298 m and 1328 m a fibrous dark greenish mineral has been detected, but due to the very small grain size there is still unclear, whether it is actinolite.

2.6.3 Alteration mineral zonation

Alteration zones refer to the secondary minerals forming and dominating at a certain range of depth within the hydrothermal system, giving clues regarding the formation temperature. Alteration mineral zonation can differ from one geothermal system to another depending on the parent rock, the chemistry and temperature of the area. Icelandic geothermal systems are dominated by basaltic rock formations. From the group of alteration minerals identified in this study, and with respect to their temperature of formation and sometimes the contradictory XRD clay analysis, the alteration zones in well SV-26 will be presented in two separate ways as follows:

1. Zonation depending on the distribution of alteration minerals.

- a. *Unaltered zone (0-112 m)*; this zone is mainly comprised of surface alteration minerals forming from cold groundwater with temperature ranging from 0 to 40°C.
- b. *Smectite–Zeolite (112-622 m)*; defined by the first appearance and abundance of smectite clay where at a depth of 82 m it was identified by petrographic analysis in a slight amount (considered as first appearance), confirmed by the XRD analysis at 94 m. Temperature for the

formation of smectite clay is less than 200°C.

- c. *Chlorite – Epidote (622-1394 m)*; Epidote was first spotted at 564 m but only below 634 m as crystalline epidote.

2. Zonation depending on clay analysis.

Twenty-one samples were chosen for XRD-analysis to locate the transition from smectite, mixed-layer clays and chlorite within the well. X-ray diffractions results (Table 3, Appendix III) indicate that above 400 m smectite is present as the dominant clay mineral. The appearance of mixed-layer clay is detected in a sample at 452 m, indicative of a temperature increase. Analysed samples from depths 506, 566, 600, 678, 758 and 816 m show that chlorite is present. The sample at a depth of 604 m shows that chlorite and mixed-layer clays are both presented. Appearance of mixed layer clay before the chlorite at 452 m is odd because it forms below the chlorite. This could indicate fluctuations in the temperature condition of the geothermal system. This may be caused by cutting mixing or disequilibrium within the hydrothermal system. Based on the XRD analysis two mineral zones can be defined. A smectite zone from 284 to 400 m and a chlorite-mixed layer zone between 400 and 1380 m.

TABLE 3: Results of a XRD analysis of clays in SV-26

Sample	Depth (m) (MD)	d(001) OMH Å	d(001) GLY Å	d(002) Å	Type	Remarks
#01	284	13.74	13.84	10.18	SM	
#02	330	13.1	16.5	9.9	SM	
#03	340	12.80	13.59	10.01	SM	
#04	400	12.72	13.44	9.92	SM	
#05	452	12.90/14	14.2	10/12.4	MLC	Peak at 30.1 Å
#06	506	14.59	14.24	7.25	Chl	Unstable chlorite
#07	558	14.4	14.7	9.9	MLC	Peak at 30.9 Å
#08	566	14.68	14.68	7.25	Chl	Unstable chlorite
#09	600	14.5/12.94	14.5	7.20	Chl	Unstable chlorite
#10	604	14.4	14.3	9.9/12.3	Chl/MLC	
#11	626	13.97	14.31	7.18	Chl/MLC	Peak at 30.54 Å
#12	678	14.8		7.3	Chl	Unstable chlorite
#13	758	14.7	7.2		Chl	Unstable chlorite
#14	816	14.8	7.2		Chl	Unstable chlorite
#15	906	14.7	7.2	9.1	Chl/MLC	Peak at 31.3 Å
#16	948	14.6	7.2	9.1	Chl/MLC	Peak at 31.6 Å
#17	958	14.8	7.2		Chl/MLC	
#18	1052	14.4	14.6/7.2	10	Chl/MLC	Peak at 31.2 Å
#19	1068	14.8	15.1	7.3	Chl/MLC	Peak at 32.3/31.2 Å
#20	1300	14.8	15.1	7.3	Chl/MLC	Peak at 33 Å
#21	1380	15		7.3	Chl/MLC	

3. AQUIFERS/FEED ZONES

Feed point locations have been estimated by using the temperature logs and circulation losses. Figure 9 shows faults mapped on the surface in Mt. Thorbjörn, interpolated along their strike for estimation of the depth of penetration of well SV-26. The majority of feed points within the shallower parts (< 1000 m) are associated with the graben structure seen on the surface in Mt. Thorbjörn. Figure 9 shows (from Weisenberger et al., 2016) that the depth intervals where the well path cross-cuts faults A, B, and C are associated with feed zones. In contrast, fault D does not coincide with identified feed zones. But at slightly deeper levels, several feeds zones are detected, which may indicate that the modelled fracture location needs to be amended further east.

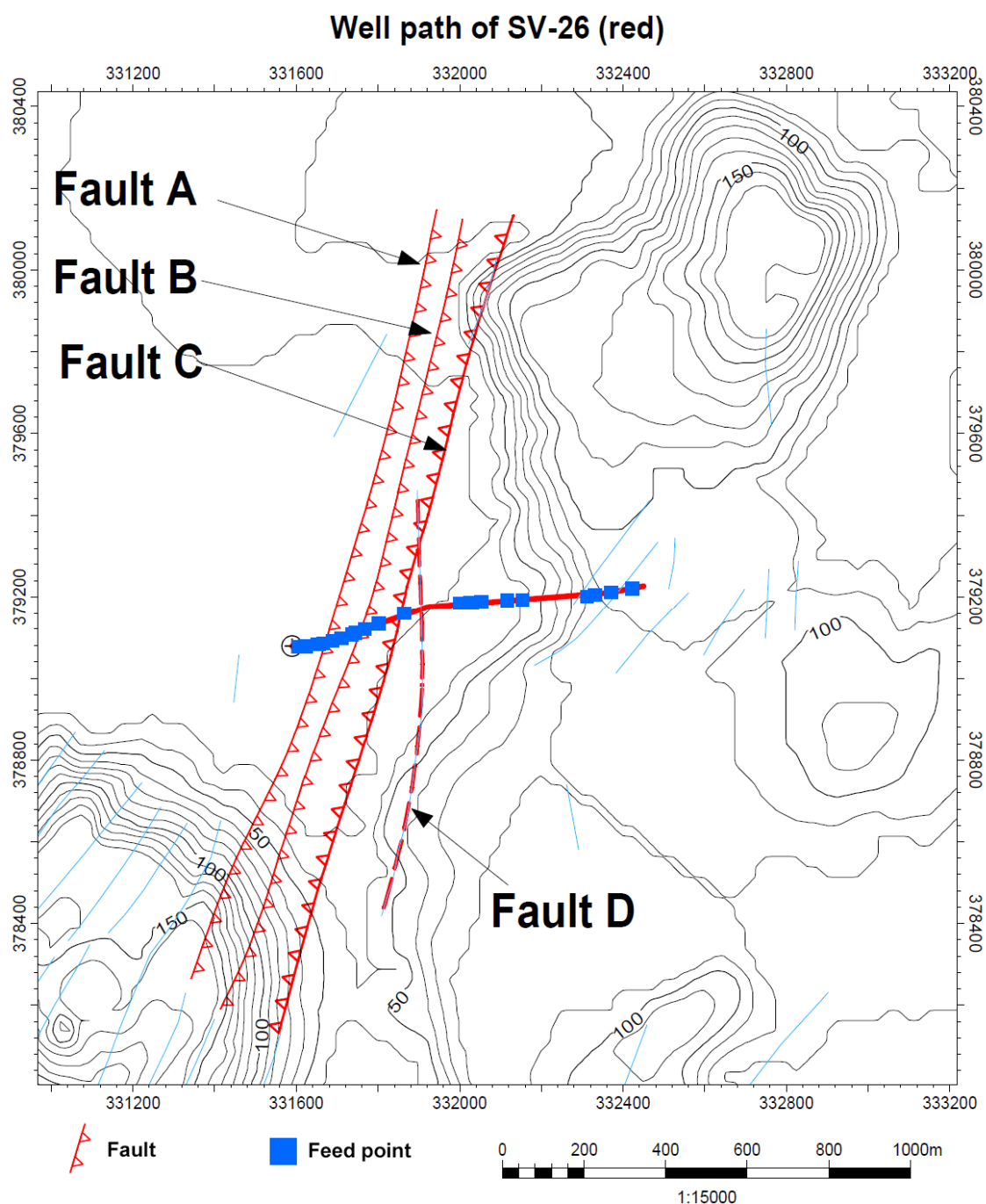


FIGURE 9: Faults mapped on the surface in Mt. Thorbjörn were interpolated along their strike for estimation of the depth of penetration of well SV-26. Feed points are given as blue squares

4. FLUID INCLUSIONS

The study of fluid inclusions shows the temperature of fluid trapped during crystallisation of the minerals, which helps us to interpret the thermal history of the system. By associating the temperatures of fluid inclusions to the present condition of the geothermal system, it is possible to predict whether the system is in equilibrium, cooling or heating. A total of 53 fluid inclusions were studied through micro thermometry in this well within depth intervals ranging from 662-666 m, 808 m, 1046 -1062 m and 1292 m. Of these, 50 inclusions are from quartz samples while the remaining 3 are from calcite and

showed a range of homogenization temperatures (T_h) from 245°C as a minimum temperature to 351°C as a maximum temperature, as described in Table 4 and Appendix II (Figure 1 and Table 4).

The quartz homogenization temperature has a wider range and is higher than the formation temperature showing temperatures above the boiling point curve in the upper section of the well at 664 m and 808 m depth but displays temperatures closer to the mineral alteration curve at deeper depths. The homogenization temperature for the calcite mineral is, however, closer to the formation temperature at around 1292 m depth.

TABLE 4: Fluid inclusion homogenization temperatures

Depth (m) MD	Homogenization temp. (T_h) ranges (°C)	No. of fluid inclusions	Type of crystals
662-666	293 - 341	17	Quartz
808	328 - 351	8	Quartz
1046 - 1062	245 - 291	25	Quartz
1292	261 -263	3	Calcite

Looking at the boiling point curve as plotted and correlated to the other temperature plots (Figure 10), one can conclude that the geothermal system has for most of its lifetime not been in boiling condition at depth, however such condition may have occurred in the uppermost part of the system below 1000 m. The main information the figure shows is that on a geological time scale the geothermal system is on a cooling trend from its hottest conditions in the past.

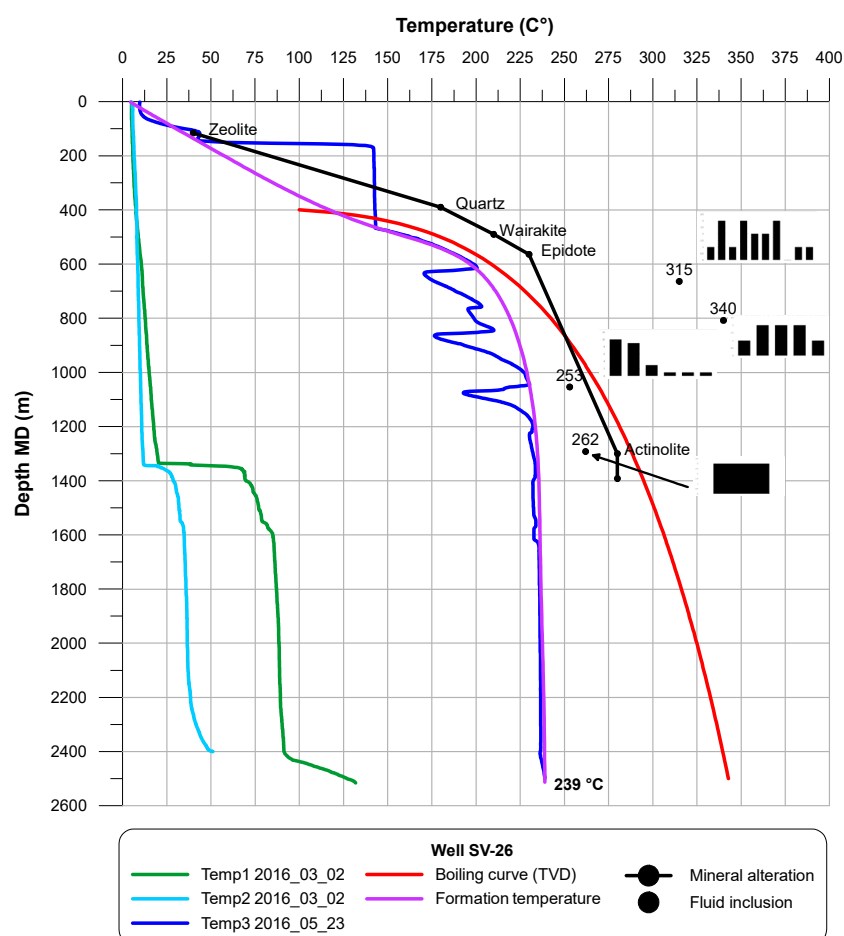


FIGURE 10: Formation temperature, alteration temperature, boiling point curve, homogenization temperatures and logging temperatures of well SV-6

5. CONCLUSIONS

The main conclusions of this report are as follows:

- The stratigraphy of well SV-26, down to 1394 m (MD), is comprised of interglacial lava series which were intersected by hyaloclastite horizons, including pillow basalt, breccia, and tuff. The hyaloclastite cap-rock of the system was reached at depth ~380 m (MD). The upper cap-rock boundary of the geothermal reservoir is therefore, found at about 380 m. However, the shallower cap-rock formation does not show any sign of significant alteration but alteration suddenly appears at a depth of about 465 m.
- The alteration in SV-26 indicates a regular progressive hydrothermal alteration with increasing depth based on the alteration mineral assembly in the well. Epidote (230–250°C) was first spotted at 564 m, and was consistently present below 634 m as crystalline epidote.
- Three alteration zones were observed: Unaltered zone (0-112 m), smectite-zeolite zone (112-622 m) and chlorite-epidote zone (622-1394 m).
- Several feed points were observed according to temperature loggings in the well with the largest at around 889, 960, and 1093 m, located behind the production casing, and in the production part the main feed zones are at 1346 and 2428 m.
- The estimated formation temperature for well SV-26 is 239°C and is in the narrow range of 235-245°C which relates to the fluid temperatures found in wells drilled at Svartsengi geothermal high-temperature field.
- A comparison shows that the alteration minerals formed at considerable higher temperatures than shown by the present formation temperature and would suggest that the reservoir is gradually cooling on a geological time scale. While temperatures at about 600 m may have been near boiling at one time, the geothermal system has probably never reached boiling conditions in deeper parts, and remained water dominated.
- Consistent data, resulting from micro-thermometry analyses done on fluid inclusions found in quartz crystals, show some abnormally high temperatures above 1000 m reaching 351°C around 800 m, which cannot be explained at the moment and should be further addressed. However, it shows conclusively that the Svartsengi system had an earlier hotter environment and has cooled.
- It is important to note that the temperature loggings and mineral sequences of the exploration well SV-26 do not show any evidences of temperature reversal in this part of the production field, which implies that the Svartsengi geothermal system may possibly extend further to the east than previously believed.
- It is important to monitor SV-26 in the future as the temperature will likely rise further still, possibly to temperatures above the Svartsengi average. Such a temperature increase is observed away from Svartsengi to the west towards the Eldvörp geothermal system.

ACKNOWLEDGEMENTS

I thank my supervisor Dr. Björn S. Hardarson for his patience, guidance and for the great time offered during fieldwork and his help in the creation of this report. Sigurdur S. Jonsson for XRD work. I would like to express my gratitude to all UNU staff for their assistance and ÍSOR staff for taking time to share their skill and knowledge with me. Special thanks to Lúdvík Georgsson for giving me the opportunity to attend the UNU Geothermal Training Programme. I gratefully acknowledge HS Orka for allowing me access to data regarding SV-26.

REFERENCES

- Björnsson, S., Guðmundsdóttir, I.D., and Ketilsson J. (eds.), 2010: *Geothermal development and research in Iceland*. Orkustofnun, Reykjavík, 39 pp.
- Browne, P.R.L., 1978: Hydrothermal alteration in active geothermal fields. *Annual Reviews of Earth and Planetary Science*, 6, 229-250.
- Franzson, H., 1990: *Svartsengi. Geological model of the high-temperature, geothermal reservoir and its surroundings*. Orkustofnun, Reykjavík, report OS-90050/JHD-08 (in Icelandic), 41 pp.
- Franzson, H., 1995: Geological aspects of the Svartsengi high-temperature field, Reykjanes Peninsula, Iceland. *Proceedings of the 8th International Symposium on Water-Rock interaction, Vladivostok, Russia, 1995*, 497-500.
- Franzson, H., 1998: Reservoir geology of the Nesjavellir high-temperature field in SW-Iceland. *Proceedings of the 19th Annual PNOC-EDC Geothermal Conference, Manila*, 13-20.
- Franzson, H., 2017: *Svartsengi – Eldvörp. A conceptual geological model of the geothermal reservoir*. Prepared for HS Orka, report ISOR-1017/017, 69 pp.
- Gebrehiwot Mesfin, K., 2010: *Subsurface geology, hydrothermal alteration and geothermal model of northern Skardsmyrarfjall, Hellisheidi geothermal field*. University of Iceland, MSc thesis, UNU-GTP, report 5, 65 pp.
- Georgsson, L.S., 1984: Resistivity and temperature distribution of the outer Reykjanes Peninsula, Southwest Iceland. *54th Annual International SEG Meeting, Atlanta, Expanded Abstracts*, 81-84.
- Guðjónsdóttir, S.R., Tryggvason, H., Gunnarsdóttir, S.H., Nielsson, S., Weisenberger, T.B., Egilson, TH., and Jónsson, S.S., 2015: *Well report – SV-25. Drilling of well SV-25 from surface down to 2004 m and geothermal studies during the drilling of the well*. ÍSOR - Iceland GeoSurvey, Reykjavík, report ÍSOR-2015/077, 263 pp.
- Hardarson, B.S., Fitton, J.G., and Pringle, M.S., 1997: Rift relocation - a geochemical and geochronological investigation of a paleo-rift in northwest Iceland. *Earth Planet Sci. Lett.*, 153, 181-196.
- Hjartarson, Á. and Saemundsson K., 2014: Bedrock map of Iceland, 1:600 000. ÍSOR – Iceland GeoSurvey, Reykjavík.
- Jakobsson, S.P., 1979: Petrology of recent basalts of the Eastern Volcanic Zone, Iceland. *Acta Naturalia Islandica*, 26, 103 pp.
- Jakobsson, S.P., Jónsson, J., and Shido, F., 1978: Petrology of the western Reykjanes Peninsula, Iceland. *J. Petrology*, 19-4, 669-705.
- Jóhannesson, H., 1989: The geology of the Reykjanes Peninsula. In: Egilsson, K. (editor), *The nature of the southern Reykjanes Peninsula*. Náttúrfraeðistofnun Íslands, Reykjavík (in Icelandic), 13-22.
- Jóhannesson H. and Sæmundsson K., 1999: Geological map of Iceland, 1:1 000 000. Icelandic Institute of Natural History, Reykjavik, 1999.
- Jónsson, J., 1978: *A geological map of the Reykjanes Peninsula*. Orkustofnun, Reykjavík, report OS/JHD 7831 (in Icelandic), 333 pp and maps.

Kristmannsdóttir, H. and Tómasson, J., 1978: Zeolite zones in geothermal areas in Iceland. In: Sand, L.B., and Mumpton (editors), *Natural zeolites, occurrence, properties, use*. Pergamon Press Ltd., Oxford, 277-284.

Kuthan, M.F., 1943: *Die Ozillation der Vulkanismus und die Tektonik von Reykjanes*. University of Bratislava, Bratislava, 108 pp.

Mnzava, F.J., 2014: Subsurface geology and hydrothermal alteration of well HE-4, Hellisheidi geothermal field, SW- Iceland. Report 20 in: *Geothermal Training in Iceland 2014*. UNU-GTP, Iceland, 30.

Mostaghel, B., 1999: Processing and interpretation of geophysical well logs from well KJ-32, Krafla geothermal field, NE-Iceland. Report 8 in: *Geothermal training in Iceland 1999*. UNU-GTP, Iceland, 193-220.

Richter, B., Gudlaugsson, S.Th., Steingrímsson, B., Björnsson, G., Bjarnason, J.Ö. and Thórhallsson, S., 1999: Svartsengi. Hla SJ.18: Borun, rannsóknir og vinnslueiginleikar: Lokaskýrsla. OS.99117/JHD.08.

Rodas M, N.R., 1996: Borehole geology and hydrothermal alteration of well SV-14, Svartsengi, SW-Iceland. Report 15 in: *Geothermal Training in Iceland 1996*. UNU-GTP, Iceland, 22.

Saemundsson, K., 2015: *Revised map of the Svartsengi, Eldvörp and Reykjanes geological map, unpublished. Based on the Eldvörp and Reykjanes geological map (bedrock), 1:25.000*. Orkustofnun, Hitaveita Sudurnesja and Landmaelingar Íslands, 1995.

Saemundsson, K., 1979: Outline of the geology of Iceland. *Jokull* 29, 7-28.

Sigurdsson, F., 1985: *Groundwater and hydrogeology of the outer Reykjanes Peninsula*. Orkustofnun, Reykjavík, report OS-85075/VOD-06 (in Icelandic), 194 pp.

Sigurdsson, Ó. and Fridleifsson, G.Ó., 2015: *Design criteria for production well SV.26, revised*. HS Orka, HF., Memorandum 9.12.2015.

Steingrímsson, B., 2011: Geothermal well logging cement bond and caliper logs. *Papers presented at Short Course on Geothermal Drilling, Resource Development and Power Plants, organized by UNUGTP and LaGeo, Santa Tecla, El Salvador*, 11 pp.

Thórdarson, T., 2012: *Outline of geology of Iceland*. Chapman Conference, 2012.

Weisenberger, T.B., Gudjónsdóttir, S.R., Tryggvason, H., Hardarson, B.S., Gunnarsdóttir, S.H., Nielsson, S., Sigurgeirsson, M.Á., Einarsson, G.M., Kristinsson, B., Pétursson, F., Ingólfsson, H., Stefánsson, H.Ö., Jónasson, H., Tulinius, H., and Gunnarsson B.S., 2016: *Well report – SV-26. Drilling of well SV-26 in Svartsengi from surface down to 2537 m and geothermal studies during the drilling of the well*. ÍSOR – Iceland GeoSurvey, Reykjavík, report ÍSOR-2016/022, prepared for HS Orka Ltd., 143 pp.

Weisenberger, T. and Selbekk, R.S., 2009: Multi-stage zeolite facies mineralization in the Hvalfjörður area, Iceland. *International Journal of Earth Sciences*, 98, 985–999.

Worku, S., 2012: Borehole geology and hydrothermal mineral alteration of well HN-3, Hellisheidi Iceland, geothermal field, SW-Iceland. Report 37 in: *Geothermal training in Iceland 2012*. UNU-GTP, Iceland, 953-986.

APPENDIX I: Temperature and geophysical logs



Svartsengi Well SV-26

December 7th 2015
HT/FP

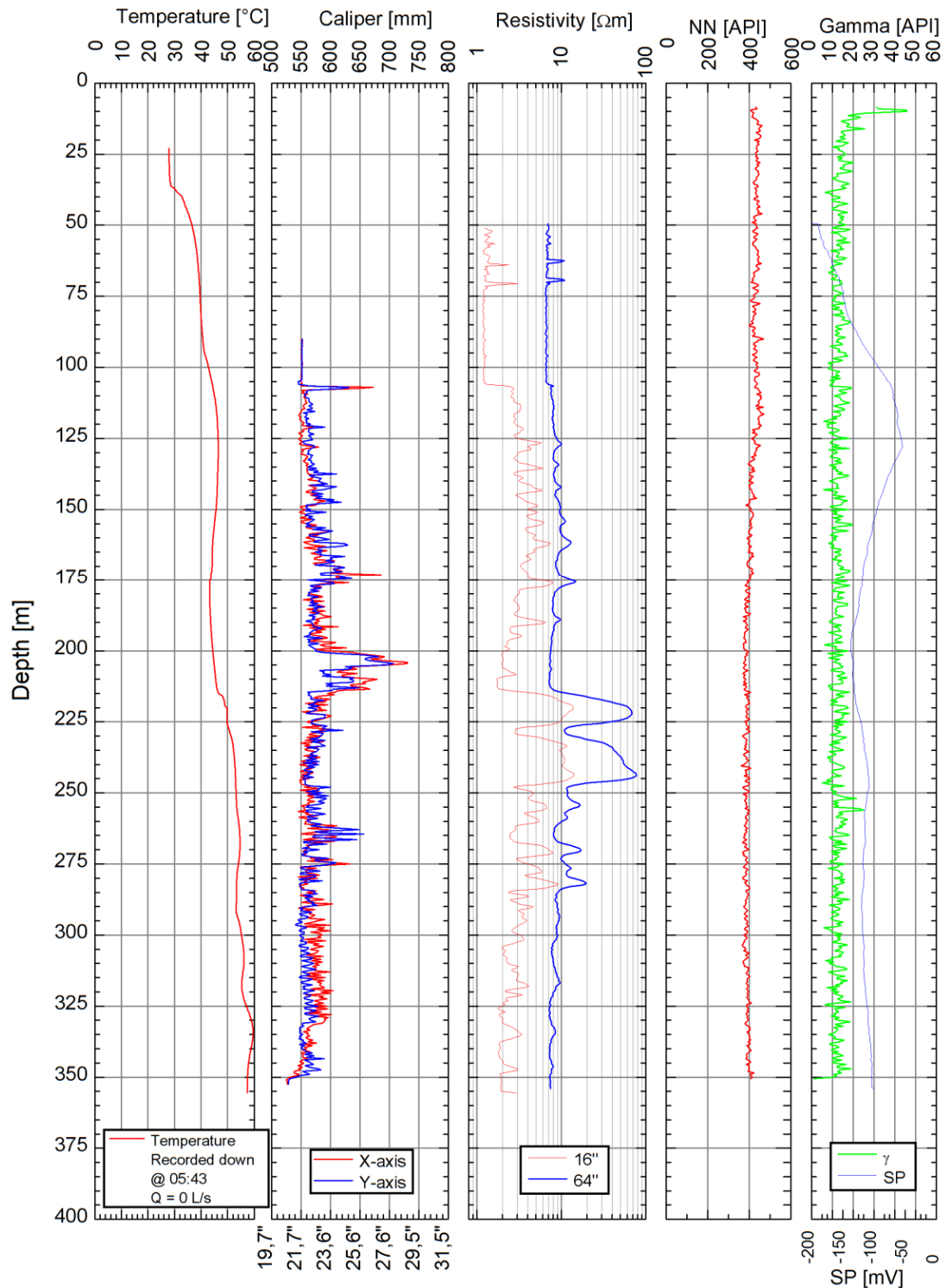


FIGURE 1: Geophysical logs after phase 1 of the drilling of well SV-26.
(Weisenberger et al., 2016)



Svartsengi Well SV-26

January 13th 2016
HI/HÖS/BMS

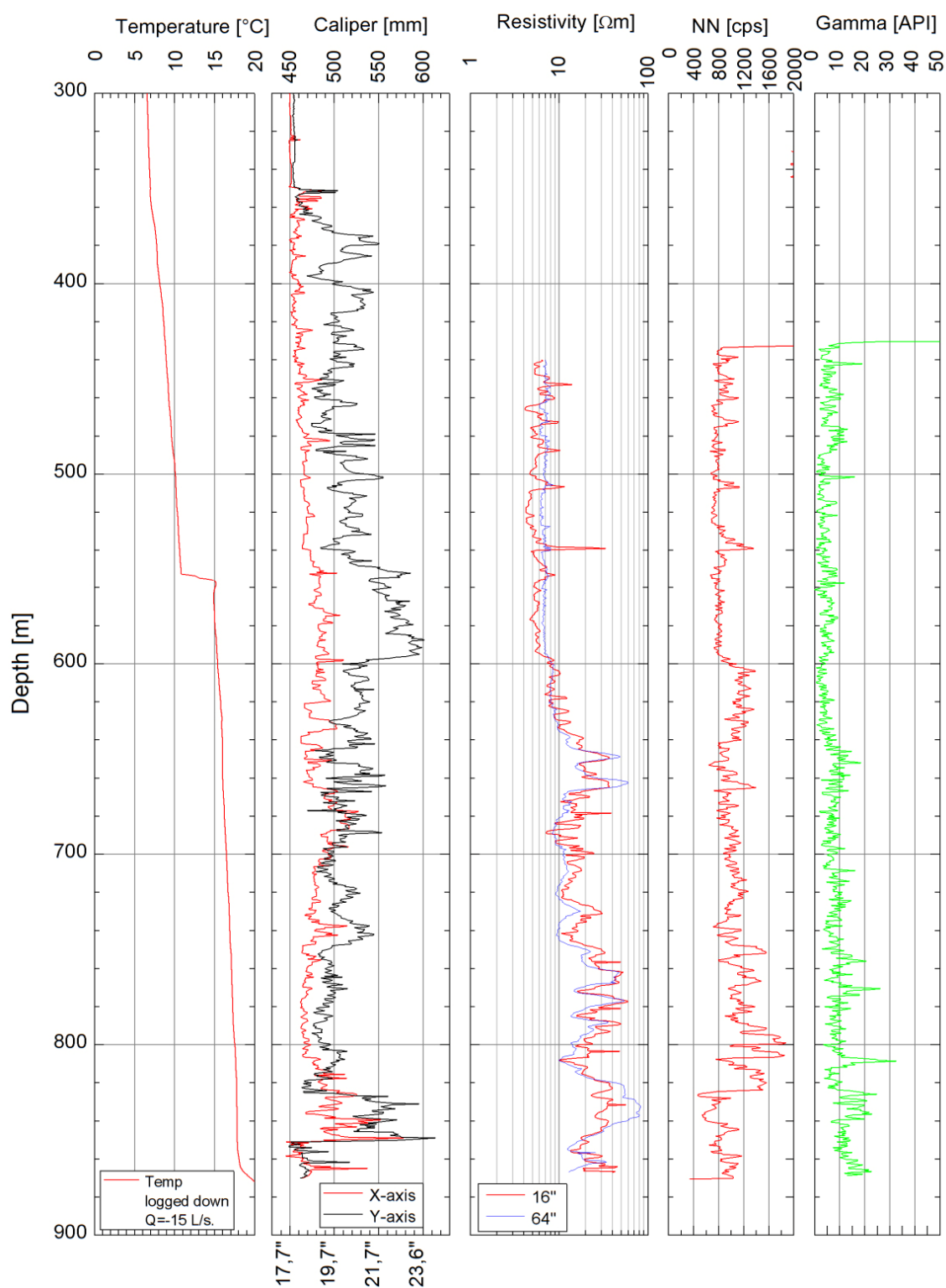


FIGURE 2: Geophysical logs after phase 2 of the drilling of well SV-26.
(Weisenberger et al., 2016)



Svartsengi Well SV-26

February 9th 2016
HI/HÖS

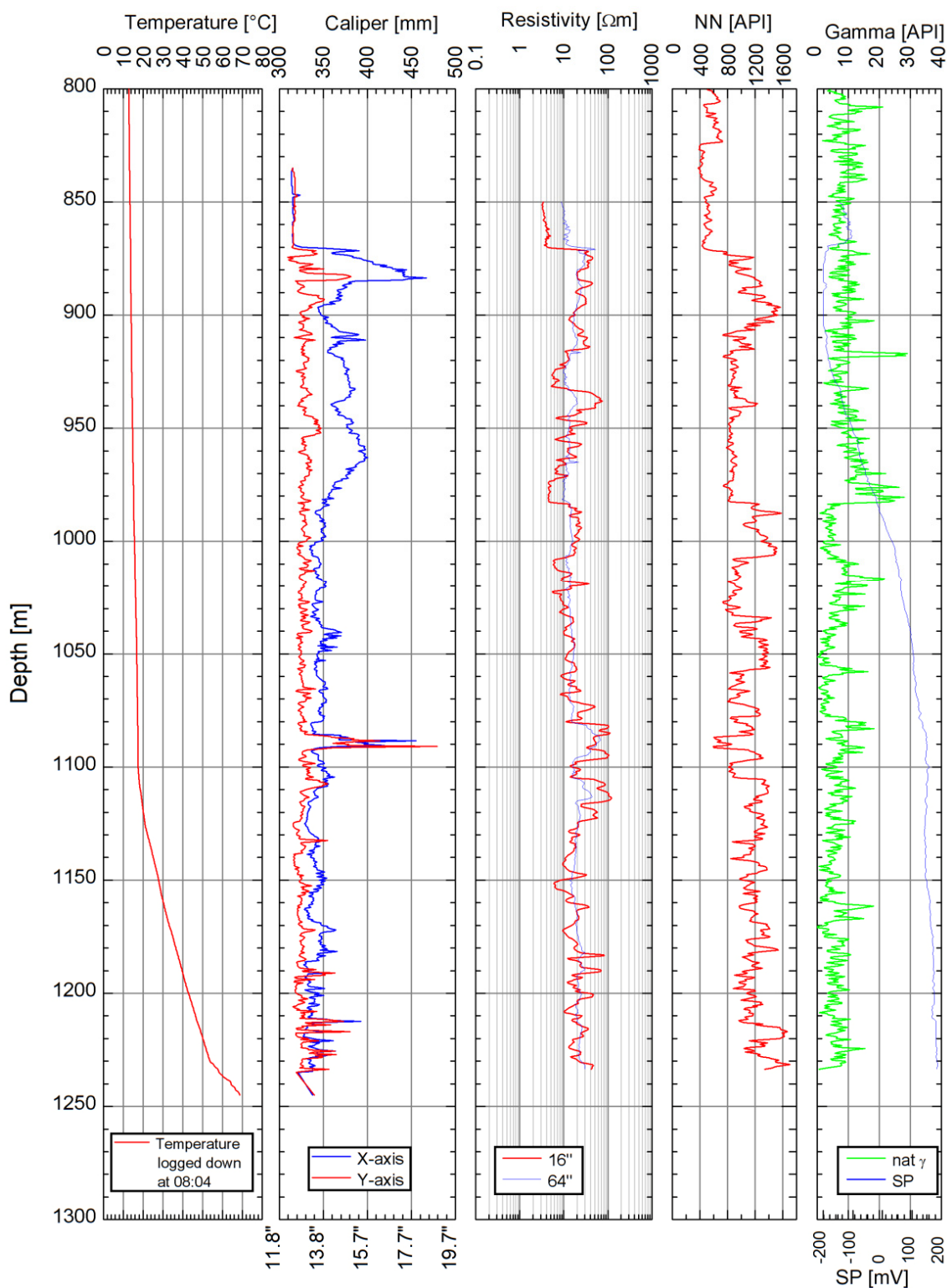


FIGURE 3: Geophysical logs after phase 3 of the drilling of well SV-26.
(Weisenberger et al., 2016)



Svartsengi Well SV-26

February 27th 2016
BJKr/FP/HaJ/HÖS

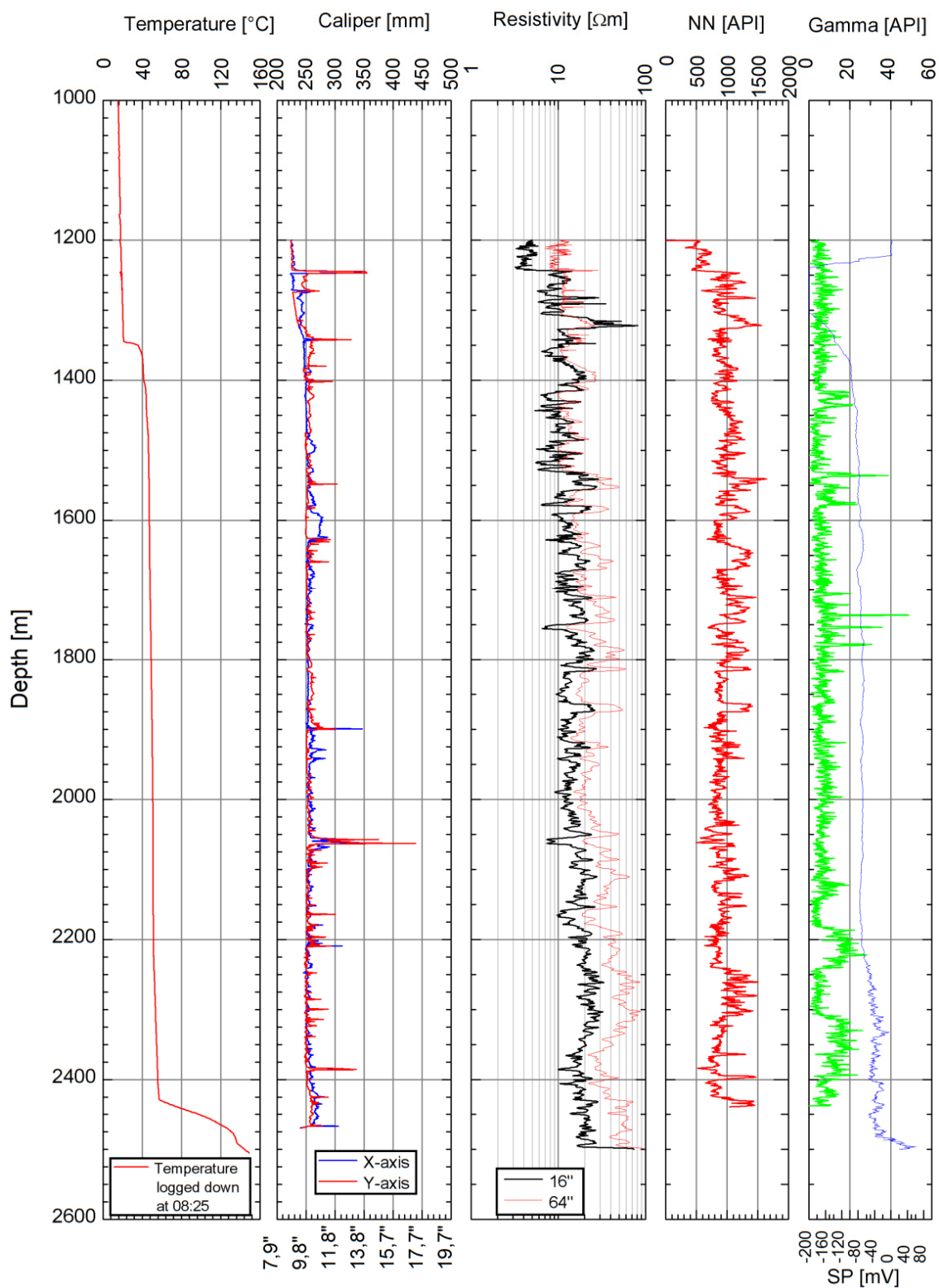


FIGURE 4: Geophysical logs after phase 4 of the drilling of well SV-26.
(Weisenberger et al., 2016)

APPENDIX II: Fluid inclusion results

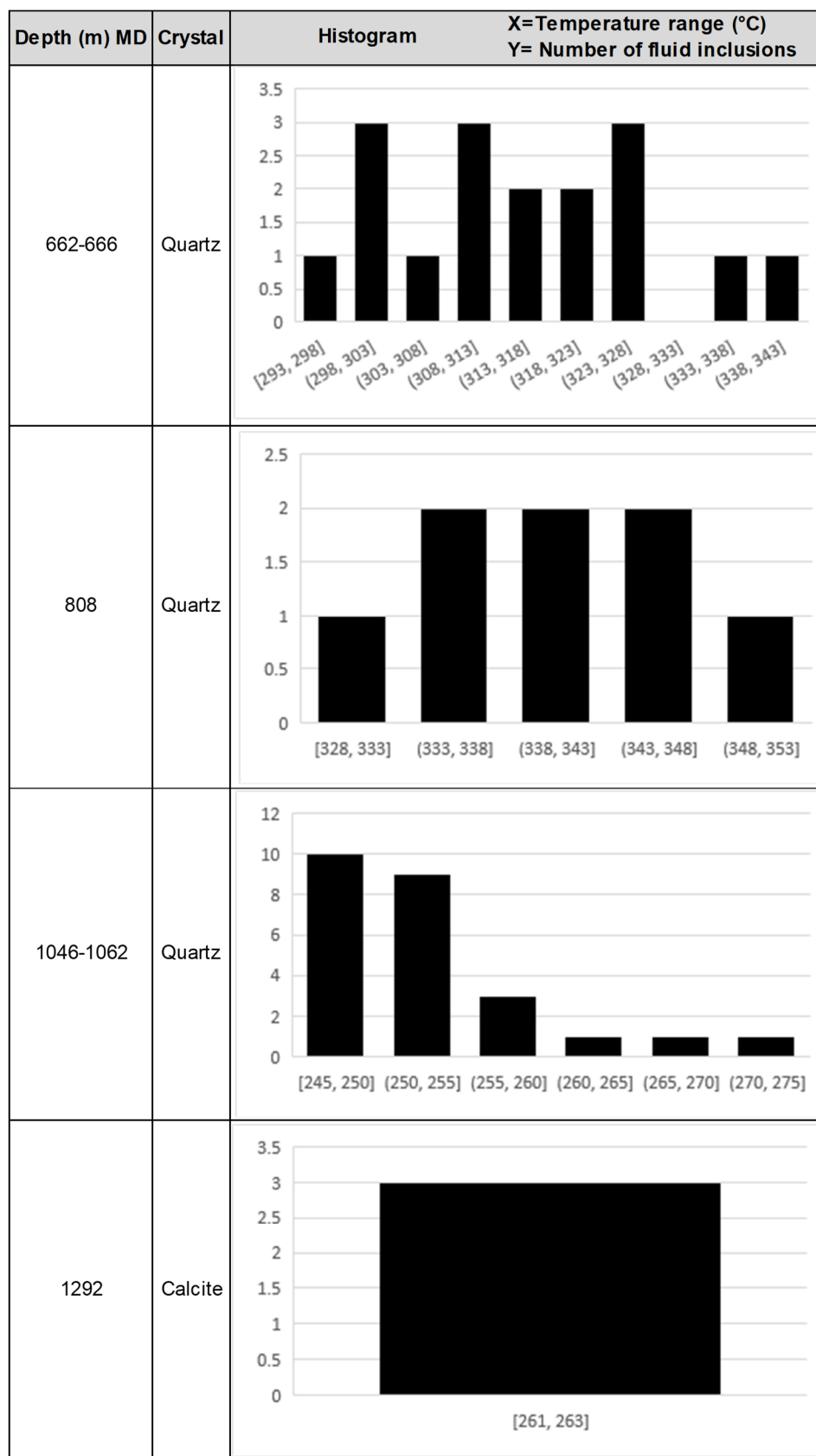


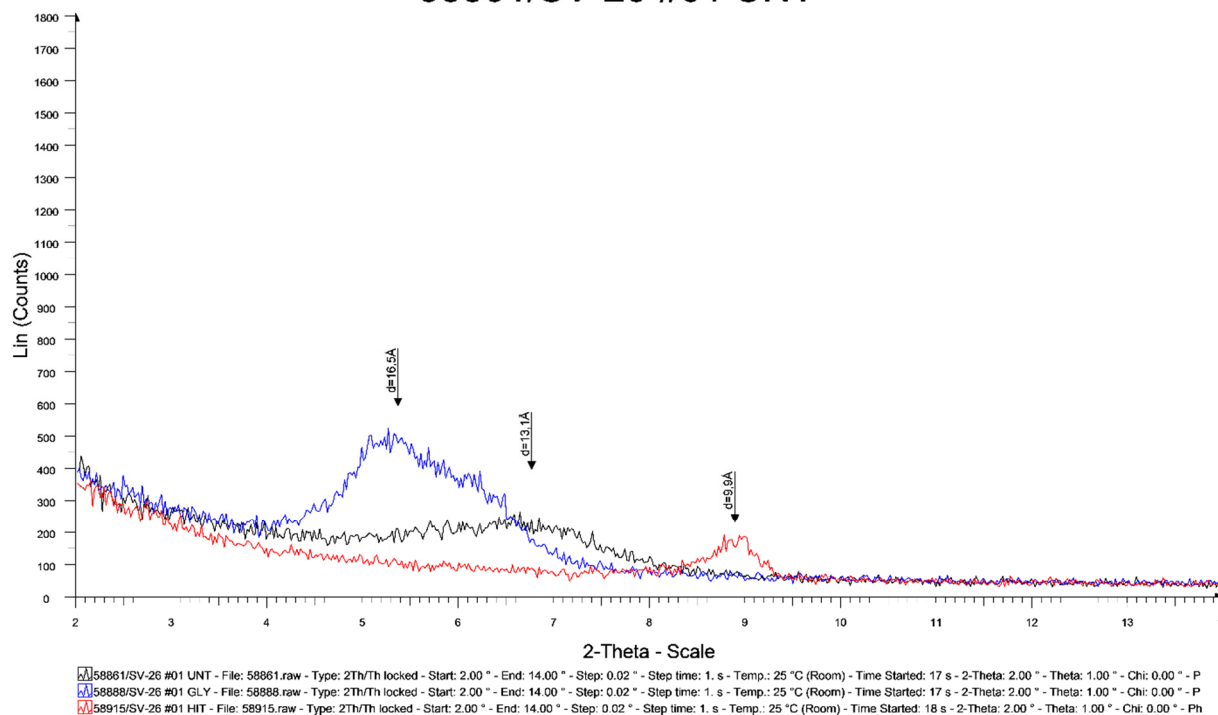
FIGURE 1: Histogram diagram showing the variations of homogenization temperatures in well SV-26

TABLE 2: Homogenization of fluid inclusion

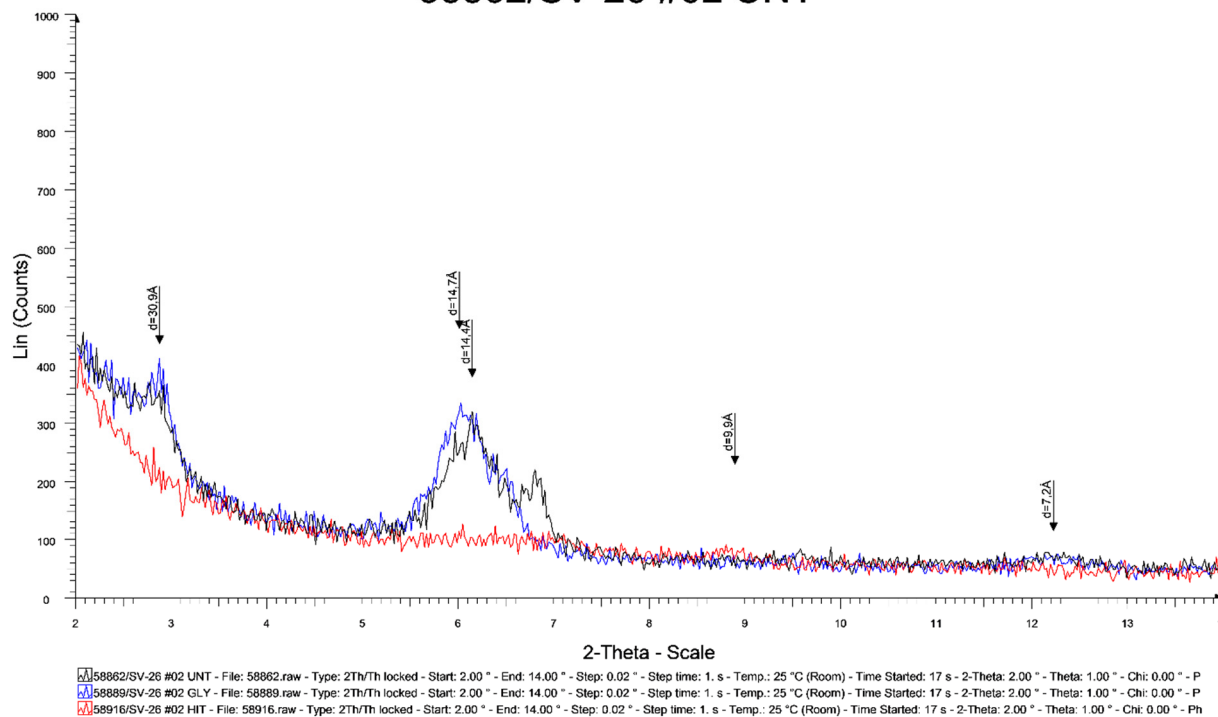
Depth (m) MD	Sample	Mineral	Inclusion	Homogenization Temperature (°C)
662	1	Quartz	1	313
	1		2	299
	1		3	308
	1		4	300
	1		5	300
	1		6	318
	1		7	293
	1		8	319
666	1	Quartz	1	325
	1		2	320
	1		3	328
	1		4	341
	1		5	336
	1		6	328
	1		7	310
	1		8	311
808	1	Quartz	1	346
	1		2	351
	1		3	328
	1		4	337
	1		5	343
	1		6	335
	1		7	342
	1		8	342
1046	1	Quartz	1	245
	2		1	262
	2		2	248
	2		3	250
	2		4	257
	2		5	266
	2		6	251
	2		7	251
1062	1	Quartz	1	256
	1		2	257
	1		3	255
	1		4	255
	1		5	255
	1		6	252
	1		7	252
	1		8	251
	2	Quartz	1	272
	2		2	250
	2		3	249
	2		4	249
	2		5	249
	2		6	249
	2		7	251
	2		8	250
1292	1	Calcite	1	261
	1		2	262
	1		3	263

APPENDIX III: XRD results

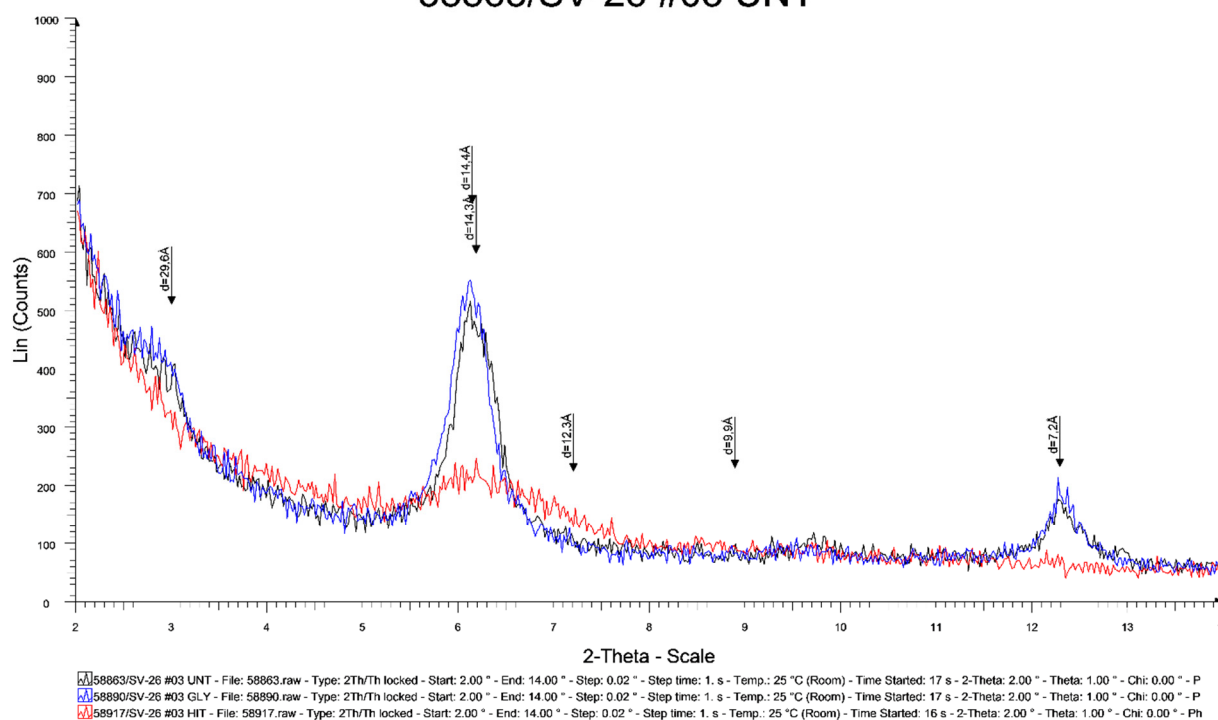
58861/SV-26 #01 UNT



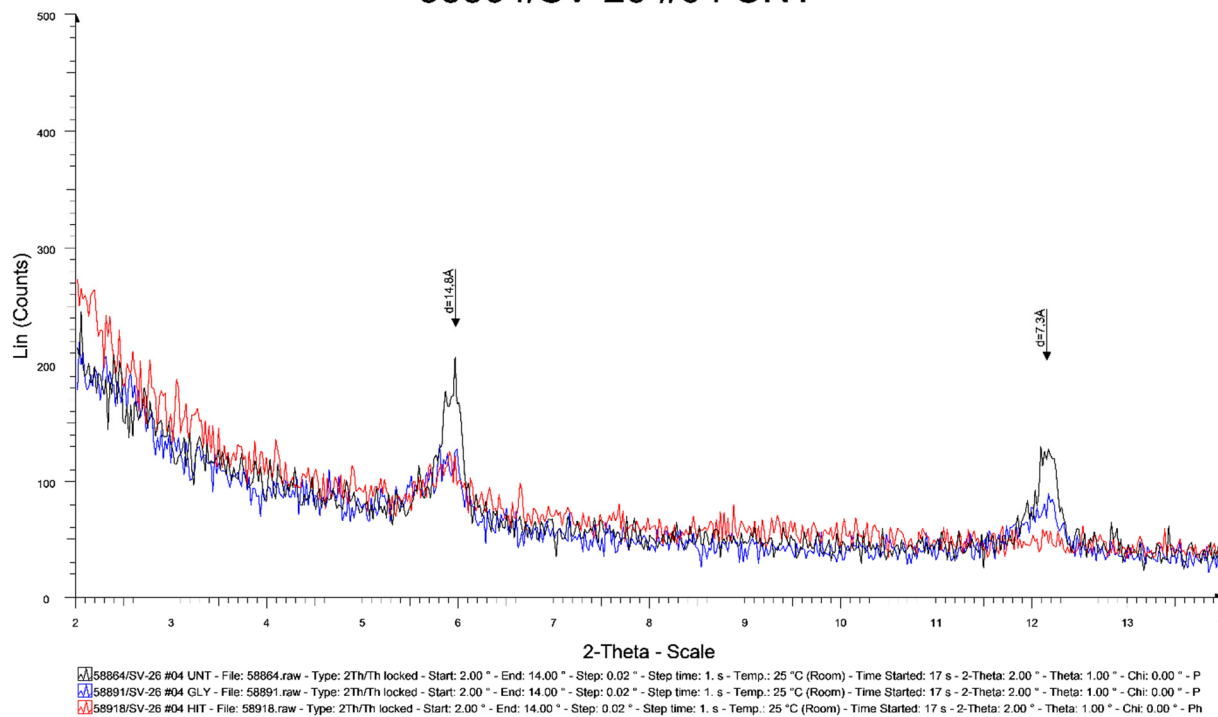
58862/SV-26 #02 UNT



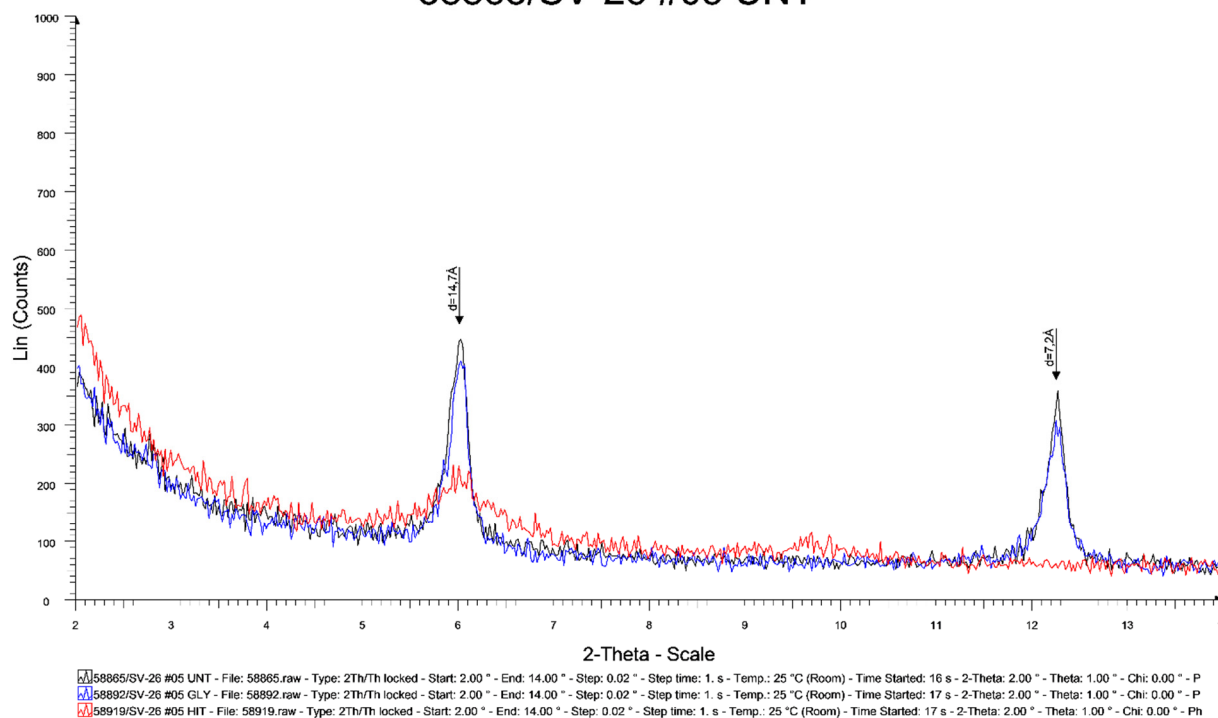
58863/SV-26 #03 UNT



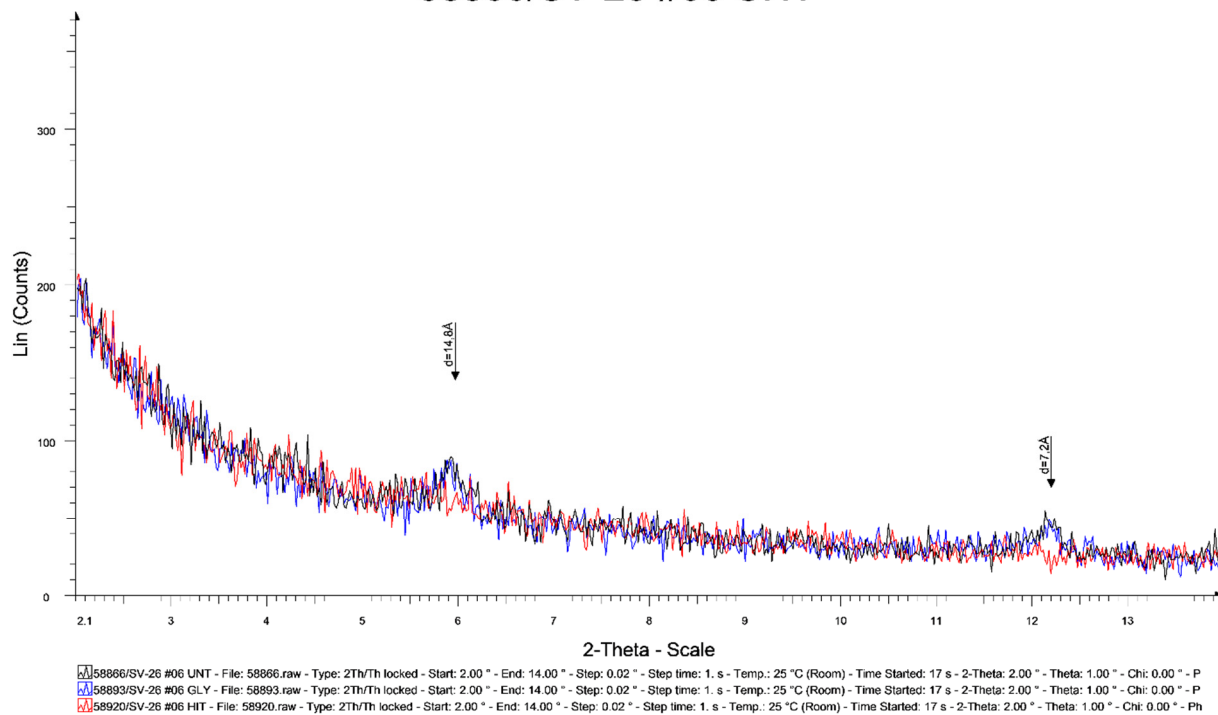
58864/SV-26 #04 UNT



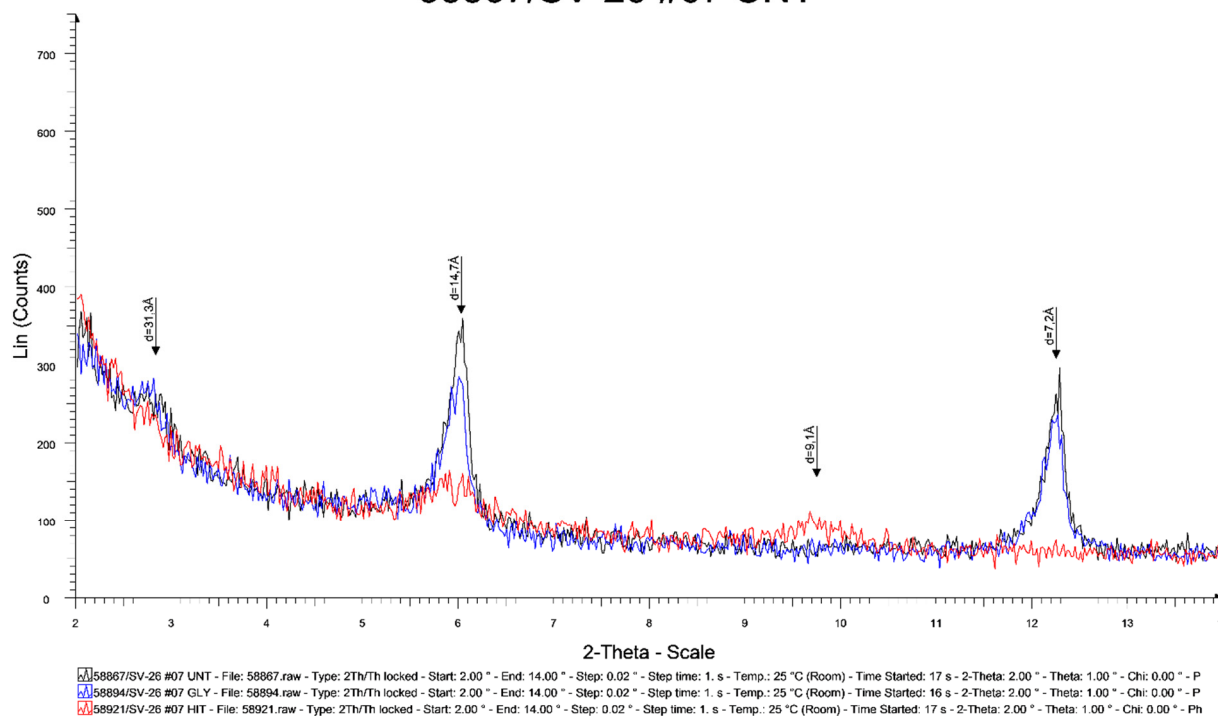
58865/SV-26 #05 UNT



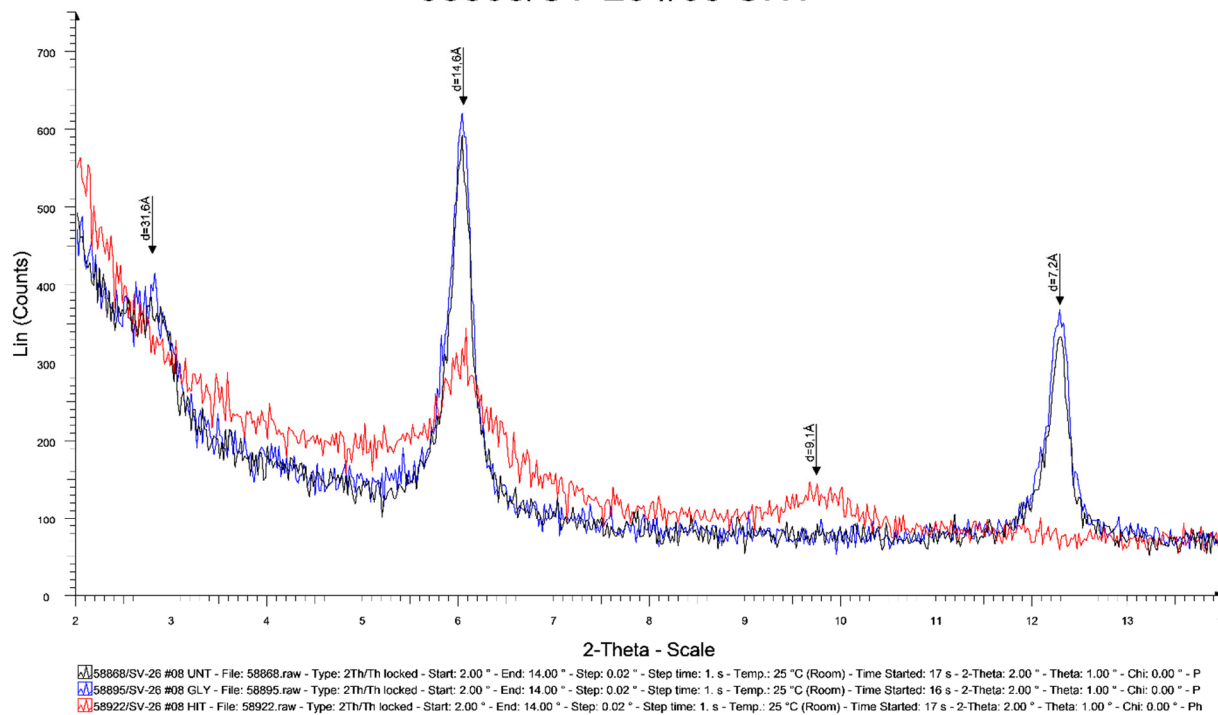
58866/SV-26 #06 UNT



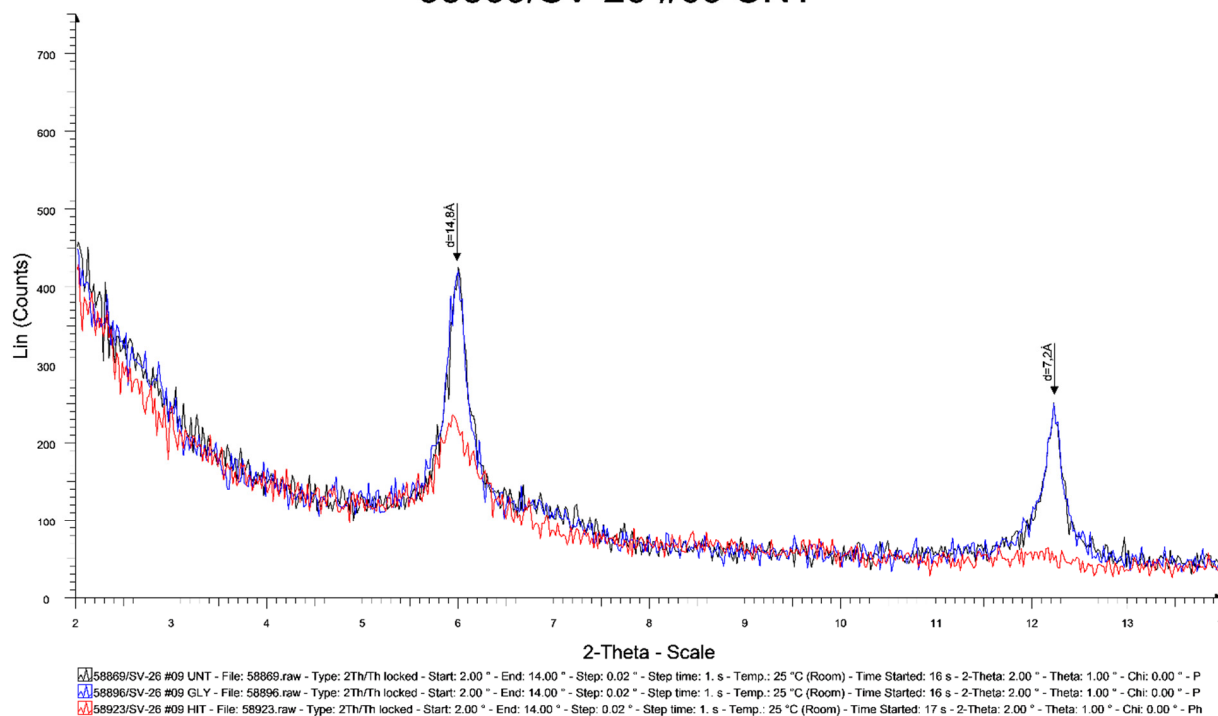
58867/SV-26 #07 UNT



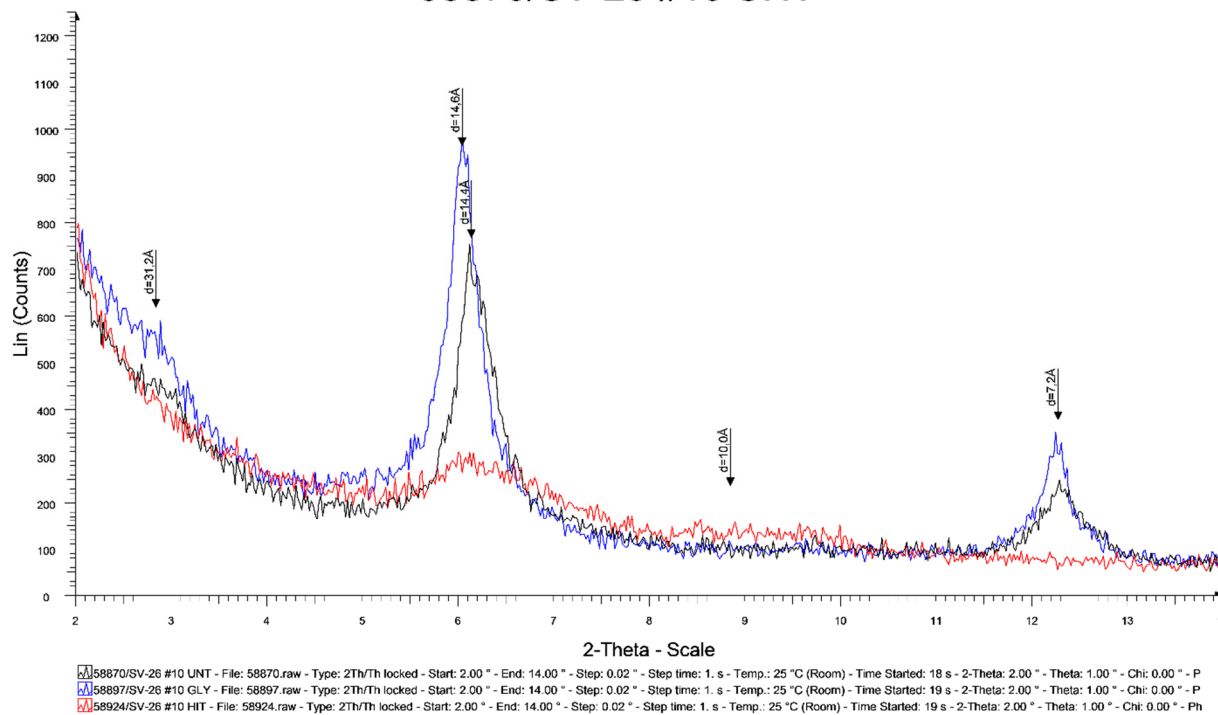
58868/SV-26 #08 UNT



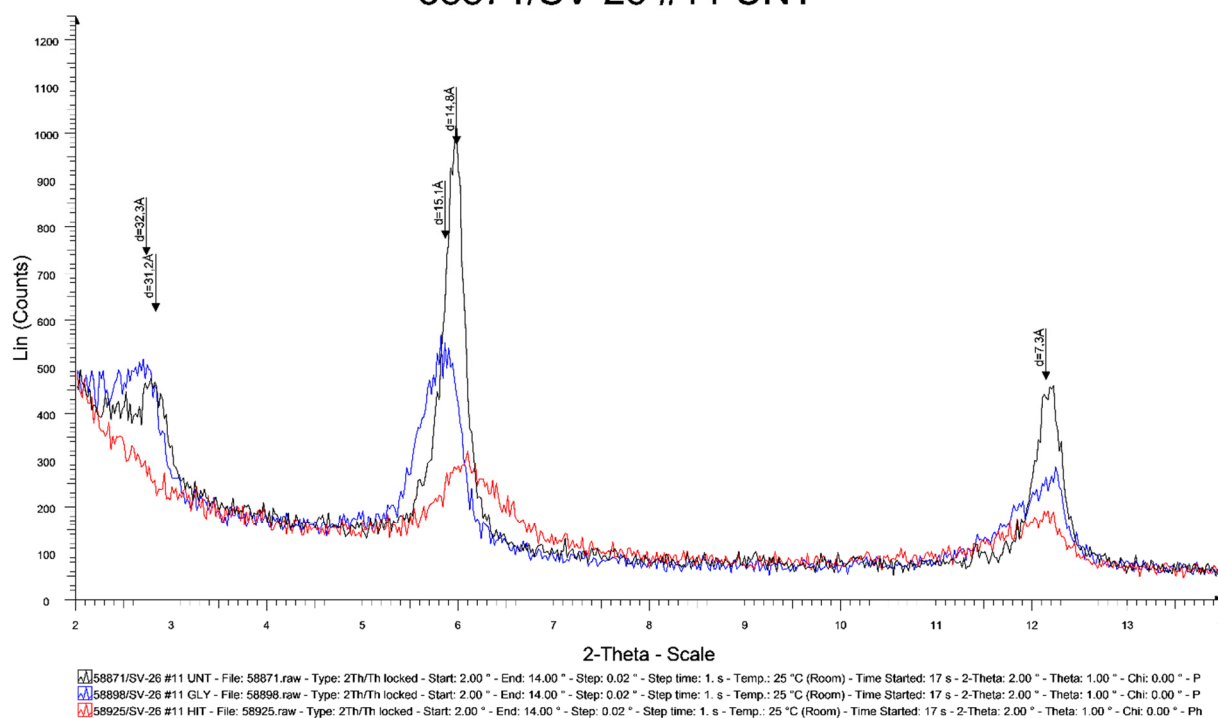
58869/SV-26 #09 UNT



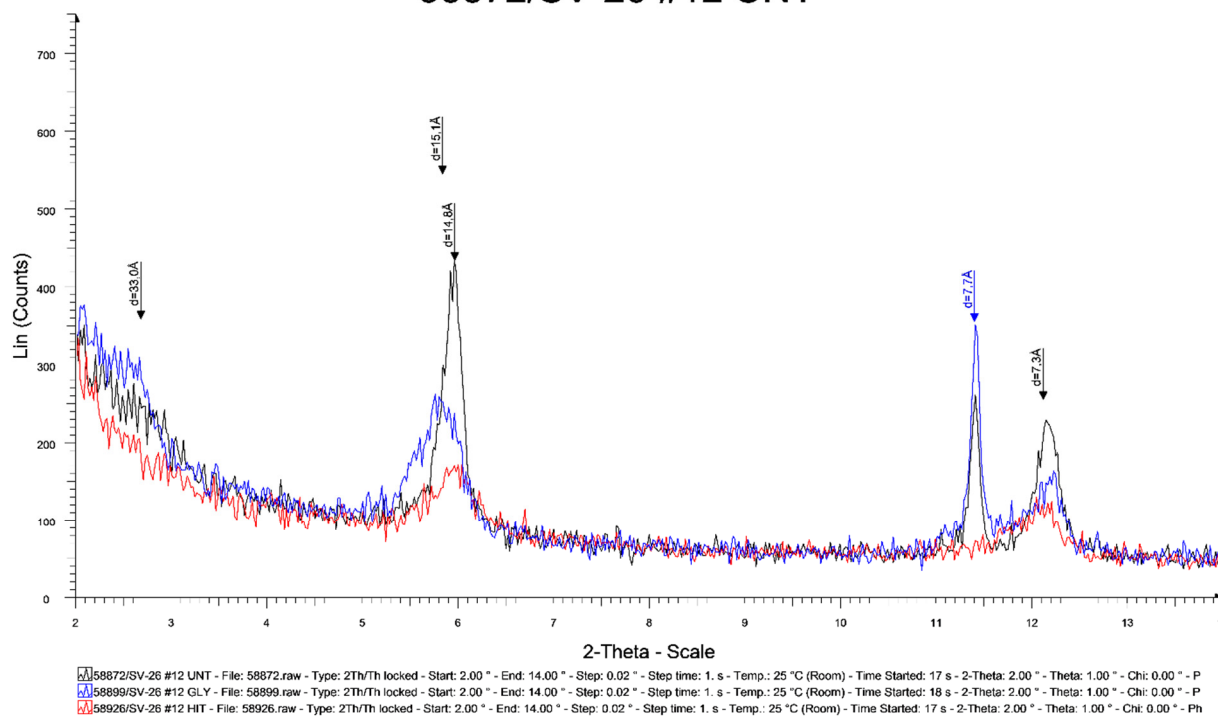
58870/SV-26 #10 UNT



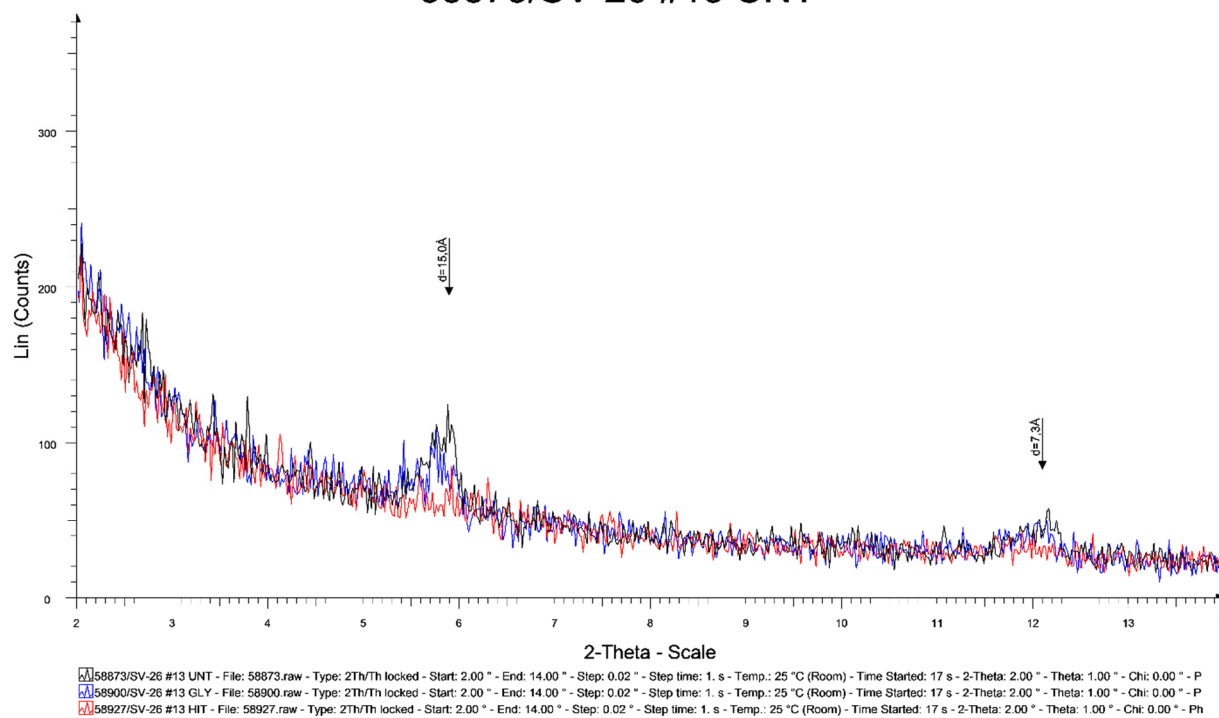
58871/SV-26 #11 UNT



58872/SV-26 #12 UNT



58873/SV-26 #13 UNT





UNITED NATIONS
UNIVERSITY

UNU-GTP

Geothermal Training Programme

Orkustofnun, Grensasvegur 9,
IS-108 Reykjavik, Iceland

Reports 2016
Number 27

COGENERATION OF POWER AND HEAT IN HUNGARY

Anna Medgyesy

41. Szolo Street

Budajeno

HUNGARY

medgyesy.anna@gmail.com

ABSTRACT

For the first time in Hungary, a geothermal ORC power plant is being built, and will have the capacity to generate 2.2-2.5 MW of electricity. It is located in Tura, 30 km east of Budapest. After a long design and optimisation procedure, some questions are still unanswered. This paper reports answer to some of these, like how much heat the power plant can provide for the greenhouse designed near to the power plant, and how much water is needed to replace the evaporated water in the evaporative condenser, as well as how the ambient temperature will influence the screw expanders power output through the condenser. To evaluate these tasks, a Scilab code was written. The main parameters were provided by Mannvit Consulting Engineers.

1. INTRODUCTION

Hungary is a country with a good low-temperature geothermal potential, suitable for direct use, such as district heating or bathing. Recently, new possibilities have opened up, as in Tura, 30 km east of Budapest, where Hungary's first geothermal electric power plant is being built, or in Dombóvár, where plans have also been proposed for electricity production (Unyi, 2016).

Tura is a small town and the site of first ORC power plant to be built in Hungary. The power plant is scheduled to generate up to 2.5 MW of electricity to the network. Commissioning the power plant has an added value, not just because it will raise the share of renewables in electricity generation, but it will also serve as good practice, and give new knowledge to Hungary. This report presents a hypothetical investigation of a planned Organic Rankine Cycle power plant in Hungary. The main task was to determine the needed heat supply for an 11-ha. greenhouse complex intended for tomato growing, with the geothermal water provided by the power plant. Additional task was to assess the net power output of the power plant versus ambient temperatures. The ambient temperature influences the greenhouse heat requirements as well as the working efficiency of the planned evaporative condenser. Many parameters are unknown here, like the exact design of the greenhouse, or the mass flow and pressure ratio of the ORC fluid in the power plant, hence this discussion must be looked at as hypothetical.

The ORC plant has two loops, a high-temperature one and a low-temperature one, a total nominal rated output at generator of 3350 kW and design gross power of 2619 kW. The geothermal fluid mass flow is 86 kg/s, the inlet temperature 124°C. When the plant is operating only 45 kg/s are available at 78°C, flowing to the greenhouse. The plant investment cost based on the latest news is around 10 billion HUF

(circa 3,225,000 EUR), 5.5 billion HUF is expected to cover the capital cost of the ORC plant, the rest will be spent on the greenhouse complex, which is designed to cover 11 ha. (Magyar Idők, 2016; Alternatív Energia, 2016). The project will be financed by foreign investors, EU assistance, bank loans and Hungarian investors. To know the possible heat supply, and the temperature effect on the power output can be crucial in the ROI (Return On Investment) calculations. Scilab free software was used for the calculation, with Coolprop fluid properties extension. Scilab is more or less similar to Matlab and CoolProp is similar to REFPROP (Scilab, 2016; CoolProp, 2016; MATLAB, 2016; REFPROP, 2016).

This project was carried out as the final project of the author's six-month geothermal training in Iceland at the United Nations University Geothermal Training Programme (UNU-GTP). The main project objectives were the following:

- How much income can the scheduled Tura power plant possibly have from selling heat to an 11-ha. tomato greenhouse complex?
- How much water evaporates in the evaporative condenser as a function of the ambient temperature?
- How will ambient temperature through the condenser influence power output of the power plant?

2. PRESTUDY

2.1 The greenhouse

Before determining the energy requirements of the greenhouse complex, Mr. Keszthelyi Krisztián, Department Engineer at Faculty of Economics and Social Sciences, Szent István University, was contacted to gain information on mainstream greenhouse design in Hungary. He provided a lot of useful information, which can influence decisions, and an important part of the model, including the following: During the winter season, there is no tomato production in greenhouses in Hungary, as the Spanish and Jordanian farms control the market, with their cheap prices. They have a competitive advantage, based on their warmer and less radical weather conditions. However, in the winter period Hungarian greenhouses need heat to avoid freezing damage. Using light is not common, as the electricity price is quite high compared to the heat price, and during the greenhouse heating period this is not necessary, as the number of sunny hours is efficient for growing plants inside. Nowadays, typical greenhouses are of Venlo type, with 5×8 m² blocks, 22° roof angle, 7.5 m total height, and 4 mm glass layer on the roof and two glass layers on the sides, which can be more than 100 meter long. In Hódmezővásárhely, the new greenhouses, based on measurement made through the Google Earth ruler function, are of the size 140×78 m², a size which consequently was used in this project (Google Earth, 2016). It is common to use energy curtains to reduce the heat loss during the night. From practical experience, 20-70% of the heat loss can be reduced by the curtain during night (Sanford, 2011). The tomato plants' optimal growth is depending of course on the species, and the greenhouses are usually operated with daytime temperature of 20-27°C and night-time temperature of 16-18°C (Mariani et al., 2016).

2.2 Energy prices

Some energy prices in Hungary are regulated by law. The renewable energy investment costs can be higher than those for regular natural gas, coal fired or nuclear power plants, depending on the circumstances. This applies especially to places where potential is not high, the renewable energy is seasonable, etc. (OECD, 2015). To enforce the growth of renewable energy against their relative high capital cost, in the European Union there is a common practice, called a *Feed in Tariff*. It is arguable, whether it is a good or bad practice, but it is to be expected that anybody tries to label/emphasize health, environment and risk tax after spreading carcinogenic and health damaging pollutants or causing global

warming etc., as the nuclear, natural gas or coal industry, which has a serious effect, not like the CO₂ quota. Life is not just about money and profitability.

Cutting this discussion short, the main point is to make sure the investment will be paid back, support non-government renewable energy investments (independent companies), and ensure that the renewable energy is not lost, and will be used right away in the net, which means almost unlimited access to the network. The renewable electricity prices are presented in Figure 1.

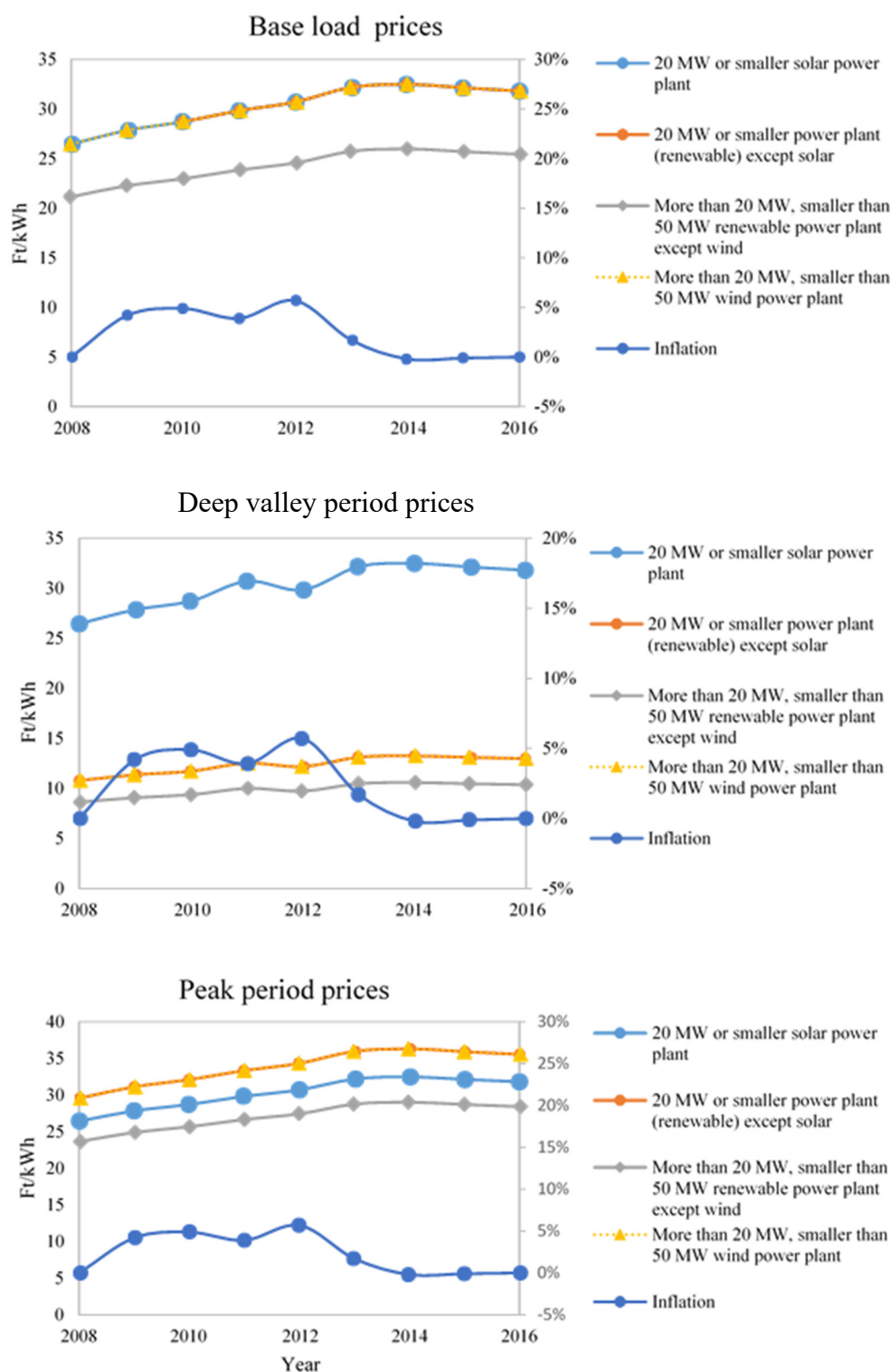


FIGURE 1: Renewable electricity prices

In Hungary district heating is also getting government support, through a regulation intended for regulating the heat price of power plants (Hungarian Ministry of National Development, 2011). District heating is not popular in Hungary, and one of the reasons can be seen in Figure 2. It shows that the sales heating fee is regulated by the government, fixed by the *Regulation of district heating sale fees*. If somebody has his own natural gas boiler, for a non-household consumer with more than 20 m³/h consumption, the average gas price is between 2540 and 2670 Ft/MJ +VAT (Főgaz, 2016). In all, 69% of the district heating fees are higher than the natural gas fee (and this was even higher before, as the regulation aims to reduce the profits of the companies). This resulted in people leaving the district heating systems in the past.

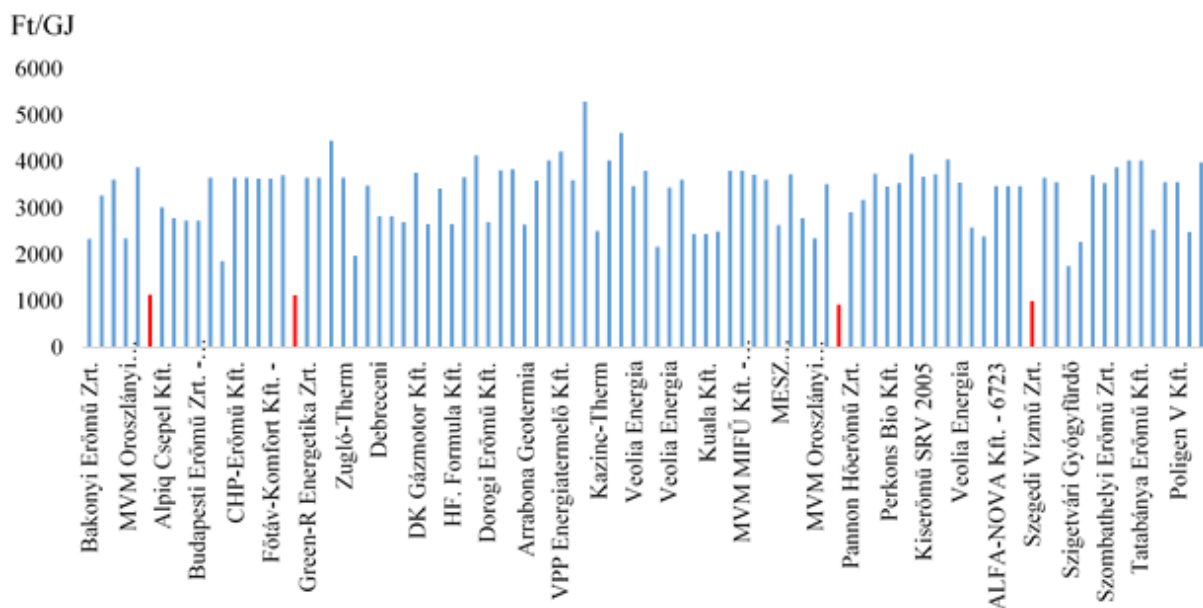


FIGURE 2: District heating suppliers' fixed rate by law

Figure 3 shows non-household consumer gas prices from 1992. It illustrates very well the effect of the economic crisis in 2008. After 2011 the government started to regulate the energy prices to minimise the cost of the households as much as possible. To summarize, the natural gas price in Hungary does not always follow the market trend, but what the politicians want to achieve, and then it depends of course also mostly on the price of Russian natural gas and the contract between the two nations.

In my opinion, in future the natural gas' market price could decrease, as the frozen Siberian gas will be available, and has to be utilised. The renewable energy share is also growing in Europe. In wealthier and environmentally cautious countries, ground source heat pumps may replace the conventional heating systems eliminating the need for the Russian or Dutch natural gas in Europe, which could cause surplus in the system and reduce the prices. The future is unpredictable, everything can happen, the prices can go up or down because of embargo, war, economic crisis, political change, etc. From a capitalist's point of view, if somebody plans a commercial greenhouse and competes on the free market with tomatoes, he/she would choose the cheap natural gas, if the prognosis of the gas price appears cheap in the long term. Consequently, the power plant cannot sell at a higher price than the price would be for laying down the gas pipes (similar as for geothermal water utilisation), paying the fee for the storage capacity, and the fee of the used gas. Comparison of the electricity and gas price gives (Főgaz, 2016):

- 17 Ft/kWh_e on the electricity market;
- 25-37 Ft/kWh_e renewable feed in tariff (peak, baseload, valley);
- 9.18-9.61 Ft/kWh_{th} natural gas price.

The decree online about the Tura project (Tura organic garden, 2015) makes it clear that it was prepared to get the *feed in tariff*. From these prices, it can be seen, that the power plant will focus on electricity

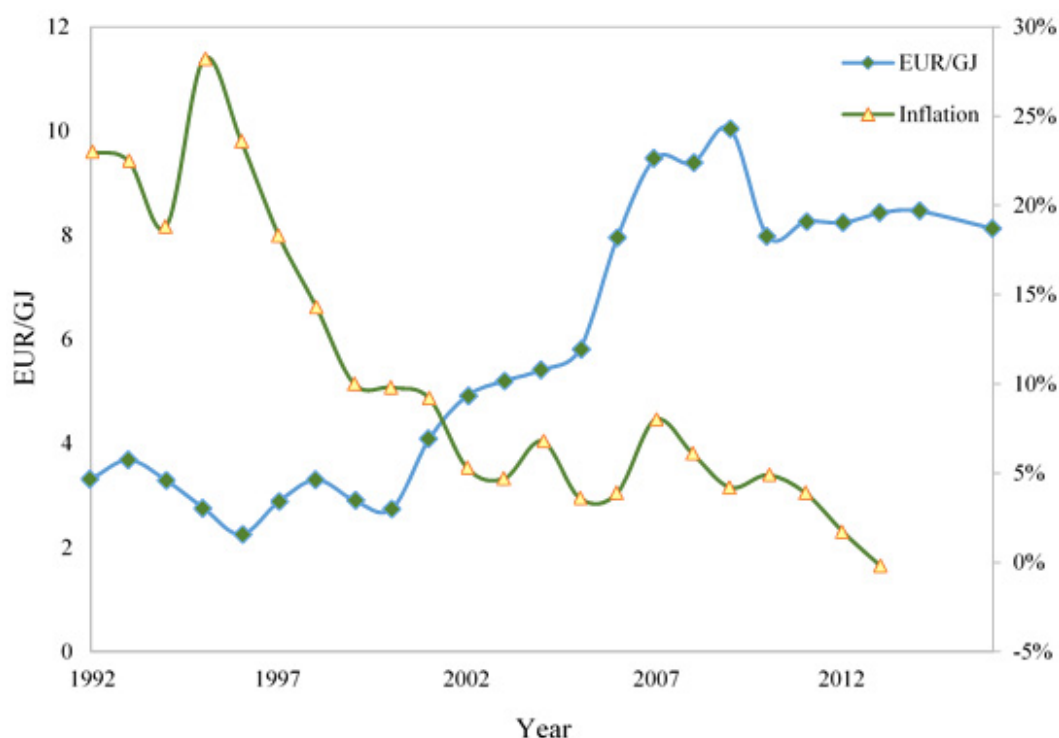


FIGURE 3: Non-household consumer's gas price in Hungary

production, even if the gas price / heat price will be 150-200% higher (for the combined heat and electricity production). It can also be assumed the power plant has to sell the energy at a price close to the actual gas price or lower to be a good choice for the greenhouse owner, unless the greenhouse owner is really environmentally aware or is able to sell the tomatoes with some “green design”, which could cover the additional expense.

3. GREENHOUSE HEAT REQUIREMENTS AND GEOTHERMAL HEAT SUPPLY

To estimate the heat requirements of the greenhouse a dynamic model was using Scilab software. The geothermal water inlet mass flow and temperature were the only fixed parameters.

The necessary heat requirements in a greenhouse depend on many factors. There are heat losses by transmission, filtration and ventilation, radiation and vegetable transpiration, evaporation, and water condensation on the surfaces. Heat is gained by solar radiation, and when necessary by the heating system in the greenhouse. I chose to build up a simple model, which doesn't take into account the transpiration and condensation losses but the rest is evaluated. Some assumptions had to be made, including:

- The walls and roof are from glass, the heat transmission across the aluminium frame wasn't taken into account.
- The temperature control system is PID controlled, mass flow is regulated with a fixed inlet temperature in the radiator, depending on the heat requirement.
- It is presumed that the greenhouse owner is planning to utilise the geothermal heat and the design of the heating system is adapted to this idea. To do that, the design inlet/outlet temperature of the radiator system has to be sufficiently low, not the 90/70°C system, conventional in Hungary. This requires a higher heat exchanger area, which makes it more practical to utilise the geothermal energy, as more energy can be transferred with the same mass flow. A good example can be found

in Iceland, where district heating systems are conventionally run at 80/40°C, successfully for at least 30 years. One of the key factor in the success, is that they use higher heat exchanger surfaces, based on 40°C temperature change in the system, which enables them to utilize twice as much energy, as with the Hungarian 90/70°C forward/return based systems.

- If the geothermal system cannot cover the necessary heat through the heat exchanger, a peak boiler will raise the temperature to the designed water temperature.
- Transpiration of the plants was not considered.
- An 11-ha. greenhouse complex is to be built up from 10 different 140×78.5 m² greenhouse blocks.
- Radiation loss was only considered for the roof. It was assumed that all solar radiation is absorbed as heat, which is not reflected by the ground, air or the wall of the greenhouse.
- Air temperature by an ideal ventilator is mixed and uniform everywhere, resulting in no delay in sensing temperature changes.
- If the air temperature exceeds 28°C, the greenhouse roof windows must open, with 28°C being kept preventing the employees suffering from higher temperatures.
- The price of the geothermal heat is assumed to be the same as for natural gas in the income calculation.

Definitions of variables are found in Nomenclature at the end of the report.

For stable conditions, the sum of the heat gain and loss should be zero, as shown in Equation 1:

$$Q_{sr} + Q_{add} - Q_f - Q_t - Q_r = 0 \quad (1)$$

Transmission heat loss from the greenhouse is calculated with Equation 2, where the temperature difference is between the inside temperature in the greenhouse and the outdoor ambient air temperature based on Equation 3. The U value was calculated separately for the wall, roof and the ground:

$$Q_t = U \cdot A \cdot \Delta T \quad (2)$$

$$\Delta T = T_{in} - T_{out} \quad (3)$$

The U value in Equation 2 is dependent on the air/ground temperature, the pressure and the velocity of the fluid, in the boundary layers and outside of it. Many theoretical formulae exist for these calculations. In this paper, Equation 4 was used, where δ is the thickness of the wall layer, λ is the conduction heat transfer coefficient of the wall material, and α is the convection heat transfer coefficient of the two sides of the surface. The convective heat transfer coefficient calculations based on the Nusselt number - Reynold number are applicable to liquids, but in the case of gas, often these do not give correct results. Empirical numbers exist for the overall heat transfer coefficient for the greenhouses, with many authors using Rafferty (1998). To the given data a polynomial curve can be fitted and used to estimate the overall heat transfer coefficient in different wind speeds. From the zero wind speed value, the inside convective heat transfer can be calculated from the glass convective heat transfer coefficient. With knowledge on that base value, the roof outside temperature can be determined to estimate the radiative heat loss:

$$U(v_{wind}) = \frac{1}{\frac{1}{\alpha_{in}} + \frac{\delta}{\lambda} + \frac{1}{\alpha_{out}}} \quad (4)$$

The air heat convective heat transfer coefficient is calculated from Equations 5-6:

$$U = -0.017 * v_{wind}^2 + 0.3877 * v_{wind} + 4.4635 \quad (5)$$

$$\alpha_{in} = \frac{2}{\frac{1}{U_0} - \frac{\delta}{\lambda}}, \quad U_0 \text{ is evaluated at } v_{wind} = 0 \quad (6)$$

The filtration heat loss is calculated by Equation 7. The heat exchange rate for modern glasshouses is usually $1/h$, but it can change due the ventilation duty, to remove the moisture, avoiding mould and fungus:

$$Q_f = n \cdot c_{p,air} \cdot \rho_{air} \cdot V \cdot \Delta T \quad (7)$$

The radiation heat loss is calculated by Equations 8-9:

$$Q_r = \delta \cdot \varepsilon_{glass} \cdot A \cdot F \cdot (T_{roof,out}^4 - T_{sky}^4) \quad (8)$$

$$T_{roof,out} = T_{out} + \frac{U \cdot A_{roof} \cdot \Delta T}{\alpha_{out}} \quad (9)$$

where the sky temperature is dependent on the opaque cloudiness (and results in lower radiation loss).

The glass temperature can be calculated by the conduction heat transfer coefficient (Equation 9). The sky temperature can be calculated by using Equations 10-12, where C , the opaque sky factor (range between 0 and 1), is recorded, usually in historical temperature databases:

$$CF = 1 + 0.00224 \cdot C + 0.0035 \cdot C^2 + 0.0028 \cdot C^3 \quad (10)$$

$$T_{sky} = T_{amb} \cdot \varepsilon_{sky}^{0.25} \cdot CF^{0.25} \text{ (MW)} \quad (11)$$

$$\varepsilon_{sky} = 0.711 + 0.56 \cdot \frac{T_{air,dew}}{100} + 0.73 \cdot \frac{T_{air,dew}^2}{100} \quad (12)$$

The solar radiation heat gain across a surface is given by Equations 13-20, based on the studies of Zelzouli et al. (2012) and Duffie and Beckman (2013):

$$Q_{sr} = A \cdot (I_{direct} + I_{diffuse,sky} + I_{diffuse,ground}) \quad (13)$$

$$\begin{aligned} \cos \theta = & \sin \delta \cdot \sin \varphi \cdot \cos \beta - \sin \delta \cdot \sin \beta \cdot \cos \varphi \cdot \cos \gamma + \cos \delta \cdot \cos \varphi \cdot \cos \beta \\ & \cdot \cos w + \cos \delta \cdot \sin \varphi \cdot \sin \beta \\ & \cdot \cos \gamma \cdot \cos w + \cos \delta \cdot \sin \beta \cdot \sin \gamma \cdot \sin w \end{aligned} \quad (14)$$

$$w = 15(time - 12) \quad (15)$$

$$\delta = 23.45 \cdot \sin\left(\frac{284 + n}{365}\right) ; n \text{ is the day of the year} \quad (16)$$

$$A = I_{direct} / (I_{global}) \quad (17)$$

$$fm = \left(\frac{I_{direct}}{I_{direct} + I_{diff}} \right)^2 \quad (18)$$

$$\cos \theta_z = \cos \varphi \cdot \cos \delta \cdot \cos w + \sin \delta \cdot \sin \varphi \quad (19)$$

$$\begin{aligned} I_s = & I_{direct} \cdot (1 - r) + I_{diff} \cdot A_s \frac{\cos \theta}{\cos \theta_z} + I_{diff} \cdot (1 - A) \cdot \frac{(1 + \cos \beta)}{2} \cdot (1 \\ & + fm \cdot \sin \frac{\beta}{2})^3 + (I_{direct}(1 - r) + I_{diff}) \cdot \rho_{ground} \\ & \cdot \frac{(1 - \cos \beta)}{2} \end{aligned} \quad (20)$$

The radiator system is unknown, so was assumed, that an effort will be made to try to fit it to the geothermal heat source and work at design temperatures 73/35 (as the geothermal water is 78°C). It is better not to have direct geothermal flow in the pipe system, as the geothermal fluid in Hungary contains a lot of minerals, and to avoid precipitation the pressure should be kept above 9 bar, which results in higher cost, if the whole system would be designed at 9 bar. The U value in the radiator system is not stable at changes with regards to duty and the temperature range. Equation 21 represents an empirical formula, which avoids the use of numerical simulation to determine the pipeline thermodynamic properties in different mass flow and temperatures conditions (Anon 1977), but instead determines the log-mean temperature difference without knowing the exact U value in different conditions, where $Q_{0,GH}$ is the design condition:

$$\frac{Q_{GH}}{Q_{0,GH}} = \left(\frac{\Delta T l g}{\Delta T l g_0} \right)^{4/3} \quad (21)$$

Through optimization it is decided which case would require a higher built-in capacity, the winter season when the temperature is rarely below -15°C, and a minimum inside temperature of 5°C needs to be kept to avoid freezing, or the autumn/spring season when the minimum temperature is -5°C as a design condition and the heat should be 22°C without radiation heat gain. In different heat duties, a different temperature difference is necessary and different mass flow. Equation 21 determines the necessary temperature difference between the radiator inlet and outlet temperatures and the room-required temperature, and with a basic iteration, the unknown radiator outlet temperature can be defined. By Equation 22 the necessary mass flow can be determined:

$$Q_{GH} = m_{rad} * c_p * (T_{in} - T_{out}) \quad (22)$$

The geothermal heat exchangers traditionally used in Hungary are shell and tube heat exchangers, as the more compact flat-plate collectors can have a high pressure drop and it could cause massive deposition, with the water usually having high mineral content. Here it is assumed, that the pinch point in the heat exchanger is 5°C, and the pinch point is between the lowest radiator return temperature at maximum radiator flow capacity. For that condition, a design UA value can be calculated by Equation 23:

$$Q_{HX} = UA * \Delta T l g_{HX} \quad (23)$$

At a fixed geothermal mass flow and inlet temperature, the most important factor is the geothermal outlet temperature in the heat exchanger in off-design conditions. The outlet temperature of water from the heat exchanger, circulated in the radiators, is also an unknown parameter. The unknown temperatures were determined by Equations 24-25:

$$\Delta T l g_{HX} = \frac{(T_{g,in} - T_{rad,x}) - (T_{g,out} - T_{rad,return})}{\ln\left(\frac{T_{g,in} - T_{rad,x}}{T_{g,out} - T_{rad,return}}\right)} \quad (24)$$

$$m_{rad}(T_{rad,x} - T_{rad,return})c_p = m_g(T_{g,in} - T_{g,out})c_p \quad (25)$$

Different functions were written in Scilab to determine all necessary parameters. The model inlet parameters were the recorded temperature data (EnergyPlus, 2016), an excel sheet containing the year recorded, hourly measured temperatures, relative humidity, wind speed, cloudiness, direct and diffuse solar radiation. The control model used, was a PID mass flow control based on the temperature difference between the reference temperature and the actual temperature, during winter period ($T_{ref} = 5^\circ\text{C}$) and the summer period (from March till November), where the reference temperature was set to 16°C in night and 22°C in day mode, and the day mode was between 6 AM and 6 PM.

4. RESULTS AND DISCUSSION OF THE GREENHOUSE HEAT REQUIREMENTS

The greenhouses were evaluated separately first and the heat losses and gain were calculated, with the necessary mass flow and temperature change for each greenhouse. After some runs it was clear that no significant heat loss or temperature change can be detected if the greenhouses were handled separately. Consequently, this simplification was made and also their heat loss and solar gain handled in the same way, which reduced greatly the time of the calculation runs. Figure 4 shows the heating need of the 11-ha. greenhouse complex per hour for a winter day (January 3rd) without using energy curtains.

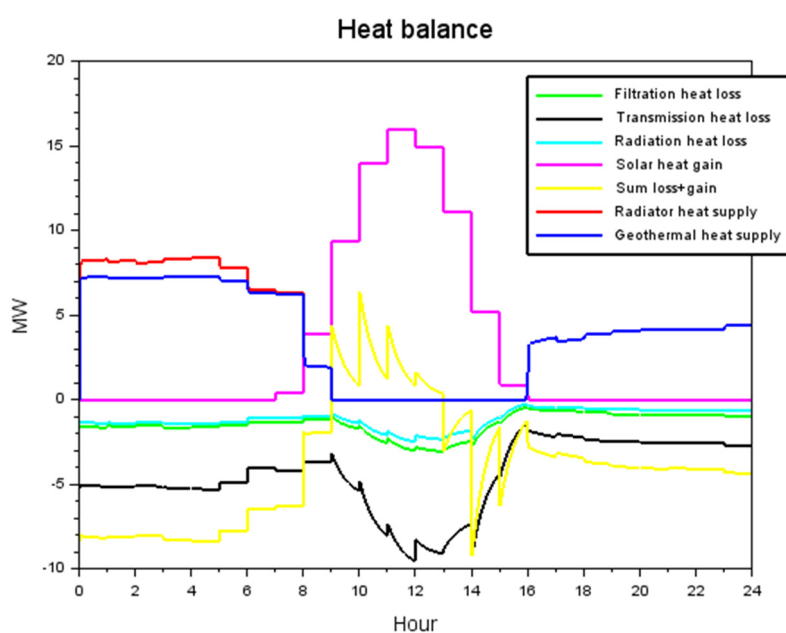


FIGURE 4: Simulation results for heat losses on January 3rd

Even though a dynamic model was made, the data used is not smooth enough, which results in big and sudden step changes in the heat losses, and also in the dynamic response of the system. Transmission and filtration heat loss is dependent on the actual temperature inside, which changes less rapidly than the outlet temperature or wind speed, as can be seen in Figure 5 based on the thermal heat storage effect. Figure 5 represents the influencing parameters of the dynamic model, like the minimum reference temperature, which in the winter season was set to be 5°C, the outlet ambient temperature and the wind speed.

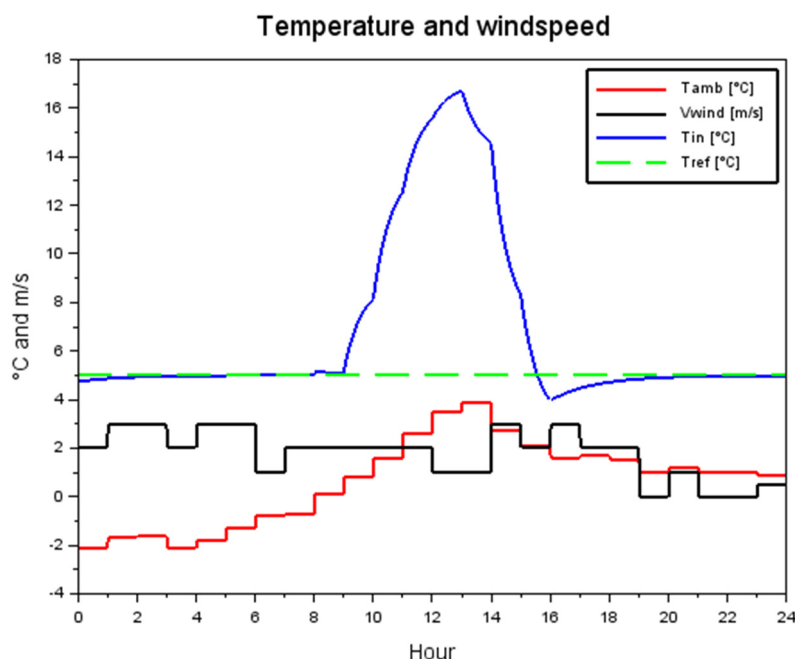
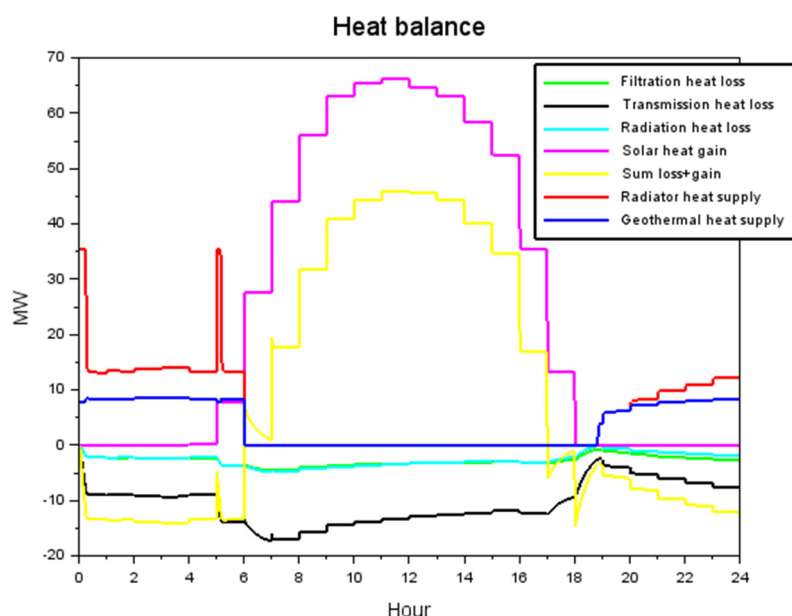


FIGURE 5: Simulation results for influencing factors on January 3rd

Due to the solar radiation and the heat stored in the greenhouse, the inside temperature of the greenhouse rises above the reference temperature. Because of this phenomenon, no additional heat was needed between 8 AM and 4 PM. Figures 6 and 7 show similar simulations for the April 20th heat parameters. The sharp (red) radiator heat supply is due to the change in the reference temperature, and is to warm up the greenhouse. Two different runs were made. In the first case, the heat loss was calculated without the energy curtain and its decreasing heat loss influence. For the other one, the energy curtain was assumed to decrease the heat loss by 45% during the nights. The total supplied energy by the ORC power plant in the first case is 92,436 GJ during a year. If the energy curtain was used, this value was reduced to 65,850 GJ, a decrease of almost 30%. For current



natural gas prices this would mean 250 million HUF (805,000 EUR) in the first case and 178 million HUF (573,500 EUR) in the second case.

FIGURE 6: Simulation results for heat losses on April 20th

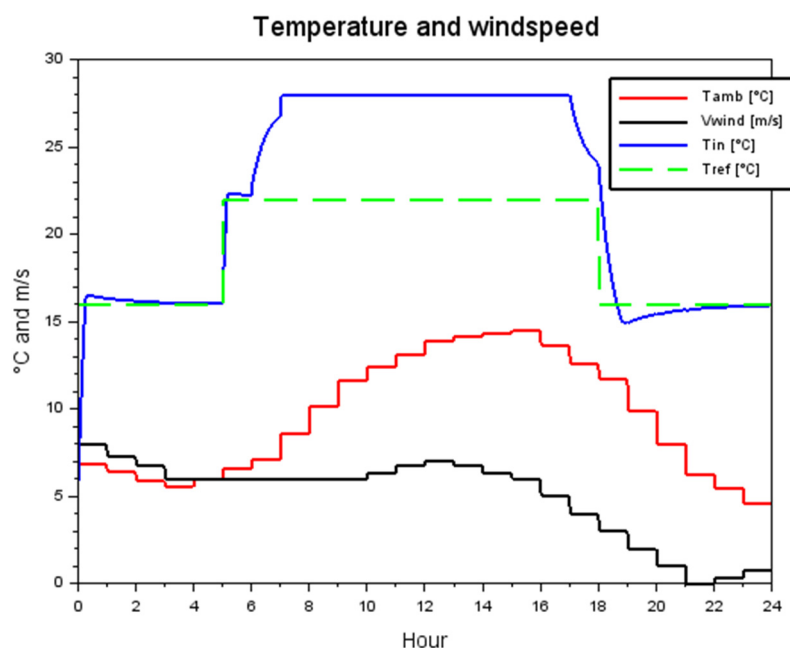


FIGURE 7: Simulation results for influencing factors on April 20th

5. EVAPORATIVE CONDENSER AND POWER OUTPUT

The evaporative condenser is somewhat different from a conventional one because the heat and mass transfer are happening at the same time (Equations 26-27). The condensate gives its heat through the pipe wall to the deluge water, by convection and conduction. The deluge water by conduction and evaporation gives the heat to the airflow (Equations 28-32). Detlev G. Kröger gave a brief description on the process in his book *Air cooled heat exchangers and cooling towers* (Kröger, 2004). Figure 8 shows an elementary control volume and the heat and mass transport in it. The principle of the evaporative condenser is the cooling effect of the water evaporation to the air stream and the high (-er)

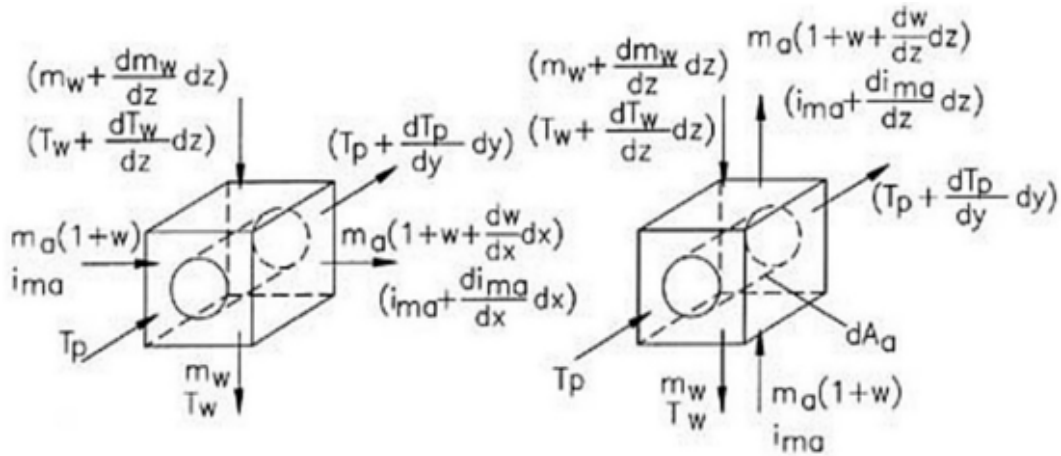


FIGURE 8: Evaporative condenser's heat and mass flows (Kröger, 2004)

conductive heat transfer coefficient at the wall-water surface. The driving force of the evaporation is the difference between the air absolute humidity and the air humidity at the water surface (which is assumed to have 100% relative humidity) and the water surface. The basic equations of the evaporative condenser can be found in Kröger's book and in a thesis by Johan Heyns (Heyns, 2008), but here only the final equations are presented, neglecting the derivation of the formulae which are given in the book or paper.

Some assumptions were made:

- The evaporated water flow compared to the deluge water (circulating) or air mass flow is 10 times smaller, the water flow change can be neglected (but not the evaporation itself);
- The temperature of the water is the same through the tube bundles;
- The air properties values used are the average between the inlet and outlet; and
- The air mass flow is saturated with water at the outlet.

The final simplified case is, that through the whole heat exchanger, the total heat coming from cooling down the ORC fluid and condense it, is equal to the heat transfer through the pipeline given to the deluge water. It is also equal to the heat necessary for evaporation and also the heat transfer from the water to the air. The last two processes mentioned can be expressed as the airstream enthalpy change. The evaporation rate is represented in Equation 29 and the related energy transport by Equation 30. The conductive heat transport is determined by Equation 31.

The equations referred to above are the following:

$$m_{air}(1+w) + \left(m_w + \frac{dm_w}{dz} dz\right) = m_{air} \left[1 + \left(w + \frac{dw}{dz} dz\right)\right] + m_w \quad (26)$$

$$m_{air}h_{air} + \left(m_w + \frac{dm_w}{dz} dz\right)(h_w + dh_w) = m_a \left[h_{air} + \frac{dh_{air}}{dz} dz\right] + m_w h_w \quad (27)$$

$$dQ_{cond} (ORC \text{ fluid side}) = dQ_{mass} + dQ_{conductive} = Q_{heat+mass \text{ transfer (air side)}} \quad (28)$$

$$\frac{dm_w}{dz} dz = h_d(w_{ws} - w) * dA \quad (29)$$

$$dQ_{mass} = h_v \frac{dm_w}{dz} dz = h_v h_d (w_{ws} - w) * dA \quad (30)$$

$$dQ_{conductive} = \alpha_a (T_w - T_a) dA \quad (31)$$

$$\begin{aligned}
Q_{cond} &= m_{R245fa} \cdot (\Delta L_{cond} + \Delta h_{R245fa,cool}) \\
&= Q_{heat\ transfer} = UA_{bundles}(T_c - T_{wm}) \\
&= Q_{heat+mass\ transfer} = m_{air} \cdot (h_{air,in} - h_{air,out})
\end{aligned} \tag{32}$$

The mass transfer coefficient can be calculated by Equation 33 and the necessary fluid properties by Equations 34-37 (Heyns, 2008):

$$h_d = \frac{5.5439/10^8 Re_{wm}^{0.15} Re_{awm}^{0.9}}{d_o^{1.6}} \tag{33}$$

$$Nu_c = \frac{\alpha_c d_i}{k_c} = 0.023 * Re_c^{0.8} Pr_c^{0.4} \left(0.55 + 2.09 \left(\frac{p_{crit}}{p_{vap}} \right)^{0.38} \right) \tag{34}$$

$$Re_{awm} = \frac{\rho_{avm} \cdot v_{avm} \cdot d_o}{\mu_{wm}} \text{ where } v_{avm} = \frac{m_{air}}{\rho_{avm} A_{air}} \tag{35}$$

$$Re_{wm} = \frac{4\Gamma_m}{\mu_{wm}} \tag{36}$$

$$\Gamma_m = \frac{m_w \cdot d_o}{A_{bundles}} \tag{37}$$

The air outlet enthalpy is calculated by Equation 38:

$$h_{air,out} = h_{air,avm} - (h_{air,avm} - h_{air,in}) e^{\frac{A_{bundles} h_d}{m_{air}}} \tag{38}$$

The condensation heat transfer coefficient is given by Equations 40 for $Re_{ss} < 35000$. Equation 41 is used for Reynolds numbers higher than 35000. The Reynolds number is given by Equation 39 (Bergman et al., 2006):

$$Re_{cv} = \frac{\rho_{cv} \cdot v_{cv} \cdot d_i}{\mu_{cv}} \text{ and } Re_{cl} = \frac{\rho_{cl} \cdot v_{cl} \cdot d_i}{\mu_{cl}} \tag{39}$$

$$\alpha_c = \frac{\left[\frac{0.555((g\rho_{cl}(\rho_{cl} - \rho_{cv}))(h_{vap} + 0.68 * cp_{cl}(T_c - T_{wall}))d_i^3)}{\mu_{cl}k_{cl}(T_c - T_{wall})} \right]^{1/4}}{d_i} k_{cl} \tag{40}$$

$$\alpha_c = \frac{0.023 Re_{cl}^{0.4} Pr_{cl}^{0.8} (0.55 + \left(\frac{p_{crit}}{p_{cv}} \right)^{0.38})}{d_i} k_{cl} \tag{41}$$

The deluge water heat transfer coefficient and the tube wall overall heat transfer coefficient are given by Equations 42-43:

$$\alpha_w = 2102.9 \left(\frac{\Gamma_m}{d_o} \right)^{0.333} \tag{42}$$

$$U = \frac{1}{\left(\frac{1}{\alpha_w} + \frac{d_o}{d_i k_{pipe}} + \frac{1}{\alpha_c} \right)} \tag{43}$$

One of the main questions was quantity of the evaporated water, which is given by Equation 44:

$$m_{water} = m_{air}(w_{air,out} - w_{air,in}) \tag{44}$$

In dry mode, the mass transfer doesn't take place, the air absorbs the rejected heat by condensation. The important parameters in this case are described by Equations 45-47 (Bergman et al., 2006):

$$\begin{aligned} Q_{cond} &= m_{R245fa} \cdot (\Delta L_{cond} + \Delta h_{R245fa,cool}) = Q_{heat\ transfer} \\ &= UA(T_c - T_{air,avg}) = Q_{heat+mass\ transfer\ (air\ side)} \\ &= m_{air} \cdot (h_{air,in} - h_{air,out}) \end{aligned} \quad (45)$$

$$\alpha_{a,dry} = \left(0.3 + \frac{0.62 Re_{air,wall}^{0.5} Pr_{air,wall}^{\frac{1}{3}}}{\left(1 + \left(\frac{0.4}{Pr_{air,wall}} \right)^{\frac{2}{3}} \right)^{0.25}} \right) \left(1 + \left(\frac{Re_{air,wall}}{282000} \right)^{\frac{5}{8}} \right)^{4/5} \frac{k_{air,wall}}{d_o} \quad (46)$$

$$U = \frac{1}{\left(\frac{1}{\alpha_{a,dry}} + \frac{d_o}{k_{pipe}} + \frac{1}{\alpha_c} \right)} \quad (47)$$

In the calculation, many parameters are unknown, like the mean deluge water temperature, or the condensation temperature (as it changes by the inlet air temperature) and the air average temperature, where Re_{awm} was evaluated, the air outlet temperature and the wall temperature. The wall temperature doesn't really change the coefficient, which is related to it, but the other parameters have a crucial role. To find the condensation temperature for a given air temperature, a nested loop iteration was used, with the deluge water temperature and the condensation temperature changed in the iteration.

The given data of the condenser didn't contain the exact geometric parameters of the evaporative condenser, like number of tubes, just one tube diameter. To overstep this problem, a surface was suggested, which can fulfil the criterion to use the condenser at 22°C when the design outlet temperature is 11.2°C, as was suggested by Mannvit. When choosing the surface size, it was also considered, that during winter it must work in a dry mode, as the water could freeze in the tubes and destroy them. This would reduce the efficiency of the plant very much, as the overall heat transfer coefficient can be two orders of magnitude less if on one side there is gas instead of liquid. The mass flow of the ORC fluid was also unknown, but Mannvit Consulting Engineers provided official data on the power output of the two screw expanders in the plant, and the geothermal fluid inlet and outlet temperatures and pressures in many points. To determine the mass, a flow reverse calculation was used, where the following parameters were fixed:

- The design condensation temperature;
- The geothermal water mass flow temperature and pressure values in most of the brines.

During the calculation the pressure drop on the ORC side was neglected, the turbine isentropic efficiency was estimated based on typical values found on-line (Hsu et al., 2014).

The ORC high-temperature loop was calculated with the following routines, based on the schematic drawing of the power plant (Appendix I). The red marks show the known parameters, while the blue circles show states with unknown parameters. In the high-temperature loop in the evaporator the geothermal water goes with full capacity and evaporates and slightly superheats the ORC fluid as defined in Equation 48:

$$m_{g1}(h_{g1} - h_{g2}) = m_{r245fa}(h_3 - h_{4SH}) \quad (48)$$

After the evaporator, a bigger portion of the geothermal water goes to the low-temperature loop, and a smaller fraction preheats the ORC fluid (Equation 49):

$$m_{g2}(h_{g2} - h_{g3}) = m_{r245fa}(h_2 - h_3) \quad (49)$$

The expander work's is given by Equation 50, with the screw expander power output known (W_0):

$$W_t = m_{r245fa}(h_{4SH} - h_5) \quad (50)$$

6. RESULTS OF THE EVAPORATIVE CONDENSER SIMULATION

The pump work was assumed to be isentropic (this assumption doesn't make significant change in the temperature of point 2), $s_1=s_2$. With numbers of points referring to the figure in Appendix I, the ORC fluid pressure at 2, 3, 4 and 4SH points was set to be the same, temperature at 3 and 4 is the same, while the temperature difference between the superheated vapour and the evaporated vapour was assumed to be 2°C. By iterating with the mass flow, the optimal pressure was found by an iterative method, which gave the right pressure, which results in the known power output ($W_t=W_0$). By plotting the temperatures of the geothermal fluid and the ORC fluid versus the ORC mass flow, and also represent the known geothermal temperatures ($T_{g2}=104^\circ\text{C}$, $T_{g3^*}=78^\circ\text{C}$, and $T_{g3}=T_{g4^*}=38^\circ\text{C}$, respectively), the cross point of the mass flow dependent geothermal fluid temperature and the designed geothermal fluid temperature gives the possible ORC mass flow. The two known geothermal temperatures in a precise calculation would cross the calculated geothermal temperatures at the same mass flow, but as any losses etc. at the evaporator and preheater were not taken into account, it could result in some difference, adding also that the expander efficiency has great effect on the results. The stronger boundary is the higher fixed geothermal temperature, as it has to be an evaporative medium in the low-temperature loop. As can be seen, the temperature difference between the calculated geothermal water temperature at (T_{g3}) and the reference temperature is not crucial. This was also done for the low-temperature loop. The reverse calculations resulted in 52 and 43 kg/s mass flow for the high- and low-temperature loops, respectively, and 11.9 and 6.46 bar inlet pressure to the expander. With the known mass flow, temperature and pressure values, the behaviour of the evaporative condenser was modelled.

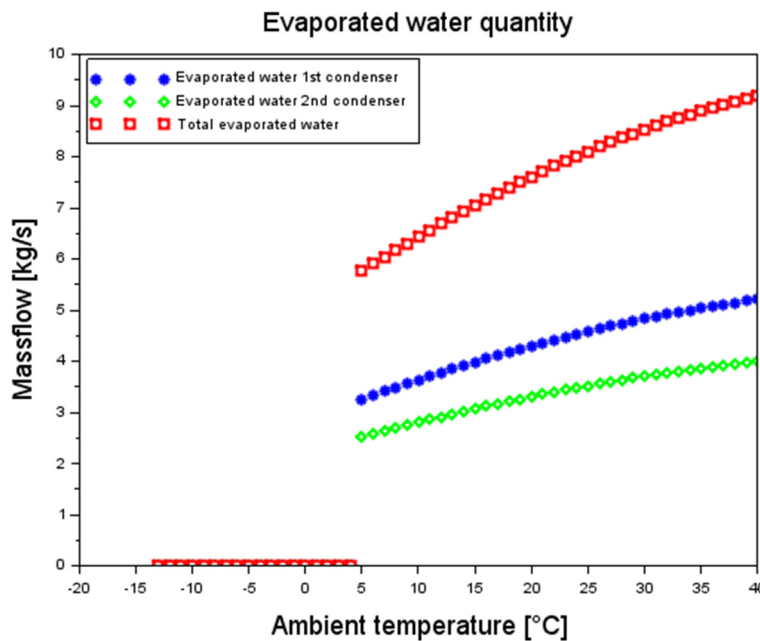


FIGURE 9: Evaporated water mass flow vs ambient temperature

As seen in Figure 9, the model shows that the evaporated water mass flow is around 8-9 kg/s. It is influenced mostly by the heat exchanger surface area and the air mass flow. As the air temperature increases, the air can carry more water vapour. Therefore, higher temperature will result in a higher water evaporation rate. The condenser temperature will also rise, as it physically cannot be lower than the air inlet wet bulb temperature. It will raise the condenser pressure and reduce the power plant efficiency as presented in Figures 10 and 11. In the dry mode, the efficiency will also be reduced, as the overall heat transfer coefficient is controlled by the air side conduction heat transfer coefficient, which is two magnitudes lower than water conduction heat transfer coefficient. The temperature duration curve and the related

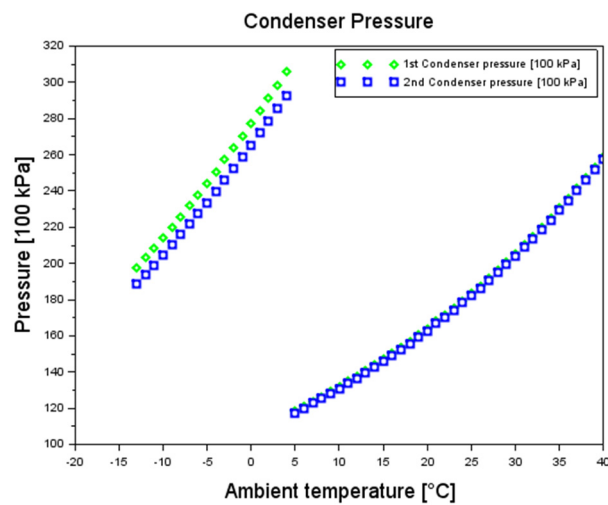


FIGURE 10: Condenser pressure vs ambient temperature

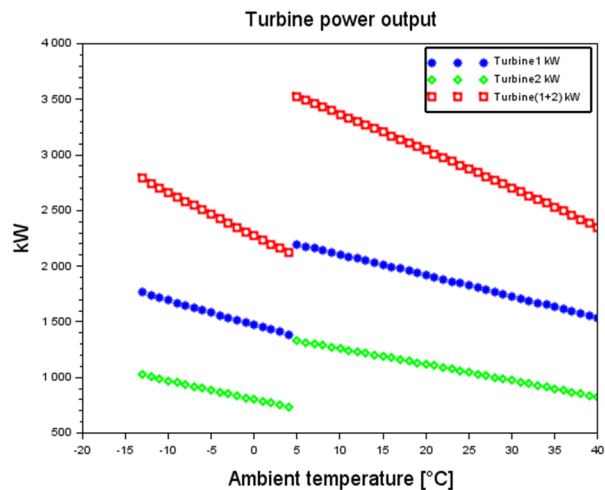


FIGURE 11: Turbine power output curve vs ambient temperature

performance duration curve can be seen in Figure 12. The power plant will work close to the design power output most of the time.

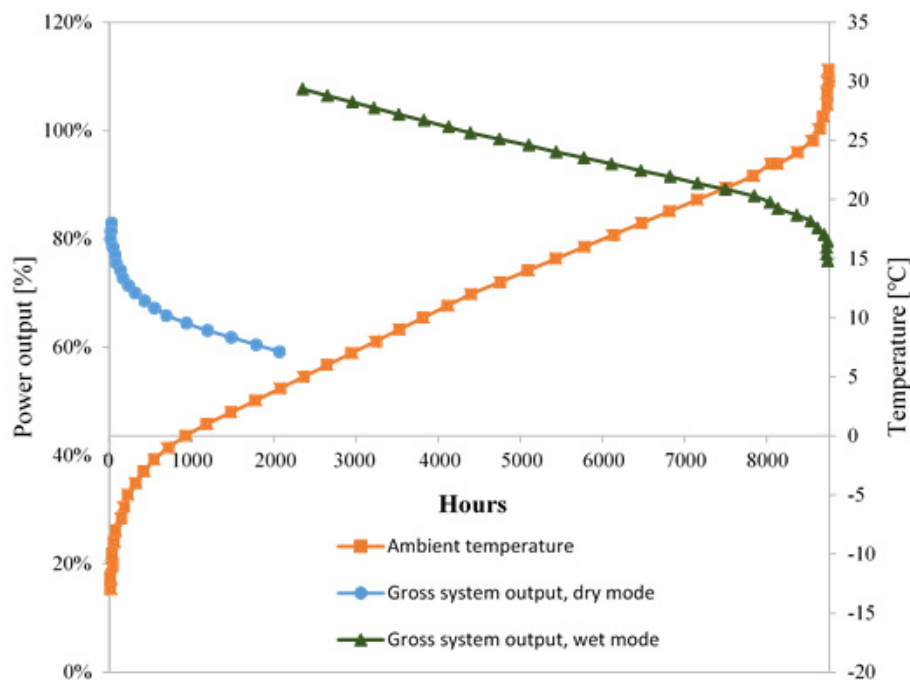


FIGURE 12: Temperature and power output duration curve

7. CONCLUSIONS

The project was conducted to find the possible heat that the ORC power plant in Tura can supply to a planned greenhouse complex and investigate the behaviour of the evaporative condenser. Scilab dynamic simulations were used to determine the heat requirements of the greenhouses and a static model was designed to evaluate the evaporative condenser behaviour and the effect on the turbine output. The calculated income is between 574 000 and 805 000 EUR per year. The evaporated water quantity varies greatly by the ambient temperature as well as the turbine power output.

The simulation of the greenhouse could be supplemented if the transpiration heat loss of the plants was more accurately calculated, and with a smoother temperature data.

The lack of power plant data resulted in many assumptions in the evaluation of the evaporative condenser. With more precise data, the calculations could be refined and give a more accurate result. But as it the case for every model, it needs validation with real measurements.

The calculated low power output for the dry operation of the evaporative condenser at low air temperatures is highly interesting. Either elimination of the dry mode by a condenser design which can tolerate some freezing on the outside of the tubes has to be made, or a way found to have fins on the tube outside to enhance the performance in the dry mode.

ACKNOWLEDGEMENTS

I would like to thank the UNU-GTP for granting me the opportunity to participate in the six-month training program. Special thanks to the director Mr. Lúdvík S. Georgsson, his deputy Mr. Ingimar G. Haraldsson, Ms. Thórhildur Ísberg, Mr. Markús A. G. Wilde and Ms. Málfríður Ómarsdóttir and every teacher who was involved in the training.

I would like to express my gratitude to Páll Valdimarsson for being my supervisor and Kristinn Ingason at Mannvit Consulting Engineers for the help and the project. I would also like to say thanks for help and professional assistance to Nasim Saber, her friend Argineh Shabandari and Gideon Gitonga Gitobu.

I would also like to thank all the students that made this time wonderful, special thanks to Zsófi Erzsébet Unyi, Byron Fabian Pilicita Masabanda, Sarantseteseg Lkhagvasuren. the whole geothermal utilisation group: Gideon Gitonga Gitobu, Nasim Saber, Winnie Adhiambo Apiyo, Daniel Wanga Odongo, Harrison Kiplimo Keter, and Zoltán Békés.

And last but not least thanks to my family and friends, who supported me the whole year, not least during my time in Iceland!

REFERENCES

Alternatív Energia, 2016: *Vegetables produced by thermal water in Tura (in Hungarian)*. Alternatív Energia, website: www.alternativenergia.hu/termalvizzel-termelnek-zoldseget-turan/76093

Anon, 1977: *DIN 4703 Teil 3. Varmeleistung von Raumheizkörper* (in German). Beuth Verlag, Berlin, Germany.

Bergman, T.L., Lavine, A.S., Incropera, F.P., and DeWitt, D.P., 2006: *Introduction to heat transfer* (6th ed.). John Wiley & Sons, NY, 912 pp.

CoolProp 2016: *CoolProp C++ library*. CoolProp, website: www.coolprop.org.

Duffie, J.A., and Beckman, W.A., 2013: *Solar engineering of thermal processes* (4th edition). John Wiley & Sons, New Jersey, 928 pp.

EnergyPlus, 2016: *Weather data*. EnergyPlus, website: energyplus.net/weather.

- Fögáz, 2016: *Present heat prices. FÖGÁZ*, website: www.fogaz.hu/Egyetemes-Szolgalatas/Ugyintezes/Arak-dijszabasok/Aktualis-arak?download
- Google Earth, 2016: *Google Earth software*. Google Earth, website: www.google.com/earth
- Heyns, J.A., 2008: *Performance characteristic of an air-cooled steam condenser incorporating a hybrid (dry/wet) dephlegmator*. University of Stellenbosch, S-Africa, MSc thesis, 129 pp.
- Hsu, S.-W., Chiang H.-W.D., and Yen, C.-W., 2014: Experimental investigation of the performance of a hermetic screw-expander Organic Rankine Cycle. *Energies* 2014, 7, 6172-6185.
- Hungarian Ministry of National Development, 2011: *Regulation about the support of district heating, "51/2011, (IX. 30.)*. NFM, website: net.jogtar.hu.
- Kröger, D.G., 2004: *Air cooled heat exchangers and cooling towers* (vol. 1). PennWell Corp. Tulsa, OK, 502 pp.
- Magyar Idők, 2016: *Ten billion investment to utilise the thermal water in Tura* (in Hu.). Magyar Idők, website: magyaridok.hu/gazdasag/tizmilliardos-beruhazas-turai-termalviz-hasznositasara-691921
- Mariani, L., Cola, G., Bulgari, R., Ferrante, and Martinetti, L., 2016: Space and time variability of heating requirements for greenhouse tomato production in the Euro-Mediterranean area. *Science of the Total Environment*, 562, 834-844.
- MATLAB, 2016: *MATLAB, the language of technical computing*. MATLAB, website: se.mathworks.com.
- OECD, 2015: *Projected costs of generating electricity*. Nuclear Energy Agency, OECD, website: www.oecd-neo.org/ndd/pubs/2015/7279-proj-costs-electricity-2015-es.pdf.
- Rafferty, K.D., 1998: Greenhouses. In: Lienau, P.J., and Lunis, B.C. (eds.), *Geothermal direct use engineering and design guidebook*. Geo-Heat Center, Klamath Falls, OR, 307-326.
- REFPROP, 2016: *NIST Reference fluid thermodynamic and transport properties database (REFPROP), version 9.1*. National Institute of Standards and Technology – NIST, website: www.nist.gov/srd/refprop.
- Sanford, S., 2011: *Using curtains to reduce greenhouse heating and cooling costs*. Energy Efficiency in Greenhouses, article, 8 pp, website: articles.extension.org/sites/default/files/4.%20A3907-03.pdf.
- Scilab, 2016: *Scilab 5.5.2*. Scilab Enterprises, website: www.scilab.org.
- Tura Organic Garden, 2015: *Decisions*. Middle-Danube-Valley Inspectorate for Environmental Protection, Nature Conservation and Water Management, website: kdvktf.zoldhatosag.hu/dokumentumok/hirek/5114/4425/34020_20_2014.pdf
- Unyi, Z.E., 2016: Geothermal reservoir model of Dombovar area, SW-Hungary. Report 40 in: *Geothermal training in Iceland 2016*. UNU-GTP, Iceland, 875-890.
- Zelzouli, K., Guizani, A., Sebai, R., and Kerkeni, C., 2012: Solar thermal systems performances versus flat plate solar collectors connected in series. *Engineering*, 4-12, 881-893.

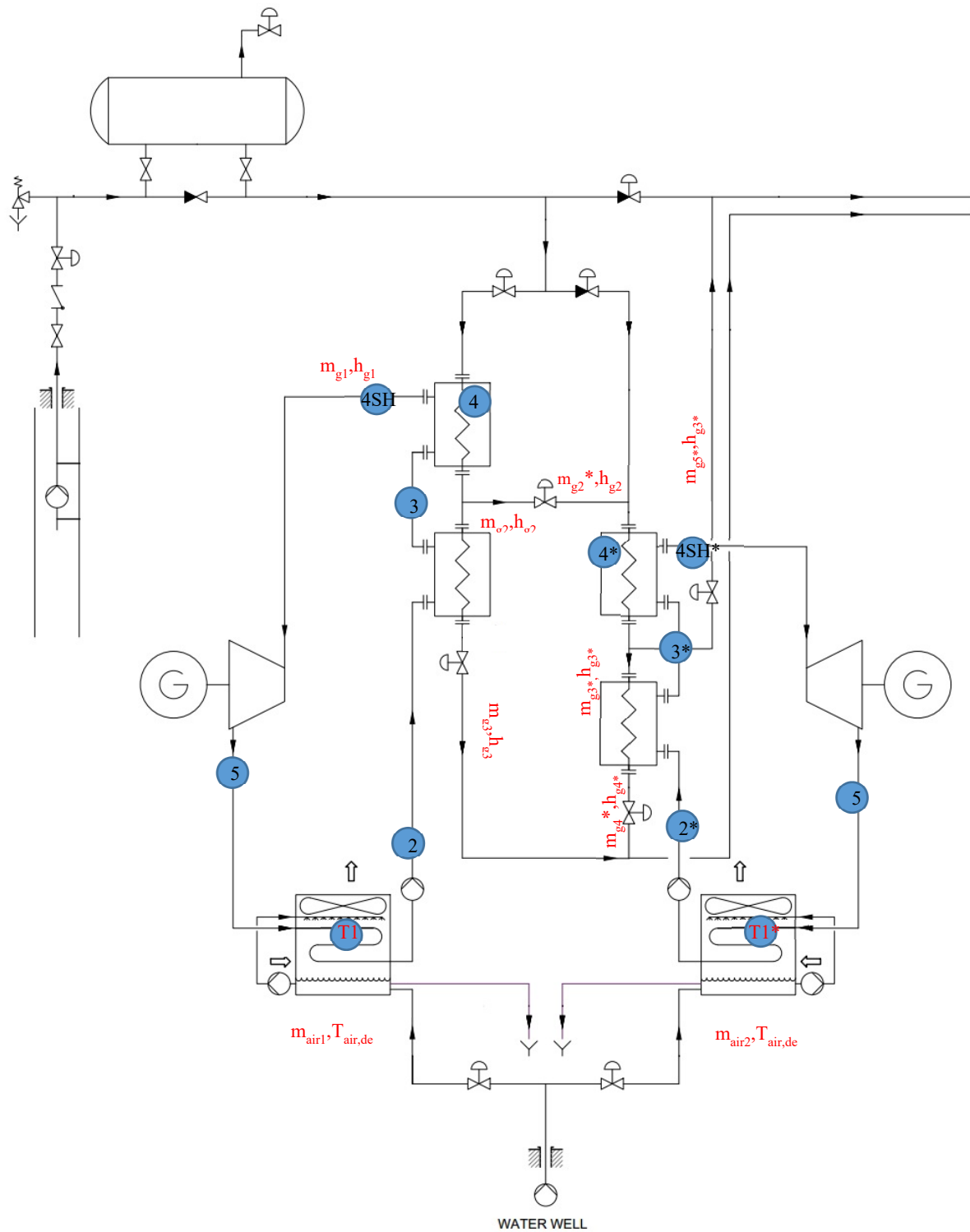
NOMENCLATURE

Symbol	Description	Unit
A	Surface	m ²
A_{roof}	Surface of the greenhouse roof	m ²
A_{bundles}	Surface of the tube bundles in the condenser	m ²
A_{air}	Surface where the air can pass in the condenser	m ²
α	Convective heat transfer coefficient	W/(m ² K)
α_a	Conductive heat transfer coefficient of air	W/(m ² K)
$\alpha_{a,dry}$	Conductive heat transfer coefficient of air	W/(m ² K)
α_c	Conductive heat transfer coefficient of ORC medium	W/(m ² K)
α_w	Conductive heat transfer coefficient of water	W/(m ² K)
β	Angle between the horizon and the surface	°
C	Opaque sky factor	
CF	Constant	
c_p	Specific heat	J/(kgK) or J/(kg°C)
cp_{cl}	Heat capacity of ORC condensate	J/(kgK) or J/(kg°C)
δ	Thickness or Stefan Boltzmann constant	m or W/(m ² K)
ΔT_{lg}	Logarithmic mean temperature difference	°C
ΔT_{lg0}	Logarithmic mean temperature difference design condition	°C
ΔT_{lgHX}	Logarithmic mean temperature difference in the heat exchanger	°C
ΔL_{cond}	Latent heat of vaporization	J/kg
$\Delta h_{R245fa,cool}$	Specific enthalpy change of ORC fluid during cooling	J/kg
d_i	Inlet diameter	m
d_o	Outer diameter	m
ϵ_{glass}	Emissivity of the glass	
ϵ_{sky}	Emissivity of the sky	
F	View factor	
g	Gravity	m/s ²
φ	Latitude of the place in degrees	°
Γ_m	Deluge water mass flow per unit length	kg/(m s)
γ	Surface azimuth angle	°
h_d	Mass transfer coefficient	kg/(sm ²)
h_v	Specific enthalpy of vapour	J/kg
h_{air}	Specific enthalpy of air	J/kg
h_{air,avm}	Specific enthalpy of air at mean water temperature	J/kg
h_{vap}	Specific enthalpy of vaporisation of water	J/kg
h_{g1}, h_{g2}	Specific enthalpy of the geothermal fluid in different points	J/kg
	Specific enthalpy of superheated ORC fluid	J/kg
h₃, h₅, h_{4SH}	Specific enthalpy of ORC fluid in different points	J/kg
I_{direct}	Direct radiation	W/m ²
I_{diffuse,sky}	Diffuse radiation from the sky	W/m ²
I_{diffuse,ground}	Diffuse radiation from the ground	W/m ²
I_{global}	Global radiation	W/m ²
I_{diff}	Diffuse radiation	W/m ²
I_s	Sum of radiation	W/m ²
k_{cl}	Thermal conductivity of the condensate	W/(mK)
k_{pipe}	Thermal conductivity y of pipe material	W/(mK)
k_{air,wall}	Thermal conductivity of air at the bundle's wall temperature	W/(mK)
λ	Conductive heat transfer coefficient	W/(mK)
m_{rad}	Mass flow in the radiator	kg/s
m_g	Mass flow of geothermal fluid	kg/s
m_w	Mass flow of deluge water	kg/s
m_{air}	Mass flow of air	kg/s
m_{R245fa}	Mass flow of ORC fluid	kg/s

Symbol	Description	Unit
\dot{m}_{water}	Mass flow of evaporated water	kg/s
μ_{wm}	Dynamic viscosity	N s/m ²
μ_{cv}	Dynamic viscosity of the condensing ORC vapour	N s/m ²
μ_{cl}	Dynamic viscosity of the condensed ORC liquid	N s/m ²
Nu_c	Nusselt number	
n	Air exchange rate, or number of the day in a year sequence	1/s or 1/h
Pr_c	Prandtl number	
Pr_{ws}	Prandtl number	
$Pr_{\text{air,wall}}$	Prandtl number	
p_{crit}	Critical pressure	Pa
p_{cv}	Vapour pressure	Pa
Q_{sr}	Heat gain rate by solar radiation	W, MW
Q_{add}	Heat supply rate by the greenhouse heating system	W, MW
Q_f	Heat loss by rate filtration	W, MW
Q_t	Heat loss by rate transmission	W, MW
Q_r	Heat loss rate by radiation	W, MW
Q_{GH}	Heat power requirement of the greenhouse	W
$Q_{0,\text{GH}}$	Heat power requirement of the greenhouse design cond.	W
Q_{HX}	Heat power supply by the geothermal heat exchanger	W
$Q_{\text{heat+mass transfer}}$	Sum of heat and mass transfer rate	W
$Q_{\text{heat transfer}}$	Heat transfer rate between deluge water and condensate	W
Q_{cond}	Heat rate of cooling and condensing of ORC fluid	W
Re_{awm}	Reynolds number of air at mean water temperature	
r	Reflectance	
Re_{wm}	Reynolds number of mean water	
Re_c	Reynolds number of condensate	
Re_{cv}	Reynolds number of condensing vapour	
$Re_{\text{air,wall}}$	Reynolds number of air at wall temperature	
ρ_{cv}	Density of ORC vapour	kg/m ³
ρ_{avm}	Density of air at mean water temperature	kg/m ³
ρ_{cl}	Density of ORC condensate	kg/m ³
ρ_{air}	Density of air at ambient temperature	kg/m ³
T	Temperature	K
$T_{\text{roof,out}}$	Temperature of the roof	°C
T_{sky}	Temperature of the sky	°C
T_{amb}	Ambient temperature	°C
$T_{\text{air,dew}}$	Dew temperature of the ambient air	°C
$T_{\text{g,in}}$	Temperature of geothermal fluid at the inlet	°C
$T_{\text{rad,x}}$	Temperature of radiator fluid after the heat exchanger	°C
$T_{\text{g,out}}$	Temperature of geothermal fluid at the outlet	°C
$T_{\text{rad,return}}$	Temperature of radiator coming from the greenhouse	°C
T_w	Temperature of water	°C
T_a	Temperature of air	°C
T_c	Temperature of condensate	°C
T_{wm}	Mean water temperature	°C
T_{wall}	Temperature of the wall	°C
$T_{\text{air,avg}}$	Average air temperature	°C
θ	Angle of incidence	°
θ_z	Zenith angle	°
U	Overall heat transfer coefficient	W/(m ² K)
v_{wind}	Wind velocity	m/s
V	Volume of air in the greenhouse	m ³
w	Absolute humidity	g/kg air
w_{ws}	Absolute humidity at water surface	g/kg air
v_{avm}	Velocity of air at the water surface	m/s
v_{cv}	Velocity of the condensing ORC vapour	m/s

Symbol	Description	Unit
v_{cl}	Velocity of the condensed ORC liquid	m/s
w_{air}	Absolute humidity of air	g/kg air
W_t	Power output of turbine	W

APPENDIX I: Schematic design of Tura ORC power plant





UNITED NATIONS
UNIVERSITY

UNU-GTP

Geothermal Training Programme

Orkustofnun, Grensasvegur 9,
IS-108 Reykjavik, Iceland

Reports 2016
Number 28

MONITORING AND EVALUATION FRAMEWORK FOR GEOTHERMAL PROJECTS: OLKARIA I UNIT 6, KENYA

Damaris Wacera Njoroge

Kenya Electricity Generating Company – KenGen

P.O. Box 785-20117

Naivasha

KENYA

dnjoroge@kengen.co.ke, damarisnjoroge@gmail.com

ABSTRACT

A monitoring and evaluation framework serves as a guide in project management and is a tool that ensures control in all the phases of a project. For capital intensive geothermal projects, a framework has proven to be beneficial in their management. The development of the framework borrows concepts and ideas from public management systems that have been and are being developed.

A framework was developed for management of geothermal projects through the use of a project being implemented in Kenya (Olkaria I unit 6). A description is given on management of phases staged in geothermal projects. Different tools and methodologies were applied to develop the framework from the initiation, execution and completion phases. Time and scope management through the use of decomposition and critical path is utilised. In cost management earned value analysis was used as a means of cost control. A profitability model was also developed that gives the economic viability of the project and is essential at the project initiation.

A reporting method with the use of performance indicators for project monitoring is discussed and guidance on reporting of the indicators as well as reporting frequency. A dashboard report for the Olkaria I unit 6 project was developed and is presented with assumed data.

1. INTRODUCTION

1.1 Development strategy

The geothermal activity in Kenya lies within the East African Rift system. Fourteen geothermal sites, shown in Figure 1, have been identified within the Kenyan rift with potential power of over 10,000 MWe while the current installed geothermal capacity stands at about 623 MWe. It is expected that the installed capacity will grow to 5,500 MWe by 2030 (MoEP, 2015). Overall power generation in Kenya is expected to grow to 19,200 MWe by 2030 from the 2,200 MWe in 2015. The growth will be necessitated by a long-term development policy, Vision 2030, which is geared towards improving living conditions in Kenya and ensuring energy sustainability. The aim of the policy is transforming the country to an industrialised middle income economy with a high quality of life, and a clean and secure environment.

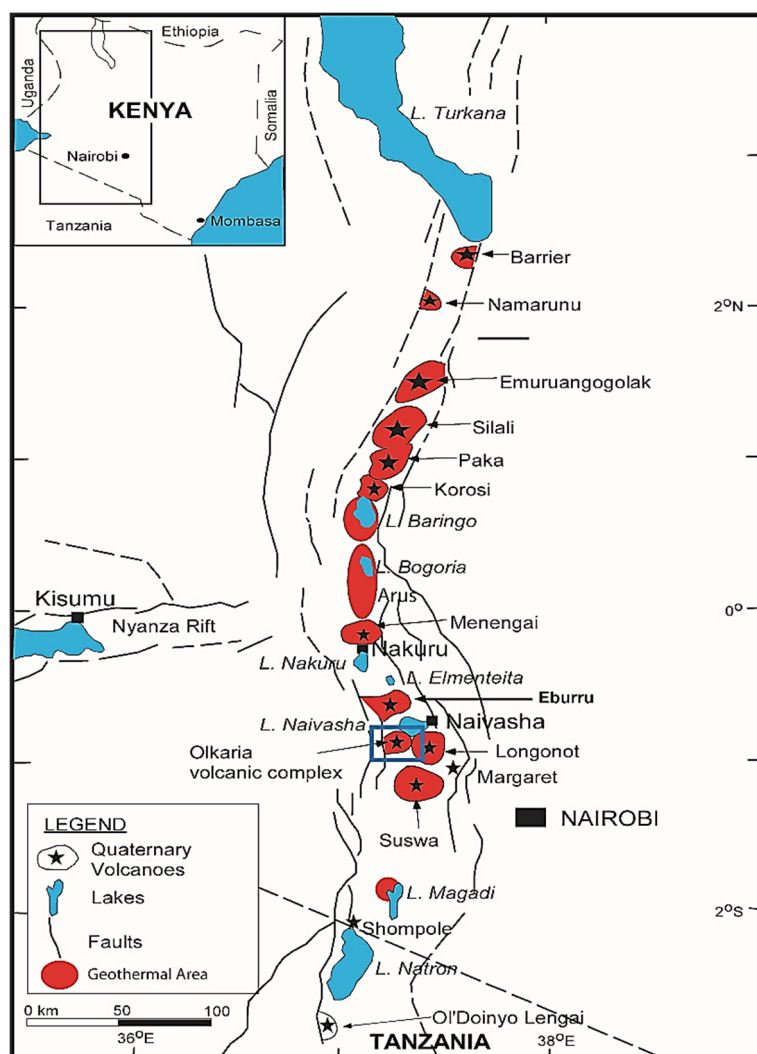


FIGURE 1: Geothermal sites along the Kenyan rift

One key pillar of the strategy is growth in electricity generation, especially from geothermal power. The government is ensuring the injection of 5000+ MWe power by 2018. This is a plan to inject an energy mix of about 5000 MWe, mostly green energy, through enhancement of various forms of energy while exploiting the current resources in the country. Prominent on this plan is the exploitation of geothermal energy and it is expected that 1,746 MWe will be injected by 2018. The plan has resulted in fast-tracking implementation of power projects in the country to ensure the attainment of this ambitious plan. Under this plan, 280 MWe was added into the grid in 2015 from Olkaria I Unit 4 & 5 and Olkaria IV projects. The government has been in the forefront to encourage the development of geothermal power for electricity generation and direct use. Favourable legislations and policies supporting geothermal development are amongst the initiatives made to ensure achievement of the plan. The government has also encouraged the involvement of Independent Power Producers (IPPs) to invest in the sector.

1.2 Management of geothermal projects

Geothermal projects are capital intensive and require keen management to ensure appropriate dispensation of resources and efficient management of time for the intended results to be attained. This creates the need to have proper mechanisms of planning, monitoring and evaluation. A good monitoring and evaluation framework ensures that the project intended goals and objectives are met, while ensuring at the same time learning opportunity, traceability and that decision making is done with good and reliable information.

The Monitoring and Evaluation framework (M&E framework) described in this work seeks to address how geothermal projects can be evaluated/monitored at the Olkaria Geothermal field and serves as a link between the resource and products. It provides the basis for evaluation and decision-making and links all processes inherent in geothermal utilisation and weighs the project risks. The framework depicts a reporting method through the use of dashboards. This gives highlights on the implementation and status of projects at a given time. The elements in the framework serve as a means of evaluation and project reporting in terms of:

- i. Economic viability and return on investment over a given period;
- ii. Giving clear indicators of areas of improvement in technology;
- iii. Defining the progress of plants and wells over a period of time;
- iv. Enabling management of resources earmarked for the different projects;
- v. Raising alarm on fields or areas that require monitoring.

2. DEVELOPMENT OF MONITORING AND EVALUATION SYSTEMS

Monitoring is the continuous analysis of information regarding implementation of a project with the aim of reaching set targets. It can be defined as the ongoing process through which stakeholders obtain regular feedback on progress made towards achieving goals and objectives (UNDP, 2009). It entails reviewing progress made in implementing actions or activities against goals.

Evaluation is the assessment of either completed or ongoing activities to determine the extent to which they are achieving stated objectives and contributing to decision making (UNDP, 2009). Evaluation involves analysis of projects with the aim of establishing fulfilment of objectives, efficiency, effectiveness impact and sustainability (OECD, 2009). The benefits of project evaluation include:

- Providing feedback on the project performance;
- Measuring failure or success with regard to set goals and objectives;
- Establishing a learning platform through documented experience.

A monitoring and evaluation framework is a guide to manage projects during implementation. According to the Project Management Body of Knowledge (PM BOK) this could be equated to the project monitoring and control phase, which is defined as the process of comparing project progress against the planned progress. The process is replicated throughout the project life cycle.

Various approaches of developing M&E frameworks have been established. A critical element in their development is the use of mixed methods. Mixed methods involve the use of both quantitative and qualitative data for evaluation of attributes influencing the project. This eventually gives real-time feedback on implementation and on how well a project worked (Bamberger et.al, 2010).

Development of M&E frameworks have been within the public sector management systems where accountability, performance feedback and impact assessment is critical (Hailey and Sorgenfrei, 2004). M&E frameworks have been continuously developed within public sector management systems. The evolution of management systems has taken place over a period of time. In the 1960s emphasis was put on financial and cost accounting through the Planning, Programming and Budgeting Systems (PPBS) while Programme Management by activities emphasised schedule management in the 1970s. Later, there was the development of Management by Objectives and Logical Framework Approach which introduced setting of objectives and identification of performance indicators (Meier, 2003). Commonly adopted strategies, results-based management, managing for development results and the log frame approach are discussed.

2.1 Results-based management (RBM)

RBM is a management strategy based on the use of results oriented tools aimed at improving performance (Meier, 2003). RBM targets to track progress and performance with the goal of demonstrating outcome and impact. It places emphasis on outcomes and impacts as opposed to inputs and outputs (Kusek and Rist, 2004). It was one of the principles adopted during a series of UN conferences for developing countries in the 1990s. During the conferences, various development priorities such as: education and environment, social development and women rights were discussed and

targets for development set. In 2000, the Millennium Development Goals (MDGs) were adopted during the United Nations Millennium Summit. The developing countries were encouraged to adopt RBM as a means of promoting good governance and results oriented public sector management (Meier, 2003).

As portrayed in the RBM life-cycle, Figure 2, the strategy ensures that all contribution to a project is geared towards the achievement of set results. According to the RBM Handbook by UNDG (2011) monitoring involves regular and systematic assessment based on actual performance and regular reporting. Monitoring results in RBM is a process that commences from the planning stage where a results framework and theory of change (toc) are developed. The results framework can be in the form of a matrix with targets, baselines and verification terms set. During the implementation stage monitoring and evaluation provides information for decision making and platform for documentation of lessons learnt.

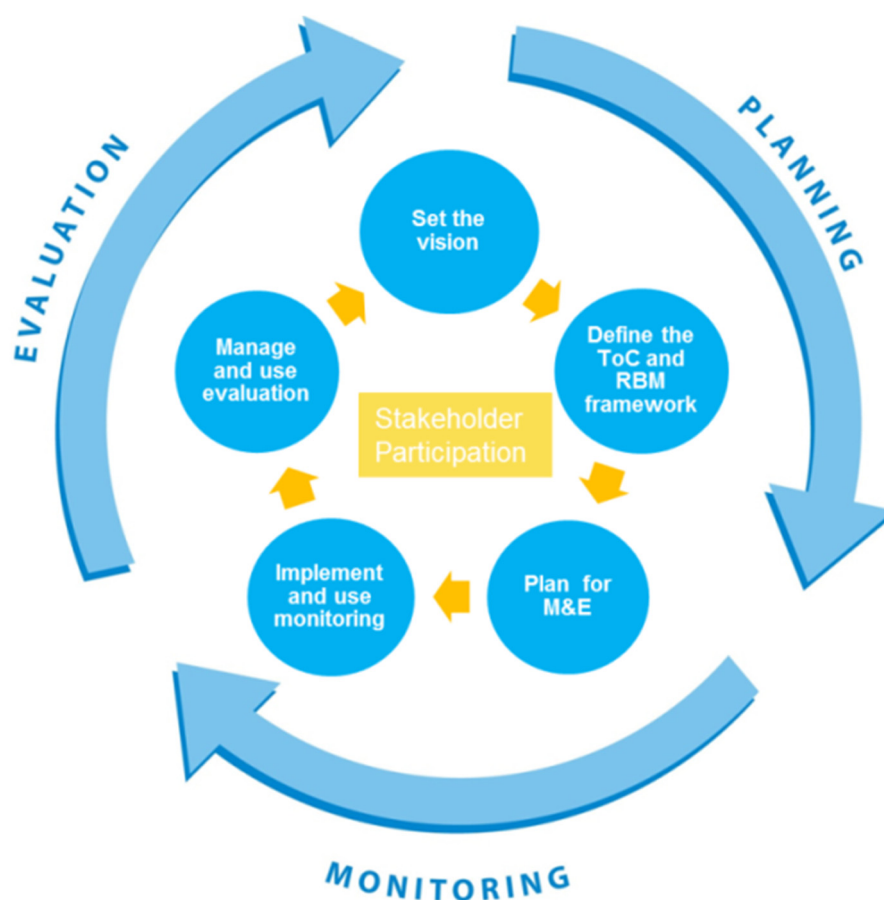


FIGURE 2: RBM life-cycle (UNDG, 2011)

In RBM, evaluation is defined as systematic assessment of a project, strategy or policy, focusing on accomplishments while examining results (UNEG, 2005). Evaluation in this context has three functions as defined in the RBM Handbook (UNDG, 2011); programme improvement, accountability and organisational learning. Key principles defined for RBM according to RBM Handbook are: accountability, ownership and inclusiveness.

2.2 Managing for development results

Managing for Development Results (MfDR) focuses on development performance and on sustainable improvement. It provides a framework for development efficiency in which performance information is used to improve decision making (OECD, 2009). The MfDR concept is based on effective global

development through enhancing ownership, aligning assistance with priorities, harmonizing agencies, policies and procedures, focusing on achievement of development outcomes. The principles of MfDR are (MfDR, 2015):

- Focusing on results at all phases of the development process;
- Aligning programming, monitoring and evaluation with results;
- Keeping measurement and reporting simple;
- Managing for achievement of results;
- Using results information for learning and decision making.

MfDR is commonly used by national governments and development agencies to measure effectiveness of projects relating to poverty reduction and economic sustainability. It is based on four main features: shared goals and strategies, performance-based budgets, evidence-based decision making and public accountability. For success of MfDR, there is a need for credible data and procedures to enhance development of performance monitoring and evaluation systems.

2.3 Logical frame approach

The LFA has been used as a project appraisal document by the World Bank. It was created in 1969 for the U.S Agency for International Development. It has been used for design, implementation, monitoring and evaluation (Team Technologies, 2005). The Logical Framework Approach (LFA) is an objective-oriented instrument for project management.

LFA is used to develop the design, improve implementation, monitor and evaluate projects. It is an engaging instrument used for problem identification, setting priorities, planning and implementing projects, follow up and evaluating progress. (Örtengren, 2003). The LFA tool (Logframe) is developed as a matrix (Table 1) which is interrelated with changes in one item resulting in changes in another.

TABLE 1: Structure of LogFrame matrix (EuropeAid, 2004)

Project description	Indicators	Source of verification	Assumptions
Overall objective – The project's contribution to policy or programme objectives (impact)	How the OO is to be measured including quantity, quality, time.	How will the information be collected, when and by whom	
Purpose – Direct benefits to the target group(s)	How the purpose is to be measured incl. quantity, quality, time.	As above	If the purpose is achieved, what assumptions must hold true to achieve the OO
Results – Tangible products or services delivered by the project	How the results are to be measured incl. quantity, quality, time.	As above	If results are achieved, what assumptions must hold true to achieve the Purpose
Activities – Tasks that have to be undertaken to deliver the desired results			If activities are completed, what assumptions must hold true to deliver the results

The first column in the matrix describes the project; the strategy or goal, impact and deliverables or output. The indicators column outlines the performance indicators and target for the levels while the third column gives the sources of data during implementation either reporting or effects of an activity.

The fourth column describes the conditions for project success i.e. the assumptions and risks are outline in the fourth column.

The process of development of the logframe is a two-stage process that involves:

- i. The first stage is the analysis. This involves stakeholder analysis, problems, objectives and strategy analysis. This process requires constant review and is refined throughout the project.
- ii. The second stage is the planning which involves the practical operation of the plan. The project structure is developed, activities and resource scheduling is also done.

A major problem with implementation of the LFA is that the process should be done prior to project documents preparation and requires stakeholder participation.

2.4 Dashboard development

The process of reporting for M&E frameworks can be inherent in the tool that is used, however there is a shift in reporting methods to dashboard reporting. Dashboard reporting involves the summing and integration of key performance indicators to communicate performance (Wind, 2005). Dashboards have been defined as a collection of interconnected key performance metrics and underlying performance drivers that reflect both short and long-term interests to be viewed in common throughout the organization (Pauwels et al., 2009). Dashboards are visual and attuned to give specific and precise information on a subject.

3. GEOTHERMAL PROJECT IMPLEMENTATION – MANAGEMENT OVERVIEW

Geothermal projects take the course of a project cycle; initiation, planning, execution and closing. However, at each stage of development one or more process groups may be part of the phase. The phases are as classified in Table 2 and nine key steps outlined:

TABLE 2: Phases of geothermal development (Ngugi, 2008)

Resource exploration	Resource assessment	Power plant construction	Operations
Review of existing information Detailed surface exploration Exploration drilling	Appraisal drilling Feasibility study and Environmental Assessment	Production drilling Power plant design and construction	Reservoir & steam field management Power plant operations

- i. *Resource exploration* entails review of existing data on the field from previous studies as well as geological and geophysical mapping and geochemical sampling of the area. It also involves exploratory drilling to confirm availability of a resource.
- ii. *Resource assessment*: involves appraisal drilling which helps in approximating the size of the resource, approximate the cost of production and ascertain chemical composition of the geothermal fluid. A feasibility study of the project is done to verify the viability of the project, environmental impact and power plant technologies available.
- iii. *Power plant construction*
 - a. Production drilling focuses on provision of sufficient steam for the sized plant;
 - b. Power plant construction entails, design, construction of the steam gathering system, the power plant and the electrical substation and transmission lines.

iv. *Operations*

- a. Reservoir management involves monitoring the steam field to ensure that steam quality to the plant is maintained and drilling for make-up wells due to drawdown;
- b. Operations and maintenance of the power plant to ensure continuous power generation.

3.1 Profile of the Olkaria I Unit 6 project

Olkaria I Unit 6 is on the east side of the Olkaria field. The plant is an additional unit to the first geothermal plant in Kenya, Olkaria I containing three 15 MWe units. The plant was commissioned between 1981 and 1985 and is due for upgrade. In 2015, additional units 4 and 5 were commissioned, each 70 MWe. The new unit (unit 6) is expected to be commissioned in December 2018. Through the development of the framework and reporting, dashboard performance indicators and measures are established at various stages of development. Economic and cost analysis is done and a visual reporting mechanism generated.

3.2 Initiation and project planning

The concept of the project as discussed in the previous chapter is based on the country's geothermal growth strategy. This forms the basis of development of the geothermal expansion programme and the execution plan. Development of Olkaria I unit 6 was incorporated as part of the projects in the Olkaria geothermal programme. The steps in the planning process are described as:

- i. *Review of existing information:* Throughout the development of a geothermal field it is a practice to study the subsurface and gain information on the resource. Continued drilling in the field gives more information on the extent and the characteristics of the field. Conceptual and numerical models give information on the resource extent, the characteristics and estimate the energy content and capacity. This phase gives the basis for developing planning inputs. The Olkaria field has been studied over the years and currently the conceptual and numerical models are being updated.
- ii. *Master programme* defines the planned projects, the expected commissioning dates and the number of wells to be drilled for both production and re-injection based on optimisation studies carried out for the field. The number of production wells depends on the planning assumptions developed from studies on the field:
 - a. Average expected output for each production well in the field is 5 MWe
 - b. Two hot re-injection wells are required for every 35 MWe. Cold and shallow re-injection wells depend on brine productivity in the field.
- iii. *The drilling programme* outlines resources (drilling rigs) and a drilling schedule with tentative dates for the entire drilling process, including procurement/contracting, rig mobilisation and move, actual drilling periods and well testing. Different resource optimisation scenarios are developed with time and cost as major factors for consideration.
The wells for the project were drilled and managed through various drilling contracts, run consecutively, as well as with the company owned rigs. The average depth of the existing holes in the field is about 3000 m. The master plan and the programme are defined in Table 3.
- iv. *Profitability models* are developed at the onset of a project. They form part of the economic analysis and provide an overview of project performance in terms of return on investment. The models assist in deciding whether a project is worthwhile and the best means of financing the project. The profitability model for the Olkaria I unit 6 is based on an Excel model by Páll Jensson (2016). It defines the expected cost of development and expected return on operation. The model includes drilling, power plant construction and operational costs. Assumptions made include that the cost of drilling is distributed within 2014 and 2015, thirty years of operation from 2019 and that costs associated with taxes and depreciation are accounted for based on Kenyan laws. The model predicts that the project will be profitable within the time frame with a net present value of 8.2 of total capital and 10% internal rate of return.

TABLE 3: Project master plan and resource allocation

Olkaria I unit 6	Number of wells required	2009/10	2010/12	2011/12	2012/13	2013/14	2014/15	2015/16
Planned	25			9	9	7		comm
Actual	28	1	1	4	4	11	7	
Number of rigs required		1	1	3	3	3	2	
Rig allocation	Rig-1		1	1	0	4	0	
	Rig-2	1		0	3	3	3	
	Rig-3			3	1	4	4	
	Total	1	1	4	4	11	7	

Resource allocation								Total per rig
Estimated cost per Rig/Year (MUSD)	Rig-1	0	4.5	4.5	0	18	0	27
	Rig-2	5.52	0	0	16.56	16.56	16.56	55.2
	Rig-3	0	0	10.56	3.52	14.08	14.08	42.24
	Total per year	5.52	4.5	15.06	20.08	48.64	30.64	124.44

The model can be used in comparison with the actual performance of the plant once it starts operating for readjustment on financial position of the company. Figure 3 shows the net present value of the project equity by 2017 and of total investment 2042.

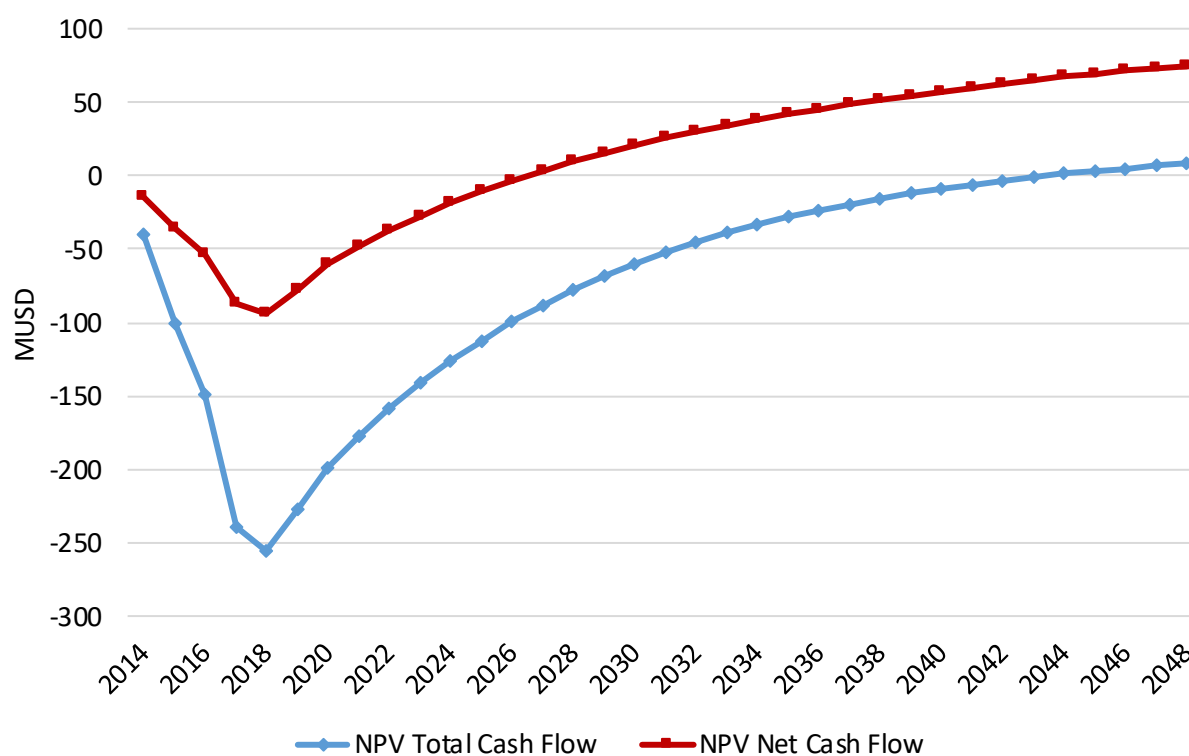


FIGURE 3: Accumulated net present value

3.3 Execution

3.3.1 Phase definition – drilling

The process of drilling can be divided into three phases (Kipsang, 2013): the pre-spud phase, the drilling phase and the completion phase, Figure 4.

- i. *Pre-spud*. The pre-spud phase mainly entails well siting (identification of the preferred location of the wells), review of the drilling programme and development of infrastructural works plan. The well design, infrastructural works, such as roads, waterlines and cellar, and rig mobilisation is done. Figure 4 depicts all the phases in the development of geothermal.
- ii. *Drilling* process involves getting to target depth with the design of the well that has been approved. A drilling schedule gives progress of overall drilling in terms of schedule and cost. This includes: delays, critical path and effects on the entire project completion and cost indices. Drilling software enhances the drilling process through data collection during the drilling period. The software can be used for materials management, control of directional drilling and obtaining geological data on the well profile.
- iii. *Completion*. This involves completion and discharge testing. Completion tests take about 2-3 days and consist of running water loss surveys, injectivity tests and transient pressure tests to confirm the results of drilling. Discharge tests take about 2-3 months depending on the characteristics of the well and persist until the equilibrium of the well is attained. During the test, steam/water flow, pressure, temperature and chemical content of the well are measured and analysed.

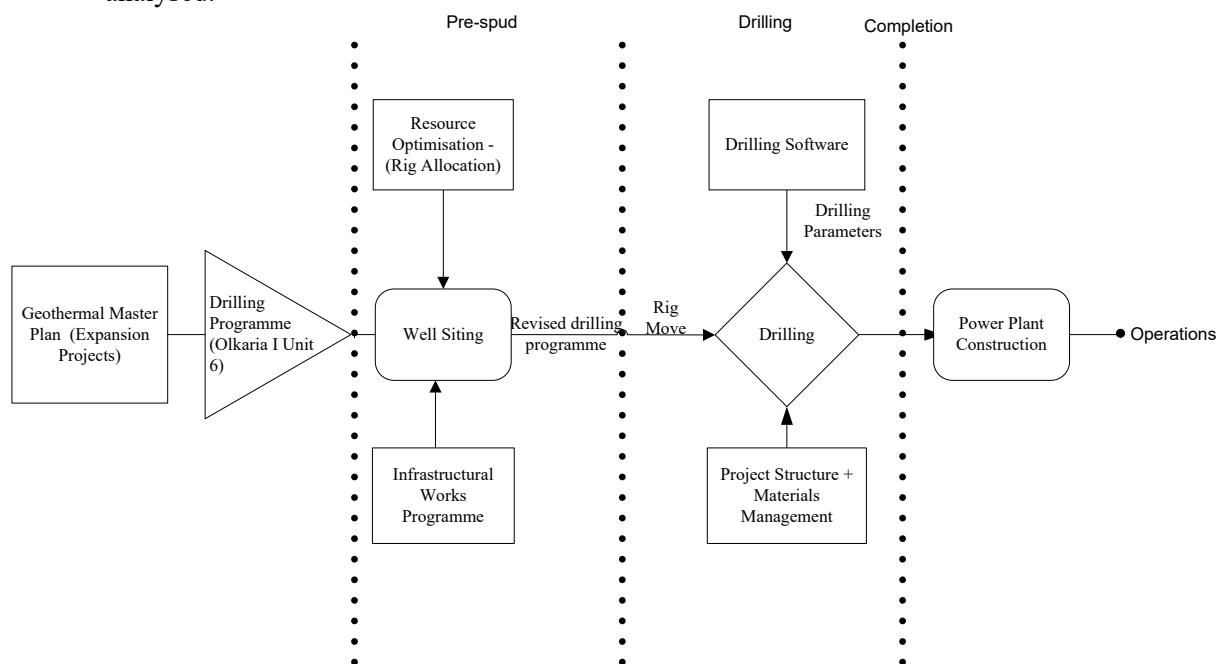


FIGURE 4: Geothermal development phases

3.3.2 Time and scope management

Time and scope management can be managed in a similar way as described below. The scenario described depicts the power plant construction phase. The construction phase of a geothermal power plant comprises the design, construction, installation and commissioning. These phases involve a large scope of various works, commonly managed through EPC (Engineering, Procurement and Construction) contracts. EPC contracts have been used in KenGen's previous geothermal projects in Kenya, such as Olkaria IV and Olkaria I units 4 & 5. The contracts are based on dividing the works into sizable lots,

award them to different contractors and manage them through a consultant. Some of the methods used are:

- i. *Decomposition technique*, this is the breaking down of the project to manageable parts based on the project. WBS system is integrated in the scope, time and cost management. Figure 5 depicts a level 1 schedule for the power plant construction. The breakdown shows major activities of individual contracts for:
 1. Construction of steam gathering system;
 2. Construction of power plant;
 3. Construction of switch yard and transmission line.
- ii. *The Critical Path Method* estimates the longest path of planned activities to the end of a project and reflects the shortest time to complete a project. Delays on activities on the critical path directly impact the planned project completion date. The method analyses the earliest and latest dates that each activity can start and finish without affecting the overall progress of the project. Critical activities within the project are highlighted in Figure 5. This shows areas where flexibility in scheduling can be exercised.

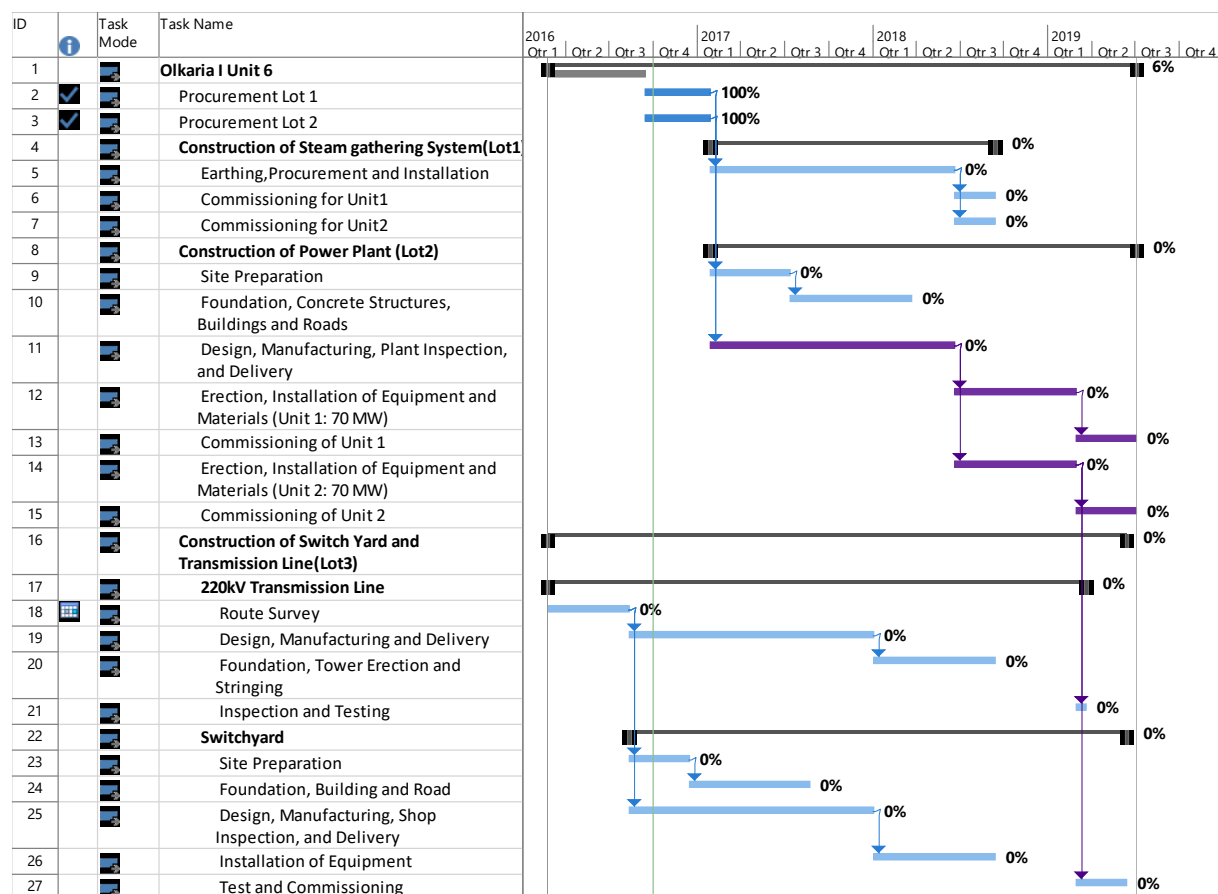


FIGURE 5: High level power plant construction project schedule

3.3.3 Cost management:

Cost management varies within the project with regard to the stage of development. Below is the means of cost management during implementation and analysis after implementation.

- i. *Earned Value Management (EVM)*
This is a method combining scope, schedule, and resource cost measurements to assess project performance and progress (PMI, 2013). Three dimensions of performance measure established are:

- a. *Planned Value*, or performance measurement baseline; this is the budget assigned to scheduled work either for an activity or to a specific WBS item. Total planned value for a project is referred to as budget at completion.
- b. *Earned Value*; this is the measure of progress of work performed based on the budget. It is the budget associated with work performed. (PMI, 2013). Progress measurements for each WBS enables a measurement of the overall progress of the work.
- c. *Actual Cost*; this is the cost incurred for work performed. It is related directly to actual work that has been performed.
- d. *Schedule Variance*: this is one of the indicators of performance. It gives progress of a project at a particular time expressed in terms of cost. It indicates progress that is behind or ahead of schedule.

$$SV = EV - PV$$

where SV = Schedule variance;
 EV = Earned value;
 PV = Planned value.

- e. *Cost Variance*: This is a cost measure of budget surplus or deficit at a given time.

$$CV = EV - AC$$

where AC = Actual cost.

The cost variance at the end of the project is the difference between the *Budget at Completion* (*BAC*) and the actual amount spent and indicates the relationship of physical performance to the cost.

Efficiency indicators include the schedule performance index and the cost performance index. The *Schedule Performance Indicator* (*SPI*) is a measure of time efficiency. It is a ratio of earned value to planned value. $SPI < 1.0$ implies that less work was completed than was planned while $SPI > 1.0$ indicates that more work was completed than was planned.

$$SPI = EV/PV$$

where SPI = Schedule performance index.

Cost Performance Index (*CPI*) is a measure of the cost efficiency of budgeted resources.

$CPI < 1.0$ indicates cost overrun for work completed.

$CPI > 1.0$ indicates a cost underrun of performance

$$CPI = EV/AC$$

where CPI = Cost performance index.

The *EVM* analysis for the construction phase is depicted in Figure 6

ii. Cost Analysis

Cost analysis involves interpreting the results of the actual costs. The process gives a basis of future project costs. It also indicates areas of improvement in terms of higher efficiency where the costs are higher than anticipated. The cost of drilling for Olkaria I unit 6 is analysed in Figure 7. The cost analysis is based on the major activities during the drilling process and includes the cost of equipment hire. Similar analysis for power plant construction can be undertaken.

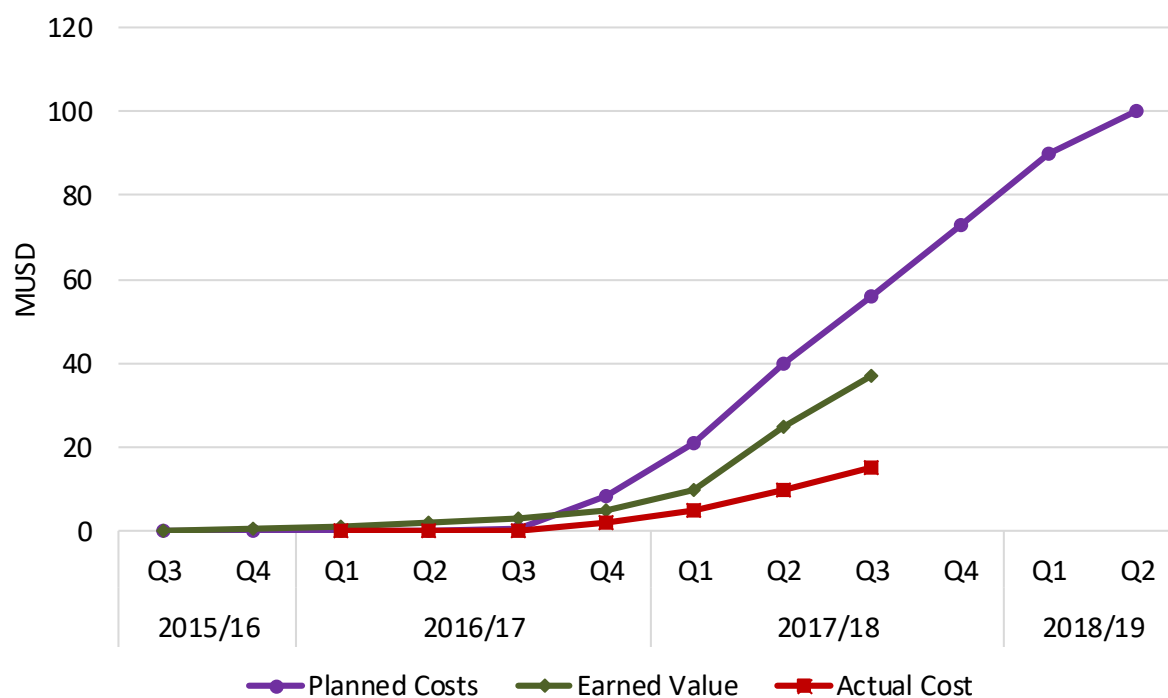


FIGURE 6: Assumed EVM analysis for Olkaria I unit 6 power plant construction

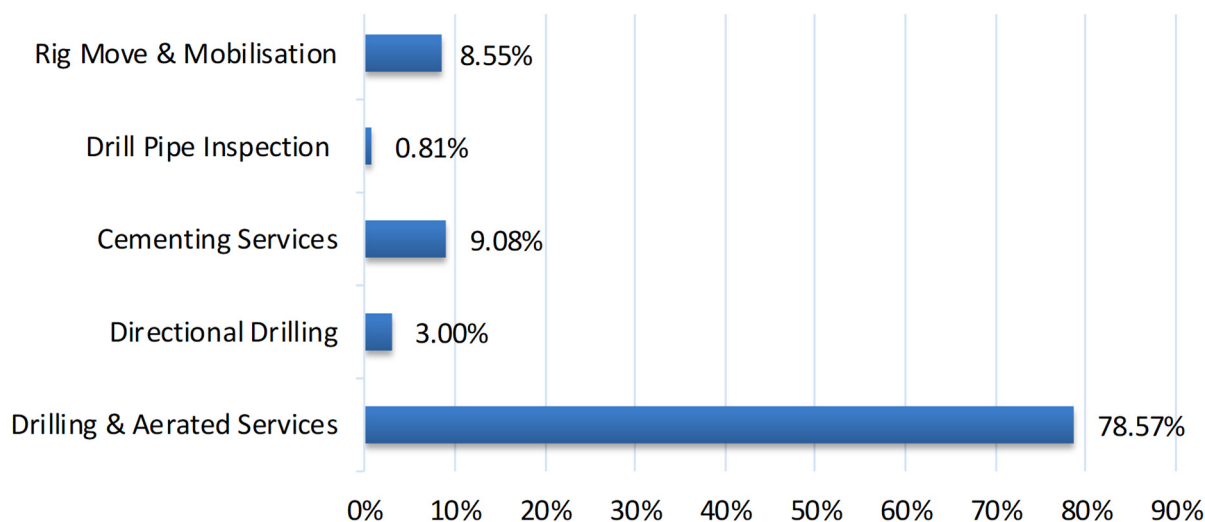


FIGURE 7: Drilling cost analysis

3.4 Reporting

Reporting for the analysed project indicators through a dashboard gives an overall overview of the project status and forecast. However, for the purpose of enhancing and providing adequate information on the project, various reports and reporting procedures are deemed important. Table 4 gives procedure and performance indicators that could be adapted for different phases of development.

TABLE 4: Reporting template

	Olkaria I unit 6 reporting	Unit of measure	Target	Reporting duration	Status	Notes
1	Drilling			Project duration		
	a. No. of wells drilled	No.	25		28	13 wells to be connected
	b. Success rate of drilling	%	100%		96.4%	Total depth: 3000 m
	c. Schedule progress	SPI	>1		1.05	
	d. Budget management	CPI	>1		0.62	
2	Power plant			Project duration		
	a. Timeliness	SPI	100%			Consultant hired
	b. Cost efficiency	CPI	100%			—
	c. Completion rate	%	100%			
	d. Delays	%	100%			
3	Operation Efficiency			Monthly		
	a. Availability	%	100%			Overhaul schedule
	b. Total units sent out	MWe	100%			Planned outages schedule
	c. Units used on works	MWe	100%			—
4	Reservoir management	MWe	85.2			
	a. Steam availability 84 MW			Project duration	85.2	
	b. Success rate		1.42	Project duration	75.6 MWe	3 wells WHP <5 Bar, 13 wells to be connected
	c. Reinjection strategy	Volume	T/hr	Bi-annual		No. of wells for reinjection
	d. Field performance			Bi-annual		Wellhead pressure and temperature
	e. Make-up connection	No.		Annual		Dependent on drawdown

4. GEOTHERMAL MANAGEMENT DASHBOARD

The consecutive dashboards highlight the different information that could be incorporated for complete reporting. The first part of the dashboard as in Figure 8 gives the planning parameters an extent to which the goals have been achieved. An overall success rate in reference to drilling is also given. This is with regard to expected depth of the wells drilled, that is 3000 m. In Olkaria I unit 6, one well was abandoned after an obstruction was encountered. The drilling project costs given are evaluated through EVM analysis, the activities in drilling and the time analysis for the twenty-eight wells drilled.

The second part of the dashboard gives details on the power plant construction, the wells to be connected to the plant giving a success rate of 1.42 since only 13 wells are to be used for the connection. Further evaluation is required to ascertain the success rate of both the East and Northeast fields, where the wells are located, individually. A depiction of the EVM analysis to be used during construction and the progress schedule is also shown, this, however, is based on invented data.

Various parameters will be monitored during operation of the plant. A graphical analysis of these has been developed. The dashboard gives a view of the phases of development and numbers used are assumed. The dashboard should give details at each stage of the geothermal project development/progress and may change according of information required.

PROJECT : Olkaria Unit 6

Capacity	70MWe
Wells	
Production Wells	17
Reinjection	
Hot	4
Cold	1
Shallow	3
Total	25
Assumptions	
1 Well	5MWe
20% Reserve	

a) Project Plan

Year	Total	2009/10	2010/11	2011/12	2012/13	2013/14	2014/15
Planned Wells	25	0	02	9	93	7	Commissioning
Actual Wells	28	1	1	4	4	11	7
Phugged	1		1				

Drilling Success Rate 96%

RAG STATUS

Red Not Acceptable

Amber Moderate

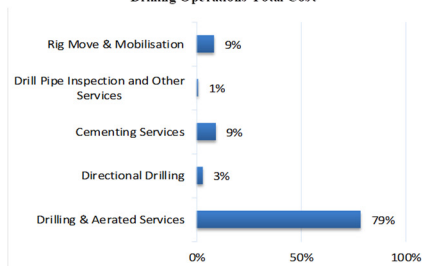
Green Acceptable

b) Drilling

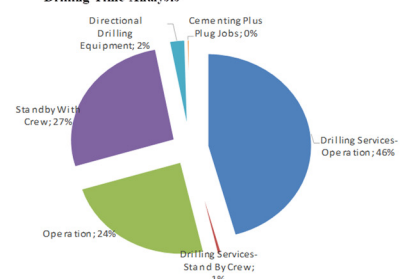
Project Cost

Budgeted Cost of the Project	USD 155.75
Actual Cost of Work Performed	USD 143.63
Budgeted Cost of Work Spent	USD 84.83
Budgeted Cost of Work Planned	USD 89.19
Cost Variance	-54.44
Cost Performance Index(CPI)	0.62

Drilling Operations Total Cost



Drilling Time Analysis

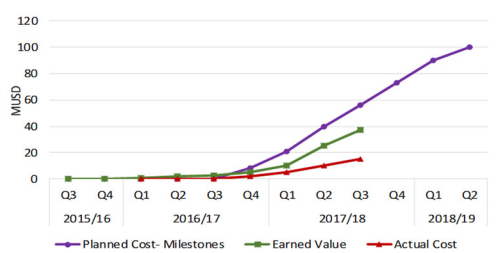


c) Plant Design

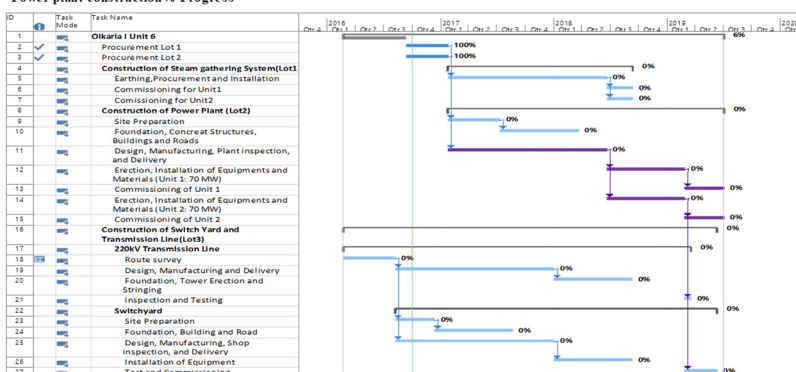
	No.	Capacity
Wells for Production	12	85.2
Wells for Re-injection	1	
Field Success Rate		142%

d) Power Plant Construction

Schedule and Scope Management



Power plant construction% Progress



e) Operation

Power Plant Assumed Parameters

Months	Jan	Feb	Mar	Apr	May	Jun	Jul
Sent Out Units	68	60	70	70	65,000	65,000	
Used Units on Work	3.29	3.27	3.69	3.43	3.35	3.00	2.52
Availability	97.14%	85.71%	100.00%	100.00%	92.86%	92.86%	

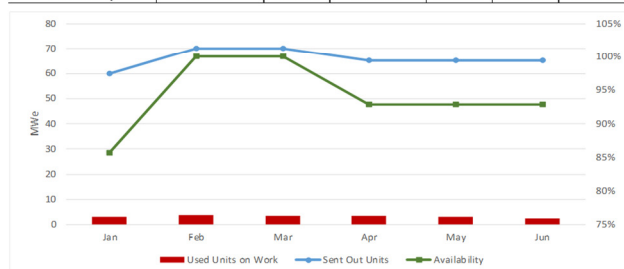


FIGURE 8: Dashboard

5. CONCLUSIONS

Olkaria I unit 6 framework is a model of how geothermal projects can be developed and managed through the different project phases. A combination of management tools has been utilised to give a comprehensive and flexible framework. The framework can be used for geothermal projects and has reporting parameters that are observed within the geothermal development and operation lifecycle.

The paper mainly presents management of scope, time and cost in the project, nevertheless details pertaining risk and quality amongst others can be incorporated into the dashboard. Qualitative measures can be developed to have these areas also represented. The reporting template defines some of the performance indicators that can be measured during and after project completion. The dashboards can be modified to give different information with regard to the process or the stage of development.

Reporting can be enhanced through the use of business objects to give live data. This requires integration of systems used within the organisation for automatic updates. Materials management, drilling software and financial and schedule management software can be integrated to feed and provide data. It is also essential to have properly managed databases that can be queried to provide the different information required for the reporting.

ACKNOWLEDGEMENTS

My sincere appreciation goes to my supervisor, Dr. Thröstur Gudmundsson, for his guidance and sharing his valuable knowledge. I express gratitude to the United Nations University, Geothermal Training Programme (UNU-GTP), under the leadership of Director, Mr. Lúdvík S. Georgsson, for offering me the chance to take part in the 2016 UNU-GTP Fellowship. Many thanks go to Mr. Ingimar Haraldsson, Ms. Málfríður Ómarsdóttir, Mr. Markús A. G. Wilde and Ms. Thórhildur Ísberg for their assistance during my stay in Iceland.

I acknowledge my employer, KenGen, for granting the sponsorship and opportunity to be part of this training. I am grateful to my family and friends, my mother Jane and sister Gladys for their support and encouragement.

I thank the Almighty for His divine favour and blessings and for making all things possible.

REFERENCES

Bamberger, M., Rao, V., and Woolcock, M, 2010: *Using mixed methods in monitoring and evaluation: experiences from international development*. World Bank, Policy research working paper No. 5245, webpage: www-wds.worldbank.org/servlet/WDSCContentServer/WDSP/IB/2010/03/23/000158349_20100323100628/Rendered/PDF/WPS5245.pdf.

EuropeAid 2004: *Aid delivery methods, vol. 1, Project cycle management guidelines*. European Commission.

Hailey, J., and Sorgenfrei, M., 2004: *Measuring success: Issues in performance measurement*. INTRAC, Occasional Papers Series No. 44, 34 pp.

Jensson, P., 2016: *A model for profitability assessment*. UNU-GTP, Iceland, unpubl. lecture notes, 18 pp.

Kipsang, C., 2013: Cost model for geothermal wells. Report 11 in: *Geothermal training in Iceland 2013*. UNU-GTP, Iceland, 177-199.

Kusek, J.Z., and Rist, R.C., 2004: *A handbook for development practitioners: Ten steps to a results-based monitoring and evaluation system*. World Bank, Washington, DC, USA, 268 pp.

Meier, W., 2003: *Results-based management: Towards a common understanding among development cooperation agencies*. Results-Based Management Group, prepared for the Canadian International Development Agency, 26 pp.

MfDR, 2015: *Managing for Development Results*, webpage: www.mfdr.org.

MoEP, 2015: *Draft national energy and petroleum policy*. Ministry of Energy and Petroleum, Energy Regulatory Commission, Nairobi, Kenya, 130 pp.

Ngugi P.K., 2008: Planning of geothermal projects in Kenya. *Paper presented at, Short Course III for Exploration for Geothermal Resources, organized by UNU-GTP and KenGen, Lake Naivasha, Kenya*. UNU-GTP, SC-6, 20 pp.

OECD, 2009: *Management for development results*. Organisation for Economic Co-operation and Development, Observer, webpage: www.oecd.org/.

Örtengren, K., 2003: *A summary of the theory behind the LFA method: The logical framework approach*. SIDA, Sweden, website: www.sida.se/publications.

Pauwels, K., Ambler, T., Clark, B.H., Lapointe, P., Reibsteind, D., Skiera, B., Wierenga, B., and Wiesel, T., 2009: Dashboards as a service: why, what, how, and what research is needed? *J. Service Research*, 12-2, 175-189.

PMI, 2013: *A guide to the project management body of knowledge* (5th ed.). Project Management Institute, publication, 217 pp.

Team Technologies, 2005: *The log frame handbook: A logical framework approach to project cycle management*. World Bank, report, 113 pp, website: documents.worldbank.org/.

UNDP, 2009: *Handbook on planning, monitoring and evaluating for development results*. UNDP, publication, 232 pp, webpage: www.undp.org/eo/handbook/.

UNDG, 2011: *Results-based management handbook*. United Nations Development Group, publication, 68 pp, webpage: www.ilo.org/global/.

UNEG, 2005: *Norms for evaluation in the UN system*. United Nations Evaluation Group, publ., 11 pp.

Wind, Y., 2005: Marketing as an engine of business growth: A cross-functional perspective. *J. Business Research*, 58-7, 863-873.

APPENDIX I: Financial model parameters

TABLE 1: Investment

Assumptions and results		Discounting rate (MARR)				10%				Planning horizon				35	Years
Assumptions:		2014	2015	2016	2017	2018	2019	2020	2021	2022	2023	2024			
Investment:															
	MUSD														
Buildings		39.60	59.40	47.64	95.29	15.88									
Equipment	100%		8.15	9.28	20.38	5.21									
Other				0.73	4.38	2.19									
Total investment		39.60	67.55	57.66	120.05	23.28	0.00	0.00	0.00	0.00	0.00	0.00	0.00	0.00	0.00
Financing:															
Working capital (Inv from Op)		0.67	1.33	3.33	4.96	8.37									
Total financing		40.27	68.88	60.98	125.01	31.65	0.00	0.00	0.00	0.00	0.00	0.00	0.00	0.00	0.00
Equity	100%	0.35													
Loan repayments	100%	20.00	years												
Loan interest	100%	0.04													
Operations:		2014	2015	2016	2017	2018	2019	2020	2021	2022	2023	2024			
Sales quantity	1.000														
Sales price	100%														
Variable cost	100%														
Fixed cost	100%	0.04	MUSD/MWh												
Inventory build-up (MUSD)		0.235	MUSD/MWh												
		0.000		0.000		0.000									
Other assumptions:															
Debtors	8.33%	of turnover													
Creditors	8.33%	of variable cost													
Dividend	0%	of profit													
Income tax	30.00%	of taxable profit													
Depreciation buildings	4.00%														
Depreciation equipment	6.70%														
Depreciation other	6.70%														
Loan management fee	1.00%														

Main Results:			
NPV of cash flow		Total Cap.	Equity
Internal rate		8.22	74.35
Internal value of shares after 10 years		10%	16%
			2.74

APPENDIX II: Drilling dashboard

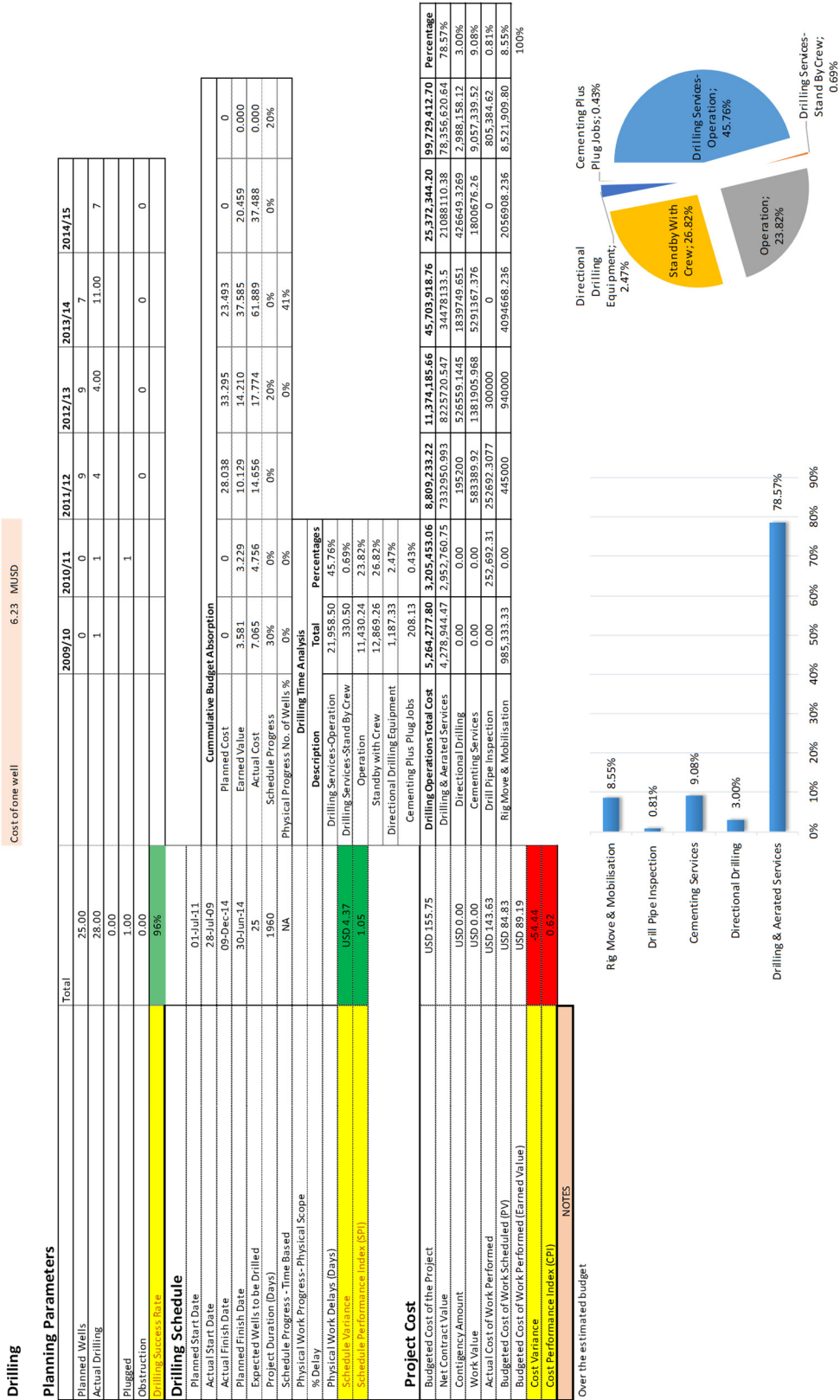


FIGURE 1: Drilling dashboard



UNITED NATIONS
UNIVERSITY

UNU-GTP

Geothermal Training Programme

Orkustofnun, Grensasvegur 9,
IS-108 Reykjavik, Iceland

Reports 2016
Number 29

THE BASIS FOR WELL DESIGN AND DRILLING PROGRAMME FOR GEOTHERMAL EXPLORATION IN KINIGI, RWANDA

Theoneste Nzayisenga

Rwanda Energy Group/Energy Development Corporation, Ltd.
EDCL KCT, 10th Floor KN 2 ST,
Nyarugenge District, P.O. Box 3855 Kigali
RWANDA

tnzayisenga@edcl.reg.rw, nzayitheo@gmail.com

ABSTRACT

The western branch of the East African Rift System is expected to flourish in geothermal resources as it is the case on the eastern branch. However, unlike the eastern branch, these resources are not yet developed. Even though exploration has been undertaken recently in countries like Rwanda and Uganda several setbacks were encountered and the worst was the deep exploration drilling in Karisimbi, Rwanda in 2013-2014. An intensive geoscientific exploration process is being performed and ultimately drilling will be carried out and therefore, a drilling programme specific to the area needs to be prepared. The African Union has provided the code of practice, the African Union Code of Practice for Geothermal Drilling, to guide engineers in the design of drilling programmes and this report is about the basis of the design of the casing programme, the cementing programme and the mud programme for future Kinigi exploration drilling. The casing programme is made up of 3 cemented strings of casings, namely: surface casing (100 m), anchor casing (450 m) and production casing (1230 m). A slotted liner is hung from the production casing from 1200 m depth down to the bottom at 3000 m. The choice for the design of the 3000 m deep well at Kinigi is based on minimum design factors and possible worst load scenarios.

Drilling fluids play a key role for the success of the drilling process, and well cleaning together with well stability are top considerations. Poor selection of drilling fluids either in quality or in quantity may result in well collapse, a stuck drill string or worse. While designing the drilling fluids programme for exploration wells in Kinigi, a number of factors has to be considered including the formation pressure, temperature, and expected loss zones in the well. Apart from those technical consideration, the cost also must be considered because some fluids e.g. the air drilling package required for pressure balance drilling with aerated drilling fluids is expensive. The design for the cementing programme focused mainly on the estimated volume of cement slurry necessary for the annular volume to be cemented plus the excess of 150%. Therefore, the estimated volume of the slurry is 180 m³ per well and considering the planned density of the slurry of 1.87 kg/l, the amount of dry cement required for each well is estimated at 250 tonnes. The success of getting a sound cement around the casing at the end of the cementing process was the priority and the inner string cementing method was chosen. The slurry pumping and displacement time also were explored and the calculated pumping time is less than 3 hours per well.

1. INTRODUCTION

The western branch of east African rift system is expected to flourish in geothermal resources as it is the case on eastern branch. However, unlike the eastern branch, these resources have not yet been developed, even though exploration drilling has been attempted recently in countries like Rwanda and Uganda. Several setbacks were encountered and the worst was the deep exploration drilling in Karisimbi, Rwanda in 2013-2014.

The eastern branch of the Africa rift system is being exploited successfully with Kenya putting on grid hundreds of MWe from successfully drilled wells and Ethiopia having built its first pilot plant. As geological conditions have been shown to be different on the western branch, it is necessary to anticipate the conditions and produce a drilling programme suitable for drilling of exploration wells in that area. The main aim of this work is a contribution to the establishment of a drilling programme specifically designed according to the conditions and lithology of the area based on the available data.

Geothermal exploration in Rwanda started in 1982 and continued during the following years until 2008 when conclusions of the various studies were indicating a geothermal system with temperatures over 200°C in the Karisimbi volcano, and 150-200°C near Lake Karago with a heat source at about 5 km depth. All surveys indicated that the drilling at Karisimbi would intersect a hot reservoir which turned out to be the opposite, unfortunately. Nevertheless, results related to the lithology of the area will be pursued in this work while calculating basic formulations and designs for a drilling programme for the Kinigi area which is to the east of Karisimbi.

Kinigi geothermal area is not chosen randomly, instead it was ranked as the best prospect by a new complementary survey prepared for Rwanda Energy Group (REG) by the Japan International Cooperation Agency (JICA) in March 2016. Furthermore, the Geothermal Risk Mitigation Facility (GRMF) sanctioned an award to the exploration drilling proposal which was prepared and submitted by the Rwandan Energy Development Corporation which is in charge of exploration and development of geothermal resources. In 2015, JICA prepared a geothermal master plan in which they ranked Kinigi as the most promising area among other prospects in Rwanda, with potential energy close to 60 MWe at the confidence level of 50%.

This United Nations University – Geothermal Training Programme (UNU-GTP) document will focus specifically on the Kinigi area but it can be adapted and used in the region of the western branch of the Africa rift system as well. Basically, drilling programmes are documents subject to modifications once firm data is obtained to replace earlier assumptions made before wells were drilled and to address new challenges encountered in the field.

In the Kinigi area, the heat source is expected to be at 5 km depth (JICA, 2014), therefore, it is necessary to drill exploration wells up to 3 km deep in order to prove the existence or absence of the resource. A target depth of 3000 m will guide the choice of the rig, the materials to be used as well as the parameters to be used throughout the drilling process. The wells will be drilled in 4 sections; namely surface casing, anchor casing, production casing and the production section with a slotted liner. The first three sections are cased and cemented back to the surface while the last one is open and allows the geothermal fluid to flow in the well to the surface. The depth for every section is determined by a number of factors including: well safety, environmental protection, and eventually, success of production and well testing. This document will summarise all basic calculations which govern the design of the drilling programme and associated programmes including the mud programme, cementing programme, casing programme etc. The aim of this paper is to have a good understanding of design calculations as part of selecting a casing programme and preparation of the drilling programme document, and to know how changes may affect the whole process and especially the success and/or the cost of the well drilling.

2. BACKGROUND OF GEOTHERMAL EXPLORATION IN RWANDA

2.1 Methods used for geothermal exploration in Rwanda

For geothermal resource development, exploration is a compulsory step. Different methods are used for the exploration process including geoscientific methods like geology, geochemistry, geophysics, drilling etc. Like elsewhere in the world, geothermal resource exploration in Rwanda went through all procedures and steps since the launching of the survey series initiated by BRGM (French Bureau of Geology and Mines) in 1982.

That survey included a geochemical reconnaissance survey at different sites like Mashyuza (Bugarama), Gisenyi, Kibuye, Ntaresi and Musanze. At the conclusion of the survey, Gisenyi and Bugarama were identified as potential sites for geothermal development with an estimated reservoir temperature beyond 100°C. A new survey was conducted by Chevron in 2006 at the hot springs of Bugarama and Gisenyi using geothermometry and the results indicated low to moderate temperature. The most promising prospects in Rwanda were identified as Bugarama, Gisenyi, Karisimbi and Kinigi (Figure 1).

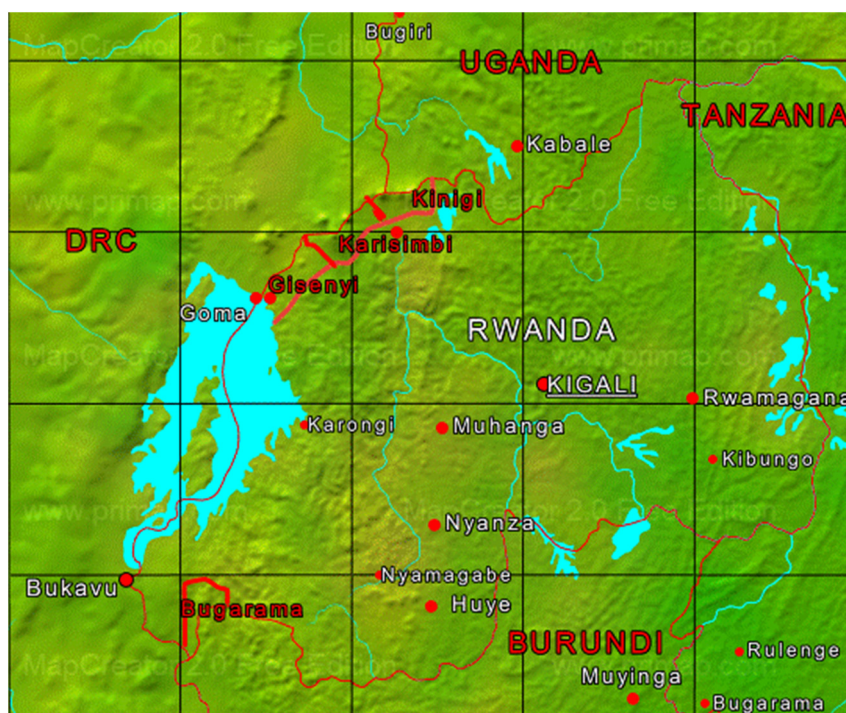


FIGURE 1: Location map of geothermal areas in Rwanda (Namugize, 2011)

In 2008, the Germany Institute for Geosciences and Natural Resources (BGR) collaborated with Kenya Electricity Generating Company (KenGen), Iceland GeoSurvey (ÍSOR) and the Institute for Technology and Renewable Energies (ITER) to conduct geochemical, geophysical and soil gas surveys in Gisenyi, Karisimbi and Kinigi. They concluded that (BGR, 2008):

- (1) A geothermal system with a temperature over 200°C is located south of Karisimbi volcano;
- (2) The temperature of the geothermal system near Lake Karago is 150 to 200°C; and
- (3) The depth of heat source in these geothermal systems is about 5 km.

In 2009, KenGen conducted additional surface surveys (geophysical and geochemical) and an environmental impact assessment south of Karisimbi volcano. In a workshop held in Kigali in February 2010, a geothermal conceptual model based on those results and drilling targets for three wells were discussed.

In 2010, KenGen conducted geophysical (MT and TEM), geochemical (soil gas: CO₂, mercury and Radon) and hydrogeological surveys. They concluded that the geothermal system is possibly distributed to the regions around the southern slopes and trends to the southeast through the town of Mukamira toward Lake Karago. Therefore, it was recommended that the exploration wells should be drilled directionally ranging between 2,000 and 3,000 m in depth to intersect as many structures as possible.

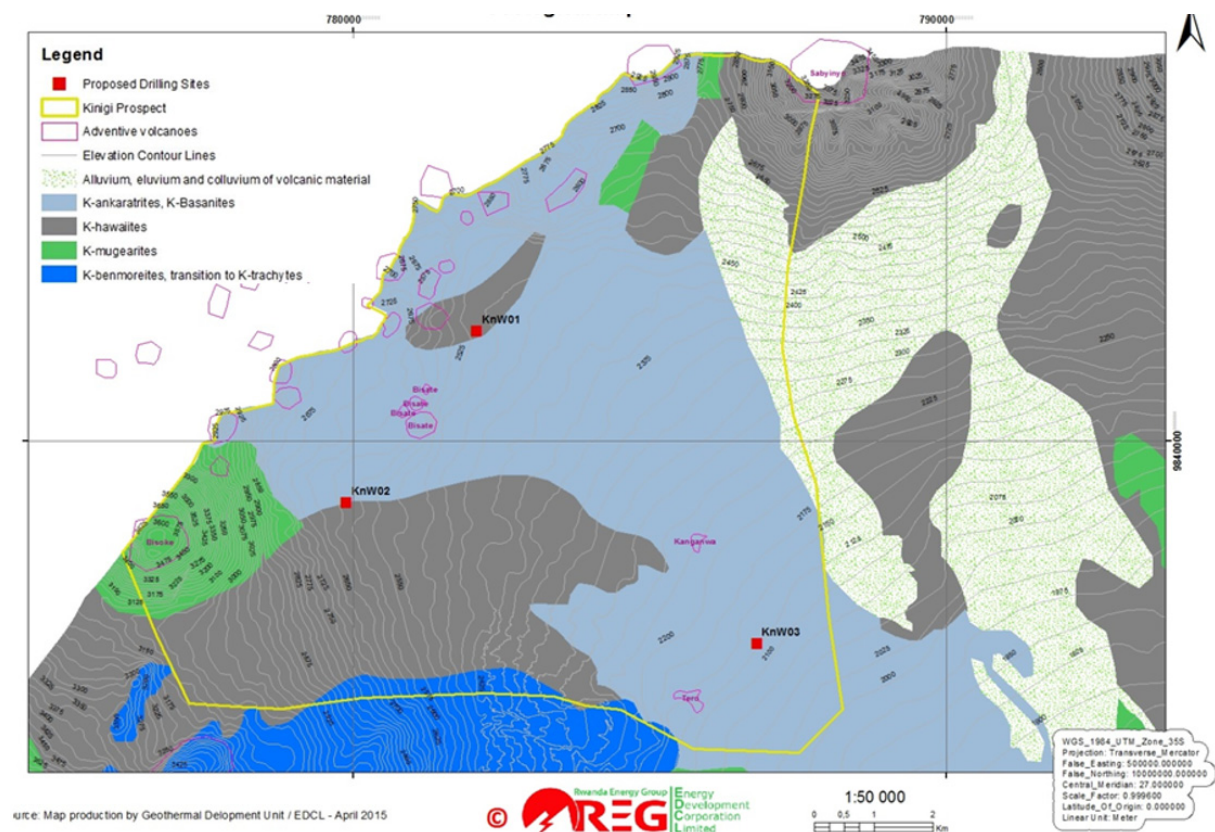


FIGURE 2: Geological map of Kinigi prospect modified from (EDCL, 2015)

From 2011 to 2012, IESE (Institute of Earth Science and Engineering) conducted additional geological, geochemical and geophysical (MT, TEM and CSAMT) surveys as part of a microseismic and heat flow study with boreholes at Kinigi, Gisenyi and Karisimbi. As a result, a geothermal conceptual model regarding geological structure and geothermal fluid flow was elaborated and targets for three vertical exploratory wells were proposed to confirm the reservoir.

In April 2012, the first validation workshop was held in Kigali with different stakeholders in order to verify previous survey results and enable the elaboration of a geothermal conceptual model of the area around Karisimbi and the targeting of three exploratory wells. However, the geophysical analytical results were thought to be insufficient. In January 2013, another validation workshop was held by UniServices, Geothermal Development Company (GDC), Reykjavik Geothermal (RG), KenGen and EWSA to verify the re-analysed results.

The outcome can be summarized as follows:

- 1) The resistivity model around Karisimbi volcano consists of a high resistivity layer (recent volcanic), a low resistivity layer (may be the clay cap) due to hydrothermal alteration of low-temperature clays and a higher resistivity layer (reservoir) due to a higher degree of hydrothermal alteration;
- 2) There is a deeper low resistivity layer (heat source) which becomes shallower toward Karisimbi volcano and dips sharply to the south; and
- 3) Drilling targets were confirmed: future drilling should be directional toward Karisimbi volcano targeting the NW and NE trending interpreted fractures and go to a depth of 3,000 m.

The first exploratory well was drilled in Karisimbi (KW01) starting July 18th, 2013 and reached the target depth of 3,015 m on October 23rd, 2013. The second exploratory well (KW02) was drilled from December 14th 2013 until March 22nd 2014 and was stopped at 1,367 m. The data from these two wells

showed that the area was rather cold (a gradient of 30°C/km) and with low permeability. Among the lessons learned is to carry out additional surveys prior to new exploration drilling.

Among the additional surveys, a gravity survey was carried out in Kinigi area by JICA and concluded that the heat source of the geothermal system is related to the Quaternary activity of the Sabinyo volcanoes (JICA, 2014).

2.2 Geology of the Kinigi area

The geology of Kinigi area as shown on the map (Figure 2) is dominated by the upper tertiary to quaternary volcanic rocks which originated from the explosive volcanism of the Karisimbi, Bisoke, Sabyinyo, Gahinga and Muhabura volcanoes (EWSA, 2014). The volcanic rocks in Kinigi area are dominated by pyroclastites of different ages and trachytes. They are probably related to a caldera collapse phase and also indicate magmatic differentiation while latites indicate silica-rich melts from local upper crust (Rogers et al., 1998).

The latites from Sabyinyo and trachytes from Karisimbi are results of fractional crystallization. The abundant pyroclastites which also occur in shallow ground water boreholes up to a depth of 100 m are expressed as volcanic ashes, lapilli and volcanic bombs (Rogers et al., 1998).

High temperature, pressure and gas content were the main engines of explosivity, possibly in the upper mantle. This together with the recent whole rock chemistry studies by Shalev et al. (2012) support the theory that magmatic differentiation could be the heat source for the geothermal system.

The rocks around Kinigi were dated to be between 100,000 and 200,000 years old in the case of the latites and the K-basanites less than 100,000 years (Rogers et al., 1998).

Most of the cold, warm and mineralised springs occur in lowlands generally at the boundary of the volcanic and the basement rocks and along NS tectonic features in the Kinigi area. Cold springs, generally with high flow rate, are sourced by the porous volcanic rocks and open faulting systems. The very high permeability and rainfall would mask any geothermal manifestations like fumaroles (EDCL, 2015).

Based on the geology, hydrogeology, geochemistry, active volcanism and geophysics there are three possible hydrogeological models for the Kinigi area (EDCL, 2015):

- (1) Thermal fluids may ascend below the volcanic zone and move to the south east along fault zones at the contacts of the different strata.
- (2) Geothermal fluids may ascend via near vertical channels along the northeast trending fault zones between Bisoke and Sabinyo volcanoes with many cones that could be associated with hot intrusive rocks. This geothermal system may be discharging to the south east along the fault zones towards the tepid springs in the basement.
- (3) The model relates to the heat source provided by a mafic-magmatic heat source (associated with demagnetised zones with low magnetic anomaly) that could be related to the mineralisation in the NE trending tungsten belt. In this model, the discharge is still expected to be to the south east along the regional NW faults and at the contacts of the lava flows.

However, it is uncertain which hydrogeological model is correct but all the three models are applicable to this area (EDCL, 2015).

The main outcome of all efforts was a recommendation in favour of an exploration drilling in the area targeting the interpreted high permeability zones to assess the geothermal potential. The geothermal system between the Bisoke and Sabyinyo volcanos appears to be controlled by a near orthogonal set of

fault zones. The main up flow of the system appears to be between Bisoke and Sabyinyo along the NW and NE trending fault zone.

From the experience of Karisimbi drilling we know that from the surface to 3000 m depth, the lithology of the area is characterised by the following different rock types: the top 60 m are basanite rock, from 60 to 1000 m Hawaiiite and basanite rocks can be found, while the layer from 1000 m and deeper is made of granite rocks (Table 1). The geophysical surveys show a resistivity structure with a low resistivity anomaly interpreted as a mafic-magmatic heat source at a depth of 5000 m. Unaltered and un-fractured basement rocks, granites and fresh volcanic rocks have very high resistivity (Figure 3).

TABLE 1: Comparison of rock type discoveries from Karisimbi drilling and the estimate for the entire region (EWSA, 2014)

Depth (m)	KW01 rock type	KW02 Rock type	Estimate of the area lithology
0-56	K-basanite	Basanite	Basanite
56-156	Scoraceous basanite	Basanite and scoria	Basanite and scoria
156-180	Scoria of K-basanite	Basanite	Basanite
180-212	K-Hawaiiite and K-basanite	Basanite	Hawaiiite and basanite
212-325	Scoria of Hawaiiite	Basanite	Hawaiiite and basanite
325-334	K-Hawaiiite	Basanite	Hawaiiite and basanite
334-960	None	Scoria, Hawaiiite, pyroclastic deposits, mugearite, Granite	Hawaiiite, scoria and granite
960-3015	Granite	Granite (to bottom at 1367)	Granite

Figure 4 shows the resistivity map of the Kinigi area and Table 2 shows the potential energy in Kinigi area as estimated by JICA, 2014.

2.3 Design alternatives for geothermal wells

The geothermal well design includes the casing programme, i.e. the size of the borehole, casing diameters and depths, connections and type of steel. The design is influenced by the expected formation temperature and pressure, subsurface rock type and needed minimum temperature for the intended exploitation scheme.

Secondary factors influencing the drilling programme are the availability of drilling rigs and drilling materials like drilling fluids, a drill string assembly, cementing materials and other necessary drilling tools and equipment.

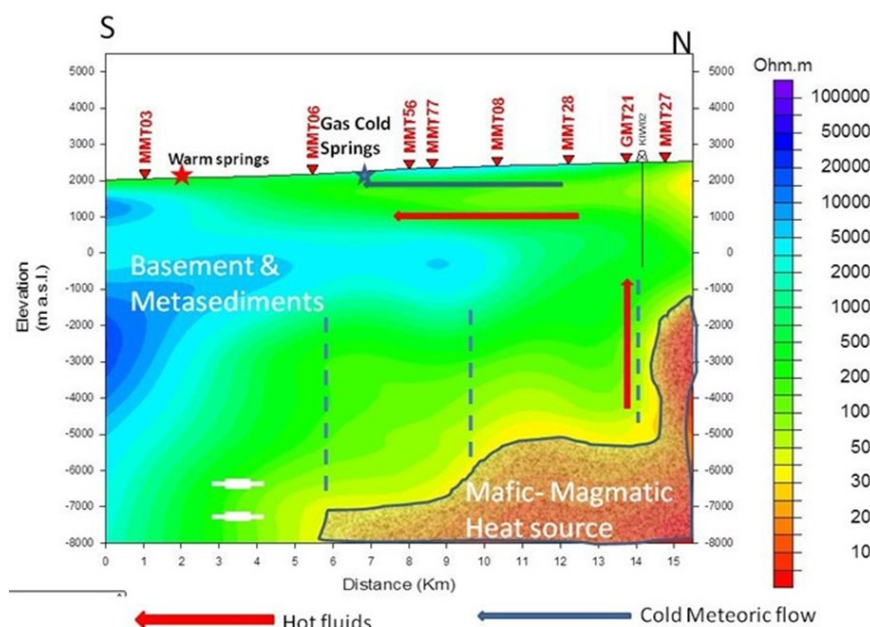


FIGURE 3: NS resistivity cross section showing a deep low resistivity interpreted as a mafic-magmatic heat source that is shallower to the north than the south (EDCL, 2015)

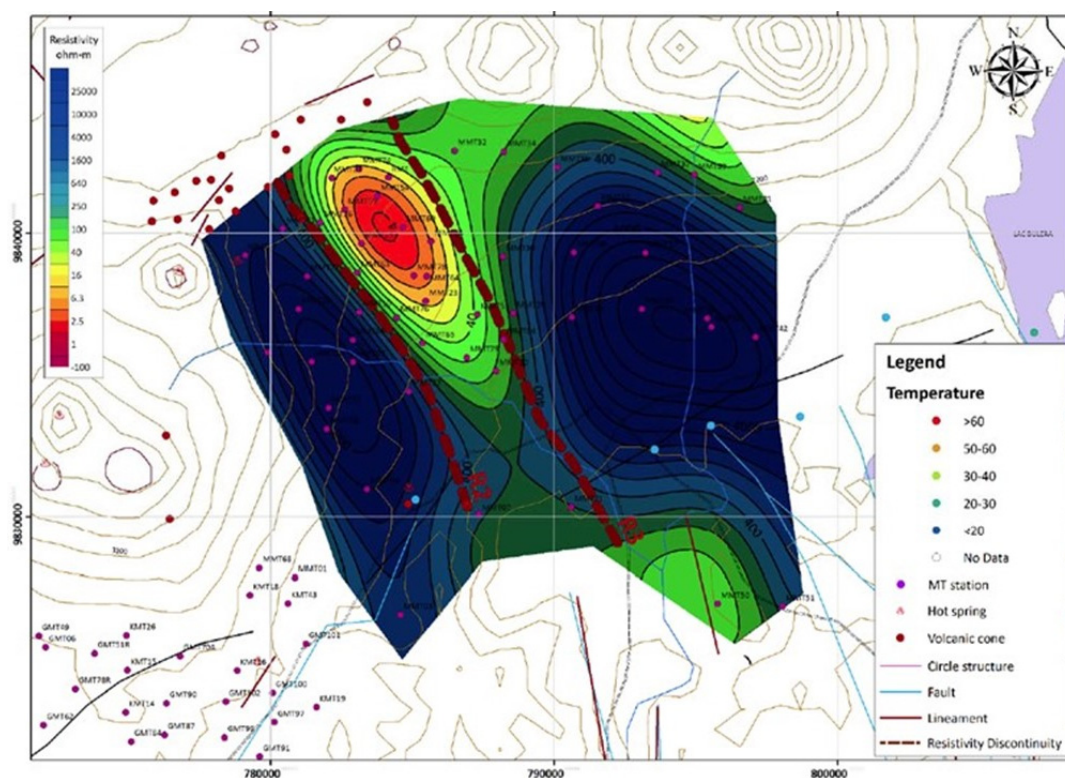


FIGURE 4: Estimated geothermal resource area extent in Kinigi prospect; resistivity map at 3000 m (JICA, 2014)

TABLE 2: Summary of resource evaluation for 5 prospects of Rwanda (modified from JICA 2014)

Field name	Potential energy (MWe) at 80% confidence level	Potential energy (MWe) at 50% confidence level
Kinigi	32.6	58.6
Bugarama	6.6	15.1
Gisenyi	1.9	3.7
Karago	2.5	4.9
Iriba	3.7	7.2
Total	47.3	89.5

A typical geothermal well has 3 types of cemented casings with various diameters set at different depths: surface or conductor casing, anchor or intermediate casing, and production casing (Hole, 2008a). In the open hole section there is a slotted liner. In a hot water or two phase field with boiling conditions the maximum temperature is assumed to follow the boiling point depth curve (BPD). The pressure at depth and the boiling point is dictated by the water column (saturation pressure). Only a few reservoirs are filled with steam (vapour dominated). The casing depth must be set in order to seal off unwanted fluid with not high enough temperature, which for high-temperature wells is about 200°C. The rock competence and loss of circulation may also influence the casing depth. This rock competence often lies between the theoretically derived fracture gradient and a theoretical overburden pressure. This hypothetical situation of BPD in a 2,500 m deep well would require the production casing shoe being set at a depth of 800 m, the anchor casing shoe at 300 m depth and the surface casing shoe at around 60 m according to the African Union Code of Practice for Geothermal Drilling (African Union, 2016). The diameters for geothermal exploration wells are chosen considering the desired fluid flow and the annular clearances for the cementing of concentric casings. Generally, geothermal wells may be classified into four categories according to the casing programme diameter selection: regular, large, slim and cored (Figure 5).

		CASING DIAMETER IN DIFFERENT GEOTHERMAL HOLES					
		No		[1]	[2]	[3]	[4]
		Name		Surface	Anchor	Production	Liners
[1]	Large holes	(inches)		26"	20"	13-3/8"	9-5/8"
		(mm)		660,4	508	339,73	244,48
[2]	Regular holes	(inches)		20"	13-3/8"	9-5/8"	7"
		(mm)		508	339,73	244,48	177,8
[3]	Slim holes	(inches)		13-3/8"	9-5/8"	7"	4-1/2"
		(mm)		339,73	244,48	177,8	114,3
[4]	Cored holes	(inches)		11-7/8"	8-5/8"	6-5/8"	4-1/2"
		(mm)		295,28	219,08	168,28	114,3

FIGURE 5: Possible casing programme for geothermal wells

3. WELL DESIGN

The African Union Code of Practice for Geothermal Drilling (African Union, 2016) indicates steps and requirements to be followed for well design in order to safely drill a successful and stable well. This code is based on the New Zealand Code NZS 2403:2015 and the steps include determination of expected geological formation, anticipated subsurface conditions, e.g. temperature versus depth, pressure versus depth, interval of lost circulation and anticipated problem zones, targeted well depth and wellhead location.

3.1 Anticipated subsurface conditions in Kinigi area

The volcanic area of Kinigi geothermal prospect is characterized by many caves, unconsolidated rocks and boulders in the top 100 m section. The water table is expected to be deeper or located between 200 and 300 m depth. This water level estimate for the first drill site in Kinigi is projected from the elevation of the nearest water body (Rugezi swamp) which is at 2050 m a.s.l. (Hategekimana and Twarabamenye, 2007) while the elevation of the drill site in Kinigi is at 2300 m a.s.l. The Karisimbi drilling showed the water level at 400 m with the well site elevation being 2622 m a.s.l. (EWSA, 2014). The elevation of the nearest water body (lake Kivu) was at 1460 m a.s.l.

A number of drilling challenges are expected during the drilling operation of the Kinigi area and the most likely include total loss of circulation, very low rate of penetration (ROP), difficulties in cleaning the hole and trouble during cementing or running the casing.

It is important to identify alternative actions in order to overcome these challenges and this report suggests some possible solutions; for instance the use of air hammer drilling technology for the surface casing (top 100 m), the use of Icelandic policy for loss of circulation and methods of cementing losses, procedures for casing cementing, how to maintain a clean hole when drilling blind (no circulation returns) and so on.

This programme is for exploratory wells which is the term used for the first 2-3 wells in a new field, therefore no data is available to support the prediction of important parameters, e.g. pressure and temperature vs. depth. For that reason, we assume that the subsurface fluid pressures are the hydrostatic values for a column of water at the boiling point (BPD) below the ground water level with no artesian condition (Africa Union, 2016). The assumptions for maximum subsurface temperature values follow saturation conditions for a column of boiling water below the same level defined by the pressure (Table 3).

TABLE 3: Standard hydrostatic pressures (gauge) and BPD temperatures for a column of pure water with no dissolved gas with water table at 200 m (African Union, 2016)

Hole depth	Hydrostatic fluid Pressure at 20°C	Hydrostatic fluid pressure at BPD	BPD temperature
(m)	(MPa)	(MPa)	(°C)
200	0.00	0.00	100
210	0.10	0.09	119
220	0.19	0.19	132
240	0.39	0.36	149
260	0.58	0.54	162
280	0.78	0.72	172
300	0.98	0.89	180
350	1.47	1.32	196
400	1.95	1.75	208
500	2.93	2.57	227
600	3.91	3.37	242
700	4.89	4.16	254
800	5.87	4.93	264
1000	7.82	6.43	281
1200	9.78	7.87	295
1400	11.70	9.26	306
1700	14.70	11.27	321
2200	19.60	14.40	339
2700	24.50	17.30	354
3200	29.30	19.90	365

3.2 Casing design

The target is to reach the low resistivity layer between 3 and 5 km as interpreted by JICA (2014) and thus the planned vertical depth for Kinigi exploration wells is 3000 m. While drilling deep wells, safety dictates that the wellbore pressure be maintained between the natural occurring pressure of the formation fluids and the maximum wellbore pressure that the formation can withstand without fracturing (Bourgoyne et al., 1986). The knowledge of how formation fluid pressure and fracture pressure vary with depth is extremely important for safe drilling of deep geothermal wells and serves as the basis for determination of minimum casing depths (Hole, 2008a).

In order to understand subsurface fluid pressure in a given area, ground elevations and previous geological processes must be considered. The pore pressure in a highly porous formation at depth, such as in a geothermal reservoir, is the same as the hydrostatic pressure which depends only on the depth and fluid density. With greater depth the porosity decreases due to high geostatic loads and the formation pore pressure increases but the hydrostatic equilibrium is maintained as the pores do not become geopressed.

For the formation pore pressure data to have the greatest utility, it must be available as early as possible. However, direct measurement of formation fracture pressure is only possible after a well has been drilled in the area. Therefore, general assumptions have to be made for the very first wells, which include the pore pressure following the boiling point depth (BPD) curve and the fracture pressure being equal to the overburden pressure. The older version of the New Zealand standard (NZS 2403:1991) considers only the overburden pressure, which depends on the soil density and that criteria has been in use for 30 years. The new version, NZS 2403:2015 (New Zealand Standards, 2015), which the AU standard is based on considers however the pore pressure following the BPD curve and the formation fracture pressure is considered instead of the overburden pressure. A comparison of results for calculations made based on

both the African Union, 2016 code of practice and the old version of the New Zealand standard (1991) (NZS 2403:1991) will be given further in this section.

Conventional practice for drilling deep wells requires the setting of successive, separate casing strings as the well gets deeper. The length of each string is determined by several factors, including rock properties (fracture gradient, sloughing, swelling, unstable, or unconsolidated formation), formation fluids (pore pressure much less or much greater than drilling fluid pressure) and well control considerations (Finger and Blankenship, 2010). Therefore, the minimum casing shoe depth for each casing string is calculated to be at the depth where the geological formation has sufficient effective containment pressure (fracture pressure or overburden pressure) equal to the maximum design fluid pressure expected to be encountered in the next open hole section (African Union, 2016).

The basis of the maximum fluid pressure to be encountered in the open hole is a steam filled well from the total depth of that section where the starting pressure at bottom of the well is at the BPD curve hydrostatic fluid pressure (African Union, 2016).

Nevertheless, the actual casing shoe depth may be adjusted slightly deeper either to target the competent formation, to avoid the problem zones or to avoid any other conditions requiring more attention. The actual depth of the production casing shoe is very much dictated by the formation temperature which should be above 200°C in order for the wells to sustain stable self-flow. For the “regular” casing programme different hole sizes and casing shoe depths for different strings are presented in Table 4. Details on the casing design calculations will be given in the casing programme section.

TABLE 4: Well plan and planned casing shoe depths for Kinigi exploration wells

Casing sections	Minimum shoe depth	Hole diameter	Casing diameter
	(m)	(inches)	(inches)
Surface	100	26	20
Anchor	450	17-1/2	13-3/8
Production	1230	12-1/4	9-5/8
Liners	3000	8-1/2	7

The formation fracture pressure in Kinigi area is not yet known. For this reason the formula of Eaton (1969) was used and later different depths for casing shoes were determined as shown in Figure 6. Thus, the hydrostatic pressure in the BPD curve serves as the lower margin of the minimum casing shoe as observed in Figure 6, while the maximum (containment pressure or formation fracture pressure (African Union, 2016)) serves as the upper margin. The old version of the New Zealand standard (NZS 2403:1991) stipulates to use the hydrostatic pressure at 20°C as lower margin and the overburden pressure curve as upper margin.

$$P_{frac} = P_f + \frac{V}{1-V} (S_v - P_f) \quad (1)$$

The overburden pressure $p(z)$ (Bourgoyne et al., 1986)) is calculated according to the formula below:

$$p(z) = p_0 + g \int_0^z \rho(z) dz \quad (2)$$

where $\rho(z)$ is the density of the overlying rock at depth z , g is gravity and p_0 is the datum pressure or pressure at the surface.

The new African Union Code of Practice for Geothermal Drilling (2016) stipulates techniques to be followed while designing the casing programme and Figure 6 shows the theoretical minimum depth of casing shoes for Kinigi exploration wells.

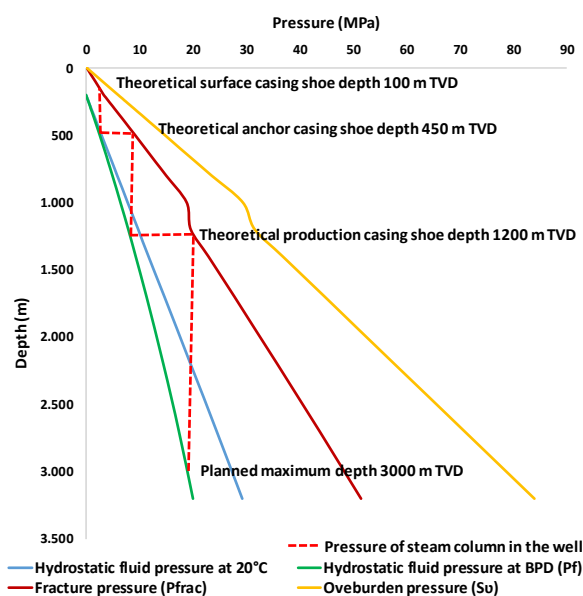


FIGURE 6: Minimum casing shoe depth for Kinigi area calculated using AU (2016) code of practice

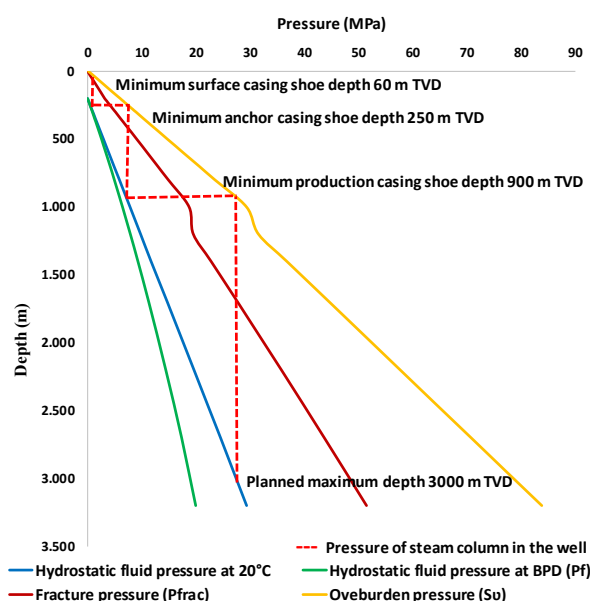


FIGURE 7: Comparative casing shoe depth set as stipulated by the NZS 2403:1991 code of practice (New Zealand Standard, 1991)

For comparison, results obtained by the method of the old New Zealand standards (NZS 2403:1991) for Kinigi area are shown in Figure 7. It is clear that this old method would set the minimum casing shoe depth at the slightly shallower levels. For instance, the production casing shoe would have been set to a depth of approximately 900 m, the anchor casing shoe to 250 m and the surface casing shoe to 60 m.

Comparing the results of the two methods, the old version of the New Zealand standard (NZS 2403:1991) set cemented casing strings at shallower depths and that can play a part financially (the cost of casing and materials) and also technically because short casing strings are more resistant to loads but their minimum setting depths are likely to be above the cold aquifer and thus would produce cooler fluids. Nevertheless, both methods, the NZS 2403:1991 code of practice and this new African Union code of practice, set minimum casing shoe depths theoretically and each has advantages and disadvantages.

3.2.1 Tackling anticipated drilling challenges in the surface casing section (0-100 m)

Considering the anticipated subsurface conditions in the Kinigi area which are volcano boulders, hard and unconsolidated rocks and total loss of circulation, alternatives to conventional rotary drilling are explored in order to see if any of them can help to overcome or alleviate these challenges. In such formations, it is advisable to apply percussion drilling because this technology presents advantages compared to rotary drilling. Air hammer technology (DTH) is probably the most versatile percussion drilling method available because it can be used in medium to hard rock formations where rotary drilling has been slow. Its benefits are directly linked to the increased rate of penetration (ROP) at the shallow depth where the weight on bit (WOB) is still low where it can even be five or seven times faster than conventional rotary drilling (Bar-Cohen and Zacny, 2009). Large fluid losses in the cavities expected are less of a problem by drilling with foam.

The use of DTH hammer does not require large rigs and sometimes pre-drilling or pre-holing for the surface casing is done before the large rig is brought in. Another advantage is the low water consumption which is only to prepare drilling soap to create the required foam to bring out the cuttings. However, every technology has its own pros and cons and air hammer drilling also has some drawbacks associated with pneumatic drilling including its use at increased drill depth, hole deviation, dust etc. (Thompson, 2010).

3.2.2 Tackling anticipated drilling challenges in the anchor casing section (0-450 m)

Anticipatively, this section will be characterised by big caves and total loss of circulation. Drilling with air hammers (DTH) is a possibility worth considering as the water table is low. If that does not succeed it is easy to switch over to conventional rotary drilling with mud or water. For large losses sweeps of foam at every joint will be applied but if the loss is not healed after 10-30 m then a cement plug job will be required as a solution. Large loss zones have been proven to be difficult to heal and a novel method used in Iceland may need to be applied. A mixture of sand and cement from a ready-mix truck is placed in the well using concrete pumps from the construction industry.

Cementing the anchor casing, with expected caves and loss zones, will require much care in planning and application of the most suitable method. A common method is to cement in the conventional way by pumping through the casing and up the annulus but only enough to reach the loss zone and then revert to a top-job to fill the annulus. A full reverse circulation of cement technique (RCC) has several advantages compared to conventional practices (Wreden et al., 2014). While using this technique, the fluids are pumped into the annulus of the well and water returns are taken through the casing. Benefits of this technique include: lowering bottom-hole placement pressure, reducing cement retarder concentration, lowering the time for cement placement etc. (Davis et al., 2004). Scenarios of different methods and calculations of slurry quantity to be used will be presented in the section on the cementing programme.

3.3.3 Tackling anticipated drilling challenges in the production casing section (0-1,230 m)

This is the most troublesome section where different drilling challenges are expected, e.g. loss of circulation, hole instability, risk of stuck drill string, low ROP and hole cleaning. Cementing this section is also very problematic but the cementing programme section will describe alternative methods to use. Issues related to well cleaning in the production casing section was observed in Karisimbi (EWSA, 2014) and in Kinigi, there is high expectation of facing similar nightmares. The section on drilling fluid will put more light on fluid to use, lag time for the travel of casing and so on.

3.3.4 Tackling anticipated drilling challenges in the slotted liners casing section (0-3,000 m)

The main drilling issues to be expected in this particular section is low rate of penetration (ROP) due to an extended granitic layer, hole cleaning etc. Other issues may be dealt with by improved drilling parameters but the granitic layer cannot be drilled with a tricone bit for more than 100 m before wearing out. Unless the permeability is greater and the formation temperatures higher the formation will be similar to the one observed at Karisimbi (EWSA, 2014). Because of the Karisimbi results there is a possibility that the basement formation in the Kinigi area is also made of granite and drilling into the basement will not result in a productive geothermal well, but only drilling will tell.

4. CASING PROGRAMME

A casing string is designed from the bottom to the top and from the innermost casing to the outside ones (Hole, 2008a). In general, casing sizes are chosen taking into consideration a number of factors, e.g. expected down hole pressure, economical objectives, pumping capacity, prevention of collapse or burst, buckling or any other deformation, support drilling and permanent wellheads, control contaminations from aquifers, counter circulation losses during drilling and protection of the integrity of the well against corrosion, erosion or fracturing (African Union, 2016).

In order to choose the right steel grade for the casing string, one has to be very careful considering the fact that casing was initially designed for the petroleum industry where parameters like fluid pressure,

casing weight and tensile loads have to be taken into account. In geothermal wells, the most severe service is high temperature loading (Hole, 2008a).

In this section, generic case methods for calculation of the design or safety factors of the casing string will be used. All calculations will be defined to find the minimum design factor below which every casing string is at high risk of damage and the maximum design line above which every casing string is an economical waste because of much unnecessary investment. Therefore, any casing design between the two lines is considered to be safe but field data update will be necessary to make precise decisions between the two limits. Figure 8 shows theoretical casing strings for geothermal exploration wells in Kinigi with depth of casing shoes, diameter of various casings and the cementing job.

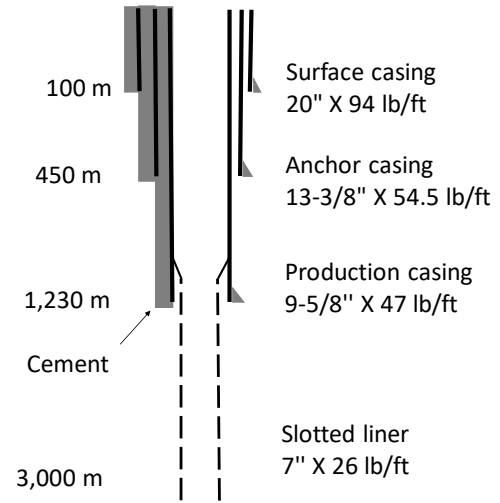


FIGURE 8: The proposed casing program for exploratory wells in Kinigi

4.1 Casing design factor calculation formulas as per the African Union code (2016)

The casing design factors are calculated in order to ensure that the casing will withstand all anticipated stresses. Among those stresses we include: radial and circumferential stress, uniform axial stress due to all sources except bending, axial bending stress for a Timoshenko beam and torsional shear stress due to a moment aligned with the axis of the pipe (African Union, 2016).

The axial stress in casings is caused by three main parameters: the weight of the casing, the temperature (expansion and contraction) and restraint due to cement or connection at the wellhead or downhole hanger. African Union (2016) stipulates that casing stresses have to be assessed either by calculating each individual stress or calculating the triaxial stress using API TR 5C3 or equivalent methods. The triaxial stress calculation combines all the stresses acting on the casing. The scope of this report will be limited to the method which uses the calculation of each individual stress. While checking the axial stress, it is paramount to separate two sets of conditions, namely before and after cementing the casing (Hole, 2008a).

4.2 Axial stress conditions

4.2.1 Axial loading before and during cementing the casing

Before the cement sets in the annulus around the casing, the tensile force at any depth includes the weight of the casing in air plus the weight of the casing contents minus the buoyancy effect due to any fluid displaced by the casing in the well (African Union, 2016).

$$F_{\text{hookload}} = F_{\text{csg air wt}} + F_{\text{csg contents}} - F_{\text{displaced fluids}} \quad (3)$$

and

$$F_{\text{csg air wt}} = L_z \times W_p \times g \times 10^{-3} \quad (4)$$

$$F_{\text{csg content}} = \sum \rho_{\text{if}} \times L_{\text{if}} \times \frac{\pi d^2}{4} \times g \times 10^{-6} \quad (5)$$

$$F_{\text{displaced fluids}} = \sum \rho_{\text{ef}} \times L_{\text{ef}} \times \frac{\pi D^2}{4} \times g \times 10^{-6} \quad (6)$$

Negative F_{hookload} means that the casing is floating and steps should be taken to hold the casing down against this floatation. Buoyancy force (F_{buoyancy}) is the difference between air weight of the casing ($F_{\text{csg air wt}}$) and the hook load (F_{hookload}) (African Union, 2016):

$$F_{\text{buoyancy}} = F_{\text{hookload}} - F_{\text{csg air wt}} = F_{\text{csg contents}} - F_{\text{displaced fluids}} \quad (7)$$

The buoyancy force is considered to be applied as a point load at the depth within the casing that is holding differential pressure either at the float collar, float shoe or at the surface (Hole, 2008b). Thus, prior to cement setting the tensile force applied at any point in the casing under hydraulic and gravitational loads is defined as:

$$F_p = [L_z W_p - (L_z - L_w) A_p / n] g \quad (8)$$

Nevertheless, the above tensile force does not include any stress which may be due to bending.

In non-vertical hole, the maximum bending stress induced is:

$$f_b = 0.291 \times E \times q \times D \times 10^{-6} \quad (9)$$

This stress is applied both as additional compressive stress and additional tensile stress. These additional stresses have to be added to the casing stress created by weight, hydraulic loads and thermal loads (African Union, 2016).

Where the axial loadings before cementing can occur simultaneously they have to be added together and the resultant maximum axial load checked against the minimum tensile strength of the casing. The design factor applied to this is 1.8 and is given by the following formula (African Union, 2016):

$$\text{Design factor} = \frac{\text{minimum tensile strength}}{\text{maximum tensile load}} \quad (10)$$

4.2.2 Axial loading after cementing the casing

According to African Union 2016 code of practice, axial forces imposed after cementing have to be checked for applicability and magnitude near both the shoe and the top of the casing. And to calculate the resultant net force, each of the loadings have to be combined with the static force present in the casing (F_p) at the time of cement setting. Hole (2008b) suggests that thermal stress can be calculated using the coefficient of thermal expansion and estimated temperature difference but it is worth to consider that due to cement constraints, the casing is forced back to the original length by axial compression (modulus of elasticity). Stress from thermal expansion, for example a temperature change of 150°C, can be calculated as follows (Hole, 2008b):

$$\begin{aligned} \text{Unit extension} &= \text{strain} = \text{coefficient} \times \text{temperature change} \\ &= 12 \times 10^{-6} \text{ } ^\circ\text{C}^{-1} \times 150^\circ\text{C} = 1.8 \times 10^{-3} \end{aligned} \quad (11)$$

$$\text{Stress} = \text{modulus} \times \text{strain} = (200 \times 10^3) \times 1.8 \times 10^{-3} = 360 \text{ MPa} \quad (12)$$

The total axial stress in a cemented string varies with depth and with the difference in temperature at any time between the time when the casing was fixed in position (neutral temperature value) and the temperature at any subsequent time (Hole, 2008b). Stress relaxation will occur if the steel is loaded at high temperature over a long period of time. Further stresses also may be induced if the geological formation in the place is faulting or moving by subsidence (Hole, 2008b). The compressive force due to temperature rise in the situation of partial longitudinal and lateral constraint is given by:

$$F_c = C_t (T_2 - T_1) A_p \quad (13)$$

$$C_t = E \times a = 200 \times 12 \times 10^{-6} = 2.4 \text{ MPa per } ^\circ\text{C} \quad (14)$$

The tensile loading as calculated for the pre-cementing time remains in the casing even after cement set. Therefore, the resultant axial force F_r on the casing after cement set and heating is given by (African Union, 2016):

$$F_r = F_c - F_p \quad (15)$$

The design factor is given by:

$$\text{Design factor} = \frac{\text{minimum compressive strength}}{\text{resultant compressive force}} \quad (16)$$

The minimum strength refers to the lesser of the strength of the pipe body or connection. In any means the design factor may not be less than 1.2 (African Union, 2016).

One of the main causes of casing failure is rapid cooling of the well, therefore cooling of a hot hole for any reason whether subsequent drilling activities, pumping tests or reinjection must be done in accordance with a strict well quenching and cooling programme thus allowing the stress to be uniformly distributed over the full length of the casing (Hole, 2008b). As the temperature rises it causes a compressional force. Cooling exerts tension to the casing, therefore the axial tension is calculated ignoring any relaxation of stress with time due to temperature reduction caused by circulation of cooling fluids. This axial tension is given by the following formula (African Union, 2016):

$$F_t = E \times a \times (T_1 - T_3) \times A_p \times 10^{-3} \quad (17)$$

At every other depth except the wellhead, the resultant force is given by (African Union, 2016):

$$F_r = F_p + F_t \quad (18)$$

The tensile axial loading of the top section of the casing due to lifting forces applied by the fluid to the wellhead is given by the formula below (African Union, 2016):

$$F_w = \left(\frac{\pi}{4}\right) \times P_w \times d^2 \times 10^{-3} - F_m \quad (19)$$

The design factor for all axial tensile and compressive loading may not be less than 1.2 (African Union, 2016).

4.2.3 Axial loading with buckling and bending

The perforated liners in the production section are not cemented and thus radially neither supported nor constrained. However, instead they must either be hung in tension on a liner hanger just above the production casing shoe or sat at the bottom of the hole with their top part sitting freely inside the production casing shoe (Hole, 2008b). In the case of the liner sitting at the bottom of the hole, it is subjected to axial self-weight compression and helical buckling and therefore must be analysed for extreme fibre compressive stress. Hole (2008b) provided the following formula for calculating this compressive stress in liners:

$$f_c = L_z \times W_p \times g \left[\frac{1}{A_p} + \frac{D \times e}{2I_p} \right] \quad (20)$$

The ratio of the hole diameter to the pipe diameter (eccentricity) determines the amount of bending and thus the bending stresses. The eccentricity e is around 1.5 times the bit diameter depending on the formation integrity and the design factor which has to be always less than 1.2 and is given by African Union (2016) as:

$$\text{Design factor} = \frac{\text{minimum yield stress} \times R_j}{\text{total compressive stress}} \quad (21)$$

R_j is the connection joint efficiency and should not exceed 1.0, but when the listed joint efficiency exceeds 1.0 it is ignored in the formula above (Hole, 2008b).

The ability of a casing string to resist loads is governed by the steel grade (which prescribes its strength), the type of connections, and the loading condition at the neutral temperature state. Since high strength steels are susceptible to corrosion due to H₂S in geothermal, API Grade K-55 and L-80 grade steels are typically utilized, manufactured according to API 5CT (API, 2005). Regarding connections, geothermal service requires a square thread form or shouldered connections to transfer the full axial loading of the pipe body. API buttress threads and various proprietary square threaded connections have been found to be suitable (Hole, 2008a).

4.3 Radial stress conditions

Hoop or circumferential loadings are applied primarily by internal or external fluid pressure. The ability of tubulars to resist differential pressures take into particular consideration the pressure that occur before and during cementing operations, and well fluid pressure in the static condition or when producing or reinjecting (Hole, 2008c). The African Union (2016) code of practice stipulates that hoop stresses which are exerted to the casing from any source have to be considered. Among the sources of hoop stress, there is pressure difference between inside and outside casing before and during cementing, well fluid pressures in static conditions or when producing or injecting, temperature changes with restraint on movement, heating of a confined liquid and dynamic loading.

4.3.1 Internal yield bursting

The casing design must ensure that adequate safety margins exist against internal yield or burst which could result from high internal fluid pressure due to a range of situations that occur during and after the cementing of casing. Those situations include but are not limited to: surface pressure plus a static fluid column, thermal expansion of trapped liquid, well pressures generated from the formation and any combination of the above (African Union, 2016). The maximum differential burst pressures usually occur near the casing shoe or stage cementing collar ports and will apply in one of the cases below:

- The casing is filled with high density cement slurry;
- The annulus is either completely filled with water back to the surface or partially filled with water as controlled by formation pressure; and
- A restriction within the casing, such as a blocked float valve or a cementing plug which will hold the differential pressure.

This last scenario is not a likely situation but it is possible, and it must be looked at as a worst case scenario. The differential burst pressure in this case is the hydrostatic pressure inside the casing at the casing shoe caused by the cement slurry plus any applied pumping pressure minus the hydrostatic pressure in the annulus at the casing shoe caused by the head of water in the annulus (Hole, 2008c).

$$\Delta P_{\text{internal}} = [(L_f \rho_c - L_f \rho_f)] \times g \times 10^{-3} \quad (22)$$

The design factor is given by the formula below and may not be less than 1.5:

$$\text{Design factor} = \frac{\text{casing internal yield pressure}}{\text{differential burst pressure}} \quad (23)$$

Once the cement has been successfully displaced to the annulus and the well completed, the maximum differential internal pressure will occur at the surface. Two scenarios are possible:

- 1) With steam at the wellhead, the design factor will be given by the formula below and may not be less than 1.8 (African Union, 2016):

$$\text{Design factor} = \frac{\text{casing internal yield pressure} \times R_i}{\text{maximum wellhead pressure}} \quad (24)$$

- 2) With cold gas at the wellhead, when the stress corrosion tensile limit of the steel should be used to determine the appropriate yield strength (African Union, 2016).

If the wellhead is fixed to the casing, a biaxial stress condition exists. The combined effects of axial tension and radial burst stress caused by the lifting force of the wellhead pressure has to be calculated with the following expression (African Union, 2016):

$$f_t = \frac{\sqrt{5}}{2} \times \left(\frac{P_w \times d}{D - d} \right) \quad (25)$$

The design factor is given by:

$$\text{Design factor} = \frac{\text{steel yield strength}}{\text{maximum tensile stress}} \quad (26)$$

The top section of the anchor casing from the surface to around 25 m depth also requires design compliance with the ASME Boiler and Pressure Vessel Code (Hole, 2008b).

4.3.2 Hoop stressing – collapse

The casing design has to ensure an adequate safety margin against pipe collapse due to external pressure from entrapped liquid expansion, applied pressure during pumping, and/or static pressure from a dense liquid column such as cement slurry. Typically, the maximum differential external pressure occurs near the casing shoe when the annulus is filled with dense cement slurry, and the inside of the casing is filled with water (African Union, 2016). The maximum differential external pressure is:

$$\Delta P_{\text{external}} = [L_z \rho_c - L_z \rho_f] \times g \times 10^{-3} \quad (27)$$

The design factor which may not be less than 1.2 is given by:

$$\text{Design factor} = \frac{\text{casing external collapse pressure}}{\text{net external pressure}} \quad (28)$$

Hole (2008b) emphasized that large diameters and especially thin walled surfaces and intermediate casings are the most vulnerable to this mode of failure.

During production, the maximum external differential pressure occurs near the casing shoe when the annulus is at formation pressure ($P_z = P_f$) and the internal pressure is controlled by well drawdown. In the worst case the internal pressure at the casing shoe can approach the operating wellhead pressure. The design factor is (African Union, 2016):

$$\text{Design factor} = \frac{\text{pipe collapse pressure}}{\text{differential external pressure}} \quad (29)$$

4.3.3 Thermal expansion of trapped fluid

Since the bulk modulus of thermal expansion of water is not constant, particularly at low temperatures and pressures, the effect of heating water in a confined space is best calculated by reference to steam tables, using a constant specific volume. However, at temperatures above 100°C, the resulting pressure rise due to change in temperature approximates to 1.6 MPa/°C (Hole, 2008b).

For instance, the rated collapse pressure of 9-5/8" 47 lb/ft Grade L-80 casing is 32.8 MPa. Assuming an event where a volume of water is trapped between an outer casing and the 9-5/8" casing, the collapse pressure of the 9-5/8" casing would be reached with a temperature rise of less than 20.5°C, although a large volume of trapped water would be required to deform the pipe until failure (Hole, 2008b).

If the temperature rises from a nominal neutral temperature of 80°C to a formation temperature of 240°C which is the typical case, the maximum pressure being possibly built up from the thermal expansion of a trapped volume of liquid between casings exceeds the strengths of normal casings strings resulting in either burst or collapse (Hole, 2008b).

Due to the importance given to the integrity of the production casing string, it is desirable that any failure should occur in the outer string. For this reason, the final pair of cemented casings has to be designed in the way that the collapse resistance of the inner string should exceed the burst resistance of the outer string with a design factor greater than 1.2. This factor is calculated by the following formula (African Union, 2016):

$$\text{Design factor} = \frac{\text{production casing collapse strength}}{\text{outer casing burst strength}} \quad (30)$$

The added resistance to 'burst' provided by the cement sheath is to a degree countered by the secondary stressing effects of the thermal axial compression, which tends to reduce the resistance to burst and increase the resistance to collapse. For the purposes of design calculations and in the interests of conservative design, this support provided by the cement sheath is ignored (Hole, 2008b).

4.4 Casing design calculation results for Kinigi exploratory wells

4.4.1 Axial loading before and during cementing

While running the casing and cementing just before the cement set, axial forces (tensile) develop and apply to the casing string. The drilling fluid in the well is basically a mixture of water and mud, let's assume the case of hot water at 50°C and apply a buoyancy factor due to its density. The density of the drilling fluid in the well is assumed to be 988 kg/m³. Table 5 below shows the calculated design factor for the casing programme in Kinigi exploratory wells. All results are based on assumptions which must be updated when the data from drilled wells will be available. It is clear that the axial forces increase with the length of the casing and the safety factor also slightly decreases.

TABLE 5: Axial forces on casing string before and during cementing

CSG Grade K55	lb/ft	Length (m)	F _{csg air wt} (kN)	F _{csg contents} (kN)	F _{displaced fluids} (kN)	F _{hookloads} F _p (kN)	Min. tensile strength (kN)	Cal DF	Min DF
20"	94	100	137	180	196	120	11,375	94.5	1.8
13-3/8"	54.5	450	358	352	395	314	6,556	20.9	1.8
9-5/8"	47	1,230	844	444	546	742	5,735	7.7	1.8

4.4.2 The axial loading after cementing

Axial load after the cement set may rise due to temperature increase or when cold water is pumped into the well. An increase in temperature results in compressive forces while a decrease of temperature results in tensile forces. Apart from these two possible forces, eventual bending of the borehole also exerts force on the casing string.

Table 6 shows assumptions made on temperatures, both the initial neutral considered to be in the well at the time of cement set (T₁) and the expected maximum (T₂) which might vary at the bottom of every casing. The thermal expansion is assumed to be 13×10⁻⁶ and the negative sign (-) shows that these are compressive forces. Results show that the higher the temperature the higher the risk. In the production casing for instance the safety factor reaches the threshold when T₁ and T₂ are assumed to be 80 and 227°C, respectively.

TABLE 6: Axial forces on casing string after cementing due to rise in temperature

CSG GRADE K55	lb/ft	E (GPa)	α (°C ⁻¹)	T1 (°C)	T2 (°C)	Ap (m ²)	Compressive force, Fc (kN)	Resulting force, Fr (kN)	Min compressive strength (kN)	Cal DF	Min DF
20"	94	210	13×10^{-6}	30	120	0.017	- 4,147	-4,146	-6,582	1.6	1.2
13-3/8"	54.5	210	13×10^{-6}	50	160	0.010	- 3,006	-2,691	-3,793	1.4	1.2
9-5/8"	47	210	13×10^{-6}	75	220	0.009	- 3,466	-2,724	-3,318	1.2	1.2

Table 7 shows tension forces resulting from a cooling fluid circulating in the hole either during drilling, testing or reinjection. Assuming that the cooling fluid is at ambient temperature of 25°C, the bottom hole temperature is assumed to be 30°C, 50°C and 75°C for respective casing strings from the surface. Results show that casing strings are robust for the assumed temperature changes. However, if the initial temperature T1 is assumed to be 120°C and the temperature of the cooling fluid T2 20°C the production casing safety reaches the minimum values.

TABLE 7: Axial forces on casing after cementing due to cooling fluid or decrease in temperature

CSG Grade K55	lb/ft	E (GPa)	α (°C ⁻¹)	T1 (°C)	T2 (°C)	Ap (m ²)	Compressive force, Fc (kN)	Resulting force, Fr (kN)	Min compressive strength (kN)	Cal DF	Min DF
20"	94	210	13×10^{-6}	30	25	0.017	237	237	11,375	32	1.8
13-3/8"	54.5	210	13×10^{-6}	50	25	0.010	683	998	6,556	6.6	1.8
9-5/8"	47	210	13×10^{-6}	75	25	0.009	1,195	1,937	5,735	3.0	1.8

After the well has been completed, the wellhead is supported by the anchor casing. Therefore, the lifting forces may be exerting to the casing string due to fluids in the well. Table 8 shows calculated forces under the maximum working pressure tolerable to the wellhead fitting (20.7 MPa) with such casing diameters as suggested by the African Union 2016 code of practice. The weight of the wellhead considered here is six tons for the Christmas tree. Tests were made with 4 tons and 8 tons which proved that the greater the weight, the higher the downward forces and thus the smaller the safety factor. Additionally, the maximum wellhead working pressure must be considered carefully since great pressure reduces the safety factor.

TABLE 8: Tension on top of the casing anchoring the wellhead

CSG Grade K55	lb/ft	P _w (MPa)	d (m)	Xmass tree weight (Tonnes)	F _m (kN)	Tension force at top F _w (kN)	Min tensile strength (kN)	Cal DF	Min DF
13-3/8"	54.5	20.7	0.32	4	39	1,629	6,556	4.02	1.8
				6	59	1,609	6,556	4.07	1.8
				8	78	1,590	6,556	4.12	1.8

4.4.3 Radial stress conditions

After drilling the well to the target depth, slotted liners are run to allow geothermal fluid to flow through the well to the surface through the production casing. Liners are often hung in the production casing, therefore they are subject to compressive forces due to axial self-weight and helical buckling. Table 9 below shows the calculated compressive forces as f_c (kN) and the calculated design factor is also shown from top, middle and bottom of the liners. Hanging the liners inside the production casing reduces the compressive forces exerted at the bottom and thus increases the design factor. For instance, if the bottom

of liners was set to 1750 m the calculated design factor (DF) would be 2.78 instead of 2.70 at 1800 m. Values for the moment of inertia are calculated as for a hollow cylinder and the eccentricity is assumed for the worst case where the liner is lying aside which is given by hole inside diameter (ID) minus liner outside diameter (OD).

TABLE 9: Compressive stress in the un-cemented liner due to axial weight and helical buckling

lb/ft	Layers	Depth of liner L_z (m)	W_p (kg/m)	g (m/s ²)	A_p (m ²)	D (mm)	e (mm)	I_p (kgm ²)	f_c (kN)	Min yield stress (MPa)	Cal DF	Min DF
26	Top	10	38.7	9.81	0.005	177.8	38	1,986	779	379	486	1.0
	Middle	900	38.7	9.81	0.005	177.8	38	1,986	70,147	379	5.4	1.0
	Bottom	1,800	38.7	9.81	0.005	177.8	38	1,986	140,293	379	2.7	1.0

Table 10 shows the maximum burst pressure for all casing strings from surface to bottom. For each casing the burst pressure and design factors are calculated for three different points, the bottom, middle and top 10 m of the casing. Assumptions are made for the case of the casing being filled with cement slurry of 1.87 kg/l density and the annulus is filled with water at 50°C and of 0.988 l/kg mean specific volume.

TABLE 10: Maximum differential burst pressure of casing near shoe or stage cementing ports

CSG Grade K55		Length of casing L_z (m)	Slurry density ρ_c (kg/m ³)	Fluid column in casing L_f (m)	Density of water ρ_f (kg/m ³)	g (m/s ²)	Differential burst pressure Δp_i (kPa)	Internal yield pressure (MPa)	Cal DF	Min DF
20"	Top	10	1,870	10	988	9.81	86.5	14.5	167.6	1.5
	Middle	50	1,870	50	988	9.81	432.6	14.5	33.5	1.5
	Shoe	100	1,870	100	988	9.81	865	14.5	16.8	1.5
13-3/8"	Top	10	1,870	10	988	9.81	86.5	18.9	218.4	1.5
	Middle	225	1,870	225	988	9.81	1,947	18.9	9.7	1.5
	Shoe	450	1,870	450	988	9.81	3,894	18.9	4.9	1.5
9-5/8"	Top	10	1,870	10	988	9.81	86.5	32.5	375.6	1.5
	Middle	615	1,870	615	988	9.81	5,321	32.5	6.1	1.5
	Shoe	1230	1,870	1230	988	9.81	10,642	32.5	3.1	1.5

Table 11 shows collapse pressure and design factors for all cemented casing strings taking into consideration the top 10 m, the middle and the shoe of the casing as reference points. Assumptions made here are the casing being filled with water at 50°C (988 kg/m³ specific volume) while the annulus is filled with cement (1870 kg/m³ density). Assumptions in the worse scenario would be that the annulus is empty due to total loss of circulation and the casing is full of cement (inner-casing cementing is reported in appendix). Of course that scenario is placed above the water table and the internal differential forces increase dramatically but stay far below the internal yield so that the design factor is still safe.

During production operation, the worst condition that can occur are when the internal pressure at the casing shoe is approaching the wellhead pressure ($P_z = P_f$) or if the fluid inside the casing is pure steam. Table 12 below shows the calculated design factors for such a scenario and shows that the casing safety factor is 6.3. Assumption are made for the case of a wellhead operating at a pressure of 5 MPa but even though that pressure would be reduced to zero the casing can still hold because the calculated design factor should be 2.6 in such a case.

TABLE 11: Hoop collapse pressure during cementing

CSG Grade K55		Length of casing L_z (m)	Slurry density ρ_c (kg/m ³)	Density of water ρ_f (kg/m ³)	g (m/s ²)	Differential pressure on casing Δ_{pex} (kPa)	Collapse pressure (MPa)	Cal DF	Min DF
20" 94 lb/ft	Top	10	1,870	988	9.81	86.5	3.6	41.6	1.2
	Middle	50	1,870	988	9.81	432.6	3.6	8.3	1.2
	Shoe	100	1,870	988	9.81	865	3.6	4.2	1.2
13-3/8" 54.5 lb/ft	Top	10	1,870	988	9.81	86.5	7.6	90.1	1.2
	Middle	225	1,870	988	9.81	1,947	7.6	4.0	1.2
	Shoe	450	1,870	988	9.81	3,893.6	7.6	2.0	1.2
9-5/8" 47 lb/ft	Top	10	1,870	988	9.81	86.5	26.8	309.7	1.2
	Middle	615	1,870	988	9.81	5,321	26.8	5.0	1.2
	Shoe	1230	1,870	988	9.81	10,6642	26.8	2.5	1.2

TABLE 12: Hoop collapse pressure during production calculated for 13-3/8" casing with $P_z = P_f$.

BPD curve Pressure (P_f) (MPa)	Min wellhead operating pressure (MPa)	Differential external pressure (MPa)	Casing collapse pressure at shoe (MPa)	Cal DF	Min DF
9.26	5	22.6	26.8	6.3	1.2

5. DRILLING FLUIDS PROGRAMME

In order to specify and select drilling equipment (mud pumps and compressors), drilling fluids and hydraulics programmes, the programme needs to be prepared for each well section according to the bit sizes and depths. The programmes should consider at least the following aspects:

- The types of drilling fluids used and their properties;
- Minimum annular velocities necessary to ensure adequate removal of cuttings from the well;
- Pressure losses in the drill string and hole (for example, through the drill string, bit jets, annulus);
- Differential pressures between the circulating fluids in the well and the fluid pressures in the formations;
- Hydraulic horsepower requirements; and
- Ability to cool and quench the well.

The drilling fluid programme design aims to serve the following functions: cleaning the hole of cuttings, cooling the bit, lubricating the drill string, maintaining the stability of the borehole, helping to collect geological information, controlling the formation pressure, protecting the drilled formation from damage, supporting partial weight of the drill-string or casing, and transmitting hydraulic power to the bit and mud motor (African Union, 2016).

Successfully drilling a geothermal well is a critical task for both the service provider and the project developer. Many factors are involved and the focus of this chapter is on the use and importance of drilling fluids. Normally, each drilled section of the well is independent with regards to behaviour, drilling parameters and fluid specifications. Drilling fluids play a key role for the success of the drilling process and well cleaning and well stability are the most important aspects. Poor selection of drilling fluids both in quality and quantity may result in well collapse, a drill string getting stuck or even worse.

While designing the drilling fluids, a number of factors have to be considered, including the formation pressure, temperature and expected loss zones in the well. Apart from those technical consideration, the cost must be considered also because some fluids like air drilling package and foam seem to be more expensive.

5.1 Drilling fluid properties and reporting

Drilling fluid properties determine fluid behaviour in and outside the borehole. Simple field tests for viscosity and density help to understand the behaviour and to generate the mud report which includes additive inventory and cost among others. Appreciating the properties and changes that take place helps to predict the situation of the well (Chemwotei, 2011).

Basically, all drilling fluids have the same properties, only the magnitude varies. These properties include density, viscosity, gel strength, filter cake, water loss, pH value and electrical resistance. For the exploration in Kinigi, normal water based bentonite drilling fluid is planned to be used in the drilling programme. Each drilling section namely surface, anchor and production will have specific mud properties. The slotted liners section will be drilled with aerated water and sweeps of foam or hi-vis polymer pills.

5.2 Hole cleaning

The aim of hole cleaning is the transportation of all cuttings from the hole in a sufficient and fast way in order to avoid severe drilling challenges like, e.g. high torque which may lead to stem snapping, a stuck pipe which may lead to the loss of the stem, hole pack off, damaged formation, excessive over pull during trips and slow rate of penetration (Dayan, 2014). The well design sets 4 different drilling sections and each will be drilled with different bit size. The fluids to be used for each section are summarised here below.

5.2.1 The drilling fluid to be used while drilling the surface casing

This section is drilled with a 26" inch bit from surface to 100 m depth and the drilling fluid to be used is air with foam. The air hammer drilling (DTH) is the preferred drilling technique because of the challenges, which are expected in this section. The amount of drilling detergent needed for this section per well is estimated at 1000 l with reference to the Karisimbi drilling experience (EWSA, 2014) which used foam and a conventional tricone bit.

5.2.2 The drilling fluid to be used while drilling the anchor casing

This section will be drilled using bentonite based mud. Calculations shown in Table 13 estimate the amount of dry bentonite needed in tons and in total mud volume and the cartoon in Figure 9 shows how volumes were estimated.

TABLE 13. Estimated amount of bentonite required to drill 17-1/2" hole from 100 to 450m with 1.05 mud density

	Length (m)	Capacity (l/m)	Amount (m ³)
Mud tanks (~1/5)			30
20" csg. 94#/ft	100	185.32	18.5
17 1/2" bit	450	155.2	54
Theoretical volume			103
Excess, open hole 200%			109
Total slurry volume			211
Bentonite 5% by weight (T)			11

5.2.3 The drilling fluid to be used while drilling the production casing

This section is the longest to be drilled with mud in this programme. Figure 10 and Table 14 show mud volume and dry bentonite amount required for the process. The total amount of dry bentonite estimated for these two sections is 23 tons. We take into account the experience of KW01 where around 37 tons of bentonite were used to drill the whole well, even in the slotted liner section (EWSA, 2014). This estimation is pretty reasonable.

5.2.4 The drilling fluid to be used while drilling the slotted liners section

In this section hole cleaning became very challenging while drilling KW01. At that point, even bentonite-based mud was used to attempt cleaning the hole (EWSA, 2014). Under normal circumstances that should be avoided because the mud cake could seal off the permeability which is highly needed for the well discharge and production. This is considered to be the reservoir section and every loss of circulation is considered as a good sign for future feed zone. To use mud could in some ways seal off the feed zones or at least reduce permeability. For the purpose of this drilling programme, no bentonite will be used in this section, instead aerated water and foam will be used and if that is not enough, sweeps with hi-vis polymers need to be considered as a contingency plan. Figure 11 and Table 15 show the calculation of the expected volume of drilling fluid in this section, the slowest lag time estimated may not be more than 35 min for a fluid to complete the trip to the total target depth of 3000 m.

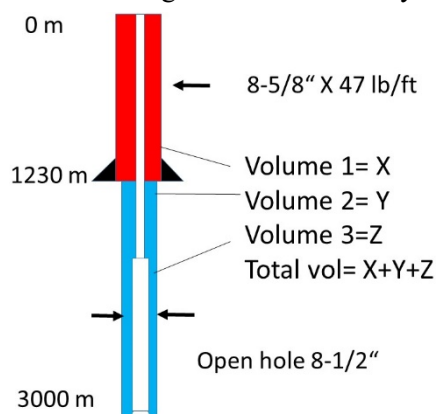


FIGURE 11: Lag time estimation for the slotted liner section

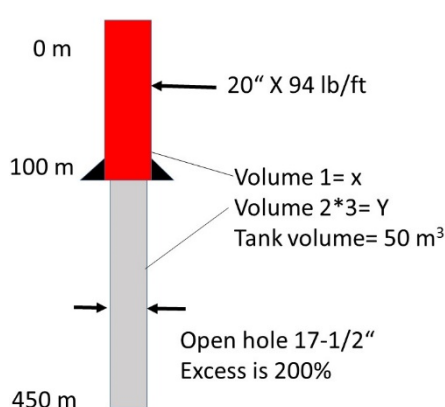


FIGURE 9: Estimated volume of mud required for anchor

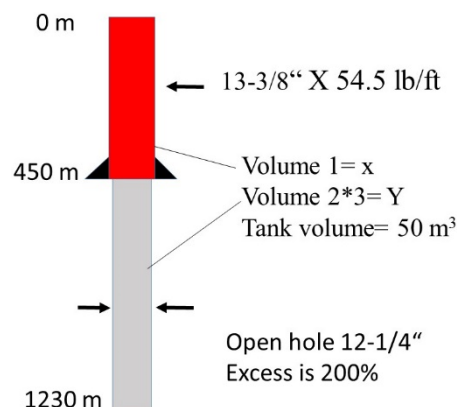


FIGURE 10: Estimation of volume of mud required for production

TABLE 14: Estimated amount of bentonite required to drill 12-1/4" hole from 450 to 1230 with 1.05 mud density

	Length (m)	Capacity (l/m)	Amount (m ³)
Mud tanks (~1/5)			30
13-3/8" csg. 54.5#/ft	450	80.64	36
12 1/4" bit	780	76.04	59
Theoretical vol.			126
Excess, open hole 200%			112
Total slurry volume			244
Bentonite 5% by weight (T)			12

TABLE 15: Estimation of lag time for the last well section

	Length (m)	Capacity (l/m)	Amount (m ³)
9-5/8" x 47 #/ft, 3 1/2" DP	1230	24.9	31
8 1/2" hole, 5" DP	1597	23.3	37
8 1/2" hole, 6 3/4" DC	173	13.5	2
Total	3000		70
Pumping rate	35	l/s	
Lag time	35	min.	

6. CEMENTING PROGRAMME

According to African Union (2016), the cementing programme shall be designed and undertaken in a manner which is most likely to ensure that the total length of annulus outside the casing is completely filled with a good quality of cement from the bottom of the respective well section to the top. Therefore, the main objective of any casing cementing is to ensure that the total length of the annulus is filled with sound cement that can withstand long term exposure to geothermal fluids and temperatures (Hole, 2008c).

6.1 Cement slurry design and composition

Cement slurry design depends mainly on well information from logs and drilling operation. That information includes but is not limited to: temperature measurements, calliper logs and cement bond logs (Khaemba, 2014). Designing a cement slurry for a geothermal well requires careful choice of cement, fluid loss additives, dispersants, silica flour, extenders, bentonite, mica flakes, friction reducers, retarders or accelerators, defoamers and mix water.

A number of properties have to be considered before the slurry is pumped into the annulus: slurry density, yield (m^3/mT), thickening time, fluid loss (m^3/h), free water (%), test temperature, compressive strength and filtration. Standardized test are carried out in a cement lab either on site or at the cementing service provider.

The cement slurry appropriate for geothermal wells has to be either mixed from neat cement or from blended cement. Portland cement manufactured accordingly to API specifications like API class A or API class G are commonly used.

The high temperature environments of geothermal reservoir systems require the in-blending of additional materials to ensure longevity of the cemented casing (Hole, 2008c). The use of blast furnace slag with class A Portland cement blended in the ratio of 30:70 provides a highly corrosion resistant cement with enhanced mixing and pumping properties. Additives other than silica flour are retarders, friction reducers, fluid loss control agents, and free water additives like Wyoming bentonite, and mica (Hole, 2008c).

6.1.1 Hole and casing volume calculations

Calculation of the total cement slurry volume requires to break the hole into a series of volume components including: casing volume (interval between the float collar and top), shoe track (interval between casing shoe and float collar), rat hole (interval between total drilled depth and casing shoe basically 2-3 m), casing-open hole annulus (volume between new casing and the open hole; just from new casing shoe depth up to the casing shoe of the previous casing) and finally casing-casing annulus (the volume of the annulus where two casings fit one inside the other) (Hole, 2008c). Therefore, the total volume of the slurry to be pumped including the excess which varies from 100% to 150% due to well conditions is given by the formula:

$$\text{Volume} = \text{shoe track} + (\text{rat hole} + \text{casing open hole annulus}) \times (1 + \text{excess}) + \text{casing casing annulus} \quad (31)$$

6.1.2 Cementing equipment

For cementing the casing, a number of equipment is important and a distinction can be made between in-hole and surface equipment. In hole equipment also known as casing accessories (Hole, 2008c) is equipment specifically designed to enable the cement placement procedure to be carried out. The float collar is fitted to the casing shoe, which has a non-return valve in order to allow the flow of the slurry

throughout the casing but prevents the flow from the well back into the casing at the end of the job. A float collar is fitted either between the first and second casing joint or between the second and third. It also has a non-return valve to ensure one-way flow of the slurry from casing to the annulus (Hole, 2008c). Other in hole equipment like casing centralisers, travelling plugs, string centralisers and tag-in adaptors for inner-string cementing are of great importance, too. On the surface, there is a cementing head for the casing or to connect to the drill pipes. Other important equipment is at the surface, including bulk pressure silos, cement mixing and pumping system just to name a few.

6.2 Cementing techniques

Casings in geothermal wells, unlike in oil and gas, are run back to the surface and are fully cemented back to the surface. This is mainly due to the high thermal stress imposed to the casing which requires a uniform cementation over its full length (Hole, 2008c). There are a number of techniques used for pumping the cement slurry into the annulus. In this section, three of them (casing cementing, inner string cementing and reverse circulation cementing) are discussed outlining the advantages of each method with regards to the situation in Kinigi and expected challenges.

6.2.1 Casing cementing

This technique involves pumping the cement slurry into the casing via a cementing head connected to the top of the casing and then at the end displacing the cement slurry from the casing into the annulus (Hole, 2008c). Travelling plugs are used to separate the cement slurry from the fluid in the casing and the displacement fluid. This technique can be carried out either in one stage or it can be done in two stages. This report will focus only on the single stage cementing as shown in Figure 12.

The procedure involves the casing string with all the required cementing accessories such as float collar,

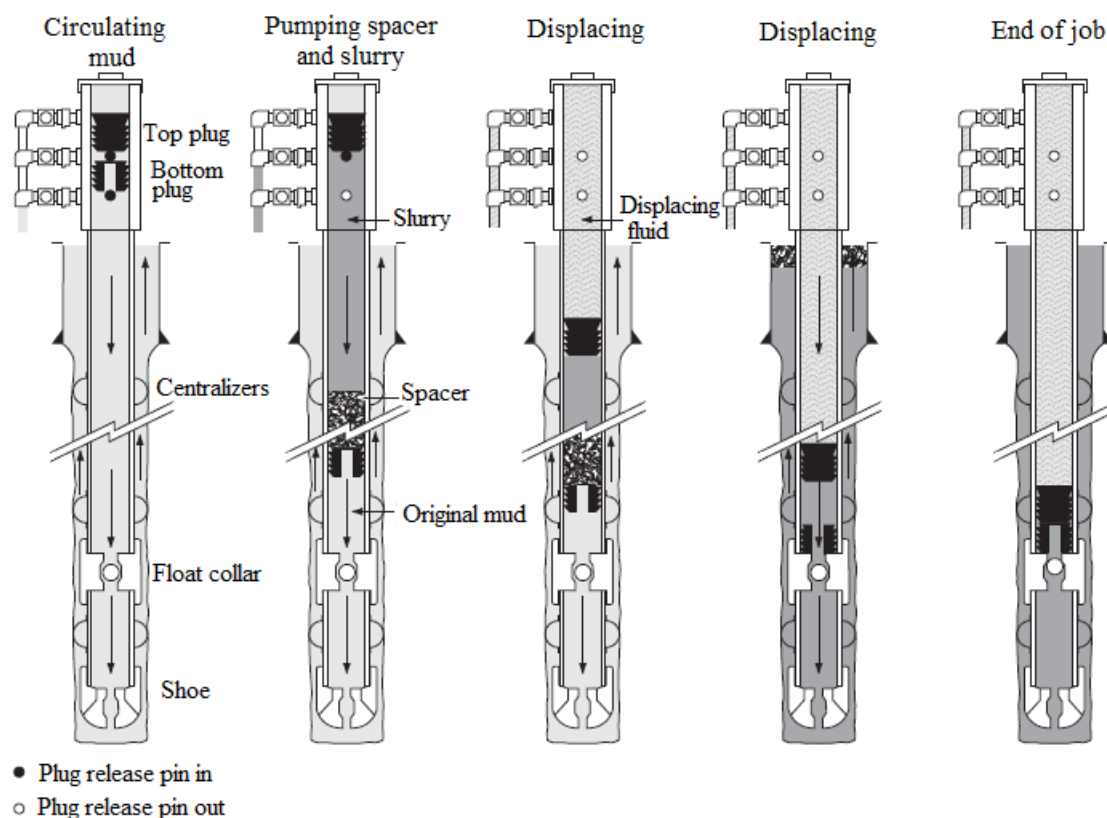


FIGURE 12: Through casing cementing single stage (Bett, 2010)

guide/float shoe and centralizers. The cementing head must be connected at the top of the casing so that cement plugs can be placed in the cementing head and released at the right moment (Khaemba, 2014).

For the success of the procedure of cementing, the well is cooled and cleaned by circulating water prior to slurry pumping. Then the bottom plug is released to wipe the casing clean and form a barrier between the spacer and the drilling fluid in the casing, followed by a spacer and then cement slurry (Khaemba, 2014). Once the bottom plug reaches the float collar, the diaphragm in the plug ruptures, allowing the spacer and slurry to flow through the plug, around the shoe and then up the annulus. The top plug is released at the end and displacing fluid is pumped. Once the plug reaches the float collar, it lands on the bottom plug and stops the displacement process.

6.2.2 Inner string cementing

When the casing has been run to depth, washed to bottom and the annulus has been circulated sufficiently, the casing is set in the rig rotary table and the inner cementing string is picked up; ran into the casing, and stabbed into the float collar receptacle (Hole, 2008c).

This technique allows large diameter casing to be cemented through and it provides a number of advantages including the reduction of the risk associated with cement slurry setting within the casing by reaching the annulus faster, no need for large diameter plugs, reduction in cement contamination, reduction of cement setting high up in the casing, reduced displacement time, and additionally, it allows

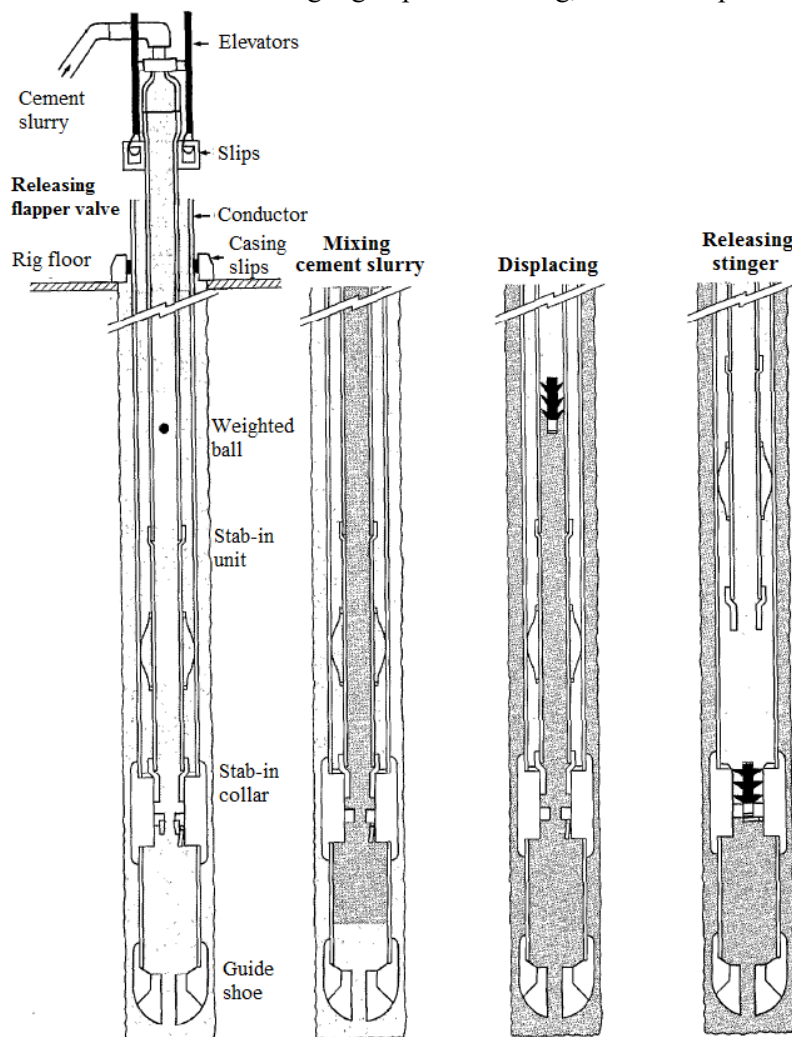


FIGURE 13: Cementing technique using inner string method (Bett, 2010)

the cement slurry to be pumped until returns are obtained on the surface (Khaemba, 2014). Possibly, only one backfill job is required, unlike the unlimited number of the ones done in Karisimbi KW01 (EWSA, 2014). Should large loss zones exist and cement returns are not seen at the surface, then the BOP is closed and the cement is immediately squeezed out of the casing/casing annulus with water to maintain an open path for reverse cementing (top-job).

Once the inner string is made up on the lower end with a sealing adapter and is stabbed into the float collar in order to seal the receptacle of the inner string adapter (Figure 13), sufficient water is circulated in the system to ensure that the stinger and annulus are clear of any debris and the well is cooled enough (Khaemba, 2014).

A variation of the inner string method is commonly in use in wells with large losses. First, a part of the calculated slurry volume is pumped to reach up to

the loss zone via the inner string. Then the rest of the slurry is pumped down the annulus via the kill line with the annular BOP closed. The cement may not reach the surface or sink a little, then it is a simple matter to fill up the annulus later as there is no water in the casing/casing annulus above the top of cement.

6.2.3 Reverse circulation cementing

This technique is mainly used in wellbores where loss of circulation has been encountered while drilling. The slurry is pumped down the annulus and at the same time the drilling fluid flows back up through the casing. Therefore, the float, differential fill up and wellhead equipment must be modified. This technique can provide advantages including the reduction of hydraulic horse power of cement slurry pumping equipment since gravitational flow works in favour of the slurry flow, reduction of the fluid pressure (equivalent circulating density-ECD), shorter slurry thickening time and shorter execution time since no displacement is required. However, this method has one main disadvantage which is the difficulty in ensuring a good cementing at the shoe (Hole, 2008c).

6.3 Calculated scenarios for the cementing of Kinigi exploration wells

Calculations presented in Table 16 show that under the same environmental conditions and while pumping the same amount of slurry the reverse method requires the shortest pumping time, then the inner string method with slightly longer pumping time, but the plug method requires considerably longer pumping time. The candidate cementing methods for Kinigi exploration are the plug method or inner string method if there are no losses at the time of cementing and a variation of the inner string method is preferred for the expected caves and loss of circulation sections. For the later method, the slurry is first pumped via the drill string and then the rest is immediately placed as a “top-job”. The reverse circulation cementing method may be considered for long production casing strings but not as a first option due to the uncertainties of good cementation at the casing shoe.

TABLE 16: Comparison between cementing techniques provided same volume of slurry and conditions

Methods	Materials	Surface casing	Anchor casing	Production casing
Inner string	Cement (T)	54	85	97
	Slurry volume (m ³)	41	65	73
	Time (min)	35	57	70
	Pump rate (l/min)	1,200	1,200	1,200
	Displacement (m ³)	0.7	4	11
In-casing	Cement (T)	54	85	97
	Slurry volume (m ³)	41	65	73
	Time (min)	45	83	100
	Pump rate (l/min)	1,200	1,200	1,200
	Displacement (m ³)	14	34	46
Reverse	Cement (T)	54	85	97
	Slurry volume (m ³)	41	65	73
	Time (min)	34	54	61
	Pump rate (l/min)	1,200	1,200	1,200
	Displacement (m ³)	-	-	-

Calculations show that 240 tons of dry cement is required for one well. The Karisimbi experience shows that for well KW01 the cement used was around 250 tons of dry cement (EWSA, 2014). As shown in EWSA (2014) cementing and WOC at KW01 took more than 15 days. Considering the day rate drilling contract that means high cost and by reducing the cementing time, especially for many backfills, by

modifying the placement procedure, the cost can be reduced. Three analysed cementing methods require the same amount of dry cement and slurry volume but there is a difference in pumping time where the reverse circulation cementing uses significantly less time. Nevertheless, both inner string and reverse circulation cementing show almost similar advantages with regards to pumping time and the choice between the two will be dictated by other conditions like loss of circulation during drilling for example. Taking all parameters into account, the inner-string cementing method, with or without the variation of the “top-job”, could be the most suitable method for the Kinigi exploration wells.

The cement of API class G is the preferred because it can be used with accelerators and retarders to cover a wider range of well depths and temperatures. Laboratory testing of the cement and water samples in special equipment is required to properly support the cementing plans.

7. PERMANENT WELLHEADS

The African Union (2016) suggests components of the permanent wellhead to include:

- The outer flanges of the master valve directly exposed to the fluid in the top of the well; and
- The bottom of the CHF (casing head flange) attaching the wellhead to the casing, plus any spools or other components included between these items.

The preferred wellhead configuration is for two side valves of at least three inches (Figure 14). It has to conform to API Spec 6A or API Spec 6D and needs to be designed to comply with maximum pressure conditions and temperature exposure possible at the surface under static or flowing conditions (Hole, 2008b).

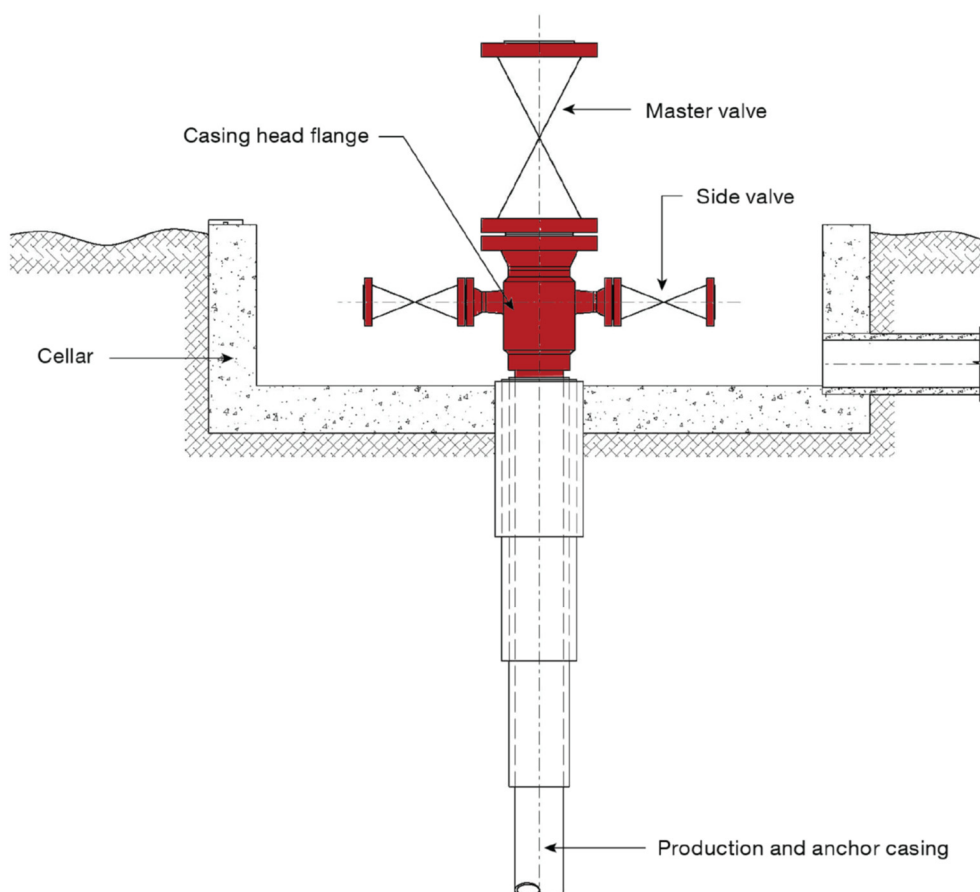


FIGURE 14: Typical permanent wellhead (African Union, 2016)

The fluids at the wellhead may vary from water, steam (either saturated or superheated), cold gas or a mixture of these fluids. In some circumstances, pressure and temperature conditions may be equal or close to downhole ones because of fluids in the well (Hole, 2008b).

7.1 Wellhead materials

Material used in wellhead components has to be suitable for use under all expected service temperatures and pressures. The pressure ratings are de-rated as temperature increases in accordance with ANSI B16.5 and API 6A (Hole, 2008b).

7.2 Wellhead design factors

According to African Union (2016), the wellhead design factor for the permanent wellhead has to include provisions for corrosive environment, it needs to minimise the rise and fall of the wellhead during operation and orientation of wellhead equipment relative to waste sumps and attachment of surface pipework to the wellhead components needs to be guaranteed.

With the assumption that the top 25 m of each casing string will expand freely through their expected temperature range, the wellhead has to provide service without interference from projecting components anchored to other casing strings. The CHF has to be connected to the anchor casing by casing threading for sizes and API pressure ratings as set out in the Table 17. However, if the design pressure exceeds these values, it is advised to connect the wellhead using a weld-on CHF.

TABLE 17: Recommended pressure limits for threaded CHFs (AU, 2016)

Casing size	Pressure rating
4-1/2" to 10-3/4"	Up to 5000 psi (34.5 MPa)
11-3/4" to 13-5/8"	Up to 3000 psi (20.7 MPa)
16" to 20"	Up to 2000 psi (13.8 MPa)

If welding is used to connect the CHF to the casing, it should be conducted using a procedure appropriate to the materials. If H₂S is expected to be present in the fluids, welding should comply with ANSI/NACE MR 175/ISO 15156. All welds have to be inspected and tested for defects including the ability to seal against an applied pressure equal to the maximum design pressure that the section will be exposed to (AU, 2016).

7.3 Wellhead valves

The entire wellhead including the master valve, expansion spool and CHF should allow for a clear bore diameter (1/8" or 3 mm) larger than any tool expected to run into or through the valve. The sealing should be accomplished by metal-to-metal seals. Figure 15 shows working pressure derated for flanges and valves conforming to above cited standards.

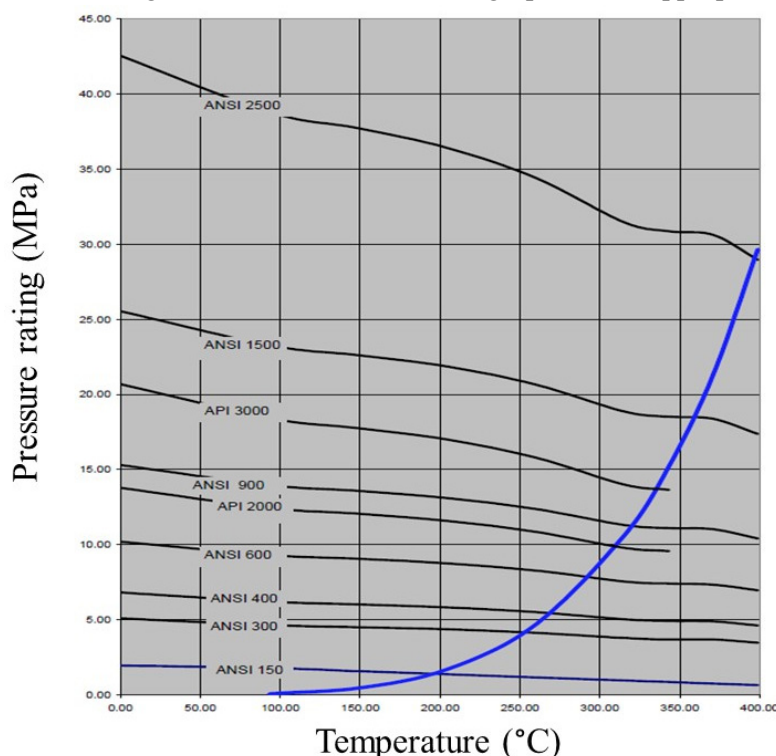


FIGURE 15: Wellhead working pressure derated for temperature modified from Hole (2008b)

8. WELL CONTROL PROGRAMME

Well control aims at preventing the flow of formation fluids into the wellbore during drilling and thereby avoiding spontaneous boiling that may lead to a kick. When the drilling process reaches a fractured or permeable layer where the pore pressure is higher than the static head of the drilling fluid, there is an inflow into the wellbore, which may result in a kick, which must be controlled. Failing to control a situation like that may result in disaster, which will at least cost money and in the worst case can even cost lives (Finger and Blankenship, 2010).

Some geothermal fields have pore pressure, which is greater than the hydrostatic column (e.g. Tiwi in the Philippines and parts of Salton Sea in California, USA) at shallow depths, usually due to high temperatures. However, most geothermal fields are under-pressured (the pore pressure is lower than the fluid pressure in the wellbore), therefore, influx may occur if there is a reduction in wellbore pressure due to either circulating hot fluids from deeper depths to the surface or loss of circulation (Finger and Blankenship, 2010).

8.1 Blowout preventer BOP

The apparatus used to control a kick is called blowout preventer (BOP) or blowout prevention equipment (BOPE). It comprises 5 types of devices to shut off the wellbore and prevent fluid flow out: rotating heads, annular preventers, pipe rams, blind rams and shear rams. The basic function of each is to shut off the wellbore but they operate in slightly different ways.

8.1.1 The rotating head or rotating BOP

This device forms a seal around the drill pipe that rotates with it. This is enabled by encasing the drill pipe seal and bearings in a sealed housing. The main purpose of this device is to keep hot fluids from reaching staff on the rig floor and can handle pressure up to 10.3 MPa.

8.1.2 Annular preventer

This is either an inflatable bladder or an elastomer that is forced into a conical cavity by a hydraulic piston; either way, the flexible element seals around drill pipe, casing, drill collars, or irregularly shaped component of the drill string.

8.1.3 Pipe rams

These are two sliding gates, each with a semi-circular cut-out that come together from each side of the drill pipe. The hole in the centre fits and seals around the outside diameter of the drill pipe.

8.1.4 Blind rams

These are also sliding gates, but there is no hole in the centre. They are used when the drill pipe is outside of the hole.

8.1.5 Shear rams

A last resort, the sliding gates have sharp, hardened, overlapping edges and are designed to sever anything hanging in the wellbore. If these are used, anything cut by them falls into the hole and becomes fish. Most of geothermal BOP stacks do not include shear rams when drilling, although they can be an important part of workovers that involve removing damaged casing from the wellbore.

8.2 Blowout preventers per well sections

The Kinigi area is not expected to have any kind of shallow high-temperature fluids which might cause a kick in the surface section drilling process. Therefore, no BOP stack is provided for this section. However, for the anchor casing, production casing and slotted liners sections BOPs are provided and they will be tested to different ranges of pressure. Table 18 below shows sizes of BOP stacks per section and the eventual pressure test it undergoes before drilling resumes. Each BOP stack connected to the casing CHF is required to fit the two cylinders, for instance the 21-1/4" BOP has a CHF of 20" since it is connected on the top of 20" casing. Figure 16 shows a typical BOP stack arrangement for a drilling process carried out with water or mud but not aerated fluid. For drilling with foam and to increase safety, a rotating head preventer is installed above the annular. The flow line connects to the rotating head so a razor is not required.

TABLE 18: BOP stack size per section and pressure test required

Section	Size of hole (inches)	OD casing (inches)	BOP stack size (inches)	Pressure test (PSI)
Anchor casing	17-1/2	13-3/8	21-1/4	500
Production casing	12-1/4	9-5/8	13-3/8	1000
Slotted liner	8-1/2	7	9-5/8	2000

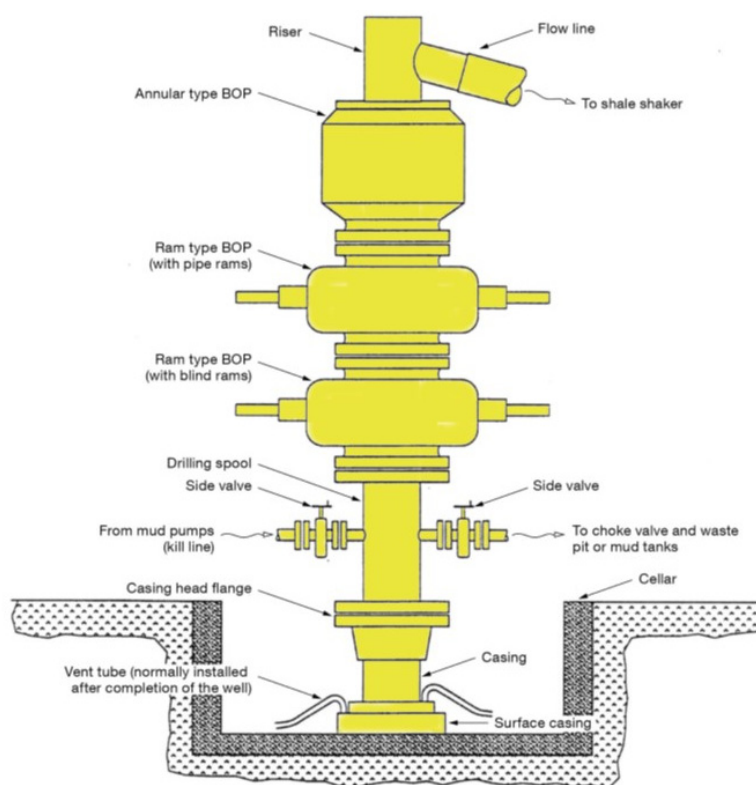


FIGURE 16: Typical drilling wellhead for use while drilling with water or mud (non-aerated) (African Union, 2016)

9. WELL COMPLETION AND WELL TESTING PROGRAMME

At the conclusion of drilling the last section and running the slotted liner, the inner cemented casing needs to be logged in order to confirm casing condition and provide a baseline record for subsequent condition monitoring (African Union, 2016). Well logs and tests carried out on geothermal wells can

include pressure and temperature surveys, and pressure measurements taken at depth of primary permeability while pumping water at stepped and variable flow rates. Well logging and testing can be done during drilling as well as after the drilling operation is completed. After the well has heated up, it may build up wellhead pressure on its own and once opened will self-flow or it may have to be stimulated to flow. The most common stimulation methods are by air compression where the water level is depressed to a level with high temperatures and then rapidly released or by air lift pumping via an air-line and using compressed air for the lift.

10. CONCLUSIONS

Exploration drilling in Kinigi prospect area around 12 km to the east of Karisimbi will be referenced to the previous experience because some of the environmental and drilling conditions are expected to be similar.

In the well, three drilled sections will be cased and cemented back to the surface; namely surface, anchor and production casing sections. The slotted liner section will be open and the liners will be hung in the production casing. Based on the AU code of practice for geothermal drilling, the surface casing minimum depth is set at 100 m, the anchor casing at 450 m and the production casing shoe at 1230 m in order to exclude cold inflows. The total planned depth is 3000 m targeting a deep geothermal reservoir estimated between 2 and 5 km in Kinigi area.

Apart from the surface section, which will be drilled with foam and air hammer in order to overcome the challenges expected to be present in that layer, the other cemented casings sections will be drilled with mud while the last open-hole section for the slotted liner will be drilled with aerated water and foam or water and hi-vis polymer pills.

Cementing the casing will be done preferably using the inner-string method. Calculations made including excess of 150% show a requirement of 180 m³ of cement slurry and 250 tons of dry cement at 1.87 kg/l of slurry density per well. By selecting a placement procedure according to the condition of the well prior to cementing the total time is expected to be considerably reduced.

This study focused on well design, casing tally and safety for the eventual mechanical loads, cementing programme and mud programme design. But other components of a drilling programme like bottom hole assembly, corrosion and erosion stress on casing due to assumed chemistry of the reservoir and so on must be assessed in further research works.

It is highly recommended that prior to exploration drilling in a new field the well design and drilling programme is established from the available data and assumptions before engaging in contract for drilling services or materials.

ACKNOWLEDGEMENTS

Allow me to use this opportunity and express my gratitude to everyone who supported me throughout the course of this geothermal training programme. I am thankful for their aspiring guidance, invaluable constructive criticism and friendly advice during the project work. I am sincerely and specifically thankful to the people listed down here for particular reasons.

On my list the first person to thank is Mr. Lúðvík S. Georgsson, Director of UNU-GTP. Sir, you and your team will always be highly ranked in my memory because of many things but the one which touched my heart the most is a well-structured and organized way of working. You handle everything

in simple and calm manner that I wish to practice in my life. I would like to express my gratitude to my supervision team: Mr. Gunnar Skúlason Kaldal, my direct supervisor and Mr. Sverrir Thórhallsson, co-supervisor, for the continuous support of my personal development and related research, for your patience, motivation, and immense knowledge. Your guidance helped me in all the time you have been there for me and the hard work you made it simple as if my life was dedicated to meet good people like you.

My wife Jeannine and children Ange, Mediateur and Darcy, you are the real sign of the benediction from God in my life and your immense love and support is the source of energy which helps me to strive and achieve goals always. I will always love you more. The Managing Director of EDCL Mr. Emmanuel KAMANZI and Mrs. Uwera Rutagarama, Manager for Geothermal Development, you are my best bosses and good friends ever, please receive here my little sign of honour and gratitude.

All of you good people from all over the world we met here at UNU and you helped me during this time, I will always remember you. I really thank you.

Prima facie, I am grateful to the Almighty God for the good health and wellbeing that were necessary to complete this training.

NOMENCLATURE

P_{frac}	= In situ fracture pressure of a formation (MPa);
P_f	= Pore pressure (MPa) and is assumed to be the boiling point pressure;
V	= Poisson's ratio values are averaged from the values of Gercek (2006);
S_V	= Overburden pressure (vertical pressure due to the weight of overlying formations (MPa));
$\rho(z)$	= Density of the overlying rock;
z	= Depth;
$F_{csg\ air\ wt}$	= Air weight of casing (kN);
$F_{csg\ contents}$	= Weight of internal contents of casing (kN);
$F_{displaced\ fluids}$	= Weight of fluids displaced by casing (kN);
$F_{hookload}$	= Surface force suspending casing that is subjected to gravitational and static hydraulic loads (kN);
ρ_{if}	= Density of a section of fluids with constant density within a casing (kg/l);
ρ_{ef}	= Density of a section of fluids with constant density within an annulus (kg/l);
L_{if}	= Vertical length of a section of fluid having the same density – within the casing (m);
L_{ef}	= Vertical length of a section of fluid having the same density – within the external annulus (m);
L_z	= Depth of casing (m);
L_f	= Height above casing shoe of cement column inside casing (m);
W_p	= Unit weight of casing (kg/m);
D	= Casing outside diameter (mm);
d	= Casing inside diameter (mm);
g	= Acceleration due to gravity (9.81 m/s ²);
F_p	= The tensile force at the surface from casing weight (kN);
L_w	= Depth of water level in well (m);
A_p	= Cross sectional area of pipe (mm ²);
n	= Mean specific volume of hot fluid (m ³ /kg);
f_b	= Maximum stress due to bending (MPa);
E	= Modulus of elasticity (MPa);
q	= Curvature of deviated hole (° per 30 m);
F_c	= Compressive force due to heating (kN);

F_r	= Resultant axial force (kN);
T_1	= Neutral temperature (temperature of casing at the time of cement setting) (°C);
T_2	= Maximum expected temperature (°C);
a	= Coefficient of linear thermal expansion (°C ⁻¹);
F_t	= Tensile force due to cooling (kN);
T_3	= Minimum temperature after cooling well (°C);
F_w	= Lifting force due to wellhead pressure (kN);
P_w	= Maximum wellhead pressure (MPa);
F_m	= Net downward force applied by the wellhead due to its own mass and pipe work reactions (kN);
f_c	= Total extreme fibre compressive stress due to axial and bending forces (MPa);
e	= Eccentricity (actual hole diameter minus D) (mm);
I_p	= Net moment of inertia of the pipe section, allowing for slotting or perforating (mm ⁴);
R_j	= The connection joint efficiency;
$\Delta P_{internal}$	= Differential on casing during cementing (MPa);
L_f	= Total vertical length of fluid column in an annulus (m);
ρ_c	= Cement slurry density (eg 1.87 kg/l);
ρ_f	= Density of water in annulus (kg/l);
R_i	= Temperature reduction factor (ratio);
F_t	= Maximum tensile stress (MPa);
P_w	= Maximum wellhead pressure (MPa);
$\Delta P_{external}$	= Differential pressure on casing during cementing (MPa).

REFERENCES

- African Union, 2016: *Code of practice for geothermal drilling*. African Union, Regional Geothermal Coordination Unit, 150 pp.
- API, 2005: *Specification for casing and tubing: ISO 11960:2004, petroleum and natural gas industries – steel pipes for use as casing or tubing for wells*. American Petroleum Institute, Washington DC, API Specification 5CT (8th ed.), 291 pp.
- Bar-Cohen, Y., and Zacny, K. (eds.), 2009: *Drilling in extreme environments – penetration and sampling on Earth and other planets*. Wiley-VCH Verlag GmbH and Co. KGaA, Weinheim, Germany, 825 pp.
- Bett, E.K., 2010: Geothermal well cementing, materials and placement techniques. Report 10 in: *Geothermal training in Iceland 2010*. United Nations University Geothermal Training Programme, Reykjavík, Iceland, 99-130.
- BGR, 2008: *Geothermal potential assessment in the Virunga geothermal prospect, Northern Rwanda*. Federal Institute for Geosciences and Natural Resources (BGR), final report, 104 pp.
- Bourgoyne, A.T., Chenevert, M.E., Milllheim, K.K., and Young Jr., F.S., 1986: *Applied drilling engineering*. Society of Petroleum Engineers, US, SPE Textbook Series, 2, 502 pp.
- Chemwotei, S.C., 2011: Geothermal drilling fluids. Report 10 in: *Geothermal training in Iceland 2011*. United Nations University Geothermal Training Programme, Reykjavík, Iceland, 149-177.
- Davis, J., Parenteau, K., Schappert, G., Tahmourpour, F., and Griffith, J., 2004: Reverse circulation of primary cementing jobs – Evaluation and case history. *Proceedings of the IADC/SPE Drilling Conference*, Dallas, Texas, United States, paper 87197, 8 pp.
- Dayan, G.M., 2014: Drilling fluid design for geothermal wells. Report 11 in: *Geothermal training in Iceland 2014*. United Nations University Geothermal Training Programme, Reykjavík, Iceland, 123-156.

- Eaton, B.A., 1969: Fracture gradient prediction and its applications in oilfield operations. *J. Petroleum Technology*, 246, 1353-1360.
- EDCL, 2015: *Kinigi geothermal exploration drilling project. Application 03-DP-06-RW*. EDCL, submitted to GRMF (unpubl. report).
- EWSA, 2014: *KW01 completion report*. Ministry of Infrastructure, Energy, Water and Sanitation Authority, report.
- Finger, J., and Blankenship, D., 2010: *Handbook of best practices for geothermal drilling*. Sandia National Laboratories, Albuquerque, New Mexico, United States, 84 pp. Web: artikel-software.com/file/geothermal%20drilling%20handbook.pdf.
- Gercek, H., 2006: Poisson's ratio values for rocks. *Internat. J. Rock Mechanics & Mining Sciences*, 44, 1-13.
- Hategekimana, S., and Twarabamenye, E., 2007: *The impact of wetlands degradation on water resources management in Rwanda: the case of Rugezi Marsh*. Pennsylvania State University, College of Information Sciences and Technology, Pennsylvania, United States, 18 pp. Website: citeseerx.ist.psu.edu/viewdoc/download?doi=10.1.1.511.9188&rep=rep1&type=pdf
- Hole, H., 2008a: Geothermal well design - casing and wellhead. In: *Petroleum Engineering Summer School, Dubrovnik, Croatia, Workshop*, 26, 7 pp.
- Hole, H., 2008b: Geothermal well completion tests. In: *Petroleum Engineering Summer School Dubrovnik, Croatia Workshop*, 26, 5 pp.
- Hole, H., 2008c: Drilling fluids for drilling of geothermal wells. In: *Petroleum Engineering Summer School, Dubrovnik, Croatia, Workshop*, 26, 8 pp.
- JICA, 2014: *Project for preparation of electricity development plan for sustainable geothermal energy in Rwanda*. JICA, interim report presented for EWSA, Rwanda (unpublished).
- Khaemba, A.W., 2014: Well design, cementing techniques and well work-over to land deep production casing in the Menengai field. Report 17 in: *Geothermal training in Iceland 2014*. United Nations University Geothermal Training Programme, Reykjavík, Iceland, 295-324.
- Namugize J.N., 2011: Preliminary environmental impact assessment of geothermal exploration and development in Karisimbi, Rwanda. Report 28 in: *Geothermal training in Iceland 2011*. United Nations University Geothermal Training Programme, Reykjavík, Iceland, 669-708.
- New Zealand Standard, 1991: *Code of practice for deep geothermal wells*. Standards Association of New Zealand, Wellington, New Zealand, 93 pp.
- New Zealand Standard, 2015: *Code of practice for deep geothermal wells*. Standards Association of New Zealand, Wellington, New Zealand, 102 pp.
- Rogers, N.W., James, D., Kelly, S.P., and DeMulder, M., 1998: The generation of potassic lavas from the Eastern Virunga province, Rwanda. *J. Petrology*, 39, 1223-1247.
- Shalev, E., Browne, T., Wameyo, P., Hochstein, M., Palmer, J., and Fenton, R., 2012: *Geoscientific surveys of the Rwanda Karisimbi, Gisenyi, and Kinigi geothermal prospects. Final Report*. Institute of Earth Science and Engineering (IESE), University of Auckland, New Zealand, 217 pp.
- Thompson, J.M., 2010: *Hydraulic hammer drilling technology to replace air hammer drilling in deep BHE design*. University of Iceland and University of Akureyri, The School of Renewable Energy Science, MSc thesis, 100 pp.
- Wreden, C., Watters, J.T., Giroux, R., Nikolaou, M., Macfarlan, K., Richardson, D.A., 2014: Deepwater reverse-circulation primary cementing: applicability and technical path forward for implementation. *Proceedings of the Offshore Technology Conference*, Houston, Texas, United States, paper OTC 25194-MS, 19 pp.

APPENDIX I: Assumed pressure on which the casing design is based

Depth below water level	Hydrostatic pressure at 20°C	Hydrostatic pressure at BPD (P _r)	BPD temperature	Hole depth from surface	Expected rock type	Average Poisson ratio (v)	Overburden pressure (S _v)	Fracture pressure (P _{frac})	Density of the overlying rock ρ(z)
m	MPa	Mpa	°C	M			MPa	MPa	(wet) (X10 ³ Kg/m ³)
		0		0	Basanite	0.35	0.08	0.04	2.98
		0		50	Basanite	0.35	1.54	0.83	2.98
		0		150	Basanite	0.35	4.46	2.40	2.98
0	0	0	100	200	Basanite	0.35	5.92	3.19	2.98
10	0.10	0.09	119	210	Hawaiite	0.35	6.22	3.39	2.98
20	0.19	0.19	132	220	Hawaiite	0.35	6.51	3.59	2.98
40	0.39	0.36	149	240	Hawaiite	0.35	7.09	3.98	2.98
60	0.58	0.54	162	260	Hawaiite	0.35	7.68	4.38	2.98
80	0.78	0.72	172	280	Hawaiite	0.35	8.26	4.78	2.98
100	0.98	0.89	180	300	Hawaiite	0.35	8.85	5.17	2.98
150	1.47	1.32	196	350	Hawaiite	0.35	10.31	6.16	2.98
200	1.95	1.75	208	400	Hawaiite	0.35	11.77	7.15	2.98
300	2.93	2.57	227	500	Hawaiite	0.35	14.69	9.10	2.98
400	3.91	3.37	242	600	Hawaiite	0.35	17.62	11.04	2.98
500	4.89	4.16	254	700	Hawaiite	0.35	20.54	12.98	2.98
600	5.87	4.93	264	800	Hawaiite	0.35	23.46	14.91	2.98
800	7.82	6.43	281	1,000	Hawaiite	0.35	29.31	18.75	2.98
1000	9.78	7.87	295	1,200	Granite	0.33	31.51	19.51	2.67
1200	11.70	9.26	306	1,400	Granite	0.33	36.75	22.80	2.67
1500	14.70	11.27	321	1,700	Granite	0.33	44.60	27.69	2.67
2000	19.60	14.40	339	2,200	Granite	0.33	57.70	35.73	2.67
2500	24.50	17.30	354	2,700	Granite	0.33	70.80	43.65	2.67
3000	29.30	19.90	365	3,200	Granite	0.33	78.65	48.84	2.67

APPENDIX II: Minimum design factors (AU, 2016)

Stress condition	Load case	Minimum DF
Triaxial	As indicated in the AU code point 2.10.1.2	1.25
Axial	Tensile force during running and cementing casing	1.8
	Fluid lifting on anchor casing	1.8
	Thermal load on anchor casing (where applicable)	1.4
	Helical buckling due to self-weight plus thermal load (uncem. liner)	1
Hoop	Internal pressure a shoe during cementing	1.5
	Wellhead internal pressure (shut-in steam/gas after drilling) where wellhead is fixed to the casing	1.8
	External pressure collapse (during cementing)	1.2
	External pressure collapse (during production)	1.2



UNITED NATIONS
UNIVERSITY

UNU-GTP

Geothermal Training Programme

Orkustofnun, Grensasvegur 9,
IS-108 Reykjavik, Iceland

Reports 2016
Number 30

OPTIMISED PIPELINE ROUTE DESIGN FOR CONNECTION OF A MAKE-UP PRODUCTION WELL: CASE STUDY OF WELL OW-906 FOR OLKARIA IV POWER PLANT, KENYA

Daniel Wanga Odongo

Kenya Electricity Generating Company Ltd. - KenGen

P.O. Box 785-20117, Naivasha

KENYA

dwanga@kengen.co.ke

ABSTRACT

Over the course of the life of a geothermal project, the steam flow will generally decline due to natural drawdown effects or changes in the reservoir as the resource is exploited. This requires that from time to time, the steam is made up by connecting additional wells to the existing steam gathering system. This process can be very challenging given the constraints offered by an already existing framework. Moreover, it requires that proper selection of the pipeline routing and tie-in points is done to ensure that the make-up well is connected in the most cost effective manner. Consideration must be given to the existing separator stations and pipelines, to ensure that there is no additional expensive construction of steam field infrastructure, unless utterly necessary. Focus should be placed on ensuring that existing spare capacities are first exhausted before more infrastructure is put up. This work attempts to give a preliminary outline for the impending connection of well OW-906 to the already existing Olkaria Domes steam field that serves the Olkaria IV plant in Olkaria, Kenya. The main focus area is the use of Variable Topography Distance Transform (VTDT) method to identify the optimal pipeline routes that would allow connection of make-up wells as cost effectively as possible. This work shows that the use of VTDT has guided the selection of the optimal route for connection of make-up well OW-906. The cheaper option is construction of a new separator station at an optimal position near the well head and then connecting the steam pipeline to the nearest main steam pipeline from separators SD1 and SD4. Brine reinjection is also to be channelled to the nearest reinjection well OW-906A. This work is intended to provide a guide for the future when new wells make-up wells are to be connected to an existing steam gathering infrastructure.

1. INTRODUCTION

1.1 General

The Olkaria geothermal resource is located in the Kenya Rift valley, about 120 km from Nairobi, the capital city of Kenya. Geothermal activity is widespread in the Kenyan rift and 14 major geothermal prospects have been identified (Figure 1). The Olkaria geothermal field is inside a major volcanic

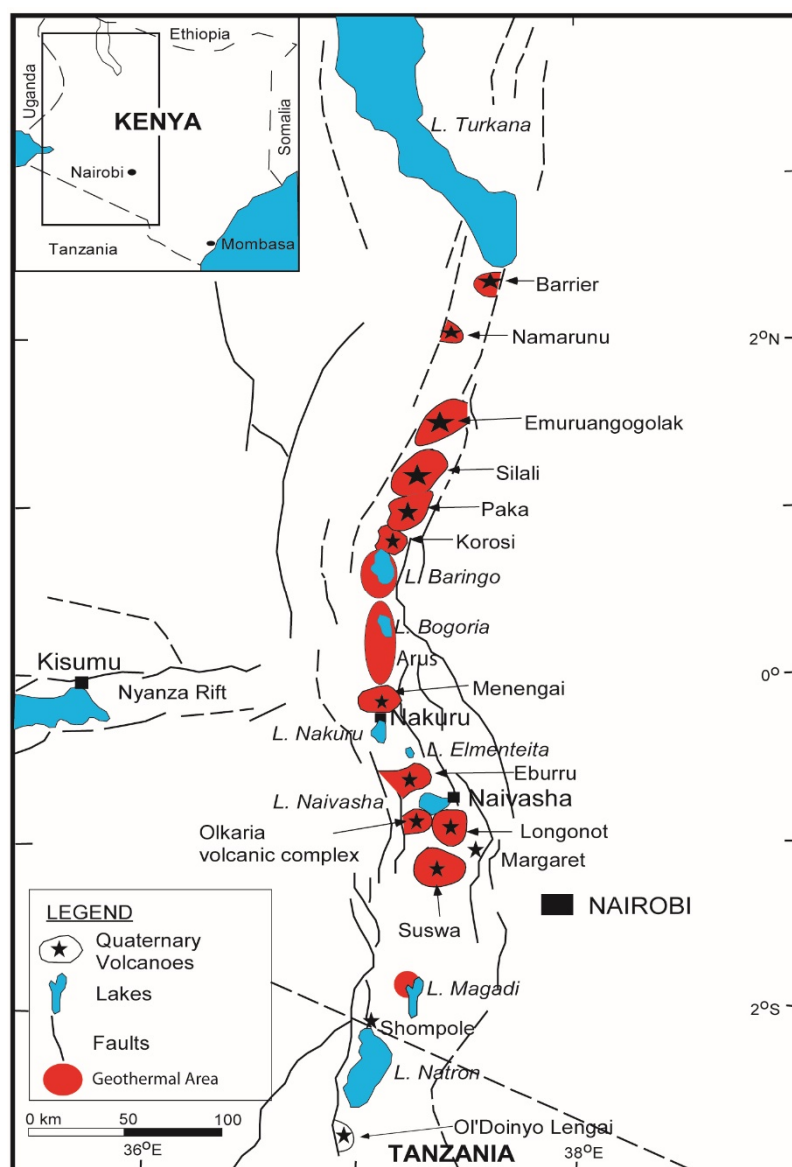


FIGURE 1: Greater Olkaria geothermal area within the Great Rift Valley of Kenya (Ofwona, 2010)

complex that has been cut by N-S trending normal rifting faults. It is characterized by numerous volcanic rhyolitic domes, some of which form a ring structure, which has been interpreted as indicating the presence of a buried volcanic caldera (Mannvit, 2012). Olkaria is surrounded by further geothermal prospects, such as Suswa, Longonot and Eburru (Figure 1).

Exploration of the Olkaria geothermal resource started in 1956 with deep drilling commencing in 1973. A feasibility study in 1976 indicated that development of the geothermal resource was feasible and consequently a 30 MWe power plant was constructed (Ouma, 2010). Three power plants were installed in the field before 2014, producing electricity; Olkaria I with 45 MWe capacity, Olkaria II with 105 MWe capacity and Olkaria III with 120 MWe capacity. The first two are operated by KenGen, the largest power producer in Kenya owned 70% by the government and 30% in private hands. The third plant is operated by OrPower 4, an independent power producer (IPP). The Olkaria I power plant consists of 3 units commissioned between

1981 and 1985 while Olkaria II, which also has 3 units, was commissioned between 2003 and 2010. The Olkaria III power plant was commissioned in two phases between 2000 and 2012. In addition, the geothermal resources of the northwest part of the Olkaria area are utilized both for direct heat and small scale electricity generation by the Oserian flower farm. KenGen has also recently started operating wellhead units of 2-5 MWe capacity which are now (mid 2016) generating about 70 MWe from 14 wells. Olkaria IAU and Olkaria IV are the latest power plants to be commissioned within the Olkaria geothermal field. Olkaria IV plant was commissioned in June 2014 as part of the Greater Olkaria 280 MW project that represented the largest one-off geothermal development project in the world. It is a 140 MWe plant utilising 2×70 MWe turbines. Olkaria IAU is an extension of Olkaria I, commissioned in December 2014, and also with 140 MWe utilized through 2×70 MWe turbines (units 4 and 5). The parts of the Olkaria geothermal field being utilized or under development have been subdivided into sectors that include Olkaria East (Olkaria I), Olkaria Northeast (Olkaria II), Olkaria West (Olkaria III) and Olkaria Domes (Olkaria IV).

The Olkaria IV plant is a single-flash plant utilising 2×70 MWe condensing double-flow double entry turbines, direct contact condenser and a wet cooling tower. Design turbine inlet pressure is 6 bar and

condenser pressure 0.075 bar. The steam field consists of 21 production wells, 7 brine reinjection wells and 2 condensate reinjection wells.

The steam field was initially designed to be operated at 7 bar. An optimisation study carried out later by Mannvit Consortium (Mannvit, 2012) recommended that the steam field pressure be raised to at least 11 bar to limit the effects of silica scaling. This was due to the fact that the wells serving these power plants were drilled to a depth of 3000 m on average. This was much deeper than the earlier average well depths of 1200 m and 2200 m for developed fields of Olkaria East and Olkaria Northeast, respectively. They therefore tapped from a more silica-rich environment due to the higher reservoir temperatures at depth. This fact had not been fully considered during the design phase. A separation pressure of 6-7 bar would cause silica supersaturation during flashing and therefore encourage silica scaling that would ultimately clog the sub-surface piping. This separation pressure change effectively reduced the available steam by reducing the steam reserve margin. KenGen has already implemented this by introducing control valves between the steam field and the power plant to maintain the steam field pressure at 12 bar. The result of this was as indicated in Table 1.

TABLE 1: Olkaria IV steam flow effects due to separation pressure change

	Separation pressure 6-7 bara	Separation pressure 12 bara
Total available steam flow (kg/s)	322	308
Plant steam demand (kg/s)	280	280
Reserve steam margin (kg/s)	42	28
Reserve steam margin (%)	15	10

The reduction in the reserve steam margin limits the flexibility of carrying out any maintenance work or dealing with emergencies. In addition, five of the production wells serving the Olkaria IV plant are wells that are not self-starting and would need to be stimulated if there is a shutdown.

The brine reinjection capacity of the wells in Olkaria IV steam field was also highly understated. Seven reinjection wells were allocated for brine reinjection but after commissioning of the system, it was confirmed that the 236 kg/s of brine generated from the separation stations of the field could comfortably be taken care of by 3 wells. Figure 2 shows the location of well OW-906 in the Olkaria IV steam field.

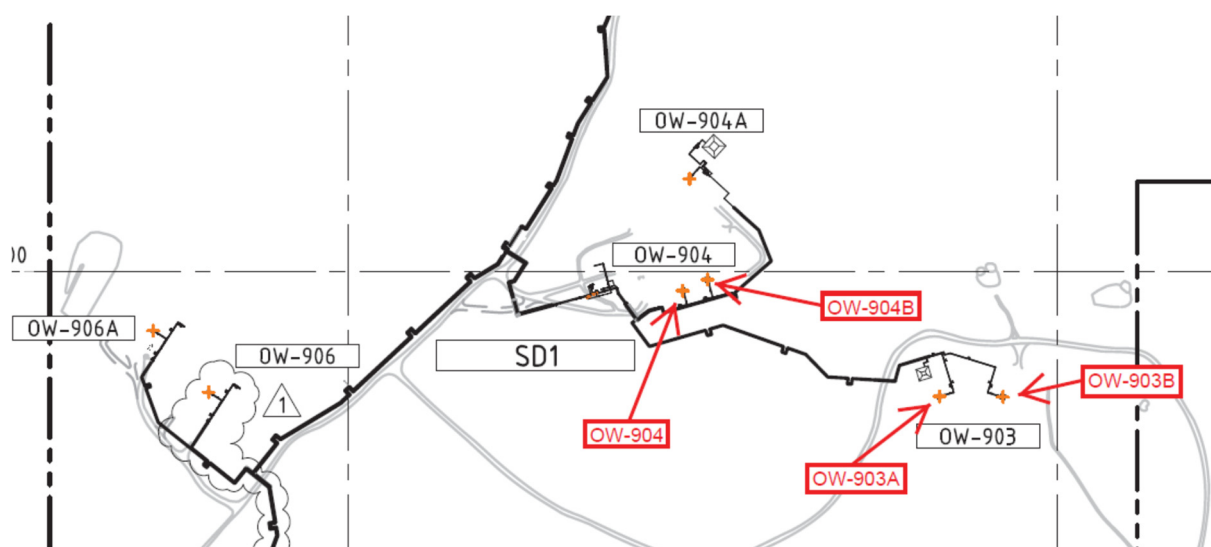


FIGURE 2: Location of well OW-906 within Olkaria IV

OW-906 was initially intended to be a production well but was connected as a reinjection well due to understated reinjection capacity. This work intends to redesign this well as a production well using the pipe design optimisation tools to find the most cost effective pipe route, pipe diameter, separator positioning, reinjection well to use and reinjection pipeline route.

1.2 Objectives

The overall goal of this work is to develop a methodology that can in the future be used to connect make-up wells optimally, considering that make-up wells would be connected within already existing infrastructure which would offer several obstacles to the intended pipeline routes. This would require that the route and placement of facilities is optimised to limit cost of connection of these wells. The main objectives of this project are the following:

- Obtain the optimal pipe route for two-phase, steam and brine to connect well OW-906 to the existing Olkaria IV steam field;
- Obtain optimal separator location for the well;
- Obtain optimal reinjection pipeline route and well for its brine;
- Determine optimal pipe sizes for two-phase pipeline and steam;
- Predict the expected pressure drops for two-phase, steam and brine pipelines;
- Ultimately increase reserve steam margin of Olkaria IV power plant.

1.3 Literature review

Geothermal wells generally produce a mixture of steam and water. The mixture is then separated into distinct phases of steam and water with minimum pressure drop. The steam is then conveyed to the power plant and the brine to suitably located reinjection wells by gravity or by pumping. A typical 30 MW plant would require about 5-6 production wells and 2-3 reinjection wells (DiPippo, 2016). These wells may be drilled on sites distributed across the field or several may be drilled from a single well pad using directional drilling. In either case, a piping system is needed to gather the fluids and transport them to the powerhouse for steam and to the points of disposal for water. The steam gathering system can therefore be defined as a network of pipelines from production wells to separator stations, separator stations to power plants for steam, separator stations to reinjection wells for separated brine, separator vessels and accompanying equipment to allow for safe operations (Onyango, 2015).

Two-phase flow

Two-phase flow in horizontal pipelines can be in different regimes. (Zarrouk and Purnanto, 2016). Bubble flow is formed when there are steam or gas bubbles moving at approximately the same velocity as the liquid. Plug flow is formed when there are alternating plugs of liquid on the upper part of the pipe. Stratified flow is formed when liquid flows on the lower part of the pipe with the steam or gas phase flowing on the upper part of the pipe. Wave flow is similar to stratified flow but the steam or gas phase moves at a higher velocity causing disturbances on the interface causing waves. Slug flow is formed when the wave of the liquid is picked up by the faster moving steam or gas and then moves faster than the average liquid velocity. Annular flow is formed when steam or gas moves at a higher velocity in the centre of the pipe, surrounded by a slower moving liquid on the walls of the pipe. Mist flow is formed when almost all the liquid is entrained as droplets in the steam or gas. Figure 3 shows two-phase flow patterns in horizontal flow.

Flow characteristics vary from annular to open channel depending on the ratio between the steam and the water. Slug flow generates a huge dynamic load and should be avoided. Baker and Mandhane maps can be used together with superficial velocity to predict the flow pattern in a two-phase pipe. Pressure drop in two-phase flow is very difficult to determine. However, correlations have been used with a fair amount of accuracy. Common methods that have been used are homogeneous method, Harrison-

Freeston method, Zhao-Freeston method, Lockhart-Martinelli method, Friedel method and Brill-Murkerjee method.

Steam flow

Pipelines are generally larger due to the higher specific volume of steam. Steam velocity is typically 30-40 m/s and pressure drop can accurately be determined using the Darcy-Weisbach equation and Colebrook friction factor equations. Pipelines are also having drain pots installed to remove condensate that develops in the steam pipelines as a result of pressure drops and losses as the steam flows along. This also helps to keep the steam as dry as possible, typically between 99.5% and 99.9% dry (Zarrouk and Purnanto, 2014).

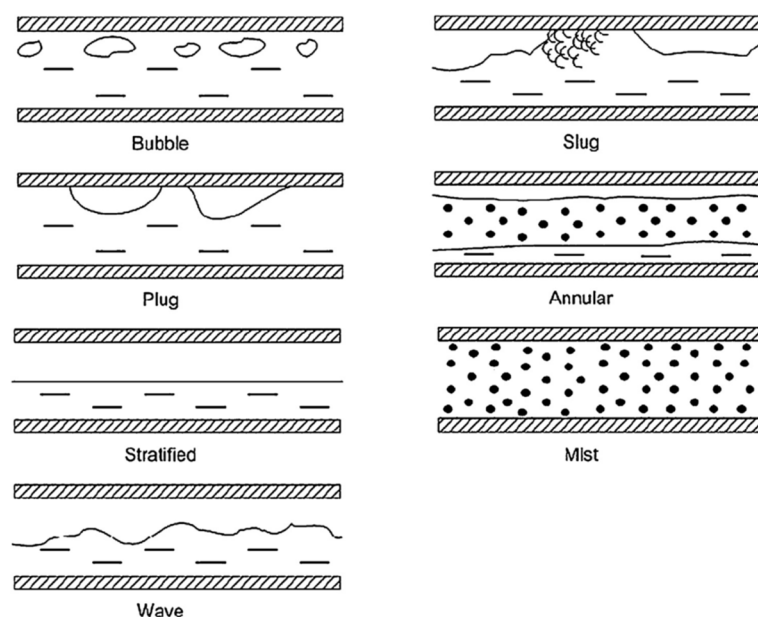


FIGURE 3: Two-phase flow patterns in horizontal flow (Zarrouk and Purnanto, 2014)

Brine flow

Brine leaving the separator is usually in saturation and care must be taken to ensure that no point along the brine pipeline is below the saturation pressure. Reinjection wells are therefore designed to gain static head (Henriquez and Aguirre, 2011). Due to the low elevation, brine reinjection wells experience the highest hydrostatic pressure. Brine flow can be anything between open channel flow and full flow depending on the geometry of the pipe. The slope required for open channel flow can be determined using the Chezy's or Manning equation. Full flow velocity is usually on the order of 2-3 m/s and the pressure drop can be estimated using the Darcy-Weisbach equation and Colebrook friction factor equations. In addition, brine pipe design should also consider erosion, corrosion, silica scaling, brine residence time, dynamic load from potential slug flow situations and provision for draining the load whenever it is required.

Pipe routes and separators

Geothermal pipe route selection has been studied extensively with algorithms developed to optimise pipe routes. One of them is the Variable Topography Distance Transform (VTDT) by De Smith (2005). Kristinsson (2005) used the VTDT to determine shortest possible route for geothermal pipelines. More work was done by Kjaernested (2011) that included incorporation of visual effect optimised codes to the VTDT algorithms. This was applied in a geothermal field in Iceland with good results. Multiple Weight Distance Transform (MWTD) was initially suggested by Kristinsson (2005) to optimally locate separators and power plants. This algorithm was later used by Kjaernested (2011) to locate separators in the Hverahlid geothermal field.

Geothermal separators are classified as either horizontal or vertical (DiPippo, 2016). The vertical cyclone design is based on reports and experience in Wairakei and Kawerau in the 1950s and 1960s by the modelling work of Lazalde-Crabtree (1984). Horizontal separators are flash vessels where the mixture will enter from the top and travel horizontally while flashing occurs. The main concern is to have the mixture velocity sufficiently lowered to give the water particles enough time to settle to the bottom before steam leaves from the top. Separators locations within the production field can be in three ways. Separators can be located near the wellhead taking two-phase fluid from individual wells, they can be at satellite locations collecting two phase fluid from a number of wells or they can be centralised and located close to the power plant and collecting two-phase fluid from long pipelines from all the wells (DiPippo, 2016). Steam and brine pipelines then move from these stations to the power plant and

reinjection wells respectively. The option that is selected depends on various design considerations like pressure drop, cost limits, environmental considerations and pipeline obstacles among others.

The cost of geothermal steam gathering systems depends on a number of factors, the key factor being distances from wells to power plant, flowing pressure of the wells and fluid chemistry. Onyango (2015) puts the estimate of steam gathering systems at about 10% of the overall project cost. Henriquez and Aguirre (2011) estimate the costs to be a lot higher at US\$600 to US\$1200 per metre, and summarise the cost to be made up of material 30%, fittings 10%, installation labour 25%, installation equipment 10%, pipe supports 15% and management 10%. Hance (2005) estimates the cost at 15-25 USD/inch of diameter, per foot of length for carbon steel which are the most commonly used material. Kalinci et al. (2007) provides estimates of pipe and bends cost and installation cost that indicates that all these costs will generally increase as the nominal pipe diameter increases. Table 2 shows a summary of pipe and pipe bends costs and installation costs for pipe and bends depending on pipe nominal diameter.

TABLE 2: Pipe and bend cost and installation costs (Kalinci et al., 2007)

Pipe nominal diameter (m)	Pipe cost (USD/m)	Pipe installation cost (USD/m)	Pipe bend cost (USD/unit)	Pipe bend installation cost (USD/unit)
0.20	50	30	150	25
0.25	70	45	300	50
0.30	90	55	450	100
0.35	115	79	700	225
0.40	150	110	950	275
0.45	175	130	1350	375
0.50	215	150	1750	403

2. DESIGN CONSIDERATIONS

Successful delivery of geothermal piping design requires a number of structured processes which are customized to the developer and to specific project requirements (Umanzor et al., 2015). These processes may vary but steps shown on Figure 4 appear to be commonly used.

Step 1: Design criteria.

The client and the designer agree on the design criteria to be applied in the entire project. Relevant criteria such as pipe sizing, layout considerations, insulation methodology, design codes and standards are typical components of this step.

Step 2: Process design

The process design should be advanced at this stage since all the required steam field data and well test reports will have been obtained. This step involves the preparation of heat balance and mass balance equations.

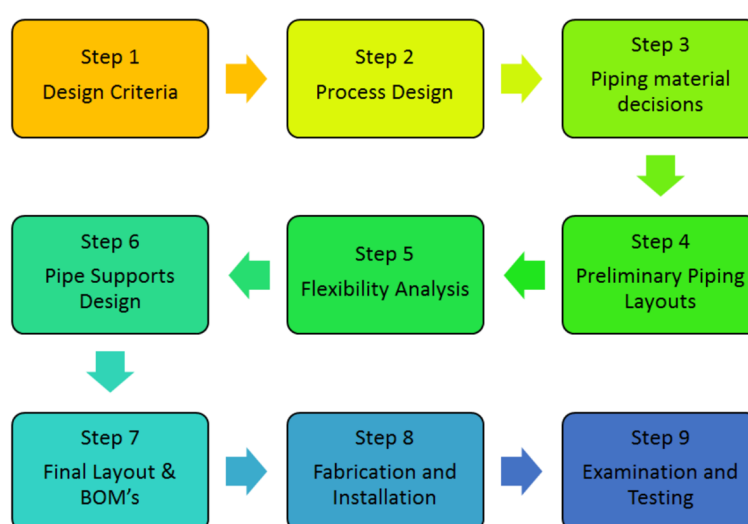


FIGURE 4: Piping design processes (Umanzor et al., 2015)

Step 3: Pipe material decision

From the well discharge reports, chemistry of the fluid at the intended operating conditions will determine the materials to be used in this design.

Step 4: Preliminary piping layout

This step is critical to ensure the constructability of the pipeline and that stakeholders are considered to avoid a redoing of the design. Variable topography distance transforms (VTDT) can be used in this stage to get a preliminary route for the pipeline and help to estimate the length of the pipeline.

Step 5: Flexibility analysis

This step uses design software to carry out stress analysis and compatibility of the design to design code requirements. This will normally be done using stress analysis computer packages and models.

Step 6: Pipe supports design

Normally the pipeline will be designed before the supports but the construction is usually the reverse. This requires that the civil engineers are involved early in the process. The loads on the pipe due to thermal and seismic loading can sometimes be unrealistically large due to insufficient flexibility or inappropriate piping layouts and restraints. This must be looked at early to avoid expensive and structurally impractical situations.

Step 7: Final layouts and Bill of Materials (BOM)

After final layouts are agreed from step 4, these can be prepared and the bill of materials also generated from this.

Step 8: Fabrication and installation

The pipe is fabricated and equipment installed. Changes can be made over the course of fabrication but should be only minor.

Step 9: Examination and testing

Pipeline is commissioned and tested. Amongst others, procedures and tests may involve steam blowing and hydro testing.

2.1 Pipe route selection

Pipe route selection depends on the fluid to be transmitted through the pipes (Onyango, 2015). Distance Transforms (DT) is one of the methods that can be used to obtain optimal paths across the landscape. DT is an image processing algorithm which works with a digital binary image that consists of object points and non-object points. The shortest (unobstructed) path across a uniform horizontal or tilted plane is a Euclidean straight line. If the surface is tilted, the surface will have a non-zero path gradient with respect to the underlying horizontal plane (Figure 5 path P_1). Calculating exact Euclidean

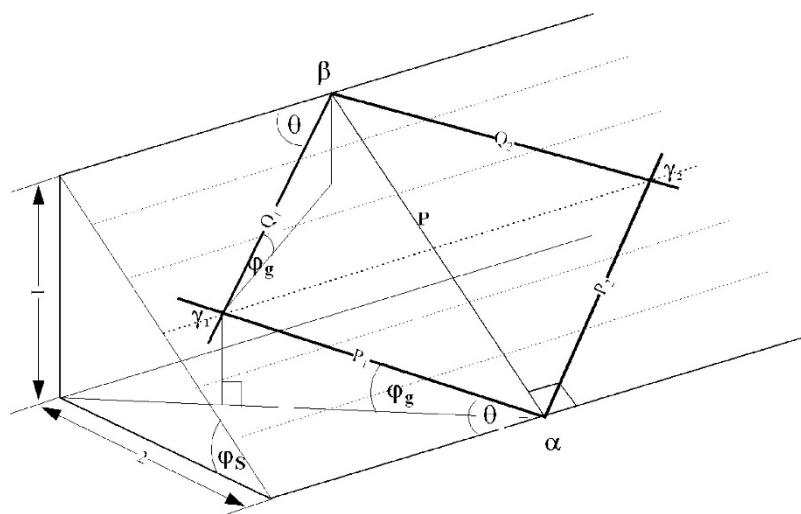


FIGURE 5: Gradient constrained path on a sloping planar surface (De Smith, 2005)

distances can be extensive and inefficient and it is better to compute local distances within space to estimate the global distances (De Smith, 2005). This can be done using Chamfer matrices.

Variable topography distance transforms

Variable topography distance transforms (VTDT) can be used to find the optimal paths across landscape when this is presented in digital elevation format. VTDT can be used to find shortest distances in cells in 3-D landscape by introducing constraints. If each cell is represented with latitude, longitude and altitude, the height difference makes it possible for the slope between two adjacent cells to be calculated by the algorithm. A VTDT algorithm gives the shortest path by using digital transforms on digital elevation models and introducing constraints. The central function in VTDT algorithm is given Equation 1:

$$S = \frac{(H_{i+m,j+n} - H_{i,j})}{c_{m,n}} \quad (1)$$

where s is slope, $c_{m,n}$ is the distance from origin to the point (i,j) , and s_{max} is maximum allowable slope.

The digital elevation model is a 2-D matrix where every element H_{ij} represents the height in the corresponding surface location (i,j) . The gradient and slope constraints are implemented in variable topography distance transform by the condition:

$$\begin{aligned} \text{If} & \quad (H_{i+m,j+n} - H_{i,j} < \Delta H_c) \\ \text{and} & \quad s < s_{max} \\ \text{then} & \quad d_{i,j} = \min(d_{i+m,j+n} + c_{m,n}, d_{i,j}) \\ \text{else} & \quad d_{i,j} = d_{j,i} \end{aligned} \quad (2)$$

where the height $(H_{i+m,j+n})$ and slope s are calculated from the altitudes of the cells in question from the digital elevation map (DEM). The critical values of height difference (ΔH_c) and slope s_{max} are user defined (Jónsson, 2014).

2.2 Pressure drop

It is important to ensure that the pressure drop in transmission pipelines is minimised. High pressure drops in the steam pipelines can cause loss of power generation if it causes the steam to get to the power plant at pressures below the design turbine inlet pressure. In the brine pipelines, high pressure drops can lead to pressure of brine going below saturation pressures. This would lead to the brine boiling and causing undesirable flow regimes.

Single-phase pressure drop

Single-phase pressure drop is fairly easy to estimate with equations available for it. The total pressure drop in single phase consists of frictional and static pressure drop. The static pressure loss will be the difference in elevation between the end and start of the pipe. Friction pressure loss will be a function of fluid velocity, pipe internal diameter, pipe roughness and Reynolds number. Single-phase pressure drop per unit length is calculated from the Darcy-Weisbach equation given in Equation 3:

$$\frac{dp}{L} = f \frac{\rho v^2}{2D_i} \quad (3)$$

where dp is pressure drop (Pa); L is length of pipe (m); f is friction factor; ρ is the fluid density (kg/m^3); v is flow velocity (m/s); and D_i is the pipe internal diameter (m).

Equation 1 above can also be rewritten in head loss terms as Equation 4 or 5:

$$dp = \rho g dh \quad (4)$$

$$\frac{dh}{L} = f \frac{v^2}{2gD_i} \quad (5)$$

where dh is head loss

Reynolds number Re is then calculated using Equation 6:

$$Re = \frac{\rho v D_i}{\mu} \quad (6)$$

The friction factor f can then be calculated from the Colebrook-White equation (Equation 7) or approximated from the Moody diagram:

$$\frac{1}{\sqrt{f}} = -2 \log_{10} \left(\frac{\epsilon}{3.7D} + \frac{2.51}{Re\sqrt{f}} \right) \quad (7)$$

where ϵ is pipe roughness height (m).

Two-phase pressure drop

Two-phase pressure drop consists of frictional, elevation change (gravitational) and momentum change terms. The main parameters extensively used are mass velocity and void fraction. Generally, two-phase flow is modelled as single phase but with a correction factor. The correction factors will vary depending on the flow regime present. The models used in pressure drop estimation can be classified as either homogeneous or separated. Homogenous ones assume that the liquid and gas phases flow at a common velocity while the separated ones assume these two phase flow at different velocities. In both models the void fraction will need to be calculated. This refers to the cross-section of the pipe occupied by the gas phase as a fraction of the total pipe cross-sectional area. Pressure drop per unit length in two phase flow can be represented by the basic conservation of momentum equation (Equation 8) as:

$$\left(\frac{dp}{dz} \right) = \left(\frac{dp}{dz} \right)_f + \left(\frac{dp}{dz} \right)_a + \left(\frac{dp}{dz} \right)_g \quad (8)$$

where $\left(\frac{dp}{dz} \right)$ = total pressure drop per unit length; $\left(\frac{dp}{dz} \right)_f$ = pressure drop per unit length due to friction; $\left(\frac{dp}{dz} \right)_a$ = pressure drop per unit length due to acceleration; $\left(\frac{dp}{dz} \right)_g$ = pressure drop per unit length due to elevation (gravity).

The equation of the individual components can be defined by means of momentum balance. The equation can be rewritten as Equation 9:

$$\frac{dp}{dz} = \frac{\tau P}{A} + m^2 \frac{d}{dz} \left(\frac{(1-x)^2}{\rho_L(1-\alpha)} + \frac{x^2}{\rho_G \alpha} \right) + g \rho_{TP} \sin \theta \quad (9)$$

where τ is wall shear stress (N/m²); P is channel periphery (m); A is channel cross-sectional area (m²); m is mass flow rate (kg/s); x is steam fraction; α is void fraction; ρ_L is liquid density (kg/m³); ρ_G is vapour density (kg/m³); ρ_{TP} is two-phase density (kg/m³); θ is angle between pipe axis and horizontal; and g is gravitational acceleration (m/s²).

The two-phase density ρ_{TP} and dynamic viscosity μ_{TP} are defined as the average density or dynamic viscosity between the two phases (liquid and gas), and is dependent on the model selected (Freeston, 1982). For the homogenous flow model it will be defined by the Equation 10 and 11:

$$\frac{1}{\rho_{TP}} = \frac{x}{\rho_G} + \frac{1-x}{\rho_L} \quad (10)$$

$$\frac{1}{\mu_{TP}} = \frac{x}{\mu_G} + \frac{1-x}{\mu_L} \quad (11)$$

where μ_G is gas phase dynamic viscosity (kg/ms); and μ_L is liquid phase dynamic viscosity (kg/ms)

For the separated flow model it will be defined by Equation 12:

$$\rho_{TP} = \alpha \rho_G + (1 - \alpha) \rho_L \quad (12)$$

From Equations 10-12 above, a void fraction α correlation is needed. Harrison modified the correlation by Butterworth (Freeston, 1982) to obtain Equation 13:

$$\alpha = \frac{1}{1 + \left(\frac{1-x}{x}\right)^{0.8} \left(\frac{\rho_G}{\rho_L}\right)^{0.515}} \quad (13)$$

Generally, the frictional pressure drop contributes to most of the total pressure drop but the calculation can be inaccurate for oversized or undersized pipes. The frictional pressure drop is usually referred to as that of a single phase flowing under certain hydrothermal conditions. The term *Two-Phase Multiplier* is the relating factor and presents two-phase frictional pressure drop as that of the gas or liquid phase flowing alone. Frictional multipliers for gas and liquid are defined by Equations 14 and 15:

$$\phi_G^2 = \frac{(dp/dz)_{TP}}{(dp/dz)_{fG}} \quad (14)$$

$$\phi_L^2 = \frac{(dp/dz)_{TP}}{(dp/dz)_{fL}} \quad (15)$$

Friction multiplier use approach is used in the *Lockhart-Martinelli* correlation as discussed by Hewitt (1982). The multiplier is obtained by defining the Lockhart-Martinelli parameter X (Equation 16) also referred to as the pressure drop ratio:

$$X^2 = \frac{(dp/dz)_{fL}}{(dp/dz)_{fG}} = \left(\frac{1-x}{x}\right)^{1.8} \left(\frac{\rho_G}{\rho_L}\right) \left(\frac{\mu_G}{\mu_L}\right)^{0.2} \quad (16)$$

From the standard Darcy-Weisbach pressure drop equation (Equation 17), and using the gas phase, single-phase pressure drop can now be rewritten as:

$$\left(\frac{dp}{dz}\right)_G = f \frac{L}{2D_i} \rho_G v_G^2 \quad (17)$$

and the resulting two phase pressure drop will then be represented by Equation 18:

$$dp_{TP} = \phi^2 f \frac{L}{2D_i} \rho_G v_G^2 \quad (18)$$

where ρ_G is gas density (kg/m³); v_G is gas flow velocity if flowing alone in pipe (m/s); D_i is pipe internal diameter (m); dp_{TP} is two-phase pressure drop (Pa), L is effective pipe length (m); f is friction factor; and ϕ is two-phase multiplier

Steam velocity can then be calculated from Equation 19:

$$v_G = \frac{4mx}{\rho_G \pi D_i^2} \quad (19)$$

The two-phase pressure drop will then be also rewritten as Equation 20:

$$dp_{TP} = \frac{8\phi^2 L f m x}{\pi^2 D_i^5 \rho_G} \quad (20)$$

Friction factor f is a function of the Reynolds number Re and pipe roughness ϵ . Reynolds number can then be calculated for the gas phase from Equation 21:

$$Re_G = \frac{\rho_G v_G D_i}{\mu_G} \quad (21)$$

Similarly as in single-phase pressure drop, the friction factor f can then be calculated from the Colebrook-White equation (Equation 7) or approximated from the Moody diagram. A simplified explicit equation (Equation 22) may also be used:

$$f = \frac{0.25}{\left(\log_{10} \left(\frac{\epsilon}{3.7 D_i} + \frac{5.74}{Re^{0.9}} \right) \right)^2} \quad (22)$$

Friedel method uses a two-phase multiplier similar to the *Lockhart-Martinelli* method to convert the liquid phase pressure drop into two-phase pressure drop. This method first defines two-phase density as in Equation 23:

$$\rho_{TP} = \left(\frac{1}{\rho_G} + \frac{1-x}{\rho_L} \right)^{-1} \quad (23)$$

The two-phase multiplier is then determined using the Weber number We , Froude number Fr and constants E , F and H , which can be calculated using inputs from saturated water and steam properties and Equations 24 and 25:

$$Fr = \frac{m^2}{g D_i \rho_{TP}^2} \quad (24)$$

$$We = \frac{m^2 D_i}{\rho_{TP} \sigma} \quad (25)$$

where σ is surface tension (kg s^{-2}).

The constants E , F and H can be calculated from Equations 26-28:

$$E = (1-x)^2 + x^2 \frac{\rho_L f_{GX}}{\rho_G f_{LX}} \quad (26)$$

$$F = x^{0.78} (1-x)^{0.24} \quad (27)$$

$$H = \left(\frac{\rho_L}{\rho_G} \right)^{0.91} \left(\frac{\mu_G}{\mu_L} \right)^{0.19} \left(1 - \frac{\mu_G}{\mu_L} \right)^{0.7} \quad (28)$$

where f_{GX} is the friction factor for mass flux with steam properties and f_{LX} is the friction factor for mass flux with liquid properties.

The two-phase multiplier is then calculated from Equation 29:

$$\phi_L^2 = E + \frac{3.24 F H}{Fr^{0.045} We^{0.035}} \quad (29)$$

The two-phase pressure drop can then be calculated using the multiplier and the liquid phase pressure drop using Equation 30:

$$dp_{TP} = \phi_L^2 \frac{2 f_{LX} (m/A)^2}{\rho_L D_i} \quad (30)$$

Recommendations from Hewitt (1982) concerning the correlations to be used are as follows:

1. For $\mu_L/\mu_G < 1000$, Friedel correlation should be used;
2. For $\mu_L/\mu_G > 1000$, and $m > 100$, Chisholm correlation should be used; and
3. For $\mu_L/\mu_G > 1000$, and $m < 100$, Martinelli correlation should be used.

Pressure loss in bends and fittings

Pressure drop in pipe bends and fittings can be done by use of the equivalent length procedure. The pipeline, discussed here, has a similar number of bends as the ones discussed in Ouma (1992). An additional 15% of the total pipe length is recommended based on earlier works by VGK Consulting Engineers of Iceland. This caters for losses from bends and fittings fairly accurately.

2.3 Pipe mechanical design

Pipe thickness

Consideration of nominal thickness of pipe is dependent on the operating pressure of the system. Pipe thickness is selected so that the pipe is able to resist the design pressure over its lifetime. ASME 31.1 power piping design codes (ASME, 2007) provide the criteria of pipe thickness selection given by Equation 31:

$$t_n \geq t_m = \frac{pD_o}{2(SE + py)} + A_c \quad (31)$$

where t_n is nominal pipe thickness (m); t_m is required pipe thickness (m); p is design pressure (Pa); D_o is outer pipe diameter (m); S is allowable stress (MPa); E is welding factor (dimensionless); y is temperature dependent coefficient; A_c is corrosion allowance (m).

For this system, wellhead pressure will be the highest pressure in the system. A margin can be added to the wellhead pressure and used as the maximum pressure the system would be subject to over its operating life.

Stress analysis

Loads acting on a pipe can be due to internal and external pressure, temperature, pipe material and contents conveyed, cladding material, fittings like valves, environmental effects like wind and snow and sudden transient effects like water hammer. Usually, the total loads would be a combination of a number of these loads. Loads acting on a pipe can be classified as either sustained or occasional loads.

(i) Sustained load criteria

The condition that must be fulfilled for the sustained loads acting on a pipe is defined by Equation 32:

$$\frac{pD_o}{4t_n} + 0.75i \left(\frac{M_A}{Z} \right) \leq S_h \quad (32)$$

where i is stress intensity factor ($0.75i \geq 1.0$); M_A is sustained bending moment, Z is section modulus; and S_h is allowable stress during operation (hot).

The section modulus Z is calculated from Equation 33:

$$Z = \frac{\pi}{32} \left(\frac{D_o^4 - D_i^4}{D_o} \right) \quad (33)$$

Vertical sustained loads

Vertical sustained loading is a combination of the weight of the pipe, weight of the insulation and weight of cladding material per unit pipe length. This can be calculated from Equation 34:

$$q_{sv} = q_p + q_e + q_c \quad (34)$$

where q_{sv} is vertical sustained load; q_p is weight of pipe; q_e is weight of insulation material; q_c is weight of cladding material.

The individual weights can be calculated from the Equations 35-37:

$$q_p = \frac{\pi}{4} g \rho_s (D_o^2 - D_i^2) \quad (35)$$

$$q_e = \frac{\pi}{4} g \rho_e (D_e^2 - D_o^2) \quad (36)$$

$$q_c = \frac{\pi}{4} g \rho_c (D_c^2 - D_e^2) \quad (37)$$

where ρ_s is density of steel; ρ_e is density of insulation material; ρ_c is density of cladding material; D_e is diameter of insulation; and D_c is diameter of cladding.

(ii) Occasional loads

The condition that must be fulfilled for the occasional loads acting on a pipe is defined by Equation 38:

$$\frac{pD_o}{4t_n} + 0.75i \left(\frac{M_A}{Z} \right) + 0.75i \left(\frac{M_B}{Z} \right) \leq kS_h \quad (38)$$

where M_B is the occasional bending moment; k is the load factor dependent on duration of operation time; $k = 1.15$ if loading is less than 10% of operational time; $k = 1.2$ if loading is less than 1% of operational time; $k = 1.0$ otherwise.

Vertical occasional loads

Vertical occasional load is a combination of the weight of the transported medium, snow load and seismic load. It is calculated from Equation 39.

$$q_{ov} = q_v + q_s + q_{ev} \quad (39)$$

where q_{ov} is vertical occasional load; q_v is weight of pipe contents; q_s is snow load; and q_{ev} is vertical seismic load.

The individual weights can be calculated from the Equations 40-42:

$$q_v = \frac{\pi}{4} g \rho_v D_i^2 \quad (40)$$

$$q_s = 0.2sD_c \quad (41)$$

$$q_{ev} = 0.5eq_g \quad (42)$$

where ρ_v is density of medium in pipe; s is snow factor; e is seismic factor; q_g is total load subject to gravity (sum of weight of pipe, medium, lagging and cladding).

Hence:

$$q_g = q_p + q_v + q_e + q_c \quad (43)$$

Horizontal occasional loads

Horizontal occasional loads refer to the maximum load calculated between the wind load, q_w and the horizontal seismic load, q_{eh} :

$$q_w = C \rho_w D_c \quad (44)$$

$$\rho_w = \frac{v_w}{1.6} \quad (45)$$

$$q_{eh} = eq_g \quad (46)$$

where v_w is wind speed (m/s).

Horizontal occasional loads can therefore be determined from Equation 47:

$$q_{oh} = \max(q_w, q_{eh}) \quad (47)$$

Bending moments

The pipeline behaves like a beam and the sustained and occasional bending moments can be calculated from Equations 48 and 49:

$$M_A = \frac{q_{sv} L_S^2}{8} \quad (48)$$

$$M_B = \sqrt{(q_{ov}^2 + q_{oh}^2)} \frac{L_S^2}{8} \quad (49)$$

where L_S is the length between supports (m).

Length between supports

Length between supports is selected to meet the conditions of Equation 50:

$$L_S^2 \leq \frac{\left(kS_h - \frac{pD_o}{4t_n}\right) \left\{\frac{\pi}{4}(D_o^4 - D_i^4)\right\}}{D_o(0.75i) \left(q_{sv} + \sqrt{q_{ov}^2 + q_{oh}^2}\right)} \quad (50)$$

Deflection

Pipe deflection can then be calculated from Equations 51 and 52:

$$\delta = \frac{2.07qL^3}{384EI} \quad (51)$$

and

$$I = \frac{\pi(D_o^4 - D_i^4)}{64} \quad (52)$$

where δ is maximum allowable deflection; E is Young's modulus; and I is the moment of inertia of the pipe cross-section.

2.4 Separator design considerations

Separator placement

Separator location is very crucial in the design of a steam gathering system. The following are critical factors that need to be taken into account when placing separators.

(i) Elevation

Separator or separating station elevation in respect to production and reinjection wells must be considered when siting separators. It is always desirable that separators are placed at a low elevation compared to the production wells to avoid going into undesirable flow regimes by flowing two-phase fluid uphill. The separators should also be placed at a higher elevation than the reinjection wells to allow reinjection brine to flow freely by gravity into the reinjection points and eliminate the need to use pumps that would otherwise increase the cost of installation and operation.

(ii) Location

Placement of separators close to the wells results in low pressure drops in two-phase pipelines while having separators close to the power plant would lead to high pressure drops in these two-phase pipelines. Both of these scenarios may be beneficial based on the reservoir pressure of the resource being utilised. Optimal separator location is desirable for separators that can handle fluid from a number of wells (Onyango, 2015).

Separator dimensions and wall thickness

Geothermal separators are generally classified as either horizontal or vertical (DiPippo, 2016). Vertical separators use the principle of centrifugal or cyclonic separation. The centrifugal force is generated using a tangential or spiral inlet to the cyclone. As the fluid rotates, the water with a higher density will tend to flow to the walls of the vessels and downwards while the steam with a much lower density will tend to flow inwards and upwards. Horizontal separators on the other hand are based on a gravitational separation process. The mixture will enter from the top and travel horizontally while flashing occurs. The design is to ensure the mixture velocity is sufficiently lowered to give the water particles enough time to settle to the bottom before steam leaves from the top on separators. The technology was in use earlier in the nuclear industry. Vertical separators are the most widely used in the world due to the simplicity of their design and construction.

Vertical separator dimensions

The key principle in vertical separators is to generate a vortex that will push the liquid to the vessel walls and concentrate the steam in the centre. Bangma (1961) and Lazalde-Crabtree (1984) methods can be used to design the dimensions of the vertical cyclone separator (Figure 6). Inlet cross-sectional area, A_i and diameter, D_t are calculated using Equations 53 and 54, respectively:

$$A_i = \frac{Q_{vs}}{v_t} \quad (53)$$

$$D_t = \left(\frac{4A}{\pi} \right)^{0.5} \quad (54)$$

where A_i is internal cross-sectional area of inlet; Q_{vs} is volumetric steam flow; D_t is inlet pipe diameter; and v_t is two-phase inlet steam velocity.

The two-phase inlet diameter D_t is calculated from the equations above, and the rest of the vessel dimension is given in terms of D_t . Purnanto et al. (2012) summarised vertical separator design guidelines from earlier works (Table 3) for the separator dimensions in terms of D_t .

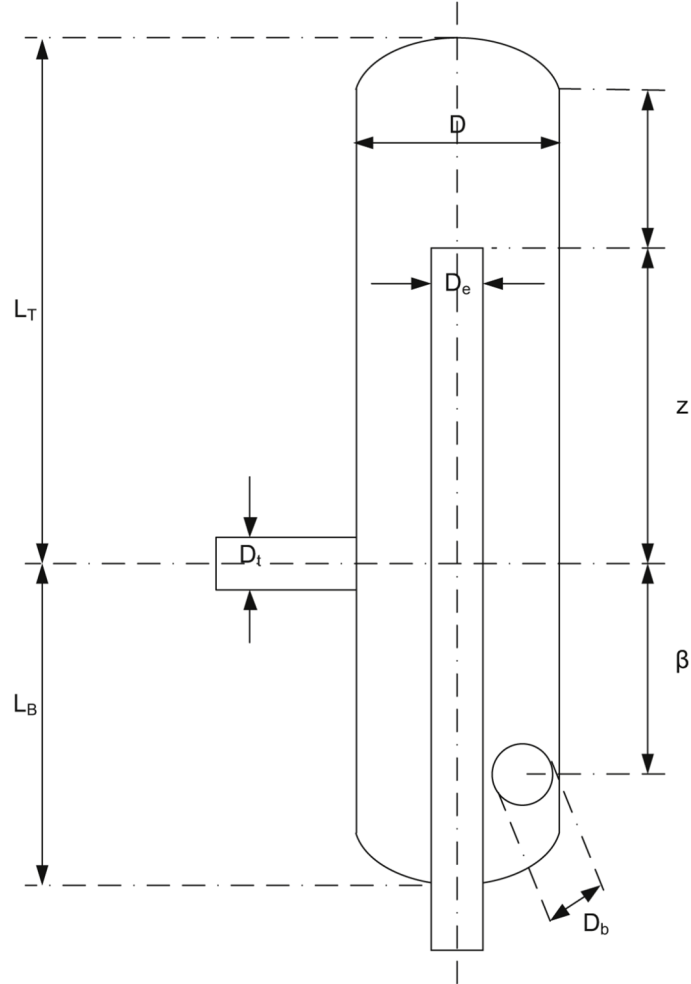


FIGURE 6: Vertical separator dimensions
(Lazalde-Crabtree, 1984)

TABLE 3: Vertical separator dimensions (Purnanto et al., 2012)

Parameter	Bangma	Lazalde-Crabtree	Spiral inlet
D	$3D_t$	$3.3D_t$	$2.95D_t$
D_e	$0.8D_t$	D_t	D_t
D_b	D_t	D_t	$0.7D_t$
α	$3.25D_t$	$0.15D_t$	$0.28D_t$
β	$3D_t$	$3.5D_t$	$3.2D_t$
Z	$3D_t$	$5.5D_t$	$5.8D_t$
L_T	$7D_t$	$6.475D_t$	$6.8D_t$
L_B	$4.5D_t$	$4.975D_t$	$4.9D_t$

Additional recommendation for fluid velocity in the separator is provided by DiPippo (2016) as summarised in Table 4.

TABLE 4: Recommended cyclone inlet and steam velocities (DiPippo, 2016)

Parameter	Velocity
Maximum steady velocity at two-phase inlet pipe	45 m/s
Recommended range of steady velocity at two-phase inlet pipe	25–40 m/s
Maximum upward annular steam velocity inside cyclone	4.5 m/s
Recommended range of upward annular steam velocity inside cyclone	2.5–4.0 m/s

Separator wall thickness

Separator wall thickness is determined using the same equations used to determine pipe wall thickness. The thickness of the walls should be sufficient to resist pressure of the vessel in working conditions. Equation 55 is used to calculate minimum wall thickness t (ASME, 2007):

$$t = \frac{pD}{2SE - 0.2p} + A_c \quad (55)$$

where t is minimum wall thickness (m); p is separator design pressure (mPa); D is separator outside diameter (m); S is material allowable stress (MPa); E is welding factor and A_c corrosion allowance (m).

3. WELL OW-906 DESIGN AND RESULTS

3.1 General information

Ambient conditions

Table 5 below gives a summary of the weather and geographical conditions that will be used in this work.

TABLE 5: Weather and geographical conditions for Olkaria Domes field

Average wet bulb temperature (°C)	35
Average dry bulb temperature (°C)	17
Atmospheric pressure (bara)	0.8
Relative humidity maximum (%)	70
Average annual rainfall (mm)	700
Wind speed maximum (m/s)	36
Wind shape facor	0.6
Seismic factors (UB, Zone 3)	0.16

Well location

Well OW-906 is situated on the eastern side of the Olkaria Domes field. Table 6 below shows the coordinates of the well. The well is a directional well drilled to a depth of 2200 meters.

TABLE 6: Well OW-906 coordinates

Northing	9899827
Easting	201803
Elevation (m a.s.l.)	1975

The well was drilled between July 2012 and January 2013 as a production well for the then proposed Olkaria IV power plant.

Well completion test data

Injection temperature profile for the well shows permeability down to about 1600 m. Below this depth, conductive heating controls the well, as indicated on the heat up profiles in Figure 7.

The major feed zone was observed to be at a depth of about 1500 m. Pressure injection test showed minimal pressure build-up while injecting water at the highest pump rate of 1900 L/min. (Figure 8).

The well has an injectivity index of 434.3 Lpm/bar (Figure 9). This is a relatively high injectivity index, in comparison to most wells in the vicinity and in the Olkaria Domes field. The well also has a high permeability. This is supported by the high injectivity index and the minimal pressure build up during the injection tests.

Well discharge test data

The well discharge tests were carried out for four days in April 2013 and two days in June 2013. The tests were, however, interrupted to allow for the connection of the reinjection pipeline for the well. The well was sacrificed to be a reinjection well due to the observed high brine outputs of the Olkaria Domes field and therefore more reinjection capacity was needed. This however changed after commissioning of the Olkaria Domes steam field where it was established that the reinjection capacity was actually excessive. In addition to the steam field pressure that was raised to 11 bar, which reduced the reserve steam margin, this justified the reconnection of the well for production. Well discharge test data in Table 7 below shows computed well output using lip pressure pipe of diameter 0.2 m. The data indicates that the well is a fairly good producer.

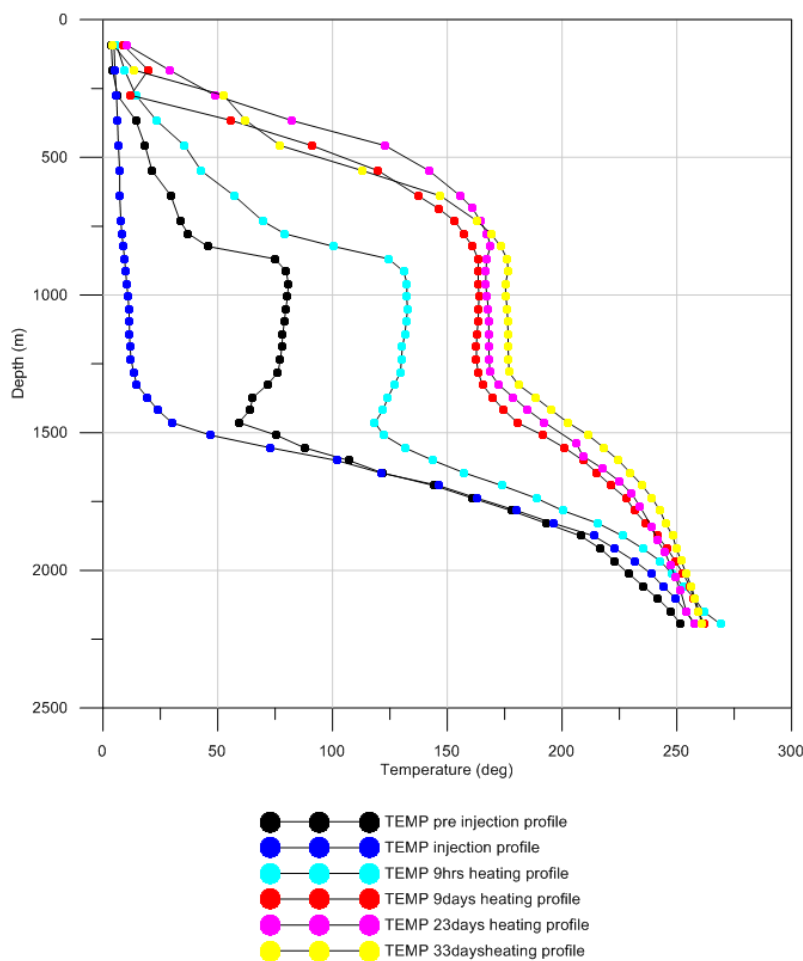


FIGURE 7: Well OW-906 temperature profiles
(KenGen, 2013)

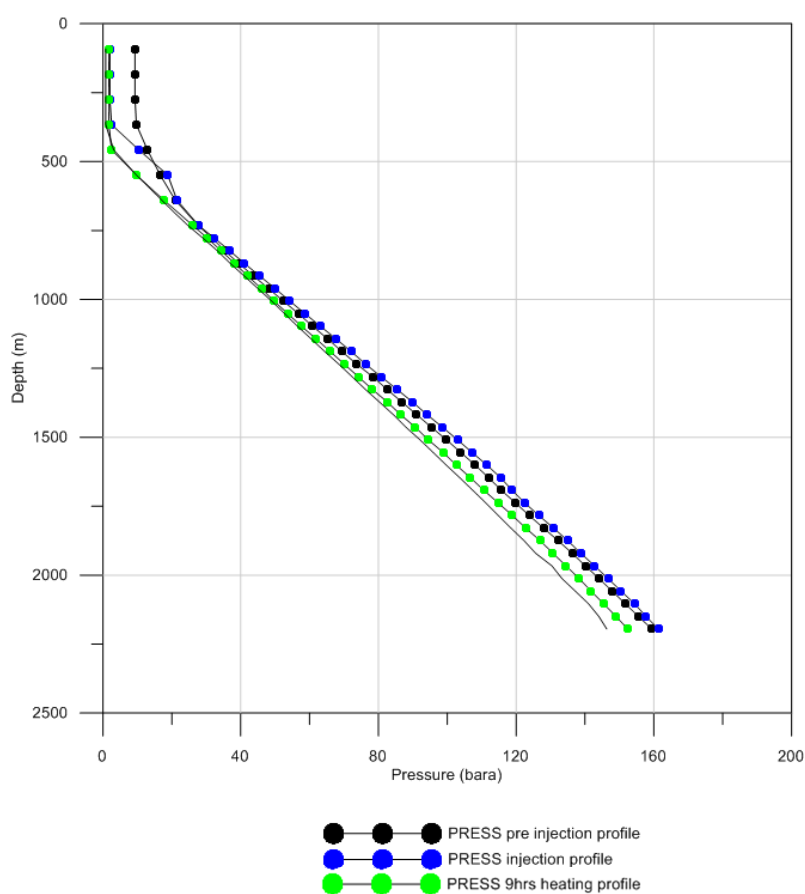


FIGURE 8: Well OW-906 pressure profiles (KenGen, 2013)

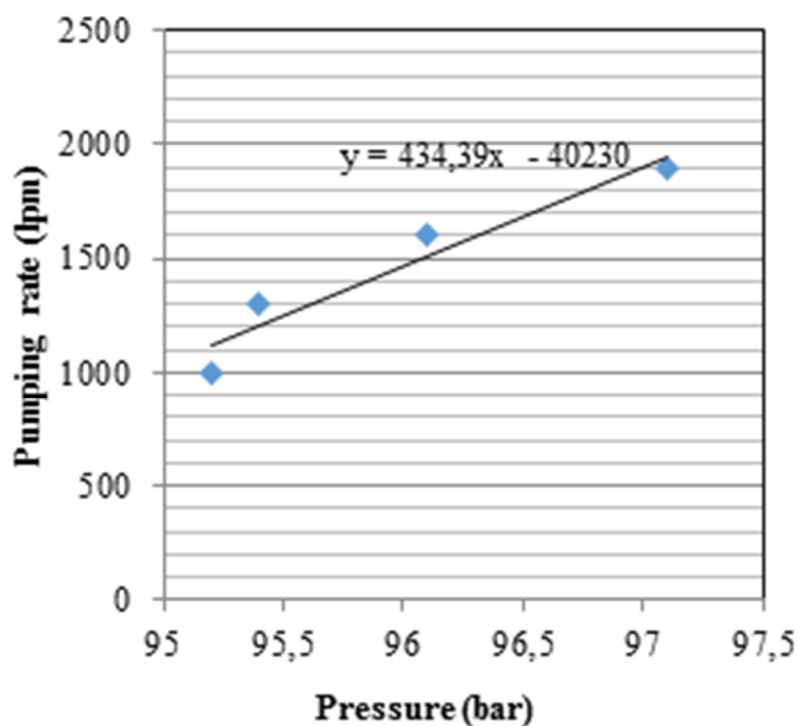


FIGURE 9: Well OW-906 injectivity index (KenGen, 2013)

The discharge tests were carried out for a very short period and the data obtained cannot be relied upon. For this work, fluid enthalpy of nearby wells was used to estimate fluid properties for 13.0 bar-a wellhead pressure as indicated in Table 8 below. The total mass flow was assumed to remain the same and was maintained at 44 kg/s. Selected fluid enthalpy used was 1350 kJ/kg and Engineering Equation Solver (EES) was used to calculate steam flow and water flow at a separation pressure of 12 bar-a. The results are as indicated in Table 8. This is the data that will be used in the design presented here.

TABLE 7: Well OW-906 discharge data with 200 mm lip pipe

Date	Well pressure (bara)	Total mass (kg/s)	Enthalpy (kJ/kg)	Water flow (kg/s)	Steam flow (kg/s)	Power output (MW)
28 Apr 13	7.3	48.2	1003	35.7	8.3	4.2
28 Apr 13	7.3	47.9	1009	35.3	8.4	4.2
29 Apr 13	7.3	46.6	1035	33.8	8.7	4.4
29 Apr 13	7.3	46.6	1035	33.8	8.7	4.4
04 Jun 13	7.5	44.1	1125	30.2	10.2	5.1
05 Jun 13	7.5	44.1	1125	30.3	10.2	5.1

TABLE 8: Well OW-906 recalculated discharge data for design

Well pressure (bar-a)	Separator pressure (bar-a)	Total mass (kg/s)	Enthalpy (kJ/kg)	Water flow (kg/s)	Steam flow (kg/s)
13.0	12.0	44.0	1350	32.0	12.0

3.2 Pipeline route selection

Pipe route selected is carried out using variable topology distance transform (VTDT) with the Olkaria IV digital elevation matrix (DEM) as the input file. The maximum height difference was set at 0.1 and the maximum slope restricted to 0.025 for the two-phase pipeline. There are no constraints in this area. Figure 10 below shows the Olkaria IV DEM with the existing separation stations. Five options will initially be considered, i.e. flow of two-phase fluid to the four existing separators and creation of an optimised separator position near the well.

The selection of the two-phase pipeline route and the brine reinjection pipeline route is done based on the optimised separator location. Two-phase and steam pipelines will be designed based on the selected existing separator stations or an optimised alternative location between the well and the closest main steam pipeline. The reinjection pipeline is limited by the fact that existing reinjection wells are to be used. Table 9 shows the locations of the existing separator stations.

Figure 10 shows the digital elevation matrix for Olkaria IV showing well OW-906 and the four existing separator stations. Results of the variable topology distance transform are shown in Figures 11 and 12.

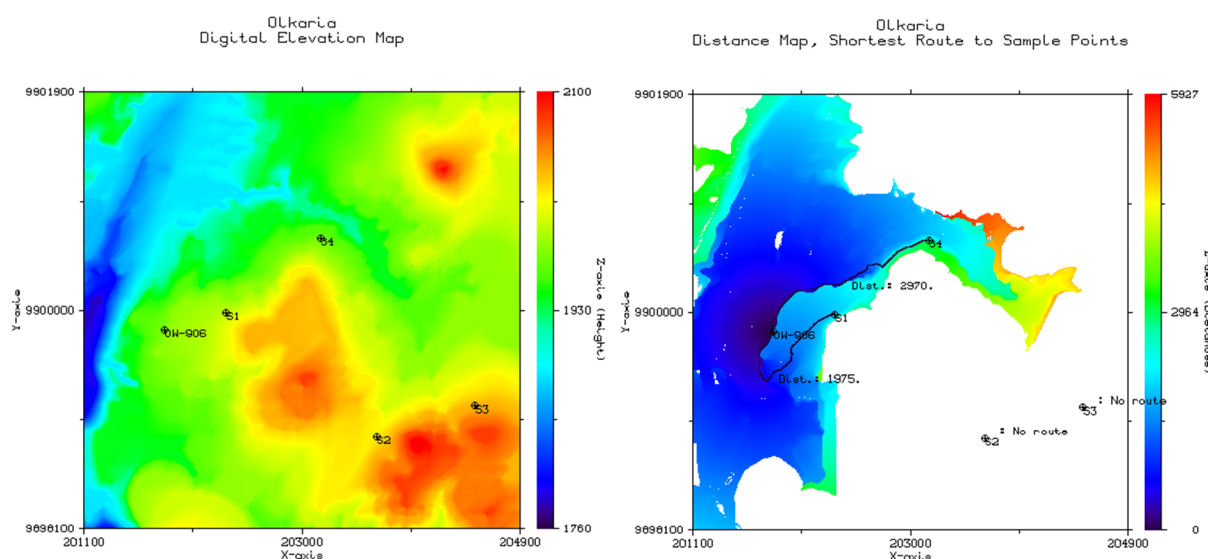


FIGURE 10: Olkaria IV Digital Elevation Matrix showing well OW-906 and existing separators

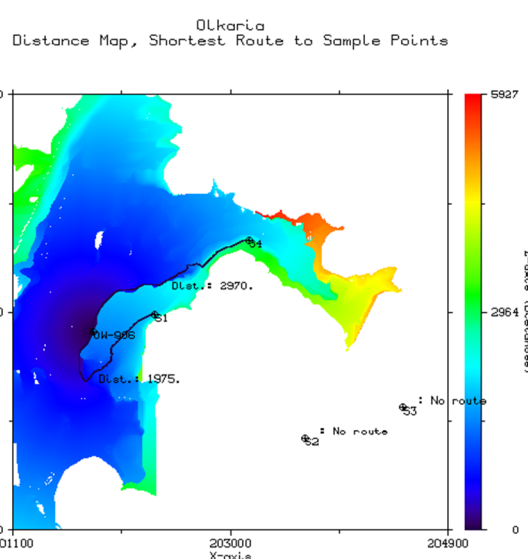


FIGURE 11: Two-phase pipelines with distances from OW-906 to separator stations SD1 and SD4

TABLE 9: Coordinates of existing separator stations

Station	Northing	Easting	Elevation
SD1	9899980	202340	1985
SD2	9898900	203650	2010
SD3	9899170	204510	2029
SD4	9900630	203160	1960

TABLE 10: VTDT results for distances from OW-906 to separator stations SD1, SD4 and SD5

Pipeline route	Fluid type	Distance (m)
OW-906 to SD1	Two-phase	1975
OW-906 to SD4	Two-phase	2970
OW-906 to SD5	Two-phase	100

TABLE 11: Coordinates of existing brine reinjection wells

Reinjection well	Northing	Easting	Elevation (m a.s.l.)
OW-901	9900842	201857	1891
OW-902	9899012	201681	1951
OW-906A	9899916	201724	1964
OW-911	9898315	202736	1979
OW-911A	9898287	202725	1979
OW-913A	9899117	202341	1980

From Figure 11, separator stations SD2 and SD3 are located at much higher elevations than the production well OW-906 and are therefore not accessible for two-phase flow from this well. The separator stations accessible to this well are SD1 and SD4. The results of the distances to these two accessible separators using VTDT is summarised in Table 10. VTDT results also indicate the optimal separator positioning is within the OW-906 well pad as shown by the black dot on Figure 12 below. This new separator station is designated as SD5 and its distance from the well is also shown in Table 10. VTDT was also used to estimate the distances to all the reinjection wells to determine the nearest reinjection well accessible to the brine from the new separator station SD5.

As Table 11 shows, all the reinjection wells are below the well pad OW-906 and are therefore available for free flow of brine by gravity. However, the well to be used is selected based on the shortest distance from the separator station. Figures 13 indicates the results of VTDT for position of the new separator station SD5 and all the reinjection wells. Figure 14 shows the optimal pipeline routes and distances from SD5 to these reinjection wells from SD5. Results of the distances of the reinjection wells are summarised in Table 12.

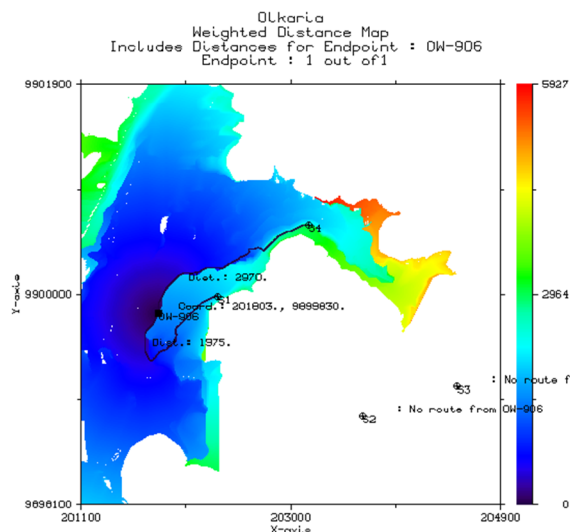


FIGURE 12: Two-phase pipelines with distances from OW-906 to separator stations SD1 and SD4 showing optimal separator location (black dot)

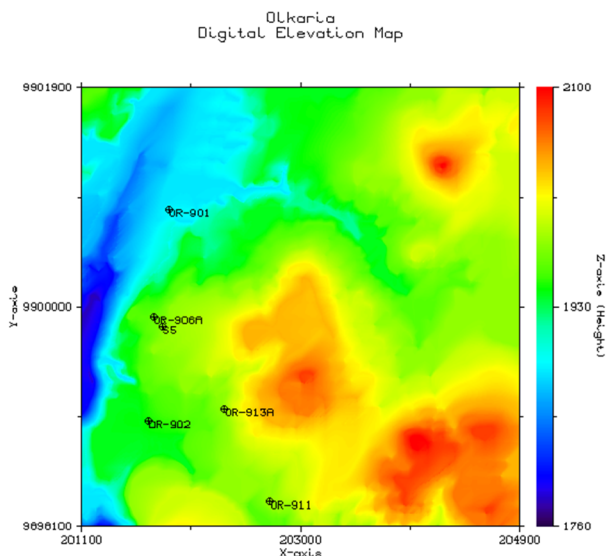


FIGURE 13: Olkaria IV DEM with new separator station SD5 and all the reinjection wells

From the VTDT results of the two-phase pipelines from well OW-906 to separator stations SD1 and SD4, only the SD4 option will be considered further. Both pipelines are fairly long for two-phase flow due to the high associated pressure drops but SD1 provided an additional problem of having to flow two-phase uphill and this is undesirable especially for long distances. The well to be used for the reinjection is selected based purely on the length of the pipeline. The shortest distance is to well OW-906A.

For the steam pipelines, VTDT is applied to find the distances from separator station SD5 to the nearest main steam pipeline towards the power plant. The closest main steam line is the main steam pipeline from separator station SD1 towards the power plant. Five anchors along this pipe are considered as possible tie-in points for this new pipeline. VTDT is therefore used to establish the shortest optimal path to the nearest anchor. For steam pipelines, the slope is not relevant. Table 13 shows the coordinates of the anchors along this main steam pipeline.

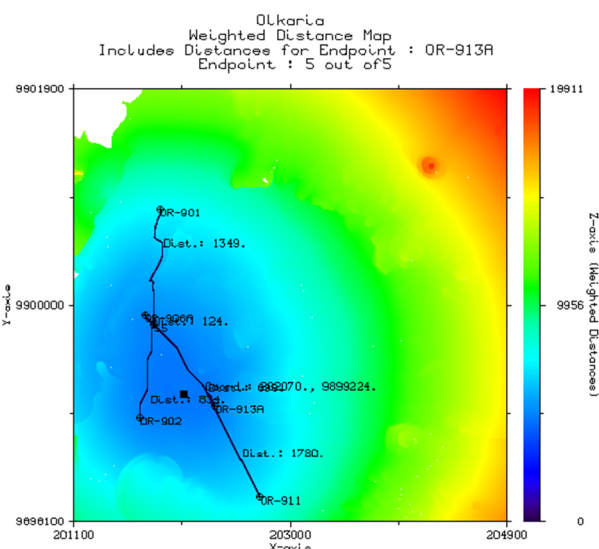


FIGURE 14: Olkaria IV DEM with new separator station SD5 and all the reinjection pipeline routes and distances from the separator

TABLE 12: VTDT results for distances from separator station SD5 to existing reinjection wells

Pipeline route	Fluid type	Distance (m)	Well elevation (m a.s.l.)
SD5 to OW-901	Brine	1349	1892
SD5 to OW-902	Brine	834	1952
SD5 to OW-906A	Brine	124	1964
SD5 to OW-911	Brine	1790	1980
SD5 to OW-911A	Brine	1797	1980
SD5 to OW-913A	Brine	899	1981

Figure 15 indicates the results of VTDT for positions of the nearest anchors on the main steam pipeline near the new separator station SD5. Figure 16 shows the optimal pipeline routes and distances from SD5 to the anchor points on the main steam pipeline near the separator station.

TABLE 14: VTDT results for distances from separator station SD5 to nearest anchor points on main steam pipeline

Pipeline route	Fluid type	Distance (m)
SD5 to A-1	Steam	341
SD5 to A-2	Steam	301
SD5 to A-3	Steam	217
SD5 to A-4	Steam	316
SD5 to A-5	Steam	535

TABLE 13: Coordinates of five anchors on the main steam pipeline considered as new steam pipeline tie-in points

Anchor identity	Northing	Easting	Elevation (m a.s.l.)
A-1	9899939	202123	1980
A-2	9899908	202090	1979
A-3	9899814	201990	1977
A-4	9899629	201900	1968
A-5	9899548	201870	1965

Results of the distances of the anchor points on the main steam pipeline to separator station SD5 are summarised in Table 14.

The two design options to be considered for optimisation and compared in this work are summarised in Table 15 and are the following:

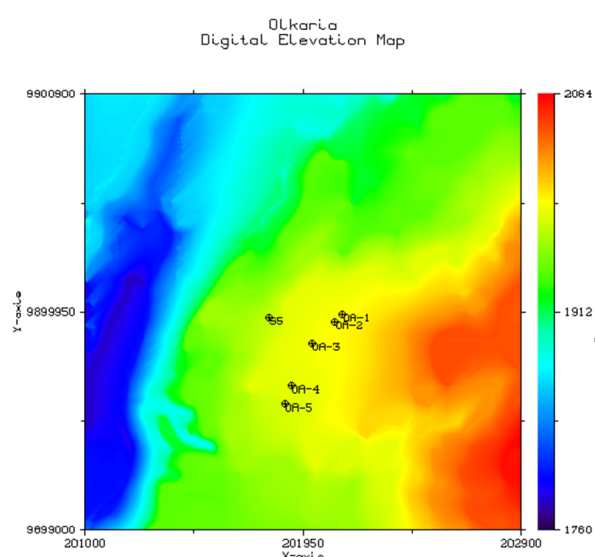


FIGURE 15: Olkaria IV DEM with anchor points on the main steam pipeline near new SD5

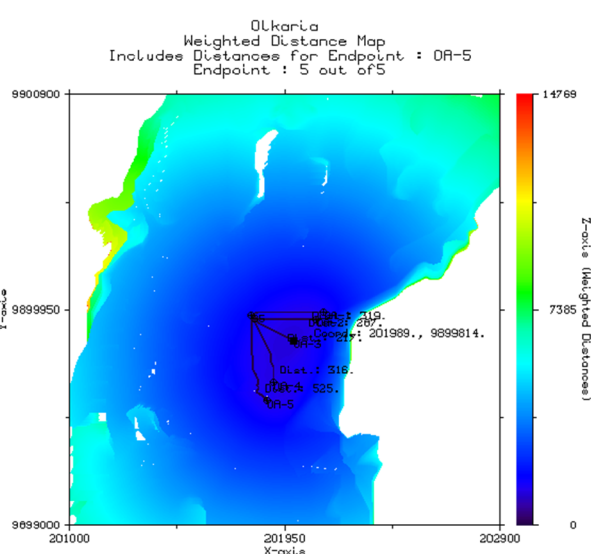


FIGURE 16: Olkaria IV DEM with optimal routes to anchor points on the main steam pipeline near SD5

TABLE 15: Summary of design items for the options to be optimised and compared

Design option	Items
1	<ol style="list-style-type: none"> 1. Design of two-phase pipeline from well OW-906 to existing separator station - SD4 – 2790 m. 2. Assess capacity of brine and steam pipeline to accommodate additional flow.
2	<ol style="list-style-type: none"> 1. Design two-phase pipeline to the new separator station SD5 located on the OW-906 wellpad – 100 m. 2. Design separator station SD5. 3. Design steam pipeline from SD5 to nearest anchor on main steam pipeline – 187 m. 4. Assess capacity of brine and steam pipeline to accommodate additional flow.

Design option 1: Flowing of two-phase fluid downhill to existing separator SD4. In this case the pipe route design will be done for two-phase flow to SD4. Brine from SD4 is already connected to flow to reinjection well OW-901. Brine and steam pipelines will be assessed to ensure they have additional capacity to accommodate the additional flow.

Design option 2: Flowing of two-phase fluid to a new optimally located separator SD5: In this case the pipe route design will be done for two-phase flow to SD5. Brine reinjection pipeline will be designed to connect to the main brine reinjection pipeline to the nearest reinjection well, OW-906A. Steam pipeline will then be optimally routed and designed to connect to the nearest anchor point along the nearest main steam pipeline.

3.3 Pressure drop and diameter selection

Pressure drop calculations have been carried out using the equations outlined in the previous chapter. All the calculations are calculated for unit pipe lengths. Two-phase pressure drop is calculated using the correlations discussed and the highest value used in this design. Steam and brine pressure drops are calculated using single-phase pressure drop equations.

3.3.1 Two-phase pressure drop

The two-phase pressure drop was carried out using the Friedel method (Appendix I). This method was selected based on the recommendations of Hewitt (1982) where the Friedel method is recommended when μ_L/μ_G is less than 1000. For this well, $\mu_L/\mu_G = 9.37$. Wellhead and separator pressure are set to 1.3 and 1.2 MPa, respectively. Diameter selected is the one that gives pressure drop values below the minimum allowable pressure drop.

Maximum allowable pressure drop is 0.1 MPa

Selected two-phase pipe diameter for Option 1 is DN800

Selected two-phase pipe diameter for Option 2 is DN500

3.3.2 Single-phase pressure drop

Steam

There was no steam pipe selection required for Option 1 because this option will use the existing pipeline from separator station DS4. For option 2, the steam pipeline was selected based on a steam velocity of 30 m/s (Appendix I). Pressure drop in this case was minimal and steam velocity was the key guiding factor in pipe size selection.

Selected steam pipe diameter for Option 2 is DN300

Brine

Brine pipeline is not considered in this work because there is an existing brine pipeline connected to the nearest reinjection well OW-906A with a 70 kg/s capacity to accommodate brine from well OW-906. The well selection is, however, done using VTDT based on distance from the new separator.

3.4 Pipe wall thickness

Pipe wall thickness was calculated using Equation 31 using Excel (Appendix II). The pipe thickness was then selected from nominal thickness tables (Appendix V). For the two-phase and steam pipelines, the design pressure used was 2 MPa corresponding to Class 150.

Calculated minimum thickness for the two-phase pipeline for Option 1 is 11.62 mm;

Selected nominal thickness for Option 1 is 12.7 mm;

Calculated minimum thickness for the two-phase pipeline for Option 2 is 7.14 mm;

Selected nominal thickness for Option 2 is 9.53 mm;

Calculated minimum thickness for the steam pipeline for Option 2 is 5.63 mm;

Selected nominal thickness for Option 2 is 6.35 mm.

3.5 Separator dimensions and wall thickness

Separator dimensions are calculated using Equations 53 and 54 with steam inlet velocity fixed at 30 m/s to calculate inlet diameter D_i . The rest of the separator dimensions were then calculated as a function of D_i . This was done for the spiral inlet option considered the most efficient (Zarrouk and Purnanto, 2014).

Calculated inlet diameter D_i is 288 mm;

Selected inlet diameter of pipe size is DN300.

Table 16 gives the results of the separator dimensions as a function of the selected inlet diameter using the spiral inlet dimensions (see also Appendix III). Pipe thickness was done based on ASME 31.3 design guidelines (Equation 55). Design pressure used was 2 MPa corresponding to Class 150.

Nominal thickness is selected from standard pipe thickness tables (Appendix V).

Calculated separator minimum wall thickness is 10 mm;

Selected nominal separator thickness is 12.7 mm.

3.6 Design options cost comparison

The two design options are compared using the cost of the piping network. The cost is based on the cost of steel per kg for equivalent pipe total lengths. Volume of steel in each of the options is first calculated using the pipe lengths obtained from the VTDT and the pipe thickness calculated from the mechanical design. Cost of steel per unit length for nominal diameters from Kalinci et al. (2007) was modified using standard world steel prices and nominal thickness of the indicated diameters.

Weight of steel was then calculated using density of steel of 7850 kg/m³ and the cost represented as cost per kg of steel as tabulated in Table 17.

TABLE 16: Vertical separator dimensions based on Spiral inlet option

Parameter	Spiral inlet	Dimensions (m)
D	$2.95D_t$	0.9
D_e	D_t	0.3
D_b	$0.7D_t$	0.2
α	$0.28D_t$	0.08
β	$3.2D_t$	0.96
Z	$5.8D_t$	1.7
L_T	$6.8D_t$	2.0
L_B	$4.9D_t$	1.5

TABLE 17: Modified pipe cost based on pipe weight
(weight/m for nominal pipe thickness (Tioga, 2014 – Appendix V)

Pipe nominal diameter (m)	Total pipe & installation cost (Kalinci et al.) (USD/m)	Pipe weight for nominal thickness (kg/m)	Calculated pipe cost based on weight (USD/kg)
0.20	80	42.5	1.88
0.25	115	60.3	1.91
0.30	145	73.9	1.96
0.35	185	81.3	2.27
0.40	240	93.3	2.57
0.45	285	105.2	2.71
0.50	345	117.2	2.94
0.55	375	129.1	3.01
0.60	424	141.1	3.10
0.65	522	152.9	3.18
0.70	567	164.4	3.21
0.75	613	176.7	3.25
0.80	658	188.8	3.30
0.85	708	212.6	3.33
0.95	754	217.6	3.36
1.00	799	236.6	3.38
1.05	844	255.6	3.40

The cost of the two options is summarized in Table 18.

TABLE 18: Summary of costs for the two options

Option	Items	Total cost of steel (USD)
1	Two-phase pipeline – DN800 Length – 3415 m Thickness – 12.7 mm	3,335,000
2	1. Two-phase pipeline – DN500 Length – 100 m Thickness – 9.5 mm 2. Steam pipeline – DN300 Length – 6.4 m Thickness – 9.5 mm 3. Separator Outside diameter – 0.9 m Thickness – 12.7 mm	64,000

3.7 Pipe stress analysis

3.7.1 Loads acting on pipe and distance between supports

Vertical sustained loads acting on the selected two-phase pipe are calculated using Equation 34. An Excel sheet was created for this calculation (Appendix IV). Insulation used is calcium silicate and a standard thickness of 30 mm is assumed. Vertical and horizontal occasional loads are calculated using Equations 39 and 47, respectively. Maximum distance between supports is calculated using Equation 50. Table 19 below gives the results of the forces acting on pipe and maximum distance between supports for both the two-phase and steam pipes.

TABLE 19: Results of forces acting on the pipe and maximum distance between supports

Pipeline	Results
Two-phase pipe	Vertical sustained load – 1488.9 N/m Vertical occasional load – 134 N/m Horizontal occasional load – 241.7 N/m Maximum distance between supports – 19.8 m Maximum allowable deflection – 2 mm
Steam pipe	Vertical sustained load – 655.5 N/m Vertical occasional load – 57.4 N/m Horizontal occasional load – 130.6 N/m Maximum distance between supports – 21.1 m Maximum allowable deflection – 2 mm

4. CONCLUSIONS

The preliminary pipe routing selection and design of production pipeline for the make-up well OW-906 to Olkaria IV steam gathering system has been carried out. This work clearly shows that it is important to carry out possible pipeline route surveys to come up with the most optimal pipe route and eventually the most cost effective option. The analysis shows that it is cheaper to build a new separator station designated as SD5 on the well pad of OW-906 and use it to separate fluid from the well, then connect the steam to the nearest main steam pipeline that goes from separator station SD4 through separator station SD1 and towards the power plant. The brine from this new separator station will flow to the

nearest reinjection well OW-906A with no additional design changes since this pipeline has sufficient capacity to accommodate the additional flow. The steam will also be accommodated by the existing steam pipeline from separator stations SD1 and SD4. The cost is estimated based on the cost of steel but there is a huge disparity observed between the two options. For this method to be accurately applied, cost must include factors such as labour, foundation costs and other accessories.

ACKNOWLEDGEMENTS

I would like to express my gratitude to the director of UNU Geothermal Training Programme Mr. Lúdvík S. Georgsson and the entire staff for the support accorded to me during the study period. Special thanks goes to my supervisor Magnús Thór Jónsson for his guidance during the period I undertook this project work. I would also like to thank the staff of Orkustofnun and ISOR for their assistance from time to time on very pertinent issues. I would like to also recognize all my colleagues and lecturers for their various inputs to the success of this study period and to the management of KenGen for according me this chance. Last but not least, I would like to express my deepest appreciation to my wife Blanche and daughter Bianca for their understanding.

REFERENCES

- ASME, 2007: *ASME 31.1-2007. Power piping*. American Society of Mechanical Engineers, NY.
- Bangma, P., 1961: The development and performance of a steam–water separator for use on geothermal bores. *Proceedings of the UN Conference on New Sources of Energy, Vol. 2, Geothermal Energy Agenda, item II*.
- De Smith, M.J., 2005: *Determination of gradient and curvature constrained optimal paths*. London University College, publication, 33 pp.
- DiPippo, R., 2016: *Geothermal power plants: Principles, applications, case studies and environmental impact*. Elsevier Ltd., Kidlington, UK, 762 pp.
- Freeston, D.H. 1982: *Lectures on geothermal energy developments in New Zealand*. UNU-GTP, Iceland, Report 12, 108 pp.
- Hance, C.N., 2005: Factors affecting cost of geothermal power development. *Geothermal Energy Association, publication for the US Department of Energy*, 64 pp.
- Henriquez M., J.L., and Aguirre L., L.A., 2011: Piping design: The fundamentals. *Paper presented at Short Course on Geothermal Drilling, Resource Development and Power Plants, organised by UNU-GTP and La-Geo, Santa Tecla, El Salvador*, UNU-GTP SC-12, CD, 14 pp.
- Hewitt, G.F., 1982: Flow regimes. In: Hetsroni, G. (ed.), *Handbook of multiphase systems*. Hemisphere Publishing Co, USA, 2.24 – 2.94.
- Jónsson, M.Th., 2014: *An approach to optimum route and site selection of steam gathering system for geothermal power plants using multiple weight distance transform*. University of Iceland, Reykjavik, 7 pp.
- Kalinci, Y., Hepbasli, A., and Tavman, I., 2008: Determination of optimum pipe diameter along with energetic and exergetic evaluation of geothermal district heating systems: Modeling and application.

Energy and Buildings, 40, 742–755.

KenGen, 2013: Well completion test report for OW-906. Kenya Electricity Generating Company, Ltd. – KenGen, Kenya, internal report, 3 pp.

Kjærnested, S.N., 2011: *A comparative study of geothermal pipeline route selection methods with visual effects optimization*. University of Iceland, Reykjavik, 57 pp.

Kristinsson, H., 2005: *Pipe route design using Variable Topography Distance Transforms*. University of Iceland, Reykjavik.

Lazalde-Crabtree, H., 1984: Design approach of steam-water separators and steam dryers for geothermal applications. *Geothermal Resource Council Bulletin*, September 1984, 11-20.

Mannvit, 2012: *Proposed field development plan for Greater Olkaria geothermal field*. Mannvit Consortium – consultancy services for geothermal resource optimisation study of Greater Olkaria geothermal fields, report 8, Kenya Electricity Generating Company Ltd. – KenGen, internal report, 59 pp.

Ofwona, C.O., 2010: Olkaria I reservoir response to 28 years of production. *Proceedings of the World Geothermal Congress 2010, Bali, Indonesia*, CD, 4 pp.

Onyango, S.O., 2015: Design of steam gathering system for Menengai geothermal field, Kenya. University of Iceland, Reykjavik, MSc thesis, UNU-GTP, report 1, 70 pp.

Ouma, P.A., 1992: *Steam gathering system for NE-Olkaria geothermal field, Kenya – preliminary design*. UNU-GTP, Iceland, report 9, 46 pp.

Ouma, P., 2010: Geothermal exploration and development of the Olkaria geothermal field. *Paper presented at Short Course V on Exploration for Geothermal Resources, organized by UNU-GTP, KenGen and GDC, Lake Bogoria and Naivasha, Kenya*, UNU-GTP SC-11, CD, 16 pp.

Purnanto, M.H., Zarrouk, S.J. and Cater, J.E., 2012: CFD modelling of two-phase flows inside geothermal steam-water separators. *Proceedings of the 34th New Zealand Geothermal Workshop, University of Auckland, Auckland, NZ*, 9 pp.

Tioga, 2014: *Pipe thicknesses*. Tioga Pipe – Pipe Supply Company, PH, USA, website: www.tiogapipe.com.

Umanzor, C., Hall, A., Buchanan, R., and Rosaria, N., 2015: Piping design considerations for geothermal steamfields. *Proceedings of the World Geothermal Congress 2015, Melbourne, Australia*, 9 pp.

Zarrouk, S.J. and Purnanto, M.H., 2014: Geothermal steam-water separators, *Geothermics*, 53, 236-254.

APPENDIX I: Pressure drop and diameter optimisation

Option 1 – Two-phase pipeline

Option 1 - Two-phase pipeline - DN800			
Wellhead pressure, P1	1.3	MPa	13bar
Separator pressure, P2	1.2	MPa	12bar
Allowable two-phase pressure drop, dP	0.1	MPa	
Total mass flow rate, m(t)	44	kg/s	
Dryness fration, x	0.28		
Pipe internal diameter, D	0.8	m	
Pipe cross-sectional area, A	0.503	m2	
Pipe roughness	0.000045	m	
Pipe relative roughness	0.000056		
Steam density, rho(g)	6.13	kg/m3	
Water density, rho(w)	878.35	kg/m3	
Steam discosity, mu(g)	0.0000153	kg/ms	
Water discosity, mu(w)	0.0001434	kg/ms	
Steam dass flow rate, m(s)	12.3	kg/s	
Water dass flow rate, m(w)	31.7	kg/s	
mu(w)/mu(g)	9.37	Less than 1000, Use Friedel	
Steam superficial velocity, v(s)	4.00	m/s	
Water superficial velocity, v(w)	0.07	m/s	
1. Friedel Method			
Two phase density, rho(tp)	21.51	kg/m3	
Surface tension, sigma	0.04	N/m	
Reynolds number steam, Re(s)	1281395		
Reynolds number water, Re(w)	351560		
Friction nactor steam, f(s)	0.0121		
Friction factor water, f(w)	0.0144		
Weber number, We	7018		
Froude number, Fr	2		
E	9.92		
F	0.34		
H	55.36		
Two phase multiplier (I)	90.89		
Two phase pressure drop	28.55	Pa/m	
Two phase pipe length	2970	m	
Additional length to cater for bends (15%)	445.5	m	
Total two phase pipe length	3415.5	m	
Total pressure drop (Pa)	97511.84	Pa	
Total pressure drop (mPA)	0.10	Mpa	

Option 2 – Two-phase pipeline

Option 2 - Two-phase pipeline - DN500			
Wellhead pressure, P1	1.3	MPa	13bar
Separator pressure, P2	1.2	MPa	12bar
Allowable two-phase pressure drop, dP	0.1	MPa	
Total mass flow rate, m(t)	44	kg/s	
Dryness fraction, x	0.28		
Pipe internal diameter, D	0.5	m	
Pipe cross-sectional area, A	0.196	m ²	
Pipe roughness	0.000045	m	
Pipe relative roughness	0.000090		
Steam density, rho(g)	6.13	kg/m ³	
Water density, rho(w)	878.35	kg/m ³	
Steam viscosity, mu(g)	0.0000153	kg/ms	
Water viscosity, mu(w)	0.0001434	kg/ms	
Steam mass flow rate, m(s)	12.3	kg/s	
Water mass flow rate, m(w)	31.7	kg/s	
mu(w)/mu(g)	9.37	Less than 1000, Use Friedel	
Steam superficial velocity, v(s)	10.23	m/s	
Water superficial velocity, v(w)	0.18	m/s	
1. Friedel Method			
Two phase density, rho(tp)	21.51	kg/m ³	
Surface tension, sigma	0.04	N/m	
Reynolds number steam, Re(s)	2050232		
Reynolds number water, Re(w)	562497		
Friction factor steam, f(s)	0.0111		
Friction factor water, f(w)	0.0132		
Weber number, We	28747		
Froude number, Fr	22		
E	9.98		
F	0.34		
H	55.36		
Two phase multiplier (I)	86.50		
Two phase pressure drop	261.01	Pa/m	
Two phase pipe length	2970	m	
Additional length to cater for bends (15%)	445.5	m	
Total two phase pipe length	3415.5	m	
Total pressure drop (Pa)	891487.72	Pa	
Total pressure drop (mPa)	0.89	Mpa	

Option 2 – Steam pipeline

Option 2 - Steam pipeline			
Wellhead pressure, P1	1.3	MPa	
Separator pressure, P2	1.2	MPa	
Allowable two-phase pressure drop, dP	0.1	MPa	
Total mass flow rate, m(t)	44	kg/s	
Dryness fraction, x	0.28		
Pipe internal diameter, D	0.307	m	
Pipe cross-sectional area, A	0.074	m ²	
Pipe roughness	0.000045	m	
Pipe relative roughness	0.000147		
Steam density, rho(g)	6.13	kg/m ³	
Water density, rho(w)	878.35	kg/m ³	
Steam viscosity, mu(g)	0.0000153	kg/ms	
Water viscosity, mu(w)	0.0001434	kg/ms	
Steam mass flow rate, m(s)	12.3	kg/s	
Water mass flow rate, m(w)	31.7	kg/s	
mu(w)/mu(g)	9.37	Less than 1000, Use Friedel	
Steam Velocity, v(s)	30	m/s	
Reynolds Number, Re	3690020		
Friction Factor	0.010		
Pressure Drop	8.58	Pa/m	
Steam pipe length	187	m	
Additional length to cater for bends (15%)	28.05	m	
Total Steam pipe length	215.05	m	
Total pressure drop	1845.474	Pa	
Total pressure drop	0.002	MPa	

APPENDIX II: Pipe wall thickness calculations

Option 1 - Pipe Thickness Work Sheet			
1. Two-phase - DN800			
Design pressure	2	mPa	
Pipe outer diameter, D	0.813	m	
Allowable stress, S	122.00	mPa	
Welding factor, E	1		
Temperature coefficient, y	0.4		
Corrosion allowance, A	0.003		
Minimum thickness, t	0.009620521	m	
Minimum thickness, t (mm)	9.62	mm	
Selected Thickness (mm)	12.7	mm	
Pipe OD (mm)	813.0	0.813	m
Pipe ID (mm)	787.6	0.788	m
Option 1 Summary			
Two phase pipe length	2970.00	m	
15% Addition for Bends	445.50	m	
Total Length	3415.50	m	
Two-phase pipe steel volume	94.85	m ³	
Steel Density	7850.00	kg/m ³	
Steel Mass	744,541.35	kg	
Steel cost/kg for DN800	3.30	USD	
Total Steel Cost	2,456,986.47	USD	
Option 2 - Pipe Thickness Work Sheet			
1. Two-phase - DN500			
Design Pressure	2	mPa	
Pipe Outer Diameter, D	0.508	m	
Allowable Stress, S	122.00	mPa	
Welding Factor, E	1		
Temperature coefficient, y	0.4		
Corrosion Allowance, A	0.003	m	
Minimum thickness, t	0.007136808	m	
Minimum thickness, t (mm)	7.14	mm	
Selected thickness (mm)	9.53	mm	
Pipe OD (mm)	508.00	0.508	m
Pipe ID (mm)	488.94	0.489	m
2. Steam - DN300			
Design pressure	2	mPa	
Pipe outer diameter, D	0.32	m	
Allowable stress, S	122.00	mPa	
Welding factor, E	1		
Temperature coefficient, y	0.4		
Corrosion allowance, A	0.003	m	
Minimum thickness, t	0.005630293	m	
Minimum thickness, t	5.63	mm	
Selected thickness (mm)	6.35	mm	
Pipe OD (mm)	323.85	0.32385	m
Pipe ID (mm)	311.15	0.31115	m
Option 2 Summary			
Two phase pipe length	100.00	m	
15% Addition for Bends	15.00	m	
Total two phase pipe Length	115.00	m	
Two-phase pipe steel volume	1.72	m ³	
Steel density	7850.00	kg/m ³	
Mass two phase pipe	13474.28	kg	
Steam pipe length	187.00	m	
15% Addition for bends	28.05	m	
Total steam pipe length	215.05	m	
Steam pipe steel volume	1.36	m ³	
Mass steam pipe	10693.82	kg	
Total Steel Mass	24168.10	kg	
Total Steel Cost	60,574.27	USD	

APPENDIX III: Separator dimensions and wall thicknesses

Separator Design Work Sheet				
Separation pressure	1.2	mPa		
Steam density@12bar	6.13	kg/m ³		
Water density@12bar	878.4	kg/m ³		
Design pressure CL150	2.0	mPa		
Mass flow rate steam, m	12	kg/s		
Volumetric flow rate, Qvs	1.96	m ³ /s		
Steam velocity (outlet)	30	m/s		
Flow area, A	0.065252855	m ²		
Diameter, Dt	0.288221692	m		
	Bangma	Lazalde - Crabtree	Spiral Inlet	Unit
D	0.86	0.95	0.9	m
D_e	0.23	0.29	0.3	m
D_b	0.29	0.29	0.2	m
α	0.94	0.04	0.1	m
β	0.86	1.01	1.0	m
Z	0.86	1.59	1.7	m
L_T	2.02	1.87	2.0	m
L_B	1.30	1.43	1.5	m
Separator Wall Thickness				
Allowable stress, S	122	mPa		
Welding factor, E	1			
Temperature coefficient, y	0.4			
Corrosion allowance, A	0.003			
	Bangma	Lazalde - Crabtree	Spiral Inlet	
Minimum thickness, tm	0.010	0.011	0.010	m
Overall height, H	3.31	3.30	3.51	m
Ellipse short radius, b	0.22	0.24	0.22	m
Ellipse long radius, a	0.43	0.48	0.44	m
Ellipse surface area	0.29	0.36	0.30	m ²
Cylinder surface area	9.00	9.86	9.76	m ²
Total surface area	9.30	10.22	10.06	m ²
Volume of steel, V	0.12	0.13	0.13	m ³
Density of steel	7850			kg/m ³
Weight of steel (rhoX volume)	927.02	1018.65	1002.98	kg
Cost/kg	3.3		3.3	USD
Total Cost	3059.16	3361.53	3309.83	USD

APPENDIX IV: Pipe stress analysis calculations

Two-phase pipeline

1. Two Phase pipeline - DN500				
Nominal diameter	500	mm	0.5000	m
Outside diameter	508	mm	0.5080	m
Inside diameter	288	mm	0.2880	m
Pipe thickness	110	mm	0.1100	m
Insulation thickness	30	mm	0.0300	m
Insulation diameter (De)	568	mm	0.5680	m
Cladding thickness	2	mm	0.002	m
Cladding diameter (Dc)	572	mm	0.572	m
Steel density	7850	kg/m ³		
Insulation density	400	kg/m ³		
Cladding density	2700	kg/m ³		
Pipe weight (Qp)	10593.0	N/m		
Insulation weight (Qe)	199.0	N/m		
Cladding weight (Qc)	95.8	N/m		
Vertical sustained load (Qp+Qe+Qc)	10887.9	N/m		
Media density	21.5	kg/m ³		
Seismic factor	0.16			
Wind velocity (Vw)	30	m/s		
Wind form factor, C	0.6			
Wind pressure (p) = $Vw^2/1.6$	562.5			
Media weight (Qm)	13.7	N/m		
Vertical seismic load (Qsv)	872.1	N/m		
Vertical occasional load (Qm+Qsv)	885.9	N/m		
Horizontal seismic load (Qsh)	1745.5	N/m		
Wind load (Qw) = $C \cdot p \cdot Dc$	193.1	N/m		
Horizontal occasional load	1745.5	N/m		
Design pressure	11000000	mPa		
Max allowable stress, hot (sh)	122000000	mPa		
Load factor (k)	1			
	109300000	A		
	0.046907956	B		
	6525.414765	C		
Length between supports $SQRT\{(A \cdot B)/C\}$	28.03	m		
Youngs modulus E	2E+11	Pa		
Uniform load (Qp+Qe+Qc)	10887.9	N/m		
Moment of inertia I	0.002931747	m ⁴		
Allowable deflection, m	0.002204517	m		
Allowable deflection, mm	2	mm		

Steam pipeline

2. Steam pipeline				
Nominal diameter	300	mm	0.3000	m
Outside diameter	323	mm	0.3230	m
Inside diameter	311	mm	0.3110	m
Pipe thickness	6	mm	0.0060	m
Insulation thickness	30	mm	0.0300	m
Insulation diameter (De)	383	mm	0.3830	m
Cladding thickness	2	mm	0.002	m
Cladding diameter (Dc)	387	mm	0.387	m
Steel density	7850	kg/m ³		
Insulation density	400	kg/m ³		
Cladding density	2700	kg/m ³		
Pipe weight (Qp)	460.2	N/m		
Insulation weight (Qe)	130.6	N/m		
Cladding weight (Qc)	64.7	N/m		
Vertical sustained load (Qp+Qe+Qc)	655.5	N/m		
Media density	6.13	kg/m ³		
Seismic factor	0.16			
Wind velocity (Vw)	30	m/s		
Wind form factor ©	0.6			
Wind pressure (p) = Vw ² /1.6	562.5			
Media weight (Qm)	4.6	N/m		
Vertical seismic load (Qsv)	52.8	N/m		
Vertical occasional load (Qm+Qsv)	57.4	N/m		
Horizontal seismic load (Qsh)	105.9	N/m		
Wind load (Qw) = C*p*Dc	130.6	N/m		
Horizontal occasional load	130.6	N/m		
Design pressure	2000000	Pa		
Max allowable stress, hot (sh)	122000000	Pa		
Load factor (k)	1			
	95083333.33	A		
	0.001201492	B		
	257.8084604	C		
Length between supports $\text{SQRT}\{(A*B)/C\}$	21.05	m		
Youngs modulus E	2E+11	Pa		
Uniform load (Qp+Qe+Qc)	655.5	N/m		
Moment of inertia I	7.50932E-05	m ⁴		
Allowable deflection, m	0.002194722	m		
Allowable deflection, mm	2	mm		

APPENDIX V: Pipe thicknesses and costs (Tioga, 2014)



Philadelphia Regional Center
2450 Wheatseaf Lane
Philadelphia, PA 19137
O 215-831-0700
F 215-533-1645
E sales@tiogapipe.com

Houston Regional Center
616 FM 1960 W, Suite 700
Houston, TX 77090
O 713-433-2111
F 281-397-0132
E sales@tiogapipe.com

Chattanooga Regional Center
1301 Riverfront Parkway, Suite 108
Chattanooga, TN 37402
O 423-899-3398
F 423-899-9695
E sales@tiogapipe.com

PIPE DIMENSIONS AND WEIGHTS

Available in commercial and nuclear

U.S./METRIC

NOMINAL PIPE SIZE	OD	SCHEDULE DESIGNATIONS	WALL THICKNESS		WEIGHT		ID	
INCH MM	INCH MM	ASME	INCH	MM	LBS/ FOOT	KG/ METER	INCH	MM
1/8 6	0.405 10.3	10 STD 40 10S XS 80 80S	0.049 0.068 0.095	1.24 1.73 2.41	0.19 0.24 0.31	0.28 0.37 0.47	0.307 0.269 0.215	7.82 6.84 5.84
1/4 8	0.540 13.7	10 STD 40 10S XS 80 80S	0.065 0.088 0.119	1.65 2.24 3.02	0.33 0.43 0.54	0.49 0.63 0.80	0.410 0.364 0.302	10.40 9.22 7.66
3/8 10	0.675 17.1	10 STD 40 10S XS 80 80S	0.065 0.091 0.126	1.65 2.31 3.20	0.42 0.57 0.74	0.63 0.84 1.10	0.545 0.493 0.423	13.80 12.48 10.70
1/2 15	0.840 21.3	5 10 STD 40 10S XS 80 80S 160 XX	0.065 0.083 0.109 0.147 0.188 0.294	1.65 2.11 2.77 3.73 4.78 7.47	0.54 0.67 0.85 1.09 1.31 1.72	0.80 1.00 1.27 1.62 1.95 2.55	0.710 0.674 0.622 0.546 0.464 0.252	18.00 17.08 15.76 13.84 11.74 6.36
3/4 20	1.050 26.7	5 10 STD 40 10S XS 80 80S 160 XX	0.065 0.083 0.113 0.154 0.219 0.308	1.65 2.11 2.87 3.91 5.56 7.82	0.69 0.86 1.13 1.48 1.95 2.44	1.03 1.28 1.69 2.20 2.90 3.64	0.920 0.884 0.824 0.742 0.612 0.434	23.40 22.48 20.96 18.88 15.58 11.06
1 25	1.315 33.4	5 10 STD 40 10S XS 80 80S 160 XX	0.065 0.109 0.133 0.179 0.250 0.358	1.65 2.77 3.38 4.55 6.35 9.09	0.87 1.41 1.68 2.17 2.85 3.66	1.29 1.97 2.50 3.24 4.24 5.45	1.185 1.097 1.049 0.957 0.815 0.599	30.10 27.86 26.64 24.30 20.70 15.22
1-1/4 32	1.660 42.2	5 10 STD 40 10S XS 80 80S 160 XX	0.065 0.109 0.140 0.191 0.250 0.382	1.65 2.77 3.56 4.85 6.35 9.70	1.11 1.81 2.27 3.00 3.77 5.22	1.65 2.69 3.39 4.47 5.61 7.77	1.530 1.442 1.380 1.278 1.160 0.896	38.90 36.66 35.08 32.50 29.50 22.80
1-1/2 40	1.900 48.3	5 10 STD 40 10S XS 80 80S 160 XX	0.065 0.109 0.145 0.200 0.281 0.400	1.65 2.77 3.68 5.08 7.14 10.15	1.28 2.09 2.72 3.63 4.86 6.41	1.90 3.11 4.05 5.41 7.25 9.55	1.770 1.682 1.610 1.500 1.338 1.100	45.00 42.76 40.94 38.14 34.02 28.00
2 50	2.375 60.3	5 10 STD 40 10S XS 80 80S 160 XX	0.065 0.109 0.154 0.218 0.344 0.436	1.65 2.77 3.97 5.54 8.74 11.07	1.61 2.64 3.66 5.03 7.47 9.04	2.39 3.93 5.44 7.48 11.11 13.44	2.245 2.157 2.067 1.939 1.687 1.503	57.00 54.76 52.48 49.22 42.82 38.16
2-1/2 65	2.875 73.0	5 10 STD 40 10S XS 80 80S 160 XX	0.083 0.120 0.203 0.276 0.375 0.552	2.11 3.05 5.16 7.01 9.53 14.02	2.48 3.53 5.80 7.67 10.02 13.71	3.69 5.26 8.63 11.41 14.92 20.39	2.709 2.635 2.469 2.323 2.125 1.771	68.78 66.90 62.68 58.98 53.94 44.96
3 80	3.500 88.9	5 10 STD 40 10S XS 80 80S 160 XX	0.083 0.120 0.216 0.300 0.438 0.600	2.11 3.05 5.49 7.62 11.13 15.24	3.03 4.34 7.58 10.26 14.34 18.60	4.52 6.46 11.29 15.27 21.35 27.68	3.334 3.260 3.068 2.900 2.624 2.300	84.68 82.80 77.92 73.66 66.64 58.42
3-1/2 90	4.000 101.6	5 10 STD 40 10S XS 80 80S 160 XX	0.083 0.120 0.226 0.318 0.436	2.11 3.05 5.74 8.08 10.63	3.48 4.98 9.12 12.52 16.15	5.18 7.41 13.57 18.64 34.33	3.834 3.760 3.548 3.364 2.728	97.38 95.50 90.12 85.44 69.30
4 100	4.500 114.3	5 10 STD 40 10S XS 80 80S 120 160 XX	0.083 0.120 0.156 0.188 0.237 0.337 0.438 0.531 0.674	2.11 3.05 3.96 4.78 6.02 8.56 11.13 13.49 17.12	3.92 5.62 7.24 8.67 10.80 15.00 19.02 22.53 27.57	5.84 8.37 10.78 12.91 16.08 22.32 28.32 33.54 41.03	4.334 4.260 4.188 4.124 4.026 3.826 3.624 3.438 3.152	110.08 108.20 106.38 104.74 102.26 97.18 92.04 87.32 80.06
4-1/2 115	5.000 127.0	STD 40 40S XS 80 80S XX	0.247 0.355 0.710	6.27 9.02 18.03	12.55 17.63 32.56	18.67 26.24 48.45	4.506 4.290 3.580	114.46 108.96 90.94

NOMINAL PIPE SIZE	OD	SCHEDULE DESIGNATIONS	WALL THICKNESS		WEIGHT		ID	
INCH MM	INCH MM	ASME	INCH	MM	LBS/ FOOT	KG/ METER	INCH	MM
5 125	5.563 141.3	5 10 STD 40 10S XS 80 80S 120 160 XX	0.109 0.134 0.258 0.375 0.500 0.625 0.750	2.77 3.40 6.55 9.53 12.70 15.88 19.05	6.36 7.78 14.63 20.80 27.06 32.99 38.59	9.46 11.56 21.77 30.97 40.28 49.12 57.43	5.345 5.295 5.047 4.813 4.563 4.313 4.063	135.76 134.50 128.20 122.24 115.90 109.54 103.20
6 150	6.625 168.3	5 10 STD 40 10S XS 80 80S 120 160 XX	0.109 0.134 0.188 0.280 0.432 0.562 0.719 0.864	2.77 3.40 4.78 7.11 10.97 14.27 18.26 21.95	7.59 9.30 12.94 18.99 28.60 36.43 45.39 53.21	11.31 13.83 19.28 28.26 42.56 54.21 67.57 79.22	6.407 6.357 6.249 6.065 5.761 5.501 5.187 4.897	162.76 161.50 158.74 154.08 146.36 139.76 131.78 124.40
7 175	7.625 193.7	STD 40 40S XS 80 80S XX	0.301 0.500 0.875	7.65 12.70 22.23	23.57 38.08 63.14	35.10 56.69 94.00	7.023 6.625 5.875	178.40 168.30 149.24
8 200	8.625 219.1	5 10 STD 40 10S XS 80 80S 120 160 XX	0.109 0.148 0.250 0.277 0.322 0.406 0.500 0.594 0.719 0.812 0.875 0.906	2.77 3.76 6.35 7.04 8.18 10.31 12.70 15.09 18.26 20.62 22.23 23.01	9.92 13.41 22.38 24.72 28.58 35.67 43.43 51.00 60.77 67.82 72.49 74.76	14.78 19.97 33.32 36.82 42.55 53.09 64.64 75.92 90.44 100.93 107.93 111.27	8.407 8.329 8.125 8.071 7.981 7.813 7.625 7.437 7.187 7.001 6.875 6.813	213.56 211.58 206.40 205.02 202.74 198.48 193.70 188.92 182.58 177.86 174.64 173.08
9 225	9.625 244.5	STD 40 40S XS 80 80S XX	0.342 0.500 0.875	8.69 12.70 22.23	33.94 48.77 81.85	50.54 72.60 121.85	8.941 8.625 7.875	227.12 219.10 200.04
10 250	10.750 273.0	5 10 STD 40 10S XS 80 80S 120 160 XX	0.134 0.165 0.188 0.250 0.307 0.365 0.500 0.594 0.719 0.844 1.000 1.125	3.40 4.19 4.78 6.35 7.80 9.27 12.70 15.09 18.26 21.44 25.40 28.58	15.21 18.67 21.23 28.06 34.27 40.52 54.79 64.49 77.10 89.38 104.23 115.75	22.61 27.78 31.62 41.76 51.01 60.29 81.53 95.98 114.71 133.01 155.10 172.27	10.482 10.420 10.374 10.250 10.136 10.020 9.750 9.562 9.312 9.062 8.750 8.500	266.20 264.62 263.44 260.30 257.40 254.46 247.60 242.82 236.48 230.12 222.20 215.84
11 275	11.750 298.5	STD 40 40S XS 80 80S XX	0.375 0.500 0.875	9.53 12.70 22.23	45.60 60.13 101.72	67.91 89.51 151.46	11.000 10.750 10.000	279.44 273.10 254.04
12 300	12.750 323.8	5 10 STD 40 10S XS 80 80S 120 160 XX	0.156 0.180 0.188 0.250 0.330 0.375 0.406 0.500 0.562 0.688 0.844 1.000 1.125 1.312	3.96 4.57 4.78 6.35 8.38 9.53 10.31 12.70 14.27 17.48 21.44 25.40 28.58 33.32	21.00 24.19 25.25 33.41 43.81 49.61 53.57 65.48 73.22 88.71 107.42 125.61 139.81 160.42	31.24 35.98 37.61 49.71 65.19 73.86 79.71 97.44 108.93 132.05 159.87 186.92 208.08 238.69	12.438 12.390 12.374 12.250 12.090 12.000 11.938 11.750 11.626 11.374 11.062 10.750 10.500 10.126	315.88 314.66 314.24 311.10 307.04 304.74 303.18 298.40 295.26 288.84 280.92 273.00 266.64 257.16
14 350	14.000 355.6	10 20 STD 40 10S XS 80 80S 120 140 160	0.188 0.250 0.312 0.375 0.438 0.500 0.594 0.750 0.938 1.094 1.250 1.406	4.78 6.35 7.92 9.53 11.13 12.70 15.09 19.05 23.83 27.79 31.75 35.71	27.76 36.75 45.65 54.62 63.50 72.16 85.13 106.23 130.98 150.93 170.37 189.29	41.36 54.69 67.91 81.33 94.55 107.40 126.72 158.11 194.98 224.66 253.58 281.72	13.624 13.500 13.376 13.250 13.124 13.000 12.812 12.500 12.124 11.812 11.500 11.188	346.04 342.90 339.76 336.54 333.34 330.20 325.42 317.50 307.94 300.02 292.10 284.18

NOMINAL PIPE SIZE	OD	SCHEDULE DESIGNATIONS		WALL THICKNESS		WEIGHT		ID	
INCH MM	INCH MM	ASME		INCH	MM	LBS/ FOOT	KG/ METER	INCH	MM
16 400	16.000 406.4	10	10S	0.188	4.78	31.78	47.34	15.624	396.84
				0.250	6.35	42.09	62.65	15.500	393.70
		20	40S	0.312	7.92	52.32	77.83	15.376	390.56
				0.375	9.53	62.64	93.27	15.250	387.34
		XS	80S	0.500	12.70	82.85	123.31	15.000	381.00
				0.656	16.66	107.60	160.13	14.688	373.08
		60	80S	0.844	21.44	136.74	203.54	14.312	363.52
		80		1.031	26.19	164.98	245.57	13.938	354.02
		100		1.219	30.96	192.61	286.66	13.562	344.48
		120		1.438	36.53	223.85	333.21	13.124	333.34
		140		1.594	40.49	245.48	365.38	12.812	325.42
18 450	18.000 457	10	10S	0.188	4.78	35.80	53.31	17.624	447.44
				0.250	6.35	47.44	70.57	17.500	444.30
		20	40S	0.312	7.92	58.99	87.71	17.376	441.16
				0.375	9.53	70.65	105.17	17.250	437.94
		30	80S	0.438	11.13	82.23	122.38	17.124	434.74
				0.500	12.70	93.54	139.16	17.000	431.60
		40	80S	0.562	14.27	104.76	155.81	16.876	428.46
		60		0.750	19.05	138.30	205.75	16.500	418.90
		80		0.938	23.83	171.08	254.57	16.124	409.34
		100		1.156	29.36	208.15	309.64	15.688	398.28
		120		1.375	34.93	244.37	363.58	15.250	387.14
20 500	20.000 508	10	10S	0.218	5.54	46.10	68.61	19.564	496.92
				0.250	6.35	52.78	78.56	19.500	495.30
		20	40S	0.375	9.53	78.67	117.15	19.250	488.94
				0.500	12.70	104.23	155.13	19.000	482.60
		XS	80S	0.594	15.09	123.23	183.43	18.812	477.82
				0.812	20.62	166.56	247.84	18.376	466.76
		60	80S	1.031	26.19	209.06	311.19	17.938	455.62
		80		1.281	32.54	256.34	381.55	17.438	442.92
		100		1.500	38.10	296.65	441.52	17.000	431.80
		120		1.750	44.45	341.41	508.15	16.500	419.10
		140		1.969	50.01	379.53	564.85	16.062	407.98
22 550	22.000 559	10	10S	0.218	5.54	50.76	75.55	21.564	547.92
				0.250	6.35	58.13	86.55	21.500	546.30
		20	40S	0.375	9.53	86.69	129.14	21.250	539.94
				0.500	12.70	114.92	171.10	21.000	533.60
		XS	80S	0.875	22.23	197.60	294.27	20.250	514.54
				1.125	28.58	251.05	373.85	19.750	501.84
		60	80S	1.375	34.93	303.16	451.45	19.250	489.14
		80		1.625	41.28	353.94	527.05	18.750	476.44
		100		1.875	47.63	403.38	600.67	18.250	463.74
		120		2.125	53.98	451.49	672.30	17.750	451.04
		140							

PIPING • TUBING • FITTINGS FLANGES • RELATED PRODUCTS

Type	Seamless & Welded
Commodity	Chrome • Stainless • Carbon • Low Temperature
Specifications	A/SA335 • A/SA312 • A/SA213 • A/SA106 • A/SA53/API5L • A/SA333
Sizes (O.D.)	1/8" (3.175mm) - 60" (1524mm) (Larger ODs Available)
Grades	Chrome: P1 • P5 • P9 • P11 • P22 • P91 Stainless: 304 • 304H • 304L • 316 • 316H • 316L • 316LN • 321 • 321H • 347 • 347H • 310 • 310s • 309 • Alloy 20 Low Temp: Grade 1/6 • Grade 3 Carbon: Grade B • Grade C • Galvanized

MILITARY SPEC PIPE & TUBING

Program	MIL-I-45208A Quality Program • Approved Level 1 Supplier
Contact Tioga for	U.S. Navy Specifications • Navy Nuclear • MIC Level 1 • Ultrasonic Testing
Fittings & Flanges	All Fittings & Flanges to Match the Pipe

NUCLEAR MATERIALS

Program	ASME Section III - ASME QSC 467
Specifications	10CFR50 Appendix B • N45.2 • NQA-1 • U.S. Navy Nuclear Specifications
Products	Pipe • Tubing • Fittings • Flanges • Structural • Fasteners • Forgings • Castings • Weld Rod • Plate
Grades	Carbon • Stainless • Chrome Moly • Nickel Alloys • Duplex • 6 Moly Alloys • Low Temperature • Special Melts • Copper • Titanium

When it has to be right.™

Call the center of your choice for our 24-hour emergency service
tiogapipe.com

NOMINAL PIPE SIZE	OD	SCHEDULE DESIGNATIONS		WALL THICKNESS		WEIGHT		ID		
INCH MM	INCH MM	ASME		INCH	MM	LBS/ FOOT	KG/ METER	INCH	MM	
24 600	24.000 610	10	10S	0.250	6.35	63.47	94.53	23.500	597.30	
		STD	20	40S	0.375	9.53	94.71	141.12	23.250	590.94
		XS	80S	0.500	12.70	125.61	187.07	23.000	584.60	
		30		0.562	14.27	140.81	209.65	22.876	581.46	
		40		0.688	17.48	171.45	255.43	22.624	575.04	
		60		0.969	24.61	238.57	355.28	22.062	560.78	
		80		1.219	30.96	296.86	442.11	21.562	548.08	
		100		1.531	38.89	367.74	547.74	20.938	532.22	
		120		1.812	46.02	429.79	640.07	20.376	517.96	
		140		2.062	52.37	483.57	720.19	19.876	505.26	
160		2.344	59.54	542.64	808.27	19.312	490.92			
26 650	26.000 660	10		0.312	7.92	85.68	127.36	25.376	644.16	
		STD	40S	0.375	9.53	102.72	152.88	25.250	640.94	
		XS	80S	0.500	12.70	136.30	202.74	25.000	634.60	
28 700	28.000 711	10		0.312	7.92	92.35	137.32	27.376	695.16	
		STD	40S	0.375	9.53	110.74	164.86	27.250	691.94	
		XS	20	80S	0.500	12.70	146.99	218.71	27.000	685.60
		30		0.625	15.88	182.90	272.23	26.750	679.24	
30 750	30.000 762	10		0.312	7.92	99.02	147.29	29.376	746.16	
		STD	40S	0.375	9.53	118.76	176.85	29.250	742.94	
		XS	20	80S	0.500	12.70	157.68	234.68	29.000	736.60
		30		0.625	15.88	196.26	292.20	28.750	730.24	
32 800	32.000 813	10		0.312	7.92	105.69	157.25	31.376	797.16	
		STD	20	0.375	9.53	126.78	188.83	31.250	793.94	
		XS	30	0.500	12.70	168.37	250.65	31.000	787.60	
		40		0.625	15.88	209.62	312.17	30.750	781.24	
		40		0.688	17.48	230.29	342.94	30.624	778.04	
34 850	34.000 864	10		0.312	7.92	112.36	167.21	33.376	848.16	
		STD	20	0.375	9.53	134.79	200.82	33.250	844.94	
		XS	30	0.500	12.70	179.06	266.63	33.000	838.60	
		40		0.625	15.88	222.99	332.14	32.750	832.24	
		40		0.688	17.48	245.00	364.92	32.624	829.04	
36 900	36.000 914	10		0.312	7.92	119.03	176.97	35.376	898.16	
		STD	20	0.375	9.53	142.81	212.57	35.250	894.94	
		XS	30	0.500	12.70	189.75	282.29	35.000	888.60	
42 1050	42.000 1067	STD		0.375	9.53	166.86	248.53	41.250	1047.94	
		XS	20	0.500	12.70	221.82	330.21	41.000	1041.60	
			30	0.625	15.88	276.44	411.64	40.750	1035.24	
			40	0.750	19.05	330.72	492.33	40.500	1028.90	
48 1200	48.000 1219	STD		0.375	9.53	190.92	284.25	47.250	1199.94	
		XS	30	0.500	12.70	253.89	377.81	47.000	1193.60	

SPECIALTY ALLOYS

Type	Seamless & Welded
Commodity	Nickel • Duplex & Titanium
Specifications & Grades	Alloy 800 • Alloy 825 • Alloy 600 • Alloy 625 • Alloy 400 • 6% Moly Grades • Duplex A790 UNS 31803 • 316LN
Sizes (O.D.)	1/8" (3.175mm) - 8" (203.2mm)
Wall Dimensions	0.035" (.89mm) - 0.875" (22.23mm)

TIOGA SPECIALTIES

<ul style="list-style-type: none"> Project Management 24/7 Emergency Service Just-In-Time Programs Inventory in Stock All Schedule Walls Special Heavy Walls to 4" (101.6mm) Header Pipe to 4" Wall (101.6mm) Special Intermediate Walls Average & Minimum Walls Saw Cut up to 40" (1016mm) Cutting: Square & Miter Custom Lengths and OD's End Preps-Variou Hard to Find Metals & Sizes Se Habla Español Exceptional Mill/Sourcing Relations 	<ul style="list-style-type: none"> Dedicated Project Solution Teams Vendor Managed Inventory Programs Mobile On-Site Inventory Programs Quick Response Programs Low Total Cost Solutions International Export & Packaging EN PED 97/23/EC ISO 9001-2008 MIC Level 1 Supplier In-House Testing Destructive Examination Non-Destructive Examination In-House Hydrostatic Testing Full EDI Capabilities Customized e-business Solutions Emergency Forged and Butt Weld Fittings
---	--

Note: Actual dimensions can vary from the figures based on specifications/manufacturing tolerances. The Data for weight is based on the following calculation for wrought steel pipe:
LB/Foot = (Outside diameter [in.] - Wall Thickness [in.]) x (Wall Thickness [in.]) x (10.69)
KG/Meter = (Outside diameter [mm] - Wall Thickness [mm]) x (Wall Thickness [mm]) x (0.0246615)

Equal Opportunity Employer © Tioga Pipe, Inc. 12/2013

Tioga™



UNITED NATIONS
UNIVERSITY

UNU-GTP

Geothermal Training Programme

Orkustofnun, Grensasvegur 9,
IS-108 Reykjavik, Iceland

Reports 2016
Number 31

MODEL REVIEW AND SENSITIVITY ANALYSIS OF THE SÁROSPATAK RESERVOIR MODEL, NE-HUNGARY

Domokos Pásztor

2131 Göd

Lánchíd utca 20

HUNGARY

pasztor.domokos@gmail.com

ABSTRACT

Hungary's favourable natural conditions for geothermal energy production and utilization are well known. The anomalously high thermal gradient and the significant expanse of deep aquifers make Hungary one of the most notable European countries regarding low-temperature geothermal resources. Among other cities, Sárospatak in northeast Hungary has utilized its deep carbonate geothermal reservoir for bathing purposes since the 1960s. In recent years, a 7-layer, three-dimensional numerical model with two proposed wells for district heating was constructed by the Icelandic company Vatnaskil Consulting Engineers. The main objective was to predict the impact of the planned well duplet on the geothermal reservoir at Sárospatak with a special focus on the existing geothermal wells associated with the thermal spa of the city. In this study, after a model and literature review, a detailed sensitivity analysis with 11 different scenarios was performed. Results of the analysis show that 1) the model is not sensitive to input parameters in its lower layers, 2) the model is not sensitive to the porosity and 3) the model is very sensitive to the hydraulic conductivity in the top model layers, especially the producing layer. It has also been shown that the proposed wells are not likely to have any negative impact on the existing thermal wells. On the other hand, the study shows that the existing thermal wells could have a significant impact on the reservoir pressure at the proposed well duplet. Lack of data related to the existing thermal wells (their actual production and the exact thickness and extent of the tuff layer from which they are producing) are crucial factors preventing their actual impacts from being known. These impacts could be the key in determining the success of the Sárospatak geothermal project.

1. INTRODUCTION

Hungary's favourable natural conditions for geothermal energy production and utilization are well known. The heat flow density within the Pannonian basin is high compared to the rest of central Europe (Figure 1). The anomalously high thermal gradient and the significant expanse of deep aquifers make Hungary one of the most notable European countries regarding low-temperature geothermal resources. According to REN21 (2016) data, Hungary is third in geothermal heat capacity per capita in the world (not including heat pumps) and sixth in direct heat capacity utilization. Although geothermal energy has been used mainly for bathing purposes in the country since historical times (e.g. the famous spas of

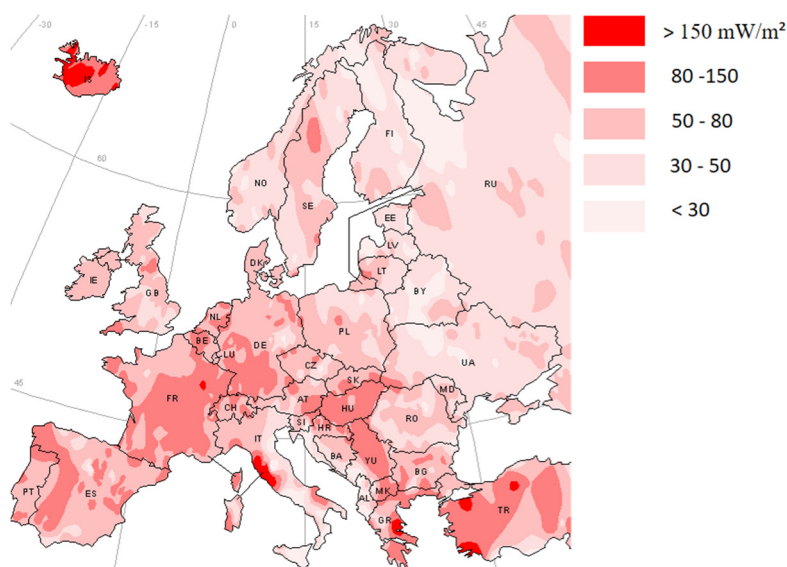


FIGURE 1: Geothermal heat flow density of Europe (Rollin et al., 1995)

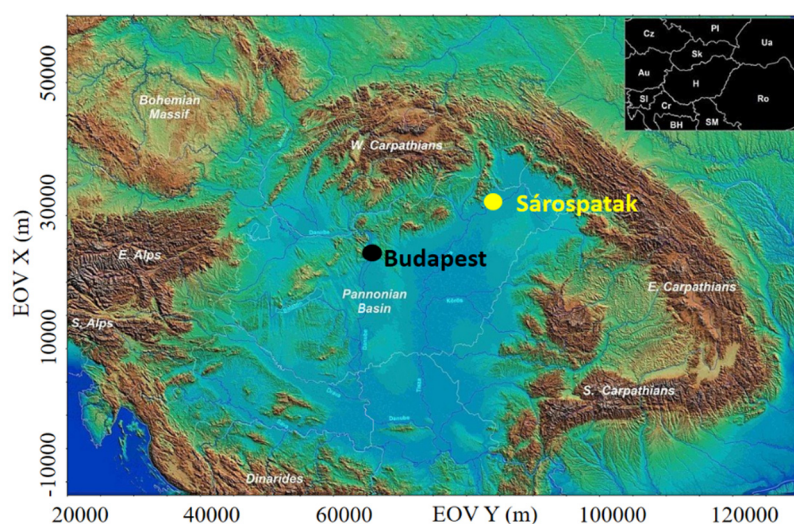


FIGURE 2: Location of the Sárospatak model in the Pannonian basin (modified after Horváth et al., 2006)

Budapest), other types of utilization have been increasing in the last decade. More and more municipalities are investigating and implementing geothermal production for alternate energy supply and for space heating in residential, public and industrial buildings. In addition, the first geothermal power plant is also about to be built near the town of Tura.

Using numerical reservoir models in order to simulate field capacity/performance under a variety of conditions is not just helpful, but is also a crucial part of successful geothermal exploration and development. With the help of numerical modelling, it is possible to predict worst- and best-case exploitation scenarios in a geothermal project, and therefore manage the development of the project in an efficient manner. Perhaps the most important and challenging part of the modelling process is the collection and integration of information compiled by all the geoscientific disciplines, leading to the development of the conceptual model.

The geothermal potential of Sárospatak in northeast Hungary (Figure 2) was first discovered in the late 1950s when geothermal wells began supplying water for a thermal spa in the city. The thermal wells have been producing from a relatively thin layer of a fractured rhyolite tuff formation. The lateral extent of this tuff formation is unknown, but it is believed to be hydraulically connected to the deeper Triassic carbonate reservoir in the basement, which is believed to have a much larger lateral extent (Erhardt, 1962). Overall, the area is lacking in detailed data from the carbonate reservoir and its exact hydraulic parameters. In 2013, an Icelandic company, Vatnaskil Consulting Engineers, constructed a numerical model of the geothermal reservoir at Sárospatak as part of a preliminary feasibility study. The model was used to simulate the effects of a proposed well duplet for use in district heating. The main objective was to predict the impact of the planned production and injection wells with a special focus on the existing geothermal wells associated with the thermal spa of the city of Sárospatak.

The goals of this study were twofold. First, the original model developed by Vatnaskil in 2013 was reviewed and analysed in an effort to determine the input parameters with the most amount of uncertainty. A literature review was performed in order to find new data which could improve the understanding of the most important model parameters. The second part of the study entailed performing a sensitivity analysis on the model in order to determine model parameters which have the most

influence on the simulated results. It is hoped that this evaluation of the model of Sárospatak helps give a better understanding of the geothermal potential of the reservoir, and therefore contribute to the energy development plan of the city of Sárospatak.

2. MODEL REVIEW

2.1 Geological setting

On a large scale, the study area is located on the northeast edge of the Pannonian Basin (Figure 2). The basin is surrounded by a mountain range, namely the Carpathians. It was formed during the Middle Miocene due to extension and thinning of the lithosphere. This thinning is the main reason for the relatively high heat flow and thermal gradient of the area (Lenkey et al., 2002).

On a smaller scale, the model area lies on the southeast margin of the Tokaj Mountains and the northeast edge of the Great Hungarian Plain, along the river Bodrog at an elevation of around 100-200 m above sea level. The surface geology consists mainly of alluvial and fluvial sediments from the Pleistocene, such as gravel, loess and clay (Lengyel, 1957). Underneath these units and on the hills of the Tokaj Mountains, Miocene-aged volcanics are common, and consist of mainly tuffs and breccias with a composition ranging from andesitic to rhyolitic. These formations are often extensively altered due to volcanic hydrothermal processes, creating silicified successions often composed of kaolinite or bentonite. These volcanic units can exceed 300 m thickness (Lengyel, 1957).

The Miocene formations directly overlie the basement units with an unconformity indicating a long chronological gap. These basement rocks consist of Triassic carbonates which are in an uplifted, horst position and are thus capable of forming a productive geothermal reservoir (Pentelényi et al, 2003, Haas et al., 2010). Figure 3 shows the elevation of the basement along with the known extent of the Triassic carbonates in the area. Besides indirect investigations of the basement formations, such as basement rock inclusions or hydrothermal veining in the younger volcanics, the only direct information available is from well Sp-5, which is the only well that penetrates into the Triassic carbonates (Figure 3). Despite that fact that Sp-5 was drilled to a depth of close to 400 m, it did not penetrate the entire sequence of

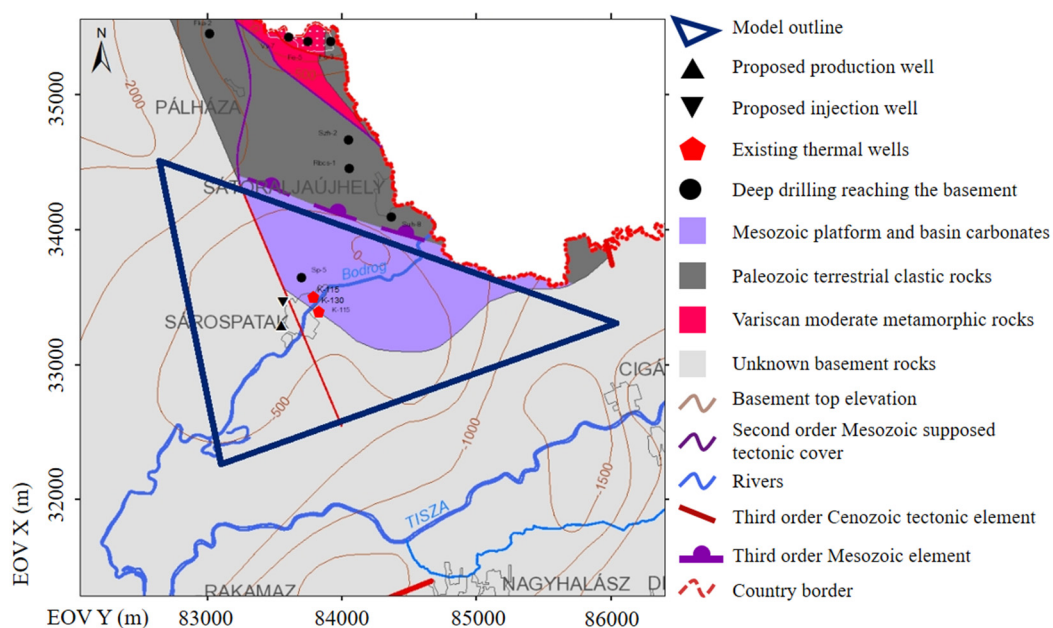


FIGURE 3: Model boundaries and the basement geology of the study area (modified after Haas et al., 2010)

Triassic carbonate rock (Csoma and Molnár, 1999; Pentelényi et al., 2003). The well has confirmed, however, that the Triassic sequence is mainly composed of the Dachstein-type platform carbonate (“Dachstein Limestone Formation”), which is known and well-studied in other parts of the Pannonian basin (Wein, 1977; Császár, 1997). Based on these studies, it is assumed that the Dachstein Formation overlies a Triassic dolomite succession, called the “Hauptdolomite” Formation. Altogether, the estimated thickness of the entire carbonate sequences exceeds 1700 m (Császár, 1997).

The geothermal potential of these types of deep carbonate reservoirs is recognized around the world. Besides the faults and fractures, the most important process that contributes to the creation of a productive reservoir is karstification (Goldscheider et al., 2010). Two different processes can be distinguished, the well-known “epigene” and the less known “hypogene” karstification. Many deep carbonate rocks were exposed to epigene karstification in earlier geologic times and then buried by younger sequences, preserving their karstic features. Thus, they create “paleokarsts” which contribute to the reservoir porosity (Smosna et al., 2005). However, several processes can enlarge fractures and conduits after burial, and these processes are called “hypogenic” karstification or speleogenesis. These processes can considerably enhance both the porosity and the hydraulic conductivity in the reservoir, thereby creating significant geothermal reservoirs. This type of reservoir has been observed all over the world (Klimchouk, 2007). In fact, one of Europe’s largest thermal systems, the “Buda Thermal Karst” in Hungary, which is partly composed of the same Triassic carbonates as occur in Sárospatak, has been mainly formed by these processes (Goldscheider et al., 2010). This also supports the assumption that the geothermal potential of Sárospatak is indeed considerable.

2.2 Model description

The original numerical model of the Sárospatak reservoir was constructed by Vatnaskil in 2013, and the following description of the reservoir dimensions and parameters is based on the Vatnaskil memo (Myer, 2013) describing the modelling work.

The modelled reservoir consists of fractured and karstified carbonate rocks of Triassic age which extend uninterrupted within the model area.

2.2.1 Dimensions and boundaries

The lateral boundaries of the model (Figures 2 and 3) were defined by using regional tectonic and structural features and were determined as no-flow model boundaries. However, because of the sparse availability of the data in the area, assumptions were made in many cases. The northeast boundary is an interpreted nappe structure described by Haas et al. (2010). The southeast boundary follows a large fault which is parallel to the mid-Hungarian tectonic line. The western boundary lies along a hydrothermal calcite vein near the village of Komlóska (Figure 2), which has been mapped by Csoma and Molnár (1999). They assumed that the origin of the vein-forming hydrothermal fluids was the Triassic carbonate and this was therefore interpreted as the last indirect proof of the basement rocks to the west.

The vertical dimensions of the reservoir model were determined using lithological boundaries. The upper part consist of the Dachstein Limestone Formation while the lower part is made of the Hauptdolomite Formation. The vertical discretization consists of 7 layers according to the distinctive hydrostratigraphic units (Table 1). The upper 4 layers belong to the Dachstein Limestone Formation. The efficiency of surface karstification decreases with depth, and therefore, the hydraulic conductivity of the limestone also decreases with depth. The lower 3 layers are built up by the Hauptdolomite Formation. The hydraulic parameters were defined according to the abundance of the fractures in the formation. The proposed production/injection well duplet targets the uppermost limestone layer.

TABLE 1: The main hydraulic parameters of the original Sárospatak model

Model layer	Rock type	Alteration	Thickness [m]	Hydraulic conductivity [m^2/s]	Porosity (%)	Rock compressibility [m^2/N]
1	Dachstein Limestone	Heavily karstified	100	1×10^{-4}	1.00	1×10^{-9}
2		Karstified	100	1×10^{-5}	0.50	1×10^{-9}
3		Poorly	100	1×10^{-6}	0.50	1×10^{-9}
4		Limestone	100	1×10^{-7}	0.10	1×10^{-10}
5	Hauptdolomite	Fractured	30	1×10^{-4}	1.00	1×10^{-9}
6		Dolomite	24	1×10^{-6}	0.25	1×10^{-10}
7		Fractured	30	1×10^{-4}	1.00	1×10^{-9}

The elevation of the top layer was made using available data on the pre-Tertiary basement map by Haas et al. (2010) (Figure 3) and the thickness of the layers were assumed constant (Figure 4). The total thickness of the 7 layers is 700 m which is a rough average between theoretical thicknesses of the Triassic carbonate formations and the measured thickness by well Sp-5 (Pentelényi et al., 1993). Two cross-sections of the modelled reservoir are shown in Figure 4. Their locations are shown in Figure 5.

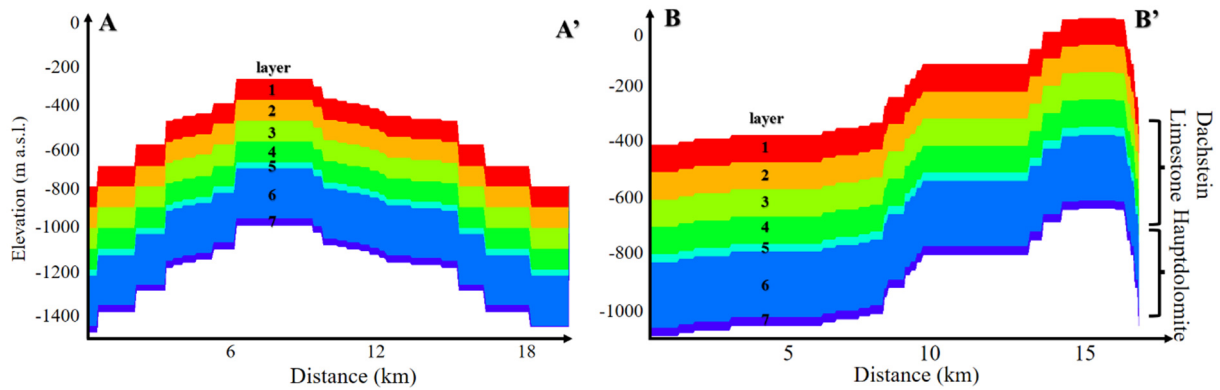


FIGURE 4: Cross-sections A-A' and B-B' showing vertical discretization of the model

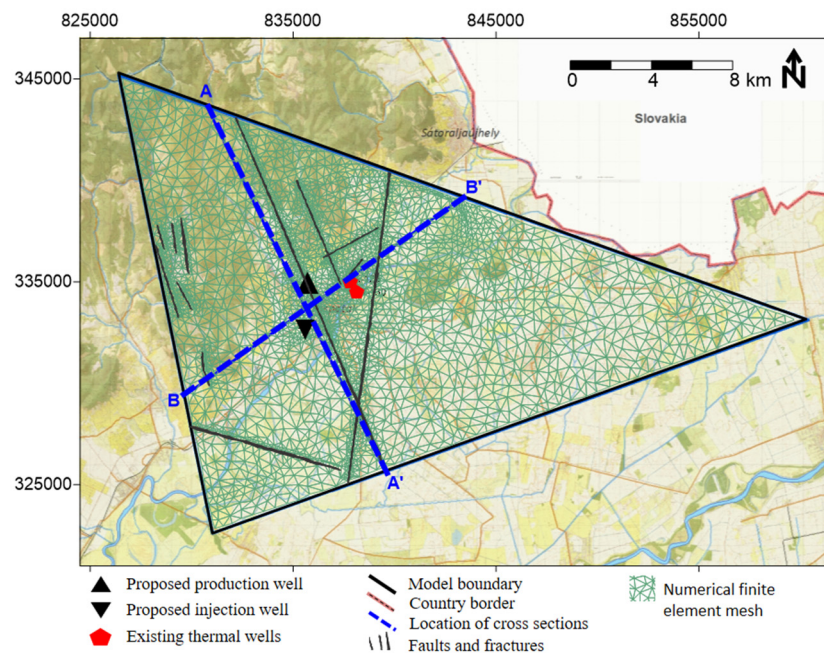


FIGURE 5: Fractures and faults, the locations of the cross sections (Figure 4) and the finite element mesh

The upper no-flow boundary of the reservoir model is the overlying Miocene tuff caprock. Most of the formation contains clay layers, which provide a barrier to vertical groundwater flow. On the other hand, the existing thermal wells in Sárospatak are producing from the lower 0-50 m of this tuff which is silicified and fractured and therefore hydraulically connected to the Triassic carbonates. However, there is no evidence that the zone exists elsewhere in the model area outside of Sárospatak so the zone was not included in the original reservoir model. This was done in an effort to take a more conservative approach in modelling the effects of the proposed well duplet. A thinner reservoir would give more drawdown with the same production.

The physical parameters of the specific layers in the model were collected from:

- Well logs
 - Hungarian Mining and Geological Authority
 - Mining Property Utilization Company
- Technical data from existing hydrocarbon and thermal wells in the area
 - Regional Agency of the National Environmental
- Seismic data
 - Hungarian Mining and Geological Authority
- Hydrogeological reports
 - Environmental and Hydrological Research Institute (VITUKI)

2.2.2 Parameters

The *hydraulic conductivity* for each layer was defined from published values for similar rock types and calculated values from well tests performed on existing hydrocarbon and thermal wells. For the main hydraulic parameters, see Table 1.

The *faults and fractures* determine the amount of anisotropy in the reservoir and thus the flow of groundwater. In the model, they were defined from interpretation of various geological maps (Lengyel, 1957; Gyarmati, 1964; Haas et al., 2010) and are shown in Figure 5. The area's regional fault system direction is NE-SW (Frits, 1964). It was assumed that the hydraulic conductivity is 5 times greater in the direction of this regional fracture system than perpendicular to it. Within individual major fractures the anisotropy was assumed even greater, with defined hydraulic conductivity 10 times greater in the direction of the fracture than perpendicular to it. It was also assumed that the vertical hydraulic conductivity is 10 times lower than the horizontal hydraulic conductivity.

The temperature of the geothermal fluid was estimated from the temperature data from well testing and drilling logs. The assumed *thermal gradient* of 20°C/km was used to calculate the background temperature of the reservoir fluid within each layer of the model.

The reservoir's *rock compressibility* is used to calculate specific storage which controls groundwater level fluctuations. Porosity is also used to calculate specific storage. The estimated porosity values for each layer in the model can be seen in Table 1.

The Triassic carbonate formations do not outcrop within the model area and are overlain by several hundred meters of low-permeability caprock, mostly the above mentioned Miocene tuffs. Therefore, it was assumed that there is no *infiltration* recharge into the reservoir model.

2.2.3 Numerical model

Numerical modelling was done using Vatnaskil's self-developed software, Aqua3D (Vatnaskil, 2013). The program is a finite-element model used to solve three-dimensional groundwater flow and mass/heat transport problems. Vatnaskil has utilized Aqua3D over the past 30 years on a number of geothermal reservoirs all around the world and it has proven to be a reliable and accurate tool.

The software uses the following three-dimensional flow equation for describing the movement of groundwater flow with constant density:

$$\frac{\partial}{\partial x} \left(k_{xx} \frac{\partial h}{\partial x} \right) + \frac{\partial}{\partial y} \left(k_{yy} \frac{\partial h}{\partial y} \right) + \frac{\partial}{\partial z} \left(k_{zz} \frac{\partial h}{\partial z} \right) = S_s \frac{\partial h}{\partial t} - Q \quad (1)$$

where k_{xx}, k_{yy}, k_{zz} , are values of the hydraulic conductivities along the principal axes [m/s]
 h is the piezometric head [m]
 Q is a volumetric flux per unit volume [m³/s/m³]
 S_s is the specific storage coefficient [m⁻¹]
 T is time [s]

Specific storage is calculated for each layer in the model using the following formula:

$$S_s = \rho g (\alpha + \varphi \beta) \quad (2)$$

where ρ density of the reservoir fluid [kg/m³]
 g acceleration due to gravity (9.81 m/s)
 α rock compressibility [m²/N]
 φ porosity
 β fluid compressibility (4.4·10⁻¹⁰ m²/N)

The solution of the three-dimensional mass/heat transport problem is based on the following partial equation:

$$\begin{aligned} & \frac{\partial}{\partial x} \left(D_{xx} \frac{\partial T}{\partial x} \right) + \frac{\partial}{\partial y} \left(D_{yy} \frac{\partial T}{\partial y} \right) + \frac{\partial}{\partial z} \left(D_{zz} \frac{\partial T}{\partial z} \right) + \\ & + Q(T_w - T) - \left(V_x \frac{\partial T}{\partial x} + V_y \frac{\partial T}{\partial y} + V_z \frac{\partial T}{\partial z} \right) = \varphi R_h \frac{\partial T}{\partial t} \end{aligned} \quad (3)$$

where D_{xx}, D_{yy}, D_{zz} are dispersion coefficients along the principal axes
 t is time [s]
 T is the temperature of the reservoir water [°C]
 T_w is the temperature of the injected water [°C]
 Q is pumping/injection rate [m³/s]
 V_x, V_y, V_z are the velocity vectors taken from the solution of the flow problem [m/s]
 φ is porosity
 R_h is retardation coefficient

The retardation coefficient is calculated by:

$$R_h = 1 + \left(\frac{c_s}{c_l} \right) \frac{(1 - \varphi) \rho_s}{\varphi \rho_l} \quad (4)$$

where c_s is the specific heat capacity of the porous medium [J/g°C]
 c_l is the specific heat capacity of the liquid [J/g°C]
 ρ_s is the density of the porous medium [kg/m³]
 ρ_l density of the reservoir fluid [kg/m³]

The three-dimensional model of the Sárospatak reservoir constructed by Vatnaskil consists of 3808 nodes and 7419 finite elements, creating a mesh (Figure 5) in 7 layers in order to define depth-varying hydrological parameters. As mentioned previously, Vatnaskil assumed that the boundaries of the model are based on tectonic and lithological features and provide no-flow conditions to the reservoir.

2.3 Results

For the preliminary reservoir modelling, two different production/injection scenarios (Scenario A and Scenario B) were simulated (Table 2). A well duplet was defined in the reservoir as shown in Figure 3 and 5. It was assumed that all the production was reinjected back into the reservoir with lower temperature according to the scenario and the heating/summer season. The reservoir parameters for the two scenarios were the same.

TABLE 2: Production rates and the injection temperatures used for Scenarios A and B by Vatnaskil in 2013

Scenario	Production [m ³ /s]		Temperature of reinjection fluid [°C]	
	Winter	Summer	Winter	Summer
A	2.43×10^{-2}	4.86×10^{-3}	40.5	34
B	3.08×10^{-2}	9.71×10^{-3}	42.5	40

The results for Scenarios A and B are shown in Figure 6. The simulation for drawdown and upconing were calculated and shown after 20 years of hypothetical operation with the given production/injection rates. The cooling effect was calculated and plotted after 50 years of operation. As the figures show, the drawdown/upconing are visible, but not drastic. In the well's immediate vicinity the change in the water

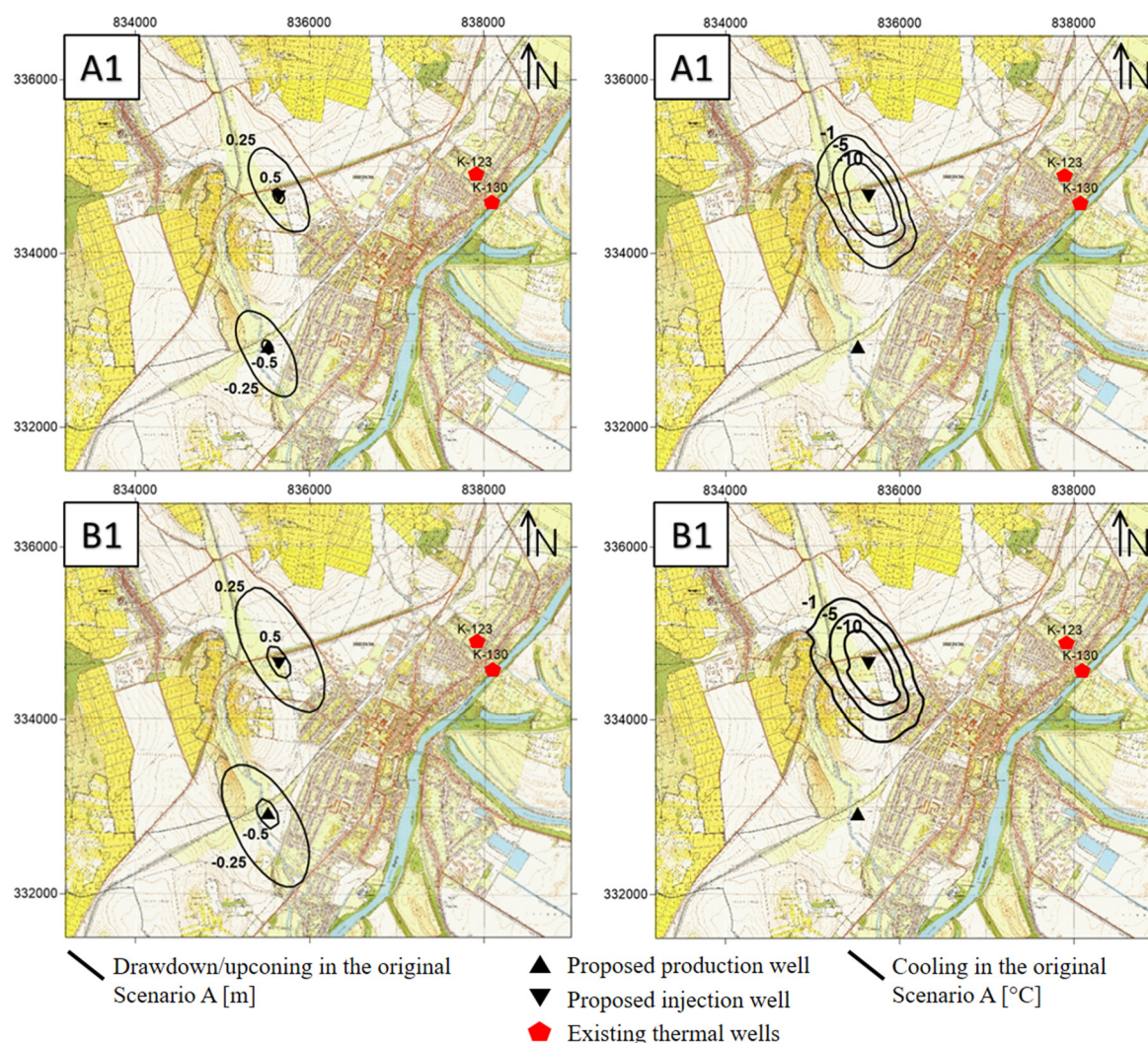


FIGURE 6: Results of the original model for Scenario A (top) and Scenario B (bottom). The drawdown/upconing effects are shown on the left and the cooling effects on the right

level is 50 cm, with a 25 cm change within roughly 1 km of each well. At a distance of greater than 1 km, the change in water level is negligible. In the case of the cooling effect around the well, the affected zone is similar. The cooling effects appear in the immediate vicinity of the injection well with a maximum cooling of 10°C, but a couple of hundred meters away from the well there is less than 1°C cooling. These areas are relatively small compared to the entire reservoir. The main conclusion of from the scenario runs is that the proposed well duplet, both in the case of the drawdown/upconing and cooling effects, has a negligible influence on the existing thermal wells in Sárospatak.

2.4 Collection of new data

As part of this study, additional research in the literature was done in order to investigate possible ways to improve the original Sárospatak model. The aim was to get a broader picture of the carbonate geothermal reservoirs abroad and in Hungary and then to gather as much information of the Sárospatak area as possible.

2.4.1 Hydraulic parameters

S. N. Ehrenberg and P. H. Nadeau (2005) collected data from 10,481 carbonate petroleum reservoirs and 30,122 siliciclastic reservoirs from all over the world. Although the petroleum industry can be quite different from the geothermal industry, from a hydrogeological point of view, the geological information can be useful for both industries. Ehrenberg and Nadeau plotted the average porosity vs. depth for all the carbonate reservoirs they investigated (Figure 7A). Although the carbonate reservoirs have less porosity than the sandstones, the average porosities above 2 km depth is between 10 and 17%. In the paper, they also plotted the average permeability vs. porosity in order to have an idea of the hydraulic conductivity (Figure 7B). It is certain that with decreasing porosity, the permeability also decreases. Below 15% porosity, the permeability varies between 10-100 mD. In order to compare these permeability values with values in the Sárospatak model, the relevant values from the paper were converted into hydraulic conductivities in units of m/s as shown in Equation 5 below. The conversion was based on Darcy's law presented in the book of Freeze and Cherry (1979). The converted hydraulic conductivities and the comparison can be seen in Tables 3 and 4.

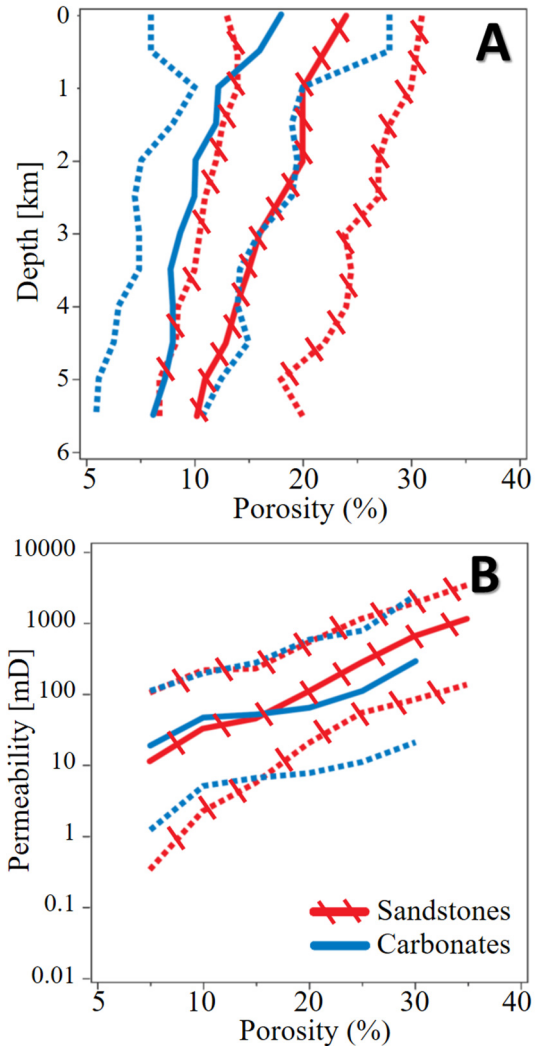


FIGURE 7: Depth vs. porosity (A) and permeability vs. porosity (B) in the sandstone and carbonate reservoirs from all over the world (Ehrenberg and Nadeau, 2005). The continuous lines represent the average values, whilst the dotted lines indicate the lower and upper 10% limits where 90% of the reservoirs fall within

$$K = \frac{k\rho g}{\mu} \quad (5)$$

where:

K is the hydraulic conductivity [m/s]
 k is the permeability [m²]
 ρ is the density [1000 kg/m³]

g is the gravitational acceleration [10 m/s^2]
 μ the dynamic viscosity [$0.5465 \text{ mPa}\cdot\text{s}$ at 50°C]

From Table 3, we can see that the average porosities of the carbonate reservoirs of the world are 10-100 times higher in the relevant depth range than in the case of the Sárospatak model, according to Ehrenberg and Nadeau. There is more similarity between the model and the values given by Ehrenberg and Nadeau for the hydraulic conductivity, however at shallower depths the model difference is roughly 2 orders of magnitude with the model values being higher.

TABLE 3: Average porosity values vs. depth of the carbonate reservoirs from all around the world (Ehrenberg and Nadeau, 2005). The highest and lowest porosities from the Sárospatak model are also shown for comparison

Depth [km]	Porosity [%]	Porosity from the Sárospatak model [%]
0.25–0.75	16	1.0 (highest)
0.75–1.25	12.2	
1.25–1.75	12	0.1 (lowest)

In 2014, Götz et al. directly examined and measured the hydraulic parameters of specific rock formations, collecting samples from the vicinity of Budapest. The work was done both in the field and in the laboratory. The one formation they investigated that exists in the Sárospatak reservoir is the Triassic Hauptdolomite. The measured permeability was $4.40\text{E-}15 \text{ m}^2$, which was converted to $8.05\text{E-}08 \text{ m/s}$ hydraulic conductivity with the same method mentioned above. This is around one order of magnitude less than the hydraulic conductivity of the unaltered Hauptdolomite defined in the Sárospatak model.

TABLE 4: Average permeability vs. porosity values, and the converted hydraulic conductivities from carbonate reservoirs from all over the world (Ehrenberg and Nadeau, 2005). The highest and lowest hydraulic conductivities from the Sárospatak model are also shown for comparison

Porosity (%)	Permeability [md]	Permeability [m^2]	Hydraulic conductivity [m/s]	Hydraulic conductivities from the Sárospatak model [m/s]
7.5–12.5	42	4.15×10^{-14}	7.58×10^{-7}	1.00×10^{-4} (highest)
12.5–17.5	46	4.54×10^{-14}	8.31×10^{-7}	1.00×10^{-7} (lowest)

In 2012, within the framework of the “T-JAM” project between Hungary and Slovenia, Nádor et al. (2012) made a geothermal reservoir model for the Mura-Zala basin which covers areas from both countries. In this model, based on their resources, they calculated hydraulic parameters for both the Dachstein Limestone and the Hauptdolomite Formations. The results can be seen in Table 5.

TABLE 5: Values of porosity and hydraulic conductivity from Nádor et al. (2012)

Rock type		Porosity [%]	Hydraulic conductivity [m/s]
Dachstein Limestone	min.	1	5.79×10^{-7}
	max.	3	1.16×10^{-6}
Hauptdolomite	min.	1	5.79×10^{-7}
	max.	3	1.16×10^{-6}

However, Péter Szűcs and György Ritter (2007) created a geothermal model for the Sárospatak (Végardó) Spa and they used slightly different parameters for the Triassic limestone. They also included the Miocene siliceous fractured rhyolite tuff layer into their model, where the spa's thermal wells are screened. The relevant parameters are shown in Table 6. Although Szűcs and Ritter modelled the same reservoir as Vatnaskil, their model covered only the area of Sárospatak and its immediate vicinity. This was probably made because of a lack of information on the lateral extent of the rhyolite tuff. The defined thickness of the karstified limestone and hydraulic conductivity are very similar to the values in the Vatnaskil model. However, the porosity is somewhat higher than the porosity defined in the Vatnaskil model.

TABLE 6: Hydraulic parameters used by Szűcs and Ritter (2007) in their model for the Sárospatak-Végardó Spa

Rock type	Thickness [m]	Hydraulic conductivity [m/s]	Porosity [%]
Miocene, siliceous, fractured rhyolite tuff	min. 40	1.16×10^{-5}	5
	max. 40	6.94×10^{-5}	
Triassic, karstified limestone	min. 100	2.31×10^{-5}	3
	max. 100	2.31×10^{-6}	

Using well data, Zoltán Fejes (2011) collected and calculated hydraulic parameters from the vicinity of the town Szerencs. This small city neighbours Sárospatak, so the reference is quite local. His calculations lead to 2.14×10^{-4} m/s hydraulic conductivity for the above-mentioned Miocene silicified and fractured rhyolite tuff. This value is very similar to the hydraulic conductivity defined in the heavily karstified limestone, which is the top layer in the Sárospatak value.

2.4.2 Existing thermal wells in the reservoir

The Sárospatak-Végardó geothermal spa operates two thermal wells which are supposedly exploiting from the reservoir. However, neither of them is actually screened within the Triassic limestone, but rather from slightly above it. The formation is often described as a silicified and fractured rhyolite tuff from the Miocene age and it overlays the Triassic carbonate rocks with an unconformity. The two formations are thought to be hydraulically connected with each other, and thus part of the same geothermal reservoir.

The first existing geothermal well was drilled in 1960 with the name Vé-27, and although it was initially very promising it had to be shut down in 1967 due to bad conditions of the well itself. In the same year, well Vé-2 (K-123) was drilled and started to operate with a temperature of 49°C and flow rate of 1000 l/min (1440 m³/day). The bottom of the well was at 290 m depth. Because the owners were experiencing significant pressure drop in the well, they drilled another well, V-3 (K-130), in 1984. This well reached a depth of 344 m and started to produce with a temperature of 45°C and flow rate of 700 l/min (1008 m³/day). Since 1984, a significant pressure drop has been experienced in both wells. In 2007, the maximum allowed production rate was 450 l/min for K-123 and 700 l/min for K-130.

After analysing the literature, it can be concluded that the values of the main hydraulic parameters used in the original Vatnaskil model of Sárospatak compare reasonably well with published values from other similar geothermal reservoirs. The exception is that the porosity values used in the Vatnaskil model are much lower than published values. Furthermore, in the Vatnaskil model, the bottom of the Miocene tuff layer from which the existing wells are producing is not included due to lack of information about the extent of the layer.

3. MODEL SENSITIVITY ANALYSIS

3.1 Overview

In order to determine which model parameters are most important with respect to their influence on the results of drawdown/upconing and cooling, a sensitivity analysis study was performed. The focus was on the parameters which have the largest variability and uncertainty (hydraulic conductivity and porosity). It was also decided to investigate the effects of the existing thermal wells on the reservoir.

The B scenario from the original Vatnaskil (2013) work was used as the base model from which all new sensitivity scenarios were constructed. Therefore, results from the new sensitivity analysis runs were plotted against the results from the B1 scenario in order to determine the effects of the changed parameters. The water level changes were plotted after approximately 20 years of production (7470 days), and the cooling effects after 50 years of production (18250 days). The results are described and shown in Section 3.3.

3.2 Altered parameters

In each scenario, only one parameter was changed at a time, with the exception of Scenarios 1-3. In total, 11 different scenarios were simulated which can be divided into three groups.

In the first group of scenarios, a new layer was added to the top of the model representing the Miocene siliceous and fractured rhyolite tuff. The parameters assigned to this new layer were based on the work of Fejes (2011) and are described in Table 7.

TABLE 7: The main hydraulic parameters of the extra layer in Scenario 1-3 (based on: Fejes, 2011)

Rock type	Thickness [m]	Hydraulic conductivity [m/s]	Porosity [%]
Siliceous, fractured rhyolite tuff	40	2.14×10^{-4}	1

In Scenario 1, the extra layer was added but no production from the existing thermal wells at the Sárospatak-Végardó spa was defined. In Scenarios 2 and 3 the production from the existing wells was defined in the model. Due to conflicting data on the actual production rates from these existing wells, two scenarios were run in order to account for this uncertainty (Table 8). For simplicity, constant production rates were defined.

TABLE 8: Production rates [m^3/s] in the first 3 scenarios

Layer	Screened Wells	Summer			Winter		
		Scenario 1	Scenario 2	Scenario 3	Scenario 1	Scenario 2	Scenario 3
Karstified limestone (Layer 2)	Production	-3.08×10^{-2}	-3.08×10^{-2}	-3.08×10^{-2}	-9.71×10^{-3}	-9.71×10^{-3}	-9.71×10^{-3}
	Injection	3.08×10^{-2}	3.08×10^{-2}	3.08×10^{-2}	9.71×10^{-3}	9.71×10^{-3}	9.71×10^{-3}
Rhyolite tuff (Layer 1)	K-123	-	-7.50×10^{-3}	-1.14×10^{-3}	-	-7.50×10^{-3}	-1.14×10^{-3}
	K-130	-	-1.17×10^{-2}	-7.57×10^{-4}	-	-1.17×10^{-2}	-7.57×10^{-4}

In the second group of the simulations, only hydraulic conductivities were altered, and in the third group only porosity values were altered. For the second and third group of scenarios, the original 7-layer model (without the silicified and fractured rhyolite tuff layer) was used. The altered parameters are shown in Table 9. In Scenarios 4 and 11, only the bottom layers were changed. Since the degree of karstification in the upper parts of the carbonates is relatively unknown, Scenarios 5-10 were used to alter parameters based on this factor. In Scenario 5 and 9, it was assumed that the top 3 layers were all poorly karstified,

TABLE 9: The altered parameters of Scenarios 4-11. The yellow cells show where the parameters were changed and the underlines show the parameters they were based on. For more details see text

Model layer	Rock type	Alteration	Thickness [m]	Hydraulic conductivity [m/s]					Porosity (%)				
				Original	Scenario 4	Scenario 5	Scenario 6	Scenario 7	Original	Scenario 8	Scenario 9	Scenario 10	Scenario 11
1	Limestone	Heavily Karstified	100	1.00E-04	1.00E-04	1.00E-06	<u>7.28E-04</u>	<u>1.00E-04</u>	1.00	<u>3.00</u>	0.50	<u>12.00</u>	1.00
2		Karstified	100	1.00E-05	1.00E-05	1.00E-06	7.28E-05	1.00E-04	0.50	1.50	0.50	6.00	0.50
3		Poorly	100	1.00E-06	1.00E-06	<u>1.00E-06</u>	7.28E-06	1.00E-04	0.50	1.50	<u>0.50</u>	6.00	0.50
4		Limestone	100	1.00E-07	1.00E-07	1.00E-07	7.28E-07	1.00E-07	0.10	0.30	0.10	1.20	0.10
5	Dolomite	Fractured	30	1.00E-04	8.05E-06	1.00E-04	1.00E-04	1.00E-04	1.00	1.00	1.00	1.00	<u>12.00</u>
6		Dolomite	24	1.00E-06	<u>8.05E-08</u>	1.00E-06	1.00E-06	1.00E-06	0.25	0.25	0.25	0.25	3.00
7		Fractured	30	1.00E-04	8.05E-06	1.00E-04	1.00E-04	1.00E-04	1.00	1.00	1.00	1.00	12.00

and in Scenarios 5, 8 and 10 it was assumed that the top layers were all heavily karstified. In Scenario 6 the model was run with the highest hydraulic conductivity that has been found in the literature for the limestone. Similarly in Scenario 10, the model was run using the average porosity of the world's carbonate reservoirs according to Ehrenberg and Nadeau (2005). A summary of the 11 scenarios with the altered parameters are shown below.

Additional model layer

- Scenario 1** An extra layer added to the top of the model to represent the siliceous fractured rhyolite tuff. No production from the two existing thermal wells. Hydraulic parameters were taken from Fejes (2011).
- Scenario 2** An extra layer added to the top of the model to represent the siliceous fractured rhyolite tuff. Define production from the two existing thermal wells with the maximum allowed production (Szűcs and Ritter, 2007).
- Scenario 3** An extra layer added to the top of the model to represent the siliceous fractured rhyolite tuff. Define production from the two existing thermal wells with an estimated current production (Vatnaskil, 2013).

Hydraulic conductivity changes

- Scenario 4** Decrease hydraulic conductivity in model layer 6 from 1E-06 to 8.05E-08 m/s which is the average published value for the Hauptdolomite (Götz et al., 2014). Scale the hydraulic conductivity values for layers 5 and 7 down by the same factor as layer 6.
- Scenario 5** Assume model layers 1 and 2 are poorly karstified. Decrease hydraulic conductivity in those layers to the same value as layer 3 (1E-06 m/s).
- Scenario 6** Increase hydraulic conductivity in model layer 1 from 1E-04 to 7.28E-04 m/s which is the calculated value for Triassic limestone from Fejes (2011). Scale the hydraulic conductivity values for layers 2-4 up by the same factor as layer 1.
- Scenario 7** Assume model layers 2 and 3 are heavily karstified. Increase hydraulic conductivity in those layers to the same value as layer 1 (1E-04 m/s).

Porosity changes

- Scenario 8** Increase porosity in model layer 1 from 1 to 3% which is the value for Dachstein Limestone from the T-JAM model (2011). Scale the porosity values for layers 2-4 up by the same factor as layer 1.
- Scenario 9** Assume model layers 1 and 2 are poorly karstified. Decrease porosity in those layers to the same value as layer 3 (0.5 %).
- Scenario 10** Increase porosity in model layer 1 from 1 to 12% which is the value for the average values for carbonates found in reservoirs all over the world (Ehrenberg and Nadeau, 2005). Scale the porosity values for layers 2-4 up by the same factor as layer 1.
- Scenario 11** Increase porosity in model layer 5 from 1 to 12% which is the value for the average values for carbonates found in reservoirs all over the world (Ehrenberg and Nadeau, 2005). Scale the porosity values for layers 6 and 7 up by the same factor as layer 5.

Figure 8 shows the legend for Figures 9-19. The results from the scenario runs are shown in Figures 9-19, where they are compared with results from the original Vatnaskil model (Scenario B). The contours represent the difference in the water level and reservoir fluid temperature in the proposed producing layer (model layer 1) before and after the simulated production. In Figures 9-19, the drawdown/upconing effects are plotted after 20 years (7470 days) and shown on the left, and the cooling effects are plotted after ~50 years (18250 days) of simulated production and are shown on the right. The results from the original model are marked with continuous black lines and results from the sensitivity analysis runs are shown with red and blue dashed lines. The proposed well duplet and the existing thermal wells are also displayed. The coordinates are in the EOV system, which is the main projection system for Hungary.

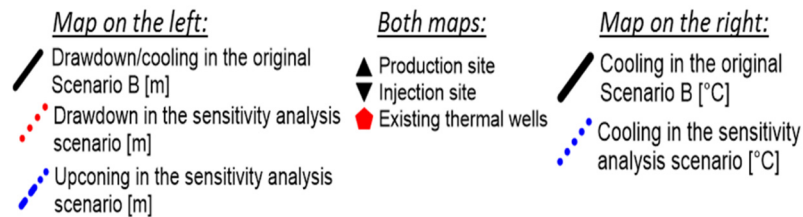


FIGURE 8: Legend of the maps showing the results in Figures 9-19

3.3 Results

Additional model layer

The results from Scenario 1 are shown in Figure 9. For this scenario, an additional layer, 40 m thick, was added to the top of the model in order to represent the siliceous, fractured rhyolite tuff formation. As a results show, the drawdown and upconing effects have significantly decreased compared to the original model. A few hundred meters away from the proposed wells, the change in the water level is less than 10 cm. Although the cooling effect has also decreased, the difference is not that large. In this scenario, adding an extra layer above the production layer of the proposed well duplet has in effect increased the thickness of the reservoir, and thus the storativity. The increased storativity clearly diminishes the drawdown effects and decreases slightly the cooling effects.

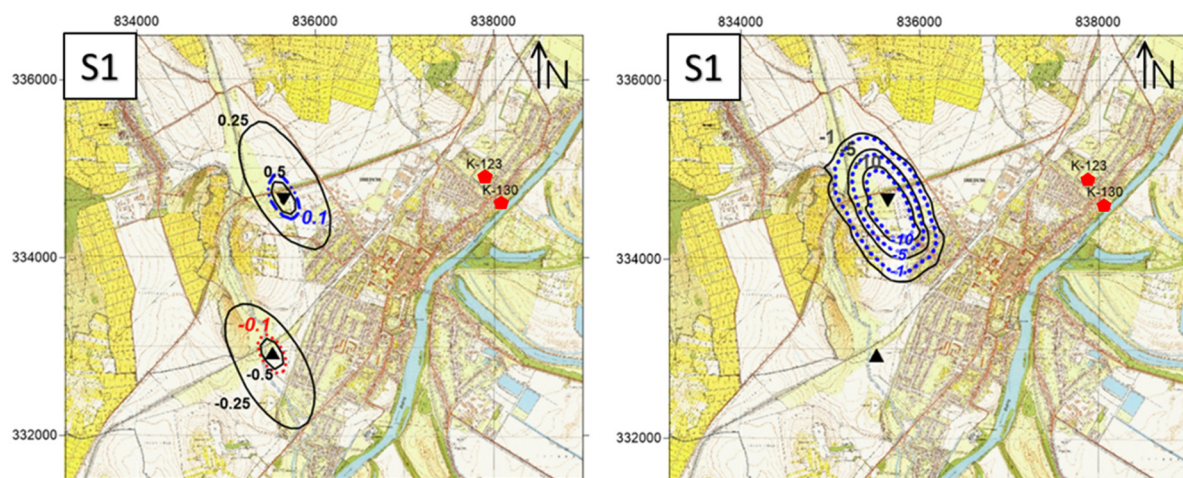


FIGURE 9: Calculated long-term effects of the proposed well duplet on the water level and temperature for Scenario 1

In Scenario 2 (Figure 10), the production from the existing thermal wells at Sárospatak was added to the model with their maximum allowed production rates. The change in the water level is significant for this scenario. The upconing has basically disappeared, and only the drawdown effect is visible now, which is drastically larger than it was in the original model. At a distance of several kilometres from the proposed production well, the water level change is 0.5 m. The effect is much less around the injection well. It seems that although adding an extra layer did increase the storativity, the drastic increase in production from the existing thermal wells outweighs this effect significantly, and they have an impact on the proposed wells (pressure decline). The magnitude of the cooling effect has not changed, it is still very small and is slightly shifted towards the existing thermal wells. This is probably due to changes in the flow direction in the system caused by the production from the existing thermal wells.

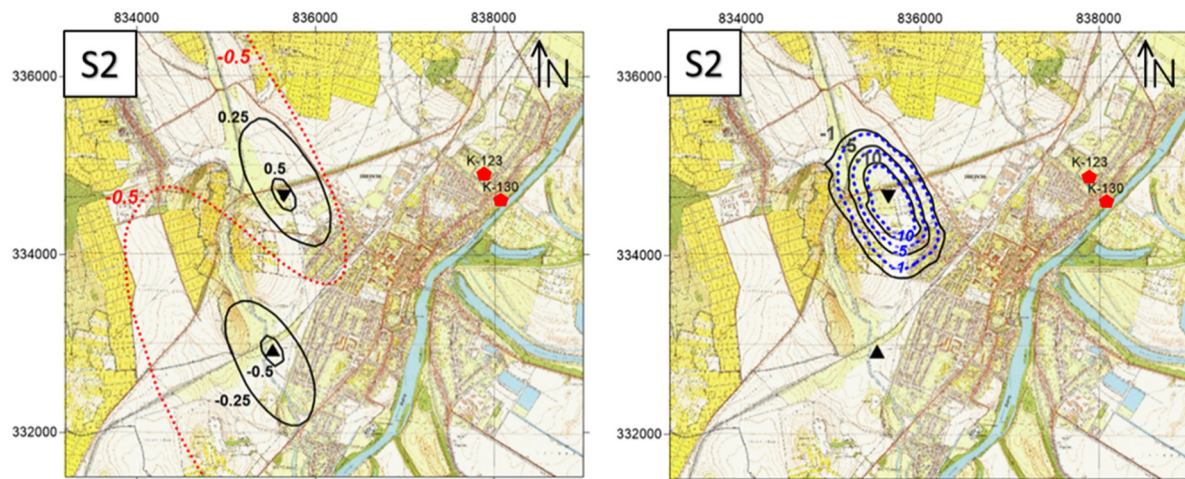


FIGURE 10: Calculated long-term effects of the proposed well duplet on the water level and temperature for Scenario 2

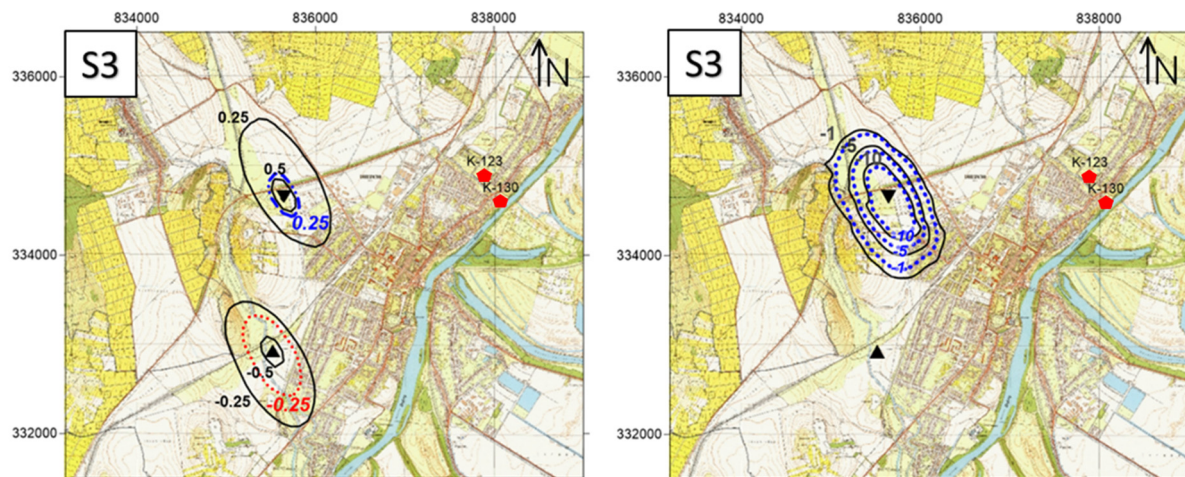


FIGURE 11: Calculated long-term effects of the proposed well duplet on the water level and temperature for Scenario 3

Figure 11 shows the results of Scenario 3. Production from the existing thermal wells was decreased by around one order of magnitude to more realistic rates. In this case, the influence of the increased storage from the extra layer outweighs the impact from the proposed wells on the water level and there is therefore less drawdown/upconing than in the original model. However, the effects on the water levels are still somewhat larger than in Scenario 1. The cooling effect of the reinjection is, however, very similar to Scenario 1.

Note that for all of Scenarios 1-3, there was some change in the cooling effect regardless of the production. The main reason for this is most likely the change in the thickness, and thus the storativity, of the reservoir.

Hydraulic conductivity changes

In Scenarios 4-11, neither the existing thermal wells of Sárospatak nor the extra layer were accounted for in the simulations. In Scenario 4 (Figure 12), the aim was to determine if the hydraulic conductivity of the lower, dolomite layers had any impact on the state of the producing layer. The results of the scenario show very little difference from the results of the original model. Thus, it can be concluded that the hydraulic conductivity of the lower dolomite layers do not influence the effects of the production/injection in the top model layer.

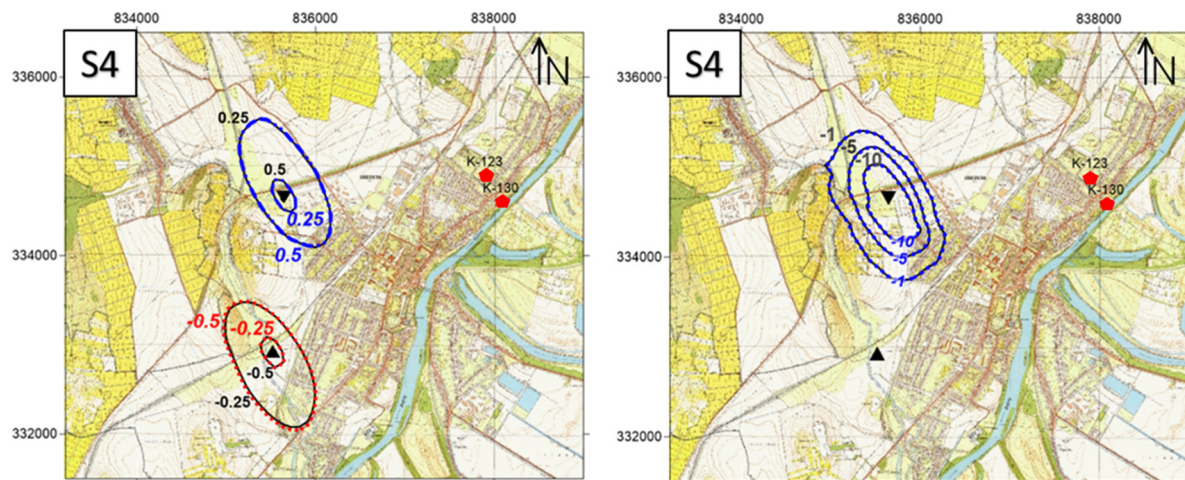


FIGURE 12: Calculated long-term effects of the proposed well duplet on the water level and temperature for Scenario 4

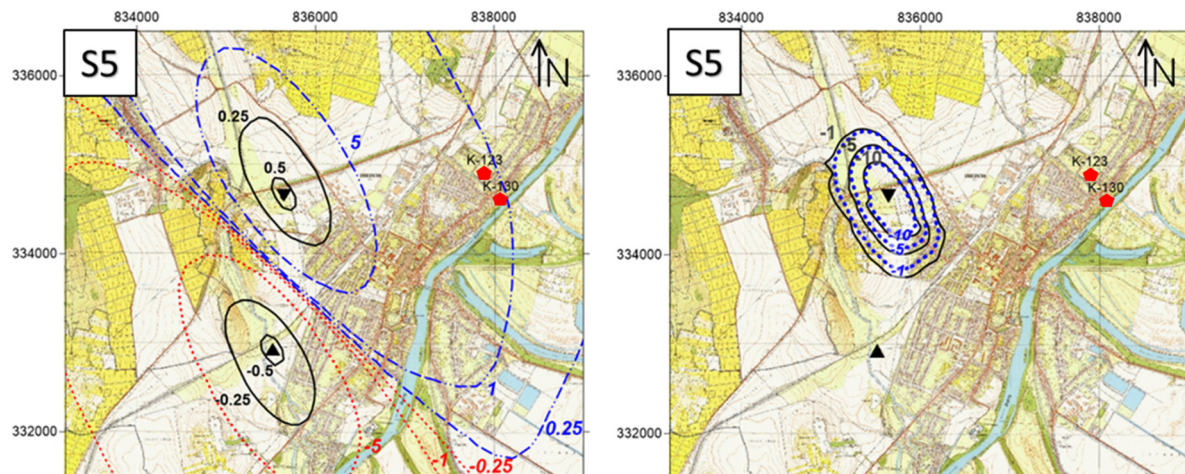


FIGURE 13: Calculated long-term effects of the proposed well duplet on the water level and temperature for Scenario 5

In Scenarios 5-7, the impact of the hydraulic conductivity of the limestone layers was investigated. In Scenario 5 (Figure 13), it was assumed that all the karstified limestone layers (layers 1-3) were poorly karstified. Accordingly, the hydraulic conductivity was lowered in layers 1 and 2 to the same value as layer 3. As a result, the amount of drawdown and upconing drastically increased as can be seen in Figure 13. Where the change in water level was ± 0.25 m in the original model, the calculated change in water level in Scenario 5 was 10 m. The influence from the well duplet reaches the existing thermal wells and causes roughly 1 m of upconing at the wells. The difference between the calculated cooling in Scenario 5 and the original model is minimal.

In Scenario 6 (Figure 14), hydraulic conductivity was increased in all the limestone layers (Table 9). The assumption was based on the highest hydraulic conductivity for limestones in the area, according to Fejes (2011). It is clearly apparent that even this relatively small change of the parameter (\sim seven times) can significantly change the calculated effects of the well duplet on the water level. The results of the scenario show that both the drawdown and upconing are minimal. However, the cooling effect has remained the same as in the original model.

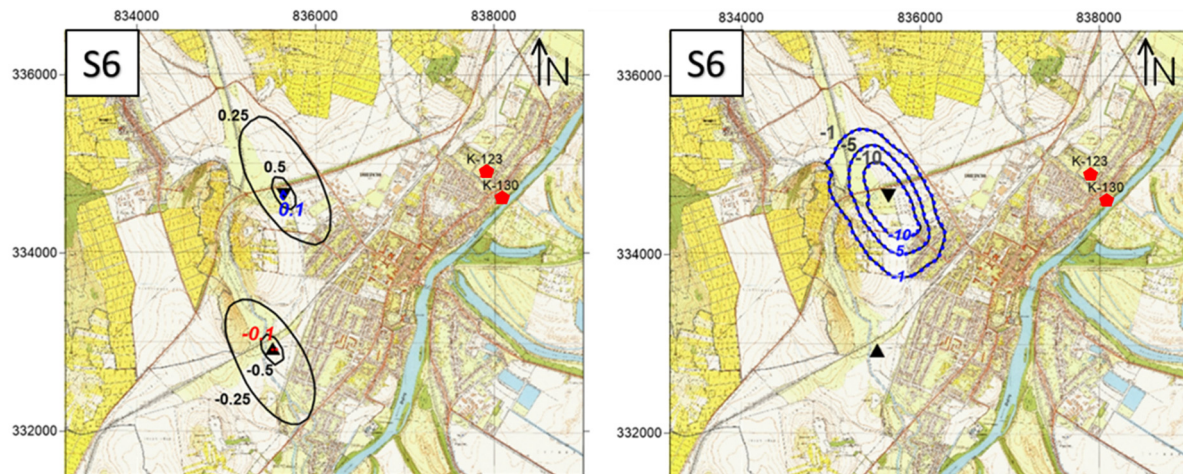


FIGURE 14: Calculated long-term effects of the proposed well duplet on the water level and temperature for Scenario 6

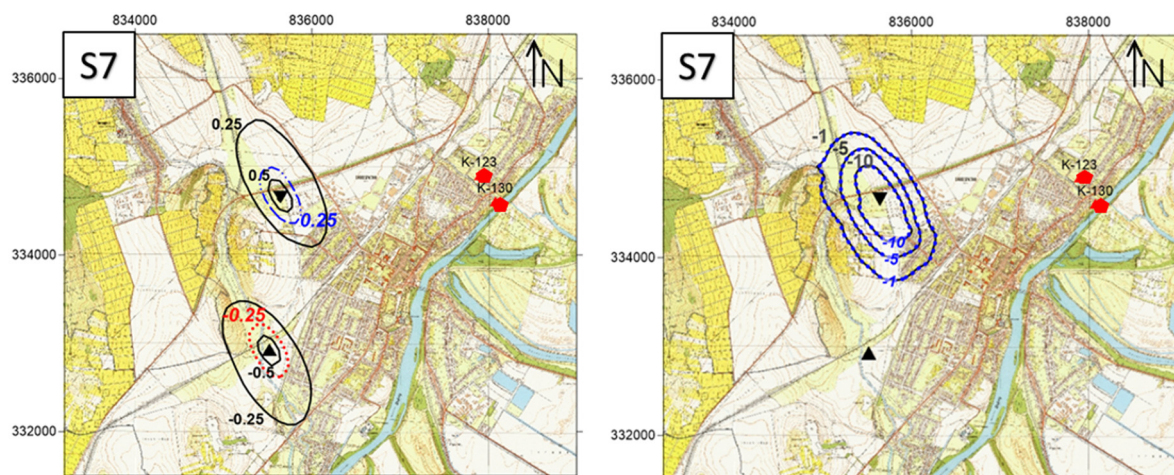


FIGURE 15: Calculated long-term effects of the proposed well duplet on the water level and temperature for Scenario 7

In Scenario 7, showed in Figure 15, the hydraulic conductivity was increased in layer 2 and 3 to the same value as layer 1, i.e. it was assumed that the upper three limestone layers were heavily karstified. In this way, the top three layers were actually unified and handled as one layer in the model, in terms of hydraulic conductivity. The drawdown and the upconing effects were very similar to the original model, although they have both slightly decreased. This is probably because the top 3 layers were behaving as one, in effect increasing the production layer's thickness and hence the storativity. There was very little change, however, in the cooling effects.

Note that among the 4 scenarios of the second group, only one (Scenario 5) caused any significant changes in the cooling effect from the original model. This fact suggests that the degree of cooling is not sensitive to the hydraulic conductivity in this model, or at least not significantly. On the other hand,

the water level change varied to a much larger degree with changes to the hydraulic conductivity. This point indicates that the water level change is sensitive to the hydraulic conductivity.

Porosity changes

In the last group of scenarios, porosity values were altered. In Scenario 8 and 10, the porosity values of the limestone layers were increased with different magnitudes. In Scenario 9 (Figure 17), they were lowered to the same level as the poorly karstified layer and in Scenario 11 (Figure 19) porosity was only altered in the lower, dolomite layers. The results from Scenarios 8-11 are shown in Figure 16-19. It is evident that in most of these cases, porosity changes made very little difference in the results for both the water level changes and the cooling effects, i.e. they gave the same results as in the original model. However, the only noticeable difference was in the case of Scenario 10 (Figure 18).

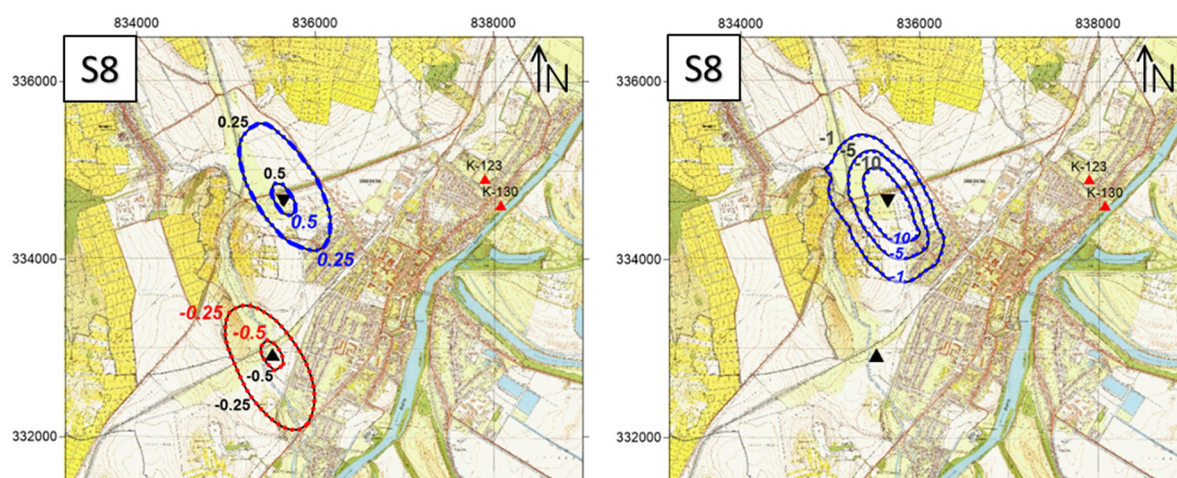


FIGURE 16: Calculated long-term effects of the proposed well duplet on the water level and temperature for Scenario 8

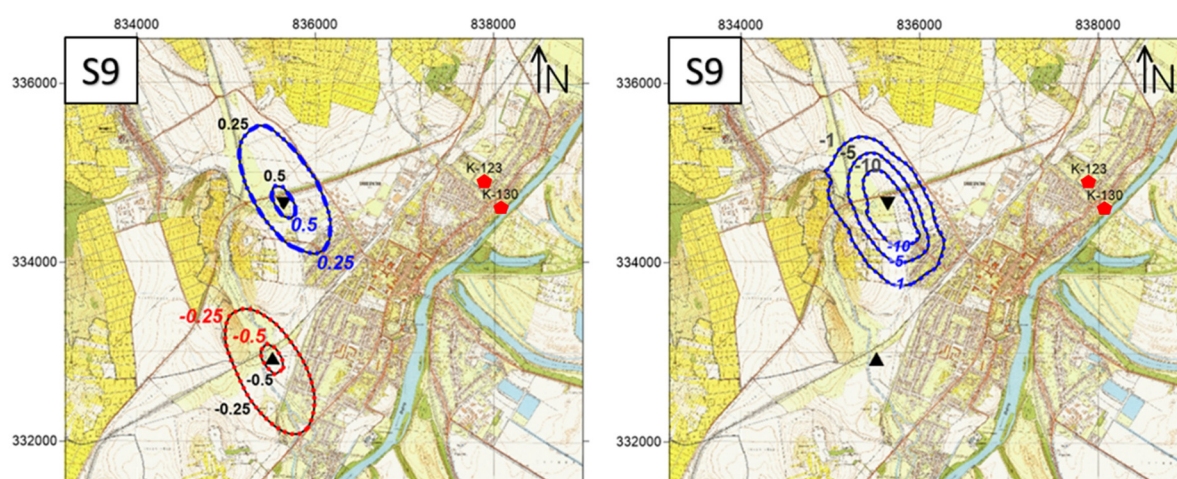


FIGURE 17: Calculated long-term effects of the proposed well duplet on the water level and temperature for Scenario 9

In this scenario, the porosity values of the limestone layers were actually increased by 12 times in layer 1. This was the largest alteration of the porosity value in all the scenarios. This was enough to cause a slight decrease in the cooling effect from the original model, although still to a very small degree. This fact indicates that the model is not sensitive to the porosity.

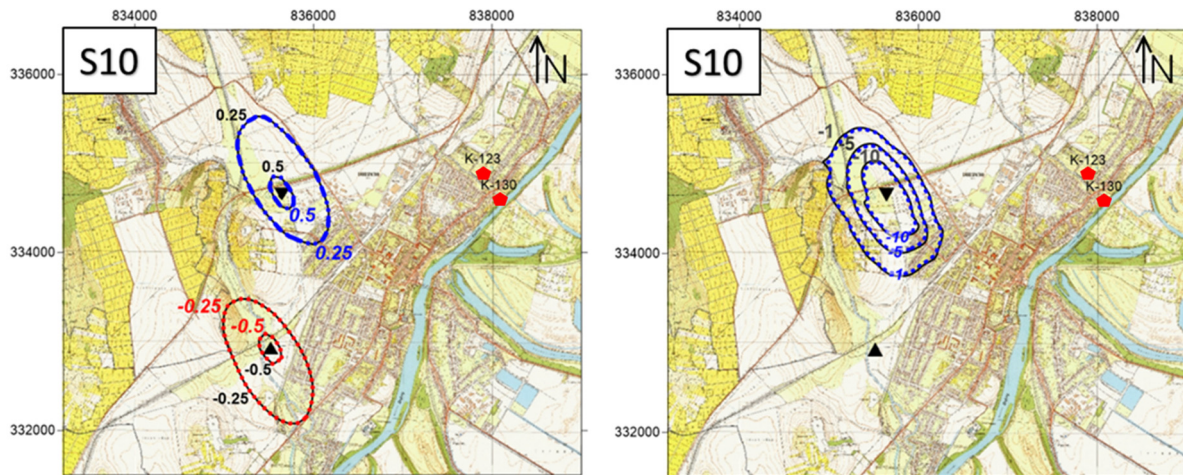


FIGURE 18: Calculated long-term effects of the proposed well duplet on the water level and temperature for Scenario 10

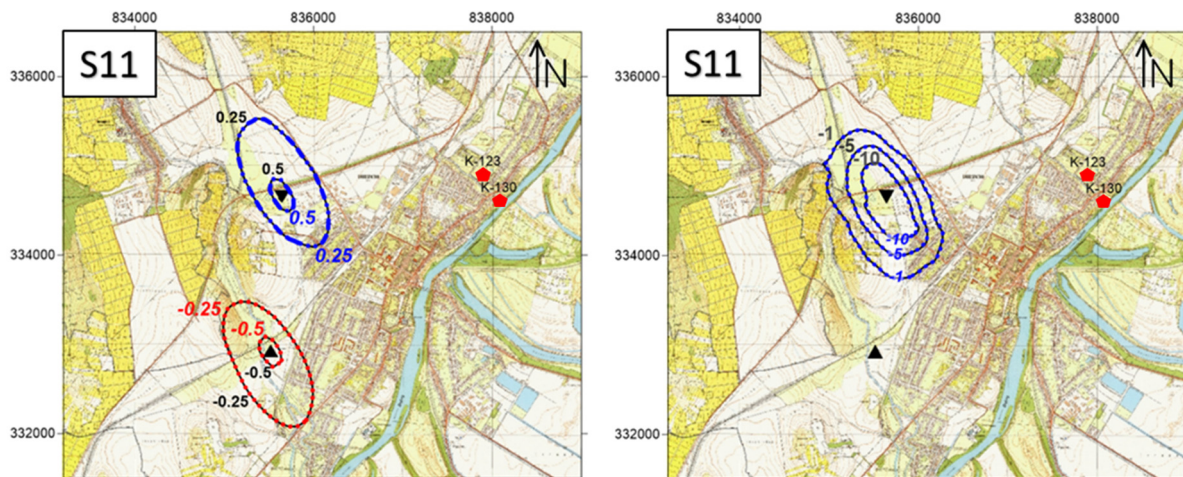


FIGURE 19: Calculated long-term effects of the proposed well duplet on the water level and temperature for Scenario 11

4. CONCLUSIONS AND RECOMMENDATIONS

The literature review showed that many of the parameters describing the geological conditions in the Sárospatak geothermal reservoir have a relatively large degree of uncertainty. After analysing the results of the sensitivity analysis, a prioritization of these parameters can be concluded.

The hydraulic parameters of the dolomite and the porosity of the limestone formation do not play key roles in the reservoir model because calculated changes in water level and cooling are not sensitive to these parameters. However, the model is sensitive to the hydraulic conductivity, hence the karstification, as well as the layer thicknesses, hence the storativity, of the top limestone layer. Therefore, these parameters have the greatest influence on the calculated drawdown/upconing and to a lesser degree on the cooling effect around the injection well. It can also be concluded that cooling is more sensitive to changes in thickness/storativity, less sensitive to changes in hydraulic conductivity and least sensitive to changes in porosity.

The main objective of the original modelling work by Vatnaskil was to determine if the proposed well duplet would have any negative impact on the existing thermal wells at Sárospatak. The results of the

sensitivity analysis indicate clearly that the production/injection of the proposed wells are very unlikely to have any impact on the existing thermal wells. Moreover, the only possible effect would be a positive change in the water level (upconing) as shown in Scenario 5 where a lower degree of karstification in the upper layers was assumed. On the other hand, it is more likely that the production from the existing thermal wells would rather have a negative effect (increased drawdown) on the water level around the proposed well duplet.

For further investigation of the use of geothermal district heating in Sárospatak, a carefully constructed numerical model is necessary. This model is a good base for that purpose, but it needs several careful improvements. In my opinion, the crucial aspects for future modelling work include the following:

- Acquire accurate historical production rates and expected future production from the existing thermal wells. Production from these wells has a high probability of negatively affecting the proposed wells.
- Future boreholes drilled into the Dachstein Limestone can provide crucial information for improving the model. Drill logs, borehole measurements and well testing can be used to determine more accurate values for hydraulic conductivity within the reservoir. This parameter mostly depends on the degree of karstification which is the central question. A better understanding of the hydraulic conductivity can also be attained by analysing the above-mentioned production history of the existing wells.
- Acquire a better understanding of the storativity of the producing layer. This mostly depends on the thickness and the horizontal extent of the Dachstein Limestone. Therefore, further geophysical investigations of the basement in the area would be advisable.

ACKNOWLEDGEMENTS

I would like to express my gratitude to the Director of UNU-GTP, Mr. Lúdvík S. Georgsson, and his staff, Mr. Ingimar Gudni Haraldsson, Ms. Málfríður Ómarsdóttir, Ms. Thórhildur Ísberg, and Mr. Markús A. G. Wilde for offering and organizing this genuine unique program. I would also like to thank other UNU-GTP staff and teachers for their support, guidance, time and help from the beginning to the end of the training that made it cheerful and successful for me.

I am deeply thankful my supervisor Eric M. Myer, for his persistent support and guidance throughout the whole project from the beginning to the last minute. Special thanks to Vatnaskil Consulting Engineering for letting me work on their data and giving me permission to use the software Aqua3D.

I would like to thank and appreciate my UNU fellows from all around the world, they have been one of the most inspiring people I have met in my life. I will not forget them. Special thanks to my Hungarian flatmates, Bandi and Zoli, whom I could share the struggles, happy and sad moments during my stay in Iceland.

I must express how greatly I am indebted to my home supervisor, Judit Mádl-Szőnyi, associate professor of Eötvös Loránd University who got my interest in hydrogeology and geothermal in the first place. She made the application for this program possible for me. Studying geothermal in Iceland had been one of the greatest dreams in my life which used to seem unattainable. With this program this dream came true.

Last, but not least, I thank to my friends and especially my family at home, who were supporting and inspiring me since the moment I was born into this life.

Above all, I praise God simply for his constant presence in my life.

REFERENCES

- Császár, G., 1997: *Basic lithostratigraphic units of Hungary*. Stratigraphic Commission of Hungary, Subcommissions of Budapest, 114 pp.
- Csoma, A., and Molnár F., 1999: Genesis of the carbonate-vein at Komlóska on the basis of fluid inclusion and stable isotopic studies (in Hungarian). *Földtani Közlöny*, 129, 41-60.
- Ehrenberg, S. N., and Nadeau, P. H., 2005: Sandstone vs. carbonate petroleum reservoirs: A global perspective on porosity-depth and porosity-permeability relationships. *AAPG Bulletin*, 89, 435-445.
- Erhardt, G., 1962: The Sárospatak-végardói thermal water (in Hungarian). *Hidrológiai Közlöny*, 4-6, 514-517.
- Fejes, Z., 2011: *Data supplement for planning of deep geothermal exploration* (in Hungarian). University of Miskolc, Miskolc, Hungary, scientific student work, 1-61.
- Freeze, R.A., and Cherry, J.A., 1979: *Groundwater*. Englewood Cliffs, NJ, Prentice-Hall, 604 pp.
- Frits, J., 1964: *Thermal line at village of Végardó* (in Hungarian). Hungarian Geological Institute, annual report of 1955-1960, 505-515.
- Goldscheider, N., Mádl-Szőnyi, J., Eröss, A., and Schill, E., 2010: Review: thermal water resources in carbonate rock aquifers. *Hydrogeology J.*, 18-6, 1303-1318.
- Götz, A.E., Török, Á., and Sass, I., 2014: Geothermal reservoir characteristics of Meso-and Cenozoic sedimentary rocks of Budapest (Hungary). *Zeitschrift der Deutschen Gesellschaft für Geowissenschaften*, 165-3, 487-493.
- Gyarmati, P., 1964: *Explanatory text for geological map of Hungary, 1: 25,000 series, Area of Háromhuta* (in Hungarian). Geological Institute of Hungary, Budapest.
- Haas, J., Budai, T., Csontos, L., Fodor, L., and Konrád, G. 2010: *Pre-Cainozoic geological map of Hungary, 1:500 000*. Geological Institute of Hungary, Budapest
- Horváth, F., Bada, G., Windhoffer, G., Csontos, L., Dövényi, P., Fodor, L., Grencs, G., Síkhegyi, F., Szafián, P., Székely, B., and Timár, G., 2006: Atlas of the present-day geodynamics of the Pannonian basin: Euroconform maps with explanatory text. *Magy Geofizika*, 47-4, 133-137.
- Klimchouk, A.B. 2007: *Hypogene speleogenesis: hydrogeological and morphogenetic perspective.*, National Cave and Karst Research Institute, Carlsbad, NM, USA, Special Paper 1, 106 pp.
- Lengyel, E., 1957: *Geological mapping around town of Sárospatak* (in Hungarian). Annual report of 1955-1956 by the Hungarian Geological Institute, 203-223.
- Lenkey, L., Dövényi, P., Horváth, F., and Cloetingh, S.A.P.L., 2002: Geothermics of the Pannonian basin and its bearing on the neotectonics. *EGU Stephan Mueller Special Publication Series*, 3, 29-40.
- Myer, E.M. 2013: *Preliminary modelling results from the Sárospatak geothermal reservoir model*. Vatnaskil Consulting Engineers, memo 13.12.
- Nádor, A., Lapanje, A., Tóth, G., Rman, N., Szöcs, T., Prestor, J., Uhrin, A., Rajver, D., Fodor, L., Muráti, J., and Székely, E., 2012: Transboundary geothermal resources of the Mura-Zala basin: a need for joint thermal aquifer management of Slovenia and Hungary. *Geologija*, 55-2, 209-224.

Pentelényi, L., Haas, J., Pelikán, P., Piros, O., and Oravecz-Scheffer, A., 2003: Re-evaluation of Triassic formations in the Hungarian part of the Zemplén unit (in Hungarian). *Földtani Közlöny*, 133, 1-19.

Smosna, R., Bruner, K.R., and Riley, R.A., 2005: Paleokarst and reservoir porosity in the Ordovician Beekmantown dolomite of the central Appalachian Basin. *Carbonates and Evaporites*, 20-1, 50-63.

Szűcs, P., and Ritter, G., 2007: *Planning of the hydrogeological protection body of the thermal wells of the Sárospatak-Végható thermal spa*. RIT-TERV Kft., report R-40 (in Hungarian), 37 pp.

Ren21, 2016: *Global status report*. Ren21 - Renewable Energy Policy Network for the 21st Century, Paris, France.

Rollin, K.E., Kirby, G.A., and Rowley, W.J., 1995: *Atlas of geothermal resources in Europe: UK revision*. British Geological Survey, Regional Geophysics Group.

Vatnaskil, 2013: *AQUA3D, a 3-dimensional finite-element groundwater flow and transport model software*. Vatnaskil, Reykjavík.

Wein, G., and Konda, J., 1977: *Tectonics of the Buda Mountains, geological maps*. Geological Institute of Hungary, Budapest.



UNITED NATIONS
UNIVERSITY

UNU-GTP

Geothermal Training Programme

Orkustofnun, Grensasvegur 9,
IS-108 Reykjavik, Iceland

Reports 2016
Number 32

COMMON GEOTHERMAL WELL DESIGN AND A CASE STUDY OF THE LOW-TEMPERATURE GEOTHERMAL RESERVOIR IN OTOPENI, ROMANIA

Valentin Cristian Petrică

Drilling Engineer

S.C DAFORA S.A

15 Piata Regele Ferdinand, Medias

ROMANIA

cristian_petrica07@yahoo.com

ABSTRACT

The report describes a design of a well for the low-temperature geothermal, Therme Balotesti reservoir in Otopeni in the Romanian Plain. The well was designed by specialists with great experience in the field using the main features from the offset wells as references. The report includes assumed design calculation regarding the drill string design and casing design characteristics based on the information gathered from various published papers and drilling handbooks. More information for the project could not be accessed due to confidentiality with regard to technical information.

Romania has the third largest potential geothermal capacity in Europe after Greece and Italy. The development of direct utilization of geothermal resources in Romania is however not far advanced due to high investments costs and the very low price of hydrocarbons. Exploration drilling for geothermal resources in Romania started in the 1960s. Over 200 drilled wells for hydrocarbons explorations have been drilled to depths between 800 and 3000 m, encountering geothermal resources of low and medium enthalpy (40-120°C). Thermal springs are the only visible manifestations of geothermal resources across the country. The main direct uses of geothermal heat are district heating and individual space heating and health and recreational bathing. Geothermal energy is also used for greenhouse heating, fish farming, industrial processes and drying. Currently further geothermal development is facing unfavourable conditions as the international market prices for fossil fuels and domestic oil and gas production have dropped dramatically.

1. INTRODUCTION

Geothermal energy is thermal energy generated and stored in the Earth. Geothermal energy extracted from the Earth's crust has a relatively stable temperature and is utilized to generate electricity and to provide heating. Geothermal fluids may be steam or hot water and can serve for electrical power generation or for different projects as space heating, aquaculture, snow melting, food processing and hot tubs and spas. Geothermal energy is a clean and renewable energy resource which can be found in

many places in the world and especially in tectonically active areas. The heat from geothermal sources has been used by mankind from the earliest days for cooking and bathing. Major development has taken place during the past 30-40 years, when significant advances have been made in deep drilling practices. The equipment and techniques used in the drilling of geothermal wells have many similarities with those used in the oil and gas industry.

Drilling operations are performed in order to open up geothermal reservoirs for energy exploitation. The drilling phase of the geothermal power plant requires heavy equipment, such as drill rigs, fuel and materials. Geothermal wells have been used for several decades for the existing heating and cooling systems. The geothermal reservoirs can be high-temperature and steam-dominated or low-temperature water-dominated reservoirs.

Geothermal wells can be expressed like other types of wells with different purposes created by drilling into the Earth's surface, cased and cemented.

There are different geothermal well types which can be utilized in various ways, ranging from wells that connect to sources of steam used to power turbines, to wells utilized for thermal energy with geothermal heat pumps. With the help of a recirculating water system a stable indoor temperature will be maintained for district heating. A geothermal production well can be considered successful when it has sufficient capacity to be connected and utilized in the respective power plant or utilization scheme.

Nowadays price for drilling geothermal wells may be approximately ~2,000 USD/m and take 35-70 days to drill (Thórhallsson, 2016). Several factors influence the costs such as the type of the drilling rig used, cost of materials, total depth of the well and additional services. The hook load capacity dictates the depth that can be reached using a specific rig, a common lifting capacity of 400 tons is quite normal in oil industry, while in geothermal industry for many different reasons to reduce the costs of drilling, smaller rigs may be adequate to reach the target depth safely.

Time spent on drilling (rotating the drill bit) is about 50% of the total, the rest is spent on installing casings, cementing, logging, mobilising the rig and other activities (Thórhallsson, 2016).

2. COMMON WELL DESIGN

The main aspects of the well design process focus on the objectives and the purpose of the well. The well design considers the casing programme selection, casing setting depths and drilling procedures to achieve satisfactory well completion and integrity of the well.

The well construction process can be split into five sequential phases of work, as follows:

1. Preliminary well design;
2. Detailed well design;
3. Preparation of drilling programme;
4. Execution of well programme;
5. Analysis and improvement of performance.

Preliminary and detailed well design are important factors for the preparation of the drilling programme. Once the geological and geophysical studies have identified a potential well location, the subsurface team will work up a basis of design. The preliminary well design will generally involve the following:

- Well name and number;
- Well objectives;

- Total depth;
- Surface location;
- Water depth;
- Target;
- Target size and tolerance;
- Target constraints;
- Geological prognosis;
- Seismic section;
- Expected hydrocarbons;
- Anticipated pore pressures;
- Anticipated temperature profile;
- Offset wells.

A review of all the available offset data and regional data is also needed and includes:

- Pore and fracture pressure plots;
- Time depth curves;
- Daily drilling reports;
- Daily mud reports;
- Mud logging records;
- Bit records;
- Casing and cementing reports;
- Survey records.

This will give an understanding of how previous wells were drilled, what problems were encountered and how they were solved, what casing programme, mud type and density was used, any directional problems experienced, how long the well took to drill, etc.

Detailed well design entails taking the preliminary well design and developing it further to the point that a drilling programme can be prepared. Detailed well design includes, but is not limited, to a detailed engineering study and design of the following areas:

- Pore and fracture pressure profiles;
- Temperature profiles (HPHT wells);
- Casing design;
- Casing running and jewellery (hardware);
- Drilling fluids;
- Hydraulics and hole cleaning;
- Cementing design;
- Trajectory and surveying;
- Torque and drag;
- Drill string design;
- Well abandonment;
- Completion design;
- Well cost and duration;
- Contingency planning.

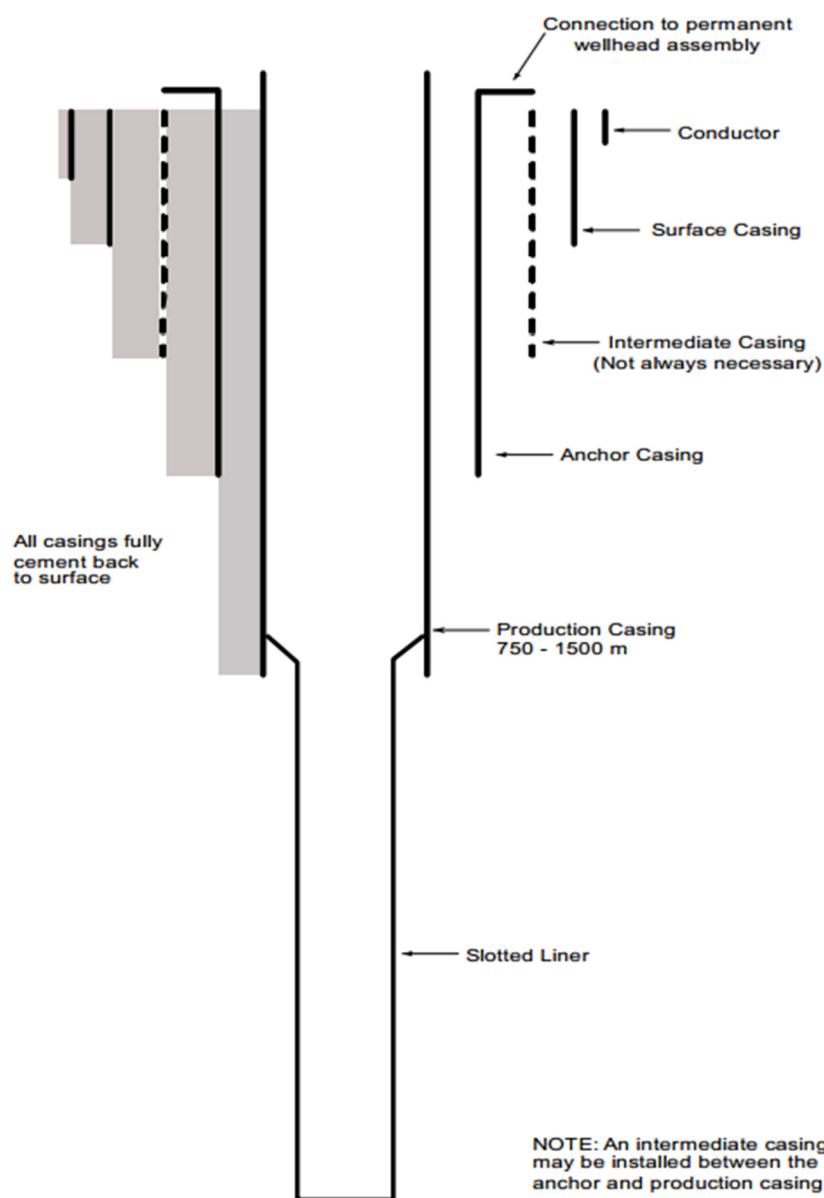
Obviously, the amount of time spent on each area is a function of the complexity of the well being planned.

The initial estimate of determining casing setting depths is best determined graphically, plotting pressure and fracture gradient, expressed in equivalent density, against depth.

Factors that may affect casing depth selection in addition to pore pressure and fracture pressure are:

- Shallow gas zones;
- Fresh water sands;
- Lost circulations zones;
- Directional well profile;
- Hole cleaning;
- High pressure zones;
- Lithology, casing shoes should, where practicable, be set in competent impermeable formations.

The initial casing setting depths need to be adjusted accordingly considering all of the above factors. The design stage involves determining the loads each casing string will be exposed to during the life of the well and the selections of tubular with suitable mechanical and physical properties that can withstand the predicted loads.



As many of these issues are inter-related it is essential that a system of change control be used to ensure that the effect of changing a parameter is carried throughout the complete design. Figure 1 illustrates a typical geothermal well design.

According to Thórhallsson (2016) in low enthalpy reservoirs in Iceland the design of well is based on installing 2-3 casing strings with casing diameters of: 18 $\frac{5}{8}$ ", 13 $\frac{3}{8}$ " and 9 $\frac{5}{8}$ ". The diameter of the open hole is 12 $\frac{1}{4}$ " or 8 $\frac{1}{2}$ " as there is no liner. For low-temperature wells under 1,500 m depth, casing sizes of 13 $\frac{3}{8}$ " and 10 $\frac{3}{4}$ " are used and an open hole of 9 $\frac{7}{8}$ ". All casings for low-temperature well have welded connections.

Prior to the well drilling, both office and rig site personnel from the operator, drilling contractor and additional service providers have a meeting to perform an exercise drilling of the well on paper, aimed to identify any problems ahead of time, obtain information from the rig site personnel as to performance improvements

FIGURE 1: Casing strings and liner for typical geothermal well (Hole, 2008)

that could be made. Regular meetings are a vital tool to maintain the team spirit and provide a vehicle for two ways communication. To reduce the drilling cost there is a need to schedule the next operations and be ahead of all activities, anticipate problems and avoid non-productive time.

2.1 Drill string

The principal components of the drill string consist of the assembled components of drill pipe, heavy weight drill pipe (HWDP), drill collars and special subs and drill bit.

The drill string is used to:

- Lower the bit into the hole and withdraw it;
- To penetrate the formations more effectively, placing weight on the bit;
- Transmit the rotation action to the bit, including axial and torsional loads;
- Transport the drilling fluid and cuttings under pressure from the bit to the surface.

The *Top Drive System (TDS)* or *kelly*, is not exactly part of the drill string but transmits and absorbs torque to or from the drill string while carrying all the tensile load of the drill string.

Drillpipes (DP) are the major component of the drill string and transmit power by rotating motion from the rig to the bit and allow mud circulation.

American Petroleum Institute (API) drill pipes and other tubular products are gauged by the nominal outside diameter (OD) of the tube. The OD of a given pipe must be a specific measurement in order for threaded fittings and pipe-handling tools, such as elevators and slips, to fit properly. Although the OD of API drill pipes is the same for each size, the inside diameter (ID) varies with the nominal weight per unit length. API seamless drill pipes are offered in five grades of steel, varying in strength from D (the weakest) through E, X, G to S (the strongest). High strength drill pipes require heavier and longer upsets than those used on grades D and E. Appendix I shows the different API Specifications Standards.

The most common used grades of steel to meet different hole requirements for drill pipes are G105 and S135. G105 is most commonly used in shallow or H₂S environments. S135 is a high strength drill pipe with heavier and longer upsets than those used on grades D and E (API RP 5A5).

U150 is relatively new grade that is being used for deep water operations.

Heavy weight drill pipes (HWDP) make the transition between drill pipe and drill collars, thus avoiding an abrupt change in cross-sectional area used with drill collars. HWDP can provide weight on the bit. This tubing product is an intermediate sized drill pipe, having the same nominal outside diameter (OD) as a drill pipe but having a smaller interior diameter (ID), thus giving it more strength.

HWDP reduce the stiffness of the Bottom Hole Assembly (BHA). They are easier and faster to handle than drill collars (DC) and one of the important factors is that they reduce the possibility of differential sticking.

Differential sticking occurs when drilling a well with a greater well bore pressure than formation pressure. As a result, the pipe becomes stuck to the wall, and requires additional force to release the stuck pipe string.

Drill collars (DC) are similar to drill pipes, but have larger outside diameters (up to 11 inches) and have small inside diameters. The drill collars provide the desired weight on the bit, keeping the drill pipe section in tension during drilling, and drilling a nearly vertical hole providing the pendulum effect

and the rigidity. The weight on bit (WOB) should not exceed 85% of the buoyed weight of the total drill collar weight to ensure the neutral point remains within the collars.

One important aspect is that the drill pipe should never be subjected to compression, as it would bend and twist-off (break) very easily. That is also the main reason for adding heavy-weight drill pipes to the drill string when deciding how many collars to run, because total drill collar weight must exceed the WOB during drilling.

Other downhole tools include: Stabilizers, crossover, jars, under reamer, measurement while drilling tool (MWD), mud motor, etc.

The word “sub” includes any short length of pipe, collar, casing; all of these drill string components in a certain arrangement below the drill pipe will form the BHA. Crossover subs have different threaded ends to change between different sizes and types of drill pipe or collars.

Stabilizers are short subs with blades which are full borehole size or a fixed amount below gauge. Configuration of blades may be straight or spiral and made from aluminium, rubber or steel with tungsten carbide inserts on the edges. In order to maintain a straight hole, centralized stabilizers are located between the collars, also to maintain a full gauge hole by a scraping action, reduce bit wobble and help prevent wall sticking.

Drilling jars are included in the drill collar string, usually having 3-5 DC above, in order to deliver a sharp blow in order to free the drill string should it become stuck. Hydraulic jars are activated by a straight pull to give an upward blow, mechanical jars may be pre-set at surface and fired downwards by a given compression load.

All the above listed components of the drill string represent an important part of the drilling equipment cost, but the consequence of a downhole failure can be even greater.

Good care must be taken while handling these tubulars, especially for the tool joint which is generally the weakest point.

2.2 Casing design

In the pre-planning stage, important decisions have to be made in selecting casing depths for each casing string to achieve the total depth of the well safely.

In order to allow the drilling and completion of a well, it is necessary to select the drilled open hole diameter with respect to the steel pipe / casing. Once in place, this pipe is cemented, supporting the casing and sealing the annulus in order to:

- Strengthen the hole;
- Isolate unstable/underbalanced / overbalanced formations;
- Prevent the contamination of freshwater reservoirs;
- Provide a pressure control system;
- Confine and contain drilling / completion / produced fluids and solids;
- Support wellhead and additional casing strings;
- Support the blow out preventer (BOP) and Christmas tree (or Xmas tree – named for its crude resemblance to a decorated tree, is an assembly of valves, spools, and fittings used in oil industry);
- Act as a conduit for associated operations (drilling, wireline, completion and further casing / tubing string) with known dimension (Serban, 2014).

Primarily six types of casings are installed in onshore/offshore wells:

- Stove pipe, marine conductor, foundation pile;
- Conductor string;
- Surface casing;
- Intermediate casing / anchor casing;
- Production casing;
- Liner, slotted or perforated with holes.

Casing properties: Casing is usually specified by the following properties:

- Outside diameter;
- Weight per unit length;
- Grade of steel;
- Type of connection;
- Length of joint.

The outside diameter refers to the pipe body and not to the coupling. Diameter of the coupling is important as it determines the minimum hole size that the casing can be run into and the wall thickness determines the inside diameter of the pipe and hence the maximum bit size that can be run through the pipe.

In API Spec 5CT the permitted tolerance on outside diameter and wall thickness is given as a general rule:

Casing outside diameter $\geq 4\frac{1}{2}$ "	Tolerance + 1.00%, - 0.50%
Casing outside diameter $< 4\frac{1}{2}$ "	Tolerance $\pm 0.031\%$
Wall thickness	Tolerance – 12.5%

The mechanical and physical properties of casings are dependent upon the chemical composition of the steel and the heat treatment it receives during manufacture.

API defines nine grades of steel for casing:

H40 J55 K55 C75 L80 N80 C95 P110 Q125

The grade has a letter, which indicates the grade, and a number which indicates the minimum yield strength in thousands of psi, e.g. K55=55,000 psi (API SPEC 5CT). In Table 1 are listed API casing grades and properties:

TABLE 1: API casing standards

API Grade	H-40	J-55	K-55	C-75	L-80	N-80	C-90	C95	P-110	Q-125
Minimum yield strength (1,000 psi)	40	55	55	75	80	80	90	95	110	125
Minimum ultimate tensile strength (1,000 psi)	60	75	95	95	100	100	105	105	125	135

Casing setting depth determination

The initial selection of casing setting is based on the anticipated pore pressure and fracture gradients. The drilling engineer is responsible for ensuring that, as far as possible, all the relevant offset data has been considered in the estimation of pore pressure and fracture gradients, and that, for directional wells, the effect of the hole angle on offset fracture gradient data has been considered.

Surface and conductor setting depth design

The minimum setting depth for surface and conductor casings is the depth at which the bottom hole pressure created by the circulating drilling fluid (ECD - equivalent circulating density) is exceeded by the fracture value of the formation. Formation fracture pressure or formation breakdown pressure is the pressure required to rupture a formation, so that the whole mud can flow into it. The ECD can be significantly affected in large diameter holes by a high rate of penetration (ROP) and poor hole cleaning.

The total depth of the well, and hence the setting depth of the production casing or liner, is driven by logging, testing, and completion requirements. The shoe must be set deep enough to give an adequate sump for logging, perforating, and test on production activities. The following information used to describe the setting depths has been extracted from IWCF Well Control (Serban, 2014).

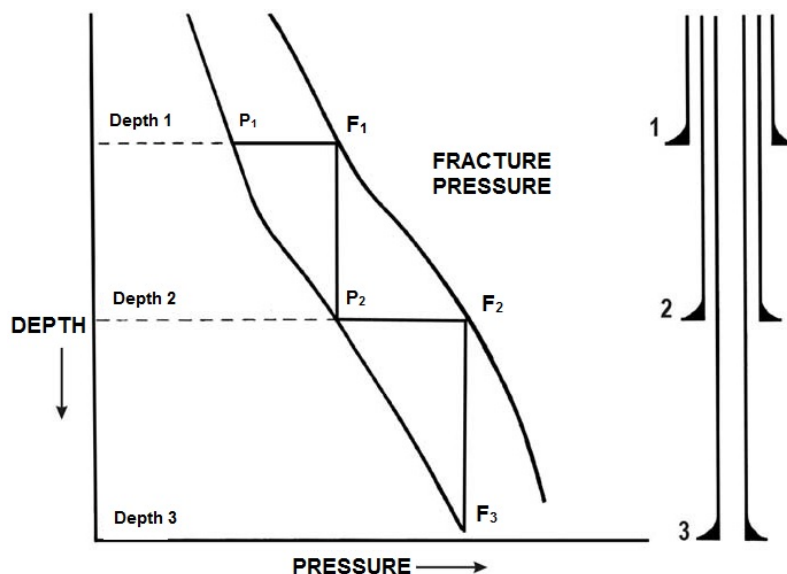


FIGURE 2: Casing Seat Selection (Serban, 2014)

The key to satisfactory casing seat selection is the assessment of pore pressure (formation fluid pressures) and fracture pressures throughout the well. Evidently, as the pore pressure in a formation being drilled approaches the fracture pressure at the last casing seat then a further string of casing is necessary. Figure 2 illustrates, an idealised casing depth selection:

Casing is set at Depth 1, where pore pressure is P_1 and the fracture pressure is F_1 . Drilling continues to Depth 2, where the pore pressure P_2 has arisen to almost equal the fracture pressure (F_1) at the first casing

seat. Another casing string is therefore set at this depth, with fracture pressure (F_2). Drilling can thus continue to Depth 3, where pore pressure (P_3) is almost equal to the fracture pressure F_2 at the previous casing seat (Serban N., 2014).

In practice, there is a need to include safety margins so take into account that this is an example.

For all casing strings a collapse load occurs when the external pressure is greater than the internal pressure. Collapse design focuses on the internal and external pressure profiles. Normally the collapse load will be highest at the casing shoe during cementing and other load cases, such as axial tension / compression, and burst load cases when the maximum load is expected.

2.3 Cementing programme

Planning a cementing job consists of evaluating a number of factors, including:

- Assessment of hole conditions (loss zones, hole cleaning, size, washouts, temperatures);
- Mud properties;
- Slurry design;
- Slurry placement;
- Additional equipment (float equipment, centralizers).

In Primary cementing the key solutions consist of:

- Isolation of casing shoe;
- Isolation of production zones – prevent cross flow between intervals at different pressure;
- Protection of water zones – prevent drilling fluid contamination of aquifers;
- Isolation of problem interval – extreme losses, well control, side-tracking;
- Protection of casing – from corrosive formation fluids e.g. H₂S, CO₂;
- Casing support – e.g. support for conductor (load bearing – bending moments derived from supporting BOP/tree/riser and potential snag loads from fishing activities), prevent thermal buckling.

For Secondary or remedial cementing, additional cementing can be done at a later stage e.g. sealing off perforations, top up job on conductor, repair casing leaks, squeeze casing shoe, setting plugs, etc. Common problems that affect all cement jobs include:

- Poor hole condition (doglegs, borehole stability, washouts, hole fill, cuttings beds, etc.);
- Poor mud condition (high gel strengths and yield point, high fluid loss, thick filter cake, high solids content, lost circulation material, mud / cement incompatibility);
- Poor centralization (cement not placed uniformly around the casing, leaving mud in place);
- Lost circulation;
- Abnormal pressure;
- Subnormal pressure;
- High temperature.

Cement types

API defines nine different classes of cement (A to H) depending on the ratio of the four fundamental chemical components (C₃S, C₂S, C₃A, C₄AF where C = calcium, S = silicate, A = aluminate and F = fluoride). Table 2 indicates API classes of cement.

TABLE 2: API cements classes.

API Class	Mix water (gal / sx)	Slurry wt. (ppg)	Depth (m)	BHST* (°C)
A (Portland)	5.2	15.6	0-1828.8	26.6-76.6
B (Portland)	5.2	15.6	0-1828.8	26.6-76.6
C (High early)	6.3	14.8	0-1828.8	26.6-76.6
D (Retarded)	4.3	16.4	1828.8-3048	76.6-110
E (Retarded)	4.3	16.4	1828.8-3048	76.6-143.3
F (Retarded)	4.3	16.4	3048-4876.8	110-160
G (Basic California)	5.0	15.8	0-2438.4	26.6-93.3
H (Basic Gulf Coast)	4.3	16.4	0-2438.4	26.6-93.3

* Bottom hole static temperature

Notes:

Class A and B – Shallow depth use. Composition 50% C₃S, 25% C₂S, 10% C₃A, 10% C₄AF.

Class C – Produces high early strength due to high C₃S content.

Class D, E and F – Retarded cements due to coarse grind or inclusion of organic retarders (lignosulphonates).

Class G and H – General purpose, compatible with most additives and able to be used over a wide range of temperature and pressure. H coarser than G – better retarding in deeper wells.

Class G is the most common type of cement used.

Other common cement variants out with API specification include:

Pozmix cement – 50% Portland, 50% pozzolan (ground volcanic ash) and 2% bentonite.

Gypsum cement – mixture of Portland cement and gypsum. Used for remedial work.

Diesel oil cement – “Gunk squeeze”. Mixture of basic cement with base oil used to seal off loss zones. Will set if water present.

Silica flour – At temperatures above 110°C cement will initially strengthen and then later weaken due to the subsequent formation of calcium silicate hydrate (C₂SH). By adding 30-40% silica flour to the cement, CSH forms in preference to C₂SH thus extending the temperature range of the mix.

2.4 Drilling problems

Additional equipment is required to be adapted for geothermal drilling in order to face conditions in geothermal reservoirs: Rotating head, blow out preventer (BOP), cooling tower for mud, air compressors and separator for aerated drilling.

During drilling, the pore pressure has to be considered in order to determine the optimum mud weight needed to face any gas or steam pressures encountered, while maximising rates of penetration and minimising loss of circulation, differential sticking and hole stability problems.

There are different aspects of the problems while drilling geothermal wells:

- Hard fractured rocks will create drill string vibrations which will affect the rig equipment;
- Drill string getting stuck in the hole;
- Loss of circulation requiring cementing;
- Breaking of the drill string requiring fishing;
- No returns while cementing the casing;
- Well problems: kicks and blow-outs;
- High concentration of H₂S;
- Slow ROP in hard rocks;
- Selecting inadequate drill bits may cause slow ROP;
- Drilling incidents as equipment failures, personal accidents.

3. GEOTHERMAL RESOURCES IN ROMANIA

The presence of the main geothermal resources in Romania is confirmed in porous and permeable sandstones and siltstones, or in fractured carbonate formations. The first shallow geothermal applications were implemented in the late 1990s.

Hydrological research for geothermal water began in 1981, when it was established that geothermal water temperature of 70-85°C could be found at depths between 3,000 and 3,300 m. Geothermal waters are a source of renewable energy regulated by the order number: 87/2008 of National Agency for Mineral Resources (NAMR). The agency was established in 1993 as the regulatory authority which administers the mineral resources of Romania and is under government subordination.

The first geothermal well was drilled in Felix in 1885. The well was 51 m deep, with a flow rate of 195 l/s, and a temperature of 49°C. It is still operating for health and recreational bathing and heating. For 14 geothermal wells drilled in Romania from 1995 to 2000 to depths of 1,500-3,000 m, the rate of success was 85%; only 2 geothermal wells were recorded unproductive (Codruta et al., 2015).

Two main companies in Romania are currently exploiting geothermal resources. They are Transgex S.A. and Foradex S.A. and have the long term concessions for practically all known geothermal reservoirs.

The geothermal resources in Romania are suitable for direct heat utilisation, low enthalpy indicating temperatures of 50-120°C, and being used for other different purposes: space heating, greenhouse heating, aquaculture, health and recreational bathing resorts, swimming pools. Figure 4 shows the main uses of geothermal energy in Romania.

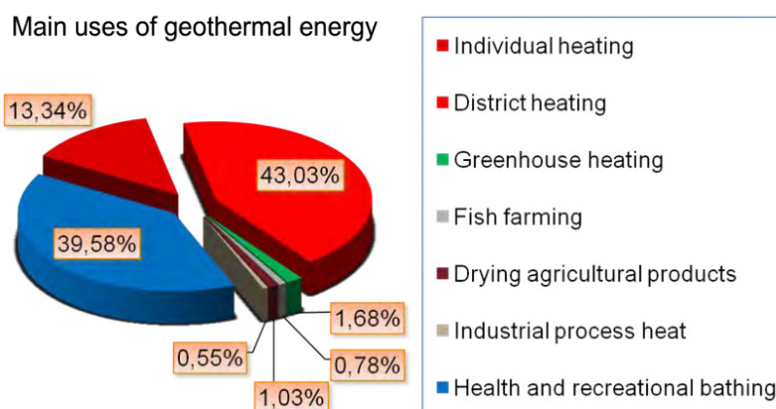


FIGURE 4: Geothermal energy distribution (Marcel, 2011)

3.1 Case history of the Therme Balotesti well in the Otopeni reservoir

The Otopeni geothermal reservoir is located north of Bucharest. Based on the offset data from wells drilled previously, both wells for oil and gas and for geothermal energy, the presence of a huge aquifer (300 km²), located in fissured limestone and dolomites has been confirmed. The existence of a geothermal field has been established evaluating hydrodynamics characteristics of carbonate collector from Jurassic Superior and Cretaceous inferior formations. The geothermal water temperature is 58-84°C. In the Otopeni geothermal reservoir 23 wells have been drilled (of which only 17 are potential producers or injectors). They confirm the aquifer being located in fissured limestone and dolomites, situated at depth of 2,000-3,200 m, belonging to the Moesian Platform. The depth to the static water level in the wells is about ~80 m, or even greater, down hole pumps being required. The geothermal water has wellhead temperatures of 58-84°C and a rather high Total Dissolved Solids (TDS) (1.5-2.2 g/l), with a high H₂S content (up to 30 ppm), for environmental protection reinjection is compulsory (Codruta et al., 2015).

The analysed well, named Therme Balotesti, was drilled in the Otopeni reservoir on the basis of an exploration license obtained from the National Agency for Mineral Resources (NAMR). The area is located in the middle of Romania Plain, the altitude is between 90 and 98 m below sea level (bsl) and the average annual temperature of the soil is 12°C, January average is -30°C and July average 23°C. The aim of the well was to explore the thermal field, evaluate hydrodynamic characteristics and hydro as well as the possibilities of exploiting geothermal waters.

In order to find the hydro geothermal potential of the area, information from previous exploration drillings were used:

- To identify the lithological sequence in this area to get an assessment of the flow capacity of the geothermal reservoir.
- Formation research to establish hydrodynamics and geochemical conditions.
- Detailed evaluation of geothermal field characteristics for evaluating the possibility for reinjection of used geothermal water.

3.1.1 The well design

A Romanian group of geologists and drilling engineers with great experience in the field have dealt with the design and the construction project supervising drilling. The respective engineers were Marin Gheorghe, Romanian Association of Hydrogeologists member (RAH) and National Agency for Mineral Resources expert (NARM), Cornel Popescu and Mircea Lungu.

The drilling Company S.C. DAFORA S.A. has successfully drilled the well Therme Balotesti with the Bentec Euro Rig 350. Below are presented the main features (Bentec Ltd., 2016).

EURO RIG™ general features:

- Climate: Temperate -20 to 40°C.
- Draw works capacities: 1,000 –2,000 hp.
- Hook Load capacities: 440,000-1,000,000 lbs/200-450 t.
- Drilling depth capacities: Up to 19,700 ft/or just over 6,000 m.

The width sections and their depths
Construction drilling activity was carried out with very few interruptions. Small inclination of the well led to successful casing of long sections of the well demonstrating professionalism of those who designed and / or supervised the construction.

Crossing areas with unconsolidated sediments, the presence of gas-bearing formations, drilling mud loss, and difficulty in cementing long sections, represented important features that needed to be considered in modifying the drilling programme.

The stratigraphic depths in the drilling project encountered some difference limits of maximum 10 m. Figure 5 illustrates the Therme Balotesti well design.

Casing design

Some of the technical features of the design and execution drilling of Therme Balotesti were presented by Marin Gheorghe in a paper published in the Romanian Association of Hydrogeologists website (RAH, 2016).

Cementing the Anchor Casing to the surface and the liners was carried out by a specialized company using two aggregates and cement silos, the cement density used was 1.75 kg/dm³. Due to lack of available data about the casing design and cementing techniques, according to Figure 5, I assumed the anchor casing was fully cemented back to surface and the liners were cemented by their entire length.

Water and bentonite with a specific weight of 1.14-1.25 kg/dm³ was used for the first 1,100 m (casing depth of the anchor casing). Mud with inhibitors for preventing potential issues up to 2,330 m and for the free hole section water was used with loss of circulation without affecting productive potential range. Table 4 shows the length and widths of the sections and the casings in the well.

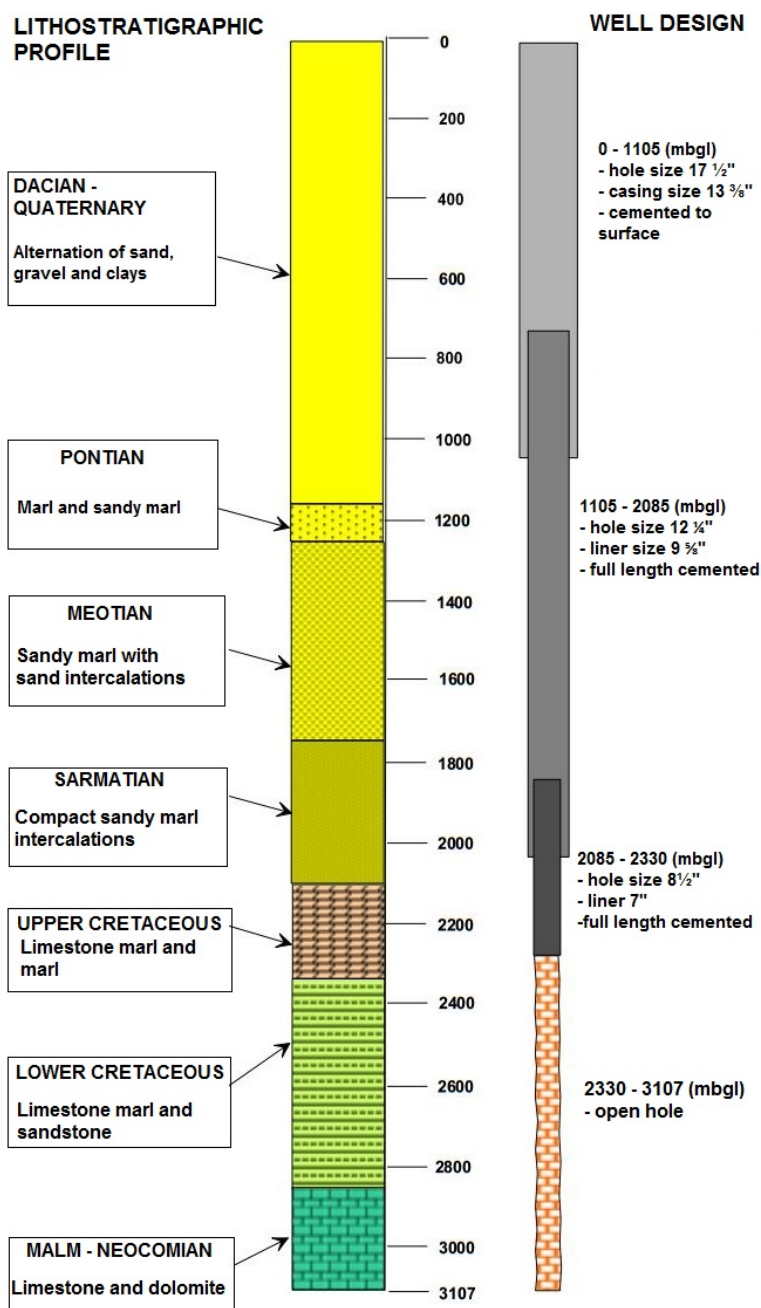


FIGURE 5: Therme Balotesti well construction and lithostratigraphic profile (RAH, 2016)

API CASING AND BIT PROGRAMS - COMBINATIONS

The figure shows possible combinations of API casing and bit sizes that can make up a casing program.

The **red** line shows the most common selection for geothermal wells.

Blue line is for slimholes.

The figure shows possible combinations of API casing and bit sizes that can make up a casing program.

The legend shows the liner size for different programs.

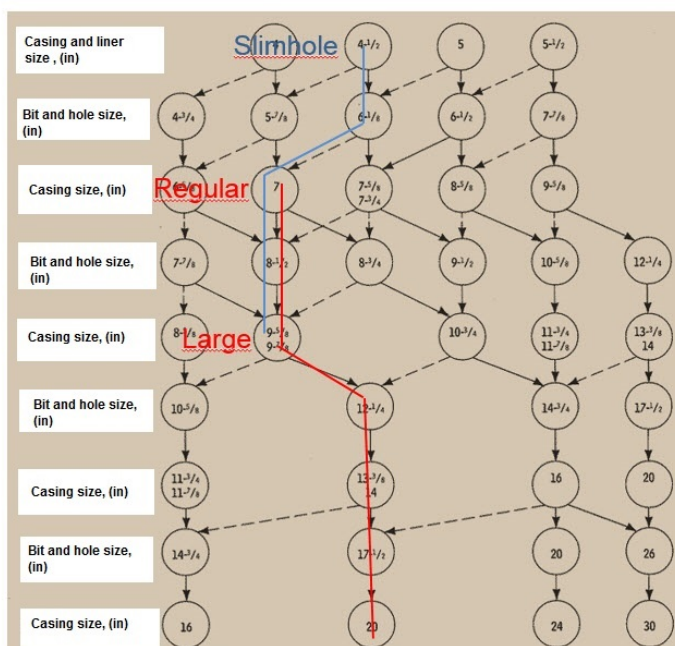


FIGURE 6: Possible combination of casing and bit sizes (Thórhallsson 2016)

TABLE 4: Length and widths of the sections and the casings in the well

Sections of the well		Casing/liner	
Depth	Width	Length	Size
(m)	(")	(m)	(")
0 – 1,105	17½	1,105	13⅜
1,105 – 2,085	12¼	2,085	9⅝
2,085 – 2,330	8½	2,330	7
2,330 – 3,107	5¾	None	

The casing string selection is specific for geothermal wells according to API where it is recommended practice for combination of casing sizes and drill bit diameter (Figure 6). The presence of H₂S requires using K55 as grade for all the casing strings. It conforms to ANSI/NACE MR 0175/ISO 15156 (NBS 2403:2015) and has resistance to H₂S environments.

3.2 Drilling history of the well

Technical details of the project required the involvement of specialized teams in all stages of construction and completion of drilling. Choosing the right rig, equipment and the regime drilling parameters demonstrated record time in drilling the Therme Balotesti well. The total depth of the well was 3,107 m and it was completed in 60 days. Construction drilling activity was carried out in shifts, (2x12 hours). During all activities very few interruptions were caused by technical problems. Well logging was performed by *Weatherford Atlas Gip* for each drilled interval before running the casing. Cementing the Anchor Casing and the two liners was carried out by specialized teams of *Rompetrol*, a Romanian Well Services Company. Completion of each stage construction according to technical project without incidents, ensures long-term operation of the well in safe conditions (RAH, 2016).

3.2.1 Drilling parameters

Figure 7 is presenting an example of a composited log with key drilling parameters recorded while drilling, the compiled log. The Log Plot program is used to display well drilling design and programme for geothermal wells and plot key drilling parameters as: rate of penetration (ROP), weight on bit (WOB), rotation per minute (RPM), drilling fluid specific gravity (SG) expressed in kg/dm^3 .

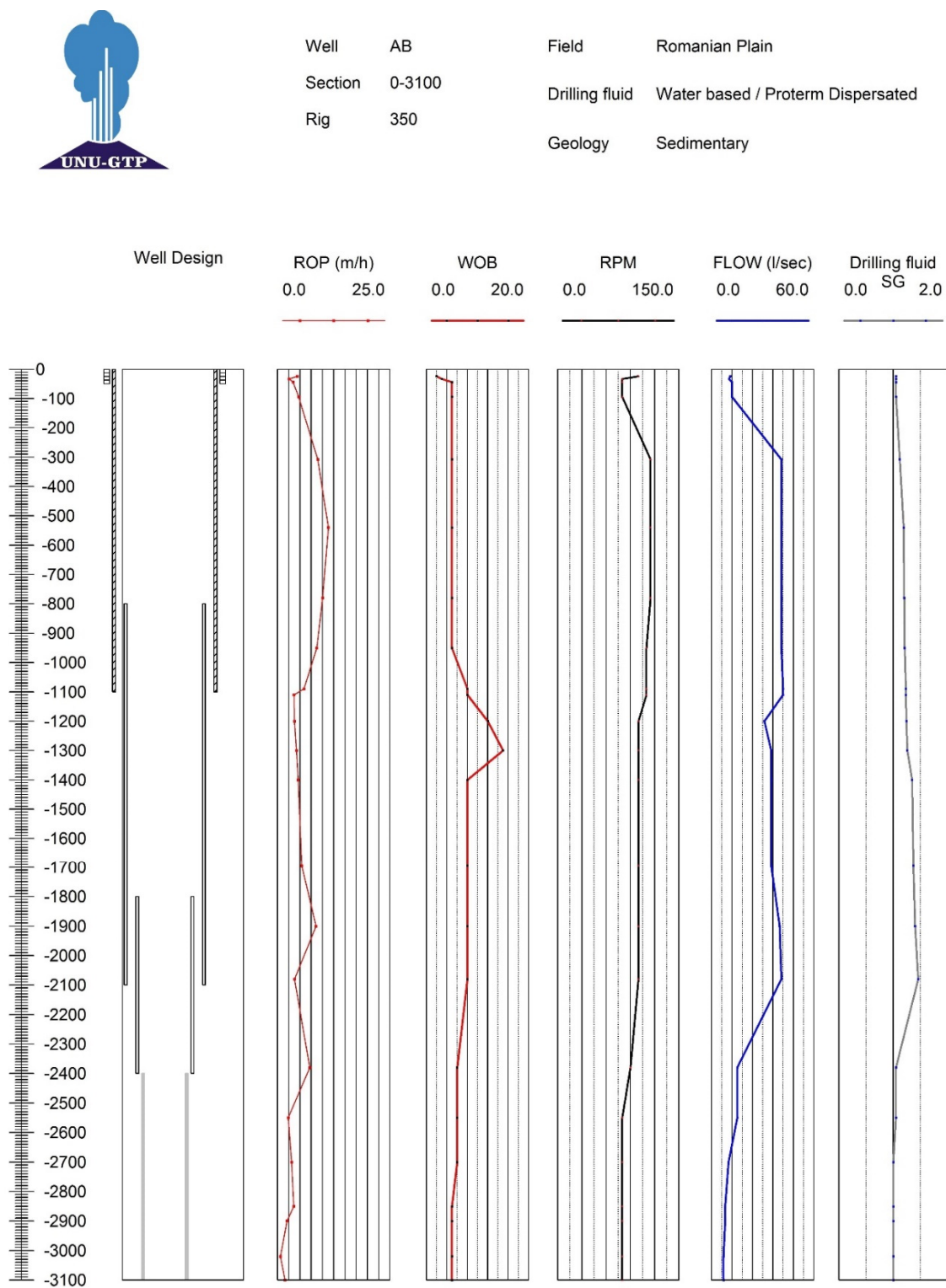


FIGURE 7: Design and drilling parameters for the Therme Balotesti well

3.2.2 Drilling evolution

As the well was being drilled, the progress was monitored with the rig instrumentation system and analysis of cuttings and reported daily, often against a time depth curve. One thing to note is any changes that may indicate the transition from one pressure regime to another, thus formations properties have to be closely monitored. The well target objective was to intercept the Jurassic Superior – Cretaceous Inferior collector which has a relatively high temperature and productivity for low-temperature geothermal fields.

Due to the different structure of the formation sections of the well, the drilling fluid characteristics had to be adapted for each interval:

- For the first interval from 0 to 1,100 m: water and bentonite at a density of 1.14-1.25 kg/dm³;
- Down to 2,330 m mud was used with inhibitors to prevent problems caused by the interaction of contractile clays with mud;
- Below 2,330 m water was used, with loss of circulation, so as not to influence the productive potential.

3.2.3 Problems encountered

Offset information from previous studies in Otopeni geothermal reservoir confirmed the presence of H₂S and other gases. During drilling through the formations due attention should be given to eruptive manifestations that may occur and adjust the drilling parameters and mud properties. In order to avoid getting stuck in the open hole section due to fractured zones, the stabilizers were excluded from the BHA.

A very important aspect that could affect completion of drilling is the perfect cementing operation of liners, especially in crossing areas of unconsolidated sediments; the water quality was not affected by the aquifers from some intervals. The Cement Bond Log (CBL) evaluating the integrity of cement work was performed by a specialised company that checked the cement integrity after each section of the well has been cased and cemented.

3.3 Success of drilling and outcome

The safety factors used for drill string assembly made the total depth of the well successfully achieved. The Air-lift pump system was used to clean the well, finally getting a flow rate of 25 l/s and a temperature of ~81°C. Chemically speaking, the water is chlorinated bicarbonate, calcium-magnesium. The reservoir conditions were known in Otopeni. The casing selection path was respected according to common selection for geothermal wells. The water properties analyses revealing the absence of any bacteriological groups considered pathogenic was confirmed by different accredited institutions, Table 5 shows the result of water analysis.

TABLE 5: Water analysis results (RAH, 2016)

Parameter	Unit	Value
Temperature	(°C)	81-82
Electrical conductivity, EC	(μS/cm)	3,900
Chloride, Cl	(mg/l)	1,090
Bicarbonate, HCO ₃	(mg/l)	268
Calcium, Ca	(mg/l)	134.88
Ammonium, NH ₄	(mg/l)	2.6
Hydrogen sulphide, H ₂ S	(mg/l)	30

Each step of well design has been successfully completed without any incidents, which guarantees safe operation and long life of the well utilization.

4. DISCUSSION

Geothermal utilization has evolved through time in different parts of the world; modern day technology has made it possible in better conditions. Drilling of geothermal wells is not such a big market, meaning that there are not so many drilling companies specialised in drilling for geothermal resources. In each country the wells are drilled with their own contractors, and the drilling rigs are the same commonly used in the oil and gas industry, including some additional equipment such as cooling towers for the mud and a rotating head preventer to provide added protection for the crew in case of a kick and also when doing aerated drilling (Thórhallsson, 2016).

Based on data from the well project, the drilling company needs to decide about important details in order to successfully complete the well, such as: rig capacities, drill string characteristics, required equipment etc. The next subchapters will present some calculations on the drill string and the casings and safety factors. Regarding drilling costs, there is a lack of open data due to confidentiality, each drilling rig having its own trend, drilling contractors and the drilling material costs are influenced by the oil and gas industry.

4.1 Calculations of the drill string

The Therme Balotesti well design was based on the design of previous wells and the anticipated geology and lithology; these are important factors to decide the setting of the casing shoe depths and to obtain a better image about the drill string design.

The next calculations are obtained with the help of formulas and drill string characteristics from Drilling Data Handbook, 7th edition (DDH) (Gabolde and Nguyen, 2006), for example of drill string used to drill a ~3,100 m deep vertical geothermal well.

Design parameters

Hole diameter: Final section from 2,330 to 3,107 m drilled with 5¾" diameter bit.

Assumed mud weight: 1.2 (kg/m³); buoyancy factor = 0.847 (DDH, A-28).

Table 6 describes the drill pipe sizes and the tensile strengths used when drilling the final section of the well.

TABLE 6: Drill pipes features

Composition of the drillstring	Outer diameter (OD)	Total length with tool joints, (L _{xxx})	Weight per m with tool joint in air (W _{xxx})	Grade	Tool joint (NC)	Tensile strength
	(")	(m)	(kg/m)			(daN*10 ³)
Drill pipes 1 (DP ₁)	5	1,781	32.55	G105	50	193.8
Drill pipes 2 (DP ₂)	3½	980	25.37	G105	38	132.0
18 Heavy weight drill pipes (HWDP)	3½	165.5	37.70	-	38	153.0
18 Drill collars (DC)	4¾	169.6	73.84	-	38	

To reduce the fatigue failure above the BHA, HWDP are used to provide a flexible transition between the drill collars and the drill pipes.

Checking for a maximum WOB in tons, rearranging formula from DDH, B-56:

$$WOB_{\max} = \frac{L_{DC} \cdot \cos(i) \cdot F_{PN} \cdot P_{DC} \cdot k}{10^5} = \frac{169.6 \cdot 1 \cdot 85 \cdot 73.84 \cdot 0.847}{10^5} = 9 \text{ tons which is very much for } 5\frac{3}{4}'' \text{ bit.}$$

For a $5\frac{3}{4}''$ bit $F_{PN} = 50$ would give 5.3 tons which is recommended. As a rule of thumb there should be used 1 ton weight on per inch of the bit diameter.

Here L_{DC} = Length of the drill collars (m);
 WOB = Maximum weight on bit (tons);
 i = Hole angle from vertical (0°);
 F_{PN} = Neutral point position as percentage of total drill collar string length (85 for 85%);
 k = Buoyancy factor (DDH);
 P_{DC} = Weight per m of drill collars (kg/m).

Checking for tensional loading, T (DDH):

Checking tensional loading for the $3\frac{1}{2}''$ drill pipes, DP_2 :

$$T_{DP2} = g \cdot (L_{DP2} \cdot W_{DP2} + L_{HWDP} \cdot W_{HWDP} + L_{DC} \cdot W_{DC}) \cdot k$$

where T_{DP2} = Submerged load hanging below the upper end of this section of drill pipe (10^3 daN);
 L_{DC} = Length of the drill collars (m);
 W_{DC} = Weight of collars per m (kg/m);
 L_{HWDP} = Length of the heavy wall drill pipes (m);
 W_{HWDP} = Weight of those pipes per m (kg/m);
 L_{DP2} = Length of the $3\frac{1}{2}''$ drill pipes (m);
 W_{DP2} = Weight of those pipes per m (kg/m);
 k = Buoyancy factor for the mud.

Hence:

$$T_{DP2} = 0.981 \cdot (980 \cdot 25.37 + 165.5 \cdot 37.7 + 169.6 \cdot 73.84) \cdot 0.847 = 36.25 \cdot 10^3 \text{ daN}$$

This is much less than the tensile strength, T_{e2} , of the pipes, $132 \cdot 10^3$ daN – *tensional loading OK*.

Checking tensional loading for the $5''$ drill pipes, DP_1 :

$$T_{DP1} = 0.981 \cdot (L_{DP1} \cdot W_{DP1} + L_{DP2} \cdot W_{DP2} + L_{HWDP} \cdot W_{HWDP} + L_{DC} \cdot W_{DC}) \cdot k$$

$$T_{DP1} = 0.981 \cdot (1781 \cdot 32.55 + 980 \cdot 25.37 + 165.5 \cdot 37.7 + 169.6 \cdot 73.84) \cdot 0.847 = 84.42 \cdot 10^3 \text{ daN}$$

which is much less than the tensile strength, T_{e1} , of the pipes, $193.8 \cdot 10^3$ daN – *tensional loading OK*.

Consideration of the weakest link in the stem, i.e. the $3\frac{1}{2}''$ drill pipes DP_1 :

Allowable load - factor of safety = 10% or 1.1. Margin of over pull (MOP) using formulas from DDH:

$$\text{Allowable load in tension (daN), } T_a = 0.9 \cdot T_{e2} = 0.9 \cdot 132 \cdot 10^3 \text{ daN} = 118.8 \cdot 10^3 \text{ daN}$$

$$\text{Calculate } R_T = \text{Margin of over pull (MOP)} = T_a - T_{DP2} = 118.8 \cdot 10^3 \text{ daN} - 36.25 \cdot 10^3 \text{ daN} = 82.55 \cdot 10^3 \text{ daN.}$$

$$\text{Calculate safety factor in tension, } F_s = \frac{T_a}{T_{DP2}} = \frac{82.55 \cdot 10^3}{36.25 \cdot 10^3} = 2.28 - \text{which is OK.}$$

Consideration of the 5" drill pipes DP₁:

Allowable load - factor of safety and margin of over pull (MOP) using formulas from DDH:

Allowable load in tension (daN), $T_a = 0.9 \cdot T_{e1} = 0.9 \cdot 193.8 \cdot 10^3 \text{ daN} = 163.8 \cdot 10^3 \text{ daN}$

Calculate $R_T = \text{Margin of over pull (MOP)} = T_a - T_{DP1} = 163.8 \cdot 10^3 - 84.42 \cdot 10^3 \text{ daN} = 79.32 \cdot 10^3 \text{ daN}$.

Calculate safety factor in tension, $F_s = \frac{T_a}{T_{DP1}} = \frac{163.8 \cdot 10^3}{84.42 \cdot 10^3} = 1.94$, which is OK.

Estimate of maximum drilling depth with this drill stem if the MOP is lowered to $30 \cdot 10^3 \text{ daN}$, using formula from DDH:

$R_T = T_a - T_{DP1*}; T_{DP1*} = T_a - R_T = 163.8 \cdot 10^3 \text{ daN} - 30 \cdot 10^3 \text{ daN} = 133.8 \cdot 10^3 \text{ daN}$

$T_{DP1*} = 0.981 \cdot (L_{DP1} \cdot W_{DP1} + L_{DP2} \cdot W_{DP2} + L_{HWD} \cdot W_{HWD} + L_{DC} \cdot W_{DC}) \cdot k = 133.8 \cdot 10^3 \text{ daN}$

$L_{DP1} \cdot 32.55 \cdot 10^3 = 117,404 \text{ kg}$

$L_{DP1} = \frac{117,404}{32.55} = 3,606.9 \text{ m}$

The maximum drilling depth is $= L_{DP1} + L_{DP2} + L_{HWD} + L_{DC} = 3,606.9 + 980 + 165.5 + 169.6 = 4,922 \text{ m}$.

Checking for collapse due to annular hydrostatic pressure for the 3½" drill pipes, DP₂ according to maximum depth, using formulas from DDH.

For drill pipe DP₂ the limit collapse pressure is $P_{ct2} = 139.7 \text{ MPa}$.

If there is no fluid in the drill pipe the pressure from outside the pipe is:

$$P_C = 9.81 \cdot d \cdot z$$

where P_C = Collapse pressure (kPa);
 z = Vertical depth of the drill pipes (m), $L_{DP1} + L_{DP2} = 3,606.9 + 980 = 4,586.9 \text{ m}$;
 d = Mud weight (kg/m³).

1. Mud weight $d = 1,200 \text{ kg/m}^3$.

The units are: $\text{m/s}^2 \cdot \text{kg/m}^3 \cdot \text{m} = (\text{kg} \cdot \text{m/s}^2) / \text{m}^2 = \text{N/m}^2 = \text{Pa} = 10^{-6} \text{ MPa}$

$P_C = 9.81 (\text{m/s}^2) \cdot 1.2 \cdot 10^3 (\text{kg/m}^3) \cdot 4,586.9 (\text{m}) = 54 \text{ MPa}$ which is OK.

2. Mud weight $d = 1,000 \text{ kg/m}^3$.

$P_C = 9.81 (\text{m/s}^2) \cdot 1 \cdot 10^3 (\text{kg/m}^3) \cdot 4,586.9 (\text{m}) = 45 \text{ MPa}$ which is OK.

Checking for safety against hydrostatic collapse for drill pipe 2.

1. Mud weight $d = 1,200 \text{ kg/m}^3$.

Drilled depth about 3,100 m.

Allowed safety factor 10% or 1.1.

$L_{DP2} = 3,100 - 165.5 \text{ m} - 169.6 \text{ m} = 2,764.9 \text{ m}$

$$2,764.9 = P_{ct1} / (9.81 \cdot 10^3 \cdot d \cdot F)$$

$F = 40 \cdot 10^6 / (9.81 \cdot 1.2 \cdot 10^3 \cdot 2,764.9) = 1.23$, which is OK

where F = Safety against collapse.

2. Mud weight $d = 1,000 \text{ kg/m}^3$.

Drilled depth about 3,100 m.

$$L_{DP2} = 3,100 - 165.5 \text{ m} - 169.6 \text{ m} = 2,764.9 \text{ m}$$

$$2,764.9 = P_{ct1} / (9.81 \cdot 10^3 \cdot d \cdot F)$$

$$F = 40 \cdot 10^6 / (9.81 \cdot 1 \cdot 10^3 \cdot 2,764.9) = 1.48, \text{ which is OK}$$

4.2 Casing calculations

With the information gathered from the paper presented in AHR and the casing features from New Zealand Standards and Drilling Data Handbook (Gabolde and Nguyen, 2014), the following was calculated for each casing:

- Axial tensile forces on casing during running and cementing;
- Axial force due to temperature rise;
- Maximum differential burst pressure of casing near shoe or stage cementing ports;
- Hoop collapse pressure during cementing.

Table 7 represents the results of axial tensile forces on casing during running and cementing:

TABLE 7: Axial tensile forces

CSG Grade	Length	$F_{\text{csg air wt}}$	$F_{\text{csg contents}}$	$F_{\text{displaced fluids}}$	F_{hookload}, F_p	Minimum tensile strength	Calculated DF	Minimum DF
K55 width (")	(m)	(kN)	(kN)	(kN)	(kN)	(kN)		
13 $\frac{3}{8}$	1,105	879	863	970	772	6,556	8.5	1.8
9 $\frac{5}{8}$	1,285	882	475	584	773	5,735	7.4	1.8
7	480	161	95	115	141	2,813	19.9	1.8

Here $F_{\text{csg air wt}}$ = Air weight of casing (kN);
 $F_{\text{csg contents}}$ = Weight of internal contents of casing (kN);
 $F_{\text{displaced fluids}}$ = Weight of fluids displaced by casing (kN);
 F_{hookload} = Surface force suspending casing that is subjected to gravitational and static hydraulic loads (kN);
 DF = Design factor.

Checking for the design factor for each casing string according to New Zealand Standards (New Zealand Standard, 2015) the minimum tensile design factor is 1.8. The results on calculated design factor as shown in Table 7 are:

- For 13 $\frac{3}{8}$ " = 8.5 which is OK;
- For 9 $\frac{5}{8}$ " = 7.4 which is OK;
- For 7" = 19.9 which is OK.

Table 8 represents the results of axial force due to temperature rise.

TABLE 8: Axial force using NZS 2403:2015

Outer diameter (")	E (GPa)	α (°C ⁻¹)	T ₁ (°C)	T ₂ (°C)	A _p (m ²)	F _c (kN)	F _r (kN)	Minimum compressive strength (kN)	Calculated DF	Minimum DF
13 ^{3/8}	210	0.000013	30	85	0.010009	-1,503	-731	3,793	5.19	1.20
9 ^{5/8}	210	0.000013	40	85	0.008756	-1,076	-303	3,319	10.95	1.20
7	210	0.000013	45	85	0.004294	-469	-327	1,627	4.97	1.20

Here E = Modulus of elasticity (GPa);
 α = Coefficient of linear thermal expansion;
T₁ = Neutral temperature (temperature of cement set (°C));
T₂ = Maximum expected temperature (°C);
A_p = Cross-sectional area of pipe (m²);
F_c = Compressive force due to heating (kN);
F_r = Resultant force (kN).

Minimum design factor is 1.20 (New Zealand Standard, 2015). Results on calculated design factor are:

- For 13^{3/8}" = 5.19 *which is OK*;
- For 9^{5/8}" = 10.95 *which is OK*;
- For 7" = 4.97 *which is OK*.

Table 9 represents maximum differential burst pressure of casing near shoe or stage cementing ports.

TABLE 9: Burst pressure using NZS 2403:2015

CSG Grade K55 width (")	L _z (m)	ρ_c (kg/l)	L _f (m)	ρ_f (kg/l)	g (m/s ²)	Differential burst pressure (MPa)	Internal yield pressure (MPa)	Calculated DF	Minimum DF
13 ^{3/8} Shoe	1105	1.75	1105	1.25	9.81	5.42	18.90	3.5	1.5

where L = Length of casing (m);
 ρ_c = Slurry density (kg/l);
L_f = Total vertical length of fluid column in an annulus (m);
 ρ_f = Density of water (kg/l);
g = Gravitational acceleration (9.81 m/s²).

Minimum design factor is 1.5 (New Zealand Standard, 2015). The results calculated on maximum differential burst pressure of 13^{3/8}" casing near the shoe = 3.5, *which is OK*.

Table 10 represents Hoop collapse pressure during cementing.

TABLE 10: Hoop collapse NZS using NZS 2403:2015

CSG Grade K55	L _z (m)	ρ_c (kg/l)	ρ_f (kg/l)	g (m/s ²)	Δ_{pe} (MPa)	Internal collapse pressure (MPa)	Calculated DF	Minimum DF
13 ^{3/8} " Shoe	1,105	1.75	0.988	9.81	8.26	7.80	0.944	1.2
9 ^{5/8} " Shoe	2,085	1.75	0.988	9.81	15.59	26.80	1.720	1.2
7" Shoe	2,330	1.75	0.988	9.81	17.42	26.80	1.539	1.2

where L_z = Total vertical length of liner (m);
 Δ_{pe} = Differential pressure on casing during cementing (MPa).

Minimum design factor is 1.20 (New Zealand Standard, 2015). The results on hoop collapse pressure during cementing are:

- For 13 $\frac{3}{8}$ " at shoe = 0.944 – assumed that water was used to calculate, it is recommended to use mud *which is not OK*.
- For 13 $\frac{3}{8}$ " at shoe = 1.439 – with mud density of 1.25 (maximum density for 13 $\frac{3}{8}$ " section), *which is OK*.
- For 9 $\frac{5}{8}$ " at shoe = 1.720 *which is OK*.
- For 7" at shoe = 1.539 *which is OK*.

5. CONCLUSIONS

Therme Balotesti is the name of a successful geothermal well drilled in Otopeni geothermal reservoir for the supply of water for a spa complex. Therme Bucharest is the name of a private project which was the development of a modern spa concept near the capital Bucharest. Therme Bucharest, a 30,000 m² wellness, relaxation and entertainment centre based on thermal waters was completed and inaugurated in January 2016 becoming the largest thermal wellness centre in Europe. The success of the well was highlighted in the final stage by getting a flow rate of 25 l/s and temperature of 81°C. Water quality was tested at recognized institutions nationally and internationally, the analyses revealing the absence of any bacteriological groups considered pathogenic.

On the surface, the well is equipped with a pump head fitted with valves and gauges. For exploiting the geothermal aquifer a submersible pump was installed with variable flow located at a depth of 150 m, operable to temperatures of 90°C.

Checking for a maximum weight on bit in tons with a neutral point of 85% in the collars with this drill string gave 9 tons which is very much for 5 $\frac{3}{4}$ " bit. As a thumb of rule it is said 1 ton's weight is needed on each diameter inch of the drill bit. For a 5 $\frac{3}{4}$ " bit $F_{PN} = 50$ would give 5.3 tons which is close to the recommended value.

Tensional loading for the 3 $\frac{1}{2}$ " drill pipes was $36.25 \cdot 10^3$ daN which is much less than the tensile strength of the pipes, $132 \cdot 10^3$ daN. Therefore, the tensional loading is OK.

Tensional loading for the 5" drill pipes was $84.42 \cdot 10^3$ daN which is much less than the tensile strength of the pipes, $193.8 \cdot 10^3$ daN. Therefore, the tensional loading is OK.

Consideration of the weakest link in the stem, i.e. the safety factor of 10% or 1.1. For the 3 $\frac{1}{2}$ " drill pipes the safety factor in tension was 2.28 which is OK. Consideration of the 5" drill pipes the safety factor in tension was 1.94 which is also OK.

The maximum length of the 5" drill pipes if the Margin of Over pull, (MOP) is lowered to $30 \cdot 10^3$ daN with the same components of the drill string is 3,609.9 and maximum drilling depth with this drill string is 4,922 m.

Checking for collapse due to annular hydrostatic pressure if there is no fluid in the drill pipe and mud weight $d = 1,200$ kg/m³ for the 3 $\frac{1}{2}$ " drill pipes, according to maximum depth of the pipes to 4,586.9 m gave 54 MPa which is much lower than the collapse limit pressure, 139.7 MPa. For a mud weight $d = 1,000$ kg/m³ the hydrostatic pressure was 45 MPa which is also much lower.

Checking for safety factor against hydrostatic collapse for the 5" drill pipes, mud weight $d = 1,200$ kg/m³ and drilled depth about 3,100 m gave safety factor 1.23. For mud weight $d = 1,000$ kg/m³ the safety factor was 1.48. The drill string composition design was successful, drilling the well safely.

The casing design programme, the mechanical and physical properties of casing was conducted by S.C. Therme Nord Bucuresti S.R.L. Each service company uses safety factors from different handbooks. The minimum acceptable casing design factors (NZS 2403:2015) are:

- Internal yield (burst) design factors 1.5 -1.8;
- Collapse design factors 1.2;
- Tensile design factor 1.8;
- Compressive factor 1.2.

Checking for the design factor for each casing string according to New Zealand Standard (New Zealand Standard, 2015) the minimum tensile design factor is 1.8.

For 13 $\frac{3}{8}$ " this means 8.5 which is OK, for 9 $\frac{5}{8}$ " 7.4 which is OK, and for 7" 19.9 which is OK.

Checking for axial force due to temperature rise, minimum design factor is 1.20 (NZS 2403:2015). The result on calculated design factors: for 13 $\frac{3}{8}$ " it was 5.19 which is OK, for 9 $\frac{5}{8}$ " it was 10.95 which is OK and for 7" it was 4.97 which is OK.

Checking for maximum differential burst pressure of casing near shoe, the minimum design factor is 1.5 (New Zealand Standard, 2015). The results calculated for 13 $\frac{3}{8}$ " at shoe was 3.5 which is OK. This load case occurs due to cement density, with the casing full of cement and the annulus full of water, creating a pressure difference that can lead to burst of casing in case of inadequate choices regarding casing features.

Checking for hoop collapse pressure during cementing the minimum design factors is 1.20 (New Zealand Standard, 2015), where: for 13 $\frac{3}{8}$ " at shoe it was 0.944, assuming that water was used for calculation. However, it is recommended to use mud, hence for 13 $\frac{3}{8}$ " at shoe it was 1.439 – with mud density of 1.25 (maximum density for 13 $\frac{3}{8}$ " section), which is OK, for 9 $\frac{5}{8}$ " at shoe it was 1.720 which is OK and for 7" at shoe it was 1.539 which is OK.

ACKNOWLEDGEMENTS

I wish to address my gratitude to the Government of Iceland, the United Nations University Geothermal Training Programme and Dafora Drilling Company, Romania for the opportunity to participate in this training programme.

My sincere gratitude to the Director, Mr. Lúdvík S. Georgsson and the Deputy Director Mr. Ingimar G. Haraldsson. I am grateful to Ms. Málfríður Ómarsdóttir, Ms. Thórhildur Ísberg, and Mr. Markús A. G. Wilde, for their generous help, guidance and support during my stay in Iceland and all the staff of Orkustofnun and ÍSOR.

I am indebted to my supervisor, Mr. Björn Már Sveinbjörnsson for the entire support and Mr. Sverrir Thórhallsson, for sharing his extensive knowledge and experience and for supervision of this work. I would like to express my gratitude to Gunnar Skúlason Kaldal from ÍSOR regarding technical calculations guide.

Cheers for the 2016 UNU-GTP fellows for the good time we enjoyed during the six months.

Thank be to God, for my family, for my life!

REFERENCES

- Bentec Ltd., 2016: *Stationary standard euro rigs*. Bentec Ltd., website: www.bentec.com/rigs/euro-rigs/stationary-standard-euro-rigs/
- Codruta, B., Cornel, A., and Marcel, R., 2015: Geothermal energy in Romania: Country update 2010-2014. *Proceedings of the World Geothermal Congress 2015, Melbourne, Australia*, 9 pp.
- Gabolde, G., and Nguyen, J.P., 2006: *Drilling data handbook* (7th ed.). Editions Technip, Paris, 576 pp.
- Gabolde, G., and Nguyen, J.P., 2014: *Drilling data handbook* (9th ed.). Editions Technip, Paris, 576 pp.
- Hole, H., 2008: Geothermal well completion tests. *Paper presented at "Petroleum Engineering Summer School", Dubrovnik, Croatia, Workshop*, 26 pp, website: <https://www.geothermal-energy.org/pdf/IGAstandard/ISS/2008Croatia/Hole02.pdf>
- Marcel, R., 2011: Geothermal resources of Romania. *Paper presented at GEOELEC Workshop, Athens*, 16 pp.
- New Zealand Standard, 2015: *Code of practice for deep geothermal wells*. Standards Association of New Zealand, Wellington, NZ, 102 pp.
- RAH, 2016: *Forajul hot springs, Bucurest*. Romanian Association of Hydrogeologists (in Romanian), website: www.ahgr.ro/media/85718/forajgeoterm_balotesti.pdf.
- Serban, N., 2014: *UPG – Ploiesti, Romania, well control training program*. International Well Control Forum (IWCF), unpublished lecture notes.
- Thórhallsson, S., 2016: *Well designs and geothermal drilling technology*. UNU-GTP, Iceland, unpublished lecture notes, 379 pp.
- Wikipedia, 2016: *Romanian plain*. Wikipedia, website: ro.wikipedia.org/wiki/C%C3%A2mpia_Rom%C3%A2n%C4%83

APPENDIX I: API SPECIFICATIONS STANDARDS

- API SPEC 5CT:** Specification for casing and tubing.
- API BULL 5C2:** Bulletin on performance properties of casing and tubing.
- API BULL 5C3:** Bulletin on formulas and calculations for casing, tubing, drill pipe and line pipe properties"
- API RP 5 A5:** Specifies requirements and gives recommendation for filed inspection of new casing, tubing and plain-end drill pipe.
- API SPEC 10A:** Specification for cements and materials for well cementing, 23rd edition. 2002 Washington, DC, API.



UNITED NATIONS
UNIVERSITY

UNU-GTP

Geothermal Training Programme

Orkustofnun, Grensasvegur 9,
IS-108 Reykjavik, Iceland

Reports 2016
Number 33

CHEMISTRY OF GEOTHERMAL FLUIDS IN DIENBIEN AND SONLA PROVINCES, NW-VIETNAM

Pham Dieu Linh

Vietnam Institute of Geosciences and Mineral Resources
67 Chien Thang Road, Ha Dong District
Hanoi
VIETNAM
phamdieulinh1981@gmail.com

ABSTRACT

North-west Vietnam is a very special area where development of geothermal energy will be significant for socio-economic activities. The data in this project is taken from a previous research in 2004. Thirty-four samples are taken from 119 hot springs for further study, with the purpose of estimating and interpreting the chemical compositions of the water, by using the methods as triangle diagrams, geothermometers, evidence of mixing and log Q/K plot. The 34 samples were divided into 5 groups based on the location and structure of geology. The study results show that Group 1 with samples S1, S2, and S3 give a good estimation of the temperature of the reservoir from 73°C to 150°C with small deviation between methods. Group 2 with samples S8, S18, and S19 give a temperature from 76°C to 111°C. In Group 3 with samples S11 and S12, reservoir temperature is from 59°C to 110°C. Group 4 with S72 and S73 samples, the temperature of reservoir drops between 60-100°C. Group 5 with samples S6, S65, S75, S77, and S78 the reservoir temperatures estimated by silica geothermometers are quite low and they might be from a different reservoir.

1. INTRODUCTION

Geothermal energy is a clean, renewable and environmentally benign energy source which is based on the heat in the earth. Geothermal energy is number fourth of the renewable energy sources in world electricity production after hydro, biomass and wind.

Vietnam is a country with an area of 331,689 km² situated on the Indochina peninsula and more than 300 thermal springs. There have been some geothermal studies done since 1986 that involve basic surveying such as mapping, sampling and analysis of geothermal water and evaluation for the areas in north and central Vietnam, with the aim of supporting socio-economic development. Until now, geothermal utilization in Vietnam is simple, such as swimming pools, spa treatments and vegetable dehydration.

The aim of this study is about working with geothermal fluid as a part of a surface exploration. During this process, sampling locations are selected, water samples are collected and analysed to find out the chemical composition of the thermal water. Geothermometers and chemical programs are applied on

the data from the analytical results. The interpretation of geochemical data aims at estimating the reservoir temperature, the properties of the geothermal fluids, fluids origin and recharge, and if possible, physical processes such as cooling, boiling or condensation, and geothermal potential of area.

2. GEOLOGICAL BACKGROUND

Vietnam is located in southeast Asia and is a part of the South China plate and Indochina plate. The plate boundary is the Red River fault zone that strikes NW-SE and extends over a length of more than 1000 km between the Gulf of Tonkin and Tibet (Tapponnier et al., 1990).

According to the model of Tapponnier et al. (1986), the whole of Indochina extruded to the southeast during the collision of India with Asia. The relationship between Indochina and South China movement along the Red River fault zone has been estimated to be from 330 km (Lacassin et al., 1993) to 500-740 km (Tapponnier et al., 1986, 1990) of left lateral motion during the Tertiary (from 65 Ma to 1.8 Ma).

According to Tran (1995) the territory of Vietnam can be divided into five units as structural blocks consisting of the Northeast (NE), Northwest (NW), Truongson (north center of Vietnam), Kontum (south center of Vietnam) and Nambo blocks (South Vietnam). The NE block includes the stratigraphy and igneous rocks ranging from the Late Proterozoic to Quaternary age, 542 Ma to 1.6 Ma. The NW and Truongson blocks involve the thickest Paleozoic strata in Vietnam which are recognized as NW-SE trending Paleozoic folded systems with some differences in tectonic development between them, especially in the late Paleozoic. The Kontum block is an uplifted massif where the oldest stratigraphy of the Archean is found, but Paleozoic rocks are almost absent. The Nambo block is defined as a continental rift filled with thick (6 km) Cenozoic deposits.

The study area is located in a part of Dienbien and Sonla provinces in the NW block which have abundant active tectonic faults (Figure 1). About 34 hot springs have been discovered in this area with temperatures ranging from 35 to 78°C. The geology of this area is quite complicated with presentation of many types of rock that are structured in NW-SE direction. With regard to geology and tectonics, the region is composed of the following zones:

The Dienbien zone is located southwest of study area which lies along the Vietnam-Laos border in southwest and Songma fault at northeast. Dienbien zone was filled up with volcano clastic and coal-bearing sediments in Triassic age, sandstone, siltstone, silicic, tuff basalt, andesite and limestone in Carbon – Permian age and sandstone, clay schist in Silurian – Devon age. Samples marked S1-S5, S7, S8, S14, S15, S16, S17, S18, S19, S20 and S82 are located in this zone.

The Songma zone belonging to the northwest Vietnam folded system (late Caledonian time), which is located in the southwestern study area, is composed of a femic (mostly ferromagnesian minerals) basement complex. This zone was mixed with ophiolite of an old subduction zone. Samples marked S77, S79, S83, S6, S78, S80, S81, S65, S74 and S75 are located in this zone.

The Songda zone was the rift of Mesozoic time which is located in the northeastern part of the study area. A superimposed depression structure overlaps the Songma zone and comprises a terrigenous-carbonate volcanic complex with a prevalence of porphyritic basalt and carbonate-terrigenous formations. Samples marked S11 and S12 are located in this zone.

The Tule zone is a volcano-tectonic depression formed in Jura-Cretaceous time. The bedrocks are alkaline-calcareous and volcano-platonic. The Fansipan mountain ridge which is a part of the Tule zone is a granite-granodiorite intrusion. Samples marked S67, S68, S69, S70, S71, S72 and S73 are located in this zone.

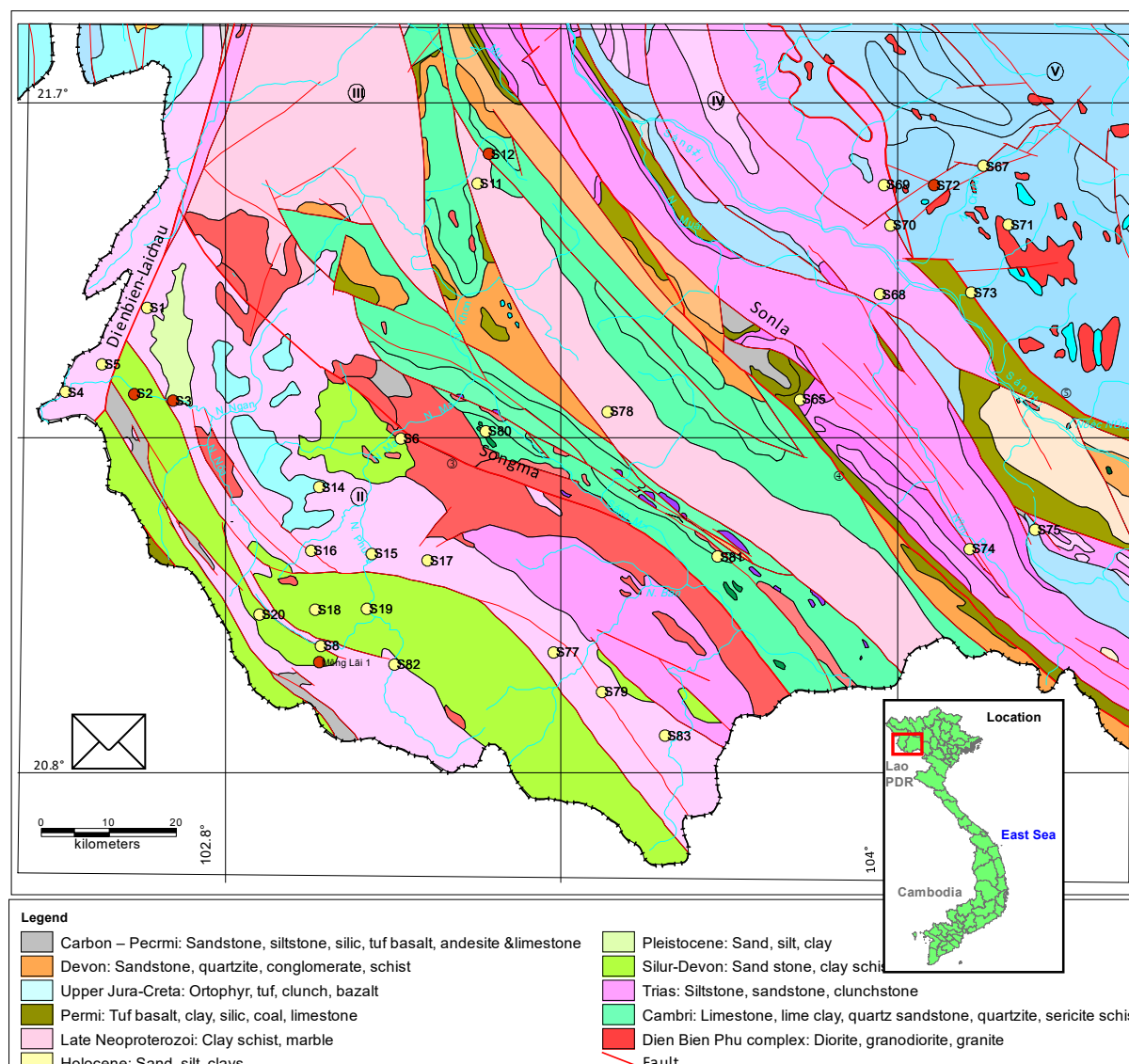


FIGURE 1: Geological map of the study area (modified from VIGMR, 2004), Vietnam map on the right and samples from S1 to S82 showing on the map

The three main active tectonic faults are the Dienbien-Laichau fault, Songma fault and Sonla fault, where earthquakes are intensively active in this region (Figure 1). The faults and their cataclastic zones are the vents for geothermal heat discharge. Anomalous heat flow is often revealed in the form of thermal springs, which are densely located near the tectonic-zoned faults (Hoang, 1996). The Pomlot (sample S3, Table 1) hot spring which appeared after an earthquake occurred in 1935 is an illustration of this.

3. CHEMICAL PROPERTIES OF THE GEOTHERMAL WATER

3.1 Sampling and analyses of geothermal waters

One hundred and twenty water samples from hot springs from northwest Vietnam (520 km × 125 km) were collected and analysed in the years 2002-2004 by the geothermal group of Vietnam Institute of Geosciences and Mineral Resources (VIGMR, 2004). It was decided to use some data from VIGMR (2004) but to concentrate on smaller areas in this report to study the chemical characters of geothermal fluid in more detail. Due to the purpose of this study 34 samples were chosen which were spread over a 100 x 165 km area in the north-western part of Vietnam. The surface temperature range for these samples were from 30 to 78°C.

According to Ármannsson and Ólafsson (2006) the various subsamples collected are described in detail in Table 2.

TABLE 2: Treatment and sub-samples from hot springs and hot-water wells
(Ármannsson and Ólafsson, 2006)

Treatment	Container	Specification	To determine
None; amber glass bottle with ground glass stopper	250-300 ml Glass	Ru	pH, CO ₂ H ₂ S (if not in field), conductivity
None	200 ml plastic	Ru	Mg, SiO ₂ if < 100 ppm
Dilution; 50 ml of sample added to 50 ml of distilled, deionized water	3x100 ml Plastic	Rd (1:10 to 1:1)	SiO ₂ if > 100 ppm
Filtration	200 ml Plastic	Fu	Anions
Filtration; 0.8 ml conc. HNO ₃ (Suprapur) added to 200 ml sample	200 ml plastic	Fa	Cations
Filtration; 2 ml 0.2 M ZnAc ₂ added to sample in 100 ml volumetric glass flask and ≥ 10 ml to ≥ 500 ml bottle containing ≥ 25 mg SO ₄ to precipitate sulphide	100 ml, >500 ml Plastic	Fp, Fpi	SO ₄ , δ ³⁴ S and δ ¹⁸ O in SO ₄
Filtration; one 60 ml and two 1000 ml amber glass bottles	60 ml, 1000 ml Glass	Fui, Fuc, Fut	δ ² H, δ ¹⁸ O, ¹³ C, ³ H

The author of this report has no information about the sampling of this data, but assumes that the major ion concentrations were analyzed by colorimetric, AAS and ICP-AES methods, and the trace elements were analyzed by ICP-MS. Oxygen and hydrogen isotopes were analyzed in New Zealand.

The 34 samples were divided to 5 groups according to the location and structure of geology shown in Table 1.

Group 1 consist of samples S1, S2, S3, S4 and S5 taken in about 20 x 20 km area in the Dienbien zone. This area is the boundary between the highland and lowland and is an active fault zone. The S2, S3, S4, S5 samples are located along the Namron river and the S1 sample was taken beside the Peluong lake.

Group 2 including samples S7, S8, S14, S15, S16, S17, S18, S19, S20 and S82 and are distributed in an area of about 20 x 30 km. This sample group lies on the Dienbien zone as well, but the location is mostly highland and between the small faults in NW-SE direction.

Group 3 includes samples S11, S12 which are located in the Songda zone in the north of study area. This is a small area with the distance between S11 and S12 is about 2 x 3 km.

Group 4 involves samples S67, S68, S69, S70, S71, S72 and S73. They are located in the Tule zone which is spread 20 x 25 km. Most of the samples lie on beside the river shelf.

Group 5 consist of samples S77, S79, S83, S6, S78, S80, S81, S65, S74 and S75. They are all disconnected samples and distributed along in NW-SE direction following the structure of rocks and located in the Songda and Songma zones.

3.2 Chemical composition of the fluids

All of the 34 samples considered are collected from hot springs with temperatures ranging from 30 to 78°C (Table 1). The charge balance can be used to evaluate the analysis (Table 1). The charge balance should be as close to zero as possible, but values between $\pm 15\%$ are used here. Some of the samples were therefore excluded because of the large differences in ionic balance. If the charge balance is higher or lower than $\pm 10\%$ it indicates the erroneous analysis of one of the major ionic species or a missing major ionic species. Five samples, S4, S5, S67, S79, and S70, have charge balance greater than 15%.

Cl-SO₄-HCO₃ diagram

Thermal waters have been classified by a ternary diagram based on the major anion concentrations Cl⁻, SO₄²⁻ and HCO₃⁻ (Figure 2) (Giggenbach 1991). Twenty seven hot springs samples from the study area are plotted on the diagram shown in Figure 2.

According to Giggenbach (1991) the best suited water samples for geothermometers are comprised of neutral, low sulfate, high chloride geothermal waters along the Cl-HCO₃ axis, close to the Cl corner.

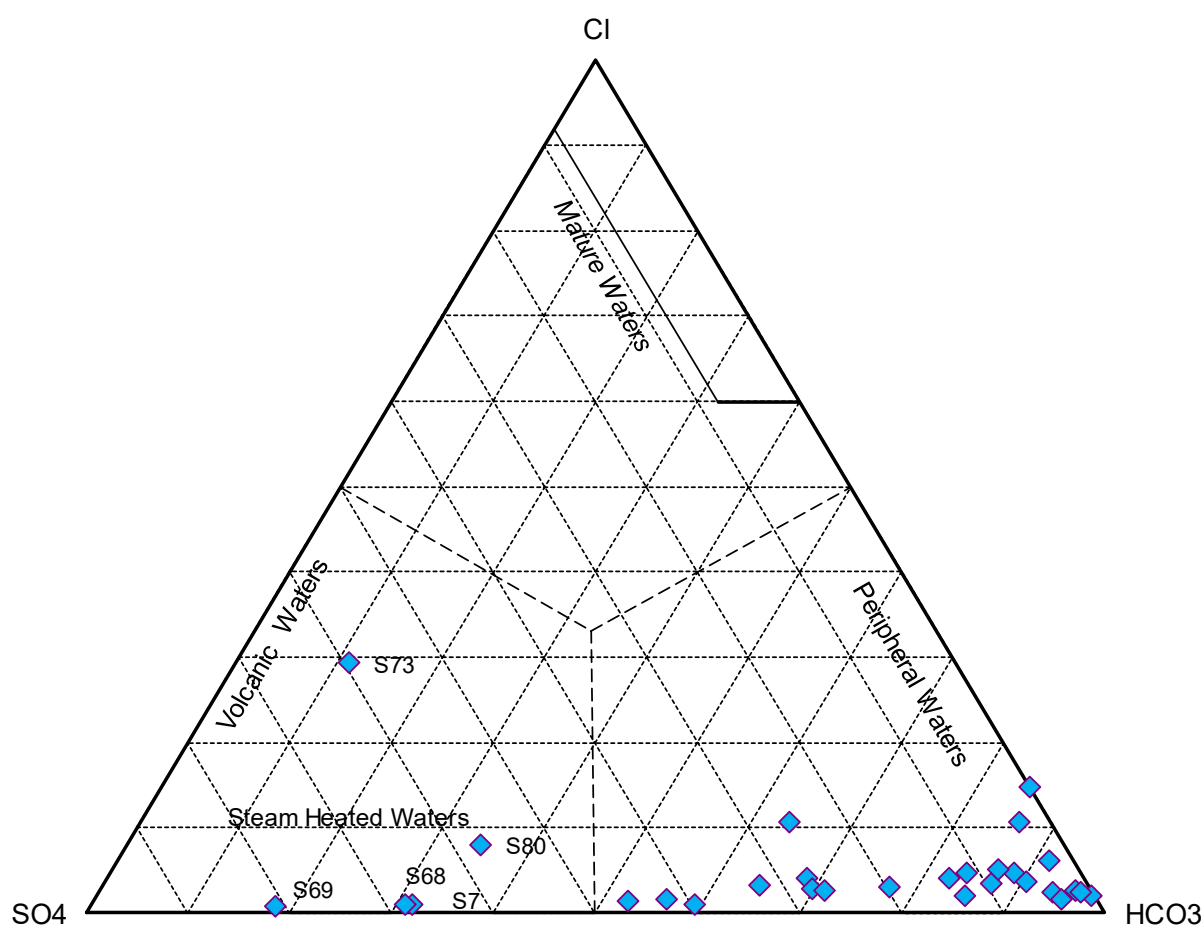
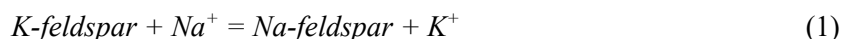


FIGURE 2: The Cl-SO₄-HCO₃ ternary diagram for twenty-seven hot springs samples in study area

The samples from the study area are mainly spread in the HCO_3 corner and a few plot in the steam heated waters part close to the SO_4 corner. This indicates that most of the samples are peripheral waters, where one can use geothermometers. Four samples S7, S69, S68, S73 and S80 which are the steam heated waters, are not suitable for geothermometers according to Giggenbach (1991).

Na-K-Mg diagram

The Na-K-Mg triangular diagram is used to classify water into fully equilibrated, partial equilibrated or immature based on three cations, Na, K and Mg (Figure 3, Giggenbach, 1991). The relationship of the cations are presented in the reactions:



and



When we use the geothermometer, most of the problems in their use arise from their application to unsuitable samples. The Na, K and Mg contents of waters in equilibrium with this assemblage are accessible to rigorous evaluation. Twenty seven hot springs samples from the study area are plotted on the Na-K-Mg triangular diagram in Figure 3.

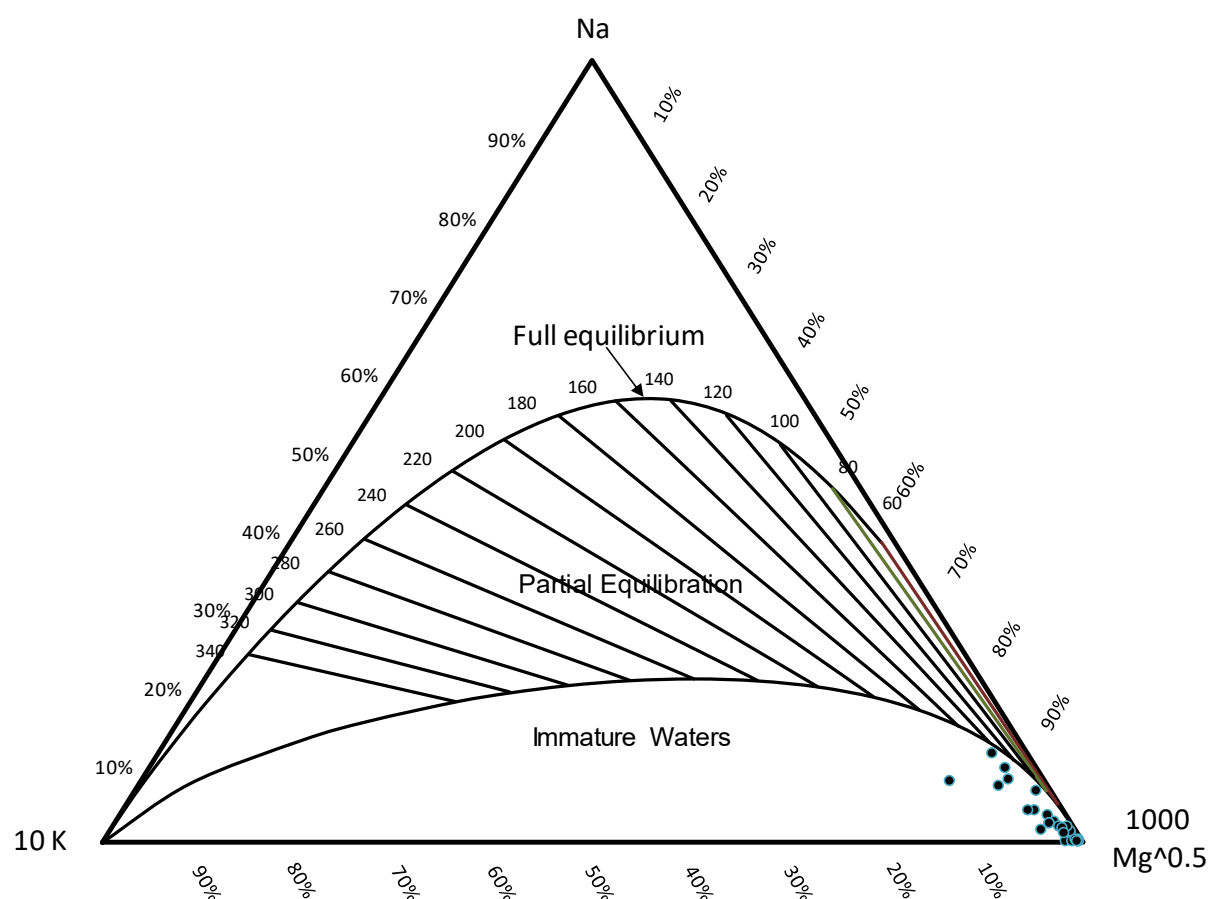


FIGURE 3: The Na-K-Mg triangular diagram for twenty-seven hot springs in study area

Figure 3 shows that most of the samples are placed as immature waters (dissolution of rock with little or no chemical equilibrium) with high Mg content. In this place, samples are frequently quite acid or CO_2 rich waters and therefore according to Giggenbach (1991) the application of both the K-Na and K-Mg geothermometers becomes doubtful.

4. APPLICATION OF GEOTHERMOMETERS

Many water geothermometers have been developed and applied in geothermal fluid study. The water geothermometers can be divided into two main groups. The first group is based on temperature-dependent variations in solubility of individual minerals, and silica minerals are ideal for geothermometry. Second group is based on temperature-dependent exchange reactions which fix ratios of certain dissolved constituents as Na/K geothermometers. The latter ones are complicated and usually calculated by a computer program. In this part the report focuses on the silica geothermometers and cation geothermometers to estimate the reservoir temperatures of study area. Excel spreadsheets by Powell and Cumming (2010) are used to do the calculation and the results are shown in Table 3. The formulas and conditionals are also described in Table 3.

TABLE 3: Reservoir temperatures calculated by various geothermometers

Sample label	Surface temp.	Temperature of reservoir (°C)														
		Amorphous Silica	Alpha Cristobalite	Beta Cristobalite	Chalcedony conductive	Quartz conductive	Quartz adiabatic	Na-K-Ca	Na-K-Ca Mg corr	Na/K Fournier, 1979	Na/K Truesdell, 1976	Na/K Gignenbach, 1988	Na/K Tonani, 1980	Na/K Nieva & Nieva, 1987	Na/K Arnórsson et al., 1983	K/Mg Gignenbach, 1988
S1	53.8	NA	NA	NA	73	103	104	71	61	178	140	196	169	165	149	54
S2	78	NA	100	NA	125	151	144	192	118	233	208	247	246	219	214	100
S3	74	NA	65	18	87	116	115	77	77	190	154	207	185	177	163	67
S8	36.5	NA	55	NA	76	106	106	52	52	169	129	187	158	157	139	58
S14	47	NA	NA	NA	NA	NA	NA	123	NA	138	94	158	118	127	105	71
S15	43	NA	NA	NA	NA	NA	NA	103	85	134	89	154	113	123	100	74
S16	38	NA	NA	NA	NA	NA	NA	NA	16	161	119	179	147	149	130	NA
S17	30	NA	NA	NA	NA	NA	NA	NA	NA	161	120	180	148	149	130	NA
S18	43	NA	60	NA	81	111	110	111	83	188	152	205	183	176	161	82
S19	46	NA	56	NA	77	107	106	103	55	201	168	218	201	189	177	72
S20	32	NA	NA	NA	45	77	81	48	48	204	172	221	205	192	180	61
S82	48.9	NA	NA	NA	NA	60	66	NA	NA	182	145	200	175	170	155	NA
S11	30	NA	39	NA	59	90	92	NA	NA	258	240	270	282	244	245	NA
S12	50.5	NA	59	NA	80	109	109	42	42	453	541	442	634	435	513	53
S71	36	NA	NA	NA	54	86	88	52	52	212	181	227	215	198	189	48
S72	55.5	NA	NA	NA	70	100	101	77	77	289	282	298	330	274	284	71
S77	37	NA	NA	NA	NA	48	56	58	58	189	153	206	184	176	162	51
S83	30	NA	NA	NA	NA	NA	NA	NA	NA	131	85	151	109	120	97	NA
S65	40.2	NA	NA	NA	42	74	78	54	NA	419	483	414	564	402	463	43
S74	33	NA	NA	NA	NA	NA	NA	44	44	178	139	195	169	165	149	46
S75	34.5	NA	NA	NA	39	71	76	NA	NA	225	197	240	234	211	204	NA
S6	61.5	NA	NA	NA	NA	84	86	68	68	204	171	220	205	191	180	NA
S78	42	NA	NA	NA	NA	63	68	NA	NA	217	188	232	223	204	195	NA
S81	43	NA	NA	NA	NA	NA	NA	61	NA	138	94	158	119	127	105	NA

NA - not applicable

4.1 Silica geothermometers

According to Fournier (1991) the solubilities of all silica minerals decrease drastically as temperature decreases below 340°C. The rate of dissolution and precipitation of quartz and amorphous silica change as logarithmic functions of absolute temperature with moderately fast rates at very high temperatures and extremely slow rates at low temperatures (Rimstidt and Barnes, 1980). The silica minerals are formed when the solution becomes saturated.

The formulas for calculating reservoir temperature are based on logarithm of dissolved silica versus the reciprocal of absolute temperature presented below in Equations 3-8, where S refers to the concentration of SiO₂ in mg/l and T is the temperature of reservoir (°C).

Amorphous silica (Fournier, 1977) for 25-250°C

$$T(^{\circ}C) = \frac{731}{4.52 - \log S} - 273.15 \quad (3)$$

Alpha-Crisobalite (Fournier, 1977):

$$T(^{\circ}C) = \frac{1000}{4.78 - \log S} - 273.15 \quad (4)$$

Beta-Crisobalite (Fournier, 1991): for 25-250°C

$$T(^{\circ}C) = \frac{781}{4.51 - \log S} - 273.15 \quad (5)$$

Chalcedony conductive, 0-250°C (Fournier, 1977):

$$T(^{\circ}C) = \frac{1032}{4.69 - \log S} - 273.15 \quad (6)$$

Quartz conductive (Fournier, 1977) for 25-250°C:

$$T(^{\circ}C) = \frac{1309}{5.19 - \log S} - 273.15 \quad (7)$$

Quartz, 25-900°C (Fournier and Potter, 1982) adiabatic:

$$T(^{\circ}C) = -42.2 + 0.28831S - 3.6686 \times 10^{-4}S^2 + 3.1665 \times 10^{-7}S^3 + 77.034 \log S \quad (8)$$

Of the 24 sample results obtained from amorphous silica, alpha-crisobalite and beta-crisobalite silica geothermometers give very low temperatures, some of them are lower than surface temperatures, even negative values. In fact, the alpha-crisobalite is a very rare mineral in nature so that the amorphous silica, alpha-crisobalite and beta-crisobalite geothermometers are not suitable in this case.

In the study area, the most of bedrocks are old sedimentary rocks. According to D'Amore and Arnórsson (2000) in mature sedimentary rock, which contain less reactive minerals than volcanic rock, equilibration with quartz may be experienced at temperatures of even less than 100°C. In fact, chalcedony is formed between 0-100°C and quartz is formed at greater than 180°C, but in the old rock where chalcedony tends to become quartz after a long time, so it is possible to use both chalcedony and quartz geothermometers.

According to D'Amore and Arnórsson (2000) when calculating temperatures from the silica content of nature water assuming equilibrium with either quartz or chalcedony, the temperatures are termed quartz equilibrium and chalcedony equilibrium temperatures. So in this study case, some geothermal water samples which give temperature of reservoir as less than surface temperature, might not be equilibrium thermal water in silica.

4.2 Cation geothermometers

In the natural systems, there are many different cations of silicates existing in solid solutions, such as Na and Ca in plagioclase and Na, Ca, Mg, K and Li in smectites (clay minerals). The mineral constitution in geothermal solutions depends on the rate of two counteracting processes; dissolution of primary

minerals and precipitation of secondary minerals. Cation geothermometers are based on ion exchange reactions with temperature-dependent equilibrium constants.

The formulas for calculating reservoir temperature by cation geothermometers are described in Equations 9-19 below. Concentrations are in ppm if not otherwise specified.

Na/K/Ca (Fournier and Truesdell, 1973):

$$T(^{\circ}C) = \frac{1647}{\log \frac{Na}{K} + \beta \log \frac{\sqrt{Ca}}{Na} + 2.24} - 273.15 \quad (9)$$

Concentrations are in mol/kg. $\beta = 4/3$ for $t < 100^{\circ}C$ and $1/3$ for $t > 100^{\circ}C$ and for $\log \frac{\sqrt{Ca}}{Na} < 0$

Na/K/Ca/Mg correction (Fournier and Potter, 1979):

Equation for calculating the Mg correction for the Na-K-Ca geothermometer. Concentrations, C , are in mg/kg.

$$R = \frac{C_{Mg}}{C_{Mg} + 0.61C_{Ca} + 0.31C_K} \times 100 \quad (10)$$

For R from 5 to 50, the Mg correction (Δt_{Mg} in $^{\circ}C$) is:

$$\begin{aligned} \Delta t_{Mg} = & 10.66 - 4.7415 \log R + 325.87 (\log R)^2 - 1.032 \times 10^5 \frac{(\log R)^2}{T} \\ & - 1.968 \times 10^7 \frac{(\log R)^2}{T^2} + 1.605 \times 10^7 \frac{(\log R)^3}{T^2} \end{aligned} \quad (11)$$

The Mg correction is not applied if Δt is negative or $R < 1.5$.

The above Mg correction is applicable only for waters which have a calculated Na-K-Ca temperature of $>70^{\circ}C$. If $R > 50$, select the measured spring temperature.

T represents the calculated Na-K-Ca temperature in Kelvin.

For R from 0.5 to 5,

$$\begin{aligned} \Delta t_{Mg} = & -1.03 + 59.971 \log R + 145.05 (\log R)^2 - 36711 \frac{(\log R)^2}{T} \\ & - 1.67 \times 10^7 \frac{\log TR}{T^2} \end{aligned} \quad (12)$$

Na/K (Fournier, 1979):

$$T(^{\circ}C) = \frac{1217}{1.438 + \log \frac{Na}{K}} - 273.15 \quad (13)$$

Na/K (Truesdell, 1976) for 100-275 $^{\circ}C$:

$$T(^{\circ}C) = \frac{856}{0.857 + \log \frac{Na}{K}} - 273.15 \quad (14)$$

Na/K (Giggenbach, 1988):

$$T(^{\circ}C) = \frac{1390}{1.75 + \log \frac{Na}{K}} - 273.15 \quad (15)$$

Na/K (Tonani, 1980):

$$T(^{\circ}C) = \frac{833}{0.780 + \log \frac{Na}{K}} - 273.15 \quad (16)$$

Na/K (Nieva and Nieva, 1987):

$$T(^{\circ}C) = \frac{1178}{1.470 + \log \frac{Na}{K}} - 273.15 \quad (17)$$

Na/K (Arnórsson et al, 1983) for 25-250°C:

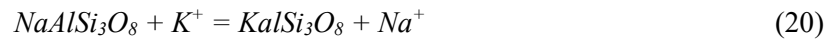
$$T(^{\circ}C) = \frac{933}{0.993 + \log \frac{Na}{K}} - 273.15 \quad (18)$$

K/Mg (Giggenbach, 1988):

$$T(^{\circ}C) = \frac{4410}{14.0 - \log(\frac{K^2}{Mg})} - 273.15 \quad (19)$$

The data from the 24 hot spring samples were calculated using the formulas above and the results are presented in Table 3.

Na-K geothermometers are based on the exchange reaction of albite and K-feldspar and Na and K in aqueous solution. The reaction involved is appropriately expressed as:



And the equilibrium constant being:

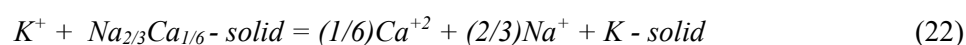
$$K \text{ alkali field} = \frac{[Na^+]}{[K^+]} \quad (21)$$

The reservoir temperatures attained from Na/K geothermometers showing in Table 3 indicate that the reservoir temperatures in the study area are quite high. Most of the results give more than 150°C in the reservoir, which will be discussed later.

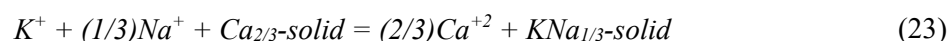
According to the classification results most of the water samples are immature water and the application of K-Na and K-Mg geothermometers becomes doubtful. Beside that, according to Fournier (1991) the exchange reactions of Na and K between alkali feldspars and solutions proceed very slowly at temperatures below about 300°C. Also, the Na/K geothermometer generally appears to take longer than the silica geothermometer to obtain a new water-rock chemical equilibrium where reservoir temperatures are changing in response to production. There is a tendency to use the Na/K ratio to estimate possible higher temperatures in a deeper part of a system where waters reside for relatively long periods of time. Therefore, K/Na geothermometer might not be suitable to apply in this study case.

The Na-K-Ca geothermometer is based on the exchange reaction of Na^+ , K^+ , and Ca^{+2} with mineral solid solutions. The geothermometer assumes one type of base exchange reaction at temperatures above about

100°C where exchange involving clay and micas is a major controlling factor in fixing Na-K-Ca concentrations in nature waters.



And a different exchange reaction at temperatures below about 100°C,



The general form of both of the above reactions is

$$\log K_{eq} = \log (Na/K) + \beta \log (\sqrt{Ca/Na}) \quad (24)$$

where $\beta = 4/3$ for $t < 100^\circ\text{C}$ and $1/3$ for $t > 100^\circ\text{C}$ and for $\log \frac{\sqrt{Ca}}{Na} < 0$.

According to Fournier (1991) Na-K-Ca geothermometer is entirely empirical and will give excellent results for most water above 200°C but also give erratic results for water at less than 200°C. The erratic results are affected by exchange reactions involving Na^+ , K^+ , or Ca^{+2} with additional ions as Mg and precipitation of calcium as carbonate where solutions boil on the way from the reservoir to the surface.

Table 3 shows that the reservoir temperatures obtained by Na-K-Ca geothermometer are less than 200°C, most of them even less than 100°C. Besides that, the Mg content in most of sample quite high, therefore the results may be erratic and it should be checked by the Mg correction for the Na-K-Ca geothermometer.

According to the water classification in the Na-K-Mg triangular diagram by Giggenbach (1991) in chapter 3, most of the water samples in study area are high in Mg content and quite acid or CO_2 rich waters. They should be applied with the Mg correction for Na-K-Ca geothermometer.

According to Fournier (1991) Mg correction is applicable only for water which have calculated Na-K-Ca temperatures $> 70^\circ\text{C}$. Therefore, from Table 3 there are samples S1, S2, S3, S14, S15, S18, S19, S72 with Na-K-Ca temperature greater than 70°C and also they have calculated R from 5 to 50, so it is possible to apply the Mg correction geothermometer. The results are shown in Table 4.

TABLE 4: Reservoir temperatures calculated by Na-K-Ca Mg correction

Sample label	S1	S2	S3	S14	S15	S18	S19	S72
Surface temp.	53.8	78	74	47	43	43	46	55.5
R	35	14	19	40	20	20	32	24
Na-K-Ca	71	192	77	123	103	111	103	77
Na-K-Ca Mg corr.	61	118	77	35	85	83	55	77

Calculation of R - see Equation 10

Most of results might be acceptable, except S14 where subsurface temperature is lower than surface temperature.

K/Mg geothermometers (Giggenbach, 1988) are based on the calculation for various temperatures the relative concentrations of K^+ and Mg^{2+} that would be in equilibrium with the mineral assemblage K-feldspar, clinocllore and muscovite. The results of the calculated temperature are shown in Table 3 and will be discussed later.

5. PROCESSES AFFECTING FLUID COMPOSITIONS

The geothermal water ascending from the reservoir to the surface may cool by some processes such as conduction of heat to surrounding rock, mixing with colder water or boiling and therefore losing steam. The chemical and physical characteristics of fluid compositions may support some information about conditions in the reservoir.

5.1 Conductive cooling

The slowly ascending geothermal water with low flows may lose heat by conduction. Calculations show that a flow of 26 kg/min (0.43 l/s) would cool conductively from 200 to 100°C during a vertical ascent from a depth of 1000 m with an initial linear temperature gradient from the reservoir to the surface (Truesdell, 1991). Also flows are no more than 8 kg/min (0.133 l/s) from shallower reservoirs of about 300 m during vertical ascent to the surface. Some chemical components are effected by conductive cooling process such as isotopic content, K and Mg.

Table 5 shows the flow rate (Q) of hot springs in the study area compared with calculations of Truesdell, 1991).

TABLE 5: The flow rate of hot springs in study area comparing with calculations of Truesdell, 1991

Q (l/s)	<0.133	0.133 <Q<0.43	>0.43
Sample	S8, S6	S4, S5, S16, S18, S19, S67, S69, S71, S77, S83, S78, S80, S81	S1, S2, S3, S7, S14, S15, S17, S20, S82, S11, S12, S68, S70, S72, S73, S79, S65, S74, S75

There are 15 samples, with flow rate being less than 0.43 l/s that are effected by conductive cooling. The other 19 samples with a flow rate more than 0.43 l/s may be less effected by conductive cooling process.

5.2 Mixing with colder water

The geothermal water may be mixed with cold water in the upflow zone on the way to discharge at the surface. The geothermal water is characteried by chemical equilibrium conditions in solutions but cold water composition is determined by the kinetics of the leaching process (Truesdell, 1991). These characteristics may be used to quantify the mixing and estimate conditions in the reservoir.

There are some indications of mixing in a solution which is based on the relations between chloride, boron, SO_4^{2-} and $\delta^{18}\text{O}$, δD , SiO_2 and so on.

The $\text{Cl-SO}_4\text{-HCO}_3$ ternary diagram and the Na-K-Mg triangular diagram by Giggenbach (1991) above show that most of the samples in study area are immature water so they might be mixed with cold water.

The linear relations between chloride and boron or δD and $\delta^{18}\text{O}$ constitutes are used as the main evidence for mixing. Chloride and boron concentrations are variable, and as a rule, higher in geothermal water and low in cold water but the Cl/B ratio is stable even in mixing water (Arnórsson, 1985). Only 8 samples in the study area have both Cl and B content (samples S1, S2, S3, S7, S8, S12, S72 and S73). The relationship between Cl and B is shown in Figure 4.

In the study area there are some results of cold water analysis but boron has not been analysed. If mixing of geothermal water with cold water is responsible for variable chloride concentration, it is to be expected that intersection at 0 ppm boron of line through the data points is in the range of 10 ppm

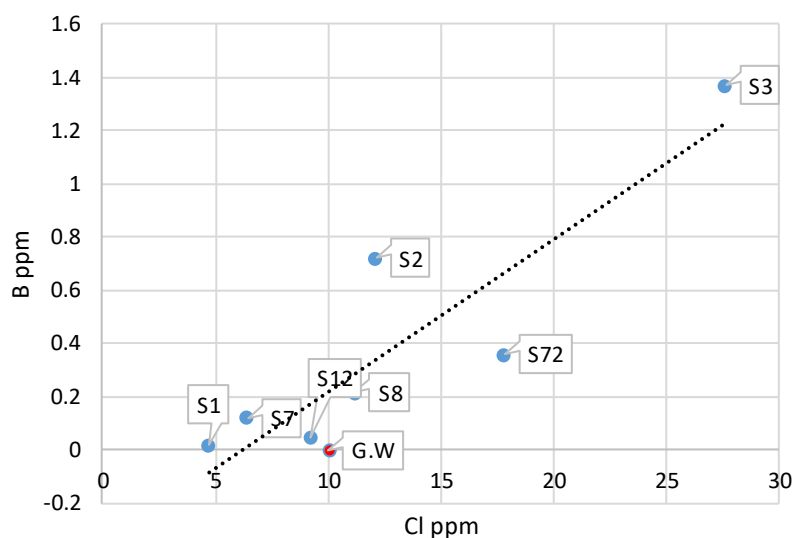


FIGURE 4: The relationship between Cl and B in warm springs in study area, red dot is groundwater sample

chloride as cold water contains chloride in that range and less than 0.01 ppm boron (Arnórsson, 1985). Figure 4 shows that both chloride and boron concentrations in these samples are very low. Sample 73 is an anomaly compared to the other and cannot be explained right now.

Figure 4 shows that the intersection of the regression line through the data points at 0 ppm boron corresponds with 6 ppm chloride. The mixing evidence showing in Figure 4 is not very clear.

The relationship between δD and $\delta^{18}O$ values for the thermal water and non-thermal water can give some information about mixing processes. Figure 5 shows the relationship between δD and $\delta^{18}O$. Of 27 samples there are 7 samples which have isotope analysis results, consisting of S1, S2, S3, S69, S72, S65, and S73. Figure 5 above shows that all of them are in the meteoric trend line and none are on the mixing line.

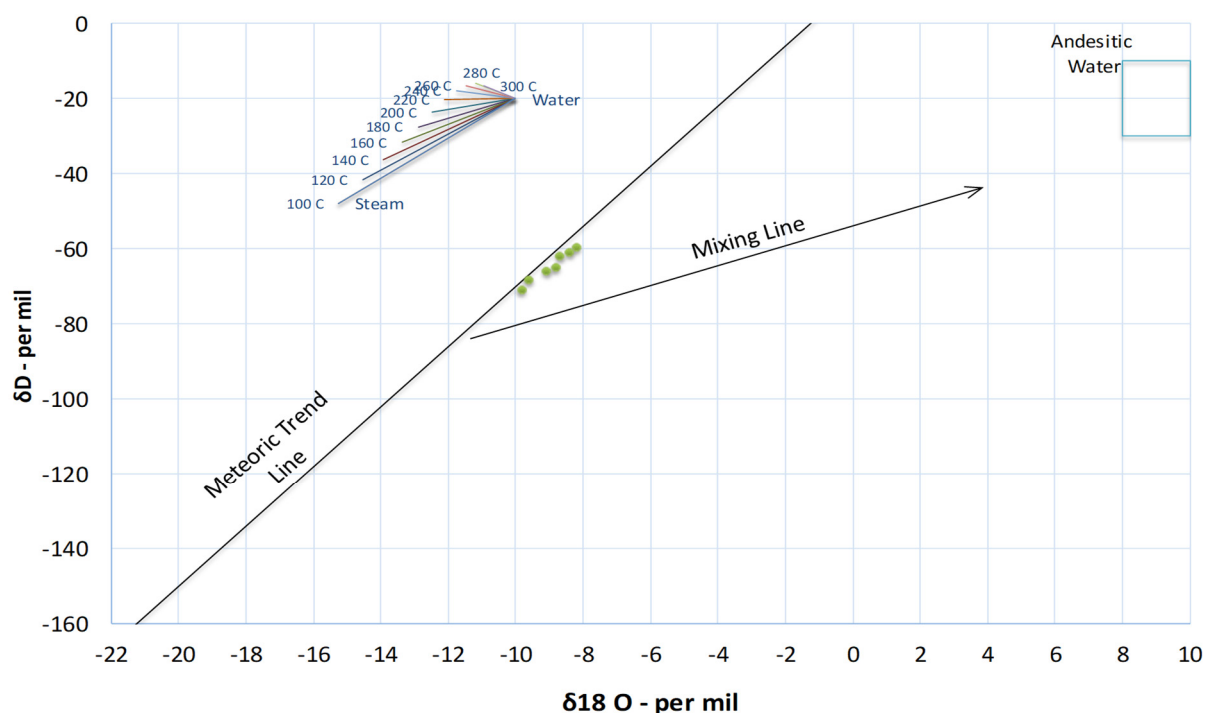


FIGURE 5: The relationship between δD and $\delta^{18}O$

Magnesium levels are usually very low in high-temperature geothermal fluids, about 0.01-0.1 mg/kg (Nicholson, 1993). In the high-temperature fluid, Mg is readily associated into secondary alteration minerals such as illite, montmorillonite and especially chlorite. Higher Mg concentrations in thermal fluid can either indicate leaching of Mg from the local rock or dilution by ground water which has much higher Mg concentration.

Of the 27 samples, Mg content in warm springs are in a range of 6.1-201 mg/l. According to the result of groundwater analysis in the same area shown in Table 6 it can be seen that Mg content in samples S1, S7, S8, S14, and S20 is quite similar with Mg content in groundwater, some are even higher (S11, S12). Table 6 shows that the thermal fluid of some warm springs in study area might be diluted by groundwater.

TABLE 6: Chemical compositions of groundwater in the study area. Sample location show groundwater located closely with some thermal water (VIGMR, 2009)

Sample	pH	Na ⁺	K ⁺	Ca ²⁺	Mg ²⁺	Fe ²⁺	Fe ³⁺	Al ³⁺	HCO ₃ ⁻	Cl ⁻	SO ₄	Sample location
LK06-DB	7.8	6.3	2.21	23.8	4.89	-	0.35	0.05	109.2	7.1	0.01	S11, S12
LK07-DB	7.65	14.81	12.66	22.09	12.11	-	0.04	0.01	175.7	3.55	0.67	S1
LK08-DB	7.15	39.46	23.47	24	9.6	0.03	8.36	0.297	140.3	11.4	0.63	S1
LK09-DB	7.18	33.29	34.2	16	12	0.018	0.392	0.243	140.3	10.4	1.39	S1
LK10-DB	9.06	63.07	25.38	40	22.8	0.06	3.914	0.297	140	17.7	23.5	S7, S8, S20
LK11-DB	9.19	69.42	27.19	36	18	0.017	0.059	0.297	170.8	7.38	1.25	S7, S8, S20
LK12-DB	9.17	40.83	27.85	14	7.2	0.02	2.078	0.297	146.4	7.09	1.75	S14
LK13-DB	8.1	46.67	27.86	16	25.2	0.017	1.134	0.253	109.8	7.15	1.63	S14

“–” no analysis

6. APPLICATION OF CHEMICAL PROGRAMS

In the geothermal solution, the activity distribution between various aqueous species and minerals is described by the equilibrium constant (K). The formation of minerals is dependent on many factors such as temperature, pressure of reservoir, activity of components or more generally enthalpy and entropy in reservoir. The mineral saturation index is calculated to give the information about dissolving forming or at equilibrium of minerals. The saturation index is defined by

$$SI = \log(Q/K) \quad (25)$$

where K is the solubility product and Q is the ion activity product.

If the SI value is greater than zero (supersaturation) the mineral may form and if the value is less than zero (undersaturation) the mineral may dissolve. If the value equals to zero the system is stable.

Reed and Spycher (1984) have presented a different approach geothermometer by using the numerical value of $\log(Q/K)$ calculated at different temperature. This method evaluates the saturation index of water of a specific composition with a large number of minerals at particular temperature, at which the water has equilibrated. Moreover, the mineral assemblage and temperature of equilibration of hot springs may be determined based on the convergence of $\log(Q/K)$ curves for the equilibrium assemblage to zero at temperature of equilibration. The effects of boiling, dilution, temperature variations and lack equilibrium are also described in this method.

The program WATCH version 2.4 (Arnórsson et al., 1982; Bjarnason, 2010) is applied in this case to compute species concentrations, activities and solubility products for minerals when the equilibrated fluids are cooled conductively from the reference temperature to a lower temperature. Nine samples in the study area, which have pretty good estimation of reservoir temperature by quartz geothermometer, are chosen to apply this method consisting of samples No. S1, S2 S3, S8, S18, S19, S11, S12 and S72. In WATCH the samples are cooled conductively from reservoir temperature with reference temperature calculated by quartz geothermometer. The value of $\log(Q/K)$ for minerals are obtained from $\log Q$ and $\log K$ calculation. The diagram of $\log(Q/K)$ versus temperature for minerals assemblage of 9 samples is shown in Figure 6.

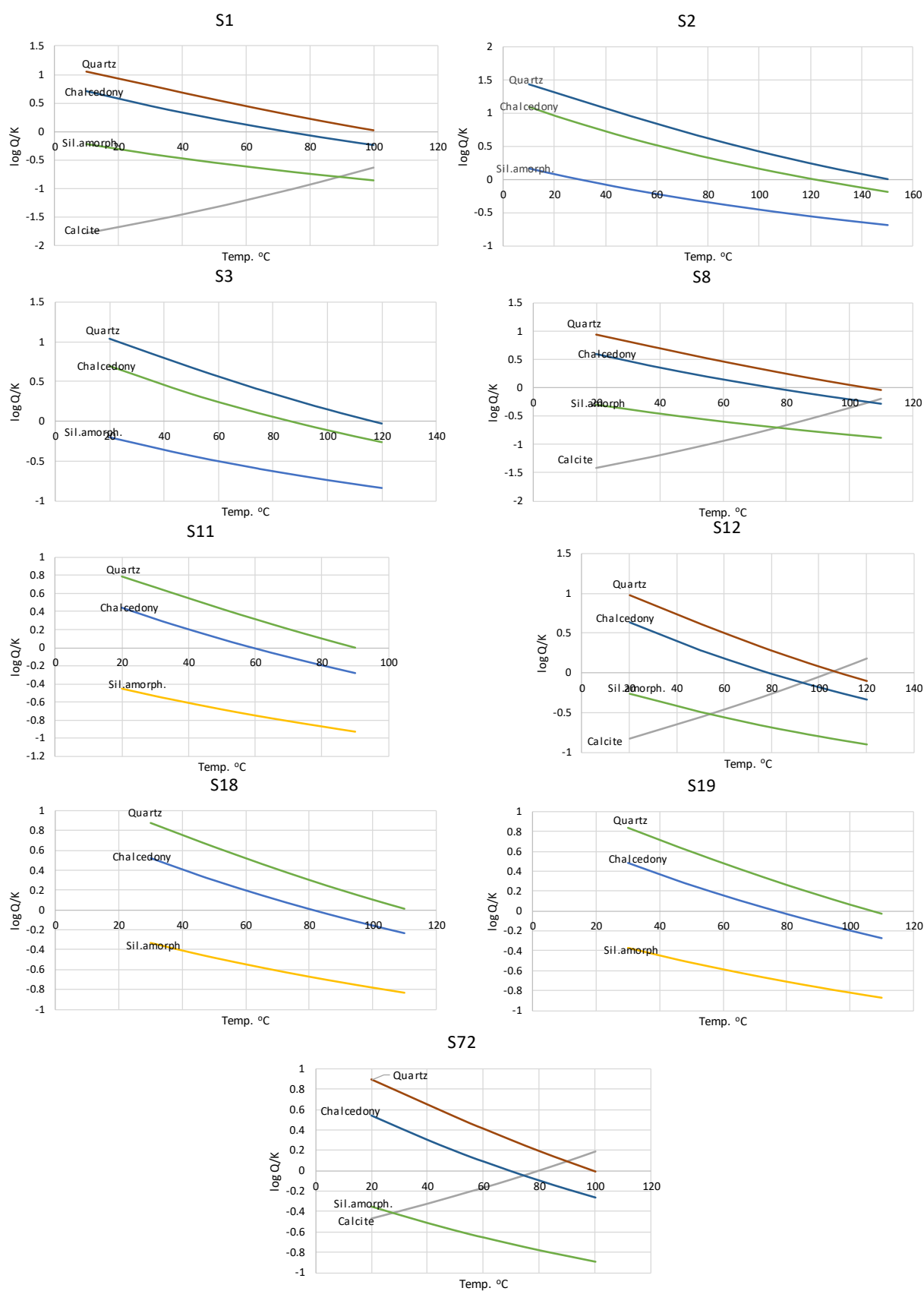


FIGURE 6: The diagram of $\log(Q/K)$ versus temperature for minerals assemblage of 9 samples (S1, S2, S3, S8, S11, S12, S18, S19, S72)

According to Reed and Spycher (1984), it is ideal when the log (Q/K) curve of mineral assemblage converges at zero line, the system is stable and the corresponded temperature will be the reservoir temperature. If the convergence point is above the zero line, the water may be boiling and the water is diluted when the convergence point is below the zero line. There are some other effects such as inaccurate water analyses, and poor thermodynamic data for minerals and aqueous ions and complexes which lead to dispersion on such plots and cloud geologic interpretations.

The calculations illustrate in Figure 6 nine simple diagrams. Figure 6 shows that solutions are in equilibrium in temperature forming chalcedony or quartz minerals. In the S1 diagram shows that the reservoir is in equilibrium with chalcedony at $\sim 75^{\circ}\text{C}$ and quartz around 100°C . These results are similar to the chalcedony and the quartz geothermometers by Fournier 1977 (formulas 6 and 7 and shown in table 3) which gives 73°C and 103°C respectively. In the S2 diagram, the reservoir temperature is estimated between $120\text{--}150^{\circ}\text{C}$ basing on the equilibrium of chalcedony and quartz and the water is mixed slightly. Similarly, in the S3 plot, the temperature of reservoir is estimated from 85 to 120°C and there is a mixing in this water. The S8 plot shows that the temperature of reservoir ranges from 80 to 110°C and water is diluted slightly. In S18, there are only two curves, quartz and chalcedony are intersection the zero line but the chalcedony curve is closer to the zero line than the quartz curve so the temperature of reservoir will be 80°C . The S19 sample shows that the reservoir temperature is about $100\text{--}110^{\circ}\text{C}$ and water is slightly diluted. In S11 the plot is similar to S18, reservoir temperature is 60°C . The S12 plot shows that temperature of reservoir ranges from 57 to 110°C but at 57°C the water is diluted. In the S72 diagram, the temperature of reservoir is between $60\text{--}90^{\circ}\text{C}$.

7. DISCUSSION AND CONCLUSIONS

The main aim of this project is to use geothermal fluids as a part of surface exploration. The author chose 34 of 119 samples to study based on location of hot springs which are spread over a 100×165 km area in the north-western part of Vietnam. Most of the bedrock in the study area is old sedimentary rock, and some tuff, basalt and granite rocks. There are manifestations of active tectonics and a lot of fractures have been formed which are vents for hot spring discharge.

The thirty four hot springs with temperatures ranging from 35 to 78°C have been divided into five groups based on the location. The silica content in most of the samples is very low, only 7 samples have silica concentration greater than 50 mg/l (samples marked S1, S2, S3, S8, S18, S19, and S12). The Mg content in most of the samples are very high, ranging between $1.6\text{--}35.6\text{ mg/l}$, some samples from 96.6 to 157.2 mg/l . Sample S73 has high Cl content (930 mg/l) and TDS (4790 mg/l) even though this area is far from sea.

Using Cl-SO₄-HCO₃ ternary Giggenbach (1991) diagram for classifying water showed that most of the samples are the peripheral waters. Geothermometers can be used for these waters except for the steam heated samples S7, S69, S68, and S80. The Na-K-Mg triangular diagram shows that all of the waters are immature waters, which are dissolution of rock with little or no chemical equilibrium so the application of both the K-Na and K-Mg geothermometers becomes doubtful.

For calculation of reservoir temperature, 15 geothermometers are used including silica and cation geothermometers as presented above. The results of cation geothermometers show that it is really doubtful when most of samples give very high temperature values. Na/K geothermometers are based on the equilibrium constant, so when the water is immature, it is impossible to apply Na/K geothermometers. On the other hand, (22) and (23) reactions usually happen in high temperature conditions and magma rock, so Na/K geothermometers cannot be used in this study area. The Mg-K geothermometer is responding extremely fast to temperature changes and normally reflects a very recent temperature, pretty often the surface temperature of the spring and this is illustrated in Table 3, where the results of K/Mg geothermometer of samples S1, S2, S3, S8, S12, S14, S15, S18, S19, S20, S65, S71,

S72, S74, and S77 give similar temperatures to surface temperatures. As explained above, chalcedony and quartz geothermometers, and some of the results in Na-K-Ca-Mg correction (S1, S2, S3, S15, S18, S19, S72), can be used for estimation of reservoir temperature. The results are shown in Table 3.

According to Figures 4 and 5 and Table 6 there is no evidence of mixing with groundwater in the samples. Maybe there were some mistakes in the sampling process or the water was diluted without re-equilibrium, but using log Q/K diagram, there were some samples that were diluted slightly.

As presented above the temperature of the reservoir can be estimated by plotting the log Q/K value of various minerals in equilibrium of solution in the reservoir and these diagrams can also be used to explain some of the processes affecting fluid compositions. Because the data lacks some information such as isotope elements for most of the samples, and/or maybe there were some mistakes in sampling and analysis process, it is not likely that one can interpret all the samples.

Below are the results of this work and it is summarised in Table 7.

Group 1 (S1, S2, S3, S4, S5) is in the western of part of the study area, spread about 20 km x 20 km. This group consisted of five samples with temperature range 54-78°C, SiO₂ concentration ranging from 28-126 mg/l, Mg concentrations from 1.8 to 7.2 mg/l and Cl concentrations from 4.7 to 28 mg/l. Two of the samples have a charge balance 17% (S4) and 34% (S5) which are too high and therefore these samples have not be used in this study. All the samples are most likely in equilibrium with quartz as indicated by the main rocks in the area, which are siltstone, sandstone and clay schist which are mainly composed of quartz and chalcedony. Therefore, quartz and chalcedony geothermometers by Fournier (1977) are the most suitable.

Group 2 (S7, S8, S14, S16, S15, S17, S18, S19, S20, S82) is south of Group 1, spread over 20 km x 30 km. The charge balances are lower but in five of the samples (S14, S15, S16, and S17) silica has not been analysed. Sample 7 is steam heated water and is not included in the study. Temperature of this group ranges between 30-49°C, with Cl contents from 6.4 to 58.1 mg/l and Mg concentrations are from 4 to 22.8 mg/l. The bedrocks in this group include clay schist, siltstone, and sandstone which are mainly formed of chalcedony and quartz so chalcedony and quartz geothermometers are the most suitable.

Group 3 includes only two samples, S11 and S12, in the northern part of the study area and they are located in a small square about 2 km x 3 km. Temperature measured 30 and 50.5°C, SiO₂ concentrations are 38 and 58.2 mg/l, Cl concentrations are 7.6 and 9.2 mg/l and Mg concentrations are 34.8 and 35.6 mg/l, which is quite high. The bedrock in this area is clay schist, limestone, lime clay, quartz sandstone, quartzite, sericite schist which are mainly composed of quartz, chalcedony, chlorite, and calcite, and as in other groups quartz and chalcedony geothermometers are most suitable.

Group 4 (S67, S68, S69, S70, S71, S72, S73) in the east of part of the study area, spread in 20 km x 25 km. This group includes 7 samples but two of them (S67 and S70) have too high charge balance (38% and 26%), charge balance of S72 and S73 are 13% and 11% but will be used. The SiO₂ concentration is ranging from 18.8 to 47.9 mg/l and Cl concentration range between 7.1-54 mg/l with the exception of sample S73 where the concentration is 930 mg/l. The bedrock in this area is siltstone, sandstone, diorite, granodiorite, granite, tuff, basalt, trachyte, silica, coal and limestone which are mainly composed of quartz, chalcedony, and K-feldspar. Therefore, quartz and chalcedony geothermometer are the most suitable.

Group 5 consist of (S77, S79, S83, S6, S78, S80, S81, S65, S74, S75) and the samples are scattered and distributed along in northwest-southeast direction of the study area. The charge balance of most of the samples are good except sample S79 which will not be included here. SiO₂ concentration of samples S74, S80, S81, and S83 was not analysed and therefore these samples are not included in this work. Temperature ranges from 30 to 61.5°C with the Cl concentrations ranging from 6 to 56 mg/l and Mg concentration ranges from 6.1 to 28.8 mg/l. The bedrocks in this area are sandstone, clay schist, diorite,

TABLE 7: Summary of samples used in this study showing among other things reservoir temperature calculated by chalcedony and quartz geothermometers, log Q/K, water classification, bedrock composition and main minerals in host rock

Sample	Temp. surf (°C)	Temp. of geothermometers in °C			Classif.	Mixing*	Bedrocks	Minerals
		Chalcedony	Quartz	Log Q/K				
S1	53.8	73	103		Peripheral waters	Diluted slightly	Siltstone, sandstone	Quartz, chalcedony
S2	78	125	151	120-150	Peripheral waters	Diluted slightly	Sandstone, clay schist	Quartz, chalcedony
S3	74	87	116	80-120	Peripheral waters	Diluted slightly	Siltstone, sandstone	Quartz, chalcedony
S7	37	54	85	NA	Steam heated waters	NA	Sandstone, clay schist	Quartz, chalcedony
S8	36.5	76	106	80-110	Peripheral waters	No mixing	Siltstone, sandstone	Quartz, chalcedony
S18	43	81	111	80	Peripheral waters	No mixing	Sandstone, clay schist	Quartz, chalcedony
S19	46	77	107	100-110	Peripheral waters	Diluted slightly	Sandstone, clay schist	Quartz, chalcedony
S20	32	45	77	NA	Peripheral waters	NA	Sandstone, clay schist	Quartz, chalcedony
S82	48.9	NA	60	NA	Peripheral waters	NA	Siltstone, sandstone	Quartz, chalcedony
S11	30	59	90	60	Peripheral waters	No mixing	Clay schist, marble	Quartz, chalcedony
S12	50.5	80	109	57-110	Peripheral waters	Diluted slightly	Limestone, lime clay, quartz sandstone, schist, quartzite, sericite	Quartz, chalcedony, chlorite, calcite
S68	45.8	NA	62	NA	Steam heated waters	NA	Siltstone, sandstone, clunchstone	Quartz, chalcedony
S69	41.5	59	90	NA	Steam heated waters	NA	Siltstone, sandstone	Quartz, chalcedony
S71	36	54	86	NA	Peripheral waters	NA	Diorite, granodiorite, granite	Quartz
S72	55.5	70	100	60-90	Peripheral waters	No mixing	Tuff, basalt, trachyte	Quartz, chalcedony, K-feldspar
S73	55	NA	NA	NA	Steam heated waters	NA	Tuff basalt, clay, silic, coal, limestone	Quartz, chalcedony
S77	37	NA	48	NA	Peripheral waters	NA	Sandstone, clay schist	Quartz, chalcedony
S6	61.5	NA	84	NA	Peripheral waters	NA	Diorite, granodiorite, granite	Quartz, andesine, hornblende, K-feldspar, biotite, plagioclase
S78	42	NA	63	NA	Peripheral waters	NA	Clay schist, marble	Quartz, chalcedony
S65	40.2	42	74	NA	Peripheral waters	NA	Tuff basalt, clay, silica, coal, limestone	Quartz, calcite chalcedony
S75	34.5	39	71	NA	Peripheral waters	NA	Tuff, basalt, trachyte	Quartz, chalcedony, K-feldspar

* Most mixing information based on Reed and Spycher (1984)

granodiorite, granite, basalt tuff, trachyte, coal, limestone which are mainly composed of quartz, chalcedony, andesine, hornblende, plagioclase, K-feldspar, and biotite. The quartz and chalcedony geothermometers might be used in this group but it gives quite low temperature estimate.

Table 7 summarizes samples used in this study and shows among other things reservoir temperature calculated by chalcedony and quartz geothermometers, log Q/K, water classification, bedrock composition and main minerals in host rock.

8. RECOMMENDATIONS

The studying of geothermal fluid is a part of a surface exploration. During this process, sampling and analysis play very important roles and it affects the research result directly. Therefore, the sampling procedures should be standard and the equipment should be sufficient in both of number and quality for collecting samples. Chemical components of hot water should be analysed adequately (major elements as well as metal and trace elements) including special stable isotopes which help to evaluate the origin and age of hot water. It is best to work with samples from boreholes.

The discharge zone of hot springs should be described carefully and photographed to have a prospect view when estimating potential of reservoirs. When drilling, cuttings should be collected, and thin sections from drill cuttings should be sampled to see the mineral assemblage in the subsurface.

It is important that thermal springs are studied in great detail with all the available methods in order to better estimate their potential for energy production.

ACKNOWLEDGEMENTS

I would like to thank the United Nations University Geothermal Training Programme and the Government of Iceland for giving me a scholarship to participate in this six months training programme. My special gratitude goes to Mr. Lúðvík S. Georgsson, Mr. Ingimar Guðni Haraldsson for giving me the opportunity to take part in this course and for their support, guidance and care throughout the course.

Many thanks go to Ms. Þórhildur Ísberg and Mr. Markús A. G. Wilde and Rósa S. Jónsdóttir for their assistance and training facilitation through the six months. Special thanks to Ms. Málfríður Ómarsdóttir, my kind neighbour for the whole six months and friendly guide in every field trip.

My special gratefulness goes to my supervisor Dr. Vigdís Hardardóttir for sharing with me her experience and knowledge of geochemistry and guiding me to complete this report. I would like to extend my special thanks to Finnbogi Óskarsson, Dr. Halldór Ármannsson and Dr. Andri Stefánsson for giving me exciting geochemical lectures and sharing their amazing knowledge of geochemistry. Also, my thanks to all of lecturers and staff members at Iceland GeoSurvey – ÍSOR for their help and willingness to share their knowledge and experience.

I am grateful to Mr. Tran Trong Thang, 1996 UNU-GTP fellow, for his support, help and providing me with the data used in this project. My thanks to my employer, Vietnam Institute of Geosciences and Mineral Resources, for nominating and granting me leave to attend this course. To my dear mum, husband, son and daughter, thanks for your encouragement, sacrifice and unconditional love during my six months of study.

To the 2016 UNU-GTP Fellows, thank you for your cheer and friendship in whole six months. Hope to see you again in near future. May God bless you all.

REFERENCES

- Arnórsson, S., 1985: The use of mixing models and chemical geothermometers for estimating underground temperature in geothermal systems. *J. Volc. Geotherm. Res.*, 23, 299-335.
- Arnórsson, S., Gunnlaugsson, E., and Svavarsson, H., 1983: The chemistry of geothermal waters in Iceland III. Chemical geothermometry in geothermal investigations. *Geochim. Cosmochim. Acta*, 47, 567-577.
- Arnórsson, S., Sigurdsson, S., and Svavarsson, H., 1982: The chemistry of geothermal waters in Iceland I. Calculation of aqueous speciation from 0°C to 370°C. *Geochim. Cosmochim. Acta*, 46, 1513-1532.
- Ármannsson, H., and Ólafsson, M., 2006: *Collection of geothermal fluids for chemical analysis*. ÍSOR – Iceland GeoSurvey, report, ÍSOR-2006/016, 17 pp.
- Bjarnason, J.Ö., 2010: *The speciation program WATCH, version 2.4*. Orkustofnun, Reykjavik, 9 pp.
- D'Amore, F., and Arnórsson, S., 2000: Geothermometry. In: Arnórsson, S.(ed.), *Isotopic and chemical techniques in geothermal exploration, development and use. Sampling methods, data handling, interpretation*. International Atomic Energy Agency, Vienna, 152-198.
- Fournier, R.O., 1977: Chemical geothermometers and mixing models for geothermal systems. *Geothermics*, 5, 41-50.
- Fournier, R.O., 1979: A revised equation for the Na/K geothermometer. *Geothermal Resources Council, Transactions*, 3, 221-224.
- Fournier, R.O., 1991: Water geothermometers applied to geothermal energy. In: D'Amore, F. (coordinator), *Application of geochemistry in geothermal reservoir development*. UNITAR/UNDP publication, Rome, 37-69.
- Fournier, R.O., and Potter, R.W. II, 1979: Magnesium correction to the Na-K-Ca geothermometer. *Geochim. Cosmochim. Acta*, 43, 1543-1550.
- Fournier, R.O., and Potter, R.W. II, 1982: A revised and expanded silica (quartz) geothermometer. *Geoth. Res. Council, Bull.*, 11-10, 3-12.
- Fournier, R.O., and Truesdell, A.H., 1973: An empirical Na-K-Ca geothermometer for natural waters. *Geochim. Cosmochim. Acta*, 37, 1255-1275.
- Giggenbach, W.F., 1988: Geothermal solute equilibria. Derivation of Na-K-Mg-Ca geothermometers. *Geochim. Cosmochim. Acta*, 52, 2749-2765.
- Giggenbach, W.F., 1991: Chemical techniques in geothermal exploration. In: D'Amore, F. (coordinator), *Application of geochemistry in geothermal reservoir development*. UNITAR/UNDP publication, Rome, 119-144.
- Hoang, H.Q., 1996: General evaluation of geothermal potential in the tectonic setting of Vietnam. *Geothermal Resources Council, Bulletin*, 63-76.
- Lacassin, R., Leloup, P.H., and Tapponnier, P., 1993: Bounds on strain in large Tertiary shear zones of SE Asia from boudinage restoration. *J. Structural Geology*, 15, 677-692.

- Nicholson, K., 1993: *Geothermal fluids: chemistry and exploration techniques*. Springer-Verlag, Berlin, 268 pp.
- Nieva, D., and Nieva, R., 1987: Developments in geothermal energy in Mexico, part 12-A: Cationic composition geothermometer for prospection of geothermal resources. *Heat Recovery Systems and CHP*, 7, 243-258.
- Powell, T., and Cumming, W., 2010: Spreadsheets for geothermal water and gas geochemistry. *Proceedings of the 35th Workshop on Geothermal Reservoir Engineering, Stanford University, Stanford, CA*, 10 pp.
- Reed, M.H., and Spycher, N.F., 1984: Calculation of pH and mineral equilibria in hydrothermal water with application to geothermometry and studies of boiling and dilution. *Geochim. Cosmochim. Acta*, 48, 1479-1490.
- Rimstidt, J.D., and Barnes, H.L., 1980: The kinetics of silica-water reactions. *Geochim. Cosmochim. Acta*, 44, 1683-1699.
- Tapponnier, P., Lacassin, R., Leloup, P.H., Sharer, U., Zhong, D., Wu, J., Liu, X., Ji, S., Zhang, L., and Zhong, J., 1990: The Ailao Shan Red River metamorphic belt: Tertiary left-lateral shear between Sundaland and South China. *Nature*, 343, 431 - 437.
- Tapponnier, P., Peltzer, G., and Armijo, R., 1986: On the mechanics of the collision between India and Asia. In: Coward, M.P., and Ries, A.C., (eds.), *Collision Tectonics*. Geological Society, London, Special Publications, 19, 115-157.
- Tonani, F., 1980: Some remarks on the application of geochemical techniques in geothermal exploration. *Proceedings, Adv. Eur. Geoth. Res., 2nd Symposium, Strasbourg*, 428-443.
- Tran, N.N., 1995: The geology of Vietnam: A brief summary and problems. *Geosci. Repts. Shizuoka Univ.*, 22, 1-10.
- Truesdell, A.H., 1976: Summary of section III - geochemical techniques in exploration. *Proceedings of the 2nd U.N. Symposium on the Development and Use of Geothermal Resources, San Francisco, I*, liii-lxxix.
- Truesdell, A.H., 1991: Effects of physical processes on geothermal fluids. In: D'Amore, F. (coordinator), *Application of geochemistry in geothermal reservoir development*. UNITAR/UNDP publication, Rome, 71-92.
- VIGMR, 2004: *Research and evaluation of geothermal potential in the North-west of Northern Plain, Vietnam with the aim to support for the socio-economic development*. Vietnam Institute of Geosciences and Mineral Resources (VIGMR), Hanoi, Vietnam, Geothermal Resource Assessment Project, internal report, 179 pp.
- VIGMR, 2009: *Analysis data, research and evaluation of groundwater resources in the Northwest and Central, Vietnam*. Vietnam Institute of Geosciences and Mineral Resources (VIGMR), Hanoi, Vietnam, internal report.



UNITED NATIONS
UNIVERSITY

UNU-GTP

Geothermal Training Programme

Orkustofnun, Grensasvegur 9,
IS-108 Reykjavik, Iceland

Reports 2016
Number 34

A 3D MODEL OF THE CHACHIMBIRO GEOTHERMAL SYSTEM IN ECUADOR USING PETREL

Byron F. Pilicita Masabanda

Corporación Eléctrica del Ecuador

Unidad de Negocio Termopichincha

Av. 6 de Diciembre N26-235 y Av. Orellana, Quito

ECUADOR

bf07epn@gmail.com

ABSTRACT

The Chachimbiro Geothermal System is the most important geothermal prospect in Ecuador. Various geothermal models have been presented based on geological, geochemical and geophysical data collected at different epochs. Currently the Chachimbiro prospect is ready to enter the exploration drilling phase. This is why it is important to identify the best drilling targets. The Petrel software allows the combination of all surface exploration data in order to identify different geothermal anomalies and create a 3D model to visualize all features of the system. This model uses lineaments as boundaries of the system based on structural mapping and locations of earthquake epicentres. The heat source is related to magma chambers that feed the main volcanic vent but is also controlled by faults, which influence possible up-flow. This up-flow is located beneath a cap rock (0-10 Ωm) and is related to a high resistivity core, which shows a concave shape (30-70 Ωm). The Na/K geothermometers show temperatures of around 240°C, however, the water in Chachimbiro has poor equilibrium with the rock. Resistivity analysis shows possible temperatures from 200 to 250°C, but this range of temperature does not represent the current temperature of the system. The origin of the fluids in Chachimbiro is meteoric based upon isotopic analysis. The interaction between this fluid, with the up-flow into the sub-surface, forms a possible reservoir. Hot springs and gas manifestations ($\text{CO}_2\text{-H}_2\text{S}$) are out-flows of the system, which also indicate volcanic activity in the system and are expressions of the reservoir at the surface. The intersection between Chachimbiro and Azufra faults and the Chachimbiro Fault have been identified as drilling targets in the system, which could be reached by directional drilling from three different locations. These location have been chosen by combining the structural features, the resistivity anomalies, possible out-flow and up-flow zones, the hydrothermal areas and temperature anomalies which were modelled and analysed in Petrel.

1. INTRODUCTION

Conceptual models are based on geological information, both from surface mapping and analysis of subsurface data, remote sensing data, results of geophysical surveying, information on chemical and isotopic content of fluid at surface manifestations and reservoir fluid samples collected from wells,

information on temperature and pressure conditions based on analysis of available well logging data as well as other reservoir engineering information. These data are processed in order to explain the heat source that feed the reservoir, to locate the recharge zones and the main flow channels, and to analyse the general flow patterns within the reservoir as well as reservoir temperature and pressure conditions. A comprehensive conceptual model furthermore, provides an estimate of the size of the reservoir. Nevertheless, not all geothermal conceptual models incorporate the whole information at the same time, in fact only a few do so. In the early stages, the conceptual models depend mostly on surface exploration data, with geological (e.g. faults/fractures) and geophysical (e.g. resistivity) data being most important. Formation temperature is e.g. unknown at such an early stage. The only indications of reservoir temperature at that stage come from chemical investigation (Axelsson, 2013).

Three-dimensional modelling software is increasingly being used to visualize, merge and jointly analyse various types of data in geothermal research. The Petrel E&P is software that provides a full range of tools to solve the most complex challenges from regional exploration to reservoir development. Petrel allows the integration of structural geology, lithology, geochemical and geophysical data obtained in the early stages of the geothermal system development (Schlumberger, 2016). Chachimbiro is a geothermal prospect is currently at the pre-feasibility stage. The area is located on the eastern slopes of the Western Cordillera, at about 70 km north of Quito, which is Ecuador's capital and 18 km west of Ibarra which is the nearest major load centre. It is bounded to the north by Chota Basin, to the east by Interandean valley, to the south and west by Cotacachi and Yanahurcu de Piñan volcanoes, respectively (Figure 1).

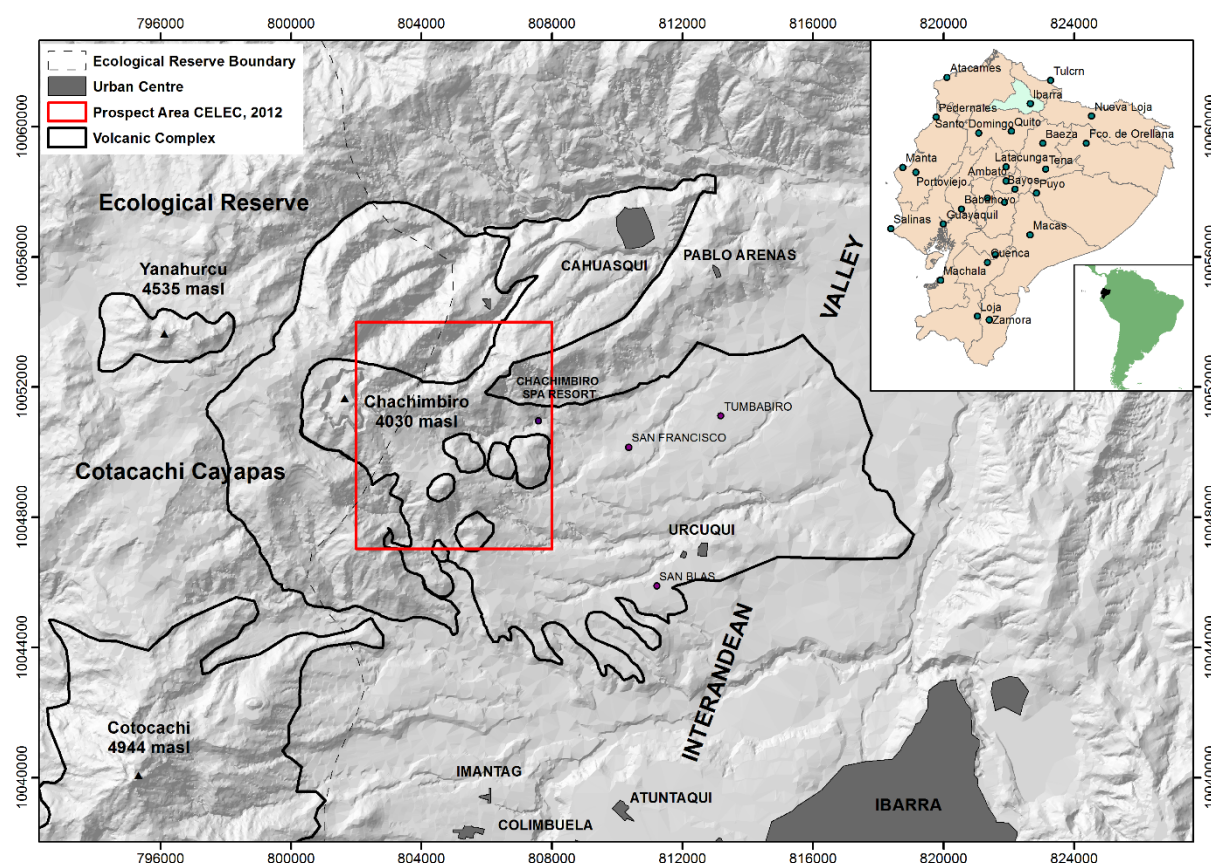


FIGURE 1: Location of the Chachimbiro volcanic complex

The area straddles the Cotacachi – Cayapas Ecological Reserve. It is only accessible by gravel and dirt roads. The climate is temperate and the vegetation cover varies from forest to grassy areas. In administrative terms, the area is divided into 3 parishes: Urcuquí, San Blas and Tumbabiro and it belongs to the Urcuquí district in the Imbabura province. The best-known hot springs in the area are located along the Cachiya River, in the Spa Resort Chachimbiro area. La Delicia de San Francisco is the nearest habitation to the hot springs.

Previous work has been carried out at Chachimbiro with the objective to assess the geothermal potential of the area. These studies were completed by government institutions between the late 70s and early 90s, within the framework of OLADE-INECEL¹, OLADE-AQUATER² and IAEA³-INECEL projects. In 2011, CELEC EP⁴ (Government Company) contracted the SYR⁵ Company to gather geoscience information and develop a Geothermal Conceptual Model, which was presented in 2012 (SYR, 2012). Currently CELEC EP is being assisted by JICA (Japan International Cooperation Agency) to gather complementary information about Chachimbiro Geothermal System together with MMC-MMTEC⁶ Consultants Company.

This report summarizes the geothermal model of the Chachimbiro Geothermal System in the Petrel E&P software platform. By integrating the results of geological, geochemical and geophysical studies obtained by CELEC EP / SYR in 2012 and results from CELEC EP / MMC in 2016, the objective is to visualize the features of the conceptual models, to propose new study areas and to recommend locations and targets of wells which may be drilled in the future.

2. GEOLOGICAL AND GEODYNAMIC SETTING

Regional features are identified as fragmentations of the Farallón Plate, forming the Cocos and Nazca Plate during the early Miocene (Lonsdale, 2005). The interaction between the South American, Cocos and Nazca plates control the cortical deformation, the high seismicity and the volcanism in the North-Andean Block (Figure 2). The convergence between the Nazca and South American plates is estimated to be 7.0 cm/year (Schellart et al., 2007). The tectonic state of stress is homogenous south of 5°N; this state results in an East-West-oriented compression which is responsible for the crustal deformation (Ego et al., 1996).

The Chachimbiro Volcanic Complex consists of 60 volcanoes associated with the Ecuadorian Quaternary Volcanic Arc. It is located 80 km north of Quito, in the northern part of the Ecuadorian Volcanic Front. Holocene activity is characterized by powerful, but low-frequency, explosive eruptions of acid andesite to dacite magmas. The long-lasting evolution of the Chachimbiro Volcanic Complex comprises three successive phases named Huanguillaro, Tumbatú, and Hugá. Recent investigations identified at least four eruptions associated to the Hugá phase in the last 6,000 years (Bernard et al., 2014).

The basement of the Chachimbiro Volcanic Complex is composed of Cretaceous rocks that accreted in a subduction zone. McCourt et al. (1997) and Vallejo (2007) defined the Pallatanga Formation as the volcanic basement of the Western Cordillera, which comprises mainly basaltic rocks. There are no outcrops in the Chachimbiro volcanic area, but it probably lies under the distal southeast flanks of the volcano. Vallejo (2007) described the Rio Cala Group, which is composed of volcanic and sedimentary sequence deposited in an intraoceanic island arc setting, overlying the Pallatanga formation. It consists of massive basaltic to andesitic lavas, volcanic breccias, and to a smaller extent, of volcanoclastic sandstones. This unit is exposed on the Southeastern flank of the volcanic complex. The Natividad formation included in the Rio Cala Group, is composed of sedimentary rocks in the north of the volcanic complex, correlated with turbidites deposited during the Eocene (Vallejo 2007). The Natividad Unit is exposed on both the southwestern and northeastern slopes of the volcano and is probably the dominant Cretaceous lithology underlying the southern and eastern slopes of the Chachimbiro Volcanic Complex (Granda, 2011). The Silante formation is restricted to the northern area of the Western Cordillera, which

¹ Latin American Energy Organization (OLADE), the Ecuadorian Institute of Electrification (INECEL)

² Decision Support System to manage water resources in Italy using remote sensing (AQUATER)

³ International Atomic Energy Agency (IAEA)

⁴ Corporación Eléctrica del Ecuador (CELEC EP)

⁵ Servicios y Remediación (SYR)

⁶ Mitsubishi Materials Corporation - Mitsubishi Materials Techno Corporation (MMC-MMTEC)

includes channelized conglomerates, breccias, red mudstones and shales, deposited during the latest Maastrichtian to Early Paleocene (Vallejo 2007). The unit is clearly exposed on the western and northern flanks of the volcanic complex and, most likely, underlies the western half of the volcano (Granda, 2011).

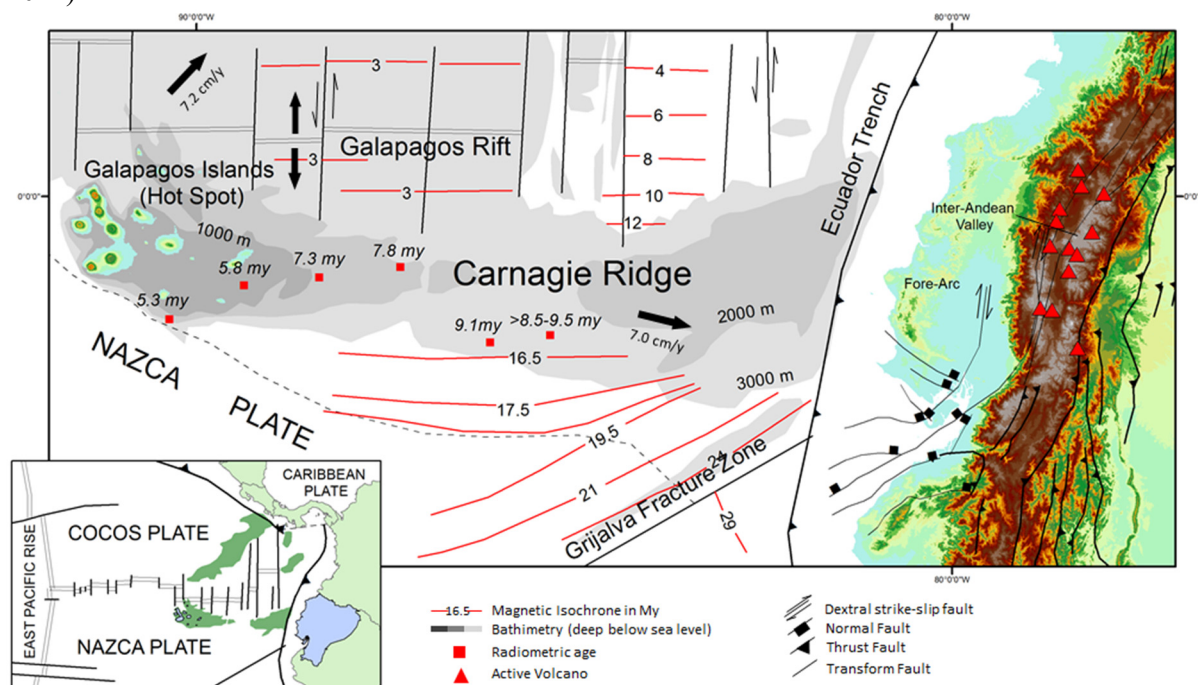


FIGURE 2: Geodynamic setting of Ecuador, showing mainland Ecuador on the South American plate and the Galapagos Islands on the Nazca plate (redrawn after the plate tectonic map of the Circum-Pacific Region (1981) and modified from Spikings et al., 2001)

The Pugaran volcanic rocks were deposited during the Tertiary, and occur both southeast and northwest of the Chachimbiro volcanic complex. This volcanic unit consists of andesitic lava flows and hornblende dacite tuffs and breccias. There is no evidence whether the Pugaran unit extends beneath the Chachimbiro volcanic complex (Granda, 2011).

Chachimbiro Phase 1 is composed of large andesite lava flows streaming radially and predominantly effusive events. These lavas form the ancestral andesitic stratovolcano known as Huanguillaro (Beate, 1990 in SYR 2012). After phase 1, an instability in the volcanic complex centre resulted in a collapse forming a horseshoe shaped scarp, which is open to the east (Figure 3 and 4).

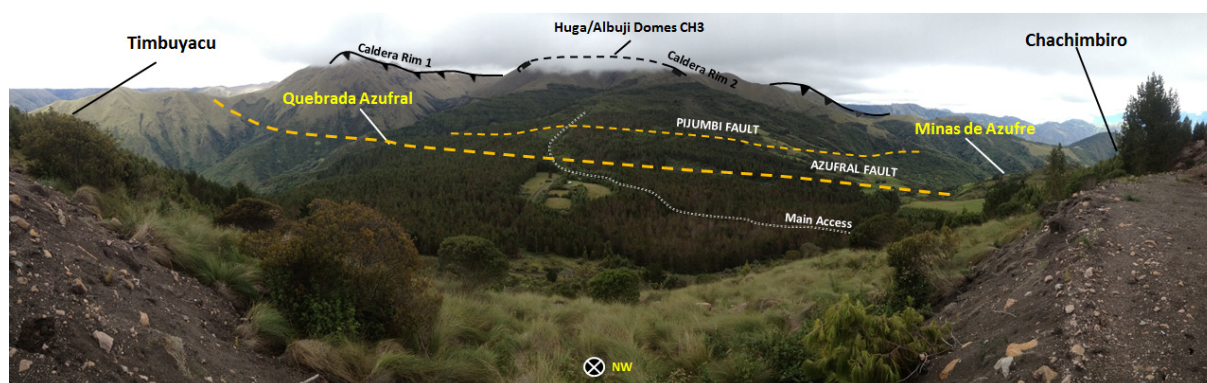


FIGURE 3: Panoramic view of Chachimbiro volcanic complex with the main geothermal manifestation areas and fault structures

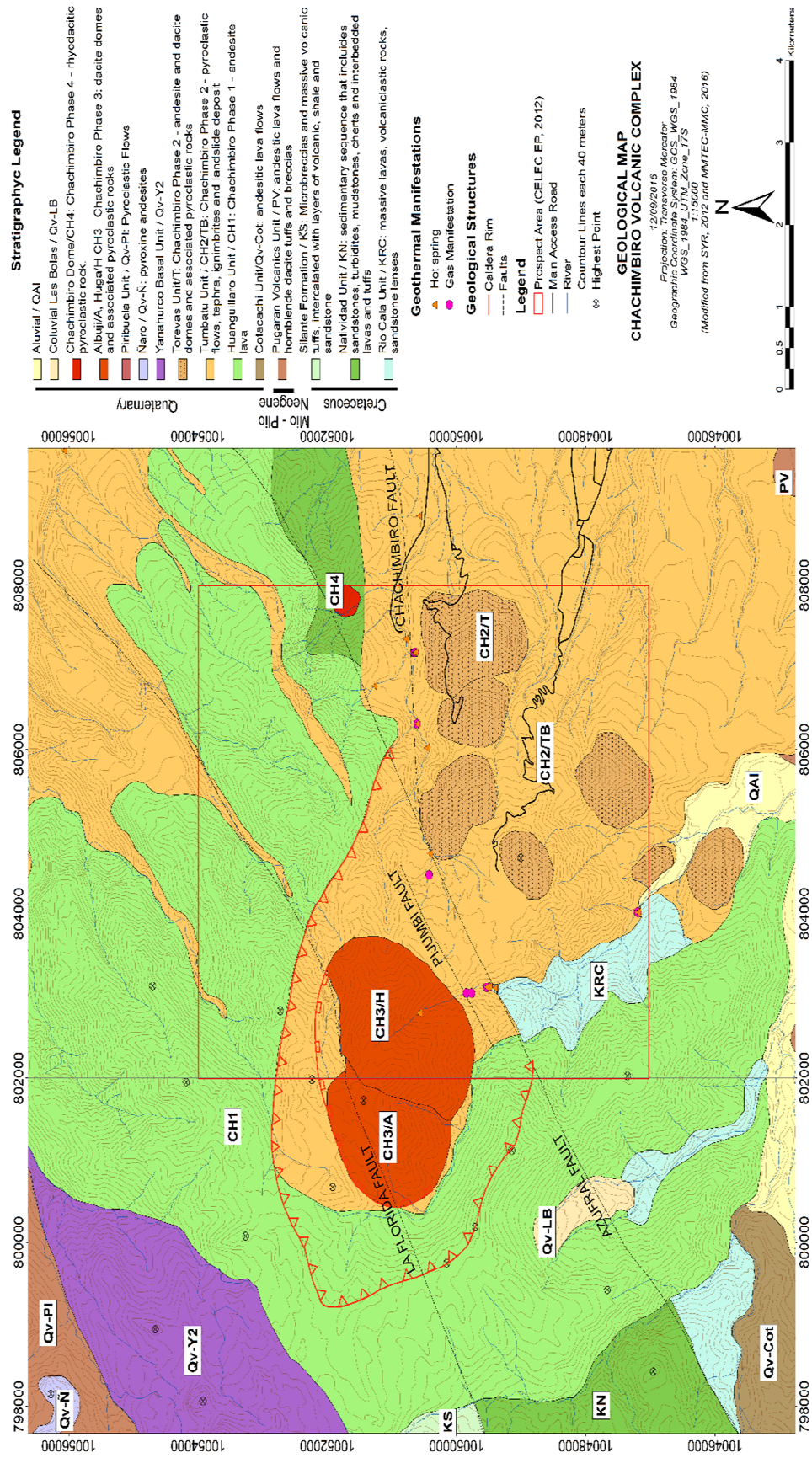


FIGURE 4: Geological Map of Chachimbiro volcanic complex, Ecuador, 1:15000 (modified from SYR, 2012)

The Quaternary volcanics evolved in four distinct phases (Bernard et al., 2010; 2014), which form the Chachimbiro Volcanic Complex and lie unconformable on the Cretaceous rocks.

Chachimbiro Phase 2 is described as either the Tumbatú or Chachimbiro volcano. Following this phase of dacitic dome building a second landslide occurred, with land mass movement to the east and the development of a smaller scarp that is sub-parallel to the scarp associated with the first collapse (Figure 3). Ruiz G. (2011), following Bernard et al. (2010), mapped these dacite domes as *torevas*, indicating that they may have been displaced from their point of origin while preserving some of their original morphology (Figure 4)

Chachimbiro Phase 3 in the evolution of the Chachimbiro Volcanic Complex is the most recent period of dome building, extending into the Holocene (Bernard et al., 2010). These large and young dacitic domes occupy the centre of the crater that resulted from the second landslide and include the large domes of Cerro Hugá and Cerro Albují (Figures 3 and 4). These domes and associated pyroclastics are predominantly dacitic, although some andesites are also observed (SYR, 2012).

Chachimbiro Phase 4 which was recently described by Bernard et al. (2014), occurred on the northeast slope of the volcano and defined the most powerful Holocene eruption of the Chachimbiro volcano, dated between 3640 and 3510 years BC. It produced a large pyroclastic density current directed to the southeast followed by a sub-Plinian eruptive column drifted westwards by the wind.

In the final report by SYR (2012), three fault systems were identified, believed to play important roles in the origin of the volcano and the potential location and circulation in the geothermal system.

The NE-SW striking Florida fault system forms the contact between the Cretaceous Natividad and Silante units. This fault complex underlies the eruptive centres of the Huanguarillo volcano and the Hugá-Albují domes (Figure 4).

The Azufral fault system in the central part of the project area also trends NE-SW. Based on structural mapping information collected by SYR it is interpreted as being a right lateral strike slip fault system. This fault zone, which may represent the transition of the Natividad to the Rio Cala formations, brings the Rio Cala unit into contact with the Quaternary volcanic unit. The fault system is described as two



FIGURE 5: Panoramic view of Chachimbiro hot springs location and Chachimbiro Fault

separate segments – the Pijumbí fault and the Crusacha fault (SYR, 2012), but according to a new report by MMC-MMTEC (2016) the Pijumbí fault is a segment parallel to the Azufral Fault (Figures 3 and 5). The third important fault zone is an unnamed fault system that extends EW through the eastern part of the Chachimbiro. Nevertheless, in the new geological report by MMC-MMTEC (2016) this system is called Chachimbiro Fault System which controls the hydrothermal alteration and hot springs found along the trace of this fault zone (Figure 5).

3. METHODOLOGY AND DATABASE

3.1 Geology data

The geology of the Chachimbiro prospect has been mapped in detail by Ruiz G. (2011) and Granda (2011). They reviewed previous reports and interpreted aerial photographs and other remote sensing images. During the field mapping, samples were collected for petrography, chemical analysis and rock dating. Databases of the lithology information from Vallejo (2007) and Bernard et al, (2010) were the source showing the Evolution of Chachimbiro Volcanic Complex. This evolution model was presented in a technical report by SYR in 2012 and a geological map in the scale 1:25000 resulting from the fieldwork.

Analysis of structural features observed in outcrops, such as the orientations of bedding features, joints, and faults is provided by Wrightson (2011). The data set includes orientations of fault segments and fractures in the Cretaceous basement rocks as well as some specifics regarding the nature of the structural features (SYR, 2012).

Hydrothermal alteration observed in the rocks was described by Ponce (2011). During the field mapping, samples of altered rocks were collected and analysed using reflectance technology. Ponce identified six different alteration assemblages:

- 1) Mesothermal propylitic (chlorite-epidote-calcite); only affects the basaltic rocks and it is not associated with current thermal activity,
- 2) Epithermal propylitic (smectite-chlorite); associated with acid fluids and contemporaneous with the current thermal features,
- 3) Argillic (smectite-kaolinite); associated with hot springs and fumaroles and considered to be contemporaneous with the thermal activity,
- 4) Steam heated advanced argillic (opal-smectite-kaolinite); associated with fumaroles showing high concentration of H_2S , and is also considered to be contemporaneous with the Argillic alteration,
- 5) Carbonization; represents the deposition of carbonate minerals that form along structures where CO_2 gas is being released and;
- 6) Supergene advanced argillic alteration; it is not hydrothermal in origin, but rather results from the weathering of rocks.

These were mapped on a 1:10,000 scale topographic map (Figure 6).

MMC-MMTEC and CELEC EP carried out geological field work from April to July in 2016, in order to improve the geological model as the area is lacking outcrops. Several rock samples were collected in order to apply the Thermoluminescence method to characterize the heat sources, alteration zones and even doing stress modelling with new geological lineaments analysed. MMC-MMTEC identified four different alterations zones:

- 1) Kaolinite Zone (kaolinite \pm halloysite); associated with alteration by fluids with temperatures from 100°C to 200°C. This zone covers the similar argillic area identified by Ponce (2011).
- 2) Steam Heat Argillic Zone (quartz \pm crisobalite \pm kaolinite); associated with acid fluids (H_2S) which altered volcanic rock, and this covers the same area as the steam heated advanced argillic alteration mapped by Ponce (2011).
- 3) Smectite Zone (smectite \pm quartz \pm halloysite \pm Trd); extends along the Chachimbiro Fault and formed at around 130°C. This zone has been described as argillic with patches of carbonization and propylitic low-temperature alteration by Ponce (2011), but the smectite zone is covering a greater area around of Chachimbiro fault that has not been identified before (Figure 6) and;
- 4) Smectite Zone Discrete (Smc \pm Qz); associated with regional metamorphism without any relation to geothermal fluids.

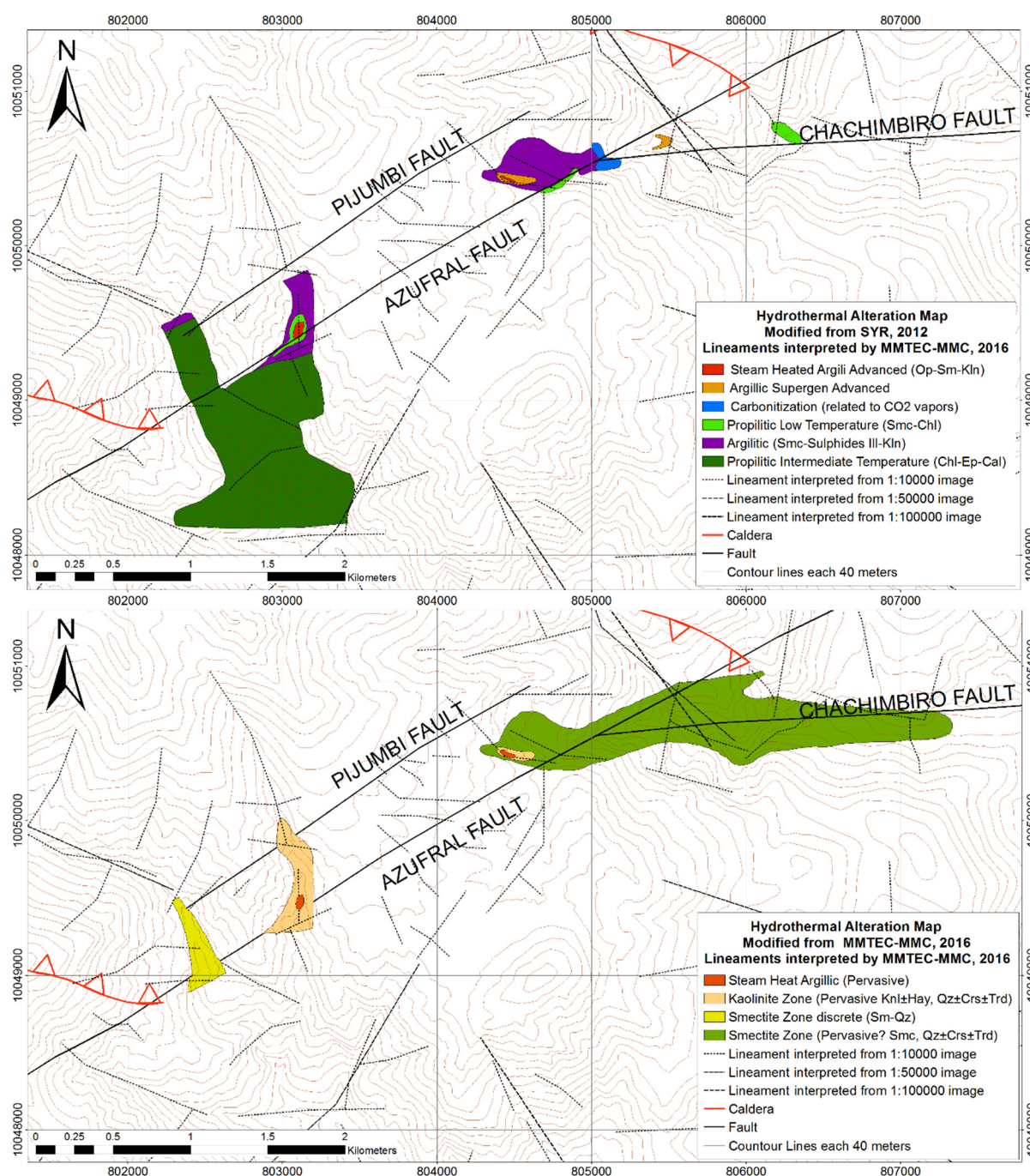


FIGURE 6: Hydrothermal alteration maps (modified from SYR, 2012 and MMTEC-MMC, 2016) which show the different zones of the hydrothermal alteration areas, except for Steam Heat Argillic Zone

All the data described above, have been provided by SYR to CELEC EP, in the form of reports and shapefile databases. In this study, these data were edited and a new dataset was generated in ArcGIS 10.3 in order to visualize the geological model in 3D using Petrel.

Geological lineaments were identified and analysed using ASTER/GDEM data and Photo-Interpretation with 1:10000, 1:50000 and 1:100000 scale by MMTC-MMC (2016) in order to locate areas with high density of lineaments and possible fractures. In this study, the data were georeferenced and plotted in order to correlate the lineaments with the main structures as well as the seismicity.

3.2 Geophysical data

Magnetotelluric data were collected in 2011 by WesternGeco Integrated EM CoE. In total 70 MT stations were installed and distributed on an irregular grid with a minimum spacing of 0.35 km between stations.

The data were processed and 1D and 3D inversions were carried out (SYR, 2012). The data were acquired as five component stand-alone remote reference MT stations with a nominal bandwidth from 0.001 to 10000 Hz. However, there are serious gaps in the survey because suitable sites were hard to find in the rugged terrain. Those gaps are northwest of Minas de Azufre, north of Timbuyacu hot spring, south of Quebrada Azufra, near MT station M33, north of Santa Susana hot spring and several locations of less conceptual interest (Figure 7).

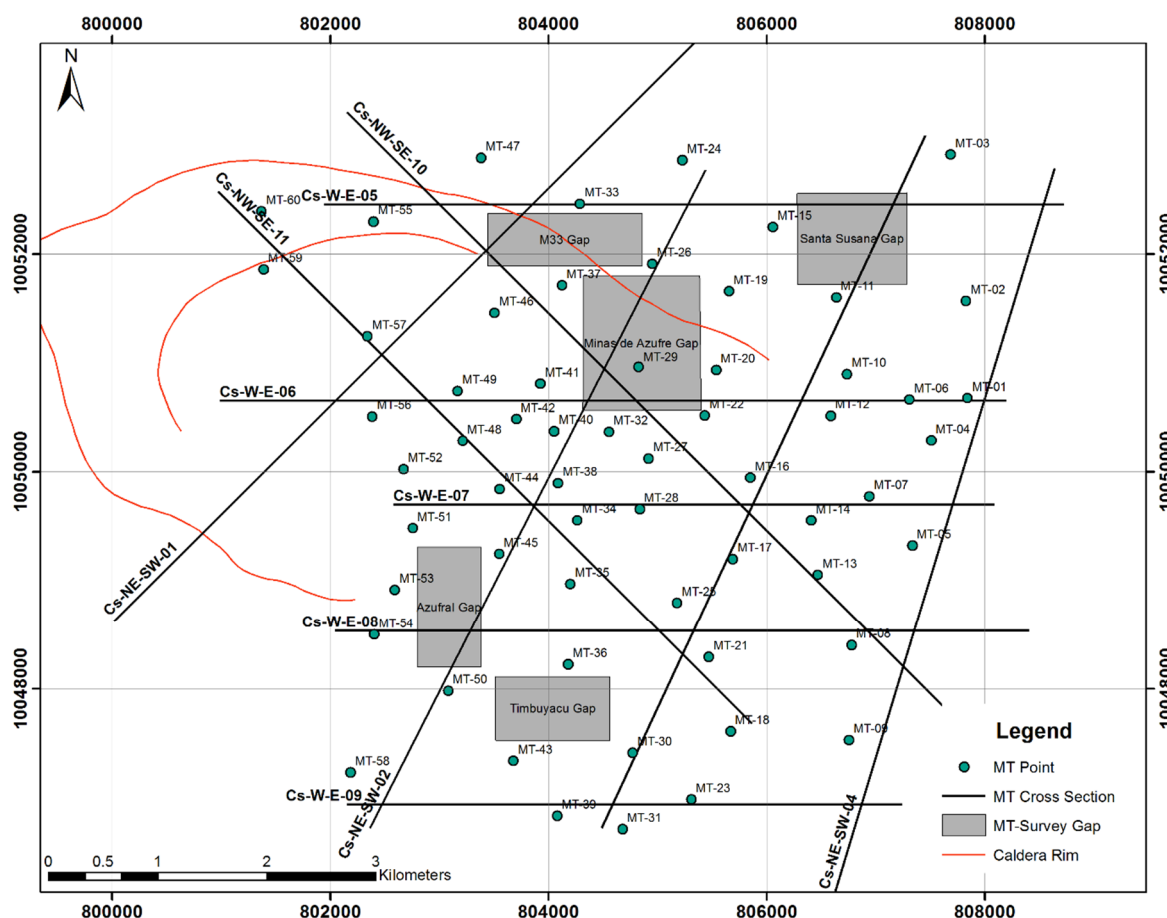


FIGURE 7: Magnetotelluric data points and cross-sections used in order to create a data grid in Petrel Software

CELEC EP has acquired a MT/TDEM equipment set which consists of six Electromagnetic Geophysical Data Acquisition Systems in order to obtain new data in the area where a low resistivity anomaly was found. These new data was collected from May to August of 2016 and are still being processed.

The present study employs eleven resistivity profiles made by Manabu Sugioka geophysicist specialist of JICA-CELEC, who is supporting the geophysical exploration in Chachimiro Prospect. The cross-sections shown below have been selected specifically for this study (Figure 7 and Table 1- Appendix I).

The MT data were processed for Petrel analysis using ASC-II files for each cross-section. They show the resistivity values as a function of depth. In order to visualize the data in 3D, two main steps had to be performed: a) to define a grid in X, Y, Z directions and b) to populate the grid with data.

The grid was defined as a cube, which covers all cross-sections from the surface (Top Limit) to 4000 m below sea level (Base Limit). The grid increment was defined to be 50 m in the X, Y and Z directions. Petrel allows the use of several interpolation methods for computing values in cells where no data was available. In this study these methods were tested on the main input data. The Gaussian Methods show distortion in the results and do not allow to clearly define the resistivity anomalies. The Closest Method shows interpolation in data blocks and distortion at the boundaries of resistivity layers. The Functional Method shows resistivity layers with soft boundaries, nevertheless in areas with low resistivity, it shows distortion and unusual forms. The User Define Algorithm and moving average methods show intercuts with cross-sections and do not define resistivity layers.

The Kriging methods produce similar results as the approaches mentioned above. The Kriging theory conducts smoothing and exact interpolation at the same time. Further, the Kriging method makes use of a very flexible gridding scheme (Yang et al., 2004). In this study, the Kriging Interpolation Method outlined low and high resistivity layers with a minimum of distortion compared to the results of other methods, allowing us to visualize the results from the MT data in the best possible way.

3.3 Geochemical data

The Chachimbiro Geothermal Prospect consists of a number of mixed chloride-bicarbonate hot and warm springs (temperatures up to 61°C) located along Quebrada Chachimbiro in the northeastern part of the prospect area. These springs are utilized for commercial thermal spas. There are also a few hot springs at Timbuyacu (temperatures up to 41°C), on the southeastern edge of the prospect area. The Chachimbiro hot springs show the highest temperature in the prospect and appear to represent the geothermal resource waters (Table 3 in Appendix I). Sulphur gas comes up along the stream wall in local fractures, but this gas has not been sampled without air contamination.

GeothermEx, Inc participated in the pre-feasibility stage of the Chachimbiro Prospect, subcontracted by SYR in 2011, to do geochemical analysis. They designed the sampling and analysis schedule, sampled the fluids (water and gas), reviewed the lab operation and results, and compiled, integrated and interpreted the geochemistry data (SYR, 2012). The areas sampled were the Chachimbiro, Timbuyacu, Pinguchela, Pilomanchi hot springs and Quebrada Azufral gas and cold fluids (Figures 8A, 8B and 8C).

During the field campaigns, data were collected to gain information on physical (Table 3 in Appendix I) and chemical parameters (T° , pH, Eh, Ec, flow estimation). The lab results show concentrations in the order of ppm of major elements (Ca, Mg, Na, K, HCO_3 , SO_4 , Cl, Si and Li) and minor elements (Fe, F, NH_4 , B, As, Al, Cs, Rb, Br, NO_3), isotopes ($\delta\text{-}^2\text{H}$, $\delta\text{-}^{18}\text{O}$) in hot and groundwater. In addition, gas dry analysis in percentage of volume (CO_2 , H_2S , NH_3 , Ar, N_2 , CH_4 , H_2 , O_2 , CO) and He isotopes ($^3\text{He}/^4\text{He}$) was carried out. From these chemistry data liquid and gas geothermometers have been calculated.

GeothermEx (2011) also took into account geochemistry data published by Aguilera et al. in 2005. These data were reviewed by SYR in order to create a complete database. Aguilera (2005) also refers to the chemistry data collected by Almeida et al. (1990) which do not have geographic coordinates.

4. INTERPRETATION USING THE PETREL SOFTWARE

4.1 Structural analysis

Hydrothermal alteration is controlled by the Azufral and Chachimbiro Fault systems and NW-SE lineaments. Low emission of CO_2 and H_2S has been found in Pijumbi and Azufral faults close to the hydrothermal alteration. The gas flow and alteration disappear in Northwest direction from this point, no hot springs or gas have been found further than Pijumbi fault and Azufral stream intersection. This

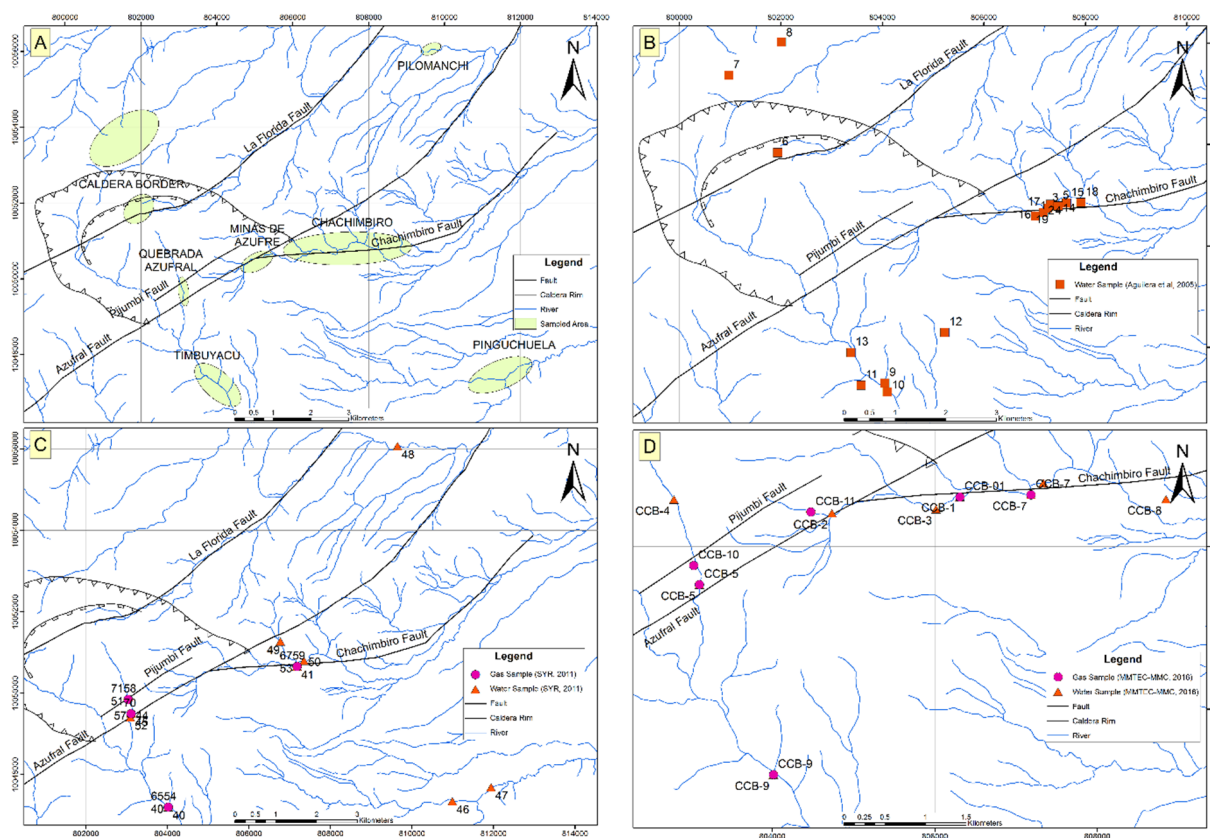


FIGURE 8: Geothermal manifestation areas (a) and area sampled (gas (b), hot springs (c) and fresh water (d)) during field campaigns in 2005, 2011 and 2016

would suggest the Pijumbi fault is a boundary of the geothermal system. Hot springs are located along the Chachimbiro Fault and the intersection with the Azufral Fault (Figure 8). This indicates that those faults control the upward movement of fluids and that the faults are permeable.

MMC-MMTEC and CELEC EP worked together and conducted a field survey from April to June 2016. The main objective was to sample gas and water at the same locations as GeothermEx (2011) and sample new hot spring locations (included Minas de Azufre gas manifestation, Figure 8D). The analysis is ongoing and some results have been shown and a preliminary interpretation has been presented by MMC-MMTEC (unpublished document). The results show the concentration of major (Na, K, Li, Ca, Mg, Cl, SO_4 , HCO_3 and T-SiO₂) and minor elements (NH₄, AL, Fe, NO₃, NO₂, F, B, and As) and isotopes (δ -²H, δ -¹⁸O) in water and gas dry analysis results in percentage of volume (CO₂, SO₂, H₂S). In this study, the ArcGIS 10.3 software was used to create shapefiles containing the element concentration as attributes. Petrel allows shapefiles to be imported with topography information and creates surfaces that show concentration of chemical elements or temperature anomalies (see Figures 21, 22, 25 and 26 in chapter 4.3).

The quantity of lineaments increases close to the intersection between faults and alteration zones, suggesting a fracture system associated with the main structures. MMTC-MMC (2016) points out a set of W-E lineaments caused by shearing activity of the Azufral Fault at Minas de Azufre area. This also indicates that permeability in the system controlled by the Azufral Fault (Figure 9). There are alignment of earthquake epicentres parallel to the Azufral and Chachimbiro faults in NE-SW and E-W directions respectively. The lineaments coincide with lineaments interpreted by MMC-MMTEC (Figures 9 and 10).

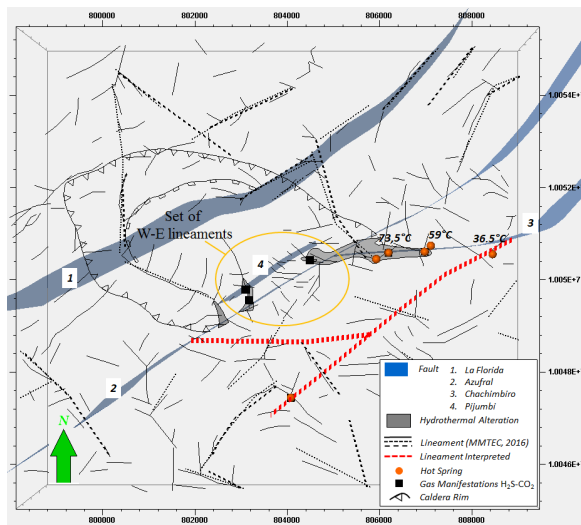


FIGURE 9: Map of interpreted lineaments that show an increase of lineaments at Azufra and Chachimbira faults and also staggering lineaments in W-E direction in the Minas de Azufre area

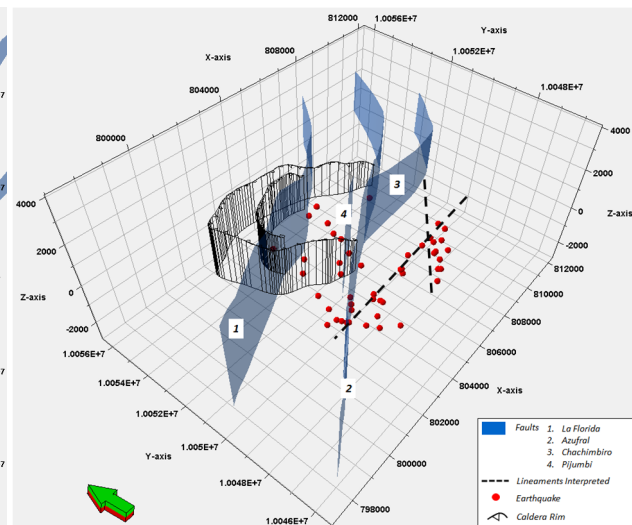


FIGURE 10: Alignments of earthquake epicenters subparallel to Chachimbira (4) and Azufra (3) faults

The seismic activity has been recorded and the locations of earthquakes have been included into the model (Ruiz M, 2011). Figure 10 shows an alignment of earthquakes with the fault systems Azufra and Pijumbi, which confirms shearing activity.

It is important to note that in the current regional structural system, the main stress is oriented in E-W direction, which creates a subparallel fault system in NE-SW direction of the Azufra and La Florida Fault and the Chachimbira Fault System at the same time. This interaction between faults results in a “pull apart” system in the Chacana volcanic complex (Hall, 2012). This is indicated by sub-parallel faults in the Azufra and Chachimbira systems, which allow permeability and upward movement of fluids in the system, and also structural barriers. This strongly suggests the existence of carriers and barriers.

4.2 Magnetotelluric data analysis

Electrical resistivity is controlled by electrical properties of the material, not only related to types of rock and their composition, but also to the overall physical conditions of the media (Tikhonov, 1950 - in Sakindi, 2015). Generally, the resistivity values in a weathered layer of igneous rock from mafic to felsic composition is ranged from 3 to 300 Ωm , in clays from 4 to 100 Ωm , in tills from 50 to 2000 Ωm and in fresh water in aquifers from 3 to 100 Ωm (EOS, 2007). High permeability and porosity (fractures) increase the conductivity. This means low resistivity, which then tends to increase with depth, due to the pressure, which closes the fractures and reduces rock porosity (Palacky, 1987).

Geothermal systems show electrical resistivity (conductivity) anomalies related to clay minerals, one of the most common being smectite. The formation of clay minerals in geothermal systems depends on the temperature and chemical conditions of the fluids that flow through the rocks. A low resistivity (high conductivity) anomaly is observed on the outer and upper margins of the reservoir. The low resistivity represents the cap rock, which is underlain by a high resistivity core (Tikhonov, 1950 - in Sakindi, 2015).

Low resistivity (generally lower than 5 Ωm) in geothermal systems is associated with the smectite-zeolite alteration zone. The resistivity increases with depth until the chlorite and epidote zones are reached, which usually forms a high resistivity core. These mineral zones also depend on temperature

conditions. The smectite-zeolite zone forms at temperatures between 50-100°C and chlorite-epidote zone forms at temperatures exceeding 250°C (Árnason et al., 2000).

To visualize the different resistivity layers in Petrel, a 3D grid was developed. Then iso-values of resistivity were generated by filtering out areas of specific resistivity. From this 3D shapes of low resistivity i.e. the distribution of the anomalies become visible. That allows the user to decide the direction of cross-sections (Figure 11). Once these have been determined, the cross-sections were completed with data previously present in the cube grid (Figure 12).

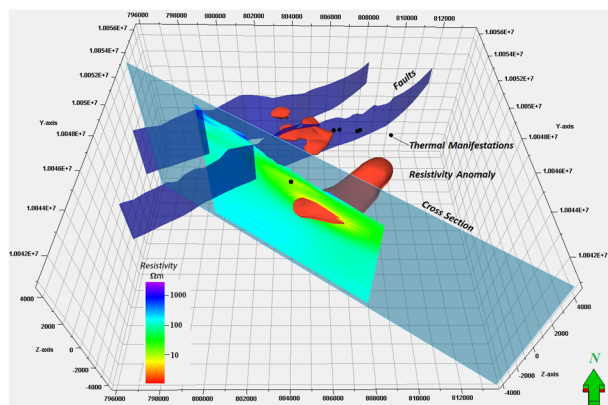


FIGURE 11: Determination process to define a cross-section in Petrel software

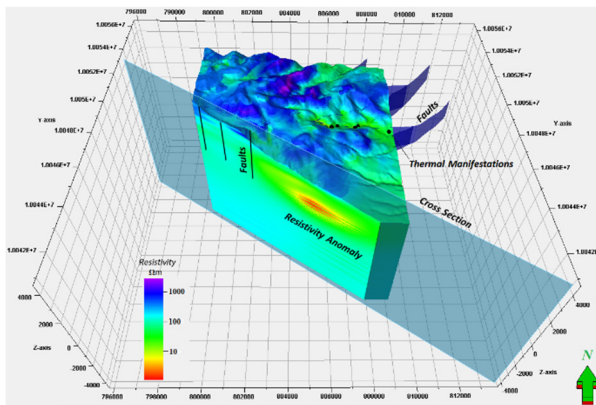


FIGURE 12: Resistivity cross-section through the cube grid populated with resistivity data

In order to visualize the low resistivity anomaly in Chachimbiro several filters were used showing different resistivity values (Figures 13, 14 and Figures 4-9 in Appendix III). Using this method, the spatial distribution of the anomalies was identified and structures and boundaries of the cap rock, and a possible reservoir, can be revealed. Table 2 in Appendix I shows the dimensions of these resistivity anomalies.

The resistivity model shows three different anomalies, two of them are large and cover extensive areas. These anomalies are separated from each other by a fault (Figure 15). The shallow anomaly, which is possibly the cap rock, covers an area of 11.07 km² and its average thickness is around 388 m.

In Figures 15 and 16, the low resistivity shows clear divisions of the anomaly by Azufral, Chachimbiro, and Pijumbi Fault and a division in NW-SE direction with a similar trend to lineaments was interpreted by MMC-MMTEC (2016). Another lineament in NW-SE direction has been interpreted in the borders of 5 to 7 Ω m resistivity anomaly (Figure 16). These lineaments could be fractures that increase the

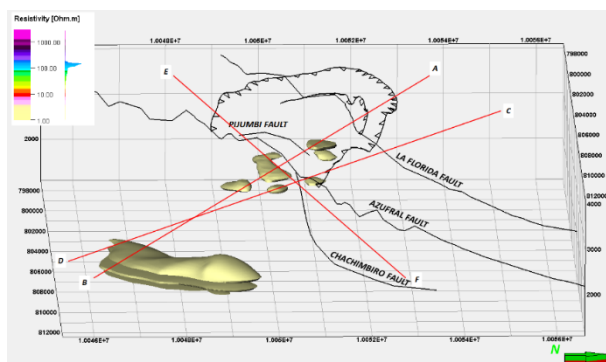


FIGURE 13: Spatial distribution of low resistivity anomalies (0-3 Ω m) and choice of cross-sections

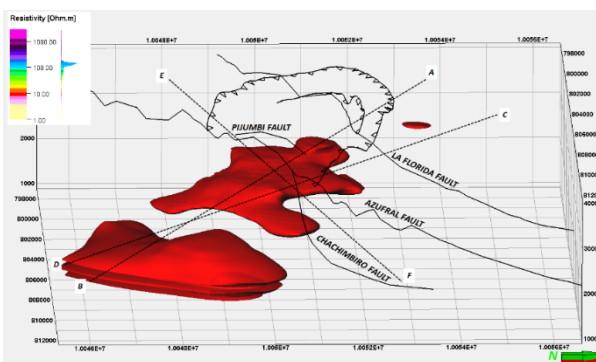


FIGURE 14: Low resistivity anomaly from 7 to 10 Ω m modelled in Petrel Software, showing its relation to faults

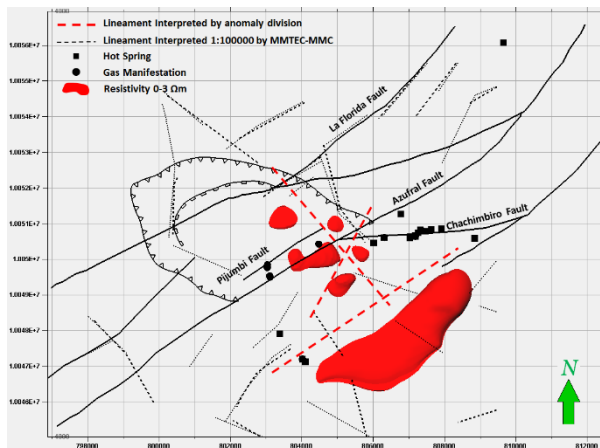


FIGURE 15: Divisions of the anomaly by Azufra, Chachimbiro, Pijumbi Fault and possible fractures in NW-SE direction

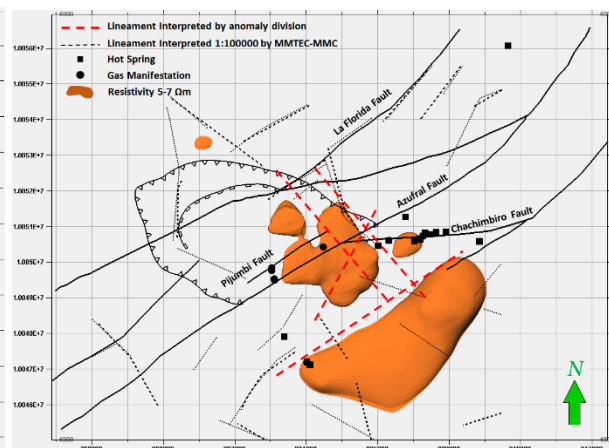


FIGURE 16: Divisions of the anomaly by Azufra, Chachimbiro, Pijumbi Fault and possible fractures in NW-SE direction

permeability of the system and outer boundaries. An important lineament has a subparallel trend to the Azufra fault that divides two resistivity anomalies (at 7-10 Ωm) and is in alignment with earthquakes, hot springs and lineaments interpreted by MMTEC (Figures 9 and 10).

Petrel can create cross-sections in any direction. Based on the analysis above, some directions of interest become apparent (Figure 13).

The resistivity distribution in Chachimbiro shows different layers. The shallow part with high resistivity ($>160 \Omega\text{m}$) corresponds to Quaternary volcanic rocks and tills. The low resistivity zone ($<10 \Omega\text{m}$) could be related to the cap rock, probably formed by smectite. Outcrops of smectite have been located and described in technical reports as personal documentation. Below the low resistivity anomaly, the resistivity increases gradually from 10 to 160 Ωm and forms a medium resistivity zone that includes a high resistivity core of 60 to 160 Ωm (Figures 17, 18 and 19).

Interpreted lineaments are present in cross-sections associated with earthquakes. The projection from the surface to the subsurface of Pijumbi, La Florida and Azufra faults, are aligned with hypocenter earthquakes concentration (Figures 17 and 18).

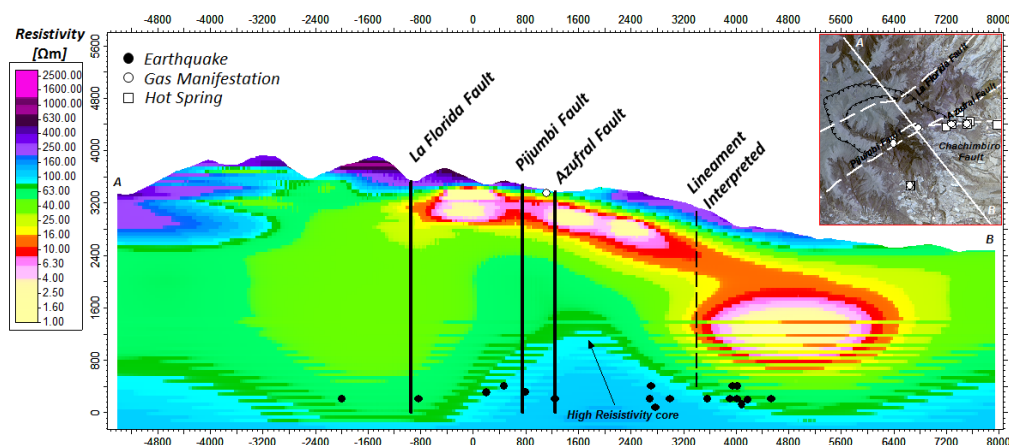


FIGURE 17: Resistivity cross-section A-B shows the high resistivity core and the relation between the interpreted lineament, earthquakes, fault, gas manifestations and resistivity anomalies

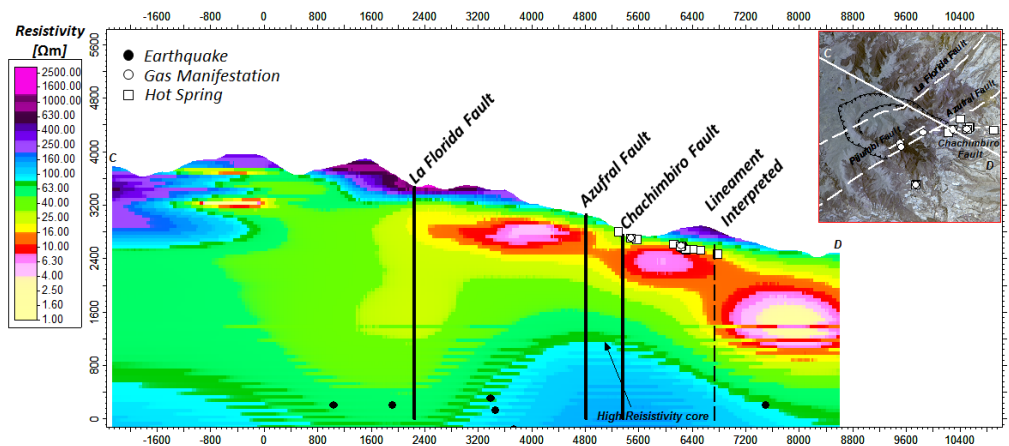


FIGURE 18: Resistivity cross-section C-D shows the high resistivity core and the relation between the interpreted lineament, earthquakes, faults, gas manifestations, hot springs and resistivity anomalies

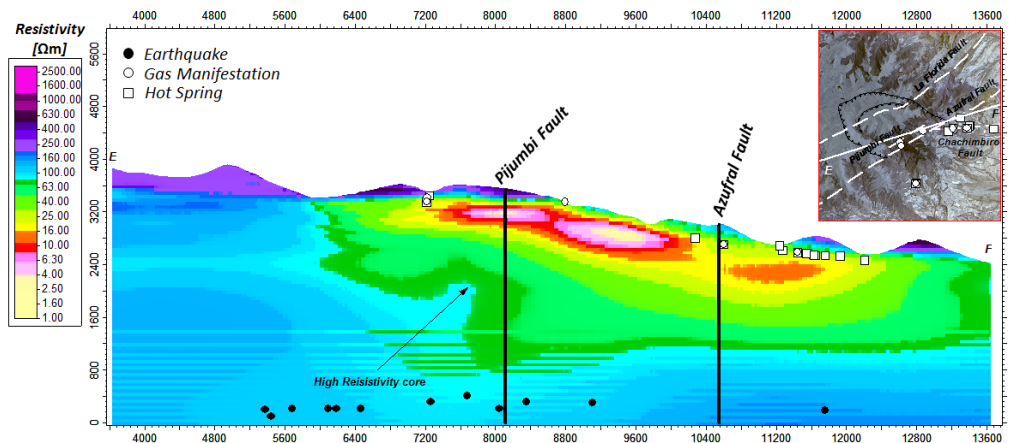


FIGURE 19: Resistivity cross-section E-F shows the high resistivity core and the relation between the interpreted lineament, earthquakes, fault, gas manifestations and resistivity anomalies

The Azufra and Pijumbi Faults are clearly affecting the low resistivity anomaly. As mentioned above an interpreted lineament (Figures 9 and 10) is also evident in the resistivity cross-sections. This inferred lineament divides the two largest low resistivity anomalies and is associated with earthquakes cutting the Chachimburo fault and Timbuyacu valley where the hot springs are found (Figure 9 and 16).

The cross-sections show a slightly concave shape of the shallow low resistivity anomaly, which overlays a high resistivity core that is wrapped in by a medium resistivity layer (Figures 17 and 18). The faults projection from the surface to subsurface reaches the high resistivity core; hot spring and gas manifestations are located on the faults which indicates that fluids in the core are connected to the surface through the Pijumbi, Azufra and Chachimburo Faults (Figures 17, 18 and 19).

4.3 Geochemical analysis

For the purpose of this report, the geochemistry data analysis will focus on: 1) geographical distribution of the geothermal manifestation, 2) origin of the geothermal fluids, 3) temperature of the reservoir and 4) the permeability zone.

Isotope analysis is an indispensable tool to understand the flow pattern in geothermal systems. Isotopes are sensitive to changes in temperature, water-rock interaction and other physicochemical processes, such as mixing and steam separation, and they are suitable as tracers detecting the source water and regional flow pattern.

The $\delta^{18}\text{O}$ values of geothermal waters are often higher (less negative) than those of local meteoric waters, an oxygen isotope shift has been termed in the diagram $\delta^{18}\text{O}-\delta^2\text{H}$. This has been interpreted as the result of isotopic exchange at high temperatures between the water and the rock (Abaya et al, 2000).

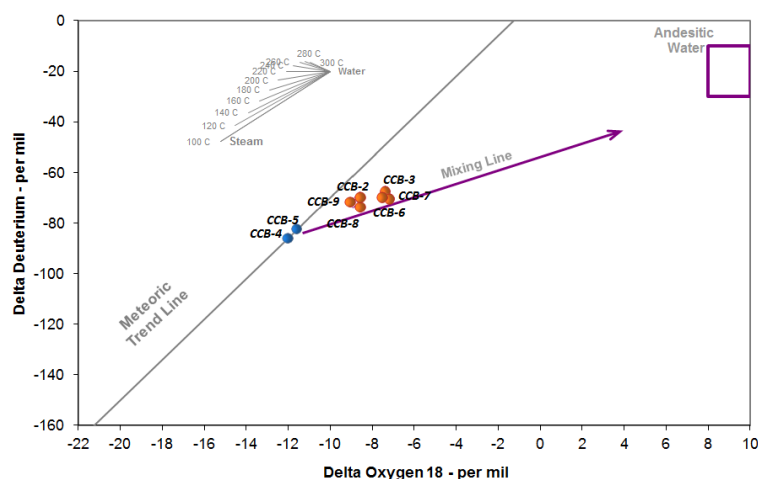


FIGURE 20: Diagram $\delta^{18}\text{O}-\delta^2\text{H}$, applied to the Chachimbiro water samples

Figure 20, shows that the Azufral water samples (CCB4 and CCB-5) are on the local meteoric trend line. These samples are cold groundwater with rock interaction at subsurface collected next to the CO_2 and H_2S gas manifestations. The hot spring samples (CCB-1, CCB-2, CCB3-CCB-6, CCB-7, CCB-8, CCB-9) in Chachimbiro and Timbuyacu areas show an oxygen isotope shift and these samples are almost in the same value range as the $\delta^2\text{H}$ isotope. That implies that these hot springs are of meteoric origin with subsurface rock interaction (Abaya et al, 2000).

Figure 20 also shows a mixing line trend to the andesitic water. That indicates input of andesitic water to the geothermal system from significant depths and mixing with geothermal fluids. Nevertheless, the oxygen isotope shift is normal compared to meteoric waters and the possibility of input from andesitic water to the geothermal system is minimal.

Geothermometers and isotope analyses probably constitute the most important geochemical tool for the exploration phase. Geothermometry is used to estimate subsurface temperature. During the ascent of geothermal waters from a deep reservoir to the surface, they may cool by conductive heat loss as they travel through cooler rocks or by boiling as the hydrostatic head decreases. When geothermometers are applied to measure subsurface or aquifer temperatures, basic assumptions are always made, namely that the temperature dependent chemical or isotopic equilibrium prevails in the source aquifers (D'Amore and Arnórsson, 2000).

SYR (2012) developed three different scenarios for Chachimbiro system based on geothermometer temperature:

- 1) The first model is a moderate temperature hydrothermal system with neutral chloride reservoir water at 225-235°C and deep temperatures as high as 260°C. It is based upon the neutral chloride chemistry of the hot springs, temperatures predicted by the Na-K and $\text{CO}/\text{CO}_2\text{-CH}_4/\text{CO}_2$ geothermometers.
- 2) The second model is that of a low temperature (110-125°C) formation water, referred to as "immature water", based upon predictions of the K-Mg and sulphate isotope geothermometers.
- 3) The final model is that of a cooling magma-hydrothermal system, with temperature of 110-125°C, supported by carbon and helium isotopes.

This report shows the temperature in the subsurface based on liquid geothermometer and using the chemical data collected by MMC-MMTEC (2016). The analysis of the results can be found in Table 5 in Appendix I and Appendix II. The chemical data were processed with Plotting Spreadsheet developed

by Powell and Cumming in 2010. Only four samples could be used for the next analyse described below because some samples are out-of-ionic balance between anions and cations (Table 4 in Appendix I). The Na and K cations usually are in high concentration in deep areas in the reservoir and they are only in low concentration in meteoric water. Thus, the Na/K ratio does not change even when there is a mixing process between hot and cold water. The geothermometers that use Na and K cations are the best for fluids derived from a thermal environment ($> 180^{\circ}\text{C}$), and also the flow rate of a spring may be less than is required for the application of the quartz geothermometer (Yock, 2009). The highest temperature based upon Na/K geothermometers is around 285°C (Tonini, 1980), but the average value is 240°C . These values are close to the temperature values reported by SYR (2012) in their first model, which is related to neutral chloride reservoir water.

The Na/K geothermometers are applicable in Chachimbiro geothermal system and the values calculated using those methods were used to create temperature iso-lines at different epochs in Petrel Software (Figures 21 and 22). Figure 21 shows core temperature areas of over 300°C . This anomaly covers Minas de Azufre, Quebrada Azufra and partially the intersection between the Chachimbiro and Azufra faults. The figure also shows an area with Na/K temperature less than 200°C that overlaps with the hydrothermal zone. Figure 22 shows high temperatures (from 250 to 300°C) next to Minas de Azufre area and here also the most extensive hydrothermal alteration area, which overlaps with the 250°C temperatures area, can be found. There is a slight correlation between the two iso-lines graphics (Figures 21 and 22). The main reason may be due to the distribution of the samples and also, the methodology used to obtain the temperature values with the K/Na geothermometer. However, it seems that the high temperature area overlaps with the large alteration zone and also the Azufra area (Figures 21 and 22).

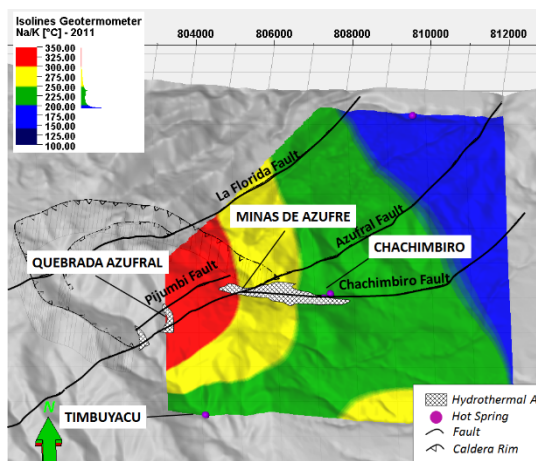


FIGURE 21: Isolines based on temperatures obtained with K/Na Geothermometer, using ion concentration from hot spring samples collected by GeothermEx in 2011

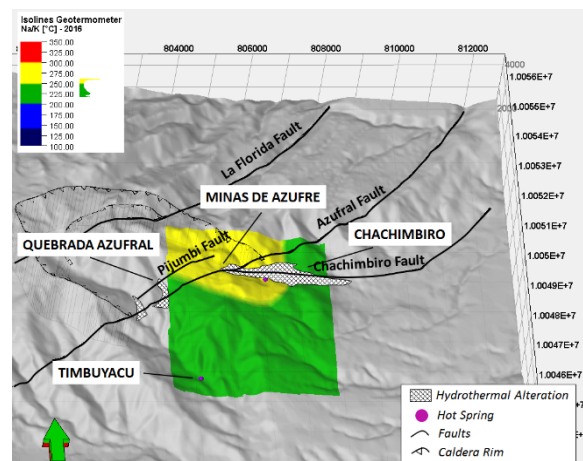


FIGURE 22: Isolines based on temperatures obtained with K/Na Geothermometer, using ion concentration from hot spring samples collected by MMC-MMTEC in 2016

The permeability can be interpreted with direct observations in the field and analysis of the distribution of the fluids at the subsurface. In the Quebrada Azufra and Minas de Azufre area there are several gas manifestations of CO_2 and H_2S at low flow rate and pressure. These are located on the stream bedrock (bubbling gas, Figure 23) and also in fractures on the stream walls, where native sulphur precipitates (Figure 23). These emissions are controlled by the Azufra fault that also controls the hydrothermal alteration in this area. It is important to mention there are no hot springs in the area.

The hottest springs are located along the Chachimbiro Fault in Chachimbiro area. These hot springs precipitated CaCO_3 and there is no emission of H_2S . Most of the hot springs are entrapped in cement boxes which feed the Chachimbiro spa (Figure 24). The Timbuyacu hot springs appear not to be related with any structures.

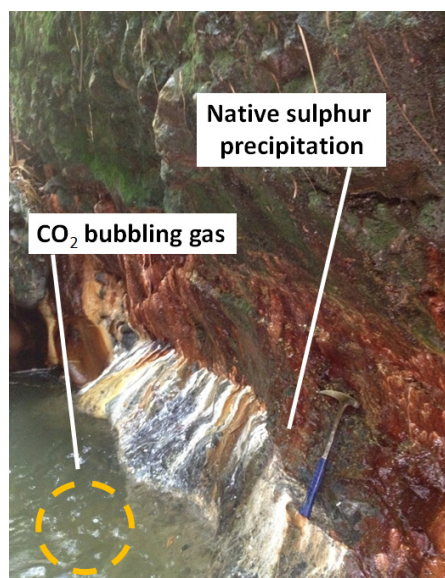


FIGURE 23: CO₂ emission on the bedrock stream at Quebrada Azufral area and Native Sulphur precipitation on fractures



FIGURE 24: Hot Springs entrapped in cement box at Chachimbiro area

The higher concentration of hot springs at Chachimbiro shows that the most permeable area is related to the Chachimbiro fault. Permeability is also related to the Azufral fault where CO₂ and H₂S indicate a degasification zone at depth.

The temperature iso-lines in Figures 25 and 26, show the Chachimbiro area as the hottest point at the different epochs, as might be expected. From Chachimbiro the high temperature trends to the North, Southeast and Southwest. The iso-lines do not represent the temperature gradient; the rock is not an isotropic environment and the iso-lines have been interpolated based on hot spring temperatures. However, it may represent a main zone of outflow such as Chachimbiro area and lateral outflows such as Timbuyacu, Pinguchuela and Pilomanchi.

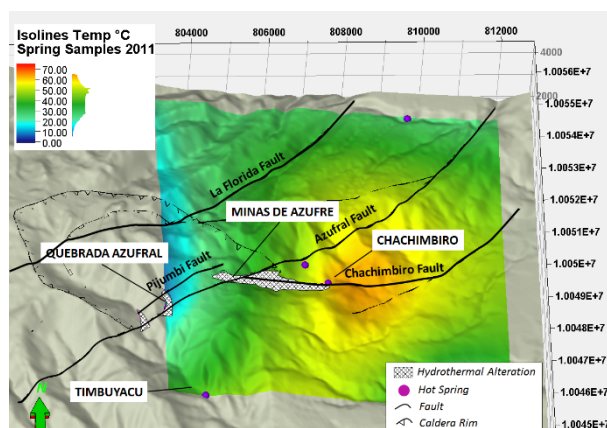


FIGURE 25: Iso-lines based on hot spring temperatures measured by Geothermex (2011)

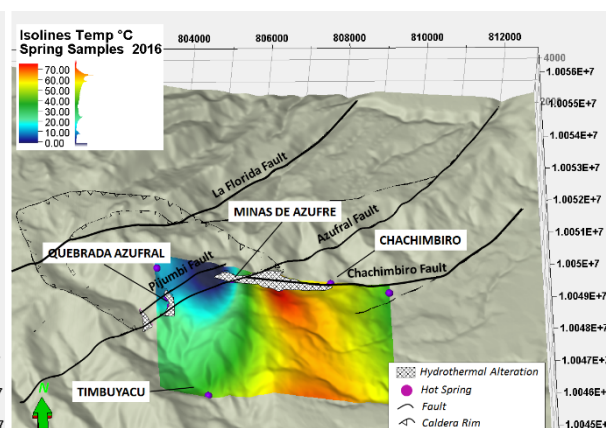


FIGURE 26: Iso-lines based on hot spring temperatures measured by MMC-MMTEC (2016)

5. GEOTHERMAL MODEL OF CHACHIMBIRO IN PETREL

The available data for the Chachimbiro geothermal prospect has been described in previous chapters. In this chapter, a conceptual model is presented. This is an early model so it is simple and based on analogies with geothermal fields that are better understood. When a resistivity survey and other surveys such as geochemistry are done, the outline of the field can be defined approximately, and geothermometers can indicate a possible reservoir temperature. After that a very simple model could yield an estimate of the potential power-generation capacity (Lumb, 1981).

Axelsson (2013) mentions the information from the geothermal systems that should be incorporated in a conceptual model. His method is applied for describing the Chachimbiro system making use of the available information. This study uses his guidelines and takes into account that not all geothermal conceptual models incorporate all the components.

5.1 Estimate of the system size

The sizes of geothermal systems worldwide tend to follow a log normal size distribution. In Chachimbiro there is considerable uncertainty concerning boundaries, temperatures and thickness. This study defines the boundaries using the dimensions of the low resistivity anomaly as the areal extent. This could be interpreted as the largest possible area of a resource. New geological, geochemical and geophysical data are under revision by MMTEC and MMC (2016) which will provide information about the size of the system and will also complement borehole information of scheduled drilling projects. Currently, the areal extent of the system is believed to be 11.06 km² based on the low resistivity anomaly (between 0-10 Ω m) and the thickness is about 3400 m from the surface to where the possible up-flow is located (resistivity anomaly 90 Ω m).

5.2 Nature of the heat source(s)

SYR (2012) suggests that the heat source is located near the Huga dome (Figure 27). This is indicated by its volcanic history (emplacement occurred 30.000 years ago) and composition (rhyodacite). These domes are interpreted as magmatic intrusions, and these have been controlled structurally by the La Florida fault (Figure 27). Bernard et al. (2014) documented volcanic activity between 3640 and 3510 years BC, which extruded a ~650-m-wide and ~225-m-high rhyodacite dome, located 6.3 km east of the magma chamber which is emplaced at two different depths (~14.4 and 8.0 km). The hot (~940°C) deep reservoir fed the central vent while the shallow reservoir (~860°C) had an independent evolution controlled by regional faults. This indicates partial migration of the heat source to the East, located below the Chachimbiro dome (CH4) at shallower depths (Figure 27).

The resistivity records show two high-resistivity anomalies of >150 Ω m (Figures 1 and 2 in Appendix III); one of them is under the Albuji and Hugá (CH3) domes and the other is under the Chachimbiro emission centre (CH4). These anomalies could relate to two intrusions, which are the heat source of the system (Figures 1 and 2 in Appendix III) and this also corresponds to the model by Bernard et al. (2014) suggesting that two different magma chambers exist. Figure 28 shows the 3D model of Chachimbiro, and it shows a clear structural control over the magma ascent. The evidence of the magma at surface is the Albuji and Hugá domes. However, the high resistivity anomalies have been modelled by extrapolation in sectors where MT data is missing. In order to strengthen this model, gaps in gravity and seismicity data need to be closed.

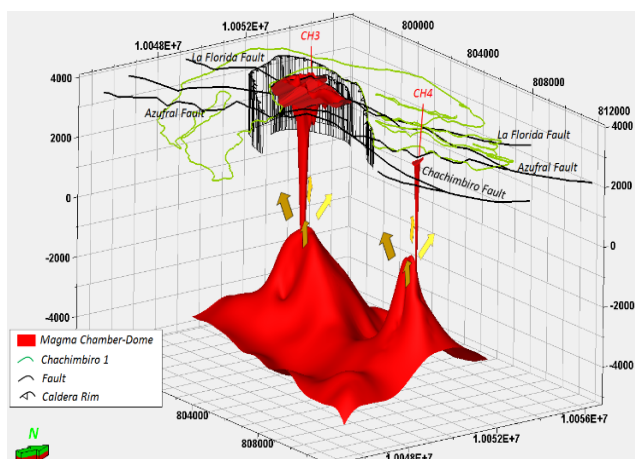


FIGURE 27: Magma intrusions that function as a geothermal system heat source and fed the emission centre in Chachimbira volcanic complex

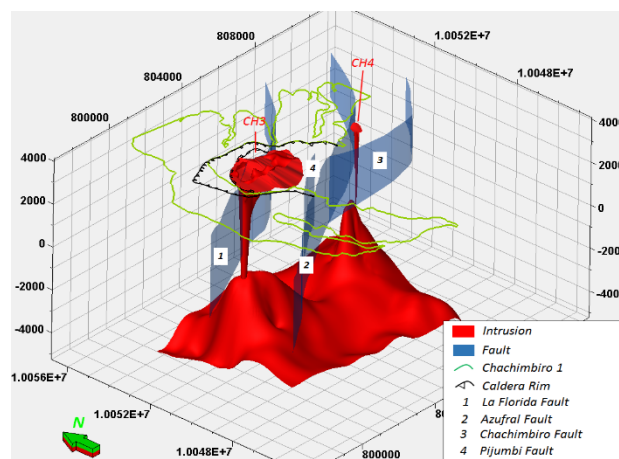


FIGURE 28: Structural control by La Florida Fault about magma rise that form Albuji and Huga domes (CH3)

5.3 Location and strength of the hot up-flow/recharge zones and origin of the fluid

The $\delta^{18}\text{O}$ and $\delta^2\text{H}$ isotopes show a clear meteoric origin of the water in the hot springs of Chachimbira (Figure 20). The geological structures allow the infiltration of the rain-ground water into the subsurface where it is heated up by convection and then rises to the surface where it forms hot springs in the Chachimbira area.

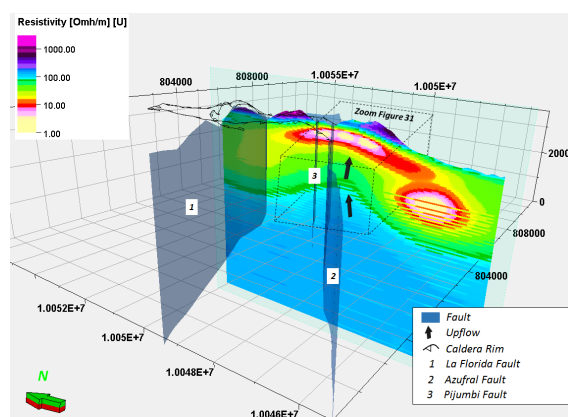


FIGURE 29: Up-flow controlled by the Azufra Fault

The low resistivity cap partitions the geothermal field hydrology into a shallower cooler meteoric zone and a deeper high temperature zone because the low resistivity (lower than $5\Omega\text{m}$) is associated with cap rock composed of clay, which has low permeability (Árnason et al., 2000). This cap rock covers a geothermal reservoir and accumulates heat by trapping the buoyant thermal up-flow. The up-flow zone is the reservoir zone in which flow is predominantly vertical and temperature generally increases with depth (Cumming, 2009). This means, in this case, that the up-flow in Chachimbira is located where the high resistivity core is identified, beneath the cap rock and is apparently controlled by the Azufra Fault (Figure 29).

5.4 Location and strength of colder recharge zones

Marginal recharge represents the influx of cooler marginal meteoric waters into the geothermal reservoir. Cooler water can flow into a geothermal up-flow zone through permeable channels, from either side of the system if the groundwater has more pressure than the reservoir. It may also enter from overlying aquifers at higher elevations (Cumming, 2009).

The Chachimbira volcanic complex is covered by the Páramo area (Andean ecosystem) which absorbs and percolates 600-1000 mm/year of rain water at more than 3000 m elevation (Hofstede et al., 2014). The river system shows several hydrography sub-basins outlined by geologic structures that both border

and exist inside the volcanic complex (Figure 3 in Appendix III). SYR (2012) documented a fracture zone that borders Caldera-1, lava flow fractures and contact zones, flow foliation in the dacite domes, contact zones between individual domes, and vertical fractures bordering the dome feeder dikes. These structures and lineaments will allow part of the groundwater to enter the host rock of the geothermal resource.

5.5 General flow pattern in the system in the natural state and changes in the pattern induced by production

As mentioned before, the low resistivity anomaly often correlates with more intensely altered up-flows. The steam dominated geothermal reservoirs are usually sealed by mineral alteration (smectite), with fumaroles, sinter, \pm mud pots and high flow of non-condensable gases such as CH_4 , H_2S , CO_2 , H_2 and N_2 . Water dominated reservoirs usually have outflow zones where buoyant hot water flows up through tabular aquifers under the smectite cap rock, without fumaroles, sinter and mud pots. The outflow is predominantly horizontal and temperature declines with depth underneath the main outflow zone (Cumming, 2009). In natural state, Chachimbiro geothermal system is dominated by liquid phase (there are no fumaroles, mud pots and low flow of non-condensable gases at surface).

In the reservoir and the core, the fluids are in convection due to the interaction between hot/basal recharge from a magmatic chamber and fluid meteoric water that percolates through open structures (see cold recharge zones in section 5.4). The geothermal fluids are accumulated beneath the cap rock, which is interpreted as the low resistivity anomaly, due to thermal buoyancy. There is no chemical evidence for magmatic fluid input. The outflow is established through the system faults. This is indicated by several hot springs and gas manifestation located on top of faults that bound the low resistivity anomaly. It suggests the existence of a subsurface connection between the upflow zone with the Chachimbiro area (hottest spring) and the Azufral and Pijumbi Fault (gas manifestations). The Timbuyacu springs do not have a structural connection to the upflow zone which is the outermost zone. It can be explained as a lateral discharge of the system through hidden structures. The Pilomanchi and Pinguchuela hot springs show lateral discharge that has been mixed with ground water, as indicated by their low temperatures (24.8 and 30°C) and high concentrations of magnesium with regard to Chachimbiro hot-springs (Figure 30).

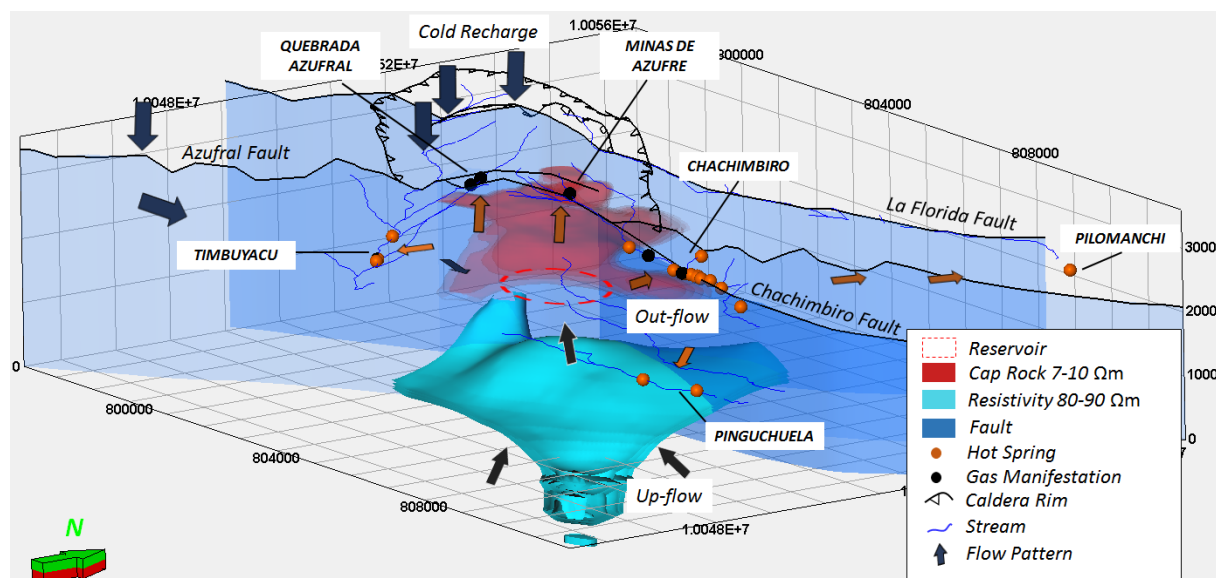


FIGURE 30: Flow pattern of fluids (perpendicular view to the main faults) that shows the cold recharge areas at the Chachimbiro highlands (Caldera Rims and Domes and the upflow zones beneath of cap rock (high resistivity)

5.6 Temperature in the system

For the purpose of this study, the temperature can be estimated by two methods. The geothermometer Na/K ratio in samples which were collected in 2016 shows temperatures of around 240°C. SYR (2012) reports temperatures of about 260°C in their first model. The resistivity method shows an increase in resistivity beneath a low resistivity layer. However, the resistivity method indicates that the maximum temperature that was reached in the past and does not reflect the current temperature of the system.

In many high temperature geothermal systems the transition between low to high resistivity anomaly core corresponds to a mixed clay/chlorite zone. Underneath the resistivity increases again considerably and stays relatively high in the chlorite and chlorite-epidote zones at temperatures exceeding 250°C (Árnason et al., 2000).

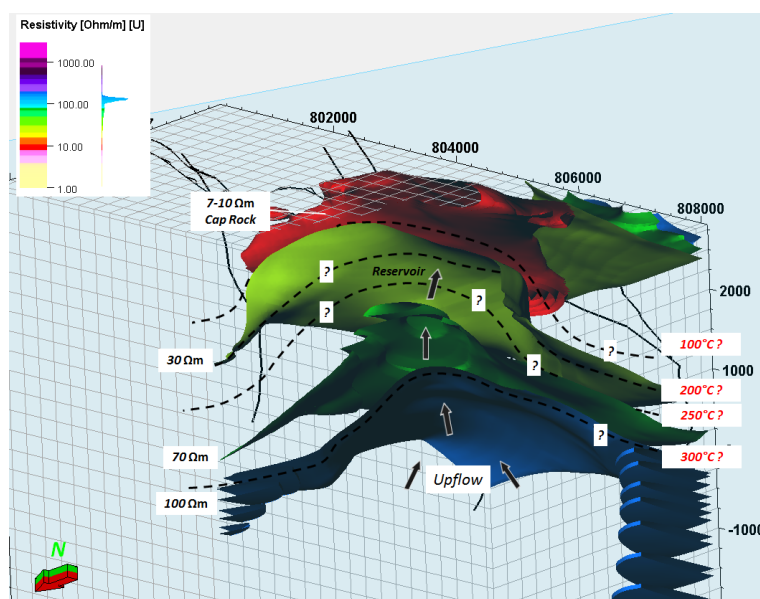


FIGURE 31: The isotherms in the Chachimbiro Geothermal System sketched based on guidelines given by Árnason (2008) and Cumming (2009)

Figure 31 shows a sketch based on the Chachimbiro resistivity maps and geochemical data following the conceptual guidelines given in Árnason et al., (2000) and Cumming (2009). Given the mapped alteration in the area, the shallow red zone (<10 Ωm) is likely to be a hydrothermal smectite clay cap. To reconcile the chemistry of the surface manifestations with the existence of a >240°C neutral geothermal reservoir, an intermediate aquifer that leaks to the surface has been assumed, which flows and carries the hot water to the permeable Chachimbiro fault where the hot springs rise to the surface.

5.7 Location of main permeable flow structures

The permeable structures in the Chachimbiro area are where the hot water rises to the surface and forms hot springs. The Chachimbiro fault controls the ascent of water in the area. The fault is E-W trending, and is limited by the Azufral fault and crosses the low resistivity anomaly (cap rock). The Chachimbiro fault seems to control the flow from the reservoir to the surface. The Minas de Azufre and Quebrada Azufral areas show hydrothermal alteration (smectite) in outcrops related to the cap rock as indicated in the magneto-telluric model. In these areas, only CO₂ and H₂S emission with low pressure are present in fractures. In these areas, lower permeability can be interpreted compared to Chachimbiro Area, and they are also controlled by the Pijumbi and Azufral faults. It is important to point out that the H₂S and CO₂ emission indicate volcanic activity in the subsurface but not an active geothermal system. The main signal of the geothermal system in Chachimbiro area is the presence of hot springs (Figure 32).

5.8 Delineate of cap-rock in the system (horizontal and vertical boundaries)

The Chachimbiro system has a horizontal boundary (cap rock) which is defined by low resistivity (0-10 Ωm) and is identified using interpolation of magnetotelluric data in the Petrel software (Figures 14, 17,

18, 19, 30, 31 and 32). The cap rock forms an irregular shape that covers 11 km² and its thickness is ~340 m. Possibly, the low resistivity cap rock corresponds to temperatures in the range of 50-100°C, depending on the intensity of the alteration. The transition from the low resistivity cap to the highly resistive core corresponds to temperatures in the range of 230-250°C (temperature interpreted based on high temperature geothermal systems surveys), where the reservoir would be emplaced. The horizontal natural boundaries are the Chachimbiro, Pijumbi and Azufral faults, which controlled the hydrothermal alteration in the past and still control the current raise of geothermal fluids to the surface. These structures partially enclose the cap rock in the north (Chachimbiro Fault) and cross cut the middle of the cap rock (Pijumbi and Chachimbiro). However, such enclosing geological structures have not been recognised in the south and east. Figures 7 and 8 show lineaments based on earthquakes epicentre alignments and anomaly divisions that could enclose the system; nevertheless, this should be confirmed by gravimetric and seismic data.

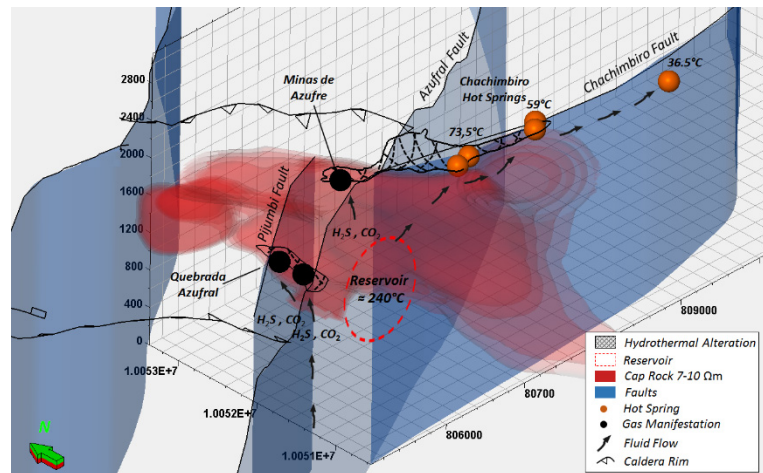


FIGURE 32: High permeability in Chachimbiro area. Hot springs are controlled by the Chachimbiro fault and low permeability at Azufral Quebrada and Minas de Azufre are controlled by the Azufral and Pijumbi faults

Axelsson (2013) mentions other components in the geothermal systems such as pressure in the system, locations of phase zones, as well as steam-dominated zones and division of systems into subsystems. The Chachimbiro project is in the surface exploration phase (preliminary study as described by Steingrímsson (2009), meaning there are no boreholes in the area. Therefore, there are not enough data available to describe all the components of the model.

6. DISCUSSION AND PROPOSAL WELL

The geothermal models of Chachimbiro area have been presented by Aguilera (2005) and SYR (2012) using surface database. They conclude that the Chachimbiro geothermal area has a small to moderate size resource with high temperature to an immature system (the geothermal fluids have not reached the chemical equilibrium) in a cooling phase, based on of the resistivity anomaly area and the geothermometers. New geochemistry data collected by MMC-MMTEC (2016) have been analysed in this report and the results are not different from SYR (2012) (reservoir temperature ~240°C). For this report the resistivity data collected by SYR (2012) was modelled using Petrel and the area extent is also comparable (11 km² to 12 km² reported by SYR in 2012). Thus, the Chachimbiro prospect should enter the exploratory drilling phase. Then the question is: Where should the first well target be located? Geothermal systems in the world have been exploited where at least two parameters (temperature and permeability) are sufficiently high. In Chachimbiro, these parameters have been in continuous discussion. Nevertheless, the only way to confirm the geothermal resource is the drilling of an exploration well.

SYR (2012) proposed to first drill a vertical well (slim hole) at location 803500E/10049900N in the WGS 84-17N (Figure 33) system. This is based on the assumption that the Azufral fault has a slight dip to the SE, and it controls the permeability in the system as well as on accessibility to the area. This point is located between the Azufral and Pijumbi faults which could ensure sufficient permeability. The well

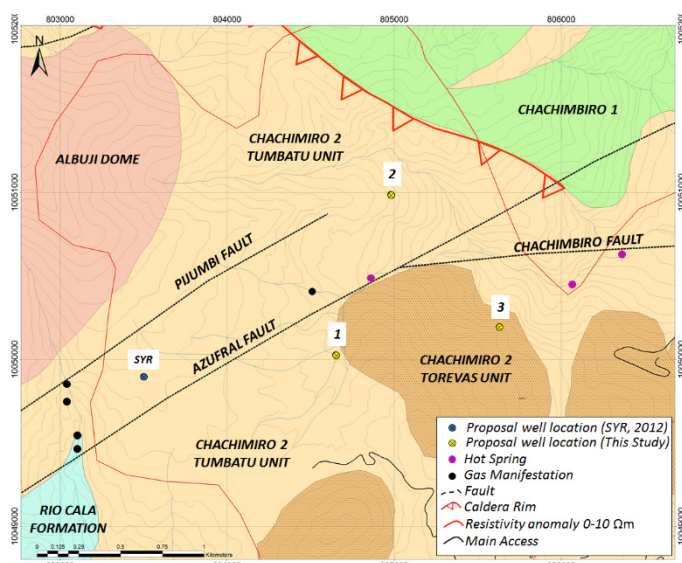


FIGURE 33: The proposed locations to drill the first geothermal well in the Chachimbiro prospect

most permeable area. This fault controls the upflow of the hottest water to the surface. Three different locations are proposed to access these targets (Figure 34).

The first proposed location is in the centre of the low resistivity anomaly (804650E/10050000N in WGS 84-17N) and beneath the high resistivity core where the upflow is located. The permeability in the sector would be controlled by the Azufral fault and the 30 Ωm resistivity anomaly (possibly 200°C) at 900 m depth and 70 Ωm resistivity anomaly (possible >250°C) at 1780 m depth would be reached.

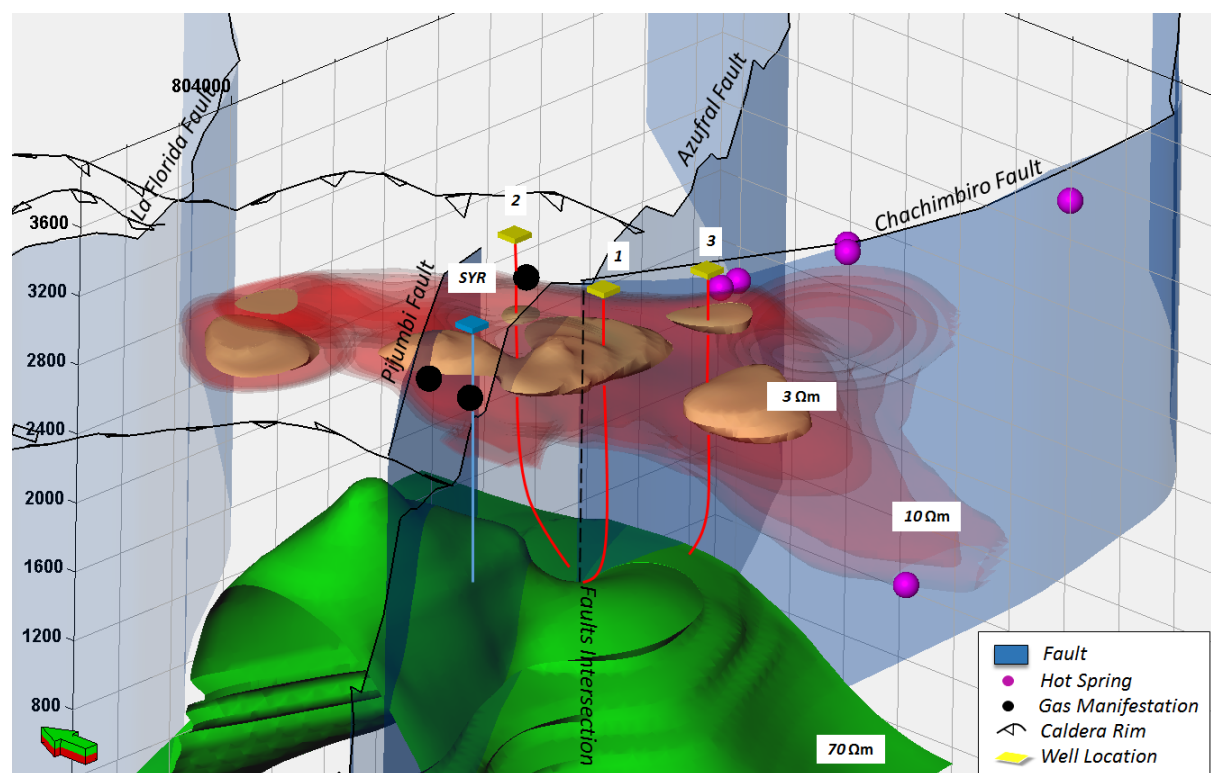


FIGURE 34: Proposed locations for the drilling of the first geothermal well in Chachimbiro prospect using Petrel

would infuse the 7-10 Ωm resistivity anomaly until it reaches the 30 Ωm resistivity anomaly, which correspond to 200°C. However, this point is on the edge of the anomaly.

The present report suggests well targets based on the permeability given by the interaction between faults, their relation with hot springs and gas manifestations, the largest hydrothermal area, the anomaly temperature by geothermometers, the possible cap rock indicated by low and high resistivity anomalies and also the suggested upflow zone. The first target is the intersection between the Chachimbiro and Azufral faults, which is covered by the cap rock and could give more permeability to the system. The second target is the Chachimbiro fault, which is apparently the

The second proposed location is at the northern border (804970E /10050950N in WGS 84-17N) but the permeability in this sector is controlled by an interaction between the Azufral and Chachimbiro faults. This location reaches the 30 Ωm resistivity anomaly (possibly 200°C) at ~1100 m depth and the 70 Ωm resistivity anomaly (possibly >250°C) at 1940 m depth.

The third is located on the opposite side of the drill point which was proposed by SYR (805600E/10050200N in WGS 84-17N), but it is closer to the resistivity anomaly centre. The permeability in the sector is controlled by the Azufral and Pijumbi faults. The 30 Ωm resistivity anomaly (possibly 200°C) is reached at 950 m and the 70 Ωm resistivity (possibly >250°C) at 1750 m depth.

The first two options are directional wells for the purpose of cutting the intersection of two faults and the third which is also a directional well that should cross the Chachimbiro fault. These wells should extend down to around 2000 m depth, where the supposed reservoir is located (Figure 34). These drill sites have been selected without consideration of road access, protected areas, relief or settlements.

7. CONCLUSIONS AND RECOMMENDATIONS

Petrel is a convenient tool to model geothermal systems. It allows the visualization in 3D including all surface data that have been collected so far to support previous interpretations as well as creating new interpretations.

Interpreted lineaments and faults are lateral boundaries of the system, which locally limit the pathways of the natural discharge of the system. However, it is necessary to correlate these interpretations with gravimetric data. A magma chamber feeds the main and lateral emission volcanic centres in Chachimbiro and is at the same time the heat source of the system. Nevertheless, the location of this magma chamber has to be confirmed with gravimetric and new passive seismicity data.

The low resistivity layer (0 to 10 Ωm) is interpreted as cap rock which covers the alleged reservoir. The resistivity model forms a concave shape where the up-flow could be emplaced. The Na/K liquid geothermometers are the most applicable in Chachimbiro and these show temperatures of around 240°C in the reservoir. This is consistent with the resistivity layers between 30 to 70 Ωm (possible 200°C to 250°C). However, the Chachimbiro hot springs show poor equilibrium with the rock and the resistivity anomalies could not represent the current temperature in the system.

The inflow in the system consists of cold recharges from the highlands in Chachimbiro area. This cold recharge of meteoric water (isotopic evidence) interacts with the up-flow under the cap rock and forms a possibly liquid dominant reservoir. The surface expressions of this reservoir are the gas manifestation in the Quebrada Azufral and Minas de Azufre areas (low permeability) and the hot springs in Chachimbiro Area (high permeability). Lateral flow discharges are located in Timbuyacu, Pinguchuela and Pilomanchi areas.

Two drilling targets are proposed in this study. The first is the intersection between the Chachimbiro and Azufral fault and the second is the Chachimbiro fault which is apparently most permeable area in the system. The choice of these targets is based on the structural, chemical and geophysical analysis done in this study. To reach these target two different locations are proposed for crossing the intersection of the faults and the third suggested a well should cross the Chachimbiro fault. From these locations, directional wells should be drilled to reach down to around 2000 m depth where the alleged reservoir is located.

A geological model derived using Petrel will be able to incorporate the new data from the well and the current conceptual model of the Chachimbiro area will be improved.

ACKNOWLEDGEMENTS

I would like to express my gratitude to Gunnlaugur M. Einarsson for his diligent assistance and advice during my research project, to Björn S. Hardarson for his support and constant monitoring of this project. I am genuinely grateful to Lúdvík S. Georgsson and Ingimar Gudni Haraldsson for the opportunity to take part in this amazing programme, to Málfríður Ómarsdóttir, Thórhildur Ísberg and Markús A.G. Wilde for their commitment and unquestionable support during my stay and study in Iceland. I wish to give my thanks to ISOR and UNU-GTP staff, who sacrificed their time to share with us some of their knowledge and experiences.

My sincere gratitude to all my classmates for enjoying the time during this incredible experience, especially to Domi, Kristof, Zsófi, Danni, Fahman, Zoly, Bondi, James and Panni who helped me and made me feel special in different ways. Thanks a lot MA for those wonderful moments.

Sincere gratitude goes to Matilde Urquiza who thrust and gave to me the opportunity to come to Iceland and also to Mario Brito for leading the development of our geothermal projects in Ecuador. Thanks to Danilo Asimbaya and Manabu Sugioka for their invaluable help during this project.

I would like to extend my gratitude to this paradise called Iceland, which is in my personal opinion one of the most extraordinary places in the world.

Finally, I want to dedicate this project to my family, to my mom Eva, my sister Michelle and my brother Richard. Everything I've done is for you.

REFERENCES

- Abaya, J.G., D'Amore, F., and Arnórsson, S., 2000: Isotopes for geothermal investigations, *In: Arnórsson, S (ed.), Isotopic and chemical techniques in geothermal exploration, development and use, International Atomic Energy Agency, Vienna*, 49-65.
- Aguilera, E., Cioni, R., Gherardi, F., Magro, G., Marini, L., and Pang Z., 2005: Chemical and isotope characteristics of the Chachimbiro geothermal fluids (Ecuador), *Geothermics*, 34, 495-517.
- Almeida, E., Sandoval, G., Panichi, C., Noto, P., and Bellucci, L., 1990: Preliminary geothermal model of the volcanic areas in Ecuador, from chemical and isotopic studies of thermal manifestations. *Geothermal Investigations with Isotope and Geochemical Techniques in Latin America, Proceedings of the final research coordination meeting held in San José, Costa Rica*, 219-236.
- Árnason, K., Karlsdóttir, R., Eysteinnsson, H., Flóvenz, Ó.G., and Gudlaugsson, S.Th., 2000: The resistivity structure of high-temperature geothermal systems in Iceland. *Proceedings of the World Geothermal Congress 2000, Kyushu-Tohoku, Japan*, 923-928.
- Arnórsson, S., Gunnlaugsson, E., and Svavarsson, H., 1983: The chemistry of geothermal waters in Iceland III. Chemical geothermometry in geothermal investigations. *Geochim. Cosmochim. Acta*, 47, 567-577.
- Axelsson, G., 2013: Conceptual models of geothermal systems – Introduction. *Paper presented at Short Course V on Conceptual Modelling of Geothermal System, organized by UNUGTP and LaGeo, Santa Tecla, El Salvador*, UNU-GTP SC-16, 12 pp.
- Beate, B., 1990: The volcanic complex Chachimbiro, first data and geothermal implications (in Spanish). *Proceedings of the 1st Conference in Earth Sciences, EPN, Quito*, November, 20-21.
- Bernard, B., Robin, C., Beate, B., and Hidalgo, S., 2010: New evolutionary model and recent eruptive activity of the Chachimbiro volcano (in Spanish). *Proceedings of the SENAYCT conference*, 6 pp.

Bernard, B., Hidalgo, S., Robin, C., Beate, B., and Quijozaca, J., 2014: The 3640–3510 BC rhyodacite eruption of Chachimbiro compound volcano, Ecuador: a violent directed blast produced by a satellite dome. *Bull. Volcanol.*, 849, 20 pp.

Cumming, W., 2009: Geothermal resource conceptual models using surface exploration data. *Proceedings of the 34th Workshop on Geothermal Reservoir Engineering, Stanford University, Stanford, CA*, 6 pp.

D'Amore, F., and Arnórsson, S., 2000: Geothermometry. In: Arnórsson, S. (ed.), *Isotopic and chemical techniques in geothermal exploration, development and use. Sampling methods, data handling, interpretation*. International Atomic Energy Agency, Vienna, 152-199.

Ego, F., Sébrier, M., Lavenu, A., Yépez, H., and Egüez, A., 1996: Quaternary state of stress in the Northern Andes and restraining bend model for the Ecuadorian Andes. *Tectonophysics*, 259, 101-116.

EOS, 2007: *Geophysics foundations: Physical properties: Electrical resistivity of geologic materials*. Department of Earth, Ocean and Atmospheric Sciences, website: www.eos.ubc.ca/ubcgif/iag/foundations/properties/resistivity.htm

Fournier, R.O., 1979: A revised equation for Na-K geothermometer. *Geoth. Res. Council, Trans.*, 3, 221-224.

GeothermEx Inc., 2011: *Initial feasibility study to develop a conceptual model for Chachimbiro geothermal project* (in Spanish). Corporación Eléctrica del Ecuador - CELEC EP and Servicios y Remediación - SYR; technical report prepared by GeothermEx, Inc., 110 pp.

Giggenbach, W.F., 1986: Graphical techniques for the evaluated water/rock equilibration conditions by use of Na, K, Mg and Ca contents of discharge water. *Proceedings of the 8th New Zealand Geothermal Workshop, Auckland, NZ*, 37-43.

Giggenbach, W.F., 1988: Geothermal solute equilibria. Derivation of Na-K-Mg-Ca geothermometers. *Geochim. Cosmochim. Acta*, 52, 2749-2765.

Granda, B., 2011: *Geological mapping 1: 25000 of the pre-Quaternary rocks, Chachimbiro geothermal project, pre-feasibility phase* (in Spanish). Technical report prepared for SyR, 18 pp.

Hofstede, R., Calles, J., Lopez, V., Polanco, R., Torres, F., Ulloa, J., Vasquez, A. and Cerra, M., 2014: *The Andean moors - what do we know? State of knowledge about the impact of climate change on the moors ecosystem* (in Spanish). UICN, Quito, Ecuador, 154 pp.

Hall, M., 2012: *Geological mapping in 1:25,000 of the Chacana geothermal project area*. Technical report for SyR, January, 94 pp.

Lonsdale, P., 2005: Creation of the Cocos and Nazca plates by fission of the Farallon plate. *Tectonophysics*, 404, 237-264.

Lumb, J.T., 1981: Prospecting for geothermal resources. In: Rybach, L, and Muffler, P.L.J. (eds.) *Geothermal systems: principles and case histories*. Wiley-Interscience, Chichester, Sussex and NY, 77-108.

McCourt, W.J., Duque, P., and Pilatasig, L.F., 1997: *Geology of the Western Cordillera of Ecuador between 1–2°S: Quito, Ecuador*. Development Corporation and Geological Research, Mining and Metalurgy, British Geological Survey, project of the Mining and Environmental Control Department, Cartographic Information Program and geology report 3; scale 1:200,000.

MMC-MMTEC, 2016: *Preparatory study for the construction project geothermal plant in Chachimbiro. Progress report (Stage 2)* (in Spanish). Mitsubishi Materials Techno Corporation - Mitsubishi Materials Corporation, report for CELEC EP, August, 178 pp.

Nieva, D., and Nieva, R., 1987: Developments in geothermal energy in Mexico, part 12-A: Cationic composition geothermometer for prospection of geothermal resources. *Heat Recovery Systems and CHP*, 7, 243-258.

Palacky, G.J., 1987: Resistivity characteristics of Geologic targets. In: *Electromagnetic methods in applied geophysics, 1. Theory*. Soc. Expl. Geophys., Tulsa, OK, USA.

Ponce, M., 2011: *Alteration map for the Chachimbiro geothermal project, Imbabura, Ecuador* (in Spanish). Technical report for SyR, September, 21 pp.

Powell, T., and Cumming, W., 2010: Spreadsheets for geothermal water and gas geochemistry, *Proceedings of the 35th Workshop on Geothermal Reservoir Engineering, Stanford University, Stanford, CA*, 393-402.

Ruiz, G., 2011: *Technical information, geological map, 1:25,000 of a part of the volcano, Chachimbiro geothermal project, prefeasibility phase* (in Spanish). Technical report for SyR, July, 1-55.

Ruiz, M., 2011: *Microseismic studies for the Chachimbiro geothermal project* (in Spanish). Technical report for SyR, November, 1-38.

Sakindi, G., 2015: *Three-dimensional inversion of magnetotelluric data: geological/geothermal interpretation of Asal geothermal field, Djibouti*, University of Iceland, MSc thesis, UNU-GTP, Iceland, report 4, 90 pp.

Schellart, W.P., Freeman, J., Stegman, D.R., Moresi L. and May, D., 2007: Evolution and diversity of subduction zones controlled by slab width. *Nature*, 446, 308-311.

Schlumberger, 2016: *Petrel E&P software platform*. Schlumberger, website: www.software.slb.com/products/petrel

SYR, 2012: *Initial prefeasibility study to develop a conceptual model for the Chachimbiro geothermal project*. Servicios y Remediación – SYR, final report prepared for CELEC EP, Ecuador, 123 pp.

Spikings, R.A., Winkler, W., Seward., and Handler, R., 2001: Along-strike variation in the thermal and tectonic response of the continental Ecuadorian Andes to the collision with heterogeneous oceanic crust. *Earth and Planetary Science Letters*, 186, 57-73.

Steingrímsson, B., 2009: Geothermal exploration and development from a hot spring to utilization. *Paper presented at “Short Course on Surface Exploration for Geothermal Resources”, organized by UNU-GTP and LaGeo, in Ahuachapan and Santa Tecla, El Salvador*, UNU-GTP SC-09, 8 pp.

Tikhonov, A. N., 1950: *The determination of electrical properties of the deep layers of the Earth's crust*. Dokl. Aad. Nauk. SSR 73: 295-297 (in Russian).

Tonani, F., 1980: Some remarks on the application of geochemical techniques in geothermal exploration. *Proceedings, Adv. Eur. Geoth. Res., 2nd Symposium, Strasbourg*, 428-443.

Vallejo, C., 2007: *Evolution of the western cordillera in the Andes of Ecuador (Late Cretaceous-Paleogene)*. Swiss Federal Institute of Technology, Zürich PhD thesis, report ETH 17023, 208 pp.

Wrightson, B., 2011: *Analysis of structural geology data for Chachimbiro geothermal project*. Technical report for SYR, December, 6 pp.

Yang, C.S., Kao, S.P., Lee, F.B., and Hung, P.S., 2004: Twelve different interpolation methods: a case study of Surfer 8.0. *Proceedings of the XX ISPRS Congress, Istanbul*, 772–777.

Yock, A., 2009: Geothermometry. *Paper presented at “Short Course on Surface Exploration for Geothermal Resources”, organized by UNU-GTP and LaGeo, in Ahuachapan and Santa Tecla, El Salvador*, UNU-GTP SC-09, 8 pp.

APPENDIX 1: Tables with geoscientific data

TABLE 1. Cross-section coordinates in Geographic Coordinate System: WGS 84 UTM zone 17S, used in order to create a resistivity data grid in Petrel

Cross-section		North	East
Cs-NE-SW-01	East	10055017.67	806411.23
	West	10048621.89	800015.45
Cs-NE-SW-02	East	10046728.61	802364.81
	West	10052774.37	805440.73
Cs-NE-SW-03	East	10046728.61	804486.13
	West	10053092.57	807455.98
Cs-NE-SW-04	East	10052790.28	808638.62
	West	10045599.53	806463.73
CS-E-W-05	East	10052456.17	801940.55
	West	10052456.17	808728.77
CS-E-W-06	East	10050653.05	800985.95
	West	10050653.05	808198.44
CS-E-W-07	East	10049698.46	802576.94
	West	10049698.46	808092.38
CS-E-W-08	East	10048531.73	802046.61
	West	10048531.73	808410.58
CS-E-W-09	East	10046940.74	807243.85
	West	10046940.74	802152.68
Cs-NW-SE-10	East	10053304.70	802152.68
	West	10047577.14	807880.25
Cs-NW-SE-11	East	10052578.15	800970.04
	West	10047683.20	805864.99

TABLE 2. Low-resistivity anomaly dimensions

Resistivity [Ωm]	Anomaly	Topography altitude above anomaly centre [m a.s.l.]	Altitude at which anomaly appears [m a.s.l.]	Thickness [m]	Estimated area [km²]
1-3	1	3559	3400	374	0.41
	2	3039	2900	129	0.17
	3	3404	3200	177	0.81
	4	3106	2900	129	0.15
	5	3372	2900	203	0.38
	6	2707	1900	622	6.88
3-5	1	3570	3500	356	0.51
	2	3330	3250	200	3.28
	3	2697	2000	736	9.13
5-7	1	3441	3234	295	5.44
	2	2691	2452	289	0.43
	3	2721	2127	1078	10.77
	4	3956	3252	52	0.13
7-10	1	3455	3414	388	11.07
	2	2794	2256	961	13.36
	3	3945	3253	65	0.34
10-15	1	3162	3420	340	31.73
	2	3958	3259	89	0.55

TABLE 3. Sample coordinates in geographic coordinate system: WGS 84 UTM zone 17S and physical parameters collected during field campaigns in 2005, 2011 and 2016

ID	X	Y	Sampling date	Location	Classification	Spring water temp [°C]	pH	EC [mS/m]
CCB-1	806309	10050611	15.4.2016	Qda. Chachimbiro	Spring water	57.9	6.37	464
CCB-2	804734	10050412	16.4.2916	Qda. Chachimbiro	Fresh water	11.2	6.16	22.9
CCB-3	806016	10050461	16.4.2916	Qda. Chachimbiro	Spring water	73.5	7.2	697
CCB-4	802789	10050579	17.4.2016	Azufral	Fresh water	9.7	7.22	18.04
CCB-5	803102	10049533	17.4.2016	Azufral	Spring water	17.6	5.6	27
CCB-6	807336	10050783	18.4.2016	Chachimbiro complex	Spring water	59.4	7.86	691
CCB-7	807184	10050638	18.4.2016	Chachimbiro complex	Spring water	58	6.43	721
CCB-8	808845	10050584	18.4.2016	Chachimbiro complex	Spring water	36.5	6.07	297
CCB-9	804014	10047195	18.4.2016	Timbuyacu	Spring water	41.3	6.69	514
CCB-10	803032	10049768	19.4.2016	Qda. Azufral	Fumarole gas	10.1	-	-
CCB-11	804474	1050426	11.6.2016	Sulfur Mine	Gas	-	-	-
40	804019	10047202	21.5.2011	Timbuyacu cement tank spr	Spring water/Gas	41	6.43	4940
45	803108	10049496	22.5.2011	Qda de Azufre stream at pt b	Spring water	-	-	-
46	810987	10047346	23.5.2011	Spr at Qda Pigunchuela	Spring water	22	6.36	1023
47	811937	10047686	23.5.2011	Qda Pigunchuela Rock Joint Spr	Spring water	30	6.04	3850
48	809642	10056070	23.5.2011	Qda Pilomachi	Spring water	24.8	33	6.16
49	806769	10051268	24.5.2011	Santa Susana 1 / Caja 1 ojo	Spring water	48.7	6.41	4020
50	807347	10050796	24.5.2011	Chachimbiro Caja 1 spr	Spring water	60.9	7.72	6760
52	803092	10049406	25.5.2011	Qda de Azufre spr below trail	Spring water	13.8	2.85	904
41	807178	10050656	21.5.2011	Chachimbiro Caja 7 spr	Spring water	56.6	6.45	6900
43	803108	10049496	22.5.2011	Qda de Azufre point a	Gas	-	-	-
56	803108	10049496	22.5.2011	Qda de Azufre point a	Gas	-	-	-
68	803108	10049496	22.5.2011	Qda de Azufre point a	Gas	-	-	-
42	803108	10049496	22.5.2011	Qda de Azufre point b	Gas	-	-	-
55	803108	10049496	22.5.2011	Qda de Azufre point b	Gas	-	-	-
69	803108	10049496	22.5.2011	Qda de Azufre point b	Gas	-	-	-
44	803108	10049496	22.5.2011	Qda de Azufre point c	Gas	-	-	-
57	803108	10049496	22.5.2011	Qda de Azufre point c	Gas	-	-	-
70	803108	10049496	22.5.2011	Qda de Azufre point c	Gas	-	-	-
51	803034	10049847	25.5.2011	Qda Pijumbi	Gas	-	-	-
58	803034	10049847	25.5.2011	Qda Pijumbi	Gas	-	-	-
71	803034	10049847	25.5.2011	Qda Pijumbi	Gas	-	-	-
53	807178	10050656	26.5.2011	Chachimbiro Caja 7	Gas	-	-	-
59	807178	10050656	26.5.2011	Chachimbiro Caja 7	Gas	-	-	-
67	807178	10050656	26.5.2011	Chachimbiro Caja 7	Gas	-	-	-
40	804019	10047202	21.5.2011	Timbuyacu cement tank spr	Gas	-	-	-
54	804019	10047202	21.5.2011	Timbuyacu cement tank spr	Gas	-	-	-
4	807317	10050820	25.7.2001	Chachimbiro	Spring water	24.8	7.31	-
18	807914	10050857	15.6.1999	Chachimbiro	Spring water	21.5	8.12	-
15	807627	10050848	14.6.1999	Chachimbiro	Spring water	23.7	7.74	-
16	807021	10050588	15.6.1999	Chachimbiro	Spring water	58.6	6.34	-
1	807021	10050588	24.7.2001	Chachimbiro	Spring water	58.3	6.21	-
17	807176	10050661	15.6.1999	Chachimbiro	Spring water	54.9	7	-
2	807176	10050661	24.7.2001	Chachimbiro	Spring water	53.4	6.37	-
19	807258	10050743	15.6.1999	Chachimbiro	Spring water	46.9	6.19	-
3	807258	10050743	25.7.2001	Chachimbiro	Spring water	47.2	6.23	-
14	807463	10050788	11.6.1999	Chachimbiro	Spring water	59.1	6.25	-
5	807463	10050788	25.7.2001	Chachimbiro	Spring water	54.4	6.7	-
6	801939	10051843	25.7.2001	-	Spring water	16.7	-	-
7	800977	10053365	25-Jul-01	-	Spring water	17.6	-	-
8	802017	10054025	25-Jul-02	-	Spring water	6.7	-	-
9	804054	10047301	26.7.2001	-	Spring water	10.9	7.76	-
11	803584	10047256	27.7.2001	-	Spring water	14.1	8.18	-
10	804098	10047122	26.7.2001	Timbuyacu	Spring water	42.2	6.46	-
13	803382	10047905	27.7.2001	Timbuyacu	Spring water	29.9	6.17	-
12	805228	10048297	27.7.2001	Timbuyacu	Spring water	17.2	-	-

TABLE 4: Chemical analysis of Chachimbiro water samples, collected during the field work by MMC-MMTEC (2016)

Sample label	Li	Na	K	Ca	Mg	SiO2	B	Cl	F	SO4	HCO3	CO3	NH4
CCB-1	2.7	677	107	74	29	141	25	1060	0.3	48	418	0	4.6
CCB-2	0	0	0	86.5	0	0	0	0	0	0	0	0	0
CCB-3	4.4	1190	187	24	14	148	39	1600	0.5	82	511	0	6.4
CCB-4	0	0	0	9	0	0	0	0	0	0	0	0	0
CCB-5	0.013	16	3.1	54.9	8.6	100	0.76	0.25	0.16	14	149	0	0.18
CCB-6	4.3	1150	148	124	52	127	41	1640	0.41	31	670	0	4.5
CCB-7	4.3	1140	136	4.5	51	123	43	1690	0.38	28	652	0	7.2
CCB-8	1.7	450	36	115.9	24	99	17	664	0.24	18	372	0	4.3
CCB-9	2	650	65	152	142	64	26	833	0.16	9.1	1700	0	3.8
Sample label	As	Rb	Cs	Sr	Ba	Fe	Mn	$\delta 18O$	$\delta 2H$	sum cations	sum anions	Charge Balance	
CCB-1	0.56	0	0	0	0	0	0	-8.6	-70	38.91	37.77	1%	
CCB-2	0	0	0	0	0	0	0	-8.6	-70	4.32	0.00	100%	
CCB-3	0.91	0	0	0	0	0	0	-7.4	-67	59.88	55.24	4%	
CCB-4	0	0	0	0	0	0	0	-12	-86	0.45	0.00	100%	
CCB-5	0	0	0	0	0	0	0	-12	-82	4.24	2.75	21%	
CCB-6	1.2	0	0	0	0	0	0	-7.2	-70	65.14	57.91	6%	
CCB-7	1.4	0	0	0	0	0	0	-7.5	-70	58.51	58.96	0%	
CCB-8	0.31	0	0	0	0	0	0	-8.6	-74	28.74	25.22	7%	
CCB-9	0.014	0	0	0	0	0	0	-8.9	-72	49.70	51.56	-2%	

TABLE 5: Resulting temperature based upon liquid geothermometer using *Plotting Spreadsheet* developed by Powell and Cumming in 2010

ID	Amorphous Silica	Alpha Cristobalite	Beta Cristobalite	Chalcedony conductivity	Quartz conductive	Quartz adiabatic	Na-K-Ca	Na-K-Ca Mg corr	Na/K Fournier 1979	Na/K Truesdell 1976	Na/K Giggenbach 1988	Na/K Tonani 1980	Na/K Nieva & Nieva 1987	Na/K Arnórsson et al. 1983	K/Mg Giggenbach 1986
CCB-1	35	107	58	133	158	150	222	71	260	243	272	285	246	247	115
CCB-3	38	110	61	136	161	152	247	129	259	242	271	284	245	246	145
CCB-7	28	99	50	124	149	143	246	21	233	207	247	245	219	214	114
CCB-9	-4	63	16	85	114	113	187	11	217	188	232	223	204	195	80

APPENDIX II: Geothermometer analysis of Chachimbiro water samples

Amorphous silica and crysobilite do not reach equilibrium in geothermal systems. These minerals are affected by the processes dilution and precipitation. These geothermometers are applicable in exploitation and production phases of the geothermal systems but not applicable to the Chachimbiro system. Also these geothermometers show very low temperature in the Chachimbiro hot spring, which indicated dilution and precipitation processes.

Quartz is the most stable and least soluble form of solid silica. This geothermometer indicates temperature from 100 to 180°C. However, the solubility is controlled by chalcedony and amorphous silica which control the silica solubility preferentially over quartz (Yock, 2009). The average temperature estimated with this quartz geothermometer is around 140°C and with the geothermometer chalcedony around 120°C. These values are closer to the second and third model proposed by SYR (2012).

The high concentration of Mg is not usual in geothermal fluids. The high concentration of Mg (> 1 ppm) in Chachimbiro fluids is explained by mixing process with cold water close to the surface. Yock (2009) mentions that the geothermometer K/Mg is useful in chloride waters with Mg concentrations <1.0 ppm and that this geothermometer is very sensitive to C_K^2/C_{Mg} ratios. Any slight addition of Mg through mixing of shallow water with the deep fluid gives cooler temperatures. Thus, this geothermometer would not applicable to Chachimbiro hot springs.

The Na/K/Ca geothermometers application would show wrong temperatures due to high partial pressure of CO₂ and ion exchange among Na-K-Ca with Mg which produces precipitation of Ca. This geothermometer is not applicable in water with high concentration of Mg either. Thus, this geothermometer is not applicable in Chachimbiro hot springs.

APPENDIX III: Resistivity and hydrographic maps from the Chachimbiro area

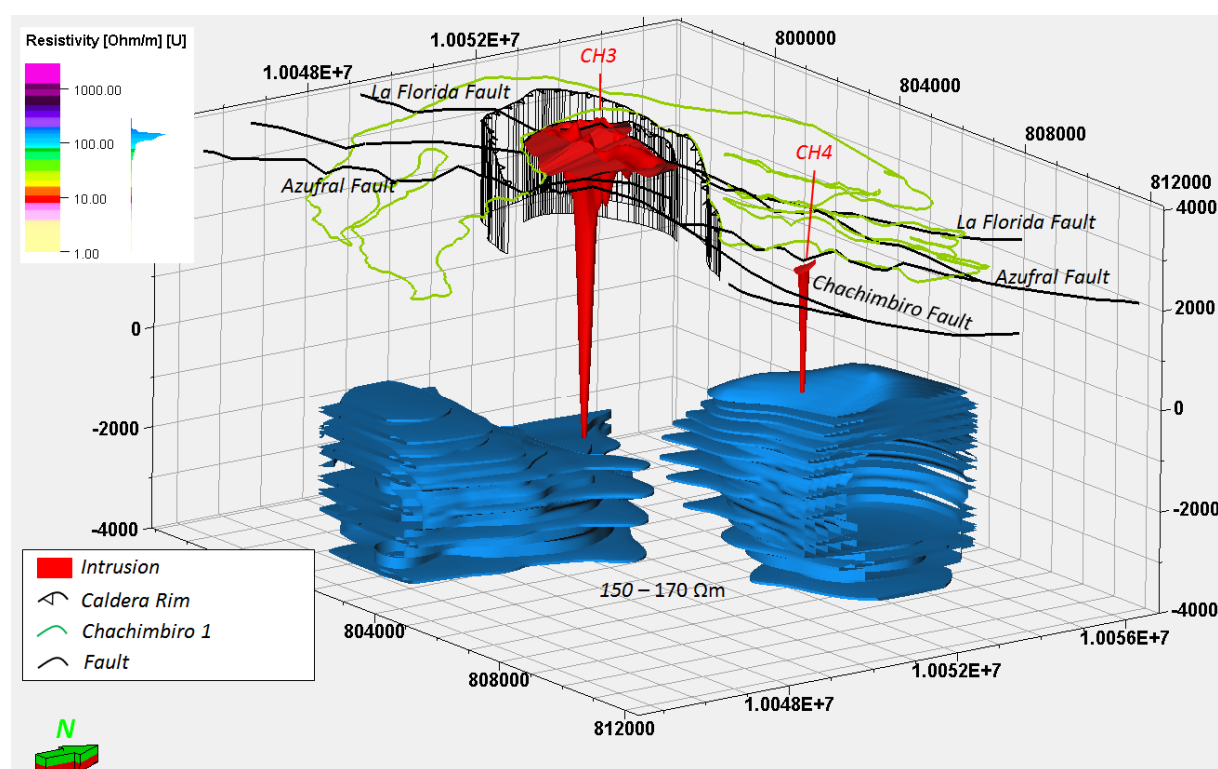
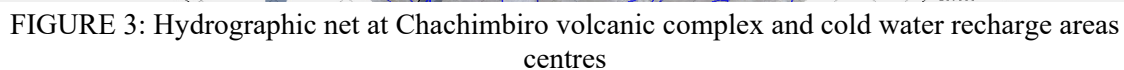
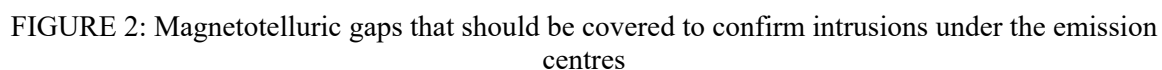


FIGURE 1: High-resistivity anomaly under Albuji/Huga domes (CH3) main emission centre and under Chachimbiro emission centre (CH4)



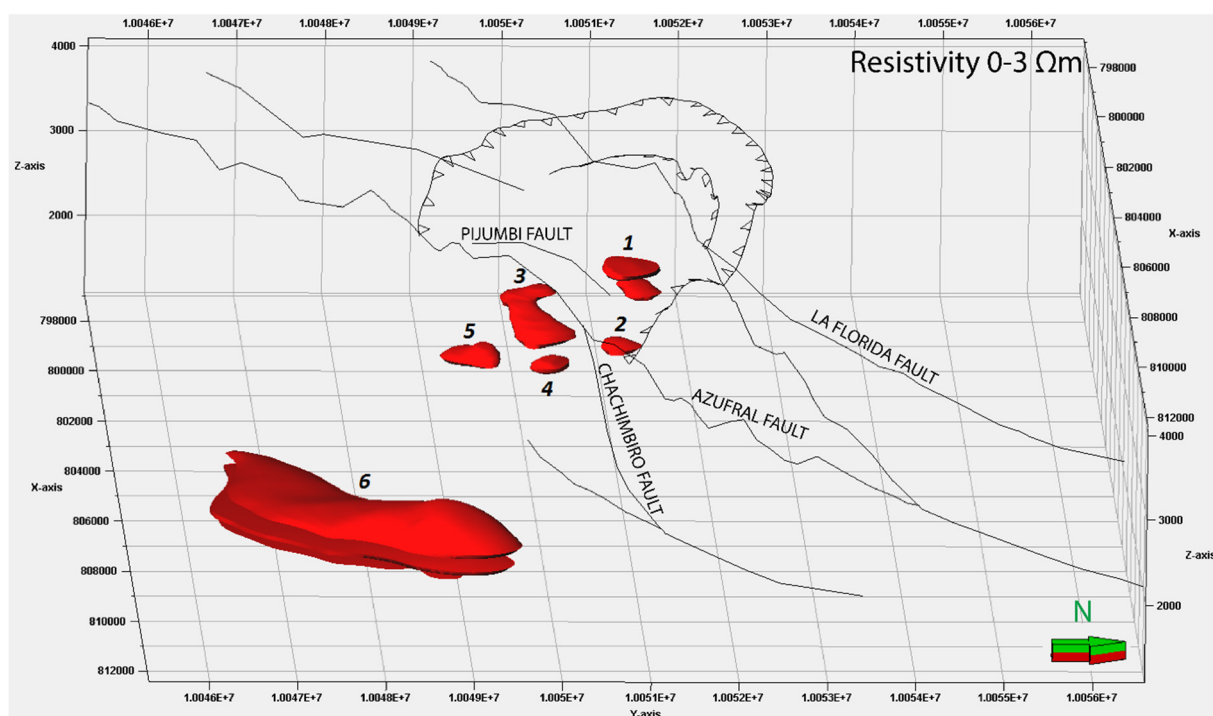


FIGURE 4: Low-resistivity anomalies for resistivity in the range 0-3 Ωm modelled in Petrel

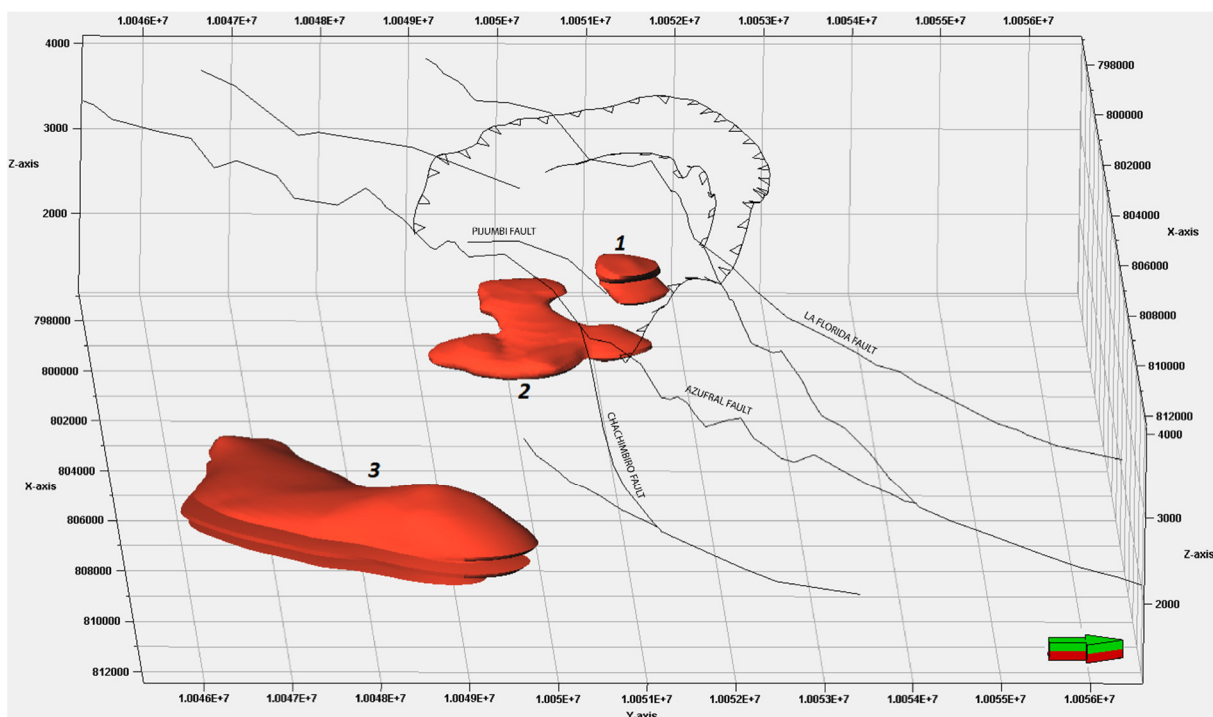


FIGURE 5: Low-resistivity anomalies for resistivity in the range 3-5 Ωm modelled in Petrel

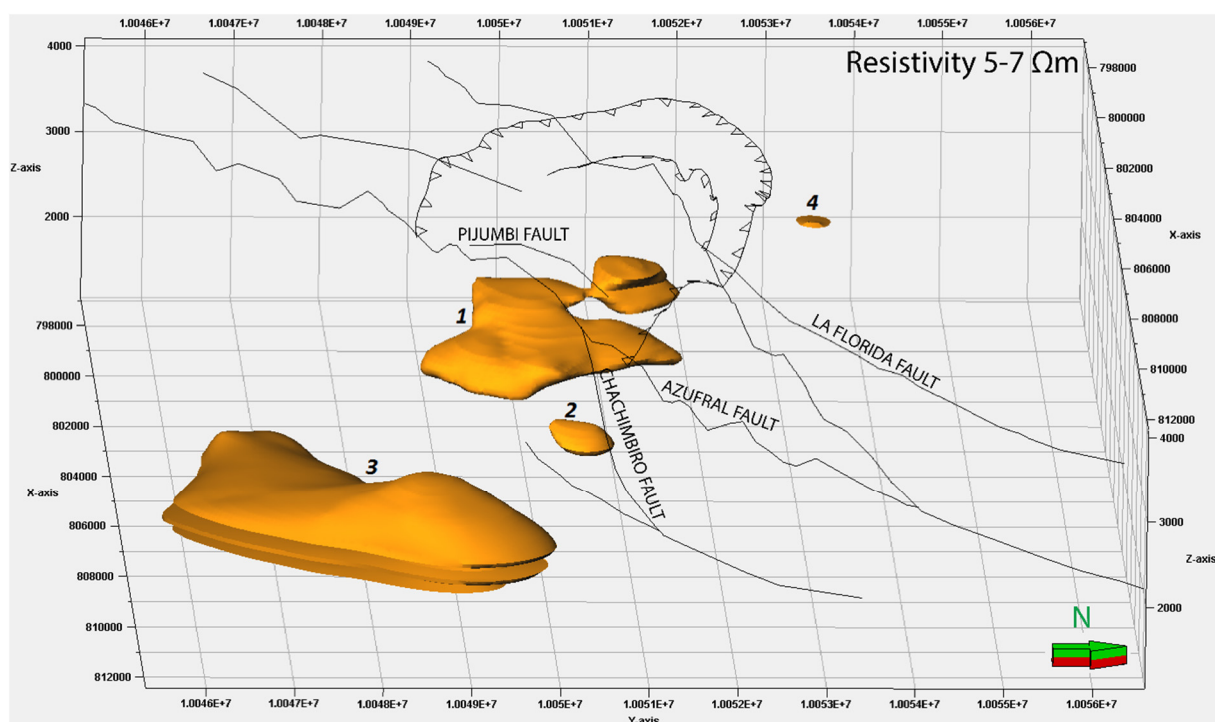


FIGURE 6: Low-resistivity anomalies for resistivity in the range 5-7 Ωm modelled in Petrel

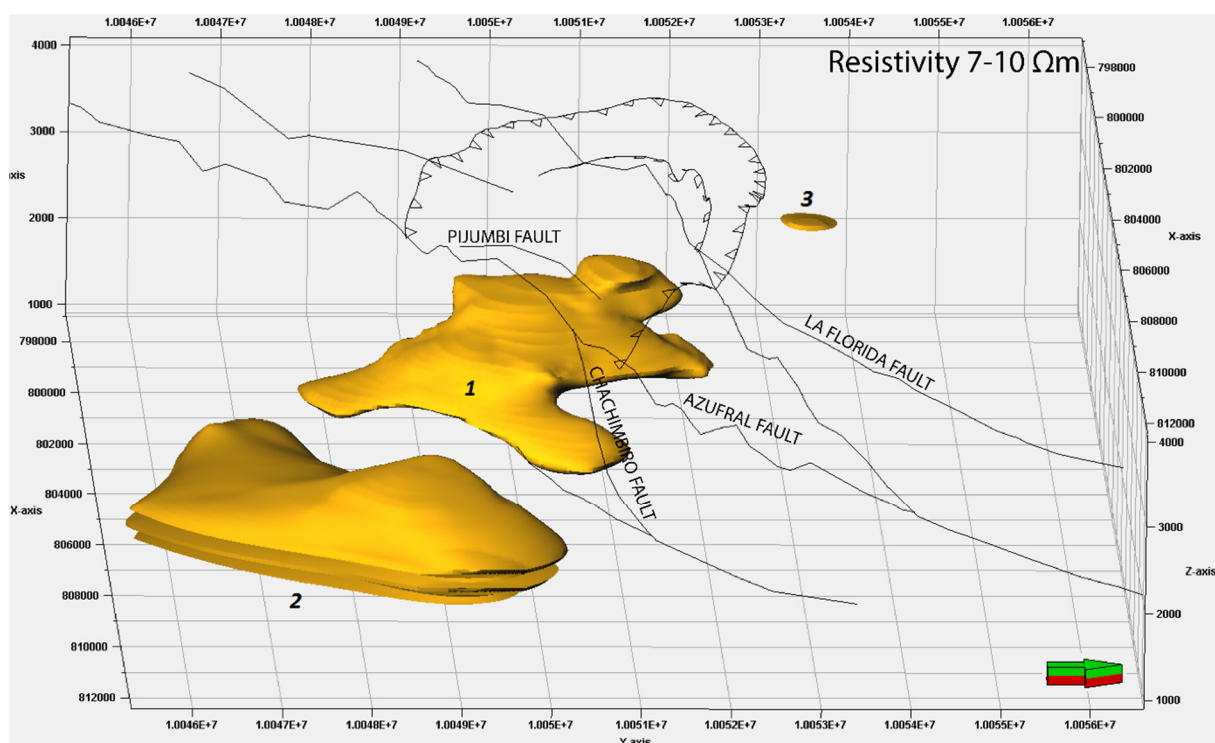
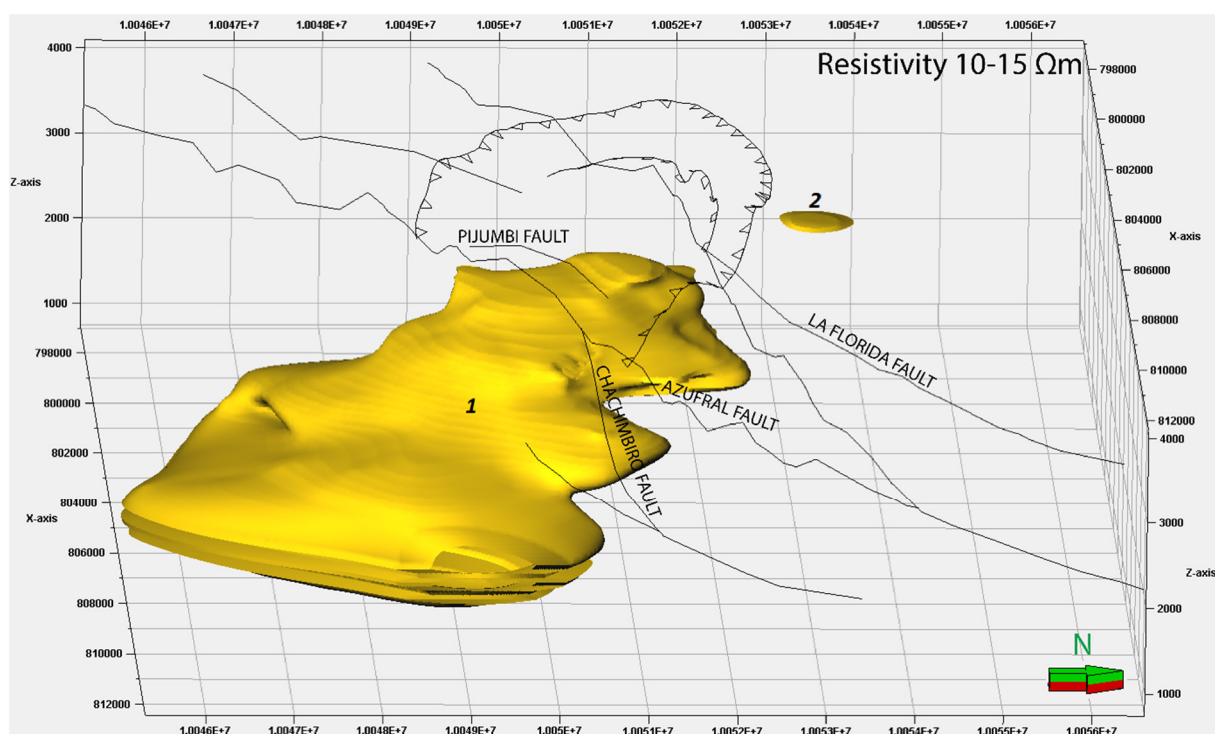
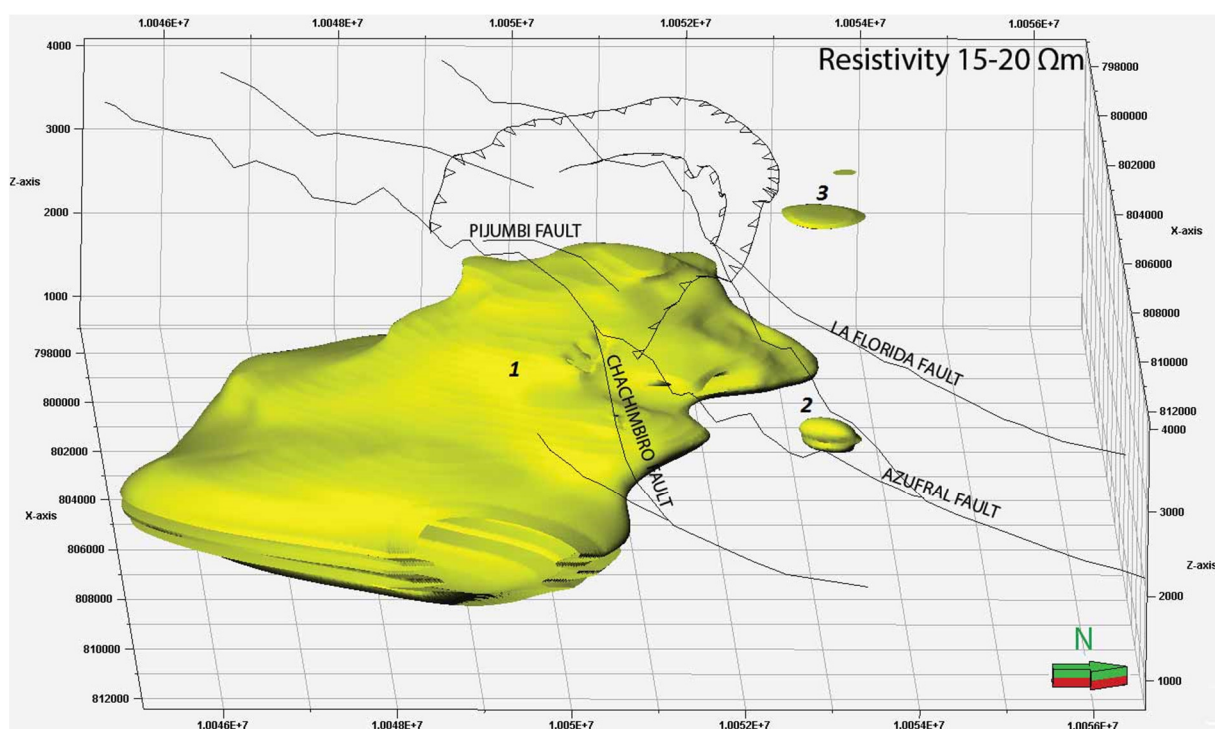


FIGURE 7: Low-resistivity anomalies for resistivity in the range 7-10 Ωm modelled in Petrel

FIGURE 8: Low-resistivity anomalies for resistivity in the range 10-15 Ωm modelled in PetrelFIGURE 9: Low-resistivity anomalies for resistivity in the range 15-20 Ωm modelled in Petrel



UNITED NATIONS
UNIVERSITY

UNU-GTP

Geothermal Training Programme

Orkustofnun, Grensasvegur 9,
IS-108 Reykjavik, Iceland

Reports 2016
Number 35

EIA OF GEOTHERMAL EXPLORATION IN TANZANIA: THE LAWS AND REGULATIONS, EIA PROCESS AND PRELIMINARY EIA OF EXPLORATION DRILLING IN NGOZI AREA, SW-TANZANIA

Esther Mtimbaru Range

Tanzania Geothermal Development Company, Ltd.

P.O Box 14801

Dar es Salaam

TANZANIA

emtimbaru2010@gmail.com

ABSTRACT

Ngozi geothermal prospect is located in the Southwest part of Tanzania. The distance from Dar es Salaam to Mbeya is 817 km. Detailed surface exploration has been carried out in the area and exploration drilling is expected to prove the existence of a geothermal resource. Environmental laws and regulations in the country that have to be taken in account during the EIA process are presented. A preliminary EIA of the three main environmental factors that the project is expected to have impact on i.e. noise, land use and social economy, is introduced. Mitigating measures are proposed for the aforementioned impacts. The report aims to provide a basis for future EIA work for geothermal exploration drilling in Tanzania. A detailed Environmental Impact Assessment based on evaluation of baseline data is recommended as a first step to provide a better understanding of the potential impacts and mitigating measures during the development.

1. INTRODUCTION

The United Republic of Tanzania is a large country in Eastern Africa, consisting of Tanzania mainland and Zanzibar. It is located between longitudes 29° and 41° east and latitudes 1° and 12° south. It is bordered by Kenya and Uganda to the north, Rwanda, Burundi and Democratic Republic of Congo to the west, Zambia, Malawi and Mozambique to the south and by the Indian Ocean to the east (NBS, 2012) as shown in Figure 1. It covers a total area of 947,303 km² and has a population of estimated 53.47 million inhabitants (2015) (Worldometers, 2016). The population is diverse, composed of several ethnic, linguistic and religious groups.

Tanzania is endowed with diverse forms of energy resources including natural gas, hydro, coal, biomass, geothermal, solar, wind and uranium, most of which have not been optimally utilised. In May 2014, Tanzania's total installed electric generation capacity was 1,583 MW composed of hydro (561.82 MW), natural gas power plants (527 MW) and liquid fuel power plants (495 MW). Tanzania also imports small amount of electricity from Uganda (10 MW), Zambia (5 MW) and Kenya (1 MW) (ESI reform strategy and road map; MEM, 2014a). On the mainland of Tanzania only 24% of the population is connected to electricity. The demand for electricity is growing by 10-15% per year and the main reason is increased



FIGURE 1: Location map (Nations Online Project, 2016)

socio-economic activities. By 2025, the demand is predicted to be around 8,000 MW. Therefore, to meet such demand, the installed capacity must increase to at least 10,000 MW. To nurture the desired socio-economic transformation, the access to modern energy services in an affordable, reliable, sustainable and environmentally-friendly manner is inevitable (MEM, 2014a). Tanzania through its implementing agency TGDC (Tanzania Geothermal Development Company) anticipates to start drilling geothermal exploration wells by the end of 2017 in Ngozi geothermal prospect.

This study is intended to gather important information on the legal issues and the Environmental Impact Assessment (EIA) process in the country to support the preparation of future geothermal development. A preliminary EIA of the most important environmental factors that the Ngozi project is likely to affect; land use, social economy and noise, is introduced.

2. GEOTHERMAL EXPLORATION IN TANZANIA

Geothermal energy has so far not been utilized in Tanzania but is estimated to be a realistic resource. The estimated geothermal potential exceeds 5000 MW (TGDC, 2014). More than 50 areas with geothermal activities, mainly hot springs, have been identified and most of these areas are located in the East African Rift system (EARS) (Figure 2). In Figure 2 are shown the 50 areas with geothermal activity, the four main areas within the red circles, the two subareas where geothermal exploration has been licensed, Rungwe and Mbeya, are shown as red dots.

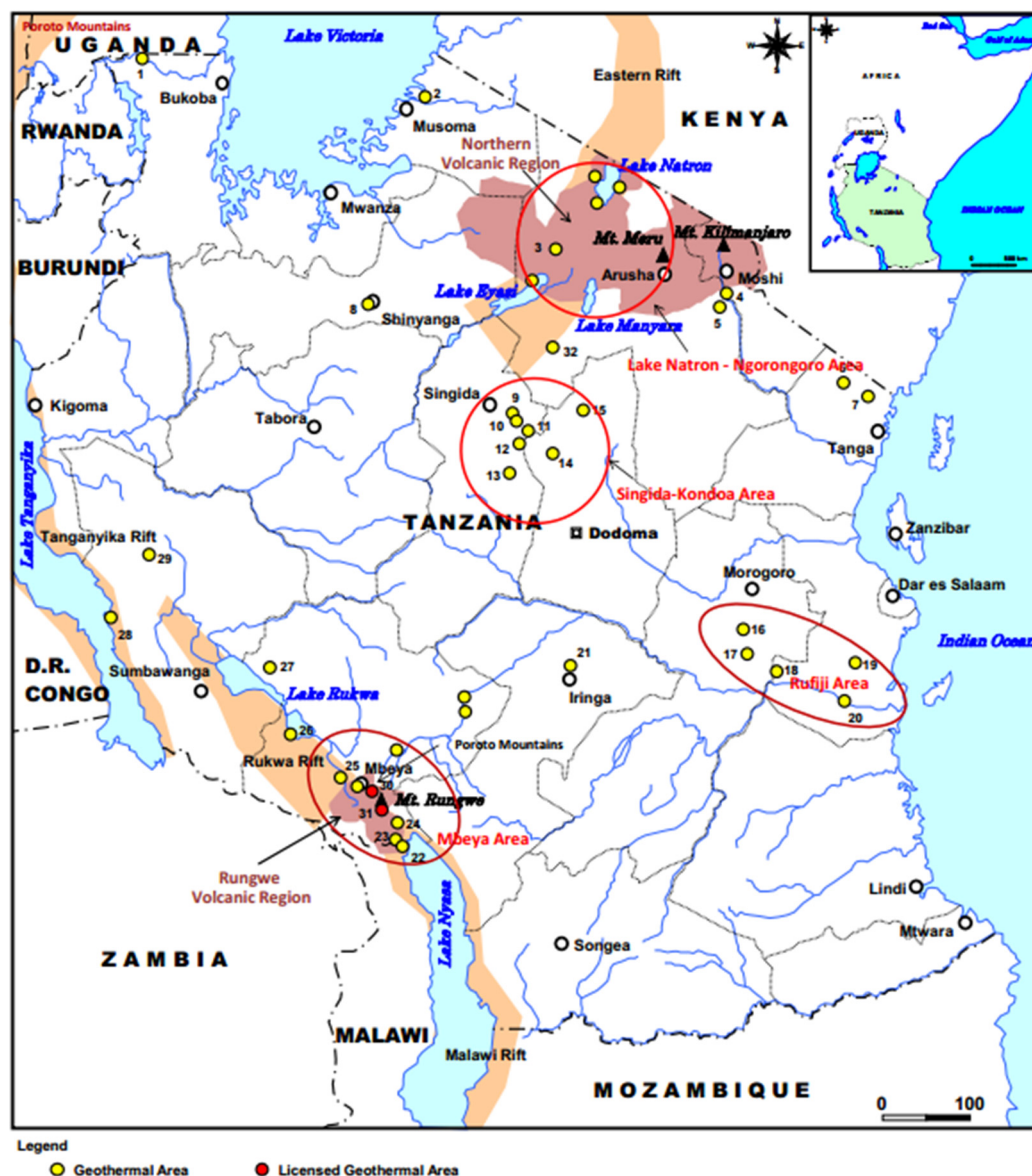


FIGURE 2: Geothermal areas in Tanzania (modified from Mnjokava, 2012)

The geothermal areas are mainly located in four parts of the country which are the Northern Volcanic regions such as Kilimanjaro and Ngorongoro near the border with Kenya, in Singida and Kondoa in the central part of the country, in Rufiji in the East Coastal belt, and in the Rungwe volcanic region and Mbeya in the Southwest part. Detailed surface exploration studies have only been carried out in the Southwest part and mostly in the Ngozi geothermal area in Mbeya as it is believed to be the most promising area.

A Swedish consulting group (SWECO) and Virkir Orkint Consulting Group of Iceland conducted geothermal surface exploration in the country from 1976 to 1978. They did temperature measurements in 50 hot springs. The result was that high-temperature areas were identified around Lake Manyara, Lake Natron, Ngorongoro crater and Mbeya. These areas are considered to be promising for further research (SWECO, 1978).

A prefeasibility study focusing on geological mapping, structural geology, rock/fluid sampling and geochemical characterization of thermal and non-thermal fluids, hydrogeological studies and preliminary geophysical surveys were conducted (Kraml et al., 2008). The results of these studies indicated the presence of active faults allowing fluid circulation, abundant meteoric recharge and a young volcanic heat source capable of driving sustained hydrothermal circulation. Chemical and isotopic analyses of surface thermal manifestations pointed to the existence of a high temperature geothermal resource in the Songwe-Ngozi area, Mbeya region. Preliminary geophysical studies pointed to the existence of a geothermal reservoir.

Detailed geophysics (MT and TEM) and additional bathymetric and hydro geochemical studies at Lake Ngozi were carried out. Bathymetric and hydro geochemical studies indicated occurrence of vent/fault structures in the caldera floor, associated with high bottom temperatures and sub lacustrine hydrothermal activity in Lake Ngozi (Kraml et al., 2012). Volcanological and isotopic investigations provide first evidences that a shallow crustal level trachytic magma chamber, associated to caldera structures at Ngozi volcano, is capable of providing a long-lived heat source for hydrothermal circulation in the Ngozi-Songwe area (Kraml et al., 2008). Tectonic investigations have shown that the fluid flow is fault-controlled (fracture permeability). Most thermal springs are aligned along the major NW-SE Rukwa-Malawi Rift trend (long-living, often reactivated, continuous faults). Thermal waters have dominant Na-HCO_3 to Na-(Ca-Mg)-HCO_3 composition, due to high dissolved CO_2 contents, which favours silicate weathering and cation exchange reactions. Additional, progressive fluid/rock interaction causes increase in salinity and Na enrichment in hot spring waters by Ca removal through precipitation of secondary minerals. CO_2 -rich fluids derive predominantly from a deep-seated mantle/magmatic source, although local crustal and biogenic contribution may be high.

3. ENVIRONMENTAL LAWS AND REGULATIONS IN TANZANIA

3.1 General

Tanzania responded to international/global environmental processes by enactment of the National Environment Management Act 1983, creating an environmental council (known as National Environment Management Council – NEMC) which became operational in 1986, the formulation and approval of the National Environmental Policy 1997 and the recent Environmental Management Act (EMA) of 2004. Additional, Tanzania has ratified several Multilateral Environmental Agreements. NEMC oversees the environmental management matters in the country. It has the responsibility in the EIA process to make decisions on screening, scoping and Environmental Impact Statements (EIS) and to advice the Minister of the Environment on whether a project should proceed or not.

3.2 Environmental policy

The National Environmental Policy (NEP) was adopted in 1997, at the same time as the country was just beginning to implement its economic transformation programs. The policy includes a framework for environmental planning and management and cross sectoral and sectoral guidelines for environmental governance and management. Table 1 lists sectoral policies that are relevant to geothermal exploration activities in the country.

TABLE 1: Sectoral policies

- | |
|---|
| <ul style="list-style-type: none"> ○ National Land Policy, 1995 ○ Agriculture Policy, 1997 ○ National Forestry Policy, 1998 ○ Health Policy, 1998 ○ National Tourism Policy, 1999 ○ National Human Settlement Development Policy, 2002 ○ National Water Policy, 2002 ○ National Energy Policy, 2003 ○ National Transport Policy, 2003 ○ Wildlife Policy of Tanzania, 2007 ○ Mineral Policy of Tanzania, 2009 |
|---|

3.3 Environmental law

The Environmental Management Act no. 20 was adopted in 2004, at the same time as the process of privatisation of economic development was advanced. The Act includes an implementation framework for the national policy and the legal and institutional framework for sustainable environmental management. Table 2 lists a number of sectoral acts that are relevant to geothermal exploration activities in the country. The key players in environmental management are the National Advisory Committee, Director of Environment, The National Environment Management Council, Regional Secretariat and local government authorities.

TABLE 2: Sectoral acts

- | |
|--|
| <ul style="list-style-type: none"> ○ The National Parks Ordinance Act No. 12, 1959 ○ Petroleum (Exploration and Production) Act No. 27, 1980 ○ Land Act No. 4, 1999 ○ Village Land Act No. 5, 1999 ○ EWURA Act No. 11, 2001 ○ Forest Act no. 14, 2002 ○ Industrial and Chemical Management Act No. 3, 2003 ○ Fisheries Act No. 22, 2003 ○ Occupational Health and Safety Act No. 5, 2003 ○ Rural Energy Act No. 8, 2005 ○ Land Use Planning Act No. 6, 2007 ○ Electricity Act No. 10, 2008 ○ Tourism Act No. 29, 2008 ○ Water Resources Management Act No. 11, 2009 ○ Water Supply and Sanitation Act No. 12, 2009 ○ The Wildlife Conservation Act No. 5, 2009 ○ Mining Act No. 14, 2010 ○ Petroleum Act No. 8, 2015 |
|--|

3.4 EIA and audit regulations

The EIA and Audit regulations were adopted in 2005 (G.N. No. 349 of 2005). They provide guidelines on how to conduct EIA and environmental audits as provided for EMA. Environmental Impact Assessment and audit regulations emphasize the importance of conducting an EIA before any development project is implemented. The regulation also gives an outline of the nature of development

projects that need an EIA study. The regulations include a public hearing. In addition, the regulations require that an EIA must be conducted by a registered environmental expert, as referred to in part IV section 14 of the regulations and the registration of environmental expert has to be conducted as stipulated in part V of the regulations (G.N. No. 348 of 2005) (United Republic of Tanzania, 2005).

3.5 International conventions

When developing a project, it is important to take into account several international agreements. In most countries, laws on EIA exist and are founded partly on Multilateral Environmental Agreements (MEAs), such as The Espoo (EIA) Convention, 1997, and the Rio Declaration, 1992. It is well known that projects have to comply with requirements from international banks if the project is to be funded by them. The investment banks, like the World Bank (WB), African Development Bank (AfDB), European Investment Bank (EIB) and Japanese Bank for International Cooperation (JBIC), have environmental safeguards to ensure that projects financed by them are not only based on the precautionary principle and preventative actions but also mitigations and sustainable development. A good example is the World Bank Operation Policy 4.01 on Environmental Assessment and the World Bank Operation Policy 4.12 on involuntary resettlement/relocation and compensation.

3.6 Conclusions on environmental laws and regulations

The key act, regulation and policy for geothermal development that need to be fulfilled are the EMA 2004, NEP 1997 and EIA and audit regulations, 2005. It is important for a developer who plans to develop geothermal resources, to study sectoral acts and policies from the very beginning to secure that the project is in accordance with these. The most important sectoral acts and policies in Table 1 and 2 that the developer must fulfil are Land Act, Industrial and Chemical Management Act, Occupational Health and Safety Act, Land Use Planning Act, Electricity Act, Water Resources Management Act, Water Supply and Sanitation Act, National Land Policy, Health Policy, National Water Policy, National Energy Policy and National Transport Policy. However, the laws and policies to be considered for geothermal development are largely dependent on where the project is located. Considering the policy and laws on environment in the country, there is a need to inform the public on all the environmental consequences of a project as it is important for the people to be aware of the economic value of the goods and services they obtain from the environment and the project could have positive and negative impacts on those. There is also a need to review, in close corporation with the government, environmental experts and development partners, the current policy, the National Environmental Policy of 1997 and update, to take into account the issues of globalisation, transformation economic and climate change.

4. ENVIRONMENTAL IMPACT ASSESSMENT (EIA) PRACTICE IN TANZANIA

4.1 General information

Environmental Impact Assessment (EIA) can simply be defined as a systematic examination to determine whether or not a policy, programme, plan or a project will have any adverse impacts on the environment, nature or society. It is also an important management tool for improving the long-term viability of projects. The role of EIA for sustainable development was highlighted at the United Nations Conference on Environment and Development (UNCED) in 1992, as principle 17 of the Rio Declaration states:

“EIA, as a national instrument, shall be undertaken for proposed activities that are likely to have significant adverse impact on the environment and are subject to a decision of a competent national authority”

Tanzania is a signatory of the Rio Declaration. In 1996, African environment ministers, including Tanzania, reaffirmed this commitment and pledged to formalise the use of EIA within legislative frameworks at the project, program and policy levels. Now the Environmental Management Act Cap 191 from 2004 and the Environmental Impact Assessment and Audit Regulations from 2005 emphasize the importance of conducting an EIA before any development project is implemented (Mwalyosi et al., 1999).

4.2 EIA process in Tanzania

The EIA process is described in the FOURTH SCHEDULE of the EIA and audit regulations G.N. No. 349, 2005. The timeframe and key responsibilities are shown in Table 3. Currently, all EIA projects are being administered at the National level by NEMC. In Figure 3 is the EIA process in Tanzania better explained and the picture makes it easy for different stakeholders to see where they are involved and what their responsibilities are in the EIA process. In the following text there are the phases I to V of the EIA process explained.

TABLE 3: The EIA process in Tanzania

Activity	Documents	Responsible	Timeframe
Phase I: Project registration	Project registration to NEMC (submit 10 copies of project brief)	Developer and EIA Expert	Unlimited time for Developer for field work and report writing
Screening decision		NEMC	45 days to do screening
Phase II: Scoping study	Scoping report with ToR (submit 5 copies to NEMC for approval)	Developer and EIA Expert	Unlimited time for Developer for field work and report writing
Scoping decision		NEMC	30 days for NEMC to review and approve/make a decision
Phase III: EIA study	Draft EIS to NEMC (submit 15 copies)	Developer and EIA Expert	Unlimited time for Developer for field work and report writing
Review (NEMC and TAC)		NEMC/TAC	30 days for NEMC and TAC to review
Phase IV: Review of Draft EIS (Developer by incorporating the comments)	Final EIS to NEMC (submit 5 copies)	Developer, EIA Expert	Unlimited time for Developer to prepare final EIS
Phase V: Review and issuance of EIA certificate	Approval process and EIA certificate	NEMC and Minister of Environment	30 days for Minister of Environment to review final EIS

Phase I

Project registration

In the first step of the EIA process a developer or proponent registers a project at the National Environment Management Council (NEMC) by submitting a project brief, a filled application form together with the pre described fee (as described in Part III Sections 5–11 of the EIA regulations). The project brief has to include information about the nature, location, activities and design of the project, the materials to be used, products and by-products, generated wastes and the methods of their disposal. It has also to include a description of the potential environmental impacts and possible mitigation measures, plan for health and safety of the workers, the economic and soci-cultural impacts to the local community and the nation in general.

Screening

NEMC does the screening, built on the project brief and the application information, to determine whether an EIA should be undertaken. NEMC submits a copy of the project brief to the relevant

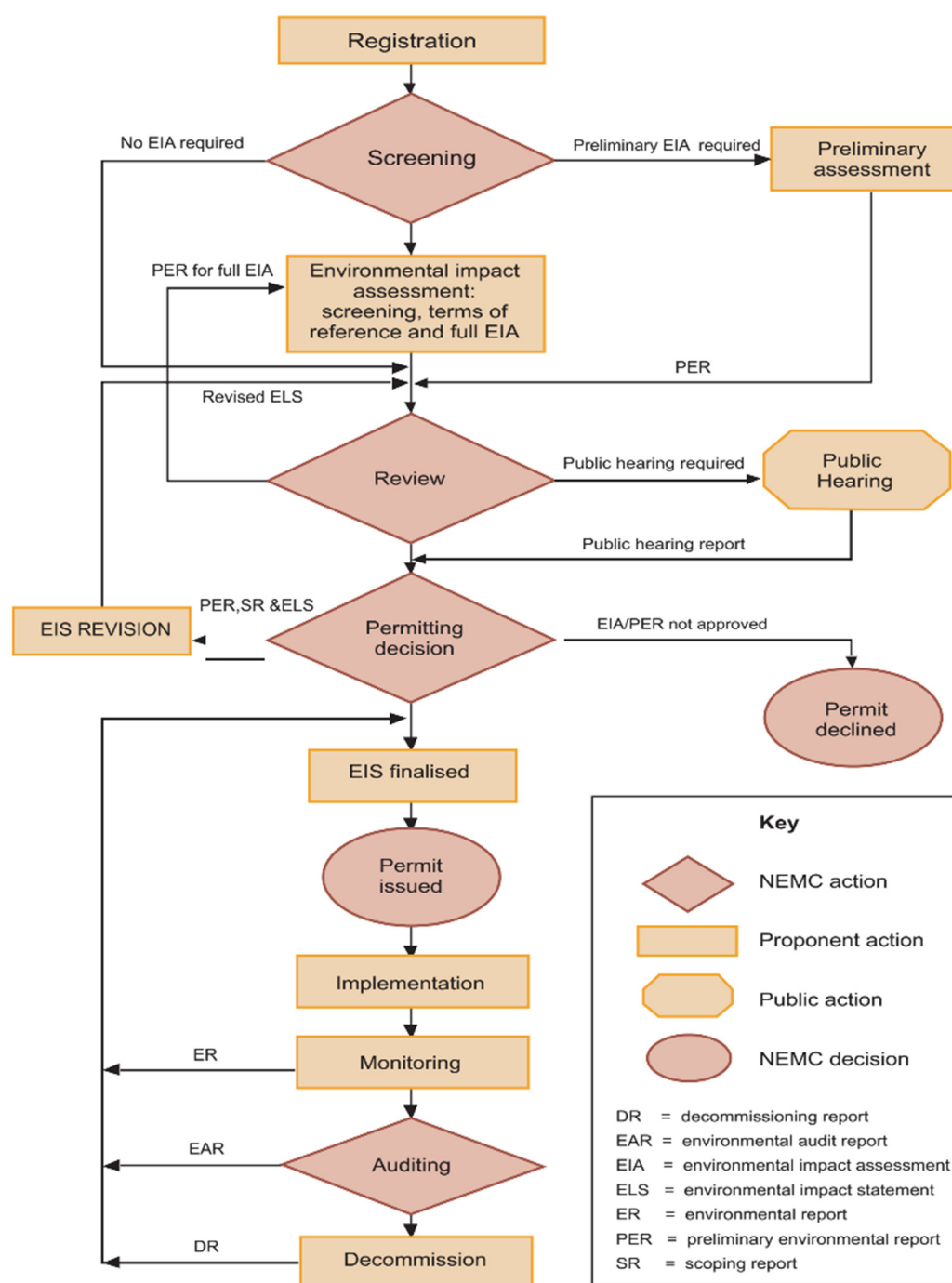


FIGURE 3: EIA administration (MEM, 2014b)

ministries or public agencies and the relevant local environmental management officer. Where more than one district is involved a copy is sent to the relevant regional secretariat, for their comments. They have 21 days to deliver their comments. The screening decision must be taken by NEMC within 45 days from the date of submission of the project brief. When NEMC finds that the project has or may have significant impacts on the environment, the proponent has to undertake EIA or undertake a preliminary assessment when more information is required to determine a screening decision. When NEMC finds that the project will not have significant negative impacts on the environment, it does not require an EIA and may be recommended to the Minister of environment for approval of the project.

Phase II*Scoping and terms of reference*

When NEMC decides that an EIA is necessary the developer carries out a scoping study. The scoping process involves the preparation of the scoping document which is submitted to the same parties as in a screening process. The document is built on the existing information and involves e.g. a description of the project and the environment where the project is planned. It includes an identification of environmental factors that the project may have potential positive and/or negative impacts on and expected boundaries of the project (special, temporal and institutional). It further contains a description of which areas might be affected by different parts of the project and a map or description of the area that needs to be studied to gain baseline information for the valuation of possible impacts on the environment. It also describes the projects' alternatives that will be assessed and compared in the EIS, list of stakeholders to be consulted, public participation and last but not least is a Terms of Reference (ToR). The ToR must be very precise because it is a description of what information will be gathered, which studies/research is needed and how the information and results will be come forward in the EIS (text, tables, pictures, maps etc.). The ToR is a checklist for NEMC to compare the EIS and to what the EIS must comply. In the EIA process and preparation of the EIS the developer must follow the scoping document or otherwise explain why he is not doing so.

Phase III*Impact assessment*

The EIA process involves impact identification, prediction, evaluation and mitigations of relevant effects of a development proposal before major decisions are taken or a project is permitted. In the process a variety of appropriate techniques and approaches are used. The assessment must be in accordance with the ToR and has to take into account the concerns and views of the key stakeholders (those who are or are likely to be affected by the project) as well as from relevant governmental agencies and the public. The main part of the assessment is the gathering of necessary information on the environment, evaluating the impacts and writing the EIS. The process also includes the assessment of relevant alternatives and leads to recommendation of the most appropriate options. An important part of the process could also include actions to minimise negative impacts of the project by changing the original project or reducing the impacts. If the project does still have negative impacts after these actions mitigation measures must be introduced. A project can also contribute to social development and environmental conservation. Preparation of a monitoring plan and environmental and social management plan can also be a part of the EIA process with details about institutional responsibilities, monitoring framework, parameters to be monitored, indicators for monitoring and costs of monitoring where appropriate. The time taken to carry out an EIA depends on the type of a project, its complexity, availability of environmental information and the research that needs to be carried out.

Preparation of an environmental impact statement

An EIS is a detailed report prepared by a developer and submitted to the NEMC. Part V of the EIA and the audit regulation of 2005 inform about the content of an EIS. It must include all important components relating to the project in accordance with the scoping decision i.e. approval of a ToR. In the EIS there has to be a non-technical summary both in Swahili and English, stating the key findings, conclusions and recommendations of the assessment.

Phase IV*Review process of environmental impact statement*

The review of an EIS is done by the NEMC in collaboration with the Cross Sectoral Technical Advisory Committee adhering to the review criteria (Part VI of the EIA and audit regulations, 2005). The NEMC has 30 days to finish the review. It may call for a public hearing and public review of the EIS. The NEMC submits to the minister of environment a review report with its recommendations and all documents used in the review process for approval or disapproval.

Phase V

Permit issued

The minister has to make a decision on an EIS within 30 days of receiving the recommendations from NEMC. The decision, including a justification, must be given out in written form. The Minister can either approve or not approve the EIS, an approval can be attached to specified conditions which the developer has to meet.

Environmental monitoring and auditing

Environmental monitoring is done by NEMC to evaluate the performance of the mitigation measures addressed in the Environmental and Social Management Plan as well as in the Monitoring Plan. The developer conducts an internal monitoring of an ongoing project to ensure that the project is in accordance with the Ministers' decision, licences and that the mitigation measures are effective. The NEMC conducts three types of auditing, an implementation/enforcement audit, a performance/regulatory audit and an impact prediction audit.

Decommissioning

Decommissioning at the end of a projects' life, involves rehabilitation of the land and ecological restoration, tearing of the project infrastructure, and dismantling of equipment and machinery. The developer prepares a decommissioning plan either as a part of the EIS or separately and submits it to the NEMC for approval. According to the Environmental Management Act, 2004, decommission will be done by the developer at his own cost (United Republic of Tanzania, 2004).

5. NGOZI GEOTHERMAL FIELD

5.1 General description of the area

Ngozi geothermal area is located in Rungwe and Mbeya rural districts in Mbeya region, in the southwest of Tanzania. The area is accessible by aeroplanes, TAZARA railway or roads from Dar es Salaam to Zambia. The distance from Dar es Salaam to Mbeya is 817 km and it takes 12 hours to travel by bus and 1.30 hours by air. However, the accessibility is difficult from Mbeya towards Ngozi and Rungwe volcanoes due to rugged and steep terrain. The existing roads are tarmacked within Mbeya town and untarmacked towards Ngozi geothermal area, thus there will be a need to rebuild the existing roads and construct new ones. The area is at the borders of the Poroto Ridge Forest Reserve and Itunza Forest Reserve. All forests belong to Tanzania Forest Services Agency of the Ministry of Natural Resources

and Tourism. These forests are core attraction for tourists, who frequently come to see the amazing landscape, scenery and vegetation. Hiking to the top of the mountains is popular among tourists to have a good view of the Great Rift Valley. Monkey and bird species are also found in the forest.

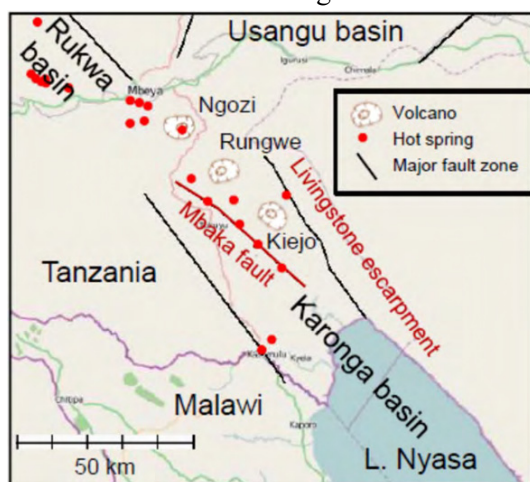


FIGURE 4: Rungwe volcanic complex with the Ngozi, Rungwe and Kiejo volcanos (Kraml et al., 2012)

5.2 Geoscientific exploration

The field is located within a rift-rift-rift triple junction (Rukwa Basin, Karonga Basin and Usangu Basin) (Fontijn et al., 2012) (Figure 3). In the area are also the quaternary volcanoes, Mbeya, Rungwe, Kiejo and Ngozi. There are many volcanic cones around volcanic mountains forming a structural line which is NW-SE oriented as shown in Figure 4. K-Ar dating of younger volcanic rocks and U-Th dating of the Songwe travertine

show that Ngozi geothermal system started to be active around 360 ka ago (Delvaux et al 2010). The magmatic activity in Mbeya area started in Miocene times. The last eruption in the Rungwe area occurred in Kiejo about 200 years ago (Harkin, 1960). Most of the thermal springs in the area are aligned along the major NW-SE rift trend. The results from the electromagnetic surveys (TEM, MT) show zones of low resistivity in the Ngozi area, which can possibly be correlated to alteration zones formed by geothermal activity (GEOTHERM, 2006).

5.3 Description of the environment

This section describes the existing environment in the area and draws a picture of what environmental factors might potentially be impacted by the exploration drilling. It gives a general overview of the study area, including the community, the climate, soil condition and land use, flora and fauna, the available water sources and the existing infrastructure (mainly the road conditions). However, detailed baseline studies should be carried out in the area to provide information for possible future changes and to minimise negative impacts.

The community

The project area is located in two districts, Rungwe and Mbeya rural in Mbeya Region. The two districts have a population of about 650,000 people and the number of each gender is equal. The population density is 39 persons per km². The region is considered to be moderately densely populated compared to the rest of Tanzania (United Republic of Tanzania, 2013). The main indigenous ethnic groups are the Nyakyusa, Ndali and Safwa. Most of the ethnic groups are predominantly agro-pastoralists and their main economic activities are agriculture and livestock keeping. The crops cultivated are maize, wheat, pyrethrum, coffee, beans, bananas and Irish potatoes. These are both food and cash crops. Small scale farming occupies the largest portion of the area but there are a few large plantations of tea and coffee (Figure 5).



FIGURE 5: A) Tea plantation in Rungwe area. B) Irish potatoes farming (field study, March 2015)

Climate

The climate of the Mbeya region is generally tropical with marked seasonal and altitudinal temperature variations and a sharply defined dry season (dry cooler conditions and a fairly constant southerly wind from June to October) and rainy season (wetter and warmer conditions from November to May). The temperatures in the region vary according to altitude but generally range from about 16°C in the highlands to 30°C in the lowlands. The rain distribution is strongly influenced by topography and is highest in high mountain ranges like the Poroto Mountains. Around Rungwe the rain is about 2500 mm/year which is more than twice the annual rain amount in the Mbeya-Songwe area (1000 mm/yr) (Branchu et al., 2005).

Soil condition and land use

The area has thick volcanic soils suitable for intensive agricultural production as well as for grazing livestock, mainly cattle, sheep and goats. In the higher areas/in the mountains there is also deep fertile soil and which is intensively used for agricultural purposes.

Flora

The most dominant vegetation types are evergreen and semi evergreen species. These include indigenous trees, planted trees, grassland, bushland, miombo woodlands, bushed grassland, bush-shrubland, shrub-grassland and rock outcrops (Figure 6). Topography, soil type, drainage and rock structure seem to have a big influence on the geographic distribution of these vegetation types. The largest open grassland consists of *Eucalyptus* spp “*mikaratusi*”, *Cynodon* spp and *Digitaria* spp and is found in the relatively flat areas of the Rungwe volcanic mountain.

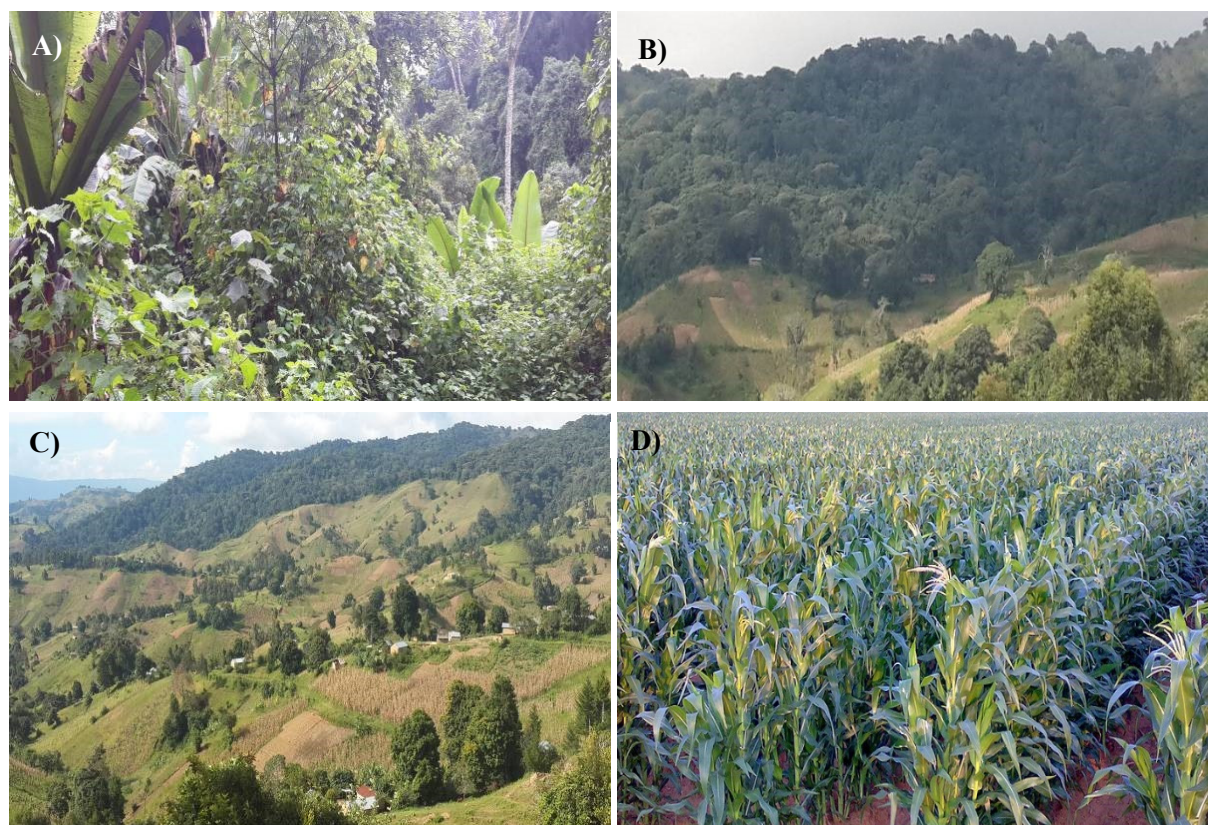


FIGURE 6: A) and B) vegetation type within Poroto forest reserve. C) Miombo woodlands with scattered settlement in the proposed project area. D) Maize plantation around the project area (field study, March 2015)

Fauna

The fauna consists of domestic animals and few wild animal species. They include different bird species, baboons and monkeys such as small black monkeys, different species of small and large snakes and wild animals like mongoose are common. Most of the domestic animals are zero grazing (indoor grazing), especially cows and chickens, however goats are mostly found grazing in the open grassland.

Water sources

The water sources in the area are mainly seasonal rivers which are the Mwanyilu, Sawazia, Mwatisi, Mawe and Mwambalizi rivers that discharge water to Lake Ngozi. There are permanent rivers close to the proposed drilling sites, namely river Halanzi, Mwanzalala, Mpwata, but also drilled well and springs that flow throughout the year can be found. However, the Mbeya urban water and sewerage authority (MBEYA UWSA) provides water services in many villages around the project area. The drainage pattern is formed mainly by the topography of the area. The drainage pattern is directed northwestward

towards Lake Rukwa, northeastward towards Usungu flat and southwards towards Lake Malawi (Gibert et al. 2002).

5.4 Description of the proposed project

Geoscientific studies were carried out to select the locations of the four exploration wells. The four wells are located in farmlands and at the border of the Poroto and Itunza forest reserves (Figure 7). The project involves drilling of 4 exploration wells by the end of 2017, and the goal is to prove/confirm the existence of a geothermal resource that can be utilized for production of electricity. The wells will be 1500-2000 m deep but before the drilling can start several activities need to be completed. The Ngozi geothermal field is in a remote area and therefore significant site preparation is required. Construction of new roads and reinforcement of current roads for carrying heavy equipment to the drilling sites is crucial. The new roads are estimated to be 2.5 km long and 6 m wide and the existing roads will be similar after the reconstruction. A typical well pad is required with an area of roughly 100 m × 50 m including buffer space around the equipment and structures. There is a need for 100,000 m³ of water for the drilling of one well and therefore construction of pump stations and pipes is necessary. A total of 50 people are working on a drill rig. A campus with temporarily houses for workers will be installed with drinking water supply and sewage. The drilling one well takes about 60 days and it is estimated that 8 months will be needed for drilling four wells. Testing of wells after drilling can be estimated to take three months. If an exploration well indicated that the geothermal resource is suitable for processing steam

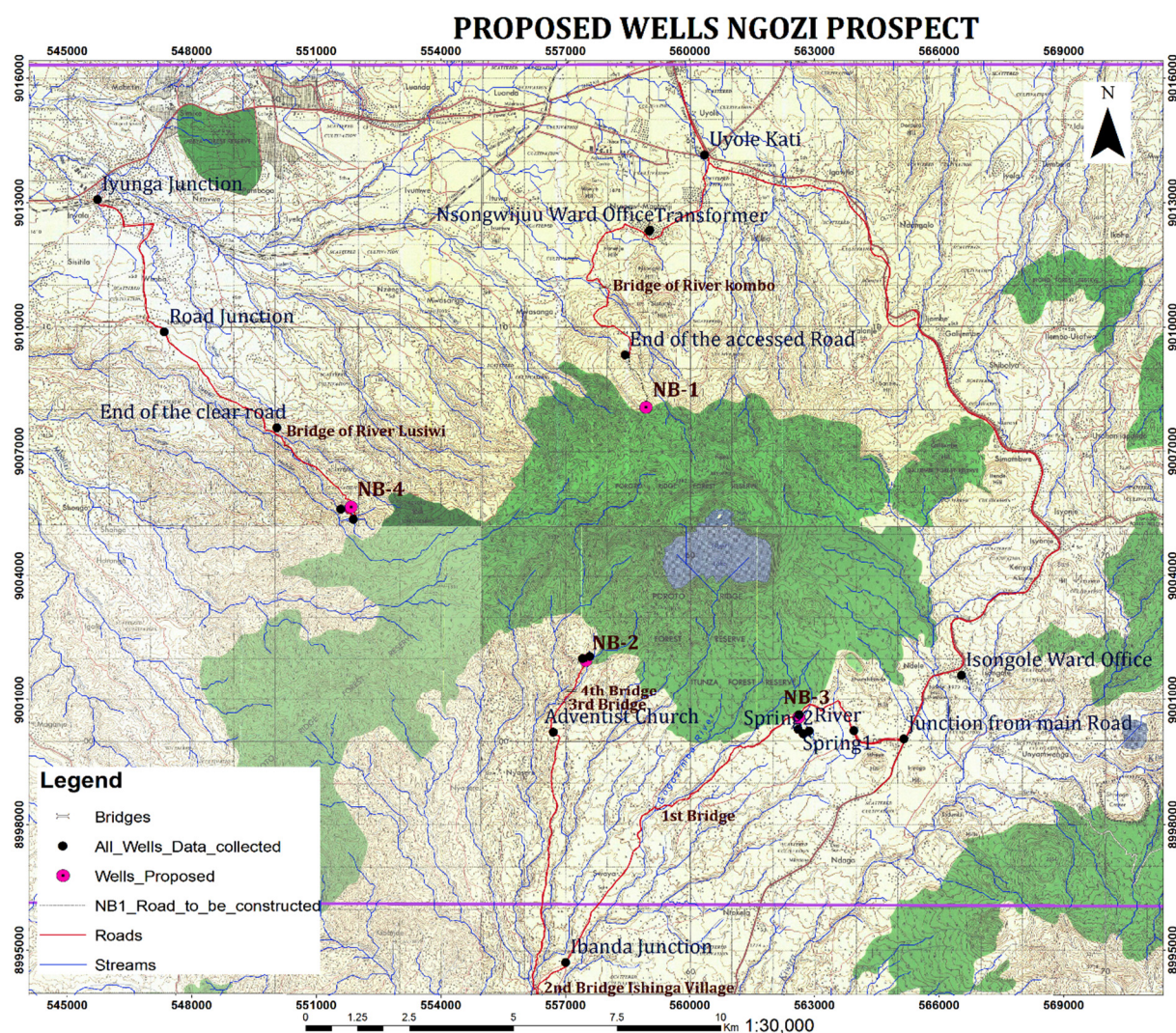


FIGURE 7: Location of the proposed drill wells (TGDC, 2016)

and generation of electricity then it is most likely that more wells will be drilled and a power plant will be built. The construction area might therefore expand depending on the size of the power plant and the need for power lines to the nearest substation.

6. PRELIMINARY ENVIRONMENTAL ASSESSMENT AND MITIGATIONS

Three environmental factors, land use, society and economics and noise, have been chosen to be dealt with in this preliminary EIA. These factors are considered to be among the key factors likely to be affected by the project and accompanying activities. When preparing the EIA of a project the scoping report is the leading document that determines the extent and approach of the EIA study. The scoping report has to be done according to part III of the EIA and Audit Regulation G.M. No. 349 from 2005.

A short review of the scoping report for the Ngozi Geothermal Prospect, May 2015, raises questions on both the structure of the report and the content. The review of that report might indicate that a review of the EIA and Audit Regulation/2005 should be made. The first remark is a lack of more detailed maps of the area in the scoping report. Detailed maps must be part of the background information as they are necessary to draw conclusions on the potential impact of the project and choose the research area for the study of different environmental factors providing necessary information in the assessment process.

The EIA and Audit Regulation of 2005, require that the scoping report includes details of potential negative and positive impacts of the project. It is necessary to explain how the developer must carry out the assessment of the environmental impact of the environmental factors; that is, whether and what available data, research, and sources he will use in the assessment process and how he could carry out data compilation and research for the purpose of the EIA. It is also necessary to describe where, when, and how the developer intends to conduct surveys or carry out measurements, how he intends to process the data, what methods will be used to assess environmental impacts, and how he intends to present the results in the EIS.

6.1 Land use

Four sites have been chosen for the drilling of wells. The drilling sites are located in cultivated land, and the sites will require the acquisition of the land from the owners. The land is needed for construction of the drilling pad, which usually requires $100\text{ m} \times 50\text{ m}$ and $30\text{ m} \times 50\text{ m} \times 2\text{ m}$ for construction ponds at the drill site. This area can become much bigger if the exploration drilling is successful and a power plant is constructed that may require several km^2 depending on the geothermal resource and the amount of electricity produced. Most of the existing roads found in the field are gravel roads that need maintenance/rebuilt to allow transport of heavy equipment to the drilling site. Sites NB-1 and NB-2 need most likely road improvement. In NB-1 the existing road is passing through populated area, with houses close to the road and widening of the road to 6 m might have impact on the people living close by. At this moment there is no information available on exactly how many people will be affected or if houses need to be moved, but such information is necessary. On the road to site NB-2 are four small bridges (Figure 8), new bridges are necessary for the transport of heavy equipment and the road needs to be rebuilt.

The roads to sites NB-3 and NB-4 need to be rebuilt, but the roads are lying through cultivated land and not very close to houses. In all cases, there is a need for a detailed survey to be included in the official EIA where markings for new roads have been set out in the land and also for the area needed for rebuilding existing roads. In this survey, the existing land use, existing infrastructure and number of houses and people affected by the project are noted. Therefore, it has to be a priority to collect various data and make maps in different scales. It is also important to see how the drilling project, with all related constructions, fits into the master plan of the area, by communication with the local authorities.



FIGURE 8: Existing bridges toward drill site NB-2 (Field Study, June 2016)

If a power plant will be built in those sites these roads will be rebuilt for additional heavy machinery traffic. The land area needed for such a power plant will also increase a lot from what is needed for an exploration well.

Land acquisition is delicate and should therefore be carefully planned at an early stage of the EIA process to fulfil national and international regulations. Negotiation on land acquisition and compensation are the best options in land acquisition. The Tanzania Land Act, 1999, confirms the National Land Policy directive which specifies that all land is public land, vested by the President as trustee on behalf of all citizens. The Act lays down fundamental principles for occupying and using the land. Among them is the principle that any land user shall ensure that land is used productively and that any use complies with the principles of sustainable development.

The project area is in agricultural land with scattered settlements. The main impact will be loss of farmland for the local community and it may cause involuntary resettlement. It is therefore important to consider in the beginning of the EIA process the process of land acquisition which must be in accordance with Section 10 (1) of the Land (Compensation Claims) Regulation, 2001. The Regulation Assessment of Value for Compensation states “...the basis for assessment of the value of any land shall be the market value of such land”. The institutional actor for population resettlement and compensation in the country is the Ministry of Lands, Housing and Human Settlements Development. However, before the compensation is paid, compensation schedules need to get approval from the Ward Executive Officer,

Land Officer, District Commissioner and Regional Commissioner of the respective ward, district and region.

The World Bank policy on involuntary resettlement (OP 4.12) applies to all land acquisition, impact on assets, negative impact on livelihood and/or any changes in access to resources due to a subproject, irrespective of whether or not affected persons must move to another location.

The project will have permanent direct impacts on the land mainly by building access roads and drilling pads. This can impact agricultural activities due to loss of available land for crops and livestock grazing in the area. Traffic on roads can also have impacts on livestock grazing because of noise, dust and possible collision.

In the official EIA process, all the main existing infrastructure and land use must be shown on maps and the proposed project, roads, drill pads etc., to assess how they fit in the environment to make it possible to evaluate the impacts they have. Improved access roads can also have positive impacts as they will reduce the transport cost for the local community making it easier to transport and sell their agricultural products and by that raising their living standard. This must be thoroughly described and assessed in the coming EIA process. The project proponent 's main goal and best result from the EIA process must be to locate all necessary constructions, roads, drilling pads, workers' facilities etc. so that they minimize the impacts on existing land use (i.e. households, agricultural, grazing land, nature reserves, surface manifestations etc.). There exist surface manifestations in the area that form recreational spots for locals and tourists. Local people used to believe bathing in hot spring water could cure skin disorders. If the result of the EIA is that the project will have unavoidable negative impacts compensation measures must be used and they must be introduced in the EIA study.

6.2 Social and economic impact

Developing a new geothermal project in an area may cause changes in the daily life and habits and even future settlement of the local people. Despite the benefits of the project to the community, it may still become difficult to get social acceptance in the short run. The area where the proposed drilling of exploration wells will take place is agricultural land with different type of food and cash crops, maize, Irish potatoes, coffee, rice etc. The ethnic groups found in the area are Safwa and Nyakyusa. Livestock keeping is also part of the activity in the area, the main animals kept are cattle, goats and sheep, mostly grazed in open grassland. The roads to the drill sites need improvement, which will have direct impact on the people living close to them, specially the roads to NB-1 and NB-4 as they located through quite densely populated areas. The best option would be to divert the road, but a detail analysis is required to come up with the best option for this. In the official EIA process we need to gather various kinds of data which form the base to build the evaluation of possible impacts on the society.

The impacts can then be divided into short- and long term, positive and negative impacts and have to be dealt with in the text. Creation of jobs during drilling, e.g. the opportunity for catering services for the workers around the drill rig can be grouped as positive impact of the project. Short term negative impacts could be fencing off grazing and agriculture areas for security which will be reopened after the drilling. A drilling project of several months may result in a small temporary increase in the local population. Long term positive impacts could be new market opportunities for the local populations as boarding needs to be provided for the workers. Improvement of roads could improve local living conditions as it can help farmers to transport and sell their agricultural products, and even national, depending on how many people are involved. Roads improvement can also increase tourism, as it could attract more tourists to the area, who come and hike in the mountains. An example of long term negative impacts could be displacement of people, land acquisition and resettlement of evacuated people. A good example of social impacts from a drilling activity can be found in Kenya, East African, where about 50 people were hired to work in connection with one drill rig. It is expected that all casual staff would work for at least six months for the completion of 3 exploration wells. It is anticipated that monitoring wells and

production wells would be drilled later, depending on exploration results and the availability of funds. The drilling activity would not require additional houses because the drill crew would have a camp site. The best way to motivate the local people is to encourage maximum recruitment of labour from the nearby community wherever necessary and reducing the number of employees moving into the project area especially casual workers. Also, the local society could benefit from the project, at least short term, by providing food to the staff, both those that come in the beginning preparing roads, well pads, water pipes, sewages construction and the people on the drill rig. The agriculture products in the area that locals provide today, e.g. Irish potatoes, maize and the grazing animals they keep could increase because of the demand from people working in the project. This could lead to a positive long term impact, more agriculture and transport to other areas by the new road.

6.3 Noise

The project is in a rural area and the background noise level can be considered very low in general. Therefore, the drilling activities will have a significant impact to the residents and livestock, as they are the potential receptors. The Tanzania Bureau of Standards (TBS) set the noise level limits for residential area to 50 dB(A) at day time and 35 dB(A) at night time, for industrial areas it is 70 dB(A) at day time and 60 dB(A) at night time (Table 4) (TZS932: 2007) (Tanzania Bureau of Standards, 2007).

TABLE 4: Maximum permissible levels for general environment

Facility	Noise limits dba (Leq)	
	Day (6:00 AM - 10:00 PM)	Night (10:00 PM - 6:00 AM)
Any building used as hospital, convalescent home, home for the elderly, sanatorium, and learning institutions, conference rooms, public library, and environmental and recreational site	45	35
Residential building	50	35
Mixed residential (with some commercial and entertainment)	55	45
Residential and Industry/small scale production and commerce	60	50
Industrial area	70	60

Noise levels will be raised during site preparation, drilling and testing (blowing) of wells. Noise distribution is dependent on the vegetation cover, topography and landscape. Therefore, the selection of drilling sites can have considerable impact on the noise level in the area. Noise from drilling is generally in the range of 70-100 dB(A) in 10 m distance from the source depending on the equipment used. In this case, all drilling equipment will fulfil strictest standards regarding noise levels. Highest noise levels can be expected to be 92 dB(A) at a 2 m distance. At 80 m distance, it has dropped to below 70 dB(A) and at 550 m distance the sound level is below 45 dB(A).

Noise from discharging wells or testing wells ranges from 70 to 100 dB(A). At a range of 1,000-1,400 m the sound level has fallen below the 45 dB(A) level.

The rise in noise level is temporary and limited to the drilling and testing period that can last for approximately 6 months at individual wells.. As mentioned above, this is quite depending on terrain and surface. The sources of noise in geothermal development activity are well drilling, testing, construction and plant operations. In drilling, the drilling fluid is either air or mud with air drilling rigs being much louder (120 dBA) than mud drilling (up to 80 dBA) (Table 5). It is important to monitor ambient noise levels to determine noise intensity, frequency and duration before and during development.

TABLE 5: Noise from different drilling activities (Hunt, 2001)

Activity	Noise level (dBA)
Air drilling	120 (80 with suitable muffling)
Discharging well after drilling	Up to 120
Well testing	70-110 (if silencer used)
Heavy machinery	Up to 90
Well bleeding	Up to 85 (65 if rock muffler is used)
Mud drilling	Up to 80
Diesel engine to operate compressors and electricity	45-55 (if suitable muffling is used)

The test wells are often bleeding for many months/years and can produce noise of high frequency which may not be harmful but disturbing in the neighbourhood. Wells that are blowing into a silencer produce low frequency sound that can travel long distance and be heard up to 15 km away but damped readjusted significantly in forested/vegetated areas. This noise is normally not harmful but can be disturbing especially for tourists/recreation people who are visiting the area for hiking in the mountain. Effects of noise range from relatively minor such as temporary task interference and irritation to more severe and permanent effects such as sleep loss, physiological stress, speech impairment and loss of hearing. The extent of harm is related directly to the frequency and duration of exposure. Animal behaviour is also affected by excessive noise, which has been shown to cause changes in the size, weight, reproductive activity and behaviour of farm animals.

7. CONCLUSIONS

This preliminary assessment was prepared to give a general picture on future EIA studies in the Ngozi area, that is to be conducted in accordance with national laws and international requirements. The laws and procedures in Tanzania provide the main guidelines that need to be followed in order to fulfil the requirements to obtain the certificate of authorization for geothermal exploration drilling. The study showed that the project will have the most impact on land use, social economics and noise. The drilling sites are in agriculture land. The most important thing is to conduct a baseline study in the area, acquire most recent detailed maps that will help predicting the impacts together with maps made in the EIA process. A more comprehensive EIA must be done for geothermal exploration drilling in the Ngozi area.

ACKNOWLEDGEMENTS

The successful completion of this project is the result from joint efforts of several experts who deserve a vote of appreciation. I cannot mention everyone separately; nevertheless, I would like to convey my appreciation and thanks to all of you who helped me during my training. My full appreciation goes to my supervisor, Thóroddur Thóroddsson, for his guidance and moral support throughout the work. Thanks to Brynhildur Davídsdóttir, the head of study line in Environmental Science, for her support and encouragement.

I am grateful to recognize the financial support provided by the United National University Geothermal Training Program to cover cost of study, upkeep and living expenses in Iceland. I thank the UNU GTP staff for the continuous assistance throughout the six months, the Director, Lúdvík S. Georgsson, Deputy Director, Ingimar G. Haraldsson, Thórhildur Ísberg, Markús A. G. Wilde and Málfríður Ómarsdóttir. My gratitude is equally extended to Ms Audur Magnúsdóttir at VSÓ Consulting for her support in this study.

I acknowledge my employer, Tanzania Geothermal Development Company (TGDC) for granting me permission to attend this training. The whole work would have been unbearable without support and

encouragement of friends and colleagues. I appreciate the cooperation from all UNU-GTP fellows of 2016.

Finally, my sincere thanks are due to my family, my husband and my daughter who patiently waited for me in the period of six months. Thank you for your support and prayers.

It's an immense opportunity to thank God for all the good achievements I have ever grasped in my life and especially during my learning period.

REFERENCES

- Branchu, P., Bergonzini, L., Delvaux, D., Batist, M., Golubev V., Benedetti M., and Klerk, J., 2005: Tectonic, climatic and hydrothermal control on sedimentation and water chemistry of northern Lake Malawi (Nyasa), Tanzania. *J. African Earth Science*, 43, 433-446.
- Delvaux, D., Kraml, M., Sierralta, M., Wittenberg, A., Mayalla, J.W., Kabaka, K., Makene, C., and GEOTHERM working group, 2010: Surface exploration of a viable geothermal resource in Mbeya area, SW Tanzania, Part I: Geology of the Ngozi-Songwe geothermal system, *Proceedings of the World Geothermal Congress 2010, Bali, Indonesia*, 7 pp.
- Fontijn, K., Williamson, D., Mbede, E. and Ernst, G.G.J., 2012: The Rungwe volcanic province, Tanzania – a review. *J. African Earth Sciences*, 63, 12-31.
- Gibert, E., Bergonzini, L., Massault, M., and Williamson, D., 2002: AMS-C-14 chronology of 40.0 ka BP continuous deposits from a crater lake (Lake Massoko, Tanzania) – modern water balance and environmental implications. *Palaeogeogr. Palaeoclimatol. Palaeoecol.*, 187, 307–322.
- Harkin, D.A., 1960: *The Rungwe volcanics at the northern end of Lake Nyasa*. Geological Survey of Tanganyika, Department of Lands and Surveys, Dar es Salaam, 172 pp.
- Hunt, T.M., 2001: *Five lectures on environmental effects of geothermal utilization*. UNU-GTP, Iceland, report 1-2000, 109 pp.
- Kraml, M., Kreuter, H., and Robertson, G., 2012: Small scale rural electrification and direct use of low temperature geothermal resources at Mbaka. *Proceedings of the ARGeo-C4 conference, Nairobi, Kenya*, 11 pp.
- Kraml, M., Schaumann, G., Kalberkamp, U., Stadtler, C., Delvaux, D., Ndonde, P.B., Mnjokava, T.T., Chiragwile, S.A., Mayalla, J.W., Kabaka, K., Mwano, J.M., and Makene, C., 2008: *Geothermal Energy as an alternative source of energy for Tanzania*. BGR, Germany, GEOTHERM project Technical Cooperation with the Republic of Tanzania, final technical report, 235 pp.
- MEM, 2014a: *Electricity supply industry reform strategy and roadmap 2014-2025*. Ministry of Energy and Minerals, The United Republic of Tanzania. 55 pp.
- MEM, 2014b: *Mineral sector environmental impact assessment guidelines*. Ministry of Energy and Minerals, report, 128 pp.
- Mnjokava, T.T., 2012: Geothermal development in Tanzania – A country update. *Proceedings of the ARGeo-C4 conference, Nairobi, Kenya*, 5 pp.

Mwalyosi, R., Hughes, R., and Howlett, D.J.B., 1999: *Introduction course on Environmental Impact Assessment in Tanzania: resource handbook*. International Institute for Environment and Development and Institute for Resource Assessment, 217 pp.

Nations Online Project, 2016: Political map of Tanzania. Nations Online, website: www.nationsonline.org/oneworld/map/tanzania-political-map.htm

NBS, 2012: *Basic facts and figures on human settlements*. National Bureau of Statistics, Ministry of Finance, Dar es salaam, Tanzania, 139 pp.

Tanzania Bureau of Standards, 2007: *Acoustics – general tolerance limits for environmental noise*. TBS, Dar es Salaam, 12 pp.

United Republic of Tanzania, 2004: *Environmental management act (EMA)*. Government Printers, Dar es Salaam, 129 pp.

United Republic of Tanzania, 2005: *Environmental Impact Assessment and Audit Regulations G.N. No 349*. Government Printers, Dar es Salaam, 53 pp.

United Republic of Tanzania, 2013: *Mbeya region socio-economic profile*. The Planning Commission, Dar es Salaam and Regional Commissioner's Office, Mbeya, 206 pp.

SWECO, 1978: *Reconnaissance of geothermal resources*. Report for the Ministry of Water, Energy and Minerals of Tanzania, SWECO, Stockholm, Sweden and VIRKIR, Reykjavík, Iceland, 51 pp.

TGDC, 2014: *Tanzania Geothermal Potential Areas*. TGDC, Dar es Salaam, unpublished map.

TGDC, 2016: *Proposed wells Ngozi prospect*. TGDC, Dar es Salaam, unpublished map.

Worldometers, 2016: *Statistics on Tanzania*. Worldometers, website: www.worldometers.info/world-population/tanzania-population/



UNITED NATIONS
UNIVERSITY

UNU-GTP

Geothermal Training Programme

Orkustofnun, Grensasvegur 9,
IS-108 Reykjavik, Iceland

Reports 2016
Number 36

ANALYSIS OF BIT OPERATIONS: LAGUNA COLORADA GEOTHERMAL PROJECT, BOLIVIA

Danny Miguel Revilla Vargas

ENDE - Empresa Nacional de Electricidad

(National Electricity Company)

Av. Ballivián N°503, Cochabamba

BOLIVIA

danny.revilla@ende.bo, dannyrevilla@hotmail.es

ABSTRACT

Twenty-seven years ago the National Electricity Company of Bolivia (ENDE) drilled four wells successfully in the Sol de Mañana geothermal field. The wells confirmed the geothermal power potential of the field and with a loan, financed by the Japanese International Cooperation Agency (JICA), new wells are planned to be drilled in order to develop the project's first stage of 50 MW. Drill bit selection and operation are essential factors for getting good performance and avoiding problems during drilling activities. Multiple linear regression (also called Bourgoyne and Young method) and Mechanical Specific Energy were the methods applied on data from the Icelandic well RN-16, finding that a theoretical research could be useful in improving drilling time and better identify when problems or dysfunction is occurring. Both methods evaluate the effects of the rate of penetration (ROP), such as: rock strength and drill ability, differential bottom hole pressure, mud flow rate, weight on bit, revolution per minute. Finally, rock strength surveys were found to be a useful tool for making bit selection more efficient, especially in new fields.

1. INTRODUCTION

1.1 Location and weather description

The Laguna Colorada Geothermal Project is located on the southwest zone of Potosi-Bolivia at a high altitude (4900-4980 m a.s.l.) between the meridians 57°26' - 69°38' western longitude and 9°38' - 22°53' southern latitude. It is inside the Occidental zone of Cordillera de los Andes, located close to the subduction zone between the South-American and Nazca Plates. The weather is relatively arid with average temperature of 0.8°C, annual rainfall between 250-300 mm and strong winds at 15 m/sec (approx.) predominantly during the afternoon.

1.2 Background

The National Electricity Company of Bolivia (ENDE) has been developing the Laguna Colorada geothermal project, which includes the Sol de Mañana field, where geoscientific exploration has been performed and five geothermal wells drilled. Four of the drilled wells have been tested, achieving an

estimated power capacity of 7 MW_e per well. Through numerical reservoir simulations it has been estimated that the Sol de Mañana field is able to generate 100 MW_e with a single-flash power plant.

The reservoir evaluation indicates a high probability of the reservoir being able to sustain a 50 MW power plant, with a possible extension to 100 MW (ENEL, 1991). In light of these promising results, ENDE is planning to drill six production wells (until 2,000 m of depth) and three reinjection wells. This is an analysis of methods for optimizing the bit performance and purpose their application on these new geothermal wells. To this end, data from the Sol de Mañana drilling data was processed and analysed. Furthermore, data from drilling at Reykjanes geothermal field was analysed to apply these methods in a near future.

1.3 The geothermal field and wells (SM-1 and SM-2)

This field is located on the Miocene-Pleistocene Andin volcanic arc and is covered by an extensive dacitic ignimbrite and andesitic lava (Ramos, 2015). Geoscientific exploration was done on Sol de Mañana and volcanic rock, fractured systems, hot springs, hot water, and other factors identified.

According to geochemical studies the geothermal fluid was classified as mature water and the geothermometers indicated reservoir temperatures in the range of 280°C.

The geophysical surveys observed an intermediate conductive layer, this layer has notable variations of thickness (TERANOV-CGG, 2014). The resistivity at deep levels indicates good signals of the geothermal resource.

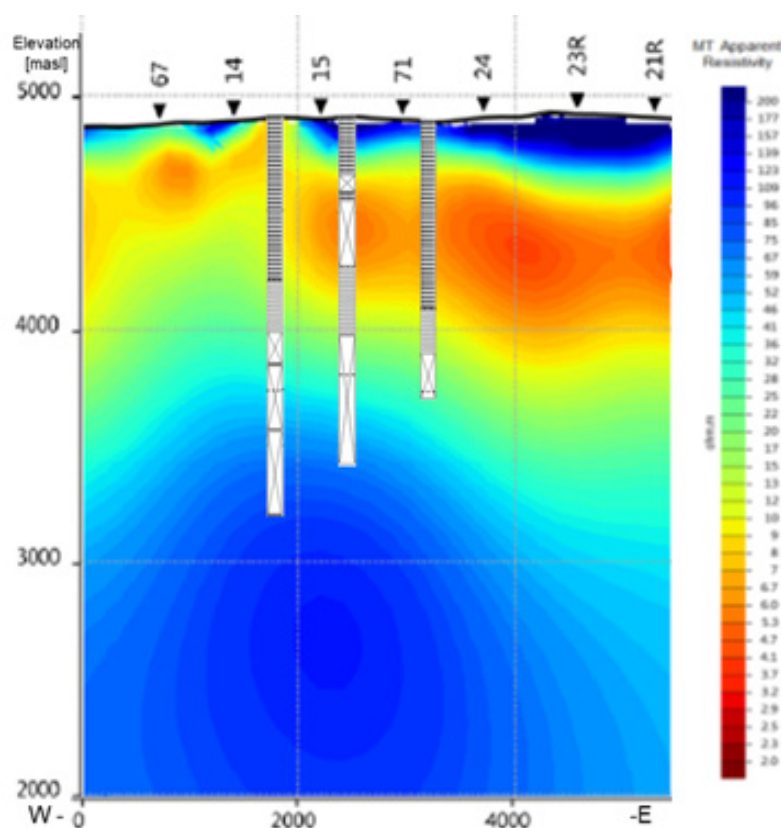


FIGURE 1: Resistivity cross-section and lithology correlation of the Wells SM-1, SM-2 and SM-5

On Sol de Mañana field five wells were drilled, four of them proved to be production wells (SM-1, SM-2, SM-3 and SM-5) finding a reservoir temperature of 245°C (West JEC, 2010). The wells were drilled with a Massarenti 7000 SP rig, with 3600 m of nominal depth capacity using 5" drill pipe. Figure 1 shows a resistivity cross-section (TERANOV-CGG, 2014) with lithological correlation (WestJEC, 2008), modified for this report.

After the surface exploration stage identified favourable conditions for geothermal power production, well SM-1 was drilled in Sol de Mañana area. The drilling began on 8th September 1988 and ended after 74 days at a depth of 1,180 m (ENEL, 1989a). Lithology information shows (Figure 2) that ignimbrite of dacite composition with variable colour, which consists of quartz crystals, plagioclase, biotite and

hornblende is predominant. Three alteration zones were identified through analysis of the cuttings gathered while drilling:

1. Heulandite zone (0-400 m);
2. Quartz – chlorite zone (400-780 m);
3. Epidote zone (780-1180 m).

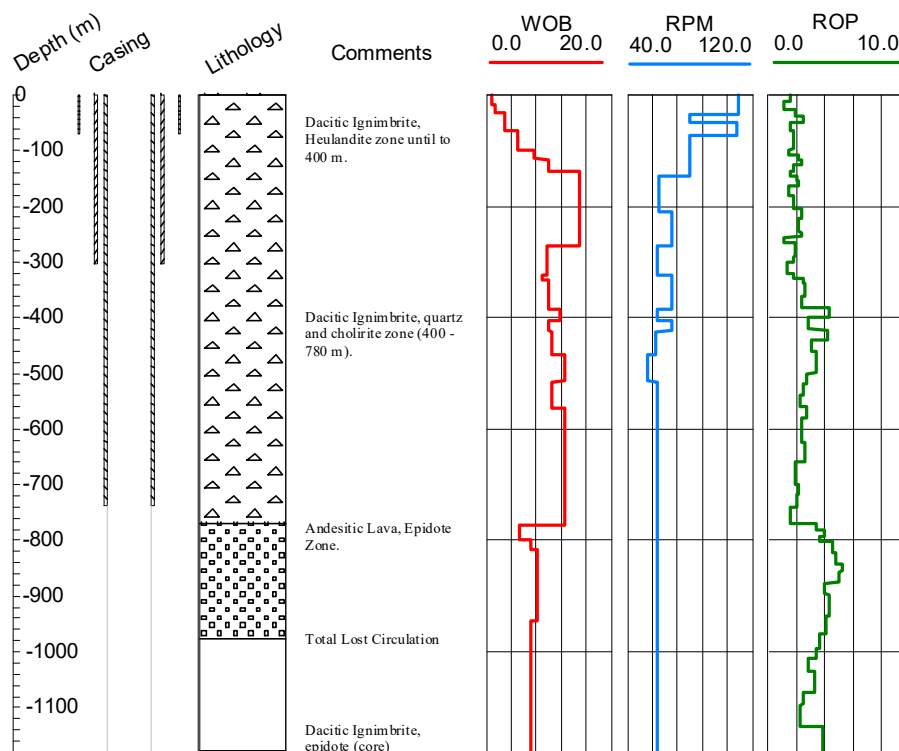


FIGURE 2: SM-1 Lithology and drilling data (ENEL, 1989a)

The well was drilled with bentonite mud down to 762 m without big losses. Successive drilling was done with water and total loss of circulation was experienced at 977 m depth. The well was drilled using hole openers for the first and second sections. As this report is focused on bit performance, Table 1 shows only the first bit used to do the first hole (without hole openers).

Well SM-2 was drilled 1100 m N-NW of SM-1, drilling began on 19th December 1988 and ended after 59.5 days at a depth of 1486.5 m, 14.5 days less than SM-1, this was attributed to lithology that was found there (ENEL, 1989b). The wells lithology is shown in Figure 3 and was similar to the lithology seen in SM-1. The alteration zones are:

1. Clay minerals zone (0-400 m);
2. Wairakite zone: (525-800 m);
3. Wairakite and epidote zone (800-900 m);
4. Epidote and adularia zone (950-1486.50 m).

Bentonite mud was used with partial losses until 242 m where total circulation loss occurred and drilling was continued with water. Similar to SM-1, well SM-2 was drilled using hole openers.

Figure 1 in Appendix I shows the drill bit data for SM-1 and SM-2. Table 1 shows the drill bits used to drill SM-1 and SM-2. Neither hole-openers nor core bits are included in the table as such drilling techniques are outside the scope of this report. Table 1 shows that several bit changes were performed in both wells, some in conjunction with tripping operations related to coring, logging or testing, all of

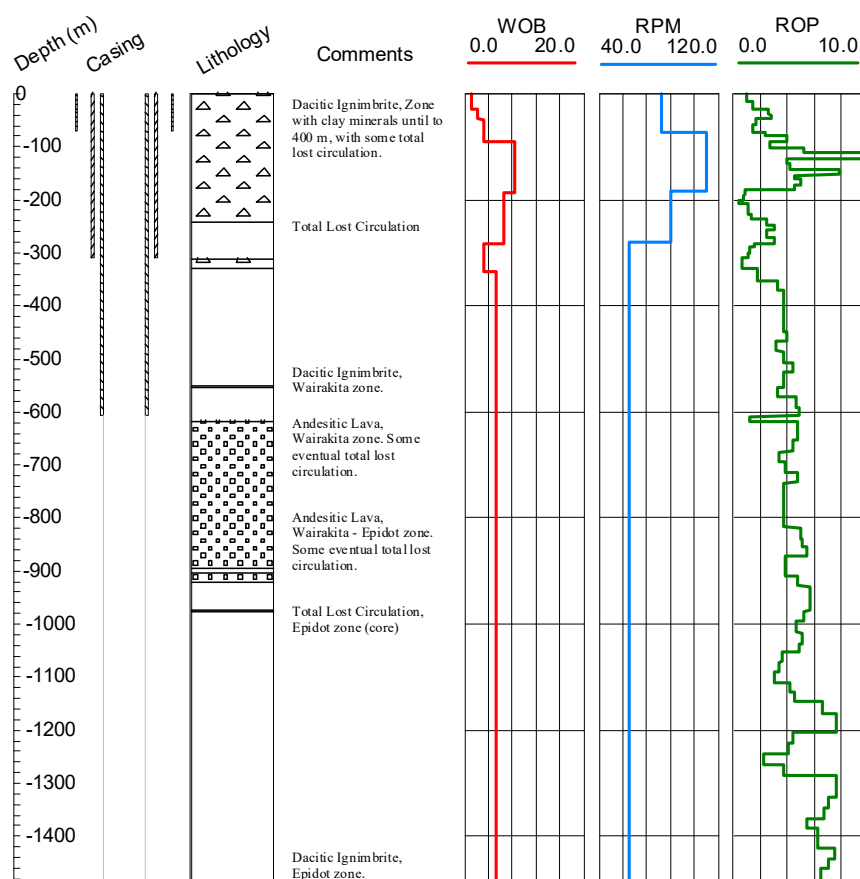


FIGURE 3: SM-2 Lithology and drilling data (ENEL, 1989b)

which are common during drilling of exploratory wells. The rate of penetration (ROP) is relatively low and according to the IADC Code (Table 1), a long steel tooth bit was used in shallow layers and a short tooth TCI bit from 300 m to bottom. Some exceptions during drilling below 300 m in SM-2, a medium steel tooth bit was used and the recorded ROP was slightly lower than for same size TCI bits.

TABLE 1: Bit record of wells SM-1 and SM-2 (ENEL, 1989a; ENEL, 1989b)

SM-1						SM-2					
IADC Code	Bit diameter ["]	Section	Depth start [m]	Depth end [m]	ROP [m/hr]	IADC Code	Bit diameter ["]	Section	Depth start [m]	Depth end [m]	ROP [m/hr]
1-3-1u	17 1/2	0	0	26.0	2.50						
1-3-1u	17 1/2	0	26.0	75.0	1.75	6-3-7	12 1/4	0	12.7	74.0	2.70
1-3-1	17 1/2	1	75.0	94.5	1.62	1-1-1u	17 1/2	1	74.0	85.0	2.50
1-3-1	17 1/2	1	94.5	195.0	1.58	1-1-4	17 1/2	1	85.0	209.0	1.70
1-3-1	17 1/2	1	195.0	255.0	1.71	1-1-1	17 1/2	1	209.0	240.0	2.00
6-1-7	12 1/4	1	255.0	307.0	1.30	6-3-7	12 1/4	1	240.0	311.0	1.70
LH2J	12 1/4	2	307.0	316.0	1.63	2-3-1	12 1/4	2	311.0	328.0	0.95
6-1-7	12 1/4	2	317.5	411.0	2.20	6-1-6	12 1/4	2	328.0	617.0	3.84
6-1-7	12 1/4	2	411.0	614.0	2.40	2-5-1	8 1/2	3	634.0	851.0	4.50
6-3-7	12 1/4	2	614.0	762.0	1.57	6-2-7	8 1/2	3	851.0	943.0	4.70
7-3-1	8 1/2	2	762.0	786.0	6.00	6-2-7	8 1/2	3	943.0	973.0	6.00
6-2-7	8 1/2	3	786.0	963.0	4.04	6-2-7	8 1/2	3	976.0	1052.0	5.30
6-2-7	8 1/2	3	963.0	1029.0	2.73	6-3-7	8 1/2	3	1052.0	1198.0	4.80
6-2-7	8 1/2	3	1029.0	1114.0	2.38	2-3-1	8 1/2	3	1198.0	1264.0	3.20
6-2-7	8 1/2	3	1114.0	1178.5	5.38	6-3-7	8 1/2	3	1264.0	1485.0	6.14

where: Section 0 with safety casing 20" on hole 26"
 Section 1 with safety casing 13 3/8" on hole 17 1/2"
 Section 2 with safety casing 9 5/8" on hole 12 1/4"
 Section 3 with on open hole 8"

2. LITERATURE OVERVIEW

2.1 Bit selection

Unfortunately, the selection of the optimal drill bit and operational parameters can only be achieved by trial and error. In the absence of bit records or if bit records are poor, several rules and methods can be applied. One method is based on collecting available drilling data in previously formations drilled (Bourgoyne et al., 1991). In addition to lithology information, the drillability and abrasiveness are the theoretical concepts to describe the formation drilled:

- Drillability: is a calculated parameter for estimating how easy or hard it is drill a specific formation and is inversely proportional to the compressive stresses of the rock formations.
- Abrasiveness: is relative to the tooth wear rate of the drill bit during operation in a specific formation. Abrasiveness tends to increase when the drillability decreases.

The drill bits are classified into Roller Cone and Drag bits (Figure 2 in Appendix I). The roller-cone has been more widely used (Ngugi, 2008) and is the bit type used on the wells that are studied in this report. Usually roller cone bits (parts of the bit are shown in Figure 3 in Appendix I) have an IADC code that consist of three digits (Tables 2 and 3):

- First digit – cutter structure (1-8): used to describe the type (Steel tooth or Tungsten Carbide Insert tooth TCI) and application of drill bit (Bourgoyne et al., 1991):
- Second digit – subdivision (1-4): is a subdivision inside to each class, where 1 is the softest formation inside each series and 4 is the hardest formation.
- Third digit – Bearing description (1-7): describe the bearing system and whether the bit is gouge protected or not.
- Optional letter could be show to describe other characteristics.

TABLE 2: IADC Code, First Digit

First digit	Type	Application
1	Steel tooth cutting structure	Soft formations with low compressive strength or high drillability.
2		Medium to medium hard formations with high compressive strength.
3		Hard formations and semi-abrasive to abrasive formations.
4	Tungsten carbide insert tooth cutting structure	Soft formations with low compressive strength or high drillability.
5		Soft to medium formations with low compressive strength.
6		Medium hard formations with high compressive strength.
7		Hard formations and semi-abrasive to abrasive formations
8		Extremely hard and abrasive formations

TABLE 3: IADC Code, third digit

Third digit	Bearing description
1	Standard roller bearing
2	Roller bearing air cooled
3	Roller bearing gauge protected
4	Sealed roller bearing
5	Sealed roller bearing – gauge protected
6	Sealed friction bearing
7	Sealed friction bearing gauge protected

In order to do guidelines to select the drill bits, it is possible to mark off the next points as some general rules according with their performance and cost (for roller cone bit):

1. Rules to use to choose the size of bit tooth (Bourgoyne et al., 1991):
 - a) Use the longest tooth size possible;
 - b) Allow small amount of tooth breakage rather than selecting a shorter tooth size;
 - c) When enough weight cannot be applied economically to a steel tooth bit to cause self-sharpening tooth wear, a longer tooth size should be used;
 - d) When the rate of tooth wear is much less than the rate of bearing wear, select a longer tooth size (improvements with a better bearing design or apply more weight on bit).
2. Rules to choose the bearing and gauge:
 - a) Bits with roller bearings can be run at a higher speed than bits with journal bearings;
 - b) Bits with sealed bearings have a longer life than bits with open bearings;
 - c) Bits with journal bearings can be run at higher weights than bits with roller bearings. For geothermal drilling sealed bearings are recommended specially for high temperature intervals.
3. Rules to choose the journal angle: Bits with relatively small journal angles are best suited for drilling in softer formations, and those with larger angles perform best in harder formations.

2.2 The main drilling parameters

Below is a brief description of the main drilling parameters being analysed:

Hook load is the total force pulling down on the hook. This includes the weight of the drill string, the drill collars and any ancillary equipment in air, less any force that reduces that weight. Example of forces that might reduce the weight include friction along the wellbore wall (especially in deviated wells) and, importantly, buoyant forces on the drill string caused by its immersion in drilling fluid.

WOB: Weight On Bit represents the weight applied on the bit i.e. the force to overcome the compressive strength of the rock. The actual measurement of the weight is made with a hydraulic gauge attached to the dead line of the drilling line (as tension increases in the drilling line, more hydraulic fluid is forced through the instrument, turning the hands of the indicator. This sensor measures a unique value, which is the overall weight (hook-load) of the drill string including the weight of the block and top drive system, therefore a correct calibration is required in order to have proper reading for the actual WOB.

RPM: Revolution Per Minute represents the rotational speed of the drill string. It is measured at the top drive system or rotary table and is read directly from the respective electronic unit. The measurement for this parameter is considered accurate as long as the acquisition system has been properly set up. If a down hole motor (DHM) is included on the bottom hole assembly (BHA), the real RPM should be calculated and include on the drilling data record.

ROP: Rate of Penetration, is measured through the relative change of the position of the block in time. Accurate calibrations are important in order to have a representative ROP parameter.

Bourgayne et al. (1991) explained the response of the ROP with changes in WOB and RPM, which is shown in Figure 4. ROP increases with increased WOB (a to c). At higher WOB increases start to show only slight improvement in ROP (c to d). In some cases a decrease in ROP is observed at too high values of WOB for a given scenario (d to e), this type of behaviour is often called bit floundering. As shown in Figure 5, ROP usually increases with rotary speed RPM (a to b). At certain RPM, ROP stops increasing linearly with increased RPM and the ROP response becomes poor (b to c).

Torque: This parameter is the torque applied to rotate the drill string. It is measured by means of a top drive system or a rotary table and its monitoring is important for detecting wellbore cleaning issues and problems related to highly deviated wellbores. If a DHM is included on the BHA, the torque of the motor can be calculated based on hydraulic parameters.

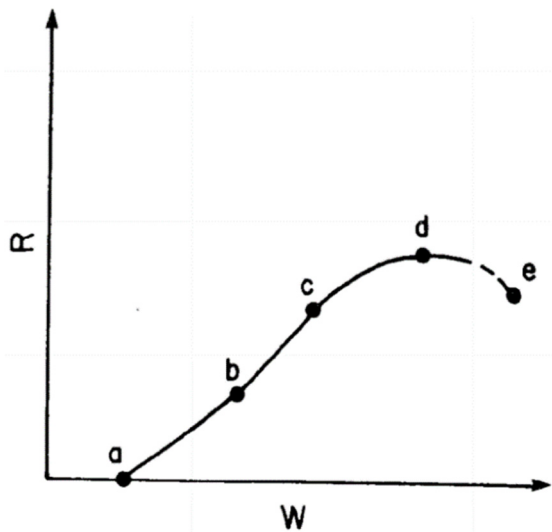


FIGURE 4: Typical response of ROP(R) with increasing WOB (W)

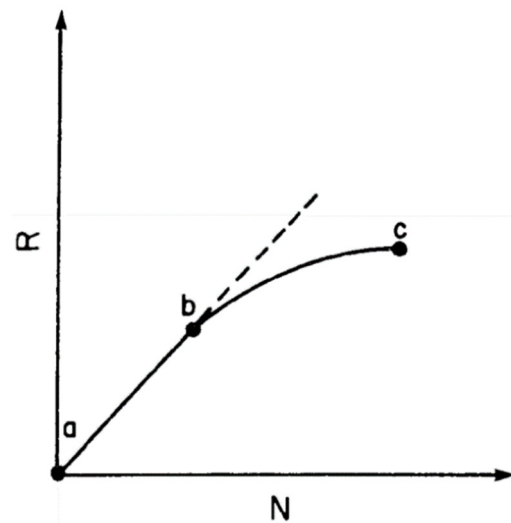


FIGURE 5: Typical response of ROP(R) with increasing RPM (N)

Pump rate represents the pump rate of the of the mud pumps. The pump rate is determined by the liner size in use and number of strokes. In case there are two pumps working simultaneously, the pump rate is the total combined flow rate of the two pumps. Use of flow meters could also be adapted for accurate flow rate measurements.

Stand pipe pressure is the total pressure pumped to the well, this pressure must be sufficient to overcome the total pressure losses in the well. Pressure losses are the sum of pressure losses in the annulus, across the bit, in the bottom hole assembly and drill string. The monitoring of this parameter helps in determining downhole problems.

The pump rate and stand pipe pressure should be determined before the start of drilling in order to select the appropriate jet bit nozzle size, determine the effective flow rate of the cleaning fluid and to ensure efficient cleaning of a wellbore. Rheological models can be used to determine the effective standpipe pressure and pump rate in a wellbore during drilling. In geothermal drilling the Newtonian Model and Bingham Plastic Model are often used.

Depth: The depth refers to the bit position. Usually it is linked to the position of the block, by means of a sensors located at the crown block.

Fluid properties: Rheological properties and the density of the drilling fluids are important parameters to be recorded for optimization purposes. Physical, chemical and rheological properties are measured in the laboratory.

2.3 Optimization of drilling parameters

Optimization of drilling parameters has a long history (Eren, 2010) through objective analysis and research in oil fields (Bourgoyne and Young, 1974) and laboratory tests (Eckel, 1968). The parameters that have been studied and found to affect the rate of penetration (ROP), include bit type, formation characteristics, drilling fluid properties, weight on bit (WOB), rotational speed (RPM), bit tooth wear and bit hydraulics. This report focuses on the methods to find the optimum WOB and RPM combinations with regards to ROP and bit life. Methods to find the optimum WOB and RPM combination include a step test and drill off test to give a starting point, which will be monitored to maintain optimum parameters.

2.3.1 Step test

A step test involves increasing the WOB at constant RPM to find the most effective WOB for a given RPM. An example is shown in Figure 6 where WOB is increased by 5,000 pounds at a time at constant RPM. The ROP responds by increasing 25 ft/hr with each step until 15,000 tons are reached, then the next ROP increase is less 10 ft/hr. The founder point is defined at the WOB after which the ROP increases are no longer a linear (IADC, 2014). This method is also called an active drill off test.

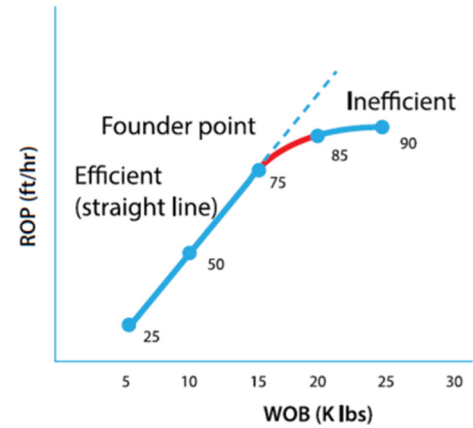


FIGURE 6: Step Test (IADC, 2014)

A drill-off (passive) test is performed in order to determine the combination of WOB and RPM which maximizes the rate of penetration (Figure 7). In geothermal drilling it could be good to do this test where a section where uniform lithology is expected or when large changes in ROP or Torque are observed. Following the recommendations of Bourgoyne et al. (1991), this test consists of the following steps:

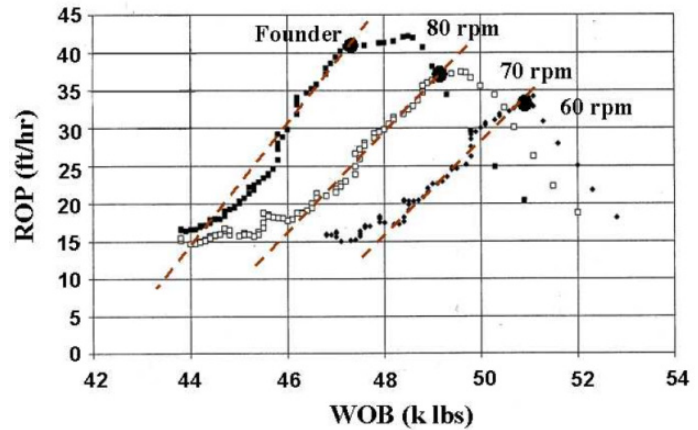


FIGURE 7: Drill off test (Guerrero, 2007)

1. While drilling with the bit weight currently in use, lock the brake and determine the time required to drill off 10% of this weight. This is called the characteristic time.
2. Increase the bit weight to the initial value of the drill off test. This initial value should be at least a 20% increase in bit weight over the bit weight currently in use.
3. Drill at this bit weight long enough to establish the new bottom hole patterns of the bit. The time allowed is usually one characteristic time per 10% increase in bit weight, an interval of twice the characteristic time would be used for a 20% increase in bit weight.
4. Lock the brake and maintain a constant rotary speed. Record each time of bit weight falls off 4,000 pounds. Continue the test until at least 50% of the initial bit weight has been drilled off.
5. Make a plot of ROP versus WOB. A straight line should result having a slope that is equal to the bit weight exponent a_5 (on a log-log plot).
6. These steps should be repeated at different RPM. Could be applicable to choose the maximum ranges recommended by manufactures.

The application of this method should not take more than five minutes. Modern drilling data acquisition allow for fast analysis, using for example an excel sheet. The ROP can be calculated using the Equation 1:

$$ROP = 0.95 \frac{L_{DP} * \Delta WOB}{E * A_s \Delta t} \quad (1)$$

Find the ROP, a_5 and a_6 can by calculated with Equations 2 and 3:

$$ROP = K * \left(\frac{WOB}{d_B} \right)^{a_5} N \quad (2)$$

$$ROP = K * N^{a_6} \quad (3)$$

Then the optimum WOB and RPM are found using Equations 4 and 5:

$$\left(\frac{WOB}{d_B}\right)_{opt} = \frac{a_5 * H_1 \left(\frac{WOB}{d_B}\right)_{max} + a_6 \left(\frac{WOB}{d_B}\right)_t}{a_5 * H_1 + a_6} \quad (4)$$

$$N_{opt} = 60 * \left[\frac{\tau_H \left(\frac{WOB}{d_B}\right)_{max} - a_6 \left(\frac{WOB}{d_B}\right)_{opt}}{t_B \left(\frac{WOB}{d_B}\right)_{max} - 4} \right]^{1/H_1} \quad (5)$$

where	WOB	=	Weight on bit [lb];
	N	=	Revolutions per minute;
	d_B	=	Bit diameter [in];
	ROP	=	Rate of penetration [ft/hr];
	L_{DP}	=	Length of drill pipe [ft];
	E	=	Young's modulus;
	A_S	=	Cross-sectional area of drill pipe [in ²];
	Δt	=	Differential of elapsed time [hr];
	τ_H	=	Formation abrasiveness constant [hr];
	t_B	=	Optimum bit life [hr];
	$\left(\frac{WOB}{d_B}\right)_t$	=	Threshold weight on bit per inch applied in the drill off test
	$\left(\frac{WOB}{d_B}\right)_{max}$	=	Maximum weight on bit per inch applied in the drill off test
	K	=	Constant of proportionality

2.3.3 Multiple linear regression

In statistics, a regression or linear adjustment is a mathematical model used to approximate the dependency relationship between a dependent variable y_i and the independent variables x_i . Using this method, Bourgoyne and Young (1974) presented an approach to get a ROP model, which can be optimized through variables which are controllable during drilling, such as weight on bit (Equation 4) and bit rotation speed (Equation 5), to obtain maximum ROP. This method is based on statistical analysis of past drilling data where a mathematical model of ROP is made through multiple linear regression analysis to find the a coefficients. Equation 6 shows the mathematical ROP model:

$$ROP = \frac{df}{dt} = e^{(a_1 + \sum_{j=2}^8 a_j x_j)} \quad (6)$$

where a_1 to a_8 are the constant coefficients; and x_2 to x_8 are the variables by different effects.

Formation strength function: a_1 primarily represents the effect of formation strength on ROP. It is inversely proportional to the natural logarithm of the square of the drillability parameter (Maurer, 1962). The coefficient a_1 includes also the effects of parameters not mathematically modelled such as the effect of drilled cuttings. Other factors which could be included for future consideration but known to be under this function could be drilling fluid details, solids content, efficiency of the rig equipment/material, crew experience and service contractors' efficiency (Bourgoyne et al., 1991).

The function f_1 is has the same unit as rate of penetration, for this reason it is called the apparent formation drillability and is defined by Equation 7:

$$f_1 = e^{a_1} \quad (7)$$

Formation compaction function: The functions f_2 and f_3 are models of the rock compaction due to depth. f_2 is an effect of normal compaction trend which is defined by Equation 8:

$$\begin{aligned} f_2 &= e^{a_2(10,000-D)} \\ x_2 &= (10,000 - D) \end{aligned} \quad (8)$$

The function f_3 assumes an exponential increase in penetration rate with pore pressure gradient. That means that for over-pressured formations, the ROP will increase (Murray, 1955). This function is defined by:

$$\begin{aligned} f_3 &= e^{a_3 D^{0.69}(g_p-9)} \\ x_3 &= D^{0.69}(g_p - 9) \end{aligned} \quad (9)$$

where D = True vertical well depth [ft];
 g_p = Gradient of pore pressure [lb/gal].

Bottom hole differential pressure function: (Also called overbalance pressure). This function has a value equal to 1 when the overbalance is zero. This function shows a reduction in ROP with increased overbalance (Bourgoyne et al., 1991). If the overbalance is expressed in terms of equivalent circulating density (ECD) and pore pressure gradient, the function f_4 is defined by:

$$\begin{aligned} f_4 &= e^{a_4 D(g_p - ECD)} \\ x_4 &= D(g_p - ECD) \end{aligned} \quad (10)$$

where ECD = Equivalent circulation density [lb/gal]

As example, for turbulent flow of Newtonian fluids, the ECD can be calculated using Equations 11-13:

$$\Delta P_{annulus} = \frac{\rho_m^{0.75} v^{1.75} \mu^{0.25}}{490 (D_2 - D_1)^{1.25}} \Delta L_s \quad (11)$$

$$v = \frac{1000 Q}{(D_2^2 - D_1^2)} \quad (12)$$

$$ECD_{SI} = \rho_m - \frac{\Delta P_{annulus}}{10.2 D} \quad (13)$$

where ECD_{SI} = Equivalent circulation density on SI units [kg/m³]
 $\Delta P_{annulus}$ = Frictional pressure losses through to annulus [kPa]
 ρ_m = Mud density [kg/m³]
 v = Velocity [m/s]
 Q = Flow rate [l/s]
 μ = Viscosity [Pa-s]
 D_1 = Outside diameter, drill pipe or drill collar [in]
 D_2 = Inside diameter, open hole or casing [cm]
 ΔL_s = Length of conduit [m]

Weight on bit and diameter function: The WOB and bit diameter are considered to have direct effect on the penetration rate. This assumes that the penetration rate is directly proportional to WOB per bit diameter (Graham and Muench, 1959). The $(WOB/d_B)_t$ is the WOB threshold and the reported values for this term is between 0.6 to 2.0. The WOB threshold can be estimated from drill off test performed using low WOB. This function has an upper limit corresponding to the floundered point, which must be estimated from drill off test (Cheraghi, 2013):

$$f_5 = \left[\frac{\left(\frac{WOB}{d_B}\right) - \left(\frac{WOB}{d_B}\right)_t}{4 - \left(\frac{WOB}{d_B}\right)_t} \right]^{a_5} \quad (14)$$

By properties of natural logarithmic, the x_5 is equal to:

$$x_5 = \ln \left[\frac{\left(\frac{WOB}{d_B}\right) - \left(\frac{WOB}{d_B}\right)_t}{4 - \left(\frac{WOB}{d_B}\right)_t} \right] \quad (15)$$

where $\left(\frac{WOB}{d_B}\right)_t$ = Threshold weight on bit per inch of bit

Rotary speed function: this function assumes that the ROP is directly proportional to rotary speed of the bit, RPM or N (Graham and Muench, 1959):

$$f_6 = \left[\frac{N}{100} \right]^{a_6} \quad (16)$$

$$x_6 = \ln \left(\frac{N}{100} \right)$$

It should be highlighted that a_5 and a_6 can be determined from a independant of this method as described in Section 2.2.1.

Tooth wear function: The tooth wear function is calculated by fractional tooth height h (adimensional). In order to calculate the respective tooth height, a bit record for a similar bit type that has been used within the same formation is necessary. For practical purposes, this report assumes zero tooth wear, that is valid when the drill bit is starting to do the hole (Bourgoyne and Young, 1974).

$$f_7 = e^{a_7(-h)} \quad (17)$$

$$x_7 = -h$$

Hydraulic function: It is based on microbit experiments performed by Eckel (1968). The hydraulics function represents the effects of the bit hydraulics. Jet impact force was chosen as the hydraulic parameter of interest with a normalized value of 1.0 for f_8 at 1,000 lbf.

$$f_8 = e^{a_8 \left(\frac{\rho Q}{350 \mu d_n} \right)} \quad (18)$$

$$x_8 = \frac{\rho Q}{350 \mu d_n}$$

where:

ρ	=	Mud density [lb/gal]
Q	=	Mud flow rate [gpm]
μ	=	Apparent viscosity at 10,000 s ⁻¹ [cp]
d_n	=	Diameter of bit nozzle [in]
h	=	Fractional tooth height worn away

2.3.4 Mechanical specific energy

Mechanical specific energy (MSE) surveillance is another method for determining drilling performance. Teale defined the MSE as the energy being used per volume of rock drilled (Teale, 1965):

$$MSE = \frac{TOTAL\ ENERGY\ INPUT}{VOLUME\ REMOVED} \quad (19)$$

where the total energy input is the vertical energy plus the rotational energy.

Then the vertical energy, or work done, is the vertical force (WOB) times distance (ROP). The rotational energy, or work done, is the bit rotation (RPM) times torque. The volume of rock removed is the area of the bit times ROP. Therefore, the MSE can be expressed by:

$$MSE = \frac{WOB \cdot ROP}{A_b \cdot ROP} + \frac{2 \pi \cdot RPM \cdot T}{A_b \cdot ROP} \quad (20)$$

Introducing the mechanical efficiency factor, the final MSE equation is given by (Bevilacqua, 2013):

$$MSE = EFF_M \cdot \left(\frac{4 \cdot WOB}{\pi d_B^2} + \frac{480 \cdot RPM \cdot T}{d_B \cdot ROP} \right) \quad (21)$$

where

		Field units	SI units
MSE	= Mechanical specific energy	[psi]	[kg/cm ²]
WOB	= Weight on bit	[lb]	[kg]
RPM	= Rotary speed	[rev/min]	[rev/min]
T	= Torque on bit	[lb-ft]	[kg-m]
d_B	= Bit diameter	[in]	[cm]
ROP	= Rate of penetration	[ft/hr]	[m/hr]
EFF_M	= Mechanical efficiency		

Currently this equation it is called the Teale MSE model, and is valid under atmospheric conditions. The torque could be an erratic measure affected by the torque and drag of the drill string along the well. Pessier (1992) defined a coefficient of sliding friction μ to express the torque as a function of WOB as shown in Equation 22:

$$T = \frac{\mu \cdot WOB \cdot d_B}{36} \quad (22)$$

The TOB (torque on bit) is used to compute the MSE in the absence of reliable torque measurements.

Then the mechanical efficiency of rock destruction is defined by:

$$EFF_M = \frac{CCS}{MSE} \quad (23)$$

In theory, at perfect drilling efficiency, the value of the MSE is equal to the rock strength. In the experience of oil and gas companies, the bits are typically 30-40% efficient at peak performance (Guerrero, 2007). In field practice, MSE is primarily used as an indicator of drilling efficiency and thus it is not necessary to know the rock strength (IADC, 2014). The rock strength can be evaluated by:

- Unconfined compressive strength (UCS) represents the force applied to a defined area necessary to deform the rock at atmospheric pressure, whose value is characteristic and fixed for each type of formation and represents the minimum value of the relative mechanical resistance.
- Confined compressive strength (CCS) is the force on a defined area needed to deform a volume of rock which is subjected to pressure in a confined medium. CCS measures the maximum value of the resistance for each rock.
- The real compressive strength (RCS), of a defined formation, will be an average value within UCS and CCS. Experience of oil drilling engineers recommend maintaining the MSE value as close as possible to RCS. Unexpected changes in MSE may indicate changes in the rock formation, or drilling inefficiency, or both.

The MSE value could be plotted by the data-acquisition tools on the rig. Modern systems can provide relatively high definition with a sampling rate typically at 1 Hz, or sometimes even higher at 10 Hz. Then as the driller makes a change he can observe the MSE to see if rock cutting efficiency improves or declines. Mainly, WOB, RPM and flow rate are the parameters to operate and change when looking for efficient ROP, then while the driller is operating he can change one parameter, holding the others constant until the best combination is found.

An increase in MSE value can be caused by (IADC, 2014):

- Bit balling: build up of material on the bit that interferes with depth of cut.
- Interfacial severity: formations with hard inclusions or layers that cause axial shocks and break cutters.
- Bottom hole balling: layer of ground cuttings held to the bottom of the hole by differential pressure.
- Whirl vibrations: lateral motion of the string and bit.
- Stick-slip vibrations: torsional motion in which the bit speed oscillates periodically.
- Axial vibrations: axial motion in which the bit depth of cut oscillates periodically.
- Changes on Overbalance Pressure: increases of mud pump pressure or decreases on the gradient pressure.

When MSE information is combined with other information, it could be useful to determine the cause of the problem.

Figure 8 shows an example of a drill off test with a MSE record. The drill off test was done when a new formation was entered and a MSE increase was noted. If the MSE remains close to the baseline value while increasing the WOB until the floundered point, then the bit is as efficient at the high load as in the previous formation.

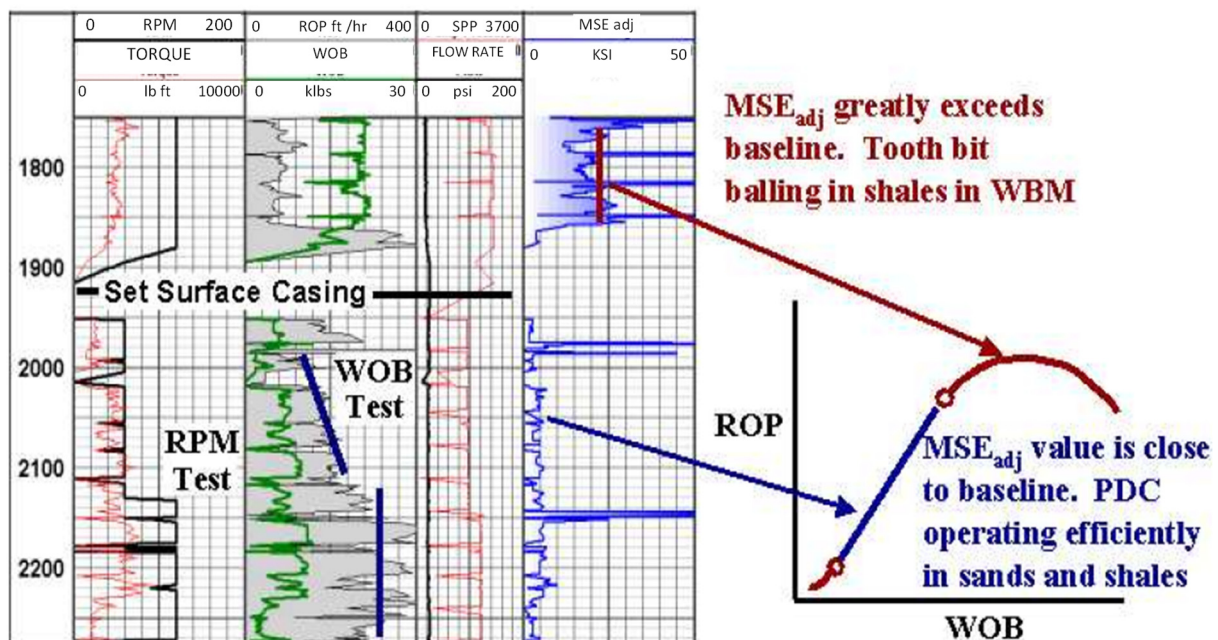


FIGURE 8: MSE analysis on a drill off test (Guerrero, 2007)

3. DATA AND RESULTS

3.1 Icelandic data – RN-16

Data from well RN-16 in Reykjanes, Iceland, is shown in this report with the purpose of trying the methods used to evaluate the drilling performance. Well RN-16 is located in Reykjanes at the south western tip of Iceland. This well was completed on May 6 of 2004 at 2627 m. The raw data was provided by ISOR and measurements were recorded with a sampling rate of 0.2 Hz (one set data per 5 seconds). It was necessary to filter the data and to delete the measurements done on connections, tripping, and other stops. After filtering, smoothing was done to get data with a width of 1 m of intervals (approx.) as is presented on Table 4.

TABLE 4: Data based by depth interval

MD [M]	WOB [ton]	RPM [rev/min]	ROP [m/h]	TORQUE [dN*m]	Flow Rate [l/s]	SPP (bar)	ECD [kg/l]	g_p [kg/l]
881.99	13.02	200.46	20.20	155.21	56.37	81.29	1.016707	0.869910
883.08	15.91	193.39	8.05	185.77	56.20	84.64	1.016728	0.869846
884.10	16.27	195.79	6.10	155.70	56.34	83.58	1.016747	0.869785
885.29	15.87	195.28	6.54	149.27	56.43	82.79	1.016770	0.869715
886.51	16.38	194.77	7.40	157.77	56.32	85.12	1.016793	0.869643
889.64	16.40	195.35	16.54	137.82	55.37	80.79	1.016852	0.869458
890.94	16.21	195.98	11.05	147.97	55.43	80.80	1.016877	0.869382
892.19	16.10	195.89	12.53	149.41	55.46	80.86	1.016900	0.869308
893.49	16.05	195.69	12.24	151.99	55.38	80.62	1.016925	0.869231
894.86	15.69	195.71	13.54	150.95	55.14	79.92	1.016951	0.869150
898.76	15.59	196.08	13.19	144.15	55.13	79.79	1.017025	0.868919
900.11	14.63	194.25	12.40	140.23	55.20	80.58	1.017050	0.868839
901.41	14.34	194.32	13.33	138.97	55.25	80.16	1.017075	0.868762
902.93	13.73	194.30	12.90	139.53	55.28	79.88	1.017104	0.868672

The lithology is mostly basalt tuff, tuffs and pillow lava. The secondary minerals found are shown in Table 5.

TABLE 5: Secondary minerals

Secondary mineral	Minimum temperature	RN-16
Quartz	100	880
Epidote	105	1074
Wollastonite	290	1050
Amphibole	290	2010
Garnet	290	1248
Calcite	300	>2532

The production casing 13 3/8" (K-55 98.46 kg/m) was set down to 870 m. The last section between 879 and 2627 m of depth was made with two TCI drill bits, 12 1/4" with nozzles 32/32", using fresh water as drilling mud. The interval from 879 to 1923 m was drilled using one 12 1/4" TCI drill bit, a 5" drill string and a bottom hole assembly including a downhole motor 9 1/2" M1XL, 9 drill collar 8", drilling jar, shock absorber (Kristjánsson et al., 2005). The drill operation was made combining the rotation of the drill string and DHM, the raw data collected included the corrections of the RPM. Appendix I shows the raw data filtered and smoothed (Table 1 and Figure 4 in Appendix I). Specifically, Table 1 in Appendix I presents a sample of the data used to show the drilling optimization methods.

3.1.1 Application of multiple regression analysis

Figure 9 shows a flow chart of the multiple regression steps. Visual basic and Excel were used to apply the ROP model described in Section 2.2.3, by taking the following steps.

The data was collected from 124 data set points (drilling parameters) from the interval between 882 to 1116 m. This section was drilled with a tricone insert bit starting at 879 m and as the wear of the bit is assumed to be minimal the value of x_7 was assumed to be equal to zero, as was explained in Section 2.3.3.

Equations 7-10 are used to find the values x_1 to x_8 . Using the x values and the ROP data, a matrix was formed which was solved

using multiple linear regression. To do this Equation 6 is modified by taking the logarithmic on both sides, such that the ROP is expressed by:

$$\ln ROP = a_1 + \sum_{j=2}^8 a_j x_j \quad (18)$$

With the ROP data base and the x values found, the multiple regression was run getting the a coefficients shown in Table 6:

TABLE 6: "a" coefficients

a1	a2	a3	a4	a5	a6	a7	a8
12446.21	-1.15	24.12	0.86	-0.1	-6.91	0	0.84

After the coefficients a_1 to a_8 are obtained, the model for the drilling rate or ROP is calculated and the results are shown in Figure 10 where they are compared with the measured ROP data. The square residuals are also displayed in Figure 10 and are considered acceptable.

The model introduced could be useful for another well in the same area, if the well prognosis, lithology, pore pressure, bit structure, drilling mud, operation, and the depth, are similar. Data from each additional well drilled in the area can be used to update the model for each interval. It is, however, necessary to validate the results by comparing the logged ROP to the ROP from model.

The a_5 and a_6 coefficients are used with Equations 4 and 5 in order to get the optimum WOB and RPM.

The optimal values are 8.5 tons and 194.7 rev/min for the WOB and RPM respectively. In other words, as an interpretation, the model helps to find the efficient point which was described in Section 2.3.1. in the literature overview. Figure 11 shows the data for the WOB versus ROP. The optimum WOB (8.5 tons) versus ROP (13.8 m/hr, average from model) is highlighted in the figure.

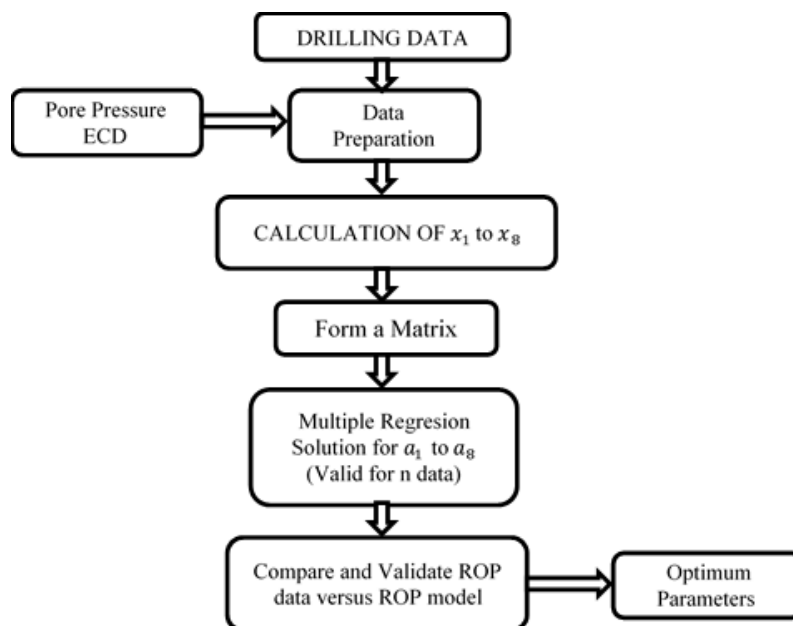


FIGURE 9: Steps of multiple regression

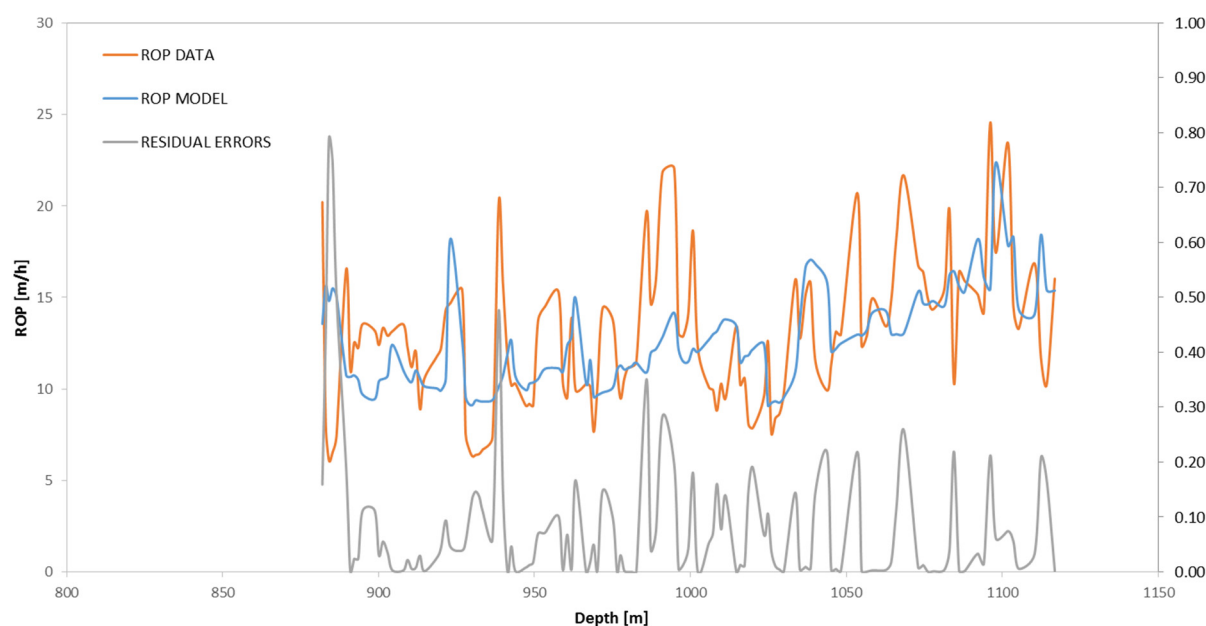


FIGURE 10: ROP data and ROP model

3.1.2 Application of mechanical specific energy

As explained before, the MSE is an indicator of the drilling performance. The log plot Figure 12 shows the drilling parameters and the behaviour of MSE calculated with Equation 21. The WOB and ROP data is plotted alongside the log plot with the aim of showing how the MSE could be a useful indicator while drilling.

As was indicated in Section 2.3.4, it is recommended to maintain the MSE value as close as possible to the estimated rock strength. For this report, it was assumed to be 24,000 psi for basalt and tuff rocks (Figure 5 in Appendix) as a relative indicator for high MSE value.

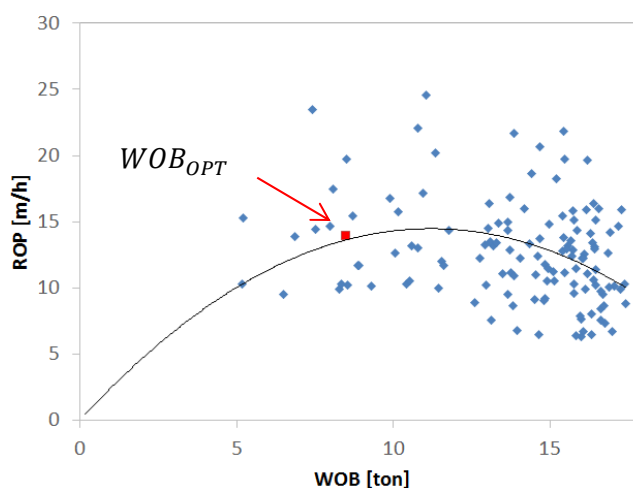


FIGURE 11: Response of the ROP at 882-1116 m (grey line is the smoothed line)

Intervals of similar lithology were selected. In Figure 12 the drilled layer Coarse Basalt (890-925 m) shows on Figure 13 that the ROP response is similar at 8, 12 or 16 tons without dependence of the depth, the low MSE is at 8 tons with a ROP response of 15 m/hr. The drilling performance on Fine-Mid Basalt (with some intercalations of Basaltic Tuff) is shown on Figure 14 where 12-16 tons have high MSE and 8-12 tons have low MSE, both scenarios have variable ROP with similar range.

Figure 15 shows intervals of Fine-Mid Basalt. Figure 16 shows that the WOB was close to 16 tons, when the driller reduced it to 12 tons and got a better ROP with lower MSE. Below this interval the same situation was repeated. Figure 17 shows a good example of optimum ROP found between 4 to 8 tons with low MSE. The lowest MSE is 8,000 psi, but it should be highlighted that a good estimation of CCS is an important factor to get a MSE baseline.

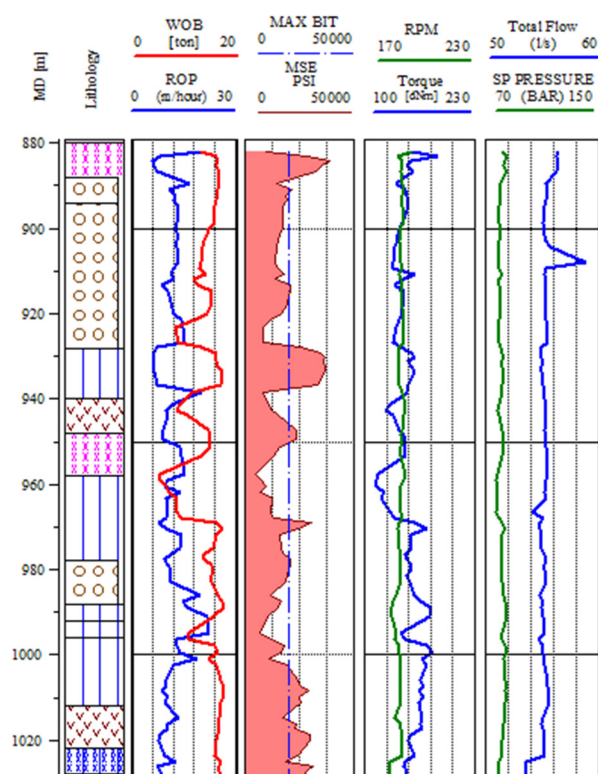


FIGURE 12: Log Plot drilling data 890-1030 m

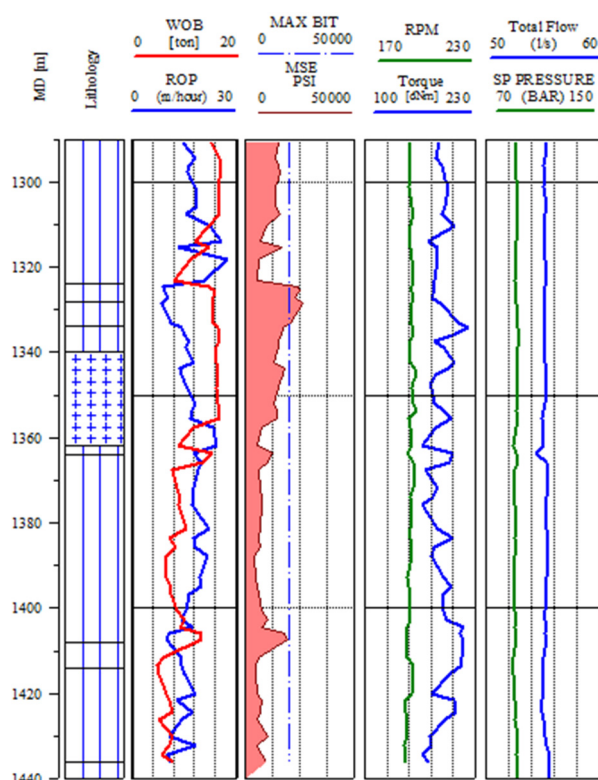


FIGURE 15: Log Plot drilling data 1290-1440 m

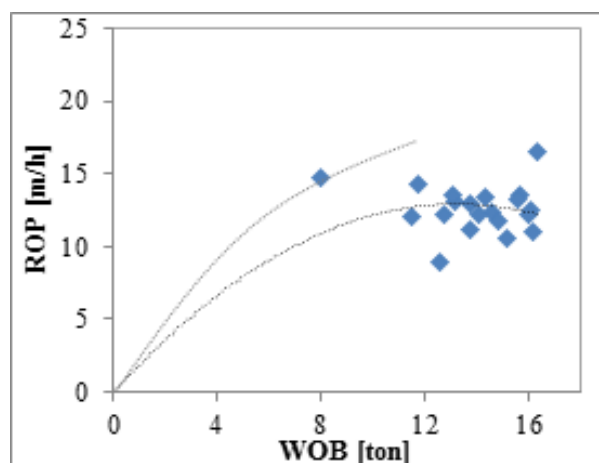


FIGURE 13: Response of ROP at 890-925 m

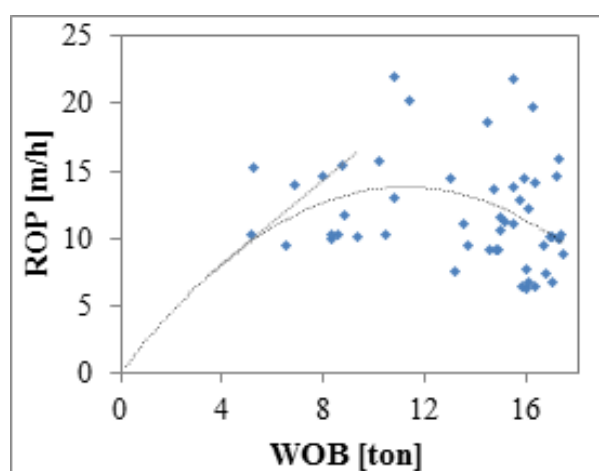


FIGURE 14: Response of ROP at 925-1010 m

In Figure 18 the combination WOB versus RPM shows the ROP performance, where the changes of these three parameters were cyclical along the interval from 890-1,500 m. At first glance it is possible to see where the lowest ROP and the highest MSE are.

Looking at the same lithology, two intervals were selected to show the difference on their operation behaviour and MSE indicator. As Figure 19 shows the WOB-RPM combinations in range A (WOB 5 to 11 tons and RPM 195 to 200) are less likely to result in low ROP (1.68-8.26 m/hr) and more likely to result in high ROP. Further, this combination results in the lowest MSE zone, which means that the drilling is efficient. It is worthy of attention to observe that the results from multiple linear regression, MSE and statistical analysis shows that high values of WOB (more than 12 tons) could be resulting in inefficient drilling. WOB in the 8-10 tons range seems to be most efficient, RPM in this section of the well does however not change significantly.

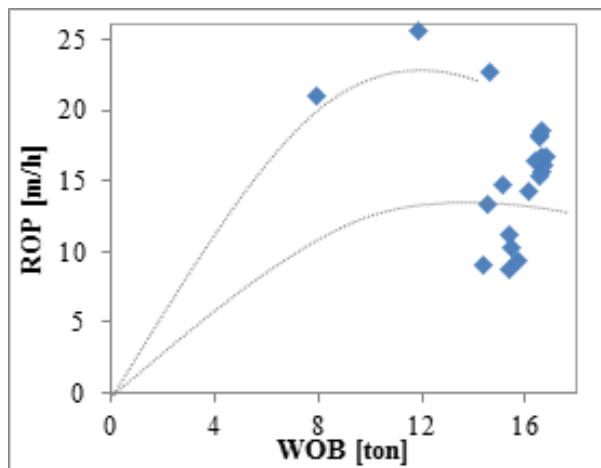


FIGURE 16: Response of ROP 1290 - 1338 m

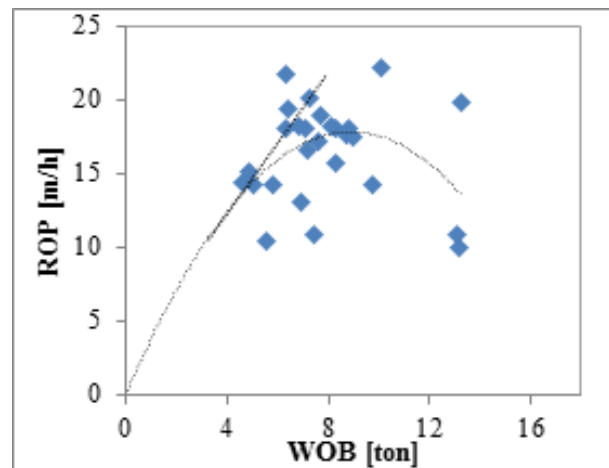


FIGURE 17: Response of ROP 1365 - 1436 m

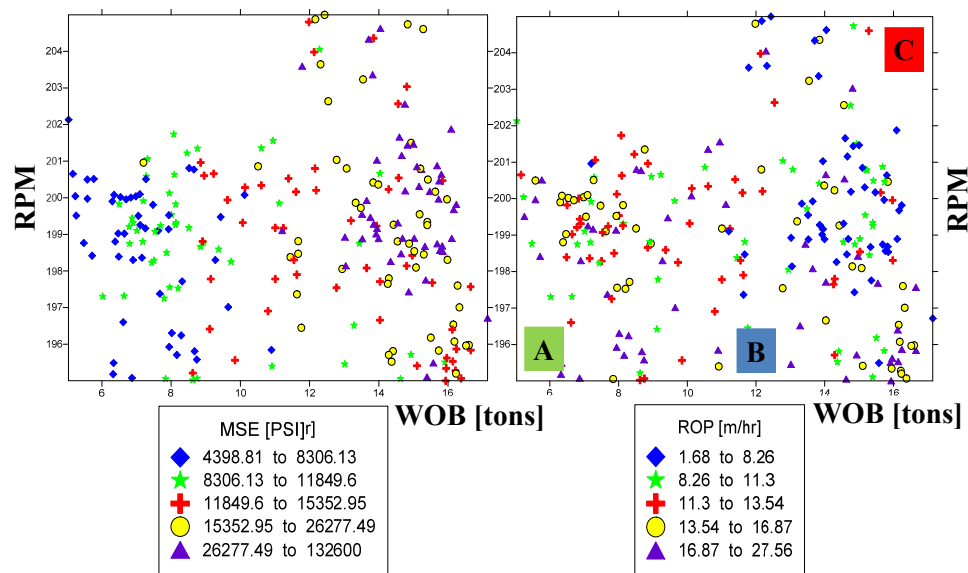


FIGURE 18: Distribution of MSE and ROP, 890-1500 m

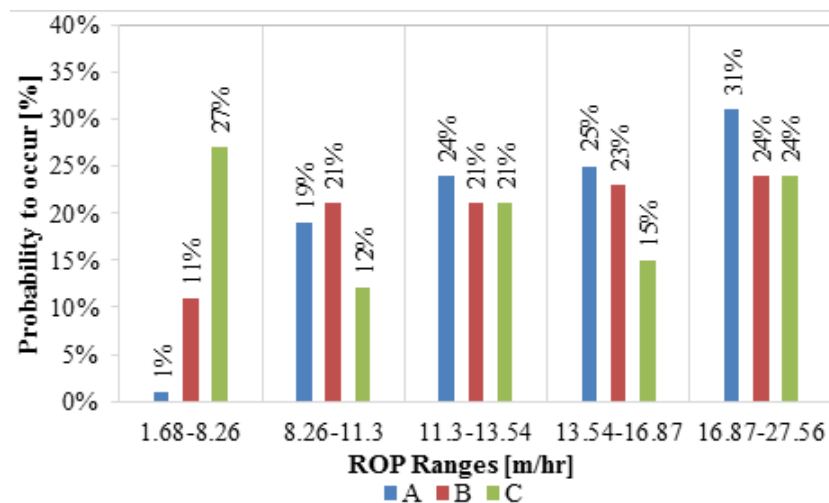


FIGURE 19: ROP probability distribution for WOB and RPM combinations

3.2 Bolivian data and results

As the raw drilling data from SM-1 and SM-2 was not available for analysis, it was not possible to apply the methods presented above. The summary in Table 7 was made from the available data, shown in Figure 2, 3 and Table 1; doing a comparison from the use of different kind of bits shows that drill bits with a long steel tooth were often used on shallow layers and short tooth TCI bit on sections 2 and 3. It is interesting that the steel bit with medium tooth was used on sections 2 and 3, and that the performance was similar to TCI bit on same section.

TABLE 7: Average performance of the bits in well SM-1 and SM-2

Bit type	Section	ROP average	Avg. drilled [m]	Avg. time used	Sum quantity
Steel bit with large tooth	0	1.77	56.86	34.80	3
	1	0.95	17.00	17.89	6
Steel bit with medium tooth	2	0.95	17.00	17.89	1
	3	3.85	141.50	34.42	2
TCI bit with short tooth	1	1.50	61.50	40.88	2
	2	2.94	127.75	51.02	5
	3	4.61	106.39	24.56	10

It is to be expected that the first wells drilled in a new field will take longer to drill than a well in a developed field. This is due to continuous improvement as the developer and personnel involved, gain a better understanding of the field and its geology. As mentioned in Section 1.3, it took 74.0 and 59.5 days to drill the SM-1 and SM-2 to 1,180 and 1,486 m of depth respectively. Figure 20 shows how the drilling time is divided between different activities on both wells, with drilling and cementing taking longest, as is usual. The aim of this report is drilling optimization that can result in reduced need for bit changes, help avoid drilling problems and mitigate non-productive time, all points that could result in reduction of cost.

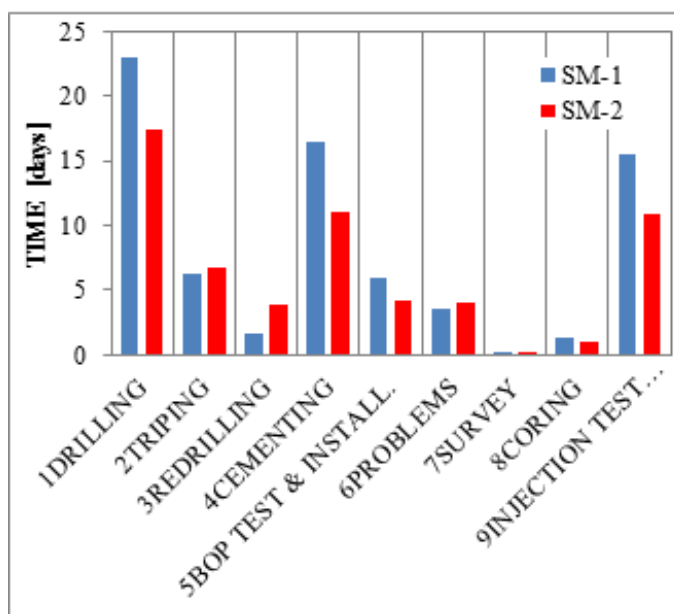


FIGURE 20: Distribution of working time on SM-1 and SM-2

The drill bit selection, for the new wells, will be done by a team studying the lithology, rock strength, fractures, drilling mud, temperature and others specific drilling needs. Below an attempt is made to provide an initial bit selection, by using the rules presented in Section 2.1 which can be thought of as an initial starting point for a selection of the drill bits:

- 26" hole (until-70 m): Steel Bit with long tooth hard formations and bearing gauge protected with the aim to drill with one trip (series 1-4-3 to 2-4-3). Due to a possible lack of WOB it might be necessary to use a bit 17.5" first and after that a 26" hole opener. Series 1-1-1 to 1-2-6 could provide more RPM with WOB reduction.
- 17 ½" hole (70-400 m): Similar to the last hole, steel tooth bit with long tooth for hard formation and bearing gauge protected with the aim to drill with one trip (series 1-4-3 to 2-4-3).

- 12 ¼" hole (400-850 m): in this section the angle will be built with KOP (kick-off point) planned at 450 m and an end of build at 30° of inclination. At least two changes of the drill bit should be planned. As it is possible to find high temperatures, a sealed bearing to journal friction bearing is recommended. Steel bit with middle tooth was used at similar depths on wells SM-1 and SM-2, thinking on the bit life and operation with down hole motor (DHM) TCI bit with longer to medium tooth could be useful (series 4-3-4 to 6-3-7).
- 8 ½" hole (850 – 2000 m): section holding 30° of inclination at high temperatures. At least two drill bits should be considered for this section. The use of DHM could improve the RPM on the bit resulting on more ROP (recommendable series 5-1-4 to 6-3-7).

The bit selection for the 12 ¼" and 8 ½" sections should be aimed at getting good ROP and bit life to avoid unexpected trips. Notice that a drilling program with estimated down hole temperatures and coring are very important to be able to choose the correct drill bit. Also for this section, the uses of PDC and hybrid drill bit should be considered.

It is recommended to analyse the rock core and do well logs such as compressional / shear travel time (Sonic log), bulk density (Density log), shale content (Gamma log) (Shrivastava et al., 2013) at least for the first wells. These results are very useful to find the unconfined compressive strength (UCS) and the confined compressive strength (CCS) which provide a better criterion for choosing a drill bit (Shrivastava, 2013). These surveys can also be useful for describing the characteristic of each formation.

4. CONCLUSIONS AND RECOMMENDATIONS

The drilling optimization methods explained in this report show similar results at the interval studied. The main points that can be highlighted are:

- Multiple linear regression model is able to predict the ROP and provide corrections especially for Weight on Bit (WOB). The model's reliability depends on data quantity and quality. When drilling in a new field, it is more reliable to find a_5 and a_6 through a drill off test, because of the reduction in the uncertainty of variables such as the drillability.
- Mechanical specific energy (MSE), was found to be a good indicator for efficient drilling and drilling rate (ROP). By including this indicator on the drillers monitor, it can facilitate the processing and analysis of drilling performance. Knowing the rock strength is valuable and provides added guidance to the driller in the form of a better established MSE baseline.
- Both methods can help improve the drilling operation by identifying the optimal ROP, reduce unexpected trips, accelerate the drilling related learning curve, reduce drilling risks and thereby mitigating NPT (nonproductive time), resulting in reduced costs per meter drilled. Both could be applied in real time while drilling.

Finally, a good drilling program and carefully selected materials and equipment should help in achieving optimum drilling time and total cost reduction. It is highly recommended to invest in scientific surveys such as well logging and coring laboratory studies to expedite knowledge build up when drilling in new fields.

ACKNOWLEDGEMENTS

Thanks to the Government of Iceland and UNU-GTP by giving me the scholarship for the six months Geothermal Training. My great gratitude goes to Mr. Lúdvík S. Georgsson and Mr. Ingimar G. Haraldsson who gave me the opportunity to participate, guidance and complete support along this training course. Thank you too much for Ms. Málfríður Ómarsdóttir, Ms. Thórhildur Ísberg and Mr. Markús A.G. Wilde for giving me their friendship and making me feel so comfortable in Iceland.

I want to give sincere thanks to my supervisor Kjartan Örn Sigurjónsson for helping and guiding me on the elaboration of this report. I extend my gratefulness to teachers from Iceland GeoSurvey ISOR and MANNVIT for sharing their knowledge.

I am very grateful to my Family, my brother and grandparents who give me support on my challenges, special thanks for my wife and children for their huge love.

I want to take this medium to express my gratitude to everyone who shared their knowledge and experience. I really appreciate their guidance, constructive criticism and friendly advice.

Finally, I wish to express my thanks to God for guiding my steps.

REFERENCES

Bevilacqua, M., Ciarapica, F., and Marchetti, B., 2013: *Acquisition, processing and evaluation of down hole data for monitoring efficiency of drilling processes*. DIISM - Università Politecnica delle Marche and Università degli Studi eCampus, Italy, 8 pp.

Bourgoyne, A.T., and Young, F.S., 1974: A multiple regression approach to optimal drilling and abnormal pressure detection. *Paper presented at the 6th SPE-AIME Conference on Drilling and Rock Mechanics, Austin, Texas*, 14 pp.

Bourgoyne, A.T., Millheim, K.K., Chenevert, M.E., and Young, F.S., 1991: *Applied drilling engineering* (2nd ed.). Society of Petroleum Engineers, Richardson, TX, US, 502 pp.

Cheraghi, M.S., and Ehteshami, P., 2013: Estimating the drilling rate in Ahvaz oil field. *J. Petroleum Exploration and Production Technology*, 2013, 169-173.

Eckel, J.R., 1968: Microbit studies of the effect of fluid properties and hydraulics on drilling rate. II. *SPE Annual Fall Meeting, Houston, October, SPE 2244*, 4 pp.

ENEL, 1989a: *Geothermal feasibility study in the área of Laguna Colorada. Report of the well SM-01, BOL/84/007*. Empresa Nacional de Electricidad - ENDE, internal report (in Spanish), 111 pp.

ENEL, 1989b: *Geothermal feasibility study in the área of Laguna Colorada. Report of the well SM-02, BOL/84/007*. Empresa Nacional de Electricidad - ENDE, internal report (in Spanish), 179 pp.

ENEL, 1991: *Geothermal feasibility study in Laguna Colorada area*. Empresa Nacional de Electricidad - ENDE, internal report (in Spanish), 395 pp.

Eren, T., 2010: *Real-time-optimization of drilling parameters during drilling operations*. Middle East Technical University, Ankara, Turkey, PhD thesis, 165 pp.

Guerrero, C., 2007: *Drilling optimization with mechanical specific energy*. SPE Drilling Studies Group, Chevron, 32 pp.

Graham, J.W., and Muench, N.L., 1959: Analytical determination of optimum bit weight and rotary speed combinations. *Proceedings of the Paper SPE 1349-G Presented at SPE-AIME 34th Annual Fall Meeting, Oct. 4-7, Dallas.*

IADC, 2014: *IADC drilling manual* (12th ed.). International Association of Drilling Contractors, 1158 pp.

Kristjánsson, B.R., Egilsson, Th., Gautason, B., Björnsson, G., Fridleifsson, G., Ásmundsson, R., Franzson, H., Danielsen, P., Jónasson, H., Hjartarson, Á., Hermannsson, G., and Jónsson, P., 2005: *Reykjanes – well RN-16 – 3. phase: Drilling of 12 ¼" production part from 879 m to 2627 m depth.* ÍSOR – Iceland GeoSurvey, Reykjavík, report, ISOR-2005/010 (in Icelandic), 99 pp.

Maurer, W.C., 1962: *The “perfect - cleaning” theory of rotary drilling.* SPE Drilling Engineering, Paper SPE-408-PA, 5 pp.

Murray, A.S., and Cunningham, R.A., 1955: Effect of mud column pressure on drilling rates. *Petroleum Transactions, AIME, 204, 196-204.*

Myora, T.O., 2014: *Modelling and optimization of geothermal drilling parameters – A case study of well MW-17 in Menengai, Kenya.* University of Iceland, Reykjavík, MSc thesis, UNU-GTP, report 6, 65 pp.

Ngugi, P.K., 2008: Geothermal well drilling. *Paper presented at “Short Course III on Exploration for Geothermal Resources”, organized by UNU-GTP and KenGen, at Lake Naivasha, Kenya, UNU-GTP, SC-07, 20 pp.*

Pessier, R.C., and Fear, M.J., 1992: Quantifying common drilling problems with mechanical specific energy and a bit-specific coefficient of sliding friction. *Paper presented at SPE Annual Technical Conference and Exhibition, Washington, D.C.* Paper SPE-24584-MS, 8 pp.

Ramos, P., 2014: *Well Data Analysis and Volumetric Assessment of the Sol De Mañana Geothermal Field, Bolivia.* Report 30 in: Geothermal training in Iceland 2014. UNU-GTP, Iceland, 665-688.

Shrivastava, S., Javed, A., and Pratap, K., 2013: Assessing rock compressive strength and predicting formation drillability using sonic, gamma & density logs. *Presented at 10th Biennial International Conference & Exposition, Drilling R&D and Technology Group, Institute of Drilling Technology, ONGC, Kochias. Uttarakhand, India, 7 pp.*

Stowe, R.L., 1969: *Strength and deformation properties of granite, basalt, limestone and tuff at various loading rates.* US Army Engineer Waterways Experiment Station, sponsored by Defense Atomic Support Agency, Vicksburg, MS, 162 pp.

Teale, R., 1965: The concept of specific energy in rock drilling. *Internat. J. of Rock Mechanics, 2, 57-73.*

TERANOV-CGG, 2014: *Geothermal project Laguna Colorada magnetotelluric survey Sol de Mañana.* CGG, internal report, submitted to ENDE, Bolivia.

West JEC, 2008: *Feasibility study for the geothermal power plant construction on Laguna Colorada.* West JEC, internal report (in Spanish), submitted to ENDE, Bolivia.

West JEC, 2010: *Preparatory study for the geothermal development of Sol de Mañana, Bolivia.* West JEC, internal report (in Spanish), submitted to ENDE, Bolivia.

APPENDIX I: Additional information and raw data

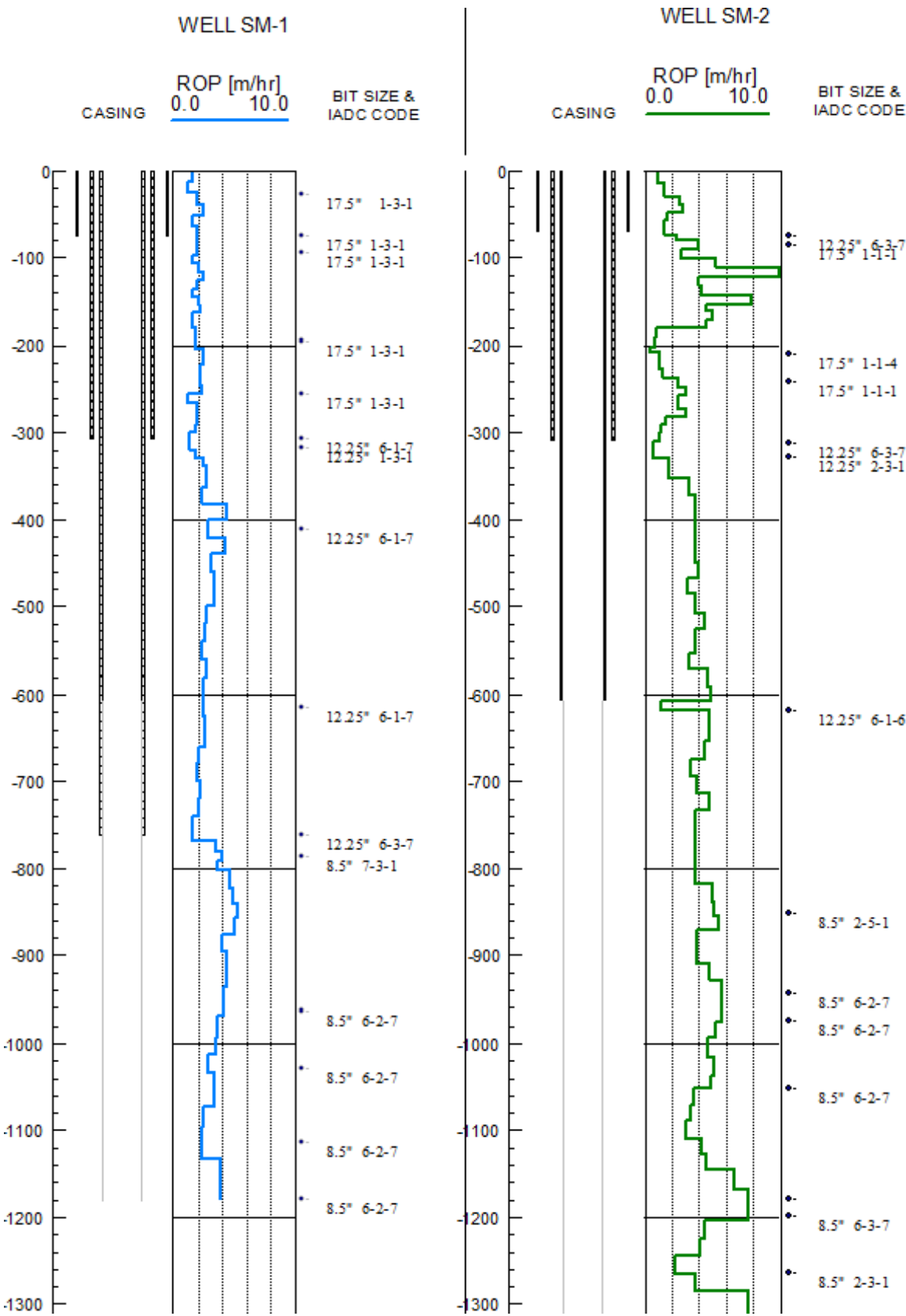


FIGURE 1: Drill bit data SM-1 and SM-2

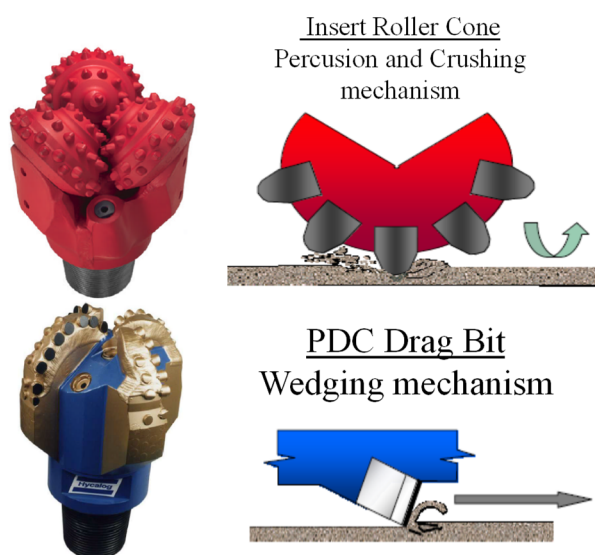


FIGURE 2: Drill mechanism of roller cone and PDC bit

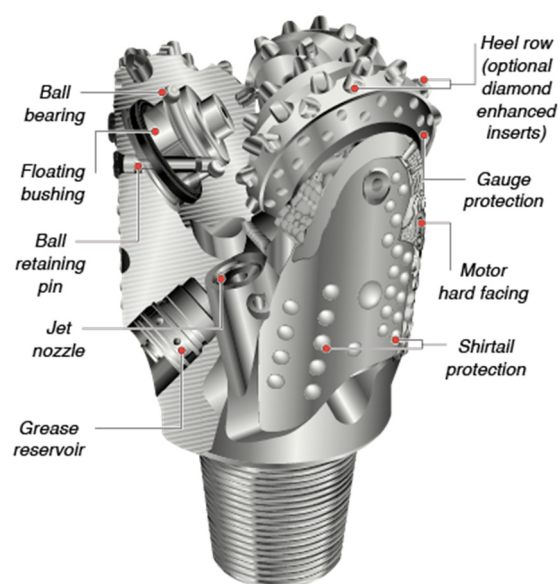


FIGURE 3: Parts of roller cone drill bit

TABLE 1: Sample of the raw data used

Data time	Depth of well	Mudpump1	Mudpump2	Mudpump3	TotalFlow Rate (l/s)	LOC (l/s)	SPP (bar)	Temperature, mud-pit (down)	Temperature, flowline (up)	Height of Kelly (m)	Total Weigh (ton)	WOB (ton)	RPM	TORQUE (dN m)	ROP (m/hr)
21/04/2004 21:22:15	885.52	28.05	28.16	0	56.22	0	85.14	10.21	16.09	3.01	30.81	16.11	39.8	157.18	7.02
21/04/2004 21:22:20	885.54	28.08	28.27	0.02	56.36	0	85.11	10.21	16.09	2.99	31.05	15.87	39.8	156.77	7.00
21/04/2004 21:22:25	885.54	28.06	28.37	0	56.43	0	84.94	10.21	16.09	2.99	31.21	15.71	39.9	155.39	6.98
21/04/2004 21:22:30	885.55	28.12	28.06	0.02	56.2	0	84.71	10.21	16.09	2.98	31.05	15.87	40	152.54	6.98
21/04/2004 21:22:35	885.55	28.06	28.14	0	56.2	0	84.53	10.21	16.09	2.98	31.53	15.4	40.1	152.86	6.97
21/04/2004 21:22:40	885.55	28.16	28.3	0	56.47	0	84.35	10.21	16.09	2.98	31.84	15.08	40.1	151.48	6.92
21/04/2004 21:22:45	885.56	28.06	28.16	0.02	56.24	0	84.1	10.21	16.07	2.97	32.08	14.84	40.1	151.32	6.87
21/04/2004 21:22:50	885.58	28.14	28.24	0.02	56.4	0	84.49	10.21	16.09	2.95	32	14.92	40.2	151.24	6.83
21/04/2004 21:22:55	885.58	27.98	28.43	0	56.41	0	84.41	10.21	16.09	2.95	32.24	14.69	40.2	151.64	6.79
21/04/2004 21:23:00	885.58	28.18	28.27	0.02	56.47	0	83.95	10.21	16.09	2.95	32.24	14.69	40.6	145.87	6.32
21/04/2004 21:23:05	885.60	28.18	28.15	0.02	56.35	0	83.68	10.21	16.09	2.94	32.47	14.45	40.6	144.56	6.26
21/04/2004 21:23:10	885.60	28.07	28.36	0	56.43	0	84.07	10.21	16.07	2.93	31.84	15.08	40.5	145.7	6.21

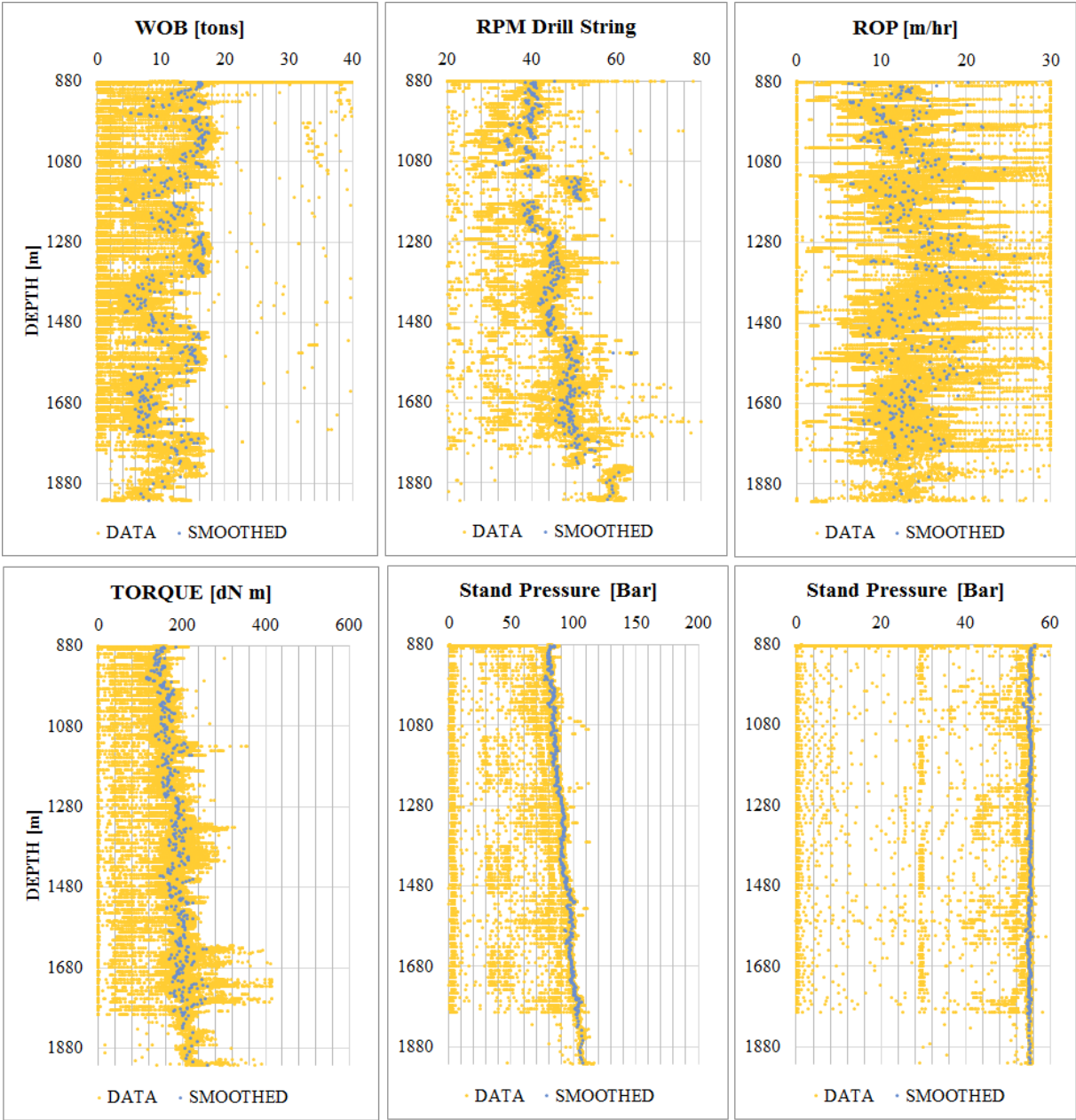
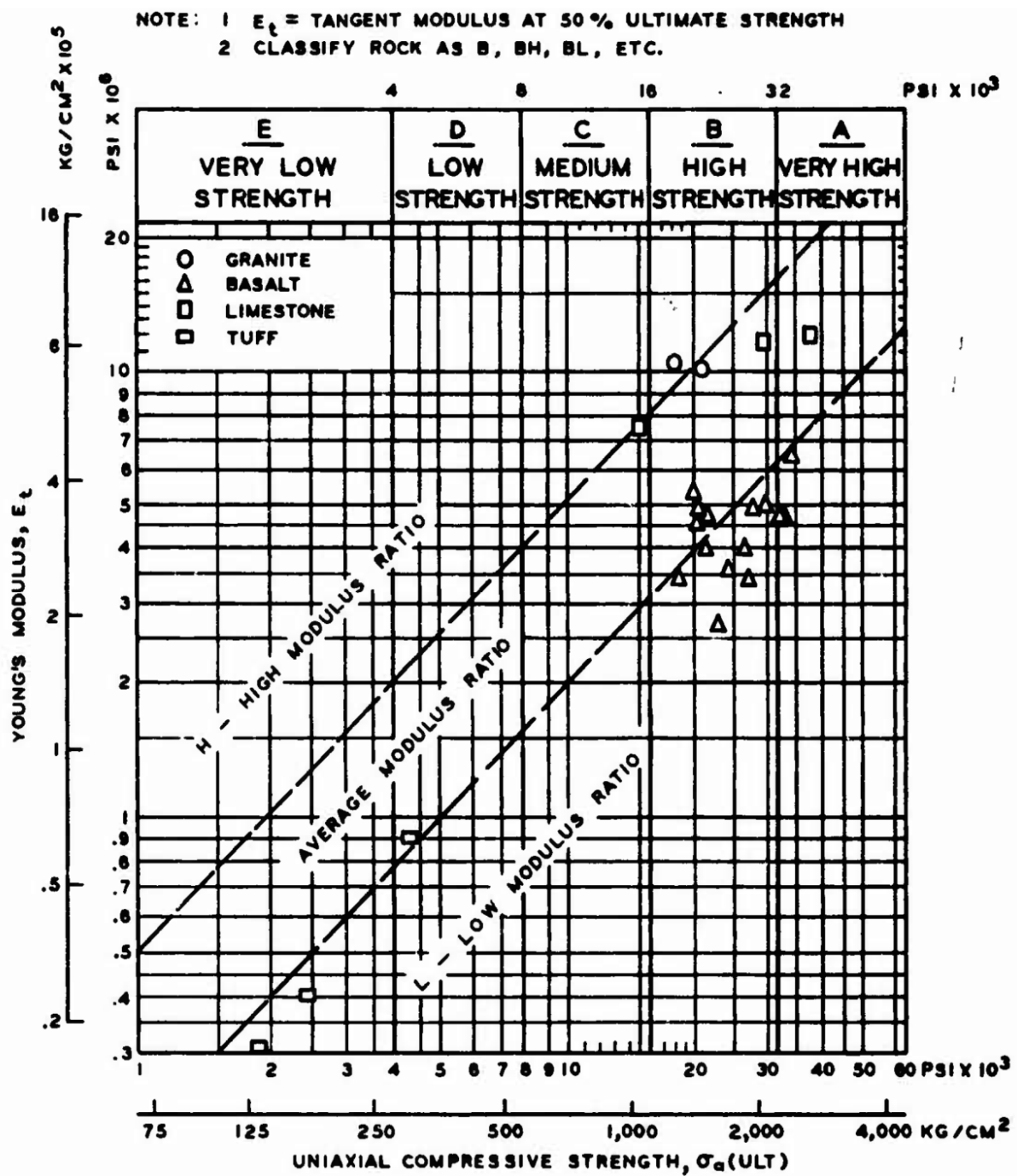


FIGURE 4: Raw data, filtered and smoothed





UNITED NATIONS
UNIVERSITY

UNU-GTP

Geothermal Training Programme

Orkustofnun, Grensasvegur 9,
IS-108 Reykjavik, Iceland

Reports 2016
Number 37

FEASIBILITY OF PRIVATE SECTOR'S PARTICIPATION IN GEOTHERMAL POWER GENERATION IN IRAN

Nasim Saber

Monenco Consulting Engineers

No. 12, Attar St., Valiasr Ave.

Tehran

IRAN

nasim.saber@yahoo.com

ABSTRACT

Iran wants to become an attractive frontier market for geothermal energy projects. The government has implemented laws guaranteeing power purchase for a period of up to 20 years but it seems not to be favourable enough to attract private sector participation. This is evident in the total lack of field developers since geothermal exploration begun in the Iran. The current system is not very attractive to prospective investors due to the unfavourable rate of return on their investments. This study gives an overview of the current conditions and procedural steps. It was also carried out with the aim of finding out the challenges towards Feed-in-Tariff law instrument to promote geothermal energy in Iran. To be attractive for the private sector, the price of electricity in Iran needs to increase, or drilling costs to be lowered to a comparable level to costs elsewhere in the world.

1. INTRODUCTION

Iran's energy mix is dominated by fossil fuels which satisfy around 97% of Iran's total primary energy demand (Figure 1). The remaining 3% come from a combination of hydropower, biofuels and other renewable sources as well as nuclear (BP, 2016).

Overreliance on fossil fuel sources is a problem for a number of reasons. For one, Iran's wealth of hydrocarbons has led the government to heavily subsidize fuel for individual energy consumption (MEI, 2016). The average price of gasoline around the world is 0.97 USD/L, while in Iran the price of gasoline is 0.39 USD/L, or close to the price of a bottle of mineral water (Globalpetrolprices.com, 2016).

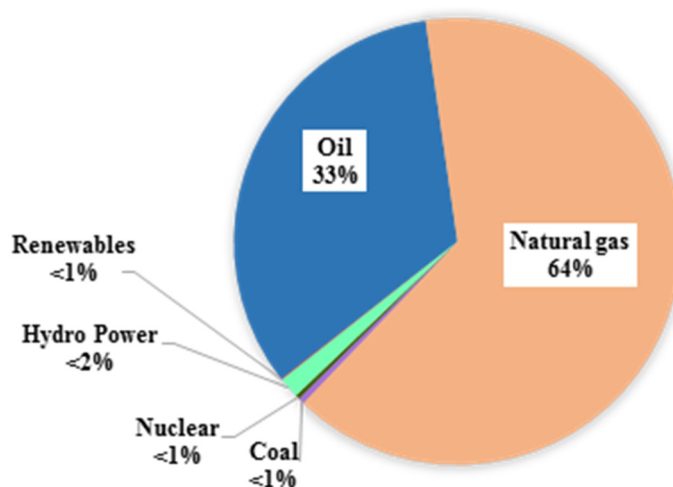


FIGURE 1: Iran's total primary energy consumption
(BP, 2016)

Iran's average wholesale electricity tariff is 8 USD/MWh which makes the electricity tariffs in Iran among the lowest in the world compared to e.g. 75 USD/MWh in Egypt or 17 USD/MWh in Russia (TradeArabia, 2016).

Additionally, Iran spends USD 30 billion annually to fuel its thermal power plant infrastructure (MEI, 2016). Demand for electricity is increasing in Iran, as the population is growing 3.5% faster than the country's GDP (gross domestic product). These numbers underline that Iran cannot reasonably sustain the use of hydrocarbons to generate electricity nationwide (MEI, 2016).

Iran will experience two major benefits by transitioning to a more diverse energy mix. First, a reduced domestic demand for fossil fuels will lead to increased competitiveness in global energy markets. In other words, reduced domestic demand will allow Iran to export more of its immense reserves of oil and natural gas to client states abroad. Second, reducing domestic fuel use will allow the government to ease its costly subsidies while simultaneously meeting a growing electrical demand through more sustainable and cost effective renewable energy sources (MEI, 2016).

The Iranian government is considering paying more attention to the utilization of renewable energies. Among the renewable sources, Iran has geothermal energy potential. The exploitable potential of geothermal energy for electricity generation is estimated to be 5,000-6,000 MW (Energypedia, 2016). Iran has also begun development on the Middle East's first geothermal power plant. This "pilot" station in the northwest Iranian province of Ardabil is expected to have an installed capacity of 50 MW (MEI, 2016).

To increase incentives for investing in renewable energy, Iran amended its laws in 2015. The previous regulations provided for a period of only five years a power purchase agreement including a uniform tariff for all types of technology. Pursuant to the new laws, a new system of feed-in tariffs, differentiating prices by type of technology, has been implemented. Moreover, the guaranteed period for power purchase has been extended to 20 years (WFW, 2016).

The present policy seems not to be favourable enough to attract private sector participation. This is evident in the total lack of field developers since geothermal exploration began in the Iran. The current fiscal incentives being enjoyed by these developers are not sufficient to warrant continuous sustainable exploration and development of this resource. The present system is not attractive to prospective investors, basically due to the unfavourable rate of return on their investments. To hasten the exploration and development of our geothermal resources, we need to improve the regulation to attract investments.

2. PRIVATE PARTICIPATION IN GEOTHERMAL ELECTRICITY GENERATION

2.1 Review of government regulations in Iran

2.1.1 Statistics of non-governmental renewable power plants

In Iran, the first non-governmental power plant became operational in 2009. Since 2009 until now, more than 440 million kWh of electricity from renewable sources have been produced and fed to the grid. The price of the electricity equalling 1270 billion Rials was paid to the power plants (SUNA, 2016). Table 1 shows the share of each renewable energy source in the generation of electricity.

TABLE 1: Summary of information related to production of non-governmental renewable power plants (SUNA, 2016)

	Wind (MWh)	Solar (MWh)	Biomass (MWh)	Small hydro (MWh)	Sea (wave) (MWh)	Geothermal (MWh)	Total (MWh)
Production	390,425	712	44,734	4,633	---	---	440,506

Until April 2016, of the received requests and issued permits for construction of non-governmental renewable energy power plants, about 68 MW were in production (Table 2) and 565 MW had obtained a power purchase agreement, based on two types of buyback contracts (3 MW) and a 133-article contract or guaranteed purchase (562 MW) (SUNA, 2016). As mentioned before, there is no non-governmental geothermal power plants in Iran (Table 1).

TABLE 2: Summary of information related to permits given to non-governmental renewable power plants (SUNA, 2016)

	Wind (MW)	Solar (MW)	Biomass (MW)	Small hydro (MW)	Sea (wave) (MW)	Geothermal (MW)	Total (MW)
Capacity	53.88	0.514	13.56	0.44	---	---	68.394

2.1.2 Feed-in tariffs

On the implementation of the legal obligations of Ministry of Energy, the guaranteed electricity purchase tariff for types of renewable are as follows (Table 3):

TABLE 3: The guaranteed electricity purchase tariff for the first 10 years for renewable energy (SUNA, 2016)

Technology type		Guaranteed purchase tariff (IRRs/kWh)	Guaranteed purchase tariff (US¢/kWh)
Biomass	Landfill	2700	9
	The anaerobic digestion of manure, sewage and agriculture	3500	11
	Incineration and waste gas storage	3700	12
Wind farm	> 50 MW capacity	3400	11
	≤ 50 MW capacity	4200	13
Solar farm	> 30 MW capacity	3200	10
	≤ 30 MW capacity	4000	13
	≤ 10 MW capacity	4900	16
Geothermal (including exploration and equipment)		4900	16
Waste recycling in industrial processes		2900	9
Small hydropower (≤ 10 MW capacity)	Installation in rivers, and through use of dams	2100	7
	Installation through pipelines	1500	5

Power Purchase Agreements of power plants subject to this announcement are extended to a 20 years' period with the specified tariffs. Tariffs will be multiplied by a factor of 0.7 after adjustment of Article 3 of the *Economic Council Directive* starting from the first day of the second 10 year period until the end of the contract. The rates of this announcement are applied to contracts, where the contracted power plant has been constructed and commercially operated within a period of a maximum of 30 months since the notification of the contract. Tariffs will be proportionately increased up to 30% in accordance to the instructions under Article 6 of the *Economic Council Directive*, for power plants constructed using local equipment, technologies, know-how, design and manufacturing (SUNA, 2016).

2.1.3 Procedural steps

Workflow for a proposed project should be as follows (Figure 2):

Phase 1: Registration and issuance of construction permit.

Phase 2: Obtaining required permits and concluding contract.

Phase 3: Project execution period and construction of the power plant (after signing the contract).

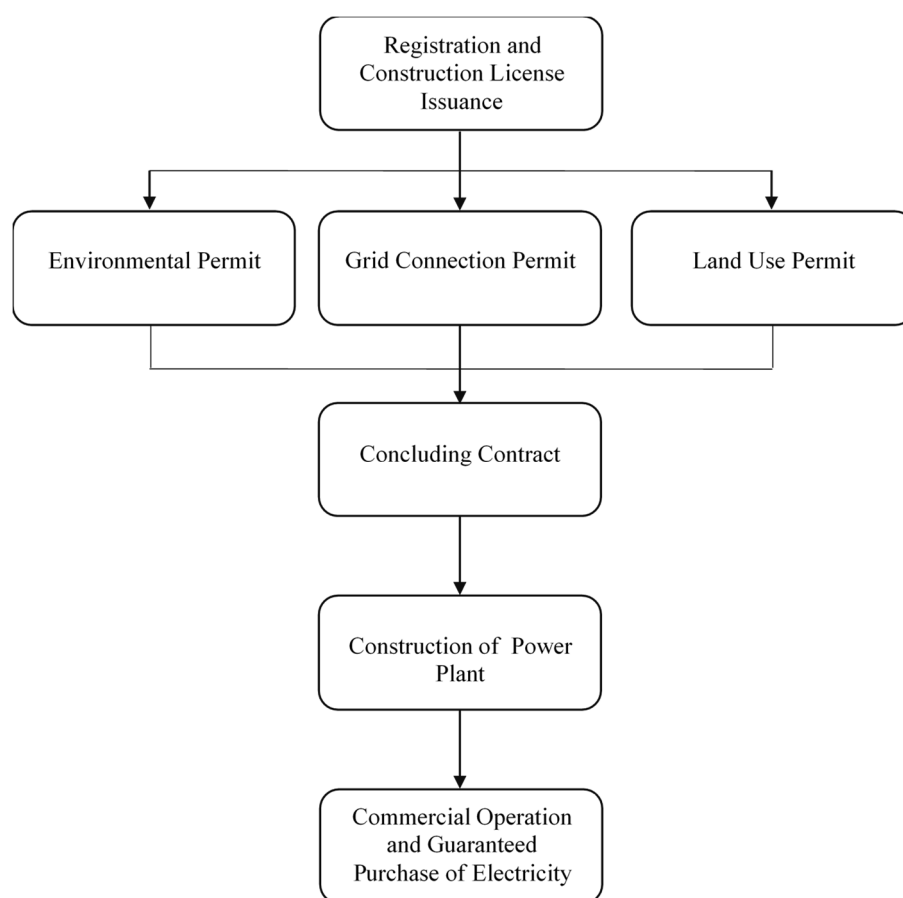


FIGURE 2: Steps of implementing renewable energy projects (SUNA, 2016)

Phase 4: Operating period.

In order to start constructing a renewable energy power plant in Iran, an application must be submitted to SUNA (Renewable Energy Organization of Iran) containing details of the project such as location and estimated capacity of the plant. The applicant must be non-governmental. Moreover, it must be an Iranian person, thus, foreign investors are required to incorporate a company in Iran (or to enter into a joint venture with a local partner). However, it is permissible for foreign investors to hold 100% of the share capital in an Iranian company. Upon verification of the aforementioned requirements and on the condition that no overlap exists with the sites of previously registered projects, SUNA will issue a construction permit to the applicant.

Following the issuance of the construction permit, the applicant has to obtain other necessary permits such as environmental preservation, grid connection and land permits. Thereafter, a power purchase agreement can be concluded with SUNA and the construction of the power plant can commence. During the construction period, the project company is required to periodically submit progress reports to SUNA. SUNA controls and supervises the construction and coordinates the grid connection tests and inspections through the Iran Grid Management Company. The plant must be commissioned within 18 months of the conclusion of the power purchase agreement, otherwise the tariff valid at the time of commissioning will be applied, rather than the tariff valid at the time of the conclusion of the power purchase agreement (WFW, 2016).

2.2 Review of governmental regulations in other countries

Countries worldwide are increasingly turning to *feed-in tariffs* as a mechanism to develop geothermal energy. In many countries of the world feed-in tariffs play a fundamental role in raising the commercial

interest of investors in geothermal electricity production such as in Austria, Croatia, Ecuador, France, Germany, Greece, Indonesia, Italy, Japan, Kenya, Moldova, Portugal, Serbia, Slovakia, Slovenia, Switzerland, Taiwan, Turkey, and Uganda (Table 4).

TABLE 4: The guaranteed electricity purchase tariff for geothermal energy in selected countries

Country	Size of plant	Contract term	US¢ / kWh
Austria ¹	-	13	8.29 (reduced by 1% annually)
Ecuador ²	-	15	13.81
France ¹	-	15	French mainland: 22.31 + premium of up to 8.92 for energy efficiency Overseas Departments and Overseas Collectives): 14.5 + premium of up to 3.35 for energy efficiency
Germany ¹	-	20	28.11
Greece ¹	-	20	Low-temperature geothermal generation: 15.951 (no support); 14.501 (with support) High-temperature geothermal generation (>90°C): 12.27 (no support); 11.155 (with support)
Indonesia ³	-	-	I. Sumatera, Java and Bali, Sulawesi, NTB, NTT (11.8-15.9) (2015-2025) (0.4 average increase/year) II. Halmahera, Maluku, Papua and Kalimantan (17-23.3) (2015-2025) (0.6 average increase/year) III. Isolated areas within Region I and II where electricity is supplied by fuel oil power plant (25.4-29.6) (2015-2025) (0.4 average increase/year)
Italy ¹	1 kW - 1 MW	20	15.059
Japan ⁴	< 15 MW ≥ 15 MW	15	38 25
Kenya ⁵	35-70 MW	20	8.8-20% for first 12 years and 15% after
Moldova ¹	-	15	Feed-in tariffs are determined and approved annually, depending on type and capacity of power plant, amount of electricity produced and expected to be delivered.
Portugal ¹	≤ 3 MW	12	The indicative average rate is 30.117
Serbia ¹	≤ 1 MW 1-2 MW > 5 MW	12	10.79 11.58-0.77×P; where P = installed power 7.72
Slovakia ¹	-	15	17.304
Slovenia ¹	-	15	The price is based on the reference price applicable on the day on which the contract is concluded.
Switzerland ¹	≤ 5 MW ≤ 10 MW ≤ 20 MW > 20 MW	20	41 37 29 23
Taiwan ⁷	-	20	15.9081
Turkey ¹		10 years for feed-in tariff, first 5 years of operation for bonus tariff for local- content support	10.5 local-content bonus: 0.7-2.7
Uganda ⁶		20	7.7

Sources: 1) Res-Legal, 2016; 2) Campen and O'Sullivan, 2015; 3) Repit.wordpress, 2016; 4) IEA, 2016; 5) ERC, 2016; 6) ERA, 2014; 7) MOEABOE, 2015 and 2016.

In selected countries, the contract terms of feed-in tariffs for electricity generated from geothermal power are valid from 12 to 20 years. The tariffs vary significantly between countries, from 7.7 US¢ in Uganda to 41 US¢ for small geothermal power plants in Switzerland. Japan, Serbia and Switzerland have more than one tariff category, depending on the size of the power plant (Haraldsson, 2014).

3. COST ESTIMATION OF BUILDING A GEOTHERMAL POWER PLANT

3.1 Capital cost of a geothermal power plant

The primary stages of a geothermal developmental cycle are exploration, resource confirmation, drilling and reservoir development, plant construction and power production. Four phases of the geothermal energy project will be used as a baseline plan for a future feasibility models:

- 1) Exploration and confirmation cost;
- 2) Drilling cost;
- 3) Power plant cost;
- 4) Operation and maintenance cost.

The capital cost of geothermal power plants varies, depending on the resource chemistry, temperature, and technology employed. The majority of the overall cost is typically attributed to construction of the power plant, due to the high cost of raw materials including steel (46.6% of the total cost). The second highest costs are associated with the exploration and production drilling stages, which together can comprise 42% of the total cost. Low-temperature reservoirs typically use binary power plants, while moderate- to high-temperature reservoirs employ dry steam or flash steam plants, based on whether the production wells produce primarily steam or water, respectively (Cross and Freeman, 2008). Table 5 shows capital costs of a geothermal power plant according to different references. This information indicates that capital costs of binary projects are higher than those of flash technologies.

TABLE 5: Overview of some reported capital cost of geothermal power technologies

Author	Technology	Capital cost (USD/W)	Cap. cost range (USD/W)
Geo-energy, 2016	NS (not specified)	3.4	-
Chatenay and Jóhannesson, 2014	NS (50 MW uses 250°C geothermal fluid)	3.7	-
Gehringer and Loksha, 2012	NS	4	-
Salmon et al., 2011	NS	3 - 4	-
Konyali, 2010	NS	1.2 – 3	-
Average capital cost not specified (NS)		3.33	1.15 - 4
Matek and Gawell, 2014	Flash	2.7	-
IRENA, 2012	Flash	2 - 4	-
Average capital cost flash		2.83	2 - 4
Matek and Gawell, 2014	Binary	5.2	-
IRENA, 2014	Binary	5 - 10	-
Chatenay and Jóhannesson, 2014	Binary (10 MW using 150°C geothermal fluid)	5.3	-
IRENA, 2012	Binary	2.4 - 5.9	-
Average capital cost binary		5.53	2.4 - 10

3.1.1 Exploration and confirmation cost

Exploration is the initial development phase and seeks to locate a geothermal resource that can provide sufficient energy to run a power plant and produce electricity. This phase begins with various kinds of exploration methods and field analysis, and ends with the drilling of the first successful full-size commercial production well. Resources defined during the exploration phase, can be divided into three sub-phases: regional reconnaissance, district exploration, and prospect evaluation. Recent interviews with geothermal developers provided exploration cost estimates averaging 150 USD/kW. Total exploration cost figures may thus range from 100 to 200 USD/kW according to the nature of the project (greenfield vs. expansion), the amount of information available initially, the selection of technologies involved in each exploration phase, and the size of the project and resulting economies of scale (Hance, 2005).

The confirmation phase includes the drilling of additional production wells and testing their flow rates until approximately 25% of the resource capacity needed by the project is achieved. It also involves reservoir design, engineering, and the drilling of some injection capacity to dispose of fluids from production well tests. Other activities and costs consist of well testing, reporting, regulatory compliance and permitting, and administration. Confirmation cost estimates for commercially viable projects are considered to average 150 USD/kW (Hance, 2005). An average cost of 346 USD/kW can be considered when the confirmation phase is done in tandem with the exploration phase (Salas, 2012). In this study, exploration and confirmation cost is considered 346 USD/kW.

3.1.2 Drilling cost

Exploration cost related to drilling is usually the single largest cost and a highly risky component in any geothermal development. Given the circumstances, it is expected that the cost of drilling will be very variable; while this is certainly true to some degree, there are general tendencies (Salas, 2012).

Two major factors will affect the total drilling costs:

- 1) The cost of drilling individual wells; and
- 2) The number of wells to drill.

The cost of an individual well is mainly related to the depth and diameter of the well as well as the properties of the rock formation. The number of wells to drill is determined by the average well productivity and the size of the project. Well productivity directly depends on the resource temperature and the rock permeability (Hance, 2005).

The productivity of each well (P_{well}) expressed as a function of estimated reservoir temperature (T_{well}) can be written as:

$$P_{well} = \frac{9}{250} T_{well} - 2.86 \quad (1)$$

Additional wells are drilled for production purpose. One reinjection well is usually required for every 4-5 production wells (Ngugi, 2013).

For estimation presented here, based on information from industrial partners, it is assumed that the average depth of the wells in Sabalan area is 2,400 m and the estimated reservoir temperature is 265°C. In addition, drilling cost in Iran is 5,000 USD/m, while it is not so high in other countries as will be better discussed in Section 5.2. Most fields have an overall success rate of over 50% and 80-90% is the most common (Avato, 2013). For the study presented in this report, the success rate is assumed to be 75%.

3.1.3 Power plant cost

Equipment purchase cost estimation is the key driver of the capital cost estimation for a given power plant project. There are three main sources of equipment estimation data: vendor contacts, open literature, and computerized estimating systems (Salas, 2012). In this section, the prices of the main geothermal power plant components are collected from home country purchase documents for the 5 MW Sabalan geothermal pilot plant.

There is an important concept to take into account when estimating costs: economy of scale. Economy of scale refers to the idea that “bigger is cheaper” per unit output. In quantitative terms (Geirdal, 2013):

$$\left(\frac{C_i}{K_i}\right) = \left(\frac{C_0}{K_0}\right) \left(\frac{K_i}{K_0}\right)^{n-1} \quad (2)$$

where C_i = The cost of the unit of size i ;
 C_0 = The cost of the reference unit;
 K_i = The size or rating of unit i ;
 K_0 = The size or rating of the reference unit;
 n = The scale exponent.

Scale exponent is often about 0.6 for chemical processing plants. In general, n has a range of 0.5 to 0.9, for different types of equipment and each type of processing plant has its characteristic value (Berthouex, 1972). In this study, economy of scale is used for estimating the cost of a 50 MW power plant and n is assumed 0.9.

3.2 Operation and maintenance costs

The operation and maintenance cost (O&M cost) factors may be categorized as ordinary O&M costs which include staff, administrative and cost of spares, the plant inefficiency, reservoir management costs and cost of capital associated with increased working capital.

The rate of operation and maintenance is fairly low for geothermal power plants in comparison to conventional power plants. The Kenyan experience indicates the cost to be about 0.00763 USD/kWh (Ngugi, 2012). According to ESMAF, total O&M costs for a 50 MW power plant in a developing or developed country would be in the range of USD 3.5-10.5 million per year. These costs can be translated into USD 0.009-0.027 per generated kWh, based on a 90% capacity factor (Gehringer and Loksha, 2012). For this estimation, it is assumed 0.009 USD/kWh.

4. FINANCIAL FEASIBILITY ASSESSMENTS

Before an investment decision is made it is necessary to determine whether or not the planned investment idea is feasible. A financial feasibility analysis is an effective analytical tool which can be used to evaluate investments from various perspectives, such as technical, social, legal, financial, market, and organizational (Björnsdóttir, 2010).

The finances necessary to make an investment must be paid right away, while benefits accrue over time. Benefits are based on future events and the ability to predict the future is imperfect; therefore, it is crucial to carefully evaluate investment alternatives (Salas, 2012).

For investors to engage in a new investment project, the project has to be financially viable. Invested capital must show the potential to generate an economic return to investors at least equal to that available from other similarly risky investments, i.e. the return on investment needs to be equal or higher. Financial feasibility analysis is an analytical tool used to evaluate the economic viability of an investment. It consists of evaluating the financial conditions and operating performance of the investment and forecasting its future conditions and performance. A financial decision is dependent on two specific factors, expected return and expected risk, and a financial feasibility analysis is a means for examining these two factors (Björnsdóttir, 2010).

The model used in this study is a mathematical model which makes it easier and less time consuming to update the analysis. It is designed for Microsoft Excel in a spreadsheet form. In this model the Net Present Value (NPV) and Internal Rate of Return (IRR) are used as profitability criteria. Both of them are calculated with Excel's built-in functions. Two scenarios will be calculated for profitability in order to figure out the viability of this project:

- *Scenario 1: 5 MW geothermal power plant*
- *Scenario 2: 50 MW geothermal power plant*

4.1 Net Present Value

The Net Present Value (NPV) is the difference between the present value of all cash inflows and cash outflows associated with an investment project. The formula for the NPV is (Björnsdóttir, 2010):

$$NPV(i) = \frac{A_0}{(1+i)^0} + \frac{A_1}{(1+i)^1} + \dots + \frac{A_N}{(1+i)^N} = \sum_{n=0}^N \frac{A_n}{(1+i)^n} \quad (3)$$

where A_n = Net cash flow at the end of period n ;
 i = MARR (Marginal Attractive Rate of Return);
 N = Service life of the project.

If the NPV(i) is positive for a single project, the project is financially feasible, since a positive NPV means that the project has greater equivalent value of inflows than outflows and therefore makes a profit (Björnsdóttir, 2010).

The calculation of the NPV requires a value for the discount rate i and its selection is the main difficulty for this method. Discount rate value selection is essentially a strategic function and is done from the viewpoint of the entire organization. The value of the discount rate that is used can be the financial cost of capital, the economic cost of capital or the risk adjusted discount rate (Salas, 2012).

4.2 Internal Rate of Return

The Internal Rate of Return (IRR or i^*) is defined as the compound rate of return i that makes the NPV equal to zero (Salas, 2012) which is expressed as:

$$NPV(i^*) = \sum_{n=0}^N \frac{A_n}{(1+i^*)^n} = 0 \quad (4)$$

Investors usually want to do better than breaking even in their investments. Their investment policy usually defines a minimum acceptable rate of return (MARR), in which case the IRR and the MARR can be used to decide whether a project is feasible or not. The decision rule for a simple project is as follows (Björnsdóttir, 2010):

If $IRR > MARR$, accept the project;
 If $IRR = MARR$, remain indifferent;
 If $IRR < MARR$, reject the project.

4.3 Model inputs and assumptions

As with any model calculations, some assumptions regarding the model have to be made. The assumptions made for the financial model are stated here below.

The planning horizon is the amount of time an organization will look into the future when preparing a strategic plan and is set to 20 years in this study based on the contract terms of the feed-in tariffs. The construction time of the power plant is assumed to be one year (2016) for Scenario 1 and seven years for Scenario 2 (2016-2022).

Capital cost. The total cost in this model is divided into three categories: buildings costs, equipment costs and other costs.

Working capital is the capital needed to pay short-term debts and continue operations. It is assumed to be 0 MUSD for Scenario 1 and 36 MUSD for Scenario 2.

Financials. The financial inputs and assumptions include requirements of the owners, tax and accounting regulations of the respective country, etc. (Björnsdóttir, 2010). Following are the required inputs regarding the project's financials which are based on Iran's laws and regulations (see Table 6):

- *MARR*: the minimum acceptable rate of return for both project and equity needs to be determined by the project owners.
- *Equity percentage*: the part of the project's capital cost that will be paid with equity from owners. The financing for both scenarios in this project is considered to be 25% equity and 75% loan.
- *Dividend percentage*: the proportion of profits that will be paid to owners in the form of dividends.
- *Income (corporation) tax*: determined in compliance with the respective country's laws and regulations.
- *Depreciation*: determined in compliance with the respective country's laws and regulations. Depreciation categories may have to be defined as applicable for each project, e.g. buildings, equipment and other investment.
- *Loan interests*: different interests are available for different projects, depending on the project's estimated return and risk, as well as conditions on financial markets. If the project owners plan to refinance the project after some time, the refinancing interests also need to be determined.
- *Loan life*: the time from when repayments of a loan start until the loan is fully paid.

TABLE 6: Financials inputs

Input	Value
Discounting rate project, MARR project	17%
Discounting rate equity, MARR equity	24%
Equity	25%
Loans	75%
Loan repayments	5 years
Loan interest	6%
Debtors	10%
Creditors	10%
Dividend	30%
Depreciation buildings	4%
Depreciation equipment.	10%
Depreciation other	20%
Loan management fees	2%
Income tax	25%

5. RESULTS

5.1 Financial feasibility assessments in Iran – capital cost

The previous sections provided a methodology to estimate all expenses related to the capital cost for development of a geothermal power plant (PP). Capital cost for geothermal power plant includes exploration and confirmation, drilling and power plant costs. Most of the estimations are based on related literature, which present average cost figures. Table 7 shows a summary of costs for the two different PPs, 5 MW and 50 MW. The estimated capital costs will be used as input in the financial modelling. Figure 3 illustrates the breakdown of the total capital cost for the two scenarios. This includes

TABLE 7: Estimated cost of the two different geothermal power plant

Power plant capacity (MW)	Category	Cost (MUSD)
5	Exploration and confirmation	1.7
	Drilling	12
	Power plant	15.7
	Capital cost	29.5
	Capital cost per MW	5.9
	Operation and maintenance (every year)	0.4
50	Exploration and confirmation	17.3
	Drilling	144
	Power plant	124.9
	Capital cost	286.2
	Capital cost per MW	5.7
	Operation and maintenance (every year)	3.9

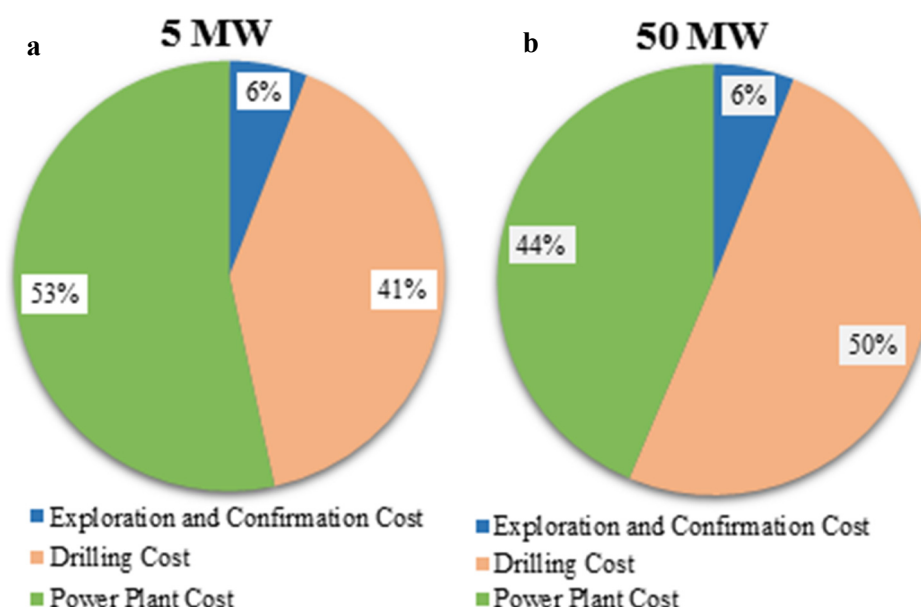


FIGURE 3: Breakdown of the total capital cost for, a) a 5 MW PP; and b) a 50 MW PP

all the costs associated with total investment where the drilling cost is approximately 50%. In the case of Iran drilling cost is the dominant factor. The bigger power plant is more cost effective, so the share of the power plant cost (percentage wise) for the 50 MW PP is lower than for the 5 MW PP. Therefore the share of the drilling costs (percentage of the total costs) for the 50 MW PP will be bigger than for 5 MW.

5.1.1 Scenario 1 - 5 MW geothermal power plant

The cash flows of the investment project for the 5 MW power plant are illustrated in Figure 4. The chart shows two cash flows, one for capital investment and the other for equity. As seen from the chart, there is outflow of cash during the construction of the project, i.e. in the first year (2016). When the construction is finished, the project starts to generate income but just for one year (2017) because after a year the loan received must be paid. The loan received, which accounts for 75% of the investment cost and working capital, is paid over 5 years after a year of start-up in 2018, so this is the reason why there is a dip in the net cash flow and equity from 2018 to 2022. After that the power plant begins to make profit as revenues from sales. Tariffs will be multiplied by 0.7 from the first day of the second 10 years

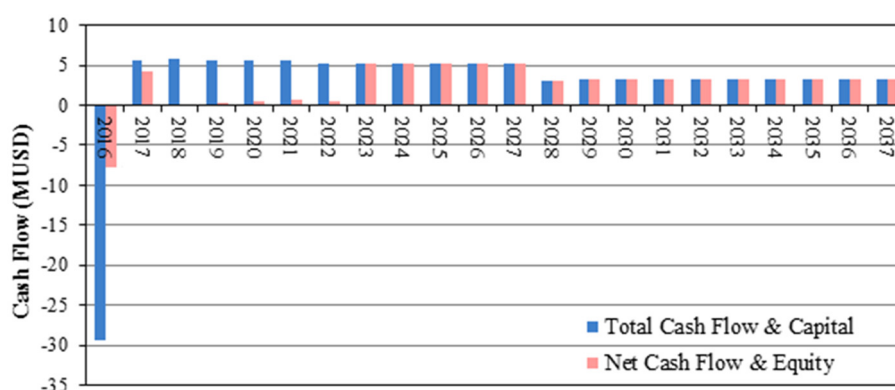


FIGURE 4: The cash flows of the project for a 5 MW PP

period until the end of the contract which explains the dip in net cash flow and equity from 2027 to 2028.

Figure 5 shows the accumulated NPV over the planning horizon. The NPV of net cash flow becomes positive over the planning horizon but the NPV of the total cash flow increases over the planning horizon without ever becoming positive. Since the NPV of total cash flow is zero the project remains balanced. The necessary payback period to recover investments is higher for the project (end of year contract) than for the equity investors but still payback period for the equity is high (10 years after operation began).

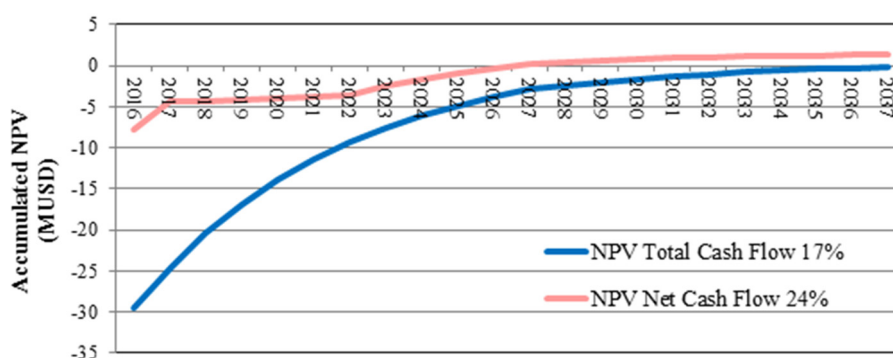


FIGURE 5: Accumulated NPV over the planning horizon for a 5 MW PP

The IRR is of much interest to the investors. Figure 6 shows how the IRR rises throughout the planning horizon for the 5 MW PP. The MARR for Net Cash Flow is 24% and the MARR for Total Cash Flow is 17%, see Table 6. Since the IRR of Net Cash Flow is higher than the MARR (or the discount rate), this project can be considered a profitable project for the equity investors but since the IRR of the total

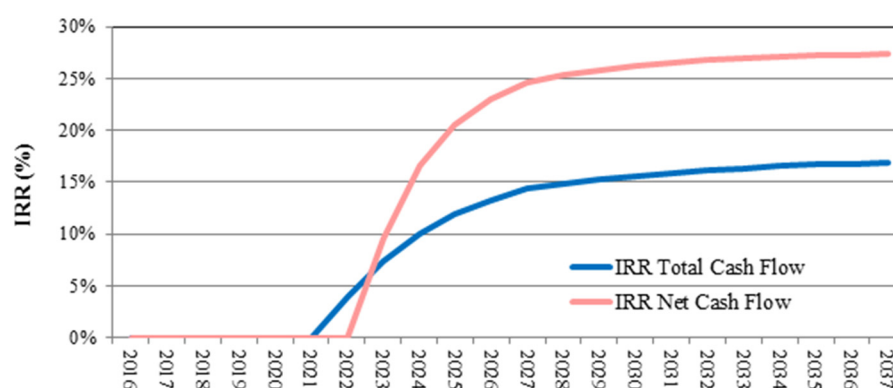


FIGURE 6: Internal Rate of Return for 5 MW

Cash Flow equals the discount rate, the project remains balanced. By comparing Figure 5 and Figure 6 it can be seen that the NPV of net cash flow reaches zero at the same time as the IRR reaches the MARR.

Both cash flow ratios and financial ratios for the 5 MW PP show that based on these results there is not much foundation for investment and the project remains balanced.

5.1.2 Scenario 2 - 50 MW geothermal power plant

The cash flows of the investment project for a 50 MW PP are illustrated in Figure 7. The chart shows two cash flows, one for capital investment and the other for equity. As seen from the chart, there is outflow of cash during the construction of the project, i.e. in the first seven years (2016 - 2022).

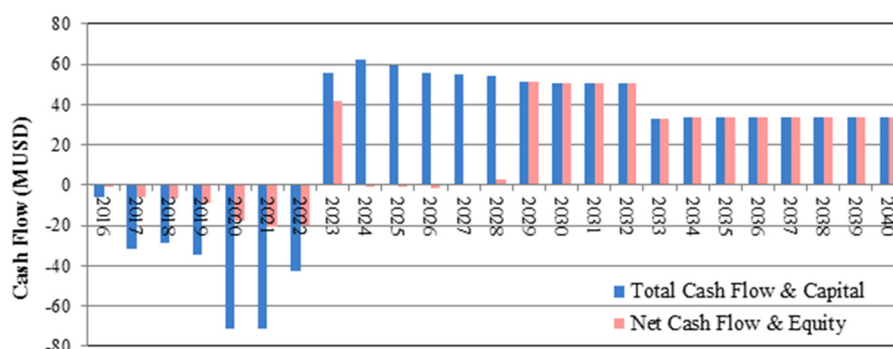


FIGURE 7: The cash flows of the project for a 50 MW PP

The loan received, which accounts for 75% of the investment cost and working capital, is paid back over a period of 5 years, starting a year after the start-up in 2024, which is the reason why there is a dip in the net cash flow and equity from 2024 to 2028. When the construction is finished, the project starts to generate income but just for one year (2023) until the received loan must be paid. The project does not generate net profits from 2024 until 2026 and due to the accumulated losses the project is still in the red numbers at the end of the planning horizon. Tariffs will be multiplied by 0.7 from the first day of the second 10 years until the end of the contract which shows the dip in net cash flow and equity from 2032 to 2033.

Figure 8 shows the accumulated NPV of the project over the planning horizon. The graph shows how the project increases its NPV over the planning horizon without ever becoming positive. At the end of this period the NPV of total capital is -48 MUSD and NPV of equity is -12 MUSD.

The IRR is of much interest to the investors. Figure 9 shows how the IRR rises throughout the planning horizon for a 50 MW PP. The IRR for Net Cash Flow is 18% and the IRR for Total Cash Flow is 12%.

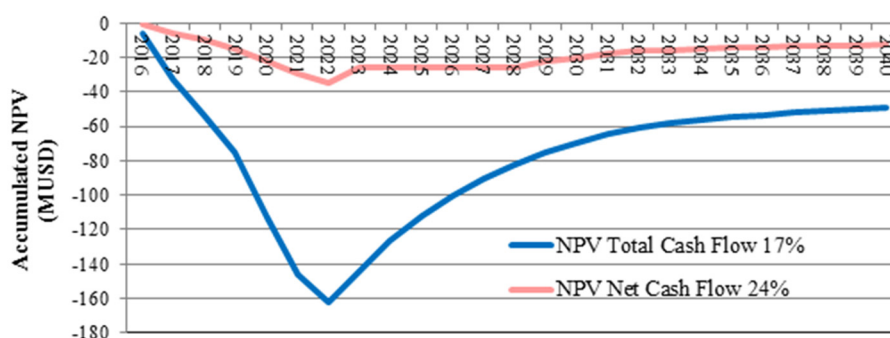


FIGURE 8: Accumulated NPV over the planning horizon for a 50 MW PP

Since the IRR of Total Cash Flow and Net Cash Flow are lower than the discount rate (for equity and total capital they are 24% and 17%, respectively), this project cannot be considered a profitable project.

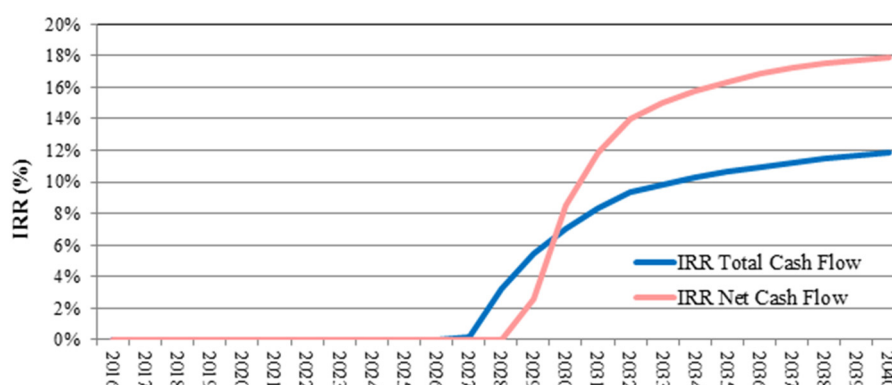


FIGURE 9: Internal rate of return for a 50 MW PP

Both cash flow ratios and financial ratios for a 50 MW PP show that based on these results there is not much foundation for investment. The ratios are all lower than the present acceptable minima and therefore the project would have difficulties meeting its obligations with regard to repayment of loans and other financial obligations.

5.2 Comparing financial feasibility study in Iran with other countries

Drilling costs in the Middle East are more expensive because the demands are very high compared to other countries and the competition with the oil and gas industry. Drilling cost in Iran is around 5000 USD/m, while this cost is not as high in other countries. Based on information from industrial partners, the drilling cost in other countries is estimated around 1300-3500 USD/m. This is the reason why the geothermal power plant construction is too expensive in Iran. In addition to drilling costs, some financial parameters are also different which affect the results. For example, discount rates for projects and equity are 10% in some countries while in Iran these are higher. Also loan repayments time in Iran is only 5 years while in some countries it can be more than 10 years.

Given the current situation, our present system is not very attractive to prospective investors - leading to favourable rate of return on their investments. To hasten the exploration and development of our geothermal resources, Iran needs to provide an environment that will attract investments, with proposed legislative measure offering a package of incentives, both in fiscal and contractual arrangements.

5.3 Sensitivity analysis

The most effective way to present the results of a sensitivity analysis is plotting sensitivity graphs. All variables are then plotted on the same graph, each as a separate line. The slopes of the lines show how sensitive the output is to a change in each variable; the steeper the slope is the more sensitive is the outcome to a change in a particular variable. It is therefore very good for the decision maker to take the results of the sensitivity analysis into account in the decision-making process, and if possible arrange to mitigate risk associated with changes in key parameters (Björnsdóttir, 2010).

Figure 10 shows a sensitivity graph for Scenario 2 (50 MW PP). Input parameters that are known to have most effect on the outcome of a geothermal project were selected for the analysis. As seen from the graph, the IRR of this project is most sensitive to changes in electricity price and buildings costs, which includes drilling cost. These parameters affect the outcome in a different way, as an increase in the electricity price increases the IRR, but an increase in drilling cost decreases the IRR.

As seen from the sensitivity analysis in Figure 10, small changes in input values can affect the outcome of the analysis significantly. If the electricity price or drilling costs change, the project can become profitable. The sensitivity analysis in Figure 10 for the electricity price and drilling costs shows that a relatively modest increase in the price of electricity or decrease in drilling costs can change the financial aspect of the project. If the price of electricity can be raised from the current 16 US¢/kWh to 24 US¢/kWh (1.5 times) or if the drilling costs can be decreased from 5000 to 1600 USD/m, the economics of the project can change significantly. Tables 8 and 9 show a summary of a sensitivity analysis of this project. The result of the calculation are shown in Appendix I.

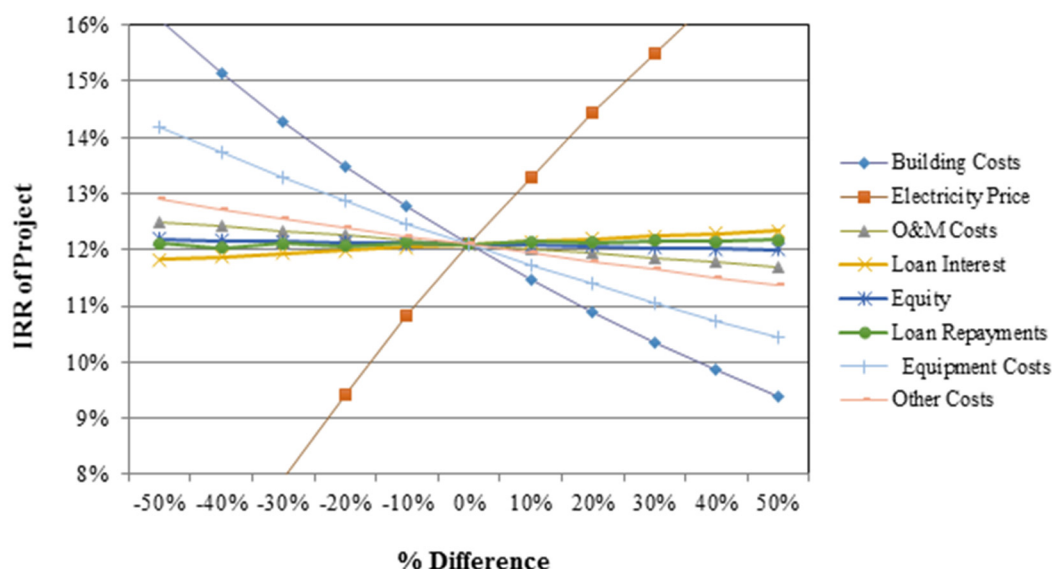


FIGURE 10: Sensitivity graph for a case study for a 50 MW PP

TABLE 8: Summary of a sensitivity analysis for a 50 MW PP when the electricity price is changed

Electricity price (US¢/kWh)	NPV Total Cash Flow (MUSD)	NPV Net Cash Flow (MUSD)	IRR Total Cash Flow	IRR Net Cash Flow
16	-48	-12	12%	18%
24	6	16	18%	31%

TABLE 9: Summary of a sensitivity analysis for a 50 MW PP when the drilling cost is changed

Drilling cost (USD/m)	NPV Total Cash Flow (MUSD)	NPV Net Cash Flow (MUSD)	IRR Total Cash Flow	IRR Net Cash Flow
5000	-48	-12	12%	18%
1600	4	13	18%	34%

Loan repayment is also important for the financial analysis, therefore it is assumed that the government gives loan for renewable energy projects with a longer repayment period (for example 10 years). But this will not affect the result much.

As mentioned in previous sections, the MARR for Net Cash Flow is 24% and the MARR for Total Cash Flow is 17%. Since the IRR of Total Cash Flow and Net Cash Flow after changing the price of electricity or drilling cost are higher than the discount rate, this project can now be considered profitable with an energy price of at least 24 US¢/kWh, or with drilling costs not exceeding 1600 USD/m.

6. CONCLUSIONS

Based on the abundant resources of geothermal, Iran should be attractive for geothermal business. The government has implemented laws guaranteeing power purchase for a period of up to 20 years but it does not seem to be favourable enough to attract private sector participation. Financing the initial investment is the main barrier. The main goal of this study was to find out whether or not there is a financial foundation for the private sector's participation in geothermal power generation in Iran.

The conclusion of this study is that geothermal power development projects in Iran are not very attractive for private investors when the potential investor takes into consideration the costs of exploration and confirmation, drilling into an unknown field, and running a power plant with the current electricity tariffs.

The profitability model came up with an indifferent result for Scenario 1 (a 5 MW geothermal PP) and an infeasible result for Scenario 2 (a 50 MW geothermal PP). Risk analysis suggests that the most important financial factors that affect the project profitability are the energy price and the drilling costs.

In order for the scenarios to be successful in the real world the price of electricity in Iran would have to increase at least 1.5 times to 24 US\$/ kWh or drilling costs have to be lowered to a comparative level to costs elsewhere in the world. This means they would have to decrease at least to 1600 USD/m. It can also be added, that bigger power plants can be more economic since the highest value of the scale exponent was selected for scaling.

These are some problems which could be solved with the will and determination of the Iranian government. Important factors where the government could help to generate a positive impact on profitability and risk of the investment are: energy price, taxes and reduction of drilling costs. Numerous alternatives could be evaluated such as: improved tax incentive laws, large period energy contracts, public funds for exploration and confirmation phases, and different scenarios like:

- 1) Geothermal reservoir exploration by private developers;
- 2) Drilling for steam and hot water production by private developers;
- 3) Buying steam and water and generating electricity through private developers;
- 4) Drilling for steam and hot water production and generating electricity through private developers.

The decision-making process for large projects is very complicated and obviously, all aspects could not be covered in this paper. Many assumptions were also made, some based on little available information.

ACKNOWLEDGEMENTS

Foremost, I would like to express my sincere gratitude to the United Nation University Geothermal Training Programme for giving me the opportunity to attend the 6-month training programme in 2016. My special thanks goes to the head of programme, Mr. Lúdvík S. Georgsson, Mr. Ingimar Gudni Haraldsson, Ms. Málfríður Ómarsdóttir, Mr. Markús A. G. Wilde and Ms. Thórhildur Ísberg for not only making prior arrangement for this training programme but also for accompanying us and providing guidance, moral support and proper understanding of what we were taught by explaining further.

I would like to express the deepest appreciation to my supervisors Dr. María Sigríður Gudjónsdóttir and Dr. Páll Jensson for their patience, motivation, enthusiasm, and immense knowledge.

I also want to thank all 2016 UNU fellows, especially Damaris Wacera Njoroge and Moses Kipsang Kachumo for their support, and all others for their kind company and friendship.

My thanks and appreciations also go to Soheil Porkhial and Mohsen Taghaddosi for giving me this opportunity to undergo geothermal training in Iceland

Last but not the least; I would like to thank my family: my parents Majid Saber and Masume Mirzai, for supporting me spiritually throughout my life. This project is dedicated to my dear husband, Mohammad Karimi, for his support, and encouragement throughout these six months in Iceland.

REFERENCES

- Avato, P., 2013: *Success of geothermal wells: a global study*. International Finance Corporation, report, 80 pp.
- Berthouex, P.M., 1972: Evaluating economy of scale. *J. Water Pollution Control Federation*, 44-11, 2111-2119.
- Björnsdóttir, A.R., 2010: *Financial feasibility assessments. Building and using assessment models for financial feasibility analysis of investment projects*. University of Iceland, Reykjavík, MSc thesis, 82 pp.
- BP, 2016: *Statistical review of world energy* (65th ed.). BP statistical review of world energy, 48 pp, website: www.bp.com.
- Campen, B.V. and O'Sullivan, J., 2016: *Geothermal capacity needs assessment methodology*. IRENA - International Renewable Energy Agency, report.
- Chatenay, C. and Jóhannesson, T., 2014: How do financial aspects of geothermal compare with other energy sources? *Paper presented at "Short Course VI on Utilization of Low- and Medium-Enthalpy Geothermal Resources and Financial Aspects of Utilization", organized by UNU-GTP and LaGeo, in Santa Tecla, El Salvador, UNU-GTP, SC-18*, 6 pp
- Cross, J., and Freeman, J., 2009: *2008 geothermal technologies market report*. US Department of Energy, report DOE/GO-102009-2864.
- Energypedia, 2016: *Iran energy situation*. Energypedia, website: energypedia.info/wiki/Iran_Energy_Situation#cite_note-inter3._Konzeptpapier_-_Potenziale_f.C3.BCr_Erneuerbare_Energien_und_M.C3.B6glichkeiten_des_Kompetenzaufbaus_im_Iran-3.
- ERA, 2014: *Feed-in-tariff*. Electricity Regulatory Authority - ERA, Uganda, website: www.era.or.ug/index.php/statistics-tariffs/tariffs/2014-09-08-13-29-51/feed-in-tariff.
- ERC, 2016: *Feed-in tariff policy*. Energy Regulatory Commission – ERC, Kenya, website: www.erc.go.ke/index.php?option=com_content&view=article&id=148&Itemid=637.
- Gehringer, M. and Loksha, V., 2012: *Geothermal handbook: planning and financing power generation*. Energy Sector Management Assistance Program (ESMAP), technical report 0 02/12, 150 pp.
- Geirdal, C.A.C., 2013: *Economic comparison between a well-head geothermal power plant and a traditional geothermal power plant*. Reykjavik University, Reykjavík, MSc thesis, 100 pp.
- Geo-Energy, 2016: *Geothermal basics power plant costs*. Geothermal Energy Association, website: geo-energy.org/geo_basics_plant_cost.aspx.
- Globalpetrolprices.com 2016: Gasoline prices. Globalpetrolprices.com, website: www.globalpetrolprices.com/gasoline_prices/
- Hance, C.N., 2005: *Factors affecting costs of geothermal power development*. Geothermal Energy Association, publication for the US Department of Energy.

Haraldsson, I.G., 2014: Government incentives and international support for geothermal project development. Presented at “Short Course VI on Utilization of Low- and Medium-Enthalpy Geothermal Resources and Financial Aspects of Utilization”, organized by UNU-GTP and LaGeo, in Santa Tecla, El Salvador, UNU-GTP, SC-18, 12 pp.

IEA, 2016: *Policies and measures*. International Energy Agency – IEA, website: www.iea.org/policiesandmeasures/pams/japan/name-30660-en.php.

IRENA, 2012: *Renewable power generation costs in 2012, an overview*. International Renewable Energy Agency – IRENA, report, 92 pp.

IRENA, 2014: *Renewable power generation costs in 2014*. International Renewable Energy Agency – IRENA, report, 164 pp.

Konyali, A., 2010: Financial evaluation of Kizildere geothermal power plant. Izmir Institute of Technology, Izmir, MSc thesis, 70 pp.

Matek, B. and Gawell, K., 2014: *The economic costs and benefits of geothermal power*. Geothermal Energy Association, publication, 9 pp.

MEI, 2016: *Iran’s renewable energy potential*. Middle East Institute – MEI, Washington DC, website: www.mei.edu/content/article/iran%E2%80%99s-renewable-energy-potential#_edn6.

MOEABOE, 2015 and 2016: *Formula for calculating feed-in tariffs of renewable energy electric power*. Bureau of Energy, Ministry of Economic Affairs, Taiwan, website: web3.moeaboe.gov.tw/ECW/english/content/Content.aspx?menu_id=3008.

Ngugi, P.K., 2012: What does geothermal cost? - the Kenya experience. Paper presented at “Short Course on Geothermal Development and Geothermal Wells”, organized by UNU-GTP and LaGeo, in Santa Tecla, El Salvador. UNU-GTP, SC14, 13 pp.

Ngugi, P.K., 2013: Geothermal well drilling. Paper presented at “Short Course VIII on Exploration for Geothermal Resources”, organized by UNU-GTP, GDC and KenGen, at Lake Bogoria and Lake Naivasha, Kenya. UNU-GTP, SC17, 23 pp.

Res-Legal, 2016: *Legal sources on renewable energy, search by country*. Res-Legal, website: www.res-legal.eu/en/search-by-country/.

Repit.wordpress, 2016: *Feed-in tariff (FIT)*. Indonesia Power Generation, website: repit.wordpress.com/projects/feed-in-tariff-fit/.

Salas, R.J.E., 2012: *Geothermal power plant projects in Central America: technical and financial feasibility assessment model*. University of Iceland, Reykjavík, MSc thesis, 108 pp.

Salmon, P.J., Meurice, J., Wobus, N., Stern, F. and Duaiame, M., 2011: *Guidebook to geothermal power finance*. National Renewable Energy Laboratory (NREL), US DoE, subcontract report NREL/SR-6A20-49391.

SUNA, 2016: *Guidelines on renewable power plants investment*. SUNA – Renewable Energy Organization of Iran, website: www.suna.org.ir/en/investment1-%D8%B3%D8%B1%D9%85%D8%A7%DB%8C%D9%87-%DA%AF%D8%B0%D8%A7%D8%B1%DB%8C.

TradeArabia, 2016: *Analysis*. TradeArabia, business news information, website: www.tradearabia.com/news/REAL_299110.html

WFW, 2016: *Renewable energy in Iran, May 2016*. Watson Farley & Williams, briefing, 6 pp.

APPENDIX I: Results of a sensitivity analysis based on 24 US¢/kWh electricity price

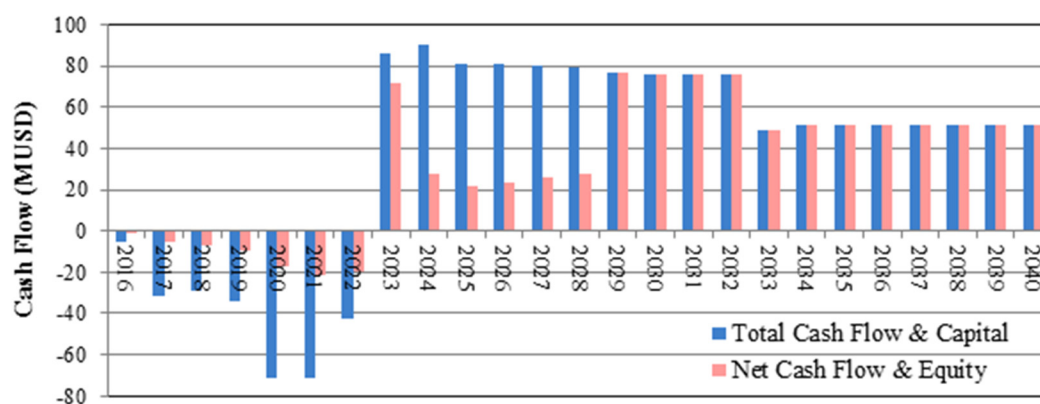


FIGURE 1: The cash flows of the project for a 50 MW PP with 24 US¢/kWh electricity price

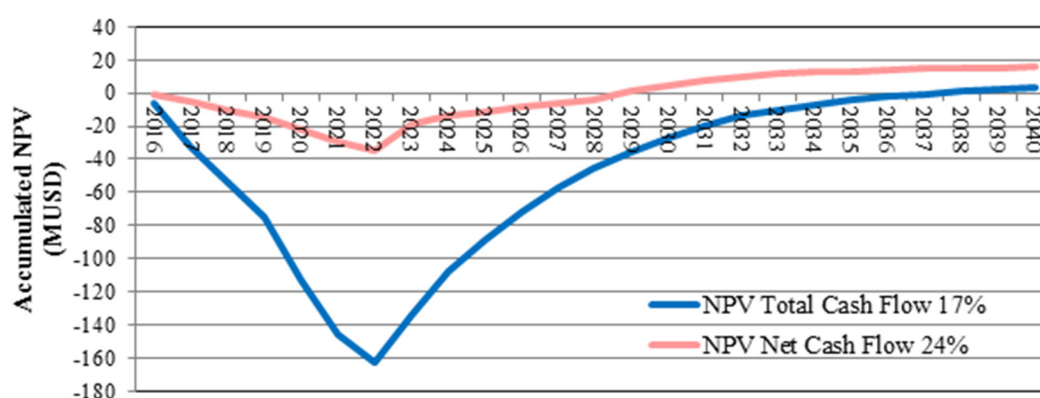


FIGURE 2: Accumulated NPV over the planning horizon for a 50 MW PP with 24 US¢/kWh electricity price

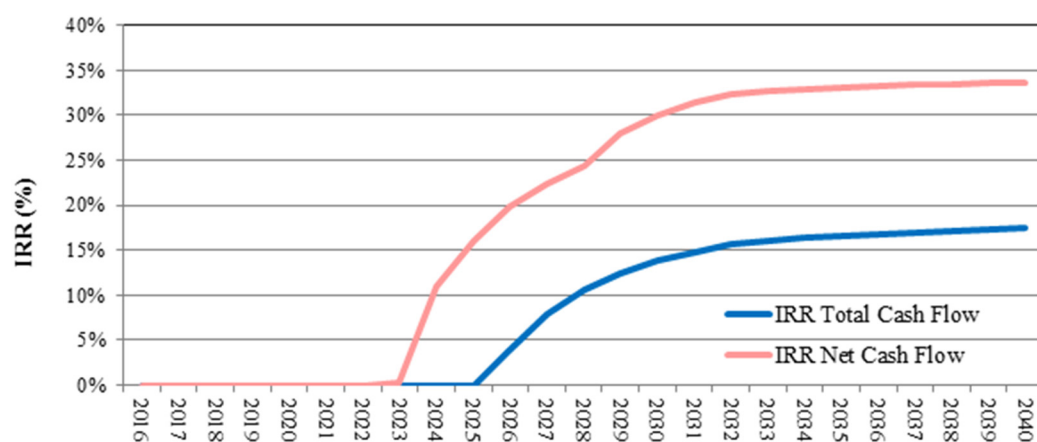


FIGURE 3: Internal Rate of Return for 50MW with 24 US¢/kWh electricity price



FIGURE 4: The cash flow of the project for a 50 MW PP with 1600 USD/m in drilling costs

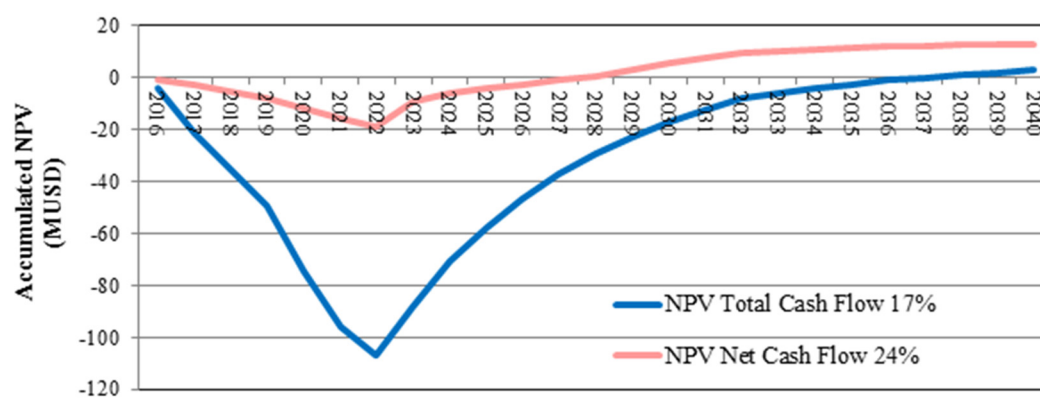


FIGURE 5: Accumulated NPV over the planning horizon for a 50 MW PP with 1600 USD/m in drilling costs

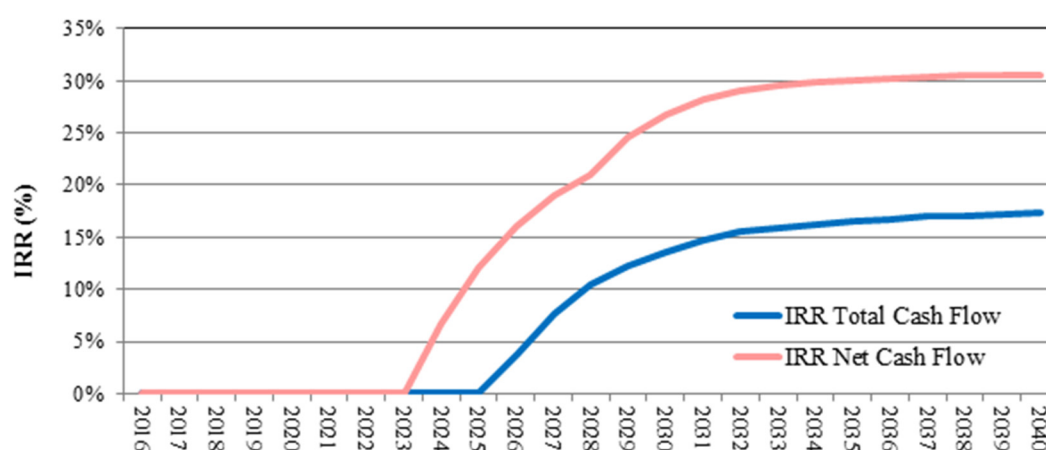


FIGURE 6: Internal Rate of Return for a 50 MW PP with 1600 USD/m in drilling costs



UNITED NATIONS
UNIVERSITY

UNU-GTP

Geothermal Training Programme

Orkustofnun, Grensasvegur 9,
IS-108 Reykjavik, Iceland

Reports 2016
Number 38

BOREHOLE GEOLOGY, HYDROTHERMAL ALTERATION AND STRUCTURAL MAPPING OF WELL HE-30, HELLISHEIDI, SW-ICELAND

Erios Naiga Sembatya

Ministry of Energy and Mineral Development,
Directorate of Geological Survey and Mines
P. O. Box 9, Entebbe
UGANDA
eriesembatya@gmail.com

ABSTRACT

Well HE-30 is located in the Hellisheidi high-temperature geothermal field, SW-Iceland. It is a directional production well which was drilled to 2318 m to explore faults at the western margin of the Hengill fissure system as well as to investigate the Reykjafell mini-graben. HE-30 is composed of hyaloclastites (basaltic tuff, basaltic breccia and pillow basalt) and interglacial lavas, occasionally intruded by fine- to medium-grained crystalline basalts. Permeability is provided through faults, formation boundaries and intrusions. Thirteen feed zones were identified in HE-30. Five intrusions were observed and four alteration zones: smectite-zeolite (116 – 456 m), mixed layer clay (456 – 718 m), chlorite - epidote (718 – 1014 m), and epidote – actinolite (1014 – 1328 m). Fluid inclusion homogenization temperatures are lower than in the formation and alteration temperatures, which may indicate an old formation temperature. Alteration and formation temperatures indicate that the system is in thermodynamic equilibrium.

1. INTRODUCTION

Surface exploration surveys, investigation of subsurface geothermal and production characteristics of the reservoir, have to be carried out before utilization of the geothermal field since geothermal systems usually have complicated geology. These include lithology, hydrothermal alteration of the rocks, fluid characteristics such as flow into the system (natural recharge), within the system (fluid convection) and out of the system to the surface (surface manifestations), permeability and hydrological characteristics of the reservoir characteristics. Joint interpretation of the data is then done by various disciplines to decide if the system should be utilized (Steingrímsson and Gudmundsson, 2006). Hengill is an active central volcano located about 30 km southeast of Reykjavik. In the Hengill area there are four main geothermal fields; Hellisheidi, Nesjavellir, Bitra and Hverahlíð (Figure 1) (Franzson et al., 2010). There are over 100 boreholes drilled in Hengill for exploration and production and more than 20 for reinjection (Helgadóttir et al., 2016). A total of 420 MWe electricity and 430 MWt thermal energy are produced from the Hengill geothermal field from three power plants operated by Reykjavik Energy (Hardarson et al., 2015). Well HE-30 was drilled as a production well and to explore faults at the western margin of the Hengill fissure system as well as to investigate the Reykjafell mini-graben. The objective of this

project was to explore the lithology and understand the permeable zones in well HE-30 by locating the fractures and faults in its path and linking them to surface structures.

2. GEOLOGY AND TECTONICS OF ICELAND AND HENGIL

2.1 Geology of Iceland

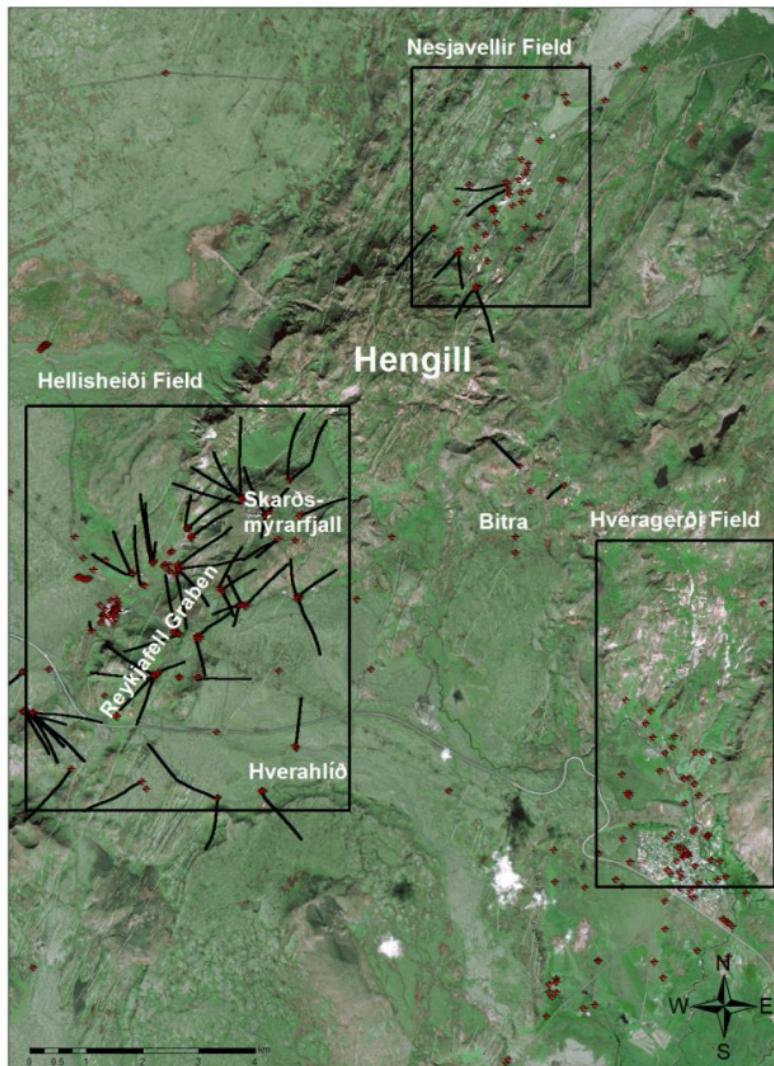


FIGURE 1: Satellite image showing the location of the different fields in the Hengill central volcano and the Reykjafell mini-graben (Hardarson et al., 2015)

Iceland is located on the Mid-Atlantic ridge and above a mantle plume which for about 24 million years has caused intense magmatism and complex tectonism (Hardarson et al., 2015) with sea floor spreading of about 1 cm per year in opposite directions (Saemundsson, 1979). Iceland is composed of three geological formations which date back 16 my (Hardarson et al., 1997). First are the basalt lavas (covering 80-85%) which occur in three types. There is olivine tholeiite which erupted as pahoehoe lava flows, simple tholeiitic flows with little or no olivine which erupted as aa fissure lavas and the porphyritic flows with plagioclase and/or pyroxene which formed in fissures as thick and massive flows. Second are the acidic lavas with intermediate rocks (which cover 10%) of which 60-70% are lavas and intrusions. There are dolerite, gabbro and granophyre that are exposed in the eroded central volcanoes, then 30-40% being pyroclastites deposited in and around vents as ash flows or tuff sheets and transported over long distances (Figure 2). Third (5-10%) are the alkaline rocks found in the neovolcanic zones

underlain by the tertiary tholeiites. There are four stratigraphic series based on climatic evidence (Figure 2) (Saemundsson, 1979). *Tertiary rocks* were formed more than 3.1 my ago and cover half of Iceland or about 50,000 km². They vary in lithology from the tholeiitic lavas to intermediate and acidic rocks. The *Plio-pleistocene lavas* were formed around 0.7 – 3.1 my ago and cover 25,000 km². They are made up of tillites interstratified with pillow lavas, various types of breccia and hyaloclastites. The *Upper Pleistocene lavas* were formed about 0.7 my ago. They are marked by an unconformity with the Plio-pleistocene lavas. During their eruption, they covered the fissure swarms forming table mountains. They occur in central, western and south western Iceland. From their structure and morphology, they were classified into two types, the grey basalts erupted during interglacial periods and the subglacial

palagonites (pillow lavas and hyaloclastite tuffs). Lastly to mention are the *Postglacial lavas* (less than 12,000 years old) which occur in the active rift zones of Iceland. They cover 12000 km² (10%) of Iceland and are 90% basalts and 10% intermediate and acidic lavas (Saemundsson, 1979).

2.2 Tectonics of Iceland

Neovolcanic zones together with the graben structures, oblique and transverse fissure zones are tectonically active unlike the Tertiary and Pleistocene zones except where younger tectonic zones cross cut them (Saemundsson, 1979). The axial rifts in the neovolcanic zones, where active plate growth occurs, mainly erupt tholeiitic rocks and fracturing is localized in fissure swarms. Volcanic fissures, non-eruptive gaping cracks and faults are the dominant structures in these swarms and they are associated with dyke injection, as seen in the old lava piles (Saemundsson, 1979). These dykes are 1-20 m wide and can be several km long. Central volcanoes host most fissure swarms. These fissure swarms are about 10-30 km wide and 50-100 km long. Sometimes narrow grabens are found within the fissure swarms, for example the Mt. Reykjafell mini-graben (Figure 3). The volcanoes sometimes form calderas with about 5-10 km diameter, which in turn, develop cone sheets stretching beyond caldera margins (Saemundsson, 1979). Transforms and seismic zones are zones where active strike-slip tectonic activities occur. These include the South Iceland Fracture Zone (SIFZ) and the Tjörnes Fracture Zone (TFZ). The largest earthquakes in Iceland occur along these transforms (Figure 2).

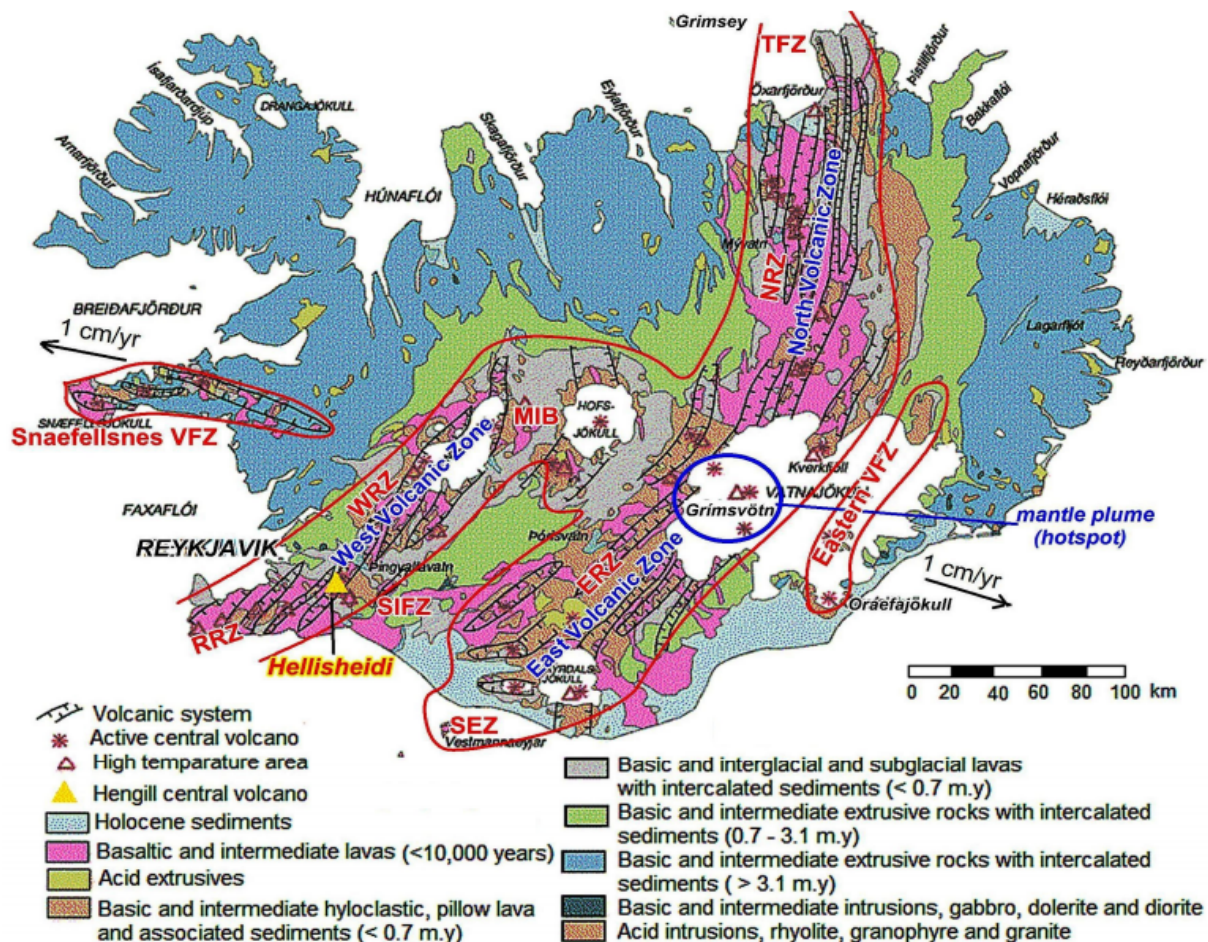


FIGURE 2: Map of Iceland showing the volcanic systems and fissure swarms, location of the mantle plume, rift systems, direction of spreading and location of the Hellisheidi high-temperature geothermal field in the Hengill central volcano (modified from Saemundsson, 1979; Bawasu, 2010)

2.3 Hengill geology and structural setting

2.3.1 Geology of Hengill central volcano

Hengill volcano is about 400,000 years old. The highlands (about 800 m a.s.l.) are covered by hyaloclastites that erupted during the glacial periods and the interglacial lava flows, which are found in the lowlands (Franzson et al., 2010). Hyaloclastites are comprised of pillow basalts, breccia and tuff, which have high porosity but low permeability when altered (e.g. Gebrehiwot Mesfin, 2010). Three volcanic systems are found in the area. One is called the Hveragerdi-Grensdalur volcanic system, which is no longer volcanically active but is seismically. Here the oldest rocks are found (about 0.8 my). The other two systems are the Hrómundartindur volcanic system with rocks younger than 0.2 my and the Hengill volcanic system which is still active (e.g. Gebrehiwot Mesfin, 2010). Hengill is a complex volcano with a fissure swarm that is 5 – 10 km wide and 40 - 60 km long (Franzson et al., 2010; Hardarson et al., 2015). The main fractures trend NNE-SSW. Other structures strike N-S and WNW-ESE (Árnason, 2007; Spichak et al., 2013). Hellsheidi is a high-temperature field found in the Hengill central volcano (Figures 1 and 2). It is located at the intersection of the Western Iceland volcanic zone

(an axial rift zone), the Reykjanes Peninsula (an oblique spreading ridge), and the South Iceland seismic zone (a seismically active transform zone). This triple junction of the American-Eurasian plate boundary has been described by Hardarson et al. (2015) and Gasperikova, et al. (2015).

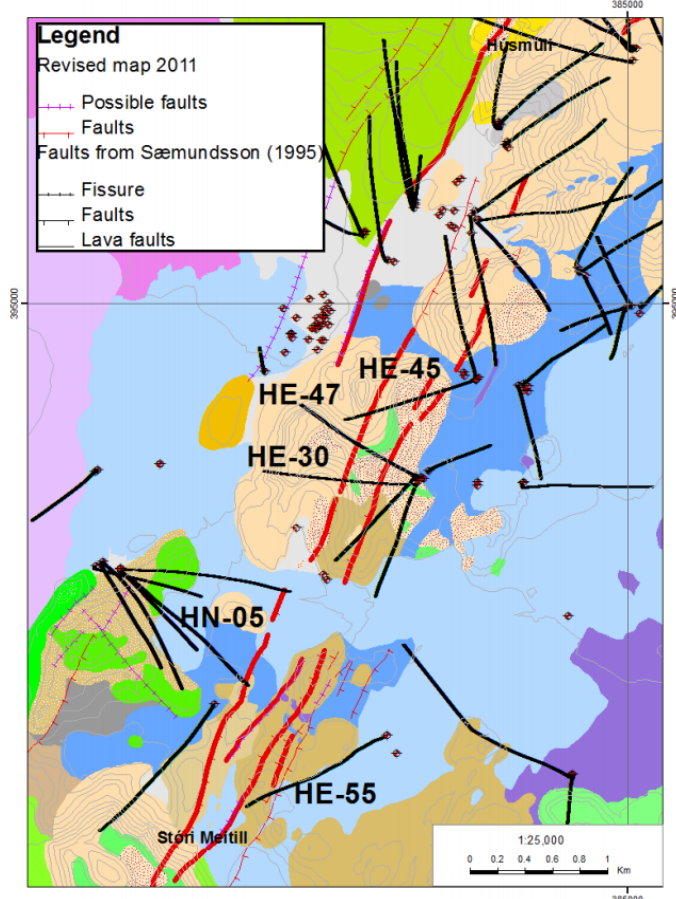


FIGURE 3: Map showing the Reykjafell mini-graben (red lines) (Hellsheidi field) which is located on the western flank of the Hengill fissure swarm. It strikes NE-SW, through Mt. Reykjafell, and wells that penetrate the Reykjafell mini-graben are very productive (about 10 MW). Postglacial lavas (<12000 years) are drawn in blue-purple, subglacial hyaloclastites in brown and interglacial lavas in green (Hardarson et al, 2015)

2.3.2 Hengill structural setting

Reykjafell mini-graben: Several geological surveys have been conducted in this area including a detailed surface mapping of the Mt. Reykjafell mini-graben (Figure 3), which transects Mt. Reykjafell towards the southwest, covering the Gráuhnúkar area, Mt. Stóri Meitill and Mt. Litli Meitill (Hardarson et al., 2015). There are a number of surface manifestations on the eastern rim of the graben. South of Mt. Reykjafell and the subglacial craters that are >10,000 years old, striking NE to SW additionally to some others which are within the graben (Gunnarsdóttir, 2012). The Reykjafell mini graben probably extends northeast towards Nesjavellir (Hardarson et al., 2015). It trends NNE-SSW with a 20-40 m down-throw on the surface and are 150-400 m wide (Hardarson et al., 2015). Three volcanic fissure swarms erupted after the last glaciation or about 9,000, 5,000 and 2,000 years ago (Figure 4). Permeability is provided by formation boundaries, intrusions, faults and feeder dykes in the Hengill volcano (Franzson et al., 2010; Gasperikova et al., 2015). Holocene

volcanic fissure eruptions have increased the permeability and geothermal activity in the volcano. This was confirmed by the renewed heating in the Nesjavellir geothermal field by the fissure swarms which are 5,000 and 2,000 years old (Figure 4). The Reykjafell mini graben provides up-flow zones as has been confirmed by geophysical data (Hardarson et al., 2015). Analysis of drill cuttings and drill data was done to understand the subsurface and indicates that the wells which penetrate the graben and its faults have an output of >10 MWe and also show a down throw of greater than 200 m at 1300 m depth (Hardarson et al., 2015).

3. LITERATURE REVIEW ON HENGILL GEOTHERMAL FIELD

Work has been ongoing in Hengill central volcano since 1975 including surface exploration surveys such as geological, geochemical and geophysical exploration, TEM/MT surveys, borehole resistivity measurements, subsurface geology analysis and hydrothermal alteration mapping (Haraldsdóttir et al., 2015). Worldwide, there is a similarity in the responses of resistivity and P-wave velocities at temperatures below 350°C (e.g. Gasperikova et al., 2015). Resistivity survey results show that the Hengill volcano has a high-temperature geothermal source. Relating resistivity, well temperatures and alteration mineralogy show that the resistivity features in the volcano is more dependent on the hydrothermal mineral alteration than the temperature (e.g. Gasperikova et al., 2015). When a geothermal system cools, alteration minerals that remain indicate the maximum temperatures when these minerals were formed (Haraldsdóttir, et al., 2015). Both the resistivity and reservoir models indicate similar results (Björnsson and Hersir, 1981). Figure 5 shows low resistivity in the first 1-2 km which is due to the smectite-zeolite zone and mixed layer clays formed at temperatures <200°C. This zone is called the clay cap, which is caused by the conductivity of loosely bound cations in smectite and zeolite minerals (Haraldsdóttir, et al., 2015). Underneath is a high resistivity core caused by chlorite and other alteration minerals that are compacted and with little water, like epidote which forms at temperatures >250°C (Haraldsdóttir et al., 2015). Another low resistivity anomaly is found at even greater depth. The eruption in Bitra geothermal system about 13,000 years ago re-activated this system that had cooled during the glacial period (e.g. Gasperikova et al., 2015). Microearthquakes are common in Hengill volcano because of its location and they are linked to the geothermal surface manifestations (e.g. Gebrehiwot Mesfin, 2010). This is indicated by the dense fissure swarm and recent eruptions (e.g. Hardarson, 2014). These occur at about 5 km depth, and strike E-W or N-S. Seismological surveys revealed two seismic vibrations, the infrequent and intense earthquakes caused by movement of the crust as a result of release of stress along plate boundaries and the small quakes in the Hveragerdi central volcano (e.g. Gebrehiwot Mesfin, 2010).

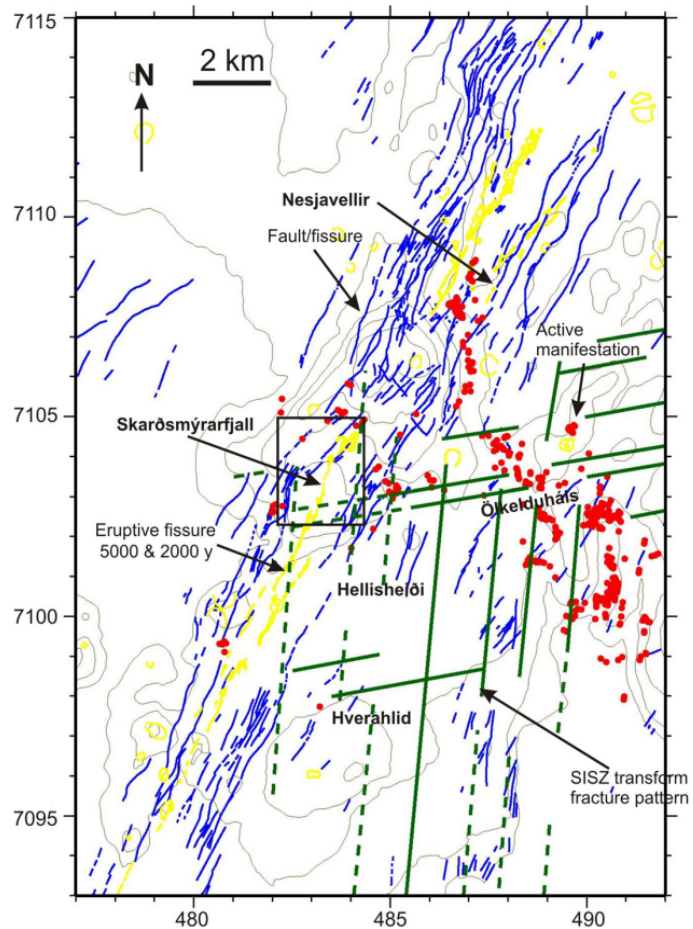


FIGURE 4: The Hengill volcanic system. Red dots tag surface manifestations, blue lines indicate surface fissures and faults, fissures and faults defined by earthquake locations are sketched in green and yellow lines mark postglacial fissures (Franzson, et al., 2010)

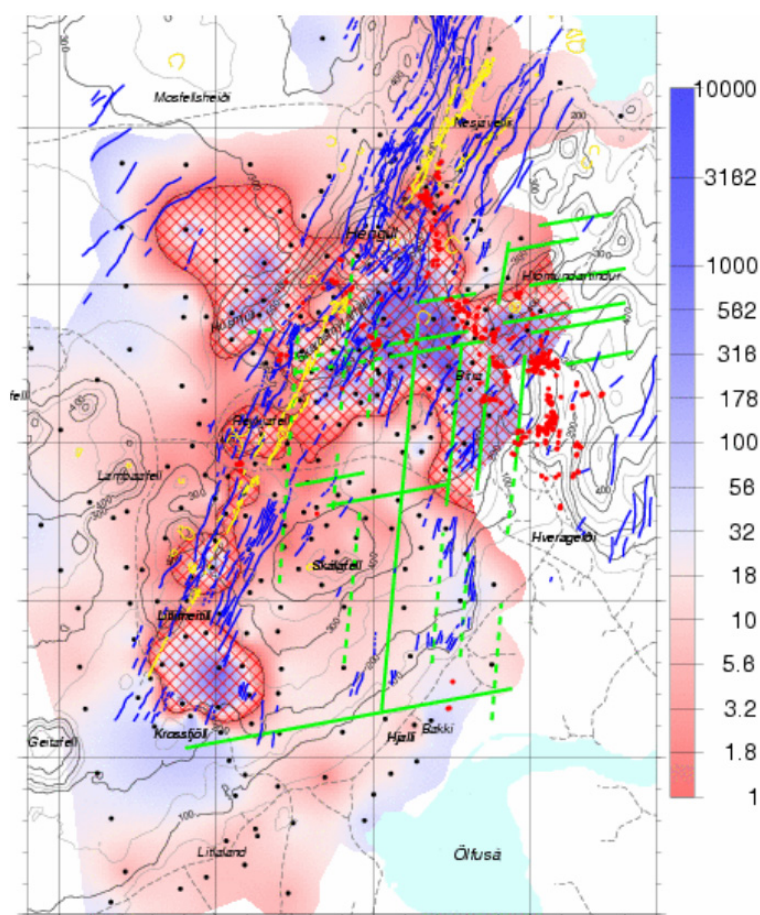


FIGURE 5: Map showing resistivity variations in Hengill central volcano at 850 m b.s.l., high resistivity cores (cross-hatched) below low resistivity indicate alteration temperatures above 230°C, surface geothermal springs (red dots), fissures (blue lines) and faults (green lines) earthquake locations and post glacial (< 12 ka) fissures (yellow lines) (Árnason, 2007)

(Measurement While Drilling) in the BHA (Bottom Hole Assembly). The well was drilled to 707 m and cased with a 13 $\frac{3}{8}$ " production casing, which was set at 705 m depth and cemented with 71 m³ of slurry. The well design assumed a KOP (Kick Off Point) at 320 m with a 2.5°/30 m build-up reaching the final inclination of 30° at 690 m depth. The direction was 270° west. Gyro surveys showed that by the end of phase 2 the inclination was 30.8° and azimuth 268° which are very acceptable results. Phase three commenced on March 16th on workday 29 and a 12 $\frac{1}{4}$ " bit was used. Aerated drilling with foam and water was chosen. The well was drilled to 2318 m and the 9 $\frac{5}{8}$ " slotted liner extends to a depth of 2256.5 m. There was loss of circulation at 1288 m (Gunnarsdóttir, 2012). Total loss of circulation occurred at 1328 m and no drill cuttings were retrieved below that depth. Well HE-30 was completed on April 4th on workday 48.

TABLE 1: Drilling depth, casing depth and drill bits in well HE-30. Depths refer to the platform of Ódinn, 6.7 m above ground level (Hardarson et al., 2007a, 2007b)

Rig	Drill Phase	Drill bit	Drill depth	Casing	Casing depth
Ódinn	Pre-drilling	26"	91 m	22 $\frac{1}{2}$ "	90,7 m
Ódinn	1. Phase	21"	300 m	18 $\frac{5}{8}$ "	300 m
Ódinn	2. Phase	17 $\frac{1}{2}$ "	707 m	13 $\frac{3}{8}$ "	705 m
Ódinn	3. Phase	12 $\frac{1}{4}$ "	2318 m	9 $\frac{5}{8}$ "	2256,5 m

4. BOREHOLE GEOLOGY

4.1 Drilling of HE-30

The drilling of HE-30 was carried out in four phases during February and March 2007. Drilling depths, casing depths and drill bits in well HE-30 are presented in Table 1. The well path according to gyro surveys is shown in Figure 3. The well was drilled using the rig Ódinn Drillmec HH-220 series. Well HE-30 was spudded on the 20th of February 2007 and was completed on the 48th working day, April 4th. Pre-drilling with a 26" drill-bit commenced on the 5th working day, and drilling down to 91 m depth was completed in one day. The well was cased with 22 $\frac{1}{2}$ " pipes (surface casing) to 90.7 m depth and cemented using 20.5 m³ of cement slurry. Phase one, when a 21" bit and motor was used, started on February 26th and was completed, at a depth of 300 m, late in the evening of the following day. The well was cased with 18 $\frac{5}{8}$ " pipes (anchor casing) down to 300 m. Subsequently 28 m³ of cement slurry was used to set the casing. No circulation losses were encountered during pre-drilling and phase one. Phase two commenced on March 3rd using a 17 $\frac{1}{2}$ " bit, motor and MWD

4.2 Methodology

Binocular microscope: A total of 606 drill cutting samples from 0 to 1328 m depth, which were sampled at a 2 m depth interval, were analysed in detail to determine rock type, alteration, oxidation, intrusions, fractures and vein fillings. Lithological and alteration logs were prepared.

Petrographic analysis: In well HE-30, 21 thin sections from the first 1278 m were analysed to provide a detailed description of the rock including mineral type, texture, fractures, porosity, alteration minerals and alteration sequences (Table 3).

X-ray diffractometer (XRD) analysis: Clays were not easily distinguished by binocular and petrographic microscopes. A X-ray diffractometer was used to analyse clays to delineate the alteration zones which aided the interpretation of alteration temperatures in the geothermal field. Three categories of samples were analysed (at Icelandic GeoSurvey – ISOR): untreated, treated with the glycol solution and heated samples. Sample preparation was done for 24 to 48 hours before placing the samples in the XRD for measurement. Twenty-two samples from the first 1282 m depths in HE-30 were analysed and the results indicate smectite, chlorite, illite (minute amount) and mixed layered clays.

Fluid inclusion analysis: Fluid inclusions (FI) are bubbles of liquid or gas trapped in a crystal. The inclusion may be primary (formed during crystal growth) or secondary (formed after crystal growth), pseudosecondary inclusions exist as well but are not used in this analysis. FI were used to understand the thermal evolution of the geothermal system by carrying out microthermometric analysis where they are used as geothermometers to measure the homogenization temperature (T_h) (Shepherd et al., 1985; Bodnar, 2003) by heating quartz and calcite crystals, which contained the inclusions until the trapped bubble(s) disappeared. The maximum temperature was recorded which gives an estimate of the temperature at the time of the mineral formation.

4.3 Lithology of well HE-30

HE-30 is composed of fine- to medium-grained crystalline basalts (postglacial/interglacial lavas and intrusions) and hyaloclastites (tuff, breccia and pillow lavas). They were identified by their physical properties such as grain size, minerals and crystal shape, colour, extent of alteration, alteration minerals and oxidation and many other factors were noted using a binocular microscope. The results are summarised in Figure 6.

0 – 12 m: No cuttings.

12 – 48 m: Fine- to medium-grained crystalline basalt; Greyish brown fine- to medium-grained crystalline basalt with phenocrysts of plagioclase, pyroxene and olivine. Samples from 14 -16 m and 22-26 m were slightly oxidized thus indicating the presence of magnetite in them. At 18m, 34 – 38 m and 46 – 48 m there were few scattered pores filled with calcite.

48 – 58 m: Glassy basalt (Pillow basalt); Porous brownish fine- to medium-grained pillow lava with calcite and silica in vesicles. Plagioclase, pyroxene and olivine phenocrysts with some calcite were observed.

58 – 70 m: Basaltic tuff; Greyish to dark coloured fine- to medium-grained tuff with plagioclase, pyroxene and olivine phenocrysts. 60 – 66 m had patches of fresh glass. 66 – 70 m were highly fractured and veins were filled with calcite.

70 – 80 m: Fine- to medium-grained crystalline basalt; Dark grey fine- to medium-grained microcrystalline olivine tholeiite with plagioclase and pyroxene phenocrysts. 78 m was highly fractured, veins were filled with calcite.

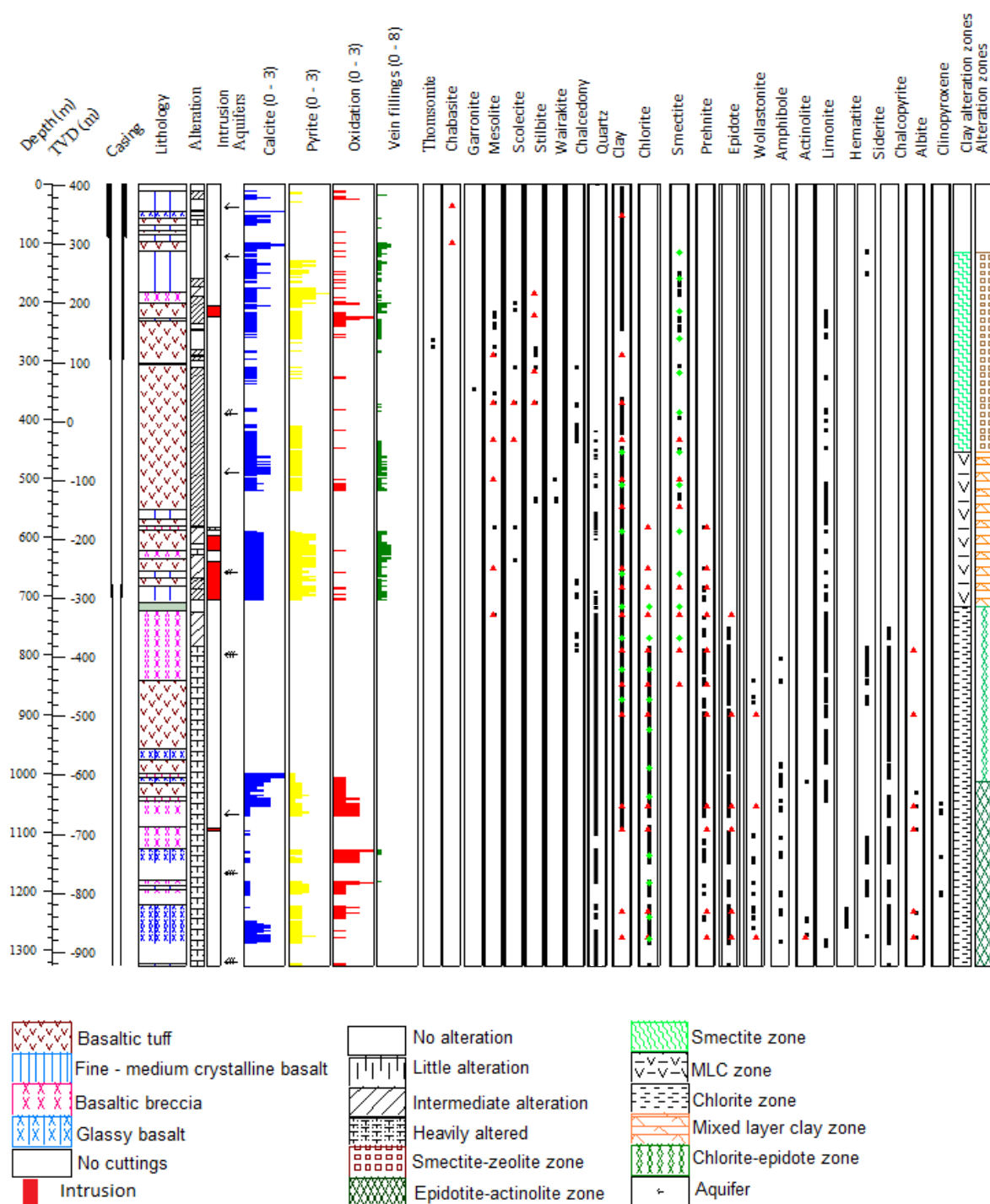


FIGURE 6: Lithology, alteration mineral distribution, intrusions, aquifers and alteration zones of well HE-30 from 0 to 1328 m;

◆ XRD analysis, ▲ petrographic analysis and ■ binocular analysis

80 – 86 m: *Basaltic tuff*; Very porous greyish brown tuff. Slight oxidation observed at 82 m, thus limonite is present. There was occurrence of fresh scoria.

86 - 98 m: *Fine- to medium-grained crystalline basalt with cement.*

98 – 114 m: *Basaltic tuff*; 98 – 110 m samples were highly fractured greyish tuff with few pores. Cuttings at 110 – 114 m were crystalline, slightly fractured and oxidized with presence of siderite, limonite and less glass. The veins were filled with silica and calcite.

114 – 184 m: *Fine- to medium-grained crystalline basalt*; Slightly fractured fine- to medium-grained olivine tholeiite. It is slightly oxidized in the first 10 metres with silica and calcite in the veins. 136 – 138 m were more fractured. The lower part was porous with plagioclase and pyroxene phenocrysts and clay, calcite and pyrite filled the vesicles. Pyrite appeared at 128 m.

184 - 204 m: *Basaltic breccia*; Very porous greyish brown basaltic breccia with phenocrysts of plagioclase and olivine. It is slightly oxidized resulting into limonite. There was occurrence of calcite and pyrite, vesicles and quartz and scolecite in veins.

204 – 228 m: *Basaltic tuff with scoria*; Highly fractured greyish to dark brown crystalline basaltic tuff with olivine and plagioclase phenocrysts. Scoria was observed in this rock. The rock was intruded by a dark grey, less altered, fine-grained crystalline basalt. The secondary minerals were chabazite, stilbite and limonite. Veins were filled with calcite and pyrite with clays forming a thin lining in the vesicles.

228 – 234 m: *Pillow basalt*; Highly fractured and slightly oxidized dark grey to black crystalline pillow basalt with olivine, pyroxene and plagioclase phenocrysts. There was presence of amorph silica, smectite, limonite, calcite, and pyrite, veins were filled with calcite. Grains from a fine- to medium-grained crystalline basalt intrusion were also observed.

234 – 240 m: *Fine- to medium-grained crystalline basalt*; Fractured, less oxidized and less altered dark grey fine- to medium-grained crystalline basalt with phenocrysts of olivine, plagioclase and pyroxene. Secondary minerals were chabazite, mesolite, quartz, smectite with calcite and pyrite filling the veins.

240 – 300 m: *Basaltic tuff*; Porous greyish brown crystalline basaltic tuff with phenocrysts of plagioclase and pyroxene. 240 – 262 m and 284 – 286 m were fractured with calcite, pyrite and quartz in the veins. Smectite, mesolite, quartz and calcite filled some pores. It was slightly oxidized thus presence of magnetite and limonite was indicated.

300 – 304 m: *No cuttings*.

304 – 308 m: *Basaltic breccia*; Brownish crystalline basaltic breccia with abundant cement.

308 – 554 m: *Basaltic tuff*; Greyish brown, fairly fractured and slightly oxidized (presence of limonite) basaltic tuff with little cement in the upper part. It is crystalline and very fine in the middle and highly fractured at the bottom. There were no cuttings at 494 m and 498 m depths. Wairakite, chalcedony, calcite, and pyrite were observed in the vesicles and the veins were filled with quartz, calcite and pyrite. There were numerous grains of fine- to medium-grained crystalline basalt.

554 – 570 m: *Fine- to medium-grained crystalline basalt*; Fractured and altered rock with phenocrysts of plagioclase and numerous calcite and pyrite grains. The bottom was oxidized thus showing limonite. There were sedimentary grains and calcite in veins.

570 – 582 m: *Basaltic tuff*; Fractured and oxidized (limonite shown) brown crystalline basaltic tuff with olivine phenocrysts. There were calcite and pyrite grains in veins and vesicles. No cuttings could be retrieved from 582 m.

582 – 588 m: *Tuffrich breccia*; Very altered and fractured dark grey to greyish tuffrich breccia which was intruded by dark coloured compact fine-grained crystalline basalt (possible intrusion). Calcite and pyrite filled the vesicles and veins.

588 – 622 m: *Basaltic tuff*; Highly fractured and very altered greyish brown basaltic tuff with phenocrysts of pyroxene, abundance of calcite and pyrite grains in vesicles and in veins. It was intruded by a fresh dark grey fine-grained crystalline basalt, probably a dyke. 620 – 622 m were slightly oxidized (presence of limonite).

622 – 636 m: *Basaltic breccia*; Very altered and highly fractured greyish brown basaltic breccia. It had abundant calcite and pyrite grains, quartz, calcite and pyrite in veins. Fresh dark grey fine-grained crystalline basalt, probably a dyke intrusion was seen throughout this rock.

636 – 658 m: *Basaltic tuff*; Very altered and fairly fractured greyish brown basaltic tuff with calcite and pyrite grains and scolecite, quartz and calcite in veins. Prehnite was observed in the tuff. An intrusion of fresh dark grey fine-grained crystalline basalt, probably a dyke, was also observed in this rock.

658 – 668 m: *Fine- to medium-grained crystalline basalt*; Very altered and fairly fractured dark grey crystalline basalt (olivine tholeiite) with calcite and pyrite grains and in veins. An intrusion of fresh dark grey fine-grained crystalline basalt, probably a dyke, is also observed in this rock.

668 – 684 m: *Basaltic tuff*; Very altered and fractured fine-grained brownish basaltic tuff which was intruded by a fresh and compact dark grey fine-grained crystalline basalt, with phenocrysts of plagioclase and olivine. There was chalcedony, quartz, abundance of calcite and pyrite in the veins. 682 – 684 m were slightly oxidized showing limonite.

684 – 707 m: *Fine- to medium-grained crystalline basalt*; Altered, fractured and slightly oxidized (showing limonite) dark grey grained crystalline basalt (olivine tholeiite) with phenocrysts of plagioclase and pyroxene. Chalcedony, quartz, abundance of calcite and pyrite was observed in the veins. There was a dyke intrusion present.

707 – 712 m: *No cuttings*.

712 – 724 m: *Cement*.

724 – 844 m: *Basaltic breccia*; Altered, slightly oxidized and more fractured greenish brown to dark grey very fine-grained rock with some epidote. The samples from 788 – 844 m were more altered. There was prehnite at 818 – 820 m. Calcite, chalcopryrite and quartz were observed in the veins while in the vesicles, there was chalcedony, calcite, quartz, chlorite, chalcopryrite, epidote and prehnite.

844 – 958 m: *Basaltic tuff*; Very altered, oxidized (presence of siderite and limonite) and highly fractured greenish grey rock with less calcite and chalcopryrite. Calcite, chalcopryrite and quartz were observed in veins while chalcedony, calcite, quartz, chlorite, chalcopryrite, epidote and prehnite were observed in vesicles. Other secondary minerals included wollastonite.

958 – 978 m: *Pillow basalt*; Very altered and slightly oxidized dark to grey coloured rock with quartz, chlorite, calcite, chalcopryrite and epidote filling the vesicles. Other secondary minerals were prehnite, and siderite.

978 – 1000 m: *Basaltic tuff*; Very altered greenish grey and very fine-grained tuff with a lot of calcite and less chalcopryrite. Other minerals that were observed here were prehnite, epidote, quartz and amphibole.

1000 – 1008 m: *Tuff-rich breccia*; Very altered dark grey to greyish tuff-rich breccia with abundance of calcite and to a smaller extent chalcopryrite. Quartz, amphibole, prehnite and epidote were observed in this rock.

1008 – 1018 m: *Pillow basalt*; Very altered and slightly oxidized (limonite shown) pillow basalt with more calcite and less chalcopryrite. Other secondary minerals that were observed were chlorite, epidote, prehnite and amphibole.

1018 – 1040 m: *basaltic tuff*; Very altered and slightly oxidized (limonite shown) greenish brown tuff. There was less chalcopyrite and calcite. Other secondary minerals that were observed were chlorite, epidote, prehnite and amphibole.

1040 – 1048 m: *Tuff-rich breccia*; Very altered and oxidized dark grey to greyish rock with more calcite and less chalcopyrite. Chlorite, prehnite and epidote were also seen.

1048 – 1072 m: *Basaltic tuff*; Very altered and very oxidized microcrystalline greenish grey to dark aphyric basaltic breccia. 1040 – 1048 m has more calcite than the bottom part. Chalcopyrite, chlorite, quartz and prehnite were observed.

1072 – 1092 m: *No cuttings*.

1092 – 1128 m: *Basaltic breccia*; Very altered greenish breccia with traces of calcite at the bottom. At 1094 – 1098 m, it was intruded by dark grey fine-grained crystalline basalt that was fresh and compact.

1128 – 1152 m: *Pillow basalt*; Very altered and oxidized greyish black pillow basalt with pyroxene phenocrysts. Few traces of calcite were observed at the bottom and 1130 – 1138 m were fractured. Secondary minerals observed were quartz, chalcopyrite, chlorite, epidote, siderite, prehnite, wollastonite and amphibole. There were several crystals of wollastonite at 1144 m.

1152 – 1182 m: *No cuttings*.

1182 – 1192 m: *Basaltic breccia*; Very altered and much oxidized greyish brown, fine material of basaltic breccia with abundance of epidote in the upper part and with phenocrysts of pyroxene and olivine at the bottom. Quartz, calcite (few traces), epidote, chlorite, chalcopyrite, prehnite, wollastonite and siderite were the secondary minerals that were observed. A vein in 1184 m was filled with quartz and epidote.

1192 – 1198 m: *Fine- to medium-grained crystalline basalt*; Very altered and fairly oxidized dark coloured aphyric crystalline basalt with few traces of calcite. Quartz, epidote, chlorite, chalcopyrite and siderite were the secondary minerals that were seen.

1198 – 1208 m: *Basaltic breccia*; Very altered greyish brown very fine material of basaltic breccia with abundance of epidote and quartz and less calcite and chlorite. It was slightly oxidized and the other secondary minerals include siderite, quartz, chalcopyrite, prehnite, amphibole and wollastonite.

1208 – 1224 m: *No cuttings*.

1224 – 1288 m: *Basaltic breccia*; Very altered and much oxidized greenish grey pillow basalt which was aphyric with abundance of chlorite, quartz and epidote. There was not any chlorite at the bottom (1282 -1288 m). Other secondary minerals observed were wollastonite, actinolite, amphibole, prehnite, siderite and chalcopyrite. Traces of calcite were seen at 1228 m.

1288 – 1324 m: *No cuttings*.

1324 – 1328 m: *Pillow basalt*; Very altered and slightly oxidized, greyish black aphyric pillow basalt with a lot of quartz and epidote and little chlorite. Actinolite was observed as well as chalcopyrite and siderite.

No further cuttings were retrieved from the well due to total loss of circulation.

4.4 Intrusions

Intrusions are usually compact with oxidized margins. They can be indicators of good permeability. In HE-30, these intrusives were observed in the cuttings, using a binocular microscope, as dark grey fine- to medium-grained microcrystalline basalts (Figure 6). Oxidation was observed at 208-226 m and at 528-588 m. Peaks were observed in the neutron log at 598-622 and 642-707 m. Another peak was observed at 1094-1098 m in the resistivity curve (Hardarson et al., 2007a; 2007b; Gunnarsdóttir, 2012). Figure 7, as obtained from leapfrog, shows HE-30 intercepting the intrusions (642-707 and 1094-1098 m) and faults.

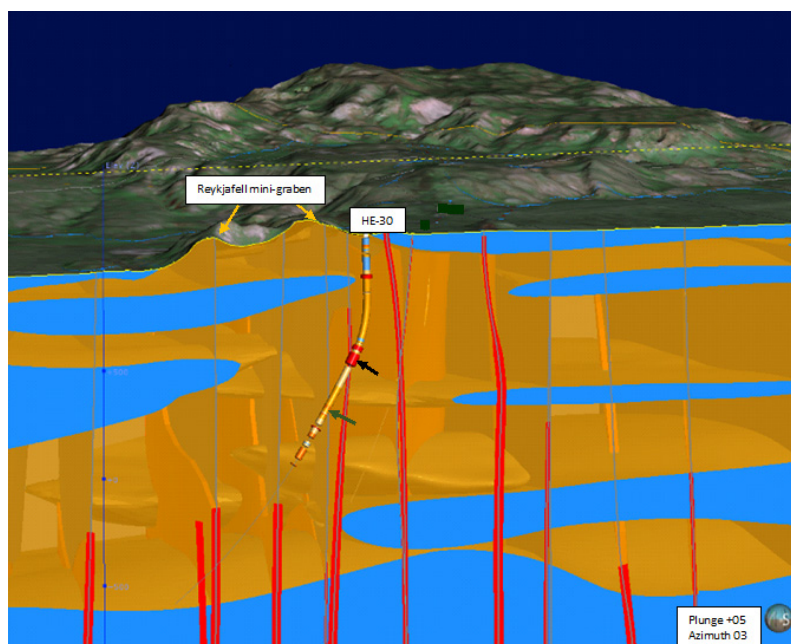


FIGURE 7: Path of well HE-30, fine – medium crystalline basalt (blue), hyaloclastites (yellow), intrusions in Hellisheidi field (red), faults (light blue), Reykjafell mini-graben (yellow arrows) and intrusion in HE-30 at 632 – 707 m (black arrow) and 1094 – 1098 m (dark green arrow)

4.5 Aquifers / feed zones

Thirteen feed zones were observed from temperature logs (Figure 8). They are at 40, 125, 390, 490, 660, 800, 1070, 1170, 1310, 1460, 1550, 1680 and 1960 m depth. The aquifers in the zones of loss of circulation (Figure 6) are in 1070, 1170 and 1310 m depth while 490 and 1070 m had abundance of calcite and pyrite which indicates permeability. There was total loss of circulation below 1328 m. Temperature logs showed that there are feed zones at 1460, 1550, 1680, and 1960 m depth. There are no details on the circulation losses on Figure 8 which shows small aquifers located at 40, 125 and 490 m, medium ones at 390, 660, 1460, 1680 and 1960 m and largest ones at 800, 1070, 1170, 1320 and 1550 m.

4.6 Alteration mineralogy

Minerals that crystallize from magma are called primary minerals (rock forming minerals) while those that result from deposition from geothermal activity and from hydrothermal reactions and/or hydrothermal alteration in host rock inside amygdales, vesicles and fissures are called secondary minerals (Reyes, 2000). Primary minerals alter when subjected to different conditions like temperature, pressure, fluid composition and many more. HE-30 is composed of hyaloclastites and basalts with the primary minerals being volcanic glass, olivine, plagioclase, pyroxene and opaque minerals.

4.6.1 Primary minerals

Below is the description of the primary minerals with their alteration products (Figure 9). *Glass*: Glass forms when magma cools rapidly. It is translucent, unstable and easily altered with vitreous lustre and conchoidal fractures. It alters to clay, calcite, zeolites and quartz. *Olivine*: When magma solidifies, olivine crystallizes first. In HE-30 these were small (a few millimetres) yellowish green crystals with indistinct cleavage and conchoidal fractures. It alters to clay, calcite, zeolites and quartz. *Plagioclase*: The most common primary mineral was the calcium rich feldspar with phenocrysts that occurs singly or as clusters. The crystals are white to colourless, flat, columnar or granular and have parallel cleavage,

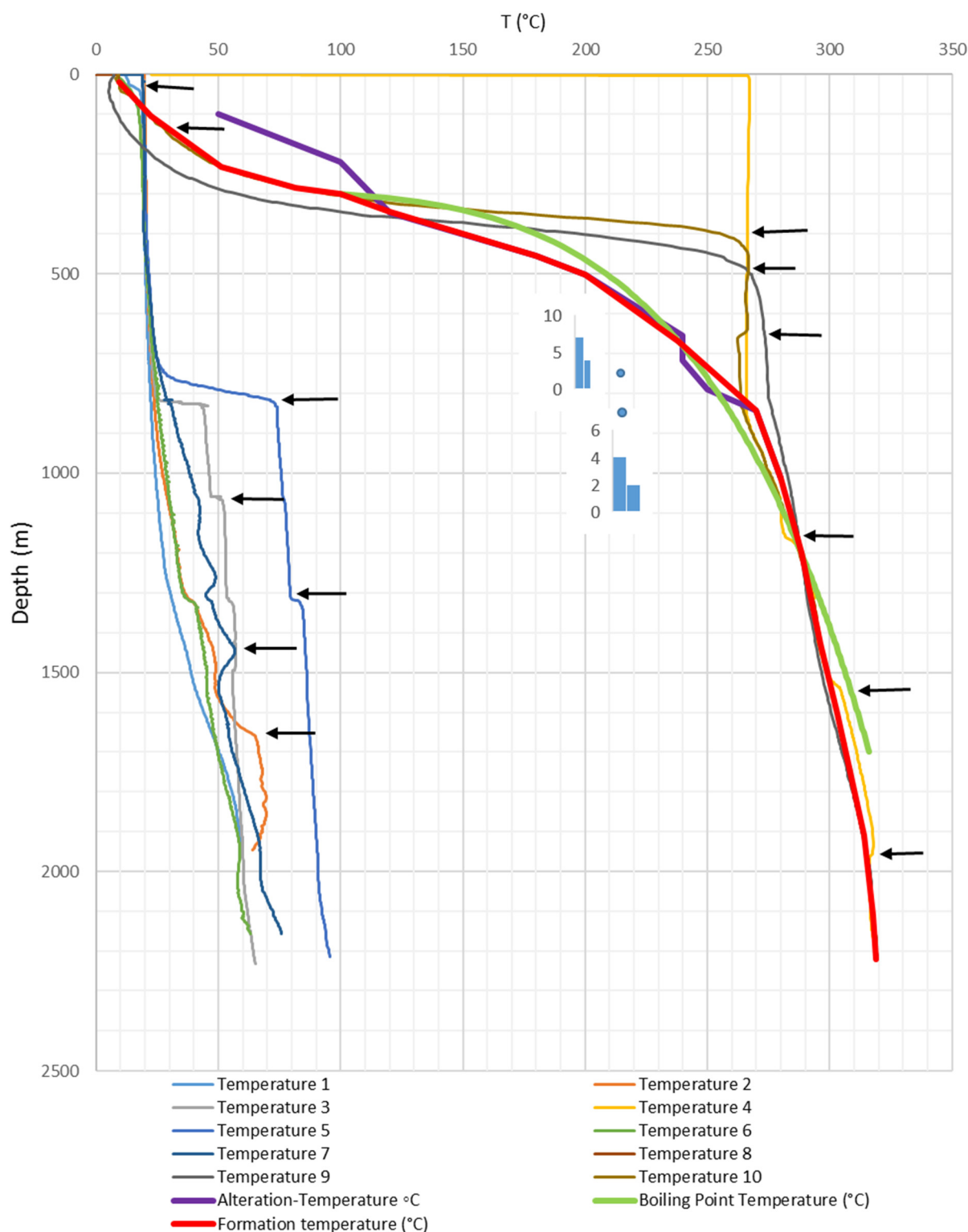


FIGURE 8: Location of feed zones from 0 to 1960 m in HE-30 based on temperature logs at different times in the well including heating-up curves, alteration temperature, formation temperature and homogenization temperature (T_h) (blue dots)

oscillatory zoning and polysynthetic twinning with a low relief (Saemundsson and Gunnlaugsson, 2010). Plagioclase is observed throughout well HE-30. It was altered to albite, wairakite, chlorite and epidote. *Pyroxene*: These were very small black to dark green prismatic crystals of augite. The cleavage was perfect (parallel cleavage) with vitreous lustre observed throughout the well. It was altered to clay,

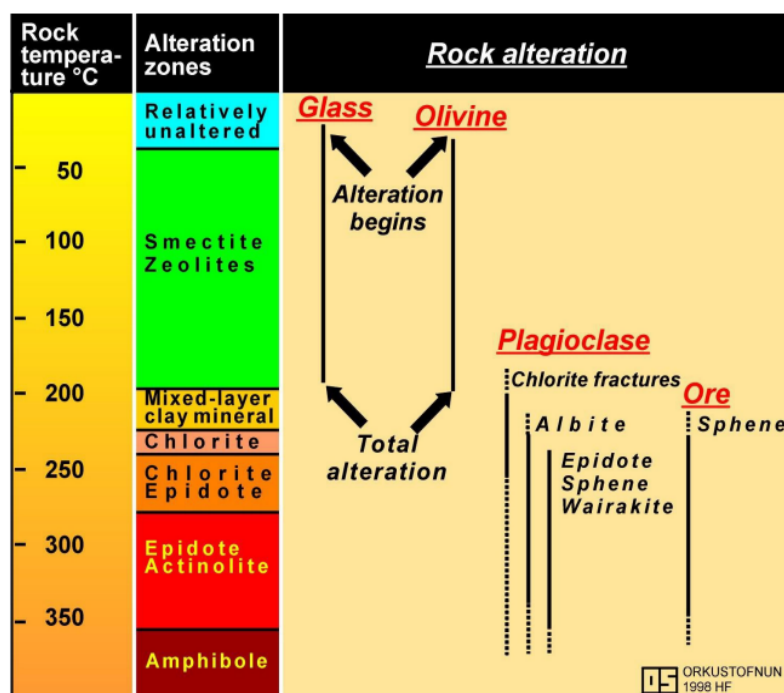


FIGURE 9: Alteration temperatures of primary minerals (Franzson, 1998)

oxidation of iron and chemical weathering of the rocks. Limonite and hematite were observed in HE-30. *Limonite* is yellowish to reddish brown of round shape with a dull metallic lustre and forms as surface coating as well as in fractures and vesicles. It was first seen at 114 m then occasionally throughout the well. It usually occurs together with siderite. *Hematite* is an opaque coarse crystalline of reddish brown to blackish colour, with shiny metallic lustre and occurs in between grains. It was seen at 250 m and towards the bottom of the well.

Carbonates are formed by reaction of carbonic acid with metals, weathering of metallic sulphides and alteration of other rock minerals (Saemundsson and Gunnlaugsson, 2010). Calcite and siderite were seen in HE-30. *Calcite* is the most common carbonate with an extreme birefringence and change in relief when it reacted with weak acids. It is white but coloured when it has impurities with dull lustre, rhomboidal cleavage or conchoidal fracture and occurs in many forms, for example as precipitation in amygdals, fissures and vein fillings. In HE-30, it was seen, evenly distributed, from the top to 1228 m with close association to the sulphides and other minerals. Platy calcite was seen at 108 m and thus representing boiling in the formation. *Siderite* is yellowish to reddish brown spherical or tabular crystals with perfect cleavage and vitreous lustre. It is found together with limonite and in veins or at intrusion margins. It was found from 114 m towards the bottom of the well.

Clays occurred as blueish/brown or greenish soft laminar very fine-grained particles with perfect cleavage. It forms as a result of alteration of the primary minerals. Smectite, chlorite and mixed layered clays (MLC) were observed throughout the well at different depths as seen from the binocular microscope and XRD analysis (Figure 6). *Smectite* is a greenish clay, formed as thin lining in amygdals and rock surfaces. It is brown in plain polarized light and green in crossed polar light. It was first observed from 116 to 772 m (Appendices I and II). *MLC* result from high-temperature hydrothermal alteration. They were seen from 456 to 876 m (Appendices I and II). There was a blue, unidentified, clay that was observed occasionally between 248 and 256 m. *Chlorite* has greenish to greenish brown fibre-like crystals that is found on rock surfaces, in vesicles and veins. It is associated with quartz, calcite and the high-temperature minerals. It was observed from 718 m (first appearance XRD analysis) (Appendices I and II) and from 754 m (first appearance in cuttings) to the bottom. It is indicative of temperatures $\geq 230^{\circ}\text{C}$ (Table 2).

calcite, quartz, chlorite, chlorite, epidote and actinolite. *Opaque minerals*: They were dark coloured and opaque and encountered throughout the well. *Magnetite* occurred as very tiny black cubic crystals with a metallic lustre and precipitated in vesicles or fractures. It was altered to limonite and siderite.

4.6.2 Hydrothermal mineral alteration

The distribution of the alteration minerals with regard to the order of occurrence, which represents the temperatures at which they were formed, is presented in Table 2. In HE-30, they occur as described below (Figure 6).

Oxides: These are formed from alteration of magnetite and

Zeolites are hydrated aluminium silicates which are colourless or white but coloured if containing impurities with variable cleavage, pearly or vitreous lustre and with uneven or conchoidal fractures. They are translucent or opaque. They form from precipitation and alteration in vesicles and veins at relatively low temperatures, below 200°C (Table 2) (Saemundsson and Gunnlaugsson, 2010). They occur in clusters in variable shapes and are associated with calcite, and sometimes quartz. They were observed from 100 m to 732 m. Chabazite, stilbite, scolecite, mesolite, thomsonite, garronite and phillipsite were seen in HE-30 from 100 to 732 m. *Chabazite* of white cubic shaped was found at 100 m (first appearance). It forms at around 50°C. *Scolecite* and *mesolite* are small elongated fibrous clustered crystals with a centred divergent radiation. They usually form at 70 – 80°C. *Scolecite* had thicker fibrous clustered crystals that were colourless or white and were first seen at 204 m. *Mesolite* occurred as white or greyish thin fibrous clustered crystals, which were seen at 220 m (first appearance). *Stilbite* was seen as thick tabular milky white crystals in bow tie form. It forms at around 90°C and was first seen at 312 m. *Thomsonite* occurred as flattened round milky white crystals and its first appearance was at 266 m depth and forms at around 100°C. *Phillipsite* occurred as thick blocky crystals that were colourless to white in colour. Its first appearance was at 346 m depth. *Garronite* was found in form of radiating concentric fractured milky white clustered crystals. It is a rare zeolite which forms at 120°C. It was seen at 348 m depth. *Wairakite* (>200°C) is found commonly in olivine tholeiites, in vesicles and fractures as transparent cubic crystal clusters with conchoidal fracture and has strong vitreous lustre with a conspicuous cross hatched twinning. It is a high temperature zeolite which usually occurs together with epidote, prehnite, calcite, quartz. It was first seen in 502 m in thin sections (Figures 6, 10 and 11) and at 534 m in cuttings.

Sulphides are found at margins of intrusions (Saemundsson and Gunnlaugsson, 2010). They sometimes occur in dykes and at geothermal springs in high-temperature areas (due to the presence of the H₂S in geothermal fields) and they are usually associated with calcite thus being indicator of permeability (Reyes, 2000; Saemundsson and Gunnlaugsson, 2010). In HE-30, pyrite and chalcopyrite were observed. *Pyrite* is cubic yellow with a strong metallic lustre and no cleavage. It is also formed from the deposition of hydrogen sulphide and/or from the alteration of oxides (Saemundsson and Gunnlaugsson, 2010). It was found as shiny coatings on fracture surfaces and in vesicles. It was seen from 128 m down to 790 m. *Chalcopyrite* forms by solidification of late magma gas-rich liquids (Saemundsson and Gunnlaugsson, 2010). It has indistinctive cleavage but is soft, yellow and tetragonal, though darker than pyrite. It was seen from 790 m to the bottom.

TABLE 2: Temperature dependant minerals in high-temperature geothermal fields in Iceland (Kristmannsdóttir, 1979; Franzson, 1998)

Minerals	Min. temp. (°C)	Max. temp. (°C)
Zeolites	40	120
*Laumontite	120	180
*Wairakite	200	
Smectite		<200
**MLC	200	230
Chlorite	230	>300
Calcite	50-100	280-300
Quartz	180	>300
Prehnite	240	>300
Epidote	230-250	>300
Wollastonite	270	>300
Actinolite	280	>300
*Belong to the zeolite group		
**Mixed-layer clay		

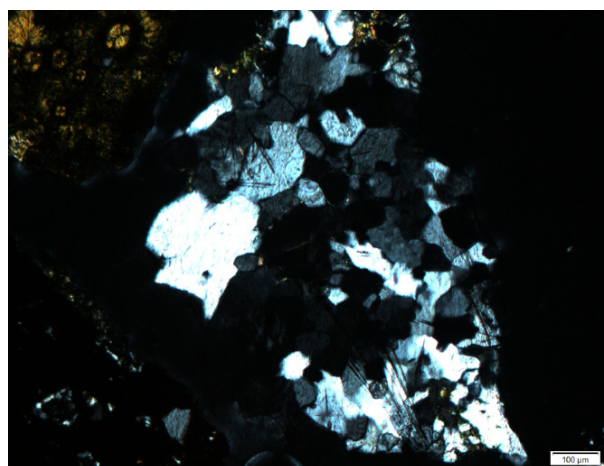


FIGURE 10: Wairakite at 502 m under crossed polars showed conspicuous cross hatched twinning in HE-30

Albite occurs as a transparent to translucent mineral as either a primary mineral (precipitation filling in vesicles) and/or an alteration of plagioclase. It has polysynthetic cleavage formed with low refractive index and is cloudy what differentiates it from quartz.

Silicates: *Chalcedony* is found in amygdaloids and cavities (as a coating) as white to grey translucent to opaque milky amorphous convex crystals (Saemundsson and Gunnlaugsson, 2010). The other colours are caused by oxidation. It is hexagonal with a greasy and waxy lustre and no cleavage. It was seen sparsely distributed from 314 to 788 m. *Quartz* (formed at 180°C) occurs in vesicles and fissures as hexagonal transparent, colourless, milky, greyish white crystals. It is deposited in cavities or as an alteration of chalcedony. It was well distributed in the well and was abundant in the bottom part of the well due to its temperature stability.

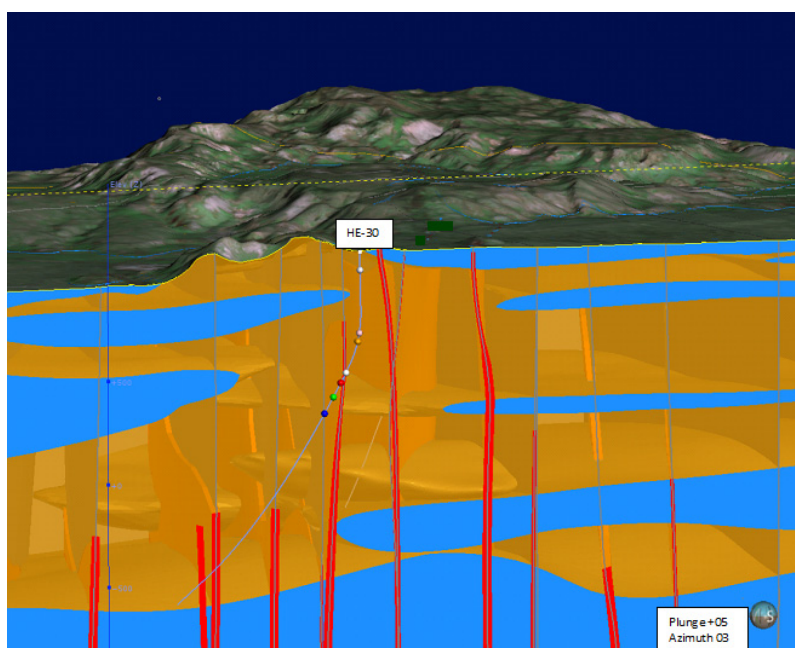


FIGURE 11: First appearance of alteration minerals in HE-30. Quartz (grey), wairakite (pink), prehnite (yellow), epidote (white and red), wollastonite (green), amphibole (blue)

Prehnite is made of white to grey rounded (orthorhombic) crystal clusters with distinct cleavage, irregular fracture and a strong birefringence which differentiates it from quartz. It was associated with the other high-temperature minerals, calcite, quartz, oxides and sulphides indicating temperatures $\geq 240^{\circ}\text{C}$. In HE-30, it was first seen at 654 m (Figures 6 and 11). *Epidote* are greenish yellow to pale green, translucent, microcrystalline (monoclinic) elongated prismatic fibrous crystals, with a high relief, vitreous lustre and unidirectional cleavage. It is an alteration product of feldspars, pyroxene and amphibole. It is stable at higher temperatures and indicates temperatures $\geq 240^{\circ}\text{C}$. It was

widely distributed from 790 m (first appearance) (Figures 6 and 11) and well distributed towards the bottom. It occurred together with other high-temperature minerals like quartz, calcite, oxides and sulphides.

Wollastonite is found as very thin white fibres and occurs together with quartz, calcite and epidote. In He-30, it was associated with silicates, oxides, chalcopryrite, prehnite, epidote and actinolite at 844 m depth (first appearance, Figures 6 and 11) and at the bottom of well. It represents temperatures $\geq 270^{\circ}\text{C}$.

Amphiboles: *Actinolite*, which is a high-temperature mineral, was observed at 1014 m (first appearance), indicating $\geq 280^{\circ}\text{C}$. It occurred as thin, needle shaped, dark green crystals that resulted from the alteration of clinopyroxenes (Figures 6 and 11).

4.6.3 Alteration mineral zones

Hot hydrothermal fluids react with the host rocks forming hydrothermal minerals. There are a number of factors that influence the formation of alteration minerals such as permeability, temperature, duration of activity, rock composition, pressure, hydrothermal fluid composition and hydrology (Reyes, 2000; Marosvölgyi et al., 2010) resulting in mineral zonation with an increase of alteration with depth and

temperature in the well. In HE-30, 4 alteration zones (Figure 6 and Appendix I) were observed as shown below.

Unaltered zone (0 – 116 m): In this zone, there was no or slight oxidation and alteration which could be a result of interaction of run off or ground water with the host rock, thus magnetite, limonite, calcite and siderite occur.

Smectite – zeolite zone (116 – 456 m): In this zone there are zeolites (chabazite, stilbite, scolecite, phillipsite and mesolite) and low-temperature clays, smectite being the dominant one as seen from the XRD results (Appendices I and II). They represent a temperature range of 40 – 150°C. Other minerals in this zone include wairakite, chalcedony, quartz, hematite, limonite, siderite, calcite and pyrite.

Mixed layered clays zone (456 – 718 m): This zone is characterized by high-temperature clays (Appendices I and II) representing temperatures from 150 – 230°C. They are associated with quartz, chalcedony, calcite, pyrite, zeolites and prehnite.

Chlorite - epidote zone (718 – 1014 m): Chlorite (Appendices I and II) and epidote became more evident in this zone representing a temperature $\geq 250^\circ\text{C}$. They are found together with prehnite, chalcopryrite and limonite.

Epidote – actinolite zone (1014 – 1328 m): Chlorite and epidote were dominant in this zone. They define temperatures $\geq 280^\circ\text{C}$. The rocks in this zone were greatly altered and the upper part was intensely fractured, with abundance of chlorite and epidote. At the bottom, there was less epidote and chlorite and no calcite. Wollastonite and actinolite were observed together with prehnite, quartz, limonite and siderite.

4.7 Vesicles, vein fillings and mineral deposition sequences

4.7.1 Vesicles and vein fillings

Veins and vesicles contribute greatly to porosity and permeability, which control the transportation and storage of fluids within the rocks. Due to different conditions of the rock and fluids, for example temperature, pressure, fluid composition and many others, alteration minerals are deposited and/or replace the primary minerals in fractures and vesicles resulting in deposition sequences of secondary minerals. Hydrothermal mineral deposition in geothermal fields is mostly controlled by temperature. The most common minerals that were found in the vesicles and veins in HE-30 were calcite, pyrite, chalcedony, quartz, zeolites, chlorite and epidote. Clay formed a thin layer lining the vesicles. In the cuttings, veins were observed at different depths (42 m, 60 m, and 76 m) in fine- to medium-grained crystalline basalt at 66, 203 – 264, 284 – 286, 328 – 330, 352 – 376, 386, and 420 m in basaltic tuff, at 728 and 1184 m in basaltic breccia, at 1130 – 1138, 1268, 1280 and 1326 – 1328 m in pillow basalt, at 1002 – 1024 m in basaltic tuff and fine- to medium-grained crystalline basalt, at 132 – 220 m in fine- to medium-grained crystalline basalt and basaltic breccia, at 738 – 892 and 1008 – 1072 m in basaltic tuff and basaltic breccia and at 434 – 707 m in basaltic tuff, basaltic breccia and fine- to medium-grained crystalline basalt (Figure 6). For example, in the petrographic analysis, a vein was observed in 1096 m depth (Figure 12).

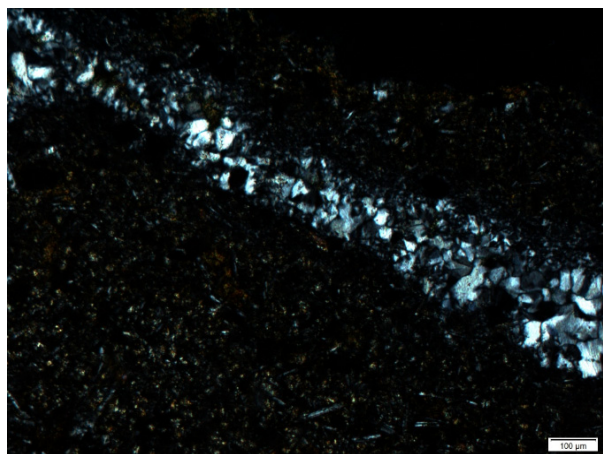


FIGURE 12: Vein filled with quartz in fine-grained crystalline basalt at 1096 m in HE-30

4.7.2 Mineral deposition sequence

Fractures and vesicles are conduits for the hydrothermal fluids, which react with the host rock causing deposition and replacement of minerals and wall rock alteration. This process determines the sequence of mineral deposition in relation to time and temperature. The sequences of mineral deposition (Table 3) in veins and vesicles in HE-30 were observed in the binocular and petrographic analyses, which included clay, calcite, quartz, zeolites, chlorite and epidote.

4.8 Fluid inclusions

Microthermometric analysis from 17 fluid inclusions in two crystals (quartz at 758 – 762 m and calcite at 842 – 846 m) were conducted. Homogenization temperature (T_h)

showed a range of 178 – 197, 202 – 220 and 254 – 255°C. The 254 – 255°C temperature range coincides to the estimated formation temperature at that depth range (758 – 762 m) which is around 250°C as seen in Figure 10, while the 178 – 197 and 202 – 220°C temperature ranges as well as the T_h at 842 – 846 m were low compared to the estimated formation temperature.

Comparison of alteration, fluid inclusion and formation temperatures

Fluid inclusion analysis, homogenization temperatures (T_h) at which the alteration minerals first appeared and the formation temperature were used to understand the thermal history of the system, showing if it was heating up, cooling or in equilibrium. Other factors have to be considered when interpreting the thermal history of the system, as there could be eruptive fissures or a magma chamber causing increased heating or a cold inflow leading to cooling of the system. The formation and alteration temperature are almost identical (Figure 8). Homogenization temperatures (T_h) being lower than formation and alteration temperatures could represent an old formation temperature (Figure 8). However, by comparing alteration temperature, formation temperature and the boiling point curve it is concluded that the system is presently in thermal equilibrium.

5. DISCUSSION

HE-30 is composed of alternating interglacial lavas and hyaloclastites, occasionally cut by intrusions, and the sequence is partly covered by postglacial lava flows. The alteration intensity and mineral deposition increases with depth (Figures 6 and 11). There were four alteration zones observed in HE-30, smectite- zeolite at 116 – 456 m, mixed layer clay at 456 – 718 m, chlorite- epidote at 718 – 1014 m and epidote – actinolite 1014 – 1328 m.

TABLE 3: Sequence of mineral deposition in HE-30

Depth (m)	Host rock	Sequence of mineral deposition
54	Basaltic tuff	clay → calcite
100	Basaltic tuff	calcite → chabazite
186	Basaltic tuff	calcite → stilbite
224	Basaltic tuff	smectite → quartz
292	Basaltic tuff	calcite → mesolite
372	Basaltic breccia	clay → calcite → zeolites
434	Basaltic breccia	clay → mesolite
502	Basaltic breccia	clay → calcite
548	Fine -medium crystalline basalt	clay → calcite
584	Basaltic breccia	clay → calcite → quartz
654	Fine -medium crystalline basalt	clay → calcite → quartz
686	Fine -medium crystalline basalt	smectite → calcite
732	Fine -medium crystalline basalt	clay → calcite → zeolites
792	Basaltic breccia	clay → calcite
850	Basaltic breccia	clay → calcite
900	Basaltic tuff	clay → calcite → chlorite
1034	Basaltic breccia	clay → chlorite → calcite
1056	Basaltic breccia	clay → quartz
1184	Basaltic breccia	clay → quartz → epidote
1096	Basaltic breccia	clay → chlorite → calcite
1236	Basaltic breccia	clay → chlorite → calcite
1278	Basaltic breccia	clay → chlorite

Faults, lithological boundaries and intrusions were the major cause of permeability in HE-30. Different sizes of feed-zones were seen at different depths in different lithologies from 0 to 1960 m in HE-30 as seen from circulation losses and temperature logs. Table 1 shows that the aquifers above 705 m were sealed off by casing and cementing the well with production casing.

Alteration and formation temperatures are almost identical and the alteration mineralogy indicates that the well temperature is $> 250^{\circ}\text{C}$ at 700 m depth.

The homogenization temperature (T_h) derived from the fluid inclusions is $178^{\circ}\text{C} - 197^{\circ}\text{C}$, 202°C and $254^{\circ}\text{C} - 255^{\circ}\text{C}$ in quartz crystal at 758 - 762 m and $213^{\circ}\text{C} - 220^{\circ}\text{C}$ in calcite crystal at 842 - 846 m. It was lower than the estimated formation temperature which could indicate older alteration.

The objective of drilling HE-30 was achieved as seen in Figures 7 and 11, which show that the faults and the Reykjafell minigraben were intercepted. This resulted in a well with a productivity above average in the Hellisheidi geothermal field.

6. CONCLUSIONS

The main conclusions in this report are as follows:

- Hyaloclastites (basaltic tuff, basaltic breccia and pillow lavas) and fine- to medium-grained crystalline basalts are the major geological formations in HE-30.
- The intrusions were fine- to medium-grained crystalline basalts.
- Permeability is caused by faults, intrusives and lithological boundaries.
- Thirteen feed zones were found down to 1960 m depth.
- The sequence of mineral deposition is dependent on the rock type, permeability and temperature resulting in four alteration zones.
- The sequence of mineral deposition is dependent on the rock type, permeability and temperature.
- Hydrothermal alteration compared to formation temperature indicates that the system is in thermodynamic equilibrium.
- The low homogenization temperatures (T_h) could be representing old temperature conditions.

ACKNOWLEDGEMENTS

I am grateful to the management and staff of United Nations University Geothermal Training Programme (UNU-GTP) for sponsoring me and giving me the precious opportunity to undertake this training and the knowledge, especially Mr. Lúdvík S. Georgsson, Mr. Ingimar G. Haraldsson, Ms. Thórhildur Ísberg, Mr. Markús A.G. Wilde, and Mrs. Málfríður Ómarsdóttir, who never stopped attending to me whenever I needed their assistance; the Icelandic GeoSurvey (ISOR) not forgetting Ms. Sveinborg H. Gunnarsdóttir, Mr. Bastien Poux, Mrs. Saeunn Halldórsdóttir, Mrs. Helga M. Helgadóttir and Dr. Hjalti Franzson for their technical assistance. Special thanks to my supervisor Dr. Björn S. Hardarson for his parental and generous technical guidance and support. I also thank Reykjavik Energy for allowing me to access HE-30 data.

I am grateful to my employer Ministry of Energy and Mineral Development - Directorate of Geological Survey and Mines (DGSM) for permitting me to attend this training. I am forever and greatly indebted to my God sent husband Mr. Timothy Sembatya for taking care of the children and for being supportive and understanding throughout this time, my sweet sister Dr. Justine N. Busingye for sacrificing

everything else whenever we needed you and my colleagues at DGSM for the overwhelming support. I thank my UNU fellows for your cooperation throughout the training.

Finally, I give God the glory for sustaining me and my family through this training.

REFERENCES

Árnason, K., 2007: *TEM resistivity surveys at the Hengill area 2006 and proposed experimental drilling by Eldborg*. ÍSOR – Iceland GeoSurvey, Reykjavík, report, ISOR-04001 (in Icelandic), 34 pp.

Bawasu, M.L., 2010: Borehole stratigraphy and alteration mineralogy of well HE-6, Hellisheidi, SW-Iceland. Report 9 in *Geothermal training in Iceland 2010*. UNU-GTP, Iceland, 65-90.

Björnsson, A., and Hersir, G.P., 1981: Geophysical reconnaissance study of the Hengill high temperature area, SW-Iceland. *Geothermal Resources Council, Transactions*, 5, 55-58.

Bodnar, R.J., 2003: Introduction to fluid inclusions, Analysis and Interpretation. *Mineral Association of Canada, Short Course Series 32*, 8 pp.

Franzson, H., 1998: Reservoir geology of the Nesjavellir high-temperature field in SW-Iceland. *Proceedings of the 19th Annual PNOC-EDC Geothermal Conference, Manila*, 13-20.

Franzson, H., Gunnlaugsson E., Árnason, K., Saemundsson, K., Steingrímsson, B., and Hardarson, B.S., 2010: The Hengill geothermal system, conceptual model and thermal evolution. *Proceedings of the World Geothermal Congress 2010, Bali, Indonesia*, 19 pp.

Gasperikova, E., Rosenkjaer, K.G., Árnason, K., Newman, A.G., and Lindsey, J.N., 2015: Resistivity characterization of Krafla and Hengill geothermal fields through 3D MT inverse modelling, *Geothermics*, 57, 246-257.

Gebrehiwot Mesfin, K., 2010: *Subsurface geology, hydrothermal alteration and geothermal model of northern Skardsmyrarfjall, Hellisheidi geothermal field*. University of Iceland, MSc thesis, UNU-GTP, report 5, 65 pp.

Gunnarsdóttir, S.H., 2012: *Geology and alteration of Mount. Reykjafell, Hellisheidi, Iceland*. University of Iceland, Reykjavík, MSc thesis (in Icelandic), 197 pp.

Haraldsdóttir, S., Franzson, H., and Árnason, K., 2015: Comparison of down hole data and surface resistivity data from S-Hengill, a high temperature geothermal field in SW-Iceland. *Proceedings of the World Geothermal Congress 2015, Melbourne, Australia*, 12 pp.

Hardarson, B.S., 2014: Geothermal exploration of the Hengill high temperature area. *Presented at Short course IX on exploration for geothermal resources 2014, organized by UNU-GTP, KenGen and GDC, Naivasha, Kenya*, UNU-GTP SC-19, 9 pp.

Hardarson, B.S., Fitton, J.G., Ellam, R.M. and Pringle, M.S, 1997: Rift relocation - a geochemical and geochronological investigation of a paleo-rift in northwest Iceland. *Earth Planet Science Letters*, 153, 181-196.

Hardarson, B.S., Franzson, H., Gudbrandsson, S., Pétursson, F., Sigurdsson, G., Kjartansson, O., Sigurdsson, Ó., Jónsson, P., Danielsen, P.E., and Brynleifsson, T., 2007a: *Hellisheidi – Well HE-30. Predrilling, Phase 1 and 2: Drilling for 22½" surface casing to 90 m, 18⅝" safety casing to 300 m and*

13½" production casing to 707 m depth. ÍSOR – Iceland GeoSurvey, Reykjavík, report ISOR/2007/033 (in Icelandic), 81 pp.

Hardarson, B.S., Júlíusson, E., Einarsson, G.M., Jónsson, S.S., and Gudbrandsson, S., 2007b: *Hellisheidi – Well HE-30. Phase 3: Drilling of production part from 707 m to 2318 m depth for a 9½" liner*. ÍSOR – Iceland GeoSurvey, Reykjavík, report ISOR/2007/037 (in Icelandic), 118 pp.

Hardarson, B.S., Kristinsson, S.G., Karlsdóttir, R., and Einarsson, G.M., 2015: Geothermal implications of rift zone mini-grabens. Geological and geophysical structure of the Reykjafell mini-graben, Hengill geothermal field, SW Iceland. *Proceedings of the World Geothermal Congress 2015, Melbourne, Australia*, 11 pp.

Helgadóttir, M.H., Hardarson, B.S., and Franzson, H., 2016: *Lectures notes on logging drill cuttings*. UNU-GTP, Iceland, unpublished lecture notes, 19 pp.

Kristmannsdóttir, H., 1979: Alteration of basaltic rocks by hydrothermal activity at 100-300°C. In: Mortland, M.M., and Farmer, V.C. (editors), *International Clay Conference 1978*. Elsevier Scientific Publishing Co., Amsterdam, 359-367.

Marosvölgyi, K., Kristmannsdóttir, H., and Lacasse, C., 2010: Retrograde alteration of basaltic rocks in the Theistareykir high-temperature geothermal field, North-Iceland. *Proceedings of the World Geothermal Congress 2010, Bali, Indonesia*, 9 pp.

Reyes, A.G., 2000: *Petrology and mineral alteration in hydrothermal systems: from diagenesis to volcanic catastrophes*. UNU-GTP, Iceland, report 18, 1998, 77 pp.

Saemundsson, K., 1979, Outline of the geology of Iceland, *Jökull*, 29, 7-28.

Saemundsson, K., and Gunnlaugsson, E., 2002: *Icelandic rocks and minerals*. Edda and Media Publishing, Reykjavík, Iceland, 233 pp.

Shepherd, T.J., Rankin, A.H., and Alderton, D.H.A., 1985: *Practical guide to fluid inclusion studies*. Blackie and Sons, Glasgow, UK, 239 pp.

Spichak, V.V., Zakharova, K.O., and Goidina, G.A., 2013: A new conceptual model of the Icelandic crust in the Hengill geothermal area based on the indirect electromagnetic geothermometry *J. Volcan. Geoth. Res.* 257, 99-112.

Steingrímsson, B. and Gudmundsson A., 2006: Geothermal borehole investigations during and after drilling. *Workshop for decision makers on geothermal projects in Central America, organized by UNU-GTP and LaGeo in San Salvador, El Salvador, 2006*, 10 pp.

APPENDIX I: Details of XRD analysis of clay

Sample #	Depth (m)	d(001) OMH	d(001) GLY	d(001) HT	d(002)	Type	Other minerals
#01	58	-	-	-	-	-	
#02	116	13.81	15.93	10.04		sm	
#03	162	13.9	13.9	10.04		sm	
#04	218	13.98	13.98	10.04		sm	
#05	264	14.76	14.76	9.86		sm	
#06	322	13.6	13.6	10.1		sm	Å=9.1 zeol.?
#07	388	13.12	13.62	10		sm	Å=9.1 zeol.?
#08	456	30.91 / 13.24	30.91 / 13.87	9.97	7.2 HIT=0	MLC	Å=9.1 zeol.?
#09	512	13.13	13.78	9.98		sm	
#10	590	32.53 / 14.54	32.53 / 14.54	12.74	7.2 HIT=0	MLC	
#11	662	13.55	13.97	10.2	7.12 HIT=0	sm/ML C	Å=9.1 og 8.97 zeol.?
#12	718	14.34	14.34		7.23 HIT=0	Chl. unst.	
#13	772	15.14	15.85	10.79	7.29 HIT=0	sm/ML C	
#14	824	30.80 / 14.57	30.80 / 14.57	14.57	7.2 HIT=0	MLC	
#15	876	30.79 / 14.86	30.79 / 14.86		7.27 HIT=0	MLC	Å=7.75 ?
#16	926	14.57	14.57	14.57	7.19	Chl	
#17	992	14.76	14.76	14.76	7.22	Chl	Å=7.73 ?
#18	1040	14.6	14.6	14.6	7.2	Chl	Å=7.71?
#19	1140	14.65	14.65	14.65	7.22 HIT=0	Chl. unst.	
#20	1186	14.65	14.65	14.65	7.20 HIT=0	Chl. ill	Å=10.05 illite
#21	1244	14.43	14.43	14.43	7.15 HIT=0	Chl. unst.	
#22	1282	14.81	14.81	14.81	7.26 HIT=0	Chl. unst.	

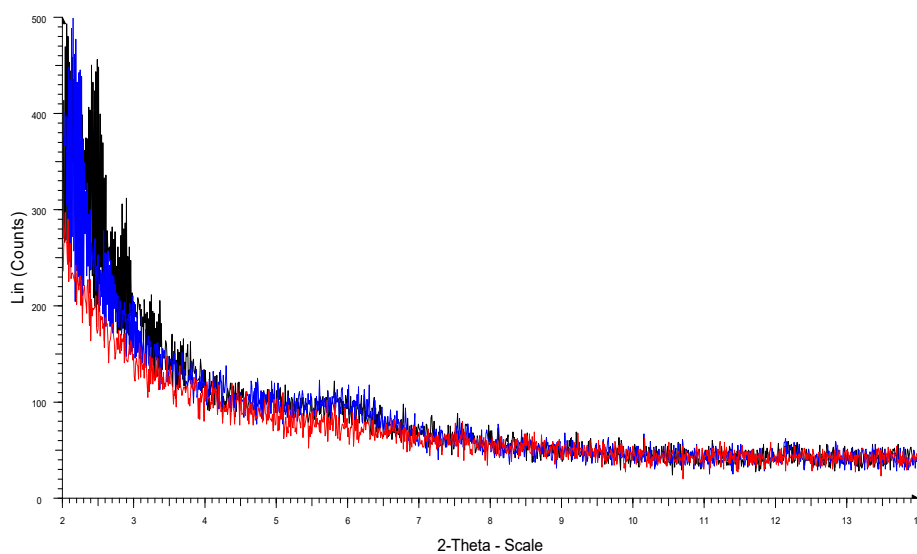
Appendix II: Graphs from XRD analysis of samples at different depths in HE-30

FIGURE 1: HE-30 at 58 m

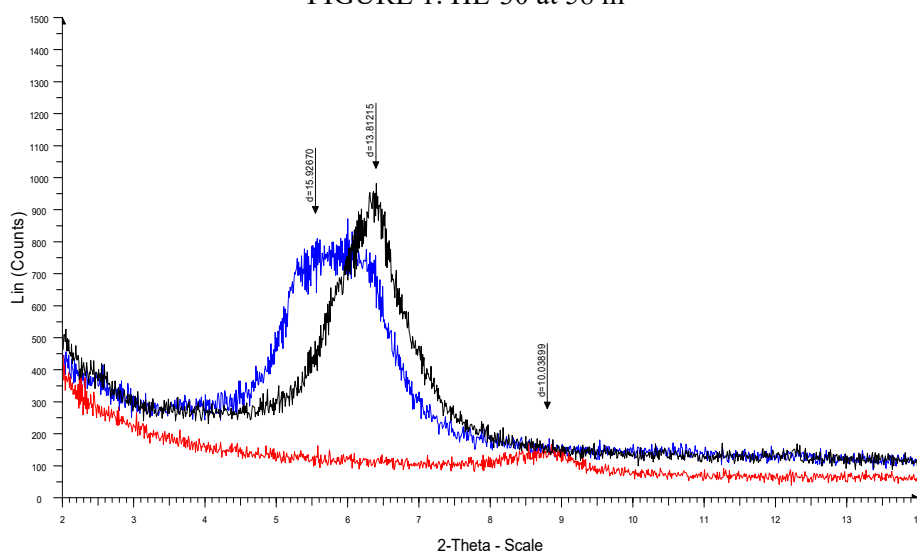


FIGURE 2: HE-30 at 116 m

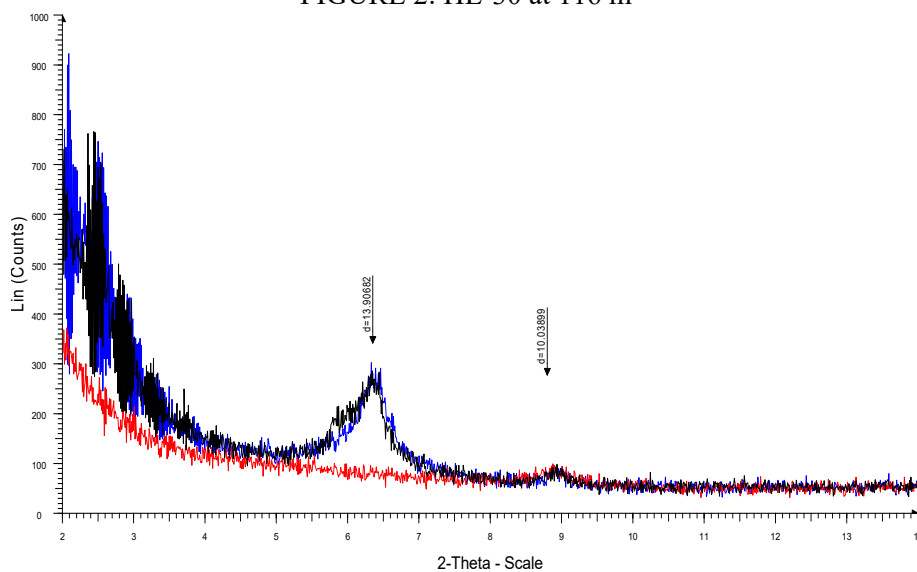


FIGURE 3: HE-30 at 162 m

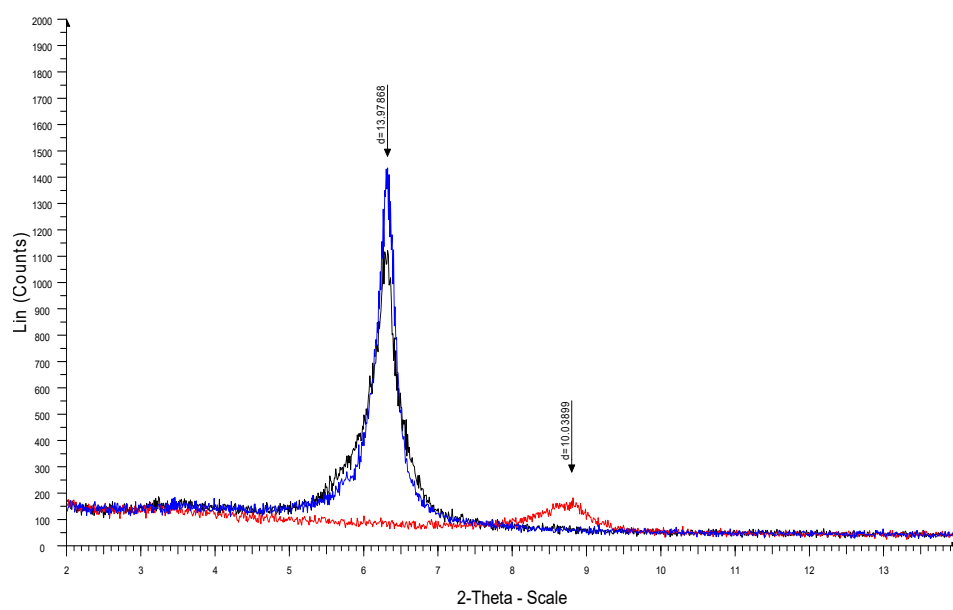


FIGURE 4: HE-30 at 218 m

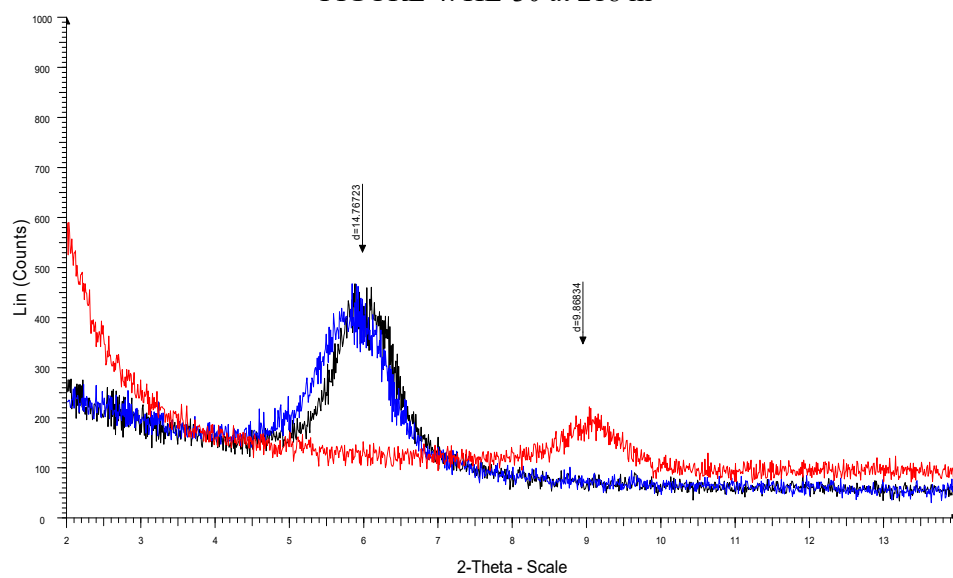


FIGURE 5: HE-30 at 264 m

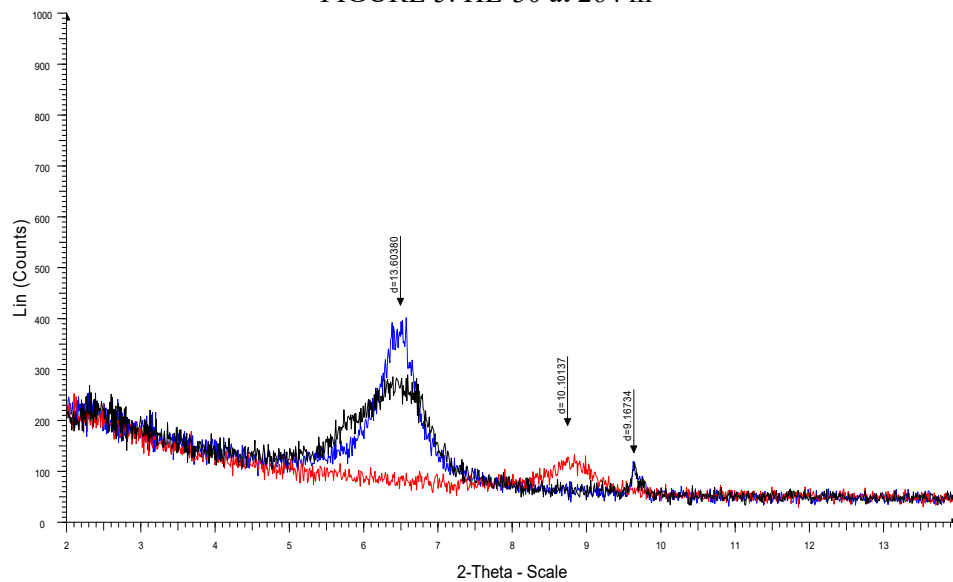


FIGURE 6: HE-30 at 322 m

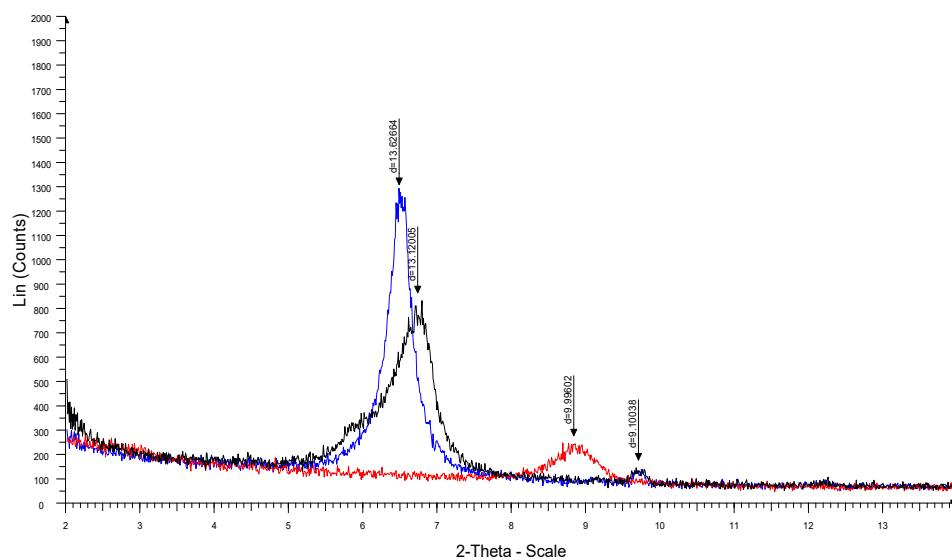


FIGURE 7: HE-30 at 388 m

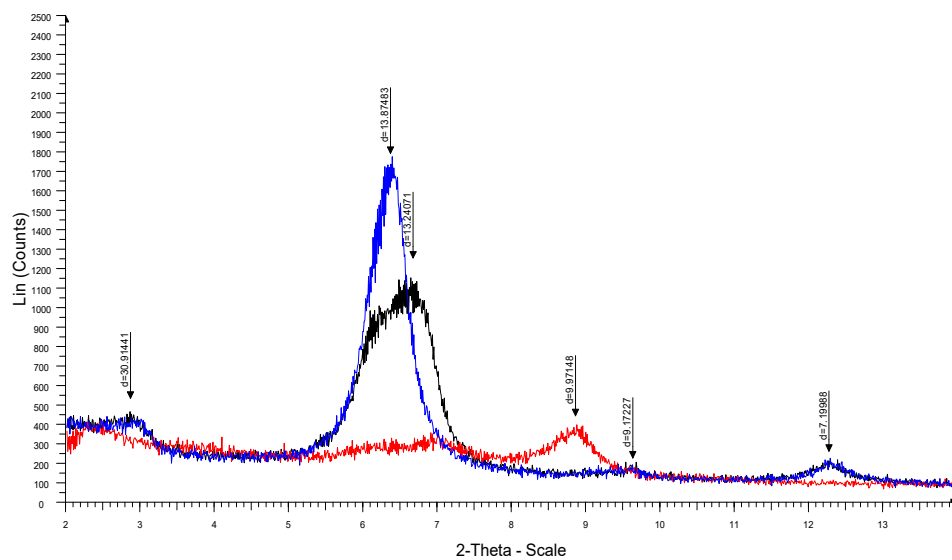


FIGURE 8: HE-30 at 456 m

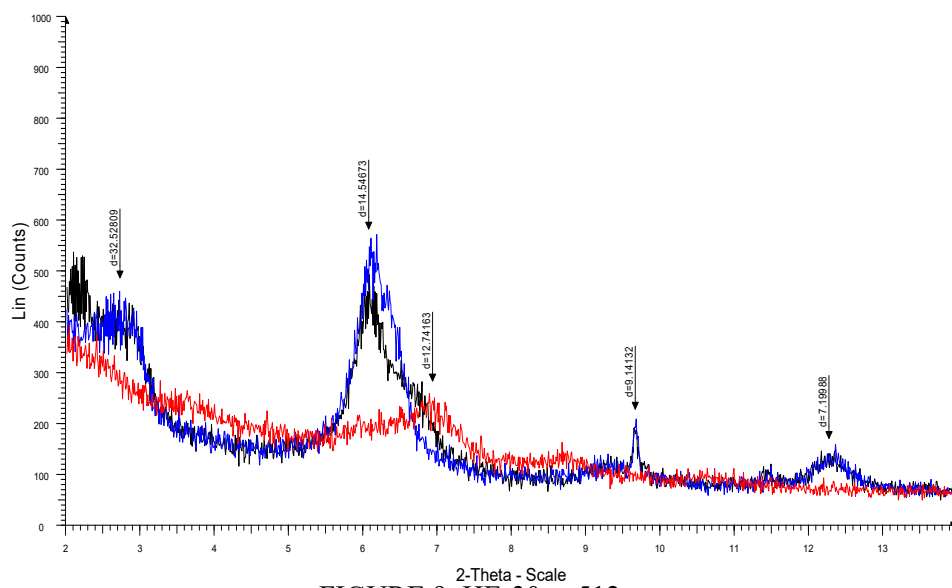


FIGURE 9: HE-30 at 512 m

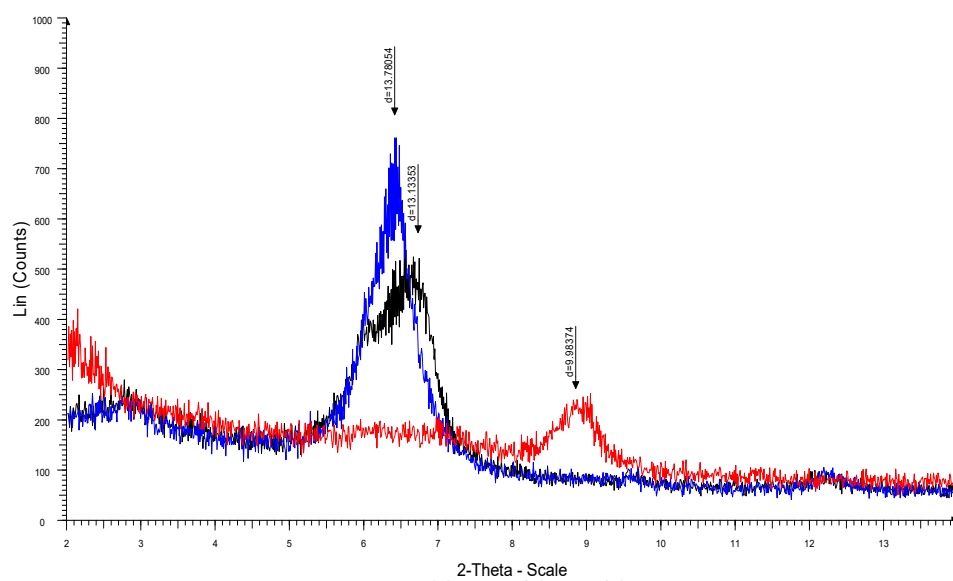


FIGURE 10: HE-30 at 590 m

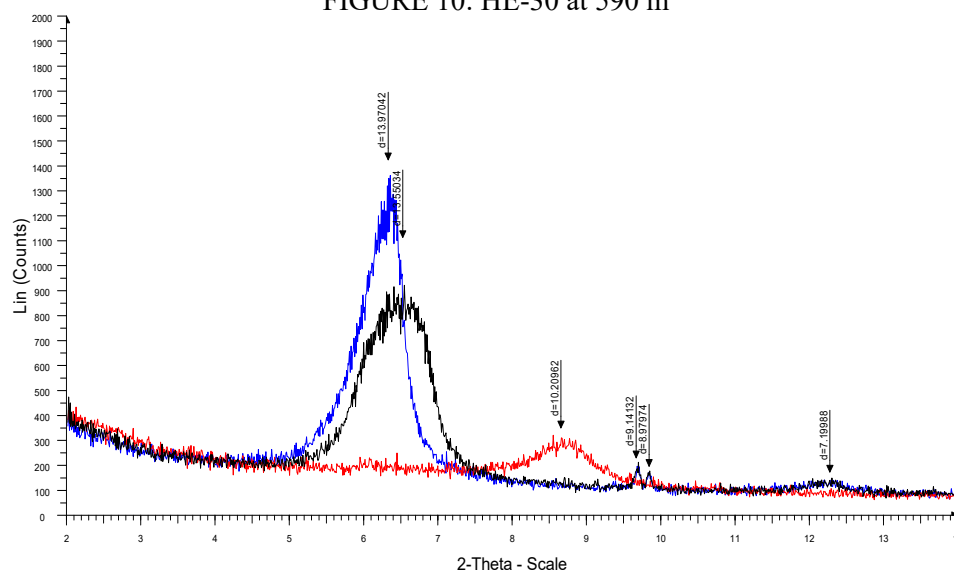


FIGURE 11: HE-30 at 662 m

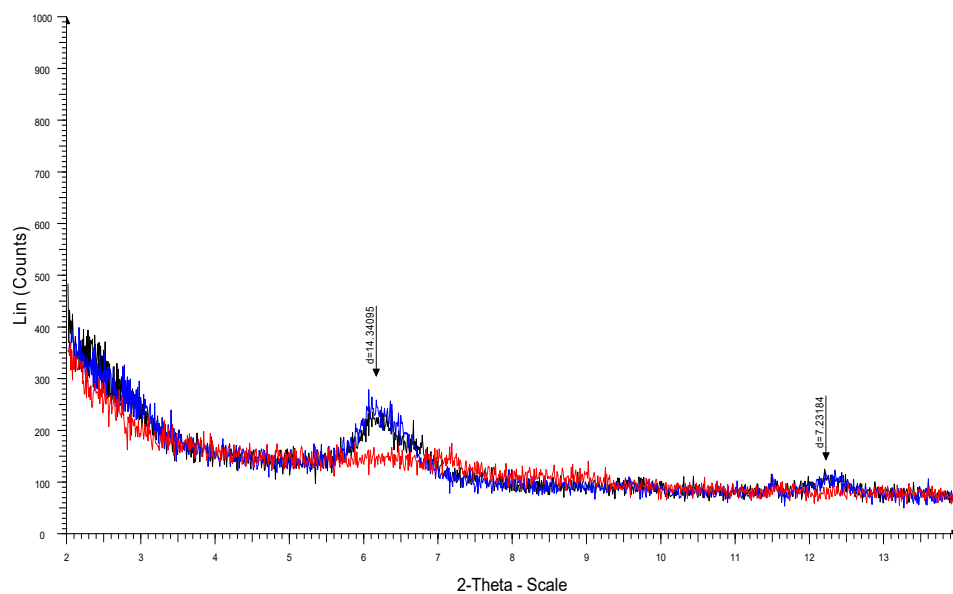


FIGURE 12: HE-30 at 718 m

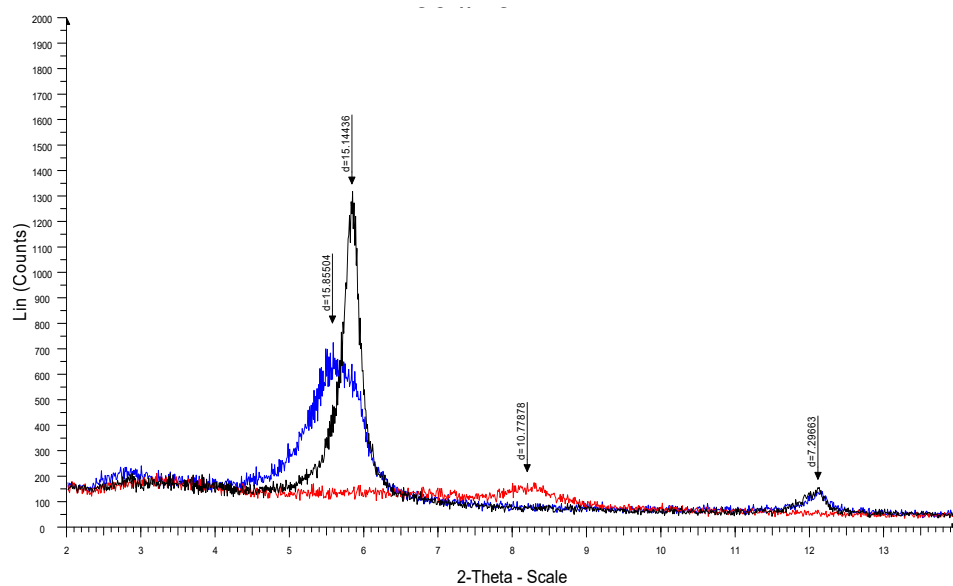


FIGURE 13: HE-30 at 772 m

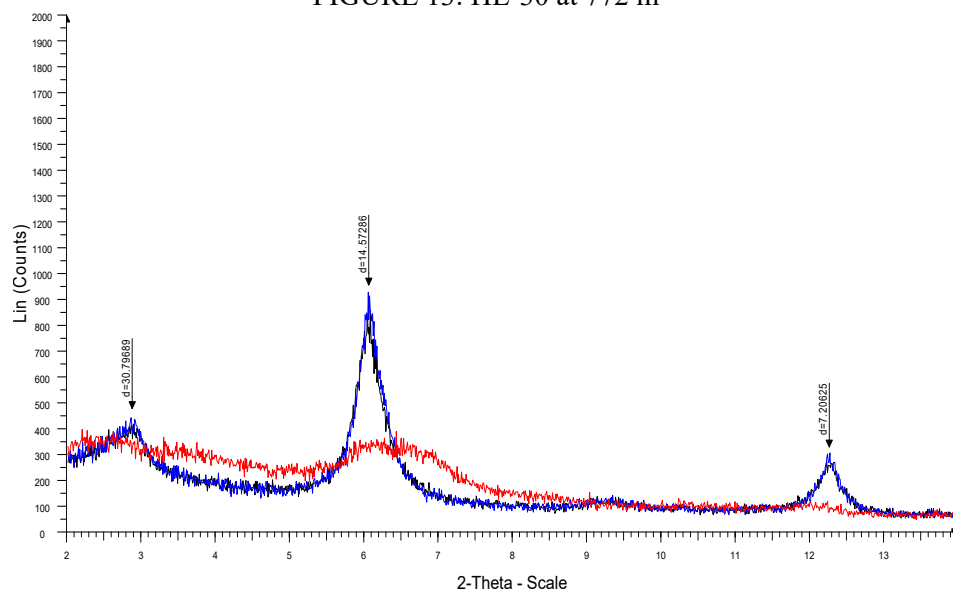


FIGURE 14: HE-30 at 824 m

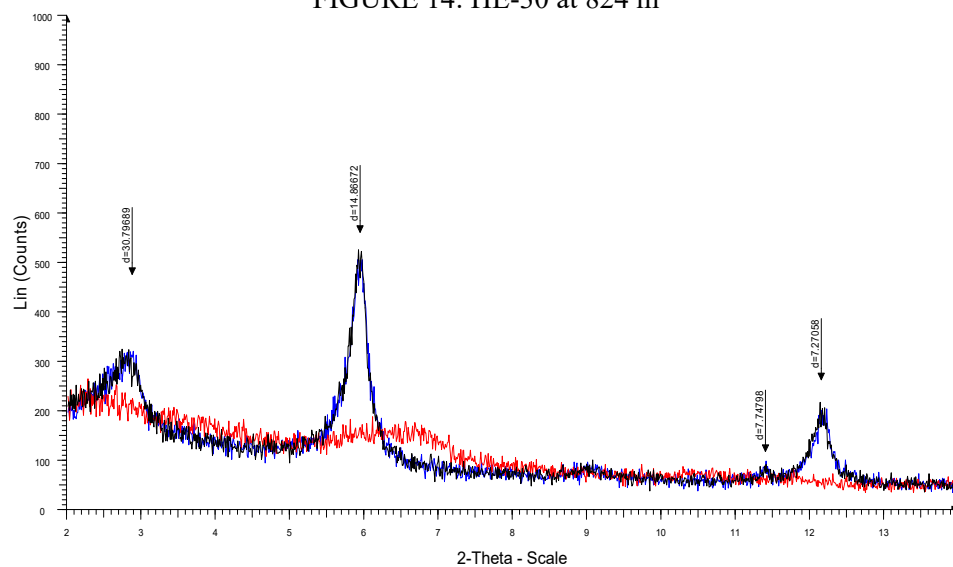


FIGURE 15: HE-30 at 876 m

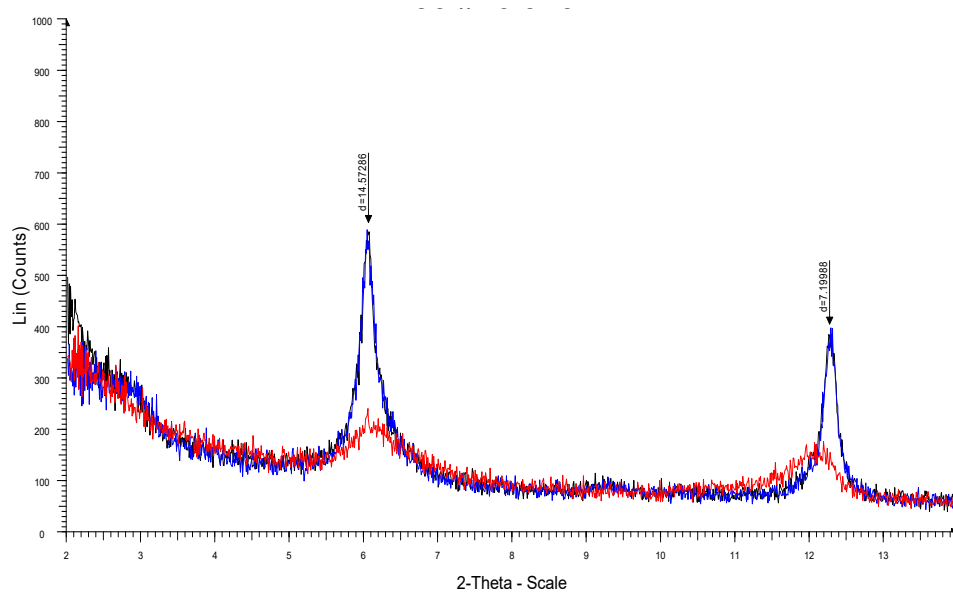


FIGURE 16: HE-30 at 926 m

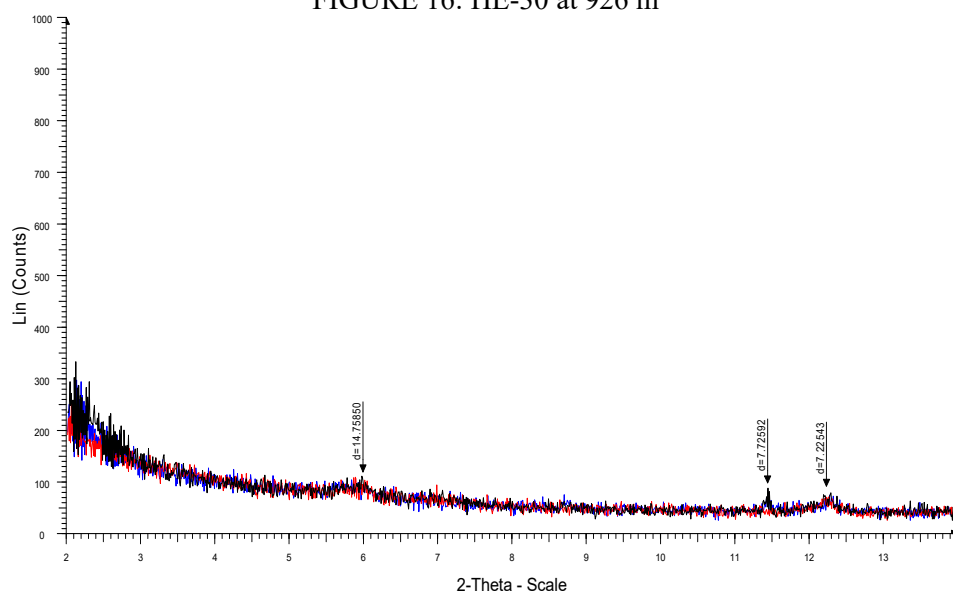


FIGURE 17: HE-30 at 992 m

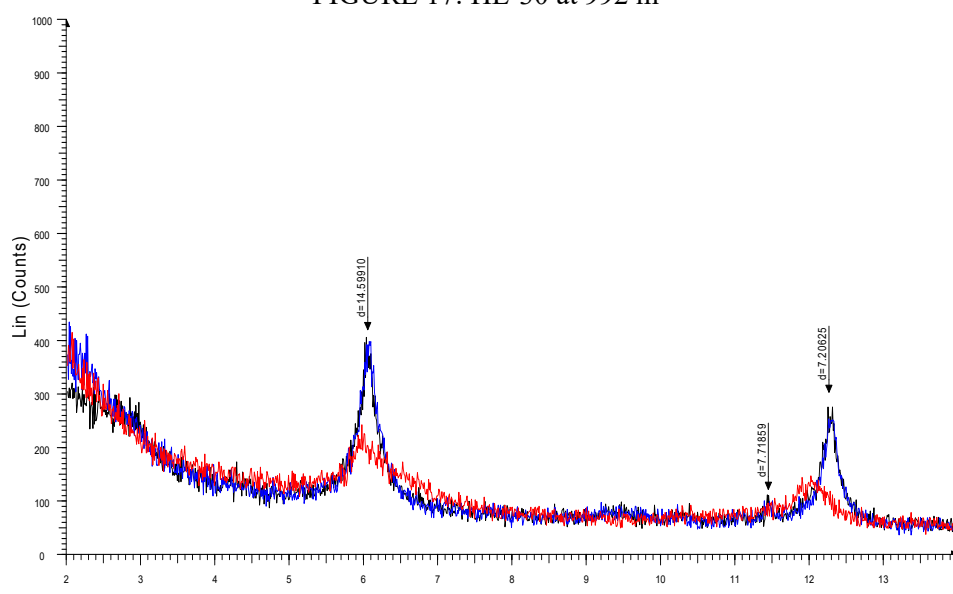


FIGURE 18: HE-30 at 1040 m

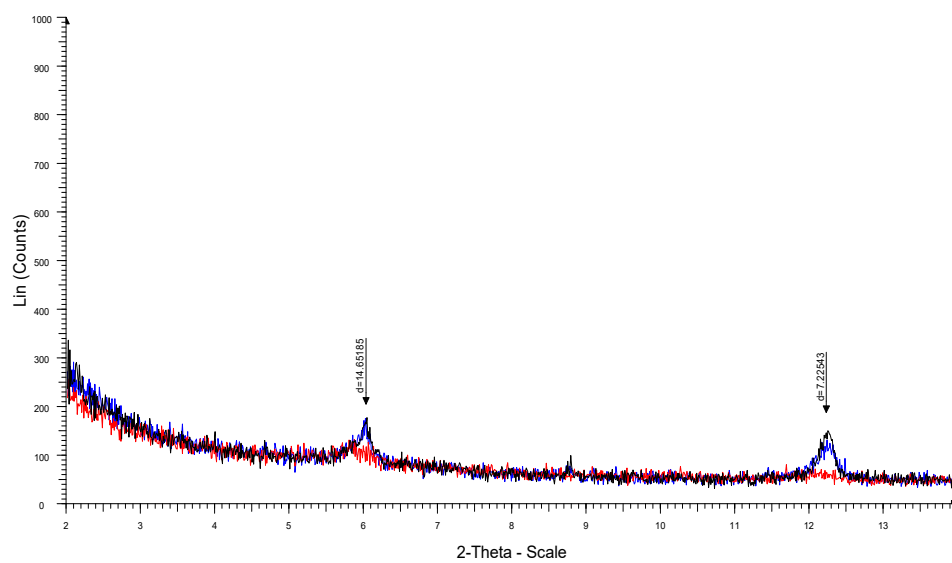


FIGURE 19: HE-30 at 1140 m

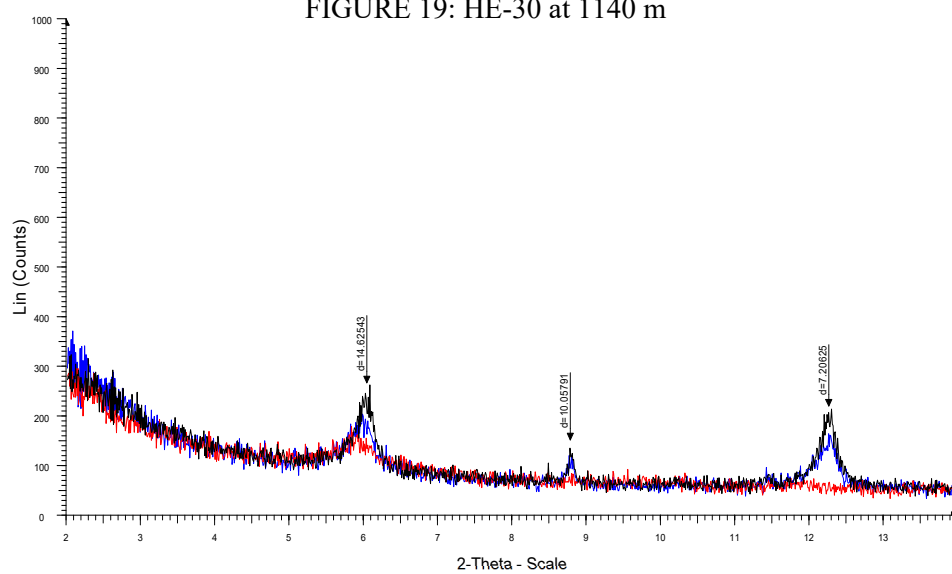


FIGURE 20: HE-30 at 1186 m

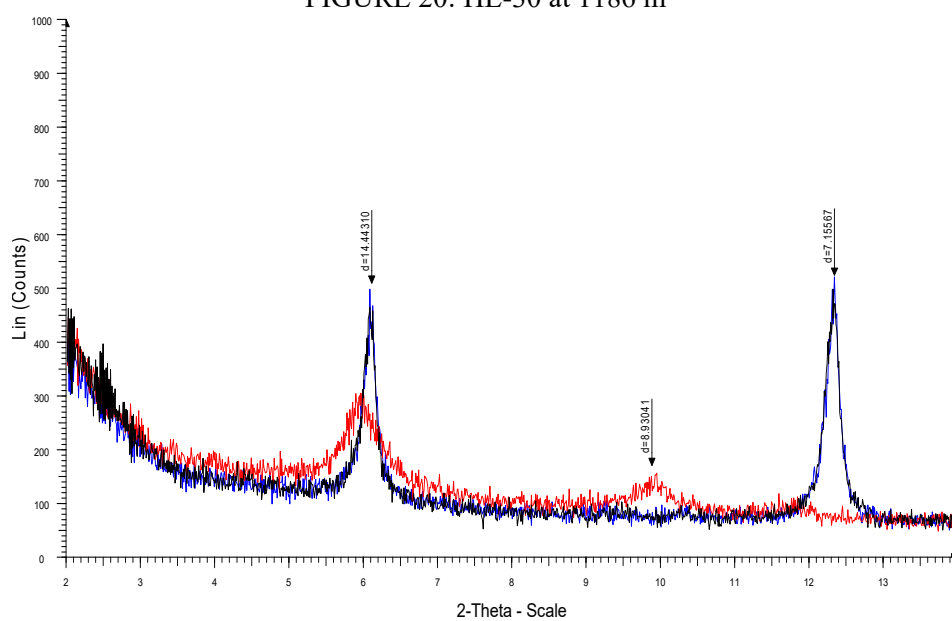


FIGURE 21: HE-30 at 1244 m

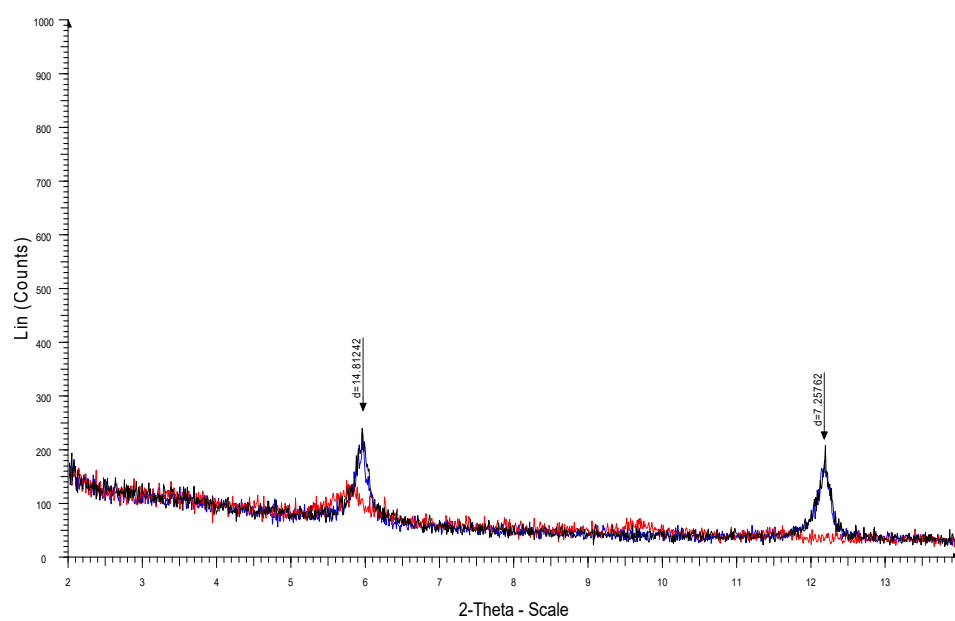


FIGURE 21: HE-30 at 1282 m



UNITED NATIONS
UNIVERSITY

UNU-GTP

Geothermal Training Programme

Orkustofnun, Grensasvegur 9,
IS-108 Reykjavik, Iceland

Reports 2016
Number 39

GEOHERMAL REINJECTION IN SEDIMENTARY BASINS

Ionut Emil Tanase

Ilfov County Council

18, Gheorghe Manu Street

010446 Bucharest

ROMANIA

tanaseionutcji@gmail.com, ionut.tanase@cjilfov.ro

ABSTRACT

Low-temperature sedimentary geothermal systems belong to one of the main types of geothermal resources worldwide. Experience from reinjection practices is important to understand the main characteristic parameters of a geothermal system, in order to avoid a failure of its utilization, e.g. through overexploitation. This report presents examples of good reinjection practices in sedimentary systems in different European countries, where reinjection is a part of the sustainable management of geothermal resources. Besides this, the report presents information on the geothermal potential in Romania, with main emphasis on reservoirs and geothermal specifics in the Balotesti area, north of the capital of Bucharest. The experience of countries such as France and Germany has shown that reinjection should be planned simultaneously with production for geothermal district heating systems. The lessons learned in these countries should be the basis of developing geothermal reinjection in countries with limited experience of reinjection, such as in Romania. The reinjection design should focus on maintaining the reservoir pressure, but it is also important to predict the long-term thermal breakthrough time for the production wells used. The report also presents recommendations aimed at supporting a considerable increase in the utilization of geothermal resources in Romania as well as their sustainable management.

1. INTRODUCTION

Geothermal energy refers to the thermal energy that is flowing and contained within the Earth. It is a renewable energy source, available worldwide. Exploitable geothermal resources can be found especially in regions where the geothermal gradient is normal or high. Volcanic regions have the highest geothermal potential, but geothermal energy may also be found in sedimentary regions as warm ground water, often sufficiently warm to be used for heating. Shallow thermal energy can be utilized through shallow boreholes and ground source heat pumps.

Geothermal systems can be classified based on the geological settings as (Saemundsson et al., 2011):

1. Volcanic geothermal systems associated in general with volcanic activity where the heat source is hot intrusions or magma. The reservoir temperature in those systems at 1 km depth is above 200°C.

2. Convective fracture systems located in tectonically active areas with above average geothermal gradient. The heat source is the hot crust where water has circulated down to at least 1000 m depth through fractures. In general, these are intermediate- or low-temperature systems with reservoir temperature below 150°C at 1000 m depth
3. Sedimentary geothermal systems are the most common geothermal systems, which can be found worldwide. In general, these are low-temperature systems.
4. Geo-pressured systems are fairly deep and are located where there is an impermeable layer of sedimentary cap rock that traps the geothermal reservoir. The temperatures in these systems range from 90 to 200°C at 1000 m.
5. Hot Dry Rock (HDR) or Enhanced Geothermal System (EGS) consist of volumes of rocks heated by volcanism or other high heat sources. This kind of geothermal resource often has low permeability or is virtually impermeable, hence it cannot be used in a conventional way. EGS systems usually have production-reinjection doublets.
6. Shallow geothermal is related to the normal heat flux near the surface or energy stored in the groundwater systems. Shallow geothermal is exploited using ground source heat pumps.

The proper and sustainable exploitation of geothermal resources involves production and reinjection of geothermal fluids. Geothermal reinjection involves injecting energy-depleted fluid back into the geothermal reservoir system. The quantity of geothermal water injected into a geothermal reservoir is not equal to the amount of produced water in most cases, and often just some portion is returned into the reservoir. Reinjection started out as solution for wastewater disposal and but in recent years it has become a necessary part of sustainable and environmentally friendly utilization of geothermal resources.

In most cases reinjection is considered a part of comprehensive geothermal resource management as well as sustainable utilization of geothermal resources. Reinjection provides an additional recharge to the geothermal systems and reservoir pressure support. In this way, more thermal energy can be extracted from geothermal systems. Reinjection will increase production capacity of geothermal reservoirs, which counteracts the costs for reinjection and exploitation projects. In enhanced geothermal systems (EGS) reinjection is a crucial part.

Some operational problems can appear in projects which involve reinjection, such as cooling of production wells and scaling in reinjection equipment and injection wells, because of the precipitation of chemicals in the water. Before starting a reinjection project some extensive studies and research regarding successful reinject operation need to be performed.

The status of reinjection at the end of last century was described by Stefansson (1997). Axelsson (2008 and 2012) and Rivera-Diaz et al. (2016) provide more recent reviews, including information on associated technology, research and reinjection testing. This paper reviews the key role of geothermal reinjection into the reservoir, geothermal resource management and management of long-term reinjection. The most important tool available for studying the relation between production and reinjection is tracer testing, discussed also in the paper mentioned above (Axelsson, 2012).

This report reviews some projects from sedimentary geothermal systems in different European countries, where geothermal reinjection is used in the projects. The purpose of this report seeks to exemplify these projects as good practice of geothermal reinjection in sedimentary basins in order to develop geothermal district heating systems. For this project twenty European countries were analysed: Austria, Belgium, Bulgaria, Croatia, Czech Republic, Denmark, France, Germany, Hungary, Ireland, Macedonia, Netherlands, Norway, Poland, Serbia, Slovakia, Slovenia, Sweden, Switzerland and Romania. Some of these countries perform geothermal reinjection on a small scale and in these cases the geothermal water is used mainly for recreational and health purposes. For the countries which perform geothermal reinjection the main geothermal reservoirs are presented, including successful projects which started in last decades in order to ensure the heat supply for municipalities. In this paper projects from ten European countries are reviewed: Austria, Croatia, Czech Republic, Denmark, France, Germany, Hungary, Poland, Slovenia and Hungary. The report also shows the Romanian geothermal

potential with main reservoirs and geothermal specific to the Balotesti area of Ilfov County. The main purpose of this paper is to show the importance of reinjection when utilizing geothermal resources for district heating system.

2. EVOLUTION OF REINJECTION

Sedimentary basins are, as mentioned above, the most common geothermal systems found in the world. Sedimentary basins are layered sequences of alternate permeable (limestone, sandstone) and impermeable strata (shale or mudstone). Geothermal water found in sedimentary rocks is commonly brine with variable temperatures. The temperatures depend on the depth of the permeable rocks in the geothermal system. Existence of these permeable sedimentary layers at depth of >1 km combined with average geothermal gradients ($>30^{\circ}\text{C}/\text{km}$), or above that, explains the existence of sedimentary geothermal resources. The systems are more conductive in nature than convective.

Several sedimentary basins exist in Europe, for example the Aquitaine basin, Molasse basin, Paris basin, Vienna basin, Pannonian basin and N-German basin, which are used for geothermal utilisation. The depth of geothermal systems may vary from 1 up to 5 km, the heat flow differs widely and the level of fluid salinity varies from relatively fresh ground water to high salinity brine (250,000 ppm).

Natural recharge of geothermal fluid in sedimentary system is not the same as for volcanic or convective systems, which leads to minimal recharge and therefore reinjection is needed in order to maintain the reservoir pressure level. Geothermal waste water disposal is often mandatory after using it for the main purpose of harnessing geothermal energy (heating, producing electricity, greenhouses etc.). For sedimentary geothermal systems, reinjection doublets are commonly used (production-injection well doublet). In this way the utilization of a geothermal system is ensured as sustainable during long-term operation and also environmentally friendly.

Figure 1 presents a schematic sketch of a sedimentary basin with a geothermal reservoir located at 2-4 km depth, including faults and fractures, which can play a role in the recharge of the geothermal basin reservoir. The figure also shows how the geothermal temperature profile in sedimentary basins is usually related to depth.

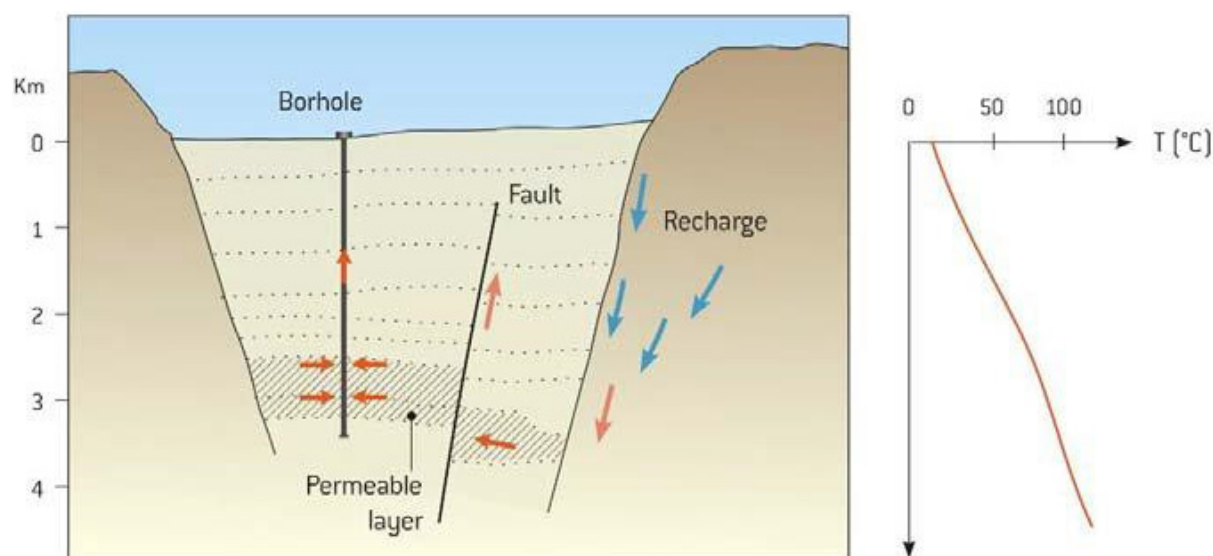


FIGURE 1: Sedimentary basin geothermal reservoir with recharge and geothermal gradient profile in the basin (Saemundsson et al., 2011)

Sedimentary rocks with pore pressure exceeding the normal hydrostatic pressure gradient contained in geothermal sedimentary basins are classified as geo-pressured geothermal systems. In such sedimentary reservoirs fluid is caught in stratigraphic traps similar to geo-pressured oil and gas reservoirs and the fluid pressure may be close to lithostatic values. Geo-pressured geothermal sedimentary systems are e.g. known in Hungary and the northern part of the Gulf of Mexico basin, but these fields are not exploited at the moment (Saemundsson et al., 2011).

Even if geothermal reinjection has focused on high-temperature geothermal fields, reinjection in low-temperature fields, especially in sedimentary basins, has become the norm in many countries, because of sustainability. Reinjection in geothermal sedimentary systems started in 1969, first in the Paris Basin in France, which includes a large geothermal resource associated with the Dogger limestone formation covering a surface greater than 15,000 km². Geothermal water is mainly used for district heating in the Dogger reservoir and the production is based on using production-injection doublets. The utilisation started as a result of the first oil crisis. The Paris doublets are separated by a distance of close to 1 km. This distance is maintained to prevent or minimise the cooling of the reservoir due to the reinjection and has so far caused no cooling in the production wells (Ungemach et al., 2005). Another example where reinjection has become an important part of harnessing geothermal fields is in Tianjin in China (Axelsson, 2008; Wang and Lin, 2010).

Reinjection provides supplemental recharge to the geothermal field and is used to counteract draw-down due to production. Pressure response of a geothermal system controls its production capacity, with reinjection being able to increase the production capacity of a geothermal reservoir. Most of the thermal energy of a geothermal system is stored in the reservoir rocks, while only a small percent (10-20%) is stored in the reservoir fluid (Axelsson, 2012). Injection wells or injection zones are located in different locations depending on their intended purpose. They are designed and drilled to intersect feed zones or aquifers. The main problems which may occur during reinjection are:

1. Cooling of production wells;
2. Silica scaling in surface pipelines and injection wells, especially in high-temperature systems;
3. Corrosion and types of scaling in both, low- and high-temperature geothermal fields;
4. Clogging of aquifers next to the reinjection wells in sandstone reservoirs.

In geothermal studies, research, development and resource management regarding reinjection and tracer testing is an important tool because it provides information on the connections between the production and reinjection wells and on the possible rate of cooling of the production wells during long-term reinjection of cold fluid back into reservoir. Reinjection is a part of modern geothermal system management for geothermal energy production, which can improve the efficiency and increase the long-term utilisation of the geothermal resources.

3. STATUS OF GEOTHERMAL REINJECTION IN DIFFERENT EUROPEAN COUNTRIES

Injection has been a part of many geothermal projects in Europe in geothermal fields of both volcanic and sedimentary type. Optimal development and management of geothermal resources led to development of the projects, which have harnessed geothermal water for district heating in some countries for more than 30 years. It is important to evaluate the past experience of reinjection practices, understanding the characteristic parameters of the reinjection systems for sustainable development. This applies especially in countries where large-scale reinjection hasn't started yet, such as Romania. The geothermal doublet system is the system commonly used for reinjection in sedimentary system in European countries. Here, it can be mentioned that reinjection is not compulsory in some countries but has become the key of long-term running of district heating systems in others. Certainly, there are some risks involved with reinjection practices but these can be mitigated by forerunner studies.

3.1 Austria

Austria (area 83,871 km², 8.5 million inhabitants in 2014) is subdivided into different geological units with different conditions for hydrogeological and geothermal water. In Austria utilisation of deep geothermal water is mainly from the Molasse basin of Upper Austria and to a minor extent in the Styrian basin. In 2014, Austria has drilled 75 geothermal wells, as summarised in Figure 2 and Table 1, with a total length of 129 km (Goldbrunner, 2015).

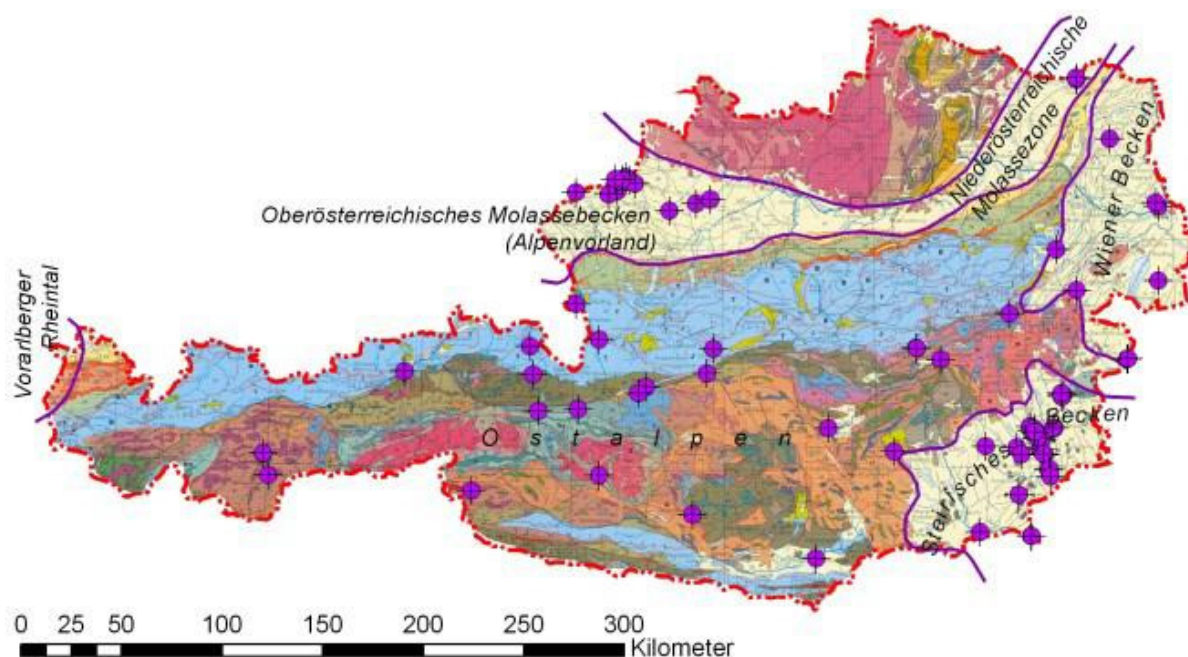


FIGURE 2: Location of the geothermal wells in Austria (Goldbrunner, 2015)

TABLE 1: Number and total length of geothermal wells in Austria (Goldbrunner, 2015)

Geological unit	Total wells drilled	New wells drilled 2010-2014	Total length of new wells [m]	Total length of all wells [m]
Styrian basin	28	2	6,578	48,100
Upper Austrian Molasse basin	3	2	4,810	28,236
Vienna basin and lower Austrian Molasse basin	8	1	4,223	12,605
N-Calcareous Alps and upper Austroalpine units (mainly carbonate rocks)	7			14,802
Lower, middle and upper Austroalpine units (mainly crystalline rocks)	18			24,618
Pannonian basin	1			860
Total:	75	5	15,611	129,221

The Geinberg project started in 1980 and is located in the upper Austrian Molasse basin. The first well in this project was drilled as a hydrocarbon exploration well into the Malm aquifer. Hot water discovered in this well, has been used for geothermal direct use. Decrease of pressure in the reservoir together with the growing demand for geothermal utilisation led to the drilling of a second well in the area, completing a doublet (production-reinjection). The new well "Geinberg Thermal 2" was planned as a deviated reinjection well located in the vicinity of the existing well, "Geinberg 1". The reinjection well was drilled at a distance of 1600 m from the production well, into a deep-groundwater carbonate aquifer to a total depth of 3155 m. The wellhead temperature is around 100°C.

The utilization in Geinberg is cascaded, including industrial processes in the dairy industry, district heating in the village of Geinberg and the thermal resort and spa of Geinberg. The use of water in the spa and greenhouse heating require a maximum temperature of 70°C. In this case, reinjection of geothermal water reaches a temperature of minimum 30°C, thus allowing the reinjection to be done without pumping, only by gravity (Goldbrunner et al., 1999).

In the Upper Austria project in Altheim a decision to drill a well for geothermal production was taken in 1989. The production well was drilled to a depth of 2300 m and the temperature obtained was 106°C. In 1994 it was decided to drill a reinjection well in order to maintain the water level in the Malm reservoir. The project for the reinjection well was financed by the European Commission (35%), the local government of Upper Austria and the federal government of Austria. In 1998 one more well was drilled, 40 m from the first one and after 8 months of drilling the final depth of 3100 m was reached. The tests performed after drilling revealed that the well could produce hot water with a flow of 100 L/s at 93°C.

The Altheim project was the first geothermal power plant in Europe which harnesses low-enthalpy geothermal water for producing electricity with a Rankine turbogenerator. Information about the ORC turbogenerator used in the Altheim project is presented in Table 2. After using the geothermal water for producing electricity the waste water is reinjected into the Malm reservoir at 70°C (Pernecker and Uhlig, 2002).

TABLE 2: The Altheim ORC turbogenerator performance data sheet (Pernecker and Uhlig, 2002)

Geothermal water inlet temperature	106°C
Geothermal water outlet temperature	70°C
Geothermal water flow rate	81.7 kg/s
Cooling water flow rate (about)	340 kg/s
Cooling water inlet temperature	10°C
Cooling water outlet temperature	18°C
Electric generator	Synchronous, low voltage
Net electric power output	1000 kW

Another geothermal district heating project is found in the district town Ried im Innkreis (11,400 inhabitants in 2013). The first well (Mehrnbach Th 1) of the geothermal doublet was intended to reach the Malm aquifer at 2,500 m. After encountering Malmian limestones at a depth of only 1,765 m it had to be recognized that the bore had landed on the up-thrown block of the Ried fault. Mehrnbach 1a cut across some 600 m of upper Cretaceous mainly sedimentary rocks and tapped the Malm aquifer at 2,354 m and penetrated the whole thickness (245 m) of Malm carbonate rocks (limestones and dolomites) and some 20 m of Basal sandstone and finally tapped the top of the crystalline basement at 2,598 m. The horizontal displacement at end depth was some 300 m. The second well (Mehrnbach Th 2) was located at the up-thrown block of the Ried fault some 1,300 m apart from well Mehrnbach Th1/1a.

From October to December 2012 a combined pumping and reinjection test was performed using Mehrnbach 1/1a as a production well and Mehrnbach 2 for injection. The production temperature was 105°C at a flow rate of 64 L/s. Upon detection of pressure reductions in Bavarian balneological wells some 16 km from Mehrnbach the function of the boreholes was reversed now using Mehrnbach Th 2 as production well and Mehrnbach Th 1/1a for reinjection. The trial operation of the geothermal doublet started in February 2014 (Goldbrunner, 2015).

3.2 Croatia

Croatia has both intermediate- and low-temperature geothermal fields, as shown in Figure 3. They are located in the north-eastern part of the Pannonian basin and in the south-western Dinaric Alps

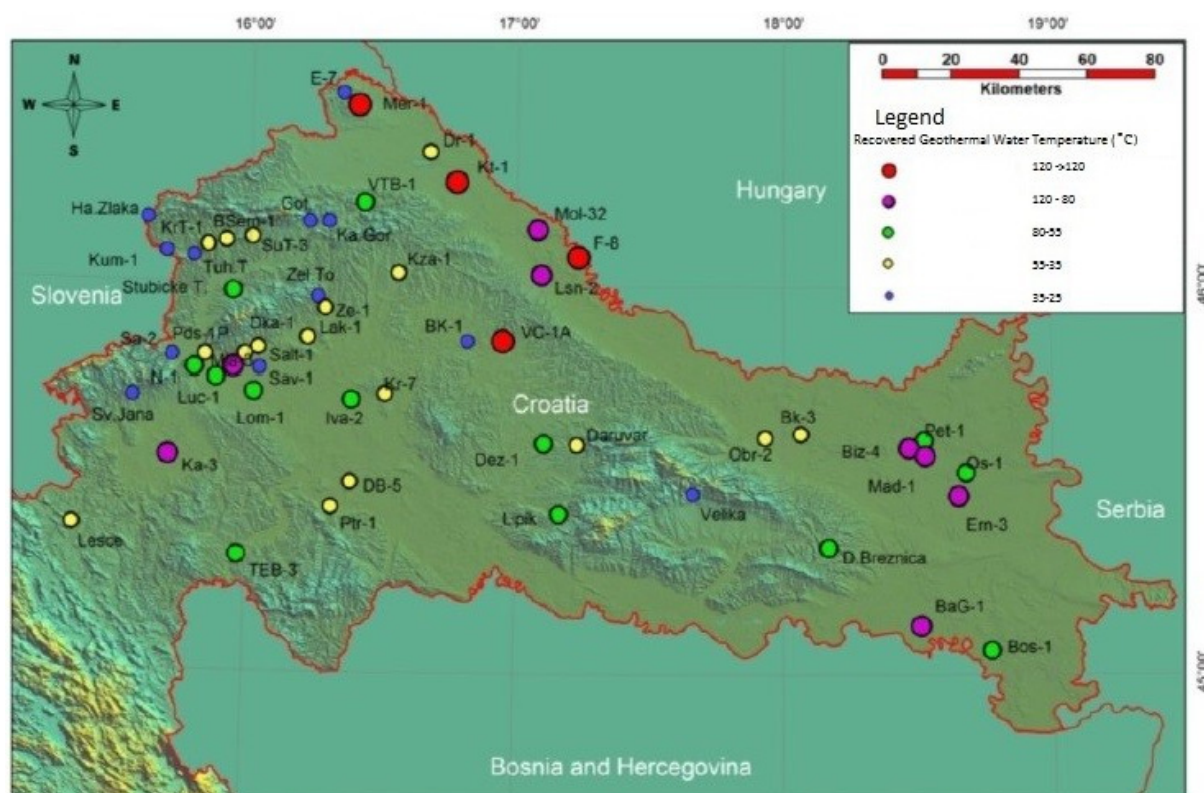


FIGURE 3: Geothermal water resources in the Republic of Croatia (Kolbah et al., 2015)

(Dinarides). In the Dinaric part (low-temperature fields) an ongoing collision of the Adriatic carbonate platform with the Eurasian plate accounts for crustal thickening. In the carbonate rocks encountered in the Dinaric part, fracture porosity caused by tectonic events has been enhanced by carbonate dissolution and this kind of fracturing increases rainwater infiltration into the ground causing reservoir cooling. Because of this, geothermal projects are mainly in the northeastern part of the country. The most common geothermal utilisation in Croatia is recreation and balneotherapy (Serpen and Aksoy, 2016).

Even though the geothermal potential to produce electricity is relatively high (Lunjkovec – Kutnjak and Velika Ciglena), Croatia has not built an electric power plant, until the first geothermal plant was planned in the Velika Ciglena geothermal field after 2015. Croatia has 27 locations with developed geothermal direct use and the development is growing through new exploration licenses: Bošnjaci Sjever (Bos-1) and Sveta Nedelja (N-1) (Kolbah et al., 2015).

In the last 80 years more than 3500 wells have been drilled for oil and gas in Croatia and in the Velika Ciglena geothermal field four oil wells were drilled in the 1990s, now abandoned. The first exploration well, VC-1, was drilled to a depth of 4790 m with a temperature of 170°C. The second well, VC-1A, was drilled at the same location. Analysis of geophysical logs indicated a porosity of 30% in the upper zones, with temperature and well logging indicating five permeable zones in well VC-1A. Constant temperature was observed from the top of the reservoir down to 3600 m indicated that the permeable zones in both wells were connected, through the same reservoir. In 1995 it was decided to harness geothermal water for a geothermal power plant with a capacity of 4.7 MWe using well VC-1A for production and VC-1 for reinjection. In 2013 a new project was scheduled and developed, using two other abandoned oil wells for reinjection, namely Ptk-1 and VC-2 located at a distance of 2 km from the production wells. As a result, Velika Ciglena became the first geothermal power plant project in Croatia with 16.5 MWe gross and 14 MWe net capacity, where wells drilled for oil exploration are used for producing electricity (Serpen and Aksoy, 2016).

Another example of a geothermal system which harnesses water (80°C) from a low-temperature field for heating in a sports centre including sport halls and swimming pools, is in Zagreb (locality Mladost), the Croatian capital. There, a geothermal doublet has been in operation since 1987 without problems during reinjection. Utilisation of geothermal waters and/or energy in new locations such as Terme Zagreb (using the wells located in Mladost), Draškovec (Međimurje County in the north of Croatia) and Šmithen (near Slovenian border) will use geothermal waters in cascaded systems for facility heating, hot water preparation, spa and recreation, greenhouse heating and/or fish farming.

At Harina Zlaka in NW-Croatia, near the Slovenian border (Sutla River), hot springs in Croatia which yielded 3.7 L/s of 33°C hot water dried up as a result of production from two wells drilled in 1970 in Slovenia to supply a spa, tapping the same aquifer that fed the spring. In 1997, on the Croatian side of the Sutla River, two exploration wells were drilled. These wells produced cold water and the studies conducted showed that wells located on the Slovenian side had reduced the pressure in the geothermal aquifer causing a mixing of cold and hot water. This case showed the need of a bilateral management of geothermal water between Croatia and Slovenia, such as is in place between Hungary and Slovenia, which established a bilateral Slovenian-Hungarian Water Management Commission in order to maintain water quantities, chemical composition and temperatures in transboundary geothermal aquifers (Borović and Marković, 2015).

3.3 Czech Republic

Geological structures of the Czech Republic include two different geothermal domains: the Bohemian Massif, formed by granite bedrock of the Bohemian Massif and covered by sedimentary formations, and the Moravian part of the Carpathian structure with variable thicknesses (few hundred metres to >6000 m) of sedimentary layers. The geothermal potential of the Czech Republic is variable depending on the geothermal and geological fields; highest heat flux being measured in the Bohemian Massif in the northern part of West Bohemia. Just one project, located at Litomerice, has been under development for power generation, the other geothermal resources are used for spas, wellness centres, swimming pools and heating (Jirakova et al., 2015).

The Pasohlavky geothermal area was discovered 20 years ago during mining for oil and gas. The area is located in the south-eastern part of the Czech Republic, in the Vienna Basin. Two wells, Musov-3G and Pasohlavky-2G, located at distance of 2600 m from each other, supply hot water for a spa in Pasohlavsky village. The well logs performed in well Musov-3G confirmed a heat flux of 48.4 mW/m² and a temperature of 49.7°C (48°C at wellhead) at a depth of 1,455 m. The outflow reached 7-17.2 L/s with a water-level draw-down of 47.8 m. Well Pasohlavky 2G was drilled for reinjection in the area and during hydrodynamic testing 40 L/s were pumped without significant draw-down in water level, with an outflow temperature of 40°C (Jirakova et al., 2015).

3.4 Denmark

Geothermal potential in Denmark is mainly related to two deep sedimentary basins, the Norwegian-Danish subsurface basin and the northern rim of the North German Basin, which constitutes the southernmost part of the country. The Norwegian-Danish basin contains formations with sandstones which can be used as geothermal reservoirs. These are primarily the Lower Triassic Bunter sandstone formation, the Triassic Skagerak formation, the Upper Triassic – Lower Jurassic Gassum formation, the Middle Jurassic Haldager sand formation and the Upper Jurassic – Lower Cretaceous Frederikshavn formation (Figure 4). The Bunter Sandstone formation located in the North German Basin represents the main geothermal reservoir, while the Gassum Formation is only sporadically preserved at shallow depths (Røgen et al., 2015).

Denmark has moderate geothermal temperature gradients and utilization of geothermal resources will be mainly for district heating, possibly supplying more than 60% of Danish houses. Danish aquifers have not been found suitable for power production but a study conducted in 2010 has assessed the reserves in a licence for the Greater Copenhagen area to be 60,000 PJ, or 1/3 of the heat demand for about 5000 years. Today Denmark has three geothermal plants with deep wells (Mahler et al., 2013).

The first of them started production in Thisted, in 1984, and later expanded to produce up to 7 MWth from a flow of 55 L/s at 44°C from the Gassum sandstone reservoir. In 2005 production started in the second geothermal plant, located in Copenhagen, for production of 14 MWth from 65 L/s 73°C, 19% saline, geothermal water from the Bunter sandstone reservoir at 2.6 km depth (Mahler et al., 2013). The latest geothermal plant, located in Sønderborg, started production of up to 12 MWth in 2013 from 48°C geothermal water produced from the Gassum reservoir at 1.2 km depth.

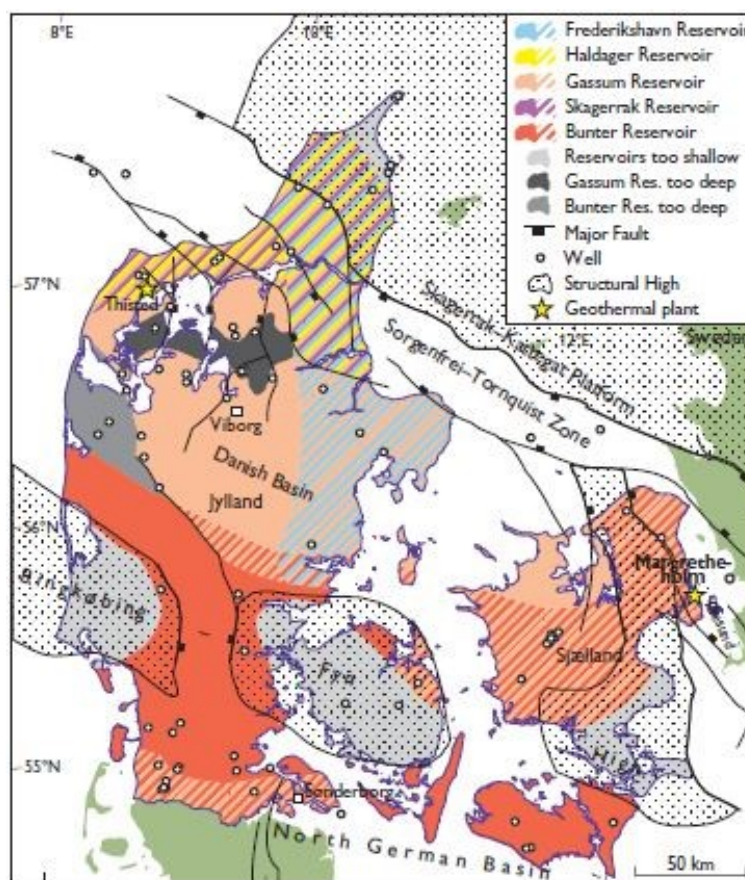


FIGURE 4: Geothermal reservoirs in Denmark
(Røgen et al., 2015)

The geothermal reservoir exploited at Thisted is a Lower Jurassic Gassum formation sandstone at 1,250 m depth producing saline water at 43°C. The geothermal plant functions with two wells, as a doublet, one for production and one for injection, located 1.5 km apart. It produces heat from the sandstone reservoirs through heat exchangers and/or LiBr based absorption heat pumps, where the driving heat primarily comes from biomass boilers for heat and/or combined heat and power production (Røgen et al., 2015).

The geothermal plant located in Copenhagen was inaugurated in 2005, using 19% saline water at 74°C from a geothermal reservoir in the Lower Triassic Bunter Sandstone formation at 2.6 km depth. The production is from a deviated well and the injection is into a vertical well next to it at ground level, and 1.3 km apart at reservoir level. The injectivity of the injection well has increased over the years, reflected by increasing injection pressure, after an initial clean-up of the injection well. This is believed to be linked with low injection pressure and high injection temperature during summer plant shutdown periods (Røgen et al., 2015).

The injectivity has been increased by acidizing several times but the well completion with perforations carries a risk of perforation collapses. Acidizing of the well has not maintained a low injection pressure and an effort is put into studying and avoiding the issues, which are believed to have caused the high injection pressure (Røgen et al., 2015).

3.5 Poland

Poland is characterized by low-temperature geothermal systems encountered in sedimentary basins. The main geothermal regions in Poland are located in sedimentary formations and contain geothermal aquifers in the following areas: The Polish Lowland Province (Triassic – Cretaceous); the Fore-Carpathians (Mesozoic - Tertiary) and the Carpathians (Mesozoic – Tertiary). Poland is built of three geostructural units: Precambrian platform of Northwestern Europe, Palaeozoic structures of Central - Western Europe covered by the Permian - Mesozoic and Cainozoic sediments as well as the Carpathians (part of the Alpine system).

The heat flow values which can be found in sedimentary basin from Poland vary from 20 to 90 mW/m² and geothermal gradients vary from 1 to 4°C/100 m. The temperature encountered at the depths of 1 to 4 km may vary from 30 to 130°C, while the geothermal water flow can reach up to 150 L/s.

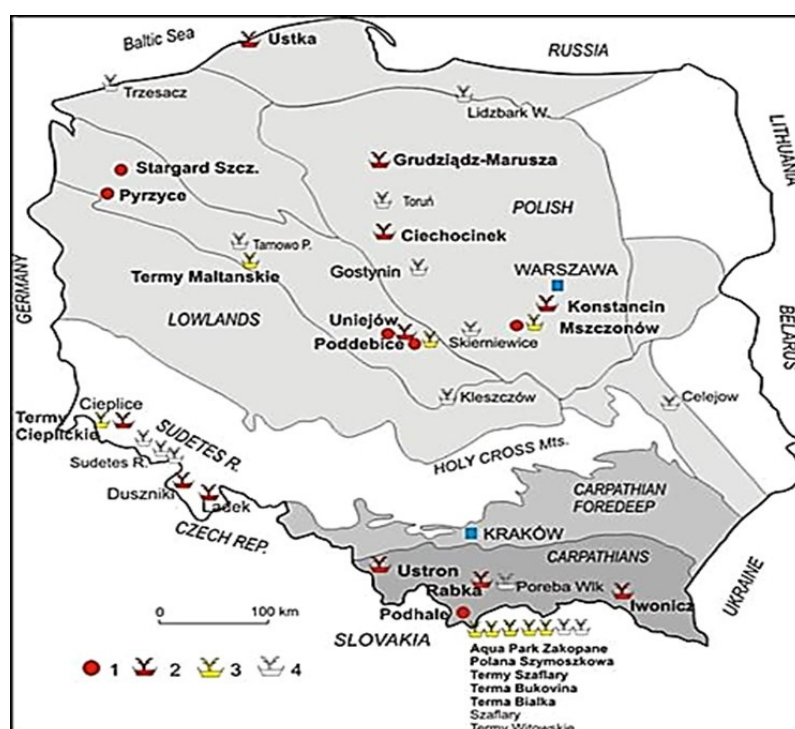


FIGURE 5: Main geothermal utilisation in Poland, 2014;
1) geothermal district heating plants, 2) health resorts;
3) recreation centres; and 4) geothermal recreation/
balneotherapy centres under construction (Kepinska, 2015)

opened after closure in 2008), and in Poddebice (since 2013). In 2014, nine geothermal recreation centres and 11 geothermal health centers (balneotherapy) used geothermal water due to their therapeutic properties. Geothermal exploitation for district heating in Poland is mainly based on reinjecting return water back into the geothermal aquifers (Kepinska, 2015).

3.6 Slovenia

Slovenia is located in the convergent area of the African and Eurasian tectonic plates. The Slovenian area is subdivided into several tectonic units: the Mura-Zala basin (the southwestern part of the Pannonian basin) in the northeast part, while the Eastern Alps (incl. magmatic rock complexes), the Southern Alps, the External and Internal Dinarides and Adriatic foreland represent parts of the Adriatic microplate. The 24 thermal (natural and captured through shallow wells) springs have temperatures

Geothermal utilisation in Poland is mainly related to space heating, bathing and balneology (Figure 5). In recent years geothermal utilisation has increased in the country with five new wells (two for production and three for exploration) drilled in the 2005-2009 period (Kepinska, 2010). The deep geothermal development was continued between 2010 and 2014, when thirteen new geothermal wells were drilled. Ten were drilled for exploration, of which one was unproductive, one for production, and two for injection and in addition one old well was deepened.

In 2014, six district heating geothermal plants were found, in the Podhale region (since 1994), in Pyrzyce (since 1996), in Mszczonow (since 1999), in Uniejow (since 2001), in Stargard Szczecinski (since 2012, re-

close to, or above, 20°C, with 36°C as a maximum. Geothermal resources of Slovenia are at present used only for direct use for space and district heating and for thermal spas, from 53 production wells and 3 thermal springs, implemented at 32 localities, shown in Figure 6, despite the hydrogeological characteristics of the northeastern part of the country indicating potential geothermal resources exploitable for electricity production.

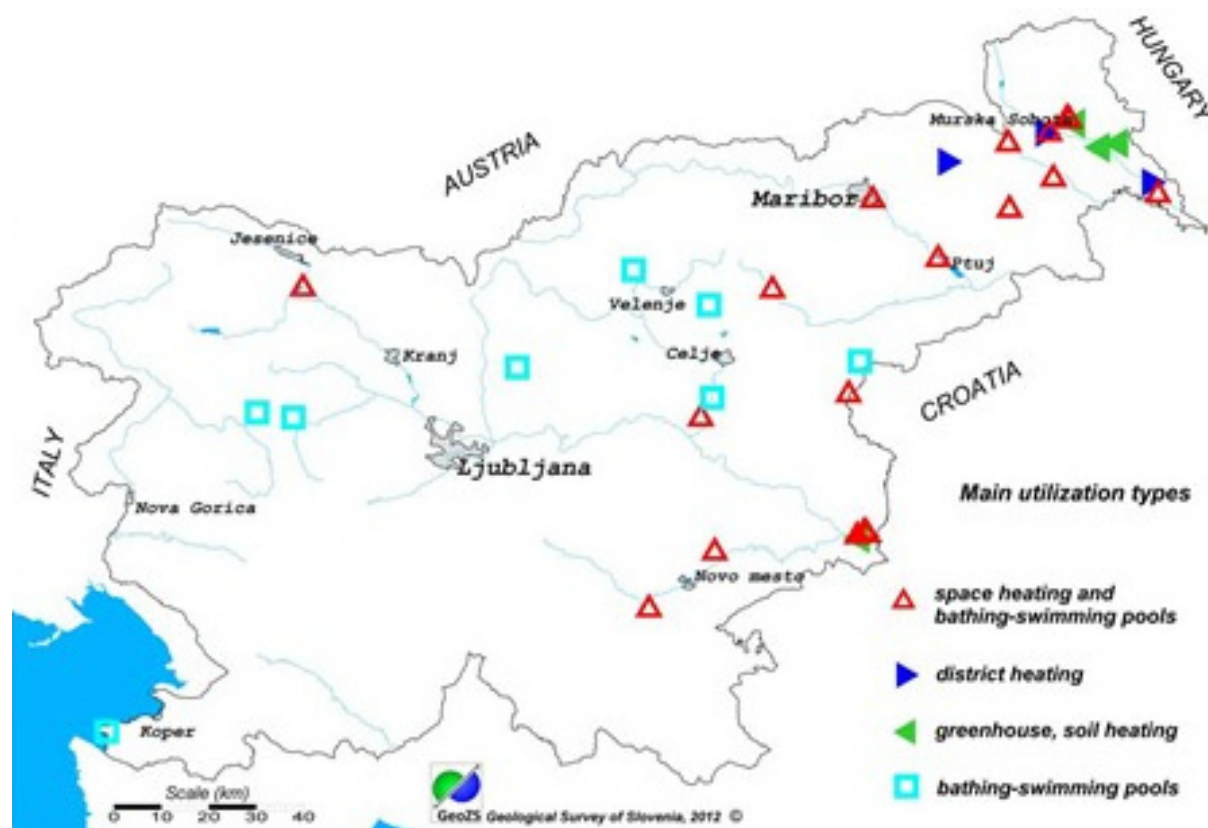


FIGURE 6: Geothermal utilization in Slovenia (2013) (Rajver et al., 2015)

The geothermal studies performed in recent years reveal geothermal and hydrogeological conditions in the Mura-Zala sedimentary basin that can support the exploitation of thermal water from a Neogene aquifer at temperature of 80°C, at 2 km depth, east of Maribor and Ptuj towns. Upper Pannonian-Pontian geothermal sandy aquifers, utilized by Hungary and Slovenia, and composed of 50-300 m thick sand-prone units, are found in a depth interval of about 700-1400 m in the interior parts of the Pannonian basin, with temperatures from 50 to 70°C (Rajver et al., 2015).

There has been a discussion on reinjection in Slovenia because many localities in the northeast part of the country are vulnerable to over-exploitation due to utilization by different companies from the same aquifer. A doublet scheme is operational in downtown Lendava while the Murska Sobota community drilled two new wells, production well (SOB-3g/12, 1.5 km deep) and a reinjection well (SOB-4g/13, 1.2 km depth), for enlarging the district heating system in the northern part of the town. A test performed in 2013 revealed that the SOB-4g well can reach maximum flow rate of 43 L/s and wellhead temperature of 57°C. It is planned to use well SOB-4g as an injection well with a temperature drop of 30°C.

Projects T-JAM and TRANSENERGY, supported by the European Union, and conducted between 2009-2013, treated geothermal aquifers in the Mura-Zala basin as a transboundary resource between Hungary, Austria and Slovenia. As a result of these projects the geothermal maps of the region were updated and a sound hydrogeological conceptual model of the groundwater flow was developed. The negative trends of geothermal resources in different locations, and also negative trends at a regional level in north-eastern and eastern parts of Slovenia, must be managed for sustainable transboundary

resource utilization, and doublet technology in the Pannonian basin is expected to provide best practices for sustainable utilization of the geothermal resources (Rajver et al., 2015).

3.7 Sweden

Sweden is characterized by the massive Baltic rock shield and its diverse crystalline eruptive and metamorphic rocks, whereas the southern part is characterized by sedimentary rock formations of significant thickness. The porous sandstone rocks found in the southern parts have very good hydraulic properties and also a geothermal gradient of 28-30°C/km, while the geothermal gradient is around 15-16°C/km in the Baltic shield regions.

Even though research for a deep geothermal project has been going on at Lund University since 1977, the lack of favourable geological conditions does not make Sweden suitable for deep geothermal exploitation (Gehlin et al., 2015).

The first geothermal plant in Sweden, which uses deep geothermal resources, started in 1984. It uses four production and five injection wells (Figure 7) for district heating the municipality of Lund, covering around 20% of the heat demand. The geothermal water is harnessed from sandstone reservoir located at a depth of 650-800 m, with a temperature of 21°C from production wells and injected back into reservoir at 5-7°C (Alm, 2011).

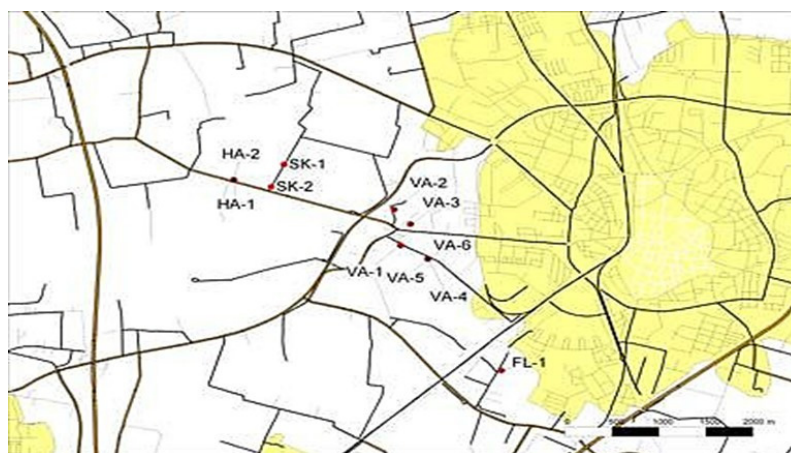


FIGURE 7: Production and injection wells in Lund in Sweden (Alm, 2011)

3.8 Germany

Geothermal utilisation of deep resources in Germany is related to the existence of natural geothermal systems (Figure 8) of three type of reservoirs (hot water aquifers, faults, and crystalline rocks) with temperatures above 100°C and at depths down to 7,000 m. Geothermal reservoirs are located in the North German Basin, the Upper Rhine Graben, and the South German Molasse Basin. Geothermal water from the North German Basin is characterized by high salinity and temperatures between 40 and 120°C, while the geothermal resources in the South German Molasse Basin are characterized by high temperature and low salinity. It is difficult to develop geothermal projects in large scale because of the characteristics represented by faults and heterogeneous geology of Upper Rhine Graben (Seibt et al., 2005, Weber et al., 2015).

The first production and injection tests in Germany were performed in 1982 in a sandstone reservoir in order to ensure the district heating for a residential area in the town of Waren (Muritz).

Sandstones reservoirs that can be found in the North German Basin at depths of around 3000 m have the following properties: effective porosity >20%, permeability > $0.5 \times 10^{-12} \text{ m}^2$ and effective thickness > 20 m, indicating good conditions for injection purposes. As was mentioned above the Mesozoic deep waters contained in the North German Basin are classified as high salinity Na-(Ca-Mg)-Cl water (salinity greater than 300 g/L) with a high pH caused by dissolved gases. Injection of the cooled waters back into the reservoir can affect the permeability of the rocks, mainly because of excessively high

injection and production flow rates, chemical incompatibility between injected fluid and reservoir aquifer, oxidation materials and bacterial activity. Due to these properties, special submersible pumps made of corrosion-resistant material have to be used (e.g., red bronze for the running wheels). The pipes used are made of coated or inert material for the same reason and to prevent eventual leakage into other aquifers, in particular groundwater-bearing beds with usable freshwater resources.

The first project which injected geothermal water after utilisation started in 1985 in order to supply heating in the town of Waren. Geothermal water is harnessed from an aquifer composed of Hettangian sandstones at a depth of 1470 m, providing flow rates of around 17 L/s at a temperature of 62°C. After utilisation the cooled water is successfully injected at temperatures of 20-40°C. The salt content of this NaCl brine is 158 g/L, and iron content is 12 mg/L.

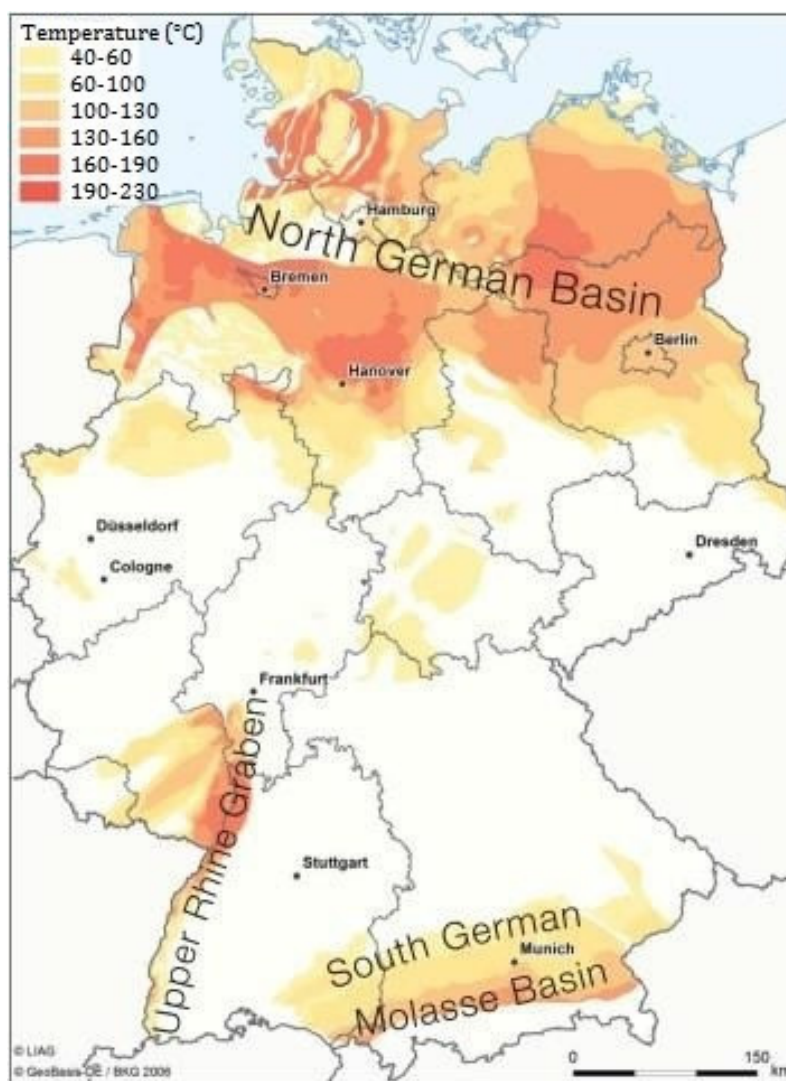


FIGURE 8: Geothermal resources in Germany
(map adapted from Suchi et al., 2014, Weber et al., 2015)

The site of Neustadt-Glewe geothermal field was explored in 1989 and the power plant started operations in 1995. The properties of geothermal resources from this site are characterized by a temperature of 100°C, a high salinity content (salt content of 220 g/L) iron content of 80 mg/L and high gas concentration in the fluid. In 1998, the oxygen entered through a defective regulating valve over a short period of time causing iron precipitation, which made it necessary to increase the injection pressure. After acidizing operations the injectivity of the well was restored and geothermal water injected back into a sandstone layer at a depth of 2200 m with a maximum flow rates of 35 L/s.

Neubrandenburg geothermal plant was commissioned in 1989. Geothermal water is harnessed from two fine sandstone horizons located at depths of 1,150 and 1,250 m, with flow rates up to 28 L/s with a salt content of 113 and 133 g/L, respectively, and after utilisation the water is injected back into the aquifers. The injectivity deteriorated continuously until the plant was rehabilitated in the 1990s. This included the installation of a nitrogen pressurizing system. The geothermal plant was reactivated and retrofitted for combined use as geothermal plant and waste heat aquifer of a gas and steam cogeneration plant for producing brine for therapeutic purposes. A new thermal water loop was installed and it is planned to heat the thermal water up to 80°C by waste heat during summer operation and to inject it. This heat will be recovered during winter, therefore increasing the efficiency of the plant significantly (Seibt and Kellner, 2003).

3.9 France

Geothermal development in the Paris basin started in the early 1970s. Since then 55 doublet systems have been implemented, 34 are still in operation using the Dogger aquifer of the Paris Basin. The Paris Basin is a sedimentary basin which occupies a large part of Northern France (110,000 km²) and extends northward below the English Channel. It is connected with the Aquitaine basin to the southwest with the “Poitou High” and the Southeast basin with the “Burgundy High”. The existence of Paris Basin is related to a period of rifting in Permo-Triassic times. The central part of the Basin, where the subsidence was the greatest, is filled with about 3000 m of sediments. The Dogger strata were deposited in a marine environment and is recharged along the eastern border of the Paris Basin where the formation outcrops.

Fluid density, variations caused by different salinities or temperature gradients may induce local perturbations, but on a basin wide scale the flow is directed towards the discharge area on the seafloor of the English Channel, in the north-western part of the basin. In the recharge part, the fluid reaches depths of 2000 m where it acquires its geothermal potential. Between 1970 and 1985, 110 geothermal wells were drilled in the Paris Basin (Figure 9), targeting the Dogger aquifer, but 42 wells were abandoned for technical (corrosion and scaling) or economical (low profitability of geothermal plants compared with low price for fossil fuels) reasons. As was mentioned above, 55 doublets were in operation in the 1980s, but just 34 of these are still exploiting the Dogger aquifer. Twenty-nine geothermal plants are used for district heating, by exploiting the Dogger Aquifer (1,600-1,900 m depths) with fluid temperatures above 65°C. Each plant uses one or more doublets and a few of them have been using triplets (three wells, one new well drilled for production and the existing wells used for injection). Abandoned wells are located in the northwest part of the basin, where the geothermal water reaches 60–65°C or less (Lopez et al., 2010, Vernier et al., 2015).

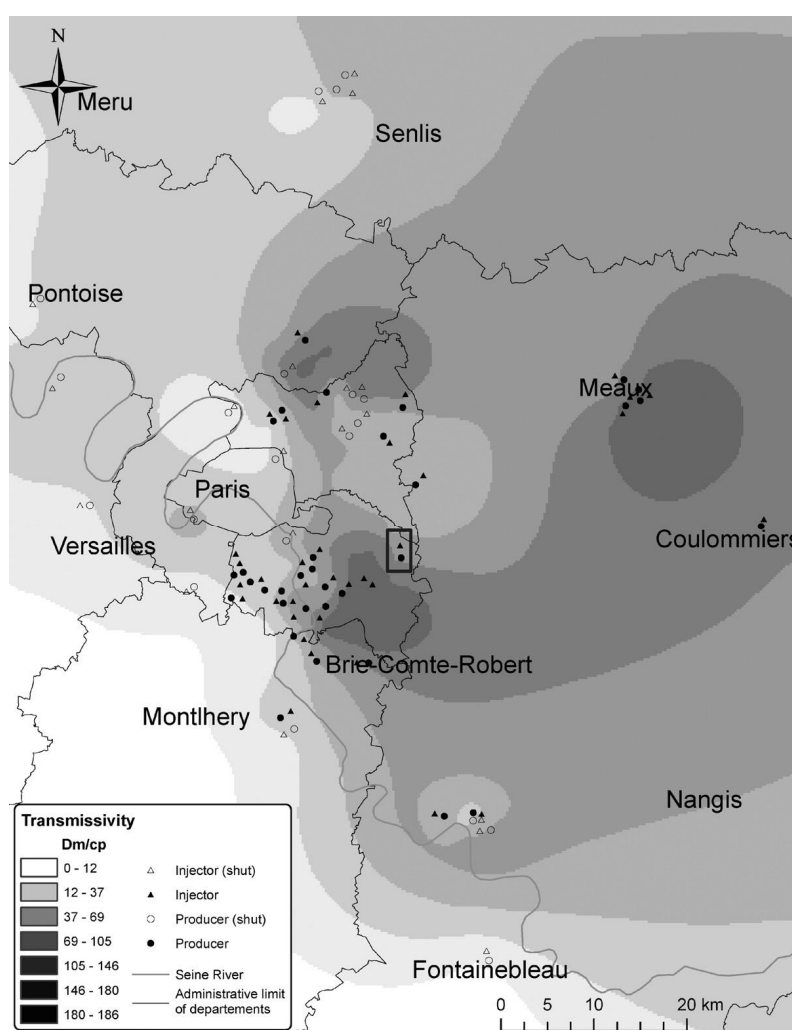


FIGURE 9: Temperature map and geothermal well locations in the Paris Basin; the grey rectangle highlights the Champigny doublet (Rojas et al., 1989)

Some new geothermal plants for heating have been commissioned since 2007 in the Paris basin. Orly Parisian airport now uses the heat produced by a new doublet developed by ADP in order to ensure heat demand for the airport. Strategies for rehabilitation of old wells involve the following: some doublets are transformed into a triplet, as in Champigny-sur-Marne, a new production well has been drilled and

both the existing wells are used for injection, some doublets are closed, while a new doublet was drilled in the vicinity (e.g. in Coulommiers) in a case where wells were damaged.

In order to prevent conflicts of use from the Dogger aquifer, the data on running operations is collected by BRGM and thermo-hydraulic modelling of the aquifer is conducted to show where new wells can be drilled. In addition, some operations are carried out in the intermediate aquifers of the Paris basin, one doublet which uses geothermal water from the Albien aquifer (650 m depth), for district heating in Issy-les-Moulineaux. This doublet provides a temperature of 28°C and a flowrate of 55 L/s, giving a thermal capacity of 5.4 MWth for heating and 1.3 MWth for hot sanitary water. Another doublet has been realized in the Neocomian aquifer (900 m depth, 34°C temperature), which provides heat for 3,500 social households in Plessis-Robinson, close to Paris (Vernier et al., 2015).

3.10 Hungary

The main utilisation of geothermal energy in Hungary is based on utilizing resources in the Pannonian basin (Carpathian Basin). The main reservoirs with geothermal resources are in Mesozoic carbonate-karstic basement rocks and the Pliocene – Upper Pannonian porous sedimentary layers, with medium temperature of water between 30 to 100°C. Pannonian sediments are multi-layered, composed of sandy, shale and silty beds with different permeability. The lower Pannonian sediments are mostly impermeable; the upper Pannonian and Quaternary formations contain porous layers of permeable sand and sandstone. The upper Pannonian aquifer has an area of 40,000 km², an average thickness of 200-300 m, a bulk porosity of 20-30% and a permeability of 500-1,500 mD. In 2014, 672 wells (179 wells abandoned and 220 temporarily closed) in Hungary could produce geothermal water with a temperature of more than 30°C (Toth, 2015).

A high-enthalpy reservoir with over-pressured steam and a temperature of 189°C has been drilled into in the south-eastern part of the country. This reservoir was discovered in 1985 in the Fabiansebestyen exploratory well when over-pressured steam at 360 bar was discharged at around 100 L/s, from a 3,800 m deep reservoir in a fractured dolomite formation. The well was killed after 47 days and at present, feasibility studies are being carried out in order to determine the geothermal potential for this area.

The Miskolc-Mályi project (installed capacity of 21 MWth) is a recent project which uses geothermal water for district heating. The geothermal plant uses two wells for production drilled to a depth of 2,305 m and 1,514 m, yielding 110-150 L/s of fluid with a temperature between 90 and 105°C from a karstified-fractured Triassic limestone reservoir. At Miskolc-Mályi three geothermal wells were drilled, also for injection purposes (Toth, 2015).

For balneology and sport purposes, Hungary uses around 295 thermal wells and 132 natural springs, with outflow temperature between 30 and 50°C. These wells mostly discharge from the Miocene porous sandstone reservoirs between an average depth of 500-1500 m. For agricultural utilisation in Hungary 181 geothermal wells are used providing heating for over 70 ha greenhouses and 250 ha of soil-heated plastic tents. Hódmezővásárhely is another city where the water used has been injected back into sedimentary reservoir for the last 60 years, without problems. Since 1969, geothermal water has been used in secondary oil production technology in the Algyő oilfield. At present 5,400 m³/s of hot water are injected into the oil reservoir for oil displacement. Problems occur in the Hungarian sandstone aquifer when the pressure decreases in the reservoir when the fields have been exploited for a long time. One case is represented by Hajdúszoboszló field, where the piezometric head of the reservoir has subsided almost 70 m and the production can just be sustained by artificial lifting. Even though 672 geothermal wells have been drilled in Hungary, only 34 wells are (partly) used as injection wells. Efforts are being made in order to develop sustainable projects using geothermal energy. Due to this, from 2010 to 2014, four injection wells were drilled and the number of these is expected to increase in the future (Toth, 2015).

4. GEOTHERMAL ENERGY IN ROMANIA

4.1 Geothermal potential in Romania

The geothermal potential in Romania is associated with low-temperature geothermal systems, located in porous permeable formations such as the Pannonian sandstone, and siltstones specific for the Western Plain and for Olt Valley, or in fractured carbonate formations specific for the Oradea, Bors and North Bucharest (Otopeni) areas. The first well for geothermal utilisation in Romania was drilled in 1885 to a depth of 51 m, yielding water of 49°C. The maximum flow rate of this well is 195 L/s but it was never used with this flow rate. This well is located at Felix Spa, close to the municipality of Oradea, and is still in operation. It was followed by three additional wells; one drilled in 1893 at Caciulata with water at temperature of 37°C, one in 1897 at Oradea with water at temperature of 29°C and one in Timisoara in 1902 with water at temperature of 31°C (Rosca et al., 2005).

As part of a geological programme for hydrocarbon resource exploration from the 1960s geothermal research, aimed at using geothermal resources on a large scale, began. Since then, over 250 wells have been drilled with a depth range of 800-3,500 m, through which were discovered low-enthalpy geothermal resources with a temperature between 40 and 120°C. Most of them are located in the western part of Romania, while three wells are located in the southern part of the country. A recent study conducted by University of Oradea and S.C. Transgex S.A. identified 223 wells drilled after 1965. Over 80% of the wells are artesian producers, 68 of them were drilled in the Pannonian basin and require anti-scaling treatment, and four are injection wells. The total installed geothermal capacity in Romania is around 480 MWth for existing wells, at a reference temperature of 25°C. Currently, only about 200 MWth are used from 96 production wells with a temperature in the range of 40-120°C.

In Romania, around 40 wells are used for health and recreational bathing in 16 spas, most of them in the western part. According to the data presented in a country update for 2005-2009 regarding geothermal energy in Romania (Rosca et al., 2010), seven geothermal wells have been drilled to depths ranging from 1,500 m to 2,800 m. Three were unsuccessful (dry or cold), three are producing geothermal water with wellhead temperatures of about 70°C and the drilling of one started in late 2008. This well was planned to be drilled to at around 3,000 m depth. At 1,700 m, due to circulation losses, the well was completed and tested (without acidizing). It produced (in artesian discharge) about 10 L/s of geothermal water with about 90°C wellhead temperature (Rosca et al., 2010).

Between 2010-2016 (October), two geothermal wells were drilled to a depth of 2,500 m and 3,100 m, respectively, producing geothermal water with a wellhead temperature in the range of 80-90°C. Two more wells were drilled during this period for injection purposes. The first injection well from this period was completed in 2010 in the town of Beius (Bendea et al., 2015), and the second well, which is located in the municipality of Oradea (financed under the RO 06 Renewable Energy Programme through the EEA Grants Financial Mechanism 2009-2014), will be completed this year (2016).

As mentioned above, the geothermal systems of Romania (Figure 10) are found in the porous and permeable sandstones of the Pannonian basin, along the western border of Romania, interbedded with clays and shales specific for the Western Plain, or in carbonate formations of Triassic age in the basement of the Pannonian basin, and of Malm-Aptian age in the Moesian Platform.

In the western part of Romania the following geothermal reservoirs are known: Pannonian aquifer Oradea reservoir, Bors reservoir, Beius reservoir and Ciuneghiu reservoir. In the central and south part of the country the following reservoirs have been discovered: Cozia-Calimanesti reservoir (central) and North Bucharest reservoir (south).

The Pannonian geothermal aquifer is multi-layered, confined and is located in the sandstones at the basement of the Upper Pannonian (late Neocene age), with an approximate area of 2,500 km² along the western border of Romania. The main geothermal areas are, from north to south: Satu Mare, Tasnad,



FIGURE 10: Location of the main geothermal reservoirs in Romania (Bendea et al., 2015)

Acas, Marghita, Sacuieni, Salonta, Curtici-Macea-Dorobanti, Nadlac, Lovrin, Tomnatic, Sannicolau Mare, Jimbolia and Timisoara. The Pannonian aquifer has been explored by over 100 geothermal wells and currently 33 (mainly artesian) of them are exploited. This aquifer is encountered in the depth range of 800-2,400 m and the thermal gradient is 45-55°C/km. The geothermal water exploited is of sodium bicarbonate-chloride type, with a mineralisation (TDS) of 4-5 g/L and wellhead temperatures between 50 and 85°C. Due to this mineralization, most of the water shows carbonate scaling, prevented by downhole chemical inhibition. Utilisation of geothermal water in this areas is mainly for district heating (around 2,500 flats), sanitary hot water supply for 2,200 flats, greenhouse heating, covering 10 ha., health and recreational bathing, and fish farming.

The Oradea geothermal reservoir covers around 75 km² and is located in the Triassic limestone and dolomites at depths of 2,200-3,200 m. The reservoir is exploited by 14 geothermal wells with a total maximum artesian flow rate of 140 L/s with wellhead temperatures ranging from 70 to 105°C. The water is of calcium-sulphate-bicarbonate type with mineralization ranging from 0.9-1.2 g/L, without dissolved gases. The Oradea Triassic aquifer is hydrodynamically connected to the Felix Spa Cretaceous aquifer, and together they are part of the active natural flow of water. The water is about 20,000 years old and the recharge area is in the northern edge of the Padurea Craiului Mountains and the Borod Basin. Despite the fact that natural recharge of the geothermal system is significant for this reservoir, the exploitation with a total flow rate of over 300 L/s has generated a pressure draw down in the reservoir that is counteracted by reinjection of water into reservoir after utilisation. The first successful doublet started operation in 1992, in the Nufarul district, located near the south east corner of Oradea City. This doublet harnesses geothermal water from the Oradea reservoir for heat suppling 3,000 flats for 8,000 people (Bendea et al., 2015).

A new geothermal heating plant has been operating since 2005 in the Iosia district in the same city. The geothermal plant can supply 80% of the heat demand (at the design value of -15°C for outside

temperature) and 100% for house tap water. The peak load for space heating is supplied by two natural gas fired boilers, which increase the supply temperature of the secondary fluid from 102 to 110°C. In 2012, a 50 kWe demonstration ORC power plant was installed to complete the heating plant, being the first operational geothermal electric generation plant in Romania (GEODH, 2016). The Felix Spa reservoir is at present exploited by over ten wells, drilled to depths between 50 and 450 m. The total flow rate available from these wells is 210 L/s, with wellhead temperatures of 36-48°C.

In the municipality of Oradea, the annual utilisation of geothermal energy is around 30% of the total geothermal energy produced in Romania (Bendea et al., 2015). Currently the municipality of Oradea is implementing a project for geothermal reinjection, with a final project date of 30.04.2017, financed under the RO06 Renewable Energy Programme developed by the Environment Fund Administration, through the EEA Grants Financial Mechanism 2009-2014. The well will be drilled to a depth of 2900 m and is expected to accept a flow rate of 45 L/s (Oradea, 2016).

The Bors geothermal reservoir is located at around 6 km north-west of Oradea and despite being located in fissured carbonate formations like the Oradea geothermal reservoir, these geothermal reservoirs are different. The Bors reservoir is a tectonically closed aquifer, covering a surface area of 12 km². The geothermal water contained in this reservoir has a mineralization of 13 g/L of dissolved salts, dissolved gases of 70% CO₂ and 30% CH₄ and high scaling potential, prevented by chemical inhibition. The reservoir temperature in Bors is over 130°C at depth of 2,500 m. The dissolved gasses are partially separated at 7 bars, which is the operating pressure, and then the fluid is passed through heat exchangers before being reinjected. The artesian production of the wells could only be maintained by reinjecting the whole amount of extracted geothermal water, and of colder water from shallower wells during the summer. In the past, three wells were used to produce a total flow rate of 50 L/s, and two other wells were used for injection, at a pressure that did not exceed 6 bar. Geothermal water from this reservoir has been used for greenhouse heating covering 12 ha., though with operations stopped for some time. In 2014, S.C. Transgex S.A. restarted the production from one well to supply heat to two companies in the area (about 17 TJ/yr).

The Beius geothermal reservoir is located about 60 km south-east of Oradea, in fissured Triassic calcite and dolomite at a depth range between 1,870-2,370 m. The first well was drilled in 1996 to 2,576 m depth. A line shaft pump was put in the well in 1999, now producing up to 45 L/s with a wellhead temperature of 83°C. A second well was drilled in early 2004, and a line shaft pump was installed later that year. This well can also produce up to 45 L/s geothermal water with an 85°C wellhead temperature. A third well was drilled in 2010 and is used to reinject the heat depleted geothermal water from the closed-loop systems. The geothermal water from the two production wells has low mineralization (462 mg/L TDS), and 22.1 mg/L non-condensable gases (NCG), mainly CO₂ and 0.01 mg/L of H₂S. The geothermal water from both wells is currently used to supply district heating to a large part of the town of Beius.

The Ciumeghiu geothermal reservoir is located in the Western Plain, about 50 km south to Oradea. The aquifer is located in Lower Pannonian age gritstone, at an average depth of 2,200 m. The geothermal water has a wellhead temperature of 105°C and high mineralization (5-6 g/L TDS), with strong carbonate scaling potential (prevented by chemical inhibition at the depth of 400 m). The main dissolved gas is CH₄. The reservoir was explored by four wells, but only one has been in use (as the greenhouses in the area have been closed).

The Cozia-Calimanesti geothermal reservoir (Olt Valley) is located in fissured siltstones of Senonian age. The reservoir depth is 2,700-3,250 m, the wells produce geothermal water with flow rates between 8.5 and 22 L/s, wellhead temperatures of 70-95°C and TDS of 15.7 g/L, without major scaling (only minor deposition and some corrosion). Despite the fact that the reservoir has been exploited for more than 25 years, there is no interference between the wells and no significant pressure draw down. The thermal potential possible to achieve from the four wells is about 14 MWth (of which 3.5 MWth are from the combustible gases – if used), but only about 7 MWth are used at present. The geothermal water

is mainly used for district heating (2,250 equivalent flats), and for health and recreational bathing (Bendea et al., 2015).

The Otopeni reservoir near Bucharest will be described in the next chapter.

In Romania the main direct uses of geothermal heat are: district heating and individual space heating, health and recreational bathing, greenhouse heating (about 10 ha.), fish farming (a few farms), industrial processes, and drying. Detailed data on installed capacity and annual energy used is not available by type of utilisation. In areas where the available wellhead temperature is rather low, geothermal water is only used for health and recreational bathing (e.g. Felix spa), or for fish farming. In other areas, even where the temperature is higher, the geothermal water is still used only for bathing (e.g. Acas-Beltiug and Tasnad), or for fish farming (e.g. Santandrei). In larger communities where wellhead temperatures of the wells are higher, the geothermal water is first used for district heating, some industrial processes, with only a part of the heat depleted water used for bathing (or for fish farming), the rest being reinjected.

As a summary of the information presented above Table 3 shows comparative characteristics of the main geothermal aquifer in Romania.

TABLE 3: Characteristics of the main geothermal aquifer in Romania
(Rosca et al., 2005; Bendea et al., 2015)

Parameters	U/M	Oradea	Bors	Beius	Western Plain	Olt Valley	North Bucharest
Type of reservoir		carbonate	carbonate	carbonate	sandstone	gritstone	carbonate
Area	km ²	7	12	47	2,500	10	300
Depth	km	2.2 - 3.2	2.4 - 2.8	2.4 - 2.8	0.8 - 2.1	2.1 - 2.4	2.0 - 3.2
Drilled wells	Total	15	6	3	88	4	18
Well head temperat.	°C	70 - 105	120	84	50 - 90	70 - 95	51-84
Temperature gradient	°C/100 m	3.5- 4.3	4.5-5.0	3.3	3.75-4.15	3.0-3.5	2.3 - 2.6
TDS	g/L	0.8 - 1.4	12 -14	0.46	2 - 6	15.7	2.2
Exploitable reserves (for 20 years)	MW/day	570	110	52	4,700	300	840
Flow rate	L/s	4 - 20	10 - 15	4 - 12	4 - 18	12 - 25	22 - 28
Type of production		artesian	artesian	pumping	artesian+ pumping	artesian	pumping
Total installed power (with existing wells)	MW _t	58	25	10	12.5	18	35

Exploitation of shallow geothermal resources in Romania started in the 1990s with ground source heat pumps (GSHP) applications, with ground water wells preferred instead of horizontal heat exchangers. Currently in Romania, GSHP applications are not regulated by technical rules and therefore it is impossible to obtain data from all companies which are installing and utilizing such systems. No specific authority or institute has especially been appointed to collect data/information, to certify, authorize and monitor the performance of these applications, which result in the lack of reliable data for these applications. Table 4 shows the total length of the largest GSHP systems, with borehole exchangers longer than 10,000 m, built in Romania.

Since 2010, the Romanian Government has supported the utilization of renewable energy sources, including ground source heat pumps, for new systems installed by individuals. Because the Government did not allocate the necessary funds in 2014 to continue the program, the geothermal heat pump market dropped to about half. Based on available data, the heat capacity of the ground source heat pumps installed in Romania by the end of 2014 is estimated at about 40 MWth.

TABLE 4: Largest GSHP systems with borehole heat exchanger in Romania (Bendea et al., 2015).

City – beneficiary name	No. of BHE	Depth BHE [m]	Total BHE [m]
Magurele – Bucharest, ELI-NP (under construct.)	1,080	125	13,500
Valul lui Traian, Cardinal Motors (2009)	357	70	24,990
Snagov, Vila 23 Hotel (2008)	224	70	15,680
Focsani, ARTIFEX (2012)	120	125	15,000
Bucharest, Midocar Est (2008)	144	75	10,800
Bucharest, Green City Hall (under construction)	80	125	10,000

The Romanian Geoexchange Society is a non-governmental organisation established in 2002 aiming to promote the HVAC GSHP systems, create a national regulatory framework, educate the users and direct them to RES, represent the Romanian market abroad, train Romanian specialists as well as contribute at the European training and certification frame.

During 2009-2014, the investment and employment in geothermal projects in Romania totalled about 5.7 million EUR, less than in any 5 year interval before. This was mainly from the State Budget, intended for drilling (field development). Out of the total investments in common geothermal projects, the cost of drilling the two wells needed, represents about 70% of the total capital cost. Successful wells can be leased from the National Agency for Mineral Resources, usually by the company that drilled them (Bendea et al., 2015).

Approximately additional 6.4 million EUR, for investments in geothermal projects (drilling new well, research and development) in the current period, are supported by the RO06 Renewable Energy Programme, financed through the State Budget (15%) and the EEA Grants Financial Mechanism 2009-2014 (85%) (RONDINE, 2016).

4.2 Geothermal utilization in Balotesti area (Ilfov County)

Balotesti is an administrative territorial unit located in the northern part of Ilfov County, around 20 km away from Bucharest. It is neighboured by Snagov to the north, Otopeni to the south, Moara Vlasiei to the east, Corbeanca to the south-west, Peris to the north-west and Stefanestii de Jos to the south-east. Balotesti Commune has an area of 53 km² and it consist of three villages: Balotesti, Saftica and Dumbraveni. According to data from the National Institute of Statistics, in 2011, Balotesti Commune has a total population of 8314 inhabitants (Ilfov-Insse, 2016).

The geothermal utilisation in Balotesti area is based on the Otopeni geothermal reservoir, located in the northern part of Bucharest. The Otopeni, or North Bucharest, geothermal reservoir is partially delimited (about 300 km²), with aquifers in fissured limestone and dolomites (carbonate rocks) at depth range of 2,000-3,200 m, belonging to the Moesian Platform. In this reservoir, through time, 24 wells have been drilled (of which only 18 are potential producers or injectors) demonstrating an important geothermal aquifer (Bendea et al., 2015).

Production has been carried out in the Otopeni area using downhole pumps, because the water level in the wells is at 80 m below surface. Geothermal water is exploited with a well flow rates between 22 and 28 L/s, a wellhead temperature of 58-84°C, and a rather high TDS (1.5-2.2 g/l) as well as a high H₂S content (up to 30 ppm). Here, it is recommended to inject the water after use into reservoir for environmental protection (Bendea et al., 2015). In the near future, three wells will be used in this northern area, one of these being drilled this year (2016) for recreational purposes. One of the other two wells (old wells) is used almost all the year for health and recreational bathing and another well will be used for district heating and domestic hot water supply for an emergency hospital. Through several wells drilled between 1981 and 1994, a high capacity geothermal reservoir has been discovered with a flow

rate range of 20-60 L/s and wellhead temperatures of: 66°C near Otopeni airport, 76°C at Moara Vlasiei, 80°C north of Balotesti and 83°C at Snagov.

Three wells have been drilled in the Balotesti north area focused on geothermal research, named wells 2669, 2684 and 2685. Well 2669 was drilled between 1989 and 1991 to a depth of 3304 m, with production samples showing satisfactory results. Well 2684 was drilled north of Balotesti between 1995 and 1998 to a depth of 3052 m with better results in terms of thermal power capacity. Well 2685 was drilled as an injection well north of Balotesti between 1998 and 1999 to a depth of 3002 m. The production tests yielded unsatisfactory result regarding injectivity. Of these three wells, currently well 2684 has been rehabilitated and will be used for district heating and domestic hot water supply for a local hospital. According to existing data from the National Agency for Mineral Resources construction of well 2684 was performed as shown in Table 5.

TABLE 5: Design of well 2684 at Balotesti

Well	Depth (m)	Diameter casing (") /cased interval (m)					Open hole interval (m)	Cemented interval (m)
		20	13 ^{3/8}	9 ^{5/8}	7	6 ^{5/8}		
2684	3052	-	0-1140	642-2230	-	1.639-2318.7	2318.7-3052	0 – 2318.7

After drilling, well 2684 in Balotesti was tested in the depth range of 3052-2318.7 m (open hole). Concentric air-lift pump was used to stabilize temperature, flow and dynamic level. The results are as follows: flow rate of 20 L/s, dynamic fluid level at 87 m, static fluid level at 65 m and wellhead temperature in the range of 82-84°C. These wells were drilled as a part of a geothermal research programme and following the testing the governmental agencies responsible decided to cement the wells in order to preserve them.

From 2014, the administrative territorial unit of Ilfov County Council started a project in order to harness geothermal water from well 2684 for district heating and domestic hot water supply for an emergency hospital located in north Balotesti, close to well 2684. The project is financed under the RO 06 Renewable Energy Programme developed by the Environment Fund Administration as programme operator, through the EEA Grants Financial Mechanism 2009-2014 (RONDINE 2016). The project has a grant of around 1.7 million EUR for eligible costs and is planned to be completed in 2016, by starting operations. The project involves construction of a geothermal plant, which will use the geothermal water produced by well 2684 for heat and hot water supply. The geothermal plant will replace the current plant that uses gas for heating and hot water. Realization of this project will include rehabilitation and testing of well 2684, geothermal installations (consisting of an uncovered storage tank with a capacity of 500 m³, well 2684 fully equipped and a geothermal station), pipe-line for used geothermal water, round trip circuit for heat and hot water, distribution network and connection to the consumers. The completion of this project aims at ensuring sustainable energy development while protecting the environment. According to recent data (2013) the annual number of beneficiaries of this investment will be around 11,000 persons (Hidroservices, 2014).

This year (2016) a new well to a depth of 3107 m has been drilled in the same area of Balotesti. This well will exploit geothermal water in order to supply water for a new spa (private investment) built in Balotesti. According to the production test performed this year, the new well yielded hot water with a temperature of 81-82°C and a flow rate of around 25 L/s. The geothermal aquifer is exploited with a submersible pump of 48 kW with variable flow (frequency converter) placed at a depth of about 150 m, operable up to temperature of 90°C (AHGR, 2016).

4.3 Thermal breakthrough time in Balotesti area

The main detrimental effect due to reinjection is the cooling of a geothermal reservoir, and even of production wells. Although reinjection is not performed now in the Balotesti area, reinjection will be needed in the future, if the reservoir will be used mainly for district heating and hot water supply through a doublet (production-injection) scheme. Therefore, cooling may occur in the long term so it is necessary to estimate the long-term thermal breakthrough time for the field (North Bucharest-Otopeni reservoir).

For this area a simple porous model with an infinite, homogeneous, isotropic, fluid-saturated, hot (at temperature T_r), horizontal layer of porous material with porosity \emptyset and thickness H , was used. At time $t = 0$, injection of cold (at temperature T_o , cold relative to the initially hot layer) water at a rate Q (kg/s) is initiated at the location $r = 0$ (location of the injection well) (Zheng, 2015). By assuming that heat transport by conduction is negligible compared to the advection heat transport, one can show that a cold front travels radially away from the reinjection well (two-dimensional flow). On the inside of the front, the temperature is T_o , while on the outside, the temperature is undisturbed at T_r . The distance to the cold front is then given as (Bödvarsson, 1972):

$$rT = \sqrt{\frac{\beta_w Q t}{\pi H < \rho \beta >}} \quad (1)$$

where rT = Radial distance of cold front (m);
 H = Reservoir thickness (m);
 $< \rho \beta >$ = Average volumetric heat capacity of reservoir, or
 $\emptyset \beta_w \rho_w + (1 - \emptyset) \beta_r \rho_r$ (J/m³/°C);
 β_w = Heat capacity of water (J/kg/°C);
 ρ_w = Water density (kg/m³);
 \emptyset = Rock porosity;
 β_r = Heat capacity of rock (J/kg/°C);
 ρ_r = Rock density (kg/m³);
 Q = Injection rate (kg/s).

Currently, according to the result of the production test carried out for the two production wells in the Balotesti area, the production flow rate ranges from 25 to 34 L/s with temperatures between 81 and 85°C. Assuming that the reservoir thickness is between 200 and 400 m and using three injections rates of 10, 15 and 25 kg/s we can estimate the distance that is needed between production and injection wells to avoid thermal breakthrough time. The breakthrough time is calculated as a function of the distance between production and injection wells.

The result of estimated cold front breakthrough time are presented in Figures 11 and 12. To avoid thermal breakthrough in 100 years, the estimated safe distance between the injection and reinjection wells should be more than 450 m for the case with a reservoir thickness of 200 m and more than 300 m for the case with a reservoir thickness of 400 m. The results of this model are optimistic, because in this model a homogeneous and isotropic system without fractures is assumed. In reality injection rates will be variable, not constant, and the active reservoir thickness may be quite different from what is assumed here.

Based on these results, it is recommended that the reinjection wells should be located at more than 450 m distance from the production wells in the Balotesti area. However, these results are uncertain because the reservoir thickness and other system parameters are quite poorly known. Once reinjection wells have been drilled, tracer tests should be conducted to estimate these parameters more accurately.

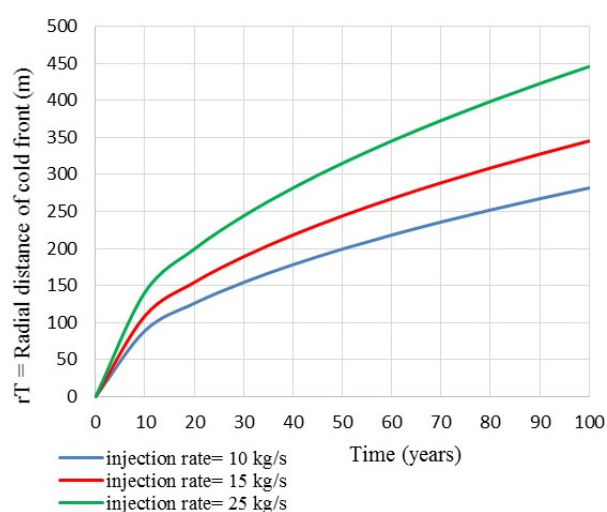


FIGURE 11: Estimated cold front breakthrough time for a reservoir thickness of 200 m with different reinjection rates in Balotesti area

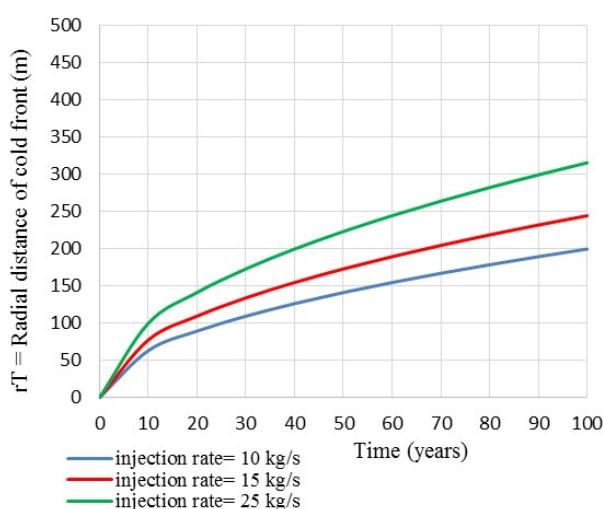


FIGURE 12: Estimated cold front breakthrough time for a reservoir thickness of 400 m with different reinjection rates in Balotesti area

4.4 Governing laws and development opportunities

Romania became a member of the European Union in 2007 and since then the Romanian legislation has been harmonized with the European Union legislation. Romania adopted and included in the Energy Strategy for 2007-2020, the European energy targets, to increase the share of renewable energy to at least 20% of the total consumption. By 2020, the EU aims to combat climate change and air pollution, decrease its dependence on foreign fossil fuels, and keep energy affordable for consumers and businesses. Even though Romania still uses fossil fuels for district heating and hot water supply, efforts to reach the European target are being made by the Romanian authorities. On this line, the Romanian government has launched national programmes in order to increase the renewable energy consumption, to reduce the emission of greenhouse gases and to reduce pollution. A part of these programs have been implemented from the State Budget, by the Environment Fund Administration, governmental agency under the Ministry of Environment, Waters and Forests. Also, the Environment Fund Administration, implemented the RO 06 Renewable Energy Programme with a total value of around 12 million EUR, financed by the State Budget (15%) and EEA Grant Financial Mechanism 2009-2014 (85%). The RO 06 Renewable Energy Programme supports two energy components, hydropower and geothermal, through which the utilisation of renewable energy resources will be increased (RONDINE, 2016; European Commission, 2016).

The Operational Programme Large Infrastructure has been developed in accordance with the identified development needs of Romania, through the Partnership Agreement 2014-2020, and in line with the Common Strategic Framework and the Position Paper of the European Commission services. To promote clean energy and energy efficiency, through the Operational Programme Large Infrastructure, Priority Axis 6 “Promote clean energy and energy efficiency in order to support a low-carbon economy”, Romania has allocated around 197 million EUR. Through the specific objective “Increasing production of less exploited renewable energy (biomass, biogas, geothermal)” of the axis mentioned above, territorial administrative units located in regions with geothermal energy will have the opportunity to develop projects for harnessing geothermal energy (MFE, 2016).

In Romania, geothermal resources are owned by the state and explored and exploited under a Mining Law license issued by the National Agency for Mineral Resources, which is required for exploration and exploitation. The drilling operations for underground production are subject to environmental

evaluation except wells drilled to depths of less than 50 m. As they are classified as mineral resources in accordance with the Mining Law, data regarding geothermal resources from the deep aquifers are currently confidential and can only be accessed by accredited persons in accordance with the same law.

In the *Country update of 2010-2014 for geothermal energy in Romania*, presented at the World Geothermal Congress 2015 in Melbourne, Bendea et al. (2015) describe the utilisation of shallow geothermal with GSHP and also mention the fact that Romania does not have any institutions especially appointed to regulate, to keep a database, to certify, authorize and monitor the performances of ground source heat pump applications. Despite this fact, considerable information about implementation of ground source heat pump applications is available on the Romanian Geoexchange Society database (Geoexchange, 2016).

5. CONCLUSIONS

Utilization of geothermal systems on a large scale for district heating started worldwide during the 1970s, after the first oil crisis. The important development of geothermal projects, therefore, took place when the world passed through the oil crisis. In contrast the price of oil has continuously decreased during the last two years. Hence, it will be interesting to see how geothermal will develop in the following years.

Reinjection is an important part of any geothermal exploitation project and it may turn into a key factor in the success or failure of geothermal operations. Even though reinjection started as a method of waste water disposal, it has now become an important part of sustainable management of geothermal resources, mainly by providing additional recharge and maintaining reservoir pressure. Other benefits include environmental management, such as when the water has high content of salts, minerals, H₂S etc., as well as to minimize subsidence. Each field has a different response to reinjection but the reservoir permeability defines the connection between production and the injection areas. Selecting the distance from injection wells to production wells is a challenge when the geothermal reinjection system is designed.

Reinjection may cause difficulties and problems such as cooling of the production areas, high pressure required for water injection, groundwater contamination, increase of possible seismic activity in the area (induced seismicity) and changes in the water chemistry. Although reinjection is a part of modern geothermal exploitation, some countries do not yet require reinjection in their geothermal operations. This is at least partly due to the fact that geothermal projects which include reinjection require at least two wells from the start, one for production and another for injection, which will increase the initial project cost.

Countries such as France and Germany have now used geothermal water from sedimentary systems for district heating for several decades, utilizing geothermal systems consisting of production and injection wells in the same area. Throughout time, these countries have not encountered significant problems during exploitation. The principal exception is associated with injection into sandstone. But technical solutions have been developed for this problem in Germany and Denmark.

The European Commission set the three following key targets in order to ensure that the European Union meets its climate and energy targets for the year 2020:

- A 20% cut in greenhouse gas emissions (from 1990 levels);
- 20% of EU energy should come from renewables; and
- 20% improvement is expected in energy efficiency.

The 2030 climate and energy framework of EU sets three key targets for the year 2030:

- At least 40% cuts in greenhouse gas emissions (from 1990 levels);
- At least 27% share for renewable energy; and
- At least 27% improvement in energy efficiency.

Geothermal energy is a renewable and a nearly carbon free, form of energy available worldwide, which can be utilized in a sustainable manner and which can contribute significantly to the European Union being able to reach its energy targets for the year 2020 (European Union, 2016).

6. RECOMMENDATIONS FOR ROMANIA

Based on the examples of geothermal utilisation and reinjection in European countries, which harness geothermal resources from sedimentary basins, the following is recommended to support a considerable increase in the utilization of the geothermal resources in Romania as well as their sustainable management:

1. To maintain district heating systems as public property (may be partly privatized but municipality should remain the main owner).
2. Utilise reinjection wells for used geothermal water and use geothermal doublets (production and injection wells) in the district heating systems, with 100% reinjection, where possible.
3. Apply experience and technologies developed, mainly in Germany and Denmark, to maintain injectivity (by avoiding clogging) of sandstone reinjection wells.
4. Create a regulatory framework for ground source heat pump applications, especially when these applications use groundwater aquifers as energy source.
5. Appoint one institution to manage and apply the regulatory framework for GSHP, preferably an already existing institution which is involved in implementing renewable energy programs.
6. Open access to existing data that can be used for studying and assessing geothermal resources (i.e. use different classification than for mineral resources).
7. Increase fund allocation for geothermal research.
8. Increase geothermal utilisation to replace biomass, as a solution for a low-carbon emission and low environment impact.
9. Develop annual programmes for exploration drilling as a part of the state energy plan.
10. Develop annual programmes for ground source heat pump applications.
11. Include geothermal utilisation in regional development strategies.
12. Take into consideration ground source heat pumps applications as an energy source in feasibility studies for new or rehabilitated buildings.
13. Reduce the number of the approval papers (permits) required in development of geothermal projects.
14. Identify, launch or create national and regional geothermal programmes of cooperation between municipalities to implement integrated geothermal projects (district heating systems).
15. Set up a national network (with universities, research institutes, governmental agencies, non-governmental organisations, municipalities, private companies) to share data, analysis and studies for geothermal development projects.

ACKNOWLEDGEMENTS

I would like to express my gratitude to the UNU-GTP staff, Mr. Lúdvík S. Georgsson, director of the United Nations University Geothermal Training Programme (UNU-GTP), Mr. Ingimar G. Haraldsson, Ms. Thórhildur Ísberg, Mr. Markús A. G. Wilde and Ms. Málfríður Ómarsdóttir for their support during this programme.

A special thanks to my supervisors, Ms. Helga Tulinius and Mr. Guðni Axelsson, for their guidance, patience and support to complete this report and also the ÍSOR staff for their lectures.

I am grateful to all those who made the participation in this programme possible. On this path I would like to express my appreciation to the University of Oradea, Environment Fund Administration and Ilfov County Council staff.

Special thanks to my family, friends and colleagues from Romania

REFERENCES

AHGR, 2016: *Forajul Therme*. Romanian Association of Hydrogeologists, website: www.ahgr.ro/media/85718/forajgeoterm_balotesti.pdf

Alm, P.G., 2011: Gravel pack maintenance and stimulation by air lifting. *Proceeding of the 36th Workshop on Geothermal Reservoir Engineering, Stanford University, Stanford, CA*, 7 pp.

Axelsson, G., 2008: The importance of geothermal reinjection. In: Fridleifsson, I.B., Holm, D.H. Wang Kun and Zhang Baiming (eds.), *Workshop for Decision Makers on Direct Heating Use of Geothermal Resources in Asia, Tianjin, China*. UNU-GTP, TBLRREM and TBGMED, CD, 16 pp.

Axelsson, G., 2012: Role and management of geothermal reinjection. *Presented at "Short Course on Geothermal Development and Geothermal Wells", organized by UNU-GTP and LaGeo, in Santa Tecla, El Salvador*, UNU-GTP SC-14, 21 pp.

Bendea, C., Antal, C., and Rosca, M., 2015: Geothermal energy in Romania: country update 2010-2014. *Proceedings of the World Geothermal Congress 2015, Melbourne, Australia*, 9 pp.

Bödvarsson, G., 1972: Thermal problems in the siting of reinjection wells. *Geothermics*, 1, 63–66.

Borović, S., and Marković, I., 2015: Utilization and tourism valorisation of geothermal waters in Croatia. *Renewable and Sustainable Energy Reviews*, 44, 52–63.

European Commission, 2016: *Climate action*. European Commission, website: ec.europa.eu/clima/policies/strategies/2020/index_en.htm

Gehlin, S., Andersson, O., Bjelm, L., Alm, P.G., and Rosberg, J.E., 2015: Country update for Sweden *Proceedings of the World Geothermal Congress 2015 Melbourne, Australia* 6 pp.

GEODH, 2016: *District heating systems in Oradea: Iosia Nord, geothermal district heating*. GEODH, website: geodh.eu/project/oradea/

Geoexchange, 2016: *Base data (in Romanian)*. Romanian Geoexchange Society, website: geoexchange.ro/wp-content/uploads/2013/12/Baza-de-date-sisteme-GSHP-centralizare-21-aprilie-2016.pdf

Goldbrunner, J., 2015: Austria – country update. *Proceedings of the World Geothermal Congress 2015 Melbourne, Australia*, 13 pp.

Goldbrunner, J., Bauer, R., Kolb, A., and Achim Schubert, A., 1999: Geothermal cascade use at Geinberg. *Austria Bulletin d'Hydrogiologie*, 17, 209-216.

Hidroservices, 2014: *Summary of feasibility study for project „Harnessing geothermal water resources from Balotesti Perimeter, Ilfov County for heat production”*. Hidroservices, unpublished report, 57 pp.

Ilfov-Inse, 2016: *Population and housing census 2011* (in Romanian). National Institute of Statistics, County Department for Statistics – Ilfov.

Jirakova, H., Stibitz, M., Frydrych, V., and Durajova, M., 2015: Geothermal country update for the Czech Republic. *Proceedings of the World Geothermal Congress 2015, Melbourne, Australia*, 7 pp.

Kepinska, B., 2010: Geothermal energy country update report from Poland, 2005 – 2009. *Proceedings of the World Geothermal Congress 2010 Bali, Indonesia*, 8 pp.

Kepinska, B., 2015: Geothermal energy country update report from Poland, 2010 – 2014. *Proceedings of the World Geothermal Congress 2015 Melbourne, Australia*, 11 pp.

Kolbah, S., Živković, S., Golub, M., and Škrlec, M., 2015: Croatia country update 2015. *Proceedings of the World Geothermal Congress 2015 Melbourne, Australia*, 7 pp.

Lopez, S., Hamm, V., Le Brun, M., Schaper, L., and Boissier, F., 2010: 40 years of Dogger aquifer management in Ile-de-France, Paris Basin, France. *Geothermics*, 39-4, 339–356.

Mahler, A., Røgen, B., Ditlefsen, C., Nielsen, L.S., and Vangkilde-Pedersen, T., 2013: Geothermal energy use, country update for Denmark. *European Geothermal Congress 2013, Pisa, Italy*, 12 pp.

MFE, 2016: *The operational programme large infrastructure*. The Ministry of European Funds, Romania, website: www.fonduri-ue.ro/poim-2014.

Oradea, 2016: *Informare PT 902*. Municipality of Oradea, website: www.oradea.ro/fisiere/module_fisiere/20561/Informare%20PT%20902.doc

Pernecker, G., and Uhlig, S., 2002: Low enthalpy power generation with ORC turbogenerator, the Altheim project, Upper Austria. *Geo-Heat Center, Quarterly Bulletin*, 16-1, 12-15.

Rajver, D., Rman, N., Lapanje, A., and Prestor, J., 2015: Geothermal development in Slovenia: country update report 2010-2014. *Proceedings of the World Geothermal Congress 2015 Melbourne, Australia*, 14 pp.

Rivera-Diaz, A., Kaya, E., and Zarrouk, S.J., 2016: Reinjection in geothermal fields – A worldwide review update. *Renewable and Sustainable Energy Reviews*, 53, 105–162.

Røgen, B., Ditlefsen, C., Vangkilde-Pedersen, T., Nielsen, L.H., and Mahler, A., 2015: Geothermal energy use, 2015 country update for Denmark, *Proceedings of the World Geothermal Congress 2015 Melbourne, Australia*, 9 pp.

Rojas, J., Giot, D., Le Nindre, Y.M., Criaud, A., Fouillac, C., Brach, M., Menjoz, A., Martin, J.C., Lambert, M., 1989: *Characterization and modelling of the Dogger geothermal reservoir, Paris Basin, France*. BRGM, Orléans, France, final report BRGM/RR-30169-FR (in French), 240 pp.

RONDINE, 2016: *Rondine RO 06, renewable energy programme RONDINE*. Environment Fund Administration, website: www.rondine.ro/en.

Rosca, M., Antal, C., and Bendea, C., 2010: Geothermal energy in Romania: country update 2005-2009. *Proceedings of the World Geothermal Congress 2010, Bali, Indonesia*, 9 pp.

Rosca, M., Antics, M., and Sferle, M., 2005: Geothermal energy in Romania: country update 2000-2004. *Proceedings of the World Geothermal Congress 2005 Antalya, Turkey*, 8 pp.

Saemundsson, K., Axelsson, G., and Steingrímsson, B., 2011: Geothermal systems in global perspective. Presented at „Short Course on Geothermal Drilling, Resource Development and Power Plants“, organized by UNU-GTP and LaGeo, in Santa Tecla, El Salvador, UNU-GTP SC-12, 13 pp.

Seibt, P., Kabus, F., and Hoth, P., 2005: The Neustadt-Glewe geothermal power plant – practical experience in the reinjection of cooled thermal waters into sandstone aquifers. *Proceedings of the World Geothermal Congress 2005, Antalya, Turkey*, 4 pp.

Seibt, P., and Kellner, T., 2003: Practical experience in the reinjection of cooled thermal waters back into sandstone reservoirs. *Geothermics*, 32/4-6, 733–741.

Serpen, U., and Aksoy, N., 2016: Developing geothermal energy in Croatia by using old oil wells for power generation. *Proceedings of the 41st Workshop on Geothermal Reservoir Engineering Stanford University, Stanford, CA*, 6 pp.

Stefansson, V., 1997: Geothermal reinjection experience. *Geothermics*, 26, 99-130.

Suchi, E., Dittmann, J., Knopf, S., Müller, C. and Schulz, R., 2014: Geothermal Atlas to visualise potential conflicts of interest between CO₂ storage (CCS) and deep geothermal energy in Germany. *Z. Dt. Ges. Geowiss.*, 165-3, 439-453.

Toth, A.N., 2015: Hungarian country update 2010-2014. *Proceedings of the World Geothermal Congress 2015, Melbourne, Australia*, 8 pp.

Ungemach, P., Antics, M., and Papachristou, M., 2005: Sustainable geothermal reservoir management. *Proceedings of the World Geothermal Congress 2005, Antalya, Turkey, April*, 12 pp.

Vernier, R., Laplaige, P., Desplan, A., and Boissavy, C., 2015: France country update. *Proceedings of the World Geothermal Congress 2015 Melbourne, Australia*, 8 pp.

Wang, L., and Lin, L., 2010: Discussion on reinjection of geothermal fluids into sandstones in Tianjin, P.R. China. *Proceedings of the World Geothermal Congress 2010, Bali, Indonesia*, 4 pp.

Weber, J., Ganz, B., Schellschmidt, R., Sanner, B., and Schulz, R., 2015: Geothermal energy use in Germany. *Proceedings of the World Geothermal Congress 2015 Melbourne, Australia*, 15 pp.

Zheng T., 2015: Assessment of the Urban Dezhou sandstone geothermal reservoir in North China. Report 35 in: *Geothermal training in Iceland 2015*. UNU-GTP, Iceland, 809-836.



UNITED NATIONS
UNIVERSITY

UNU-GTP

Geothermal Training Programme

Orkustofnun, Grensasvegur 9,
IS-108 Reykjavik, Iceland

Reports 2016
Number 40

GEOHERMAL RESERVOIR MODEL OF DOMBÓVÁR AREA, SW-HUNGARY

Zsófia Unyi

Gólya dűlő 51., 7635

Pécs

HUNGARY

zsofi.unyi@gmail.com

ABSTRACT

Dombóvár is a town in the southwestern part of Hungary with a population of 19,000 people. As part of a geothermal development plan, MVM (Hungarian Power Engineering and Consulting Ltd.) is planning to change the existing heating system of Dombóvár's industrial park into a geothermal supplied system, and possibly make the same changes to the district heating system of the entire town in the future. The goal of this study was to perform a feasibility study on the geothermal reservoir at Dombóvár to determine if it has the capacity to support a proposed geothermal well duplet. A conceptual model of the reservoir was created using available data and then a preliminary numerical model was constructed using MODFLOW. Results of the model simulations indicate that the reservoir is capable of supporting the proposed production, and therefore it is recommended to move forward with the development plan.

1. INTRODUCTION

Dombóvár is a town in SW-Hungary with a population of 19,000 people. A detailed geothermal development plan has been created with the goal of fulfilling the heating requirement of 2.1 MWth to an industrial park in Dombóvár. As part of the development plan, a detailed cost-benefit analysis was performed taking into account all physical and economical variables in the system. Estimated ranges of production rates and intake temperatures were analyzed in order to determine usage options for the geothermal fluid. Complementary usage of the geothermal fluid was analyzed, including agricultural usage and electricity generation using an ORC cycle. As geothermal production is a single source supply and heat delivery is mandatory, a backup heating source is required in case of system failure. The most likely backup system is a boiler station operated by oil, gas or wood. Costs associated with infrastructure were also analyzed.

According to preliminary calculations from the development plan, the heating demand for the industrial park can be reached with 17 l/s and 50°C heatsteps. According to the Hungarian legislation, 100% of the produced geothermal fluid must be reinjected back into the reservoir. This requires an injection well, which has to be included in the total investment cost on top of the district heating pipeline system. In order to achieve these goals and requirements, a proposed well duplet with the following dimensions is recommended:

F-1 (injection well):*Depth:* 2300 m*Coordinates:* EOY: X=112194, Y=580691, Z: 114 m a.s.l. (mBf)*Planned yield:* -17 l/s*Casing plan – using steel casings:*

0 - 40 m diameter 550 mm;

0 - 1100 m diameter 341 mm;

900 - 1400 m diameter 244 mm;

1200 - 2100 m diameter 178 mm;

1900 - 2300 m diameter 114 mm.

F-2 (production well):*Depth:* 2500 m*Coordinates:* EOY: X=112194, Y=580691, Z: 114 m a.s.l.*Planned yield:* 17 l/s*Casing plan – using steel casings:*

0 - 40 m diameter 550 mm;

0 - 1150 m diameter 341 mm;

950 - 1500 m diameter 244 mm;

1300 - 2300 m diameter 178 mm;

2100 - 2500 m diameter 114 mm.

According to the development plan, the expected lifetime of the proposed geothermal plant is 30 years. The goal of this study was to assess the geothermal reservoir at Dombóvár to determine if it has the capacity to support this proposed geothermal well duplet. A conceptual model of the reservoir was created using available data and a preliminary numerical model was constructed using MODFLOW.

2. CONCEPTUAL MODEL

2.1 Geological setting

The Pannonian basin (Figure 1) in eastern Central Europe is a large sedimentary depression from the Neogene inside the Alpine orogenic belt. It is surrounded by the mostly linear chains of the Eastern Alps and Dinarides and the strongly arcuate belts of the Carpathians. The formation of the basin on the Alpine orogenic edifice occurred during the Pannonian extension and coeval compression in the Outer Carpathian arc (Horváth, 1995).

The Pannonian basin system was formed by rifting during the late Early and Mid-Miocene. Extension was controlled by the retreat and roll-back of the subducted lithospheric slab along the Carpathian arc (Fodor, 1999). Two corners, the Bohemian and Moesian promontories, formed gateways towards this open space. At both the northern and southern corners, broad shear zones developed. The initial northeast directed tension was gradually replaced by a later east- to southeast-directed tension as a consequence of the progressive termination of subduction roll-back along the arc from the western Carpathians towards the southern Carpathians. There is growing evidence that an E-W-oriented short compressional event occurred during the earliest Late Miocene but during most of the Late Miocene extension was renewed. Starting at the end of the Miocene, roll-back terminated and a compressional stress field propagated from the Southern Alps gradually into the Pannonian Basin, followed by tectonic inversion of the entire basin system in the Pliocene and Quaternary (Horváth et al., 2006). A geological cross-section of the Dombóvár area is shown in Figure 2.

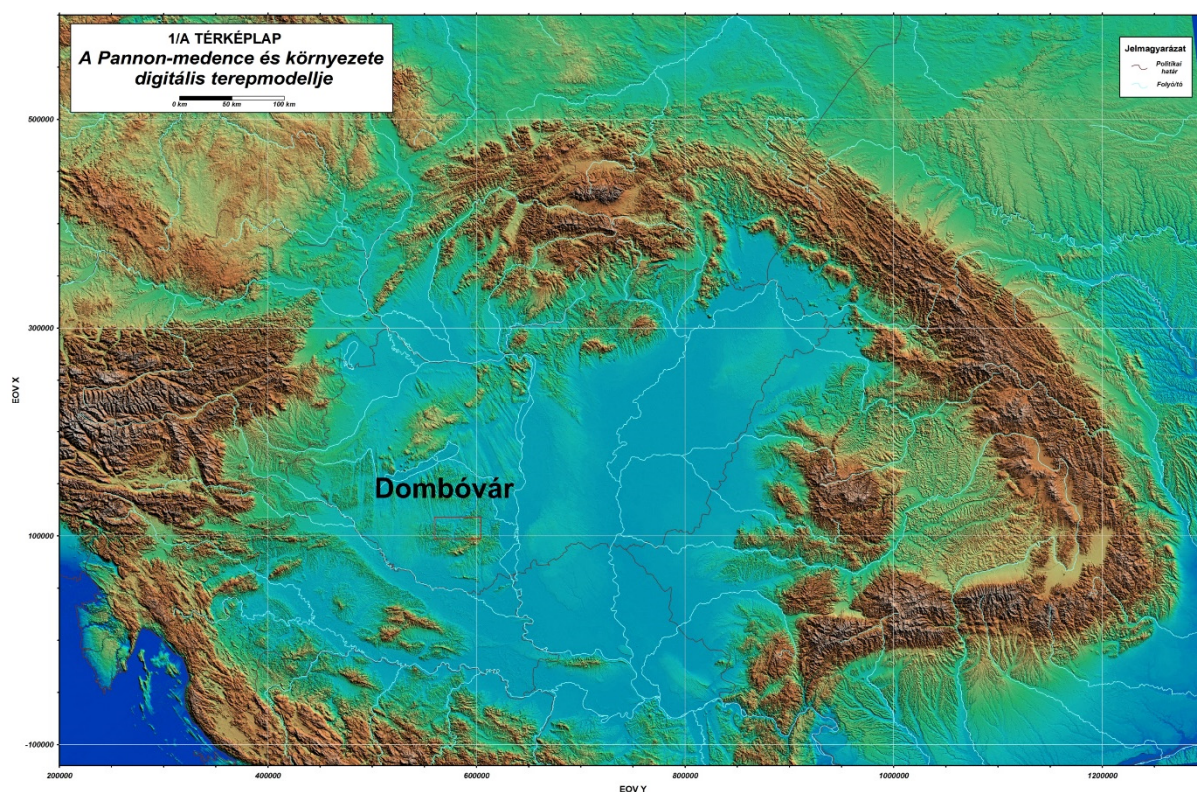


FIGURE 1: Topographical map of the Pannonian basin showing location of Dombóvár area

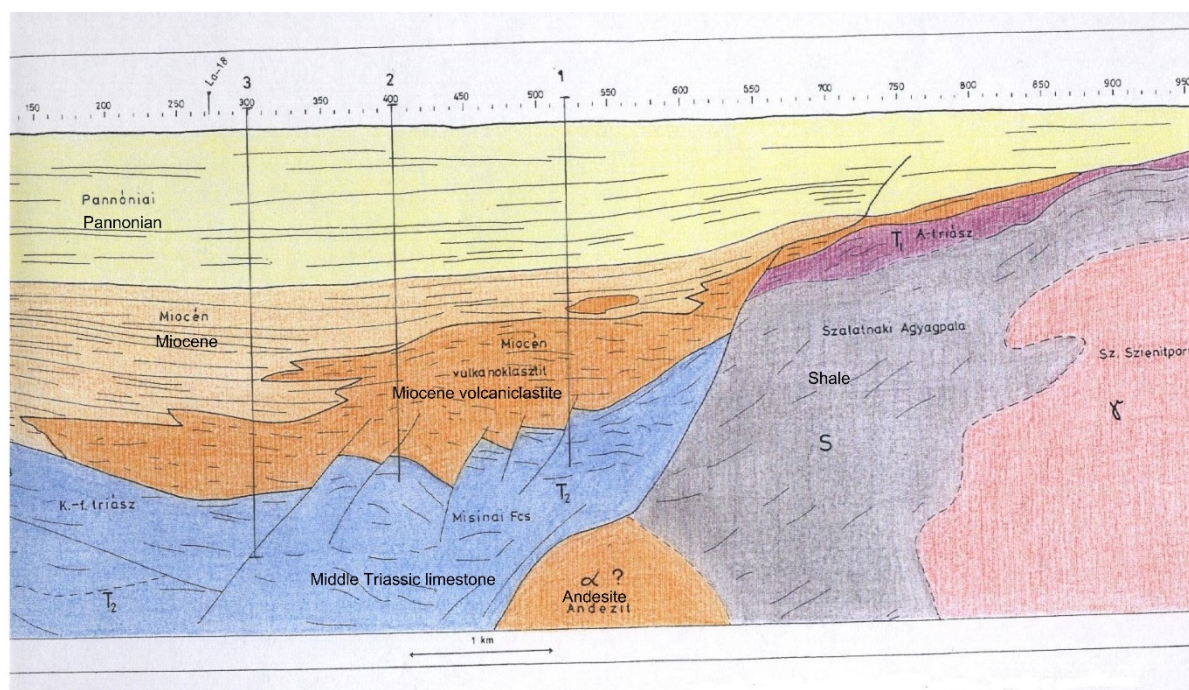


FIGURE 2: Geological cross-section of the Dombóvár area (Waterplan Ltd., 2016)

The area of interest has been analyzed by means of two 2D seismic lines, shown in Figure 3, which along with other geological data provide a general knowledge of the regional underground structure. According to the seismic interpretations, the target area of the reservoir is located at the eastern rim of

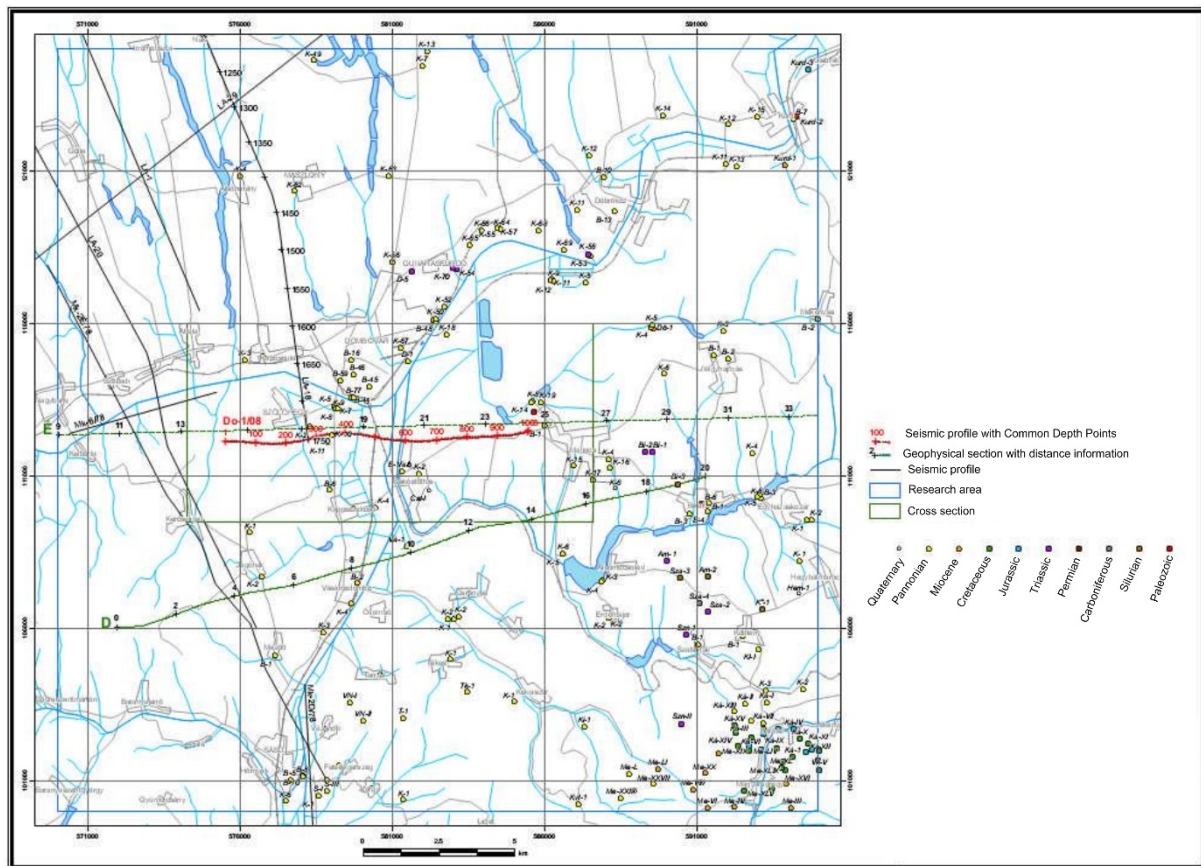


FIGURE 3: Local map showing the east-west trending seismic line Do 108 in red. The town of Dombóvár is located some 3 km north of the slight bend in the seismic line. North-south trending seismic line La – 18 (shown in black) is located just to the west of Dombóvár (Waterplan Ltd., 2016)

a basin, which is assumed to have been highly fractured due to tectonic uplifting. In addition, the basin itself has been confirmed by gravimetric and magnetic measurements carried out in the area.

The west-east cross-sections in Figures 4 and 5 show that the fractures on the eastern side of the basin reach from the basement through the Miocene up to the Pannonian, which indicates that some massive movement took place and leads to the assumption that the fractures should provide a good hydraulic connection into the lower basement.

The target geothermal reservoir is the Triassic limestone formation, which is not well defined in the area because few wells have been drilled into it. It is thought that after a small sedimentary hiatus, the Triassic sedimentary cycle of the Mecsek developed into the so-called German facies with continental Lower and Upper Triassic compression of shallow marine carbonate Middle Triassic rocks (Less, 2009). There are two wells in the area which have been drilled into the Triassic limestone to a depth of 2,250 and 2,450 meters, and both have confirmed a temperature of 120°C at a depth of 2000 m. With reference to these data and the experience from other geothermal projects in the area, the chances of finding hot water bearing fractures with good productivity is considered good.

With reference to the seismic cross-section of line Do-108 (Figure 4), there are two target areas for the establishment of the geothermal project. The first is between CDP (common depth point) 320 and 400 and the other between CDP 430 and 520. Both areas show highly faulted zones stretching from the upper Pannonian down to the lower Miocene and possibly into the basement.

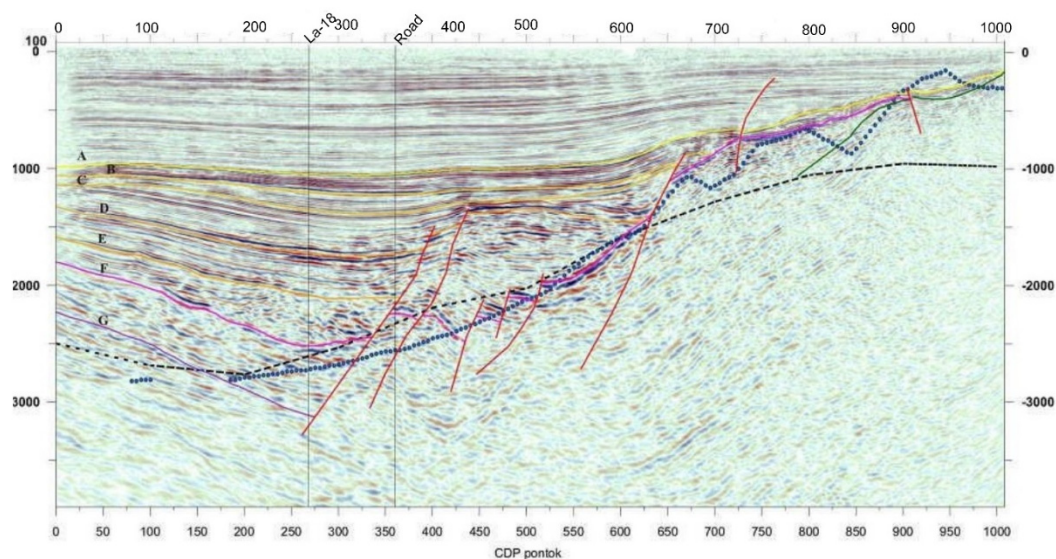


FIGURE 4: Seismic cross-section line Do-108 (west to east) (Waterplan Ltd., 2016)

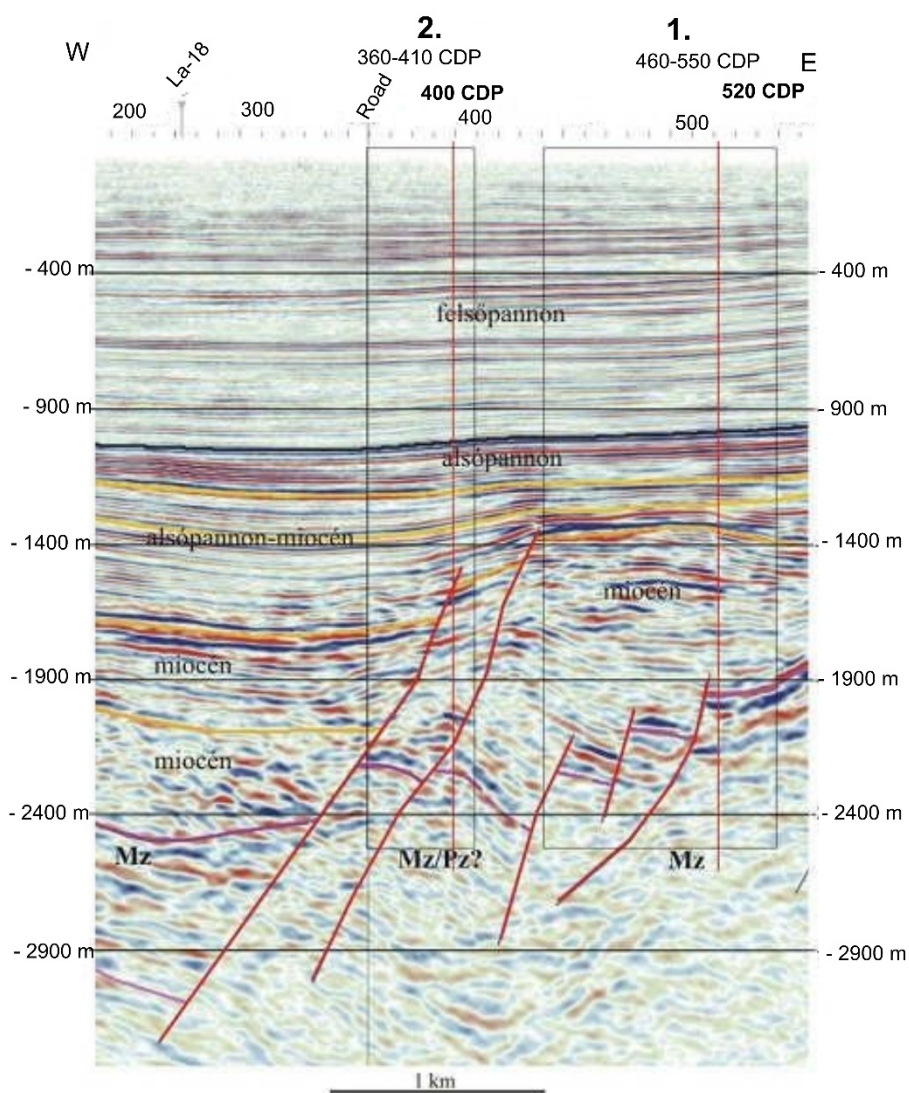


FIGURE 5. Seismic cross-section showing a close-up view of the basin between wells CDP 250 and 550 (Waterplan Ltd., 2016)

In addition to the geological and geophysical information referred to above, there are several shallower wells surrounding Dombóvár, e.g. Dombóvár K-47, K-54, K-60 and K-70, which comprise a depth range from 400 to 1500 m and which confirm a temperature gradient between 45 and 68°C/km with a production rate between 10 and 70 l/s. The regional temperature conditions are shown in Figure 6 and confirm a temperature of 120°C at 2000 m. The general trend of the surrounding wells confirms the assumption of a geothermal gradient of 50°C/km and a reservoir depth of 2300-2600 m, which would be the target depth for a geothermal well in this region according to the seismic cross-section. This would yield a minimum reservoir temperature of 125-140 or 145-160°C, assuming a temperature gradient of 60°C/km.

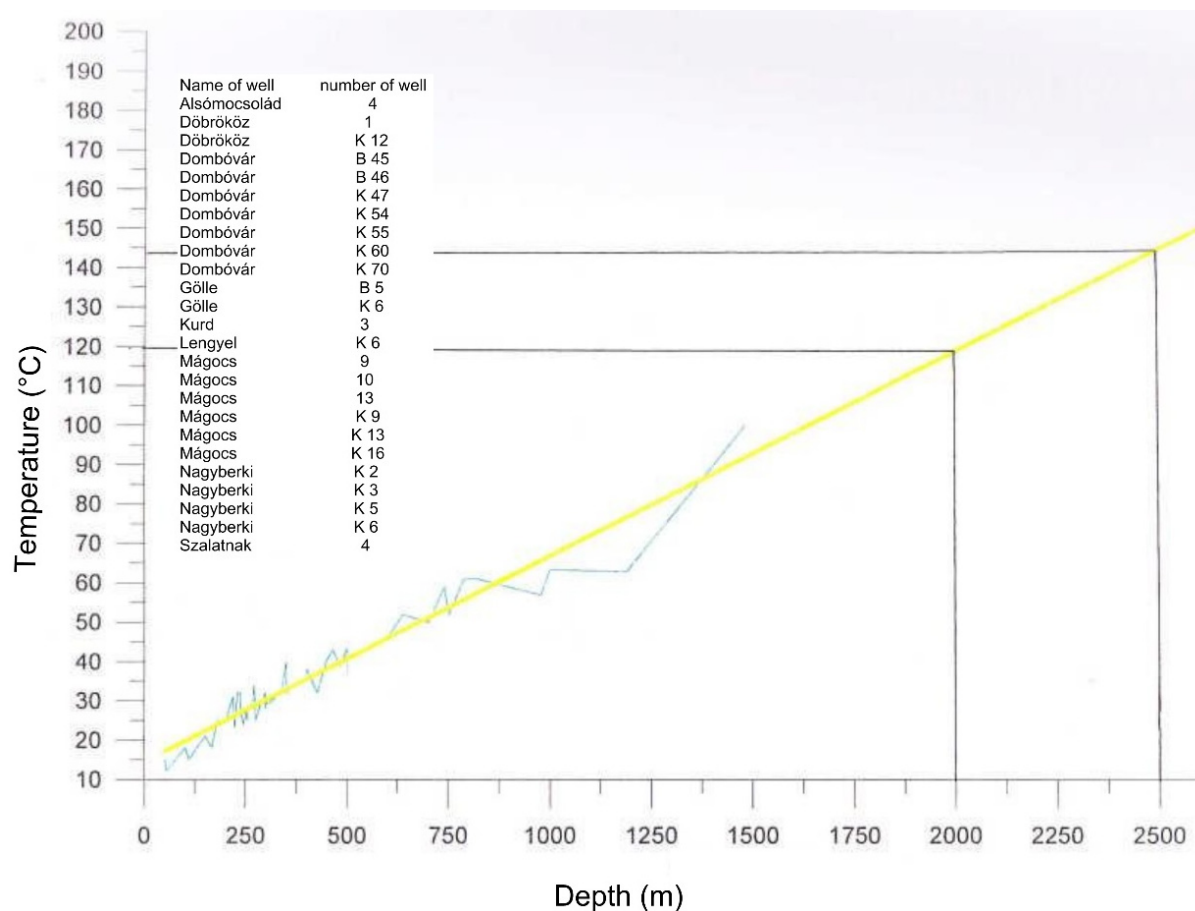


FIGURE 6: Temperature vs. depth measured in the Dombóvár region (Waterplan Ltd., 2016)

Rock temperature and water temperature data collected from wells which extend deeper than 100 m are shown on Figure 6. These wells were very scarce and unevenly distributed across the study area. However, the data do show an approximate straight line correlation between rock temperature and depth, indicating that they are close to equilibrium temperature. Using this relationship, the rock temperature from 0-2500 m depth can be estimated. According to this diagram, in the 2000-2500 m depth range, the temperature will be in the range 120-145°C.

With reference to the overall geological setting at Dombóvár, it can be stated that there is a reasonably big basin containing highly karstified limestone with good hydrological connection to the Miocene rocks, which should allow for relatively high production rates (above 70 l/s) with a reasonably acceptable drawdown.

3. NUMERICAL MODEL

A preliminary numerical reservoir model was created using available data in order to estimate the capacity of the reservoir and determine the next steps forward in the geothermal development plan.

3.1 Modelling software

The modelling software utilized for this study was VISUAL MODFLOW, MODPATH and MT3D for the heat transport. MODFLOW is a modular three-dimensional finite-difference groundwater model from the U.S. Geological Survey, and is used globally to describe and predict the behaviour of groundwater systems. The early versions of MODFLOW, MODFLOW-88 (McDonald and Harbaugh, 1988) and MODFLOW-96 (Harbaugh and McDonald, 1996a, 1996b) simulate groundwater flow including among other things, the effects of wells, rivers, drains, head-dependent boundaries, recharge and evapotranspiration. Since the publication of MODFLOW, various codes have been developed by numerous investigators. These codes are called packages, modules or sometimes simply programs. Packages are integrated with MODFLOW and each package deals with a specific feature of the hydrologic system to be simulated, such as wells, recharge or rivers. Models or programs can be stand-alone codes or can be integrated with MODFLOW. A stand-alone model or program communicates with MODFLOW through data files (Chiang and Kinzelbach, 1998).

3.2 Model construction

The total thickness of the model is 800 m, which represents the Triassic limestone formation in the area. The total thickness was divided into 4 layers with constant thicknesses. The top two model layers are each 200 m thick, layer 3 is 350 m thick, and the bottom layer (layer 4) is 50 m thick. It was assumed that the proposed production well is extracting from the upper layer (layer 1) and the reinjection well is injecting into model layer 2. The bottom layer (layer 4) was used to simulate heat transport from the deep basement formations below the reservoir.

A well duplet was defined in the model, consisting of a production well (well F2) and a reinjection well (well F1). A production rate of 1440 m³/day was assigned to the production well and the same amount is injected into the reinjection well. Because the proposed wells are both targetting the same reservoir, it can be assumed that there is a good hydrologic connection between the two. The expected temperature of the reservoir at the production depth is between 120 and 145°C and the expected temperature of the produced water at the wellhead is around 110°C. The reinjection fluid temperature was defined as 50°C in the model.

It was decided to model a 10 km × 10 km area around the proposed well duplet. The model area is therefore a square with a total area of 100 km². The eastern model boundary corresponds to a lithological boundary with impermeable rock (clay) to the east. Therefore, a no-flow model boundary was defined along this boundary.

It was assumed that lateral recharge enters the reservoir from the north, west and south. Therefore, the north, west and south model boundaries were defined as constant pressure boundary conditions. Impermeable formations lie above and below the geothermal reservoir, so the model assumes no vertical leakage into the reservoir.

All four model layers were given the same hydraulic parameters because they all consist of the same Triassic limestone formation. There is no available data to suggest major differences in the limestone formation with depth. Therefore, average values taken from the literature for fractured, karstified limestone were assigned in the model (Waterplan Ltd., 2016). The hydraulic conductivity defined in each model layer was 5×10^{-7} m/s, which should be a conservative estimate. The porosity was set to 1%

in all model layers. The constant pressure boundaries were difficult to estimate since there is no available data. It was, however, decided that a fixed pressure of 120 m a.s.l. was appropriate.

The model area, numerical grid and boundary conditions are shown in Figure 7, while a vertical cross-section of the model is shown in Figure 8. The green area, the zone around the reinjection well, is where the maximum cooling is expected to take place, and the red lines are the constant pressure boundary conditions. In Figure 8, the yellow area shows the location of the point source for the reinjection well and the grey area the point source for the production well. The blue area in Figure 8 (model layer 4) shows the constant heat source from below the reservoir.

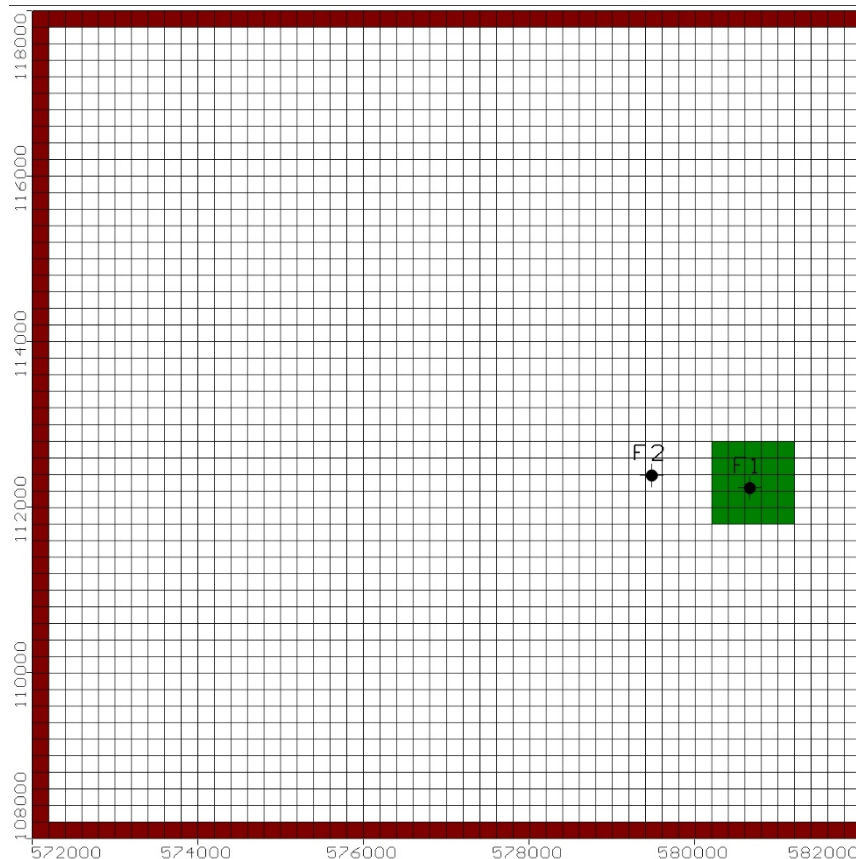


FIGURE 7: Reservoir model area and numerical mesh

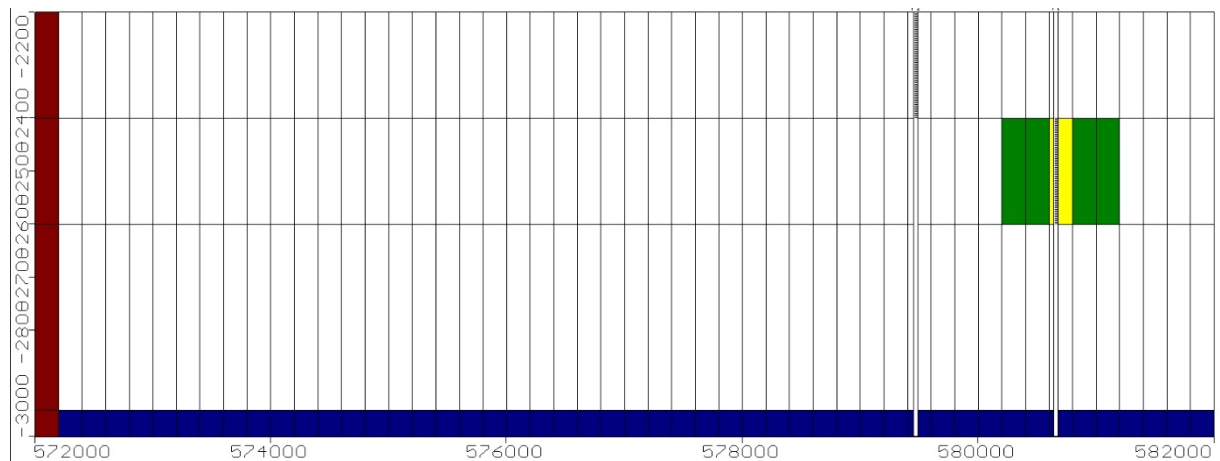


FIGURE 8: Cross-section of the reservoir model

4. RESULTS

4.1 Effects on reservoir pressure

The model was run for a simulation period of 100 years in order to determine the long-term effects of the production and reinjection. The effects of the proposed well duplet on the reservoir pressure in model layer 1 are shown in Figure 9 (groundwater contours are shown in m a.s.l.). The production causes approximately 50-60 m pressure decrease at the production well in the production layer.

Figure 10 shows calculated streamlines within layer 1 indicating the direction of groundwater flow in the vicinity of the wells. The red lines indicate flow into the production well and the green lines indicate flow from the injection well. The distance between the arrows on the lines indicate the flow path traveled during a 10-year period.

4.2 Effects on reservoir temperature

The MODFLOW software package used for modelling does not include a module for simulating temperature changes in the reservoir. However, the water-soluble contaminant transport program MT3D has been used in previous studies to simulate heat transport in low-temperature geothermal reservoirs and it was decided to use this approach (Hecht-Méndez et al., 2010).

Figures 11-17 show the results of the heat flow simulation at different time increments. Figure 11 shows the calculated reservoir temperature in layer 2 after 10 years. As the figure shows, the reinjection well is cooling the reservoir around it, with the cooling effect reaching out radially approximately 0.2 km from the reinjection well. Figure 12 shows the results in cross-section view after 10 years. In addition to lateral spreading of the cooling zone, the cooling also extends vertically from layer 2 into layers 1 and 3 above and below.

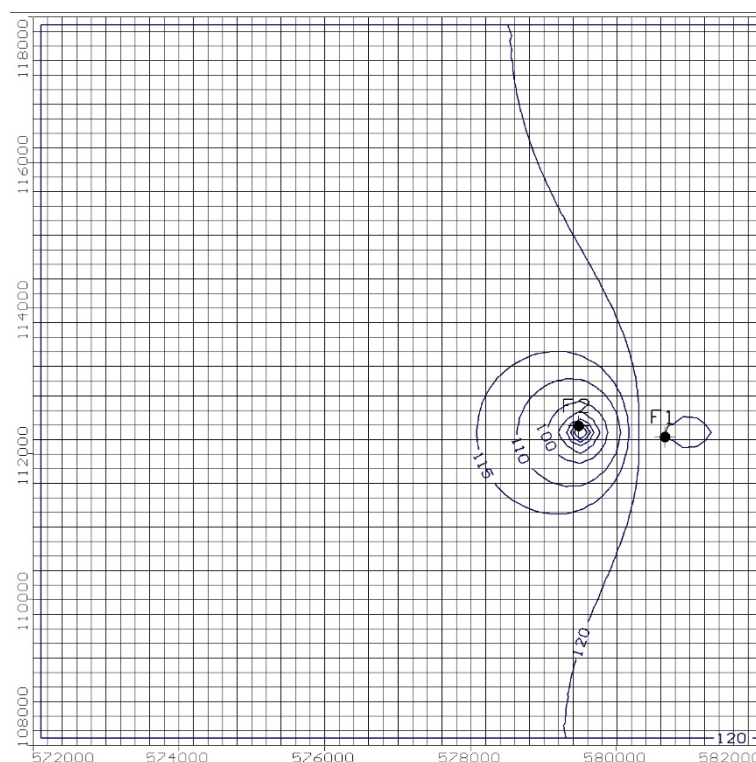


FIGURE 9: Calculated groundwater levels in model layer 1

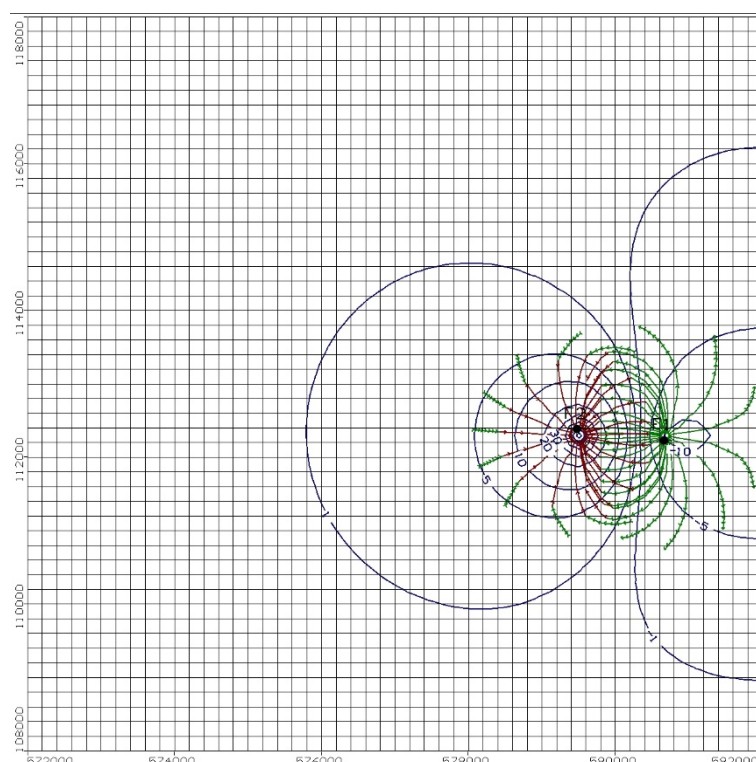


FIGURE 10: Calculated groundwater streamlines in model layer 1

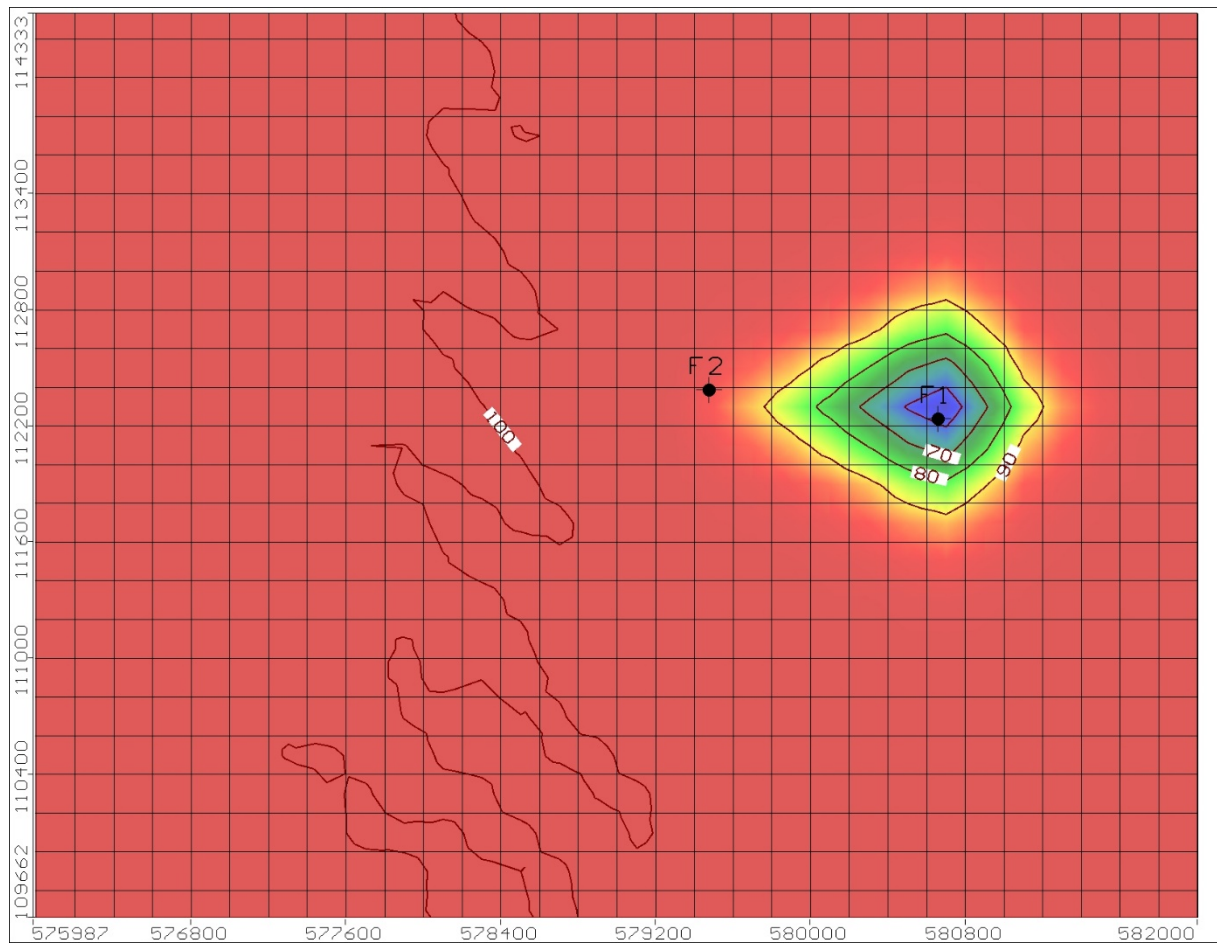


FIGURE 11: Calculated reservoir temperature in layer 2 after 10 years

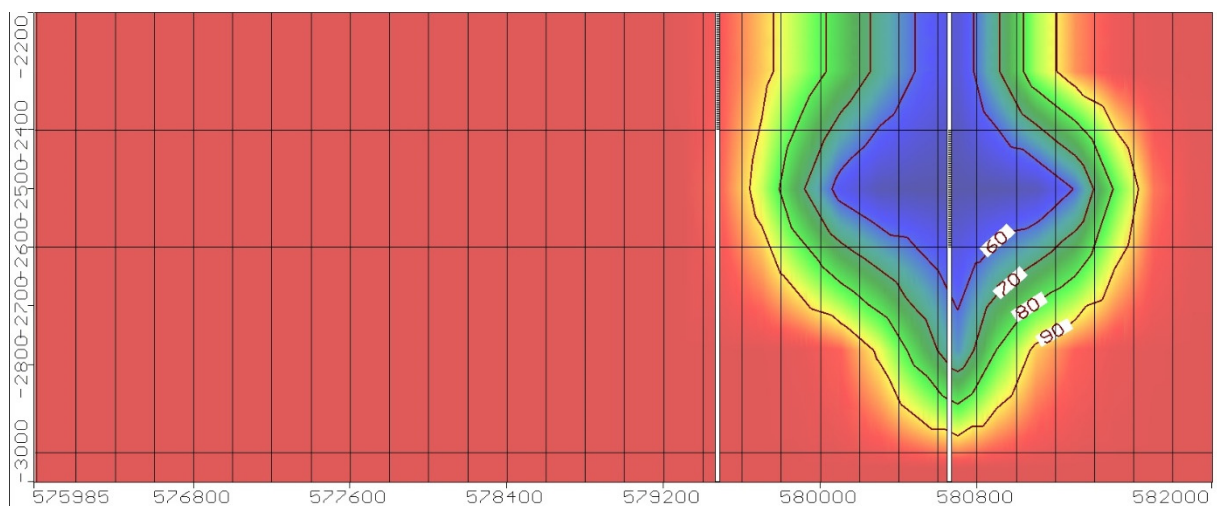


FIGURE 12: Cross-section showing calculated reservoir temperature after 10 years

Figure 13 shows the calculated reservoir temperature in layer 2 after 50 years. As the figure shows, the cooling effect is spreading further out into the reservoir with time, with the cooling effect reaching out approximately 0.8 km from the reinjection well. Figure 14 shows the results in cross-section view after 50 years.

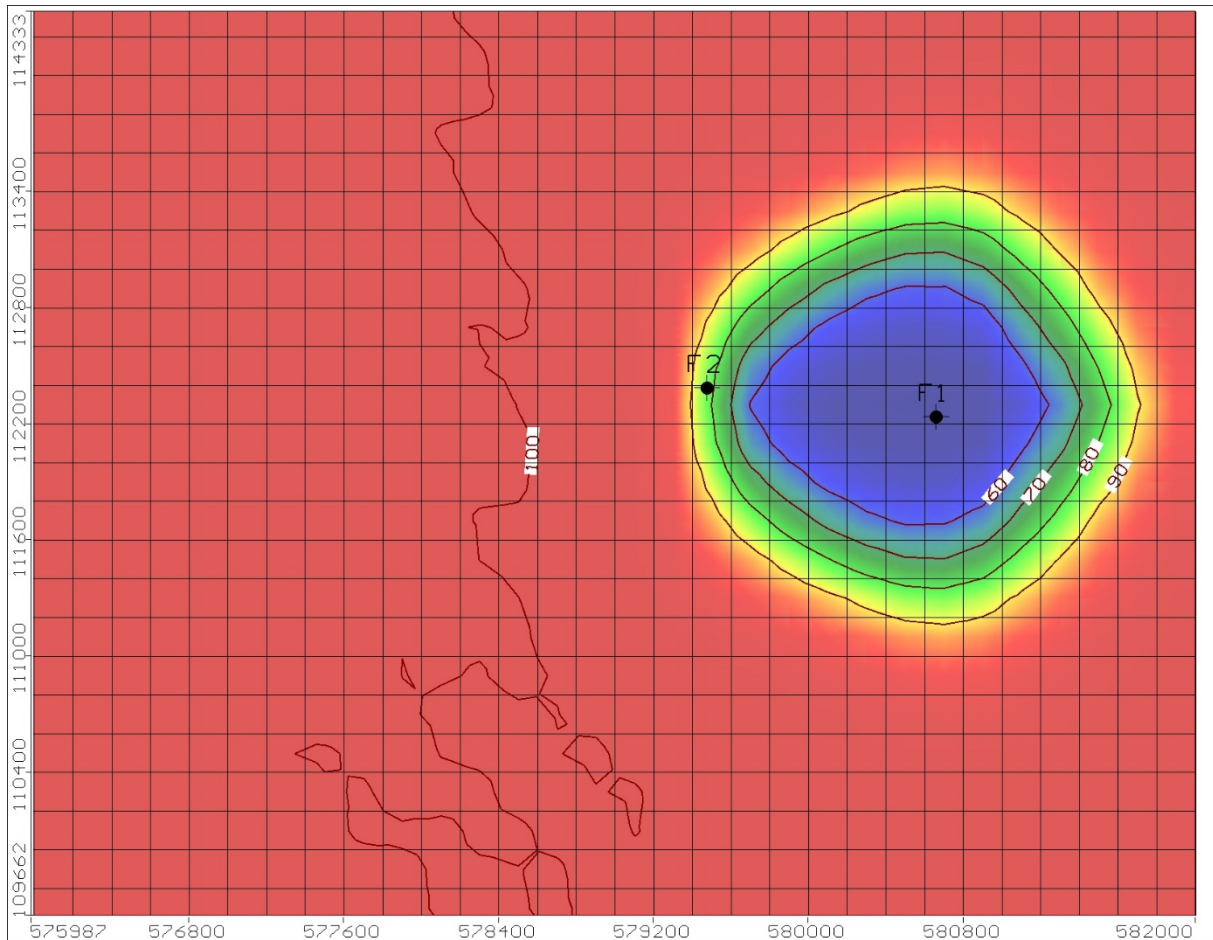


FIGURE 13: Calculated reservoir temperature in layer 2 after 50 years

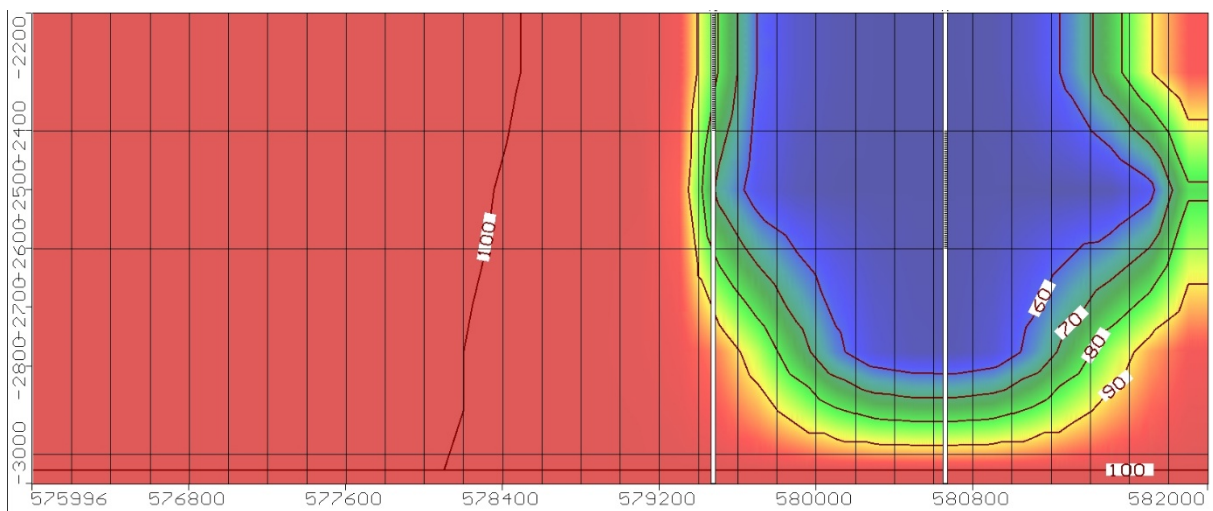


FIGURE 14: Cross-section showing calculated reservoir temperature after 50 years

Figure 15 shows the calculated reservoir temperature in layer 2 after 100 years, while Figure 16 shows the results in cross-section view after 100 years. The cooling effect now reaches out approximately 1 km from the reinjection well.

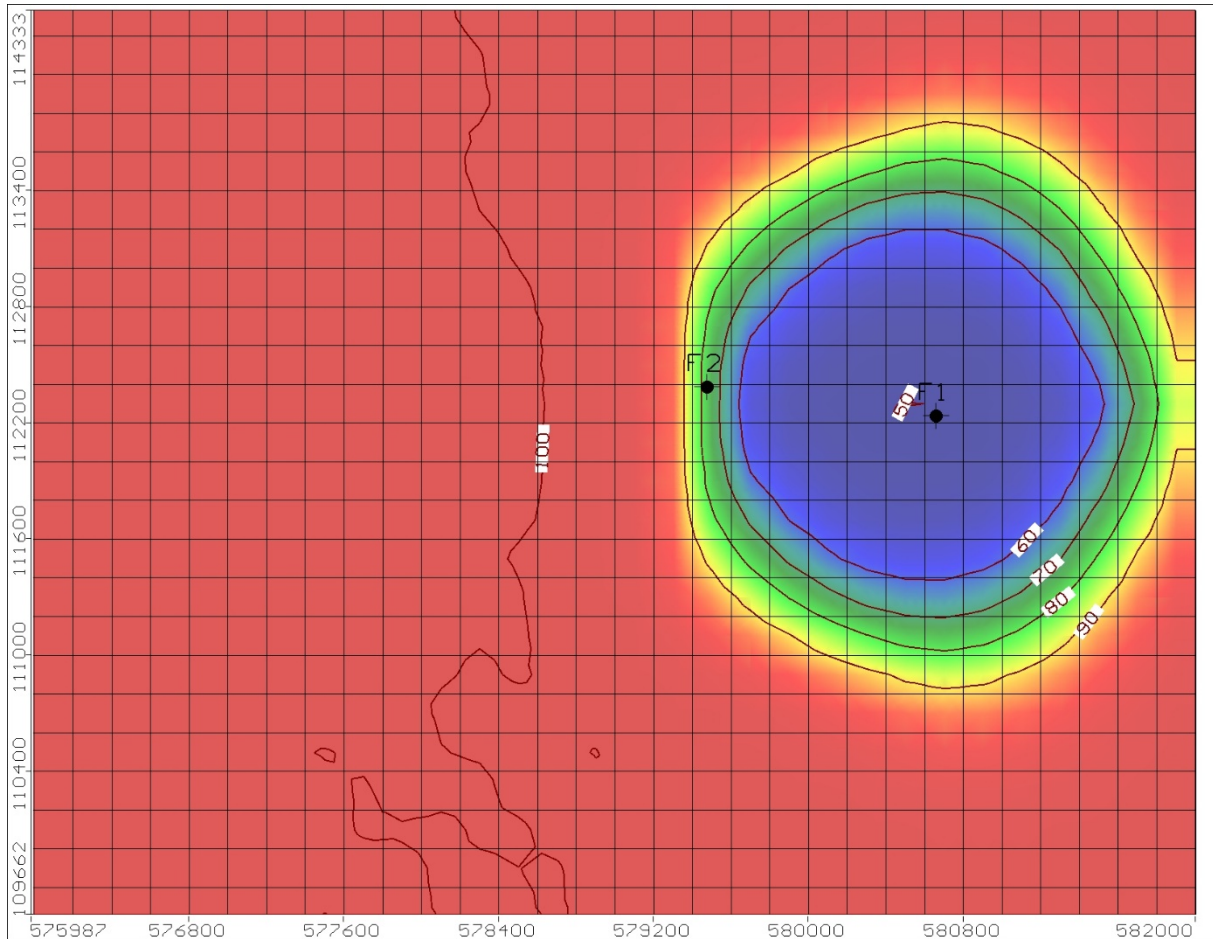


FIGURE 15: Calculated reservoir temperature in layer 2 after 100 years

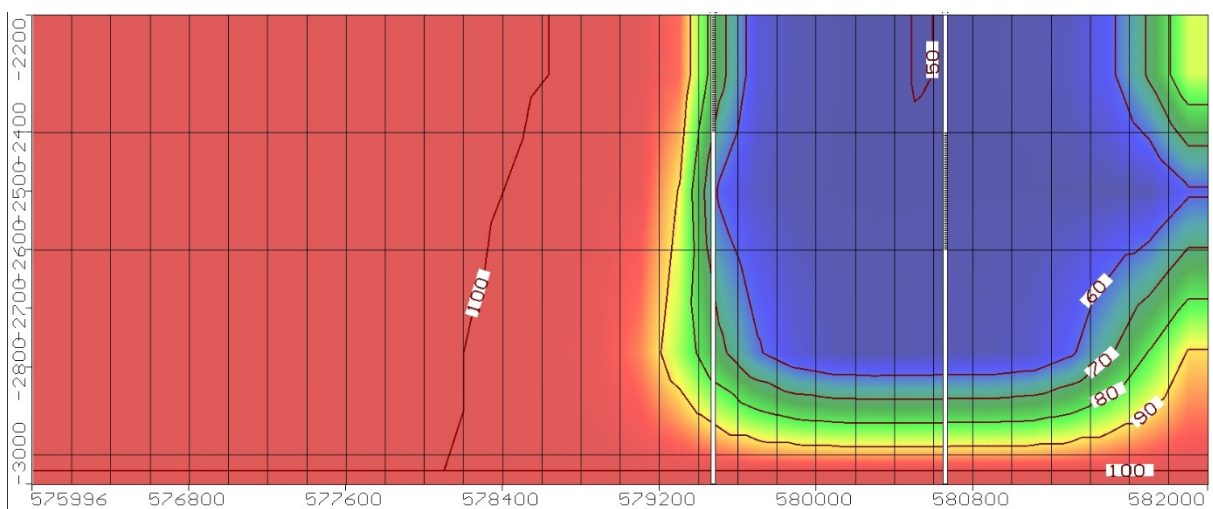


FIGURE 16: Cross-section showing calculated reservoir temperature after 100 years

The calculated mixing zone in the reinjection layer after 100 years is shown in Figure 17. As expected, the cooling of the reservoir extends furthest laterally within the layer where the reinjection is taking place (model layer 2). The cooling spreads less within the other layers. Therefore, we define the impact area of the reinjection as the mixing zone in the reinjection layer (layer 2) as shown on Figure 13. Using this definition, the impact area is a circular area centred on the reinjection well with a radius of approximately 2000 m.

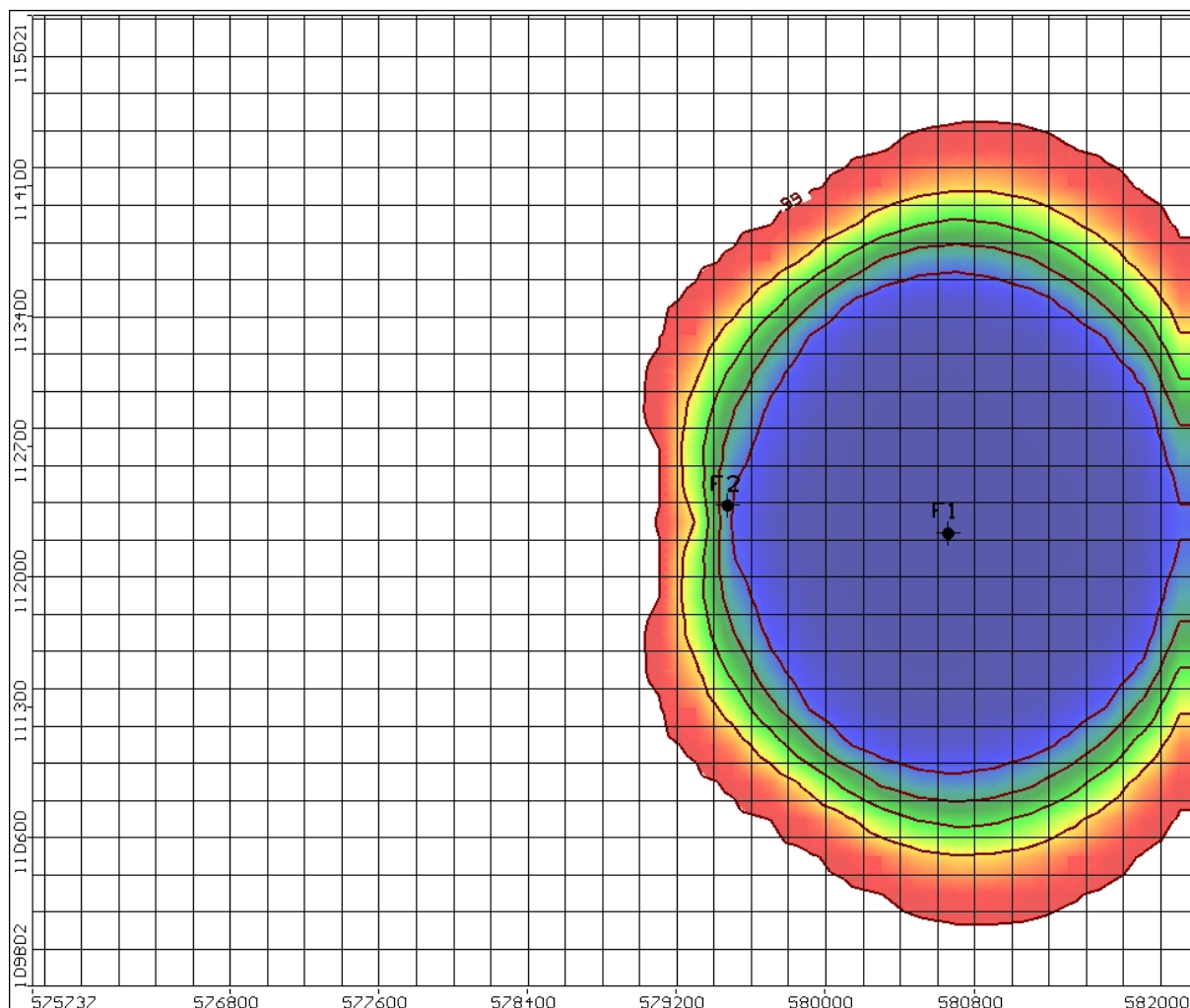


FIGURE 17: Calculated mixing zone in the reinjection layer (layer 2)

The streamlines of groundwater flow between the wells (Figure 10) indicate that there is a hydrological connection between the wells. This connection means that the cooling effects from the reinjection well are likely to lower the temperature of the reservoir fluid at the production well with time. The calculated temperature decrease at the production well is plotted in Figure 18. Calculated temperature is given in percentage of the original background temperature in the reservoir. The expected temperature values after 10 years (3650 days), 50 years (18,250 days) and 100 years (36,500 days) are marked on the diagram. According to these results, the temperature of the produced water will decline by about 20% after 50 years of production.

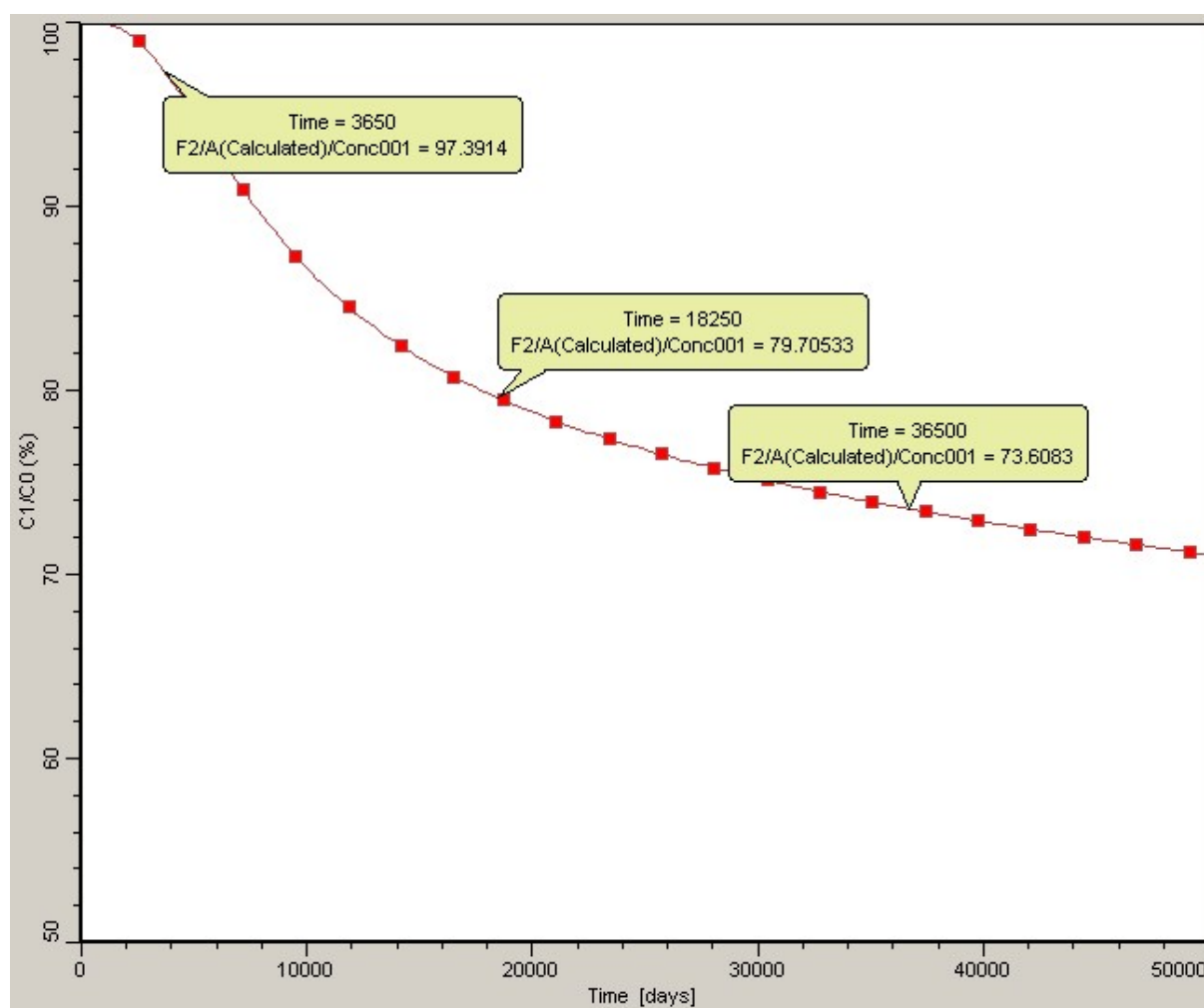


FIGURE 18: Calculated temperature decrease at the production well after 10, 50 and 100 years

5. CONCLUSIONS

Results from this preliminary modelling work indicate that the geothermal reservoir at Dombóvár can support the proposed well duplet and serve as a long-term sustainable resource for geothermal heat production. The effects of the proposed well duplet on the pressure and temperature in the reservoir are within acceptable limits for maintaining production. Therefore, it can be recommended that the next phase of the resource development plan be implemented. This next phase should focus on geological and geophysical measurements and data collection from the local reservoir in order to gain a better understanding of the system. Hydrological parameters used in the model were based on best-guess estimates due to lack of data. Updating the model with actual measured values for hydraulic conductivity and porosity from the reservoir would improve the reliability model.

The first step in the MVM geothermal development plan is to supply the industrial park with geothermal space heating. The proposed well duplet is expected to supply this demand, but additional wells could be needed. In that case, an updated reservoir model would be a good tool for determining the location and capacity of additional wells. There is an ongoing contract between the town and a local district heating company, which uses gas-driven engines for heating water. It is expected that within the next 8 years, this system will be outdated and will need to be replaced. The future goal of the town is to change the entire district heating system to a "green" geothermal energy system.

ACKNOWLEDGEMENTS

I would like to thank my supervisor Eric M. Myer from Vatnaskil for the patient guidance, encouragement and advice he has provided throughout my time as his student. I have been extremely lucky to have a supervisor, who cared so much about my work and who responded to my questions and queries so promptly.

I would also like to thank all the members of staff at UNU-GTP for the past half year, I will always keep this memory in my heart.

To my dad, Peter Unyi, and his company, Waterplan Ltd., thanks for the data and for the support from home, as well as to my mom Monika Unyi and my siblings, Laura and András, for the support.

And last but not least, to all of my new friends here at UNU-GTP, thanks for all the great memories, the running team for unforgettable races, and lots of laugh.

Thank you all!

REFERENCES

Chiang, W.-H., and Kinzelbach, W., 1998: *Processing Modflow, a simulation system for modelling groundwater flow and pollution*. ETH, Zürich.

Fodor, L., Csontos, L., Bada, G., Györfi, I., and Benkovics, L., 1999: Tertiary tectonic evolution of the Pannonian Basin system and neighbouring orogens: a new synthesis of palaeostress data. In: Durand, B., Jolivet, L., Horváth, F., and Séranne, M. (eds.): *The Mediterranean basins: Tertiary extension within the Alpine Orogene*. *Geol. Soc. London, Spec. Publ.*, 156, 295-334.

Harbaugh, A.W., and McDonald, M.G., 1996a: *User's Documentation for MODFLOW-96, an update to the U.S. Geological Survey modular finite-difference ground-water flow model*. US Geological Survey, Reston VA, open-file report 96-485, 63 pp.

Harbaugh, A.W., and McDonald, M.G., 1996b: *Programmer's documentation for MODFLOW-96, an update to the U.S. Geological Survey modular finite-difference ground-water flow model*. US Geological Survey, Reston VA, Open-File Report 96-486, 220 pp.

Hecht-Méndez, J., Molina-Giraldo, N., Blum, P., and Bayeret, P., 2010: Use of MT3DMS for heat transport simulation of shallow geothermal systems. *Proceedings of the World Geothermal Congress 2010, Bali, Indonesia*, 8 pp.

Horváth, F., 1995: Phases of compression during the evolution of the Pannonian Basin and its bearing on hydrocarbon exploration. *Marine and Petroleum Geology*, 12-8, 837-844.

Horváth, F., Bada, G., Windhoffer, G., Csontos, L., Dombrádi, E., Dövényi, P., Fodor, L., Grenerczy, G., Sikhegyi, F., Szafián, P., Székely, B., Timár, G., Tóth, L., and Tóth, T., 2006: Atlas of the present-day geodynamics of the Pannonian basin: Euroconform maps with explanatory text. *Magy Geofiz.*, 47-4, 133-137.

Less G., 2009: *Geology of Hungary*. TÁMOP, 16 pp.

McDonald, M.G., and Harbaugh, A.W., 1988: *A modular three-dimensional finite-difference ground-water flow model*. U.S. Geological Survey Techniques of Water-Resources Investigations, book 6, Chapter A1, Reston VA, 586 pp.

Waterplan, Ltd., 2016: *Preliminary study of Kaposszekcső geothermal well drilling* (in Hungarian). Waterplan, Ltd., report, 63 pp.



UNITED NATIONS
UNIVERSITY

UNU-GTP

Geothermal Training Programme

Orkustofnun, Grensasvegur 9,
IS-108 Reykjavik, Iceland

Reports 2016
Number 41

MODELLING OF TRACER TESTS IN A GEOTHERMAL RESERVOIR IN TIANJIN, CHINA

Wang Wanli

Institute of Hydrogeology and Environmental Geology - IHEG
268 North Zhonghua Street, Shijiazhuang
050061, Hebei Province
P.R. CHINA
Wanliwang2010@163.com

ABSTRACT

The Wumishan (Jxw) geothermal reservoir in the Dongli Lake area is an extensive, low-temperature geothermal system hosted mainly by Mesoproterozoic dolomitic limestone. In order to study the flow paths and predict the cooling due to long term injection, tracer tests were performed on the 17th of December, 2015. 700 kg of Ammonium Molybdate (Mo) were injected into well DL-48B. No obvious tracer recovery was detected in the water samples collected during the 90 days of tracer test. In order to interpret the tracer testing quantitatively, both an analytical method developed by ISOR (Iceland GeoSurvey) and a numerical method using Visual MODFLOW flex software were applied. For the analytical model, it was assumed that the recovery is very slow and would appear after 90 days. In the three cases of longitudinal dispersivity, 77, 230 and 384 m, the tracer concentration began to increase after 150 days. When the dispersivity was 77 m, thermal breakthrough would occur in 80 years for a narrow flow channel scenario and 27 years for a wide flow channel scenario with an average annual production and injection rate of 10 kg/s. Using an automatic parameter estimation tool along with the numerical model, errors were minimized between the observed and the simulated data to estimate the distribution of the reservoir parameters. There is reasonable agreement between the simulated and observed water levels and therefore the numerical model was used to predict the tracer concentration in the production well. For the most pessimistic case (longitudinal dispersivity of 384 m), the tracer will take more than a year to arrive at the production well with concentration values outside of the detection limit, according to the model. Results show that there is no direct connection between production and injection wells and neither of the models predicts cooling in the next 24 years.

1. INTRODUCTION

Geothermal reinjection is important in geothermal reservoir management because it helps maintain reservoir pressure. It has become an integral part of sustainable and environmentally friendly geothermal utilization projects. However, it poses the possible danger of cooling production wells (Axelsson, 2012a). An optimum reinjection strategy should balance the requirements of sustaining the reservoir pressure and preventing early thermal breakthrough of reinjected water (Diaz et al., 2016).

Tracer testing has been widely used and proved to be an important and useful tool in studying the impact of reinjection (Axelsson et al., 2005; Mondejar, 2012; Koech, 2014; Pang, 2010). In conventional geothermal development, tracer testing can provide information on the flow-paths between injection and production wells and help predicting the danger and rate of cooling of the production wells during long-term reinjection (Axelsson, 2013).

Most tracer test interpretations are only used in a qualitative manner to assess injector-producer connectivity without taking advantage of other information carried within a full tracer response curve (Alamadhan et al., 2015). To interpret the tracer testing quantitatively, both an analytical method developed by ISOR (Iceland GeoSurvey) and a numerical method using Visual MODFLOW flex software were applied. The results are described in this report.

The study area, Dongli Lake, is located in Tianjin Binhai New District with an area of 62 km² (Figure 1). This area is rich in low-temperature geothermal resources, which are stored in sedimentary reservoirs consisting mostly of Mesoproterozoic dolomitic limestone (Duan et al., 2011). Geothermal wells are mostly located in the regional structural high, known as the Cangxian uplift (Minissale et al., 2008). The geothermal water is mainly used for space heating during winter and also for bathing and agriculture (Axelsson and Dong, 1998).

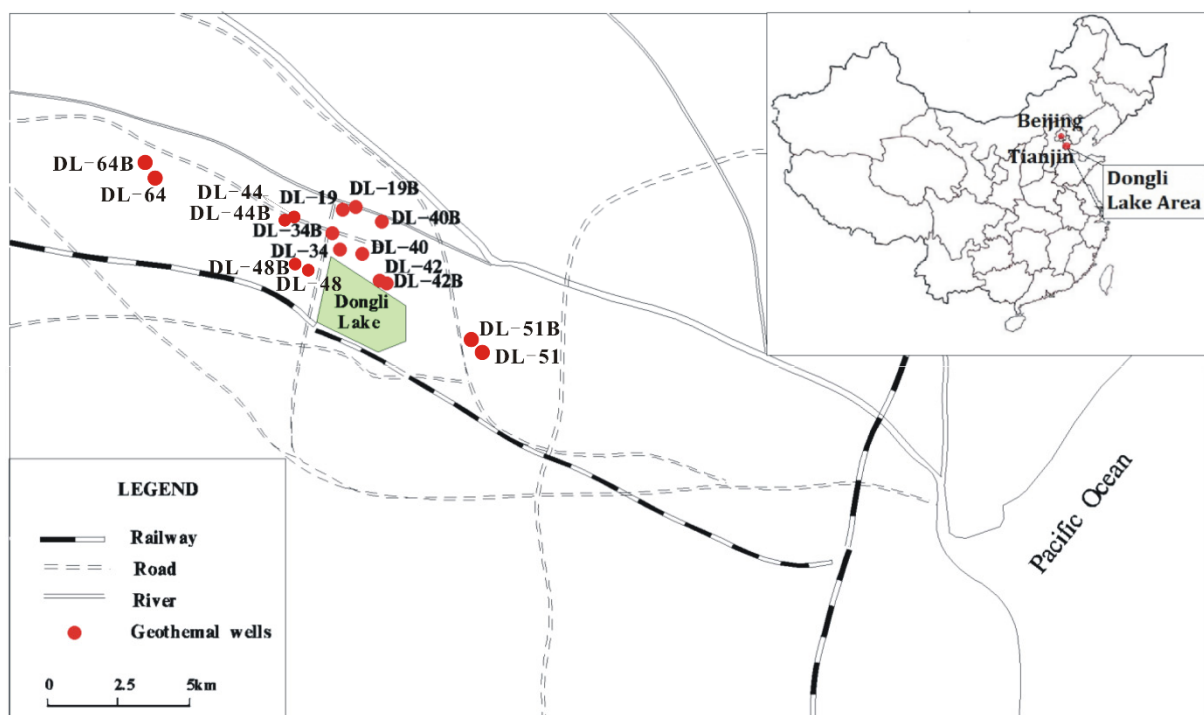


FIGURE 1: Map of the study area (modified after Zhao, 2010)

Due to gradually increased production and development, the water level has been falling 6-9 m per year since 1997 and a regional cone of depression has formed (Cheng et al., 2010). Therefore, in order to maintain reservoir pressure and prolong the lifetime of the production wells, reinjection of the used geothermal water started in 2001 (Duan et al., 2011). Reinjection provides an additional recharge to geothermal reservoirs. However, the water level has still been dropping nearly 3 m per year since 2011 due to large scale development (Ruan et al., 2015).

In order to study the flow paths and predict the cooling of long term injection, tracer testing was performed. The test started on December 17, 2015, with 700 kg of Ammonium Molybdate (Mo) injected

into the injection well DL-48B (Figure 1). Water samples were collected from eight production wells within a 3.3 km radius from the injection well for up to 3 months.

In this project, the aim is to model the flow patterns and predict the cooling time in the geothermal reservoir. Since no tracer was detected in the samples, tracer recovery was simulated and predicted based on several assumptions for the analytical method. Furthermore, a numerical model was built in order to demonstrate physical processes in the study area, and predict the change of concentration over a long time period after tracer injection.

2. THE GEOTHERMAL FIELD

2.1 Geological setting of the study area

The geothermal reservoir in Tianjin can be divided into a porous part and a bedrock part (An et al., 2016) (Figure 2). According to borehole data (Tian, 2014), the porous geothermal reservoir consists of continental sediments (Cenozoic Mesozoic Minghuazhen Group (Nm) and Guantao Group (Ng)) and their permeability is dominated by primary porosity. The Karstic-fracture geothermal reservoir (Paleozoic Ordovician (O), Cambrian (ϵ) and Mesoproterozoic Jixian Wumishan Group (Jxw)), is up to 6000 m thick with fracture-dominated secondary permeability (Minissale et al., 2008).

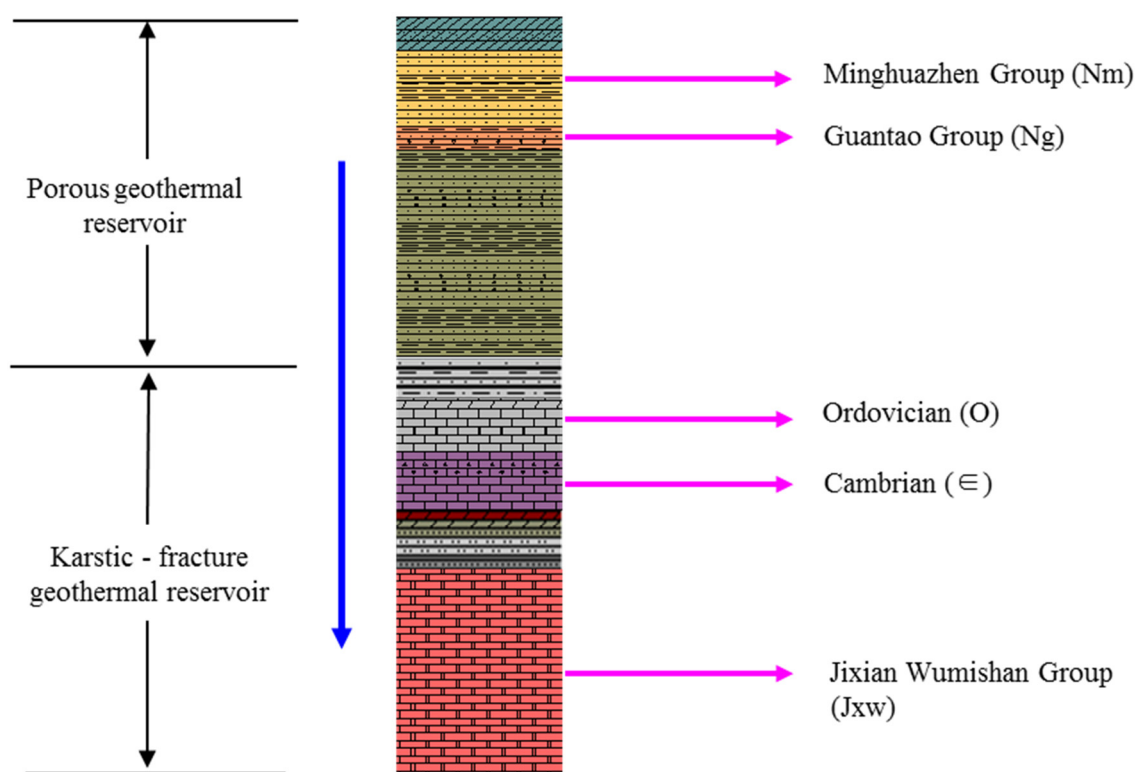


FIGURE 2: Geologic setting of the main geothermal reservoir

The Tianjin reservoir is bounded by the Tianjin fault in the west, by the Haihe fault in the south, and by the Hangu fault in the north (Zhao, 2010) (Figure 3). The most important one is the Cangdong fault, which crosses the study area and has a great impact on both the strata and heat (Figure 3). The Wumishan formation lies at a much shallower depth in the west of the Cangdong fault than in the east side of the fault. Near the fault, the strata has high permeability and conductivity.

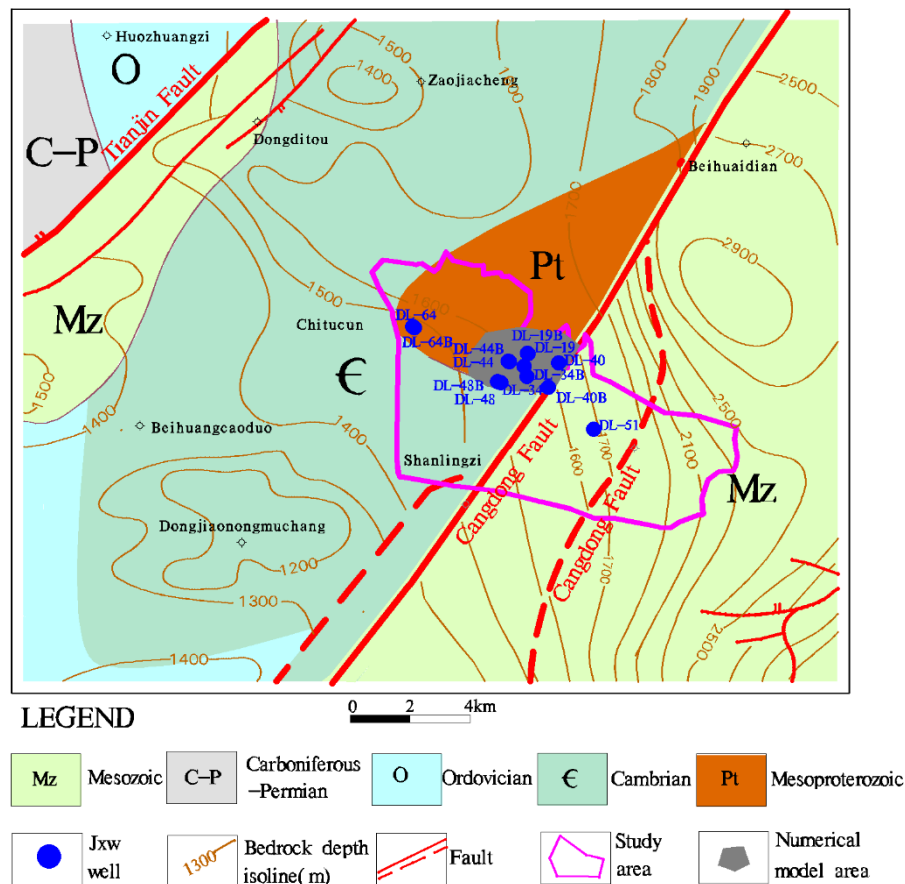


FIGURE 3: Geological formations and structures of the study area

2.2 The geothermal reservoir – Jxw

The Wumishan geothermal reservoir (Jxw) is the area of study in this project. It mostly consists of Mesoproterozoic dolomitic limestones (Duan et al., 2011). Therefore, the reservoir has good karst features, i.e. high temperature and high production rates (Zhao, 2010). From the previous study in this area, it is known that the fracture rate of this reservoir varies from 40 to 70% and in some wells, the rate is up to 80-90% (Lin, 2006).

The Quaternary and Tertiary formations consist of clay and sandstone, forming a good caprock of the geothermal reservoir. They are of low thermal conductivity and low permeability with thickness of 280-320 m. The Cangdong fault is a major fault in this area which can conduct heat from the bottom of the reservoir to the shallow part by heat convection. Heat convection becomes weaker with increasing distance from the fault (Zhao, 2010). The heat source of the reservoir is presumably an upper mantle heat-flow anomaly and radioactive decay from granite (8-16 km depth). According to isotopic analysis, the origin of the water in the reservoir is meteoric from ancient times.

Geothermal wells are mostly located near the Cangdong fault (Figure 3). Thirteen geothermal wells have been drilled into the reservoir (see Table 1). Average well production rates are in the range of 70-120 m³/h, with wellhead temperatures between 88 and 102°C (Fan, 2006; Tian, 2014). However, no well completely penetrates the reservoir and its thickness is unknown. Drilling data shows that west of the Cangdong fault, the top depth of the reservoir varies from 1752 to 2016 m, with a thickness of 480 to 1032 m. However, on the east side of the fault, only well DL-51 penetrates the reservoir, here the depth to the top is 3581 m and the thickness 153 m.

TABLE 1: Details of geothermal wells in the Dongli Lake area (Jxw) (Tian, 2014)

Well	Reservoir	Depth (m)	Temperature at wellhead (°C)	Max flow rate (m ³ /h)	Thickness of the reservoir (m)
DL-44	Jxw	2373.14	98	112.78	462
DL-44B	Jxw	2495	98	112.78	468
DL-34	Jxw	2327.1	100	204.61	
DL-34B	Jxw		96.5	140 [*]	
DL-19	Jxw	1842	83	49.2	
DL-19B	Jxw	2384.36	88	117.98	
DL-40	Jxw	2328.01	98.5	126.04	534
DL-40B	Jxw	2278.99	101	126.04	509
DL-51	Jxw	3634	97	70.71	153
DL-48	Jxw	2328.7	93	121.97	374
DL-48B	Jxw	2533.7	93	112.78	671
DL-64	Jxw	2564.6	93	126	798.6
DL-64B	Jxw	2783.81	96	119	1031.81

* Zhao (2010)

The water types in the study area of the Wumishan formation thermal reservoir are mainly $\text{HCO}_3\cdot\text{Cl}\cdot\text{SO}_4\cdot\text{Na}$ and $\text{HCO}_3\cdot\text{Cl}\cdot\text{Na}$, and the mineralization degree is 1600-2200 mg/L. The further the distance is to the Cangdong fault, the higher mineralization degree is observed in the geothermal wells (Ruan et al., 2015).

2.3 Reservoir temperature

Reservoir temperature analysis is based on data from injection well DL-48B. Figure 4 shows the warm-up temperature logs of well DL-48B. It is assumed that the well had reached thermal equilibrium in November 2015, hence the profile measured on November 2015 should reflect the true formation temperature.

Formation temperature increases gradually from the surface to about 1875 m depth, this indicates that conduction is the dominant heat transfer process within the formation. The top of the Jxw reservoir and the main feed zone seems to be intersected, as a fast increase of temperature indicates, reaching the maximum of 99.92°C at 1900 m depth. At greater depth, a temperature reversal is observed, most likely associated with the development of fissures in the well causing cold water to enter. Considering other wells nearby, the temperature stays constant when the depth increases, which indicates that convection dominates heat transfer in this formation, not conduction.

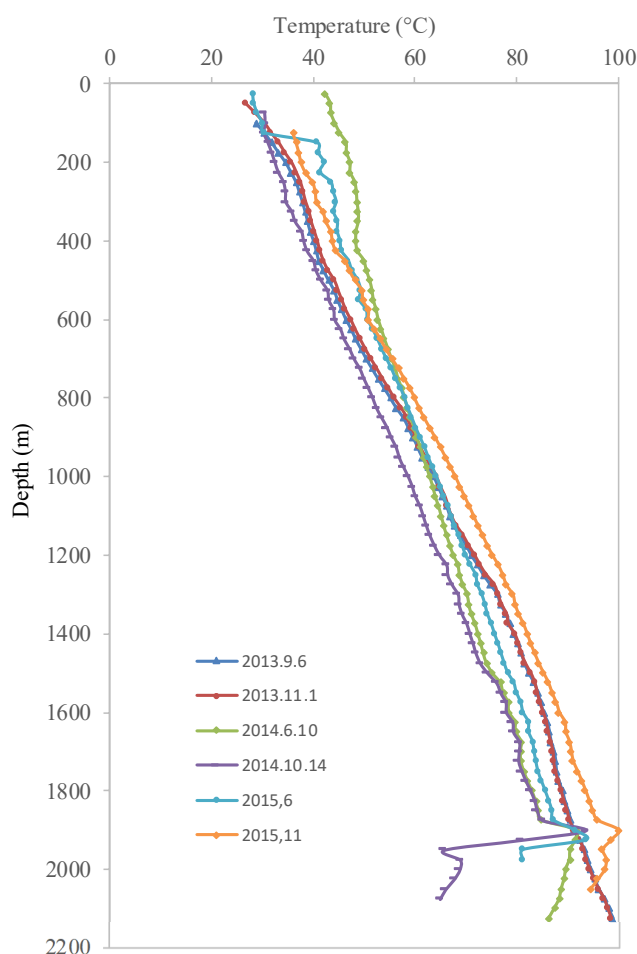


FIGURE 4: Warm-up temperature profiles from injection well DL-48B

2.4 Production in the study area

The exploration of the geothermal resources in the Dongli Lake area started in the 1980s (Zhao, 2010). With the increasing water demand for space heating and domestic water supply, the total production and the number of wells gradually increased.

Currently, there are 22 geothermal wells in this area, including 13 wells in the Wumishan geothermal formation – 7 production and 6 injection wells. In 2008 and 2009, the total annual production and injection were only $59.4 \times 10^4 \text{ m}^3$ and $53.4 \times 10^4 \text{ m}^3$, respectively (Zhao, 2010). In 2012, the total production rapidly increased and reached $140.7 \times 10^4 \text{ m}^3$ (Ruan et al., 2015). In 2013, the production increased to $157.4 \times 10^4 \text{ m}^3$, with a slight decrease in the production in 2014, to $147.0 \times 10^4 \text{ m}^3$.

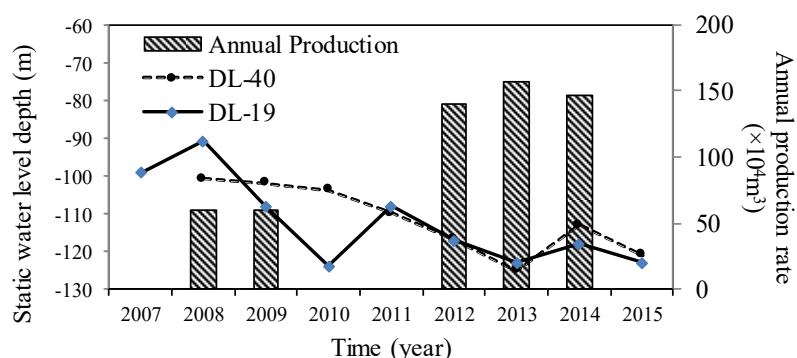


FIGURE 5: Static water level depth and annual production rate from 2007 to 2015

production rate from 2007 to 2015. Most of the production wells were shut off after the domestic heating period, from 15th November until 15th March, so the water level fluctuates significantly between seasons.

Due to intensive development and continuous increase in production, the water level has gradually declined in the reservoir. According to the dynamic monitoring data from 2012, the water level in the Jxw reservoir was at about 110 m below the surface, while in 2015 it was at around 120 m depth. Hence, the annual decline is about 3 m/year (Ruan et al., 2015). Figure 5 shows the static water level and corresponding

3. TRACER TESTING

Before starting a tracer test, the proper tracer has to be chosen. The tracer needs to meet a few basic criteria, such as:

- Not be present in the reservoir or at a concentration much lower than the expected tracer concentration;
- Not react with or be absorbed by reservoir rocks;
- Be thermally stable at reservoir conditions;
- Be relatively inexpensive;
- Be easy (fast/inexpensive) to analyse;
- Be environmentally benign (Axelsson, 2013); and
- The tracer should be detectable at low concentrations (Nottebohm et al., 2012).

Ammonium Molybdate (Mo) was used for the tracer test. It is nontoxic at low concentrations and could be used safely in the aquifer. The natural concentration of the tracer was low (background concentration is around $0.5 \mu\text{g/L}$) so it was assumed that the tracers introduced for this test could be followed over a reasonable distance and still be detected (Leblanc et al., 1991).

On December 17, 2015, 700 kg of Ammonium Molybdate were injected into well DL-48B over a period of 2 hours (Figure 3). The injection flow rate was approximately $100 \text{ m}^3/\text{h}$. Then, eight production wells were sampled every 2 hours throughout the subsequent 3 months (Figure 3). Only 1/6 of the samples were tested and analysed. If the tracer had been detected, the frequency of the analysis could have been increased.

No recovery was detected in the samples after 90 days of sampling which took place until March 18, 2016. There are a couple of possible explanations. One is that the tracer needs longer time to arrive at the production wells. Another possibility is that there is no direct flow from the injection well to production wells as the reservoir is highly fractured.

3.1 Simulation of tracer recovery and interpretation

3.1.1 Basic theory of tracer transport

The theory of tracer transport is the same as solute transport in porous and fractured hydrological systems. The principal models include transport by advection and convection, mechanical dispersion and molecular diffusion (Axelsson et al., 2005).

Various analytical models and solutions have been developed to interpret tracer test data after highly simplifying the geometry, dispersion, etc. The simple one-dimensional flow-channel tracer transport model is a rather powerful tool (Axelsson et al., 2005). This model assumes that the flow between injection and production wells can be approximated by one-dimensional flow and flow channels could be parts of near-vertical fracture-zones or parts of horizontal interbeds or layers. This one-dimensional tracer transport model is governed by the following equation (Axelsson et al., 2005):

$$D \frac{\partial^2 C}{\partial x^2} = \mu \frac{\partial C}{\partial x} + \frac{\partial C}{\partial t} \quad (1)$$

where D is the dispersion coefficient (m^2/s), C is the tracer concentration in the flow-channel (kg/m^3), x is the distance along the flow channel (m), μ is the average fluid velocity in the channel (m/s) and t is the time (s). Furthermore, $\mu = q/\rho A\phi$, where q is the injection rate (kg/s), ρ is the water density (kg/m^3), A is the average cross-sectional area of the flow-channel (m^2) and ϕ is the flow-channel porosity.

Molecular diffusion is neglected in this simple model so that $D = \alpha_L \mu$, where α_L is the longitudinal dispersivity of the channel (m).

Assuming instantaneous injection of a mass M (kg) of tracer at time $t=0$, the solution is given by:

$$c(t) = \frac{\mu M \rho}{Q} \frac{1}{2\sqrt{\pi D t}} e^{-(x-\mu t)^2/4Dt} \quad (2)$$

where $c(t)$ is the tracer concentration in the production well fluid (kg/m^3) and Q the production rate (kg/s). Conservation of the tracer according to $c \times Q = C \times q$ has been assumed.

Considering that the initial (background) tracer concentration of the production well fluid is not always 0, Equation 2 can be revised as follows:

$$c(t) = \frac{\mu M \rho}{Q} \frac{1}{2\sqrt{\pi D t}} e^{-(x-\mu t)^2/4Dt} + c(0) \quad (3)$$

3.1.2 Assumptions and simulation

This report will focus on data from injection well DL-48B and nearby production well DL-48 (Figure 3). Even though no tracer recovery was detected in the water samples during the 90 days' tracer test, it can be assumed that the recovery is very slow and if sampling had been continued, recovery would have appeared later. For assessing possible flow-paths between production and injection wells and predicting the cooling time, three assumptions are made for injection well DL-48B and production well DL-48:

1. Based on the sampling, tracer concentration is similar to the background concentration during the 90 days period. So we assume that from $t=\text{day } 1$ to $t=\text{day } 90$, the concentration is $0.5 \mu\text{g}/\text{L}$.

2. According to tracer tests from other geothermal fields, the value of dispersivity α_L is usually between $0.1x$ and $0.5x$ (where x is the channel length), so it can be assumed that the value of α_L is $0.1x$, $0.3x$ and $0.5x$, respectively (Pang, 2010).
3. The flow pattern is more complicated when all the wells are working and there will be water flowing through other parts of the reservoir outside the main flow paths (Koech, 2014). So not all tracer injected into DL-48B can be recovered in DL-48. Since the annual production of DL-48 accounts for approximately 15% of the total production in the area, it is assumed that the total tracer recovery in well DL-48 will be approximately 15% of that injected.

The distance between the injection and production wells DL-48B and DL-48 is 776 m, both the injection and the production rate are 30 kg/s during the period of domestic heating, which is 4 months of the year. According to Equation 3 and proposed assumptions, possible μ values and possible tracer concentration after 90 days can be calculated. Results are shown in Table 2 and Figures 6 and 7.

TABLE 2: Parameters of the simulated models for tracer recovery data with different dispersivity

Parameter	Simulation 1 $\alpha_L=76.7\text{m}$	Simulation 2 $\alpha_L=230.1\text{m}$	Simulation 3 $\alpha_L=383.5\text{m}$
Fluid velocity, μ (m/day)	1.04	0.43	0.29
$A\phi$ (m ²)	2600	6240	9460

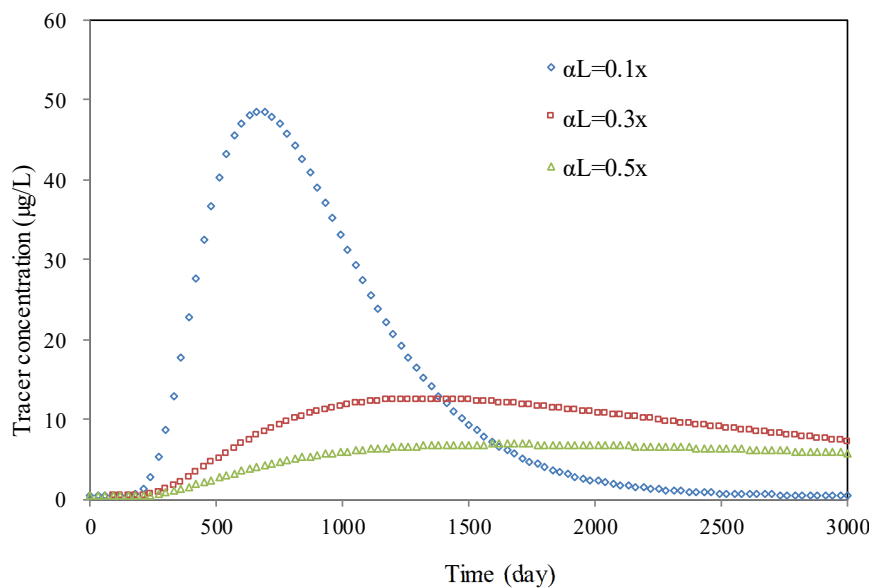


FIGURE 6: The results of the simulation of tracer recovery within 3000 days based on different dispersivity values

normally reflects the flow path dispersion, and the tracer recovery is a function of time (Axelsson et al., 2005).

Figure 7 demonstrates tracer recovery within 250 days based on different dispersivity rates. After 150 days the tracer concentration has begun to increase. This explains why no recovery in the tracer test was seen after 90 days of sampling.

In comparison with hydraulic conductivity, which is 1.29 m/day in well DL-48B (Tian, 2014), and the fluid velocity μ shown in Table 2, the simulation which assumes a longitudinal dispersivity of 0.1 times the channel length seems to be much more reliable than the other two cases.

According to Figure 6, different dispersion coefficients give significantly different results. When the longitudinal dispersivity of the channel is 0.1 times the channel length, the breakthrough time is earlier and the peak concentration is much higher than in the other two cases. As Equation 3 shows, tracer breakthrough time depends on maximum fluid velocity and time of maximum concentration reflects the average fluid velocity. The width of the tracer pulse

3.2 Cooling predictions

One of the main goals of a tracer test is to predict thermal breakthrough and temperature decline during long-term injection. The heat transfer between injection and production wells not only depends on the properties of the flow channels involved, but is also determined by the surface area and porosity of the flow channels. Therefore, it is important to have additional information on the flow path properties or geometry which is of geological or geophysical nature (Axelsson, 2013). Previous simulations of tracer recovery provide useful information about the cross-section that can be used for cooling predictions (Pang, 2010).

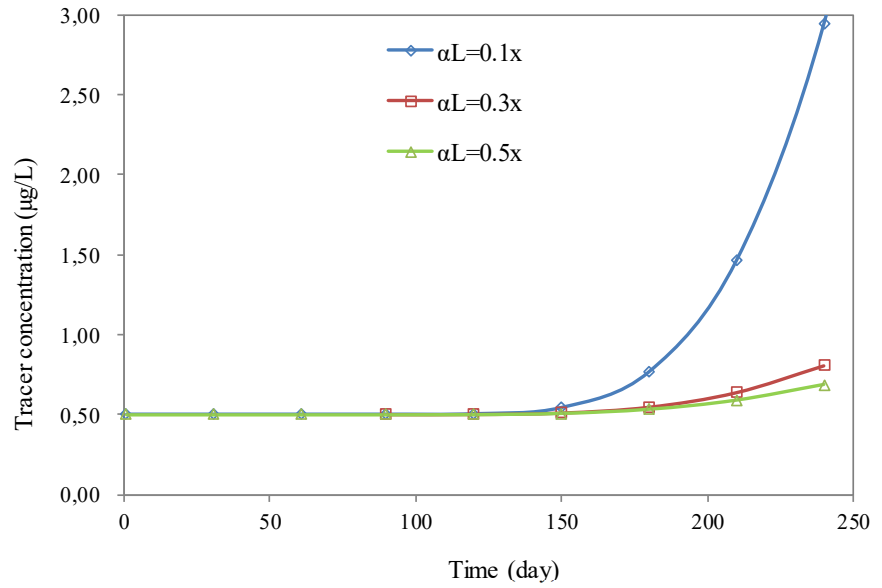


FIGURE 7: The results of the simulation of tracer recovery within 250 days based on different dispersivity values

3.2.1 Analytical model description

The model simulates a flow path along a fracture-zone, an interbed or permeable layer. Actually, it is a geometrically more restrained variant of the flow channel model described in Section 3.1.1. A detailed discussion of this model and the solution is provided in the paper by Axelsson et al. (2005). The mathematical equations giving the response of the model for cooling prediction are:

$$T(t) = T_0 - \frac{q}{Q} (T_0 - T_i) \left[1 - \operatorname{erf} \left\{ \frac{kxh}{c_w q \sqrt{\kappa(t - \frac{x}{\beta})}} \right\} \right] \quad (4)$$

$$\beta = \frac{q c_w}{(\rho c)_f h b} \quad (5)$$

with

$$(\rho c)_f = \rho_w c_w \phi + \rho_r c_r (1 - \phi) \quad (6)$$

where $T(t)$ is the production fluid temperature, T_0 is the undisturbed reservoir temperature, T_i is the injection temperature, q and Q are rates of injection and production, respectively, erf is the error function, k is the thermal conductivity of the reservoir rock, κ is the thermal diffusivity of the reservoir rock, x is the distance between injection and production wells, ρ and c are density and heat capacity, respectively, with the indices w and r standing for “water” and “rock”.

3.2.2 Prediction of temperature change and propagation from injection well

The program Tracer (TR) part of the ICEBOX software was used to calculate the theoretical temperature decline for production well DL-48. Relevant parameters are discussed according to the hydrogeological information and development situation as follows and shown in Table 3:

- 1) During the heating season, the injection is 100% with a rate of 30 kg/s. While in other seasons, production rate is decreased due to lower demand. Thus, the average annual production rate is taken as 10 kg/s. Thus, 10 and 30 kg/s are both used to simulate the extreme cases for the cooling prediction.
- 2) Based on geological information, the Wumishan geothermal reservoir (Jxw) consists mostly of Mesoproterozoic dolomitic limestone. It is assumed, that thermal conductivity of the reservoir rock is 3.2 W/m K, density of the rock is 2677 kg/m³ and porosity of the reservoir 6% (Lin, 2006).
- 3) The flow channel length is 767 m, and cross-sectional area of the flow-channel $A\phi$ is assumed to be 4336 m² based on a dispersivity equalling 76.7 m. Considering the uncertainty of predictions, two extremes regarding different flow-channel dimensions were calculated. A pessimistic scenario was assumed, where the ratio between height (h) and width (b) of the flow channels was given by $h = 5b$ and an optimistic scenario, where the ratio was given by $h = 20b$.

TABLE 3: Model parameters used for the cooling predictions

Injection/production rate (kg/s)	Scenario	Flow channel distance (m)	Flow channel width b (m)	Flow channel height h (m)	Cross-section area (m ²)
30	Pessimistic	767	93.1	466	43400
	Optimistic		46.6	931	
10	Pessimistic	767	93.1	466	43400
	Optimistic		46.6	931	

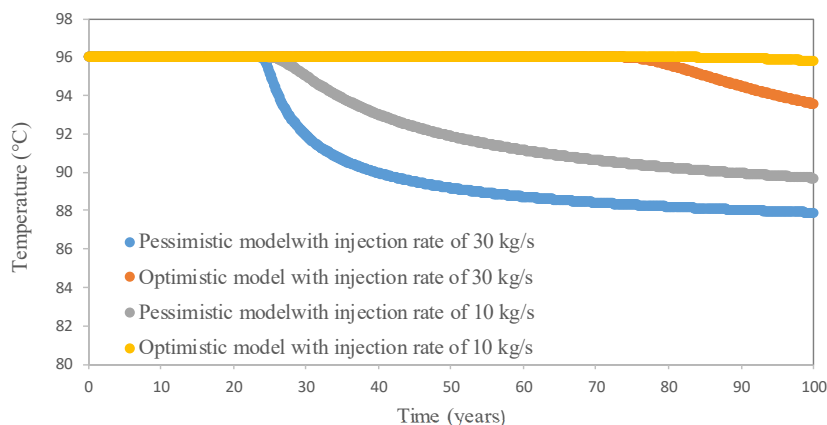


FIGURE 8: Cooling prediction for production well DL-48, with injection rates 10 and 30 kg/s, respectively, for 100 years

The cooling predictions (Figure 8) indicate that for an average annual production and injection rate of 10 kg/s, thermal breakthrough would occur in 80 years in case of a wide flow channel for an optimistic scenario and 27 years in case of a narrower flow channel for a pessimistic scenario. The cooling effect is relatively small for the optimistic model. Temperature stays nearly constant for the next 100 years, indicating no direct

connection between injection and production wells, while with the pessimistic model, the water in the production well cools down faster in the first 50 years with a temperature decline of 4°C.

With the highest production and injection rate of 30 kg/s, temperature drops faster and more rapidly compared to the lower injection rate of 10 kg/s. Thermal breakthrough would occur in 72 years in case of a wide flow channel for an optimistic scenario and in 24 years in case of a narrower flow channel for a pessimistic scenario. Temperature in the production well decreases faster in the first 50 years with declines of 6.8°C in the more pessimistic case. If the injection rate increases, the thermal breakthrough time will be earlier and the influence on cooling will become higher. Hence, it is recommended to keep the injection rate as it is.

It is important to note that the production rate always decreases after the heating period because of lower demand of geothermal energy which is beneficial for temperature recovery. This means that the cooling influence will be smaller than the model predicted.

4. NUMERICAL MODELLING

4.1 Background of numerical modelling with MODFLOW

MODFLOW is a FORTRAN program developed by the United States Geological Survey (USGS), which can simulate groundwater flow and levels under complex hydrogeological conditions with various hydrological processes and is widely used in regulatory situations (Jang et al., 2016).

The equation governing groundwater flow through saturated porous media in three dimensions is derived from Darcy's law and the continuity equation, and is given as (Harbaugh et al., 2000):

$$\frac{\partial}{\partial x} \left(K_{xx} \frac{\partial h}{\partial x} \right) + \frac{\partial}{\partial y} \left(K_{yy} \frac{\partial h}{\partial y} \right) + \frac{\partial}{\partial z} \left(K_{zz} \frac{\partial h}{\partial z} \right) + W = S_s \frac{\partial h}{\partial t} \quad (7)$$

where K_{xx} , K_{yy} and K_{zz} are the hydraulic conductivities (m/d) along the x, y, and z axes that are assumed to be parallel to the principal axes of the hydraulic conductivity tensor, h is the hydraulic head (m), W is the volumetric flux per unit volume representing sources and/or sinks of water (1/d), S_s is the specific storage of the material (1/m) and t is time (d). Here, K_{xx} , K_{yy} and K_{zz} are the functions of space (x , y , z) and W is a function of space and time (t).

In this study, the Visual MODFLOW Flex (2015.1) software has been used for simulating the groundwater dynamics. This version includes the simulation of saturated-unsaturated flow processes, density dependent flow processes, parameter optimization processes and solute transport processes (Zhou and Li, 2011). A finite difference grid was used and MODFLOW 2000 was chosen as an engine to run a transient state numerical model from 26th August, 2013 to 26th August, 2015. Two additional packages were used in this project:

- 1) MT3DMS: Visual MODFLOW Flex supports MT3DMS v.5.2. MT3DMS is a transport model for simulating advection, dispersion, and chemical reactions of contaminants in groundwater flow systems. This package was used to model the concentration of the observation wells after tracer injection (Zheng and Wang, 1999).
- 2) PEST: An effective tool of automating parameter estimation, calibration and sensitivity analysis, it allows running parameter estimation using results from both groundwater flow and contaminant transport simulations (Doherty et al., 2010).

4.2 Numerical reservoir modelling and calibration

4.2.1 Conceptual model

The Jxw geothermal reservoir in the Dongli Lake area is an extensive, low-temperature geothermal system hosted mainly by Mesoproterozoic dolomitic limestone. It belongs to semi-opened and semi-closed bedrock subsystems, where the geothermal karst fluids exist (Ruan, 2011). Considering that most of the wells are distributed on the western side of the Cangdong fault, a small area with intensive production and injection wells was chosen for the conceptual and numerical modelling (Figure 3).

In order to create a conceptual model, the study area was vertically divided into four layers. Based on borehole geology, a 3D structural model was created (Figure 9). Hence, layer 1 is the Quaternary porous formation. Layer 2 includes Cenozoic Minghuazhen Group (Nm) and Guantao Group (Ng). Layer 3 is the karstic-fracture geothermal reservoir, including Paleozoic Ordovician (O) and Cambrian (€). Layer 4 which is the main study reservoir consists of the Mesoproterozoic Jixian Wumishan Group (Jxw).

From pumping test results of the wells in this area (Tian, 2014), hydraulic conductivity of the reservoir is between 0.59 m/d and 3.3 m/d with permeability between 4.89×10^{-13} and 1.25×10^{-13} m². Porosity is around 5-6%, and the thickness of the reservoir is from 1050 to 2250 m.

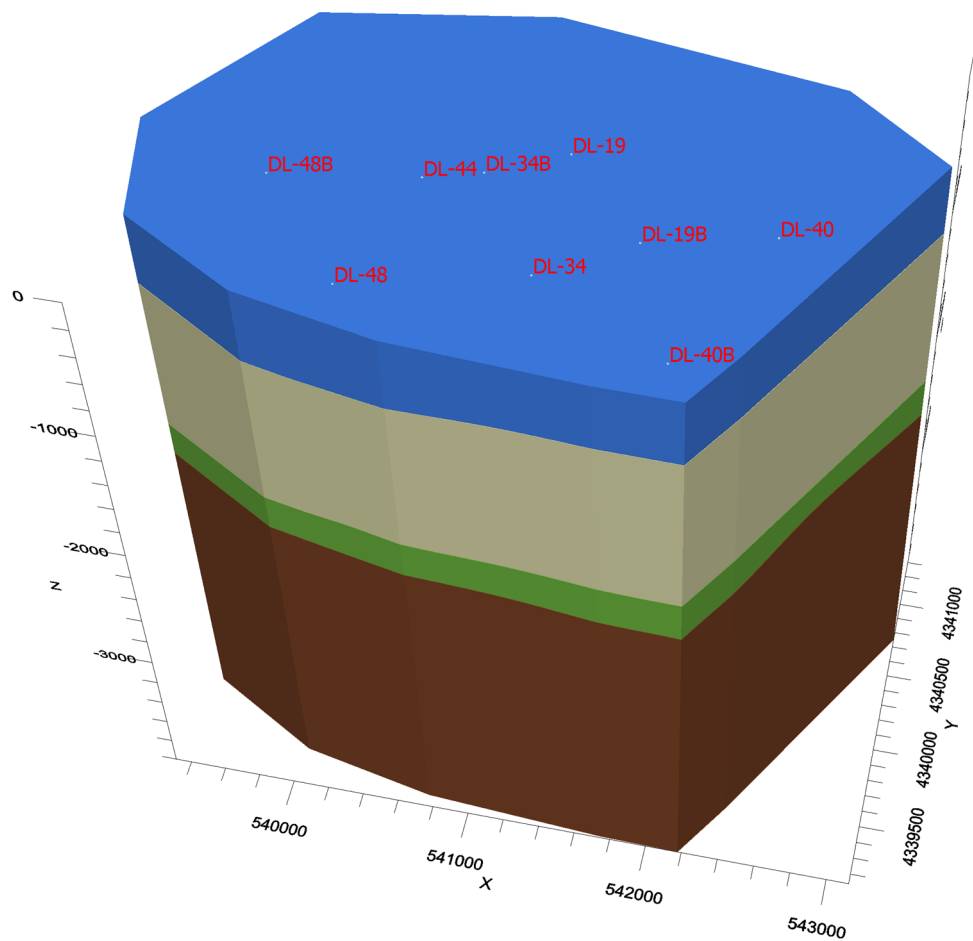


FIGURE 9: The 3D model of the Jxw geothermal reservoir

4.2.2 Numerical model

A finite difference grid was used for numerical modelling. Each layer of the conceptual model was discretized horizontally into a grid of 100×120 cells with cell height of 22.13 m and cell width of 31.78 m. For more accurate simulation of the water levels and tracer concentration between the injection and production well, a grid around well DL-48 and DL-48B was refined by a factor of two (Figure 10).

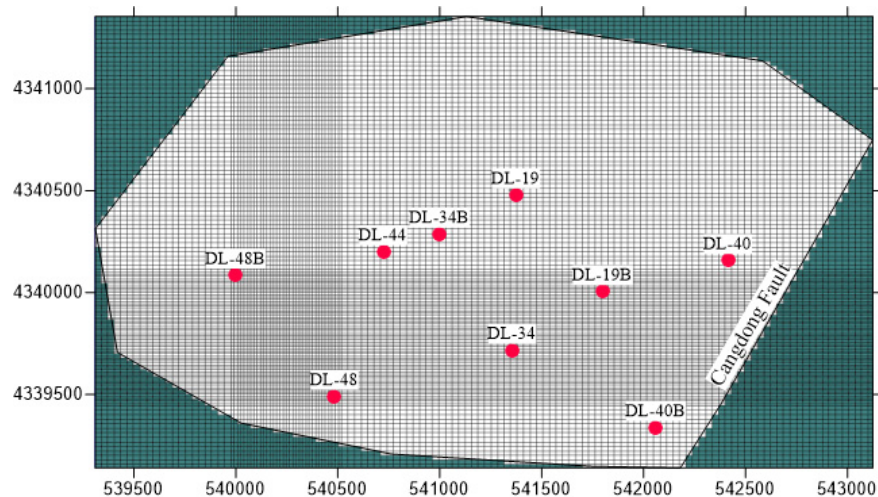


FIGURE 10: Numerical model grid

Based on the information of the deepest well with depth of 4040 m in this area, the reservoir below 4000 m depth is poorly developed with pores and fissures. Consequently, the bottom boundary was considered as no-flow boundary.

The flow direction is mainly from northwest to southeast according to the initial water level contours and the inflow and outflow flux of each boundary can be calculated by Darcy's Law. The specified flux boundary was used with these fluxes in the model and a small adjustment was made during the process of calibration. Horizontal hydraulic conductivity $K_{x,y}$, vertical hydraulic conductivity (K_z) and storativity (S_s) were defined as 1.2 m/d, 0.12 m/d and $1 \times 10^{-5} \text{ m}^{-1}$, respectively, in layer 4 (the main reservoir).

After all hydrogeological parameters were implemented into the numerical model, MODFLOW 2000 was used to run numerical engines and simulate groundwater level changes in the reservoir. Where observation data was available (from DL-19, DL-40, DL-44, DL-48), it was possible to evaluate how reliable the numerical model is. Therefore, calculated water levels are plotted against observed levels. In the perfect case scenario, there is a linear relationship between the calculated and observed heads. After a first MODFLOW 2000 run, the deviation was too high (Figure 11). Most calculated water levels are higher than the observed values, and both the absolute residual mean (ARM) and the root mean square error (RMSE) are very high, 6.14 m and 13.24 m, respectively. Thus the input parameters (hydrogeological parameters) had to be adjusted.

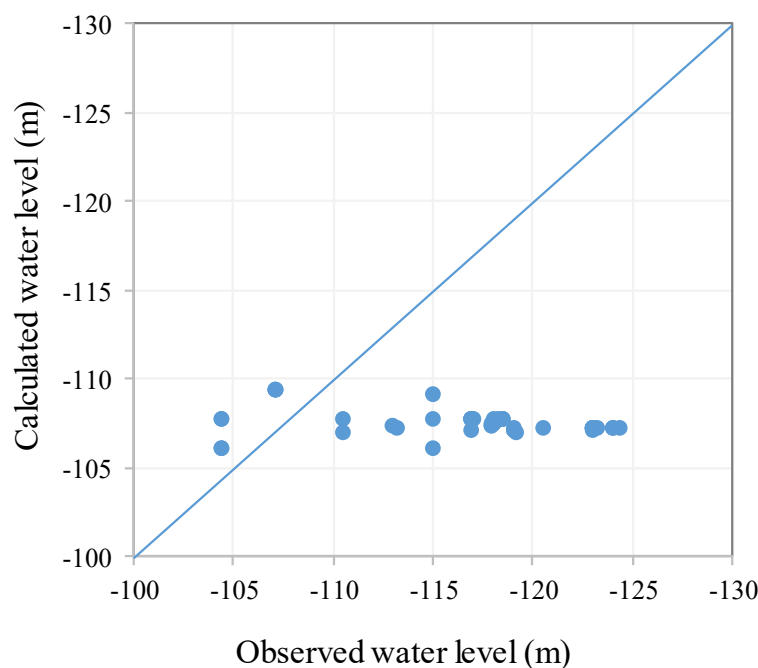


FIGURE 11: The fitting of the observed water levels and simulated water levels before calibration

Hydrogeological parameters of layer 4 (main reservoir) were manually adjusted until acceptable fit between observed and simulated water levels was reached. After manual calibration $K_{x,y}$ was 1 m/d, K_z was 0.1 m/d and S_s was $5 \times 10^{-6} \text{ m}^{-1}$ in layer 4.

In order to increase the accuracy of the model, an automatic parameter estimation tool (PEST) was used to minimize errors between the observed and simulated data. This was also used to estimate the distribution of reservoir parameters. Pilot points were placed and fixed in the wells with known $K_{x,y}$, which were obtained from pumping test data reported by Tian (2014) (Table 4). Additional pilot points were then added scattered over the study area. $K_{x,y}$, K_z and S_s in layer 4 were constrained in the range of 0.1-10 m/d, 0.01-1 m/d and 1×10^{-7} - $1 \times 10^{-4} \text{ 1/m}$, respectively. This resulted in 15 pilot points with 3 types of parameters to be calibrated. The spatial hydraulic conductivity and storativity fields were derived by interpolation among pilot points using kriging variograms (Woodward et al., 2016).

TABLE 4: The hydraulic conductivity of fixed pilot points from well test data

Well	Hydraulic conductivity (m/d)	Well	Hydraulic conductivity (m/d)
DL-40B	2.85	DL-40	1.03
DL-48	3.3	DL-34	0.85
DL-19B	1.38	DL-44	0.77
DL-48B	1.29	DL-44B	0.73

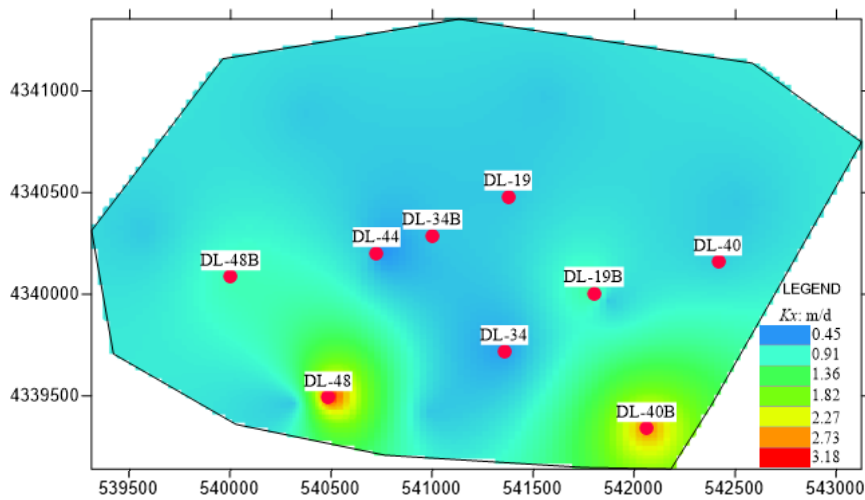


FIGURE 12: A map of simulated hydraulic conductivity ($K_{x,y}$) in the Jxw reservoir after model calibration

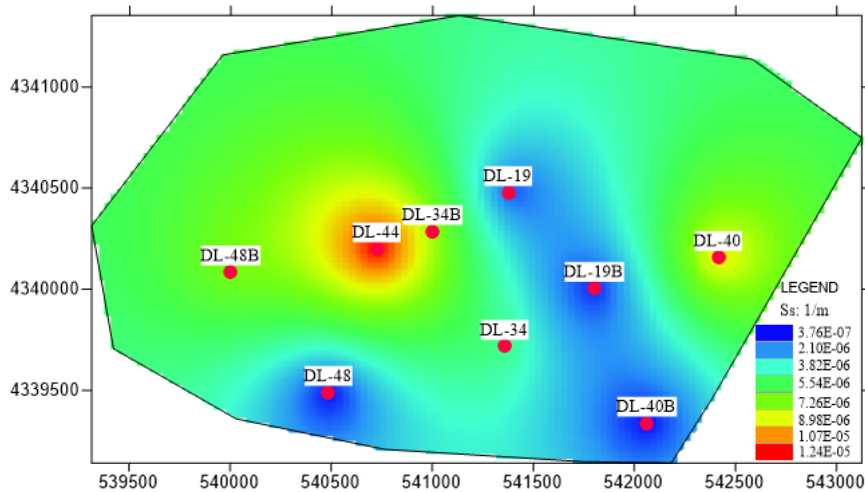
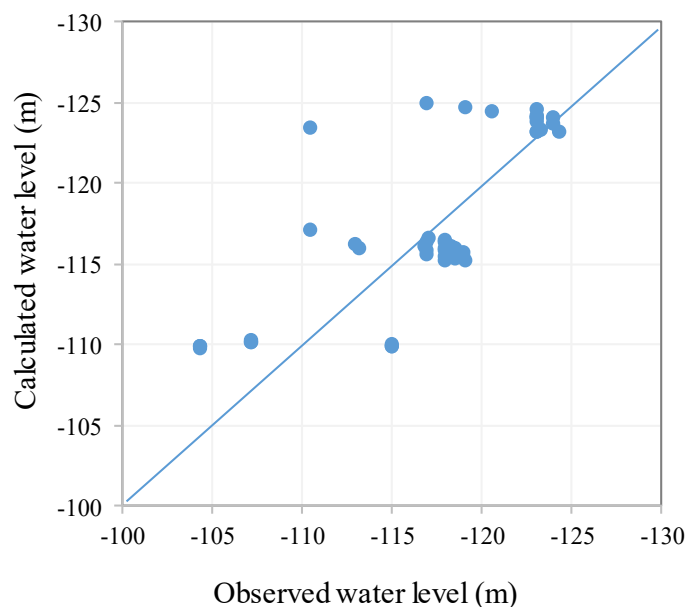


FIGURE 13: A map of simulated storativity in the Jxw reservoir (S_s) after model calibration



After running PEST, a new distribution of parameters was received and they were applied to the new model. Figures 12 and 13 show the distribution of $K_{x,y}$ and S_s used in the model after calibration. The range of $K_{x,y}$, K_z and S_s in layer 4 is mostly between 0.45 and 3.18 m/day, 0.05 and 0.33 m/day and 2.09×10^{-6} – $1.24 \times 10^{-5} \text{ m}^{-1}$, respectively, which can be reflected better by the heterogeneity of the reservoir rather than a zonal approach.

The final calibrated model produced reasonable agreement between the simulated and observed water levels at the calibration targets (Figure 14). The absolute residual mean (ARM) was 2.94 m, while the root mean square error (RMSE) was 3.84 m. For a model with an area of 6.32 km^2 a standard error estimate of 0.57 m and correlation coefficient of 0.77 were considered to be acceptable. Comparing to the model before the PEST running, both the parameter distributions and water levels are closer to the actual situation.

FIGURE 14: The fitting of the observed water levels and simulated water levels in the Jxw reservoir after PEST

4.3 Prediction of tracer concentration in the production well

The MT3DMS numerical engine was used to estimate the recovery time and the tracer concentration in the production wells. For further modelling, it was assumed that the tracer is conservative and no adsorption or desorption occurs in the reservoir, only convection and dispersion were considered. Hydraulic conductivity and storativity were deduced from the groundwater flow model. Total porosity was used to determine the chemical reaction coefficients and for calculating the average linear groundwater flow velocity (Waterloo Hydrogeologic, 2015). The longitudinal dispersivity was set the same as in the analytical method, i.e. 76.7, 230.1 and 383.5 m for the three different simulation scenarios.

The injection of tracers was set on the first day of injection with a maximum dissolved concentration of $3 \times 10^8 \mu\text{g/L}$. There are two different boundary conditions that can be used in this software, well boundary condition and constant concentration boundary condition. For the first one, tracer concentration was set at the injection well, but the concentration was diluted quickly to be $1.26 \times 10^7 \mu\text{g/L}$ after one day of injection. While, for the other one, the grid cell with the injection well was set to have a constant concentration of $3 \times 10^8 \mu\text{g/L}$ during the first day of injecting water. This difference also affected the results of tracer recovery concentration, as shown in Table 5. It can be seen that the recovery time is the same in both of these cases, but the concentration is almost one order of magnitude smaller when setting a well boundary condition compared to when setting a constant concentration.

TABLE 5: Recovery time and corresponding concentration of production well with two methods

Scenarios	Recovery time (years)	Concentration of well DL-48 ($\mu\text{g/L}$)		
		$\alpha_L=76.7 \text{ m}$	$\alpha_L=230.1 \text{ m}$	$\alpha_L=383.5 \text{ m}$
Tracer injected with well	1.1			2.51×10^{-31}
	2.1		4.26×10^{-30}	3.57×10^{-21}
	5.3	3.14×10^{-32}	2.01×10^{-14}	1.47×10^{-8}
	9.7	1.33×10^{-21}	4.68×10^{-8}	4.63×10^{-4}
Tracer as constant concentration	1.1			1.68×10^{-30}
	2.1		5.78×10^{-29}	3.60×10^{-20}
	5.3	4.96×10^{-31}	1.87×10^{-13}	1.74×10^{-7}
	9.7	6.05×10^{-21}	3.44×10^{-7}	4.24×10^{-3}

We can also notice that the tracer concentration was diluted very quickly and it moved very slowly. For the most pessimistic case ($\alpha_L=384 \text{ m}$), it takes the tracer more than a year to arrive at the production well, with very small concentration which is below the detection limit. Even at the end of 10 years, the concentration is still below detection limit (Figure 15). This means that more than 10 years are needed to get recovery with the tracer testing.

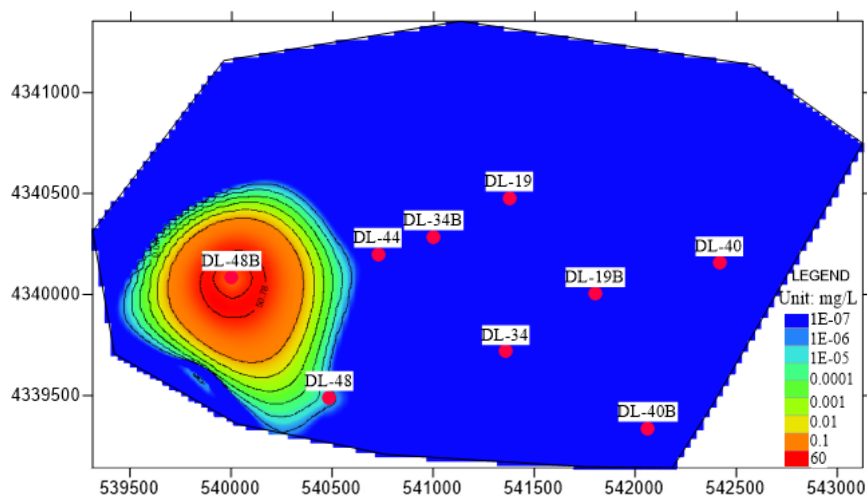


FIGURE 15: Tracer concentration contours in the Jxw reservoir after 10 years ($\alpha_L=384 \text{ m}$)

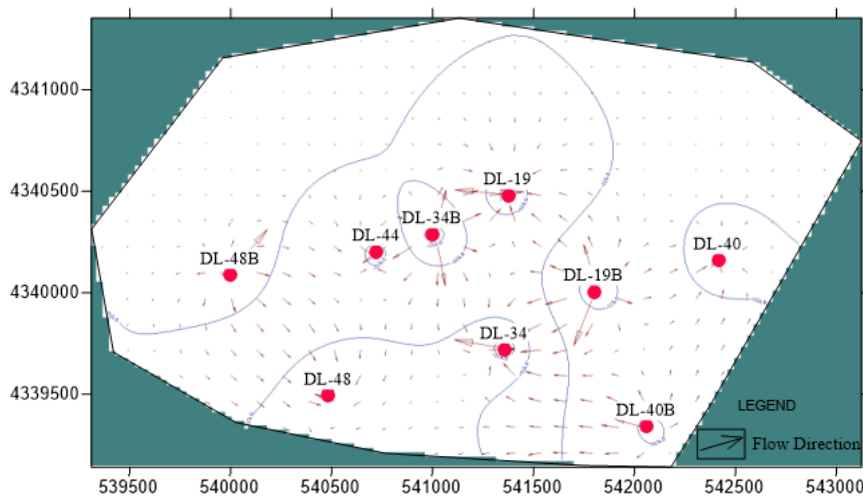


FIGURE 16: Flow directions during production and injection periods (day 127, scale factor 0.4)

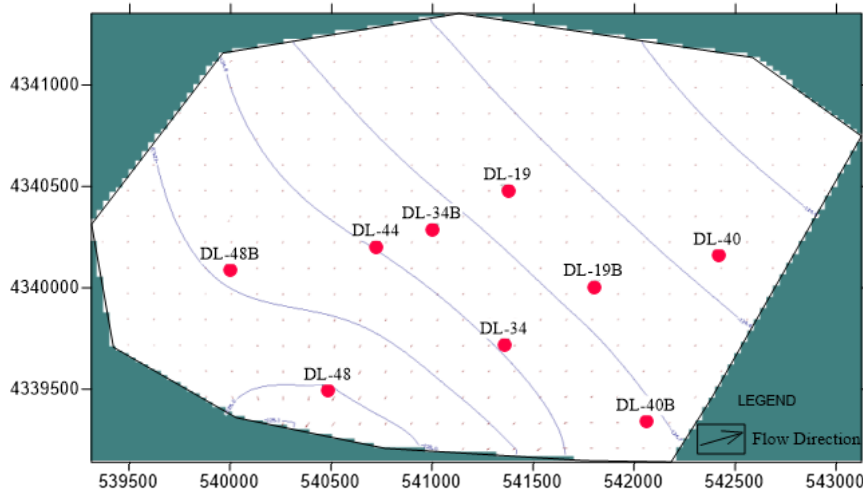


FIGURE 17: Flow directions without production and injection (day 730, scale factor 0.4)

From the flow directions, which also show velocities of the water flow at different times (Figures 16 and 17), we can find that production and injection change the flow pattern around the wells compared to other times. However, the volume of the reservoir is so big and injection or production influential radius are rather small. The flow is relatively slow with the biggest rate of 0.12 m/d around wells, while in other place and at other times this value is only around 0.01 m/d. Compared with the analytical model, this velocity only accounts for 3.4% of simulation 3 (0.29 m/d), which also explains why the tracer needs such a long time to arrive at the production well. Results show that there is no direct connection between the production and injection wells and neither model predicts cooling in the next 24 years.

5. DISCUSSION

Tracer testing in the Wumishan (Jxw) geothermal reservoir in the Dongli Lake area of Tianjin has been interpreted with respect to concentration change and cooling of the production well, using both an analytical and a complex numerical method. The analytical method, with the assumption that recovery would appear after 90 days, showed that thermal breakthrough would occur after 80 years for an optimistic scenario (narrow flow channel) and after 27 years for a pessimistic scenario (wide flow channel) assuming an average annual production and injection rate of 10 kg/s.

Although the heat transfer was not simulated with the numerical model, information was received from the tracer concentration prediction. The results show that when the longitudinal dispersivity is 384 m, the recovery time is more than 10 years. As thermal changes are known to be extremely slow, compared to pressure and chemical changes, due to the thermal inertia of the rock formation involved (Axelsson, 2012b), hence the thermal breakthrough time is estimated to be much longer than 10 years. Thus, these two different models show that there is no direct connection between the production and injection wells, which also explains why no tracer recovery was observed in the samples.

The analytical method assumes that the flow paths are directly from the injection point to the pumping wells and the influence of a regional gradient is not taken into account (Haerens, 1999). It provides a simple and effective way to interpret tracer testing results. While a numerical model can better reflect the reservoir conditions and flow patterns and thus provide better results, but it takes longer to implement data and make a run. The results depend heavily on the reliability of the model, which is why the model should be calibrated with enough observation data. If the model is considered to fit well with the observation data, it can be used for cooling prediction and consequently play an important role in the reservoir management.

6. CONCLUSIONS AND RECOMMENDATIONS

The Wumishan (Jxw) geothermal reservoir in the Dongli Lake area is an extensive, low-temperature geothermal system hosted mainly by Mesoproterozoic dolomitic limestone. It belongs to semi-open and semi-closed bedrock subsystems, where geothermal karst fluids exist. The heat source of the reservoir is presumably in the upper mantle and radioactive decay in granite (at about 8-16 km depth). The origin of the water is meteoric from ancient times. The Quaternary and Tertiary formations consist of clay and sandstone, forming a good caprock for the geothermal reservoir. The Cangdong fault is a major fault which can conduct heat from the bottom of the reservoir to the shallow part by heat convection.

In order to study the flow paths and predict the cooling due to long term injection, tracer tests were performed. To interpret the tracer tests quantitatively, both an analytical method, developed by ÍSOR (Iceland Geosurvey), and a numerical method using the Visual MODFLOW flex software were applied and discussed in the report.

For the analytical model, it was assumed that the recovery was very slow and would appear after 90 days. For the three cases of longitudinal dispersivity, 77, 230 and 384 m, the tracer concentration began to increase after 150 days. The breakthrough time was earlier and the peak concentration was much higher, with a longitudinal dispersivity of 76.7 m or 0.1 times the channel length, than for the other two cases where the longitudinal dispersivity is higher, or 0.3 times and 0.5 times the channel length. When the dispersivity was 76.7 m, thermal breakthrough would occur after 80 years for an optimistic scenario (narrow flow channel) and after 27 years for a pessimistic scenario (wide flow channel) for average annual production and injection rates of 10 kg/s.

A numerical reservoir model was developed for the Dongli Lake geothermal area. It covers an area of 6.32 km². An automatic parameter estimation tool (PEST) was used to minimize errors between observed and simulated heads and to estimate the distribution of reservoir parameters. After calibration, the range of hydraulic conductivity ($K_{x,y}$, K_z) and storativity (S_s) in the Jxw reservoir were found to be in the range 0.45-3.18 m/day, 0.05-0.33 m/day and 2.09×10^{-6} - 1.24×10^{-5} m⁻¹, respectively. This better reflects the heterogeneity of the reservoir than a zonal approach, where it is assumed that these parameters are constant within the zones. The final calibrated model produced reasonable agreement between the simulated and observed water levels and was applied to predict the tracer concentration in the production well.

For the most pessimistic case of a longitudinal dispersivity of 384 m, the tracer will take more than a year to arrive at the production well, according to the model, with very small concentration, outside the detection limit. Results show that there is no direct connection between production and injection wells and neither model predicts cooling in the next 24 years. Based on the results of this study, some recommendations are put forward:

- 1) A numerical model is helpful when designing tracer tests. It can be used to estimate the minimum quantity of tracer required, the breakthrough time and the peak arrival time. In the meantime, tracer tests data can also help to improve the calibration of a numerical model, which, in turn, could provide more information about the flow paths.

- 2) In this case study, sampling is suggested to be continued over the next one to two years at a low sampling frequency. More information should be collected to improve the numerical model.
- 3) SEAWAT software (Langevin et al., 2008) is suggested to be used to predict the cooling of the production well. It is a computer program intended to simulate multi-species solute and heat transport which couples MODFLOW-2000 with MT3DMS. Heat transport calculations with SEAWAT are based on the analogy between solute and heat transport (Vanderbohede et al., 2011) with the temperature being treated as one of the species.

ACKNOWLEDGEMENTS

I would like to thank the United Nation University for supporting me to accomplish this training programme. Thanks to Mr. Lúdvík S. Georgsson, director, as well as to all the technical staff of UNU-GTP, Mr. Ingimar G. Haraldsson, Ms. Málfríður Ómarsdóttir, Ms. Thórhildur Ísberg and Mr. Markús A. G. Wilde, for giving me a family feeling in Iceland.

Sincere thanks to Dr. Gudni Axelsson and Ms. Saeunn Halldórsdóttir, from ÍSOR, for the supervision and guidance during the preparation of the present project. I would like to express the deepest and sincerest gratitude to my supervisors, Ms. Vaiva Čypaitė and Ms. Valdís Guðmundsdóttir. Thanks for providing me with patient guidance and advice, and sharing knowledge and experience, thanks for all the help and assistance.

Thanks to my colleagues of the Institute of Hydrogeology and Environmental Geology (IHEG) staff members, especially to Mr. Wang Guiling, Mr. Lin Wenjing, Mr. Lu Chuan, Mr. Liu Feng, for their support given during the training in Iceland. Thanks for the support given by Tianjin Geothermal Exploration and Development Designing Institute for allowing the use of the data for the purpose of the present work.

Thanks to the other UNU Fellows for their support and friendship over the last six months.

Finally, I would like to express my deepest appreciation to my family. Thanks to my husband and my son for their support.

REFERENCES

- Alramadhan, A.A., Kilicaslan, U., and Schechter, D.S., 2015: Analysis, interpretation, and design of inter-well tracer tests in naturally fractured reservoirs. *J. Petroleum Science Research*, 4-2, 97-122.
- An Q.S., Wang Y., Zhao J., Luo C., and Wang Y., 2016: Direct utilization status and power generation potential of low-medium temperature hydrothermal geothermal resources in Tianjin, China: a review. *Geothermics*, 64, 426-438.
- Axelsson, G., 2012a: Role and management of geothermal reinjection. *Presented at "Short course on geothermal development and geothermal wells", organized by UNU-GTP and LaGeo, Santa Tecla, El Salvador*, UNU-GTP SC-14, 21 pp.
- Axelsson, G., 2012b: The physics of geothermal energy. In: Sayigh, A., (ed.), *Comprehensive renewable energy*. Elsevier, Oxford, 3–50.
- Axelsson, G. 2013: *Tracer tests in geothermal resource management*. *EPJ Web of Conferences*, EDP Sciences, 50, 8 pp.

Axelsson, G., Björnsson, G., and Montalvo, F., 2005: Quantitative interpretation of tracer test data. *Proceedings of the World Geothermal Congress 2005, Antalya, Turkey*, 12 pp.

Axelsson, G., and Dong Z., 1998: The Tanggu geothermal reservoir (Tianjin China). *Geothermics*, 27, 271–294.

Cheng, W., Tedesco, D., and Poreda, R., 2008: The Tianjin geothermal field (north-eastern China): water chemistry and possible reservoir permeability reduction phenomena. *Geothermics*, 37, 400–428.

Diaz, A.R., Kaya, E., and Zarrouk, S.J., 2016: Reinjection in geothermal fields - A worldwide review update. *Renewable and Sustainable Energy Reviews*, 53, 105-162.

Doherty, J.E., Hunt, R.J., and Tonkin, M.J., 2010: *Approaches to highly parameterized inversion: A guide to using PEST for model-parameter and predictive-uncertainty analysis*. US Geological Survey Scientific Investigations, report 2010-5211, 71 pp.

Duan Z., Pang Z., and Wang X., 2011: Sustainability evaluation of limestone geothermal reservoirs with extended production histories in Beijing and Tianjin, China. *Geothermics*, 40, 125–135.

Fan Y., 2006: *A study of the storage capacity of geothermal reservoirs and the exploitation dynamics of thermal water in Tianjin* (in Chinese). China University of Geosciences, Beijing, MSc thesis, 66 pp.

Haerens, B., Brouyere, S., and Dassargues, A., 1999: Detailed calibration of a deterministic transport model on multi-tracer tests: analysis and comparison with semi-analytical solutions. *Proceedings of Model CARE 99: Calibration and Reliability in Groundwater Modelling, ETH, Zurich, Switzerland*, 6 pp, website: hdl.handle.net/2268/2560.

Harbaugh, A.W., Banta, E.R., Hill, M.C., and McDonald, M.G., 2000: *MODFLOW-2000, the US Geological Survey modular ground-water model – user guide to modularization concepts and the ground-water flow process*. US Geological Survey, open-file report 00-92, Reston, VA, 121 pp.

Jang C., Chen C., Liang C., and Chen J., 2016: Combining groundwater quality analysis and a numerical flow simulation for spatially establishing utilization strategies for groundwater and surface water in the Pingtung Plain. *J. Hydrology*, 533, 541-556.

Koech, V.K., 2014: *Numerical geothermal reservoir modelling and infield reinjection design, constrained by tracer test data: case study for the Olkaria geothermal field in Kenya*. University of Iceland, MSc Thesis, UNU-GTP, report 5, 80 pp.

Langevin, C.D., Thorne Jr., D.T., Dausman, A.M., Sukop, M.C., and Guo, W., 2008: *SEAWAT vs.4: a computer program for simulation of multi-species solute and heat transport*. US Geological Survey techniques and methods, Book 6, Chapter A22, 39 pp.

Leblanc, D.R., Garabedian, S.P., Hess, K.M., Gelhar, L.W., Quadri, R.D., Stollenwerk, K.G., and Wood, W.W., 1991: Large-scale natural gradient tracer test in sand and gravel, Cape Cod, Massachusetts. *Water Resources Research*, 27, 895-910.

Lin L., 2006: *Sustainable development and utilization of thermal groundwater resources in the geothermal reservoir of the Wumishan Group* (in Chinese). China University of Geosciences, Beijing, PhD thesis, 133 pp.

Minissale, A., Borrini, D., Montegrossi, G., Orlando A., and Tassi, F., 2008: The Tianjin geothermal field (north-eastern China): Water chemistry and possible reservoir permeability reduction phenomena. *Geothermics*, 37, 400-428.

Mondejar, G.C., 2012: Hydrological flow and thermal interference modelling in the Mahanagdong geothermal field, Philippines, using four types of Naphthalene disulfonate tracer. Report 22 in: *Geothermal training in Iceland 2010*. UNU-GTP, Iceland, 467-500.

Nottebohm, M., Licha, T., and Sauter, M., 2012: Tracer design for tracking thermal fronts in geothermal reservoirs. *Geothermics*, 43, 37-44.

Pang J., 2010: Reinjection into well ST0902 and tracer testing in the Xiongxi geothermal field, Hebei Province, China. Report 25 in: *Geothermal training in Iceland 2010*. UNU-GTP, Iceland, 493-524.

Ruan C., 2011: Numerical modelling of water level changes in Tianjin low-temperature geothermal system, China. Report 31 in: *Geothermal training in Iceland 2011*. UNU-GTP, Iceland, 775-798.

Ruan C., Sun B., Shen J., Gao X., and Liu R., 2015: The injection research of Dongli Lake bedrock reservoir in Binhai New Area. *Proceedings of the World Geothermal Congress 2015, Melbourne, Australia*, 9 pp.

Tian G., 2014: *Sustainable development and utilization of geothermal resources in the Donglihu resort in Tianjin* (in Chinese). China University of Geosciences, Beijing, MSc thesis, 106 pp.

Vandenbohede, A., Hermans, T., Nguyen, F., and Lebbe, L., 2011: Shallow heat injection and storage experiment: Heat transport simulation and sensitivity analysis. *J. Hydrology*, 409, 262-272.

Waterloo Hydrogeologic, 2015: *Visual MODFLOW Flex user manual*. Waterloo Hydrogeologic, software, 569 pp.

Woodward, S.J.R., Wöhling, T., and Stenger, R., 2016: Uncertainty in the modelling of spatial and temporal patterns of shallow groundwater flow paths: The role of geological and hydrological site information. *J. Hydrology*, 534, 680-694.

Zhao N., 2010: Geochemical simulation of lake water injection into the geothermal reservoir in Tianjin, China. Report 32 in: *Geothermal training in Iceland 2010*. UNU-GTP, Iceland, 711-730.

Zheng C., and Wang P.P., 1999: *MT3DMS: A modular three-dimensional multispecies model for simulation of advection, dispersion and chemical reactions of contaminants in groundwater systems: Documentation and user's guide*. US Army Engineer Research and Development Center, Vicksburg, MI, contract report SERDP-99-1, 239 pp.

Zhou Y., and Li W., 2011. A review of regional groundwater flow modelling. *Geoscience Frontiers*, 2-2, 205-214.